

Copyright
by
Vishal Bang
2007

**The dissertation committee for Vishal Bang certifies that this is the approved
version of the following dissertation:**

**Development of a Successful Chemical Treatment for Gas Wells with
Condensate or Water Blocking Damage**

Committee:

Gary A. Pope, Supervisor

Mukul M. Sharma, Supervisor

Steven L. Bryant

Kamy Sepehrnoori

Keith P. Johnston

**Development of a Successful Chemical Treatment for Gas Wells with
Condensate or Water Blocking Damage**

by

Vishal Bang, B.S.; M.S.

Dissertation

Presented to the Faculty of the Graduate School of

The University of Texas at Austin

in Partial Fulfillment

of the Requirements

for the Degree of

Doctoral of Philosophy

The University of Texas at Austin

December 2007

Dedication

To my family

Acknowledgements

I would like to express my gratitude to Dr. Gary A. Pope and Dr. Mukul M. Sharma for their invaluable guidance and support. Working under their supervision has been a great experience and I have really enjoyed every moment of it. Their continuous encouragement and support, especially during the difficult phases of this research project, was a great source of motivation for me. Their guidance helped me think rationally about complex problems and solve them in a correct and yet simple manner. I would also like to thank my committee members Dr. Steven L. Bryant, Dr. Kamy Sephernoori and Dr. Keith Johnston for putting time and effort in my research.

I am extremely thankful to Harry Linnemeyer and John Rohan for their help with the experimental setup and the experiments. Their guidance and help was instrumental in setting up the laboratory and performing successful experiments. I will also like to acknowledge Dr. Bruce Rouse, Tony Bermudez, Glen Baum and Bob Savicki also for their help. I would also like to thank Ms. Esther Barrientes for helping with the administrative matters and Ms. Joanna Castillo for her help with the computers and the software packages.

I am extremely grateful to Dr. Jimmie Baran from 3M Corp. for his invaluable help and guidance in this research project. His guidance helped in solving many difficult and complex problems encountered in the research project. His contribution was instrumental in understanding and in the development of this

successful chemical treatment. I probably would not have made so much progress in my research work without his help and guidance. So, I am indebted to him for his great contribution to this research project. I am also thankful to and Dr. Larry Britton and Chris Britton for their invaluable help at various stages of this research project.

I am extremely grateful to Dr. D. Stern, Dr. N. Djabbarah and Dr. S. Lyons for giving me an opportunity to do an internship with the Upstream Research Company of ExxonMobil during the summer of 2006. It was a great learning experience for me to work with highly qualified and experienced professionals.

I would like to extend special thanks to the members of the gas condensate research project: Harry Linnemeyer, Mohabbat Ahmadi, Chengwu Yuan, Viren Kumar and Jitendra Mohan for helping me understand difficult topics and clearing my doubts through many useful discussions. Working with all of them has been a wonderful experience. I am also thankful to Corey, Alex and Ondrej for their invaluable help in the laboratory with the experiments. I would also like to thank my colleagues Abraham, Raman, Navneet, Robin, Kazuhiro, Rohit, Nitin, Elif, Waleed, Harshad, Hourshad and Yousef for their support and good company.

I will like to specially acknowledge the help provided by 3M corp. in this research project. I would also take this opportunity to thank the sponsors of the gas-condensate joint industry project: 3M, Chevron, Shell, Saudi Aramco, PDO, Schlumberger, Total, BP and Petrobras. I would also like to thank Calsep Inc. and

CMG for providing the PVTSim and GEM simulators, respectively for this research.

Finally, I am indebted to my parents, sisters and friends for their love, encouragement and support.

December

2007

**Development of a Successful Chemical Treatment for Gas Wells
with
Condensate or Water Blocking Damage**

Publication No. _____

Vishal Bang, PhD.

The University of Texas at Austin, 2007

Supervisors: Gary A. Pope and Mukul M. Sharma

During production from gas condensate reservoirs, significant productivity loss occurs after the pressure near the production wells drops below the dew point of the hydrocarbon fluid. Several methods such as gas recycling, hydraulic fracturing and solvent injection have been tried to restore gas production rates after a decline in well productivity owing to condensate and/or water blocking. These methods of well stimulation offer only temporary productivity restoration and cannot always be used for a variety of reasons.

Significant advances have been made during this study to develop and extend a chemical treatment to reduce the damage caused by liquid (condensate + water) blocking in gas condensate reservoirs. The chemical treatment alters the wettability of water-wet sandstone rocks to neutral wet, and thus reduces the

residual liquid saturations and increases gas relative permeability. The treatment also increases the mobility and recovery of condensate from the reservoir. A non-ionic polymeric fluoro-surfactant in a glycol-alcohol solvent mixture improved the gas and condensate relative permeabilities by a factor of about 2 on various outcrop and reservoir sandstone rocks. The improvement in relative permeability after chemical treatment was quantified by performing high pressure and high temperature coreflood experiments on outcrop and reservoir cores using synthetic gas mixtures at reservoir conditions. The durability of the chemical treatment has been tested by flowing a large volume of gas-condensate fluids for a long period of time.

Solvents used to dissolve and deliver the surfactant play an important part in the treatment, especially in the presence of high water saturation or high salinity brine. A screening test based on phase behavior studies of treatment solutions and brines has been used to select appropriate mixtures of solvents based on reservoir conditions.

The adsorption of the surfactant on the rock surface has been measured by measuring the concentration of the surfactant in the effluent.. Wettability of treated and untreated reservoir rocks has been analyzed by measuring the USBM and Amott-Harvey wettability indices to evaluate the effect of chemical treatment on wettability.

For the first time, chemical treatments have also been shown to remove the damage caused by water blocking in gas wells and for increasing the fracture conductivity and thus productivity of fractured gas-condensate wells. Core flood

experiments done on propped fractures show significant improvement in gas and condensate relative permeability due to surface modification of proppants by chemical treatment.

Relative permeability measurements have been done on sandstone and limestone cores over a wide range of conditions including high velocities typical of high rate gas wells and corresponding to both high capillary numbers and non-Darcy flow. A new approach has been presented to express relative permeability as a function three non-dimensionless terms; capillary number, modified Reynolds Number and PVT ratio.

Numerical simulations using a compositional simulator have been done to better understand and design well treatments as a function of treatment volume and other parameters. Injection of treatment solution and chase gas and the flow back of solvents were simulated. These simulations show that chemical treatments have the potential to greatly increase production with relatively small treatment volumes since only the near-well region blocked by condensate and/or water needs to be treated.

Table of Contents

List of Tables.....	xvii
List of Figures	lv
Chapter 1: Introduction	1
1.1 Introduction	1
1.2 Research Objectives	3
1.3: Review of Chapters:	4
Chapter 2: Literature Review	8
2.1 Productivity Decline in Gas Condensate Reservoirs:	8
2.2 Relative Permeability Studies:	11
2.3 Phase Behavior Studies of Gas Condensate Fluids	17
2.4 Methods to Treat Condensate Blockage:.....	21
2.4.1 Chemical stimulation by altering wettability	30
2.5 Modeling of Gas Condensate Well Deliverability:	34
Chapter 3: Theory and Experimental Setup for Corefloods.....	39
3.1 Theory	39
3.2 Coreflood Experimental Setup	43
3.2.1 Core Holder	44
3.2.2 Back Pressure Regulators	44
3.2.3 Accumulators	44
3.2.4 Pressure Transducers	45
3.2.5Pumps	45
3.2.6 Oven	46
3.2.7 Pressure Gauges	47
3.3 Experimental Procedure	47
3.3.1 Core Preparation.....	47

3.3.2 Establishing Initial Water Saturation	47
3.3.3 Gas Mixture Preparation	48
3.3.4 Treatment Solution Preparation	50
3.3.5 Coreflood Procedure	50
3.4 PVT Software	51
3.5 Equation of State	52
Chapter 4: Chemical Treatment of Sandstones with Methanol based Treatment Solutions.....	68
4.1 Introduction	68
4.2 Chemical Treatment of Dry Sandstone Rocks	70
4.2.1 Chemical Treatment at Low Temperature.....	71
4.2.1 Chemical Treatment at High Temperature	72
4.3 Initial Attempts to Chemically Treat Sandstone Rocks With Connate Water	74
4.3.1 First Approach: Imitating Dry Core Treatment.....	74
4.3.2 Second Approach: Solvent Pre-flush before Chemical Treatment	75
4.3.3 Third Approach: Removing Salt from Initial Water	76
4.3.4 Fourth Approach: Preflush with larger residence time	77
4.3.5 Fifth Approach: New Fluorocarbon surfactant	78
4.3.6 Sixth Approach: Toluene flush	79
4.3.7 Seventh Approach: New solvents	80
4.4. Summary	81
Chapter 5: Selection of Solvents for the Treatment Solution.....	96
5.1 Introduction:	96
5.2 Phase Behavior Studies to Identify Optimum Solvent.....	98
5.3 Sensitivity Study	101
5.4 Summary	105

Chapter 6: Chemical Treatment of Sandstones with Connate Water	153
6.1. New Solvent systems for Delivering Surfactant to Rock Surface.....	153
6.2. Chemical Treatment of Berea Sandstones Cores	154
6.3. Chemical Treatment of Reservoir Sandstone Cores.....	157
6.3.1 Chemical Treatment of North Sea Reservoir Sandstone Cores	157
6.3.2 Chemical Treatment of Hatter's Pond Reservoir Core	164
6.4. Effect of Surfactant Concentration on Chemical Treatment	167
6.5. Effect of Shut-in Time on Chemical Treatment.....	170
6.6. Adsorption Measurements of FC4430 on Berea Sandstone.....	171
6.7. Wettability Measurements on Un-Treated and Treated Reservoir Cores.....	177
6.8 Summary	182
Chapter 7: Remediation of Water Blocking in Gas Condensate Reservoirs by Chemical Treatment	215
7.1 Introduction	215
7.2 Effect of High Water Saturation and Mobile Water on Gas Relative Permeability:	216
7.2.1 Effect of high initial water saturation on an untreated reservoir core.....	216
7.2.2 Effect of mobile water on gas relative permeability	218
7.3 Chemical Treatment to Treat Damage Caused by Water and Condensate Blocking.....	220
7.3.1 Chemical treatment of Berea Sandstone at high water saturation using FC4430.....	220
7.3.2 Chemical treatment of Berea Sandstone with high water saturation using surfactant X3.....	225
7.3.3 Chemical treatment of Tunu reservoir core.....	228
7.4 Chemical Treatment Using a Non-fluorinated Surfactant.....	231
7.5 Summary	233
Chapter 8: Chemical Treatment of Propped Fractures	254
8.1 Introduction:	254

8.2 Preparation of Propped Fractures:.....	255
8.3 Effect of non-Darcy flow and net confining stress on fracture conductivity:.....	256
8.4 Reduction in Gas Relative Permeability Due to Condensate Buildup in Propped Fractures:	258
8.4.1 Measurements on propped fractures with sand as proppant: ...	260
8.4.2 Measurements on propped fractures with Bauxite as proppant:.....	261
8.5 Chemical Treatment to Improve Two-Phase Flow Conductivity of Propped Fractures:.....	263
8.5.1 Chemical treatment propped fractures with sand as proppant:	264
8.5.2 Chemical treatment of propped fractures with Bauxite as proppant:.....	267
8.6. Summary	268
Chapter 9: Chemical treatment for volatile oil and dead oil reservoirs.....	286
9.1 Introduction:	286
9.2 Chemical Treatment of Volatile Oil Reservoirs.....	288
9.3 Chemical Treatment of Dead Oil Reservoirs	289
9.4: Summary	292
Chapter 10: Analysis of the Relative Permeability of Gas-Condensate Fluids...	303
10.1 Introduction:	303
10.2 Ratio of Gas to Oil Relative Permeabilities Expressed as a Function of PVT Properties:.....	303
10.3 Effect of Capillary Number on Gas and Oil Relative Permeabilities:	306
10.4 Relative Permeability Expressed as a Function of PVT Ratio and Capillary Number:	309
10.4.1 Results for Sandstones	312
10.4.2 Results for Limestones	315
10.5 Replacing k_{rg}/k_{ro} Ratio with PVT Ratio to Account for Non-Darcy Flow:.....	321

10.6 Relative Permeability Expressed as a Function of Three Non-Dimensionless Groups:	322
10.7 Summary	323
Chapter 11: Chemical Treatment of Limestone Rocks	340
11.1 Gas Relative Permeability Measurements on Texas Cream Limestone Rocks:	340
11.2 Chemical Treatment of Texas Cream Limestone Rocks:.....	341
11.3 Summary	343
Chapter 12: Simulation study of chemical treatments to remove liquid blocking from gas reservoirs	349
12.1 Introduction:	349
12.2 GEM Compositional Simulator.....	350
12.3 Simulation Model Setup.....	351
8.3.1 EOS Model and Fluid Properties	352
12.3.2 Simulation Grid (Reservoir Model)	353
12.3.3 Initialization	353
12.3.4 Relative Permeability Model.....	354
12.4 Simulation Results.....	356
12.4.1 Base Case	356
12.4.2 Simulating Treatment Injection Process	358
12.4.3 Results of Chemical Treatment	359
12.4.4 Flow Back of Solvents	361
12.5 Summary	363
Chapter 13: Summary, Conclusions and Recommendations for Future Work ...	388
13.1: Summary	388
13.2: Conclusions	391
13.3: Future Work	392

Nomenclature	395
Appendix A	397
A1. Flow Rates Equations	397
A2. Phase behavior data	401
Appendix B	439
Appendix C	888
References	919
Vita	931

List of Tables

Table 3.1: Composition of synthetic gas mixture 1	56
Table 3.2: Composition of synthetic gas mixture 2	56
Table 3.3: Composition of synthetic gas mixture 3	57
Table 3.4: Composition of synthetic gas mixture 4	57
Table 3.5: Composition of synthetic gas mixture 5	58
Table 3.6: Composition of synthetic gas mixture 6	58
Table 3.7: Composition of synthetic gas mixture 7	59
Table 3.8: Composition of synthetic gas mixture 8	59
Table 3.9: Composition of synthetic gas mixture 9	60
Table 4.1: Composition of treatment solution.....	82
Table 4.2: Comparison of gas and oil relative permeabilities before and after chemical treatment on dry cores.....	82
Table 4.3 Effect of flowing time on improvement factor at 145oF and 1200 psig (Exp #3)	82
Table 4.4 Effect of chemical treatment on end point gas relative permeability at 145°F and 1200 psig (Exp #3).....	83
Table 4.5 Effect of flowing time on improvement factor at 250°F and 1500 psig (Exp#11)	83
Table 4.6: Composition of synthetic Britannia reservoir brine.....	84
Table 4.7: Comparison of gas and oil relative permeabilities before and after chemical treatment on Britannia reservoir cores with connate water	84

Table 4.8: Effect of solvent pre-flush on chemical treatment of Berea sandstone with connate water at 275°F and 1500 psig	85
Table 4.9: Effect of solvent pre-flush and chemical treatment of Berea sandstone with connate water at 275°F and 1500 psig	85
Table 4.10: Comparison of gas and oil relative permeabilities before and after chemical treatment using L16829 on Berea sandstone at 275°F and 1500 psig (Exp#14)	86
Table 4.11: Composition of treatment solution for experiment-19	86
Table 4.12: Composition of treatment solution for experiment-20	86
Table 4.13: Effect of chemical treatment using new solvents on Berea sandstone with connate water at 275°F and 1500 psig	87
Table 4.14: Experimental specifications for chemical treatments	87
Table 4.19: Summary of chemical treatment on sandstone rocks	88
Table 5.1: Composition of Britannia Brine	106
Table 5.2: Cloud point measurement of FC4430 in methanol-water mixture	106
Table 5.3: Solubility of Britannia Brine and treatment solution containing 2% FC4430, 88% methanol and 10% water	106
Table 5.4: Cloud point measurement of FC4430 in IPA-toluene-water mixtures	107
Table 5.5: Cloud point measurement of 2 wt% FC4430 in Propylene glycol- Ethanol mixtures	107
Table 5.6: Cloud point measurement of 2 wt% FC4430 in Propylene glycol- IPA mixtures	108

Table 5.7: Solubility of Britannia Brine and the following treatment solutions containing 2% FC4430.....	108
Table 5.8: Solubility of Britannia Brine and the following treatment solutions containing 2% FC4430.....	109
Table 5.9: Solubility of Britannia Brine and treatment solutions containing 2% FC4430 in a mixture of Dipropylene glycol monomethyl ether (DGGME) and ethanol	110
Table 5.10: Solubility of Britannia Brine and treatment solutions containing 2% FC4430 in a mixture of Dipropylene glycol monomethyl ether (DPGME) and IPA	111
Table 5.11: Solubility of Britannia brine and treatment solutions containing 2% FC4430 in a mixture of 2-butoxyethanol (EGMBE) and ethanol	112
Table 5.12: Solubility of Britannia brine and treatment solutions containing 2% FC4430 in a mixture of 2-butoxyethanol (EGMBE) and IPA.	113
Table 5.13: Solubility of Britannia brine and treatment solutions containing 2% FC4430 in a mixture of 70/30 2-butoxyethanol (EGMBE) and Ethanol.....	113
Table 5.14: Solubility of Britannia brine and treatment solutions containing 2% FC4430 in a mixture of 80/20 polypropylene glycol (PPG 425) and PG.....	114

Table 5.15: Solubility of Britannia brine and treatment solutions containing 2% FC4430 in a mixture of 65/35 polypropylene glycol (PPG 425) and PG.....	114
Table 5.16: Solubility of Britannia brine and treatment solutions containing 2% FC4430 in a mixture of 50/50 polypropylene glycol (PPG 425) and PG.....	114
Table 5.17: Solubility of 18% NaCl brine and treatment solutions containing 2% FC4430 in a mixture of 2-butoxyethanol (EGMBE) and ethanol	115
Table 5.18: Solubility of 18% NaCl brine and treatment solutions containing 2% FC4430 in a mixture of Dipropylene glycol monomethyl ether (DPGME) and ethanol.....	115
Table 5.19: Solubility of 18% NaCl brine and treatment solutions containing 2% FC4430 in a mixture of propylene glycol (PG) and ethanol....	116
Table 5.20: Solubility of 18% NaCl brine and treatment solutions containing 2% FC4430 in a mixture of propylene glycol (PG) and IPA	116
Table 5.21: Solubility of 18% NaCl brine and treatment solutions containing 2% FC4430 in a mixture of 2-butoxyethanol/ethylene glycol/propylene glycol (50/37.5/12.5)	117
Table 5.22: Solubility of 18% NaCl brine and treatment solutions containing 2% FC4430 in a mixture of 75/25 polypropylene glycol (PPG425) and ethylene glycol.....	117
Table 5.23: Composition of Hatter's Pond Brine.....	118

Table 5.24: Brine composition for Reservoir B	118
Table 5.25: Solubility of Hatter’s Pond brine and treatment solutions containing 2% FC4430 in a mixture of 70/30 2-butoxyethanol and ethanol	118
Table 5.26: Solubility of Hatter’s Pond brine and treatment solutions containing 2% FC4430 in a 70/30 mixture of polypropylene glycol (PPG 425) and IPA.....	119
Table 5.27: Solubility of Hatter’s Pond brine and treatment solutions containing 2% FC4430 in a 50/50 mixture of 2-butoxyethanol and methanol	119
Table 5.28: Solubility of Hatter’s Pond brine and treatment solutions containing 2% FC4430 in a mixture of 60/40 polypropylene glycol (PG425) and methanol	120
Table 5.29: Solubility of Hatter’s Pond brine and treatment solutions containing 2% FC4430 in a mixture of 50/50 polypropylene glycol (PG425) and methanol	120
Table 5.30: Solubility of Hatter’s Pond brine and treatment solutions containing 2% FC4430 in a mixture of 70/30 propylene glycol and IPA.....	121
Table 5.31: Solubility of Hatter’s Pond brine and treatment solutions containing 2% FC4430 in a mixture of 50/50 propylene glycol and IPA.....	121

Table 5.32: Solubility of Reservoir B reservoir brine and treatment solutions containing 2% FC4430 in a mixture of 50/50 2-butoxyethanol and ethylene glycol.....	122
Table 5.33: Solubility of Reservoir B reservoir brine and treatment solutions containing 2% FC4430 in a mixture of 50/50 2-butoxyethanol and 1,3-propanediol.....	122
Table 5.34: Composition of surfactant solution 1	123
Table 5.35: Composition of surfactant solution 2	123
Table 5.36: Composition of surfactant solution 3	123
Table 5.37: Composition of surfactant solution 4	124
Table 5.38: Composition of surfactant solution 5	124
Table 5.39: Composition of surfactant solution 6	124
Table 5.40: Composition of surfactant solution 7	125
Table 5.41: Composition of surfactant solution 8	125
Table 6.1: Synthetic Bruce Reservoir brine	184
Table 6.2: Summary of chemical treatment on Berea sandstone cores at 175°F at Swi=19%	184
Table 6.3: Properties of Bruce reservoir cores and characteristics of chemical treatment.....	185
Table 6.4: Comparison of Bruce reservoir and synthetic fluid properties at 175°F	185
Table 6.5: Summary of chemical treatment on Bruce reservoir core#7 at 175°F (Exp #24).....	186

Table 6.6: Summary of chemical treatment on high permeability Bruce reservoir cores 1 and 3 at 175°F (Exp #23)	186
Table 6.7: Effect of chase gas on chemical treatment of Bruce reservoir core at 175°F (Exp #27)	187
Table 6.8: Effect of chemical treatment on oil-wet Bruce reservoir core at 175°F (Exp #45)	187
Table 6.9: Comparison of pre-treatment and corrected post-treatment relative permeabilities for Exp #45	188
Table 6.10 Properties of Hatter's Pond reservoir cores and experimental conditions	188
Table 6.11- Comparison of Hatter's Pond reservoir and synthetic fluid properties at 308°F and 1140 psig	189
Table 6.12- Composition of characterized Hatter's Pond reservoir fluid	189
Table 6.13- Synthetic Hatter's Pond reservoir brine	190
Table 6.14: Summary of chemical treatment on Hatter's Pond reservoir cores at 308°F and 1140 psig (Exp #25)	190
Table 6.15: Characteristics and experimental conditions for experiments to study the effect of surfactant concentration on chemical treatment	191
Table 6.16: Effect of surfactant concentration on improvement factor	191
Table 6.17: summary of chemical treatment with 1% surfactant concentration (Exp #41)	192

Table 6.18: summary of chemical treatment with 0.1% surfactant concentration (Exp #42)	192
Table 6.19: Experimental conditions for chemical treatments on Berea sandstone at 175°F to study the effect of shut-in time	192
Table 6.20: Summary of chemical treatment done on Berea sandstone at 175°F with shut-in time of 1 hour (Exp-37)	193
Table 6.21: List of reservoir cores used for wettability study using centrifuge..	193
Table 6.22: Synthetic brines for Reservoir B and POH reservoir cores.....	193
Table 6.23: Properties of reservoir cores and results of centrifuge tests.....	194
Table 6.24: Characteristics of Treatment solutions used to treat Berea and reservoir cores	194
Table 6.25: Summary of chemical treatment on Berea and Reservoir cores using FC4430	196
Table 7.1: Properties of Tunu reservoir cores and experimental conditions.....	235
Table 7.2: Comparison of Tunu reservoir and synthetic fluid properties at 275°F and 1200 psig	235
Table 7.3 Gas and condensate relative permeabilities on Tunu core#7 at $S_{wi}=55\%$ (Exp #35) at 275°F and 1200 psig	236
Table 7.4: Properties of Berea cores and experimental conditions	236
Table 7.5: Bruce Synthetic brine	236
Table 7.6: Two-phase and three-phase relative permeabilities measured in Exp # 26	237

Table 7.7: Two-phase and three-phase relative permeabilities measured in Exp # 28	237
Table 7.8- Composition of treatment solution for Exp # 26	237
Table 7.9: Summary of two-phase and three-phase relative permeability data before and after treatment at 175°F and 400 psig for Exp #26.....	238
Table 7.10- Composition of treatment solution for Exp #28	238
Table 7.11- Solvent used to flush out brine in Exp #28	238
Table 7.12: Summary of two-phase and three-phase relative permeability data before and after treatment at 175°F and 420 psig for Exp #28.....	239
Table 7.13- Composition of treatment solution for Exp #30	239
Table 7.14: Solvent used to flush out brine in Exp #30	239
Table 7.15: Summary of two-phase relative permeability data before and after treatment at 175°F and 420 psig for Exp #30.....	240
Table 7.16: Composition of treatment solution used to treat Tunu reservoir core (Exp #34)	240
Table 7.17: Comparison of pre-treatment and post treatment relative permeability measured on Tunu core#4 at 2750F and 1200 psig (Exp #34).....	240
Table 7.18: Comparison of pre-treatment and post treatment relative permeability measured on Tunu reservoir cores at 2750F and 1200 psig	241

Table 7.19: Comparison of pre-treatment and post treatment relative permeability measured on Tunu reservoir cores at $S_{wi}=55\%$ at 2750F and 1200 psig	241
Table 7.20: Comparison of post treatment gas relative permeabilities measured on Tunu reservoir core#4 at 2750F and 1200 psig	242
Table 7.21: Composition of treatment solution with hydrocarbon surfactant.....	242
Table 7.22: Effect of chemical treatment using a non-fluorinated surfactant on gas and condensate relative permeabilities at 175°F and 410 psig.	242
Table 7.23: Effect of chemical treatment using a non-fluorinated surfactant on gas and water relative permeabilities at $f_w = 0.038$ and 175°F.....	243
Table 8.1: Properties of propped fracture used for Experiment 39	270
Table 8.2: Experimental conditions for Experiments 29, 31 and 39	270
Table 8.3: Comparison of Reservoir B reservoir and synthetic fluid properties at 279°F and 1450 psig	270
Table 8.4: Properties of propped fracture and rock matrix for Experiments 29 and 31	271
Table 8.5: Composition of synthetic Reservoir B brine	271
Table 8.6: Results of two-phase flow measurements on sand filled propped fracture at 279°F and 1500 psig (Exp#29).....	272
Table 8.7: Results of two-phase flow measurements on sand filled propped fracture at 279°F and 1450 psig (Exp#31).....	272

Table 8.8: Results of two-phase flow measurements on Bauxite filled propped fracture at 279°F and 1450 psig with a net confining stress of 1000 psig (Exp#39)	273
Table 8.9: Results of two-phase flow measurements on Bauxite filled propped fracture at 279°F and 1450 psig with a net confining stress of 3000 psig (Exp#39)	273
Table 8.10: Results of two-phase flow measurements on Bauxite filled propped fracture at 279°F and 1450 psig with a net confining stress of 5000 psig (Exp#39)	274
Table 8.11: Results of two-phase flow measurements on sand filled propped fracture before solvent pre-flush at 279°F and 2600 psig (Exp#29)	274
Table 8.12: Composition of solvent used for pre-flush in Experiment 29	274
Table 8.13: Composition of treatment solution used in Experiment 29	275
Table 8.14: Results of post-treatment two-phase flow measurements on sand filled propped fracture at 279°F and 1500 psig (Exp#29)	275
Table 8.15: Composition of treatment solution used in Experiment 31	275
Table 8.16: Results of post-treatment two-phase flow measurements on sand filled propped fracture at 279°F and 1450 psig (Exp#29)	276
Table 8.17: Results of post-treatment two-phase flow measurements on Bauxite filled propped fracture at 279°F and 1450 psig with a net confining stress of 1000 psi (Exp#39)	276

Table 9.1: Composition of original gas condensate (mixture-5) fluid and the equilibrium fluid in core at steady state at 400psig and 175°F	294
Table 9.2: Synthetic volatile oil fluid mixture (Exp #46)	294
Table 9.3: Core properties and experimental conditions for Experiment#46	295
Table 9.4- Composition of treatment solution (Exp #46)	295
Table 9.5: Effect of chemical treatment on two-phase gas and oil relative permeabilities for a volatile oil (Exp #46).....	296
Table 9.6 - Core properties and experimental conditions for Experiment #47 ...	296
Table 9.7: Pre-treatment oil-water relative permeability values (Exp #47)	297
Table 9.8- Post-treatment oil-water relative permeability values (Exp #47)	297
Table 10.1: Sources of Relative Permeability Data on Sandstone and Limestone cores.....	325
Table 10.2: Relative permeability model parameters tuned to match relative permeability data without non-Darcy Correction.....	326
Table 10.3 Properties of Sand filled propped fracture (Exp#43)	327
Table 10.4: Relative permeability model parameters tuned to match relative permeability data after non-Darcy Correction.....	328
Table 11.1: Summary of chemical treatments on Texas Cream Limestone cores	344
Table 11.2: Treatment solution	345
Table 12.1 Composition of characterized Bruce reservoir fluid	365
Table 12.2: Equation of states parameters for the characterized Bruce fluid and solvents	365

Table 12.3: Binary interaction coefficients between components	366
Table 12.4: Reservoir Properties	367
Table 12.5: Pre and Post treatment relative permeability parameters	367
Table 12.6: Volume of treatment solution for different treatment radii.....	368
Table A2.1: Composition of surfactant solution 1	401
Table A2.2: Composition of surfactant solution 2	401
Table A2.3: Composition of surfactant solution 3	401
Table A2.4: Composition of surfactant solution 4	401
Table A2.5: Composition of surfactant solution 5	402
Table A2.6: Composition of surfactant solution 6	402
Table A2.7: Composition of surfactant solution 7	402
Table A2.8: Composition of surfactant solution 8	402
Table A2.8: Solubility data for D.I. water and surfactant solution 1	403
Table A2.9: Solubility data for 25,000 ppm NaCl brine water and surfactant solution 1	403
Table A2.10: Solubility data for 50,000 ppm NaCl brine water and surfactant solution 1	404
Table A2.11: Solubility data for 75,000 ppm NaCl brine water and surfactant solution 1	404
Table A2.12: Solubility data for 100,000 ppm NaCl brine water and surfactant solution 1	405
Table A2.13: Solubility data for 150,000 ppm NaCl brine water and surfactant solution 1	405

Table A2.26: Solubility data for 150,000 ppm NaCl Brine and surfactant	
solution 3	412
Table A2.27: Solubility data for 175,000 ppm NaCl Brine and surfactant	
solution 3	412
Table A2.28: Solubility data for 200,000 ppm NaCl Brine and surfactant	
solution 3	413
Table A2.29: Solubility data for D.I. water and surfactant solution 4	413
Table A2.30: Solubility data for 25,000 ppm NaCl brine and surfactant	
solution 4	414
Table A2.31: Solubility data for 50,000 ppm NaCl brine and surfactant	
solution 4	414
Table A2.32: Solubility data for 75,000 ppm NaCl brine and surfactant	
solution 4	415
Table A2.33: Solubility data for 100,000 ppm NaCl brine and surfactant	
solution 4	415
Table A2.34: Solubility data for 125,000 ppm NaCl brine and surfactant	
solution 4	416
Table A2.35: Solubility data for 125,000 ppm NaCl brine and surfactant	
solution 4	416
Table A2.36: Solubility data for 150,000 ppm NaCl brine and surfactant	
solution 4	417
Table A2.37: Solubility data for 175,000 ppm NaCl brine and surfactant	
solution 4	417

Table A2.38: Solubility data for 200,000 ppm NaCl brine and surfactant	
solution 4	418
Table A2.39: Solubility data for 225,000 ppm NaCl brine and surfactant	
solution 4	418
Table A2.40: Solubility data for 250,000 ppm NaCl brine and surfactant	
solution 4	419
Table A2.41: Solubility data for D.I. water and surfactant solution 5	419
Table A2.42: Solubility data for 25,000 ppm NaCl brine and surfactant	
solution 5	420
Table A2.43: Solubility data for 50,000 ppm NaCl brine and surfactant	
solution 5	420
Table A2.44: Solubility data for 75,000 ppm NaCl brine and surfactant	
solution 5	421
Table A2.45: Solubility data for 100,000 ppm NaCl brine and surfactant	
solution 5	421
Table A2.46: Solubility data for 125,000 ppm NaCl brine and surfactant	
solution 5	422
Table A2.47: Solubility data for 150,000 ppm NaCl brine and surfactant	
solution 5	422
Table A2.48: Solubility data for 175,000 ppm NaCl brine and surfactant	
solution 5	423
Table A2.49: Solubility data for 200,000 ppm NaCl brine and surfactant	
solution 5	423

Table A2.50: Solubility data for 225,000 ppm NaCl brine and surfactant	
solution 5	424
Table A2.51: Solubility data for 250,000 ppm NaCl brine and surfactant	
solution 5	424
Table A2.52: Solubility data for D.I. water and surfactant solution 6	425
Table A2.53: Solubility data for 25,000 ppm NaCl brine and surfactant	
solution 6	425
Table A2.54: Solubility data for 50,000 ppm NaCl brine and surfactant	
solution 6	426
Table A2.55: Solubility data for 75,000 ppm NaCl brine and surfactant	
solution 6	426
Table A2.56: Solubility data for 100,000 ppm NaCl brine and surfactant	
solution 6	427
Table A2.57: Solubility data for 125,000 ppm NaCl brine and surfactant	
solution 6	427
Table A2.58: Solubility data for 150,000 ppm NaCl brine and surfactant	
solution 6	428
Table A2.59: Solubility data for 175,000 ppm NaCl brine and surfactant	
solution 6	428
Table A2.60: Solubility data for 200,000 ppm NaCl brine and surfactant	
solution 6	429
Table A2.61: Solubility data for 225,000 ppm NaCl brine and surfactant	
solution 6	429

Table A2.62: Solubility data for 250,000 ppm NaCl brine and surfactant	
solution 6	430
Table A2.63: Solubility data for D.I. water and surfactant solution 7	430
Table A2.64: Solubility data for 25,000 ppm NaCl brine and surfactant	
solution 7	431
Table A2.65: Solubility data for 50,000 ppm NaCl brine and surfactant	
solution 7	431
Table A2.66: Solubility data for 75,000 ppm NaCl brine and surfactant	
solution 7	432
Table A2.67: Solubility data for 100,000 ppm NaCl brine and surfactant	
solution 7	432
Table A2.68: Solubility data for 125,000 ppm NaCl brine and surfactant	
solution 7	433
Table A2.69: Solubility data for 150,000 ppm NaCl brine and surfactant	
solution 7	433
Table A2.70: Solubility data for 175,000 ppm NaCl brine and surfactant	
solution 7	433
Table A2.71: Solubility data for D.I. water and surfactant solution 8	434
Table A2.72: Solubility data for 25,000 ppm NaCl brine and surfactant	
solution 8	434
Table A2.73: Solubility data for 50,000 ppm NaCl brine and surfactant	
solution 8	435

Table A2.74: Solubility data for 75,000 ppm NaCl brine and surfactant	
solution 8	436
Table A2.75: Solubility data for 100,000 ppm NaCl brine and surfactant	
solution 8	436
Table A2.76: Solubility data for 125,000 ppm NaCl brine and surfactant	
solution 8	437
Table A2.77: Solubility data for 150,000 ppm NaCl brine and surfactant	
solution 8	437
Table A2.78: Solubility data for 175,000 ppm NaCl brine and surfactant	
solution 8	438
Table A2.79: Solubility data for 175,000 ppm NaCl brine and surfactant	
solution 8	438
Table B1.1: Core properties	441
Table B1.2: Result of methane flood	441
Table B1.3: Synthetic fluid properties at experimental conditions	442
Table B1.4: Results of initial two-phase flow of gas and condensate.....	442
Table B1.5: Composition of treatment solution	443
Table B1.6: Results of post-treatment two-phase flow of gas and condensate...	443
Table B2.1: Core properties	449
Table B2.2: Result of methane flood	449
Table B2.3: Synthetic fluid properties at experimental conditions	450
Table B2.4: Results of initial two-phase flow of gas condensate mixture	450

Table B2.5: Results of post-solvent flood two-phase flow of gas condensate mixture	451
Table B2.6: Composition of treatment solution	451
Table B2.7: Results of post-treatment two-phase flow of gas condensate mixture	452
Table B3.1: Core properties	460
Table B3.2: Result of methane flood	460
Table B3.3: Synthetic fluid properties at experimental conditions	461
Table B3.4: Results of initial two-phase flow of gas condensate mixture	461
Table B3.5: Composition of the equilibrium gas mixture	462
Table B3.6: Results of pre-treatment equilibrium gas flood	462
Table B3.7: Composition of treatment solution	462
Table B3.8: Results of post-treatment two-phase flow of gas condensate mixture	463
Table B3.9: Results of post-treatment equilibrium gas flood	463
Table B4.1: Core properties	470
Table B4.2: Result of methane flood	470
Table B4.3: Synthetic fluid properties at experimental conditions	471
Table B4.4: Results of initial two-phase flow of gas condensate mixture	471
Table B4.5: Composition of the equilibrium gas mixture	472
Table B4.6: Results of pre-treatment equilibrium gas flood	472
Table B4.7: Composition of treatment solution	472

Table B4.8: Results of post-treatment two-phase flow of gas condensate mixture	473
Table B4.9: Results of post-treatment equilibrium gas flood	473
Table B5.1: Core properties	480
Table B5.2: Result of methane flood	480
Table B5.3: Synthetic fluid properties at experimental conditions	481
Table B5.4: Results of initial two-phase flow of gas condensate mixture	481
Table B5.5: Composition of treatment solution	482
Table B5.6: Results of post-treatment two-phase flow of gas condensate mixture	482
Table B6.1: Core properties	487
Table B6.2: Result of methane flood	487
Table B6.3: Synthetic Brine	487
Table B6.4: Result of methane flood at Swi	488
Table B6.5: Synthetic fluid properties at experimental conditions	488
Table B6.6: Results of initial two-phase flow of gas condensate mixture	489
Table B6.7: Composition of treatment solution	489
Table B6.8: Results of post-treatment two-phase flow of gas condensate mixture	490
Table B7.1: Core properties	496
Table B7.2: Result of methane flood	496
Table B7.3: Synthetic Brine	496
Table B7.4: Result of methane flood at Swi	497

Table B7.5: Synthetic fluid properties at experimental conditions	497
Table B7.6: Results of initial two-phase flow of gas condensate mixture	498
Table B7.7: Composition of treatment solution	498
Table B7.8: Results of post-treatment two-phase flow of gas condensate mixture	499
Table B8.1: Core properties	505
Table B8.2: Result of methane flood	505
Table B8.3: Synthetic Brine	505
Table B8.4: Result of methane flood at Swi	506
Table B8.5: Synthetic fluid properties at experimental conditions	506
Table B8.6: Results of initial two-phase flow of gas condensate mixture	507
Table B8.7: Composition of treatment solution	507
Table B8.8: Results of post-treatment two-phase flow of gas condensate mixture	508
Table B9.1: Core properties	514
Table B9.2: Result of nitrogen flood	514
Table B9.3: Result of nitrogen flood at Swi	514
Table B9.4: Synthetic fluid properties at experimental conditions	515
Table B9.5: Results of initial two-phase flow of gas condensate mixture	515
Table B9.6: Composition of treatment solution	516
Table B9.7: Results of post-treatment two-phase flow of gas condensate mixture	516
Table B10.1: Core properties	522

Table B10.2: Result of methane flood	522
Table B10.3: Synthetic Brine	522
Table B10.4: Result of methane flood at Swi	523
Table B10.5: Synthetic fluid properties at experimental conditions	523
Table B10.6: Results of initial two-phase flow of gas condensate mixture	524
Table B10.7: Composition of treatment solution	524
Table B10.8: Results of post-treatment two-phase flow of gas condensate mixture	525
Table B10.9: Results of post second treatment two-phase flow of gas condensate mixture	525
Table B11.1: Core properties and Experimental conditions	532
Table B11.2: Result of methane flood	532
Table B11.3: Synthetic fluid properties at experimental conditions	533
Table B11.4: Results of initial two-phase flow of gas condensate mixture	533
Table B11.5: Composition of treatment solution	534
Table B11.6: Results of post-treatment two-phase flow of gas condensate mixture	534
Table 11.7 summary of all the post-treatment two-phase floods	535
Table B12.1: Core Properties and Experimental conditions	540
Table B12.2: Result of nitrogen flood	540
Table B12.3: Synthetic fluid properties at experimental conditions	541
Table B12.4: Results of initial two-phase flow of gas condensate mixture	541
Table B12.5: Composition of treatment solution	542

Table B12.6: Results of post-treatment two-phase flow of gas condensate mixture	542
Table B13.1: Core properties	548
Table B13.2: Result of nitrogen flood.....	548
Table B13.3: Result of nitrogen flood at Swi.....	548
Table B13.4: Synthetic fluid properties at experimental conditions	549
Table B13.5: Results of initial two-phase flow of gas condensate mixture	549
Table B13.6: Composition of treatment solution	550
Table B13.7: Results of post-treatment two-phase flow of gas condensate mixture	550
Table B13.8: Results of post-second treatment two-phase flow of gas condensate mixture.....	551
Table B13.9: Result of methane flood to measure post-treatment permeability.	551
Table B13.10: Results of post-third treatment two-phase flow of gas condensate mixture.....	552
Table B13.11: Results of two-phase flow of gas condensate mixture after toluene flood.....	552
Table B13.12: Results of post-fourth treatment two-phase flow of gas condensate mixture.....	553
Table B14.1: Core properties	564
Table B14.2: Result of nitrogen flood.....	564
Table B14.3: Result of methane flood at Swi	564
Table B14.4: Synthetic fluid properties at experimental conditions	565

Table B14.5: Results of initial two-phase flow of gas condensate mixture	565
Table B14.6: Composition of treatment solution	566
Table B14.7: Results of post-treatment two-phase flow of gas condensate mixture	566
Table B15.1: Core properties	574
Table B15.2: Result of nitrogen flood.....	574
Table B15.3: Result of nitrogen flood at Swi.....	574
Table B15.4: Synthetic fluid properties at experimental conditions	575
Table B15.5: Results of initial two-phase flow of gas condensate mixture	575
Table B15.6: Results of two-phase flow of gas condensate mixture after methanol pre-flush.....	576
Table B15.7: Composition of treatment solution	576
Table B15.8: Results of post-treatment two-phase flow of gas condensate mixture	577
Table B15.9: Results of two-phase flow of gas condensate mixture after toluene flood.....	577
Table B15.10: Results of post-second treatment two-phase flow of gas condensate mixture.....	578
Table B16.1: Core properties	586
Table B16.2: Result of nitrogen flood.....	586
Table B16.3: Synthetic fluid properties at experimental conditions	587
Table B16.4: Results of gas condensate two-phase floods at 145°F and 2600 psig	587

Table B17.1: Core properties	590
Table B17.2: Result of nitrogen flood.....	590
Table B17.3: Synthetic fluid properties at experimental conditions	590
Table B17.4: Results of gas condensate two-phase floods at 145°F	591
Table B19.1: Core properties	595
Table B19.2: Result of nitrogen flood.....	595
Table B19.3: Result of nitrogen flood at Swi.....	595
Table B19.4: Synthetic fluid properties at experimental conditions	596
Table B19.5: Results of the initial two-phase gas condensate flood.....	596
Table B19.6: Composition of treatment solution	597
Table B19.7: Results of post-treatment two-phase flow of gas condensate mixture	597
Table B20.1: Core properties	603
Table B20.2: Result of nitrogen flood.....	603
Table B20.3: Result of nitrogen flood at Swi.....	603
Table B20.4: Synthetic fluid properties at experimental conditions	604
Table B20.5: Results of the initial two-phase gas condensate flood.....	604
Table B20.6: Composition of treatment solution	605
Table B20.7: Results of post-treatment two-phase flow of gas condensate mixture	605
Table B21.1: Core properties	611
Table B21.2: Result of nitrogen flood.....	611
Table B21.3: Synthetic Bruce brine	611

Table B25.1: Core properties	636
Table B25.2: Result of nitrogen flood.....	636
Table B25.3: Synthetic Hatter's Pond brine.....	637
Table B25.4: Result of nitrogen flood at Swi.....	637
Table B25.5: Synthetic fluid properties at experimental conditions	637
Table B25.6: Results of the initial two-phase gas condensate flood.....	638
Table B25.7: Composition of treatment solution	638
Table B25.8: Results of post-treatment two-phase flow of gas condensate mixture	639
Table B25.9: Composition of second treatment solution	639
Table B25.10: Results of two-phase flow of gas condensate mixture after second treatment.....	640
Table B25.11: Result of toluene flood	640
Table B26.1: Core properties	648
Table B26.2: Result of nitrogen flood.....	648
Table B26.3: Result of nitrogen flood at Swi.....	648
Table B26.4: Synthetic fluid properties at experimental conditions	649
Table B26.5: Results of the initial two-phase and three-phase floods	649
Table B26.6: Composition of treatment solution	650
Table B26.7: Results of post-treatment two-phase flow of gas condensate mixture	650
Table B27.1: Core properties	656
Table B27.2: Result of initial methane flood at Swi = 12%	656

Table B27.3: Synthetic fluid properties at experimental conditions	657
Table B27.4: Results of the initial two-phase gas condensate flood.....	657
Table B27.5: Composition of treatment solution	658
Table B27.6: Results of post-treatment two-phase flow of gas condensate mixture	658
Table B27.7: Result of methane flood to measure final permeability.....	658
Table B28.1: Core properties	665
Table B28.2: Result of nitrogen flood.....	665
Table B28.3: Result of nitrogen flood at Swi.....	665
Table B28.4: Synthetic fluid properties at experimental conditions	666
Table B28.5: Results of the initial two-phase and three-phase floods	666
Table B28.6: Composition of treatment solution	667
Table B28.7: Results of post-treatment two-phase flow of gas condensate mixture	667
Table B28.8- Composition of the solvent used to flush out brine.....	668
Table B28.9: Results of condensate flood-3	668
Table B28.10: Results of condensate flood-4	669
Table B28.11: Results of condensate flood-5	669
Table B28.12: Results of gas condensate flood after second treatment.....	670
Table B29.1: Core and fracture properties	681
Table B29.2: Result of nitrogen flood.....	681
Table B29.3: Composition of synthetic brine	682
Table B29.4: Result of nitrogen flood at Swi.....	682

Table B31.4: Synthetic fluid properties at experimental conditions	712
Table B31.5: Results of the initial two-phase gas condensate flood.....	713
Table B31.6: Composition of treatment solution	713
Table B31.7: Results of post-treatment two-phase flow of gas condensate mixture	714
Table B31.8: Result of methane flood to measure final permeability.....	714
Table B33.1: Core properties	723
Table B33.2: Result of nitrogen flood.....	723
Table B33.3: Result of nitrogen flood at $S_{wi} = 20\%$	723
Table B33.4: Results of gas condensate floods at 175°F and 420 psig	724
Table B33.5: Results of gas condensate floods at 175°F and 200 psig	724
Table B33.6: Composition of equilibrium gas mixture at 200 psig and 175°F...	725
Table B33.7: Results of equilibrium gas condensate floods at 175°F and 200 psig	725
Table B33.8: Composition of treatment solution	725
Table B33.9: Results of post-treatment gas condensate floods at 175°F and 420 psig	726
Table B34.1: Core properties	733
Table B34.2: Result of methane flood	733
Table B34.3: Result of methane flood after solvent flush.....	734
Table B34.4: Result of methane flood at S_{wi}	734
Table B34.5: Synthetic fluid properties at experimental conditions	734
Table B34.6: Results of the initial two-phase gas condensate flood.....	735

Table B34.7: Composition of treatment solution	735
Table B34.8: Results of post-treatment two-phase flow of gas condensate mixture	736
Table B34.9: Results of post-treatment gas condensate flood after injecting 2 cc of brine	736
Table B34.10: Results of post-treatment gas condensate flood after injecting 1PV of brine	737
Table B34.11: Results of gas condensate flood after second treatment	737
Table B34.12: Result of methane flood to measure final permeability	738
Table B35.1: Core properties	747
Table B35.2: Result of nitrogen flood	747
Table B35.3: Synthetic fluid properties at experimental conditions	748
Table B35.4: Results of the initial two-phase gas condensate flood	748
Table B36.1: Core properties	752
Table B36.2: Result of nitrogen flood	752
Table B36.3: Synthetic fluid properties at experimental conditions	752
Table B36.4: Results of the initial two-phase gas-water flood	753
Table B36.5: Result of methane flood	753
Table B36.6: Synthetic fluid properties at experimental conditions	753
Table B36.7: Results of the initial two-phase gas condensate flood	754
Table B36.8: Composition of treatment solution	754
Table B36.9: Results of post-treatment gas condensate flood	755
Table B36.10: Result of methane flood to measure final permeability	755

Table B40.5: Results of the initial two-phase gas condensate flood.....	802
Table B40.6: Composition of treatment solution	803
Table B40.7: Results of post-treatment two-phase flow of gas condensate mixture	803
Table B40.8: Results of post-treatment two-phase flow of gas condensate mixture	804
Table B41.1: Core properties	811
Table B41.2: Result of nitrogen flood.....	811
Table B41.3: Result of nitrogen flood at Swi.....	811
Table B41.4: Synthetic fluid properties at experimental conditions	812
Table B41.5: Results of the initial two-phase gas condensate flood.....	812
Table B41.6: Composition of treatment solution	813
Table B41.7: Results of post-treatment two-phase flow of gas condensate mixture	813
Table B42.1: Core properties	819
Table B42.2: Result of nitrogen flood.....	819
Table B42.3: Result of nitrogen flood at Swi.....	819
Table B42.4: Synthetic fluid properties at experimental conditions	820
Table B42.5: Results of the initial two-phase gas condensate flood.....	820
Table B42.6: Composition of treatment solution	821
Table B42.7: Results of post-treatment two-phase flow of gas condensate mixture	821
Table B42.8: Result of methane flood to measure final permeability.....	821

Table B47.7: Saturation measured based on mass basis at the end of two- phase flow	871
Table B47.8: Results of third oil flood.....	871
Table B47.9: Composition of treatment solution	871
Table B47.10: Result of post-treatment brine flood at 250 c/hr.....	872
Table B47.11: Result of post-treatment oil flood at 650 c/hr.....	872
Table B47.12: Results of the initial two-phase oil-water flood	873
Table B47.13: Saturation measured based on mass basis at the end of two- phase flow	873
Table B48.1: Core properties	882
Table B48.2: Result of nitrogen flood.....	882
Table B48.3: Result of nitrogen flood at S_{wi}	882
Table B48.4: Synthetic fluid properties at experimental conditions	883
Table B48.5: Results of the initial two-phase gas condensate flood.....	883
Table B48.6: Composition of treatment solution	884
Table B48.7: Results of post-treatment two-phase flow of gas condensate mixture	884

List of Figures

Figure 1.1: World's energy consumption for the last 25 years showing a significant increase in natural gas demand (BP statistical review of world energy 2007)	7
Figure 2.1: Phase diagram of a gas-condensate system	37
Figure 2.2: Conceptual flow regions around a gas condensate well	37
Figure 2.3 Effect of wettability on residual oil saturation in Berea sandstone	38
Figure 3.1: Photograph of HTHP coreflood laboratory	61
Figure 3.2: Photograph of HTHP coreflood apparatus inside the oven	61
Figure 3.3: Photograph of transducer network used to measure pressure drop across the sections and the whole core	62
Figure 3.4: Schematic of coreflood setup.....	62
Figure 3.5: Liquid dropout of fluid-1 calculated using PREOS at 145°F	63
Figure 3.6: Liquid dropout of fluid-2 calculated using PREOS at 275°F	63
Figure 3.7: Liquid dropout of fluid-3 calculated using PREOS at 250°F	64
Figure 3.8: Liquid dropout of fluid-4 calculated using PREOS at 175°F	64
Figure 3.9: Liquid dropout of fluid-5 calculated using PREOS at 175°F	65
Figure 3.10: Liquid dropout of fluid-6 calculated using PREOS at 308°F	65
Figure 3.11: Liquid dropout of fluid-7 calculated using PREOS at 275°F	66
Figure 3.12: Liquid dropout of fluid-8 calculated using PREOS at 250°F	66
Figure 3.13: Liquid dropout of fluid-9 calculated using PREOS at 279°F	67

Figure 4.1: Steady state pressure drop measured during pre-treatment gas condensate flood at 145°F and 1200 psig	89
Figure 4.2: Effect of chemical treatment using FC4430 on condensate accumulation at 145°F and 1200 psig (Exp #3)	89
Figure 4.3: Durability of chemical treatment showed by flowing for a long period of time (Exp #3)	90
Figure 4.4: Comparison of pre-treatment and post-treatment pressure drop measured during equilibrium gas flood at 145°F and 1200 psig (Exp #3).....	90
Figure 4.5: Comparison of pre-treatment and post-treatment condensate buildup at 250°F and 1500 psig (Exp #11).....	91
Figure 4.6: Comparison of pre-treatment and post-treatment condensate accumulation in reservoir core with connate water at 275°F at 1500 psig (Exp #10)	91
Figure 4.7: Comparison of pre-treatment and post-treatment condensate accumulation in Berea sandstone with connate water at 275°F at 1500 psig (Exp #8)	92
Figure 4.8 Comparison of pre-treatment and post-treatment condensate accumulation in Berea sandstone with connate water at 275°F at 1500 psig (Exp #9)	92
Figure 4.9: Comparison of pre-treatment and post-treatment condensate accumulation in Berea sandstone with connate water at 275°F at 1500 psig (Exp #13)	93

Figure 4.10: Comparison of pre-treatment and post-treatment condensate accumulation in Berea sandstone with connate water at 275°F at 1500 psig (Exp #15)	93
Figure 4.11: Effect of chemical treatment using L19829 on condensate accumulation in Berea sandstone with connate water at 275°F at 1500 psig (Exp #14)	94
Figure 4.12: Effect of chemical treatment using FC4430 in a mixture of IPA and toluene on condensate accumulation in Berea sandstone with connate water at 275°F at 1500 psig (Exp #19).....	94
Figure 4.13: Effect of chemical treatment using FC4430 in a mixture of IPA and water on condensate accumulation in Berea sandstone with connate water at 275°F at 1500 psig (Exp #20).....	95
Figure 5.1: Phase behavior results of treatment solution-1 (2% FC4430, 69% 2-butoxyethanol and 29% ethanol) with NaCl brines of different salinities.....	126
Figure 5.2: Phase behavior results of treatment solution-2 (2% FC4430, 49% 2-butoxyethanol and 49% ethanol) with NaCl brines of different salinities.....	126
Figure 5.3: Phase behavior results of treatment solution-3 (2% FC4430, 29% 2-butoxyethanol and 69% ethanol) with NaCl brines of different salinities.....	127

Figure 5.4: Phase behavior results of treatment solution-4 (2% FC4430, 69% propylene glycol and 29% isopropanol) with NaCl brines of different salinities	127
Figure 5.5: Phase behavior results of treatment solution-5 (2% FC4430, 49% propylene glycol and 49% isopropanol) with NaCl brines of different salinities	128
Figure 5.6: Phase behavior results of treatment solution-6 (2% FC4430, 29% propylene glycol and 69% isopropanol) with NaCl brines of different salinities	128
Figure 5.7: Compatibility of treatment solutions with different ratio of solvents (2-butoxyethanol/ethanol) with 0 ppm salinity NaCl brine (D.I. water)	129
Figure 5.8: Compatibility of treatment solutions with different ratio of solvents (2-butoxyethanol/ethanol) with 25000 ppm salinity NaCl brine	130
Figure 5.9: Compatibility of treatment solutions with different ratio of solvents (2-butoxyethanol/ethanol) with 50000 ppm salinity NaCl brine	131
Figure 5.10: Compatibility of treatment solutions with different ratio of solvents (2-butoxyethanol/ethanol) with 75000 ppm salinity NaCl brine	132

Figure 5.11: Compatibility of treatment solutions with different ratio of solvents (2-butoxyethanol/ethanol) with 100,000 ppm salinity NaCl brine	133
Figure 5.12: Compatibility of treatment solutions with different ratio of solvents (2-butoxyethanol/ethanol) with 150,000 ppm salinity NaCl brine	134
Figure 5.13: Compatibility of treatment solutions with different ratio of solvents (PG/IPA) with 0 ppm salinity NaCl brine (D.I. water)	135
Figure 5.14: Compatibility of treatment solutions with different ratio of solvents (PG/IPA) with 25000 ppm salinity NaCl brine.....	136
Figure 5.15: Compatibility of treatment solutions with different ratio of solvents (PG/IPA) with 50000 ppm salinity NaCl brine.....	137
Figure 5.16: Compatibility of treatment solutions with different ratio of solvents (PG/IPA) with 75000 ppm salinity NaCl brine.....	138
Figure 5.17: Compatibility of treatment solutions with different ratio of solvents (PG/IPA) with 100,000 ppm salinity NaCl brine.....	139
Figure 5.18: Compatibility of treatment solutions with different ratio of solvents (PG/IPA) with 125,000 ppm salinity NaCl brine.....	140
Figure 5.19: Compatibility of treatment solutions with different ratio of solvents (PG/IPA) with 150,000 ppm salinity NaCl brine.....	141
Figure 5.20: Compatibility of treatment solutions with different ratio of solvents (PG/IPA) with 200,000 ppm salinity NaCl brine.....	142

Figure 5.21: Compatibility of treatment solutions with different ratio of solvents (PG/IPA) with 225,000 ppm salinity NaCl brine	143
Figure 5.22: Phase behavior results of treatment solution-7 (1% FC4430, 69.5% 2-butoxyethanol and 29.5% ethanol) with NaCl brines of different salinities	144
Figure 5.23: Phase behavior results of treatment solution-7 (1% FC4430, 49.5% 2-butoxyethanol and 49.5% ethanol) with NaCl brines of different salinities	145
Figure 5.24: Comparison of the phase behavior of treatment solutions with 2% FC4430 and 1% FC4430 in a 70/30 mixture of 2-butoxyethanol/ethanol and D.I water	146
Figure 5.25: Comparison of the phase behavior of treatment solutions with 2% FC4430 and 1% FC4430 in a 70/30 mixture of 2-butoxyethanol/ethanol and 25000 ppm NaCl brine.....	147
Figure 5.26: Comparison of the phase behavior of treatment solutions with 2% FC4430 and 1% FC4430 in a 70/30 mixture of 2-butoxyethanol/ethanol and 50,000 ppm NaCl brine.....	148
Figure 5.27: Comparison of the phase behavior of treatment solutions with 2% FC4430 and 1% FC4430 in a 70/30 mixture of 2-butoxyethanol/ethanol and 75,000 ppm NaCl brine.....	149
Figure 5.28: Comparison of the phase behavior of treatment solutions with 2% FC4430 and 1% FC4430 in a 70/30 mixture of 2-butoxyethanol/ethanol and 100,000 ppm NaCl brine.....	150

Figure 5.29: Phase behavior results of (90/10) NaCl/CaCl ₂ brines of different salinities with treatment solution-7 (1% FC4430, 69.5% 2-butoxyethanol and 29.5% ethanol).....	151
Figure 5.30: Phase behavior results of (90/10) NaCl/CaCl ₂ brines of different salinities with treatment solution-8 (1% FC4430, 49.5% 2-butoxyethanol and 49.5% ethanol).....	152
Figure 6.1: Visual inspection of effluent samples during treatment flood using 70/30 2-butoxyethanol/ethanol (Exp #29).....	197
Figure 6.2: Effect of chemical treatment on Berea sandstone at Swi=19% using 2% FC4430 in a mixture of 70/30 2-butoxyethanol and ethanol (Exp#21)	197
Figure 6.3: Effect of chemical treatment on Berea sandstone at Swi=50% using 2% FC4430 in a mixture of 50/50 2-butoxyethanol and ethanol (Exp#28)	198
Figure 6.4: Effect of chemical treatment on Berea sandstone at Swi=19% using 2% FC4430 in a mixture of 70/30 2-butoxyethanol and ethanol (Exp#30)	198
Figure 6.5: Calculated phase envelopes for characterized reservoir fluid and synthetic lab fluid	199
Figure 6.6: Calculated liquid dropout curves for characterized reservoir fluid and synthetic lab fluid at 175°F	199

Figure 6.7: Effect of chemical treatment on Bruce reservoir core at 175°F and 1930 psig using 2% FC4430 in 70/30 2-butoxyethanol and ethanol (Exp#24)	200
Figure 6.8: Effect of chemical treatment on Bruce reservoir core at 175°F and 460 psig using 2% FC4430 in 70/30 2-butoxyethanol and ethanol (Exp#24).....	200
Figure 6.9: Effect of chemical treatment on a high permeability Bruce reservoir core at 175°F and 1985 psig (Exp#23).....	201
Figure 6.10: Condensate buildup in a Bruce reservoir core at different PVT ratios (Exp#28).....	201
Figure 6.11: Effect of chase gas injection on chemical treatment of Bruce reservoir core at 175°F and 550 psig (Exp#27).....	202
Figure 6.12: Effect of capillary number and non-Darcy flow on condensate buildup in a Bruce reservoir core (Exp#45)	202
Figure 6.13: Effect of chemical treatment on an oil-wet Bruce reservoir core at 175°F and 393 psig (Exp#45).....	203
Figure 6.14: Calculated phase envelopes for characterized Hatter's Pond reservoir fluid and synthetic lab fluid.....	203
Figure 6.15: Calculated phase volume fractions for characterized Hatter's Pond reservoir fluid and synthetic lab fluid at 175°F	204
Figure 6.16: Effect of chemical treatment on an oil-wet Hatter's Pond reservoir core at 308°F and 1140 psig (Exp#25).....	204

Figure 6.17: Effect of second chemical treatment on an oil-wet Hatter's Pond reservoir core at 308°F and 1140 psig (Exp#25)	205
Figure 6.18: Effect of chemical treatment with 1% FC4430 on Berea sandstone at 175°F and 420 psig (Exp#41)	205
Figure 6.19: Effect of chemical treatment with 0.1% FC4430 on Berea sandstone at 175°F and 420 psig (Exp#42)	206
Figure 6.20: Effect of surfactant (FC430) concentration in treatment solution on improvement factor	206
Figure 6.21: Effect of chemical treatment on Berea sandstone at 175°F and 410 psig with 1 hour of shut-in time (Exp#37)	207
Figure 6.22: Calibration curve for detecting FC440 concentration using HPLC.....	207
Figure 6.23: Surfactant concentration profile in effluent while treating a dry Berea core at 250°F with treatment solution containing 2wt% surfactant (exp-32)	208
Figure 6.24: Surfactant concentration profile in effluent while treating a Berea core with $S_{wi}=19\%$ at 175°F with treatment solution containing 2wt% surfactant (exp-37)	208
Figure 6.25: Surfactant concentration profile in effluent while treating a Berea core ($S_{wi}=19\%$) at 175°F with treatment solution containing 1wt% surfactant (exp-41)	209

Figure 6.26: Surfactant concentration profile in effluent while treating a Berea core ($S_{wi}=19\%$) at 175°F with treatment solution containing 0.1wt% surfactant (exp-42)	209
Figure 6.27 Effect of surfactant concentration on adsorption on rock surface ...	210
Figure 6.28 Effect of temperature on surfactant adsorption on rock surface for treatment solution containing 2% FC4430	210
Figure 6.29 Effect of surfactant adsorption on improvement factor	211
Figure 6.30 Imbibition and drainage capillary pressure data measured on a treated Bruce reservoir core	211
Figure 6.31 Imbibition and drainage capillary pressure data measured on a treated Britannia reservoir core	212
Figure 6.32 Imbibition and drainage capillary pressure data measured on an Untreated Hatter's Pond reservoir core	212
Figure 6.33 Imbibition and drainage capillary pressure data measured on an Untreated Bruce reservoir core.....	213
Figure 6.34 Imbibition and drainage capillary pressure data measured on an Untreated Reservoir B reservoir core	213
Figure 6.35 Imbibition and drainage capillary pressure data measured on an Untreated POH reservoir core	214
Figure 7.1: Residual water saturation as a function of drawdown pressure.....	244
Figure 7.2: Comparison of P-T phase diagram for characterized reservoir fluid and the lab fluid calculated using PREOS	244

Figure 7.3: Comparison of liquid dropout for characterized reservoir fluid and the lab fluid calculated at 275°F using PREOS	245
Figure 7.4: Pressure drop across the core during gas condensate flood at Swi=55% on Tunu reservoir core#7 at 275°F and 1200 psig	245
Figure 7.5: Pressure drop across the core during two-phase at 400 psig and three-phase flow at fw=0.1 at 175°F for Exp#26	246
Figure 7.6: Pressure drop across the core during two-phase at 420 psig and three-phase flow at fw=0.038 at 175°F for Exp#28	246
Figure 7.7: Pressure drop during the treatment flood for Exp#26 shows plugging.....	247
Figure 7.8: Effect of chemical treatment on two-phase and three-phase flow in Exp#26	247
Figure 7.9: Pressure drop during the treatment flood for Exp#28 shows no plugging.....	248
Figure 7.10: Effect of chemical treatment on two-phase and three-phase flow in Exp#28	248
Figure 7.11: Comparison of condensate accumulation before and after treatment and after three phase flow for Exp#28	249
Figure 7.12: Pressure drop for 2PV's of three-phase followed by two-phase flow in Exp#28	249
Figure 7.13: Comparison of two-phase flow pressure drops before and after treatment at 175°F and 420 psig for Exp#28.....	250

Figure 7.14: Effect of chemical treatment on condensate accumulation at 175°F and 420 psig (Exp#30).....	250
Figure 7.15: Comparison of condensate accumulation before and after treatment and after three phase flow for Exp#30	251
Figure 7.16: Effect of 1PV brine injection on condensate accumulation after chemical treatment (Exp#30)	251
Figure 7.18: Effect of 10 PV brine injection on condensate accumulation after chemical treatment (Exp#30)	252
Figure 7.18: Comparison of two-phase flow pressure drops before and after treatment (Exp#30).....	252
Figure 7.19: Effect of high water saturation on treated and untreated Tunu reservoir cores at 275°F and 1200 psig	253
Figure 7.20Effect of chemical treatment using a non-fluorinated surfactant on methane-water two phase flow at fw=0.038 (Exp#36)	253
Figure 8.1: Step 1 of the preparation of propped fractures. Place spacers of the required fracture width between two halves of the core.	277
Figure 8.2: Step 2 of the preparation of propped fractures. Put the two halves of the core together with spacers between them and wrap them with a Teflon tape.....	277
Figure 8.3: Step 3 of the preparation of propped fractures. Fill up the fracture space with proppant. Then wrap the core with a heat shrink tube.	278
Figure 8.4: Deviation from Darcy's law at high gas velocities showing effect of non-Darcy flow	278

Figure 8.5: Effect of gas velocity and net confining stress on apparent gas permeability.....	279
Figure 8.6: Correcting gas permeability measurement for non-Darcy flow	279
Figure 8.7: Effect of net confining stress on fracture permeability	280
Figure 8.8: Effect of gas velocity and net confining stress on apparent gas permeability at S_{wi}	280
Figure 8.9: Effect of net confining stress on endpoint gas relative permeability at S_{wi}	281
Figure 8.10 Comparison of P-T phase envelope calculated using PREOS for the characterized reservoir fluid and the synthetic lab fluid	281
Figure 8.11 Comparison of liquid dropout at 279°F calculated using PREOS for the characterized reservoir fluid and the synthetic lab fluid.....	282
Figure 8.12 Variation of true gas relative permeability with gas velocity (Exp#29).....	282
Figure 8.13 Variation of true gas relative permeability with gas velocity (Exp#31).....	283
Figure 8.14 Variation of true gas relative permeability with Capillary number (Exp#29).....	283
Figure 8.15 Variation of true gas relative permeability with Capillary number (Exp#31).....	284
Figure 8.16 Effect of gas velocity and net-confining stress on true gas relative permeability for Experiment 39	284

Figure 8.17 Effect of Capillary number and net-confining stress on true gas relative permeability for Experiment 39	285
Figure 9.1: Comparison of P-T phase diagram of the original synthetic lab fluid-5 and the equilibrium fluid in the core at steady state at 400 psig and 175°F	298
Figure 9.2: Comparison of P-T phase diagram of the original synthetic lab fluid-3 and the equilibrium fluid in the core at steady state at 1500 psig and 250°F	298
Figure 9.3: Comparison of P-T phase diagram of the original Bruce reservoir fluid and the equilibrium fluid in the near wellbore region at 400 psig and 230°F	299
Figure 9.4: Calculated P-T phase diagram of synthetic lab fluid used as volatile oil (Exp #46).....	299
Figure 9.5: Calculated CCE liquid dropout for the lab fluid at 154°F	300
Figure 9.6: Comparison of pre-treatment and post-treatment steady state pressure drop at 154°F and 687 psig (Exp #46)	300
Figure 9.7: Pre-treatment oil-water relative permeability curve measured on Berea sandstone (Exp #47).....	301
Figure 9.8: Post-treatment oil-water relative permeability curve measured on Berea sandstone (Exp #47).....	301
Figure 9.9: Comparison of oil-water relative permeability curves before and after chemical treatment	302

Figure 10.1: Comparison of measured gas relative permeability for $k_{rg}/k_{ro}=2$ with the relative permeability model.....	329
Figure 10.2: Comparison of measured oil relative permeability for $k_{rg}/k_{ro}=2$ with the relative permeability model.....	329
Figure 10.3: Comparison of measured gas relative permeability for $k_{rg}/k_{ro}=1$ with the relative permeability model.....	330
Figure 10.4: Comparison of measured oil relative permeability for $k_{rg}/k_{ro}=1$ with the relative permeability model.....	330
Figure 10.5: Comparison of measured gas relative permeability for $k_{rg}/k_{ro}=3$ to 4 with the relative permeability model.....	331
Figure 10.6: Comparison of measured oil relative permeability for $k_{rg}/k_{ro}=3$ to 4 with the relative permeability model.....	331
Figure 10.7: Comparison of measured gas relative permeability for $k_{rg}/k_{ro}=8$ to 10 with the relative permeability model.....	332
Figure 10.8: Comparison of measured oil relative permeability for $k_{rg}/k_{ro}=8$ to 10 with the relative permeability model.....	332
Figure 10.9: Comparison of measured gas relative permeability for $k_{rg}/k_{ro}=20$ to 60 with the relative permeability model.....	333
Figure 10.10: Comparison of measured oil relative permeability for $k_{rg}/k_{ro}=20$ to 60 with the relative permeability model.....	333
Figure 10.11: Comparison of gas relative permeability measured on limestone for $k_{rg}/k_{ro}=1$ and 2 with the relative permeability model	334

Figure 10.12: Comparison of oil relative permeability measured on limestone for $k_{rg}/k_{ro}=1$ and 2 with the relative permeability model	334
Figure 10.13: Effect of capillary number and non-Darcy flow at high gas velocities on gas relative permeability	335
Figure 10.14: Combined effect of capillary number and non-Darcy flow on steady state pressure drop measurement for two-phase gas condensate flow	335
Figure 10.15: Comparison of gas relative permeability before and after correction for non-Darcy flow.....	336
Figure 10.16: Effect of capillary number on corrected and non-corrected gas relative permeability	336
Figure 10.17: Effect of capillary number on corrected and non-corrected gas relative permeability measured at different PVT ratios on propped fracture (Exp#43)	337
Figure 10.18: Comparison of corrected gas relative permeability with the modified relative permeability model for PVT ratio of 2 to 3	337
Figure 10.19: Gas relative permeability as a function of capillary number	338
Figure 10.20: Gas relative permeability as a function of PVT Ratio	338
Figure 10.21: Gas relative permeability as a function of oil saturation and capillary number.....	339
Figure 10.22: Oil saturation as a function of PVT ratio and capillary number ...	339
Figure 11.1: Pressure drop across TCL core during dynamic condensate accumulation at 145°F and 1200 psig (Exp#1)	346

Figure 11.2: Pressure drop across TCL core during dynamic condensate accumulation at S_{wi} -14% at 175°F and 420 psig (Exp#48).....	346
Figure 11.3: Effect of chemical treatment using FC4432 on gas relative permeability at 145°F and 1200 psig (Exp#1).....	347
Figure 11.4: Pressure drop across TCL core during pre-treatment dynamic condensate accumulation at 145°F and 1200 psig (Exp#2).....	347
Figure 11.5: Pressure drop across TCL core during dynamic condensate accumulation at 145°F and 1200 psig after treating with FC4430 (Exp#2).....	348
Figure 12.1: P-T phase diagram of Characterized Bruce reservoir fluid calculated using PREOS.....	369
Figure 12.2: Liquid dropout of the Characterized Bruce reservoir fluid calculated using PREOS at 230°F	369
Figure 12.3: Gas viscosity of the Characterized Bruce reservoir fluid calculated using PREOS at 230°F	370
Figure 12.4: Oil viscosity of the Characterized Bruce reservoir fluid calculated using PREOS at 230°F	370
Figure 12.5: Interfacial tension between gas and oil calculated using PREOS at 230°F for the Characterized Bruce reservoir fluid	371
Figure 12.6: Schematic of the 6 layered simulation model for a gas condensate well in Bruce field	372
Figure 12.7: Schematic showing the refined grids near the well and increasing logarithmically away from the well	373

Figure 12.8: Gas and oil relative permeabilities calculated using the capillary number dependent relative permeability model after 13 years of production.....	374
Figure 12.9: Capillary number calculated in the near wellbore region after 13 years of production.....	374
Figure 12.10: Comparison of gas and oil relative permeabilities calculated with the capillary number dependent relative permeability model option on and off	375
Figure 12.11: Comparison of pre and post-treatment relative permeability curves	375
Figure 12.12: Comparison of gas relative permeability near the well with and without treatment after 50 days	376
Figure 12.13: Comparison of oil relative permeability near the well with and without treatment after 50 days	376
Figure 12.14: Comparison of simulated gas production rate with the actual production data of well AO3 of Bruce field.....	377
Figure 12.15: Comparison of simulated oil production rate with the actual production data of well AO3 of Bruce field.....	377
Figure 12.16: Comparison of simulated reservoir pressure depletion with the actual well test data	378
Figure 12.17: Flowing bottom hole pressure data and those used in simulation	378
Figure 12.18: Oil saturation profile around the production well at different times	379

Figure 12.19: Simulated bottom hole pressure during the injection of treatment solution and chase gas	379
Figure 12.20: Effect of chemical treatment and treatment radii on gas production rate.....	380
Figure 12.21: Effect of chemical treatment and treatment radii on oil production rate.....	380
Figure 12.22: Improvement in productivity index due to chemical treatment for different treatment radii	381
Figure 12.23: Effect of treatment radius on improvement in Productivity index	381
Figure 12.24: Effect of treatment volume on improvement in Productivity index	382
Figure 12.25: Effect of chemical treatment and treatment radii on net gas production.....	382
Figure 12.26: Effect of chemical treatment and treatment radii on net oil production.....	383
Figure 12.27: Initial high gas production for the first few days after treatment calculated using default BIC's from PVTSim.....	383
Figure 12.28: Flow back of solvents in the gas phase after treatment calculated using default BIC's from PVTSim.....	384
Figure 12.29: Initial low liquid production for the first few days after treatment calculated using default BIC's from PVTSim	384
Figure 12.30: Flow back of solvents in the liquid phase after treatment calculated using default BIC's from PVTSim.....	385

Figure 12.31: Gas production rate for the first few days after treatment calculated by changing the BIC's between solvents and hydrocarbons to zero	385
Figure 12.32: Composition of the the gas phase after treatment calculated by changing the BIC's between solvents and hydrocarbons to zero...	386
Figure 12.33: Oil production rate for the first few days after treatment calculated by changing the BIC's between solvents and hydrocarbons to zero	386
Figure 12.34: Composition of the oil phase after treatment calculated by changing the BIC's between solvents and hydrocarbons to zero...	387
Figure A1.1: A schematic of the upstream back-pressure regulator (BPR-1) during two-phase flow	400
Figure B1.1: Pressure drop across the core during initial methane flood	444
Figure B1.2: Pressure drop across the core during the initial two-phase flow at 1200 psig flowing pressure	444
Figure B1.3: Pressure drop across the core during surfactant treatment.....	445
Figure B1.4: Pressure drop across the core during post-treatment two-phase flow at 1200 psig flowing pressure.	445
Figure B1.5: Pressure drop across the core during the final methane flood at 1200 psig.	446
Figure B2.1: Pressure drop across the core during initial methane flood	453
Figure B2.2: Pressure drop across the core during the initial two-phase flow at 1200 psig flowing pressure.	453

Figure B2.3: Pressure drop across the core during (methanol-water) solvent flood	454
Figure B2.4: Pressure drop across the core during post- solvent flood two- phase flow at 1200 psig flowing pressure	454
Figure B2.5: Pressure drop across the core during surfactant treatment	455
Figure B2.6: Pressure drop across the core during post-treatment two-phase flow at 1200 psig flowing pressure.	455
Figure B2.7: Pressure drop across the core during the final methane flood at 1200 psig.	456
Figure B3.1: Pressure drop across the core during initial methane flood	464
Figure B3.2: Pressure drop across the core during the initial two-phase flow at 1200 psig flowing pressure	464
Figure B3.3: Pressure drop across the core during the pre-treatment equilibrium gas flood.	465
Figure B3.4: Pressure drop across the core during surfactant treatment	465
Figure B3.5: Pressure drop across the core during post-treatment two-phase flow at 1200 psig flowing pressure.	466
Figure B3.6: Pressure drop across the core during post-treatment equilibrium gas flood	466
Figure B3.7: Pressure drop across the core during the final methane flood at 1200 psig	467
Figure B4.1: Pressure drop across the core during initial methane flood	474

Figure B4.2: Pressure drop across the core during the initial two-phase flow at 1200 psig flowing pressure	474
Figure B4.3: Pressure drop across the core during the pre-treatment equilibrium gas flood	475
Figure B4.4: Pressure drop across the core during surfactant treatment.....	475
Figure B4.5: Pressure drop across the core during post-treatment two-phase flow at 1200 psig flowing pressure	476
Figure B4.6: Pressure drop across the core during the post-treatment equilibrium gas flood	476
Figure B4.7: Pressure drop across the core during the final methane flood at 1200 psig	477
Figure B5.1: Pressure drop across the core during initial methane flood	483
Figure B5.2: Pressure drop across the core during the initial two-phase flow at 1200 psig flowing pressure	483
Figure B5.3: Pressure drop across the core during surfactant treatment.....	484
Figure B5.4: Pressure drop across the core during post-treatment two-phase flow at 1200 psig flowing pressure	484
Figure B6.1: Pressure drop across the core and the sections during initial methane flood	491
Figure B6.2: Pressure drop across the core and the sections during methane flood at $S_{wi}=26.1\%$	491
Figure B6.3: Pressure drop across the core and the sections during the initial two-phase flow at 275°F and 1500 psig	492

Figure B6.4: Pressure drop across the core and the sections during surfactant treatment.....	492
Figure B6.5: Pressure drop across the core and the sections during post-treatment two-phase flow at 275°F and 1500 psig	493
Figure B7.1: Pressure drop across the core and the sections during initial methane flood.....	500
Figure B7.2: Pressure drop across the core and the sections during methane flood at $S_{wi}=26.1\%$	500
Figure B7.3: Pressure drop across the core and the sections during the initial two-phase flow at 275°F and 1500 psig	501
Figure B7.4: Pressure drop across the core and the sections during surfactant treatment.....	501
Figure B7.5: Pressure drop across the core and the sections during post-treatment two-phase flow at 275°F and 1500 psig	502
Figure B8.1: Pressure drop across the core during initial nitrogen flood	509
Figure B8.2: Pressure drop across the core during methane flood at $S_{wi}=26.1\%$	509
Figure B8.3: Pressure drop across the core during the initial two-phase flow at 275°F and 1500 psig	510
Figure B8.4: Pressure drop across the core during solvent preflush	510
Figure B8.5: Pressure drop across the core during surfactant treatment.....	511
Figure B8.6: Pressure drop across the core and the sections during post-treatment two-phase flow at 275°F and 1500 psig	511

Figure B9.1: Pressure drop across the core during initial nitrogen flood	517
Figure B9.2: Pressure drop across the core during nitrogen flood at Swi=26.1%	517
Figure B9.3: Pressure drop across the core during the initial two-phase flow at 275°F and 1500 psig	518
Figure B9.4: Pressure drop across the core during solvent preflush	518
Figure B9.5: Pressure drop across the core during surfactant treatment.....	519
Figure B9.6: Pressure drop across the core during post-treatment two-phase flow at 275°F and 1500 psig.....	519
Figure B10.1: Pressure drop across the core during initial nitrogen flood	526
Figure B10.2: Pressure drop across the core during nitrogen flood at Swi.....	526
Figure B10.3: Pressure drop across the core during the initial two-phase flow at 275°F and 1500 psig	527
Figure B10.4: Pressure drop across the core during first surfactant treatment ...	527
Figure B10.5: Pressure drop across the core during post-treatment two-phase flow at 275°F and 1500 psig.....	528
Figure B10.6: Pressure drop across the core during second surfactant treatment.....	528
Figure B10.7: Pressure drop across the core during post-second treatment two- phase flow at 275°F and 1500 psig.....	529
Figure B11.1: Pressure drop across the core during initial nitrogen flood	536
Figure B11.2: Pressure drop across the core during the initial two-phase flow at 250°F and 1500 psig	536

Figure B11.3: Pressure drop across the core during first surfactant treatment ...	537
Figure B11.4: Pressure drop across the core during post-treatment two-phase floods at 250°F and 1500 psig	537
Figure B12.1: Pressure drop across the core during initial nitrogen flood	543
Figure B12.2: Pressure drop across the core during the initial two-phase flow at 250°F and 1500 psig	543
Figure B12.3: Pressure drop across the core during first surfactant treatment ...	544
Figure B12.4: Pressure drop across the core during post-treatment two-phase floods at 250°F and 1500 psig	544
Figure B13.1: Pressure drop across the core during initial nitrogen flood	554
Figure B13.2: Pressure drop across the core during nitrogen flood at Swi=26.1%	554
Figure B13.3: Pressure drop across the core during the initial two-phase flow at 275°F and 1500 psig	555
Figure B13.4: Pressure drop across the core during methanol preflush.....	555
Figure B13.5: Pressure drop across the core during the two-phase flow at 275°F and 1500 psig after methanol pre-flush	556
Figure B13.6: Pressure drop across the core during surfactant treatment.....	556
Figure B13.7: Pressure drop across the core during the post-first treatment two-phase flow at 275°F and 1500 psig	557
Figure B13.8: Pressure drop across the core during the second surfactant treatment.....	557

Figure B13.9: Pressure drop across the core during the post-second treatment	
two-phase flow at 275°F and 1500 psig	558
Figure B13.10: Pressure drop across the core during the methane flood at	
275°F and 1500 psig to measure the post-treatment core	
permeability.....	558
Figure B13.11: Pressure drop across the core during the third surfactant	
treatment.....	559
Figure B13.12: Pressure drop across the core during the post-third treatment	
two-phase flow at 275°F and 1500 psig	559
Figure B13.13: Pressure drop across the core during the two-phase flow at	
275°F and 1500 psig after toluene flood	560
Figure B13.14: Pressure drop across the core during the fourth surfactant	
treatment.....	560
Figure B13.15: Pressure drop across the core during the post-fourth treatment	
two-phase flow at 275°F and 1500 psig	561
Figure B14.1: Pressure drop across the core during initial nitrogen flood	567
Figure B14.2: Pressure drop across the core during nitrogen flood at	
$S_{wi}=26.1\%$	567
Figure B14.3: Pressure drop across the core during the initial two-phase flow	
at 275°F and 1500 psig	568
Figure B14.4: Pressure drop across the core during methanol preflush.....	568
Figure B14.5: Pressure drop across the core during two-phase flow at 275°F	
and 1500 psig after methanol pre-flush.....	569

Figure B14.6: Pressure drop across the core during surfactant treatment.....	569
Figure B14.7: Pressure drop across the core during post-treatment two-phase flow at 275°F and 1500 psig.....	570
Figure B15.1: Pressure drop across the core during initial nitrogen flood	579
Figure B15.2: Pressure drop across the core during nitrogen flood at S_{wi}	579
Figure B15.3: Pressure drop across the core during the initial two-phase flow at 275°F and 1500 psig	580
Figure B15.4: Pressure drop across the core during methanol preflush.....	580
Figure B15.5: Pressure drop across the core during the two-phase flow at 275°F and 1500 psig after methanol pre-flush	581
Figure B15.6: Pressure drop across the core during surfactant treatment.....	581
Figure B15.7: Pressure drop across the core during the post-first treatment two-phase flow at 275°F and 1500 psig	582
Figure B15.8: Pressure drop across the core during the toluene flood	582
Figure B15.9: Pressure drop across the core during the two-phase flow at 275°F and 1500 psig after toluene flood	583
Figure B15.10: Pressure drop across the core during the second surfactant treatment.....	583
Figure B15.11: Pressure drop across the core during the post-second treatment two-phase flow at 275°F and 1500 psig	584
Figure B16.1: Pressure drop across the core during initial nitrogen flood	588
Figure B16.2: Pressure drop across the core during the two-phase floods at 145°F and 2600 psig	588

Figure B17.1: Pressure drop across the core during initial nitrogen flood	592
Figure B17.2: Pressure drop across the core during the two-phase floods at 145°F	592
Figure B19.1: Pressure drop across the core during initial nitrogen flood	598
Figure B19.2: Pressure drop across the core during nitrogen flood at Swi=26.1%	598
Figure B19.3: Pressure drop across the core during the initial two-phase flow at 275°F and 1500 psig	599
Figure B19.4: Pressure drop across the core during surfactant treatment.....	599
Figure B19.5: Pressure drop across the core during post-treatment two-phase flow at 275°F and 1500 psig.....	600
Figure B20.1: Pressure drop across the core during initial nitrogen flood	606
Figure B20.2: Pressure drop across the core during nitrogen flood at Swi=26.1%	606
Figure B20.3: Pressure drop across the core during the initial two-phase flow at 275°F and 1500 psig	607
Figure B20.4: Pressure drop across the core during surfactant treatment.....	607
Figure B20.5: Pressure drop across the core during post-treatment two-phase flow at 275°F and 1500 psig.....	608
Figure B21.1: Pressure drop across the core during initial nitrogen flood	614
Figure B21.2: Pressure drop across the core during nitrogen flood at Swi=19%	614
Figure B21.3: Pressure drop across the core during the initial two-phase flow at 175°F and 1985 psig	615

Figure B21.4: Pressure drop across the core during surfactant treatment.....	615
Figure B21.5: Pressure drop across the core during post-treatment two-phase flow at 175°F and 1985 psig.....	616
Figure B23.1: Pressure drop across the core during initial nitrogen flood	623
Figure B23.2: Pressure drop across the core during nitrogen flood at $S_{wi}=19\%$	623
Figure B23.3: Pressure drop across the core during the initial two-phase flow at 175°F and 2000 psig	624
Figure B23.4: Pressure drop across the core during surfactant treatment.....	624
Figure B23.5: Pressure drop across the core during post-treatment two-phase flow at 175°F and 2000 psig.....	625
Figure B23.6: Pressure drop across the core during final methane flood	625
Figure B24.1: Pressure drop across the core during methane flood at $S_{wi}=22\%$	631
Figure B24.2: Pressure drop across the core during the initial two-phase flow at 1930 psig and 460 psig flowing pressures.....	631
Figure B24.3: Pressure drop across the core during surfactant treatment.....	632
Figure B24.4: Pressure drop across the core during post-treatment two-phase flow at 1930 psig and 460 psig flowing pressures	632
Figure B24.5: Pressure drop across the core during final methane flood	633
Figure B25.1: Pressure drop across the core during initial nitrogen flood	641
Figure B25.2: Pressure drop across the core during nitrogen flood at $S_{wi}=20\%$	641
Figure B25.3: Pressure drop across the core during the initial two-phase flow at 308°F and 1140 psig	642

Figure B27.5: Pressure drop across the core during post-treatment two-phase flow at 550 psig	661
Figure B27.6: Pressure drop across the core during final methane flood	661
Figure B28.1: Pressure drop across the core during initial nitrogen flood	671
Figure B28.2: Pressure drop across the core during nitrogen flood at $S_{wi}=19\%$	671
Figure B28.3: Pressure drop across the core during the initial two-phase and three-phase floods at 175°F and 420 psig.....	672
Figure B28.4: Pressure drop across the core during surfactant treatment.....	672
Figure B28.5: Pressure drop across the core during post-treatment two-phase and three-phase floods at 175°F and 420 psig.....	673
Figure B28.6: Pressure drop across the core during solvent flood-1	673
Figure B28.7: Pressure drop across the core during condensate flood-3	674
Figure B28.8: Pressure drop for 2PV's of three-phase followed by two-phase flow.....	674
Figure B28.9: Pressure drop across the core during brine injection	675
Figure B28.10: Pressure drop across the core during solvent flood-2	675
Figure B28.11: Pressure drop across the core during condensate flood-5	676
Figure B28.12: Pressure drop across the core during second chemical treatment.....	676
Figure B28.13: Pressure drop across the core during the gas condensate flood after second chemical treatment.....	677
Figure B29.1: Pressure drop across the propped fracture during initial nitrogen flood	685

Figure B29.2: Correcting gas permeability measurement for non-Darcy flow...	685
Figure B29.3: Pressure drop across the propped fracture during the brine flood	686
Figure B29.4: Pressure drop across the propped fracture during nitrogen flood at Swi.....	686
Figure B29.5: Correcting gas permeability measurement at Swi for non-Darcy flow.....	687
Figure B29.6: Pressure drop across the propped fracture during the initial two- phase flood at 279°F and 2600 psig	687
Figure B29.7: Pressure drop across the propped fracture during the solvent flood	688
Figure B29.8: Pressure drop across the propped fracture during the gas condensate flood after solvent flush at 279°F and 1500 psig	688
Figure B29.9: Pressure drop across the propped fracture during the gas condensate flood in the reverse flow direction at 279°F and 1500 psig	689
Figure B29.10: Pressure drop across the propped fracture during surfactant treatment.....	689
Figure B29.11: Pressure drop across the propped fracture during post- treatment two-phase flood at 279°F and 1500 psig	690
Figure B30.1: Pressure drop across the core during initial nitrogen flood	699
Figure B30.2: Pressure drop across the core during nitrogen flood at Swi=19%	699
Figure B30.3: Pressure drop across the core during the initial gas condensate flood at 175°F and 420 psig.....	700

Figure B30.4: Pressure drop across the core during surfactant treatment.....	700
Figure B30.5: Pressure drop across the core during post-treatment gas condensate flood at 175°F and 420 psig	701
Figure B30.6: Pressure drop for 2PV's of three-phase followed by two-phase flow.....	701
Figure B30.7: Pressure drop across the core during solvent flood-1	702
Figure B30.8: Pressure drop across the core during condensate flood-4	702
Figure B30.9: Pressure drop across the core during injection of 1 PV of brine..	703
Figure B30.10: Pressure drop across the core during solvent flood-2	703
Figure B30.11: Pressure drop across the core during condensate flood-5	704
Figure B30.12: Pressure drop across the core during injection of 10 PV of brine.....	704
Figure B30.13: Pressure drop across the core during solvent flood-3	705
Figure B30.14: Pressure drop across the core during condensate flood-6	705
Figure B30.15: Pressure drop across the core during solvent flood-4	706
Figure B30.16: Pressure drop across the core during condensate flood-7	706
Figure B31.1: Pressure drop across the propped fracture during initial nitrogen flood	715
Figure B31.2: Correcting gas permeability measurement for non-Darcy flow...	715
Figure B31.3: Pressure drop across the propped fracture during nitrogen flood at $S_{wi}=25\%$	716
Figure B31.4: Correcting gas permeability measurement at $S_{wi}=25\%$ for non- Darcy flow	716

Figure B31.5: Pressure drop across the propped fracture during the initial two- phase flood at 279°F and 1450 psig	717
Figure B31.6: Pressure drop across the propped fracture during the initial two- phase flood in the reverse flow direction at 279°F and 1450 psig ..	717
Figure B31.7: Pressure drop across the propped fracture during surfactant treatment.....	718
Figure B31.8: Pressure drop across the propped fracture during post-treatment two-phase flood at 279°F and 1450 psig	718
Figure B31.9: Pressure drop across the propped fracture during the second surfactant treatment	719
Figure B31.10: Pressure drop across the propped fracture during gas condensate flood after second treatment at 279°F and 1450 psig ..	719
Figure B31.11: Pressure drop across the propped fracture during second gas condensate flood after second treatment at 279°F and 1450 psig ..	720
Figure B31.12: Pressure drop across the propped fracture during final methane flood	720
Figure B33.1: Pressure drop across the core during initial nitrogen flood	727
Figure B33.2: Pressure drop across the core during nitrogen flood at $S_{wi}=20\%$	727
Figure B33.3: Pressure drop across the core during the gas condensate floods at 420 psig and 200 psig	728
Figure B33.4: Pressure drop across the core during the equilibrium gas floods at 175°F and 200 psig	728
Figure B33.5: Pressure drop across the treatment flood	729

Figure B33.6: Pressure drop across the core during the post-treatment gas condensate floods at 175°F and 420 psig	729
Figure B34.1: Pressure drop across the core during initial methane flood	739
Figure B34.2: Pressure drop across the core during solvent flood.....	739
Figure B34.3: Pressure drop across the core during methane flood after the solvent flush	740
Figure B34.4: Pressure drop across the core during methane flood at Swi=30%	740
Figure B34.5: Pressure drop across the core during the initial gas condensate flood at 275°F and 1200 psig.....	741
Figure B34.6: Pressure drop across the core during surfactant treatment.....	741
Figure B34.7: Pressure drop across the core during the first post-treatment gas condensate flood at 275°F and 1200 psig.....	742
Figure B34.8: Pressure drop across the core during the second post-treatment gas condensate flood at 275°F and 1200 psig	742
Figure B34.9: Pressure drop across the core during the post-treatment gas condensate flood after injecting 2 cc of brine at 275°F and 1200 psig	743
Figure B34.10: Pressure drop across the core during the post-treatment gas condensate flood after injecting 1PV of brine at 275°F and 1200 psig	743
Figure B34.11: Pressure drop across the core during the second surfactant treatment.....	744

Figure B34.12: Pressure drop across the core during the gas condensate flood after the second treatment at 275°F and 1200 psig.....	744
Figure B34.13: Pressure drop across the core during final methane flood	745
Figure B35.1: Pressure drop across the core during initial nitrogen flood	749
Figure B35.2: Pressure drop across the core during the gas condensate flow at 275°F and 1200 psig	749
Figure B36.1: Pressure drop across the core during initial nitrogen flood	757
Figure B36.2: Pressure drop across the core during the initial two-phase gas- water flood (fw=0.038) at 175°F and 410 psig.....	757
Figure B36.3: Pressure drop across the core during methane flood.....	758
Figure B36.4: Pressure drop across the core during the initial gas condensate flood at 175°F and 410 psig.....	758
Figure B36.5: Pressure drop across the core during surfactant treatment.....	759
Figure B36.6: Pressure drop across the core during post-treatment gas condensate flood at 175°F and 410 psig.....	759
Figure B36.7: Pressure drop across the core during final methane flood	760
Figure B36.8: Pressure drop across the core during the post-treatment two- phase gas-water flood (fw=0.038) at 175°F and 410 psig.....	760
Figure B37.1: Pressure drop across the core during initial nitrogen flood	766
Figure B37.2: Pressure drop across the core during nitrogen flood at Swi=19%	766
Figure B37.3: Pressure drop across the core during the initial two-phase flow at 175°F and 400 psig	767
Figure B37.4: Pressure drop across the core during surfactant treatment.....	767

Figure B37.5: Pressure drop across the core during post-treatment two-phase flow at 175°F and 400 psig.....	768
Figure B38.1: Pressure drop across the core during initial nitrogen flood	774
Figure B38.2: Pressure drop across the core during nitrogen flood at $S_{wi}=20\%$	774
Figure B38.3: Pressure drop across the core during the initial two-phase flow at 175°F and 500 psig	775
Figure B38.4: Pressure drop across the core during surfactant treatment.....	775
Figure B39.1: Pressure drop across the propped fracture during initial nitrogen flood at different net confining stresses	789
Figure B39.2: Correcting gas permeability measurement for non-Darcy flow at net confining stress of 1000 psig.....	789
Figure B39.3: Correcting gas permeability measurement for non-Darcy flow at net confining stress of 2000 psig.....	790
Figure B39.4: Correcting gas permeability measurement for non-Darcy flow at net confining stress of 3000 psig.....	790
Figure B39.5: Correcting gas permeability measurement for non-Darcy flow at net confining stress of 4000 psig.....	791
Figure B39.6: Correcting gas permeability measurement for non-Darcy flow at net confining stress of 5000 psig.....	791
Figure B39.7: Correcting gas permeability measurement for non-Darcy flow at net confining stress of 7000 psig.....	792
Figure B39.8: Correcting gas permeability measurement for non-Darcy flow at net confining stress of 9000 psig.....	792

Figure B39.9: Pressure drop across the propped fracture during initial nitrogen flood at Swi at different net confining stresses	793
Figure B39.10: Correcting gas permeability measurement at Swi for non-Darcy flow at net confining stress of 1000 psig	793
Figure B39.11: Correcting gas permeability measurement at Swi for non-Darcy flow at net confining stress of 3000 psig	794
Figure B39.12: Correcting gas permeability measurement at Swi for non-Darcy flow at net confining stress of 5000 psig	794
Figure B39.13: Correcting gas permeability measurement at Swi for non-Darcy flow at net confining stress of 7000 psig	795
Figure B39.14: Pressure drop across the propped fracture during the initial gas condensate flood at 279°F and 1450 psig and different net confining stresses	795
Figure B39.15: Pressure drop across the propped fracture during surfactant treatment	796
Figure B39.16: Pressure drop across the propped fracture during the post-treatment gas condensate flood at 275°F and 1450 psig and a net confining stress of 1000 psi	796
Figure B39.17: Pressure drop across the propped fracture during final methane flood	797
Figure B39.18: Pressure drop across the propped fracture during second surfactant treatment	797

Figure B39.19 Pressure drop across the propped fracture during the gas condensate flood after second treatment	798
Figure B40.1: Pressure drop across the core during initial nitrogen flood	805
Figure B40.2: Pressure drop across the core during nitrogen flood at $S_{wi}=20\%$	805
Figure B40.3: Pressure drop across the core during the initial two-phase flow at 175°F and 970 psig	806
Figure B40.4: Pressure drop across the core during surfactant treatment.....	806
Figure B40.5: Pressure drop across the core during the post-treatment two- phase flow at 175°F and 970 psig.....	807
Figure B40.6: Pressure drop across the core during second surfactant treatment.....	807
Figure B40.7: Pressure drop across the core during the gas condensate flood after the second treatment at 175°F and 970 psig.....	808
Figure B41.1: Pressure drop across the core during initial nitrogen flood	814
Figure B41.2: Pressure drop across the core during nitrogen flood at $S_{wi}=19\%$	814
Figure B41.3: Pressure drop across the core during the initial two-phase flow at 175°F and 420 psig	815
Figure B41.4: Pressure drop across the core during surfactant treatment.....	815
Figure B41.5: Pressure drop across the core during post-treatment two-phase flow at 175°F and 420 psig.....	816
Figure B42.1: Pressure drop across the core during initial nitrogen flood	822
Figure B42.2: Pressure drop across the core during nitrogen flood at $S_{wi}=19\%$	822

Figure B42.3: Pressure drop across the core during the initial two-phase flow at 175°F and 420 psig	823
Figure B42.4: Pressure drop across the core during surfactant treatment.....	823
Figure B42.5: Pressure drop across the core during post-treatment two-phase flow at 175°F and 420 psig.....	824
Figure B43.1: Pressure drop across the propped fracture during initial nitrogen flood at different net confining stresses	837
Figure B43.2: Correcting gas permeability measurement for non-Darcy flow at net confining stress of 1000 psig.....	837
Figure B43.3: Correcting gas permeability measurement for non-Darcy flow at net confining stress of 2000 psig.....	838
Figure B43.4: Correcting gas permeability measurement for non-Darcy flow at net confining stress of 3000 psig.....	838
Figure B43.5: Correcting gas permeability measurement for non-Darcy flow at net confining stress of 4000 psig.....	839
Figure B43.6: Correcting gas permeability measurement for non-Darcy flow at net confining stress of 5000 psig.....	839
Figure B43.7: Pressure drop across the propped fracture during initial nitrogen flood at S_{wi} at different net confining stresses	840
Figure B43.8: Correcting gas permeability measurement at S_{wi} for non-Darcy flow at net confining stress of 1000 psig.....	840
Figure B43.9: Correcting gas permeability measurement at S_{wi} for non-Darcy flow at net confining stress of 3000 psig.....	841

Figure B43.10: Correcting gas permeability measurement at S_{wi} for non-Darcy flow at net confining stress of 5000 psig	841
Figure B43.11: Pressure drop across the propped fracture during the initial gas condensate flood at 175°F and 3200 psig	842
Figure B43.12: Pressure drop across the propped fracture during the initial gas condensate flood at 175°F and 3750 psig	842
Figure B43.13: Pressure drop across the propped fracture during the initial gas condensate flood at 175°F and 400 psig	843
Figure B43.14: Pressure drop across the propped fracture during the second gas condensate flood at 175°F and 3200 psig	843
Figure B43.15: Pressure drop across the propped fracture during the second gas condensate flood at 175°F and 3750 psig	844
Figure B43.16: Pressure drop across the propped fracture during surfactant treatment	844
Figure B43.17: Pressure drop across the propped fracture during the post-treatment gas condensate flood at 175°F and 3200 psig	845
Figure B43.18: Pressure drop across the propped fracture during final methane flood	845
Figure B45.1: Pressure drop across the core during initial nitrogen flood	851
Figure B45.2: Pressure drop across the core during nitrogen flood at $S_{wi}=19\%$	851
Figure B45.3: Pressure drop across the core during the initial two-phase flow at 175°F and 400 psig	852
Figure B45.4: Pressure drop across the core during surfactant treatment	852

Figure B45.5: Pressure drop across the core during post-treatment two-phase flow at 175°F and 400 psig.....	853
Figure B45.6: Pressure drop across the core during final methane flood	853
Figure B46.1: Pressure drop across the core during initial nitrogen flood	860
Figure B46.2: Pressure drop across the core during nitrogen flood at $S_{wi}=19\%$	860
Figure B46.3: Pressure drop across the core during the initial two-phase flow at 154°F and 687 psig	861
Figure B46.4: Pressure drop across the core during surfactant treatment.....	861
Figure B46.5: Pressure drop across the core during post-treatment two-phase flow at 154°F and 687 psig.....	862
Figure B46.6: Pressure drop across the core during final methane flood	862
Figure B47.1: Pressure drop across the core and the sections during first brine flood	874
Figure B47.2: Pressure drop across the core and the sections during first oil flood	874
Figure B47.3: Pressure drop across the core and the sections during second brine flood	875
Figure B47.4: Pressure drop across the core and the sections during second oil flood	875
Figure B47.5: Pressure drop across the core and the sections during initial two-phase oil-water flood at different fractional flows.....	876
Figure B47.6: Pressure drop across the core and the sections during third oil flood	876

Figure B47.7: Pressure drop across the core and the sections during treatment flood	877
Figure B47.8: Pressure drop across the core and the sections during ethanol flood	877
Figure B47.9: Pressure drop across the core and the sections during first post- treatment oil flood	878
Figure B47.10: Pressure drop across the core and the sections during first post-treatment brine flood	878
Figure B47.11: Pressure drop across the core and the sections during second post-treatment oil flood	879
Figure B47.12: Pressure drop across the core and the sections during the post- treatment two-phase oil-water flood at different fractional flows..	879
Figure B48.1: Pressure drop across the core during initial nitrogen flood	885
Figure B48.2: Pressure drop across the core during nitrogen flood at Swi=19%	885
Figure B48.3: Pressure drop across the core during the initial two-phase flow at 175°F and 420psig	886
Figure B48.4: Pressure drop across the core during surfactant treatment.....	886
Figure B48.5: Pressure drop across the core during post-treatment two-phase flow at 175°F and 420 psig.....	887

Chapter 1: Introduction

1.1 INTRODUCTION

Natural gas has become an important source of global energy and is projected to be the fastest-growing component of primary world energy consumption. At present, natural gas provides approximately a quarter (25%) of the world's energy and its share is increasing significantly. **Figure 1.1** shows the world's energy consumption for the last 25 years (**BP statistical review of world energy 2007**). Oil still remains as the world's leading energy source but it has lost a significant amount of its market share to gas and coal. Over the last couple of years the gas consumption has increased by an average of 3% compared to less than 1% increase in global oil consumption. Natural gas has also become the most desirable source of energy from the standpoint of global environmental problems as it is the cleanest of all the fossil fuels. A rapid increase in worldwide demand of natural gas has resulted in significant growth of international gas trade and encouraged long-term contracts for its sales. Hence, it becomes important to accurately predict the production performances of these reservoirs and meet the predicted production rates.

Many of the natural gas reservoirs have reservoir conditions, which result in retrograde condensation as the pressure decreases during the production of gas. During depletion of gas condensate reservoirs as the pressure falls below the dew point pressure of the reservoir gas, condensate drops out of the gas phase and forms a condensate bank near the well bore. The condensed liquid is trapped by the capillary forces or is retained in the rock as a result of low liquid permeability. Condensate formation results in build up of a liquid phase around the wellbore; leading to a decrease in the effective permeability to gas. The liquid continues to accumulate, occupying portions of the rock pores that otherwise would be available for gas flow, and thus impeding gas flow, until a

critical liquid saturation is reached that is similar to the value for residual oil saturation that would form in the same rock under the same flow conditions. Once the critical liquid saturation is exceeded, both the condensate and gas flow towards the wellbore, but condensate continues to form and accumulate until a steady state saturation is reached that is somewhat higher than the critical condensate saturation. This phenomenon is called "Condensate Banking." Condensate banking can reduce the well productivity significantly, in several instances by a factor of 2 to 4. Afidick *et al.* (1994), Barnum *et al.* (1995), Engineer (1985) and Ayyalasomayajula *et al.* (2005) have reported field data that show significant productivity loss due to condensate accumulation.

The decline in well productivity because of liquid build up around the near wellbore region depends on several factors including fluid phase behavior, flow regime (Darcy or non-Darcy), interfacial forces between fluids, Capillary number, basic rock and fluid properties, wettability, gravitational forces and well type (well inclination, fractured or non-fractured). Depending on the reservoir conditions, some of these factors play a more significant role in condensate accumulation than the others.

Predicting production from gas-condensate wells requires an accurate relative permeability model when a condensate bank forms. The difficulty arises in capturing this near well bore phenomenon accurately since it is a two-phase flow problem with large changes in relative permeability. At high flow rates typical of many gas-condensate wells, the relative permeability is rate dependent. capillary number dependent relative permeability models are required to model the decrease in the residual saturations and the corresponding increase in relative permeability as viscous forces become dominant over the interfacial forces.

Several methods have been proposed to restore gas production rates after a decline owing to condensate and/or water blocking. The most common approach to treat damage caused by condensate blocking are either to change the phase behavior of the gas condensate fluid or to reduce the pressure drawdown and maintain pressure above the dew point pressure. Gas recycling, hydraulic fracturing and methanol injection have been tried but with limited success. These methods of treatment offer only temporary restoration of well productivity.

Altering the wettability of rocks in the near wellbore region of gas condensate wells, from strongly water-wet or oil-wet to neutral wet can provide a long-term solution to the problem. Wettability alteration to intermediate or neutral wet will decrease the total liquid saturation (condensate + water) in the near wellbore region, where maximum damage occurs, and result in increase in gas relative permeability. Such treatments will also increase the mobility and recovery of condensate from the reservoirs.

1.2 RESEARCH OBJECTIVES

The objective of this research work is to develop an effective and durable treatment for gas wells, which face a severe damage caused by liquid blocking (condensate + water). The main objectives can be summarized as:

- Development of a chemical treatment to stimulate gas condensate wells with condensate and/or water blocks. The motive is to increase the oil and gas relative permeabilities for a fluid flowing below the dew point pressure by reducing the total residual liquid (condensate + water) saturation. The research intends to evaluate surfactants that strongly and permanently adhere to the rock surface and at the same time impart oil and water repellency to the rock surface by altering the rock wettability from

oil or water wet to neutral wet. The research also aims at designing the appropriate solvent for delivering the surfactant to rock surface in presence of water, including high salinity brines.

- Perform coreflood experiments with synthetic gas condensate mixtures on outcrop rocks and reservoir rocks under reservoir conditions to study the effect of wettability alteration on gas and condensate relative permeability.
- Perform wettability measurements of treated rocks to evaluate the effectiveness of chemicals in altering the wettability of the rocks.
- Develop an accurate relative permeability model that accounts for the change in relative permeabilities due to capillary number and non-Darcy flow effects both before and after chemical treatment.
- Simulate the chemical treatment for gas condensate wells to study the effect of treatment at field scale.

1.3: REVIEW OF CHAPTERS:

The dissertation is organized into 13 chapters.

Chapter 2 reviews the studies related to productivity decline in gas condensate reservoirs, coreflood studies done to measure gas-condensate relative permeabilities in laboratory, studies on the phase behavior of gas condensate fluids, treatments proposed to remove condensate blocks and performance predictions from gas condensate wells using compositional simulators. The chapter also summarizes past chemical treatments proposed to mitigate the problem of condensate blocking.

Chapter 3 describes the experimental apparatus and the procedure used for conducting the coreflood experiments. The chapter describes the high-pressure and high-

temperature apparatus used for the experiments followed by a description of the experimental setup, and procedure for the preparation of the gas mixture and surfactant solution. The chapter also summarizes the Equation of states model used for this study and the various synthetic gas condensate mixtures designed and used in this study.

Chapter 4 presents the results of coreflood experiments conducted to evaluate the effect of chemical treatment on sandstone rocks with and without connate water using methanol based treatment solutions. The chapter also gives an introduction to the surfactant used in this study. The chapter describes the preliminary approaches tried to treat rocks with connate water.

Chapter 5 presents the results of phase behavior study conducted to evaluate the appropriate solvents for delivering the surfactant to the rock surface in presence of connate water including very high water saturations and high salinity brines under reservoir conditions.

Chapter 6 presents the results of coreflood experiments conducted to evaluate the effect of chemical treatment using treatment solutions developed based on the phase behavior studies (presented in Chapter 5) on both Berea and reservoir sandstone rocks with connate water. The chapter also presents the results of adsorption measurements conducted under various conditions and the results of wettability measurements on treated reservoir cores.

Chapter 7 presents the results of coreflood experiments conducted to evaluate the effect of chemical treatment in reducing the damage caused by water blocking along with condensate blocking on gas relative permeability. The chapter also discusses the effect of mobile water on the durability of the chemical treatment.

Chapter 8 presents a new approach developed for preparing propped fractures and improving the multi-phase flow conductivity of propped fractures by surface

modification of proppants. Results of two-phase flow measurements conducted on propped fractures before and after the chemical treatment are also presented.

Chapter 9 presents coreflood experiments conducted to evaluate the applicability of chemical treatment for volatile oil and dead oil reservoirs.

Chapter 10 presents a new approach for modeling gas and condensate relative permeabilities accurately, to account for the effects of capillary number, non-Darcy flow and PVT ratio (fluid properties) on two-phase flow. The chapter presents gas and oil relative permeability data measured over a wide range of capillary numbers and PVT ratios and the UT relative permeability model calibrated against the data.

Chapter 11 presents coreflood experiments conducted to evaluate different surfactants for treating limestone cores.

Chapter 12 presents results of the compositional simulation study of gas condensate well using a single well model. The chapter investigates effect of chemical treatment for different treatment radii on the improvement in well productivity. Simulations also model the injection of the treatment solution followed by chase gas injection and the flow back of solvents.

Chapter 13 presents a summary and the main conclusions of this research work. The chapter also proposes the future work for this research project.

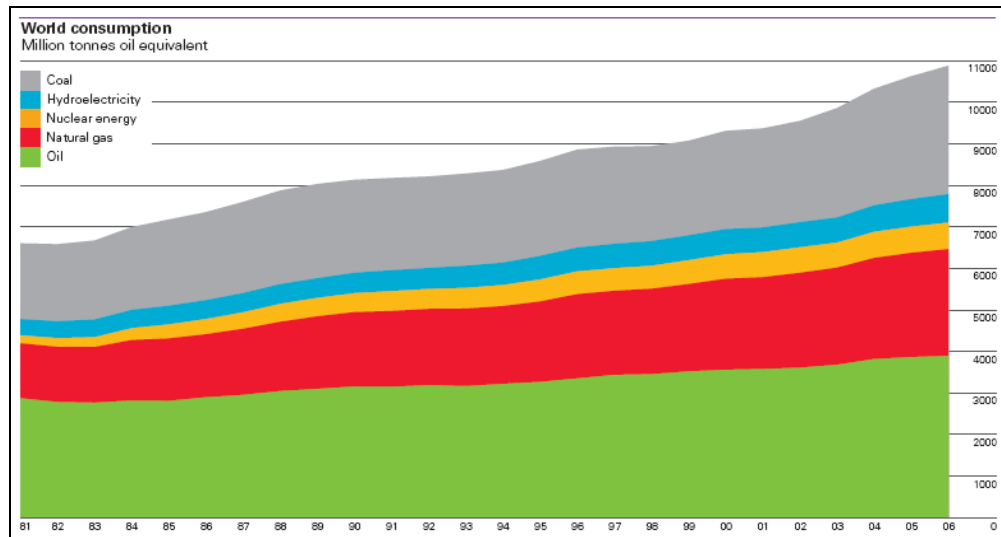


Figure 1.1: World's energy consumption for the last 25 years showing a significant increase in natural gas demand (BP statistical review of world energy 2007)

Chapter 2: Literature Review

2.1 PRODUCTIVITY DECLINE IN GAS CONDENSATE RESERVOIRS:

As a gas reservoir produces, the pressure in the reservoir decreases due to depletion. In some kind of gas reservoirs, known as retrograde gas-condensate reservoir, when the pressure decreases to a certain point, called the saturation pressure or dewpoint, a liquid phase rich in heavier hydrocarbons drops out of gas and depletes the gas of heavy ends (**Figure 2.1**). This liquid rich phase is commonly known as condensate. The condensed liquid is trapped by the capillary forces or is retained in the rock as a result of low liquid mobility. As the largest pressure drop occurs near producing wells, the formation of condensate phase usually starts as a near wellbore phenomenon. Thus, condensate formation results in build up of a liquid phase around the wellbore; leading to a decrease in the effective permeability to gas.

Conceptually, flow in gas-condensate fields can be divided into three reservoir regions, although in some situations not all three are present (**Figure 2.2**). The two regions closest to a well can exist when bottom hole pressure is below the dewpoint of the fluid. The third region, away from producing wells, exists only when the reservoir pressure is above the dewpoint.

Region 1: This is the near-well bore region characterized by the steady state flow of gas and condensate. It has condensate saturation at or above critical saturation. In this region, high flow rate conditions prevail.

Region 2: This region is characterized by pressure slightly below the dew point pressure, low condensate saturation, low interfacial tension and high gas velocity. At these low saturations, condensate remains immobile and only gas flows.

Region 3: An outer region containing single-phase gas. Average reservoir pressure is above the dew point pressure. Gas velocity is low.

There may also exist a region immediately near the wellbore where high trapping (capillary) number leads to decreased condensate saturation and increased gas mobility through “velocity stripping”.

In some cases the average reservoir pressure can drop below the dew point pressure, which results in dropout of condensate throughout the reservoir and the condensate that forms away from the well is not easily recoverable because of its low mobility and small pressure gradient deep in the reservoir. Therefore reservoir pressure dropping below the dewpoint has two disadvantages; gas and condensate production decrease because of near-well blockage, and the produced gas contains fewer valuable heavy ends because of dropout throughout the reservoir, where the condensate has insufficient mobility to flow toward the well.

Depending on the reservoir fluid composition, pressure and temperature, the liquid dropout from the gas phase may be as high as 30-40% (rich gas condensate fluid) or less than 1% (lean gas condensate fluid). The loss of productivity due to liquid blockage for rich gas condensates is well known and has been studied extensively. However, a common misconception is that, the damage due to liquid drop out for lean gas condensate fluids is not significant. In contrast, field data reported by Afidick *et al.* (1994) and Boom *et al.* (1996) show that even for lean fluids with low condensate dropout, high condensate saturations may build up as many pore volumes of gas pass through the near wellbore region. As the condensate saturation increases, the gas relative permeability decreases and thus the productivity of the well decreases.

Afidick *et al.* (1994) studied the decline in productivity of Arun gas condensate reservoir due to condensate accumulation. Experimental PVT analysis of the reservoir

fluid showed that the reservoir fluid was a lean gas condensate with a maximum liquid dropout of 1.1%. The decline in the productivity of the wells by a factor of around 2 as the reservoir pressure fell below the dewpoint pressure was attributed to accumulation of condensate around the wellbore. The accumulation of condensate around the wellbore was confirmed by well tests and the analysis done on the reservoir cores.

Barnum *et al.* (1995) found that production loss is severe for low productivity reservoirs i.e. those with a kh less than 1000 md-ft. They reported that the critical condensate saturation ranged from 10-30% and can decrease the productivity by a factor up to five due to condensate accumulation near the wellbore.

Engineer (1985) studied Cal Canal Field in California, which produced a very rich gas condensate fluid and had a very high water saturation of 59%. Due to high condensate and water saturation in the near wellbore region, the total gas recovery expected from the field is as low as 10%. Boom *et al.* (1996) showed that even for lean fluids with low condensate dropout, high condensate saturations could build up as many pore volumes of gas pass through the near wellbore region.

Shell and Petroleum Development Oman reported a 67% productivity loss for wells in two fields (Smits *et al.*, 2001). Chevron reported a loss of productivity for some of the well in a gas condensate field in North Sea (Ayyalasomayajulla *et al* 2005). Other large gas-condensate resources which have reported significant reduction in productivity due to condensate blocking include Shtokmanovskoye field in the Russian Barents Sea, Karachaganak field in Kazakhstan, the North field in Qatar that becomes the South Pars field in Iran, and the Cupiagua field in Colombia (Elliot *et al.* 1998).

Cvetkovic *et al.* (1990) studied production from rich gas condensate reservoirs ($\gamma > 0.75$). They concluded from their radial simulation studies that composition of a gas condensate can significantly affect the relative permeability to gas. They claimed that the

condensate problem is not significant for lean gas. Their results contradict the significant production loss reported in the lean gas condensate fields such as Arun and North Sea.

2.2 RELATIVE PERMEABILITY STUDIES:

The most important and complex phenomena associated with condensate banking and productivity reduction is relative permeability in the region affected by condensate blocking and thus there have been many investigations of gas-condensate relative permeability. As the flow process in the near wellbore region (Region 1, **Figure 2.2**) is eventually a steady-state flow process and therefore the relative permeability data needed for near wellbore region should be measured with a steady-state method.

Ham *et al.* (1967) conducted one of the earliest laboratory measurements done on gas condensate fluids. The authors used nitrogen and separator liquid from a reservoir condensate for their study. They evaluated the characteristic effect of several parameters including condensate saturation, pressure, apparent velocity, flowing liquid-vapor volume ratio, fluid composition and core type on the mobility of gas. The authors showed that relative mobility and liquid-vapor volume ratio relationships are dependent on pressure, saturation and, to a lesser extent, on velocity. The authors also showed that the critical condensate saturation is dependent on pressure and velocity.

Gravier *et al.* (1986) studied rock samples (0.4-50 md) from a carbonate gas field to determine gas and condensate relative permeabilities using a ternary pseudo-reservoir fluid of methane/pentane/nonane. They measured the critical condensate saturation and the extent of the reduction of permeability to gas in the presence of immobile condensate saturation. Their results showed that the gas relative permeability decreased from an average value of 0.68 to about 0.10 when the condensate saturation increased from 0 to 30%. The gas relative permeability decreased when the initial water saturation increased.

The measured critical condensate saturation was found to be high, ranging from 24.5% to 50.5%.

Asar and Handy (1988) conducted experiments using methane-propane mixtures to understand the effect of interfacial tension (IFT) on gas and oil relative permeability. The measurements were done over a range of pressures close to the saturation pressure to get values over a range of interfacial tensions. The authors show that the relative permeability curves approach straight line as the IFT approaches zero i.e. the fluids approach miscible conditions. They also observed that the oil relative permeability decreases faster than the gas relative permeability with the increase in IFT. The authors show an increase in residual gas and oil saturations with the increase in IFT showing that residual saturations are least when the fluids are close to miscibility and highest when they approach immiscible conditions.

Danesh *et al.* (1988) studied the phenomenon of retrograde condensation and flow of gas condensate fluids in porous media using glass micromodels and sandstone cores. The authors observed that the initial formation of condensate in pores is a film-wise process with a hydraulic conductivity thorough out the pores. The authors show that at low IFT values the effect of capillary forces become negligible compared to viscous and gravitational forces. The authors also suggest that as condensate forms as a film over the interstitial water, the flow of gas condensate fluid is expected to be different than that of low IFT gas-oil displacements.

Munkerud (1989) showed that the relative permeability curves for the gas condensate model system in a depletion process are similar to curves of ordinary gas/oil systems and that gravitational segregation of condensate is pronounced even at liquid saturation below the critical saturation. The author also observed that relative permeability to both gas and oil show strong dependence on IFT.

Hanif and Ali (1990) measured gas and condensate relative permeability for methane-propane mixtures at low interfacial tensions of 0.05 dynes/cm. They concluded that at these interfacial tensions, the capillary forces become negligible and gravitational forces are more significant. The liquid forms a film on the grains and gas occupies the center of the pores, that is, a complete wetting phenomena. The authors performed another study in 1993 with a multi-component system. They concluded that gravity has a strong effect on low interfacial tension systems (0.04 dynes/cm).

Fischlock and Smith (1993) conducted experiments to investigate the effect of condensate formation on gas and oil relative permeability in presence of connate water and three-phase flow in gas condensate systems under combined effect of waterflooding and pressure depletion. The authors observed a reduction in gas relative permeability by almost 60% for condensate saturation of about 23% in presence of 19% water saturation. They also observed that the presence of condensate phase reduced both residual gas saturation to waterflood and critical gas saturation during depressurization.

Bourbaix *et al.* (1994) and Kalaydjian *et al.* (1996) designed an experimental procedure to measure the critical condensate saturation (S_{cc}) and the relative permeabilities of gas and condensate. The authors also measured on-stream condensate dropout and local condensate saturation using a gamma ray attenuation technique with a specific method of calibration. The authors found that S_{cc} is related to initial water saturation (S_{wi}), with the total critical liquid saturation remaining constant around 26% of the pore volume for the cases they studied.

Henderson *et al.* (1998) measured steady state relative permeabilities for gas condensate fluids over a wide range of CGR (condensate to gas ratio), IFT (interfacial tension) and velocities. The authors found that relative permeabilities of both gas and

condensate phases are rate sensitive and increase with velocity. The relative permeabilities were also sensitive to the IFT and increased with lowering of IFT.

Chen *et al.* (1999) performed relative permeability measurements for two North Sea gas condensate fluids to investigate the effects of rock and fluid characteristics on critical condensate saturation and gas and condensate relative permeability. The authors used recombined fluids from two North Sea gas condensate reservoirs and 29' composite cores for their study. Their results showed that critical condensate saturation and relative permeability are sensitive to flow rate and interfacial tension. The authors also showed the condensate relative permeability curve exhibits an unusual convex curvature when plotted against condensate saturation. The authors suggest that high interfacial tension caused the decrease in condensate relative permeability with increasing condensate saturations.

Saevareid *et al.* (1999) conducted steady state coreflood experiments for gas condensate fluids and measured gas and condensate relative permeability as a function of gas-oil interfacial tension and velocity. The authors showed significant improvement in gas and condensate relative permeability with capillary number.

Mott *et al.* (2000) and Cable *et al.* (2003) conducted steady state coreflood experiments for gas condensate fluids to examine the effect of capillary number on relative permeability and distinguish the effect of high capillary number and inertial effects on relative permeabilities at high flow rates. The authors concluded that at fixed IFT, gas relative permeability increases with velocity and at a fixed capillary number, gas relative permeability decreases with velocity due to inertial flow. Cable *et al.* (2003) also did X-ray in-situ condensate saturation measurements at steady state conditions. Their results showed that condensate saturation increases with higher capillary number at a fixed value of k_{rg}/k_{ro} and therefore the authors concluded that improved gas relative

permeability at high capillary number is not due to lower condensate saturation. This result is in contradiction with the general perception that condensate saturation decreases at higher capillary number.

Du *et al.* (2000), Walker *et al.* (2000) and Al-Anazi *et al.* (2003) showed from their coreflood experiments that condensate dropout reduced the gas relative permeability by an order of magnitude and the reduction is even more severe in presence of high water saturation. The authors also showed that the decline in normalized PI (ratio of PI during two phase flow to PI during single phase flow i.e. ratio of damaged PI to original PI) is almost the same for both high and low permeability rocks. Al-Anazi (2003) also showed that non-equilibrium mass transfer phenomenon occurred in the cores at high flow rates and required more pore volumes of injected fluid to reach steady state than if local equilibrium existed in the cores.

Ayyalasomayajula *et al.* (2003) conducted steady state coreflood experiments for gas condensate fluids and measured gas and oil relative permeability as a function of capillary number for several different reservoir rocks and for a wide range of k_{rg}/k_{ro} values. The authors showed significant improvement in gas relative permeability with capillary number for all the rock types.

Nagarajan *et al.* (2004) compared gas condensate relative permeability measurements for rich and lean reservoir fluids with synthetic fluids. They concluded that relative permeability for reservoir fluids is lower than those measured with model fluids at any given liquid saturation or for the same k_{rg}/k_{ro} ratio. The comparison presented by the authors may not be totally conclusive as there is a lot of inconsistency in these measurements. The measurements done using rich reservoir fluid are compared with synthetic fluids made of either n-heptane and water which does not represent gas-oil system or methane and n-butane binary mixture, which does not have any heavier

hydrocarbons to closely imitate heavier components of the rich gas mixture. Also the results are in contradiction with those presented by Mott *et al.* (2000) using reservoir fluids and Kumar *et al.* (2006) using synthetic gas mixtures which agree with each other over a wide range of capillary numbers.

Kumar *et al.* (2006) measured gas and condensate relative permeabilities on both sandstone and limestone rocks over a wide range of conditions and fluid type. Measurements were made over a wide range of capillary number (10^{-6} - 10^{-4}). The authors expressed the relative permeability as a function of capillary number and k_{rg}/k_{ro} ratio and show a significant improvement in relative permeability for capillary numbers greater than 10^{-4} . The authors however neglected the effects of non-Darcy flow, which can be significant at high flow rates that were used to achieve high capillary numbers.

Some researchers including Henderson *et al.* (1995, 1998), Bourbiaux *et al.* (1994) have emphasized a lot on the importance of saturation measurements to get the relative permeability curves. Whereas, other including Fevang *et al.* (1995, 1996 and 2000), Ayyalasomayajula *et al.* (2003), Mot *et al.* (2000 and 2002), Cable *et al.* 2003, Al-Anazi *et al.* (2003), Du *et al.* (2001), Kumar *et al.* (2006) show in their work that condensate saturation near the well does not play a significant role as long as the functional relationship between k_{rg} vs. k_{rg}/k_{ro} remains the same. They also show that $k_{rg}=f(k_{rg}/k_{ro})$ is the underlying relative permeability relationship determining well deliverability in gas condensate reservoirs. The ratio of k_{rg} and k_{ro} is a function of fluid properties at steady-state (Chopra and Carter, 1986)). The fluid properties can be measured by standard PVT experiments.

2.3 PHASE BEHAVIOR STUDIES OF GAS CONDENSATE FLUIDS

The phase behavior of gas condensate fluids is an important factor controlling the reservoir performance of gas condensate fields. Phase behavior study of gas condensate fluids can be grouped into two main categories:

- Experimental phase behavior study of gas condensate fluids.
- Modeling the PVT properties of gas condensate fluids accurately using an equation-of-state (EOS) or other correlation.

Ahmed (1986) did a comprehensive study using eight EOS models to model gas condensate systems. The equations of state used were: Peng–Robinson (1976), Soave-Redlich-Kwong (1976), the Schmidt-Wenzel (1980), the Usdin-McAuliff (1976), the Heyen, the Kubic (1983), the Adachi-Lu (1984) and the Patel-Teja (1982). Experimental data of four gas condensate hydrocarbon mixtures were compared with the predicted PVT properties from the above-mentioned equations of state. The author concluded from his studies that the Schmidt-Wenzel EOS gave a better prediction of the volumetric properties than the others. Reliable compressibility predictions were obtained from Patel-Teja and Schmidt-Wenzel EOS. Peng-Robinson, Patel-Teja and Schmidt-Wenzel equations were found to give good vapor-liquid equilibrium predictions.

Sarkar *et al.* (1991) used the modified Patel-Teja equation of state to model gas condensate fluid phase behavior. In their approach, the modified Zudkevitch and Joffe method was applied to determine the parameters of the EOS. The authors show better prediction of the dew point and the condensate volume for the cases studied, using the modified Patel-Teja EOS without using any binary interaction parameters compared to the Patel-Teja, Peng-Robinson and ZJRK (Redlich-Kwong EOS with Zudkevitch and Joffe method) equation of states using binary interaction parameters.

Wang *et al.* (2000) gave an optimized procedure for tuning the equation of state parameters to match the experimental phase behavior of gas condensate fluid so as to be used in reservoir simulations for more accurate well deliverability calculations.

Elsharkawy *et al.* (2000), using compositional analysis from 1200 compositions of gas condensates, evaluated several methods for estimating two-phase compressibility factors for gas condensates. The authors based their study on the large data set of gas condensate fluids and proposed a new method to calculate the pseudo-critical properties of the gas condensate fluids, which can be used in turn to calculate the compressibility factors for gas condensates.

Arcia *et al.* (2004) developed a simplistic approach to determine the saturation pressure based on easily acquired downhole data. The method is applicable to black oil, volatile oil and gas condensate types of fluids where the reservoir and bottomhole pressures are above saturation pressure and no free water is produced from the reservoir. The dynamic pressure profile of a producing well is recorded using a pressure gauge. The recorded pressure profile is then analyzed to establish pressure gradients, density and gradient derivative in the wellbore and this, in turn, is interpreted in terms of condensation, segregation, fluid convection and flow regime identification in the wellbore. The inflection point of the gradient plot corresponds to the saturation pressure. The dew point pressure obtained from this method was verified using the PVT analysis in laboratory and EOS calculations.

Kokal *et al.* (2001) performed an experimental phase behavior study for a Saudi Arabian gas condensate fluid with water/brine. For the dry gas condensate (without water) studied, there was not a significant effect of temperature on the dew point. However, there was a significant effect on the liquid dropout; the liquid dropout reduced significantly with the increase in temperature. For the gas condensate-water system

studied, the dew point pressure decreased slightly and the amount of liquid dropout increases slightly with increasing water/condensate ratio. Phase behavior of gas condensate-water mixtures was modeled using SRKEOS and reasonable agreement was obtained between the calculated and experimental results.

Lindeloff *et al.* (2001) and Pederson *et al.* (1996) proposed a thermodynamic model that can account for polar interactions and an algorithm that can generate the phase diagram for gas condensate-water systems. The model applies the Huron-Vidal method for gas condensate-water systems. Huron-Vidal (1979) derived a procedure that enables incorporating any excess Gibbs energy model, such as UNIQUAC or NRTL, into an equation of state like SRK. The authors modified the Huron-Vidal mixing rule for temperature variation. The model allows proper description of the behavior of the polar compounds while maintaining the classical model for the hydrocarbon compounds. Lindeloff *et al.* (2001) describes an algorithm to calculate the phase boundaries on a P-T diagram that separate the 1, 2 and 3 phase regions. The method is incorporated in the PVT SIM software provided by Calsep.

Ayyalasomyajula *et al.* (2002) used SAFT (Statistical Associating Fluid Theory) equation of state to model gas condensate-water-methanol mixtures. SAFT equation of state is based on statistical mechanical theories and takes into account the intermolecular potential function. It captures the major effect of non-spherical nature and association among molecules by a modified definition for the compressibility factor. The authors show that for the pure hydrocarbon gas condensate mixture Peng-Robinson EOS gave better results than the SAFT EOS. However, for the gas condensate-methanol mixtures, after regressing both the equation of states to match the experimental data, the binary interaction parameters showed less dependence on temperature for the SAFT EOS than

that for PREOS. Overall, the authors concluded that the predictions from SAFT EOS are more accurate than those from PREOS for the phase behavior of studied mixtures.

Pederson *et al.* (2004) studied the effect of salt on the mutual solubility of water and gas condensate mixtures over a wide range of temperatures and pressures. Their results show that the dissolved salts reduce the gas solubility in water, which is in agreement with the results of Kokal *et al* (2001). The gas solubility in water phase is reduced because the presence of salt in water lowers the mole fraction and fugacity coefficient of the water phase. The lowering of mole fraction is dependent on the concentration of salt and the lowering of fugacity coefficient depends on ion-water interactions. Their results also show that the mole fraction of water in the hydrocarbon phase, in equilibrium with water or brine, can be significant at high temperatures and pressures and is not sensitive to salt concentration of around 3.5mole percent. The authors modeled the phase behavior of these mixtures using SRK and PR equations of state with the Huron-Vidal mixing rules. For modeling, ions were treated as hypothetical molecules with critical properties close to glycols.

Bang *et al.* (2005) conducted PVT experiments to study the phase behavior of hydrocarbon-water-alcohol mixtures at high temperatures and high pressures corresponding to conditions in gas-condensate reservoirs. The study was done to better understand the effect of solvents like methanol and isopropanol on the phase behavior of gas condensate and water mixtures. The Peng-Robinson equation-of-state was used to model these mixtures and the EOS parameters like binary interaction coefficients and temperature dependent volume shift parameters were tuned to fit the experimental data. The authors observed that addition of methanol reduces the dew point pressure and increases the aqueous phase volume fraction significantly. This shows that methanol prefers the aqueous phase to the hydrocarbon liquid and vapor phases even at high

temperatures. The authors further observed that isopropanol affects the phase behavior of hydrocarbon-water mixtures in a significantly different manner than methanol as it prefers the hydrocarbon liquid phase over the aqueous phase. These results show that using a solvent like just methanol or isopropanol (IPA) alone may not be very efficient in miscibly displacing both water and condensate. The authors also modeled the mixtures of hydrocarbons with water and/or methanol using PR78 Peneloux EOS with both classical and Huron-Vidal mixing rules by using temperature-dependent binary interaction and volume shift parameters. The EOS models presented by the authors can be used for simulating treatments like methanol injection in gas condensate wells more accurately.

2.4 METHODS TO TREAT CONDENSATE BLOCKAGE:

Several methods have been proposed and investigated to treat damage caused by condensate accumulation. The most common approach to treat damage caused by condensate blocking are either to change the phase behavior of the gas condensate fluid or to reduce the pressure drawdown and maintain pressure above the dew point pressure.

Abel *et al.* (1970) described the two schemes of gas cycling: full pressure maintenance and partial pressure maintenance. In full pressure maintenance process, gas is continuously injected into the reservoir at the same time gas condensate is produced from the reservoir in an attempt to prevent reservoir pressure from falling below the dew point pressure. Whereas, in the partial pressure maintenance approach, gas is injected into the reservoir after primary depletion below the dewpoint, in an attempt to arrest or slow further pressure decline and revaporize or miscibly displace the condensate.

Processes that take place when injected gas contacts condensate liquid include:

- a. Displacement of reservoir fluid by the injected gas
- b. Re-vaporization of components because of mass transfer

c. Change in PVT behavior of reservoir fluid upon contact with the injected gas

Kossak *et al.* (1986) did simulations to study the performance of slug injection of methane followed by nitrogen. They studied the effect of slug injection in a homogeneous and heterogeneous layered reservoir with both isotropy and anisotropy. Their results show that the heterogeneities allow the nitrogen to mix with condensate when the methane slug is small but the incremental recovery with methane slug over nitrogen injection is large enough to pay off the cost of methane.

Sanger and Hagoort (1992) investigated the efficiency of nitrogen to evaporate gas condensate compared to methane. They found that methane can evaporate more condensate than nitrogen. The authors reported that the evaporation capacity of methane is more than 20 times higher than that of nitrogen. The disadvantage of injecting nitrogen is that the dewpoint of the mixture is higher than the reservoir gas and thus leads to in-situ condensate drop out due to mixing with gas condensate in reservoir.

Ahmed *et al.* (1998) studied the effectiveness of lean gas, N₂, and CO₂ Huff 'n' Puff injection technique in removing the liquid accumulated in and around the wellbore. Huff 'n' Puff injection techniques use the same well alternatively as producer and injector. The authors concluded that pure CO₂ is the most effective gas in reducing the liquid dropout as compared to others when injected at the same pressure. The authors also show that the huff 'n' puff injection of gases is most effective when initiated before the maximum liquid dropout (from CVD) is reached. An insufficient amount of gas injection could increase the liquid dropout.

Luo *et al.* (2000) conducted experiments on an actual rich gas condensate fluid to investigate condensate recovery, based on the two pressure maintenance strategies: full pressure maintenance and partial pressure maintenance, to quantitatively determine the revaporization efficiency of retrograde condensate by lean gas injection. Their analysis of

the produced condensate phase shows that a greater percentage of the heavier components are vaporized and recovered when gas is injected above the saturation pressure compared to when gas is injected below the saturation pressure. Their results also show that cumulative condensate recovery is higher when injection is done above the saturation pressure. The authors also observed that during gas injection at the reservoir pressure, the mass transfer between the dry-gas injected and the original gas condensate leads to a rise in dew point pressure and earlier retrograde condensation, which may reduce the condensate recovery to some extent.

Jamaluddin *et al.* (2001) did PVT experiments to study the effect of CO₂ and propane on the phase behavior of the reservoir gas condensate fluid. They found that CO₂ increases the dewpoint of the mixture but reduces the total liquid dropout below the dewpoint whereas propane reduces the dewpoint as well as the total liquid dropout. The authors suggest Huff 'n' Puff injection of propane would efficiently reduce the damage due to condensate blocking.

Marokane *et al.* (2002) studied the injection of produced gas to remove the condensate bank for lean and rich gas condensate fluids. The authors found that to achieve maximum recovery for a lean gas condensate, produced gas should be injected after the average reservoir pressure around a producing well falls below the maximum liquid dropout pressure. For rich gas condensate, gas injection is more efficient when the produced gas is injected at a pressure greater than the maximum liquid dropout pressure.

Al-Anazi *et al.* (2004) experimentally studied the revaporization of condensate in cores by methane. The authors showed that methane flood revaporizes condensate and restores the gas permeability to single-phase flow value. Revaporization of condensate was controlled by the partitioning of the hydrocarbon components into the flowing gas

phase when the injection was done below the minimum miscibility pressure (MMP). Increase in injection pressure and rate expedited the revaporization of condensate.

Hoier *et al.* (2004) studied miscible gas injection for partial pressure maintenance in an under-saturated oil (Smorbukk South Field) exhibiting compositional variation. The authors' generated MMP (minimum miscibility pressure) gradient for a given injected gas, from the compositional, reservoir pressure and saturation pressure gradients. The authors concluded that once the injected gas develops miscibility at the injection point, the developed miscible front will first-contact miscibly displace the downstream fluid, independent of whether the downstream fluid is miscible or immiscible with the injected gas.

Henderson *et al.* (1991) performed coreflood experiments to study the effect of water injection on gas condensate recovery, above and below the dew point. They found that residual hydrocarbon saturation after waterflooding depends on the prevailing IFT between the gas and condensate. Depending on reservoir characteristics, water injection may be continued throughout field life or the reservoir may be pressure depleted after a period of injection. However, full pressure maintenance by water injection suffers from the disadvantage that an appreciable amount of gas remains trapped at high pressure at the end of field life, reducing the gas recovery efficiency. Also when waterflooding is implemented with pressure above the dew point, the trapped gas saturation will still contain a high percentage of condensate, as the heavy liquid components which make up the condensate will still be present as vapor. If alternatively water injection is done below dew point, then the condensate already deposited within the reservoir may be partially recovered. However, the amount of condensate in the gas phase will depend on the pressure at which water injection is done. Therefore, there is an optimum period of water injection, dependent on the gas relative permeability curve and the PVT properties of the

fluid that maximizes the hydrocarbon recovery when the reservoir is finally blown down to the abandonment pressure. When water injection is performed for a limited time, the pressure falls once water injection ceases and, the gas saturation in this region will be affected both by gas expansion, acting to increase the saturation, and by condensation, acting to reduce the gas saturation. Gas relative permeability under these conditions is not given by standard measurements. During depressurization, the total hydrocarbon saturation will increase and water will be driven into neighboring regions. Regions further from the injection well may see water invasion resulting from the expulsion of water from the waterflooded region. This water invasion may occur before or after condensation has taken place. Special three-phase relative permeability measurements are required to describe the displacement of gas by water in the latter case and also to describe the flow in the subsequent depressurization. Thus the authors concluded that the different conditions pertaining to waterflooding and depressurization require that different relative permeability curves need to be used for the two processes.

Fishlock *et al.* (1996) studied the performance of water injection for lean and rich gas condensate fluid systems. They found that hydrocarbon recoveries are higher for leaner fluids than richer fluids because a higher proportion of oil is in the gas phase at a given pressure in a lean fluid compared to a richer fluid.

Ahmed *et al.* (2000) analyzed the effect of waterflooding in gas condensate reservoirs and compared it with gas injection. Their results showed improvement in gas and condensate production rates for both gas and water injection. Although gas injection showed higher condensate recovery factors, the authors suggest that gas injection may not be economical due to the large initial investment required, higher operating costs, and delay of gas sales. They further show that, if water injection is planned to be used in gas condensate reservoirs, the reservoir should be blown-down before water invades the

majority of the producing wells and increases the water cut. Blow-down also helps remobilize some of the gas trapped by the injected water.

Cullick *et al.* (1989 and 1993) performed simulation and experimental studies to investigate the efficiency of WAG to improve recovery from gas condensate reservoirs. They proposed to use WAG instead of dry gas injection in the full pressure maintenance process and also as an alternative to early blowdown. Their results show an improvement of about 28% to 54% in total recovery over that with continuous gas injection for full pressure maintenance.

Sohrabi *et al.* (2000) recently conducted some visualization experiments on water wet micromodels to understand the displacement process due to WAG. N-Decane was used as oil and methane as dry gas. The authors observed that major portion of the improved oil recovery is obtained only after a few cycles of WAG injection. Although these observations were made for oil recovery by WAG, a similar displacement process would be expected for condensate dropped out of the gas phase due to pressure drop in gas condensate systems.

Du *et al.* (2000), Walker *et al.* (2000) and Al-Anazi *et al.* (2002 and 2003) investigated the use of methanol to treat damage due to condensate and water blocking. The authors show that an enhanced flow period is observed in both low and high permeability cores after methanol treatment, during which condensate accumulation is delayed. Their experiments show:

- Significant improvement in oil and gas relative permeability is observed during the enhanced flow period after to methanol treatment. Also, the treatment is more effective in presence of high water saturation as methanol effectively removes the damage due to water blocking in addition to treating the damage due to condensate dropout.

- Significant improvement due to methanol treatment is achieved only till certain volume of methanol injection, after which the relative improvement is negligible or reduces significantly.

Methanol treatments remove both water and condensate by a multi-contact miscible displacement if sufficient methanol is injected. Methanol treatments resulted in a significant but temporary enhancement in productivity for both low and high permeability cores. However, removal of water-blocks would be expected to have a long lasting impact on a well's PI.

Al-Anazi *et al.* (2003) reported successful methanol treatment to improve productivity from gas condensate Hatter's Pond field in Alabama. PVT analysis performed on samples taken from the field indicated rich retrograde condensate behavior. Walker (2000) conducted compatibility tests to ensure that the injection of filtrate and methanol did not cause any damage to the core. The well chosen for treatment was producing 250 MSCFPD with 87 BPD of condensate. After methanol treatment both gas and condensate production increased by a factor of 2 to about 500 MSCFPD and 157 BPD respectively. Well tests performed on the well before and after the treatment showed improvement in total skin from 0.68 to -1.9. This indicates that the methanol treatment effectively removed the condensate/water bank near the wellbore. However, the removal of the condensate bank is only temporary as it is expected to rebuild. The results from this test indicate that the reformation of a condensate bank does not occur immediately, the reason for which is not very clear. The authors proposed that modification of the phase behavior of reservoir fluid by the residual methanol phase trapped in the pores delayed the reformation of condensate bank.

Garzon *et al.* (2006) investigated the use of diesel with EGMBE (ethylene glycol monobutyl ether) to treat condensate blocks for carbonate rocks. The authors showed that

improvements in gas PI depend on the concentration of EGMBE in the treatment solution and the solution with 40/60 mix of diesel and EGMBE gave the maximum improvement. They also report a field treatment with the proposed 40/60-Diesel/EGMBE-treatment solution. PI increased by 10% and the gas rates increased by 15% after the treatment.

Hydraulic fracturing has been used to enhance gas productivity (Mohan *et al.*, 2005; Kumar, 2000, Settari *et al.*, 1996; Barnum *et al.*, 1995). In many wells it is possible to reduce the drawdown, i.e. increase the flowing bottom hole pressure by inducing a hydraulic fracture that significantly increases the area available to flow. This allows the well to be produced at a higher bottom hole pressure for longer periods of time thereby delaying the onset of condensate formation around the wellbore. But once the pressure in the propped fracture drops below the dew point pressure, significant condensate saturation can buildup in the fracture itself and reduce the conductivity of these fractures. The success of hydraulic fracture stimulation depends on the placement of sufficient quantity of proppant without changing the integrity of the formation, the rate at which fracture fluids are produced from the fracture, and the degree to which the fracture “cleans up” after the treatment.

Settari *et al.* (1996) conducted a simulation study to investigate the improvement of PI due to hydraulic fracturing in the Smorbukk field. Their results show that fracturing can restore 50-70 % of the PI loss due to condensate blocking compared to a non-fractured well in a low permeability zone. In higher permeability zones, fracturing can increase the PI more than the single phase PI. They found that PI improvement is more sensitive to the fracture length in low permeability zones, whereas PI is more sensitive to the fracture conductivity in high permeability zones.

Kumar (2000) studied the effect of an idealized vertical fracture in a gas condensate well. The author predicted that for two-phase flow of gas and condensate, the

productivity of a fractured well can be as high as eight times the productivity of an unfractured well. Lolon *et al.* (2003) showed that the fracturing fluid that remains in the fracture and formation after a hydraulic fracture treatment blocks the gas flow into the fracture and thus reduces the effective fracture length. Pressure transient tests performed on hydraulically fractured wells also support this and reveal that the effective fracture half-lengths are substantially less than the designed length from fracture stimulation. Thus the predictions from simulating idealized fractures are too optimistic.

Al-Hashim *et al.* (2000) performed a simulation study to investigate the improvement of PI in gas condensate wells, both above and below the dew point, due to fracturing. The authors show that hydraulic fracturing increases the time at which the dew point pressure is reached during depletion as compared to the non-fractured base case.

Mohan *et al.* (2005 and 2006) investigated improvement due to hydraulic fracturing in gas condensate wells by performing single well modeling. Parameters such as fracture dimensions, fracture conductivity has the greatest effect on improvement. The authors used multiple levels of grid refinements to model fracture with width as small as 0.1 ft. The study showed that productivity improvement due to hydraulic fracturing of a gas condensate well is the greatest for low permeability reservoirs and fracture length required to optimize the productivity mainly depends on proppant volume, reservoir permeability, fracture permeability, fluid composition, and condensate bank width on improvement due to hydraulic fracturing in gas condensate wells. The authors developed an analytical expression for optimum fracture length, which included the effects of non-Darcy flow and condensate banking. The results were in good agreement with the simulation results. Effect of various factors such as fracture permeability, reservoir permeability, gas composition and condensate bank width, was studied. It was shown that the optimum fracture length required for flow above dew point was less than that for flow

below dew point. For low permeability reservoirs, a longer and narrower fracture was found to be preferable to a shorter and wider fracture. The optimum fracture length was found to increase as the width of condensate bank increased.

2.4.1 Chemical stimulation by altering wettability

Jadhunandan *et al.* (1991), Owolabi *et al.* (1993) and Chen *et al.* (2004) have shown that altering the wettability to intermediate-wet gives lower oil saturation. **Figure 2.3** shows the residual oil saturation versus wettability index. Wettability index varies from -1 (oil-wet) to +1 (water-wet), 0 being intermediate-wet. The wettability index was measured by Amott-Harvey wettability test. The data is for Berea sandstone and shows minimum residual oil saturation in the vicinity of 0 wettability index. The reader is referred to Anderson (2006) for further literature on effect of wettability on residual oil saturation.

Li and Firoozabadi (2000) proposed to enhance the gas condensate well deliverability by altering the wettability of the near wellbore region from strong liquid wetting to preferential gas wetting. They used chemicals FC 754 and FC 722 (from 3M Corp.) to alter wettability and showed that permanent gas wetting can be established in Berea and chalk through chemical treatment.

Tang and Firoozabadi (2002 and 2003) used chemicals FC 759 and FC 722 to alter the wettability from strong liquid wetting to intermediate gas wetting. These chemicals have a fluorochemical group that provides water and oil repellency, a silanol group that chemically bonds to the rock surface provides a durable treatment. The authors concluded from their experiments that treatment with the chemical FC759 can yield:

- Wettability alteration from strong liquid wetting to stable intermediate gas wetting at room temperature as well as at high temperatures.

- Neutral wetting for gas, oil, and water phases in two-phase flow
- A significant increase in oil mobility for a gas/oil system
- Improved recovery behavior for both gas/oil and oil/water systems.

Mohanty *et al.* (2004) studied wettability alteration to neutral wet in carbonates and sandstones by using surfactants. They showed that as the number of fluoro groups increases, the rock become less water-wet. They further stated that wettability alteration reduces the brine saturation near the hydraulic fracture faces and increase gas productivity.

Fahes and Firoozabadi (2005) showed that chemical 11-12P, manufactured by 3M increases the liquid mobility for sandstone rocks by altering wettability to intermediate wet. The authors evaluated the wettability alteration by comparing the liquid imbibition rate and before and after treatment. N-decane and n-tetradecane were used as oil and air as the gas phase. The authors also compare the pressure drop for liquid flow at residual gas phase i.e. the end point relative permeability for water and n-decane. Their results show that chemical treatment reduces the pressure drop for gas/water system but has no effect for oil/gas system. The authors do not report any relative permeability data.

Kumar *et al.* (2006) tested fluoro-surfactant to alter the wettability of sandstone and limestone cores and improve gas relative permeability. The authors showed that a new nonionic polymeric fluoro-surfactant, FC4430 (made by 3M) gave the most positive results. The surfactant was delivered in a methanol-water mixture to treat cores under reservoir conditions. The authors tested the surfactants under reservoir conditions using both Berea and reservoir sandstone cores and reported significant increase in the steady state gas and condensate relative permeability. They performed experiments to evaluate the effectiveness of this surfactant at high temperature and high gas flow rates over a

range of capillary numbers on the order of those near production wells. The relative permeability for both gas and condensate for sandstone cores was improved by a factor of about 2 for temperatures over the temperature range of 145 to 275 °F. The experiments were however conducted on dry sandstone cores i.e. without any connate water present. As discussed in the later chapters, the presence of connate water and the salts in connate water significantly affects the interaction of surfactant with the rock surface.

Kumar *et al.* (2006) performed simulation studies to assess the impact of chemical treatment on a well with condensate blocking. The authors used the UT relative permeability model (Pope *et al.*, 2000) for pre and post-treatment conditions. The authors concluded that treating the condensate bank out to a radius of 20 feet results in an increase in gas and condensate production rates by a factor of about 1.8 when the relative permeability in the treated zone increases by a factor of 2. Treating the well early results in higher production rates over a longer period of time. The authors also presented a simplified analytical solution to calculate the improvement in gas and condensate productivity with increased gas and condensate relative permeability in the treated zone.

Liu *et al.* (2006) tested a chemical WA12 to alter the wettability of core samples from Dongpu gas condensate reservoir with a permeability of less than 0.1md. The authors performed spontaneous water imbibition tests before and after treating the rocks samples with the chemical. They also conducted unsteady state gas-water relative permeability measurements before and after chemical treatment. The authors show that water did not imbibe into the core after chemical treatment. Also both gas and water relative permeabilities increased significantly after treating with the chemical. Their results however have a few limitations. These measurements were conducted at room temperature and the effect of chemical treatment can vary significantly with temperature. Therefore the measurements should be done at reservoir temperatures which are typically

high for gas condensate reservoirs. Secondly, no measurements were done using gas condensate fluids. The data presented by them is for gas-water system and cannot be applied for gas-oil or gas condensate fluids. Thirdly, their method of injecting the chemical solution in the core is not representative of the actual injection of such chemicals into the reservoir. The cores were cleaned and dried after the pre-treatment relative permeability measurements and then treated with the chemical. This avoids the interaction of the chemical with the reservoir fluids which could have a significant effect on the interaction of the chemical with the rock surface.

Noh and Firoozabadi (2006) studied the effect of wettability alteration on non-Darcy or high velocity flow coefficient. The authors measured high velocity flow coefficient for two-phase gas-water and gas-oil flow on untreated and treated Berea sandstones. The authors used fluorochemical L1894 and FCX from 3M corp. for altering the wettability of Berea sandstones. The authors show that high velocity coefficient for gas-water flow decreased significantly after the chemical treatment, however the reduction in high velocity coefficient for gas-oil flow was less pronounced. This qualitatively agrees with their spontaneous imbibition and contact angle tests results, which show that chemical treatment using these chemicals makes the rocks non-water wet but does not makes them strongly non-oil wet. Also, at high flow rates the effect of capillary number can become significant for gas-oil flow and thus affect the measurement of high velocity flow coefficients. The authors have not accounted for the effect capillary number on relative permeability and determination of high velocity flow coefficients. The results presented by the authors are extremely significant as they extend the benefits that can be obtained from altering rock wettability to neutral wetting.

Panga *et al.* (2006 and 2007) evaluated 41 chemicals for altering the wettability of rocks from liquid wetting to gas wetting for the remediation of the damage caused by

water blocking in gas wells. The authors conducted three types of tests to evaluate the performance of these chemicals; contact angle measurements, imbibition test and core flow tests. The chemicals were screened based on the results of contact angle measurements and the imbibition tests. The change in wettability was evaluated by visually observing the contact angle made by a drop of water on the rock surface. In imbibition tests, the wettability change was assessed by comparing the rate of brine imbibition before and after chemical treatment. Of the tested chemicals, a fluorine based surfactant A5 gave the most positive results. The authors then conducted flow test to measure the displacement of water by gas for the untreated and treated core. The core treated with A5 delivered in 2wt% KCl brine gave high recovery of trapped water due to the reduction in capillary forces. But the treatment using A5 diluted in alcoholic solvents like methanol and IPA at high temperature plugged the core due to surfactant precipitation. Thus the chemical A5 cannot be used with solvents like methanol and IPA which can help in achieving additional benefits like miscibly displacing brine and wellbore cleanup. The treatment was successful when the chemical was delivered in an aqueous based solvent but injecting aqueous based solution in gas wells can severely damage gas wells. Thus, the treatment proposed by the authors is not a prospective treatment for treating water damage in gas wells.

2.5 MODELING OF GAS CONDENSATE WELL DELIVERABILITY:

Many experimental studies have shown the effect of interfacial tension on the gas relative permeability. However, Brownell and Katz (1947) and others recognized early on that residual saturations and relative permeabilities should be a function of the ratio of viscous to interfacial forces, defined as capillary number. In some cases buoyancy forces

also can be significant on the trapped phase. To account for this, the Bond number was defined as the ratio of the buoyancy forces to the interfacial forces, which also contributed to the total force on the trapped phase (Bardon and Longeron, 1980). Capillary number and the Bond number were combined using the vector sum of the forces on the trapped phase (condensate) to give the trapping number (Jin, 1995).

Pope *et al.* (2000) developed a trapping number dependent relative permeability model. The authors showed that this model could be used to fit typical relative permeability data available in the literature at that time. Narayanaswami *et al.* (1998 and 1999) proposed an analytical approach to calculate the non-Darcy flow coefficient for heterogeneous reservoirs. The authors successfully history matched the production from a gas condensate well of Arun field with the use of capillary number dependent relative permeability curves, instead of straight line relative permeability curves, and proper modeling of non-Darcy flow effects. Mott *et al.* (2000) showed that the inertial flow coefficient in a 3-phase gas–condensate–water system is about 50% higher than in the equivalent 2-phase gas–water system.

Civan *et al.* (2001) published an analytical correlation for deposition under non-equilibrium conditions. They concluded that the difference in condensate accumulation (with and without considering non-equilibrium effects), which is significant initially decreases with dimensionless time.

Al-Anazi (2003) showed from his experiments that non-equilibrium phenomenon is important at high flow rates, which represents the conditions prevailing in the near wellbore region. Rai (2003) simulated core flood experiments done by Al-Anazi (2003) using UTCOMP. Non-equilibrium effects were found to be significant at high flow rates.

Sharma (2003) studied the decline in productivity due to condensate build up on a well in the Hatter's Pond gas–condensate reservoir. The author also developed a new

hybrid well model that captured the near well behavior accurately and was much faster than fine-grid simulation.

Fevang and Whitson (1996) proposed a pseudo pressure approach to model the deliverability of gas-condensate wells. They calculated the pseudo pressures and used them to calculate the well deliverability. The producing GOR, reservoir fluid PVT properties (modified black oil or compositional) and gas-oil relative permeabilities are needed to calculate the pseudo pressures.

Mott (2002) devised a new method to forecast performance from gas condensate wells using simple technique that can be used in a spreadsheet. The method uses a material balance model for reservoir depletion and two-phase pseudo pressure integral to for inflow performance. The author implemented the method in both modified black-oil and compositional simulators.

Chowdhury *et al.* (2004) developed a semi analytical model to accurately predict the gas and condensate production rates. The new semi-analytical model is based on ideas similar to the Fevang-Whitson-Mott pseudo pressure approach. In this method the steady state rates are calculated analytically for grid blocks with wells and used to replace the coarse grid approximation for these grid blocks to improve the accuracy of the gas and oil production well rates.

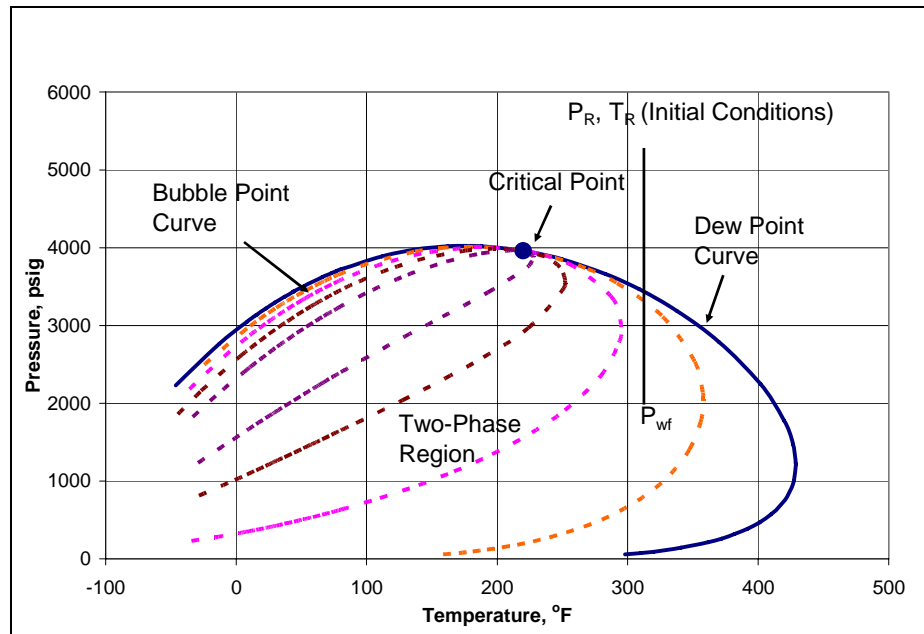


Figure 2.1: Phase diagram of a gas-condensate system

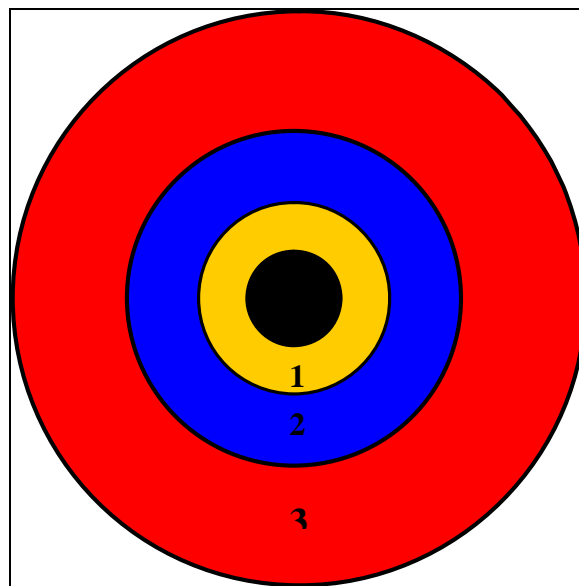


Figure 2.2: Conceptual flow regions around a gas condensate well

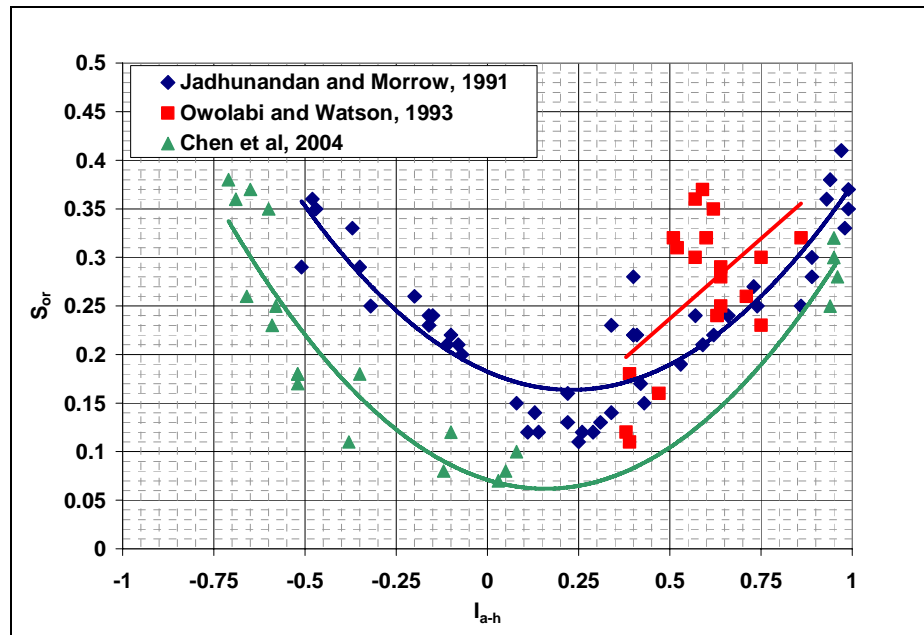


Figure 2.3 Effect of wettability on residual oil saturation in Berea sandstone

Chapter 3: Theory and Experimental Setup for Corefloods

This chapter describes the experimental setup used to perform coreflood experiments under reservoir conditions. The chapter starts with the description of equations used in the calculations used for analyzing results. The experimental apparatus section gives a detailed description of the chemicals and apparatus used in the coreflood experiments. This is followed by a section describing the detailed experimental procedure. Finally the PVT software and the equation of state used for modeling the PVT properties of the fluid have been described.

3.1 THEORY

The single-phase permeability (k) of rocks was calculated using Darcy's law:

$$k = \frac{q \mu L}{A \Delta P} \quad (3.1)$$

where q is the core flow rate, μ is the flowing fluid viscosity, L is the length of the core, A is the cross-sectional area of the core, and ΔP is the steady state pressure drop across the core.

At high velocities Darcy's law is not valid and the contribution due to non-Darcy flow has to be included to calculate the correct single-phase gas permeability. For non-Darcy flow, the single-phase permeability was calculated using Forchheimer's equation:

$$\frac{\Delta P}{L} = \frac{u \mu}{k} + \beta \rho u^2 \quad (3.2)$$

where, u is the Darcy velocity, ρ is the fluid density and β is the non-Darcy flow coefficient. This equation can be re-arranged and written as:

$$\frac{\Delta P}{uL} = \frac{\mu}{k} + \beta \rho u \quad (3.3)$$

A plot of $(\Delta P/uL)$ vs velocity (u) is a straight line with μ/k as the intercept and $\beta\rho$ as the slope. The intercept and slope were used to calculate k and β .

The relative permeability (k_{rj}) of each phase j is defined as

$$k_{rj} = \frac{k_j}{k} \quad (3.4)$$

where k_j is the permeability of fluid j and k is the initial gas permeability at 100% gas saturation at low velocity. The two-phase relative permeability of each phase j at steady-state can be calculated using Darcy's law:

$$k_{rj} = \frac{q_j \mu_j L}{k A \Delta P_j} \quad (3.5)$$

where j refers to either gas or oil (condensate) phase. Calculation of two-phase relative permeability including non-Darcy flow is described in Chapter 10. For gas condensate fluids, the interfacial tension between the phases is small and thus the capillary pressure is negligible compared to the measured pressure drop across the core. Thus, the pressure drop of each phase is equal ($\Delta P_g = \Delta P_o = \Delta P$).

The gas phase enters the backpressure regulator at a pressure above the dew point of the fluid system and flashes downstream into gas and condensate (oil) phases at a pressure below the dew point of the fluid. The flow rate of each phase (oil and gas) is calculated by performing a mass balance across the backpressure regulator. Details of the mass balance are given in **Appendix A**. Oil and gas flow rates in the core derived from the mass balance are:

$$q_o = \frac{f_o q \rho}{f_o \rho_o + f_g \rho_g} \quad (3.6)$$

$$q_g = \frac{f_g q \rho}{f_o \rho_o + f_g \rho_g} \quad (3.7)$$

where

q = total flow rate of single phase gas mixture above the dew-point pressure

q_g = flow rate of gas-phase at a pressure below the dew-point pressure

q_o = flow rate of oil-phase at a pressure below the dew-point pressure

ρ = molar density of single phase gas mixture above the dew-point pressure

ρ_g = molar density of gas-phase at a pressure below the dew-point pressure

ρ_o = molar density of oil-phase at a pressure below the dew-point pressure

f_g = fractional flow of gas-phase at a pressure below the dew-point pressure

f_o = fractional flow of oil-phase at a pressure below the dew-point pressure

At steady state the fractional flow of gas and oil (condensate) are equal to the volumes of gas and liquid obtained from constant composition expansion measurements at core pressure and temperature, expressed as a fraction of the total hydrocarbon volume.

The density of each phase and the liquid dropout were calculated using the PREOS at the experimental conditions. The flow rate of each phase through the core was calculated using Equations (3.6) and (3.7).

At steady state, the ratio of gas and oil relative permeability can be expressed as a function of the PVT ratio, if non-Darcy flow is not significant (Chopra *et al.* 1986).

$$\frac{k_{rg}}{k_{ro}} = \frac{f_g \mu_g}{f_o \mu_o} = \frac{V_g \mu_g}{V_o \mu_o} \quad (3.8)$$

where, V_g and V_o are the volumes of gas and liquid respectively obtained from constant composition expansion measurements expressed as a fraction of the total hydrocarbon volume. Thus, the ratio of gas to oil relative permeability at a given core pressure is fixed and governed by the fluid properties only. The effect of PVT ratio on gas and oil relative permeability is described in **Chapter 10**.

The capillary number is defined as the ratio of viscous forces to capillary forces. For the special case of interest here, the capillary number can be expressed as:

$$N_c = \frac{k \Delta P}{\sigma L} \quad (3.9)$$

where

- k = core permeability, cm^2
- ΔP = pressure drop across the core, dynes/cm^2
- σ = interfacial tension between the two phases, dynes/cm
- L = length of the core, cm

By using lab units: k in md, ΔP in psia, σ in dynes/cm, and L in inches, the capillary number can be written (including the conversion factor) as:

$$N_c = 2.6784 \times 10^{-7} \left(\frac{k \Delta P}{\sigma L} \right) \quad (3.10)$$

A more detailed discussion of the capillary number and its effect on gas and oil relative permeability is presented in **Chapter 10**.

3.2 COREFLOOD EXPERIMENTAL SETUP

Figure 3.1, 3.2 and 3.3 show photographs of the gas condensate coreflood setup. The coreflood apparatus was designed for high-pressure (8,000 psi) and high-temperature (350 °F) experiments. **Figure 3.4** shows a schematic diagram of the coreflood setup. High-pressure Quizix and RUSKA pumps were used to inject fluid at a constant rate. In some experiments multiple pressure ports were used to measure pressure drop across four sections (2 inches in length each) of the core. Two backpressure regulators were used to control the flowing pressure upstream (BPR-1) and downstream (BPR-2) of the core. BPR-1 maintains the fluid mixture above the dewpoint pressure and BPR-2 controls the core pressure and is maintained at a pressure below the dew point pressure. The core is kept vertical to prevent gravity segregation during two and three phase flow. The core holder, backpressure regulators, fluid accumulators, and flow lines are inside a temperature-controlled, forced-air circulation oven at a fixed temperature. The backpressure regulators were kept outside the oven for experiments after expt-15. The oven temperature is measured with a thermocouple and displayed on a digital indicator with an accuracy of $\pm 0.1^\circ\text{F}$.

3.2.1 Core Holder

A Hassler type core holder from Phoenix Instruments was used in these experiments. The core holder is rated for 10,000 psig and 400°F. There are 3 pressure taps along the length to measure pressure drop across sections of 2 inch. The maximum core length that can be accommodated is 8 inches. The core-holder material is SS-316. The core sleeve used in core-holder is a Viton rubber sleeve.

3.2.2 Back Pressure Regulators

Back-pressure regulators (BPR) used in the core flow experiments are Model BPR-05 from TEMCO, Inc. This model of back-pressure regulator has two sections separated by a diaphragm. The compressed gas is in the dome and the flowing fluid in the body section. To avoid rupturing the diaphragm, the two sections were pressurized simultaneously. The diaphragm can take a maximum pressure differential of 500 psig. Nitrogen was used as the compressed gas. The pressure of the compressed gas in the dome is monitored using a digital Heise gauge. When the desired pressure was reached, the nitrogen source was closed and the pressurized gas was allowed to reach the experimental temperature. Two back-pressure regulators were used to control the pressure upstream and downstream of the core. The upstream and downstream back-pressure regulators are called BPR-1 and BPR-2, respectively.

3.2.3 Accumulators

High-pressure and high-temperature stainless steel accumulators from Temco, Inc. were used in these experiments. The volume of the accumulators ranges from 500-

2,000 cc and has been pressure tested up to 7500 psig. These have a Teflon floating piston with viton or fluorosilicone o-rings that isolates the test fluid from the pressurizing fluid. For experiments at high temperatures, special Teflon o-ring pistons were used to provide durability and prevent leaks across the piston.

3.2.4 Pressure Transducers

Validyne DP 15, DP 363 and Rosemont Model No.300S1AAM5 pressure transducers were used to measure the pressure drop across the core in coreflood experiments. Validyne transducers have a stainless steel diaphragm that is clamped between two blocks of stainless steel. An inductance coil is embedded in each block and covered by a disc to provide a corrosion resistant surface. When a pressure difference is applied through the pressure ports, the diaphragm deflects and changes the magnetic field between the two coils. Validyne transducers are equipped with bleed ports to facilitate cleaning or filling the pressure cavity. The transducers are calibrated with a known source of pressure.

3.2.5Pumps

Five types of pumps were used in these experiments: A Ruska motorized positive displacement pump, Ruska digital positive displacement pumps, Quizix dual cylinder QX series, a vacuum pump and a gas booster pump.

Ruska motorized positive displacement pumps are driven by positive gear transmissions and are capable of delivering rates ranging from 1 cc/hr to 224 cc/hr. There are two types of Ruska motorized positive displacement pumps: single cylinder and dual cylinder. Each injection cylinder has a volume of 500 cc and has a vernier dial attached

to it. The volume measurement can be made within an accuracy of ± 0.1 cc using these vernier dials. These pumps are rated for a pressure range of 0 to 10,000 psig.

The Ruska digital positive displacement pump is driven by a D.C. servomotor. The servo motor is equipped with a resolver that ensures displacement of the exact volume at a very precise flow rate ranging from 0.1 cc/min to 8 cc/min. The volume measurements can be made with an accuracy of ± 0.001 cc. The pump has a digital display which shows the flow rate and the volume injected or retracted. The pump has a single cylinder with a volume of 1000 cc and is rated for a pressure range of 0 to 5000 psig.

Model no. QX6000SS-0-0-C-L-0 Quizix pumps also known as QX series pumps from Chandler Engineering were used. The pumps contain a pump controller, which directs the action of two completely independent, positive displacement pumps. The pump can be used at constant flow rate mode or constant pressure mode. The pumps are rated up to 6,000 psi and can inject at a maximum rate of 50 cc/min.

A vacuum pump from Central scientific equipments was used.

A single acting, single stage, gas booster pump was used to provide high-pressure nitrogen, methane and n-butane. The booster pump is made by MAXPRO Technologies (model DLE 75-1). The pump was air driven and the compression ratio at 100 psi of air was 20:1. The maximum inlet pressure allowed to the booster pump is 2175 psi.

3.2.6 Oven

BLUE M ovens were used to perform experiments at high temperatures. The ovens are 4'x4'x3' in dimensions. The temperature rating is 650°F.

3.2.7 Pressure Gauges

Heise and Mensor pressure gauges were used to measure the absolute pressure. Heise pressure gauges are rated at either 0-5,000 or 0-10,000 psig. Mensor pressure gauges are rated up to 5,000 psig.

3.3 EXPERIMENTAL PROCEDURE

3.3.1 Core Preparation

An outcrop core with 0.98 to 1 inch diameter and a length of 8 inches was cut from a source rock block. The core was dried in an oven at 180°C for 12 hrs and then was weighed. Berea Sandstone, Texas Cream Limestone and reservoir cores were used in the experiments. The core was wrapped with Teflon tape to prevent brine from contacting aluminum foil. Aluminum foil was then wrapped over the Teflon tape followed by a heat-shrink Teflon sleeve using a heat gun, to prevent diffusion of injected fluids through the Viton rubber sleeve. The wrapped core was placed into a core holder inside the oven at the experimental temperature. Then, an overburden pressure was applied using a hydraulic hand pump (the confining fluid was pump oil). For experiments where pressure taps were used, holes were drilled through the pressure taps using a small drill bit (1/32"). These holes allow gas to flow through the pressure ports to the connected pressure transducers to record the pressure drop across each section of the core.

3.3.2 Establishing Initial Water Saturation

Initial water saturation was established by injecting a known volume of brine into vacuumed core at room temperature. After measuring the initial gas permeability, a vacuum was pulled from the outlet of the core holder for 20 minutes. Then a

predetermined volume of brine was injected in the vacuumed core using a burette connected to the inlet of the core holder. The core was then shut-in for one hour to allow the injected brine to distribute uniformly throughout the vacuumed core. Finally, many pore volumes of nitrogen were flowed through the core to distribute brine more uniformly in the core.

3.3.3 Gas Mixture Preparation

Different synthetic gas mixtures were designed and used in these experiments. Gas mixtures were prepared using simple hydrocarbons like methane, propane, n-butane, n-heptane, n-decane, n-dodecane and n-pentadecane. The gas mixtures were prepared on a mass basis. Preparing the gas mixture on a mass basis is both more accurate and simpler compared to the method used by Walker (2000) and Al-Anazi (2003). In this method, the amount of each component is calculated in terms of mass from their molecular weights and number of moles only and is independent of temperature and pressure. Gas mixtures were designed using mole fractions. Then using their molecular weights and mole fractions, their corresponding mass fractions were calculated.

For preparing the gas mixture, a high-pressure high-temperature accumulator was cleaned and vacuumed. The o-rings on the end caps and on the piston were replaced. A fixed mass of total gas mixture was taken as the reference. From the mass fractions of each component, mass of each component to be injected in to the accumulator was determined.

The determined mass of hydrocarbon liquids such as n-heptane, n-decane, n-dodecane and n-pentadecane are weighed, mixed and poured in a burette. The weighed liquid hydrocarbons are then flushed through the burette nozzle and the tube connected to the burette to get rid of any air bubbles. The dispensed liquid is then returned back into

the remaining mixture in the burette. The burette is then connected to the vacuumed accumulator and the liquid hydrocarbons are transferred from the burette to the accumulator slowly and carefully making sure that no air goes into the accumulator. The final mass of the accumulator is measured to make sure the desired mass of liquid is transferred into the accumulator.

The accumulator is then placed on the weighing balance and the weighing scale is reset to zero. A pre-determined mass of n-butane and propane is then injected into the accumulator using a booster pump. Matheson Co. supplied the n-butane and propane in the form of liquid at 20 psi and 100 psi, respectively. The mass of the fluid entering the accumulator is carefully monitored on the weighing scale display to make sure the desired amount of fluid is injected into the accumulator. Finally the desired mass of methane is pumped into the accumulator using the booster pump. Matheson Co. supplied the methane in a high-pressure tank at 2,200 psig.

After injecting all the components, the accumulator is rocked to mix the components and then placed in the oven set at the experimental temperature. The pressure of the mixture is then raised above the dew point pressure using the Ruska or Quizix pump. The mixture at high temperature and high pressure is left for 9-15 hrs to equilibrate to a single phase. The accumulator is again rocked before starting the coreflood experiment. It has been observed that rocking the accumulator before starting the experiment is extremely important at both low and high temperatures to achieve a uniform fluid in the accumulator.

Tables 3.1 to 3.9 list the composition of different synthetic gas mixtures used at different temperatures and represent different reservoir fluids. Water was added in some gas mixtures to saturate them with water and prevent vaporization of water from the core during the gas mixture flood.

3.3.4 Treatment Solution Preparation

The treatment solution is prepared on a mass basis in a beaker. The required amount of solvents are poured in a beaker and mixed. Then predetermined amount of surfactant is added to the solvent mixture. Treatment solution is then mixed using a magnetic stirrer for 20 minutes before pouring it into a clean accumulator. The accumulator is placed in the oven for at least 4 hours to reach the experimental temperature before injecting it into the core.

3.3.5 Coreflood Procedure

The initial dry gas permeability of the core was measured using either nitrogen or methane at room temperature. BPR-1 and BPR-2 were typically set around 3,000 psig and 1,000 psig respectively to get high gas flow rates through the core. BPR settings changed with the type of core. Initial water saturation was then established following the method described above. The core was then shut-in for 1 hour followed with a nitrogen or methane flood to distribute water uniformly throughout the core and to measure the gas permeability at initial water saturation. The temperature of oven was then raised to the required experimental temperature.

Two-phase flow with the gas mixture was conducted using the dynamic flashing method, by flashing single-phase gas through the upstream back-pressure regular set above the dew point pressure to the core pressure set below the dew point pressure by the downstream back-pressure regulator. The gas mixture was injected at a known constant flow rate using a Ruska or Quizix pump. This allows the condensate to dynamically accumulate in the core in a way that is similar to condensate accumulation in the near

wellbore region below the dew point pressure. Steady-state pressure drop across the core was measured and relative permeabilities for gas and oil were calculated. For some experiments a gas-condensate floods were done at multiple rates and different BPR-2 pressures to measure relative permeability over a wide range of capillary number and PVT properties.

Treatment solution was then injected and the core was shut-in to soak. The soaking time varied from 1 hour to 24 hours. Post-treatment two-phase flow of gas-condensate using the same gas mixture was then conducted under the same conditions as the initial two-phase flow to measure the relative permeabilities of treated core. Finally methane was injected to measure the permeability after treatment.

3.4 PVT SOFTWARE

PVTSim, a PVT software package provided by Calsep Inc., was used for the phase behavior modeling. The original and the modified forms of the equation of state models by Peng-Robinson and Soave-Redlich-Kwong have been incorporated into the software package. The software can handle both polar and non-polar molecules as it provides an option for the type of mixing rule to be used. An important feature of the software is that it can perform three-phase flash and calculate three-phase pressure-temperature phase diagrams. The algorithm for calculating two- and three-phase boundaries for the pressure-temperature phase diagrams was given by Lindeloff and Michelson (2002).

The software provides an option for simulating various PVT operations, calculation of minimum miscibility pressure for gas injection and simulation of hydrates and asphaltenes. PVTSim also provides an option for regressing the equation of state

parameters to match the experimentally measured constant composition expansion (CCE), constant volume depletion (CVD) and other PVT experimental data.

3.5 EQUATION OF STATE

Peng-Robinson EOS, a cubic EOS developed by Peng and Robinson in 1976, has been shown to accurately model hydrocarbons and is the most widely used EOS in compositional reservoir simulators.

The PREOS is expressed as -

$$P = \frac{RT}{V-b} - \frac{a(T)}{V(V+b)+b(V-b)} \quad (3.11)$$

where

$$a(T) = a_c \alpha(T) \quad (3.12)$$

$$a_c = \Omega_a \frac{R^2 T_c^2}{P_c} \quad (3.13)$$

$$\alpha(T) = \left[1 + m \left(1 - \left(\frac{T}{T_c} \right)^{0.5} \right) \right]^2 \quad (3.14)$$

$$b = \Omega_b \frac{RT_c}{P_c} \quad (3.15)$$

and

$$\begin{aligned} \Omega_a &= 0.45724 \\ \Omega_b &= 0.07780 \end{aligned} \quad (3.16)$$

The parameter m for PREOS is found from

$$m = 0.37464 + 1.54226\omega - 0.269922\omega^2 \quad (3.17)$$

The Peng-Robinson EOS was modified in 1978 and is known as PR78 EOS. For PR78 equation m is found from the same correlation (Eq 3.9.) if $\omega \leq 0.49$. Otherwise the below correlation is used

$$m = 0.379642 + \omega(1.48503 - 0.164423\omega + 0.01666\omega^2) \quad (3.18)$$

With Peneloux volume correction the PR78 equation of state is

$$P = \frac{RT}{V-b} - \frac{a(T)}{(V+c)(V+2c+b) + (b+c)(V-b)} \quad (3.19)$$

where c is known as Peneloux volume correction and is defined as the difference between the Peneloux molar volume and the molar volume calculated without Peneloux volume correction. The parameter c is expressed as the sum of a temperature independent volume correction (c') and a temperature dependent volume correction (c'') in PVTsim software:

$$c = c' + c''(T - 288.15) \quad (3.20)$$

where T is the temperature in K.

The temperature independent volume correction for PR78 is calculated from

$$c' = 0.50033 \frac{RT_c}{P_c} (0.25969 - Z_{RA}) \quad (3.21)$$

where Z_{RA} is the Racket compressibility factor and is calculated as:

$$Z_{RA} = 0.29056 - 0.08775\omega \quad (3.22)$$

The PR78 EOS with temperature dependent Peneloux volume correction will be referred as PR78 Peneloux (T) EOS in the further sections.

The most common mixing rules used for non-polar mixtures are the classical van der Waals mixing rules. The mixing rules are based on one binary interaction parameter per pair. The parameters a, b and c for the mixture are calculated as:

$$\begin{aligned} a &= \sum_{i=1}^N \sum_{j=1}^N Z_i Z_j a_{ij} \\ b &= \sum_{i=1}^N Z_i b_i \\ c &= \sum_{i=1}^N Z_i c_i \end{aligned} \quad (3.23)$$

where z_i and z_j are mole fractions, i and j component indices, and

$$a_{ij} = \sqrt{a_i a_j} (1 - k_{ij}) \quad (3.24)$$

where k_{ij} is the binary interaction parameter between component i and j .

Figures 3.5 to 3.13 show the liquid dropout curves of different fluid mixtures calculated using PREOS with volume correction. The binary interaction coefficients between hydrocarbon components were taken as zero. Bang *et al.* (2005) showed that PVT properties of mixtures made of pure hydrocarbon components only can be accurately calculated using zero binary interaction coefficients for van der Waal's mixing rule. The liquid dropouts have been calculated at their respective experimental temperatures. In this work liquid dropout has been calculated as the ratio of liquid volume fraction to the total hydrocarbon volume at that pressure and not the volume at dew point pressure.

Table 3.1: Composition of synthetic gas mixture 1

T = 145°F	
Component	Mole %
Methane	78.5
n-Butane	15
n-Heptane	5
n-Decane	1.5

Table 3.2: Composition of synthetic gas mixture 2

T = 275°F	
Component	Mole %
Methane	93
n-Butane	4
n-Decane	2
n-Pentadecane	1

Table 3.3: Composition of synthetic gas mixture 3

T = 250°F	
Component	Mole %
Methane	83
n-Butane	4
n-Heptane	7.2
n-Decane	4
n-Dodecane	1.8

Table 3.4: Composition of synthetic gas mixture 4

T = 175°F	
Component	Mole %
Methane	89
n-Butane	5
n-Heptane	2.5
n-Decane	2.5
n-Pentadecane	1

Table 3.5: Composition of synthetic gas mixture 5

T = 175°F	
Component	Mole %
Methane	89
Propane	5
n-Heptane	2.5
n-Decane	2.5
n-Pentadecane	1

Table 3.6: Composition of synthetic gas mixture 6

T = 308°F	
Component	Mole %
Methane	70
Propane	16.5
n-Heptane	7
n-Decane	3
n-Dodecane	2
n-Pentadecane	1.5

Table 3.7: Composition of synthetic gas mixture 7

T = 275°F	
Component	Mole %
Methane	90
Propane	5.5
n-Heptane	2
n-Decane	1.5
n-Dodecane	0.5
n-Pentadecane	0.5

Table 3.8: Composition of synthetic gas mixture 8

T = 250°F	
Component	Mole %
Methane	83
Propane	4
n-Heptane	7.2
n-Decane	4
n-Dodecane	1.8

Table 3.9: Composition of synthetic gas mixture 9

T = 279°F	
Component	Mole %
Methane	95
Propane	1
n-Heptane	1.25
n-Decane	1.25
n-Pentadecane	1.5



Figure 3.1: Photograph of HTHP coreflood laboratory



Figure 3.2: Photograph of HTHP coreflood apparatus inside the oven

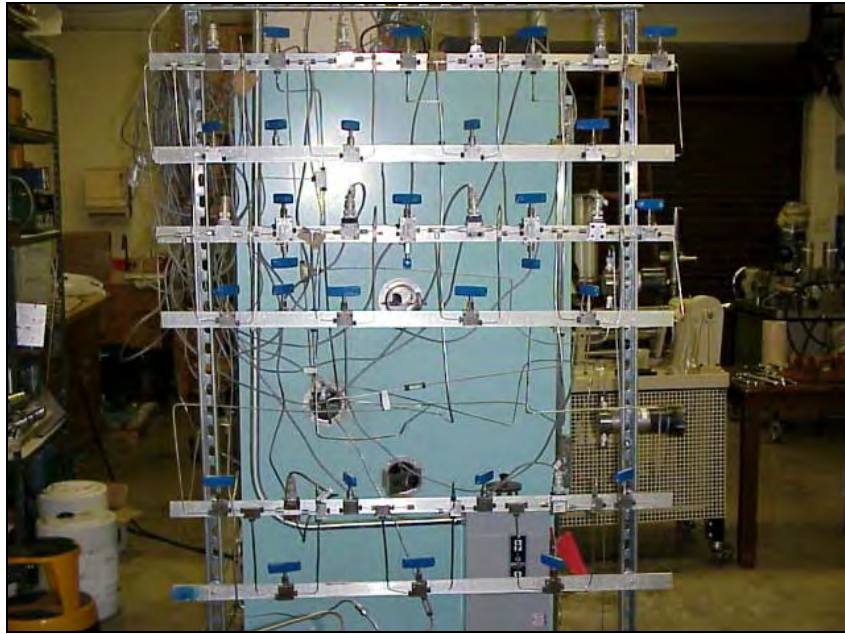


Figure 3.3: Photograph of transducer network used to measure pressure drop across the sections and the whole core

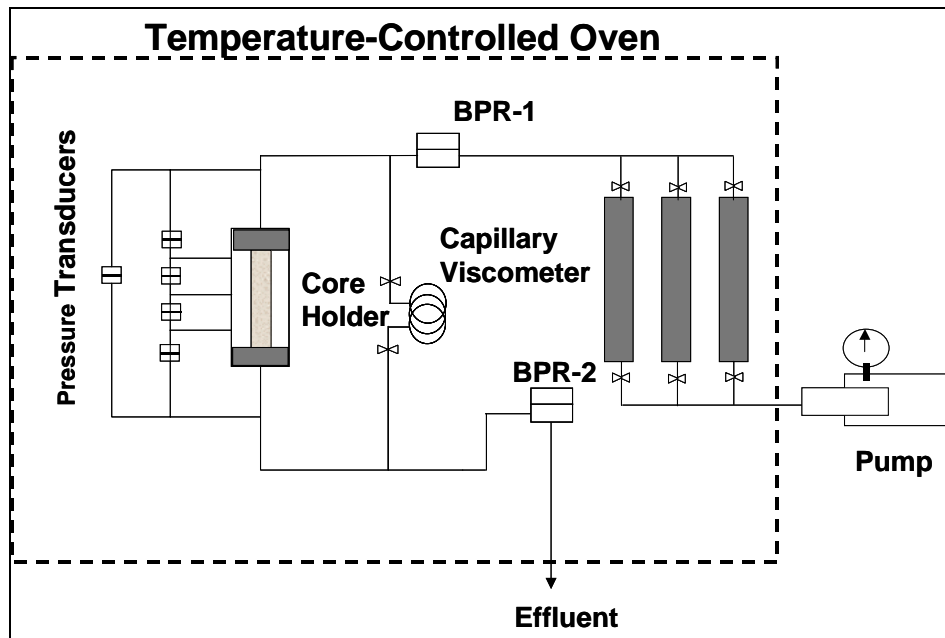


Figure 3.4: Schematic of coreflood setup

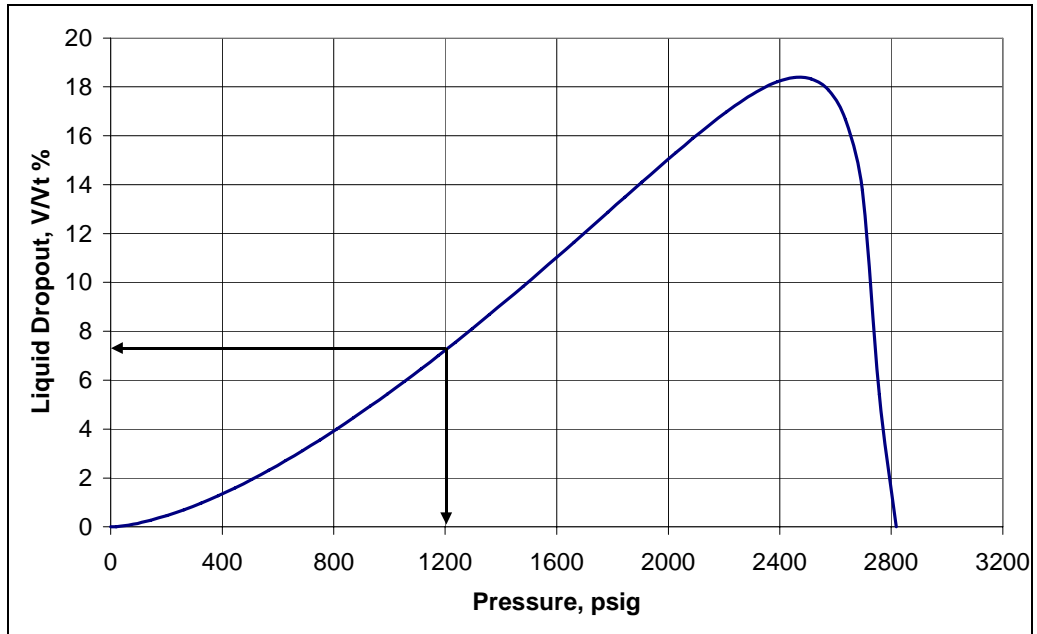


Figure 3.5: Liquid dropout of fluid-1 calculated using PREOS at 145°F

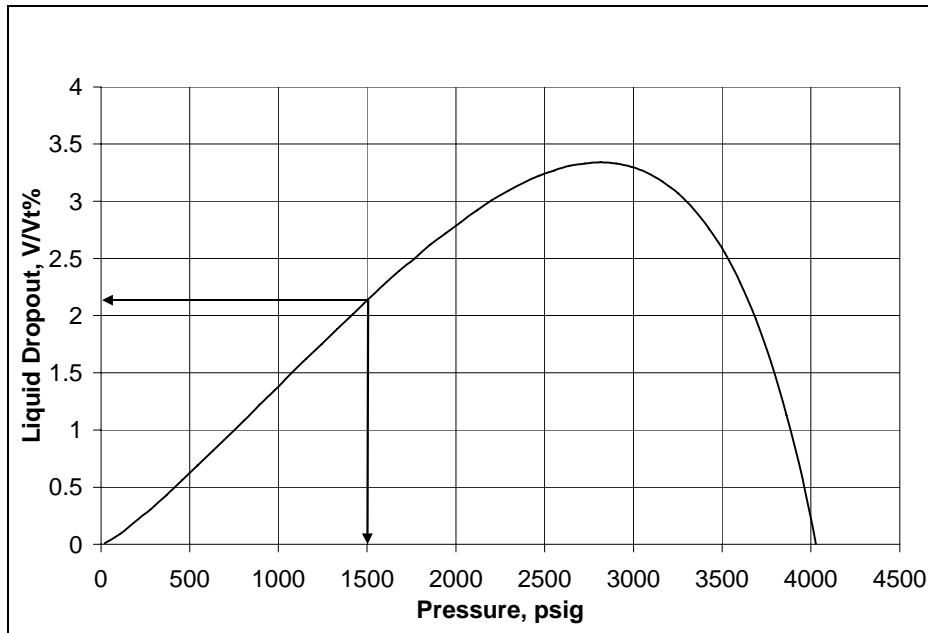


Figure 3.6: Liquid dropout of fluid-2 calculated using PREOS at 275°F

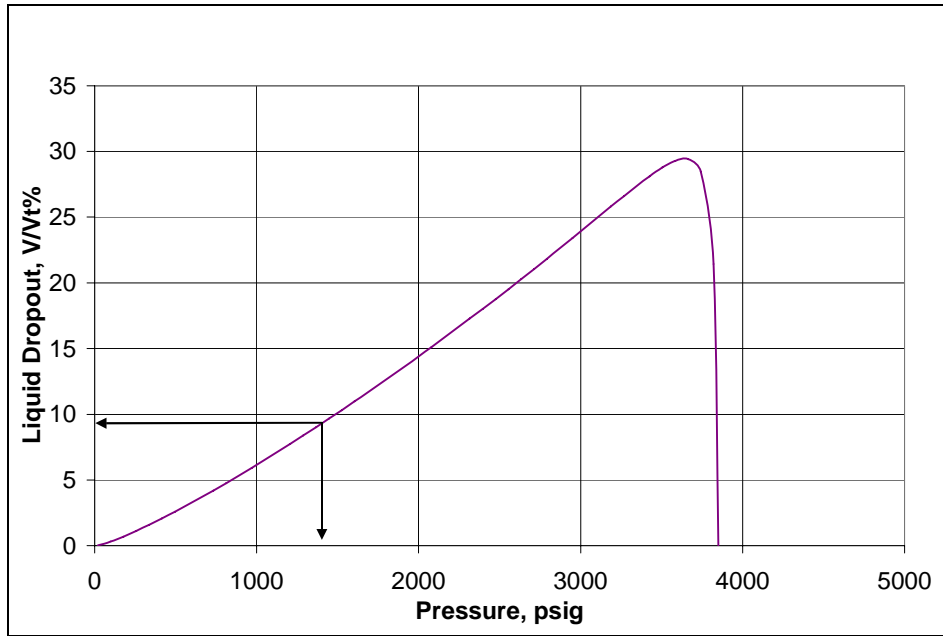


Figure 3.7: Liquid dropout of fluid-3 calculated using PREOS at 250°F

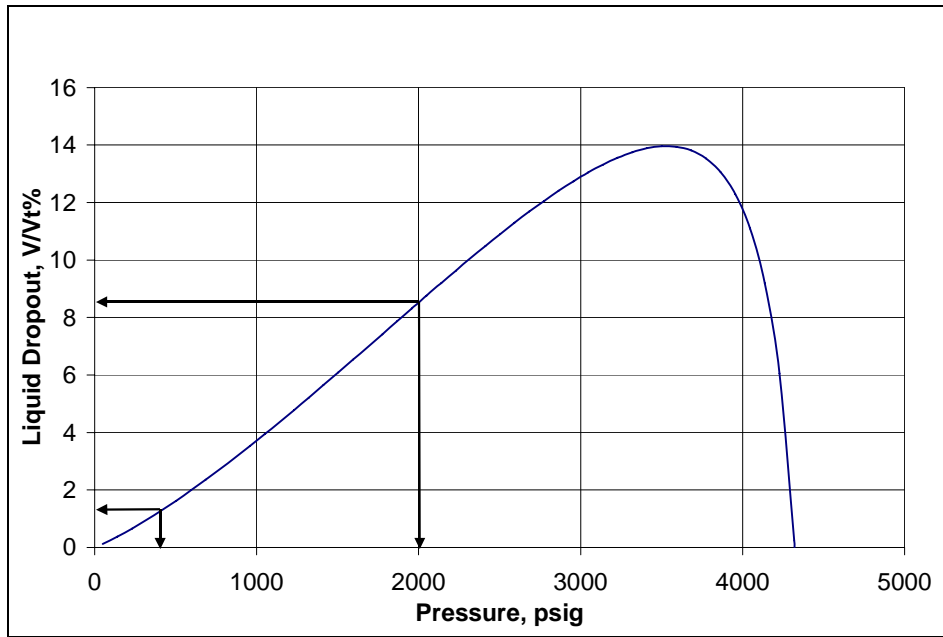


Figure 3.8: Liquid dropout of fluid-4 calculated using PREOS at 175°F

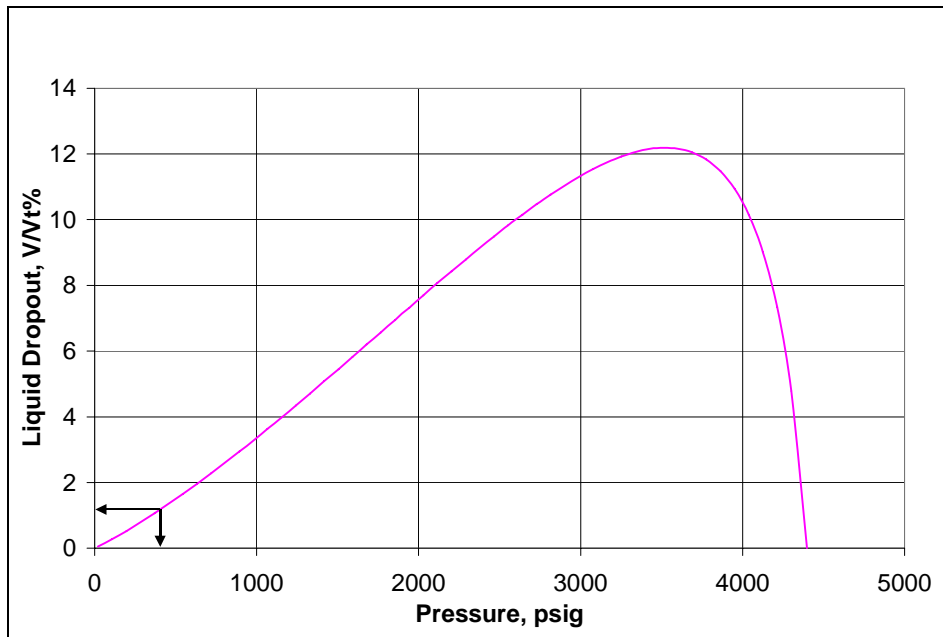


Figure 3.9: Liquid dropout of fluid-5 calculated using PREOS at 175°F

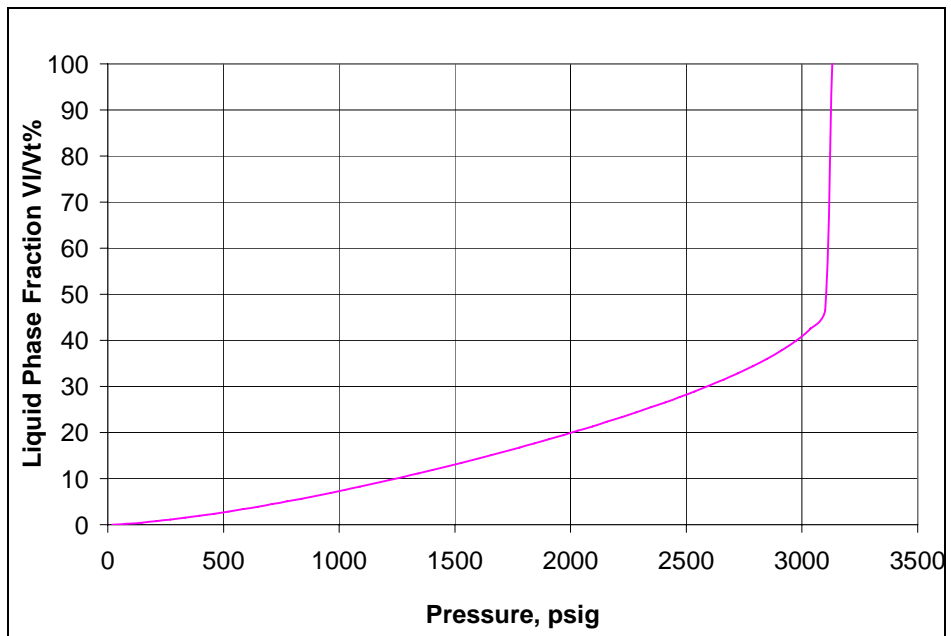


Figure 3.10: Liquid dropout of fluid-6 calculated using PREOS at 308°F

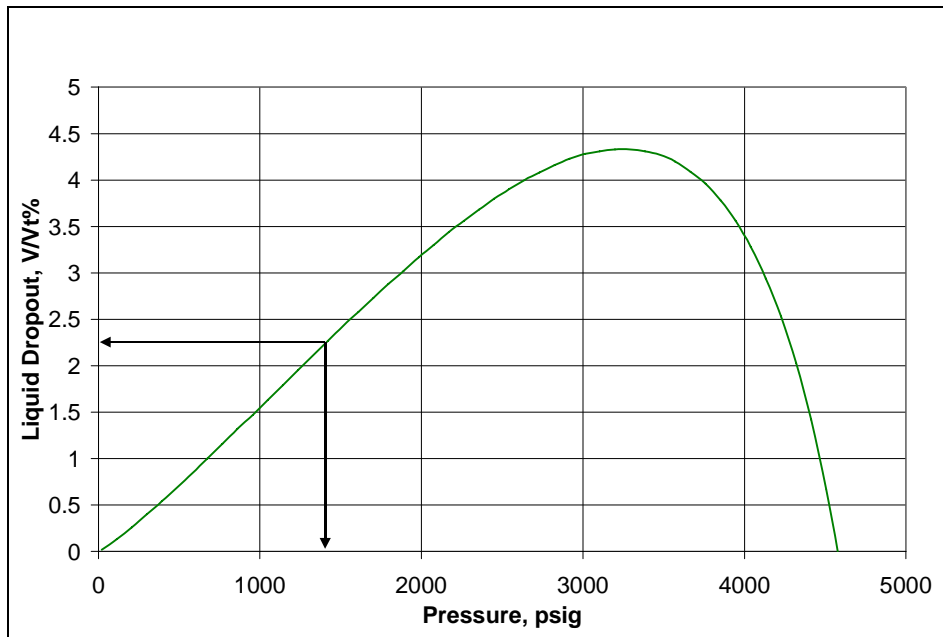


Figure 3.11: Liquid dropout of fluid-7 calculated using PREOS at 275°F

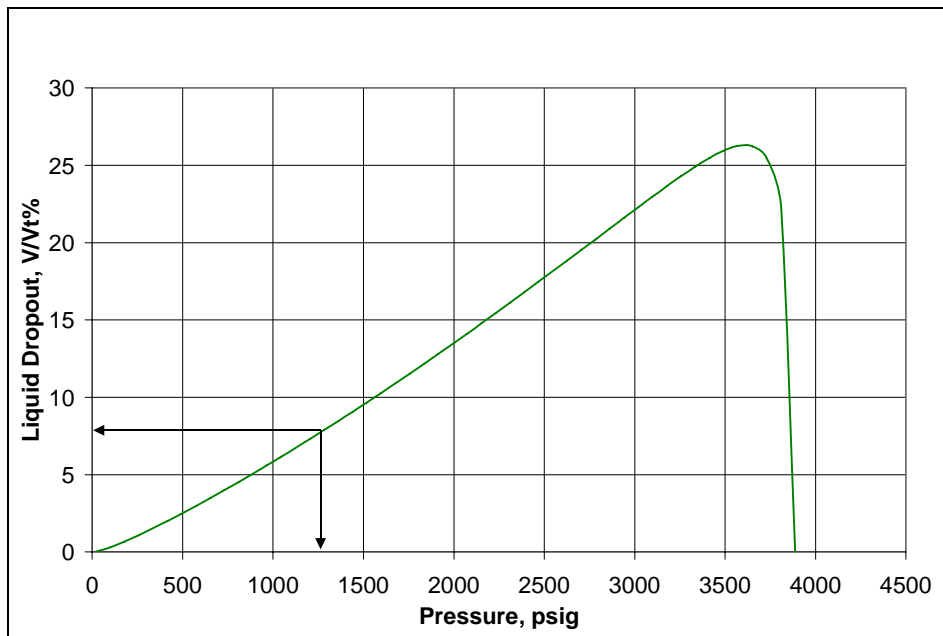


Figure 3.12: Liquid dropout of fluid-8 calculated using PREOS at 250°F

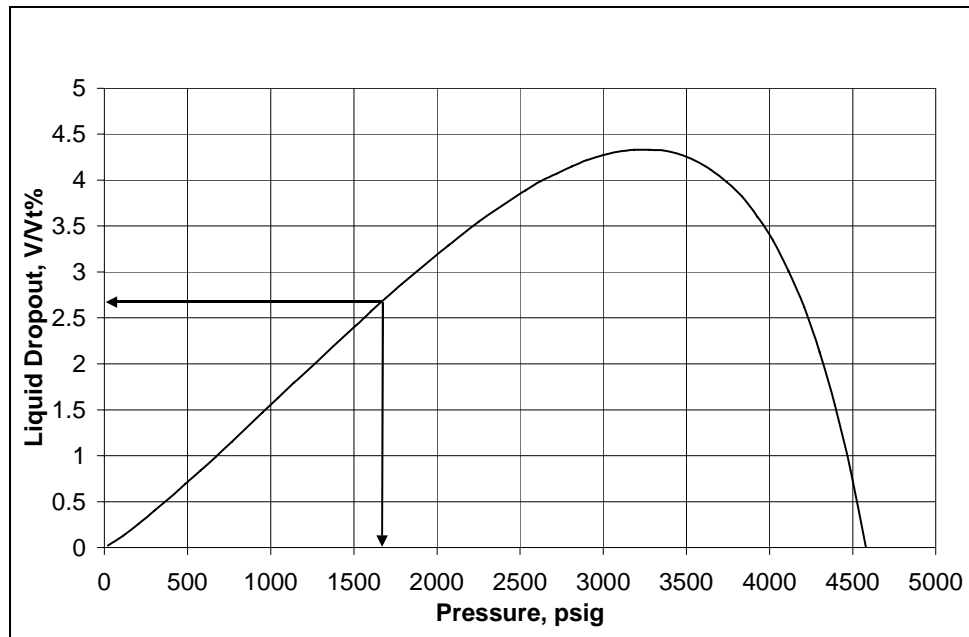


Figure 3.13: Liquid dropout of fluid-9 calculated using PREOS at 279°F

Chapter 4: Chemical Treatment of Sandstones with Methanol based Treatment Solutions

This chapter presents the results of chemical treatments done on dry sandstone cores and cores containing connate water with methanol based treatment solutions. The first section provides an introduction to the chemicals used in this study. The second section describes the results of chemical treatments on dry Berea sandstones at 145°F and 250°F. Steady-state gas and oil relative permeabilities were measured before and after treatment. The section also shows the durability of chemical treatment. The last section describes various mixtures of solvents used to treat sandstone rocks in presence of connate water before the screening test described in chapter 5 was developed.

4.1 INTRODUCTION

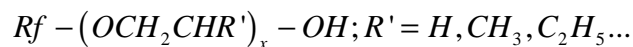
The objective of this chemical treatment is to alter the wettability of rocks from strongly water or oil wetting to intermediate wetting using a surfactant which will increase the relative permeability and thus the productivity of gas-condensate wells. For a successful chemical treatment there are a few required surfactant characteristics. The most important of them are:

- Strong interaction between the surfactant molecule and minerals on the rock surface. This is necessary for durability of the treatment.
- The surfactant should provide both water and oil repellency to make rock surfaces neutral wetting.
- It should be thermally stable at high temperatures as most of the gas and gas condensate reservoirs are at temperatures ranging from 150°F to 350°F.

- Surfactant should not cause formation damage due to undesired reactions, precipitation, emulsions, plugging or other adverse phenomena.
- Surfactant should be soluble in a non-aqueous solvent, preferably an organic solvent. Injecting an aqueous based solvent into formation can cause significant damage in gas wells as water can accumulate near the wellbore and decrease productivity. Organic solvents such as alcohol or glycols are good solvents for both water and oil/condensate and thus can displace liquid from the near wellbore region while delivering surfactant.

A non-ionic polymeric fluorinated surfactant has been used to alter the wettability of sandstone rocks to neutral or intermediate wetting. The surfactant was obtained from 3M Company, St. Paul, MN, USA under the trade name Novec FC4430. Kumar *et al.* (2006) used FC4430 in a methanol-water mixture to treat dry cores under reservoir conditions. Kumar (2006) tested the surfactants under reservoir conditions using both Berea and reservoir sandstone cores and reported a significant increase in the steady state gas and condensate relative permeability.

The general chemical structure of the non-ionic polymeric fluorinated surfactant is:



The surfactant contains a fluoroalkyl tail (R_f) and alkylene oxide head group. The head group consists of repeating units of pluronics, which consists of ethylene oxide and propylene oxide terminating in primary hydroxyl groups. Alkylene oxides in the molecule associate with sandstone via hydrogen bonding between the alkylene oxide

units and hydrated silanols on sandstone surface. The polymeric nature of the molecule results in multiple contacts with the rock surface and thus results in a durable treatment. The interaction between this type of molecule and the rock is due to adsorption out of solution, controlled in part by the cloud point of the material.

The fluoroalkyl group in the surfactant is intended to provide oil repelling and water repelling characteristics. The fluorochemical chain in this study is C_4F_9 . C_4 chemistry has been shown to be less bioaccumulative than C_8 chemistry (U.S Pat. No. 6,852,781). The fluorochemical chain is the tail of the surfactant, which repels both oil and water.

The surfactant adsorbs on the rock surface due to hydrogen bonding rather than co-valent bonds. Firoozabadi *et al.* (2002, 2005) proposed to change the wettability of rocks using alkoxysilanes, which forms covalent bonds with the sandstone rock surface, which may have some serious drawbacks and limitations. The reactivity of these materials is accelerated by temperature, water and salinity. Once the hydrolysis and subsequent condensation reactions start it is very difficult to control them under the conditions found in a reservoir. At this point the species become promiscuous and not only reacts with the substrate but also with each other. Therefore, when these materials are subjected to reservoir conditions during treatment, these materials will undergo hydrolysis and self-condensation, which could result in damage (reduced permeability) to the core.

4.2 CHEMICAL TREATMENT OF DRY SANDSTONE ROCKS

Kumar *et al.* (2006) reported an improvement in gas and oil relative permeability by about a factor of about 2 after treating dry sandstone rocks with FC4430 over a wide range of temperatures from 145°F to 275°F. The objectives of the following experiments

were to validate the results on dry sandstones and test durability of treatment by flowing large pore volumes of gas mixture over a long period of time.

4.2.1 Chemical Treatment at Low Temperature

An experiment was performed at 145°F on a Berea sandstone core. Synthetic fluid mixture-1 (Table 3.1) was used to perform a two-phase gas condensate flood. Steady state gas and oil relative permeability were measured before and after treatment. End point gas relative permeability was also measured before and after treatment by flowing equilibrium gas at core pressure. Durability of the treatment was evaluated by flowing a gas mixture for a long period of time. Details of the experiment (Expt #3) are given in **Appendix B3**.

Pre-treatment and post-treatment gas condensate two-phase floods were conducted at 489 cc/hr and 1200 psig core pressure as described in **Section 3.3**. **Figure 4.1** shows the pressure drop measured during the pre-treatment two-phase flood. Condensate accumulation at these experimental conditions decreased the gas relative permeability by more than 95%. The core was treated using 2% FC4430 in a mixture of methanol and water. **Table 4.1** gives the composition of the treatment solution. The treatment was done at a very low flow rate of 4 cc/hr to increase the residence time of the chemical in the rock. The core was shut-in for 96 hours after treatment.

To test the durability of the chemical treatment, multiple batches of post-treatment gas condensate floods were done. **Figure 4.2** shows the pressure drop across the core measured during the pre-treatment and post-treatment two-phase floods. **Figure 4.3** shows the post-treatment two-phase pressure drop data plotted against the actual flowing time. The result shows that the improvement factor was higher than 2 for the first couple of floods but the pressure drop kept increasing as more gas mixture was injected into the

core. The pressure drop stabilized after flowing about 600 pore volumes through the core and the improvement factor dropped to 1.56. A total of about 1350 pore volumes of gas mixture was injected and the actual flowing time was 52 hours. The time from the first post-treatment gas-condensate flood to the last flood was 183 hours. **Table 4.2** summarizes the results of the pre-treatment and post-treatment two-phase flow. Effect of flowing time and pore volumes on post-treatment gas relative permeability and improvement factor are given in **Table 4.3**.

An equilibrium gas flood was conducted to measure the gas end point relative permeability at residual condensate saturation before and after chemical treatment. The equilibrium gas phase composition at 145°F and 1200 psig was calculated using PREOS. The composition of the equilibrium gas mixture is given in **Appendix B3**. **Figure 4.4** compares the pressure drop measured across the core for the equilibrium gas flood before and after chemical treatment. **Table 4.4** summarizes the results of equilibrium gas floods. The end point gas relative permeability increased from 0.24 to 0.48 i.e. by a factor of 2. The result suggests that treatment reduced residual oil saturation and thus increased end point gas relative permeability. However, no saturation measurements were made to evaluate the effect of treatment on residual saturations of oil and gas.

Results of this experiment show the durability of treatment.

4.2.1 Chemical Treatment at High Temperature

This experiment (Expt #11) was performed at 250°F on a Berea sandstone core. Synthetic fluid mixture-3 (Table 3.3) was used to perform the two-phase gas condensate flood. Steady-state gas and oil relative permeability were measured before and after treatment. Durability of the treatment at high temperature was also evaluated by flowing

the gas mixture for a long period of time. Details of the experiment are given in **Appendix B11**.

Pre-treatment and post-treatment gas condensate two-phase floods were done at 640 cc/hr and 1500 psig core pressure as described in **Section 3.3**. The core was treated using 2% FC4430 in a mixture of methanol and water. **Table 4.1** gives the composition of the treatment solution. **Figure 4.5** compares the steady state pressure drop for pre-treatment and post-treatment gas condensate two-phase floods. **Table 4.2** summarizes the results of the pre-treatment and post-treatment two-phase flow. To test the durability of the chemical treatment, nine batches of post-treatment gas condensate floods were done. A total of about 1060 pore volumes of gas mixture was injected into the core and the actual flowing time was 34 hours. The time from the first post-treatment gas condensate flood to the last flood, was 232 hours. The improvement factor was more than 2 initially but stabilized at about 1.9 after flowing 250 pore volumes of fluid mixture through the core. The effect of flowing time and pore volumes on post-treatment gas relative permeability and improvement factor are given in **Table 4.5**.

The high initial improvement at both low and high temperatures is because of presence of methanol in the core. Al-Anazi *et al.* (2003) showed that a methanol treatment can delay accumulation of condensate buildup and results in an enhanced flow period of high gas and condensate relative permeability. But once methanol is flushed out of the core, there is no increase in relative permeability unless an effective surfactant treatment has been done.

4.3 INITIAL ATTEMPTS TO CHEMICALLY TREAT SANDSTONE ROCKS WITH CONNATE WATER

Results in the previous section and those reported by Kumar *et al.* (2006) show that chemical treatment using FC4430 in a mixture of methanol and water improved gas and condensate relative permeabilities by a factor of about 2 in dry sandstone cores. The following sections describe the effect of chemical treatment on rocks with connate water present. Different approaches that were tried before a successful treatment formulation was developed based on phase behavior results described in **Chapter 5**.

4.3.1 First Approach: Imitating Dry Core Treatment

These experiments (Expt #6, 7 and 10) were conducted on Britannia reservoir cores at 275°F. Synthetic fluid mixture-2 (Table 3.2) was used to perform two-phase gas condensate floods. Synthetic fluid was designed to match the actual reservoir fluid properties at reservoir temperature and pressures. An initial water saturation of 26.1% was established in the cores following the procedure described in Section 3.3. The composition of synthetic brine used in these experiments is given in **Table 4.6**. Cores were treated using 2% FC4430 in a mixture of methanol and water. 10 wt % water was used in the treatment solution in experiment 6 and 7 and 4 wt % in Experiment 10. Steady-state gas and oil relative permeability were measured before and after treatment as described in **Section 3.3**.

Figure 4.6 compares the pressure drop measured across the core for gas condensate floods before and after chemical treatment at 1500 psig for Experiment #10. No improvement in gas and oil relative permeabilities was observed after the chemical treatment. The core was then treated again and the steady-state pressure drop for the gas condensate flood was the same as that before treatment. Thus, chemical treatment using

the same treatment solution as used for dry sandstone cores did not improve relative permeabilities after treatment. Similar results were obtained in Experiment #6 and 7 conducted on Britannia sandstone reservoir cores under the same conditions. **Table 4.7** compares gas relative permeabilities before and after chemical treatment for Experiment #6, 7 and 10. Details of these experiments are given in **Appendix B6, B7 and B10**, respectively.

These results show that chemical treatment is not effective in treating a sandstone rock in the presence of initial brine. This could be due to either the presence of water or salt or both. Since the solubility of the FC4430 surfactant decreases with increasing water concentrations, eventually reaching a cloud point, it is possible that water can cause precipitation of surfactant on the rock surface. Also precipitation of salt can occur if the solvent is not miscible with high salinity brines. Precipitation of either salt or surfactant can have undesirable effects and result in the failure of the chemical treatment.

4.3.2 Second Approach: Solvent Pre-flush before Chemical Treatment

In this approach, a pre-flush of methanol/water mixture was conducted before chemical treatment to flush out brine from the core. The pre-flush was expected to either completely remove water from the core or significantly reduce water saturation in the core. This would thus prevent surfactant precipitation. The experiment (Experiment #8) was conducted at 275°F on a Berea sandstone using synthetic gas mixture-2 (Table 3.2). An initial water saturation of 26.1% was established using synthetic brine (**Table 4.6**).

Nine pore volumes of methanol/water (90/10) mixture was injected into the core after the initial gas-condensate two-phase flood. The core was then treated using the treatment solution given in **Table 4.1** followed by the post-treatment gas-condensate flood. **Figure 4.7** compares pressure drop measured across the core during pre-treatment

and post-treatment gas condensate flood at 1500 psig. No improvement was observed in gas and condensate relative permeability after chemical treatment. **Table 4.8** compares gas relative permeabilities before and after chemical treatment for the experiment. Details of the experiment are given in **Appendix B8**.

The result shows that a pre-flush of methanol-water mixture might have not been effective in removing all of the brine. Another possibility is that the solvent did not dissolve salts present in the brine during the displacement and thus resulted in salt precipitation, which affects the interaction of surfactant molecule with the rock surface.

4.3.3 Third Approach: Removing Salt from Initial Water

In this approach, initial water saturation was established using D.I. water instead of synthetic Britannia brine (given in **Table 4.6**) so that salt precipitation could be eliminated as the cause of the problem. A pre-flush of methanol was also conducted before chemical treatment to flush out water from the core and thus prevent the surfactant from reaching its cloud point.

The experiment (Experiment #9) was conducted at 275°F on a Berea sandstone core using synthetic gas mixture-2. An initial water saturation of 26.1% was established using D.I. water. 10 pore volumes of methanol was injected into the core after the initial gas condensate two-phase flood. The core was then treated using the treatment solution given in **Table 4.1** followed with the post-treatment gas condensate flood. **Figure 4.8** compares the pressure drop measured across the core for two-phase gas condensate flood at 1500 psig before and after treatment. No improvement was observed in gas and condensate relative permeability after chemical treatment. **Table 4.8** compares gas relative permeabilities before and after chemical treatment for the experiment. Details of the experiment are given in **Appendix B9**.

This result shows that the presence of salt is not the primary problem associated with treating cores with connate water. There were two explanations considered for the failure:

1. Methanol does not miscibly displace all of the water from the core.
2. Pre-flush removes all water and condensate from the core and thus reduces the surfactant adsorption on the rock because it is too soluble in the solvent and thus does not tend to interact as strongly with the rock.

4.3.4 Fourth Approach: Preflush with larger residence time

In this approach, methanol pre-flush was followed by a gas condensate two-phase flood. This was done to establish conditions similar to what exists in a dry core when treatment solution is injected into the core. Experiments were done using both D.I water and synthetic Britannia brine as connate water (Experiment #13 and #15, respectively). These experiments were conducted on Berea sandstone at 275°F using synthetic gas mixture-2 (Table 3.2).

A methanol pre-flush was conducted after the initial gas condensate flood. A pre-flush was conducted in batches to increase the residence time of methanol in the core, which may help in displacing more water. Nine pore volumes of methanol were injected into the core and then it was shut-in for 12 hours followed by nine more pore volumes of methanol. A two-phase gas condensate flood was conducted to flush out methanol and establish condensate saturation in the core. Cores were then treated using the treatment solution given in **Table 4.1** followed with the post-treatment gas condensate flood. **Figures 4.9** and **4.10** compare the pressure drop measured across the core for the two-phase gas condensate flood at 1500 psig before and after treatment for Experiments 13 and 15, respectively. **Table 4.9** compares gas relative permeabilities before and after

chemical treatment for the Experiment #13 and 15. Chemical treatment increased relative permeabilities by a factor of 1.35 and 1.1 for #Experiment #13 and 15, respectively. Details of the experiment are given in **Appendix B13 and B15**.

These partially successful results imply that a larger pore volume with increased residence time of methanol pre-flush helped to remove some water from the core. Also, the presence of condensate in the core might help in reducing the solubility of surfactant in the treatment solution and thus help in adsorption on the rock surface which resulted in some improvement.

4.3.5 Fifth Approach: New Fluorocarbon surfactant

The results presented in the above sections show that sandstone rocks with connate water are difficult to successfully treat with FC4430 in methanol-water solvent. Thus, a new fluoro-surfactant L19829 from 3M was tested for improving productivity of sandstone rocks with connate water. The surfactant is similar to FC4430 except that alkylene oxide head group has only ethylene oxide units. It is believed that the interaction between the rock surface and FC4430 is due to hydrogen bond between ethylene oxide units and hydrated silanol sites. Thus, L19829 is expected to have a stronger interaction with the sock surface than FC4430.

The experiment was conducted on Berea sandstone cores at 275°F using synthetic gas mixture-2 at 26.1% initial water saturation. Details of the experiment (Expt #14) are given in **Appendix B14**. The core was treated with L19829 in a mixture of methanol and water. **Table 4.10** gives the composition of the treatment solution used in this experiment. **Figure 4.11** compares the pressure drop for two-phase gas condensate floods before and after chemical treatment. No improvement in relative permeability was observed after chemical treatment. **Table 4.10** compares gas relative permeabilities

before and after chemical treatment and shows changing to L19289 surfactant did not solve the problem.

4.3.6 Sixth Approach: Toluene flush

Previous results showed that methanol is not a very effective solvent for flushing out water/brine from cores. In this approach, a pre-flush was done using toluene before the chemical treatment. A toluene flood was conducted in Experiments #13 and 15 after the post-treatment gas condensate flood. 10 pore volumes of toluene were injected into each core followed by the treatment solution. 1.5 cc and 2.5 cc of water were produced from the cores after the toluene flood in Experiments #13 and 15, respectively. This shows that even after injecting large pore volumes of methanol, water was not completely displaced from high permeability Berea cores. These cores were then treated with the treatment solution given in **Table 4.1**. **Table 4.9** compares gas relative permeabilities before and after chemical treatment for Experiments 13 and 15. **Figures 4.9** and **4.10** compare the pressure drop for two-phase gas condensate floods before and after chemical treatment for Experiments 13 and 15, respectively. Chemical treatment after the toluene flood increased relative permeabilities by a factor of 1.54 and 1.64 for Experiment 13 and 15, respectively.

The results showed that sandstones with connate water could be successfully treated with FC4430 if most of the water is removed from the core before treatment. The improvement factor was still less than 2 suggesting that although toluene is a better solvent than methanol, it is not completely effective in displacing all the water from cores. This result led to screening for new solvents, which could displace both condensate and water and at the same time deliver surfactant to the rock surface. The screening of new solvents is presented in **Chapter 5**.

4.3.7 Seventh Approach: New solvents

Mixtures of iso-propanol (IPA)/toluene/water and IPA/water were used as solvents in the treatment solution in Experiments 19 and 20, respectively. These experiments were conducted on Berea sandstone at 275°F using synthetic gas mixture-2 at 26.1% initial water saturation. Synthetic Britannia brine (composition given in Table 4.7) was used as connate water. Details of the experiments are given in **Appendix B19 and B20**.

Tables 4.11 and 4.12 give the composition of treatment solutions used in Experiment 19 and 20, respectively. No solvent pre-flush was conducted in these experiments. **Figures 4.12 and 4.13** show the effect of chemical treatment on two-phase flow pressure drop for Experiments 19 and 20, respectively. Chemical treatment increased gas and oil relative permeability by 30% in Experiment 19 but no improvement was observed in Experiment 20. **Table 4.13** compares gas relative permeabilities before and after chemical treatment for Experiment 19 and 20, respectively. The small improvement in experiment 19 could be due to removal of water from the core by toluene in the treatment solution. The failure of Experiment 20 shows that even a mutual solvent like IPA alone is not a good solvent for delivering the surfactant to the rock surface in the presence of connate water.

To better understand the results of chemical treatment of rock with connate water, the water concentration in the effluent samples during the treatment flood were started to be analyzed using Karl Fischer technique (Ahmadi 2008-09).

Tables 4.14 and 4.15 summarize the experimental conditions and results of chemical treatment for experiments described in this chapter.

4.4. SUMMARY

Steady state relative permeability data for Berea and reservoir sandstones were measured at different temperatures and pressures after treating with a non-ionic polymeric fluoro-surfactant FC4430 in a mixture of methanol and water. Gas and condensate relative permeability increased by a factor of 1.6 to 1.9 after chemical treatment on dry Berea sandstones. Flowing large pore volumes of gas mixture through treated cores tested the durability of the chemical treatment at both low and high temperatures.

Treatment of sandstone cores in the presence of connate water showed no improvement in gas and condensate relative permeability. Various methods such as, methanol pre-flush, removing salt from connate water, toluene pre-flush and using different solvents such as IPA and toluene to deliver surfactant were tried with only partial success. Results show that solvents such as methanol and IPA alone were unsuccessful in removing all of the water from cores and thus better solvents are needed for delivering surfactant in the presence of brine and condensate. These results imply that selection of a proper solvent for the treatment solution is an important part of the treatment and compatibility tests of treatment solution with connate water at experimental temperatures is needed for selecting appropriate solvents. **Chapter 5** describes phase behavior studies done with different solvents and brines over a wide range of temperatures to select the proper solvents depending on reservoir conditions.

Table 4.1: Composition of treatment solution

Component	Weight %
FC4430	2
D.I. Water	4
Methanol	94

Table 4.2: Comparison of gas and oil relative permeabilities before and after chemical treatment on dry cores

Exp no	Temp, °F	Pressure, psig	k_{rg}		k_{ro}		IF
			Before	After	Before	After	
3	145	1200	0.032	0.050	0.022	0.034	1.56
11	250	1500	0.035	0.066	0.039	0.074	1.89

Table 4.3 Effect of flowing time on improvement factor at 145oF and 1200 psig (Exp #3)

Post-treatment gas condensate flood	Pore Volumes Flowed	Cumulative flowing time, hrs	Absolute Time, hrs	Improvement Factor
1	132	5	5	3.83
2	262	10	28	2.64
3	387	15	36	2.47
4	510	20	60	2.09

5	610	23.7	77	1.65
6	720	28	84	1.59
7	850	33	111	1.51
8	966	37.5	132	1.50
9	1098	42.5	156	1.52
10	1345	52	183	1.56

Table 4.4 Effect of chemical treatment on end point gas relative permeability at 145°F and 1200 psig (Exp #3)

q_g , cc/hr	capillary number (Nc)	k_{rg}^o before treatment	k_{rg}^o after treatment	Improvement Factor
487	4.33×10^{-6}	0.235	0.476	2.03
1136	9.72×10^{-6}	0.244	0.433	1.77

Table 4.5 Effect of flowing time on improvement factor at 250°F and 1500 psig (Exp#11)

Post-treatment gas condensate flood	Pore Volumes Flowed	Cumulative flowing time, hrs	Absolute Time, hrs	Improvement Factor
1	105	3.60	3.6	2.78
2	248	8.10	14	2.28
3	361	11.65	64	2.09
4	466	15.30	80	2.07
5	580	18.95	86	1.93

6	692	22.55	101	1.92
7	810	26.06	126	1.88
8	950	30.56	135	1.94
9	1060	34.13	232	1.81

Table 4.6: Composition of synthetic Britannia reservoir brine

Salt	ppm
NaCl	59,000
CaCl ₂	16,000
MgCl ₂ .6H ₂ O	3,500

Table 4.7: Comparison of gas and oil relative permeabilities before and after chemical treatment on Britannia reservoir cores with connate water

Exp no	Temp, °F	Pressure, psig	k _{rg}		k _{ro}		IF
			Before	After	Before	After	
6	275	1500	0.101	0.098	0.035	0.034	0.97
7	275	1500	0.062	0.067	0.021	0.023	1.08
10	275	1500	0.072	0.083	0.072	0.025	1.00

Table 4.8: Effect of solvent pre-flush on chemical treatment of Berea sandstone with connate water at 275°F and 1500 psig

Expt #	Pre-flush	k_{rg}		k_{ro}		IF
		Before	After	Before	After	
8	Methanol/water (90/10)	0.093	0.097	0.032	0.034	1.04
9	Methanol	0.084	0.085	0.029	0.029	1.01

Table 4.9: Effect of solvent pre-flush and chemical treatment of Berea sandstone with connate water at 275°F and 1500 psig

	Expt #13	Expt #15
k_{rg} before treatment	0.102	0.074
Methanol Pre-flush	18 PV	16 PV
k_{rg} after pre-flush	0.102	0.07
k_{rg} after treatment	0.138	0.082
Improvement factor	1.35	1.1
Toluene pre-flush	10 PV	10 PV
k_{rg} after toluene pre-flush	0.139	0.10
k_{rg} after second treatment	0.157	0.121
Improvement factor	1.54	1.64

Table 4.10: Comparison of gas and oil relative permeabilities before and after chemical treatment using L16829 on Berea sandstone at 275°F and 1500 psig (Exp#14)

Swi%	Treatment solution	k _{rg}		k _{ro}		IF
		Before	After	Before	After	
26.1	L19829 (2%), Water (4%), Methanol (94%)	0.110	0.114	0.038	0.039	1.014

Table 4.11: Composition of treatment solution for experiment-19

Component	Weight %
FC4430	2
D.I. Water	10
Toluene	44
IPA	44

Table 4.12: Composition of treatment solution for experiment-20

Component	Weight %
FC4430	2
D.I. Water	10
IPA	88

Table 4.13: Effect of chemical treatment using new solvents on Berea sandstone with connate water at 275°F and 1500 psig

Expt #	k_{rg}		k_{ro}		IF
	Before	After	Before	After	
19	0.057	0.075	0.019	0.026	1.32
20	0.073	0.075	0.025	0.026	1.03

Table 4.14: Experimental specifications for chemical treatments

Expt #	Pre-flush	Treatment Solution
3	-	FC4430 (2%), Water (4%), Methanol (94%)
6	-	FC4430 (2%), Water (10%), Methanol (88%)
7	-	FC4430 (2%), Water (10%), Methanol (88%)
8	Methanol/water (90/10)	FC4430 (2%), Water (4%), Methanol (94%)
9	Methanol	FC4430 (2%), Water (4%), Methanol (94%)
10	-	FC4430 (2%), Water (4%), Methanol (94%)
11	-	FC4430 (2%), Water (4%), Methanol (94%)
13	Methanol and toluene	FC4430 (2%), Water (4%), Methanol (94%)
14	-	L19829 (2%), Water (4%), Methanol (94%)
15	Methanol and toluene	FC4430 (2%), Water (4%), Methanol (94%)

Table 4.19: Summary of chemical treatment on sandstone rocks

Experiment #	3	6	7	8	9	10	11	13	14	15	19	20
Rock	BS	Brit-A	Brit-A	BS	BS	Brit-B	BS	BS	BS	BS	BS	BS
Temperature, °F	145	275	275	275	275	275	250	275	275	275	275	275
Core Pressure, psig	1200	1500	1500	1500	1500	1500	1500	1500	1500	1500	1500	1500
k, md	150	48	51	130	213	41	196	183	186	240	216	221
S _{wi} , %	0	26.1	26.1	26.1	26.1	26.1	0	26.1	26.1	26-50	26.1	26.1
Salinity, ppm	-	78000	78000	78000	0	78000	-	0	78000	78000	78000	78000
q _{core} , cc/hr	512	720	567	365	543	528	640	528	578	578	708	708
N _c	2.81× 10 ⁻⁵	1.24× 10 ⁻⁵	1.51× 10 ⁻⁵	6.56× 10 ⁻⁶	1.15× 10 ⁻⁵	122× 10 ⁻⁵	3.25× 10 ⁻⁵	1.64× 10 ⁻⁵	6.84× 10 ⁻⁶	1.33× 10 ⁻⁵	1.93× 10 ⁻⁵	1.51× 10 ⁻⁵
Treatment rate, cc/hr	4	32	32	32	32	32	32	32	32	32	32	32
Shut-in time, hrs	96	24	24	24	24	24	24	24	24	24	24	24
PVT Ratio	1.45	2.90	2.95	2.90	2.90	2.90	0.89	2.90	2.90	2.91	2.91	2.91
k _{rg} before treatment	0.032	0.101	0.062	0.093	0.084	0.072	0.035	0.102	0.110	0.074	0.073	0.057
k _{ro} before treatment	0.022	0.035	0.021	0.032	0.029	0.025	0.039	0.035	0.038	0.025	0.025	0.019
k _{rg} after treatment	0.050	0.098	0.067	0.037	0.085	0.072	0.066	0.157	0.114	0.121	0.075	0.075
k _{ro} after treatment	0.034	0.034	0.023	0.034	0.029	0.025	0.074	0.054	0.039	0.042	0.026	0.026
IF	1.56	0.97	1.08	1.04	1.01	1.00	1.89	1.54	1.04	1.64	1.32	1.03

*BS- Berea Sandstone, *Brit- Britannia reservoir cores

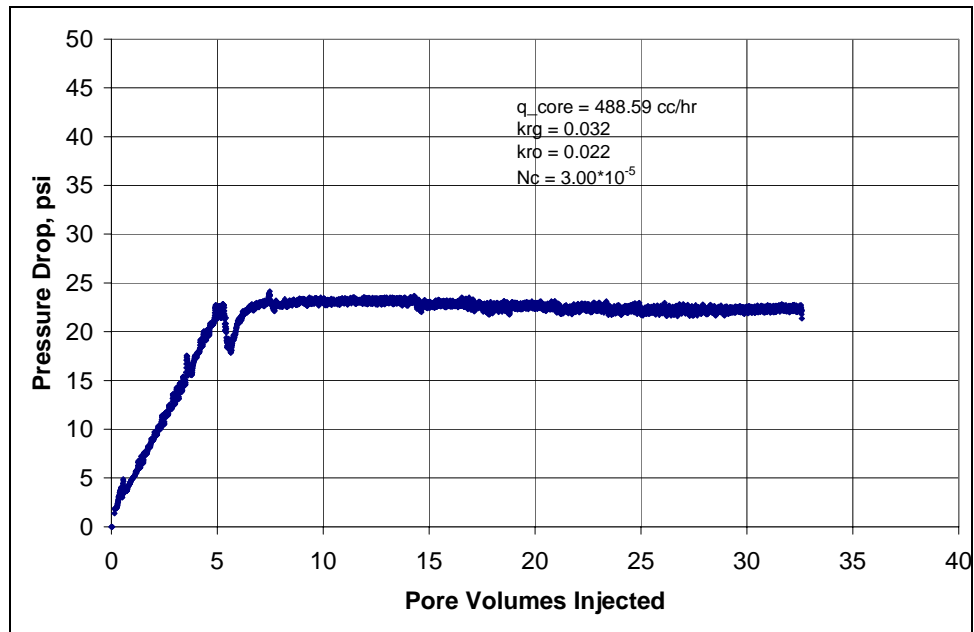


Figure 4.1: Steady state pressure drop measured during pre-treatment gas condensate flood at 145°F and 1200 psig

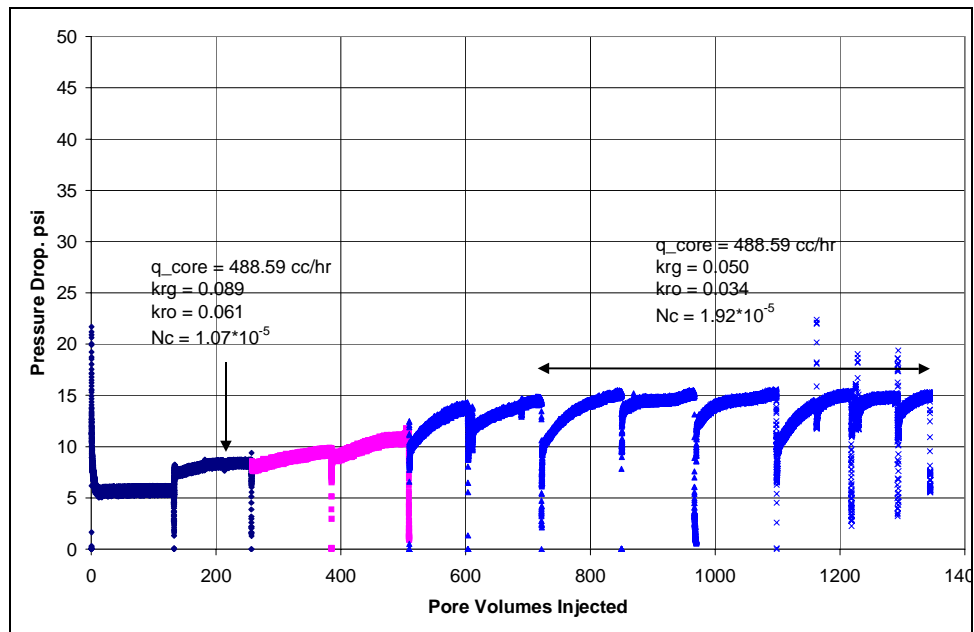


Figure 4.2: Effect of chemical treatment using FC4430 on condensate accumulation at 145°F and 1200 psig (Exp #3)

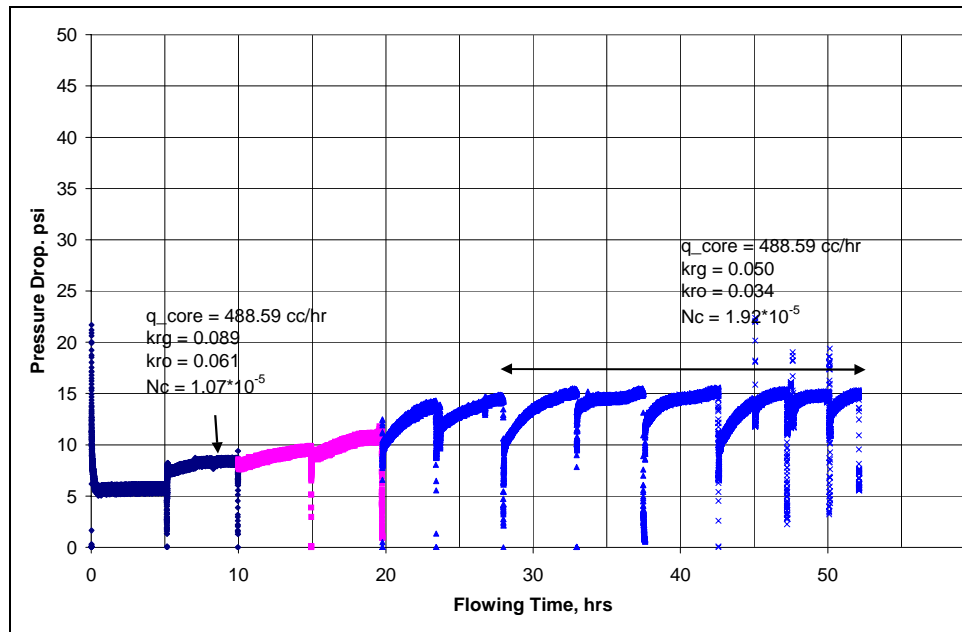


Figure 4.3: Durability of chemical treatment showed by flowing for a long period of time (Exp #3)

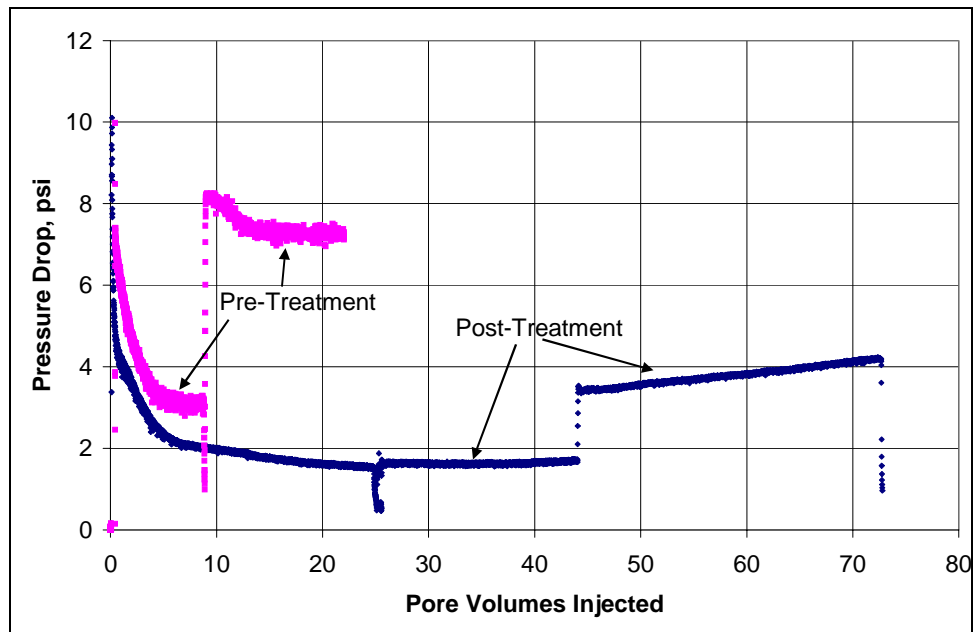


Figure 4.4: Comparison of pre-treatment and post-treatment pressure drop measured during equilibrium gas flood at 145°F and 1200 psig (Exp #3)

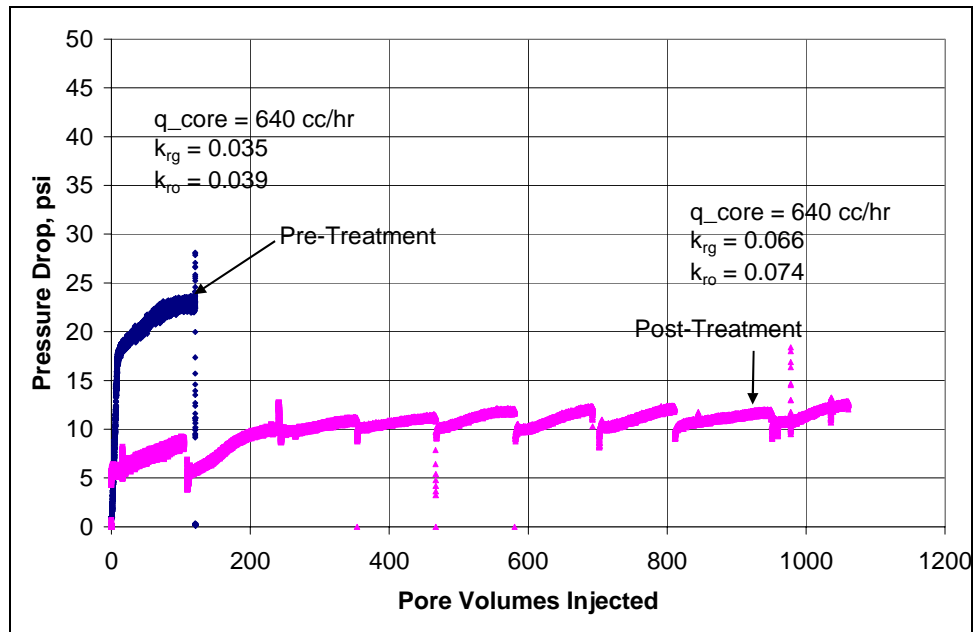


Figure 4.5: Comparison of pre-treatment and post-treatment condensate buildup at 250°F and 1500 psig (Exp #11)

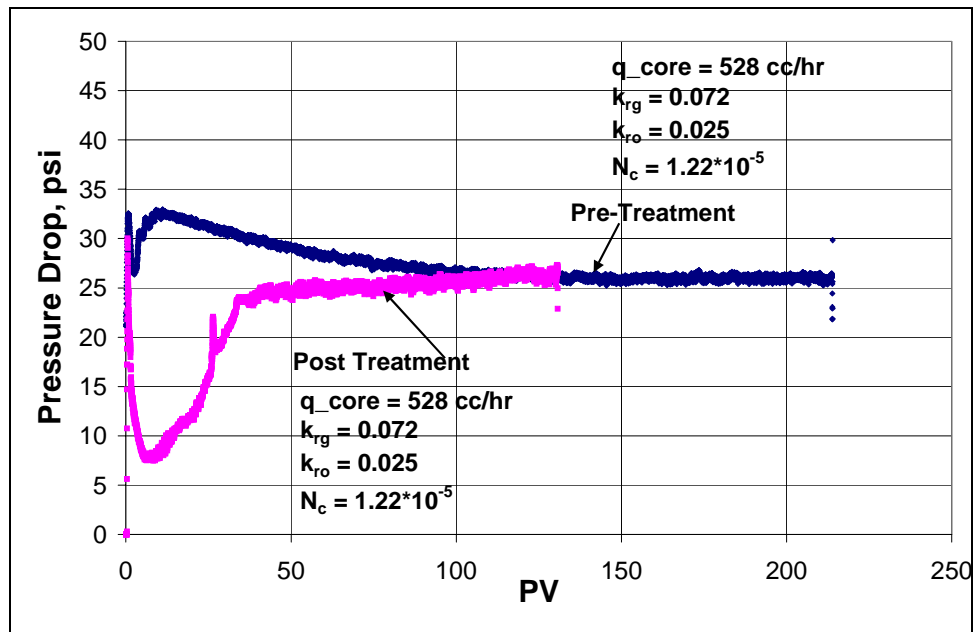


Figure 4.6: Comparison of pre-treatment and post-treatment condensate accumulation in reservoir core with connate water at 275°F at 1500 psig (Exp #10)

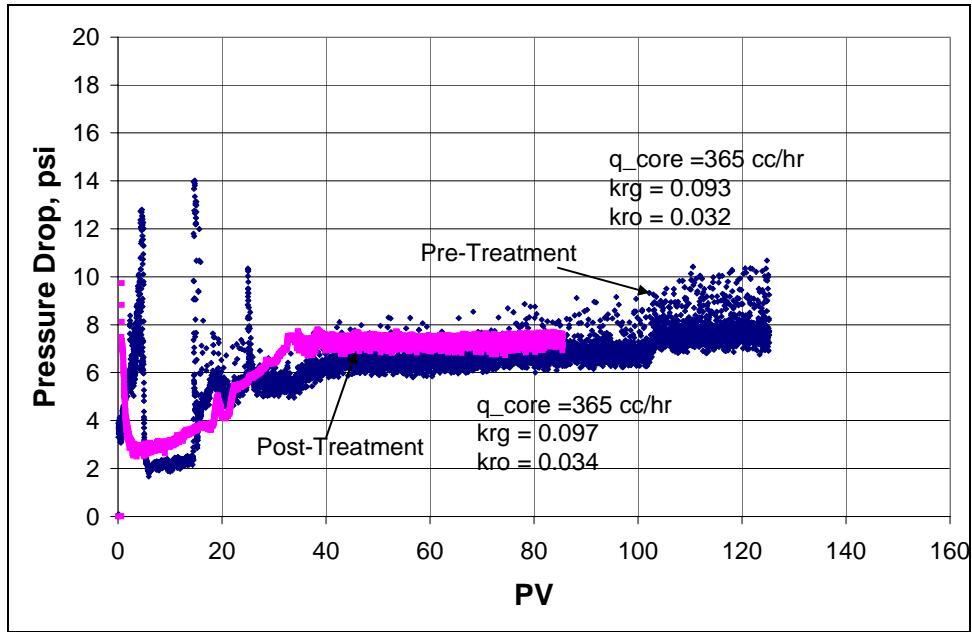


Figure 4.7: Comparison of pre-treatment and post-treatment condensate accumulation in Berea sandstone with connate water at 275°F at 1500 psig (Exp #8)

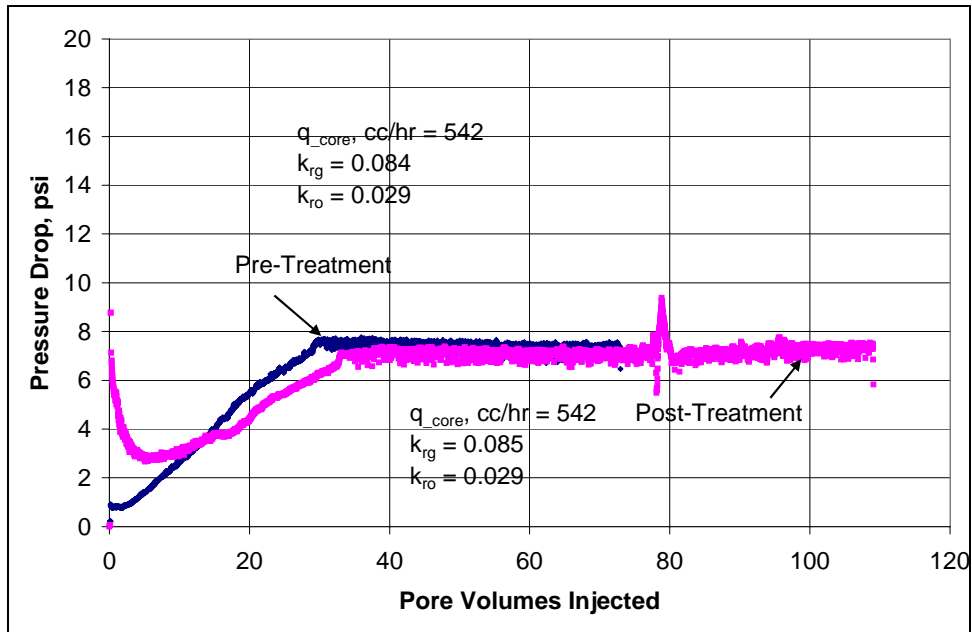


Figure 4.8 Comparison of pre-treatment and post-treatment condensate accumulation in Berea sandstone with connate water at 275°F at 1500 psig (Exp #9)

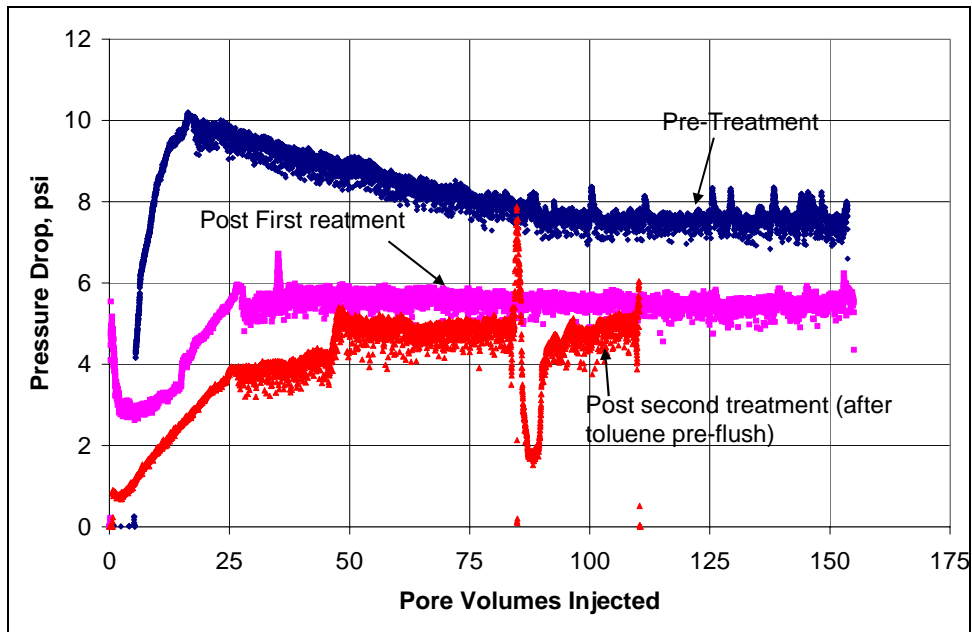


Figure 4.9: Comparison of pre-treatment and post-treatment condensate accumulation in Berea sandstone with connate water at 275°F at 1500 psig (Exp #13)

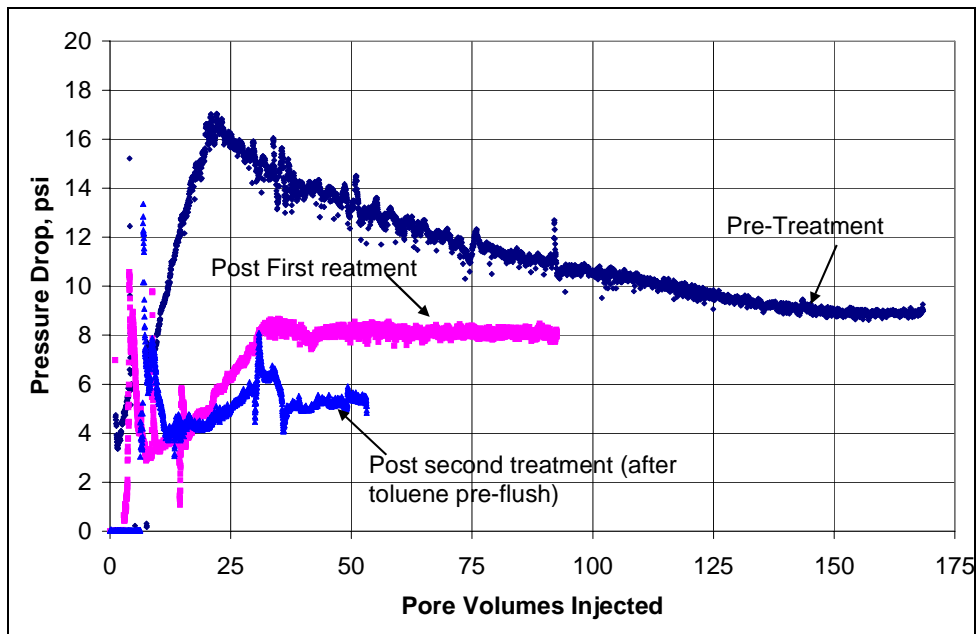


Figure 4.10: Comparison of pre-treatment and post-treatment condensate accumulation in Berea sandstone with connate water at 275°F at 1500 psig (Exp #15)

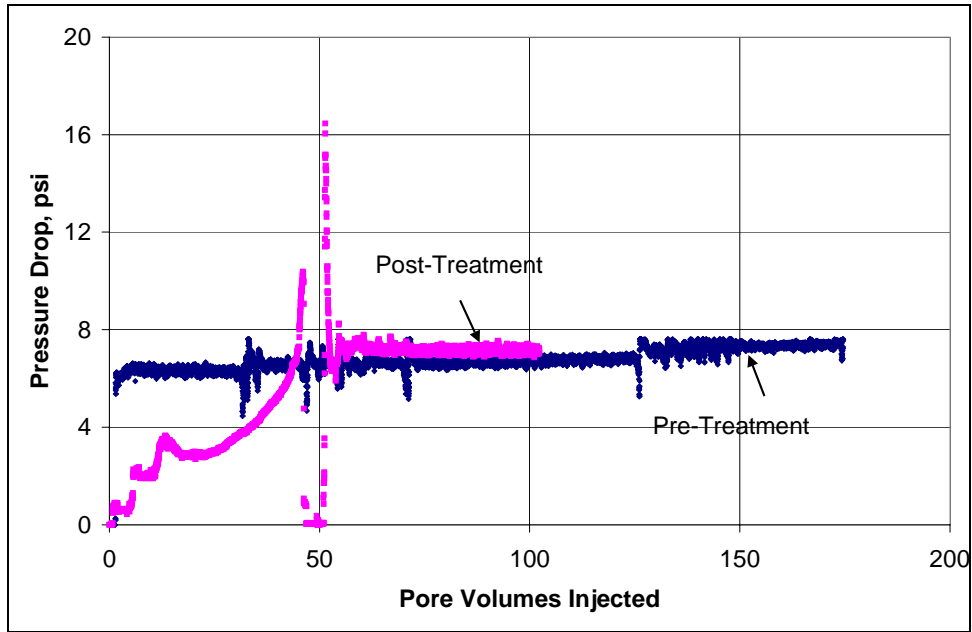


Figure 4.11: Effect of chemical treatment using L19829 on condensate accumulation in Berea sandstone with connate water at 275°F at 1500 psig (Exp #14)

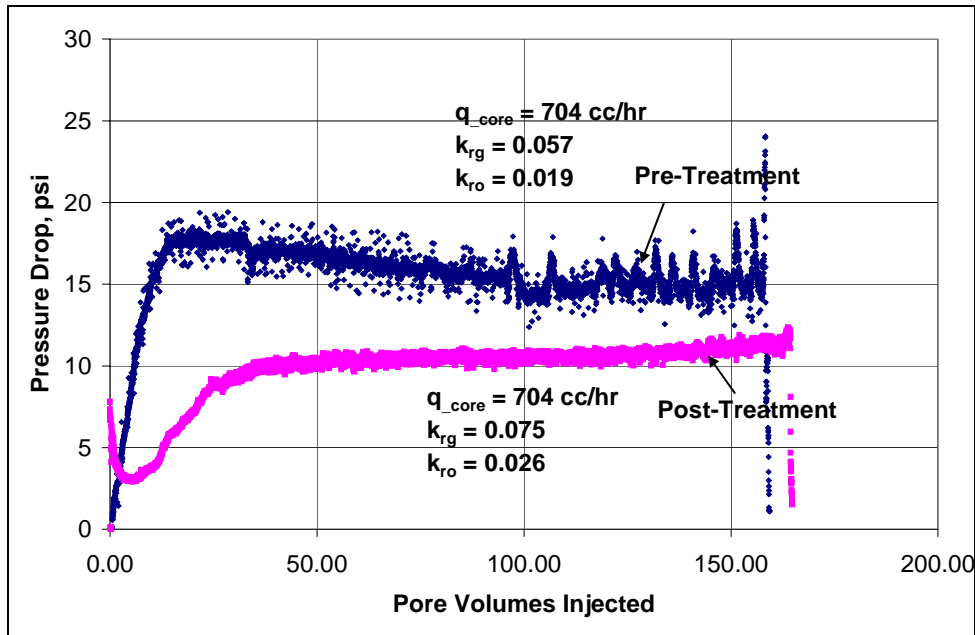


Figure 4.12: Effect of chemical treatment using FC4430 in a mixture of IPA and toluene on condensate accumulation in Berea sandstone with connate water at 275°F at 1500 psig (Exp #19)

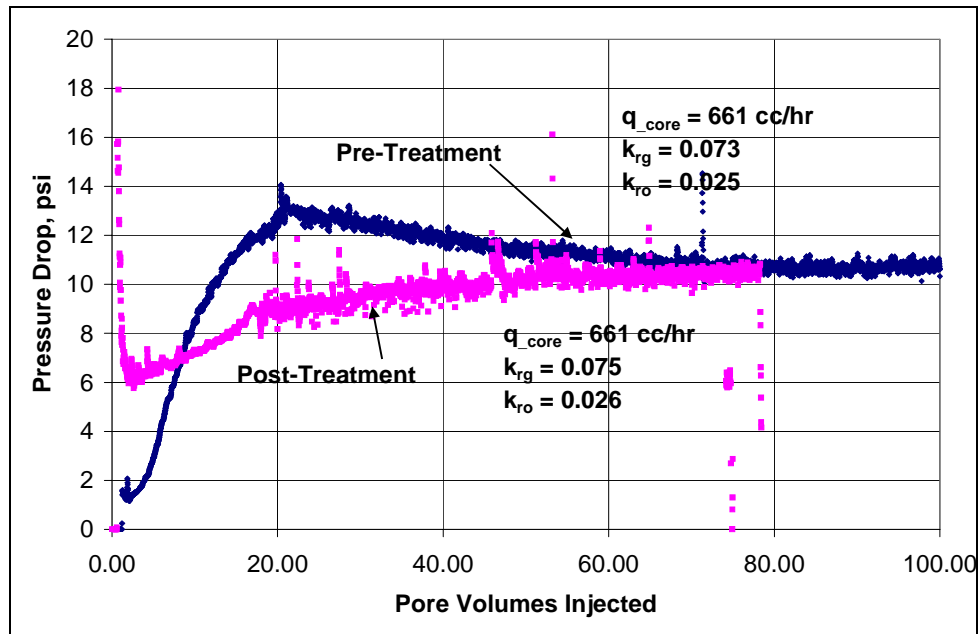


Figure 4.13: Effect of chemical treatment using FC4430 in a mixture of IPA and water on condensate accumulation in Berea sandstone with connate water at 275°F at 1500 psig (Exp #20)

Chapter 5: Section of Solvents for the Treatment Solution

This chapter describes a method that has been developed for selecting appropriate solvents for delivering the surfactant (FC4430) to the rock surface in the presence of connate water. The first section describes the important characteristics of a good solvent for delivering a surfactant to the rock surface. The second section presents the approach, based on phase behavior studies, adopted to select appropriate solvent for different experimental/reservoir conditions. The third section presents a detailed phase behavior study done using two solvent systems (2-butoxyethanol/ethanol and propylene glycol/isopropanol) over a wide range of temperature, weight percent water and brine salinity. This screening test was developed by Dr. Baran from 3M Corp. He performed a lot of initial phase behavior studies for evaluating the optimum solvent for delivering FC4430. The work was later continued at UT with the help of Dr. Larry Britton.

5.1 INTRODUCTION:

Results of chemical treatments on dry Berea sandstone rocks (**Section 4.2**) and data reported by Kumar et. al. (2006) show that treatments using FC4430 in a mixture of methanol and water were successful in improving gas and condensate relative permeabilities. However, treatment of sandstone cores containing connate water showed no improvement (**Section 4.3**). Results presented in Section 4.3 show that methanol alone or in combination with water, is not effective at solubilizing/displacing the brine and/or condensate while delivering the treatment. Failure of the treatment could be either due to the inefficiency of solvents in removing brine from the core or precipitation of surfactant and/or salt or a combination of the two.

For a successful chemical treatment there are a few required characteristics for the solvent used to deliver the surfactant to the rock surface. The most important of them are:

- The surfactant should be soluble in solvent at reservoir conditions.
- Treatment solution (surfactant + solvent) should be completely miscible with reservoir brine at reservoir temperatures. Solubility of the surfactant in the solvents decreases with increasing water concentration and temperature and eventually reaches a cloud point. This is typical of non-ionic surfactants.
- The treatment solution should be able to dissolve the salts present in the connate brine.

Many gas/gas-condensate reservoirs are associated with high water saturation and very high salinity brines. Precipitation of either the surfactant as it reaches a cloud point and/or salt, if the solvent is not able to solubilize high salt concentrations, can result in undesirable effects such as a reduction in rock permeability. Thus, depending on reservoir conditions, brine salinity, water saturation and temperature different solvent or a mixture of solvents may be required for delivering the surfactant.

A solvent that satisfies the above criteria can be used for delivering FC4430 but may not be effective in treating the rock surface as the interaction between this type of molecule and the rock is due to adsorption out of solution, controlled in part by the cloud point of the surfactant. Thus, if the surfactant is too soluble in the solvent it might not adsorb on the rock surface. Kumar *et al.* (2006) showed that treatment is not effective if surfactant is delivered in a good solvent such as methanol. Presence of water in the treatment solution caused surfactant adsorption on the rock surface due to insolubility and thus made the treatment successful. The solvent or a mixture of solvents in the treatment

solution should thus fulfill the above mentioned criteria but at the same time maintain the solution near the cloud point.

5.2 PHASE BEHAVIOR STUDIES TO IDENTIFY OPTIMUM SOLVENT

Tests were conducted to measure the solubility of FC4430 in different solvents and study its compatibility with different brines. Cloud point measurements were done in different solvent mixtures to determine the solubility of FC4430 in solvents at different temperatures. Phase behavior studies were done to test the compatibility of treatment solutions made up of different solvents and brines of different salinities.

Measurements were done either in a high-pressure, high-temperature PVT cell or glass tubes. For cloud point measurements, a constant composition of surfactant and solvents was placed in the cell and temperature was raised in steps and any visual evidence of precipitation of the surfactant was used as an indicator of the cloud point. For compatibility tests, a predetermined ratio of treatment solution (surfactant + solvent) and synthetic brine was placed in the cell or glass tubes. Temperature was then raised in steps and the solution was observed visually to detect any precipitation of surfactant or salt from the solution. Depending on the solvents used, brine salinity and water saturation (weight fraction), either salt or surfactant could precipitate out of solution. When the surfactant reaches its solubility limit, the solution turns cloudy whereas salt precipitates out as a separate phase and settles at the bottom of the solution. If the solvent is able to solubilize the surfactant and brine then the solution remains clear and is single phase. Thus by visually observing the solution, an optimum solvent mixture can be selected for delivering the surfactant depending on connate water saturation, brine salinity and temperature.

Tables 5.2, 5.4, 5.5 and 5.6 show the data for cloud point measurements of FC4430 in different solvents. The solubility of FC4430 in a methanol-water mixture decreased with increasing weight fraction of water as expected (**Table 5.2**). Solutions with 50 % or more water were cloudy at room temperature but as the water concentration decreased to 10%, no cloud point was observed till 280°F. **Table 5.4** shows the cloud point of FC4430 in IPA-toluene-water mixtures. Results show that the cloud point is affected not only by the water weight fraction in the mixture but also by the concentrations of IPA and toluene. For mixtures with IPA/toluene weight fraction ratio less than 1, the mixture was cloudy even at room temperature. As the ratio of IPA/toluene was increased to 1, no cloud point was observed till 275°F. The result shows that increasing the concentration of IPA in the treatment solution can help tolerate more water and prevent surfactant from precipitating out of solution.

Tables 5.5 and 5.6 show the results of cloud point measurements in propylene glycol (PG)-ethanol and propylene glycol-IPA mixtures. Results for both solvent mixtures are very similar i.e. solubility of the surfactant increases with increasing weight fraction of alcohol in the mixture. The surfactant is not soluble in PG alone but as the concentration of either ethanol or IPA is increased to 20% or more, the solution was clear up to 135°C.

Tables 5.7 to 5.16 present the results of phase behavior studies done using a combination of different solvents such as propylene glycol (PG), polypropylene glycol (PPG-425), ethanol, isopropanol (IPA), dipropylene glycol monomethyl ether (DPGME) and 2-butoxyethanol (EGMBE) with Britannia brine (**Table 5.1**) at both low and high temperatures. Dr. Larry Britton performed most of the tests. Results show that PG-ethanol and PG-IPA mixtures can tolerate high weight fractions of Britannia brine without precipitating out either salt or the surfactant. Also, the solubility increased with

increasing alcohol concentration in the treatment solution. Similar results are observed for treatment solutions containing 2-butoxyethanol and ethanol. However, the results were more sensitive to the concentration of ethanol in the treatment solution. The solubility increased with increasing concentration of ethanol. DPGME-ethanol and DPGME-IPA mixtures were also compatible with high brine weight fractions at high temperatures. The mixtures were, however, not completely miscible with brine at room temperature and resulted in the formation of two-phases over a wide range of water weight fractions.

From these phase behavior results, mixtures of 2-butoxyethanol-ethanol and PG-IPA looked most promising for brines such as synthetic Britannia brine. A 2-butoxyethanol-ethanol mixture may be better than a PG-IPA mixture as it is more sensitive to water and ethanol concentrations so that the ratio of solvents can be adjusted to keep the mixture close to cloud point. The ratios of solvents need to be changed depending on the operational temperature.

Tables 5.17 to 5.33 show the results of phase behavior studies done using a combination of different solvents and very high salinity brines including Hatter's Pond and Reservoir B reservoir brines (**Tables 5.23 and 5.24** respectively). Results show that for high salinity brines, the problem of salt precipitation becomes extremely important and it becomes even more significant for lower weight fractions of water in the solution. This is mainly because of the lower solubility of salts in solvents. Thus, it becomes extremely important that the ratio of solvents in the treatment solution is adjusted to prevent both salt and surfactant precipitation. Results show that mixtures of 2-butoxyethanol-methanol, PG-methanol and PG-IPA mixtures can tolerate high salinity brines up to 160°C and that the solubility again increased with increasing concentration of alcohol in the treatment solution.

Based on these phase behavior studies mixtures of 2-butoxyethanol-ethanol appear to be a better solvent for delivering the surfactant FC4430 in the presence of brines with salinity up to 78,000 ppm. PG/IPA and 2-butoxyethanol/methanol mixtures are better solvents for delivering surfactant FC4430 in the presence of very high salinity brines. The results show that the ratios of solvents in the treatment solution need to be changed depending on water saturation, brine salinity and temperature. The concentration of surfactant and the types of salts present in the treatment solution can also have an impact on phase behavior.

5.3 SENSITIVITY STUDY

This section describes the effect of various factors such as solvent ratio, brine salinity, water saturation, temperature and type of solvents on phase behavior results. Here the maximum temperature at which the solution was clear has been plotted against the water weight fraction in solution under different conditions. This maximum temperature limits the applicability of the treatment solution to those specific conditions.

Phase behavior results for a treatment solution containing 2% FC4430 and NaCl brines

Figure 5.1 shows the phase behavior results for a treatment solution made up of 2% FC4430 in a 70/30 mixture of 2-butoxyethanol/ethanol (composition given in **Table 5.34**) and NaCl brines of different salinities. The area under the curve represents the conditions under which the solution is clear or the treatment solution is applicable. Results show that the solubility of brine in the treatment solution decreases with increasing brine salinity and water weight fraction. For instance the treatment solution can take up to 50 wt% of D.I. water at 150°C whereas it can tolerate only 40wt % and 30

wt% of 50,000 ppm and 75,000 ppm brines respectively at 150°C. This treatment solution could not solubilize brine with salinity more than 100,000 ppm at any temperature.

Figure 5.2 shows the phase behavior results of a treatment solution made up of 2% FC4430 in a 50/50 mixture of 2-butoxyethanol/ethanol (composition given in **Table 5.35**) and NaCl brines of different salinities. Results show that solubility of brine in treatment solution decreases with increasing brine salinity. Solubility also decreased with increasing water concentration for low salinity brines, but for brines with a salinity of 75,000 ppm or more, the solubility first increased with water concentration and then decreased. For instance, the solution with 150,000 ppm brine was insoluble with 20 wt% water at room temperature but as the water increased to 30 wt% the solution was clear up to 125°C. The solution became cloudy again for mixtures with more than 50 wt% water. The insolubility at lower water concentration is caused by precipitation of salt from the solution, whereas at higher values the surfactant becomes insoluble and the solution becomes cloudy. Thus, the solvent has both upper and lower one-phase limits in the presence of high salinity brines. Similar results were observed from the phase behavior study of a treatment solution made up of 2% FC4430 in a 30/70 mixture of 2-butoxyethanol/ethanol mixture (composition given in **Table 5.36**) and NaCl brines of different salinities (**Figure 5.3**).

Figure 5.4 shows the phase behavior results of a treatment solution made up of 2% FC4430 in a 70/30 mixture of propylene glycol/IPA (composition given in **Table 5.37**) and NaCl brines of different salinities. Results show that the solubility of brine in the treatment solution decreases with increasing brine salinity and water concentration. The treatment solution can tolerate brines with salinity as high as 225,000 ppm and thus makes it suitable for delivering the surfactant in formations with very high salinity brines

at high temperatures. Comparing the phase behavior results with those of an analogous treatment solution made up of a 70/30 mixture of 2-butoxyethanol/ethanol (**Figure 5.1**) shows that the treatment solution made of 2-butoxyethanol/ethanol (**Table 5.34**) can tolerate higher water concentrations for lower salinity brines, but as the salinity increases to 100,000 ppm or more the treatment solution with 70/30 PG/IPA can tolerate much higher water concentrations up to much higher temperatures.

Figures 5.5 and **5.6** show the phase behavior results of NaCl brines of different salinities with a treatment solution made up of 2% FC4430 in 50/50 and 30/70 mixtures of propylene glycol/IPA respectively (composition given in **Table 5.38** and **5.39**). Results show that solubility of brine decreases with increasing brine salinity. Solubility also decreased with increasing water concentration for low salinity brines, but for higher salinity brines the solubility first increased and then decreased.

Results presented in **Figures 5.1** to **5.6** show the conditions at which a particular treatment solution can be used. A treatment solution that is applicable under a particular reservoir/experimental condition, may fail if any of the above-mentioned variables changes (depending on the phase behavior results).

Figures 5.7 to **5.12** compare the phase behavior results of treatment solutions with 2% FC4430 in 70/30, 50/50 and 30/70 mixtures of 2-butoxyethanol/ethanol with different salinity brines. The results show that for lower salinity brines, the treatment solution with 70/30 mixture of 2-butoxyethanol/ethanol is applicable up to much higher temperatures and can tolerate higher water weight percent in solution. As the salinity is increased, the treatment solutions with higher concentration of alcohol are more compatible with solutions having higher water concentration and up to higher temperatures.

Figures 5.13 to 5.21 compare the phase behavior results of treatment solutions with 2% FC4430 in 70/30, 50/50 and 30/70 mixtures of PG/IPA with different salinity brines. For lower salinity brines the treatment solution with a 30/70 mixture of PG/IPA is better than the other two in tolerating higher water concentrations up to higher temperatures. As the brine salinity increases, the treatment solution with a 70/30 mixture of PG/IPA is better than the 30/70 mixture for solutions with lower water weight percent but the 30/70 mixture of PG/IPA is better for solutions with higher water concentration.

Phase behavior results for a treatment solution containing 1% FC4430:

This section presents phase behavior studies conducted to study the effect of surfactant concentration on its phase behavior and its compatibility with different salinity brines.

Figures 5.22 and 5.23 show the phase behavior results of NaCl brines of different salinities with a treatment solution made up of 1% FC4430 in 70/30 and 50/50 mixtures of 2-butoxyethanol/ethanol respectively (compositions of treatment solution are given in **Table 5.40** and **5.41**). **Figures 5.24 to 5.28** compare the phase behavior results of treatment solutions containing 1% and 2% FC4430 in a 70/30 mixture of 2-butoxyethanol/ethanol. Results show that reducing the surfactant concentration from 2 wt% to 1 wt% has a very small effect on the phase behavior of the treatment solution. A treatment solution with 1% FC4430 does show a higher tolerance for water than one with 2% FC4430, but the difference between the two is not significant.

Figures 5.29 and 5.30 show the phase behavior results for (90/10) NaCl/CaCl₂ brines of different salinities with treatment solutions made up of 1% FC4430 in 70/30 and 50/50 mixtures of 2-butoxyethanol/ethanol, respectively (compositions of treatment solution is given in **Table 5.40** and **5.41**). These measurements were conducted to

analyze calcium chloride interaction with the surfactant and the solvents. Comparing the results of **Figures 5.22, 5.23, 5.29 and 5.30**, shows that CaCl_2 up to 10% in brine did not significantly affect its phase behavior with the treatment solutions.

Detailed data for all the above phase behavior tests presented in this section are given in **Appendix A2**.

5.4 SUMMARY

A quick and simple method of selecting solvents for delivering the surfactant FC4430 to a rock with connate water has been presented. The method is based on the phase behavior of the treatment solution with the reservoir brine at reservoir temperature. The phase behavior results showed that treatment solutions made with a combination of organic solvents such as a glycol and an alcohol can tolerate much higher water concentrations at high temperatures. Solvent mixtures of 2-butoxyethanol/ethanol and propylene glycol/isopropanol were selected for delivering the surfactant in core floods (**Chapter 6, 7 and 8**) based on the phase behavior results. A detailed phase behavior study of treatment solutions made up of these two solvent systems for different ratios of solvents in the treatment solution, different surfactant concentrations, water weight percent (saturation), brine salinities and types of salt was conducted. The results show that the 70/30 mixture of 2-butoxyethanol/ethanol is a better solvent for delivering the surfactant FC4430 in the presence of low salinity brine whereas the 70/30 mixture of PG/IPA is better for delivering surfactant to rock with high salinity brine. The results also show that the composition of the treatment solutions and the ratio of solvents need to be selected based on the particular experimental/reservoir conditions.

Table 5.1: Composition of Britannia Brine

Component	ppm
NaCl	59,000
CaCl ₂	16,000
MgCl ₂ .6H ₂ O	3500

Table 5.2: Cloud point measurement of FC4430 in methanol-water mixture

Treatment solution			75°F	250°F	280°F
Methanol wt%	Water wt %	FC4430 wt%			
23	75	2	cloudy	-	
48	50	2	cloudy	-	
73	25	2	clear	clear	-
88	10	2	clear	clear	clear

Table 5.3: Solubility of Britannia Brine and treatment solution containing 2% FC4430, 88% methanol and 10% water

Brine wt%	Treatment solution wt%	75°F	275°F
25	75	clear	clear
50	50	clear	clear

Table 5.4: Cloud point measurement of FC4430 in IPA-toluene-water mixtures

Treatment solution				75°F	275°F
IPA wt%	Toluene wt%	Water wt %	FC4430 wt%		
80	-	10	2	clear	clear
29.3	58.7	10	2	cloudy	
31.3	62.6	4	2	cloudy	
47	47	4	2	clear	
44	44	10	2	clear	clear

Table 5.5: Cloud point measurement of 2 wt% FC4430 in Propylene glycol-Ethanol mixtures

Treatment solution		25°C	135°C
PG wt%	Ethanol wt %		
100	0	cloudy	-
90	10	cloudy	-
80	20	clear	clear
70	30	clear	clear

Table 5.6: Cloud point measurement of 2 wt% FC4430 in Propylene glycol-IPA mixtures

Treatment solution		25 ⁰ C	135 ⁰ C
PG wt%	IPA wt %		
90	10	cloudy	-
80	20	clear	clear
70	30	clear	clear

Table 5.7: Solubility of Britannia Brine and the following treatment solutions containing 2% FC4430

Ratio of solvents in Treatment Solution		Brine wt%	25 ⁰ C	135 ⁰ C
PG wt%	Ethanol wt %			
89.5	10.5	5	clear	clear
88.9	11.1	10	clear	clear
78.9	21.1	5	clear	clear
77.8	22.2	10	clear	clear
88.2	11.8	15	clear	clear
87.5	12.5	20	clear	clear
76.5	23.5	15	clear	clear
75	25.0	20	clear	clear
84.6	15.4	35	clear	cloudy
75	25.0	20	clear	clear
69.2	30.8	35	clear	clear

Table 5.8: Solubility of Britannia Brine and the following treatment solutions containing 2% FC4430

Ratio of solvents in Treatment Solution		Brine wt%	25 ⁰ C	135 ⁰ C
PG wt%	IPA wt %			
89.5	10.5	5	clear	clear
88.9	11.1	10	clear	clear
78.9	21.1	5	clear	clear
77.8	22.2	10	clear	clear
88.2	11.8	15	clear	clear
87.5	12.5	20	clear	clear
76.5	23.5	15	clear	clear
75	25.0	20	clear	clear
84.6	15.4	35	clear	<i>cloudy</i>
75	25.0	20	clear	clear

Table 5.9: Solubility of Britannia Brine and treatment solutions containing 2% FC4430 in a mixture of Dipropylene glycol monomethyl ether (DGGME) and ethanol

Ratio of solvents in Treatment Solution		Brine wt% (with 2% FC4430)	25 ⁰ C	135 ⁰ C
DPGME wt%	Ethanol wt %			
87.5	12.5	20	clear	clear
84.6	15.4	35	Clear (2-phases)	clear
80.0	20.0	50	<i>cloudy</i>	<i>cloudy</i>
75.0	25.0	20	clear	clear
69.2	30.8	35	clear	clear
60.0	40.0	50	<i>cloudy</i>	<i>cloudy</i>
62.5	37.5	20	clear	clear
53.8	46.2	35	clear	clear
40.0	60.0	50	<i>hazy</i>	<i>cloudy</i>

Table 5.10: Solubility of Britannia Brine and treatment solutions containing 2% FC4430 in a mixture of Dipropylene glycol monomethyl ether (DPGME) and IPA

Ratio of solvents in Treatment Solution		Brine wt% (with 2% FC4430)	25 ⁰ C	135 ⁰ C
DPGME wt%	IPA wt %			
87.5	12.5	20	Clear (2-phases)	clear
84.6	15.4	35	Clear (2-phases)	clear
80.0	20.0	50	<i>cloudy</i>	<i>cloudy</i>
75.0	25.0	20	Clear (2-phases)	clear
69.2	30.8	35	Clear (2-phases)	clear
60.0	40.0	50	Clear (2-phases)	<i>cloudy</i>
62.5	37.5	20	Clear (2-phases)	clear
53.8	46.2	35	Clear (2-phases)	clear
40.0	60.0	50	clear	<i>cloudy</i>

Table 5.11: Solubility of Britannia brine and treatment solutions containing 2% FC4430 in a mixture of 2-butoxyethanol (EGMBE) and ethanol

Ratio of solvents in Treatment Solution		Brine wt% (with 2% FC4430)	25 ⁰ C	135 ⁰ C
EGMBE wt%	Ethanol wt %			
87.5	12.5	20	2-phase	2-phase
84.6	15.4	35	2-phase	2-phase
80.0	20.0	50	2-phase	2-phase
75.0	25.0	20	2-phase	2-phase
69.2	30.8	35	2-phase	2-phase
60.0	40.0	50	-	<i>cloudy</i>
62.5	37.5	20	Clear	clear
53.8	46.2	35	Clear	clear
40.0	60.0	50	clear	<i>cloudy</i>

Table 5.12: Solubility of Britannia brine and treatment solutions containing 2% FC4430 in a mixture of 2-butoxyethanol (EGMBE) and IPA

Ratio of solvents in Treatment Solution		Brine wt% (with 2% FC4430)	25 ⁰ C	135 ⁰ C
EGMBE wt%	IPA wt %			
87.5	12.5	20	2-phase	2-phase
84.6	15.4	35	2-phase	2-phase
80.0	20.0	50	2-phase	2-phase
75.0	25.0	20	2-phase	2-phase
69.2	30.8	35	2-phase	2-phase
60.0	40.0	50	2-phase	2-phase
62.5	37.5	20	2-phase	2-phase
53.8	46.2	35	2-phase	2-phase
40.0	60.0	50	2-phase	2-phase

Table 5.13: Solubility of Britannia brine and treatment solutions containing 2% FC4430 in a mixture of 70/30 2-butoxyethanol (EGMBE) and Ethanol

Brine with 2% FC4430 (gms)	Treatment solution, gms	Brine wt %	Amount of Britannia condensate (cc)	100 ⁰ C
1.0	4.0	20	0.5	clear
1.25	3.75	25	0.5	cloudy
1.5	3.5	30	0.5	cloudy
1.75	3.25	35	0.5	2-phase

Table 5.14: Solubility of Britannia brine and treatment solutions containing 2% FC4430 in a mixture of 80/20 polypropylene glycol (PPG 425) and PG

Brine with 2% FC4430 (gms)	Treatment solution, gms	Brine wt %	160°C
1.0	4.0	20	2-phase
1.25	3.75	25	2-phase
1.5	3.5	30	2-phase
1.75	3.25	35	2-phase

Table 5.15: Solubility of Britannia brine and treatment solutions containing 2% FC4430 in a mixture of 65/35 polypropylene glycol (PPG 425) and PG

Brine with 2% FC4430 (gms)	Treatment solution, gms	Brine wt %	160°C
1.0	4.0	20	clear
1.25	3.75	25	cloudy
1.5	3.5	30	2-phase
1.75	3.25	35	2-phase

Table 5.16: Solubility of Britannia brine and treatment solutions containing 2% FC4430 in a mixture of 50/50 polypropylene glycol (PPG 425) and PG

Brine with 2% FC4430 (gms)	Treatment solution, gms	Brine wt %	25°C	160°C
1.0	4.0	20	clear	clear
1.25	3.75	25	clear	clear
1.5	3.5	30	clear	clear
1.75	3.25	35	clear	cloudy

Table 5.17: Solubility of 18% NaCl brine and treatment solutions containing 2% FC4430 in a mixture of 2-butoxyethanol (EGMBE) and ethanol

Ratio of solvents in Treatment Solution		Brine wt% (with 2% FC4430)	25 ⁰ C	135 ⁰ C
EGMBE wt%	Ethanol wt %			
66.67	33.33	10	salt ppt	salt ppt
62.50	37.50	20	clear	clear
53.85	46.15	35	clear	clear
40	60	50	hazy	cloudy

Table 5.18: Solubility of 18% NaCl brine and treatment solutions containing 2% FC4430 in a mixture of Dipropylene glycol monomethyl ether (DPGME) and ethanol

Ratio of solvents in Treatment Solution		Brine wt% (with 2% FC4430)	25 ⁰ C	135 ⁰ C
DPGME wt%	Ethanol wt %			
66.67	33.33	10	salt ppt	salt ppt
62.50	37.50	20	salt ppt	salt ppt
53.85	46.15	35	clear	clear
40	60	50	cloudy	cloudy

Table 5.19: Solubility of 18% NaCl brine and treatment solutions containing 2% FC4430 in a mixture of propylene glycol (PG) and ethanol

Ratio of solvents in Treatment Solution		Brine wt% (with 2% FC4430)	25 ⁰ C	135 ⁰ C
PG wt%	Ethanol wt %			
66.67	33.33	10	clear	clear
62.50	37.50	20	clear	clear
53.85	46.15	35	clear	cloudy
40	60	50	cloudy	cloudy

Table 5.20: Solubility of 18% NaCl brine and treatment solutions containing 2% FC4430 in a mixture of propylene glycol (PG) and IPA

Ratio of solvents in Treatment Solution		Brine wt% (with 2% FC4430)	25 ⁰ C	135 ⁰ C
PG wt%	IPA wt %			
66.67	33.33	10	clear	clear
62.50	37.50	20	clear	clear
53.85	46.15	35	clear	cloudy
40	60	50	cloudy	cloudy

Table 5.21: Solubility of 18% NaCl brine and treatment solutions containing 2% FC4430 in a mixture of 2-butoxyethanol/ethylene glycol/propylene glycol (50/37.5/12.5)

Brine with 2% FC4430 (gms)	Treatment solution, gms	Brine wt% (with 2% FC4430)	25°C	135°C	Solution + 0.5ml of n-C7 at 135°C
1.0	4.0	20	clear	clear	clear
1.25	3.75	25	clear	clear	Hazy
1.5	3.5	30	clear	clear	2-phase
1.75	3.25	35	clear	clear	2-phase
2.0	3.0	40	clear	hazy	2-phase
2.25	2.75	45	cloudy	2-phase	2-phase
2.5	2.5	50	cloudy	2-phase	2-phase

Table 5.22: Solubility of 18% NaCl brine and treatment solutions containing 2% FC4430 in a mixture of 75/25 polypropylene glycol (PPG425) and ethylene glycol

Brine with 2% FC4430 (gms)	Treatment solution, gms	Brine wt% (with 2% FC4430)	135°C
1.0	4.0	20	2-phase
1.25	3.75	25	2-phase
1.5	3.5	30	2-phase
1.75	3.25	35	2-phase

Table 5.23: Composition of Hatter's Pond Brine

Component	g/l
NaCl	82.92
CaCl ₂	77.43
MgCl ₂ .6H ₂ O	5.2

Table 5.24: Brine composition for Reservoir B

Component	g/l
NaCl	225.2
CaCl ₂	1.5
MgCl ₂ .6H ₂ O	3.1

Table 5.25: Solubility of Hatter's Pond brine and treatment solutions containing 2% FC4430 in a mixture of 70/30 2-butoxyethanol and ethanol

Brine with 2% FC4430 (gms)	Treatment solution, gms	Brine wt% (with 2% FC4430)	160°C
1.0	4.0	20	2-phase, salt ppt
1.25	3.75	25	2-phase, salt ppt
1.5	3.5	30	2-phase
1.75	3.25	35	2-phase

Table 5.26: Solubility of Hatter's Pond brine and treatment solutions containing 2% FC4430 in a 70/30 mixture of polypropylene glycol (PPG 425) and IPA

Brine with 2% FC4430 (gms)	Treatment solution, gms	Brine wt% (with 2% FC4430)	160°C
1.0	4.0	20	2-phase, turbid
1.25	3.75	25	2-phase, turbid
1.5	3.5	30	2-phase, turbid
1.75	3.25	35	2-phase, turbid

Table 5.27: Solubility of Hatter's Pond brine and treatment solutions containing 2% FC4430 in a 50/50 mixture of 2-butoxyethanol and methanol

Brine with 2% FC4430 (gms)	Treatment solution, gms	Brine wt% (with 2% FC4430)	25°C	160°C	Solution + 0.5ml of n-C7 at 160°C
1.0	4.0	20	clear	clear	clear
1.25	3.75	25	clear	clear	clear
1.5	3.5	30	clear	clear	clear
1.75	3.25	35	clear	clear	clear
2.0	3.0	40	clear	clear	turbid

Table 5.28: Solubility of Hatter's Pond brine and treatment solutions containing 2% FC4430 in a mixture of 60/40 polypropylene glycol (PG425) and methanol

Brine with 2% FC4430 (gms)	Treatment solution, gms	Brine wt% (with 2% FC4430)	25°C	160°C	Solution + 0.5ml of n-C7 at 160°C
1.0	4.0	20	clear	clear	clear
1.25	3.75	25	clear	clear	clear
1.5	3.5	30	clear	2-phase	2-phase
1.75	3.25	35	clear	2-phase	2-phase
2.0	3.0	40	clear	2-phase	2-phase

Table 5.29: Solubility of Hatter's Pond brine and treatment solutions containing 2% FC4430 in a mixture of 50/50 polypropylene glycol (PG425) and methanol

Brine with 2% FC4430 (gms)	Treatment solution, gms	Brine wt% (with 2% FC4430)	25°C	160°C	Solution + 0.5ml of n-C7 at 160°C
1.0	4.0	20	clear	clear	clear
1.25	3.75	25	clear	clear	clear
1.5	3.5	30	clear	clear	cloudy
1.75	3.25	35	clear	clear	2-phase
2.0	3.0	40	clear	cloudy	2-phase

Table 5.30: Solubility of Hatter's Pond brine and treatment solutions containing 2% FC4430 in a mixture of 70/30 propylene glycol and IPA

Brine with 2% FC4430 (gms)	Treatment solution, gms	Brine wt% (with 2% FC4430)	25°C	160°C	Solution + 0.5ml of n-C7 at 110°C
0.75	4.25	15	clear	clear	2-phase
1.0	4.0	20	clear	clear	2-phase
1.25	3.75	25	clear	clear	2-phase
1.5	3.5	30	clear	hazy	2-phase
1.75	3.25	35	clear	cloudy	2-phase

Table 5.31: Solubility of Hatter's Pond brine and treatment solutions containing 2% FC4430 in a mixture of 50/50 propylene glycol and IPA

Brine with 2% FC4430 (gms)	Treatment solution, gms	Brine wt% (with 2% FC4430)	25°C	160°C	Solution + 0.5ml of n-C7 at 110°C
0.75	4.25	15	clear	clear	clear
1.0	4.0	20	clear	clear	2-phase
1.25	3.75	25	clear	clear	2-phase
1.5	3.5	30	clear	clear	2-phase
1.75	3.25	35	clear	clear	2-phase

Table 5.32: Solubility of Reservoir B reservoir brine and treatment solutions containing 2% FC4430 in a mixture of 50/50 2-butoxyethanol and ethylene glycol

Brine with 2% FC4430 (gms)	Treatment solution, gms	Brine wt% (with 2% FC4430)	25°C	137°C
0.75	4.25	15	clear	salt ppt
1.0	4.0	20	clear	salt ppt
1.25	3.75	25	salt ppt	2-phase, salt ppt
1.5	3.5	30	salt ppt	2-phase, salt ppt
1.75	3.25	35	salt ppt	2-phase, salt ppt
2.0	3.0	40	salt ppt	2-phase, salt ppt

Table 5.33: Solubility of Reservoir B reservoir brine and treatment solutions containing 2% FC4430 in a mixture of 50/50 2-butoxyethanol and 1,3-propanediol

Brine with 2% FC4430 (gms)	Treatment solution, gms	Brine wt% (with 2% FC4430)	25°C	137°C
0.75	4.25	15	salt ppt	salt ppt
1.0	4.0	20	salt ppt	salt ppt
1.25	3.75	25	salt ppt	salt ppt
1.5	3.5	30	salt ppt	salt ppt
1.75	3.25	35	salt ppt	salt ppt
2.0	3.0	40	salt ppt	salt ppt

Table 5.34: Composition of surfactant solution 1

Component	Weight %
FC4430	2
2-Butoxyethanol	69
Ethanol	29

Table 5.35: Composition of surfactant solution 2

Component	Weight %
FC4430	2
2-Butoxyethanol	49
Ethanol	49

Table 5.36: Composition of surfactant solution 3

Component	Weight %
FC4430	2
2-Butoxyethanol	29
Ethanol	69

Table 5.37: Composition of surfactant solution 4

Component	Weight %
FC4430	2
Propylene glycol	69
Iso-propanol (IPA)	29

Table 5.38: Composition of surfactant solution 5

Component	Weight %
FC4430	2
Propylene glycol	49
Iso-propanol (IPA)	49

Table 5.39: Composition of surfactant solution 6

Component	Weight %
FC4430	2
Propylene glycol	29
Iso-propanol (IPA)	69

Table 5.40: Composition of surfactant solution 7

Component	Weight %
FC4430	1
2-Butoxyethanol	69
Ethanol	29

Table 5.41: Composition of surfactant solution 8

Component	Weight %
FC4430	1
2-Butoxyethanol	49
Ethanol	49

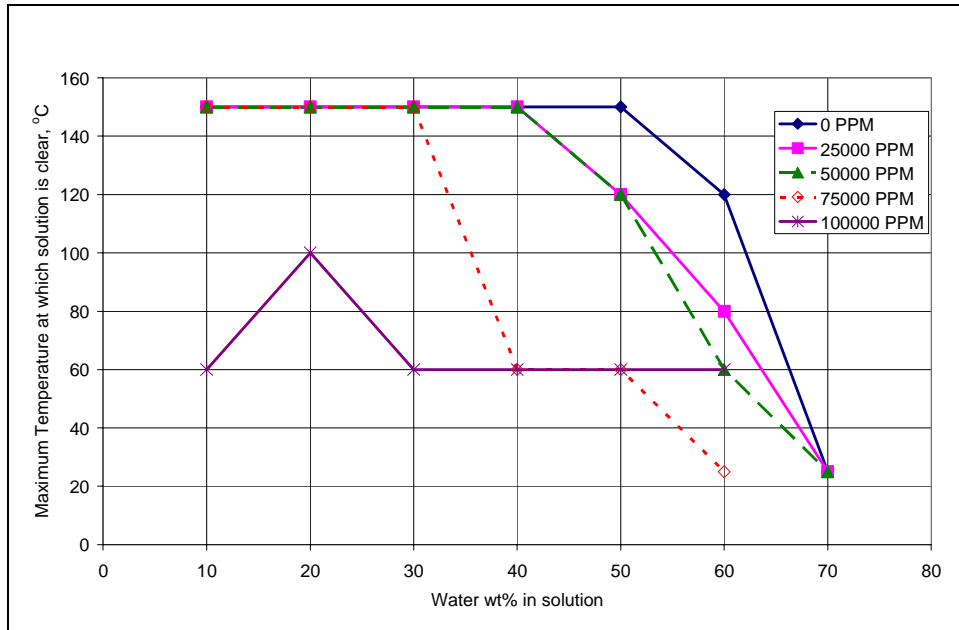


Figure 5.1: Phase behavior results of treatment solution-1 (2% FC4430, 69% 2-butoxyethanol and 29% ethanol) with NaCl brines of different salinities

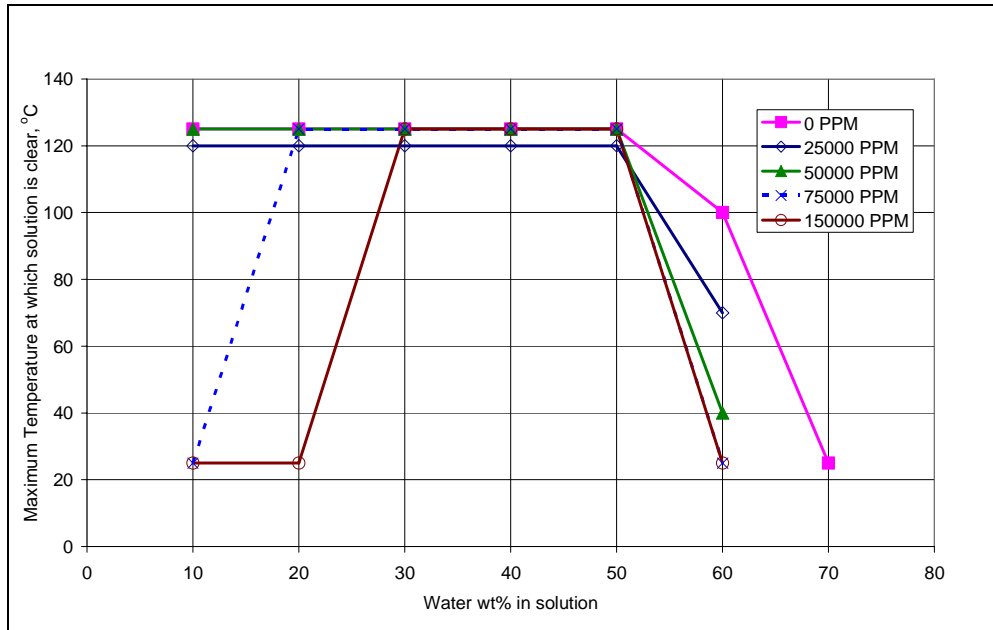


Figure 5.2: Phase behavior results of treatment solution-2 (2% FC4430, 49% 2-butoxyethanol and 49% ethanol) with NaCl brines of different salinities

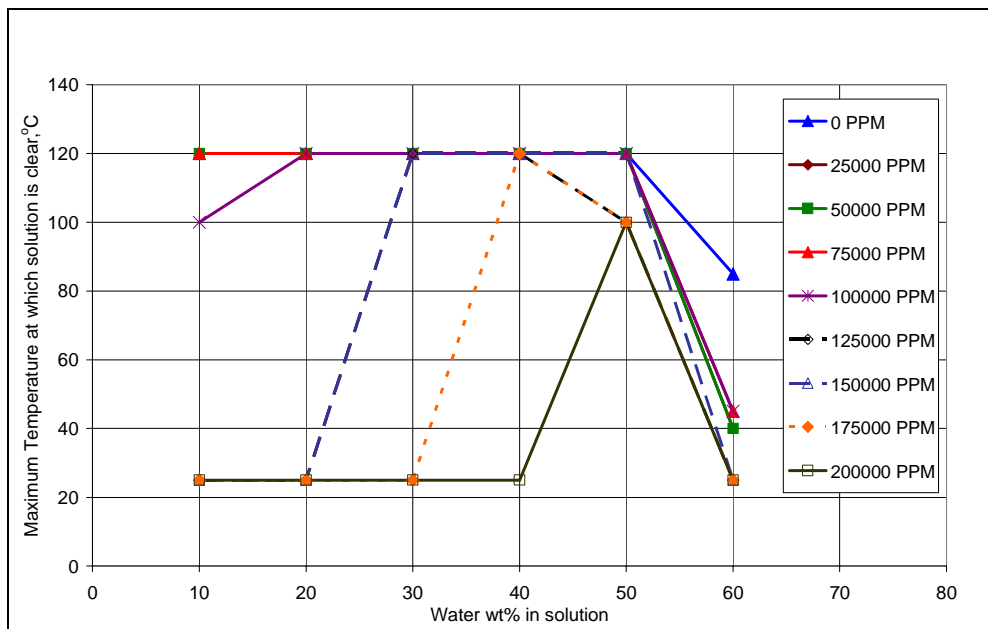


Figure 5.3: Phase behavior results of treatment solution-3 (2% FC4430, 29% 2-butoxyethanol and 69% ethanol) with NaCl brines of different salinities

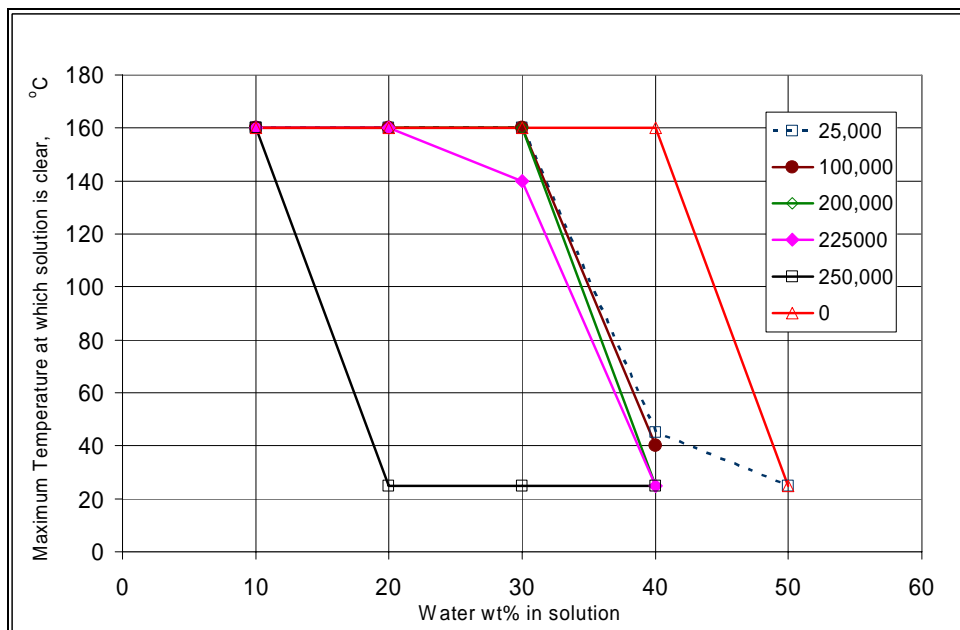


Figure 5.4: Phase behavior results of treatment solution-4 (2% FC4430, 69% propylene glycol and 29% isopropanol) with NaCl brines of different salinities

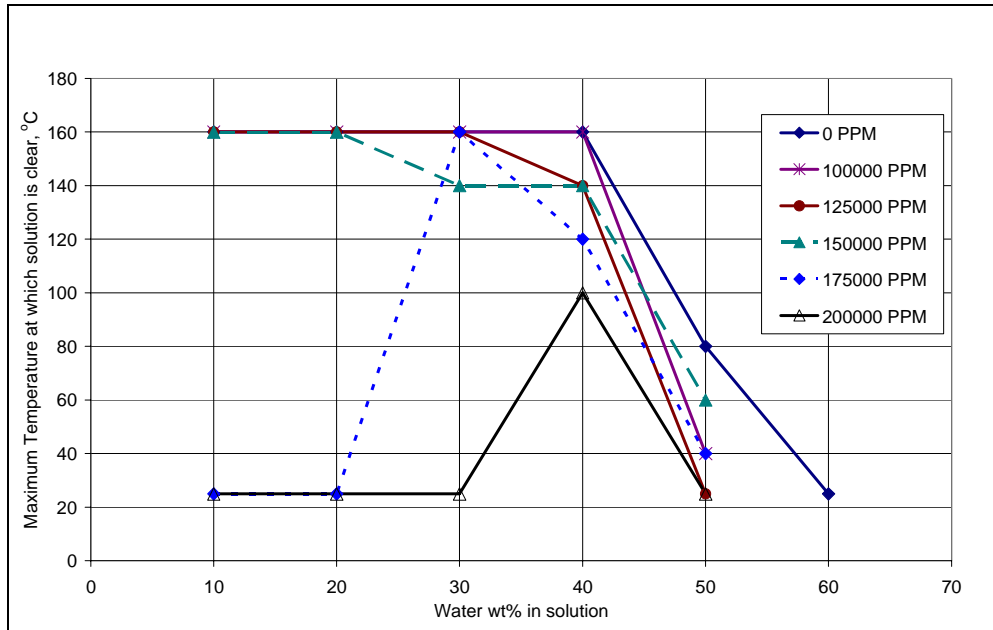


Figure 5.5: Phase behavior results of treatment solution-5 (2% FC4430, 49% propylene glycol and 49% isopropanol) with NaCl brines of different salinities

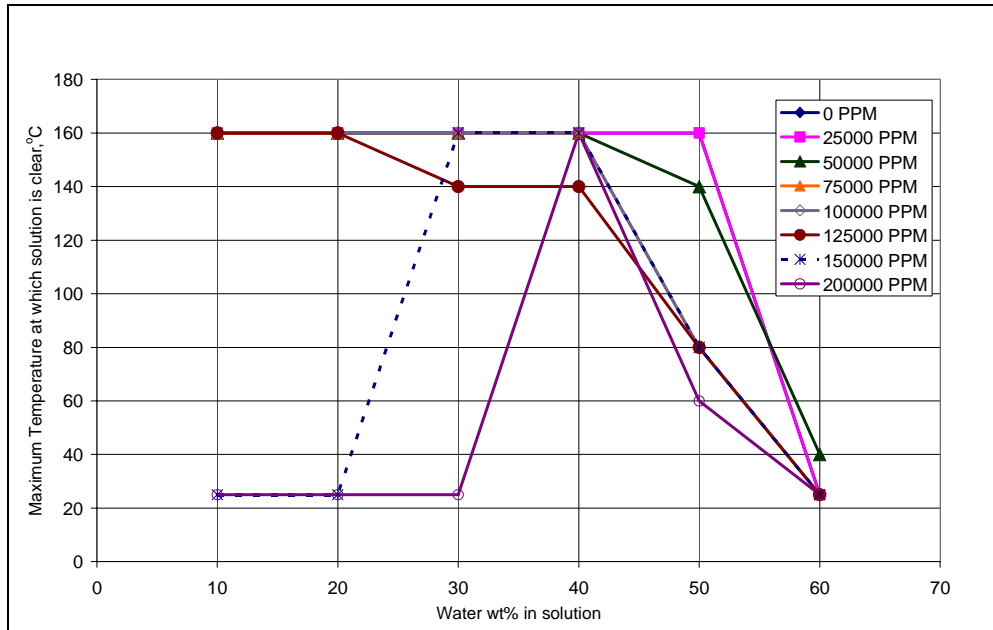


Figure 5.6: Phase behavior results of treatment solution-6 (2% FC4430, 29% propylene glycol and 69% isopropanol) with NaCl brines of different salinities

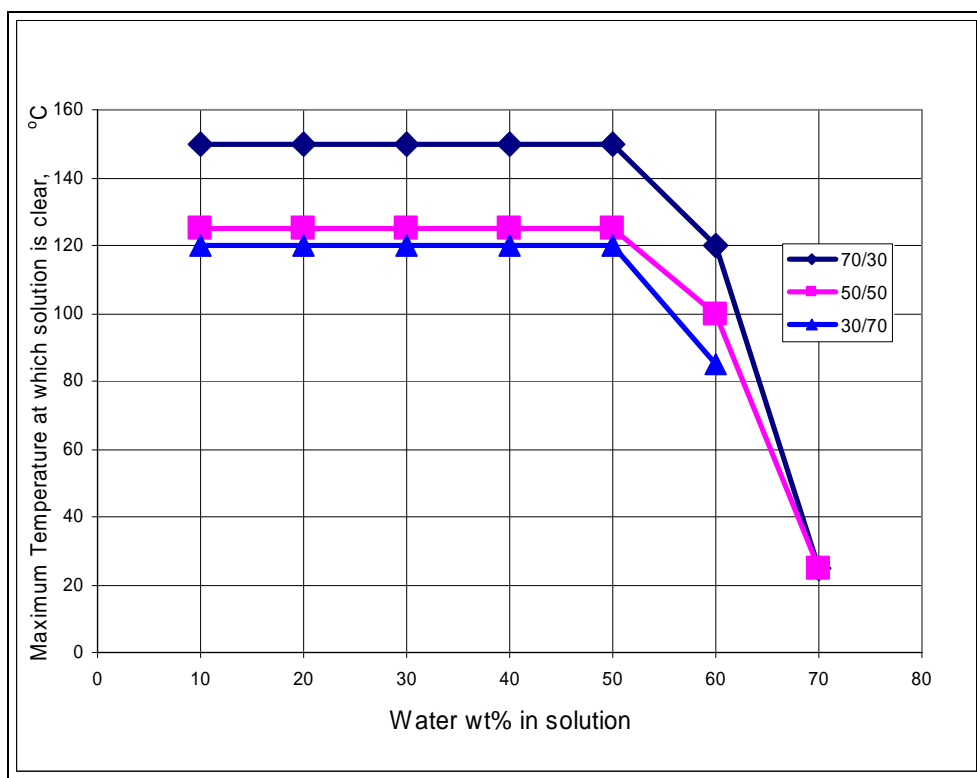


Figure 5.7: Compatibility of treatment solutions with different ratio of solvents (2-butoxyethanol/ethanol) with 0 ppm salinity NaCl brine (D.I. water)

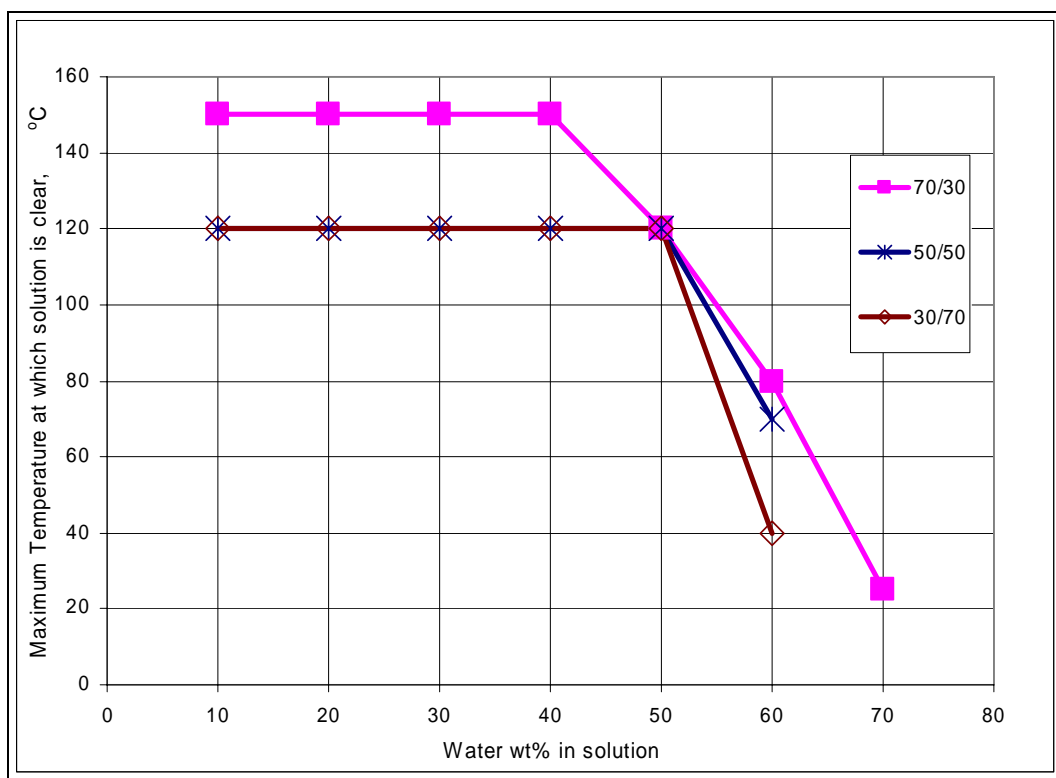


Figure 5.8: Compatibility of treatment solutions with different ratio of solvents (2-butoxyethanol/ethanol) with 25000 ppm salinity NaCl brine

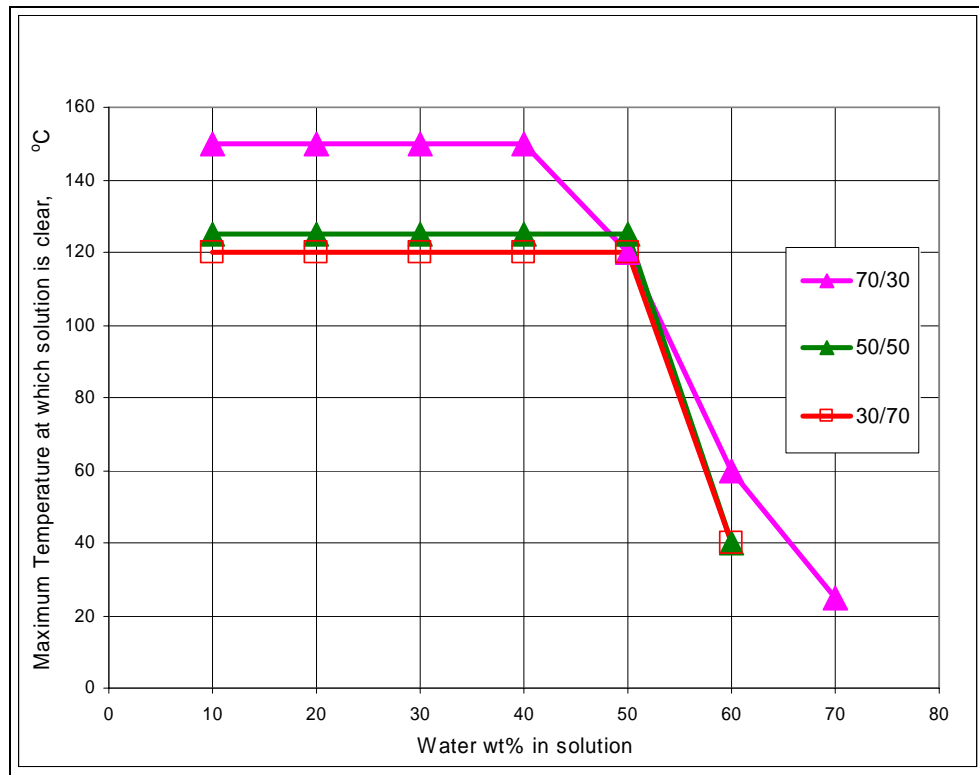


Figure 5.9: Compatibility of treatment solutions with different ratio of solvents (2-butoxyethanol/ethanol) with 50000 ppm salinity NaCl brine

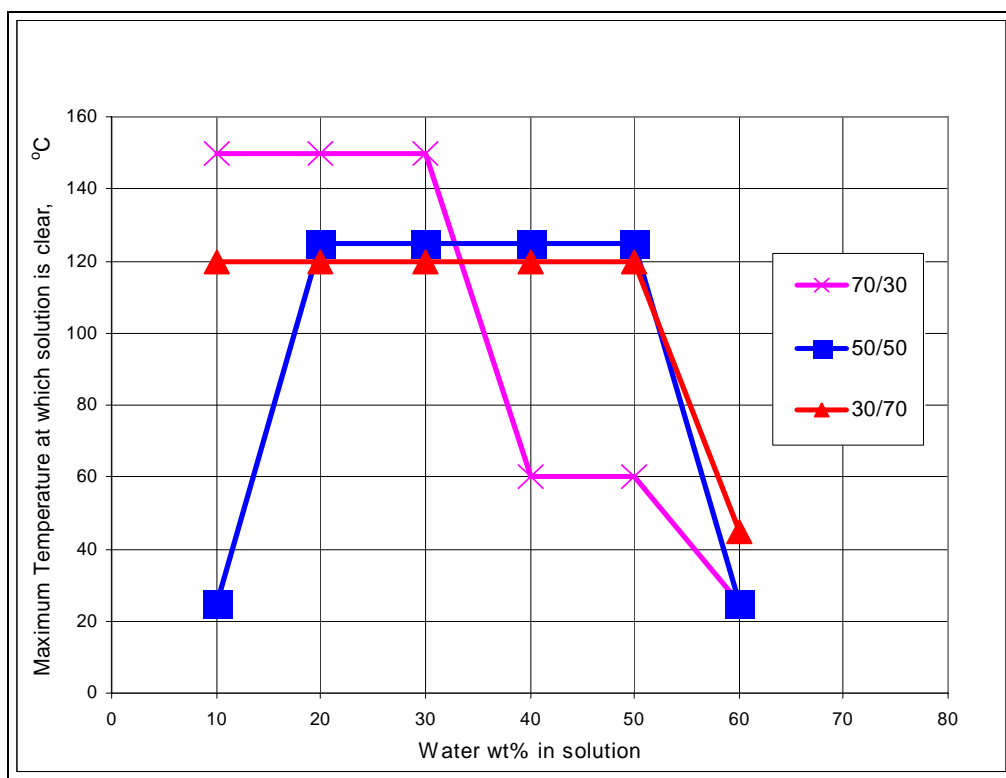


Figure 5.10: Compatibility of treatment solutions with different ratio of solvents (2-butoxyethanol/ethanol) with 75000 ppm salinity NaCl brine

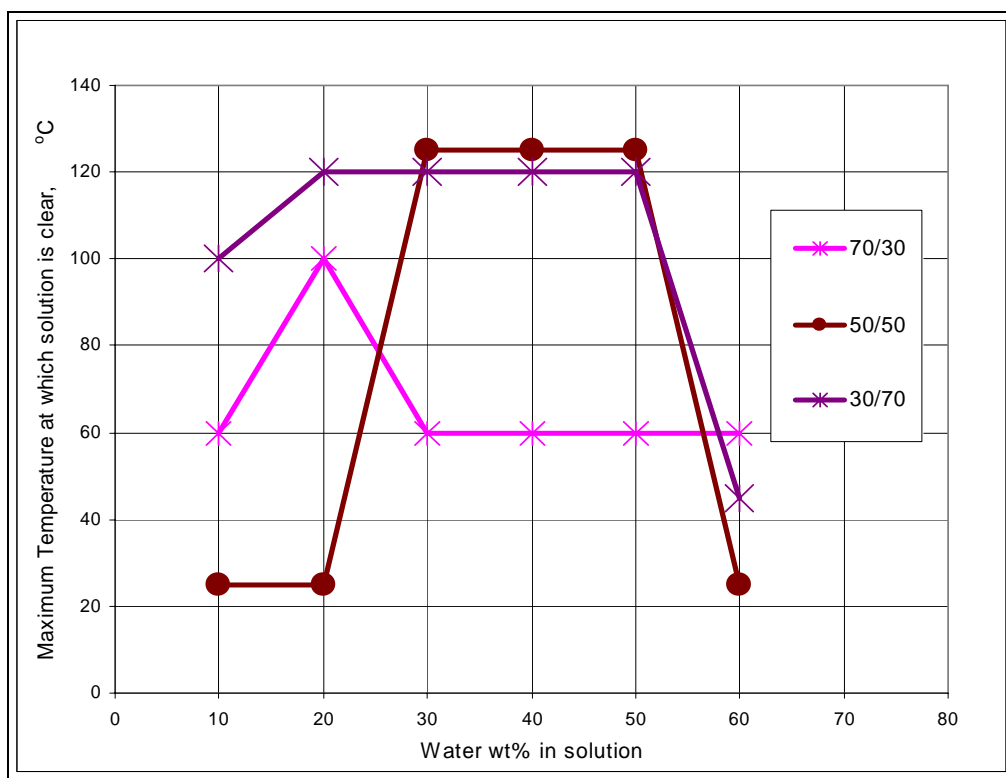


Figure 5.11: Compatibility of treatment solutions with different ratio of solvents (2-butoxyethanol/ethanol) with 100,000 ppm salinity NaCl brine

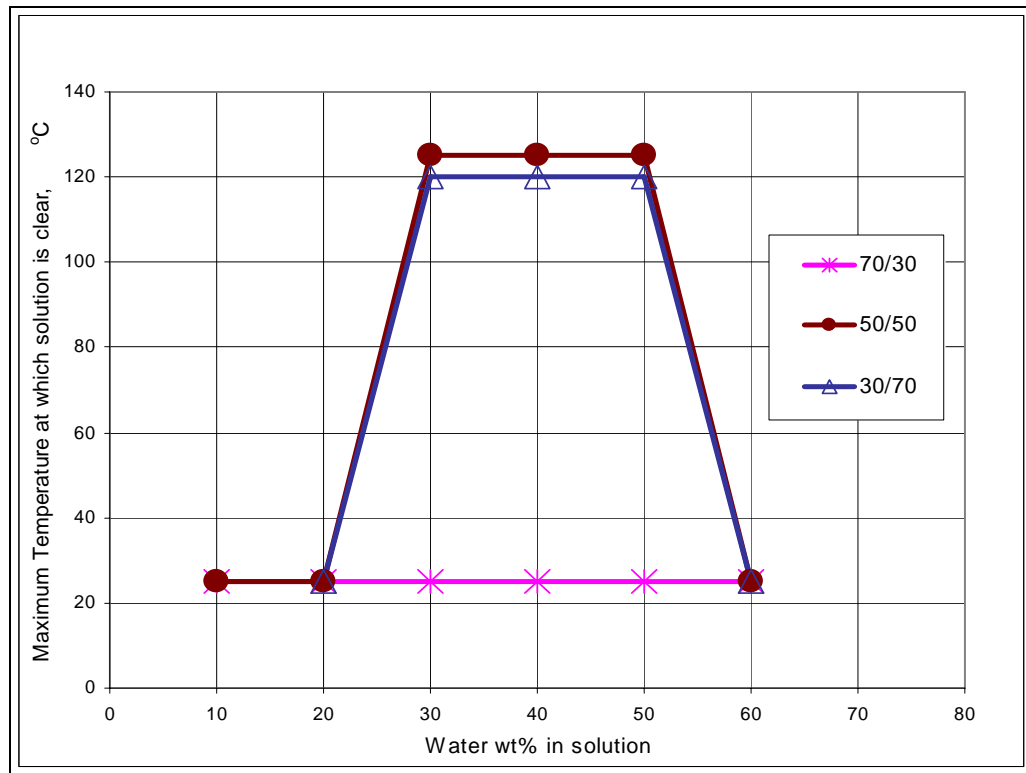


Figure 5.12: Compatibility of treatment solutions with different ratio of solvents (2-butoxyethanol/ethanol) with 150,000 ppm salinity NaCl brine

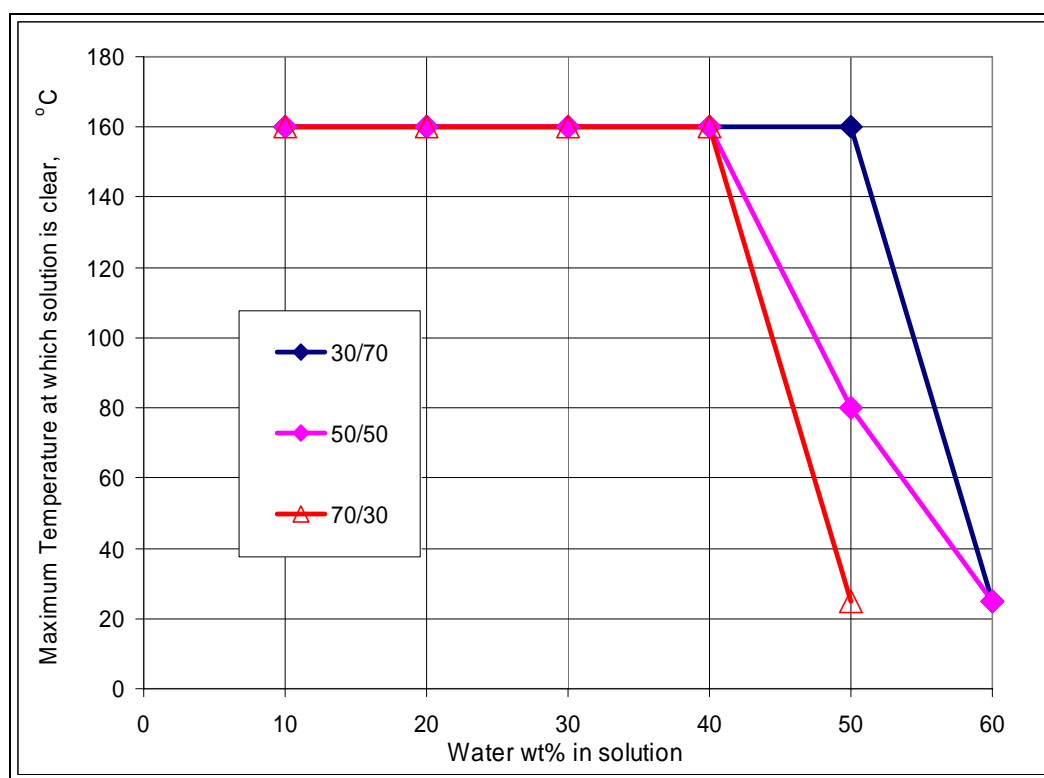


Figure 5.13: Compatibility of treatment solutions with different ratio of solvents (PG/IPA) with 0 ppm salinity NaCl brine (D.I. water)

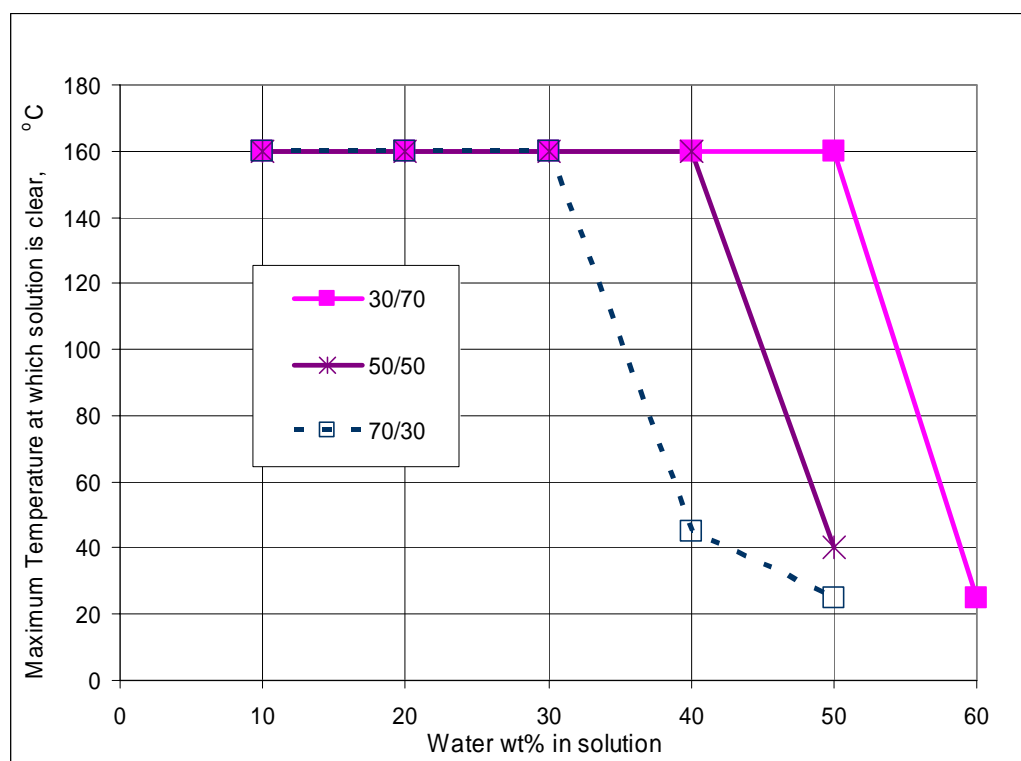


Figure 5.14: Compatibility of treatment solutions with different ratio of solvents (PG/IPA) with 25000 ppm salinity NaCl brine

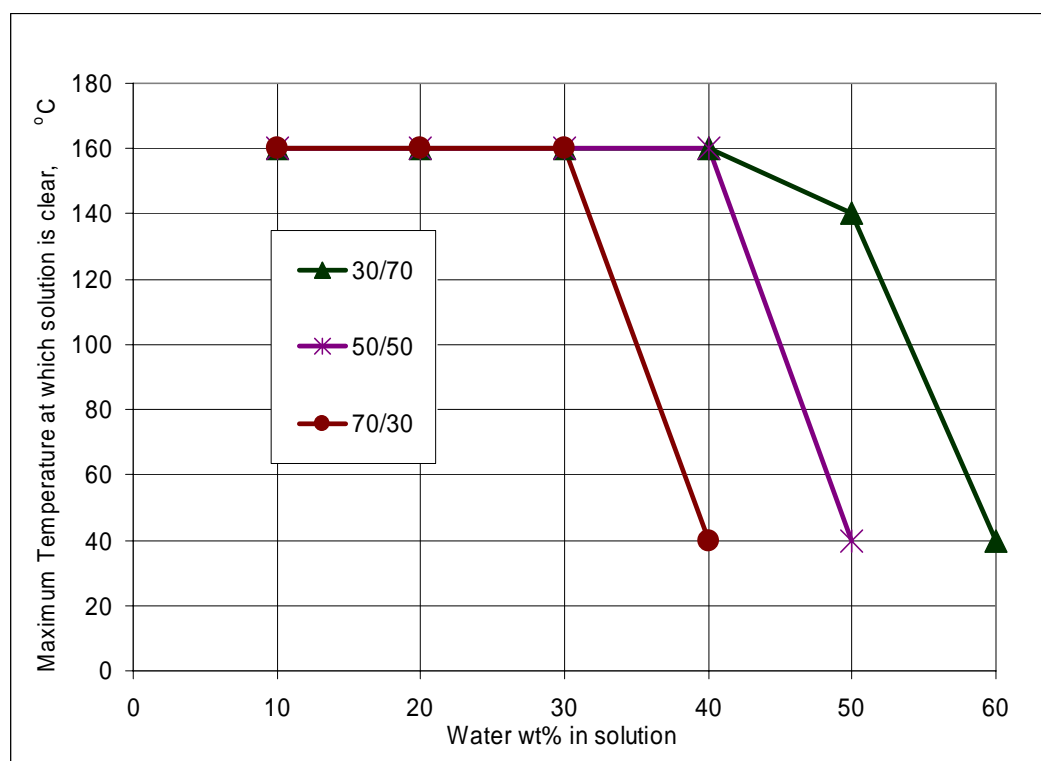


Figure 5.15: Compatibility of treatment solutions with different ratio of solvents (PG/IPA) with 50000 ppm salinity NaCl brine

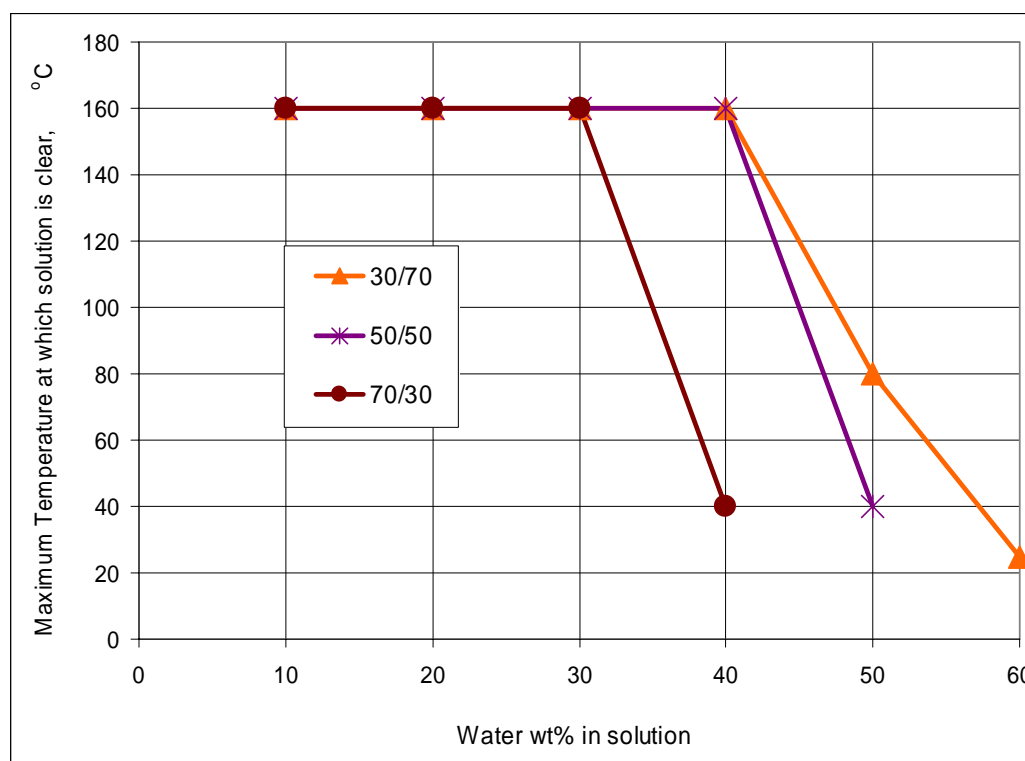


Figure 5.16: Compatibility of treatment solutions with different ratio of solvents (PG/IPA) with 75000 ppm salinity NaCl brine

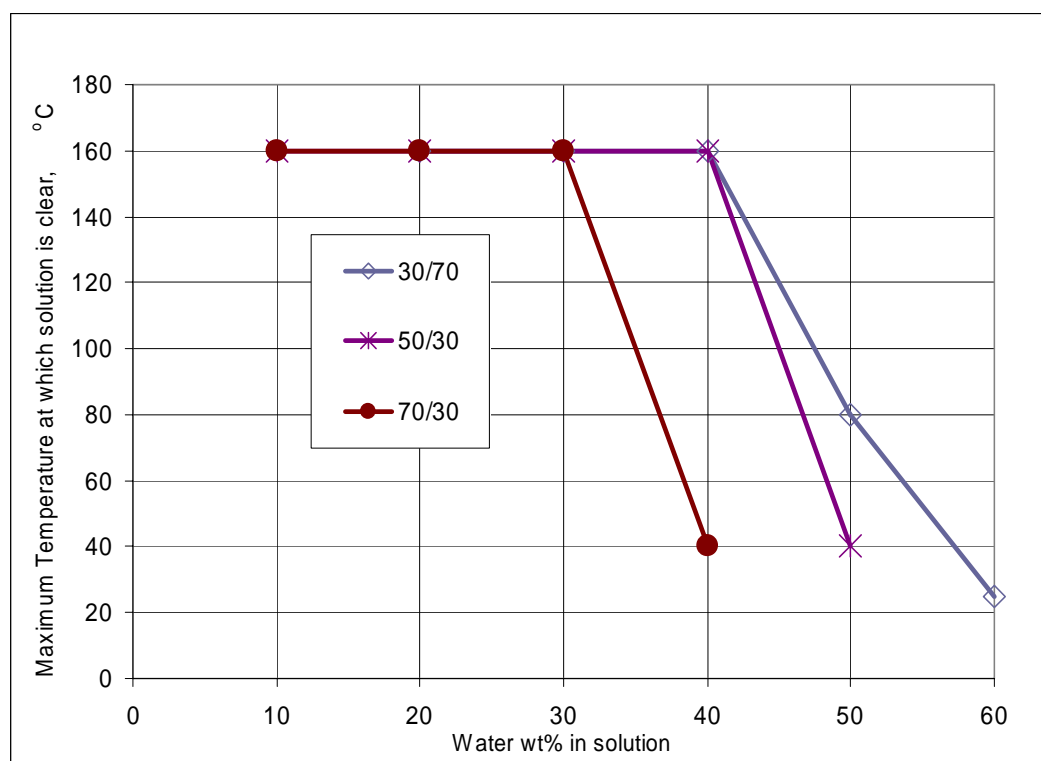


Figure 5.17: Compatibility of treatment solutions with different ratio of solvents (PG/IPA) with 100,000 ppm salinity NaCl brine

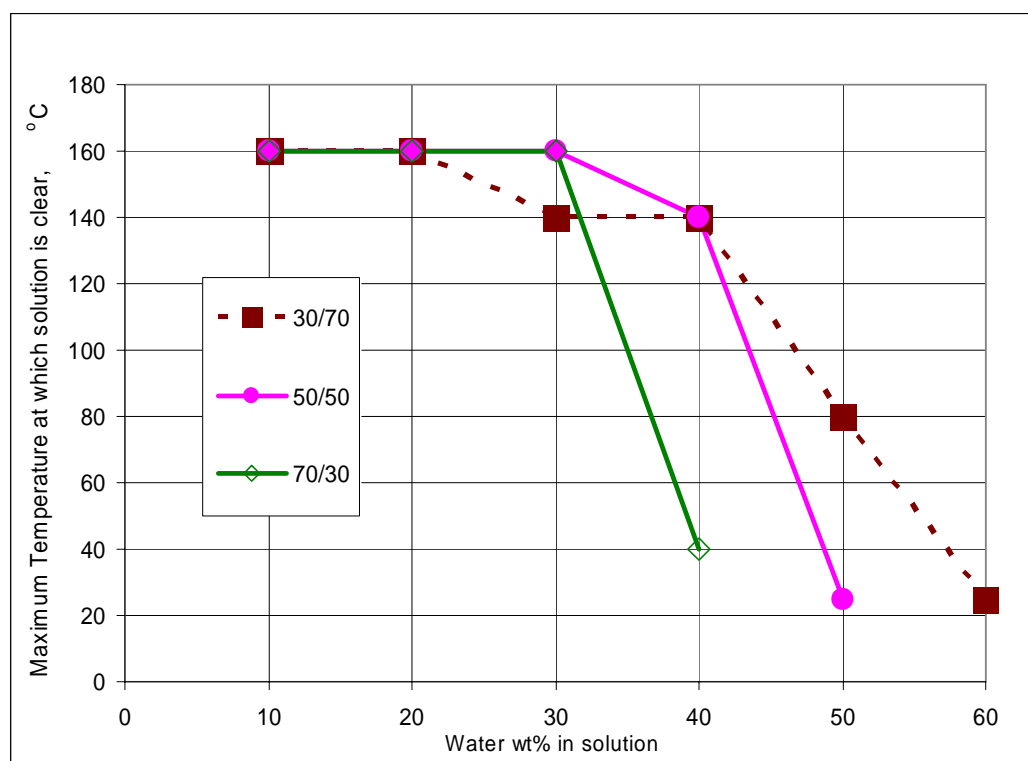


Figure 5.18: Compatibility of treatment solutions with different ratio of solvents (PG/IPA) with 125,000 ppm salinity NaCl brine

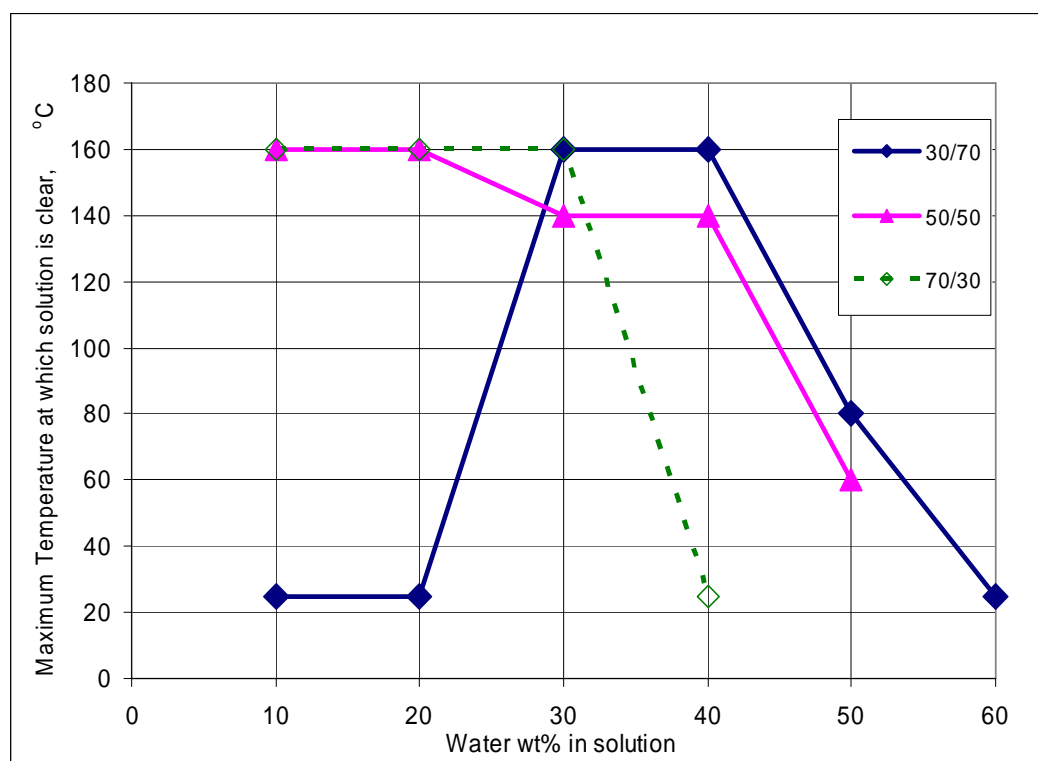


Figure 5.19: Compatibility of treatment solutions with different ratio of solvents (PG/IPA) with 150,000 ppm salinity NaCl brine

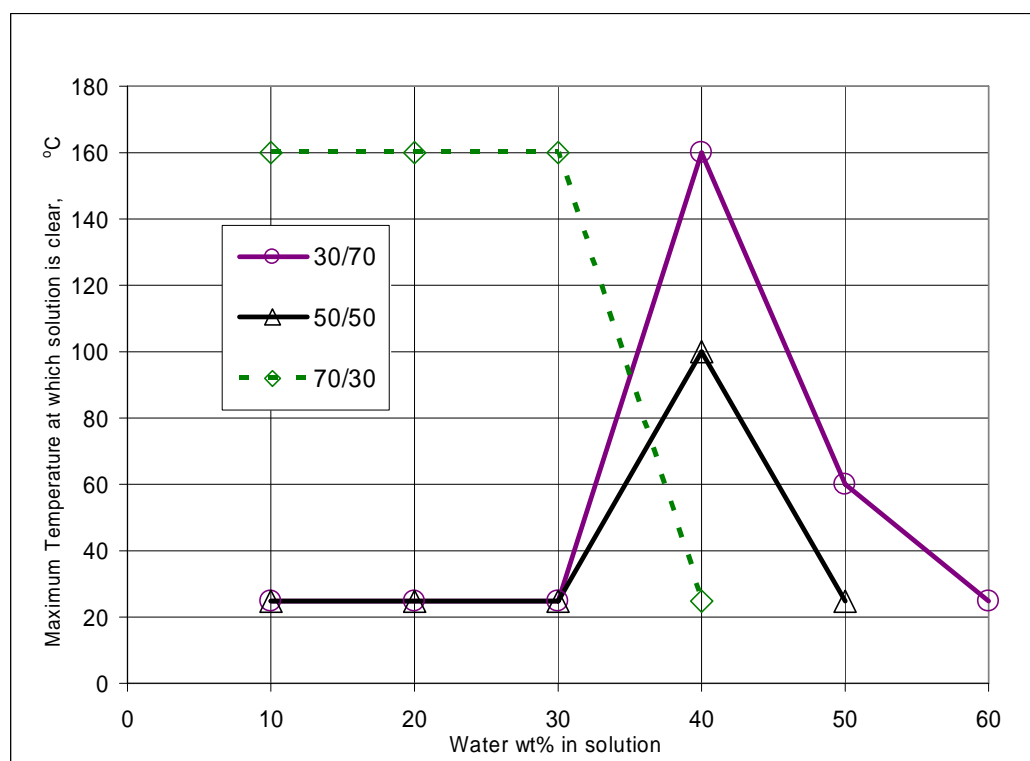


Figure 5.20: Compatibility of treatment solutions with different ratio of solvents (PG/IPA) with 200,000 ppm salinity NaCl brine

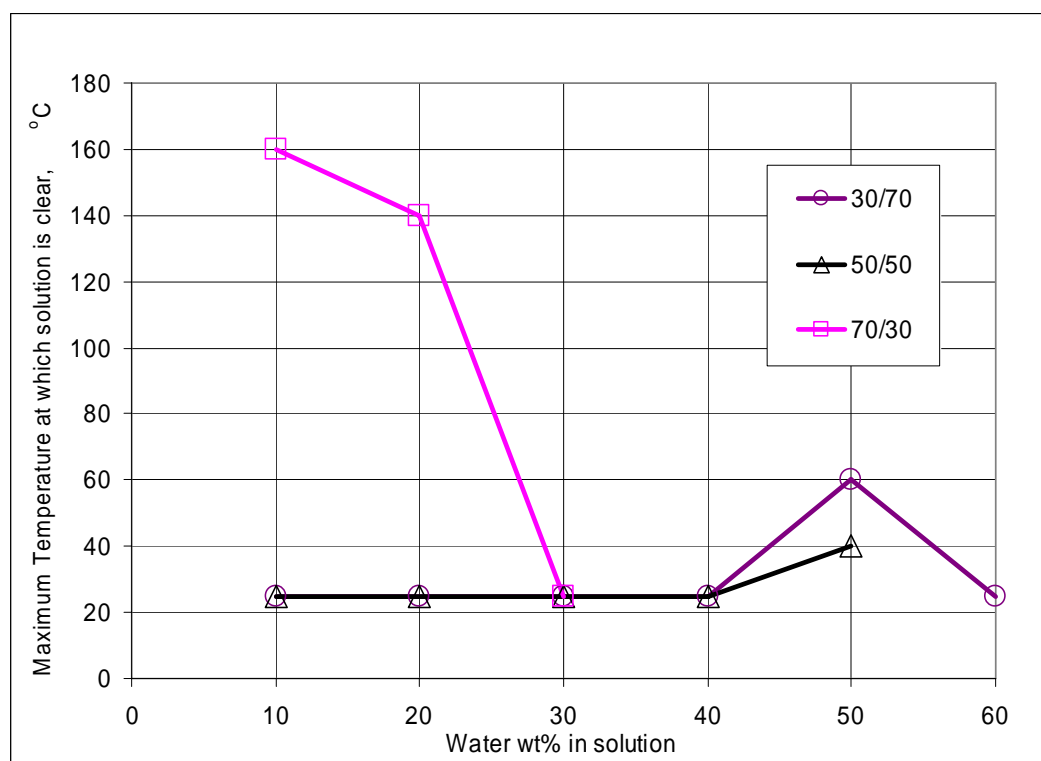


Figure 5.21: Compatibility of treatment solutions with different ratio of solvents (PG/IPA) with 225,000 ppm salinity NaCl brine

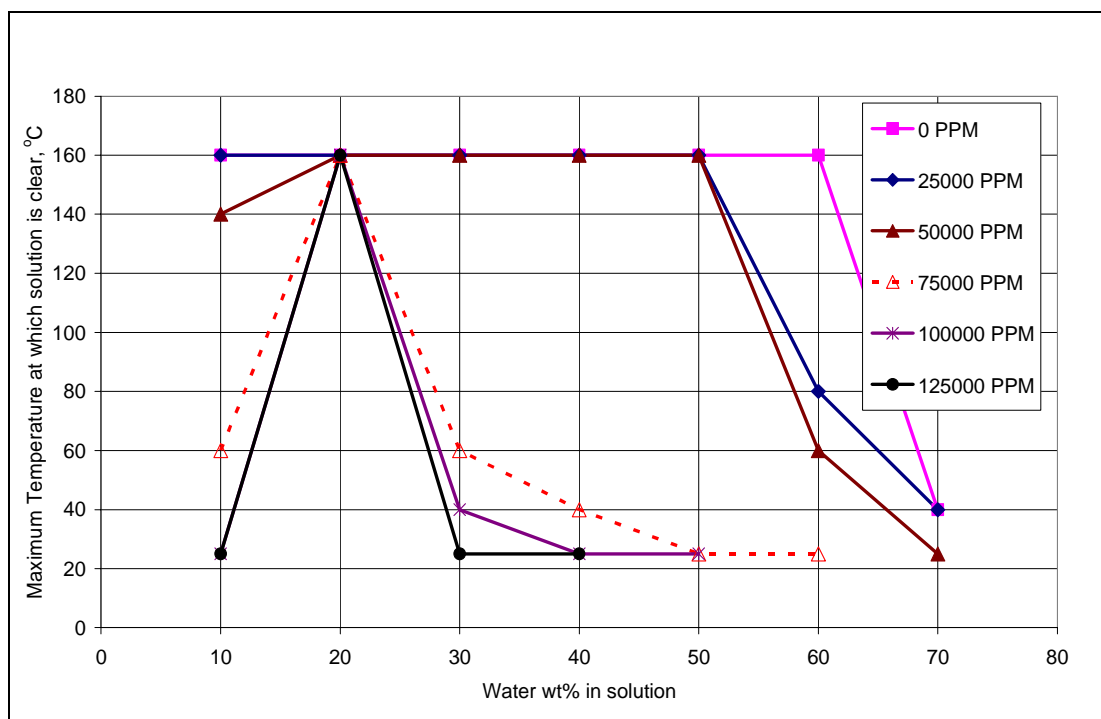


Figure 5.22: Phase behavior results of treatment solution-7 (1% FC4430, 69.5% 2-butoxyethanol and 29.5% ethanol) with NaCl brines of different salinities

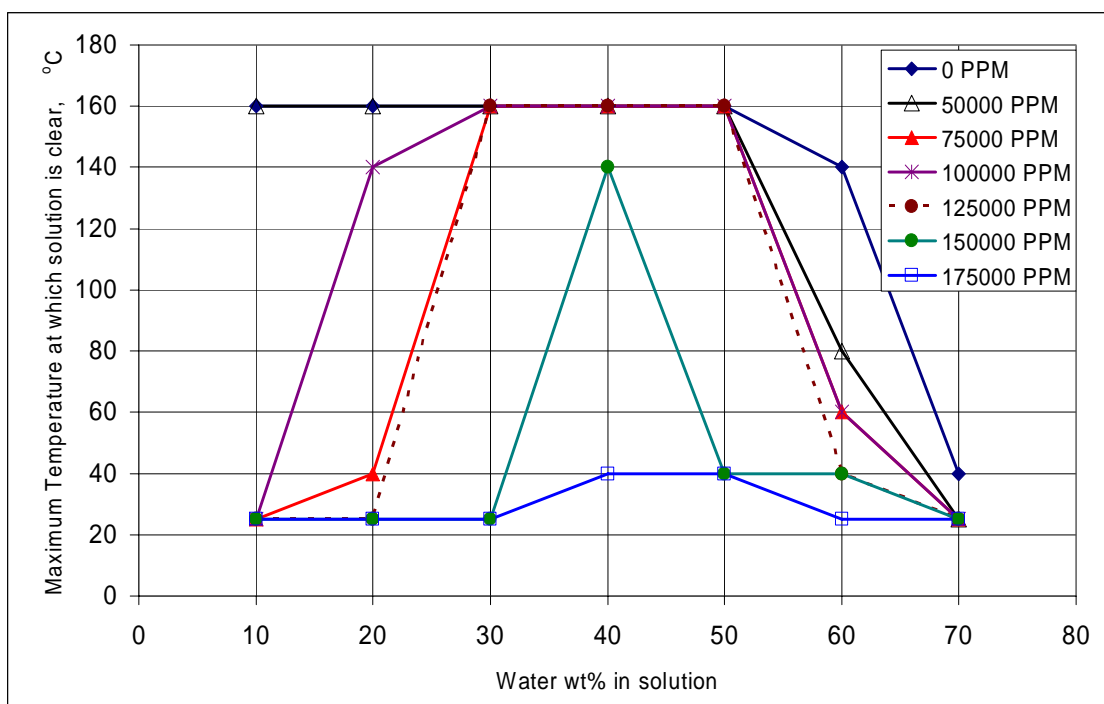


Figure 5.23: Phase behavior results of treatment solution-7 (1% FC4430, 49.5% 2-butoxyethanol and 49.5% ethanol) with NaCl brines of different salinities

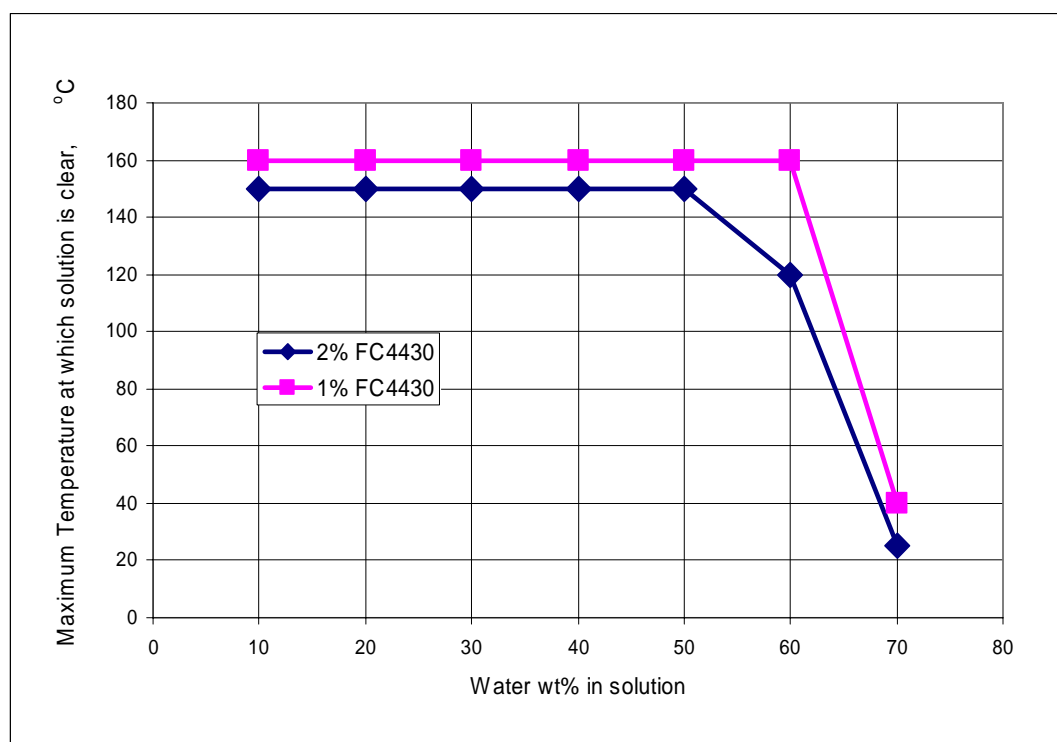


Figure 5.24: Comparison of the phase behavior of treatment solutions with 2% FC4430 and 1% FC4430 in a 70/30 mixture of 2-butoxyethanol/ethanol and D.I water

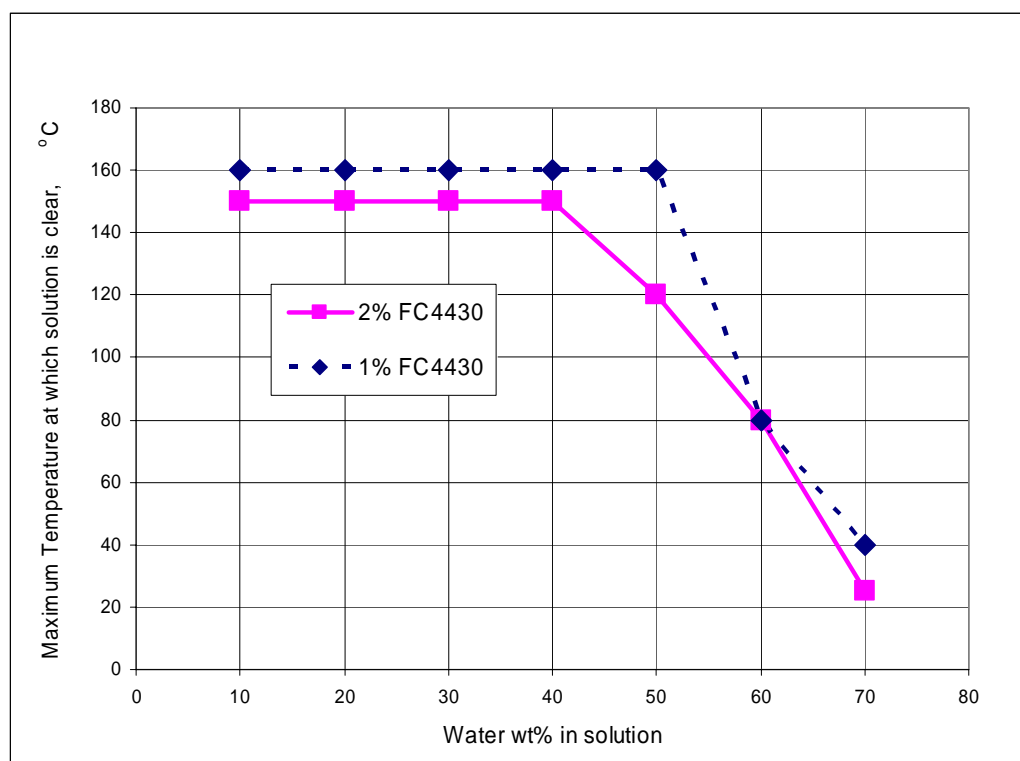


Figure 5.25: Comparison of the phase behavior of treatment solutions with 2% FC4430 and 1% FC4430 in a 70/30 mixture of 2-butoxyethanol/ethanol and 25000 ppm NaCl brine

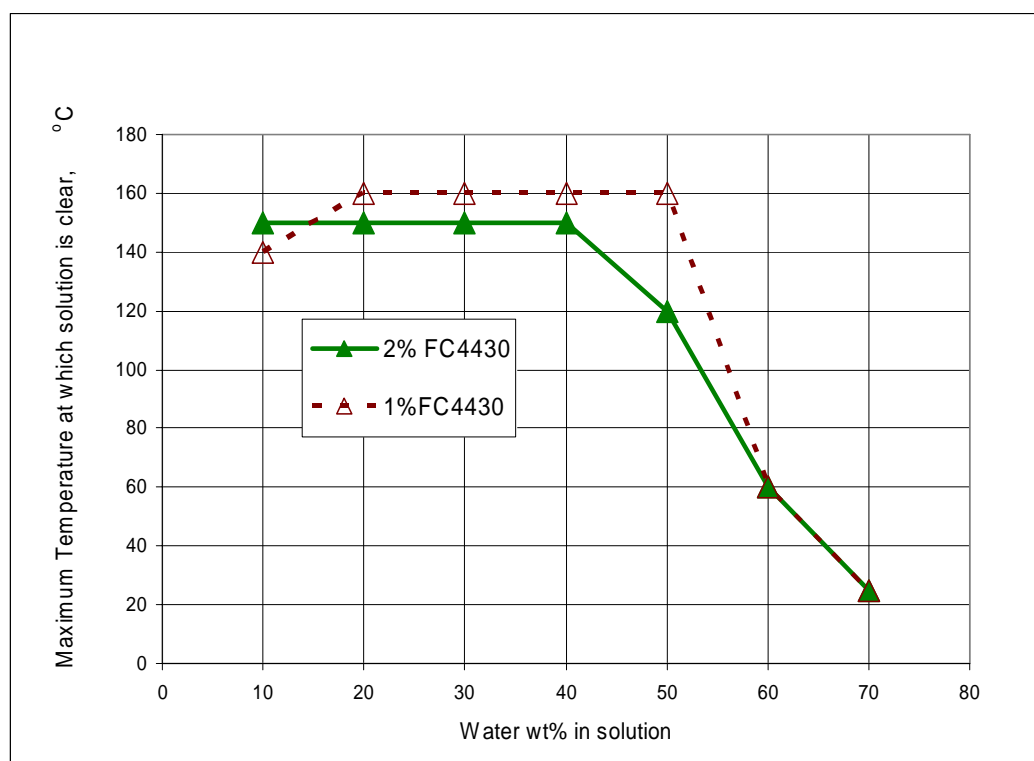


Figure 5.26: Comparison of the phase behavior of treatment solutions with 2% FC4430 and 1% FC4430 in a 70/30 mixture of 2-butoxyethanol/ethanol and 50,000 ppm NaCl brine

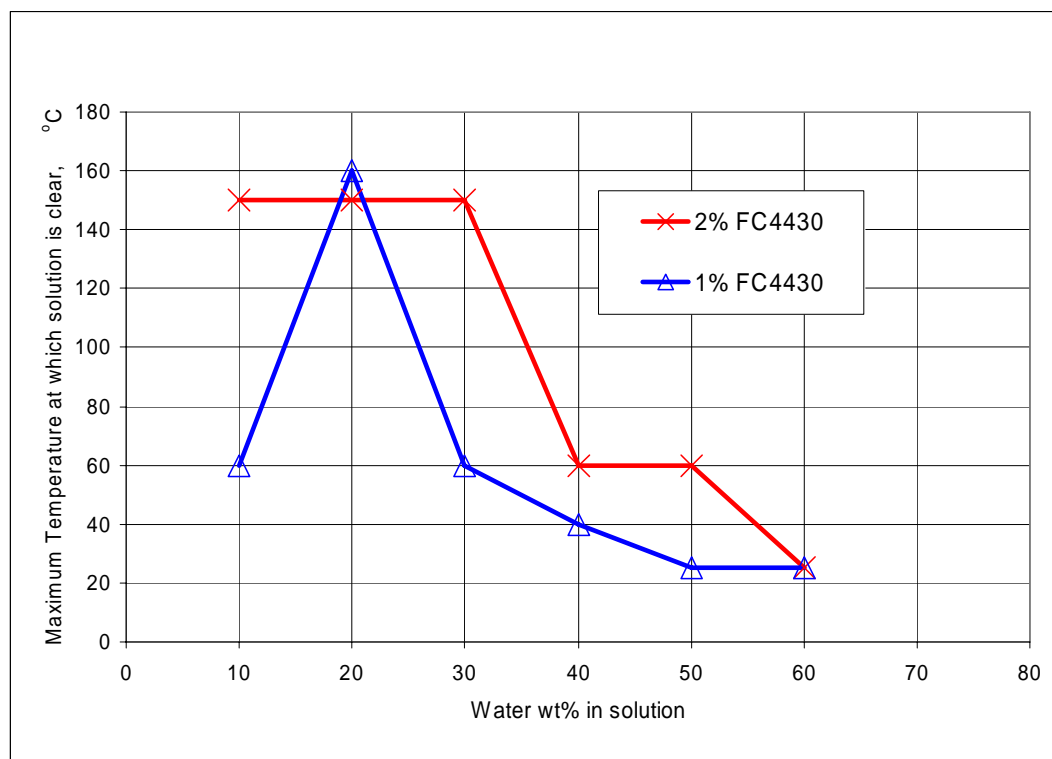


Figure 5.27: Comparison of the phase behavior of treatment solutions with 2% FC4430 and 1% FC4430 in a 70/30 mixture of 2-butoxyethanol/ethanol and 75,000 ppm NaCl brine

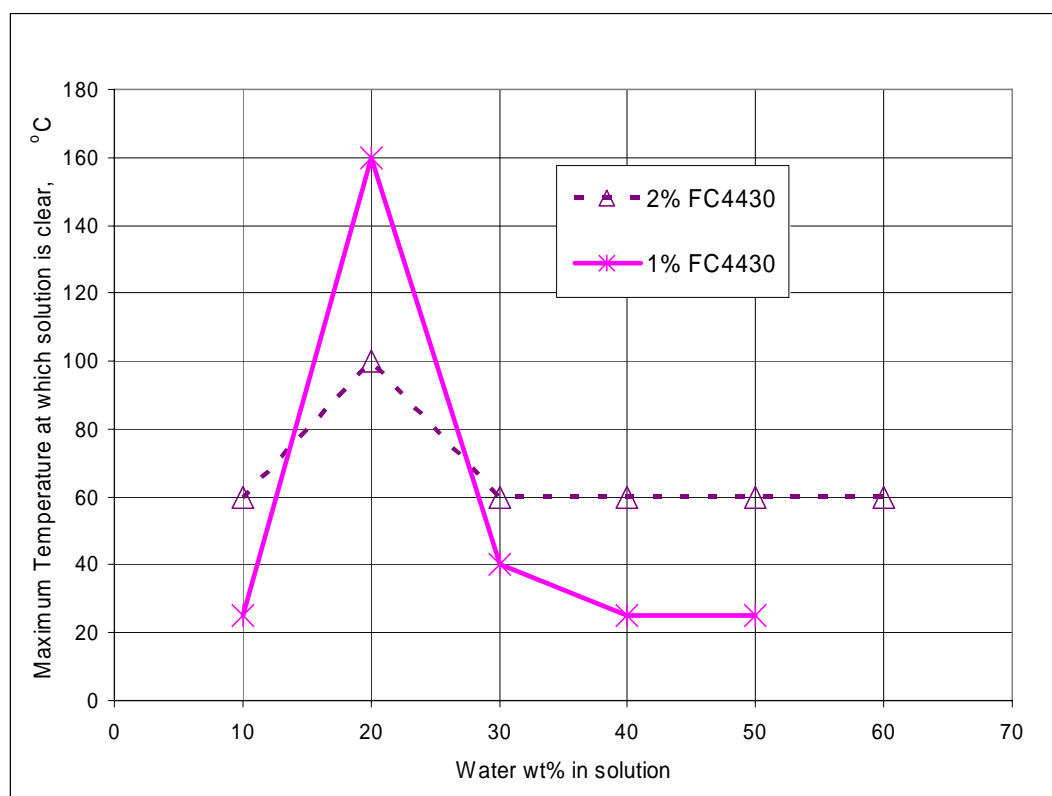


Figure 5.28: Comparison of the phase behavior of treatment solutions with 2% FC4430 and 1% FC4430 in a 70/30 mixture of 2-butoxyethanol/ethanol and 100,000 ppm NaCl brine

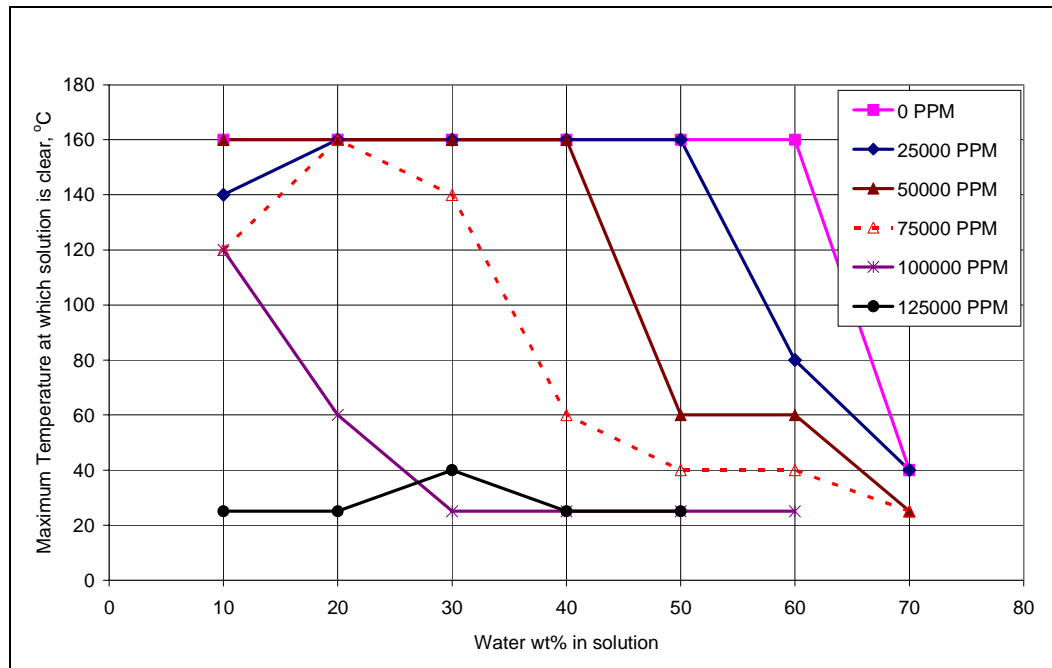


Figure 5.29: Phase behavior results of (90/10) NaCl/CaCl₂ brines of different salinities with treatment solution-7 (1% FC4430, 69.5% 2-butoxyethanol and 29.5% ethanol)

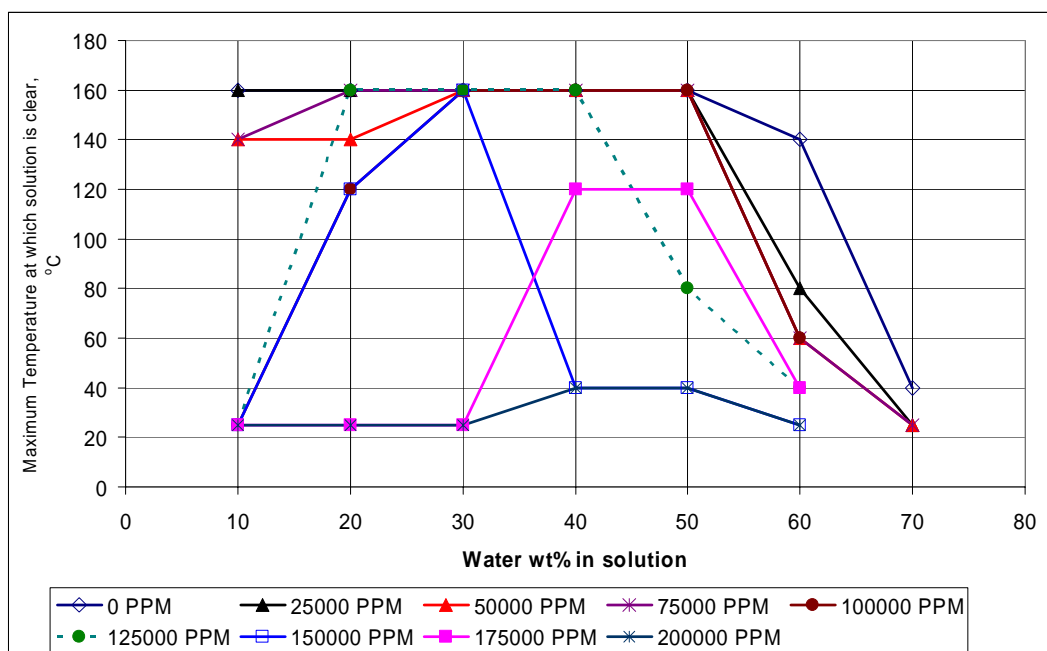


Figure 5.30: Phase behavior results of (90/10) NaCl/CaCl₂ brines of different salinities with treatment solution-8 (1% FC4430, 49.5% 2-butoxyethanol and 49.5% ethanol)

Chapter 6: Chemical Treatment of Sandstones with Connate Water

This chapter presents the results of chemical treatment using FC4430 conducted on Berea sandstone cores and reservoir rocks with connate water. The first section presents steady-state relative permeability measurements before and after chemical treatment on Berea sandstone cores with different water saturations. Next two sections presents results of chemical treatment on Bruce and Hatter's Pond reservoir cores. The effect of surfactant concentration and shut-in time on improvement in relative permeability is then discussed. Results of adsorption measurements conducted to measure the retention of surfactant on Berea sandstone cores for different surfactant concentrations are presented next. Finally, wettability measurements conducted on treated and untreated reservoir cores using a centrifuge are described. The results presented in this chapter refer to chemical treatment using FC4430 unless specified otherwise.

6.1. NEW SOLVENT SYSTEMS FOR DELIVERING SURFACTANT TO ROCK SURFACE

Results presented in Chapter 4 show that methanol alone or in combination with water does not effectively solubilize or displace brine and/or condensate while delivering surfactant to the rock surface. This led to the testing of new solvents that were more effective at removing brine from the cores. Phase behavior results described in Chapter 5 show that mixtures of a glycols and alcohols are extremely efficient in solubilizing brine. The solvent composition was varied depending on the reservoir temperature, water saturation and brine salinity.

Visual inspection of effluent samples during the treatment flood showed that treatment solution with the appropriate solvent composition displaced brine and

condensate from the core. **Figure 6.1** shows a photograph of effluent samples collected in Experiment 27 (UT Experiment #68) during the treatment flood using a 70/30 solvent mixture 2-butoxyethanol and ethanol. During the first couple of pore volumes when most of the liquid (water and condensate) in the core is flushed out, effluent samples were dark and cloudy. This corresponds to the initial high pressure drop observed during treatment injection (shown in **Appendix B27**). The effluent samples got clearer with the pore volumes of treatment solution injected and after about 5 pore volumes of treatment injection, clear effluent samples were observed. Such visual inspections were done for other experiments also and similar observations were made. Visual inspection of effluent samples show that the treatment solutions designed based on phase behavior tests (described in Chapter 5) are efficient in displacing brine and condensate from the core under the experimental conditions.

Water concentration in the effluent samples during the treatment flood using a 70/30 solvent mixture of propylene glycol and isopropanol was measured using the Karl Fisher technique (Ahmadi *et al.* 2008-09). The water concentration was about 20,000 mg/l initially but it decreased to less than 1000 mg/l after injecting 5 PV of treatment solution. The result from Karl Fischer analysis further confirms that the solvent mixtures selected based on phase behavior studies described in **Chapter 5** are suitable for displacing brine and delivering the surfactant to the rock surface.

6.2. CHEMICAL TREATMENT OF BERE A SANDSTONES CORES

These experiments (Experiment #21, 28 and 30) were performed at 175°F on Berea sandstone cores. Two-phase gas condensate flood was done using synthetic fluid mixture-4 (composition given in Table 3.4). Initial water saturation was established using synthetic brine given in **Table 6.1** following the procedure described in Section 3.3.

Steady-state gas and oil relative permeability were measured before and after treatment. The cores were treated using the non-ionic polymeric fluoro-surfactant FC4430 delivered in a mixture of 2-butoxyethanol and ethanol. Non-ionic polymeric fluoro-surfactant X3 was used in Experiment 30. Surfactant X3 from 3M Corp. is similar to FC4430, but the molecular weight of X3 is about 3 times that of FC4430. The idea was that the higher molecular weight surfactant would have more attachments to the rock surface and thus might perform better. The ratio of solvents in the treatment solution was varied depending on initial water saturation as described in Chapter 5.

Figure 6.2 compares the two-phase gas condensate flow pressure drops before and after chemical treatment for Experiment 21. Two-phase gas condensate floods were conducted at 536 cc/hr and 1985 psig core pressure. The PVT ratio for this synthetic fluid at 1985 psig and 175°F is 0.95. The core was treated with the treatment solution comprising of 2% FC4430, 69% 2-butoxyethanol and 29% ethanol. 22 pore volumes of treatment solution was flowed through the core at 224 cc/hr. The pressure drop data during the treatment flood as well as other detailed data are given in **Appendix B21**. The treatment improved the gas and condensate relative permeability by a factor of 1.93.

Figure 6.3 compares the two-phase gas condensate flow pressure drops before and after chemical treatment for Experiment 28. Two-phase gas condensate floods were conducted at 2107 cc/hr and 420 psig core pressure. The PVT ratio for this synthetic fluid at 420 psig and 175°F is 2.69. The initial two-phase flow was followed with a three-phase flow by co-injecting brine, gas and condensate through the core at a water fractional flow of 0.036 ($fw=0.036$). The water saturation in the core at this fractional flow is approximately 50% (Baker *et al.*, 1987). To tolerate such high water saturation, the ratio of 2-butoxyethanol/ethanol in the treatment solution was changed from 70/30 to 50/50.

The core was treated with 2% FC4430, 49% 2-butoxyethanol and 49% ethanol. 20

pore volumes of treatment solution was flowed through the core at 128 cc/hr. Pressure drop during the treatment flood is shown in **Appendix B28**. The treatment improved the gas and condensate relative permeability by a factor of 1.68. Improvement in this experiment is less than an expected value of 2. This could be because the change in solvent composition in treatment solution increased the cloud point and thus reduced adsorption on the rock surface. Results of three-phase flow and effect of chemical treatment on three-phase flow are discussed in Chapter 7. Details of the experiment are given in **Appendix B28**.

Figure 6.4 compares the two-phase gas condensate flood pressure drops before and after chemical treatment for Experiment 30. Two-phase gas condensate floods were conducted at 2014 cc/hr and 420 psig core pressure. The PVT ratio for this synthetic fluid at 420 psig and 175°F is 2.69. The core was treated with the treatment solution comprising of 2% X3, 69% 2-butoxyethanol and 29% ethanol. 22 pore volumes of treatment solution was injected into the core at 128 cc/hr. Pressure drop during the treatment flood is shown in **Appendix B30**. Treatment improved the gas and condensate relative permeability by a factor of 1.88. Details of the experiment are given in **Appendix B30**.

Table 6.2 summaries the experimental conditions and compares relative permeabilities before and after chemical treatment for Experiments 21, 28 and 30. These results show that sandstone rocks with connate water can be successfully treated with a proper choice of solvents used to deliver the surfactant FC4430. These results also validate the applicability of solvent selection procedure based on phase behavior studies as described in Chapter 5. Thus the phase behavior studies of surfactant solutions in different solvent mixtures with different brines presented in Chapter 5 can be used as a

screening test to design the optimum treatment solution and also predict the performance of chemical treatment depending on the experimental or reservoir conditions.

6.3. CHEMICAL TREATMENT OF RESERVOIR SANDSTONE CORES

Steady-state relative permeabilities were measured before and after the chemical treatment on reservoir cores at their respective reservoir conditions using the experimental procedure given in **Chapter 3**. Model fluids used were matched to the actual reservoir fluids on the basis of liquid dropout, viscosity, interfacial tension, dew point pressure and the PVT ratio at the reservoir conditions. Reservoir rocks from Bruce field and Hatter's Pond field were used to see the effect of chemical treatments in improving gas and condensate relative permeabilities.

6.3.1 Chemical Treatment of North Sea Reservoir Sandstone Cores

Table 6.3 gives the properties of the reservoir cores from the Bruce field in North Sea and the experimental conditions that represent the reservoir conditions. A synthetic hydrocarbon gas mixture was designed to closely represent the reservoir fluid. **Table 3.4** gives the composition of the synthetic gas mixture. **Figure 6.5** compares the calculated P-T phase diagram of the synthetic lab fluid and the characterized reservoir fluid. **Figure 6.6** compares the calculated liquid dropout of the synthetic lab fluid and the characterized reservoir fluid at 175°F. The gas condensate fluid is a moderately rich fluid with the maximum liquid dropout for the reservoir fluid of 14% at 3500 psig and 12% at 3100 psig for the synthetic lab fluid. Calculated dew point pressure for the synthetic fluid is 4318 psig compared to 5300 psig of the reservoir fluid, i.e. less by about 1000 psi. However, the dew point pressure of the fluids does not affect the steady state

measurements done using pseudo-steady state method (described in Section 3.3). **Table 6.4** compares the most pertinent fluid properties of the reservoir fluid and the synthetic fluid calculated using the Peng-Robinson EOS at the experimental conditions. All the important fluid properties of both gas and condensate phases for the synthetic gas mixture match closely with those of the actual reservoir fluid. Composition of the characterized reservoir fluid and the equation of state parameters are given in Chapter 12 (**Table 12.1**).

Effect of chemical treatment on reservoir core:

Figures 6.7 and **6.8** show the effect of chemical treatment on a reservoir core at different core pressures corresponding to different PVT ratios. Experiment-24 was performed on a 1-inch Bruce reservoir plug #7. **Table 6.3** gives the properties of the reservoir core. This core was received from BP with the initial water saturation of 22% already established by the porous plate method. The brine composition is not known but is likely to be close to the brine given in **Table 6.1**. Initial permeability of the rock at $S_{wi}=22\%$ was measured using water-saturated methane at 175°F and 1930 psig. Water-saturated methane was used to prevent vaporization of water by flowing methane. The gas condensate floods were conducted at a flowing core pressure of 1930 psig and subsequently again at 460 psig so the measurements could be done at two different PVT ratios corresponding to two different k_{rg}/k_{ro} ratios. For this fluid, the PVT ratio is 0.96 at 1930 psig and 2.37 at 460 psig.

The core was treated with a treatment solution made of 2% FC4430, 69% 2-butoxyethanol and 29% ethanol. 40 pore volumes of treatment solution was flowed through the core at 160 cc/hr. Pressure drop during the treatment flood is shown in **Appendix B23**. The core was then shut-in for 15 hours. **Figures 6.7** and **6.8** show the pressure drop measured across the core during pre-treatment and post-treatment gas

condensate two-phase flow at 1920 psig and 460 psig, respectively. Results show that the treatment reduced the steady state pressure drop by a factor of 1.75 and 2.08 at flowing pressures of 1930 psig and 460 psig, respectively. Thus, the treatment increased the gas and condensate relative permeability by the same factors.

Pressure drop for the post-treatment flood is essentially constant for more than 400 pore volumes at each flowing pressure, which indicates the treatment is very durable. **Table 6.5** summarizes the results of the chemical treatment. The final gas permeability measured using methane was 71.7 md compared to initial permeability of 58 md at S_{wi} . The result implies that the treatment did not damage the core. Details of the experiment are given in **Appendix B24**.

Effect of chemical treatment on high permeability core at high capillary number:

Figure 6.9 shows the effect of chemical treatment on high permeability reservoir cores (Exp #23). Two 1-inch cores (plug #1 and 3) were stacked together vertically for this experiment. **Table 6.3** gives the properties of these reservoir cores. These are highly permeable cores with the initial permeability to gas of 1222 md. Initial water saturation of 19% was established using synthetic brine (**Table 6.1**). An initial water saturation decreased single-phase gas permeability by about 19% as shown in **Table 6.2**. The cores were treated with a treatment solution made of 2% FC4430, 69% 2-butoxyethanol and 29% ethanol. 40 pore volumes of treatment solution was flowed through the core at 196 cc/hr. Pressure drop data during the treatment flood as well as other detailed data are given in **Appendix B23**. The core was then shut-in for 15 hours. **Figure 6.9** shows the pressure drop measured across the core during pre-treatment and post-treatment gas condensate two-phase flow at 1920 psig. Chemical treatment increased the gas and condensate relative permeability on these reservoir cores by a factor of 1.53. **Table 6.6**

summarizes the results of chemical treatment. The final gas permeability measured using methane was 1201 md compared to initial permeability of 1222 md. The result shows that the treatment did not damage the core.

Two-phase flow measurements in this experiment were done at a high capillary number of about 8×10^{-5} . At these high capillary numbers, some improvement in gas relative permeability is observed because of capillary number effect (Chapter 10). Thus, the potential for improvement at high capillary number might decrease as the residual liquid saturation decreases with increase in capillary number. This could be the reason for a lower improvement factor observed in this experiment. However, in most of the gas condensate reservoirs, high capillary number is associated with non-Darcy flow, which has an opposite effect on gas relative permeability. Thus, the impact of chemical treatment on gas relative permeability becomes difficult to predict at high flow rates or high capillary numbers, as the results will change according to the dominance of one effect over the other. The combined effects of non-Darcy flow and capillary number on gas relative permeability are explained in detail in Chapter 10.

Effect of chase gas injection on chemical treatment:

Figure 6.11 shows the effect of chase gas injection on chemical treatment. Experiment-27 was performed on the 1-inch Bruce reservoir plug #9. **Table 6.3** gives the properties of the reservoir core. This core was received from BP with an initial water saturation of 12% already established by the porous plate method. The brine composition is not known but is expected to be close to the brine given in **Table 6.1**. Initial permeability of the rock at $S_{wi} = 12\%$ was measured using water-saturated methane at 175°F and 1915 psig. Water-saturated methane was used to prevent vaporization of water by flowing methane. The initial gas condensate floods were conducted at a flowing core

pressure of 1912 psig and subsequently again at 550 psig so the measurements could be done at two different PVT ratios. For this fluid, the PVT ratio is 0.96 at 1930 psig and 2.03 at 550 psig.

Figure 6.10 shows the pressure drop during the initial gas condensate flood at different PVT ratios. The core was treated with the treatment solution made of 2% FC4430, 69% 2-butoxyethanol and 29% ethanol. 20 pore volumes of treatment solution was flowed through the core at 80 and 160 cc/hr. First 12 pore volumes of treatment solution was injected at 80 cc/hr and then the remainder at 160 cc/hr. Pressure drop during the treatment flood is shown in **Appendix B27**. The core was then shut-in for 18 hours.

In this experiment the effect of chase gas on chemical treatment was studied by injecting nitrogen at 4850 psig. The choice of chase gas (nitrogen or methane) and the volume of the chase gas are both important field design variables. Chases gas is needed to flush the treatment solution out of the well tubing and into the formation. Additional chase gas may be beneficial to a well treatment since it will displace the surfactant farther into the formation and since it may promote adsorption of the surfactant onto the rock surface before gas production is resumed. Initial field trials have been designed with these ideas in mind. More details about chase gas injection are given in Chapter 12. This experiment was designed to determine if nitrogen gas was an acceptable chase gas in terms of improvement factor in a core.

Post-treatment gas condensate flood was done after chase gas injection. **Figure 6.11** compares the pressure drop measured across the core during pre-treatment and post-treatment gas condensate two-phase flow at 550 psig. Treatment reduced pressure drop by a factor of 1.75 and thus increased relative permeabilities by the same factor. The pressure drop for the post-treatment flood is essentially constant for the last 400 pore

volumes, which indicates the durability of the treatment. **Table 6.7** summarizes the results of the chemical treatment. The final gas permeability measured using methane was 42.3 md compared to initial permeability of 39.1 md at S_{wi} . The result implies that the treatment did not damage the core. Details of the experiment are given in **Appendix B27**.

Effect of chemical treatment on an oil wet reservoir core after cleaning with solvents

Experiment 45 was performed with Bruce reservoir plug #8. **Table 6.3** gives the properties of the reservoir core. The core was contaminated with confining mineral oil due to the failure of viton rubber sleeve in the core holder, which might have changed its wettability. To remove the mineral oil and restore its wettability to a water wet state, the core was cleaned by the sequential flow of solvents. 17 pore volumes of methanol was injected first at 120 cc/hr followed by 28 pore volumes of toluene at 200 cc/hr. The core was then shut in for 12-15 hours. 17 pore volume of a mixture of methanol and toluene (50/50) was then injected at 120 cc/hr. The effluent at the end of last solvent flood was still cloudy indicating that the core was still contaminated and its original state had not been restored. A drop test was done with n-decane and water to get a quick estimate of the wettability. The core imbibed oil spontaneously, but did not imbibe water indicating that it was oil-wet.

The core was left in this state for about 9 months and then cleaned again by flowing 6 pore volumes of methanol/toluene (50/50) mixture. Yellowish colored effluent was produced initially indicating mineral oil was being flushed out. However, after a few pore volumes, the effluent became clear. A drop test was not done again to determine the wettability of the core.

An initial water saturation of 19% was established using synthetic brine given in **Table 6.1**. **Figure 6.12** shows the pressure drop during the initial gas condensate flood at different flow rates corresponding to different capillary numbers. At high flow rates, the effect of both capillary number and non-Darcy flow on gas relative permeability becomes significant. Details of non-Darcy flow effects and effect of capillary number are given in Chapter 10.

The core was treated with a treatment solution made of 2% FC4430, 69% 2-butoxyethanol and 29% ethanol. 20 pore volumes of treatment solution was injected into the core at 80 cc/hr. Pressure drop during the treatment flood is shown in **Appendix B45**. The pressure drop during the treatment flood kept increasing with the pore volumes of fluid injected indicating some kind of plugging. The reason for the plugging is not known. The treatment solution is compatible with the brine under these experimental conditions so precipitation should not have been the cause of the plugging. Plugging could be due to face plugging at the inlet face of the core caused by solids from an O-ring or other artifact since this has been observed occasionally in other experiments. The core was then shut-in for 12 hours. **Figure 6.13** shows the pressure drop measured across the core during pre-treatment and post-treatment gas condensate two-phase flow at 400 psig. Chemical treatment increased the gas and condensate relative permeability by a factor of 1.44. **Table 6.8** summarizes the results of chemical treatment.

This relatively smaller improvement in relative permeability after chemical treatment could be because of two reasons. Firstly, the original wettability, i.e. strongly water wet, of the core was not retained and thus the improvement after chemical treatment is reduced. Secondly, some damage was caused to the core permeability because of plugging. The final gas permeability measured using methane was 101 md compared to the initial permeability of 131 md. The reduction in core permeability was

probably caused by face plugging. This could be the reason for a lower improvement due to chemical treatment as the post-treatment relative permeabilities were calculated using the initial core permeability. If the final core permeability is used to calculate the post-treatment gas and condensate relative permeabilities, an improvement factor of 1.86 is obtained due to chemical treatment. **Table 6.9** summarizes the results of chemical treatment with corrected post-treatment relative permeabilities. This result is more consistent with the other results obtained with chemical treatment. Details of the experiment are given in **Appendix B45**.

6.3.2 Chemical Treatment of Hatter's Pond Reservoir Core

Table 6.10 gives the properties of reservoir core plugs from Hatter's Pond field and the experimental conditions that represent the reservoir conditions. A synthetic hydrocarbon gas mixture was designed to closely represent the reservoir fluid. **Table 3.6** gives the composition of the synthetic gas mixture. **Figure 6.14** compares the calculated P-T phase diagram of the synthetic lab fluid and the characterized reservoir fluid. **Figure 6.15** compares the calculated liquid dropout of the synthetic lab fluid and the characterized reservoir fluid at the experimental temperature of 308°F. The fluid mixture is a near-critical fluid at this temperature. EOS calculations show that the fluid is a volatile oil at this temperature. Calculated saturation point pressure for the synthetic fluid is 3130 psig compared to 3013 psig of the reservoir fluid. **Table 6.11** compares the important fluid properties of the reservoir fluid and the synthetic fluid calculated using the Peng-Robinson EOS at the experimental conditions. The fluid properties of both the gas and condensate phases for the synthetic fluid mixture match closely with those of the actual reservoir fluid. The composition of the characterized reservoir fluid is given in **Table 6.12**.

Figure 6.16 compares the two-phase gas condensate flow pressure drops before and after chemical treatment for Experiment 25. Two low permeability 1-inch Hatter's Pond cores (plug#18331A and 18331B) were stacked together vertically for the experiment. Initial water saturation of 20% was established using synthetic brine with the composition given in **Table 6.13**. Salinity of brine was 180,000 ppm and the composition of salts in the brine was selected to match the original formation brine. A 0.5 PV preflush using a 50/50 mixture of 2-butoxyethanol and methanol was injected at 12 cc/hr to prevent the interaction of treatment solution with the high salinity brine. The small preflush of 0.5 PV was selected so that the solvent would flush out some brine and reduce the water saturation and brine salinity in the cores but still leave enough brine to cause adsorption of the surfactant by inducing insolubility when treatment solution mixes with brine.

The core was treated with a treatment solution made of 2% FC4430, 49% 2-butoxyethanol and 49% methanol. 23 pore volumes of treatment solution was injected into the core at multiple flow rates varying from 12 cc/hr to 56 cc/hr. The pressure drop during the treatment flood is shown in **Appendix B25**. A different treatment formulation was used in this experiment compared to those used for treating the Bruce reservoir cores. The solvents and their ratios were changed to tolerate high salinity brine at high temperature. Compatibility tests of different treatment solutions tried with high salinity Hatter's Pond brine is presented in Chapter 5. The core was then shut-in for 15 hours. **Figure 6.16** shows the pressure drop measured across the core during the pre-treatment and the post-treatment gas condensate two-phase flow at 1140 psig. No improvement in relative permeabilities was observed after chemical treatment. **Table 6.14** summarizes the results of chemical treatment.

The failure of chemical treatment was thought to be because of the presence of high salinity brine in the core. It looked as if high salt content affected the interaction of surfactant with the rock surface. So, the cores were treated again with a treatment solution made of 2% FC4430, and 98% methanol. The solvent pre-flush and the first treatment should have displaced all the water from the core. So, it was similar to treating a dry core for which methanol based treatment solutions have given successful results (Kumar *et. al.* 2006). 18 pore volumes of second treatment solution was injected into the core at 48-80 cc/hr. **Figure 6.17** shows the pressure drop measured across the core during pre-treatment and post-second treatment gas condensate two-phase flow at 1140 psig. No improvement in relative permeabilities was observed after the second treatment either. **Table 6.14** summarizes the results of chemical treatment.

A toluene flood was done at the end to see if any water would be produced from the core. 8.5 PV of toluene was injected into the core at 64 cc/hr. No water production was observed in the effluent indicating all the water had already been produced during the initial treatment floods. Final permeability of the core measured during the toluene flood was 1.12 md compared to the original gas permeability of 3.64 md. Thus, the permeability of the core decreased by almost a factor of 3. The post treatment permeabilities were calculated using the original permeability of the core.

To understand the results of the experiment, the wettability of a new untreated Hatter's Pond core was determined by measuring the imbibition and drainage capillary pressure curves. It was observed that these cores were oil-wet, which is not common in gas reservoirs. Details of the wettability measurements are given in the last section of this chapter. The Hatter's Pond core plugs have a coating of pyrobitumen (Looney *et al.* 1995) which is not very common, and which might make the core plugs oil-wet. Thus, the reason for the failure of the treatment could be because the core plugs are oil wet.

Another possible explanation is that the treatment solution could not tolerate such high salinity brine. It is likely that water did not distribute uniformly throughout the core while establishing initial water saturation, as it is a low permeability core. This could result in contact of high water saturation with the treatment solution at the inlet of the core and possible precipitation of surfactant or salt, which decreased the core permeability and thus resulted in a failed treatment. The fact that the final permeability was three times lower indicates something caused a lot of damage to the core and thus this second possible explanation seems as likely as the first one. Perhaps both factors contributed to the failure.

6.4. EFFECT OF SURFACTANT CONCENTRATION ON CHEMICAL TREATMENT

The cost of the fluoro surfactant is a significant part of the total cost of a field treatment, so the effect of surfactant concentration on the effectiveness of chemical treatment was evaluated by decreasing the surfactant concentration by more than an order of magnitude.

Steady-state gas and condensate relative permeabilities were measured before and after chemical treatment using the procedure described in Chapter 3. Surfactant concentration in the treatment solution was varied from 0.1% to 2% on a mass basis. A mixture of 70/30 2-butoxyethanol and ethanol was used in the treatment solution to avoid any change in the results due to change in solvents. Experiments were done on Berea sandstone cores at 175°F to eliminate the effect of rock type and temperature on improvement in relative permeability after chemical treatment. Water saturation and brine salinity were also kept the same in these experiments.

Table 6.15 lists the experimental conditions and treatment specifications for Experiments 21, 30, 41 and 42 done to evaluate the effect of surfactant concentration on

improvement factor. Synthetic fluid mixture-4 was used in Experiments 21 and 30 and fluid mixture-5 was used for Experiments 41 and 42. The only difference between the two fluids is that n-butane is replaced with propane in fluid-5. The PVT properties of both the fluid at experimental conditions are very close and thus do not affect the results.

Table 6.16 shows the effect of surfactant concentration on improvement in relative permeabilities after chemical treatment. **Figures 6.2** and **6.4** compare the pressure drop during pre-treatment and post-treatment gas condensate flood for Experiments 21 and 30 respectively. The results show the effect of 2% surfactant concentration on improvement in gas and condensate relative permeabilities after treatment. A description of these experiments is given in **Section 6.2. Appendix B21 and B30** gives the details of these experiments.

Figure 6.18 compares two-phase gas condensate flow pressure drops before and after chemical treatment with 1% surfactant concentration in the treatment solution for Experiment 41. Two-phase gas condensate floods were conducted at 2713 cc/hr and 420 psig core pressure. The PVT ratio for this synthetic fluid at 420 psig and 175°F is 2.62. The core was treated with the treatment solution comprising 1% FC4430, 69.5% 2-butoxyethanol and 29.5% ethanol. 20 pore volumes of treatment solution was flowed through the core at 112 cc/hr. The pressure drop during the treatment flood is shown in **Appendix B41**. The treatment improved the gas and condensate relative permeability by a factor of 2.36. Thus, a higher improvement in relative permeabilities was observed after treating rock with 1% surfactant concentration. **Table 6.17** summarizes the results of the chemical treatment. Details of the experiment are given in **Appendix B41**.

Figure 6.19 compares two-phase gas condensate flow pressure drops before and after chemical treatment with 0.1% surfactant concentration in treatment solution for Experiment 42. Two-phase gas condensate floods were conducted at 2713 cc/hr and 420

psig core pressure. The PVT ratio for this synthetic fluid at 420 psig and 175°F is 2.62. Core was treated with the treatment solution with a composition of 0.1% FC4430, 69.9% 2-butoxyethanol and 30% ethanol. 44 pore volumes of treatment solution was flowed through the core at 128 cc/hr.

Adsorption measurements done prior to this experiment on Berea core with 2% surfactant concentration in the treatment solution showed that about 3 to 3.5 mg of surfactant is retained on the rock surface for every gram of rock. Details of adsorption measurements are described in **Section 6.6**. Thus, the minimum mass of surfactant needed to treat a core weighing 213 gm was calculated to be 0.75 gm. To deliver 0.75 gm of surfactant to the rock surface, 40 PV of treatment solution would be required at a surfactant concentration of 0.1%. A total of 0.8 gm of surfactant was injected into the core by injecting 44 PV of treatment solution. The pressure drop during the treatment flood is shown in **Appendix B42**. The treatment improved the gas and condensate relative permeability by a factor of 2.18. **Table 6.18** summarizes the results of the chemical treatment. Details of the experiment are given in **Appendix B42**.

Figure 6.20 shows the effect of surfactant concentration on improvement in relative permeabilities after chemical treatment. The result show an improvement by a factor of 2 and more over the wide range of surfactant concentrations tested, with the highest improvement of 2.36 obtained with 1% surfactant concentration. The difference in the results obtained with 0.1%, 1% and 2% surfactant concentration varies about 10% from the mean of 2.15, which is considered within the uncertainty of the individual measurements. This result is an extremely important result as it shows that the same improvement can be obtained with low surfactant concentrations, thus making the treatment more cost effective.

6.5. EFFECT OF SHUT-IN TIME ON CHEMICAL TREATMENT

The shut-in time after chemical treatment can affect the cost of treatment significantly as the loss in gas production from the wells during the shut-in time can be significant. Thus, shorter the shut-in time after treatment better it will be from the cost effectiveness point of view. Experiments were done to evaluate the effect of shut-in time on the effectiveness of chemical treatment.

Steady-state gas and condensate relative permeabilities were measured before and after chemical treatment using the procedure described in chapter 3. Shut-in time after the treatment was varied from 1 hour to 15 hours. The experiments were done on Berea sandstone cores at 175°F to eliminate the effect of rock type and temperature on improvement in relative permeability after chemical treatment. Other parameters that may affect the results of chemical treatment including treatment solution, water saturation and brine salinity were also kept the same. **Table 6.19** lists the experimental conditions and treatment specifications for Experiments 21, 30, and 37 conducted to evaluate the effect of shut-in time on improvement factor. Synthetic fluid mixture-4 was used in Experiments 21 and 30 and fluid mixture-5 was used for Experiment 37. The only difference between the two fluids is that n-butane is replaced with propane in fluid-5. The PVT properties of both the fluid at experimental conditions are very close and thus do not affect the results of these experiments.

Table 6.19 shows the effect of shut-in time on improvement in relative permeabilities after chemical treatment. **Figures 6.2** and **6.4** compare the pressure drop during pre-treatment and post-treatment gas condensate flood for Experiments 21 and 30 respectively. The results show the improvement in gas and condensate relative permeabilities with 15 hours of shut-in time after treatment. Description of these

experiments is given in **Section 6.2. Appendix B21 and B29** gives the details of these experiments.

Figure 6.21 compares the two-phase gas condensate flow pressure drops before and after chemical treatment for experiment 37. Two-phase gas condensate floods were conducted at 2682 and 5364 cc/hr and 410 psig core pressure. PVT ratio for this synthetic fluid at 410 psig and 175°F is 2.62. The core was treated with the treatment solution comprising of 2% FC4430, 69% 2-butoxyethanol and 29% ethanol. 20 pore volumes of treatment solution was flown through the core at 100 cc/hr. The pressure drop during the treatment flood is shown in **Appendix B37**. The core was then shut-in for 1 hour followed with the post-treatment gas condensate flood. Treatment improved the gas and condensate relative permeability by a factor of 1.65 at 2680 cc/hr and 1.55 at 5364 cc/hr. **Table 6.20** summarizes the results of the chemical treatment. Details of the experiment are given in **Appendix B37**.

Reducing the shut-in time from 15 hours to 1 hour decreased the improvement factor by about 15% from 1.9 to 1.65. It shows that though shut-in time of 1 hour gave a high improvement but it may not be long enough. To get a better understanding of the effect of shut-in time and determine the optimum shut-in time more experiments with shut-in times between 1 and 15 hours need to be done.

6.6. ADSORPTION MEASUREMENTS OF FC4430 ON BERE SANDSTONE

The amount of surfactant adsorption is likely to be important in terms of how much is injected into a well and in terms of the durability of the treatment. The more the surfactant adsorbed on the rock surface, the longer the treatment is expected to last. The adsorption isotherm for FC4430 is not known, but in general the adsorption of pure surfactants decreases below a certain surfactant concentration corresponding to the CMC

of the surfactant. Surfactant adsorption also depends on temperature, solvent composition, the surface characteristics of the substrate, and other variables.

Adsorption measurements were made to determine the amount of FC4430 adsorbed on the rock for different concentrations of surfactant. These measurements were done with the help of Chris Britton. Adsorption of the surfactant was measured by measuring the concentration of surfactant in the effluent coming out of the core during the injection of treatment solution. Effluent samples were collected at intervals of 0.1 to 0.3 pore volumes during the treatment flood. The surfactant concentration was then measured in the effluent samples either by drying off the solvents or running the samples through a high-pressure liquid chromatograph. From the difference between the mass of surfactant injected into the core and produced from the core, the amount of surfactant adsorbed on the rock surface was determined.

The FC4430 sample is supplied with 85-95 wt% active ingredient and has less than 10% volatile fraction. Since the treatment solution is made of non-volatile surfactant in a volatile solvent, the effluent samples were dried in a vacuum oven at 100°C to capture the non-volatile surfactant and weigh it. The sample bottles were weighed empty and then with the effluent sample to get the mass of each sample. Then from the weight of the effluent samples before and after vaporizing solvents, the concentration of the surfactant in the effluent samples was calculated. The treatment also flushes out brine from the core and thus some salt will also be observed in the effluent samples for the first few pore volumes. During drying, water will vaporize and will leave salt behind. Thus the solid residue left behind after drying will have surfactant with some salt in the first few samples and separating the two is extremely difficult. This gravimetric method was used to analyze samples from treatment solutions containing 1 wt% and 2 wt% FC4430.

However, for the lower surfactant concentration of 0.1%, the gravimetric method was not feasible due to the very low mass of surfactant in each sample.

To avoid the problem of salt interfering with results and be able to measure small surfactant concentration in the samples, effluent samples were analyzed using a high-pressure liquid chromatograph (HPLC). Chris Britton did these measurements. 2.5 cc of samples are passed through the HPLC detector and the peak area observed in response corresponds to the surfactant concentration. Standards with different surfactant concentrations were first analyzed using HPLC and the response peak was calibrated. The volume of each sample injected was 2.5 cc. **Figure 6.22** shows the calibration curve for surfactant concentration ranging from 0.0001 to 0.004 (0.01 wt% to 0.4%). The HPLC method was used for analyzing samples of treatment solution containing 0.1 wt% FC4430 (Experiment #42), so the range of standards calibrated was enough to analyze these samples.

Figure 6.23 shows the surfactant concentration profile in the effluent samples during a treatment flood on a dry Berea sandstone core at 250°F with a treatment solution containing 2% surfactant (Experiment #32). The measurements were done using the drying method. Treatment solution was made up of 2% FC4430, 69% propylene glycol and 29% iso-propanol. As the core was dry there were no issues related with salt in the effluent samples. However, the first few samples were contaminated with the fluids in the tubing of the setup left behind from the previous experiment. This was observed visually as dark colored two-phase samples were produced initially. Samples were collected for every 0.1 PV. Results show that most of the adsorption took place within the first 2.5-3 pore volumes of injection. From a mass balance on the surfactant, the adsorption of surfactant was determined to be 3.5 mg/gram of rock. .

Figure 6.24 shows the surfactant concentration profile in the effluent samples during a treatment flood on a Berea sandstone core at 175°F with a treatment solution containing 2% surfactant (experiment #37). The measurements were done using the drying method. Treatment solution was made up of 2% FC4430, 69% 2-butoxyethanol and 29% ethanol. Initial water saturation was 19% with the brine salinity of 73,000 ppm. Results show that no surfactant production was observed for about 1 PV indicating surfactant adsorption on the rock surface. Surfactant weight % reached about 2% in the effluent samples after 4 pore volumes of injection. Surfactant adsorption was calculated to be 3.1 mg/gm of rock. This is very close to the value observed on a dry core using 2 wt% surfactant concentration in the treatment solution. Details of the experiment and calculations are given in **Appendix B37**.

Figure 6.25 shows the surfactant concentration profile in the effluent samples during a treatment flood on a Berea sandstone core at 175°F with a treatment solution containing 1% surfactant (Experiment #41). The measurements were done using the drying method. Treatment solution was made up of 1% FC4430, 69.5% 2-butoxyethanol and 29.5% ethanol. The initial water saturation was 19% with a brine salinity of 73,000 ppm. Results show a lot of noise in the data for the first few pore volumes. This is because of the salt production with the treatment solution. Samples after drying off solvents show a residue weight % of more than 1 initially then a decreasing trend for the next few pore volumes till about 5 pore volumes of solution injection. This is probably because the production of salt in the effluent stream decreases with time. Residue weight % increases after 5 pore volumes of injection indicating the production of surfactant. Surfactant weight % reached about 1% in the effluent samples after 8 pore volumes of injection. This is almost twice the time taken to reach maximum adsorption compared to solution containing 2-wt% surfactant. The infection point corresponding to 0.5 wt% was

at 2.5 pore volumes. Surfactant adsorption was calculated to be 2.23 mg/gm of rock. Details of the experiment and calculations are given in **Appendix B41**.

Figure 6.26 shows the surfactant concentration profile in the effluent samples during a treatment flood on a Berea sandstone core at 175°F with a treatment solution containing 0.1% surfactant (Experiment #42). The measurements were done using HPLC. Treatment solution was made up of 0.1% FC4430, 69.9% 2-butoxyethanol and 30% ethanol. The initial water saturation was 19% with brine salinity of 73,000 ppm. Results show smooth data without any noise for the first few pore volumes as the HPLC peak corresponds to surfactant only. Some noise in the data was observed for measurements corresponding to later pore volumes and its reason is not clearly known. The surfactant weight % in the effluent stream shows an increasing trend and reaches 0.1% after about 20-25 pore volumes of injection. The inflection point, corresponding to 0.05 wt%, was at about 8 PV. Surfactant adsorption was calculated to be 0.86 mg/gm of rock. Details of the experiment and calculations are given in **Appendix B42**.

Figure 6.27 shows the adsorption of the surfactant on the Berea sandstone rock measured for different surfactant concentrations. As expected the results show an increase in surfactant adsorption with an increase in surfactant concentration in the treatment solution. **Figure 6.28** shows the effect of temperature on surfactant adsorption. The result shows that adsorption is not significantly affected by temperature in the range of temperatures studied. **Figure 6.29** relates the adsorption of surfactant to the improvement in relative permeabilities due to chemical treatment at 175°F on Berea cores. The result shows no significant change in improvement factor with the amount of adsorption. Although, the amount of adsorption has little effect on improvement factor, it might affect the durability of the treatment. To test this, de-sorption measurements need

to be conducted after treating rocks with treatment solutions containing different surfactant concentrations.

Some preliminary and rough calculations have been done to better understand the adsorption of the surfactant molecule on the rock surface i.e. if the surfactant molecules form a monolayer or a bi-layer on the rock surface. Analysis was done by comparing the surface area of the surfactant molecule in contact with the rock surface and the area of the rock surface occupied per molecule determined from adsorption measurements.

For calculating the surface area of the surfactant molecule exposed to the rock surface, it was assumed that the alkylene oxide groups adsorb linearly on the rock surface and the fluoro-carbon tails stick outwards. As a good approximation, the surface of the molecule in contact with the rock surface can be considered as a rectangular face where the length is equal to the combined length of the C-C, C-O and C-H bonds in the polymeric alkylene oxide groups and the width is equal to 2 C-H bond lengths. As per our knowledge, the polymeric alkylene oxide groups have 66 C-C bonds, 86 C-O bonds and 2 C-H bonds. The bond lengths of C-C, C-O and C-H bonds are 0.154, 0.143 and 0.109 nanometers, respectively. Thus, the total length is equal to 22.68 nm and the width is equal to 0.218 nm. Total surface area of the molecule exposed to the rock surface is therefore 4.94 nm².

The area of the rock surface occupied per molecule was calculated from the amount of surfactant adsorbed on the rock surface. As discussed earlier in this section the amount of surfactant adsorbed on the rock surface depends on the surfactant concentration. Surfactant adsorption of 3mg/g of rock has been used for the calculation here. The surface area of Berea sandstones is 0.8-1.2 m²/g (Schramm *et al.*, 2000). Surface area of 1m²/g of rock has been used in these calculations. Therefore,

$$\text{Amount of surfactant adsorbed on rock surface} = 3 \text{ mg/g} = 3\text{mg/m}^2$$

The molecular weight of FC4430 is (approximately) = 10,000 g/mole

Thus, the moles of surfactant adsorbed per square meter of rock surface

$$= 3 \times 10^{-7} \text{ moles/m}^2$$

Molecules of surfactant adsorbed per square meter of rock surface

$$= 1.8 \times 10^{17} \text{ molecules/m}^2$$

Therefore, area of the rock surface occupied per molecule is

$$= 5.5 \times 10^{-18} \text{ m}^2/\text{molecule}$$

$$= 5.5 \text{ nm}^2/\text{molecule}$$

These calculations show that the area of rock surface occupied per molecule is almost same as the surface area of the molecule exposed to the rock surface. The results suggest that FC4430 surfactant molecule forms a monolayer on the rock surface. However, there are some uncertainties in these calculations because of the assumptions made to simplify them. The results are still expected to be qualitatively valid.

6.7. WETTABILITY MEASUREMENTS ON UN-TREATED AND TREATED RESERVOIR CORES

The basic idea behind the chemical treatment is to alter the wettability of rocks from water-wet or oil-wet to neutral wet and thus increase the relative permeabilities of both gas and condensate. Coreflood results show that fluoro-surfactant FC4430 improved relative permeabilities by about a factor of about 2 on both Berea and reservoir cores. To better understand the effect of chemical treatment on wettability of rocks, wettability of treated and untreated reservoir cores were measured by measuring the Amott and USBM wettability indices.

The combined Amott / United States Bureau of Mines (USBM) method is commonly used for determining wettability of porous rocks (Anderson, 1991; Sharma and Wunderlich, 1987). The USBM method relates the free energy change produced by forcibly displacing the wetting phase (secondary drainage) to that produced by forcibly displacing the non-wetting phase (forced imbibition). The wettability is determined by taking a logarithmic ratio of the area under the secondary drainage and forced imbibition curves (Donaldson *et al.* 1969).

$$I_{\text{USBM}} = \log \left(\frac{A_1}{A_2} \right) \quad (6.1)$$

where, I_{USBM} is USBM wettability index, A_1 is the area under secondary drainage curve and A_2 is the area under forced imbibition curve. A positive wettability index indicates a water wet rock and a negative wettability index indicates an oil-wet rock. Wettability index of 0 indicates neutral or mixed wetting characteristics. Neutral and mixed wet are different but the difference cannot be determined from USBM wettability index.

The Amott index (Amott 1959) or its modification, the Amott-Harvey Relative Displacement Index (RDI) relies on the measurements of the saturation changes produced by spontaneous imbibition for both water and oil compared to the maximum saturation change by forced imbibition of these fluids in the porous rock sample. The index consists of two terms, one defined as the water index (WI) and a second defined as the oil index (OI).

$$WI = \frac{\Delta S_{wS}}{\Delta S_{wS} + \Delta S_{wF}} \quad (6.2)$$

$$OI = \frac{\Delta S_{oS}}{\Delta S_{oS} + \Delta S_{oF}} \quad (6.3)$$

where,

ΔS_{wS} and ΔS_{oS} are the saturation changes for water and oil respectively by spontaneous imbibition. ΔS_{wF} and ΔS_{oF} are the saturation changes for water and oil respectively by forced imbibition.

These indices vary from 0 to 1 for neutral to strongly wet, respectively. The relative displacement index (RDI) is a combination of the two indices and is expressed as-

$$RDI = WI - OI \quad (6.4)$$

RDI varies from 1 to -1, for highly water-wet and highly oil-wet porous media, respectively. Neutral wettability has an RDI equal to 0.

The wettability indices on 6 reservoir cores from 5 different reservoirs was measured by measuring the secondary drainage and forced imbibition capillary pressure curves for n-decane and their respective reservoir brines. A Beckman high-speed centrifuge equipped with a stroboscope and an electric timer was used to measure the imbibition and drainage capillary pressure curves. **Table 6.21** lists the reservoir cores used for wettability measurements. **Table 6.22** gives the composition of brines used for POH and Reservoir B cores. Brines used for Bruce, Britannia and Hatter's Pond cores are given in Table 6.1, 4.6 and 6.13, respectively. N-decane was used for the oil.

The cores were first weighed dry and then again after fully saturating with their reservoir brines to calculate their porosity and pore volume. **Table 6.23** gives the

properties of the reservoir cores. Then primary drainage displacement was run to get residual water saturation. In these measurements, drainage represents displacement of brine by oil and imbibition implies oil displacement by brine. To get the residual water saturations, the centrifuge was run at 10,000 rpm, which corresponds to approximately 92 psi. After measuring the residual water saturation, the forced imbibition cycle was run. Centrifuge speed was increased gradually from 200 rpm to 10,000 rpm (0.1 psi to 177 psi). Forced imbibition was followed with the secondary drainage cycle. Centrifuge speed was again increased gradually from 200 rpm to 10,000 rpm (0.04 to 92 psi) to get the whole capillary pressure curve. The saturation measurements at a low rpm (400) were taken as the spontaneous imbibition measurements for both the fluids for calculating the Amott indices and the RDI.

Figure 6.30 shows the capillary pressure curves measured on a treated high permeability Bruce reservoir core (plug#3). USBM wettability index measured on this core was 0.05 indicating it is close to neutral wet or mixed wet. The Amott water and oil indices were 0.22 and 0.13 respectively. The RDI was 0.09. These measurements suggest that the rock is mixed wet as it imbibes both water and oil. But this is a very high permeability core (1200 md) and the measurement even at an rpm of 400 may not be representative of spontaneous imbibition. The capillary pressure corresponding to an rpm of 400 is 0.28 psi and 0.15 psi for the imbibition and drainage displacements respectively. Thus, WI and OI measured at even small values of capillary pressures for this high permeability rock may not be representative of its true wettability. Chemical treatment increased the gas and condensate relative permeability by a factor of 1.53 on this core (**Section 6.3.1**). This shows that a successfully treated core was made neutral/mixed wet by the surfactant FC4430.

Figure 6.31 shows the capillary pressure curves measured on a treated Britannia reservoir core (plug#52). USBM wettability index measured on this core was 0.08 indicating it is close to neutral wet or mixed wet. WI and OI for this rock were 0 and 0.14 respectively. RDI was -0.14. Chemical treatment increased the gas and condensate relative permeability by a factor of 1.50 on this core (Ahmadi *et al.* 2008-09).

Figure 6.32 shows the capillary pressure curves measured on an untreated Hatter's pond reservoir core (plug#18352A). USBM wettability index measured on this core was -0.33 indicating it is oil wet. This is due to the coating of pyrobitumen (Looney *et al.* 1995) on the rock surface, which makes it oil wet. The Amott indices for both water and oil were 0 for this rock indicating that it does not imbibe either water or oil and is close to neutral wet. The failure of the chemical treatment of another Hatter's Pond core plug may have been because it was also neutral or oil wet.

Figure 6.33 shows the capillary pressure curves measured on an untreated Bruce reservoir core (plug#10). The core was contaminated with the confining oil, which changes the wettability to oil wet. The core was cleaned with cycles of methanol and toluene but was not cleaned completely before the capillary pressure data were measured. USBM wettability index measured on this core was -0.11 indicating it was still weakly oil wet. The Amott indices for both water and oil were 0 for this rock indicating that it does not imbibe either water or oil. Chemical treatment of another Bruce core (plug#8) contaminated with confining oil and then cleaned by flowing solvents until it was completely cleaned out increased the gas and condensate relative permeability by a factor of 1.44 (**Section 6.3.1**).

Figures 6.34 and 6.35 show the capillary pressure data measured on an untreated Reservoir B (plug#SR29-72) and a POH (plug#141) reservoir core. The measured capillary pressure data show that these rocks are water wet since both of the cores

imbibed water but did not imbibe oil even at capillary pressures as high as 178 psi. The Amott indices for both water and oil were 0 for both the rocks rock indicating they were neutral wet.

6.8 SUMMARY

Steady-state gas and condensate relative permeabilities were measured on several outcrop and reservoir cores with initial water saturation under reservoir conditions. The cores were then treated with a non-ionic polymeric fluoro-surfactant FC4430. Depending on reservoir conditions, mixtures of either 2-butoxyethanol/ethanol or 2-butoxyethanol/mthanol were used to deliver the surfactant to the core. Post-treatment gas and condensate relative permeabilities were then measured using the same gas mixture and under the same conditions as the initial gas condensate flood. **Table 6.24 and 6.25** summarize the results of chemical treatment on Berea and reservoir cores presented in this chapter. Adsorption of the surfactant on the rock surface was measured for different surfactant concentrations in the treatment solution. Wettability of the treated rocks was also determined by measuring the USBM wettability index using a centrifuge.

The major conclusions of this chapter are:

1. Reservoir and outcrop sandstone rocks with connate water were successfully treated with FC4430 delivered in a 2-butoxyethanol/ethanol mixture. Chemical treatment increased the relative permeabilities of both gas and oil by almost a factor of 2.
2. Chemical treatment showed an improvement factor of more than 2 for surfactant concentrations ranging from 0.1% and 2%.

3. Adsorption of the surfactant on the rock surface has been successfully measured. The results show that the retention of surfactant on the rock surface is on the order of 1-3 mg/gm of rock depending on surfactant concentration in the treatment solution.
4. The centrifuge test data show that the USBM wettability index for the treated cores is close to zero implying that the chemical treatment makes them neutral or mixed-wet.
5. Some field cores that were not initially water-wet showed no improvement in the gas relative permeability. This is consistent with the interpretation that the treatment works by changing the wettability of the cores to intermediate wetness.
6. The final gas permeability was the same as the original permeability of the core indicating the treatment does not cause any damage to rocks.

Table 6.1: Synthetic Bruce Reservoir brine

Component	g/l
CaCl ₂ (6H ₂ O)	7.72
MgCl ₂ (6H ₂ O)	1.67
KCl	0.659
NaCl	64.541

Table 6.2: Summary of chemical treatment on Berea sandstone cores at 175°F at
S_{wi}=19%

	Expt - 21	Exp - 28	Exp - 30
k _g , md	162	226	218
Surfactant	FC4430	FC4430	X3
Treatment solution	2% FC4430, 69% 2-butoxyethanol, 29% ethanol	2% FC4430, 49% 2-butoxyethanol, 49% ethanol	2% X3, 69% 2-butoxyethanol, 29% ethanol
Core Pressure, psig	1985	420	420
PVT Ratio	0.96	2.69	2.69
capillary number	3.29x10 ⁻⁵	5.38x10 ⁻⁵	1.78x10 ⁻⁵
k _{rg} before treatment	0.045	0.085	0.065
k _{ro} before treatment	0.047	0.032	0.025
k _{rg} after treatment	0.087	0.143	0.123
k _{ro} after treatment	0.091	0.053	0.047
Improvement Factor	1.93	1.68	1.88

Table 6.3: Properties of Bruce reservoir cores and characteristics of chemical treatment

	Exp - 23	Exp - 24	Exp - 27	Exp - 45
Plug#	1 and 3	7	9	8
k_g , md	1222	-	-	131.2
S_{wi} , %	19	22	12	19
$k_g (S_{wi})$, md	993.5	58	39.1	122.2
k_g , md after treatment	1201	71.8	42.3	101.5
Porosity, %	21.6	15	15	15.3
Length, inch	6.56	3.36	3.72	3.68
Dia, inch	1	1	1	1
Treatment Solution	2% FC4430, 69% 2-butoxyethanol, 29% ethanol			

Table 6.4: Comparison of Bruce reservoir and synthetic fluid properties at 175°F

Fluid Properties	Reservoir Fluid				Lab Fluid			
	1930 psig		460 psig		1930 psig		460 psig	
	Gas	Oil	Gas	Oil	Gas	Oil	Gas	Oil
μ (cp)	0.018	0.6	0.02	0.7	0.017	0.2	0.013	0.37
Volume fraction	0.90	0.10	0.98	0.016	0.92	0.08	0.98	0.015
IFT (dyne/cm)	3.165		13.9		3.1		12.13	

Table 6.5: Summary of chemical treatment on Bruce reservoir core#7 at 175°F (Exp #24)

	Core Pressure, psig	
	1930	460
PVT Ratio	0.96	2.37
capillary number, Nc	2.05×10^{-5}	8.66×10^{-6}
k_{rg} before treatment	0.067	0.102
k_{ro} before treatment	0.070	0.043
k_{rg} after treatment	0.118	0.209
k_{ro} after treatment	0.124	0.88
Improvement Factor	1.75	2.05

Table 6.6: Summary of chemical treatment on high permeability Bruce reservoir cores 1 and 3 at 175°F (Exp #23)

k_g , md	1222
k_g , md after treatment	1201
Core Pressure	1985
PVT Ratio	0.96
capillary number, Nc	7.63×10^{-5}
k_{rg} before treatment	0.04
k_{ro} before treatment	0.042
k_{rg} after treatment	0.061
k_{ro} after treatment	0.064
Improvement Factor	1.53

Table 6.7: Effect of chase gas on chemical treatment of Bruce reservoir core at 175°F
(Exp #27)

k_{gs} (S_{wi}) md	39.1
k_{gs} md after treatment	42.3
Core Pressure	550
PVT Ratio	2.03
capillary number, N_c	1.04×10^{-5}
k_{rg} before treatment	0.063
k_{ro} before treatment	0.031
k_{rg} after treatment	0.110
k_{ro} after treatment	0.054
Improvement Factor	1.75

Table 6.8: Effect of chemical treatment on oil-wet Bruce reservoir core at 175°F (Exp #45)

k_{gs} (S_{wi}) md	131.2
k_{gs} md after treatment	101.5
Core Pressure	393
PVT Ratio	2.77
capillary number, N_c	1.72×10^{-5}
k_{rg} before treatment	0.069
k_{ro} before treatment	0.025
k_{rg} after treatment	0.099
k_{ro} after treatment	0.036
Improvement Factor	1.44

Table 6.9: Comparison of pre-treatment and corrected post-treatment relative permeabilities for Exp #45

	Pre-treatment	Post-treatment based on initial permeability	Post-treatment based on final permeability	Improvement Factor
k_{rg}	0.069	0.099	0.128	1.86
k_{ro}	0.025	0.036	0.046	

Table 6.10 Properties of Hatter's Pond reservoir cores and experimental conditions

Plug#	18331A and 18331B
Length, inches	5.52
k_g , md	3.64
Porosity, %	9.30
S_{wi} , %	20
k_g , (S_{wi}) md	1.74
Temperature, °F	308
Core Pressure, psig	1140
PVT ratio	1.12

Table 6.11- Comparison of Hatter's Pond reservoir and synthetic fluid properties at 308°F and 1140 psig

	Reservoir Fluid		Lab Fluid	
	Gas phase	Oil phase	Gas phase	Oil phase
μ (cp)	0.017	0.174	0.017	0.153
Volume fraction	0.878	0.122	0.912	0.088
IFT (dyne/cm)	1.29		3.63	
Critical Point	308.2°F, 3013 psig		309.2°F, 3126 psig	

Table 6.12- Composition of characterized Hatter's Pond reservoir fluid

Component	Mole %
N ₂	2.830
CO ₂	6.130
C1	46.250
C2-C3	16.240
C4-C6	14.390
C7-C9	10.070
C10-C13	3.940
C14-C60	0.150

Table 6.13- Synthetic Hatter's Pond reservoir brine

Component	g/l
CaCl ₂ (6H ₂ O)	77.43
MgCl ₂ (6H ₂ O)	5.2
KCl	15.05
NaCl	89.92

Table 6.14: Summary of chemical treatment on Hatter's Pond reservoir cores at 308°F and 1140 psig (Exp #25)

k _g , md	3.64
Pre-flush	0.5 PV of 2-butoxyethanol/methanol (50/50)
First Treatment	2% FC4430, 69% 2-butoxyethanol, 29% methanol
k _{rg} before treatment	0.043
k _{ro} before treatment	0.038
k _{rg} after 1 st treatment	0.046
k _{ro} after 1 st treatment	0.041
Improvement Factor	1.08
Second Treatment	2% FC4430, 98% Methanol
k _{rg} after 2 nd treatment	0.042
k _{ro} after 2 nd treatment	0.038
Improvement Factor	0.99
Final permeability, md	1.12

Table 6.15: Characteristics and experimental conditions for experiments to study the effect of surfactant concentration on chemical treatment

	Exp-21	Exp-30	Exp-41	Exp-42
Core	Berea	Berea	Berea	Berea
Fluid	Fluid-4	Fluid-4	Flui-5	Flui-5
S_{wi} %	19	19	19	19
Temperature, °F	175	175	175	175
Core Pressure, psig	1985	420	420	420
Treatment solution	2% FC4430, 69% 2-butoxyethanol, 29% ethanol	2% X3, 69% 2-butoxyethanol, 29% ethanol	1% FC4430, 69.5% 2-butoxyethanol, 29.5% ethanol	0.1% FC4430, 69.9% 2-butoxyethanol, 30% ethanol

Table 6.16: Effect of surfactant concentration on improvement factor

	Surfactant wt%	Improvement Factor
Exp - 21	2	1.93
Exp - 30	2	1.88
Exp - 41	1	2.36
Exp - 42	0.1	2.18

Table 6.17: summary of chemical treatment with 1% surfactant concentration (Exp #41)

capillary number	Pre-Treatment		Post-Treatment		Improvement Factor
	k_{rg}	k_{ro}	k_{rg}	k_{ro}	
2.64×10^{-5}	0.057	0.022	0.135	0.052	2.36

Table 6.18: summary of chemical treatment with 0.1% surfactant concentration (Exp #42)

capillary number	Pre-Treatment		Post-Treatment		Improvement Factor
	k_{rg}	k_{ro}	k_{rg}	k_{ro}	
2.16×10^{-5}	0.071	0.027	0.154	0.059	2.18

Table 6.19: Experimental conditions for chemical treatments on Berea sandstone at 175°F to study the effect of shut-in time

	Exp #21	Exp #30	Exp #37
Fluid	Fluid-4	Fluid-4	Fluid-5
S_{wi} %	19	19	19
Pressure, psig	1985	420	410
Treatment solution	2% FC4430, 69% 2- butoxyethanol, 29% ethanol	2% X3, 69% 2- butoxyethanol, 29% ethanol	2% FC4430, 69% 2- butoxyethanol, 29% ethanol
Shut-in time	15	15	1
Improvement Factor	1.93	1.88	1.66

Table 6.20: Summary of chemical treatment done on Berea sandstone at 175°F with shut-in time of 1 hour (Exp-37)

Core Flow rate, cc/hr	Pre-Treatment		Post-Treatment		Improvement Factor
	k_{rg}	k_{ro}	k_{rg}	k_{ro}	
2682	0.096	0.036	0.160	0.06	1.66
5364	0.098	0.037	0.149	0.056	1.54

Table 6.21: List of reservoir cores used for wettability study using centrifuge

Sample No	Reservoir core	Status
1	POH (plug#141)	Untreated
2	Bruce (plug#3)	Treated
3	Hatter's Pond (plug# 18352A)	Untreated
4	Reservoir B (plug# SR29-72)	Untreated
5	Bruce (plug#10)	Untreated
6	Britannia (plug#52)	Treated

Table 6.22: Synthetic brines for Reservoir B and POH reservoir cores

	POH	Reservoir B
Component	g/l	g/l
CaCl ₂ (6H ₂ O)	-	49.52
MgCl ₂ (6H ₂ O)	0.06	2.8
KCl	1.91	-
NaCl	15.70	165.34

Table 6.23: Properties of reservoir cores and results of centrifuge tests

Sample no	1	2	3	4	5	6
k, md	0.23	1222	15	1	50-60	39.5
Length, in	1	1	1	1	1	1
Dia, in	1	1	1	1	1	1
Dry weight, gm	32.32	28.5	30.62	33.48	30.5	30.35
Brine saturated weight, gm	33.34	31.07	32.48	34.05	32.49	32.1
PV, cc	1.02	2.57	1.86	0.57	1.99	1.75
USBM wettability Index	-	0.05	-0.33	-	-0.11	0.08
WI	0	0.22	0	0	0	0
OI	0	0.13	0	0	0	0.14
RDI	0	0.09	0	0	0	-0.14

Table 6.24: Characteristics of Treatment solutions used to treat Berea and reservoir cores

Experiment no	Treatment Solution
21	2% FC4430, 69% 2-butoxyethanol, 29% ethanol
23	2% FC4430, 69% 2-butoxyethanol, 29% ethanol
24	2% FC4430, 69% 2-butoxyethanol, 29% ethanol
25	2% FC4430, 69% 2-butoxyethanol, 29% methanol
27	2% FC4430, 69% 2-butoxyethanol, 29% ethanol
28	2% FC4430, 49% 2-butoxyethanol, 49% ethanol
30	2% X3, 69% 2-butoxyethanol, 29% ethanol
37	2% FC4430, 69% 2-butoxyethanol, 29% ethanol

41	1% FC4430, 69% 2-butoxyethanol, 29% ethanol
42	0.1% FC4430, 69% 2-butoxyethanol, 29% ethanol
45	2% FC4430, 69% 2-butoxyethanol, 29% ethanol

Table 6.25: Summary of chemical treatment on Berea and Reservoir cores using FC4430

Experiment #	21	23	24	25	27	28	30	37	41	42	45
Rock	Berea	Bruce	Bruce	HP	Bruce	Berea	Berea	Berea	Berea	Berea	Bruce
Temperature, °F	175	175	175	308	175	175	175	175	175	175	175
Pressure, psig	1985	1985	1930	1140	550	420	420	410	420	420	393
k, md	162	1222	58.1	3.6	39.1	226	218	236	269	226	131.2
S _{wi} , %	19	19	22	20	12	19	19	19	19	19	19.3
Salinity, ppm	73000	73000	*	180000	*	73000	73000	73000	73000	73000	73000
q _{core} , cc/hr	536	1071	520	1512	1029	2107	2014	2682	2714	2714	2243
N _c	3.29× 10 ⁻⁵	7.63× 10 ⁻⁵	2.05× 10 ⁻⁵	6.17× 10 ⁻⁶	5.98× 10 ⁻⁶	5.38× 10 ⁻⁵	1.78× 10 ⁻⁵	1.56× 10 ⁻⁵	2.64× 10 ⁻⁵	2.16× 10 ⁻⁵	1.72× 10 ⁻⁵
FC4430 wt%	2	2	2	2	2	2	2	2	1	0.1	2
Treatment rate, cc/hr	224	196	160	24-56	160	128	128	100	112	128	80
Shut-in time, hrs	15	15	15	15	18	15	15	1	15	15	12
k _{rg} pre treatment	0.045	0.040	0.067	0.043	0.063	0.085	0.065	0.096	0.057	0.071	0.069
k _{ro} pre treatment	0.047	0.042	0.070	0.038	0.031	0.032	0.025	0.036	0.022	0.027	0.025
k _{rg} post treatment	0.087	0.061	0.118	0.046	0.110	0.143	0.123	0.160	0.135	0.154	0.099
k _{ro} post treatment	0.091	0.064	0.124	0.041	0.054	0.053	0.047	0.060	0.052	0.059	0.036
IF	1.93	1.53	1.75	1.07	1.75	1.68	1.88	1.66	2.36	2.18	1.44

* Salinity not known as cores were received with initial water saturation

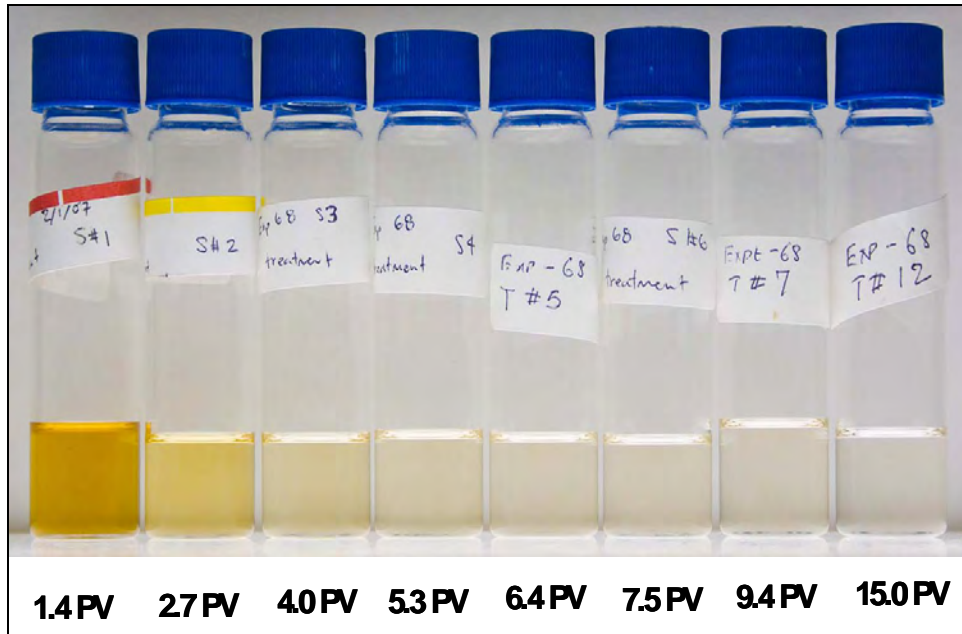


Figure 6.1: Visual inspection of effluent samples during treatment flood using 70/30 2-butoxyethanol/ethanol (Exp #29)

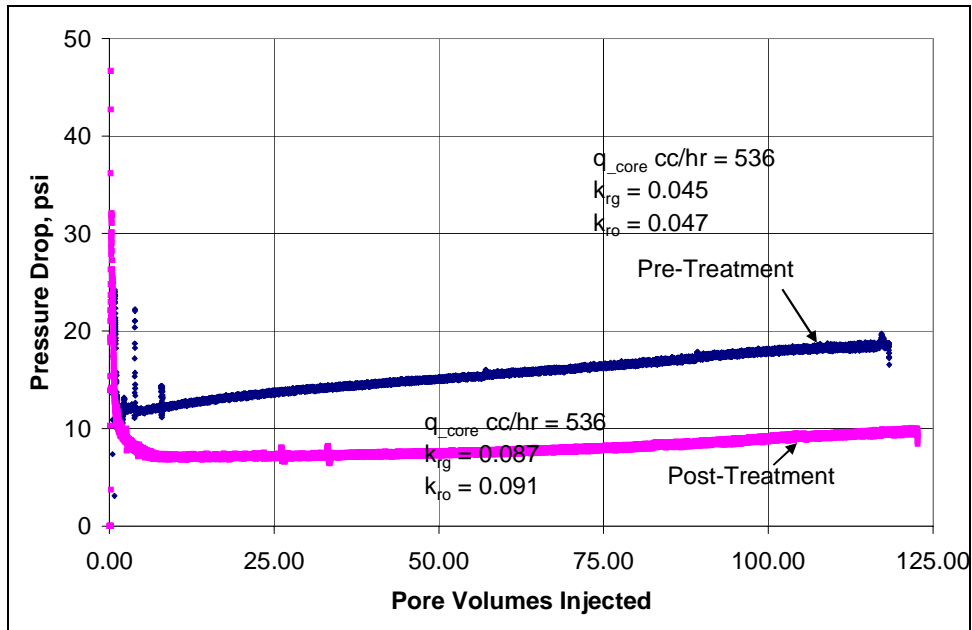


Figure 6.2: Effect of chemical treatment on Berea sandstone at $Sw_i=19\%$ using 2% FC4430 in a mixture of 70/30 2-butoxyethanol and ethanol (Exp#21)

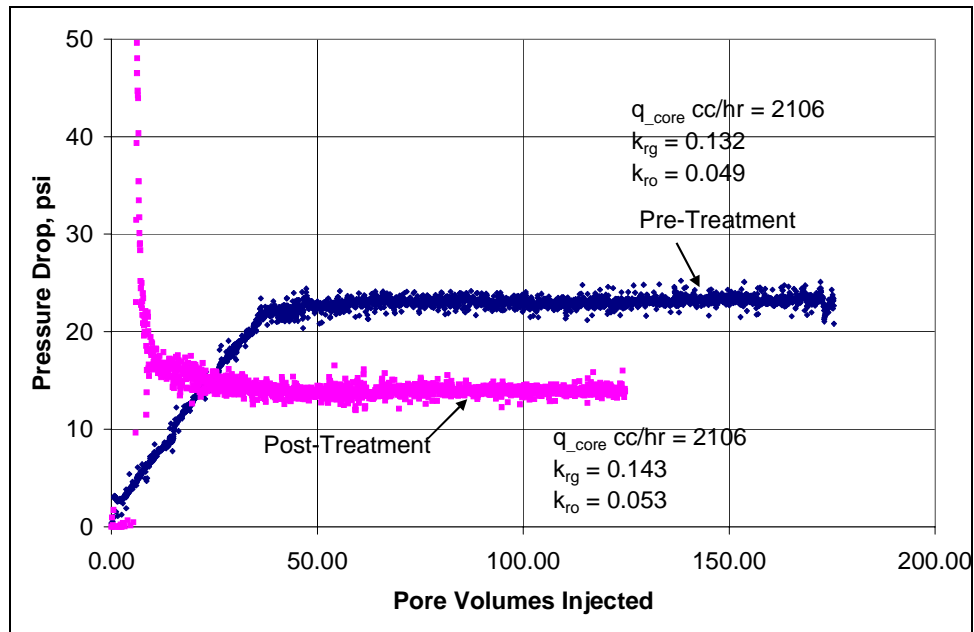


Figure 6.3: Effect of chemical treatment on Berea sandstone at $Sw_i=50\%$ using 2% FC4430 in a mixture of 50/50 2-butoxyethanol and ethanol (Exp#28)

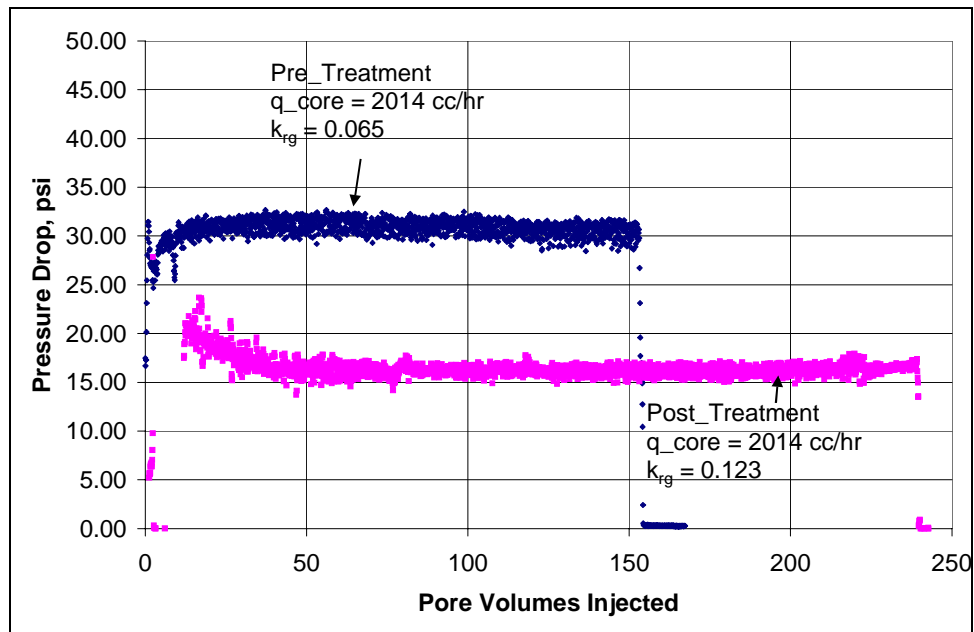


Figure 6.4: Effect of chemical treatment on Berea sandstone at $Sw_i=19\%$ using 2% FC4430 in a mixture of 70/30 2-butoxyethanol and ethanol (Exp#30)

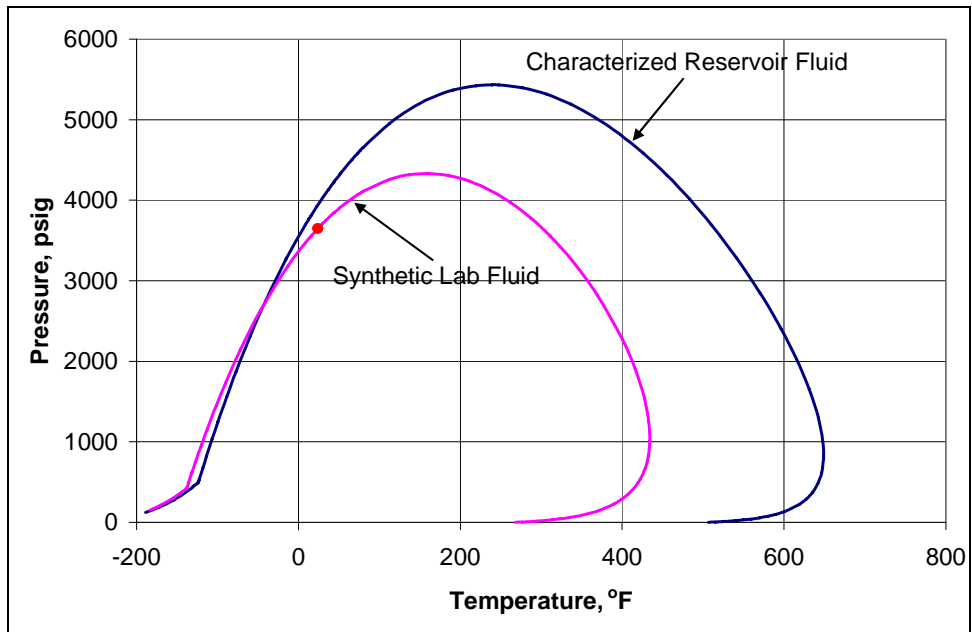


Figure 6.5: Calculated phase envelopes for characterized reservoir fluid and synthetic lab fluid

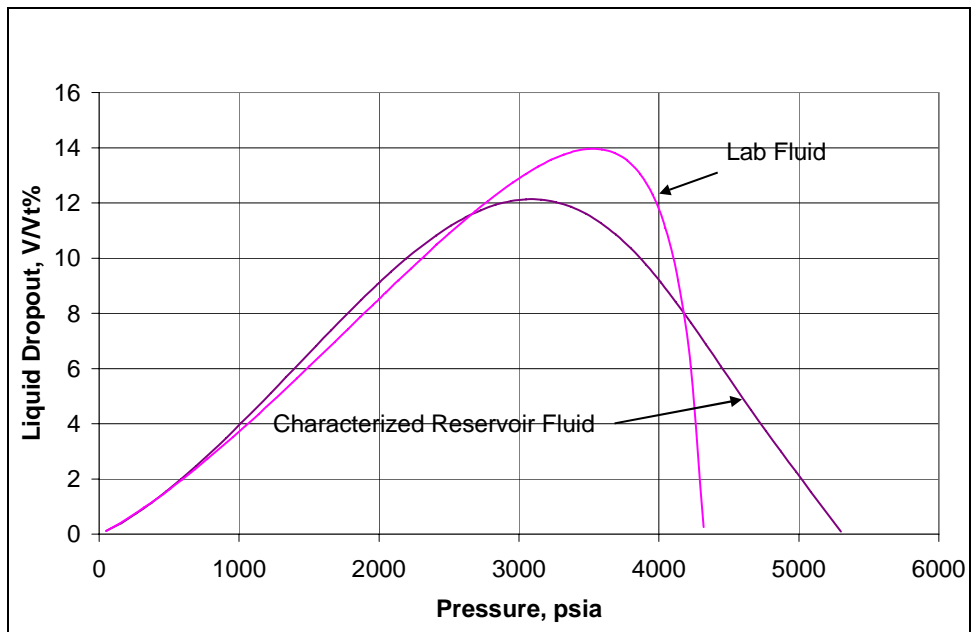


Figure 6.6: Calculated liquid dropout curves for characterized reservoir fluid and synthetic lab fluid at 175°F

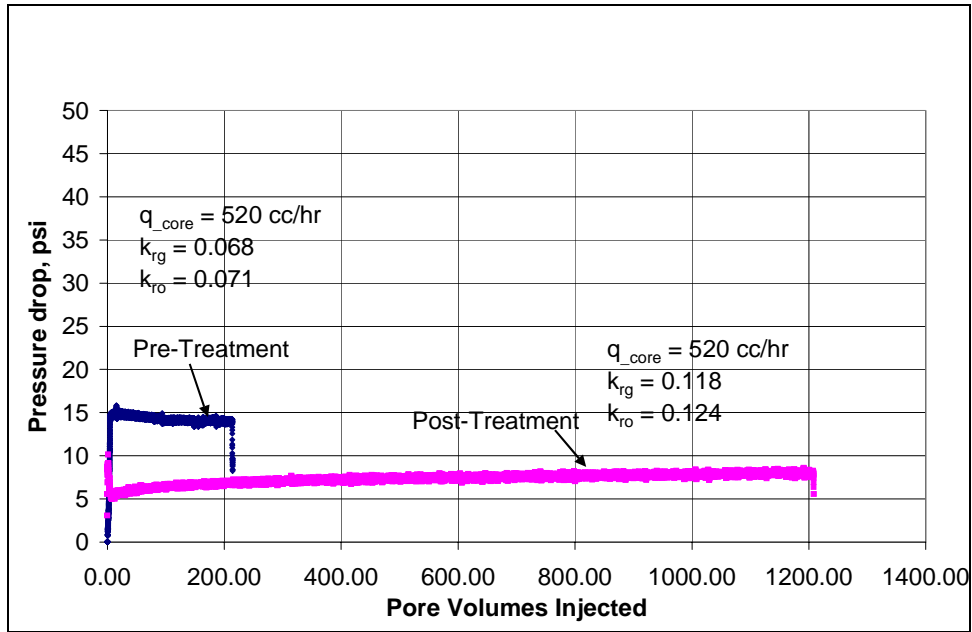


Figure 6.7: Effect of chemical treatment on Bruce reservoir core at 175°F and 1930 psig using 2% FC4430 in 70/30 2-butoxyethanol and ethanol (Exp#24)

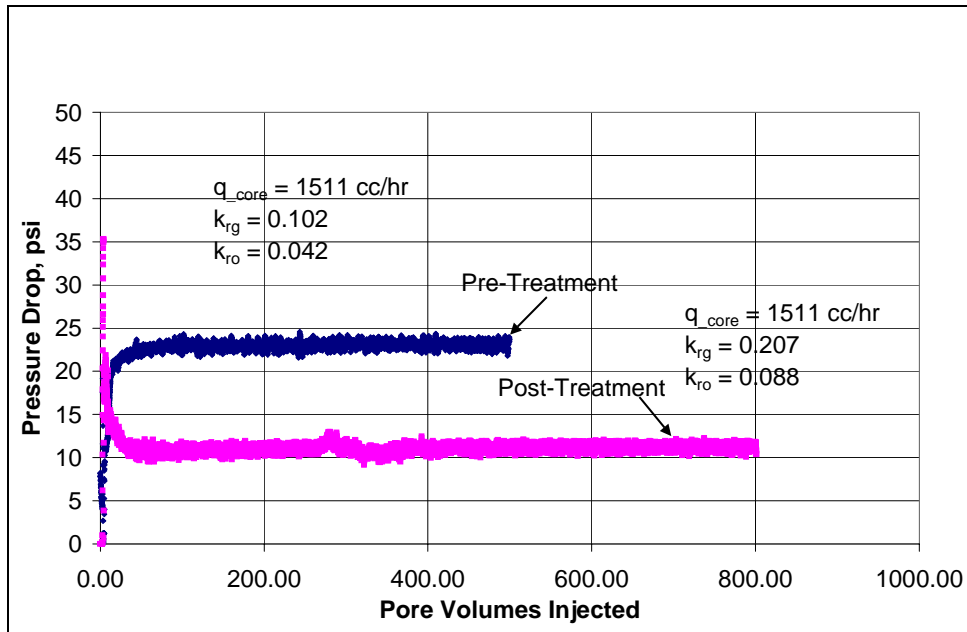


Figure 6.8: Effect of chemical treatment on Bruce reservoir core at 175°F and 460 psig using 2% FC4430 in 70/30 2-butoxyethanol and ethanol (Exp#24)

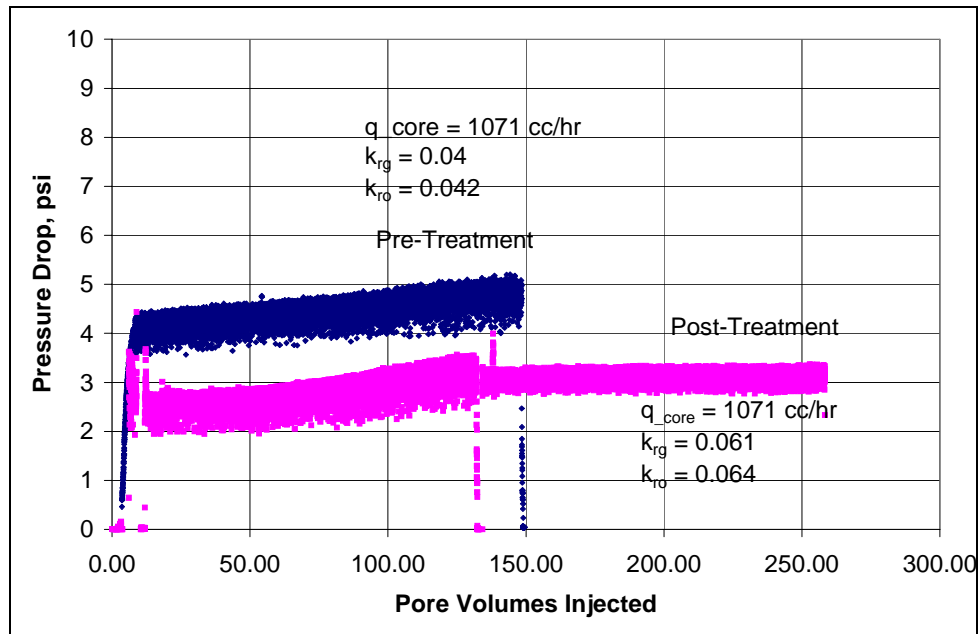


Figure 6.9: Effect of chemical treatment on a high permeability Bruce reservoir core at 175°F and 1985 psig (Exp#23)

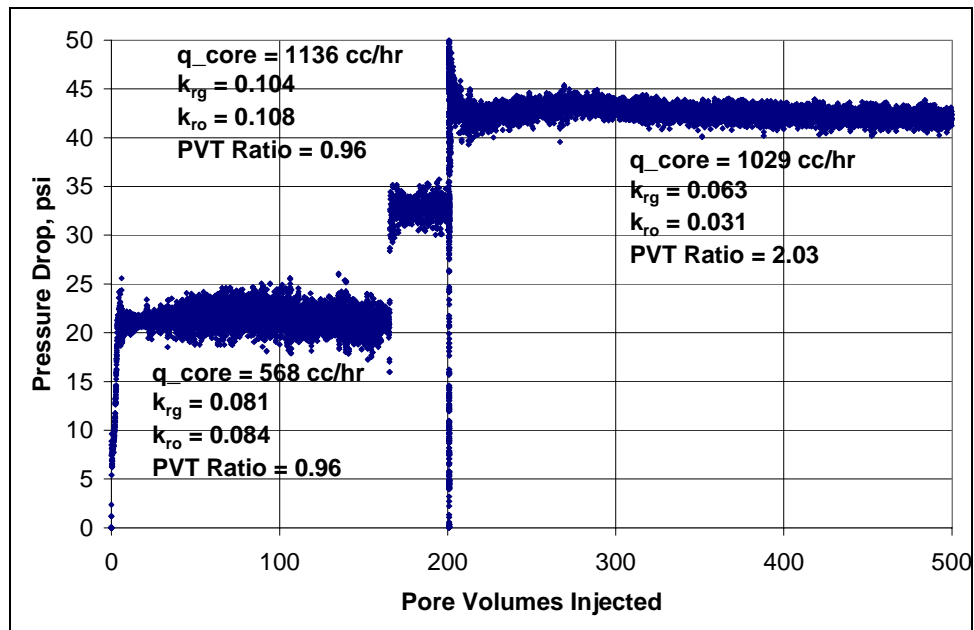


Figure 6.10: Condensate buildup in a Bruce reservoir core at different PVT ratios (Exp#28)

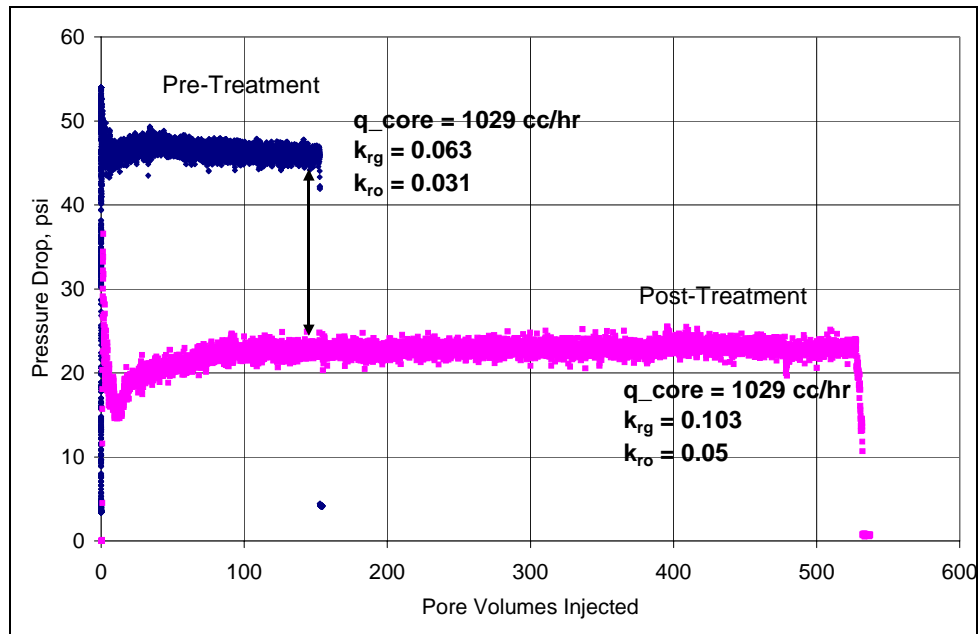


Figure 6.11: Effect of chase gas injection on chemical treatment of Bruce reservoir core at 175°F and 550 psig (Exp#27)

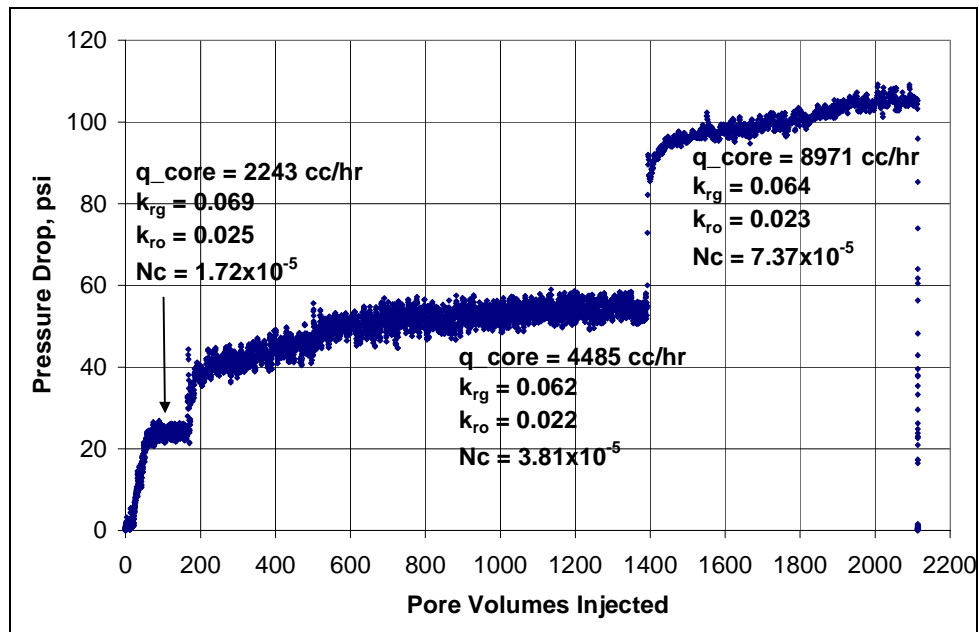


Figure 6.12: Effect of capillary number and non-Darcy flow on condensate buildup in a Bruce reservoir core (Exp#45)

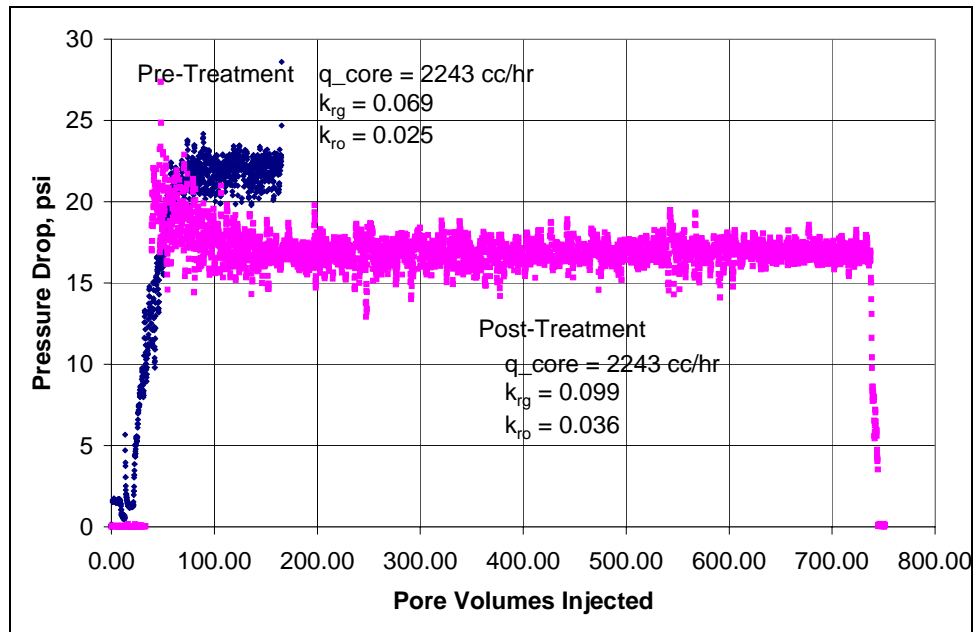


Figure 6.13: Effect of chemical treatment on an oil-wet Bruce reservoir core at 175°F and 393 psig (Exp#45)

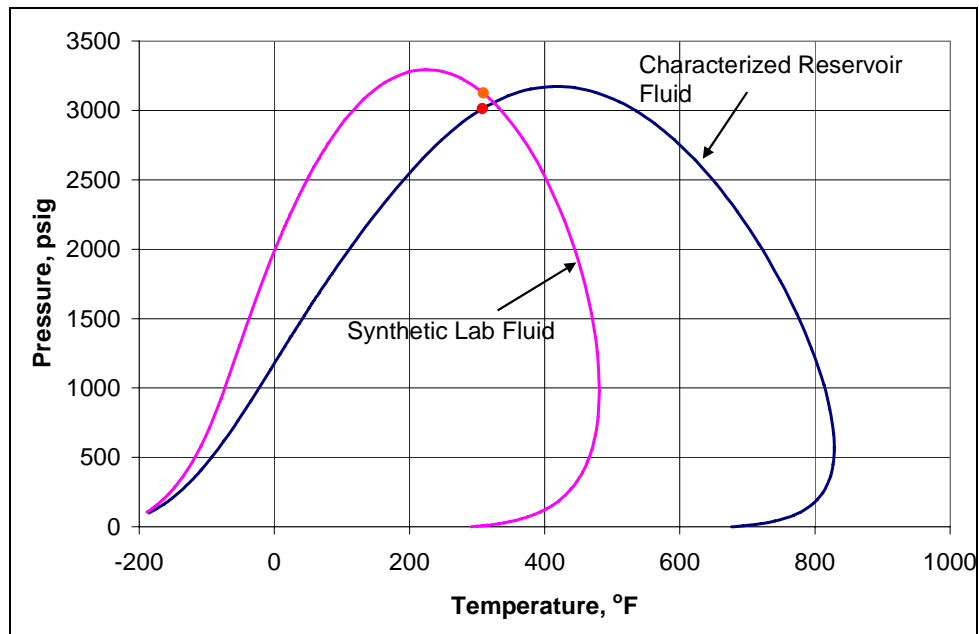


Figure 6.14: Calculated phase envelopes for characterized Hatter's Pond reservoir fluid and synthetic lab fluid

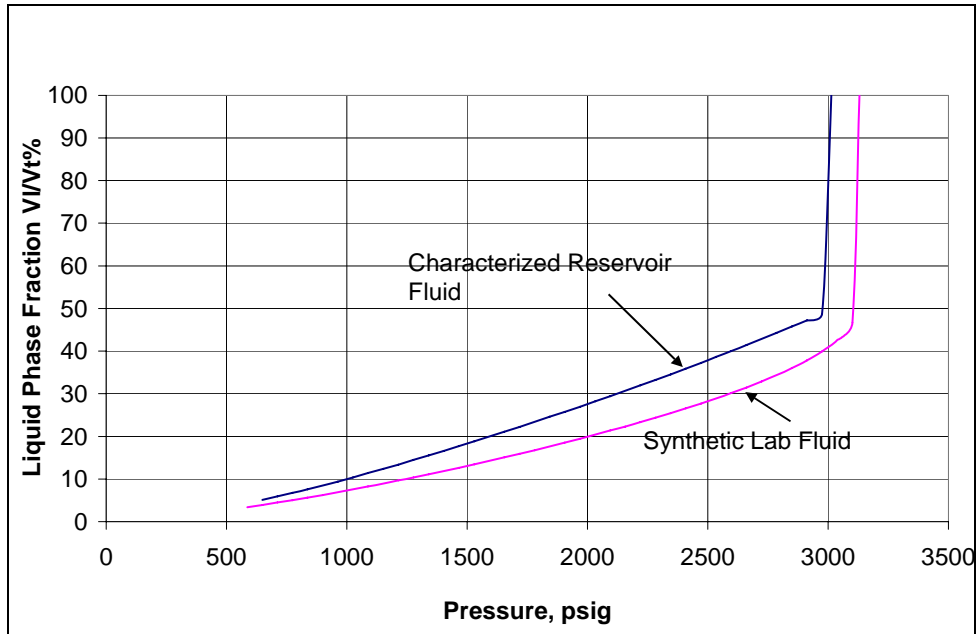


Figure 6.15: Calculated phase volume fractions for characterized Hatter's Pond reservoir fluid and synthetic lab fluid at 175°F

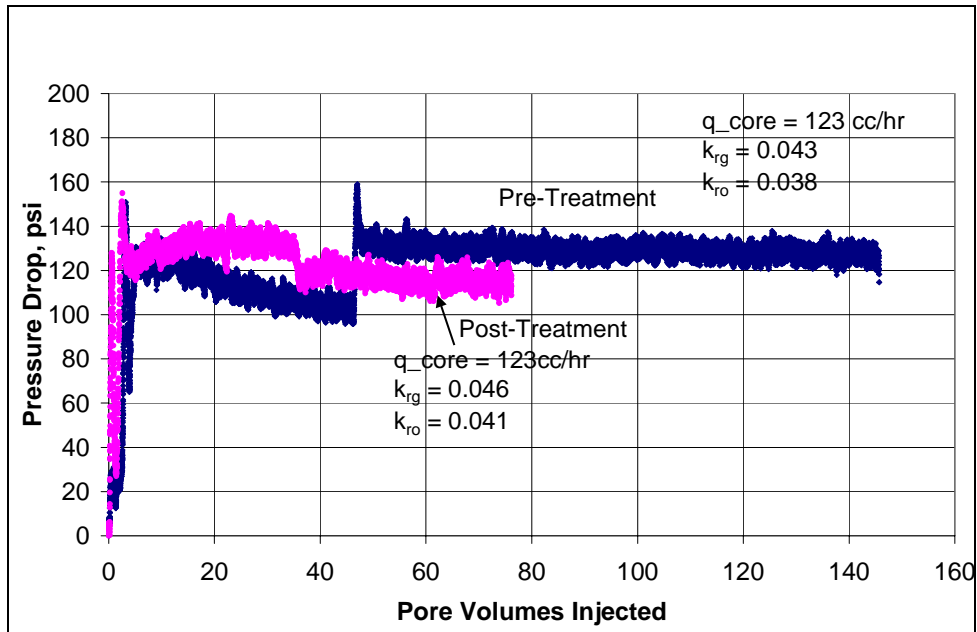


Figure 6.16: Effect of chemical treatment on an oil-wet Hatter's Pond reservoir core at 308°F and 1140 psig (Exp#25)

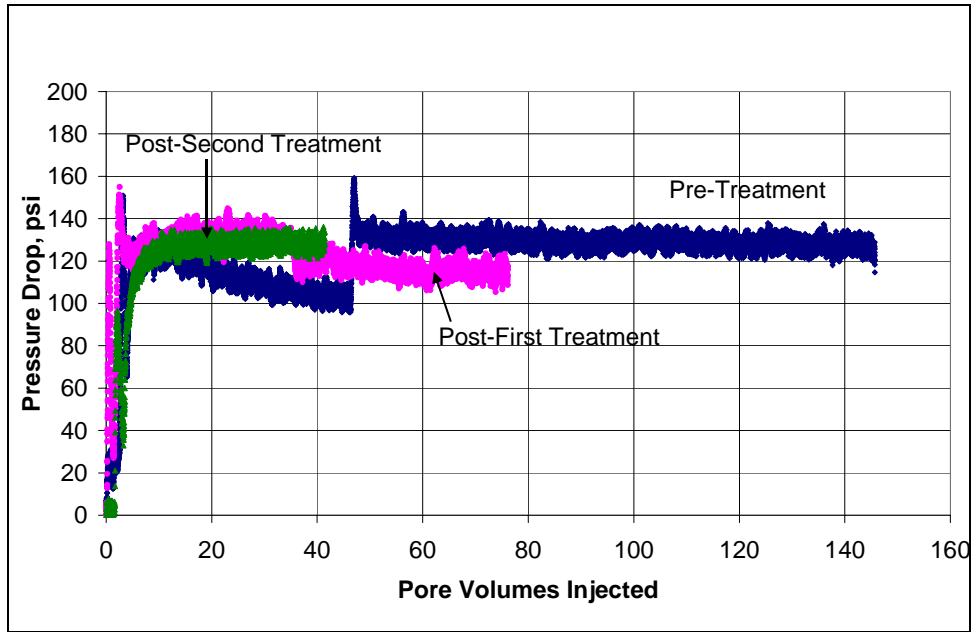


Figure 6.17: Effect of second chemical treatment on an oil-wet Hatter's Pond reservoir core at 308°F and 1140 psig (Exp#25)

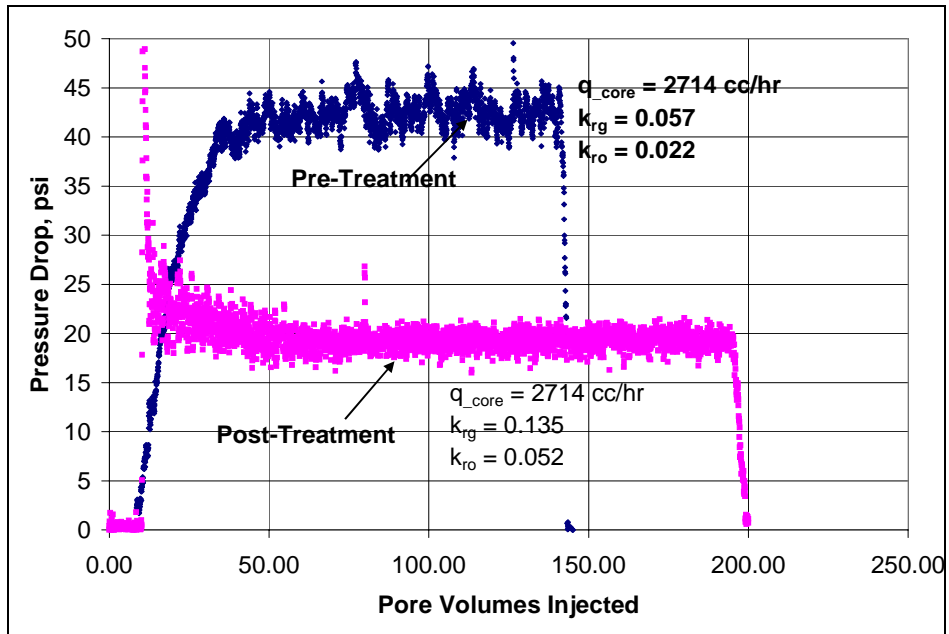


Figure 6.18: Effect of chemical treatment with 1% FC4430 on Berea sandstone at 175°F and 420 psig (Exp#41)

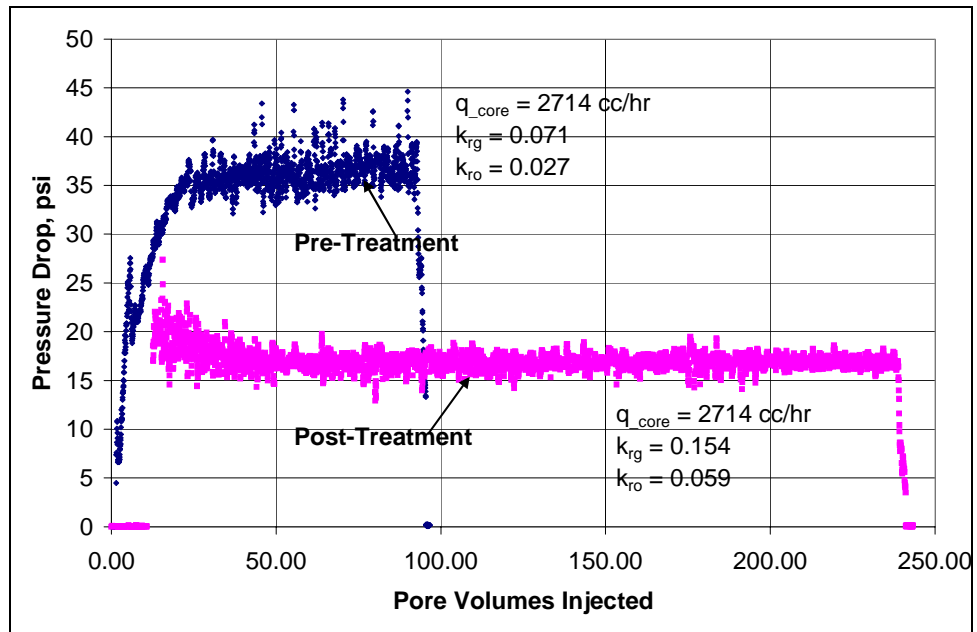


Figure 6.19: Effect of chemical treatment with 0.1% FC4430 on Berea sandstone at 175°F and 420 psig (Exp#42)

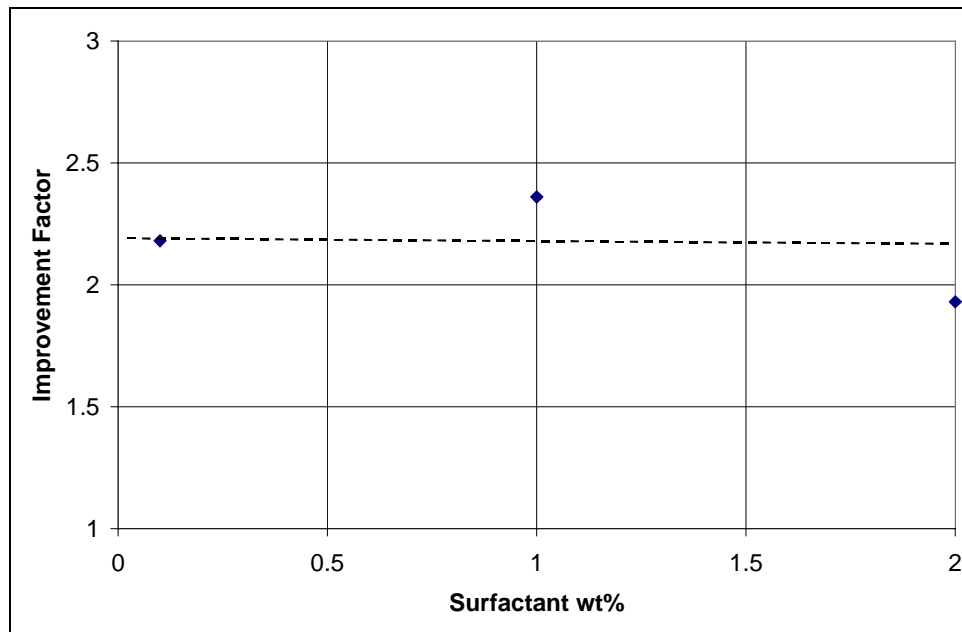


Figure 6.20: Effect of surfactant (FC430) concentration in treatment solution on improvement factor

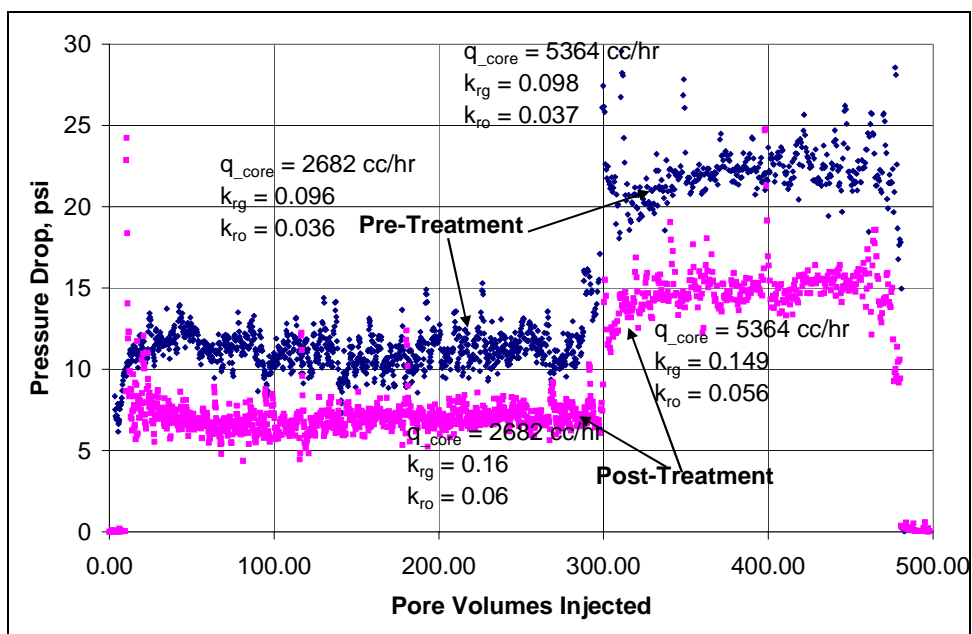


Figure 6.21: Effect of chemical treatment on Berea sandstone at 175°F and 410 psig with 1 hour of shut-in time (Exp#37)

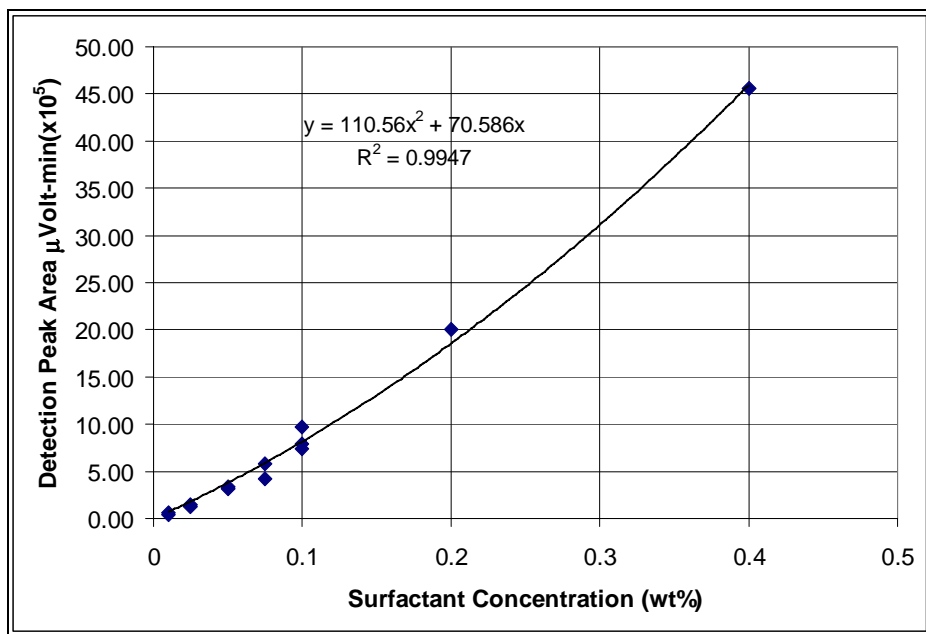


Figure 6.22: Calibration curve for detecting FC440 concentration using HPLC

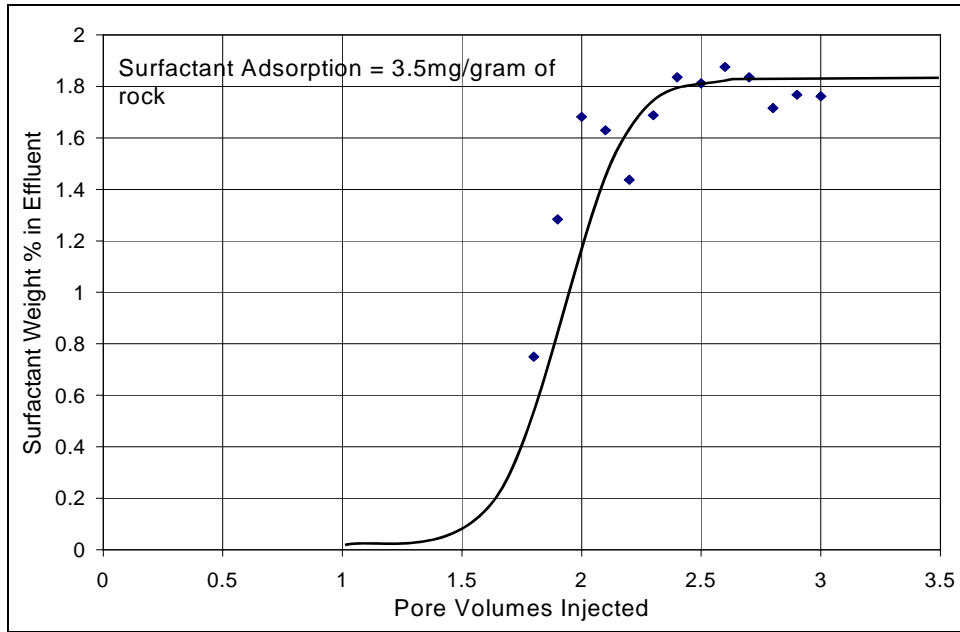


Figure 6.23: Surfactant concentration profile in effluent while treating a dry Berea core at 250°F with treatment solution containing 2wt% surfactant (exp-32)

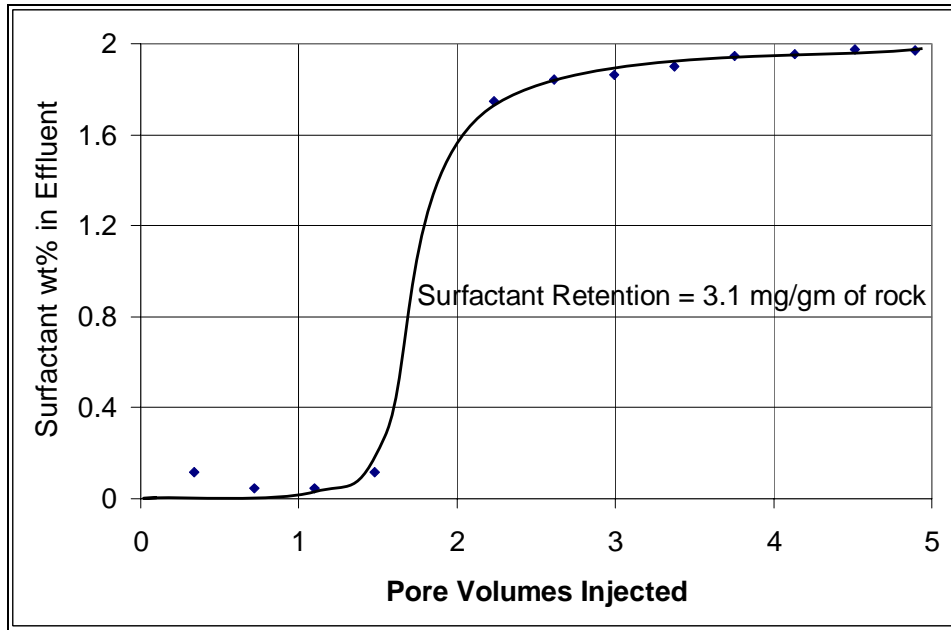


Figure 6.24: Surfactant concentration profile in effluent while treating a Berea core with $S_{wi}=19\%$ at 175°F with treatment solution containing 2wt% surfactant (exp-37)

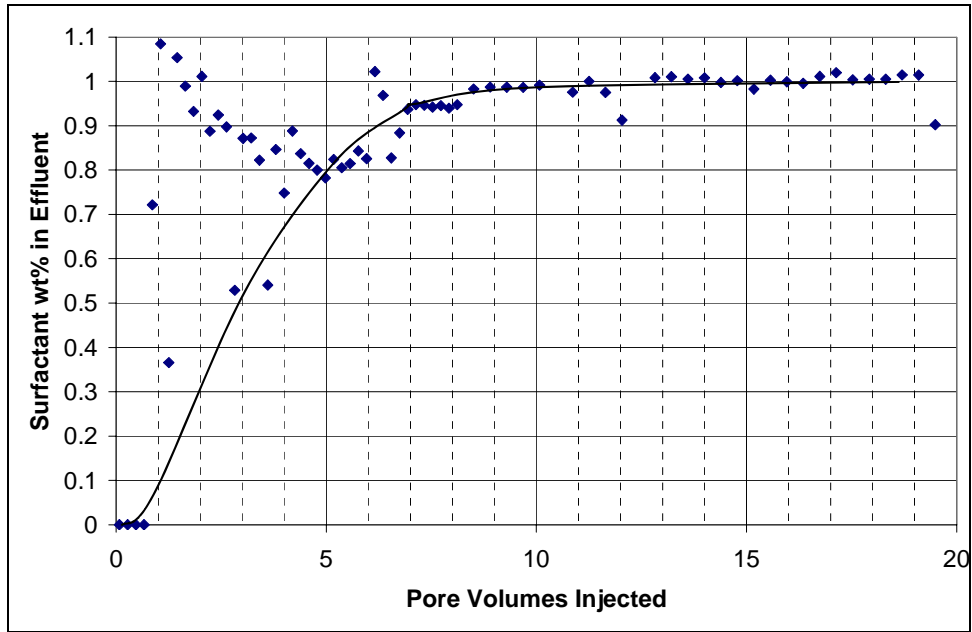


Figure 6.25: Surfactant concentration profile in effluent while treating a Berea core ($S_{wi}=19\%$) at 175°F with treatment solution containing 1wt% surfactant (exp-41)

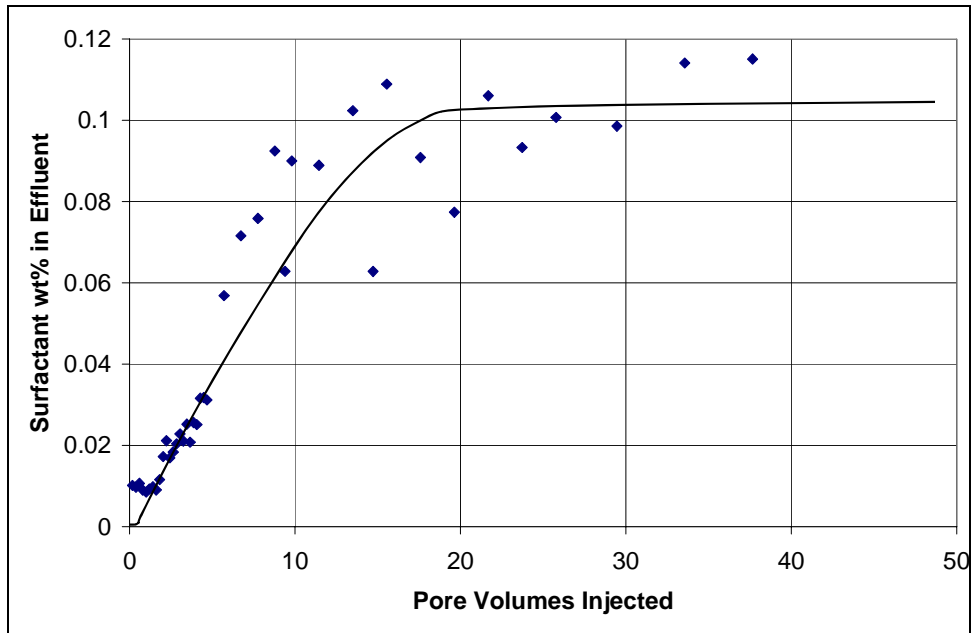


Figure 6.26: Surfactant concentration profile in effluent while treating a Berea core ($S_{wi}=19\%$) at 175°F with treatment solution containing 0.1wt% surfactant (exp-42)

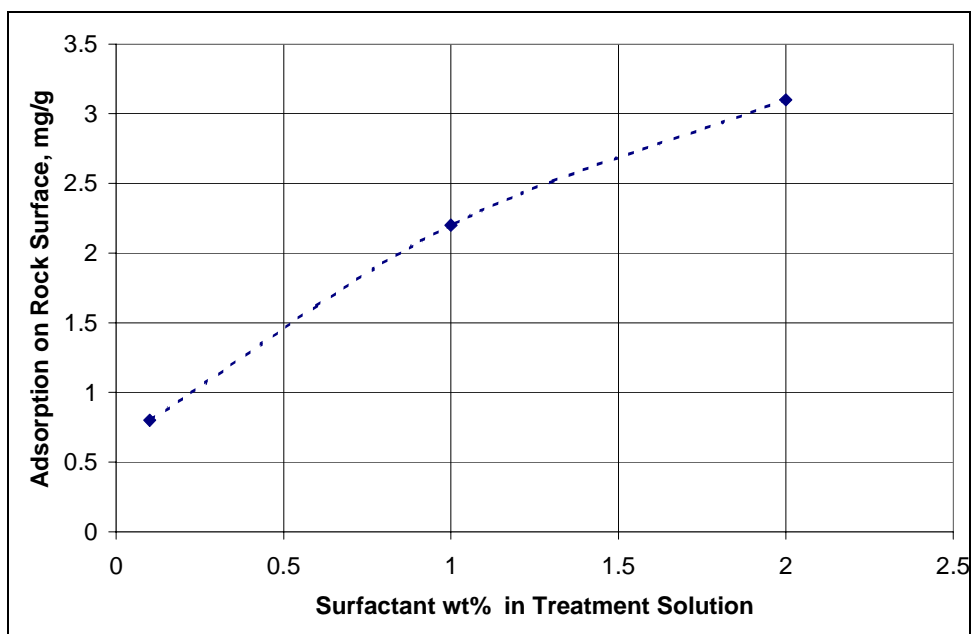


Figure 6.27 Effect of surfactant concentration on adsorption on rock surface

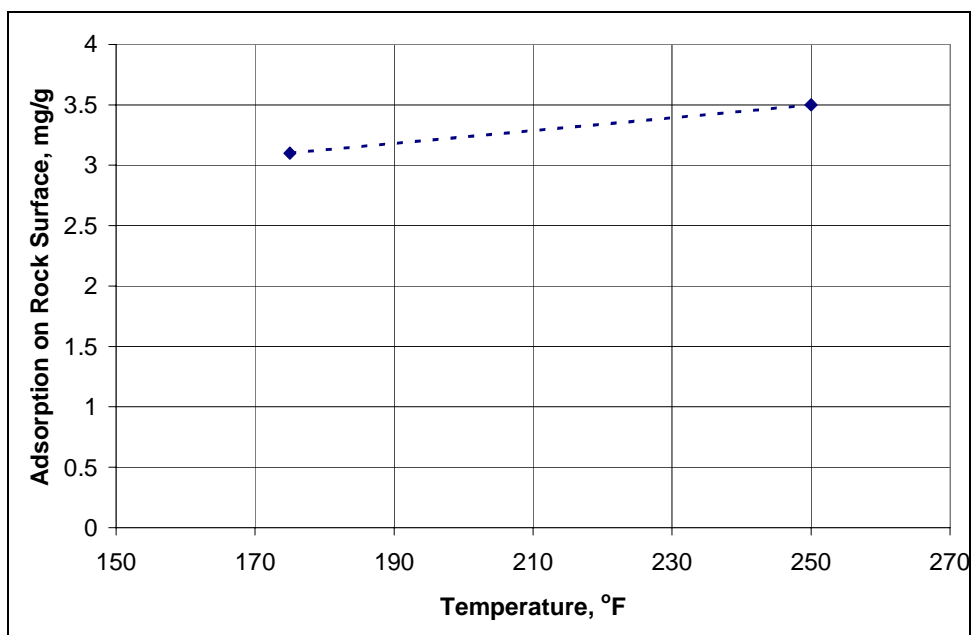


Figure 6.28 Effect of temperature on surfactant adsorption on rock surface for treatment solution containing 2% FC4430

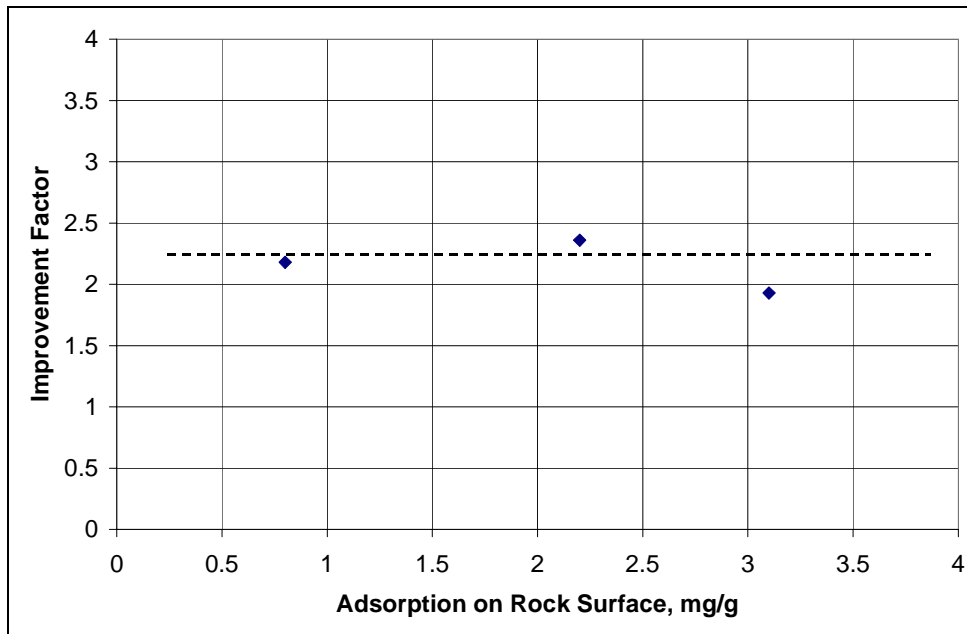


Figure 6.29 Effect of surfactant adsorption on improvement factor

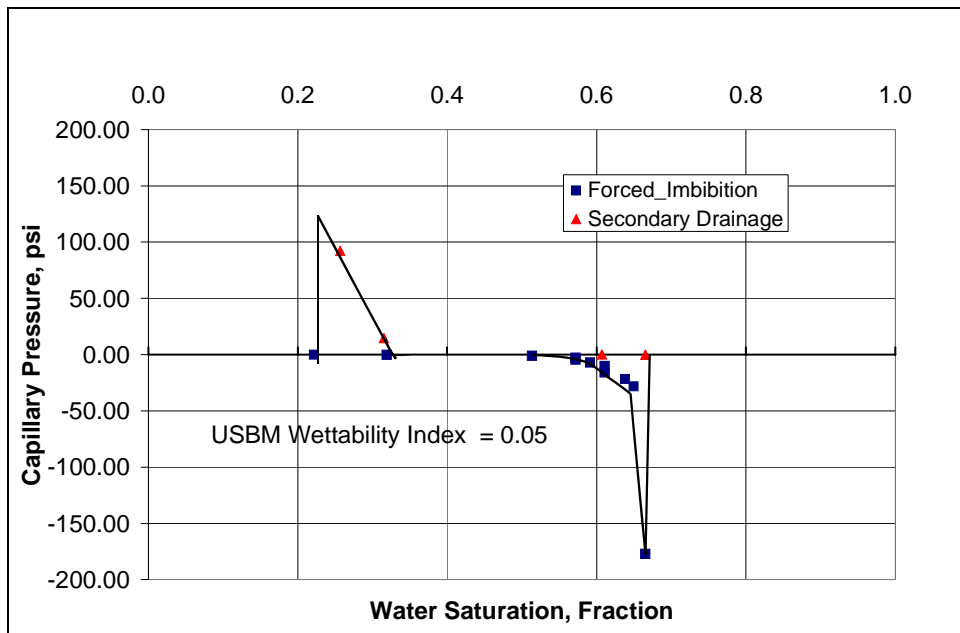


Figure 6.30 Imbibition and drainage capillary pressure data measured on a treated Bruce reservoir core

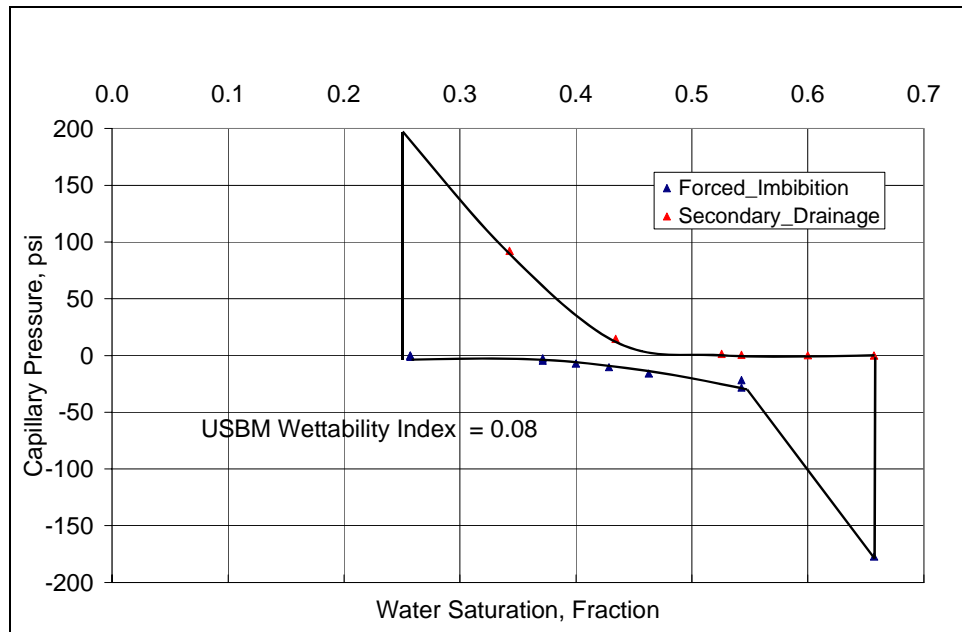


Figure 6.31 Imbibition and drainage capillary pressure data measured on a treated Britannia reservoir core

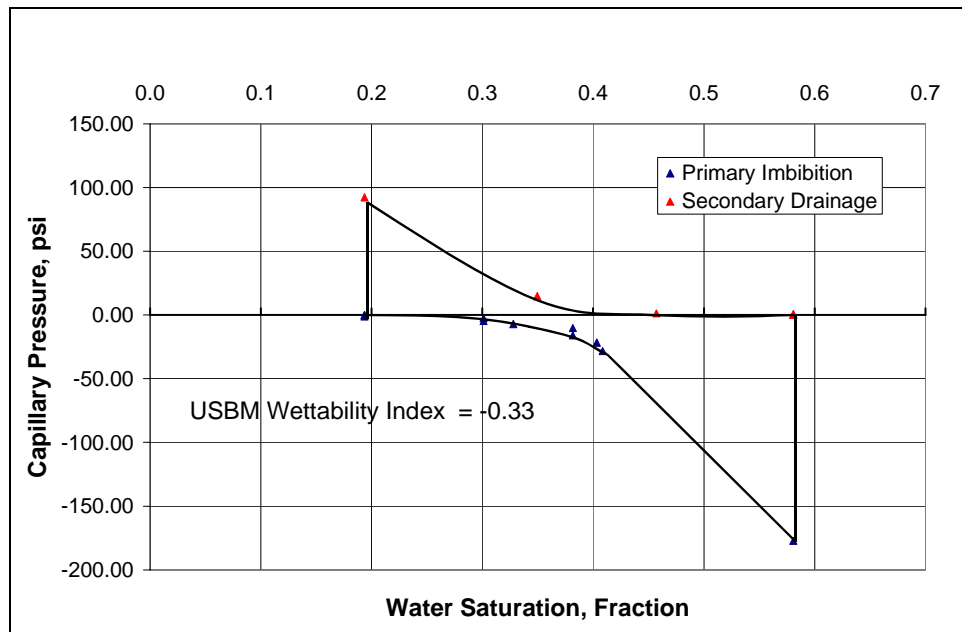


Figure 6.32 Imbibition and drainage capillary pressure data measured on an Untreated Hatter's Pond reservoir core

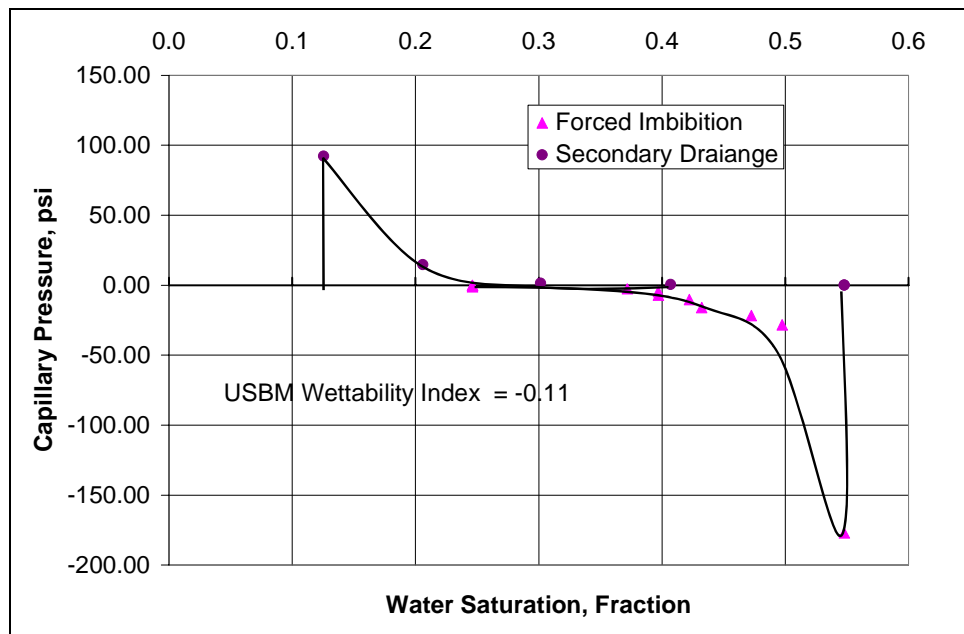


Figure 6.33 Imbibition and drainage capillary pressure data measured on an Untreated Bruce reservoir core

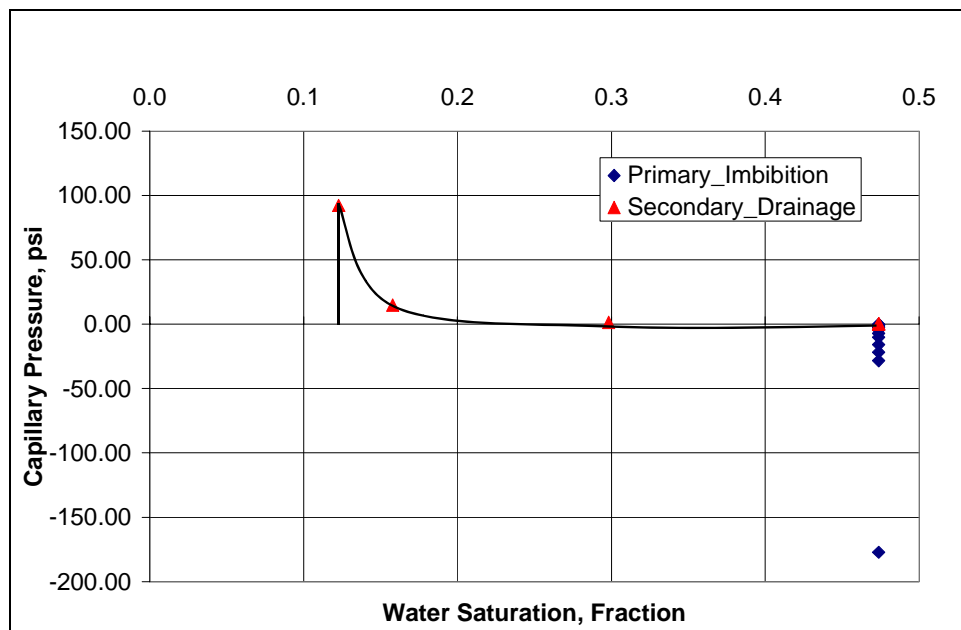


Figure 6.34 Imbibition and drainage capillary pressure data measured on an Untreated Reservoir B reservoir core

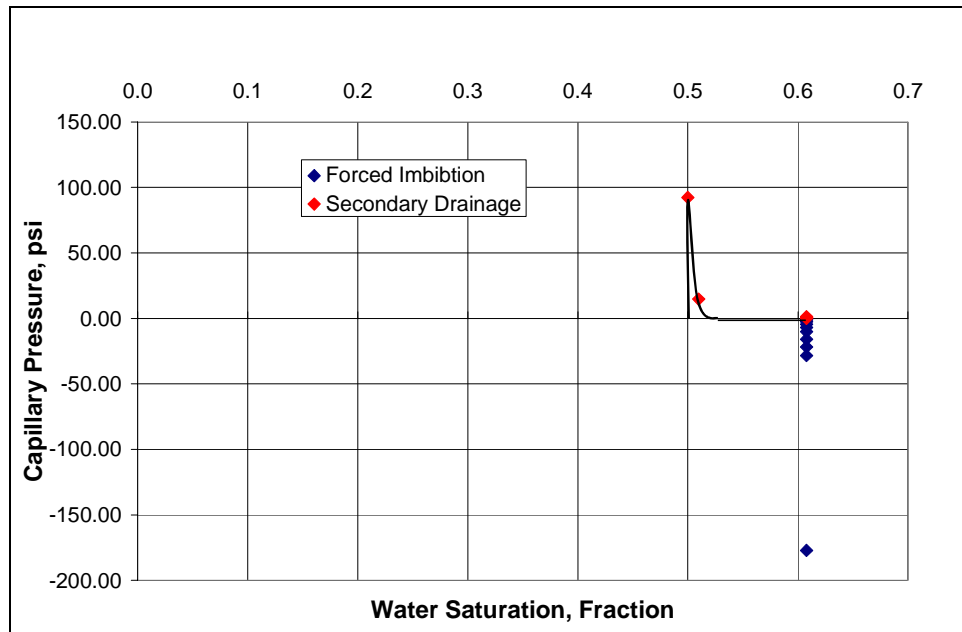


Figure 6.35 Imbibition and drainage capillary pressure data measured on an Untreated POH reservoir core

Chapter 7: Remediation of Water Blocking in Gas Condensate Reservoirs by Chemical Treatment

This chapter presents the results of chemical treatments done to reduce the damage caused by the combined effect of water and condensate blocking in gas condensate reservoirs. The first section presents an introduction to the problem of water blocking in gas and gas condensate reservoirs. The next section describes the effect of high water saturation and mobile water on gas relative permeability in low permeability reservoir cores and high permeability Berea sandstone cores. The third section presents the results of chemical treatments done using non-ionic polymeric fluoro-surfactant FC4430 and X3 to remove the damage caused by water blocking on both reservoir and Berea sandstone cores. Finally, the effect of a non-fluorinated surfactant in removing the damage caused by condensate and water blocking is described.

7.1 INTRODUCTION

Water blocking can cause significant loss in deliverability of gas and gas condensate wells. Liquids, including both condensate and water, are trapped in pores by capillary forces causing a significant reduction in gas relative permeability and this reduces well productivity. Water can be introduced into the formation during drilling, completion, or workover operations. Water can also flow into a gas-bearing zone from a high-pressure aquifer or a water-bearing zone.

The trapped water saturation in the near wellbore region is a function of the capillary pressure and the drawdown in the well. **Figure 7.1** shows a schematic of a capillary pressure curve expressing water saturation as a function of capillary pressure. Water saturation in the near wellbore region depends on the pressure gradient as shown in

Figure 7.1. A higher pressure gradient can mobilize more water and result in lower water saturation. On the other hand, lower pressure gradients can result in water saturations higher than the connate water saturation in the formation.

Water invasion along with condensate dropout in a gas bearing formation can cause a significant reduction in productivity over a long period of time. The loss in productivity can be even more pronounced in low permeability reservoirs as very high water saturations can be trapped in these reservoirs because of high capillary forces. High water saturations can also build up around the wellbore in depleted reservoirs where the pressure gradient is not high enough to mobilize the trapped water.

7.2 EFFECT OF HIGH WATER SATURATION AND MOBILE WATER ON GAS RELATIVE PERMEABILITY:

Results presented in Chapters 4 and 6 show that condensate accumulation in both high and low permeability cores decreased gas relative permeability by more than 90%. In the following section, the effect of water blocking along with condensate blocking on gas relative permeability is presented. Effects of both high water saturation and mobile water on gas and condensate relative permeabilities were analyzed.

7.2.1 Effect of high initial water saturation on an untreated reservoir core

This experiment (Exp# 35) was conducted on a Tunu reservoir core (plug#7) at 275°F to study the effect of water blocking on a low permeability reservoir core. Properties of the reservoir core are given in **Table 7.1** along with the experimental conditions representing the reservoir conditions. The model fluid was matched to the actual reservoir hydrocarbon fluid on the basis of liquid dropout, viscosity, interfacial tension, dew point pressure and the PVT ratio at reservoir temperatures and pressures.

Table 3.7 gives the composition of the synthetic gas mixture. **Figure 7.2** compares the calculated P-T phase diagram of the synthetic lab fluid and the characterized reservoir fluid. **Figure 7.3** compares the calculated liquid dropout of the synthetic lab fluid and the characterized reservoir fluid at 275°F. The gas-condensate reservoir fluid is a moderately rich fluid with a maximum liquid dropout of 2.23% at 2226 psig compared to 2.73% at 2415 psig for the synthetic lab fluid. Calculated dew point pressure for the synthetic fluid is 3473 psig compared to 3297 psig of the reservoir fluid. **Table 7.2** compares the main fluid properties affecting fluid flow in porous media calculated using the Peng-Robinson EOS at the experimental conditions. All the important fluid properties of both gas and condensate phases for the synthetic gas mixture match closely with those of the actual reservoir fluid.

The initial gas permeability of the core was measured using nitrogen at 75°F. Initial water was established by injecting 2 cc of 1.5% KCl brine into the core at 275°F. The method of establishing initial water saturation in this experiment is different than that described in Section 3.3 i.e. injecting brine with a pump in a pressurized core compared to injecting water in a vacuumed core. This was done to imitate invasion of water in a gas reservoir. 2 cc of brine was injected to obtain the initial water saturation of 55% in the core. Water introduced into the core using this method will not distribute uniformly throughout the core and will result in high water saturation at the inlet end of the core.

Two-phase gas-condensate floods were then done at a core pressure of 1200 psig. The synthetic fluid mixture was saturated with water to minimize vaporization of water from the core. The PVT ratio of the fluid mixture at this pressure is 4.1. **Figure 7.4** shows the pressure drop measured across the core during two-phase flood at different rates. **Table 7.3** summarizes the results of the gas condensate flood. Some of the initial water will be displaced by gas and condensate and some will be vaporized by gas. However, as

the gas mixture was saturated with water, most of the water will be removed by displacement only. Results show that the presence of such high water saturation in the core decreased the gas relative permeability by 98% at a low flow rate and 95% at a higher flow rate. The increase in gas relative permeability is because more water is displaced at the higher flow rate due to a higher pressure gradient causing a lower water saturation. No saturation measurements were made to actually study the effect of flow rate on water saturation

A typical gas relative permeability for a gas condensate fluid with a PVT ratio of 4.1 over this range of capillary numbers in a water-wet sandstone core is expected to be within 25% of 0.12 (details given in **Chapter 10**). The measured gas relative permeability even at the highest capillary number was only 0.045 (**Table 7.3**) at the high water saturation, which is estimated to be roughly 55%. Thus, the high water saturation reduced the gas relative permeability by a factor of about 3.

7.2.2 Effect of mobile water on gas relative permeability

Gas condensate reservoirs with an underlying aquifer can result in flow of water along with gas and condensate phases. The following experiments (Exp #26 and #28) were done to evaluate the effect of mobile water on gas relative permeability i.e. to study three-phase flow of gas, condensate and water.

These experiments were performed on a Berea sandstone core at 175°F. **Table 7.4** summarizes the properties of the cores and the experimental conditions. An initial water saturation of 19% was established using the synthetic brine (**Table 7.5**). A two-phase gas condensate flood was done using synthetic fluid mixture-4 (composition given in **Table 3.4**). **Figure 3.8** shows the calculated liquid dropout of the synthetic lab fluid.

Figure 7.5 shows the pressure drop for two-phase and three-phase flow for Experiment 26. Two-phase gas condensate floods were conducted at 1738 cc/hr and 400 psig core pressure. The PVT ratio for this synthetic fluid at 420 psig and 175°F is 2.7. The initial two-phase flow was followed with a three-phase flow by co-injecting brine along with gas and condensate through the core at a water fractional flow of 0.1 ($f_w=0.1$). Water saturation in the core for $f_w=0.1$ can build up to around 70% (Baker *et al.*, 1987). Three-phase flow was done at multiple rates. **Table 7.6** summarizes the results of steady state two-phase and three-phase flow. The relative permeabilities for both gas and condensate decreased by more than an order of magnitude compared to the two-phase flow values, even for a small fractional flow of water.

Figure 7.6 shows the pressure drop data for two-phase and three-phase flow for Experiment 28. Two-phase gas condensate floods were conducted at 2106 cc/hr and 420 psig core pressure. The PVT ratio for this synthetic fluid at 420 psig and 175°F is 2.69. The initial two-phase flow was followed with a three-phase flow by co-injecting brine along with gas and condensate through the core at a water fractional flow of 0.036 ($f_w=0.036$). Water saturation in the core for $f_w=0.036$ can build up to around 50% (Baker *et al.*, 1987). **Table 7.7** summarizes the results of steady state two-phase and three-phase flow.

Results presented in **Tables 7.6** and **7.7** show that condensate accumulation by itself reduced gas relative permeability by about 90% i.e. by an order of magnitude. Water blocking caused another 90% reduction in gas relative permeability compared to two-phase gas relative permeability. Thus, water and condensate combined decreased the gas relative permeability by more than 99%, even for such a lean fluid (liquid dropout at 420 psig and 175°F is 1.2%) and small fractional flows of water ($f_w=0.036$ and 0.1). The gas relative permeability decreased further with an increase in fractional flow of water.

These results show that water along with condensate accumulation can significantly impair the productivity of gas condensate wells even in high permeability reservoirs.

Relative permeabilities were calculated using equation 3.5. The capillary pressure between gas-water and condensate-water was neglected for calculating relative permeabilities. This assumption might result in some error in calculations, but the capillary pressure for gas-water and condensate-water in high permeability Berea sandstone cores is not significant and is negligible compared to the total pressure drop obtained during three-phase flow in these experiments. Thus, neglecting capillary pressure does not cause any significant error in the relative permeabilities.

7.3 CHEMICAL TREATMENT TO TREAT DAMAGE CAUSED BY WATER AND CONDENSATE BLOCKING

Chemical treatment of Berea sandstone and Tunu reservoir core was done to reduce the damage caused by water and condensate blocking. Effects of both high water saturations and mobile water on gas relative permeability in a treated core were studied. The effect of mobile water on the durability of chemical treatment was also studied by flowing large pore volumes of water through treated cores.

Selection of proper solvents becomes important when treating rocks with high water saturation. As described in Chapter 5, the solvent composition has to be chosen so that it is compatible with the high water saturation present in the core to avoid precipitation of either salt or surfactant.

7.3.1 Chemical treatment of Berea Sandstone at high water saturation using FC4430

These experiments (Exp #26 and #28) were conducted at 175°F. **Table 7.4** summarizes the properties of the core and the experimental conditions. Two-phase gas

condensate floods were done using synthetic fluid mixture-4 (**Table 3.4**). **Figure 3.8** shows the calculated liquid dropout of the synthetic lab fluid.

Failure due to wrong selection of solvents:

Figure 7.5 shows the pressure drop for two-phase and three-phase flow for Experiment 26. **Table 7.6** summarizes the results of steady state two-phase and three-phase flow. Two-phase gas condensate floods were conducted at 1738 cc/hr and 400 psig core pressure. Initial two-phase flow was followed with a three-phase flow by co-injecting brine along with gas and condensate through the core at a water fractional flow of 0.1 ($fw=0.1$).

The core was treated with fluoro-chemical FC4430 delivered in a 70/30 mixture of 2-butoxyethanol and ethanol solvents. The composition of the treatment solution is given in **Table 7.8**. **Figure 7.7** shows the pressure drop during treatment. Pressure drop data shows severe plugging in the core during treatment injection. The discontinuity observed in the pressure drop data is because the treatment injection was stopped when the pressure drop went too high and was then started again after it dropped to a lower value. Treatment was also injected in the reverse direction i.e. injected from the outlet end of the core to see if the increase in pressure drop is due to face plugging at the inlet end. Plugging during the treatment flood was caused by surfactant precipitation. The water saturation in the core during the three-phase flow at $fw=0.1$ can build up to around 70% (Baker *et al.*, 1987) and the treatment solution used in this experiment could not tolerate such high water saturations. Phase behavior results of this treatment solution with the synthetic brine are given in Chapter 5 (**Table 5.13**). Results show that the treatment solution reached a cloud point at about 25% weight fraction water (which is similar to

water saturation) at 100°C and thus is not suitable for treating rocks with such high water saturation.

Figure 7.8 compares pressure drops for two-phase flow and three-phase flow before and after chemical treatment for Experiment 26. No improvement in gas relative permeability was observed for either two-phase flow or three-phase flow. This is because of surfactant precipitation during the treatment flood. **Table 7.9** summarizes the pre-treatment and post-treatment relative permeabilities for both two-phase and three-phase flow. Details of the experiment are given in **Appendix B 26**.

Successful chemical treatment:

Figure 7.6 shows the pressure drop for two-phase and three-phase flow for Experiment 28 and **Table 7.7** summarizes the results of steady state two-phase and three-phase flow. Two-phase gas condensate floods were done at 2106 cc/hr and 420 psig core pressure. The initial two-phase flow was followed with a three-phase flow by co-injecting brine along with gas and condensate through the core at a water fractional flow of 0.036 ($fw=0.036$). Water saturation in the core for $fw=0.036$ can build up to around 50% (Baker *et al.*, 1987).

The core was treated with fluoro-chemical FC4430 delivered in a 50/50 solvent mixture of 2-butoxyethanol and ethanol. The composition of the treatment solution is given in **Tale 7.10**. The compatibility of the treatment solution with different amounts of water was tested before the experiment. The treatment solution showed no cloud point until 150°C for water weight fractions up to 50%. 22 pore volumes of treatment solution at 128 cc/hr were flowed through the core. **Figure 7.9** shows the pressure drop during treatment. No plugging was observed as expected from the results of the phase behavior tests. The core was then shut-in for 15 hours.

Post-treatment two-phase and three-phase flows of the gas mixture with the same fractional flow of brine were then done under the same conditions as the pre-treatment two-phase and three-phase flow. **Figure 7.10** compares the pressure drop across the core measured during the pre-treatment and post-treatment two-phase and three-phase flow. The results show that the chemical treatment reduces the pressure drop by a factor of 1.68 for the two-phase flow. Thus, the treatment increases the gas and condensate relative permeability by the same factor. This shows that the chemical treatment was successful in treating the core and improving the gas and condensate relative permeability in presence of high initial water saturation (water present in the core before the treatment due to three-phase flow).

Comparison of the pressure drop data for the pre and post-treatment three-phase flow shows that the treatment had no effect on the relative permeability of the three phases in the presence of mobile water. The results, however, are not conclusive, as they cannot be just compared on the basis of fractional flows like the two-phase gas condensate flow. This is because gas condensate mixtures follow a special relationship described by their PVT ratio (described in Chapter 3 and 10) whereas no such relationship can be applied to three-phase flow of gas, condensate and water. To understand the results of chemical treatment in three-phase flow, measurement of saturations and relative permeability curves for three phase flow are required.

Next the effect of mobile water on treated rocks was studied. This is extremely important since if water gets introduced into a treated formation it might strip out the surfactant and thus negate the effect of chemical treatment. Thus, to study the effect of mobile water on chemical treatment, the following procedure was followed.

A solvent flush (composition given in **Table 7.11**) was done after the three-phase flood to remove water from the core and this was followed by two-phase flow of gas and

condensate mixture (*condensate flood-3*). **Figure 7.11** compares the pressure drop for the pre-treatment, post-treatment and condensate flood-3 two-phase flow. The result shows that the pressure drop for the condensate flood-3 is 1.55 times lower than the pre-treatment two-phase flow and is close to the post-treatment two-phase flow. This implies that 60 PV's of mobile water at $fw=0.036$ flowed through the core during the post-treatment three-phase flow did not strip off the surfactant from the rock surface.

Then floods were done to analyze the effect a small amount of water cross-flow into a gas bearing rock on the gas and condensate relative permeabilities and how long it takes for the gas and condensate two-phase flow to reach steady-state. 2 PV of the three-phases at $fw=0.036$ were injected followed by two-phase flow of gas and condensate (*condensate flood-4*). **Figure 7.12** shows the pressure drop for the 2 PV of three-phase flow followed by the two-phase flow. The results show the two-phase gas condensate flow reached steady state in about 30 PV's and the improvement factor was about the same as that for condensate flood-3.

Finally, the effect of flowing a large volume of brine on the treatment was studied. 10 PV of brine was injected followed by 10 PV of the solvent (composition given in **Table 7.11**) to remove brine which was followed with the two-phase gas condensate flow (*condensate flood-5*) under the same conditions as the previous two-phase floods. **Figure 7.13** compares the pressure drop measured during the condensate flood-5 and other previous floods. The measured pressure drop for condensate flood-5 was higher than the post-treatment gas condensate flood but still lower than the pre-treatment gas condensate flood by a factor of 1.32. A smaller improvement factor could be due to either striping of surfactant by water or because the solvent flush was probably not sufficient to remove all the water from the core. Water saturation in the core can be as

high as 60-80% after flowing 10 PV of brine at these pressure gradients (30-90 psi/ft) and a lot more solvent may be required to remove it from the core.

These results show that even after flowing such a large volume of brine through the treated core, enough surfactant remains attached to the rock surface to improve gas and condensate relative permeabilities 1.32 to 1.55 times. These results show that high gas relative permeabilities can be restored in treated formations even if water invades these zones and also demonstrate the durability of the chemical treatment during the flow of water.

Table 7.12 summarizes the results of all the two-phase floods.

7.3.2 Chemical treatment of Berea Sandstone with high water saturation using surfactant X3

Chemical treatment using FC4430 provided a durable treatment against mobile water but the improvement factor was reduced by about 21% to 1.32 compared to 1.68 obtained before injecting brine into the core. To provide more durability to the treatment a surfactant with a higher molecular weight than FC4430 was tested. Surfactant X3 from 3M Corp. is similar to FC4430, but the molecular weight of X3 is about 3 times that of FC4430. The idea was that the higher molecular weight surfactant would have more attachments to the rock surface and thus might perform better.

Experiment #30 was performed on Berea core at 175°F. **Table 7.4** summarizes the properties of the cores and the experimental conditions. Initial water saturation of 19% established using the brine given in **Table 7.5**. A two-phase gas condensate flood was performed using synthetic fluid mixture-4 (composition given in **Table 3.4**). **Figure 3.8** shows the calculated liquid dropout of the synthetic lab fluid.

Figure 7.14 compares pressure drops for two-phase gas condensate flood before and after chemical treatment for Experiment #30. Two-phase gas condensate floods were done at 2106 cc/hr and 420 psig core pressure. The core was then treated with X3 in a 70/30 solvent mixture of 2-butoxyethanol and ethanol. The composition of the treatment solution is given in **Tale 7.13**. The compatibility of the treatment solution with different concentrations of brine was tested before the experiment. The treatment solution showed a high cloud point of 125°C with 20% water, but the cloud point decreased significantly to 95°C with 30% water. 18 pore volumes of treatment solution were injected into the core. The core was then shut-in for 15 hours. Chemical treatment reduced the pressure drop by a factor of 1.88 for the two-phase flow and thus increased the gas and condensate relative permeability by the same factor.

The chemical treatment was then tested for water blocking and the effect of mobile brine on the durability of the treatment. First the effect of a small amount of water was tested. The post-treatment gas condensate flood was followed with 2 PV of three-phase flow of gas, condensate and brine at a water fractional flow equal to 0.038 ($f_w=0.038$). This was followed by gas condensate two-phase flow (*condensate flood-3*). The pressure drop for the two-phase flow was lower than the pre-treatment two-phase flow, but did not reach steady state even after flowing 140 PV, suggesting that brine is not easily removed from the core. Thus, a solvent flush (*solvent flush-1*) (composition given in **Table 7.14**) was done to remove the brine from the core and this was followed by two-phase flow of gas condensate mixture (*condensate flood-4*). **Figure 7.15** compares the pressure drop for the pre-treatment, post-treatment and condensate flood-4 two-phase flow. The result shows that the pressure drop for the condensate flood-4 is almost same as the pressure drop for the post-treatment gas condensate flood and thus the small volume of mobile brine had no effect on the chemical treatment.

The core was then flooded with 1 PV of brine ($fw=1$) to analyze the effect of a larger volume of flowing water on the chemical treatment. The brine flood was followed with a solvent flush (*solvent flush-2*) (composition in Table-7.14) and finally with the two-phase gas condensate flood (*condensate flood-5*). **Figure 7.16** compares the steady state pressure drop for condensate flood-5 with the other gas condensate floods. The result shows that even flowing a 1 PV of brine through the core did not strip off the surfactant from the rock surface and the improvement factor for gas and condensate relative permeabilities were still about 1.9.

Finally, 10 PV of brine was flowed through the core. Flowing such a large volume of brine (at a pressure gradient of 35 psi/ft) can result in water saturations up to 60-80 %. The brine flood was followed by 10 PV of solvent (*solvent flush-3*) to remove brine, which was followed with the two-phase gas condensate flow (*condensate flood-6*) under the same conditions as the previous two-phase floods. The pressure drop for the two-phase flow and the effluent from the core showed that the solvent flush did not remove the brine completely. To remove the remaining brine, more solvent was flushed through the core (*solvent flush-4*) at a lower rate of 64 cc/hr compared to the earlier rates of 128 cc/hr. The lower rate gives more residence time for the solvent to mix with brine in the core and either solubilize or miscibly displace it. The core was shut in for 40 hrs after the condensate flood-6, which left the surfactant in contact with brine for a long period of time. Gas condensate flood (*condensate flood-7*) was done after the solvent flush-4. **Figure 7.17** shows the measured pressure drop during the condensate flood-7. The measured pressure drop for condensate flood-7 was slightly higher than the post-treatment gas condensate flood but still significantly lower than the pre-treatment gas condensate flood. This result shows that even after flowing such a large volume of brine through the treated core, there was still an improvement factor of 1.62 for the gas and

condensate relative permeabilities. **Table 7.15** summarizes the results of all the gas condensate two-phase floods. **Figure 7.18** compares all the two-phase gas condensate floods before and after treatment. Details of the experiment are given in **Appendix B30**.

Experiment #30 confirms that the X3, a chemical with a higher molecular weight than FC4430, can improve the gas and condensate relative permeabilities by a factor of 2 in the presence of connate water. The test also confirms the durability of the chemical treatment even when subjected to large volumes of flowing water. The test also showed that the large residence time of brine in the core did not remove surfactant from the rock surface.

Results presented in this section and the previous sections extend the range of applicability of such chemical treatments. Once a formation is treated, the high gas and condensate relative permeabilities due to treatment can be restored even after water invades these formations without the need of a second treatment. Invaded water can be removed and the well productivity can be restored using only solvent treatments, which are less expensive than surfactant treatments.

7.3.3 Chemical treatment of Tunu reservoir core

This experiment (Exp# 34) was done on a Tunu reservoir core (plug#4) at 275°F to study the effect of chemical treatment on a water blocked low permeability reservoir core. Properties of the reservoir core are given in **Table 7.1** along with the experimental conditions representing the reservoir conditions. **Table 3.7** gives the composition of the synthetic gas mixture modeled to match the reservoir fluid. Properties of the synthetic gas mixture along with its comparison with the reservoir fluid properties are given in **Table 7.2**. Initial water saturation of 30% was established by injecting 1.5% KCl brine into the core at 275°F.

The initial two-phase gas condensate flood was done at a core pressure of 1200 psig. The pressure drop for the gas condensate flood is shown in **Appendix B34**. The measured pressure data had a lot of fluctuations, which makes it difficult to interpret. Fluctuations were mainly caused due to a faulty back-pressure regulator, which resulted in discontinuous flow of gas mixture through the core. Gas relative permeability calculated using an average pressure drop over the last 200 pore volumes is 0.096.

The core was treated with FC4430 delivered in a 70/30 mixture of propylene glycol and iso-propanol. The composition of the treatment solution is given in **Tale 7.16**. Results of the compatibility tests of the treatment solution with the reservoir brine are presented in chapter 5. Mohabbat Ahmadi (Ahmadi *et al.* 2008-09) did the initial gas condensate and the treatment floods.

Table 7.17 compares pre-treatment and post-treatment relative permeabilities. The treatment increases the gas relative permeability by only a factor of 1.18. The result is difficult to interpret because of the poor quality of pre-treatment data. Post-treatment gas condensate flood was done at two different rates. The post-treatment gas relative permeability at the higher rate is almost 1.8 times higher than the pre-treatment gas relative permeability, however, the measurements are at different capillary numbers and thus there is some contribution of capillary number in the improvement.

A better comparison of the pre-treatment and post-treatment relative permeabilities can be done by using the initial gas condensate flood data for Exp# 35 (**Table 7.3**) as the reference. As both the experiments (Exp #34 and #35) are done on reservoir cores from the same zone with very similar petrophysical properties (**Table 7.1**), the relative permeability values measured under the same conditions are expected to be very close to each other. As the quality of data for Experiment #35 is better, pre treatment gas relative permeabilities given in **Table 7.3** have been used for comparing the

post-treatment results. Valid comparisons can be made as the measurements are made on the core from the same formation and under same conditions.

Table 7.18 compares the pre-treatment relative permeabilities measured at 55% water saturation on Tunu core#7 (Exp #35) with the post treatment relative permeabilities measured on Tunu core#4 (Exp #34) at the same flow rate and core pressure. The treatment increased the gas relative permeability by a factor of about 2.5. This significant increase is due to the removal of both water and condensate blocks from the core.

Results presented in **Table 7.3** are measured at an initial water saturation of 55%. So, to compare the effect of same water saturation on a treated core, water saturation of 55%, was established in the core by injecting 2 cc of 1.5% KCl brine into the core at 275°F followed with the two-phase gas condensate flood. **Table 7.19** compares the gas relative permeability on treated and untreated cores at same initial water saturation. Result shows that the post-treatment relative permeabilities presented in **Table 7.18** are retained back even at 55% connate water saturation.

One PV of brine ($f_w=1$) was then injected in to the core to analyze the effect of significant volume of flowing water on the chemical treatment. Brine injection was followed with a gas condensate flood to measure gas relative permeability. **Table 7.20** compares the post treatment gas relative permeability without connate water, at 55% S_{wi} and after injecting one pore volume of brine. Results show that post-treatment gas relative permeabilities are restored even in the presence of high water saturation.

Figure 7.19 compares the pre-treatment and post treatment gas relative permeabilities on Tunu cores plotted as a function of capillary number. The pre-treatment gas relative permeabilities are the ones measured in Experiment #35. Chemical treatment improved the gas relative permeability by 300-400% over the range of studied capillary

numbers. This significant increase in gas relative permeability is caused by the removal of both condensate and water blocking damage from the core due to chemical treatment.

Results obtained on Berea and Tunu reservoir cores imply that chemical treatment makes the displacement of water from both high and low permeability cores easier. Thus, high productivity from a treated gas condensate reservoir can be restored even if water invades into the formation after treatment without the need of treating it again. Chemical treatment thus becomes a better solution for treating zones that are susceptible to water blocking either due to cross flow from another zone or some other reason.

7.4 CHEMICAL TREATMENT USING A NON-FLUORINATED SURFACTANT

Results of chemical treatment presented so far are with fluorinated surfactants, which are both water and oil repelling. Results show that fluorinated surfactants are effective in increasing gas and condensate relative permeabilities and also removing damage caused by water blocking. However, such treatments are expensive due to high costs of fluorinated surfactants. Such chemical treatments can become more cost effective if similar improvements in relative permeability can be obtained using less expensive non-fluorinated surfactants.

A hydrocarbon surfactant was tested to treat the damage caused by water and condensate blocking. Surfactant 144977-75 obtained from 3M Corporation, is similar to fluoro-surfactant FC4430 with the fluorocarbon group replaced with a hydrocarbon group. Thus, the surfactant is expected to have a similar interaction with the rock surface, but may provide different interaction with pore fluids because of the difference between the tail groups.

Experiment 36 was performed on a Berea core at 175°F using synthetic brine given in **Table 7.5** and synthetic fluid mixture-5 given in **Table 3.5**. Chemical treatment was tested for both condensate and water blocking. Effect of treatment on water blocking was tested by measuring gas and water relative permeability before and after the treatment. Measurement of gas and condensate relative permeability before and after treatment for gas condensate two-phase flow tested the effect of treatment on condensate blocking.

The initial two-phase gas-water flood was done using water saturated methane and synthetic brine (composition give in **Table 7.5**) at a fractional flow of water of 0.038 ($f_w=0.038$). This was followed with methane flood to reduce to the water saturation to residual saturation. Two-phase gas condensate flood was done using the gas mixture-5 (Table 3.5) at 410 psig. Due to high pressure drop across the core, fluid properties were calculated at the average core pressure instead of the BPR-2 pressure for calculating relative permeabilities.

The core was then treated using the hydrocarbon surfactant 14477-75 in a 50/50 mixture of 2-butoxyethanol and ethanol. The composition of the treatment solution is given in **Table 7.21**. 20 PV of treatment solution was injected into the core at 150 cc/hr. The core was then shut in for 16 hours.

Table 7.22 compares the pressure drop for the pre-treatment and post-treatment gas condensate flood done at 410 psig. No improvement was observed in gas and condensate relative permeabilities. A hydrocarbon surfactant is not expected to make the surface oil repelling and this is likely the reason there was no change in the relative permeability.

Figure 7.20 compares the pressure drop for the pre-treatment and post-treatment methane-water flood done at $f_w=0.038$. **Table 7.23** compares the relative permeabilities

measured before and after treatment. The hydrocarbon surfactant is expected to make the rock surface water repelling thus increase the relative permeabilities for gas-water two-phase flow. However, no improvement was observed in gas and water relative permeabilities. The results for gas-water flood may not be totally conclusive as saturation measurements are important to fully understand the results. The same fractional flow of gas and water can be obtained for different saturations before and after the treatment and is not a function of pressure like gas condensate fluids. Details of the experiment are given in **Appendix B36**.

7.5 SUMMARY

The effect of chemical treatment using non-ionic fluorinated surfactants FC4430 and X3 on reducing the damage caused by water blocking has been studied. Experiments done on Tunu reservoir cores show that a high water saturation in a low permeability core can reduce the gas relative permeability by more than 95%. Three-phase flow measurements done on high permeability Berea cores show that even a small fractional flow of water can reduce the gas relative permeability by more than 99%.

Chemical treatment increased the gas relative permeability by a factor of 3 to 4 on Tunu reservoir cores in the presence of a high water saturation. High gas and condensate post-treatment relative permeabilities were retained even after flowing upto 10 pore volumes of brine through the treated reservoir and Berea cores. Thus, showing that high productivity from a treated reservoir can be retained even if a large volume of water invades the formation.

Chemical treatment using a non-fluorinated hydrocarbon surfactant showed no improvement in gas relative permeability for both gas condensate and gas-water two

phase flow. Results of gas-water, two-phase flow are not entirely conclusive and require saturation measurements to better understand them.

Table 7.1: Properties of Tunu reservoir cores and experimental conditions

	Exp #34	Exp #35
Plug#	4	7
k _g , md	11	9.45
Porosity, %	14.28	14
Length, inch	1.95	2.05
Dia, inch	1.00	1.00
Temperature, °F	275	275
Core Pressure, psig	1200	1200

Table 7.2: Comparison of Tunu reservoir and synthetic fluid properties at 275°F and 1200 psig

	Reservoir Fluid		Lab Fluid	
	Gas phase	Oil phase	Gas phase	Oil phase
μ (cp)	0.0164	0.2314	0.0161	0.2378
Volume fraction	0.9861	0.0139	0.984	0.016
IFT (dyne/cm)	4.43		6.23	

Table 7.3 Gas and condensate relative permeabilities on Tunu core#7 at $S_{wi}=55\%$ (Exp #35) at 275°F and 1200 psig

Core flow rate, cc/hr	Capillary number	k_{rg}	k_{ro}
146	9.7×10^{-6}	0.021	0.005
293	1.33×10^{-5}	0.031	0.007
585	1.80×10^{-5}	0.045	0.011

Table 7.4: Properties of Berea cores and experimental conditions

	Exp #26	Exp #28	Exp #30
k_g , md	192	226	218
S_{wi} , %	19	19	19
Porosity, %	20	20	20
Temperature, °F	175	175	175
Core Pressure, psig	400	420	420

Table 7.5: Bruce Synthetic brine

Component	g/l
CaCl ₂ (6H ₂ O)	7.72
MgCl ₂ (6H ₂ O)	1.67
KCl	0.659
NaCl	64.541

Table 7.6: Two-phase and three-phase relative permeabilities measured in Exp # 26

q_g , cc/hr	q_o , cc/hr	q_w , cc/hr	fw	k_{rg}	k_{ro}	k_{rw}
1716.7	21.6	0	0	0.092	0.034	0.00
429.2	5.4	48	0.1	0.004	0.001	0.011
214.6	2.7	24	0.1	0.003	0.001	0.008

Table 7.7: Two-phase and three-phase relative permeabilities measured in Exp # 28

q_g , cc/hr	q_o , cc/hr	q_w , cc/hr	fw	k_{rg}	k_{ro}	k_{rw}
2080.4	26.6	0	0.00	0.085	0.032	0.00
520.1	6.6	20	0.037	0.007	0.002	0.007

Table 7.8- Composition of treatment solution for Exp # 26

Component	Weight %
FC4430	2
2-butoxyethanol	70
Ethanol	30

Table 7.9: Summary of two-phase and three-phase relative permeability data before and after treatment at 175°F and 400 psig for Exp #26

	k_{rg}	k_{ro}	k_{rw}	fw	k_{rg}/k_{ro}	IF
Pre-Treatment 2-phase flow	0.092	0.004	-	0.0	2.73	
Pre-Treatment 3-phase flow	0.003	0.001	0.008	0.1	2.73	
Post-Treatment 2-phase flow	0.085	0.031	-	0.0	2.73	0.92
Post-Treatment 3-phase flow	0.002	0.001	0.006	0.1	2.73	0.84

Table 7.10- Composition of treatment solution for Exp #28

Component	Weight %
FC4430	2
2-butoxyethanol	49
Ethanol	49

Table 7.11- Solvent used to flush out brine in Exp #28

Component	wt%
2-butoxyethanol	50
Ethanol	50

Table 7.12: Summary of two-phase and three-phase relative permeability data before and after treatment at 175°F and 420 psig for Exp #28

	k_{rg}	k_{ro}	k_{rw}	fw	k_{rg}/k_{ro}	IF
Pre-Treatment 2-phase flow	0.085	0.032	-	-	2.69	
Pre-Treatment 3-phase flow	0.007	0.002	0.007	0.037	2.69	
Post-Treatment 2-phase flow	0.143	0.053	-	-	2.69	1.68
Post-Treatment 3-phase flow	0.006	0.002	0.006	0.037	2.69	0.87
Condensate flood-3	0.132	0.049	-		2.69	1.55
Condensate flood-4	0.126	0.047	-		2.69	1.48
Condensate flood-5	0.112	0.042	-		2.69	1.32

Table 7.13- Composition of treatment solution for Exp #30

Component	Weight %
Surfactant X3	2
2-butoxyethanol	69
Ethanol	29

Table 7.14: Solvent used to flush out brine in Exp #30

Component	wt%
2-butoxyethanol	70
Ethanol	30

Table 7.15: Summary of two-phase relative permeability data before and after treatment at 175°F and 420 psig for Exp #30

	k_{rg}	k_{ro}	k_{rg}/k_{ro}	Capillary Number	IF
Pre-Treatment 2-phase flow	0.065	0.025	2.59	1.78×10^{-5}	
Post-Treatment 2-phase flow	0.123	0.047	2.59	9.43×10^{-6}	1.88
Condensate flood-4	0.134	0.052	2.59	8.66×10^{-6}	2.05
Condensate flood-5	0.121	0.047	2.59	9.56×10^{-6}	1.86
Condensate flood-7	0.105	0.041	2.59	1.1×10^{-5}	1.62

Table 7.16: Composition of treatment solution used to treat Tunu reservoir core (Exp #34)

Component	Weight %
FC4430	2
Propylene glycol (PG)	69
iso-propanol (IPA)	29

Table 7.17: Comparison of pre-treatment and post treatment relative permeability measured on Tunu core#4 at 2750F and 1200 psig (Exp #34)

q_{core} , cc/hr	Before Treatment		After Treatment		Improvement Factor
	k_{rg}	k_{ro}	k_{rg}	k_{ro}	
594	0.096	0.023	0.113	0.028	1.18
2230	-	-	0.163	0.040	

Table 7.18: Comparison of pre-treatment and post treatment relative permeability measured on Tunu reservoir cores at 2750F and 1200 psig

q_{core} , cc/hr	Before Treatment (Exp #35)		After Treatment (Exp #34)		Improvement Factor
	k_{rg}	k_{ro}	k_{rg}	k_{ro}	
146	0.021	0.005	-	-	
293	0.031	0.007	-	-	
594	0.045	0.011	0.113	0.028	2.51
2230	-	-	0.163	0.040	

Table 7.19: Comparison of pre-treatment and post treatment relative permeability measured on Tunu reservoir cores at $S_{\text{wi}}=55\%$ at 2750F and 1200 psig

q_{core} , cc/hr	Before Treatment (Exp #35)		After Treatment (Exp #34)		Improvement Factor
	k_{rg}	k_{ro}	k_{rg}	k_{ro}	
146	0.021	0.005	-	-	
293	0.031	0.007	-	-	
594	0.045	0.011	0.081	0.020	2.51
2230	-	-	0.147	0.036	
5120			0.187	0.083	

Table 7.20: Comparison of post treatment gas relative permeabilities measured on Tunu reservoir core#4 at 2750F and 1200 psig

q_{core} , cc/hr	Post Treatment k_{rg}	Post Treatment k_{rg} at $S_{\text{wi}}=55\%$	Post Treatment k_{rg} after injecting 1PV of brine
594	0.113	0.081	0.101
2230	0.163	0.147	0.025
5120		0.187	

Table 7.21: Composition of treatment solution with hydrocarbon surfactant

Component	Weight %
Surfactant 144977-75	2
2-butoxyethanol	49
Ethanol	49

Table 7.22: Effect of chemical treatment using a non-fluorinated surfactant on gas and condensate relative permeabilities at 175°F and 410 psig

q_{core} , cc/hr	Before Treatment		After Treatment		Improvement Factor
	k_{rg}	k_{ro}	k_{rg}	k_{ro}	
4957	0.072	0.029	0.085	0.035	1.19
9640	0.097	0.041	0.094	0.040	0.97

Table 7.23: Effect of chemical treatment using a non-fluorinated surfactant on gas and water relative permeabilities at $f_w = 0.038$ and 175°F

q_{core} , cc/hr	Before Treatment		After Treatment		Improvement Factor
	k_{rg}	k_{rw}	k_{rg}	k_{rw}	
634	0.02	0.022	0.019	0.021	0.94

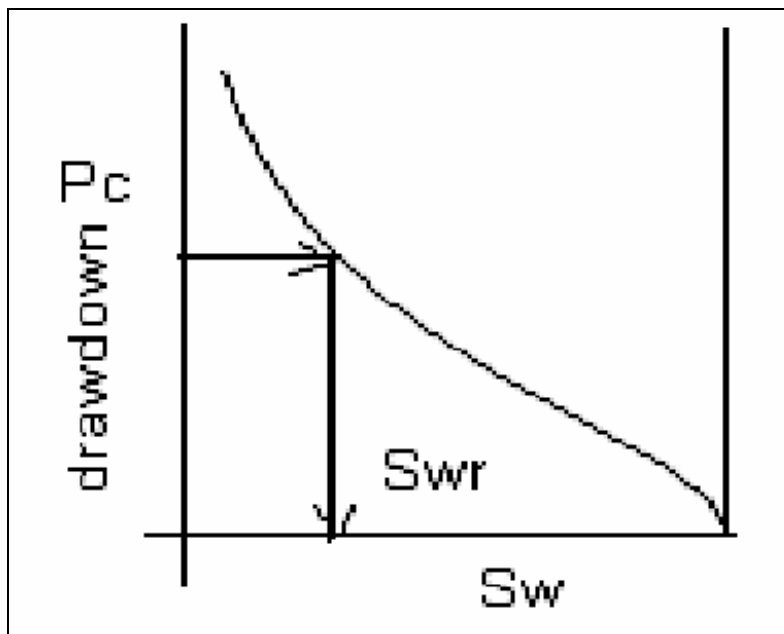


Figure 7.1: Residual water saturation as a function of drawdown pressure

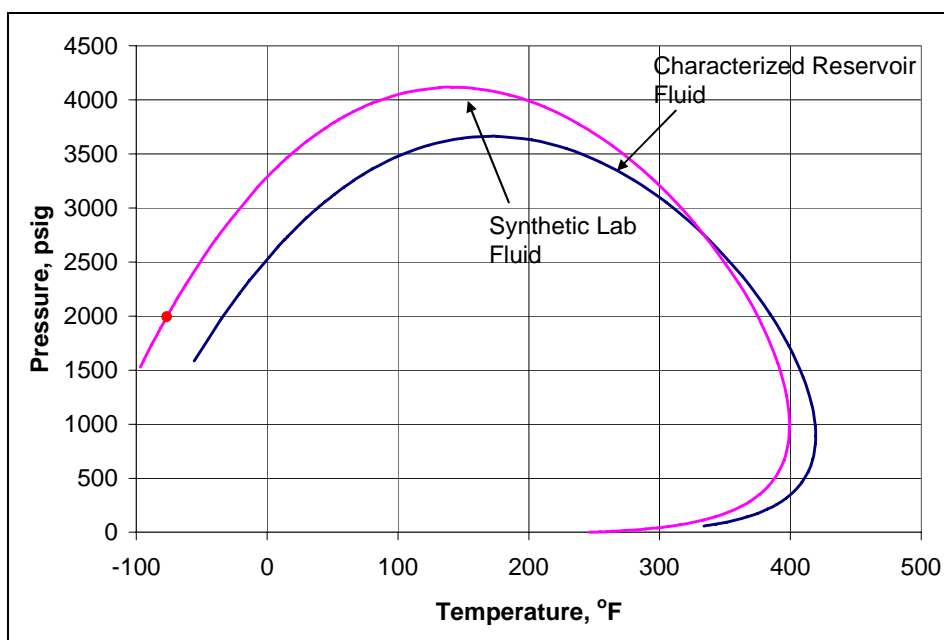


Figure 7.2: Comparison of P-T phase diagram for characterized reservoir fluid and the lab fluid calculated using PREOS

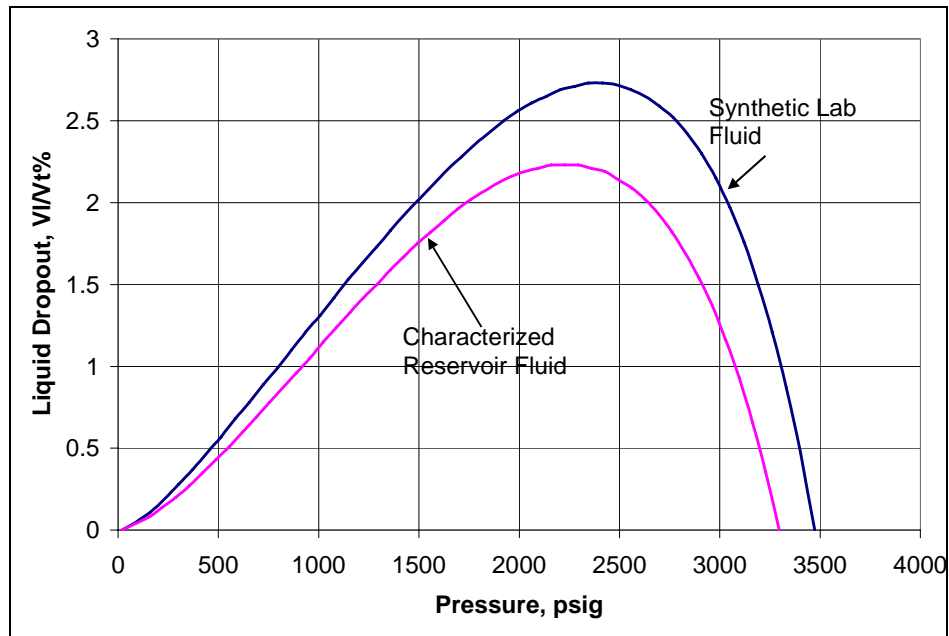


Figure 7.3: Comparison of liquid dropout for characterized reservoir fluid and the lab fluid calculated at 275°F using PREOS

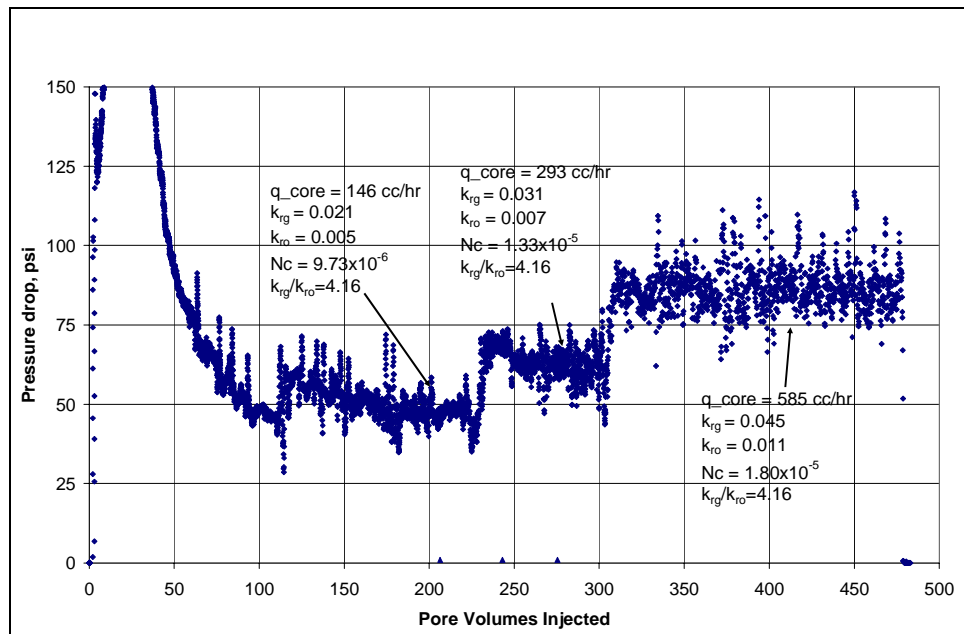


Figure 7.4: Pressure drop across the core during gas condensate flood at $S_{wi}=55\%$ on Tunu reservoir core#7 at 275°F and 1200 psig

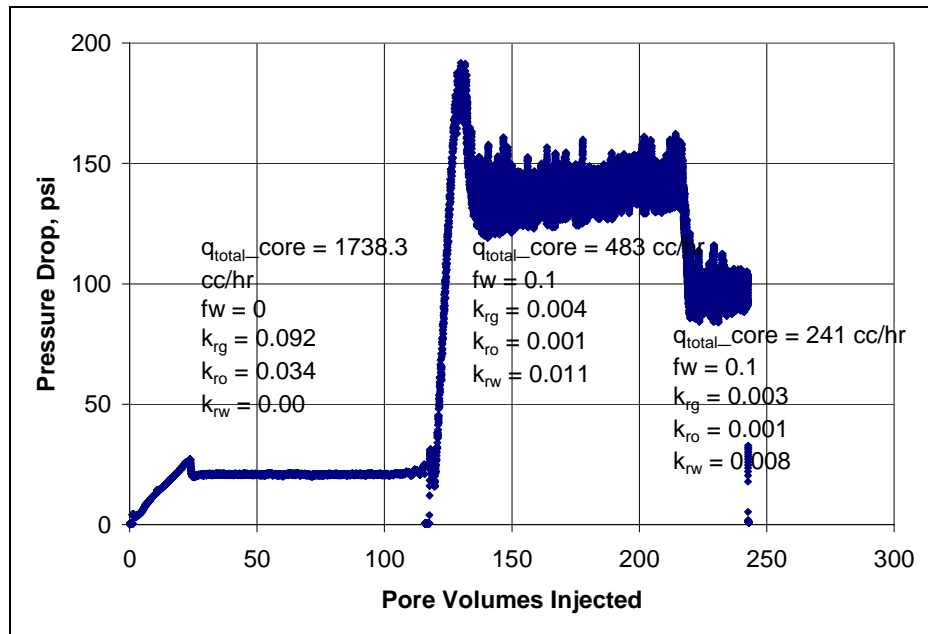


Figure 7.5: Pressure drop across the core during two-phase at 400 psig and three-phase flow at $fw=0.1$ at 175°F for Exp#26

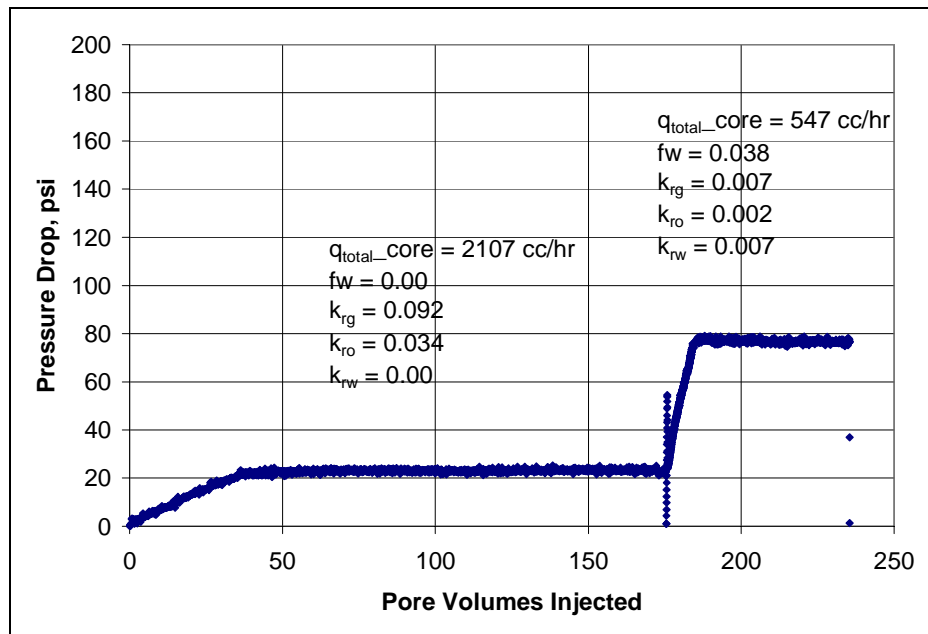


Figure 7.6: Pressure drop across the core during two-phase at 420 psig and three-phase flow at $fw=0.038$ at 175°F for Exp#28

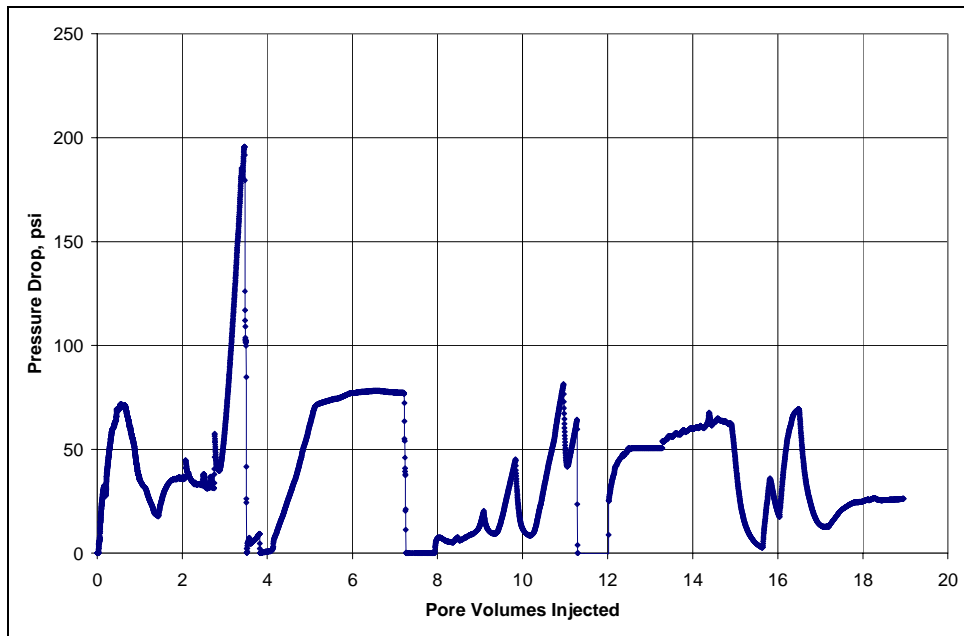


Figure 7.7: Pressure drop during the treatment flood for Exp#26 shows plugging

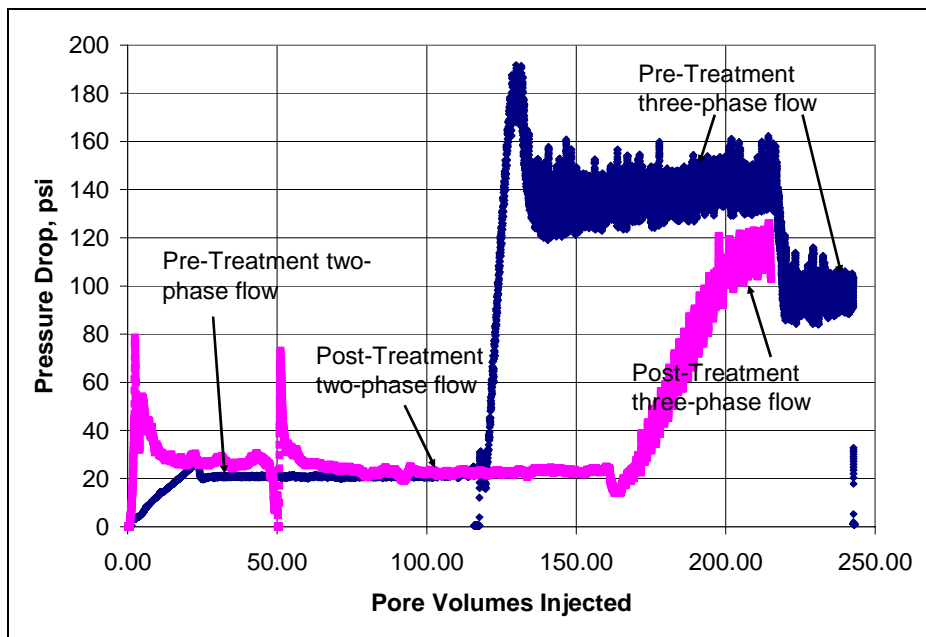


Figure 7.8: Effect of chemical treatment on two-phase and three-phase flow in Exp#26

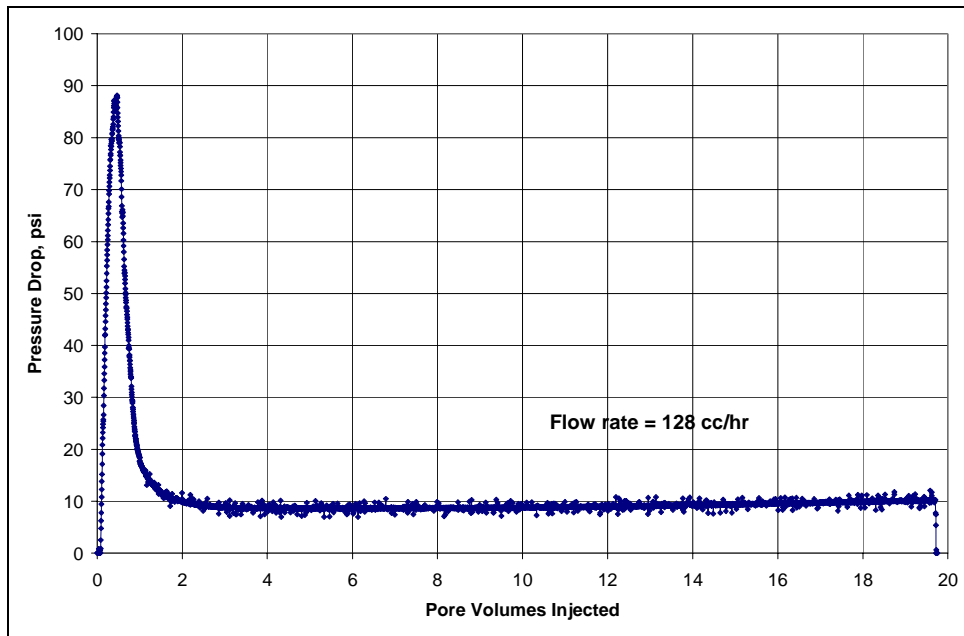


Figure 7.9: Pressure drop during the treatment flood for Exp#28 shows no plugging

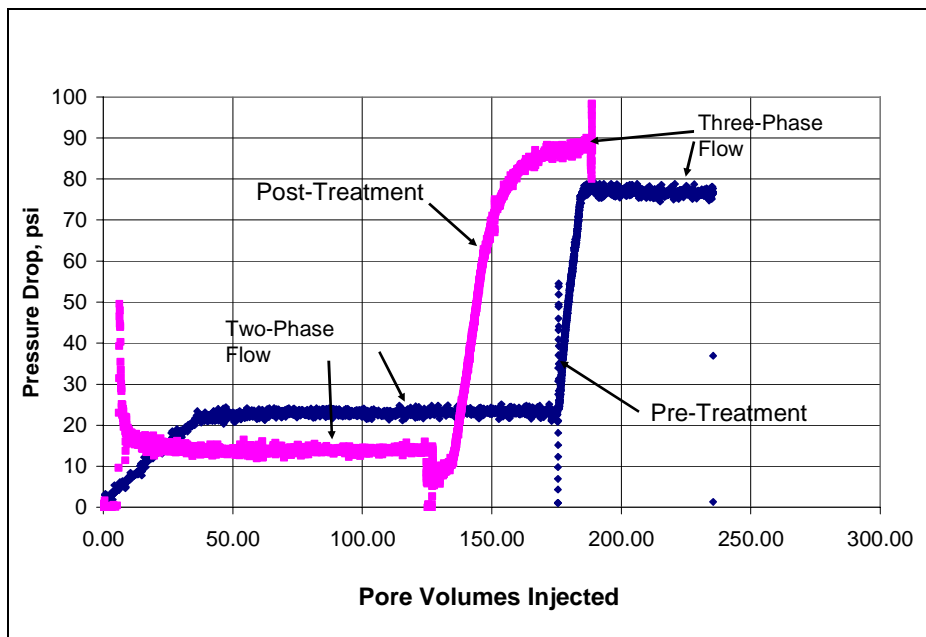


Figure 7.10: Effect of chemical treatment on two-phase and three-phase flow in Exp#28

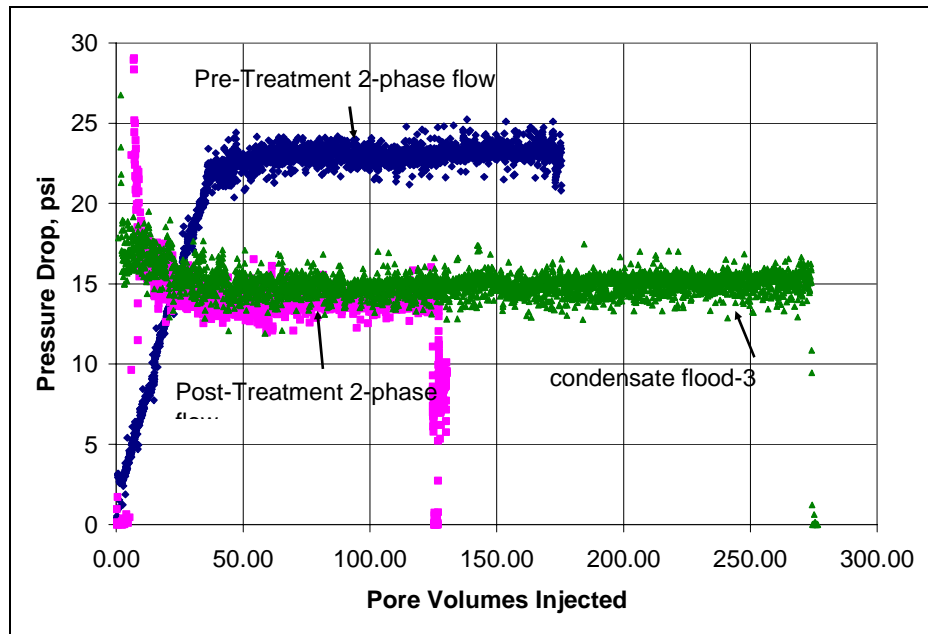


Figure 7.11: Comparison of condensate accumulation before and after treatment and after three phase flow for Exp#28

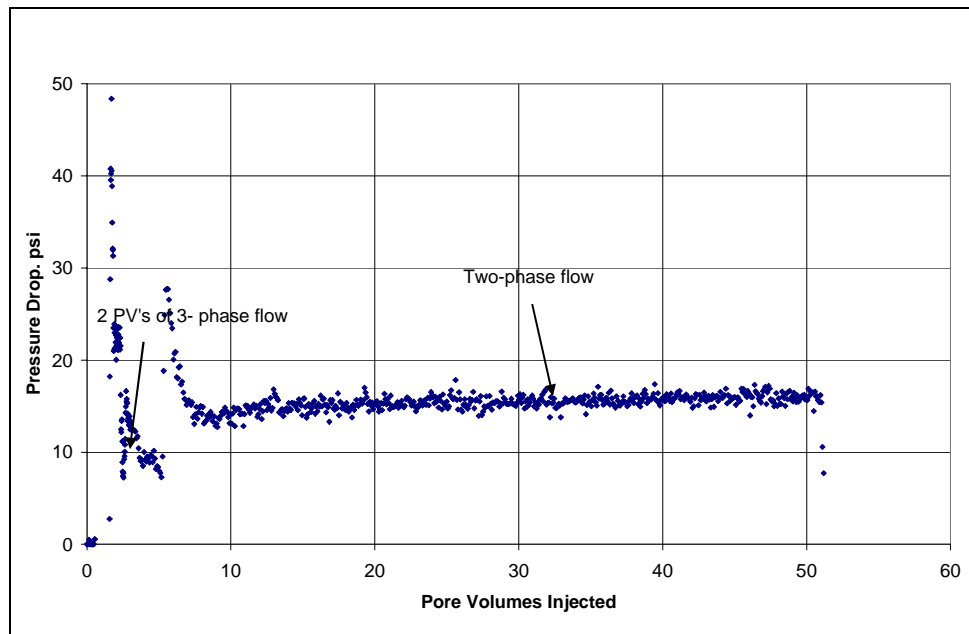


Figure 7.12: Pressure drop for 2PV's of three-phase followed by two-phase flow in Exp#28

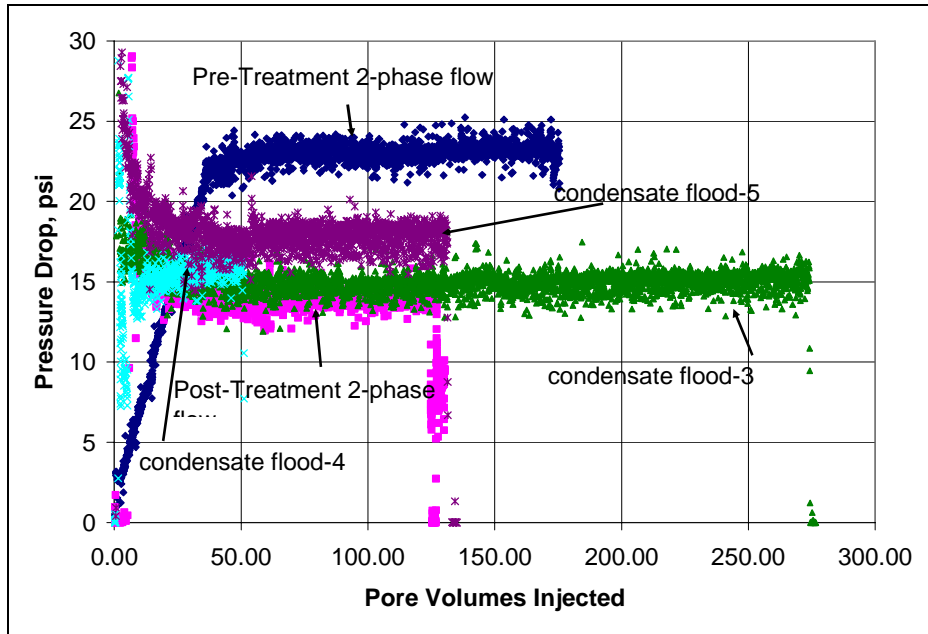


Figure 7.13: Comparison of two-phase flow pressure drops before and after treatment at 175°F and 420 psig for Exp#28

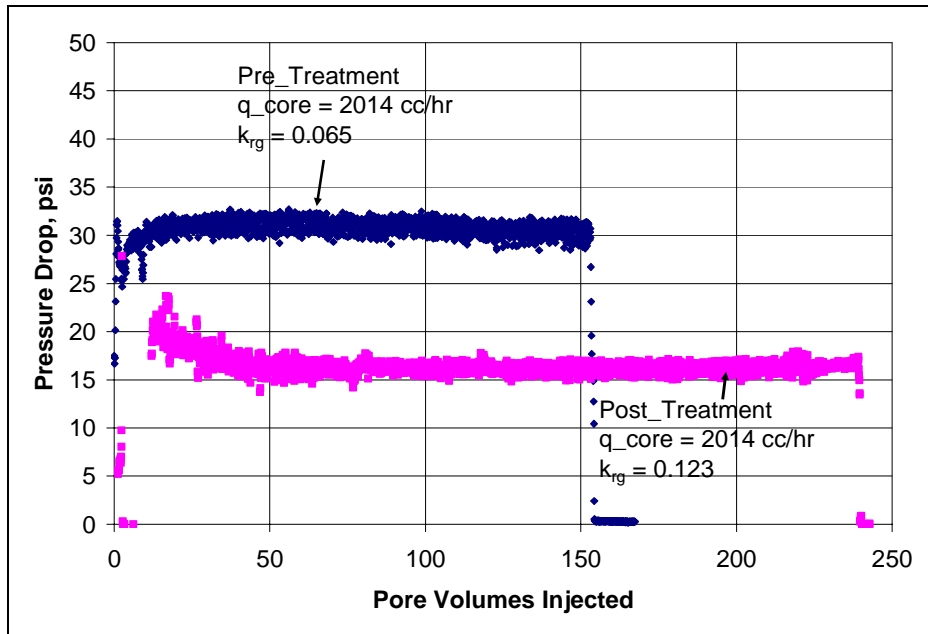


Figure 7.14: Effect of chemical treatment on condensate accumulation at 175°F and 420 psig (Exp#30)

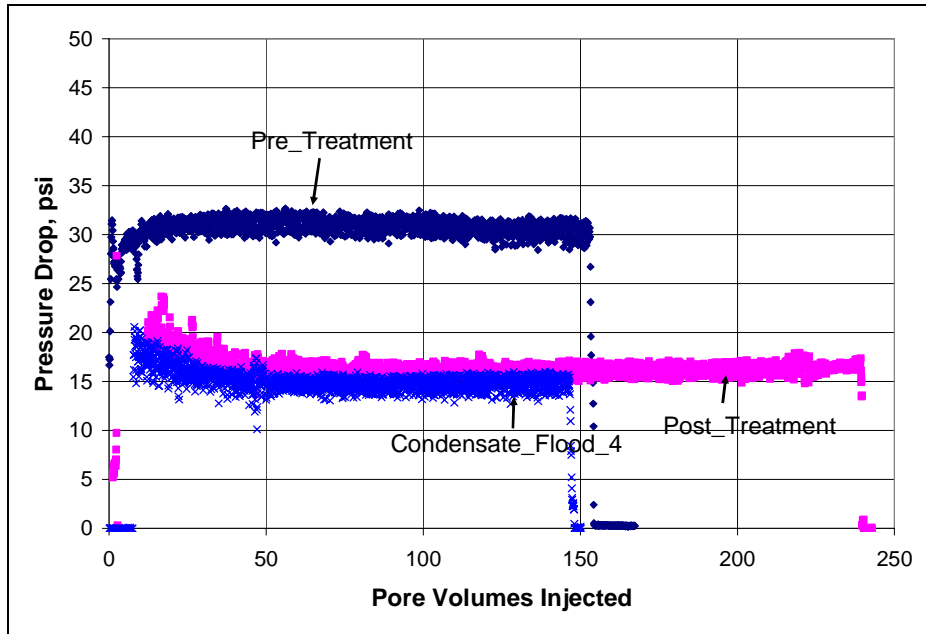


Figure 7.15: Comparison of condensate accumulation before and after treatment and after three phase flow for Exp#30

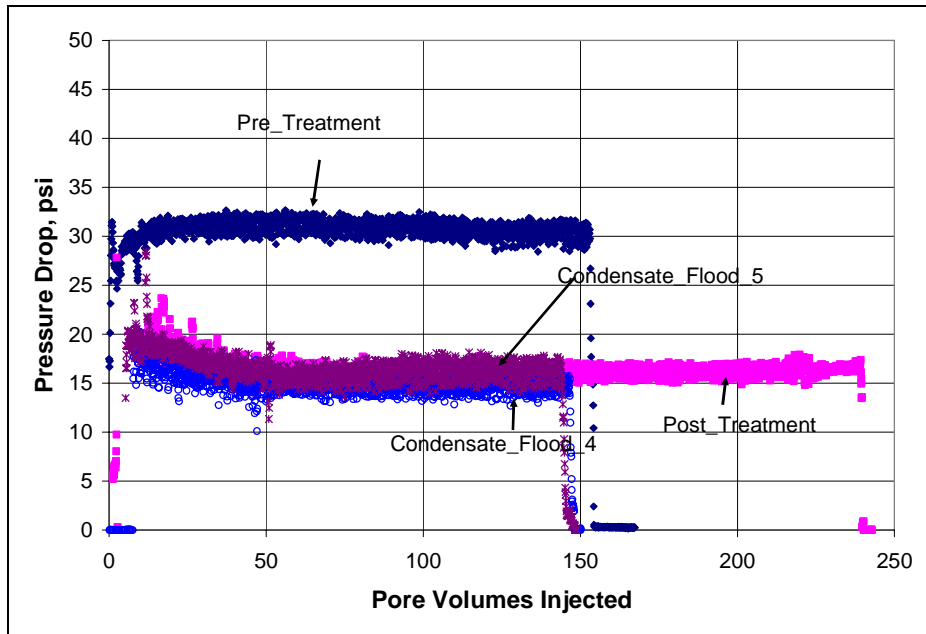


Figure 7.16: Effect of 1PV brine injection on condensate accumulation after chemical treatment (Exp#30)

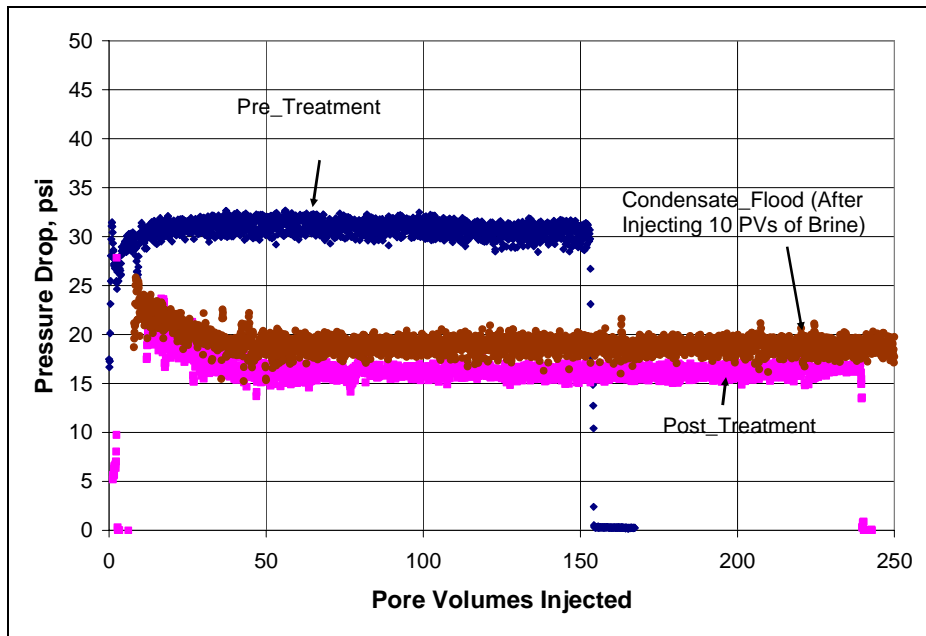


Figure 7.18: Effect of 10 PV brine injection on condensate accumulation after chemical treatment (Exp#30)

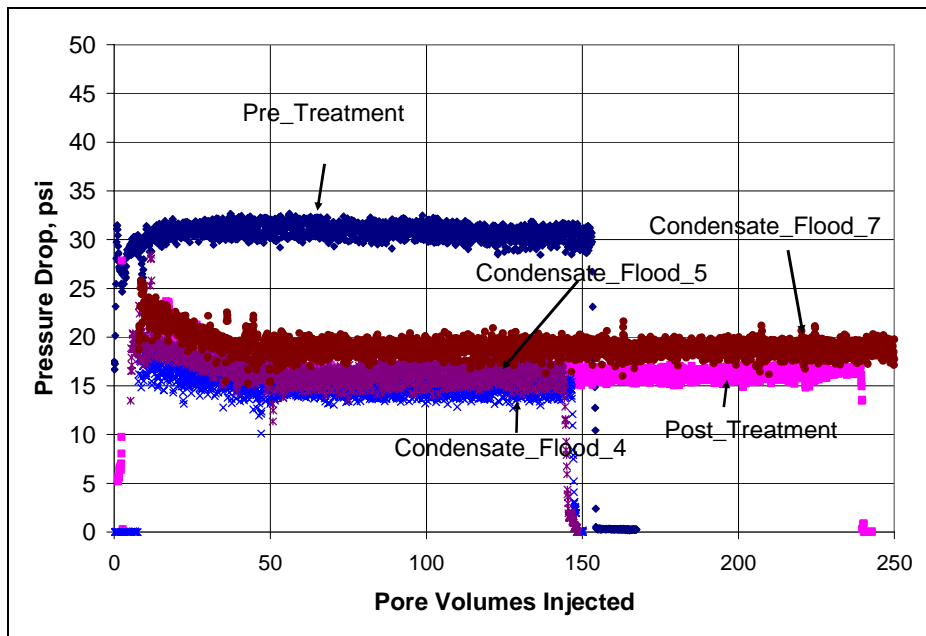


Figure 7.18: Comparison of two-phase flow pressure drops before and after treatment (Exp#30)

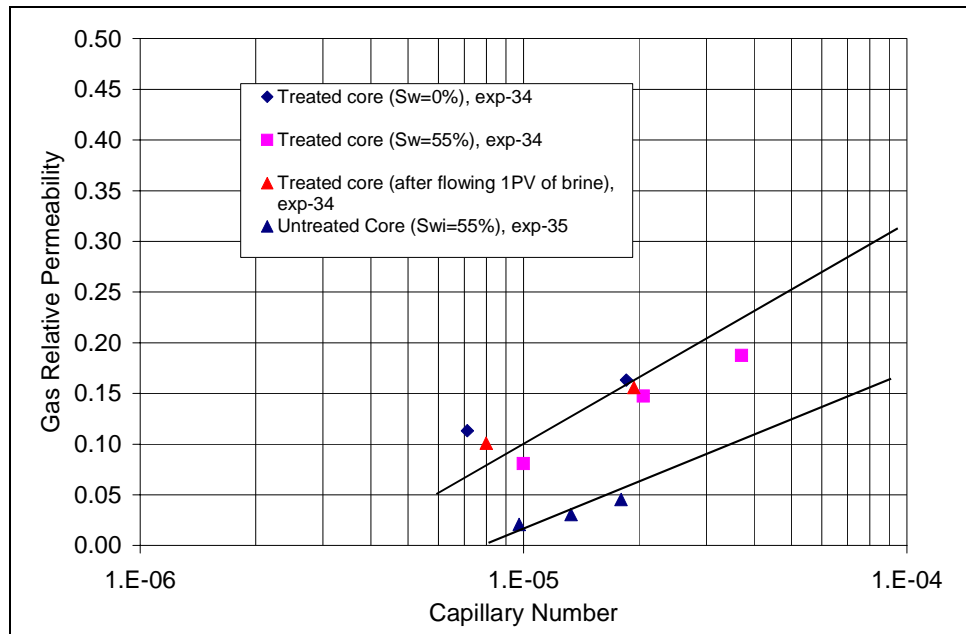


Figure 7.19: Effect of high water saturation on treated and untreated Tunu reservoir cores at 275°F and 1200 psig

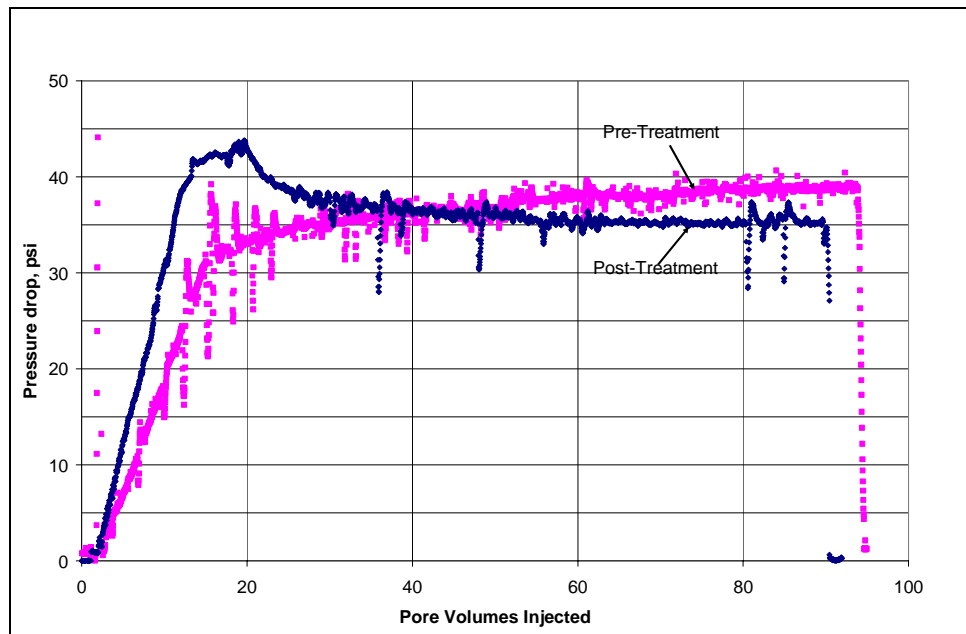


Figure 7.20 Effect of chemical treatment using a non-fluorinated surfactant on methane-water two phase flow at $f_w=0.038$ (Exp#36)

Chapter 8: Chemical Treatment of Propped Fractures

This chapter presents the results of experiments conducted to evaluate the decline in gas productivity due to condensate buildup in propped fractures and the effect of chemical treatment in restoring productivity. The first section provides an introduction to hydraulic fracturing in gas reservoirs to increase productivity. Then the experimental procedure including the method of preparing propped fractures is described. Next the effect of non-Darcy flow on single-phase and two-phase flow in fractures is presented. Finally, the effect of chemical treatment on gas relative permeability in propped fractures is discussed.

8.1 INTRODUCTION:

Hydraulic fracturing has been used to enhance productivity from gas condensate reservoirs (Mohan *et al.*, 2005; Kumar, 2000; Settari *et al.*, 1996; Barnum *et al.*, 1995 and Schechter, 1992). In many wells it is possible to reduce the drawdown, i.e. increase the flowing bottomhole pressure by inducing a hydraulic fracture that significantly increases the area available to flow. This allows the well to be produced at a bottomhole pressure higher than the dew point pressure for longer periods of time thereby delaying the onset of condensate formation around the wellbore. However, once the well pressure falls below the dew-point pressure, significant condensate saturation can build up within the fracture itself and cause a significant reduction gas productivity.

This experimental study demonstrates the effect of condensate buildup on gas relative permeability in propped fractures. This may be the first time two-phase relative permeability data for gas condensate fluids in propped fractures under reservoir

conditions and flow rates have been reported since no experimental values could be found in the literature.

For single-phase flow of gas at high flow rates through propped fractures, the effect of non-Darcy flow can be extremely important. For two-phase flow, the reduction in fracture conductivity due to non-Darcy flow is even greater than for single phase flow and is also a function of capillary number. Mohan *et al.* (2005) showed that the productivity of hydraulically fractured gas condensate reservoirs can be over estimated by about 3 times if non-Darcy flow is not taken into account. **Chapter 10** describes the effect of non-Darcy flow and capillary number on two-phase flow. In this chapter, the data are presented after correcting for non-Darcy flow as described in **Chapter 10 (Section 10.5)**.

8.2 PREPARATION OF PROPPED FRACTURES:

To study the fluid flow through propped fractures, proppant packs were designed and prepared to closely represent the actual fractures. **Figures 8.1 to 8.3** show the steps involved in preparing propped fractures. Mr. Harry Linnemeyer prepared these propped fractures using a new method he recently devised. Preparation of the propped fractures involved the following three main steps:

1. Cut a cylindrical core into two equal halves along its length. Place two spacers of the required fracture width between the two halves of the core.
2. Put the two halves of the core together with the spacers between them and wrap them with a Teflon tape. This provides the void space between the rock matrix, which represents the fracture.
3. Fill the void space with the required proppant. Shake the core and withdraw the spacers gradually while pouring in the proppant to uniformly

distribute proppant throughout the void space. Proppant filled void space between the two halves of the core represents the propped fracture. Propped fractures were not saturated with any kind of fracturing fluid to avoid complications. A 100-mesh size screen was put at the outlet end of the core to prevent any kind of proppant migration from the fracture into the flow system.

Propped fractures were prepared using F35 Ottawa sand and 30/50 Bauxite. Berea sandstone and a reservoir core were used as the matrix rock.

8.3 EFFECT OF NON-DARCY FLOW AND NET CONFINING STRESS ON FRACTURE CONDUCTIVITY:

Single-phase fracture conductivity is known to decrease significantly with increasing net confining stress and non-Darcy flow. This section shows the effect of non-Darcy flow and net confining stress on single-phase gas permeability and end point gas relative permeability at residual water saturation measured on a propped fracture. These measurements were conducted on fractures with 30/50 Bauxite proppant. **Table 8.1** gives the properties of the propped fracture and the matrix rock (Exp-39). The porosity of the propped fracture was measured from the mass of proppant used and its grain density.

Figure 8.4 shows the pressure drop as a function of gas velocity (Darcy velocity defined as $u=q/A$) through the fracture with a net confining stress of 9000 psi. As the conductivity of the fracture is about 100 times more than that of the rock matrix, most of the flow is through the fracture and the measured pressure drop data represents fluid flow properties in the fracture. The result shows that the pressure drop increases non-linearly with increasing gas velocities and thus deviates from Darcy's law. **Figure 8.5** show the effect of gas velocity on apparent single-phase gas permeability calculated using Darcy's

law under different net confining stress. As the gas velocity increases, the apparent gas permeability decreases showing the effect of non-Darcy flow at high gas velocities. Similar results were observed over a wide range of net confining stress varying from 1000 psig to 9000 psig.

Thus, at high velocities Darcy's law is not valid and contributions due to non-Darcy flow have to be accounted for to calculate the correct single-phase gas permeability. For non-Darcy flow, the single-phase permeability can be calculated using Forseheimer's equation:

$$\frac{\Delta P}{L} = \frac{u \mu}{k} + \beta \rho u^2 \quad (8.1)$$

where, v is Darcy velocity, μ is the flowing fluid viscosity, L is the length of the core, A is the cross-sectional area of the core, ΔP is the steady state pressure drop across the core, ρ is the fluid density and β is the non-Darcy flow coefficient. This equation can be re-arranged and written as:

$$\frac{\Delta P}{uL} = \frac{\mu}{k} + \beta \rho u \quad (8.2)$$

The plot of $(\Delta P/uL)$ vs velocity (u) is a straight line and the permeability of the porous medium (core/fracture) can be calculated from the intercept. The slope of the line gives the non-Darcy flow coefficient. **Figure 8.6** shows a plot of $(\Delta P/qL)$ vs flow rate (q) at a net confining stress of 9000 psi. Gas permeability is calculated from the intercept. This single-phase gas permeability is the true permeability of the propped fracture. Klinkenberg corrections are negligible at the pressures and rates used.

Figure 8.7 shows the effect of net confining stress on the true fracture permeability. Results show that no change in permeability was observed as the net-confining stress is increased from 1000 to 2000 psi. As the net-confining stress is increased further the single-phase gas permeability of the fracture decreased from about 80 Darcy to 50 Darcy (as the net-confining stress is increased from 2000 to 9000 psi). This shows a strong effect of net-confining stress on single-phase gas permeability. This suggests that measurements should be conducted at the appropriate confining stress to get accurate single-phase flow properties.

Figure 8.8 shows the effect of net confining stress on apparent gas permeability measured at S_{wi} . Apparent gas permeability at S_{wi} is calculated using Darcy's law without correcting for non-Darcy flow. Apparent gas permeability at S_{wi} shows similar trends as observed for the single-phase gas permeability. **Figure 8.9** shows the effect of net-confining stress on end-point gas relative permeability at S_{wi} calculated using the true gas permeability at S_{wi} . The gas permeability at S_{wi} was corrected for non-Darcy flow as described above for single-phase flow. Results show that no significant change is observed in end point gas relative permeability with increasing net-confining stress. This is because the effect of net-confining stress appears in both the numerator (apparent gas permeability at S_{wi}) and the denominator (apparent single-phase gas permeability) while calculating the end point gas relative permeability and therefore it cancels out. Thus, the measured gas relative permeability is relatively insensitive to the net-confining stress.

8.4 REDUCTION IN GAS RELATIVE PERMEABILITY DUE TO CONDENSATE BUILDUP IN PROPPED FRACTURES:

Results presented in Chapters 4, 6 and 7 show that liquid blocking (condensate + water) in both high and low permeability rocks can significantly reduce the gas relative

permeability. In this section, experimental data are presented to show the effect of condensate buildup on gas relative permeability in propped fractures. These measurements were conducted on both sand and bauxite propped fractures.

Experiments 29, 31 and 39 were conducted at 279°F under Reservoir B conditions. **Table 8.2** summarizes the experimental conditions. Synthetic fluid mixture 9 was used for these experiments. The model gas condensate fluid was matched to the actual reservoir fluid on the basis of liquid dropout, viscosity, interfacial tension, dew point pressure and the PVT ratio at reservoir temperatures and pressures.

Figure 8.10 compares the calculated P-T phase diagram of the synthetic fluid mixture-9 and the characterized Reservoir B fluid. **Figure 8.11** compares the calculated liquid dropout of the synthetic lab fluid and the characterized reservoir fluid at 279°F. The gas condensate fluid is a moderately rich fluid with a maximum liquid dropout for the reservoir fluid of 4.3% at 3280 psig and 4.2% at 3230 psig for the synthetic lab fluid. The calculated dew point pressure for the synthetic fluid is 4580 psig compared to 6068 psig of the reservoir fluid, i.e. less by about 1500 psi. However, the dew point pressure of the fluids does not affect the steady state measurements done using pseudo-steady state method at pressures far below the dew point pressure (described in Section 3.3). **Table 8.3** compares the main fluid properties for the reservoir fluid and the synthetic fluid calculated using the Peng-Robinson EOS at the experimental conditions. All the important fluid properties of both gas and condensate phases for the synthetic gas mixture match closely with those of the actual reservoir fluid at 1450 psig. The PVT ratio at 279°F and 1450 psig is 1.96 for the reservoir fluid and 2.38 for the synthetic lab fluid.

8.4.1 Measurements on propped fractures with sand as proppant:

Table 8.4 gives the properties of the rock matrices and the propped fractures (Exp-29 and 31). Ottawa F35 sand was used as proppant to fill the fracture. This sand has an average mesh size of about 35 corresponding to an average grain diameter of 0.02 cm. The porosity of the proppant filled fractures was measured from the mass of sand used and its grain density. Single phase gas permeabilities reported in this section have been corrected for non-Darcy flow and thus represent the true gas permeability of the fracture at the effective stress of the experiments.

Experiment 29 was performed with a low permeability Reservoir B core (1-2 mD) as the matrix rock. Initial water saturation was established by injecting 100 pore volumes (propped fracture pore volumes) of synthetic reservoir brine (composition given in **Table 8.5**) followed by a nitrogen flood to reduce the water saturation to residual. Initial water saturation was established in this manner rather than the method described in Section 3.3 because the fracture pore volume was only 0.91 cc and establishing initial water saturation of 20-30% by injecting a metered volume of water becomes very difficult. Gas permeability decreased by almost 50% due to residual water trapped in the sand proppant. A two-phase gas condensate flood was conducted using synthetic fluid mixture-9. **Table 8.6** summarizes the two-phase gas condensate flow measurements at 279°F and 1500 psig. Measurements were conducted at multiple rates to capture the effect of both capillary number and non-Darcy flow on gas relative permeability. **Table 8.6** presents gas and condensate relative permeabilities after correcting for non-Darcy flow. The method used for Non-Darcy flow corrections with two-phase flow are explained in Chapter 10. The gas relative permeability after non-Darcy flow correction represents the true gas relative permeability. Details of the experiments are given in **Appendix B29**.

Experiment 31 was performed with Berea sandstone core as the matrix rock. An initial water saturation of 20% was established using 3% (30,000 ppm) NaCl brine. A two-phase gas condensate flood was conducted using synthetic fluid mixture-9. **Table 8.7** summarizes the two-phase gas condensate flow measurements at 279°F and 1450 psig. Gas relative permeabilities in **Table 8.7** have been corrected for non-Darcy flow. Details of the experiments are given in **Appendix B31**.

Figures 8.12 and **8.13** show the variation of gas relative permeability with velocity for Experiments 29 and 31, respectively. **Figures 8.14** and **8.15** show the variation of gas relative permeability with capillary number for Experiments 29 and 31, respectively. No significant change in gas relative permeability was observed with increasing velocity or capillary number. This shows that these measurements were conducted below the critical capillary number. Some noise was observed in the measured gas relative permeability and that is because of some uncertainty involved in measuring extremely low pressure drops across the core at low flow rates. Thus, within the uncertainty of these measurements, the gas relative permeability during two-phase flow is approximately 0.08 - 0.1 over this wide range of capillary number for a PVT ratio of 2.38. These values are similar to those obtained for gas relative permeabilities measured on consolidated Berea and reservoir sandstone cores for the same PVT ratio (dependence of gas relative permeability on PVT ratio is described in Chapter 10).

8.4.2 Measurements on propped fractures with Bauxite as proppant:

Table 8.1 gives the properties of the rock matrix and the propped fracture (exp-39). Bauxite 30/50 was used as the proppant to fill the fracture. A Berea sandstone core was used as the matrix rock. An initial water saturation of 20% was established using 3%

(30,000 ppm) NaCl brine. A two-phase gas condensate flood was conducted using synthetic fluid mixture-9. **Tables 8.8, 8.9 and 8.10** summarize the two-phase gas condensate flow measurements at 279°F and 1450 psig with 1000 psig, 3000 psig and 5000 psig net confining stress, respectively. Measurements were conducted under different confining stress to study its effect on gas and condensate relative permeability. Details of the experiments are given in Appendix B39.

Figures 8.16 and 8.17 show the variation of gas relative permeability with velocity and capillary number respectively for different net confining stress. These results show that net-confining stress does not affect gas relative permeability. This is similar to what was observed for the end-point gas relative permeability. Thus, the measurement of gas relative permeability is quite insensitive to net-confining stress. No effect of velocity or capillary number was observed on gas relative permeability within the measured range of capillary numbers. Some noise was observed in the measured gas relative permeability measured at low velocities, which is primarily due to the uncertainty involved in measuring extremely low pressure drops across the core at these low flow rates.

The gas relative permeability values in the propped fracture are approximately 0.1 for a PVT ratio of 2.38 and for capillary numbers below the critical capillary number. These values are similar to those obtained for consolidated Berea and reservoir sandstone cores and for propped fractures filled with F35 sand for the same PVT ratio (dependence of gas relative permeability on PVT ratio is described in chapter 10). Details of the experiments are given in Appendix B39.

Gas relative permeability decreased by about 90% or more due to condensate blocking in both sand and bauxite filled fractures (experiments 29, 31 and 39). These results show that even in such high permeability porous media, condensate blocking can cause a significant reduction in gas relative permeability. Thus, condensate blocking is

expected to significantly reduce the productivity of wells with fractures since a fracture with a high conductivity is typically needed for such wells in the first place or they would not be fractured.

Reduction in gas relative permeability in these high permeability propped fractures is about the same as that observed in outcrop and reservoir cores (Chapter 4, 6 and 7). These results show that the damage caused by condensate dropout is as pronounced in high permeability propped fractures as it is in low permeability outcrop and reservoir cores.

8.5 CHEMICAL TREATMENT TO IMPROVE TWO-PHASE FLOW CONDUCTIVITY OF PROPPED FRACTURES:

A chemical treatment of propped fractures was conducted to reduce the damage caused by condensate accumulation and thus improve the two-phase flow conductivity of fractures. The objective of this chemical treatment is to increase the relative permeability by altering the wettability of proppants (sand or bauxite) from strongly water-wetting to intermediate-wetting using the fluoro-surfactant FC4430. The chemical treatment is based on the same principles as described in Chapters 4, 6 and 7 for treating the damage caused by liquid blocking in sandstone rocks. Experiments were conducted on both sand and bauxite filled propped fractures. In these experiments, the fluids including treatment solution were injected into both the propped fracture and the rock matrix, but because the fracture permeability is much larger than the matrix permeability, almost all of the fluid flows through the fracture and thus for all practical purposes the results represent the effect of chemical treatment on proppants only.

8.5.1 Chemical treatment propped fractures with sand as proppant:

Experiment 29 and 31 were conducted at 279°F and 1450 psig. **Table 8.4** summarizes the properties of the core and the experimental conditions. A two-phase gas condensate flood was conducted using synthetic fluid mixture-9 (composition given in **Table 3.9**). **Figure 3.13** shows the calculated liquid dropout of the synthetic lab fluid.

Table 8.11 presents the pressure drop and relative permeabilities for a two-phase gas condensate flood conducted at 2600 psig for Experiment 29. A solvent pre-flush with a mixture of propylene glycol and IPA (composition given in **Table 8.12**) was conducted after the initial gas condensate flood to remove high salinity brine from the core. A solvent flush was conducted to prevent salt or surfactant precipitation during the treatment flood. Solvent pre-flush was followed with a two-phase gas condensate flood at 1500 psig. The core pressure was decreased from 2600 psig to 1500 psig to represent the actual flowing bottomhole well pressure. **Table 8.6** summarizes the results of steady state post-preflush two-phase flow with the steady state pressure drops. Post pre-flush gas condensate flood was conducted at multiple flow rates varying from 514 to 2899 cc/hr.

The core with propped fracture was treated with fluoro-chemical FC4430 delivered in 70/30 mixture of propylene glycol and IPA. The composition of the treatment solution is given in **Table 8.13**. 40 pore volumes of treatment solution at 40 cc/hr was flowed through the core. The pressure drop during the treatment is shown in Appendix B29. No plugging was observed during treatment injection as expected from the results of phase behavior tests. The core was then shut-in for 15 hours.

Post treatment gas condensate flood was conducted under the same conditions as the post pre-flush gas condensate flood. **Table 8.14** summarizes the results of post-treatment two-phase flow and the improvement factor after the chemical treatment. The improvement factor is again described as the ratio of gas relative permeability after the

chemical treatment to that before the chemical treatment measured under the same conditions. An average improvement factor of about 1.5 was obtained after the chemical treatment. A higher improvement was observed at the lower flow rates, but the uncertainty in the measured pressure drop at the lowest rates is highest due to extremely small values. The improvement factors listed in this table are based on the comparison with the gas relative permeability after the preflush, so they underestimate the improvement. The preflush removes the water and increases the gas permeability a factor on the order of 1.4 (depending on the initial water saturation). The values of the condensate flood before the preflush were not used as the basis for comparison because it is suspected that the pressure drop data were too high during that flood due to some temporary plugging problems that were very likely caused by some sand grain movement. The problem was fixed by reversing the flow, so the pressure drop data following the preflush as well as the final pressure drop data in **Tables 8.6** and **8.14** are more reliable. Thus, the most conservative interpretation of these data is an improvement factor of 1.45. If we adjust the values for the effect of the water saturation, then the improvement factors range from about 2 to 2.4, so that the most optimistic interpretation is an improvement factor of 2.4. A detailed description of the experiment is given in **Appendix B29**.

Experiment 31 was performed with Berea sandstone core as the matrix rock. An initial water saturation of 20% was established using 3% (30,000 ppm) NaCl brine. A two-phase gas condensate flood was conducted using synthetic fluid mixture-9. **Table 8.7** summarizes the two-phase gas condensate flow measurements at 279°F and 1450 psig. Gas condensate floods were conducted at multiple flow rates varying from 206 to 2883 cc/hr.

The core with propped fracture was treated with fluoro-chemical FC4430 delivered in 80/20 mixture of propylene glycol and IPA. The composition of the treatment solution is given in **Table 8.15**. A total of 40 pore volumes of treatment solution was flowed through the core at 80 and 160 cc/hr. The pressure drop during the treatment flood is shown in **Appendix B31**. The core was then shut-in for 15 hours.

A post treatment gas condensate flood was conducted under the same conditions as the initial gas condensate flood. **Table 8.16** summarizes the results of post-treatment two-phase flow and the improvement factor after the chemical treatment. The improvement factor varied from about 1.53 to 2.53 with an average of about 1.8 to 1.9. Again, a higher improvement factor was observed at the lowest flow rates where the uncertainty in the measured pressure drop is highest due to extremely small measured values.

Analysis of improvement factors due to chemical treatment becomes complicated due to the non-Darcy flow correction of gas relative permeability. The non-Darcy flow correction is based on Geertsma's correlation which uses initial water saturation for calculating the non-Darcy flow coefficient and corrected gas relative permeability (details given in Chapter 10). There is some uncertainty in the validity of this correlation for multi-phase flow, especially in the presence of three phases. To get a more direct comparison of the chemical treatment on gas condensate flow, the improvement factor can be calculated by taking the ratio of the steady-state pressure drop during two-phase flow before and after chemical treatment. This will also account for the improvement in gas relative permeability that can be obtained by reducing the damage caused by non-Darcy flow due to higher water saturation before the chemical treatment. An improvement factor varying from 1.74 to 2.54 was observed based on the measured steady state two-phase flow pressure drop. No change in the highest improvement factor

is observed as that corresponds to the lowest rate at which the contribution of non-Darcy flow is negligible. Thus, the improvement factor based on corrected gas relative permeability and steady-state pressure drop data are the same. At higher rates, where the non-Darcy flow effects become more significant, an increase in improvement factor from 1.53 to 1.74 was observed. This increase shows the additional benefit obtained in gas relative permeability by reducing the non-Darcy flow coefficient.

8.5.2 Chemical treatment of propped fractures with Bauxite as proppant:

Table 8.1 gives the properties of the rock matrix and the propped fracture (Exp-39). Bauxite 30/50 was used as the proppant to fill the fracture. Berea sandstone core was used as the matrix rock. An initial water saturation of 20% was established using 3% (30,000 ppm) NaCl brine. Two-phase gas condensate flood was conducted using synthetic fluid mixture-9. **Tables 8.8, 8.9** and **8.10** summarize the two-phase gas condensate flow measurements at 279°F and 1450 psig with 1000 psig, 3000 psig and 5000 psig net confining stress respectively.

The core with propped fracture was treated with fluoro-chemical FC4430 delivered in a 70/30 mixture of propylene glycol and IPA. The composition of the treatment solution is given in **Table 8.13**. A total of 27 pore volumes of treatment solution was flowed through the core at 100 and 500 cc/hr. The pressure drop during the treatment flood is shown in Appendix B39. The core was then shut-in for 15 hours.

A post-treatment gas condensate flood was conducted under the same conditions as the initial gas condensate flood with a net confining stress of 1000 psig. **Table 8.17** summarizes the results of post-treatment two-phase flow and the improvement factor after the chemical treatment. No improvement in gas relative permeability was observed after the chemical treatment. A second chemical treatment was then conducted using the

same treatment solution but a much larger volume was injected this time. 90 pore volumes of treatment solution was injected through the core. The pressure drop during the treatment flood is shown in **Appendix B39**. The core was then shut-in for 15 hours followed with the post second treatment gas condensate flood. No improvement was observed after the second treatment either.

Reasons for the failure of the chemical treatment on Bauxite proppants are not known. The most likely reason could be the original wettability of these proppants. The surface properties of bauxite are different than that of sand. Initial tests indicate that it may be neutrally wet. This will thus reduce the chance of improvement from chemical treatment which aims at making the proppant neutral wet. However, the wettability of the proppants could not be determined conclusively nor is it known whether the bauxite used in these tests has the same wettability as bauxite used in propped fractures under reservoir conditions. Obviously more research is needed on the wettability and treatment of bauxite.

8.6. SUMMARY

A new approach of preparing propped fractures in the laboratory and procedures for conducting multi-phase flow measurements on them has been presented in this chapter. Measurements were conducted on both sand and bauxite propped fractures. Effects of non-Darcy flow and net-confining stress on single-phase and two-phase flow conductivity of propped fractures was studied. Net-confining stress has a significant effect on single phase flow conductivity of propped fractures whereas no effect was observed on gas relative permeability. Results presented in this chapter show that

correcting for non-Darcy flow is extremely important for both single-phase and multi-phase flow.

Results of gas condensate flow measurements show that the gas relative permeability is significantly reduced due to condensate accumulation and blocking in propped fractures. The reduction in gas relative permeability due to condensate blocking in propped fractures is of the same order as that observed in outcrop and reservoir cores. The gas relative permeability values in the propped fracture are approximately 0.1 for a PVT ratio of 2.38 and for capillary numbers below the critical capillary number. Thus liquid (condensate + water) blocking can be a significant problem in propped fractures even though they have a very high permeability.

Chemical treatment using polymeric fluoro-surfactant FC4430 was conducted to improve the multi-phase flow conductivity of propped fractures. An improvement in gas relative permeability on the order of 1.5 to 2.5 was observed due to chemical treatment of sand-filled propped fractures. At high flow rates an additional benefit of reduction in non-Darcy flow is obtained by chemical treatment. Chemical treatment of bauxite-filled propped fractures showed no improvement and the reason for this is suspected to be its original wettability. However, no conclusive measurements have been conducted on evaluating the wettability of the bauxite proppants and how the original wettability might vary with different bauxite samples made in different ways or used under different conditions. A better understanding of both bauxite and its use will be needed before any definite conclusions can be made about the benefits of chemical treatments of wells with bauxite-filled fractures can be made.

Table 8.1: Properties of propped fracture used for Experiment 39

Matrix rock	Berea Sandstone
Proppant	30/50 Bauxite
Length, inches	6.875
Fracture width, cm	0.24
Fracture porosity, %	42.82
Fracture Pore Volume, cc	4.45
Total Pore Volume, cc	17.97

Table 8.2: Experimental conditions for Experiments 29, 31 and 39

Exp #	29	31	39
Temperature, °F	279	279	279
Core Pressure, psig	1500	1450	1450

Table 8.3: Comparison of Reservoir B reservoir and synthetic fluid properties at 279°F and 1450 psig

	Reservoir Fluid		Lab Fluid	
	Gas phase	Oil phase	Gas phase	Oil phase
μ (cp)	0.017	0.348	0.0165	0.3112
Volume fraction	0.9757	0.0243	0.9782	0.0218
IFT (dyne/cm)	5.64		5.52	
PVT Ratio	1.96		2.38	

Table 8.4: Properties of propped fracture and rock matrix for Experiments 29 and 31

	Exp#29	Exp31
Matrix rock	Plug 7E	Berea Sandstone
Proppant	Ottawa F35 sand	Ottawa F35 sand
Length, inches	1.84	8
Fracture width, cm	0.22	0.24
Fracture porosity, %	36.07	36.6
Fracture Pore Volume, cc	0.97	4.42
Fracture permeability (k_g), Darcy	23.4	37.78
$K_g (S_{wi})$	11.51	33.02

Table 8.5: Composition of synthetic Reservoir B brine

Salts	g/l
NaCl	225.2
CaCl ₂	1.5
KCl	3.1

Table 8.6: Results of two-phase flow measurements on sand filled propped fracture at 279°F and 1500 psig (Exp#29)

Total Flow rate, cc/hr	Capillary Number	Pressure drop, psi	k_{rg}	k_{ro}
514	2.68×10^{-4}	0.19	0.069	0.028
815	3.67×10^{-4}	0.26	0.08	0.032
1631	7.76×10^{-4}	0.55	0.078	0.03
2899	1.69×10^{-3}	1.20	0.065	0.025

Table 8.7: Results of two-phase flow measurements on sand filled propped fracture at 279°F and 1450 psig (Exp#31)

Total Flow rate, cc/hr	Capillary Number	Pressure drop, psi	k_{rg}	k_{ro}
205.93	5.34×10^{-5}	0.23	0.054	0.022
411.86	6.87×10^{-5}	0.30	0.086	0.034
823.72	1.03×10^{-4}	0.45	0.122	0.046
1647.44	2.20×10^{-4}	0.96	0.127	0.043
2883.03	5.81×10^{-4}	2.53	0.092	0.028

Table 8.8: Results of two-phase flow measurements on Bauxite filled propped fracture at 279°F and 1450 psig with a net confining stress of 1000 psig (Exp#39)

Total Flow rate, cc/hr	Capillary Number	Pressure drop, psi	k_{rg}	k_{ro}
643.53	7.07×10^{-5}	0.13	0.139	0.052
1287.07	1.52×10^{-4}	0.28	0.144	0.048
2574.13	4.64×10^{-4}	0.82	0.113	0.033
4826.50	1.12×10^{-3}	2.06	0.106	0.025
7078.86	2.07×10^{-3}	3.80	0.100	0.02
9652.99	3.37×10^{-3}	6.20	0.099	0.016

Table 8.9: Results of two-phase flow measurements on Bauxite filled propped fracture at 279°F and 1450 psig with a net confining stress of 3000 psig (Exp#39)

Total Flow rate, cc/hr	Capillary number	Pressure drop, psi	k_{rg}	k_{ro}
643.53	8.53×10^{-5}	0.18	0.114	0.043
1287.07	1.95×10^{-4}	0.40	0.109	0.038
2574.13	4.78×10^{-4}	0.98	0.103	0.031
4826.50	1.11×10^{-3}	2.27	0.104	0.025
7078.86	1.19×10^{-3}	4.00	0.104	0.021

Table 8.10: Results of two-phase flow measurements on Bauxite filled propped fracture at 279°F and 1450 psig with a net confining stress of 5000 psig (Exp#39)

Total Flow rate, cc/hr	Capillary number	Pressure drop, psi	k_{rg}	k_{ro}
643.53	7.74×10^{-5}	0.19	0.125	0.048
1287.07	2.00×10^{-4}	0.49	0.104	0.037
2574.13	4.48×10^{-4}	1.10	0.107	0.033
4826.50	1.06×10^{-3}	2.60	0.105	0.026
7078.86	1.79×10^{-3}	4.40	0.109	0.023

Table 8.11: Results of two-phase flow measurements on sand filled propped fracture before solvent pre-flush at 279°F and 2600 psig (Exp#29)

Total Flow rate, cc/hr	Capillary number	Pressure drop, psi	k_{rg}	k_{ro}
542	1.31×10^{-3}	0.9	0.019	0.028
291	1.02×10^{-3}	0.7	0.008	0.005

Table 8.12: Composition of solvent used for pre-flush in Experiment 29

Component	Weight %
Propylene glycol	70
Isopropanol	30

Table 8.13: Composition of treatment solution used in Experiment 29

Component	Weight %
FC4430	2
Propylene glycol	69
Isopropanol	29

Table 8.14: Results of post-treatment two-phase flow measurements on sand filled propped fracture at 279°F and 1500 psig (Exp#29)

Total Flow rate, cc/hr	Capillary number	Pressure drop, psi	k_{rg}	k_{ro}	IF
514	1.55×10^{-4}	0.11	0.119	0.048	1.74
815	2.40×10^{-4}	0.17	0.124	0.049	1.54
1631	5.22×10^{-4}	0.37	0.117	0.045	1.50
2899	1.18×10^{-3}	0.84	0.095	0.035	1.45

Table 8.15: Composition of treatment solution used in Experiment 31

Component	Weight %
FC4430	2
Propylene glycol	79
Isopropanol	19

Table 8.16: Results of post-treatment two-phase flow measurements on sand filled propped fracture at 279°F and 1450 psig (Exp#29)

Total Flow rate, cc/hr	Capillary number	Pressure drop, psi	k_{rg}	k_{ro}	IF
205.93	2.10×10^{-5}	0.09	0.135	0.056	2.52
411.86	3.05×10^{-5}	0.13	0.188	0.077	2.19
823.72	5.51×10^{-5}	0.24	0.214	0.086	1.75
1647.44	1.26×10^{-4}	0.55	0.194	0.075	1.53
2883.03	2.84×10^{-4}	1.24	0.157	0.058	1.71

Table 8.17: Results of post-treatment two-phase flow measurements on Bauxite filled propped fracture at 279°F and 1450 psig with a net confining stress of 1000 psi (Exp#39)

Total Flow rate, cc/hr	Capillary number	Pressure drop, psi	k_{rg}	k_{ro}	IF
2574.13	4.90×10^{-4}	0.9	0.103	0.03	0.91
7078.86	2.39×10^{-3}	4.40	0.086	0.017	0.86

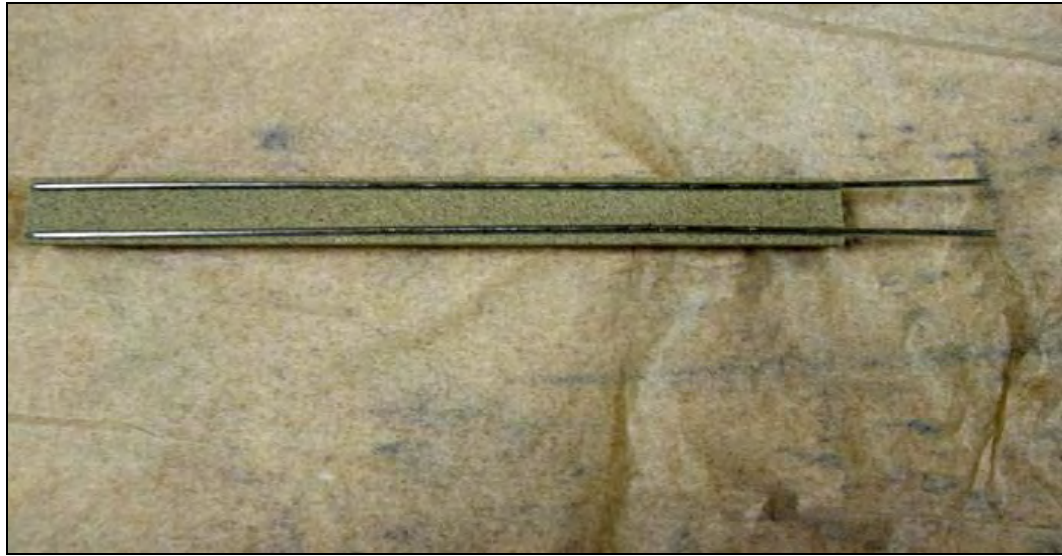


Figure 8.1: Step 1 of the preparation of propped fractures. Place spacers of the required fracture width between two halves of the core.



Figure 8.2: Step 2 of the preparation of propped fractures. Put the two halves of the core together with spacers between them and wrap them with a Teflon tape.



Figure 8.3: Step 3 of the preparation of propped fractures. Fill up the fracture space with proppant. Then wrap the core with a heat shrink tube.

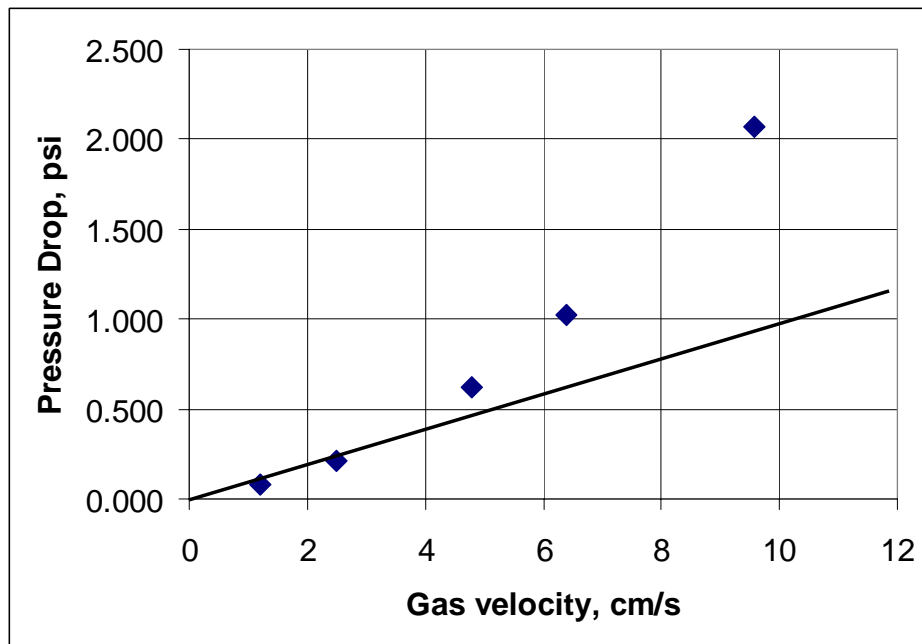


Figure 8.4: Deviation from Darcy's law at high gas velocities showing effect of non-Darcy flow

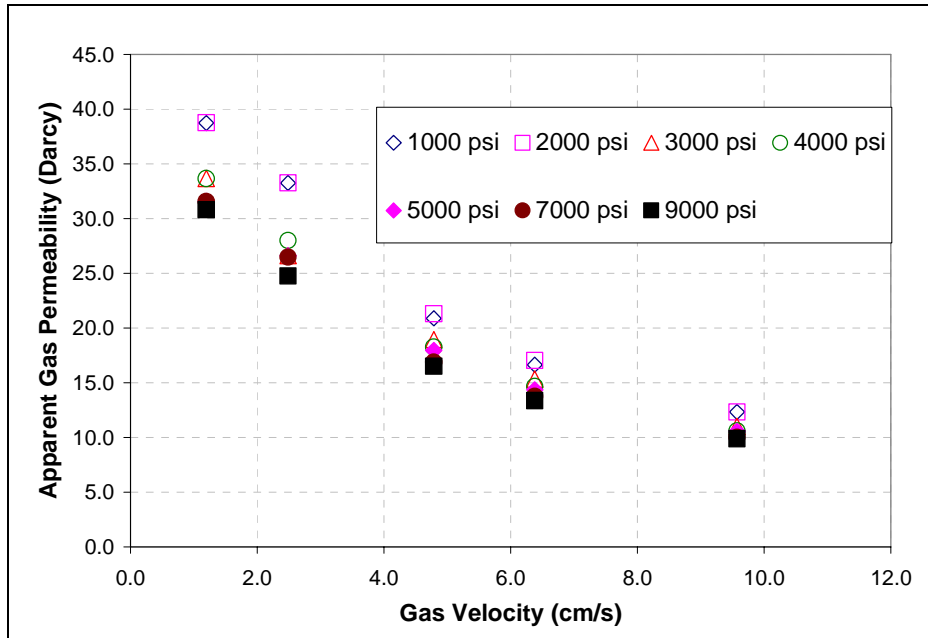


Figure 8.5: Effect of gas velocity and net confining stress on apparent gas permeability

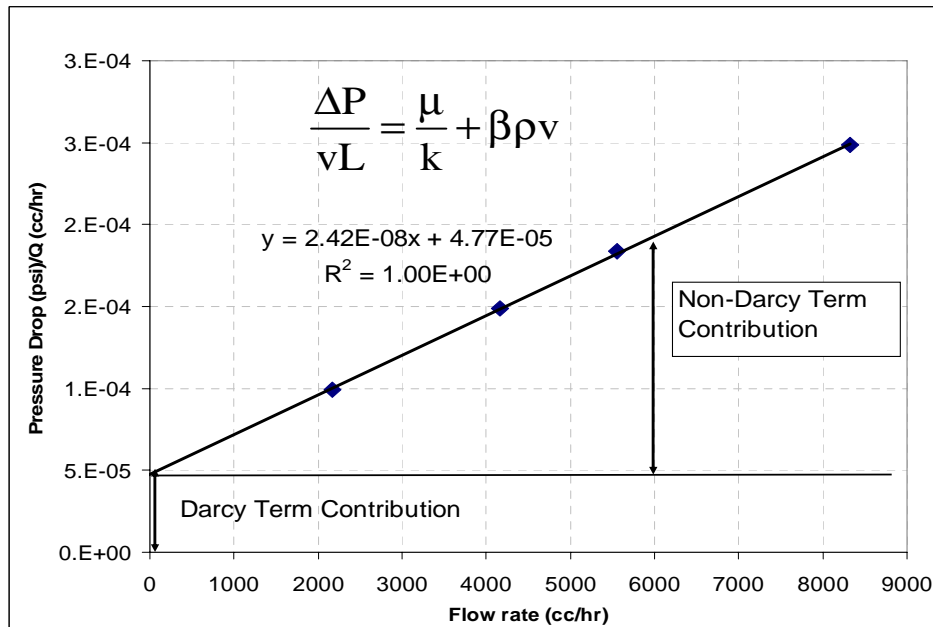


Figure 8.6: Correcting gas permeability measurement for non-Darcy flow

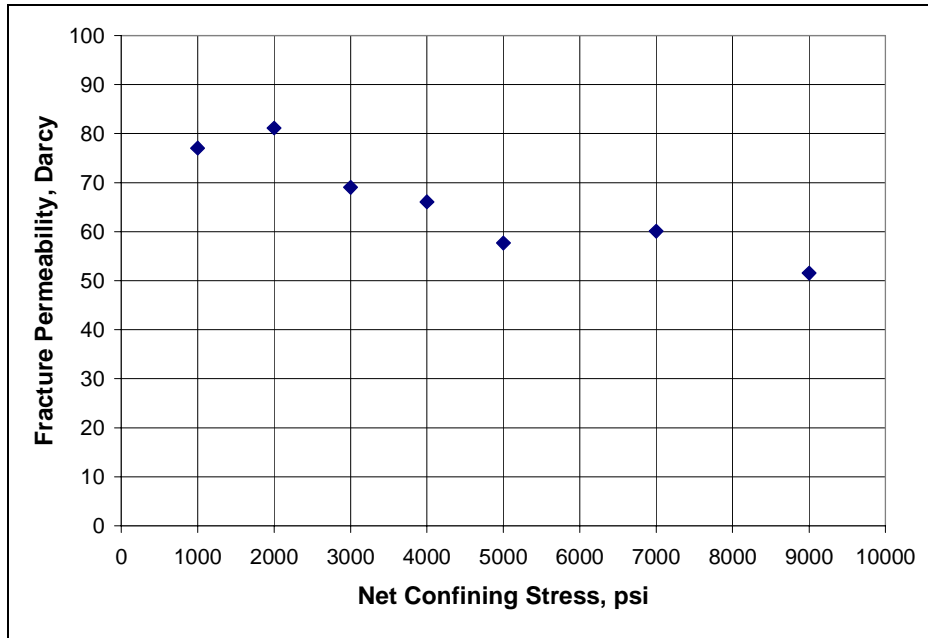


Figure 8.7: Effect of net confining stress on fracture permeability

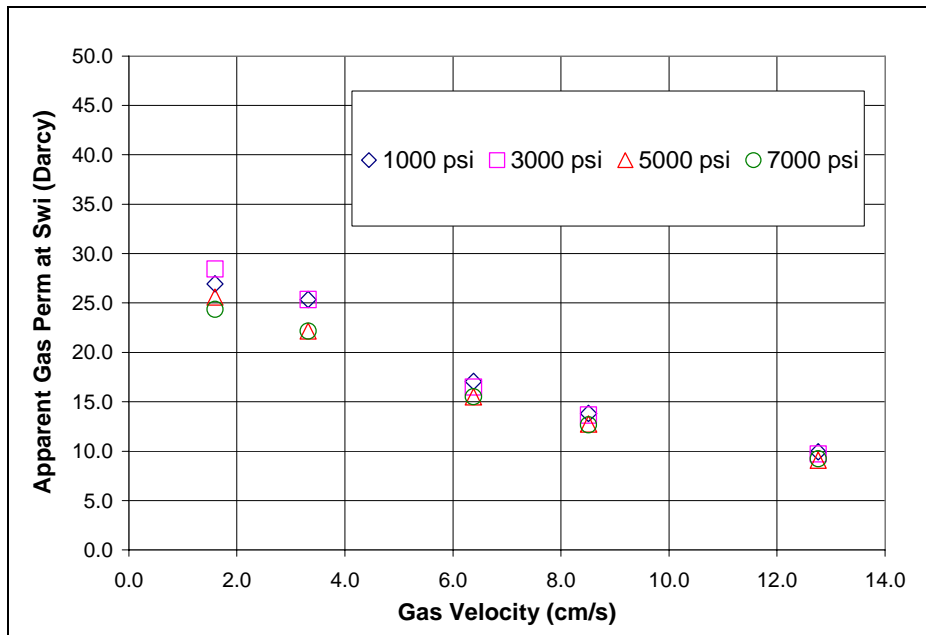


Figure 8.8: Effect of gas velocity and net confining stress on apparent gas permeability at S_{wi}

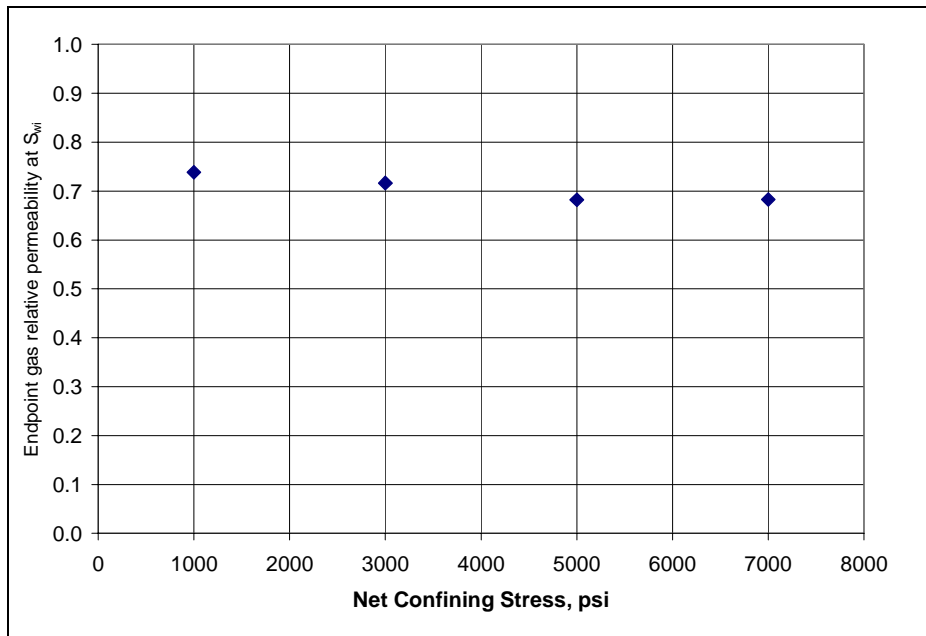


Figure 8.9: Effect of net confining stress on endpoint gas relative permeability at S_{wi}

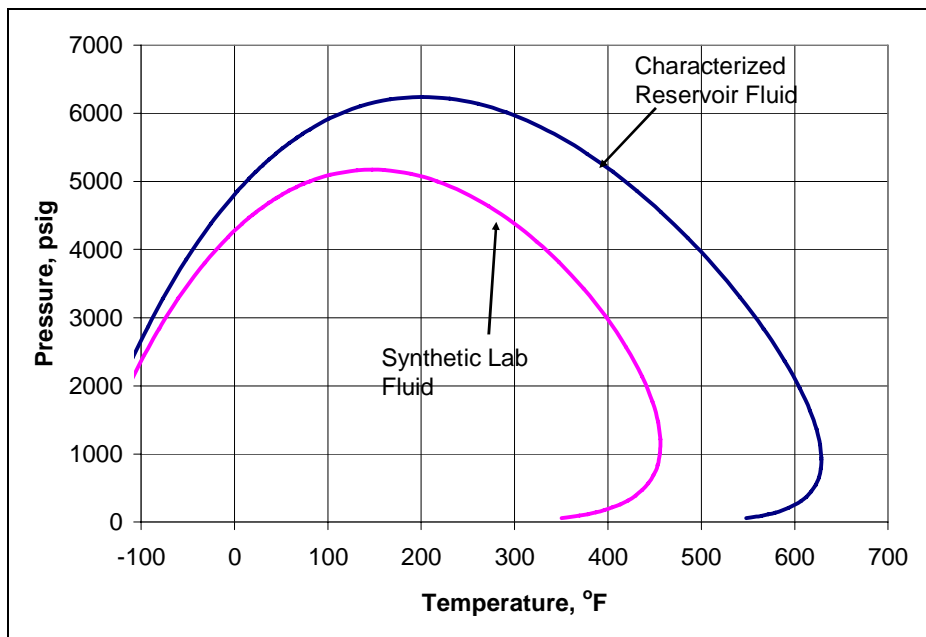


Figure 8.10 Comparison of P-T phase envelope calculated using PREOS for the characterized reservoir fluid and the synthetic lab fluid

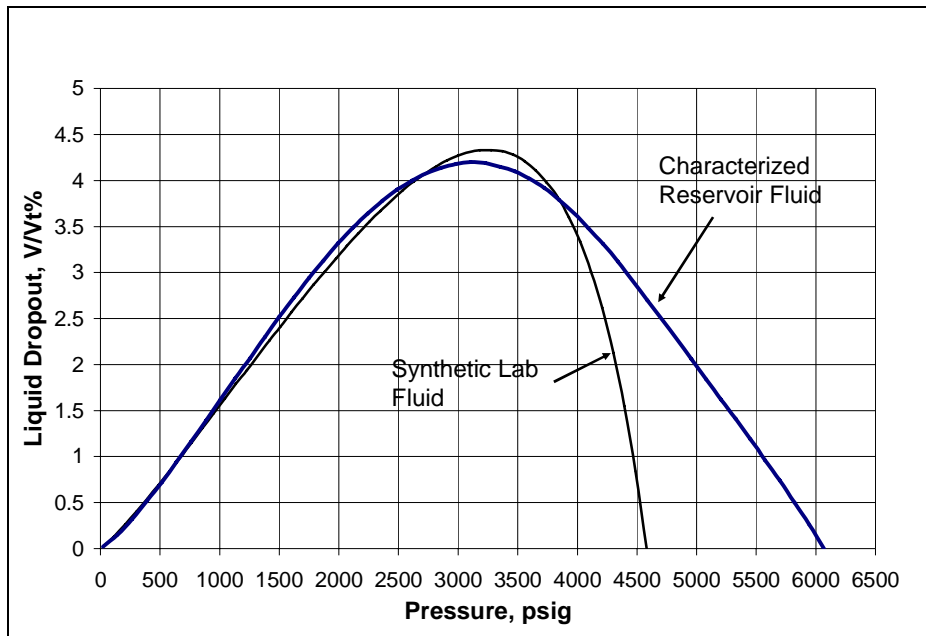


Figure 8.11 Comparison of liquid dropout at 279°F calculated using PREOS for the characterized reservoir fluid and the synthetic lab fluid

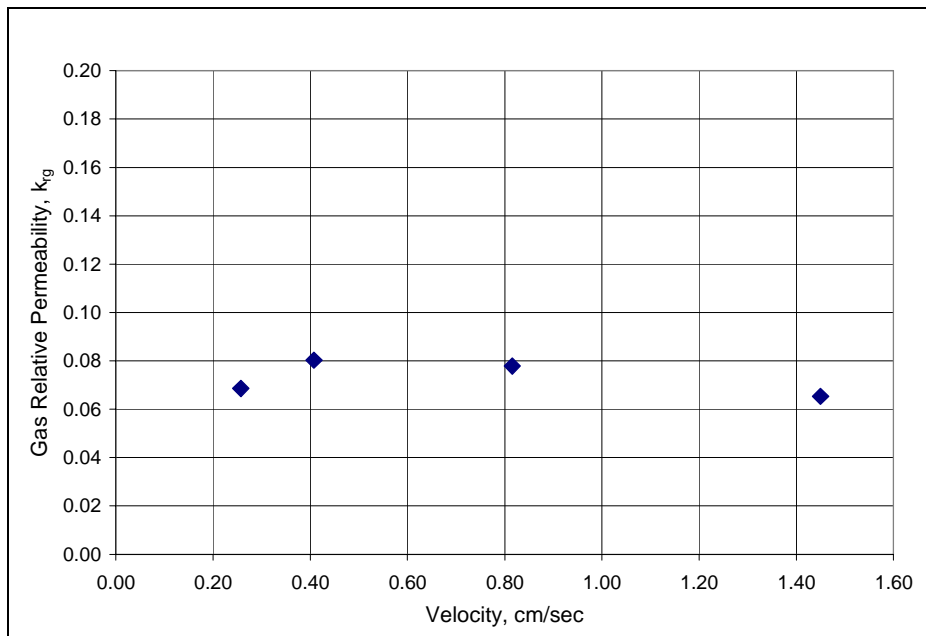


Figure 8.12 Variation of true gas relative permeability with gas velocity (Exp#29)

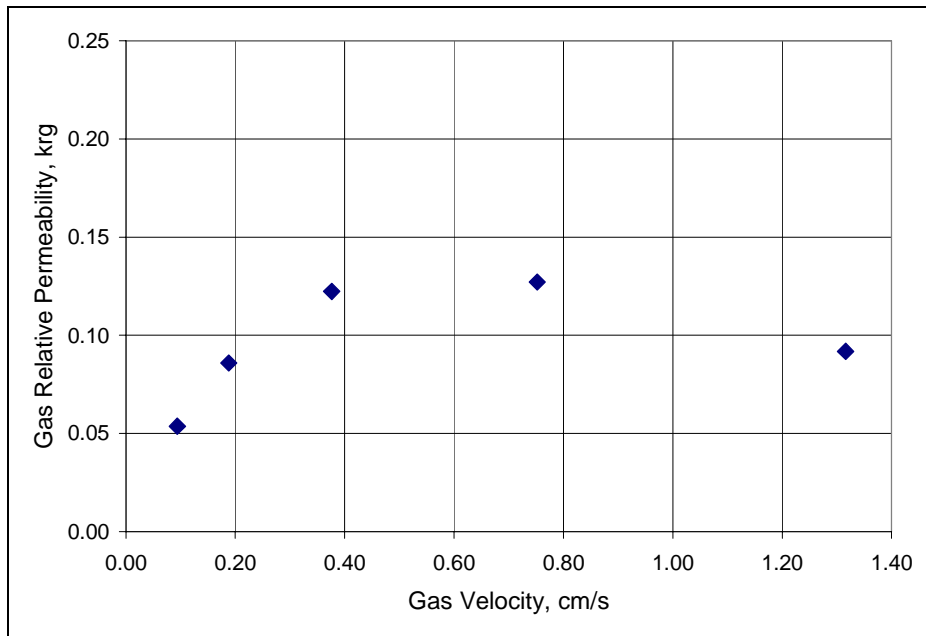


Figure 8.13 Variation of true gas relative permeability with gas velocity (Exp#31)

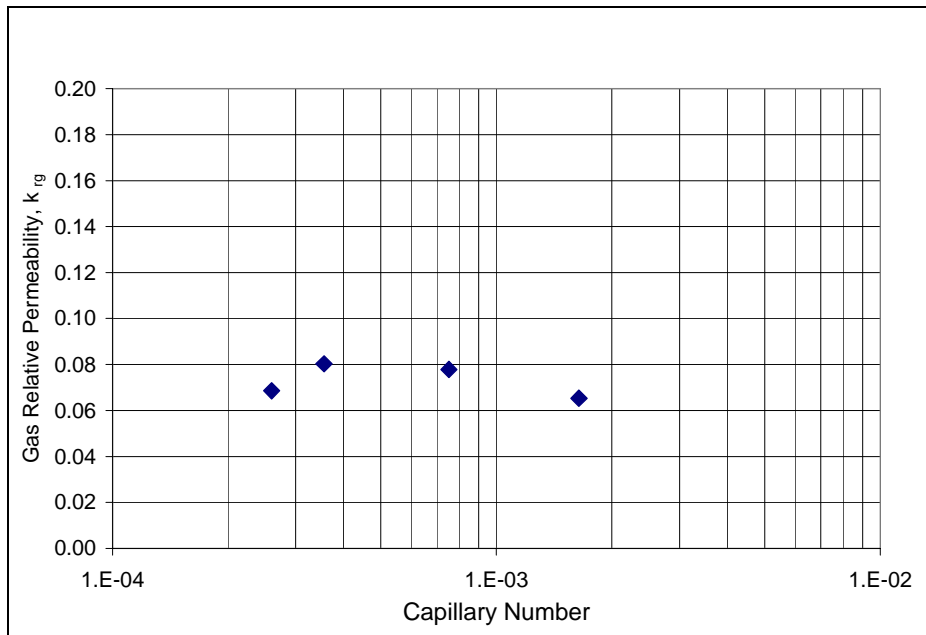


Figure 8.14 Variation of true gas relative permeability with Capillary number (Exp#29)

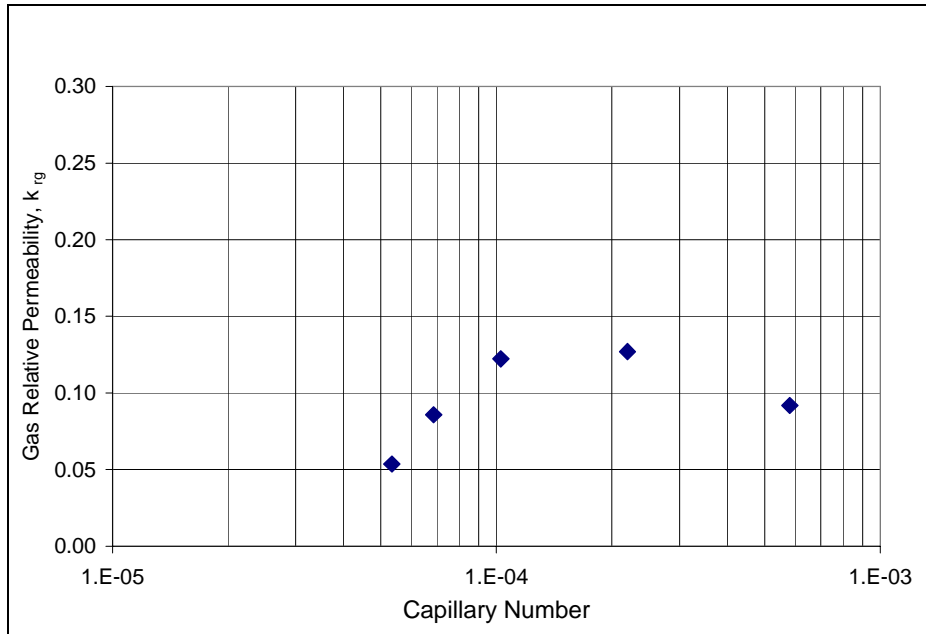


Figure 8.15 Variation of true gas relative permeability with Capillary number (Exp#31)

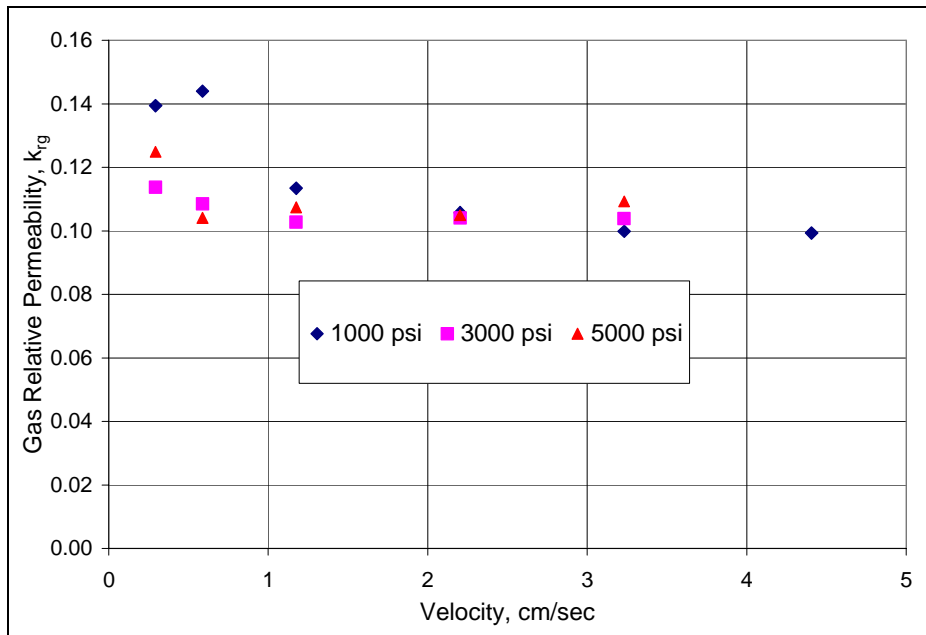


Figure 8.16 Effect of gas velocity and net-confining stress on true gas relative permeability for Experiment 39

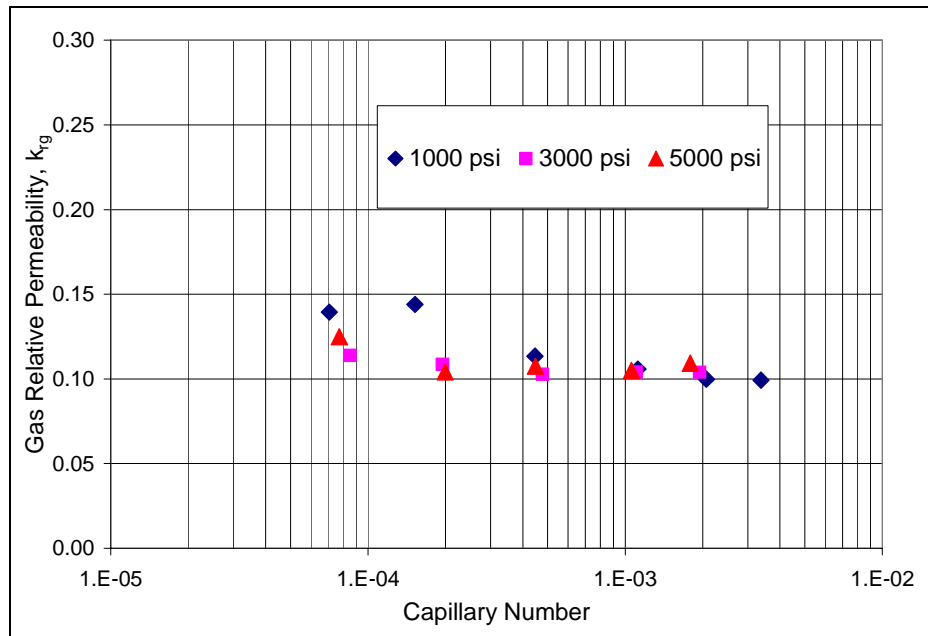


Figure 8.17 Effect of Capillary number and net-confining stress on true gas relative permeability for Experiment 39

Chapter 9: Chemical treatment for volatile oil and dead oil reservoirs

9.1 INTRODUCTION:

Dropout and accumulation in the formation of a liquid phase (condensate) from a gas phase below the dew-point pressure causes a significant reduction in gas relative permeability and thus the productivity of gas wells. A similar reduction in oil relative permeability can be caused when a gas phase bubbles out of the oil phase in volatile oil reservoirs as the pressure decreases below the bubble-point pressure. Therefore, productivity impairment of volatile oil reservoirs can be due to near wellbore gas blocking effects. Thus, the chemical treatment described in **Chapters 4 to 8** for gas condensate reservoirs was tested to determine whether it would also potentially be beneficial for wells in volatile oil reservoirs.

As condensate drops out of the gas phase below the dew point pressure, it accumulates in the pore space until it flows at some saturation above the critical condensate saturation. At steady state, (in the core or near the well) the actual fluid composition is different than the original gas condensate fluid. This change in the composition can change the phase behavior for the fluid significantly and may make it a volatile oil fluid near the well or in the core. **Figure 9.1** compares the P-T phase diagram of the original synthetic lab fluid-5 (Table 3.5), and the equilibrium fluid in the core at steady state at 400 psig and 175°F. For calculating the equilibrium fluid composition in the core, an oil saturation of 37% and gas saturation of 38% was assumed. These saturation values are the predicted steady-state saturation values calculated using the tuned relative permeability model described in **Chapter 10**. The equilibrium composition was calculated using the moles of liquid and vapor phase and the

compositions of each phase at core conditions calculated using PREOS. The overall mole fraction of each component in the core or at near wellbore conditions is given by:

$$z_i = Lx_i + Vy_i \quad (9.1)$$

Where, z_i is the overall mole fraction of component i , x_i is the mole fraction of component i in the liquid phase and y_i is the mole fraction of component i in the vapor phase. **Table 9.1** shows a comparison of the original fluid composition and the composition of the equilibrium fluid at core conditions. The comparison of the P-T phase diagrams show that the critical temperature of the equilibrium fluid at steady state in the core is about 640°F compared to -7°F for the original fluid. Thus at the experimental temperature of 175°F, the original fluid behaves as a retrograde gas condensate but the fluid in the core behaves as a volatile oil.

Figure 9.2 compares the P-T phase diagram of the original synthetic lab fluid-3 (Table 3.3) and the equilibrium fluid at steady state in the core at 1500 psig and 250°F. Again, at the experimental temperature of 250°F, the original fluid behaves as a retrograde gas condensate but the fluid in the core behaves as a volatile oil.

Figure 9.3 compares the P-T phase diagram of the characterized Bruce reservoir fluid (Table 12.1) and the equilibrium fluid at steady state around the well at a flowing bottom hole pressure of 400 psig at 175°F. The result shows that as the gas condensate fluid moves closer to the well, the fluid composition changes significantly due to higher condensate (oil) saturation around the well and makes it a volatile oil. The change in the phase behavior of the fluid, however, depends on the flowing bottom hole well pressure as a lower pressure will cause a bigger change in the fluid composition and a further shift from the original fluid.

9.2 CHEMICAL TREATMENT OF VOLATILE OIL RESERVOIRS

The reduction in well productivity for gas condensate and many volatile oil reservoirs is due to the formation of two phases around the wellbore as the pressure falls below the saturation pressure of the fluid. This results in a reduction in the relative permeability of gas and oil phases for gas and oil reservoirs, respectively. The previous section showed that many gas condensate reservoirs may actually be on the left side of the critical point in the near wellbore region making them behave like a bubble-point fluid or a volatile oil. Thus, the chemical treatment used to improve the relative permeabilities of both gas and oil in gas condensate reservoirs might also work in volatile oil reservoirs.

Experiment 46 was conducted at 154°F and 687 psig. A synthetic hydrocarbon gas mixture was designed to exhibit volatile oil or bubble point fluid behavior under the experimental conditions. **Table 9.2** gives the composition of the synthetic gas mixture. **Figure 9.4** shows calculated P-T phase diagram and **Figure 9.5** shows the calculated phase volume fractions of the synthetic lab fluid at 154°F. **Table 9.3** summarizes the core properties and the experimental conditions.

Figure 9.6 shows the steady state pressure drops measured during the two-phase flood at multiple rates. The core was then treated with the fluoro-surfactant FC4430 delivered in a 70/30 mixture of 2-butoxyethanol and ethanol. **Table 9.4** gives the composition of the treatment solution. 19 pore volumes of treatment solution was flowed thorough the core at 120 cc/hr and the core was then shut-in for 24 hours.

Post-treatment two-phase oil and gas flow of the same fluid mixture was then conducted under the same conditions as the initial two-phase flow. **Figure 9.6** compares the pressure drop across the core measured during the pre-treatment and post-treatment

two-phase floods. **Table 9.5** summarizes the results of the pre-treatment and post-treatment two-phase floods. The results show that the chemical treatment increased the oil and gas relative permeability by factor of 2.7 to 2.9. Details of the experiment are given in **Appendix B46**.

The results show that the chemical treatment can be successfully used for volatile oil reservoirs to increase their productivity. The improvement factor for gas and oil in this experiment was higher than those observed for gas condensate fluids in earlier experiments. The temperature difference between this experiment and those done under Bruce conditions at 175°F (Exp# 24, 41 and 42) is not enough to make any significant difference on the chemical treatment. So the higher improvement factor could be due to the higher oil saturation in the porous medium for volatile oil fluids before the treatment compared to gas condensate fluids. No saturation measurements were done to support this argument. Some more experimental studies should be conducted to further investigate and explore fully the possibility of such treatments in volatile oil reservoirs.

9.3 CHEMICAL TREATMENT OF DEAD OIL RESERVOIRS

Results presented in earlier chapters and in this chapter so far have shown that the chemical treatment using the fluoro-surfactant FC4430 can improve the relative permeabilities for two-phase flow of gas and oil for both gas condensate and volatile oil reservoirs. This section explores the possibility of extending the treatment to dead oil reservoirs which are associated with some mobile water. The problem associated with low relative permeability of oil in such reservoirs is not a near wellbore issue but still some improvement can be obtained by increasing the oil relative permeability in the near wellbore region where the pressure gradient driving the flow is maximum. Also, some

additional benefit can be achieved by just removing connate water from the near wellbore region.

This section presents the results of an exploratory experiment conducted to evaluate the effect of chemical treatment on oil and water relative permeabilities. Saturation measurements for such fluids become extremely important, unlike gas condensate fluids or volatile oils where the flow of gas and oil are a function of the flowing pressure (Chapter 10). Therefore, the procedure followed in this experiment was different than the one used with gas condensate and volatile oil fluids. In this experiment the entire relative permeability curve before and after the chemical treatment was measured for both oil and water. Saturation measurements were done by performing a mass balance on water.

Experiment 47 was conducted on a Berea sandstone core at 140°F. Properties of the core and the experimental conditions are given in **Table 9.6**. 25,000 ppm NaCl brine was used as an aqueous phase and n-decane was used as the oil phase. The core was vacuumed and then fully saturated with brine to measure the pore volume. Brine was then flowed through the core to measure the initial permeability. The brine flood was followed by an oil flood to reduce the water saturation to residual and measure the residual water saturation before treatment. This was followed by a second brine flood to reduce the oil saturation to residual and measure the pre-treatment residual oil saturation. This was again followed by an oil flood to reduce the water saturation to residual so that the relative permeability curve during imbibition i.e. increasing saturation of the wetting phase (water) can be measured.

Two phases, oil and water, were then flowed through the core at different fractional flows, starting with a small fractional flow of water and increasing it in steps. The fractional flow of water was increased from 0.24 to 1. Saturations at each fractional

flow were measured from the difference between the volume of water injected and produced. **Table 9.7** summarizes the measured water saturation and the corresponding oil and water relative permeability curves for the pre-treatment two-phase floods. **Figure 9.7** shows the pre-treatment oil-water relative permeability curve.

The water saturation at the end of the two-phase flood ($f_w = 1$) was 65%. This high water saturation can cause the surfactant to reach its cloud point in the treatment solution and result in surfactant precipitation. To avoid this, an oil flood was conducted to reduce the water saturation to residual. The core was then treated with FC4430 delivered in a mixture of 70/30 2-butoxyethanol/ethanol (**Table 9.4**). Fifteen pore volumes of treatment solution was flowed through the core at 250 cc/hr and 500 cc/hr. The pressure drop measured across the core and the sections during the treatment flood is shown in **Appendix B47**. The pressure drop across the inlet section of the core shows an increasing trend suggesting some kind of plugging at the inlet end. The core was then shut-in for 15 hours.

Treatment solution was then flushed out by injecting 1.5 pore volumes of ethanol. This was done to avoid precipitation of the surfactant. An oil flood was then conducted to flush out ethanol from the core. A brine flood and a second oil flood were then conducted to get the post-treatment residual oil and water saturations. Two-phase oil-water floods were then conducted under similar conditions as the pre-treatment two-phase flood to measure the post-treatment oil-water relative permeability curve. **Table 9.9** summarizes the measured water saturation and the corresponding oil and water relative permeability curves for the post-treatment two-phase floods. **Figure 9.8** shows the post-treatment oil-water relative permeability curve.

Figure 9.9 compares the pre-treatment and post-treatment relative permeability curves. The result shows that the relative permeability curves for both oil and water did

not change after chemical treatment. This suggests that the treatment failed to improve the relative permeability of oil for oil-water two-phase flow. The failure for the treatment is most probably due to plugging caused during the treatment flood (**Appendix B47**). Phase behavior tests were then done with the treatment solution and a mixture of 45/55 brine/oil at 140°F. The test showed that the mixture has two-phases and the surfactant precipitates from the aqueous phase at a lower temperature but moves into the oil phase as the temperature is increased to 140°F. This shows that a high saturation of oil (n-decane) can also cause surfactant to precipitate. The high oil saturation in the core before the treatment flood, therefore, may have caused the surfactant to precipitate out and plug the core. Thus the chemical treatment failed to give any improvement in oil relative permeability. Therefore, for successfully treating rocks with high water and oil saturations (oil-water two-phase flow or oil-water-gas three phase flow), phase behavior studies need to be done to evaluate solvents that can be used to deliver surfactant under these conditions.

9.4: SUMMARY

The chemical treatment developed for gas condensate reservoirs has been successfully extended to volatile oil reservoirs, which may face the same problem of two-phase flow in the near wellbore region. The chemical treatment increased the oil and gas relative permeability for a volatile oil by a factor of 2.7 - 2.9. The result shows that the chemical treatment can be an effective means of restoring productivity of many volatile oil reservoirs.

The chemical treatment was also extended for improving the productivity of dead oil reservoirs with oil-water two-phase flow. The idea is to increase the relative permeability of oil in the near wellbore region where the pressure gradient driving the

flow is maximum. The relative permeability curves for oil and water were measured before and after the treatment. The chemical treatment failed to change the relative permeability curves. The failure of the treatment was due to the precipitation of surfactant out of the solution as the treatment solution was not able to tolerate high oil saturations.

Table 9.1: Composition of original gas condensate (mixture-5) fluid and the equilibrium fluid in core at steady state at 400psig and 175°F

Component	At core pressure = 400 psig			
	Initial z_i	x_i	y_i	z_i
methane	0.89	0.94	0.11	0.25
propane	0.05	0.05	0.49	0.05
n-heptane	0.025	0.096	0.27	0.23
n-decane	0.025	0.014	0.40	0.33
n-pentadecane	0.01	0.001	0.17	0.14

Table 9.2: Synthetic volatile oil fluid mixture (Exp #46)

Component	Mole%
Methane	75
Propane	12
n-Heptane	9
n-Decane	4

Table 9.3: Core properties and experimental conditions for Experiment#46

Core	Berea Sandstone
Length, inches	8
Diameter, inches	0.99
Dry Weight of the core	214.36
Porosity, %	20.19
Pore volume, cc	20.46
Swi, %	20
Temperature, °F	154
Core Pressure, psig	687

Table 9.4- Composition of treatment solution (Exp #46)

Component	Weight %
FC4430	1
2-Butoxyethanol	69.5
Ethanol	29.5

Table 9.5: Effect of chemical treatment on two-phase gas and oil relative permeabilities for a volatile oil (Exp #46)

	Core Flow rate, cc/hr	
	250	125
PVT Ratio	0.94	0.94
Capillary number, N_c	2.51×10^{-5}	1.36×10^{-5}
k_{rg} before treatment	0.038	0.035
k_{ro} before treatment	0.041	0.038
k_{rg} after treatment	0.104	0.113
k_{ro} after treatment	0.111	0.120
Improvement Factor	2.73	2.96

Table 9.6 - Core properties and experimental conditions for Experiment #47

Core	Berea Sandstone
Length, inches	11.75
Diameter, inches	2
Pore volume, cc	116.85
Porosity, %	19.32
Temperature, °F	140

Table 9.7: Pre-treatment oil-water relative permeability values (Exp #47)

fw	Sw, %	k _{ro}	k _{rw}
0	37	0.564	0.000
0.25	52	0.126	0.035
0.49	56	0.060	0.050
0.63	58	0.034	0.048
1.0	65	0.000	0.060

Table 9.8- Post-treatment oil-water relative permeability values (Exp #47)

fw	Sw, %	k _{ro}	k _{rw}
0	23	0.856	0.000
0.2	46	0.178	0.037
0.4	51	0.08	0.04
0.5	53	0.055	0.046
0.6	54	0.038	0.047
0.8	56	0.015	0.049
1.0	59	0.00	0.056

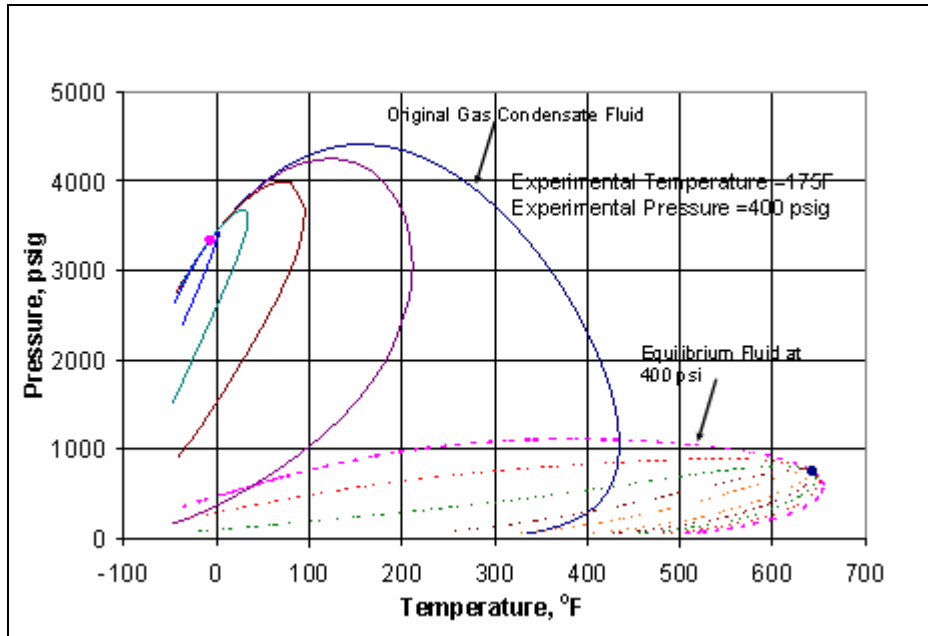


Figure 9.1: Comparison of P-T phase diagram of the original synthetic lab fluid-5 and the equilibrium fluid in the core at steady state at 400 psig and 175°F

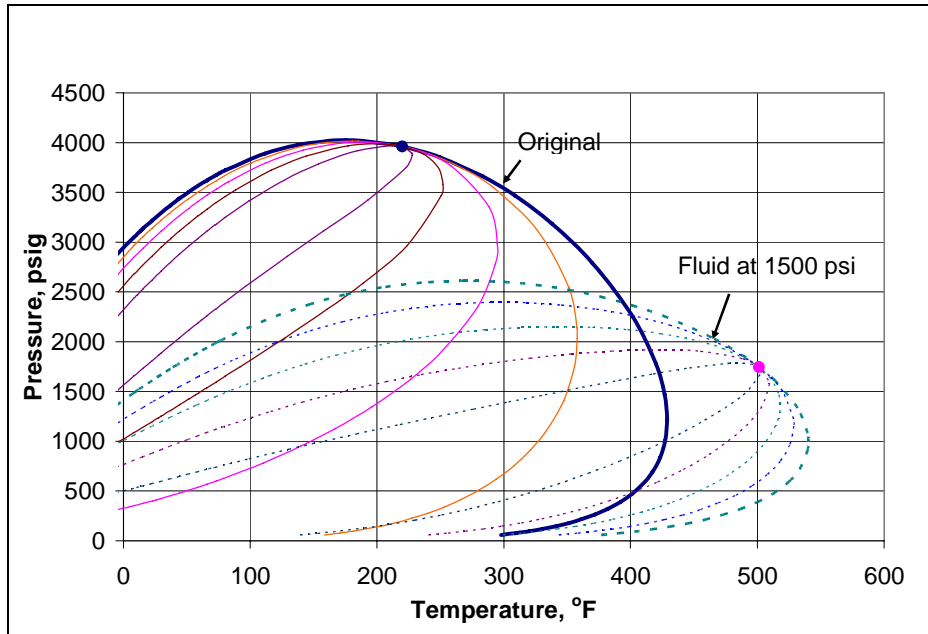


Figure 9.2: Comparison of P-T phase diagram of the original synthetic lab fluid-3 and the equilibrium fluid in the core at steady state at 1500 psig and 250°F

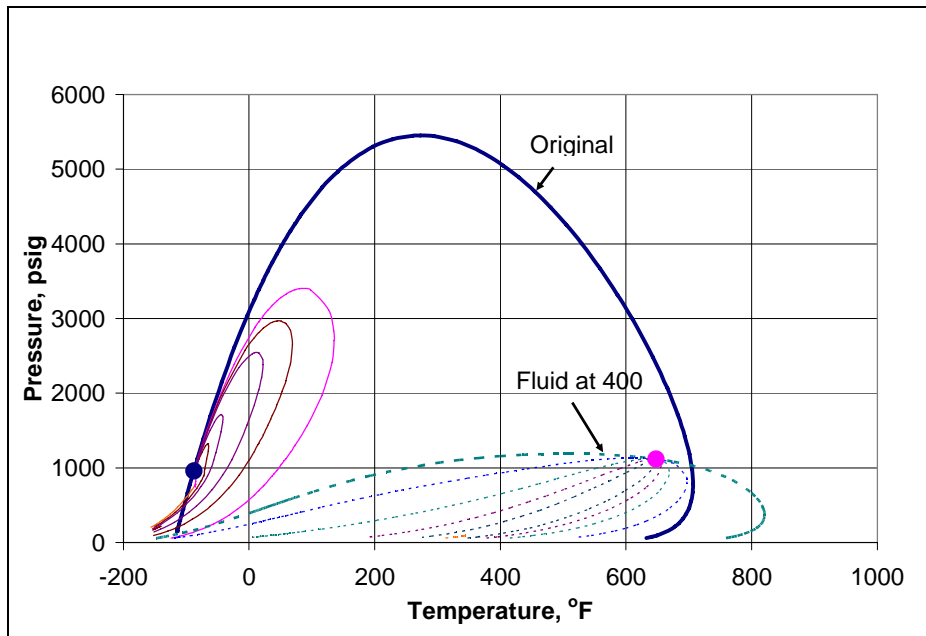


Figure 9.3: Comparison of P-T phase diagram of the original Bruce reservoir fluid and the equilibrium fluid in the near wellbore region at 400 psig and 230°F

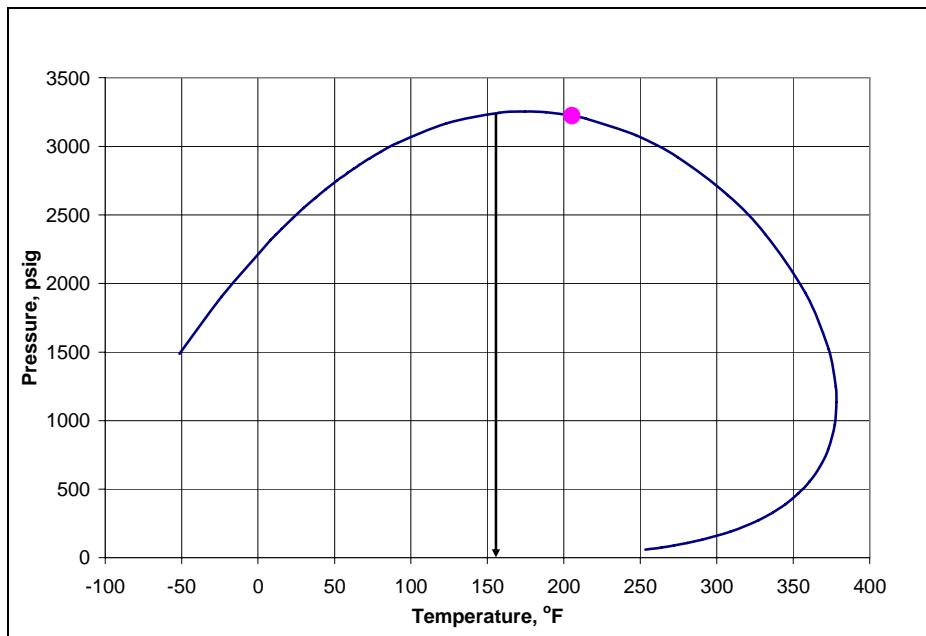


Figure 9.4: Calculated P-T phase diagram of synthetic lab fluid used as volatile oil (Exp #46)

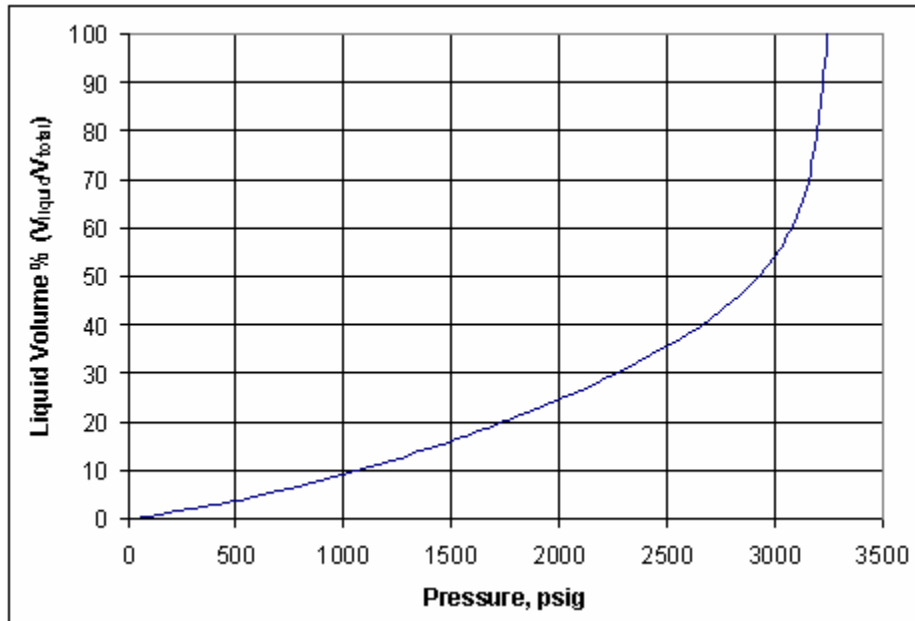


Figure 9.5: Calculated CCE liquid dropout for the lab fluid at 154°F

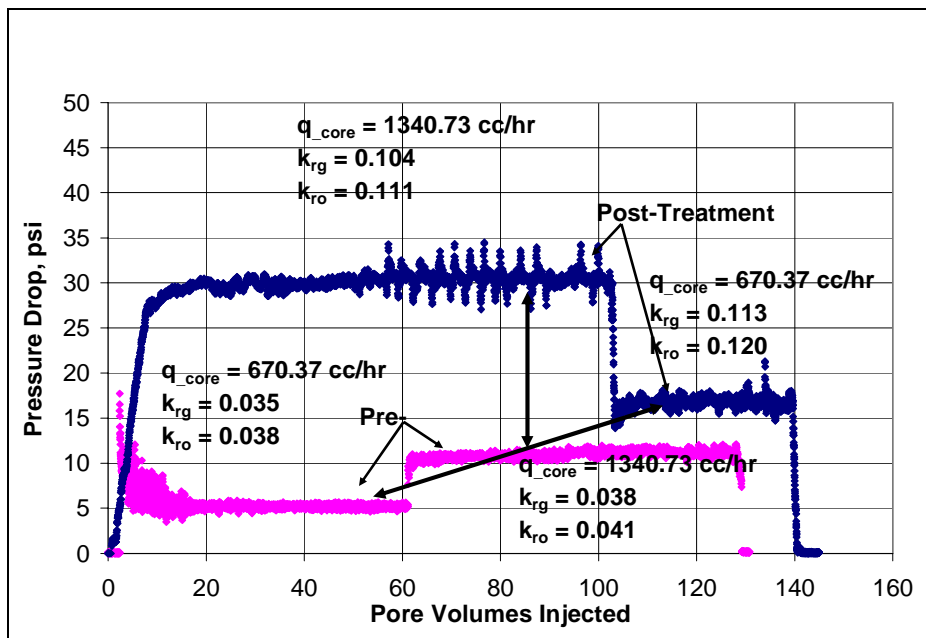


Figure 9.6: Comparison of pre-treatment and post-treatment steady state pressure drop at 154°F and 687 psig (Exp #46)

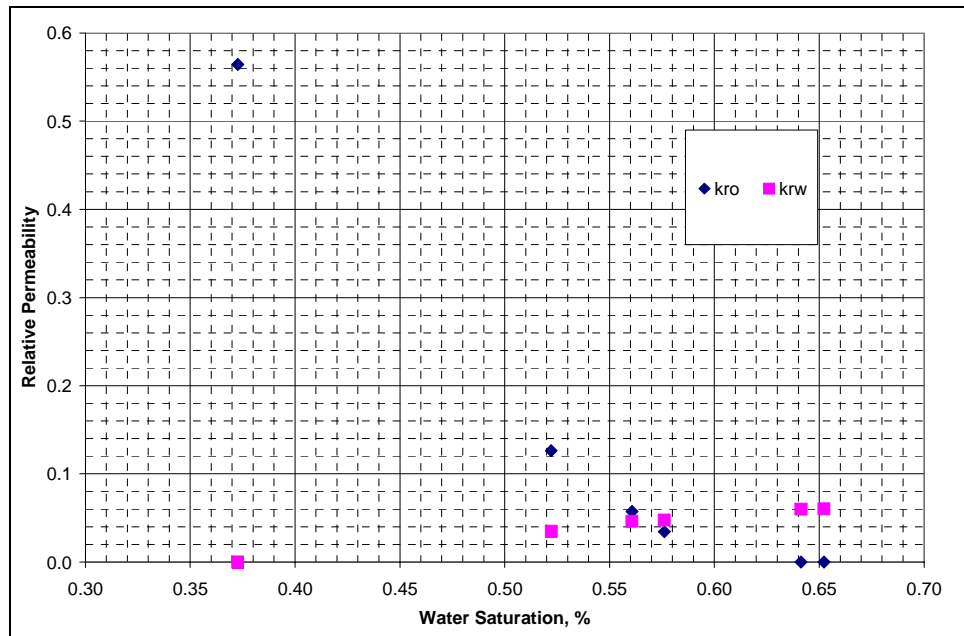


Figure 9.7: Pre-treatment oil-water relative permeability curve measured on Berea sandstone (Exp #47)

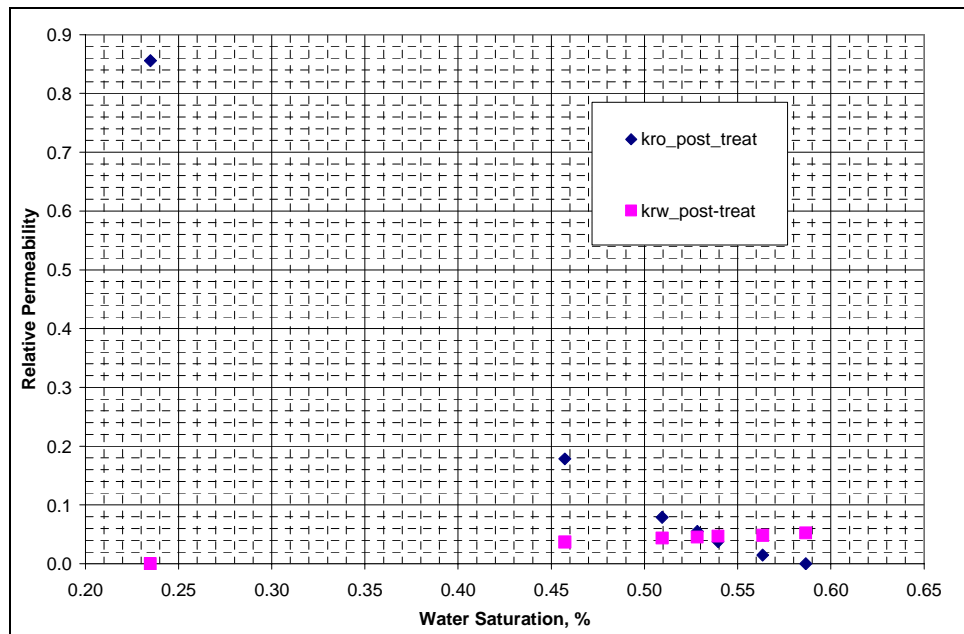


Figure 9.8: Post-treatment oil-water relative permeability curve measured on Berea sandstone (Exp #47)

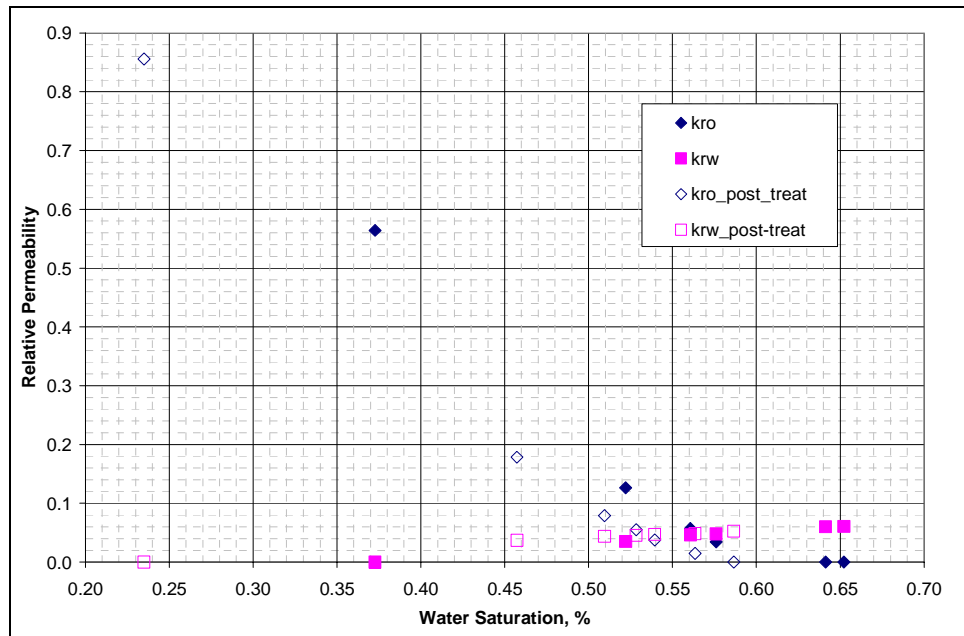


Figure 9.9: Comparison of oil-water relative permeability curves before and after chemical treatment

Chapter 10: Analysis of the Relative Permeability of Gas-Condensate Fluids

10.1 INTRODUCTION:

Predicting production from gas-condensate wells requires an accurate relative permeability model when a condensate bank forms. In the near wellbore region, due to high flow rates, both non-Darcy and Capillary number effects are significant and have opposing effects. The non-Darcy flow tends to increase the pressure loss and reduce gas relative permeability. When only non-Darcy effects are considered, the condensate bank can cause more than an order of magnitude reduction in PI. The high capillary (trapping) number, on the other hand, tends to reduce the residual saturation of the condensate and increase its relative permeability and thus counteracts the reduction in PI due to non-Darcy effects. Thus this effect mitigates the PI reduction caused by condensate buildup and makes the drop in PI more gradual. The net result on well productivity is governed by the dominance of one of the above effects over the other.

In the approach developed in this work the relative permeability has been expressed as a function of fluid properties expressed as a dimensionless PVT ratio, the Capillary number and a modified Reynolds number.

10.2 RATIO OF GAS TO OIL RELATIVE PERMEABILITIES EXPRESSED AS A FUNCTION OF PVT PROPERTIES:

Chopra *et al.* (1986) showed that at steady state the ratio of gas to oil relative permeability (k_{rg}/k_{ro}) can be calculated using only PVT data provided Darcy's law is valid, which is a good approximation at low velocities where the inertial effects are negligible.

Neglecting capillary pressure and gravity, Darcy's law for steady state flow in one dimension can be written as follows:

$$u_j = \frac{kk_{rj}\Delta P}{\mu_j L} \quad (10.1)$$

The capillary pressure between the gas and oil (condensate) phases has been neglected for the reasons explained earlier in Chapter 3. Now, the fractional flow of each phase j is defined as:

$$f_j = \frac{u_j}{u} \quad (10.2)$$

Equation 10.1 can be re-written in terms of fractional flow for gas and oil phases as:

$$f_g \mu_g = \frac{kk_{rg}\Delta P}{uL} \quad (10.3)$$

$$f_o \mu_o = \frac{kk_{ro}\Delta P}{uL} \quad (10.4)$$

Dividing equation 10.3 by equation 10.4, gives the ratio of gas to oil relative permeability expressed in terms of their fractional flow and viscosities.

$$\frac{k_{rg}}{k_{ro}} = \frac{f_g \mu_g}{f_o \mu_o} \quad (10.5)$$

At steady state the two-phase fractional flow of gas and oil is equal to the volume fraction of the phase as measured in a constant composition expansion at the temperature and pressure of the core (or reservoir) and can thus be expressed as follows:

$$f_g = \frac{V_g}{V_g + V_o} \quad (10.6)$$

$$f_o = \frac{V_o}{V_g + V_o} \quad (10.7)$$

where V_g and V_o are the volumes of gas and oil. The fractional flows are valid with or without connate water present in the rock. Substituting equation 10.6 and 10.7 into equation 10.5 gives the ratio of gas to oil relative permeability expressed in terms of the phase volumes and viscosities.

$$\frac{k_{rg}}{k_{ro}} = \frac{V_g \mu_g}{V_o \mu_o} \quad (10.8)$$

Thus, the ratio of steady state gas to oil relative permeability can be expressed as a function of a PVT ratio defined as follows:

$$\text{PVT_Ratio} = \frac{V_g \mu_g}{V_o \mu_o} \quad (10.9)$$

This relationship implies that the ratio of gas to oil relative permeability at a given core pressure is fixed and governed by the fluid properties only. This simplifies the measurement and/or modeling of gas-condensate relative permeability since the relative

permeability ratio is a function of pressure and composition only in a reservoir at fixed temperature and there is no need to know the fluid saturations. Similar relationships have been used by Fevang and Whitson (1996) and others to simplify the calculation of gas-condensate well performance. This relationship between the ratio of gas to oil relative permeability and PVT properties is however only valid as long as the non-Darcy flow effects are insignificant. Effect of non-Darcy flow on k_{rg}/k_{ro} ratio is described later in **Section 10.5**.

10.3 EFFECT OF CAPILLARY NUMBER ON GAS AND OIL RELATIVE PERMEABILITIES:

The fundamental problem with condensate buildup in the reservoir is that capillary forces can retain the condensate in the pores unless the forces displacing the condensate exceed the capillary forces. To the degree that the pressure forces in the displacing gas phase and the buoyancy force on the condensate exceed the capillary force on the condensate, the condensate saturation will be reduced and the gas relative permeability increased. Brownell and Katz (1947) recognized early on that the residual oil saturation is a function of the ratio of viscous force to interfacial force, and defined a Capillary number to capture this ratio:

$$N_{c_l} = \frac{|\vec{k} \cdot \vec{\nabla} P_l|}{\sigma_{ll}} \quad (10.10)$$

Here the displacing phase is designated by l' and the displaced phase by l .

In some cases buoyancy forces on the trapped phase can be significant or even dominant compared to viscous forces. The Bond Number is defined as the ratio of the buoyancy force to the interfacial force:

$$N_{B_I} = \frac{kg(\rho_{I'} - \rho_I)}{\sigma_{II'}} \quad (10.11)$$

The vector sum of the forces on the trapped phase (condensate) can be used to define a trapping number (Pope *et al.*, 2000).

$$N_{T_I} = \frac{\left| \vec{k} \cdot (\vec{\nabla} \Phi_I + g(\rho_{I'} - \rho_I) \vec{\nabla} D) \right|}{\sigma_{II'}} \quad (10.12)$$

The numerator of the trapping number has two opposing forces acting on the trapped phase, the pressure force in the displacing gas phase (viscous forces) favorable for the trapped phase displacement and the unfavorable gravity forces due to density difference of the displacing and the displaced phases.

For linear core floods at high flow rate where gravity and buoyancy forces are small compared to viscous forces, the trapping number simplifies to the following equation for Capillary number used in this work:

$$N_c = \frac{|\vec{k} \cdot \vec{\nabla} P|}{\sigma L} \quad (10.13)$$

The pressure drop is the only variable in Eq. 10.4 for two-phase steady state flow of gas and oil at connate water saturation at fixed temperature and pressure. There is no

advantage to expressing the Capillary Number in terms of velocity since the pressure drop is measured.

At high flow rates typical of many gas-condensate wells, the relative permeability is rate dependent. Such rate dependence can be modeled using a Capillary number to calculate the decrease in residual saturations and the corresponding increase in relative permeability as the viscous forces become dominant over the interfacial forces.

Pope *et.al* (2000) presented a relative permeability model for gas and condensate relative permeabilities as a function of Trapping Number or for special cases Capillary number. The relative permeability k_{rl} of each phase l is calculated by interpolating between the measured value at low Capillary number and a straight line corresponding to a very high Capillary number:

$$\log k_{rl} = \log k_{rl}^o + \log \bar{S}_l + \frac{\log \left(\frac{k_{rl}}{k_{rl}^o} \right)^{\text{low}} + \log \bar{S}_l}{1 + T_l (N_c)^{\tau_l}} \quad (10.14)$$

where

$$\bar{S}_l = \frac{S_l - S_{lr}}{1 - \sum_{l=1}^{n_p} S_{lr}} \quad (10.15)$$

where k_{rl} is the relative permeability and k_{rl}^o is the endpoint relative permeability for a given trapping number and saturation. \bar{S}_l is the normalized saturation and n_p is the number of phases. The residual saturation of each phase l is modeled as a function of Capillary number as shown below:

$$S_{lr} = \min \left(S_l, S_{lr}^{\text{high}} + \frac{S_{lr}^{\text{low}} - S_{lr}^{\text{high}}}{1 + T_l (N_c)^{\tau_l}} \right) \quad (10.16)$$

where S_{lr} is the residual saturation of the phase l . The superscripts low and high refer to low and high Trapping (Capillary) Numbers. Thus, the value of S_{lr}^{high} is typically zero and S_{lr}^{low} is the residual saturation measured in a core flood at low flow rate. The trapping parameters T_l and τ_l define the desaturation curves for the wetting and non-wetting phases and are obtained by fitting the residual saturation data for each phase.

The endpoint relative permeability of each phase is calculated as a function of the residual phase saturations (and thus indirectly the capillary number) as follows:

$$k_{rl}^o = k_{rl}^{\text{olow}} + \frac{S_{l'r}^{\text{low}} - S_{l'r}}{S_{l'r}^{\text{low}} - S_{l'r}^{\text{high}}} \left(k_{rl}^{\text{ohigh}} - k_{rl}^{\text{olow}} \right) \quad (10.17)$$

where $S_{l'r}$ is the residual saturation of the conjugate phase or phases. For gas, the conjugate phases are oil and water i.e. the sum of the residual oil and water saturations is used for $S_{l'r}$ in equation (10.17).

10.4 RELATIVE PERMEABILITY EXPRESSED AS A FUNCTION OF PVT RATIO AND CAPILLARY NUMBER:

For a given fluid composition, the PVT ratio (equation 10.9) is a function of pressure and temperature only. As shown earlier (eq 10.8 and 10.9) the ratio of gas to oil relative permeability can be expressed as a function of PVT ratio.

Now, at a fixed capillary number the gas and oil relative permeabilities can be expressed as a function of saturations using either measured data or a relative permeability model. For example, if Corey's model is used, then:

$$k_{rg} = k_{rg}^o (\bar{S}_g)^{n_g} \quad (10.18)$$

and

$$k_{ro} = k_{ro}^o (1 - \bar{S}_g)^{n_o} \quad (10.19)$$

where, \bar{S}_g is the normalized gas saturation which is given by equation 10.15. n_g and n_o are Corey exponents for gas and oil phases, respectively. k_{rg}^o and k_{ro}^o are the endpoint relative permeabilities for gas and oil phases, respectively.

Dividing equation 10.18 by equation 10.19 gives-

$$\frac{k_{rg}}{k_{ro}} = \frac{k_{rg}^o}{k_{ro}^o} \frac{(\bar{S}_g)^{n_g}}{(1 - \bar{S}_g)^{n_o}} \quad (10.20)$$

The only unknown variable in the above equation is the normalized gas saturation, as the k_{rg}/k_{ro} is fixed by the PVT ratio and is known from the fluid properties. Thus, equation 10.20 can be solved for gas saturation, which can be then used to calculate the gas and oil relative permeabilities at a given capillary number, flowing pressure and temperature for a given fluid. As illustrated below in section 10.4.1, the relative

permeability can be plotted either vs. capillary number for fixed PVT ratio using this approach or vs. PVT ratio for fixed capillary number. Such curves were actually generated using a spreadsheet with the PVT ratio as a parameter and compared with experimental data with the same ratio.

Several investigators (Ayyalasomayajula *et al.*, 2003; Al-Anazi *et al.*, 2002; Cable *et al.*, 2003; Henderson *et al.*, 1995 and 2000; Kumar *et al.*, 2006; Mott *et al.*, 2000 and Whitson *et al.*, 1999) measured the effect of capillary number on gas-condensate relative permeabilities. However, most of the laboratory data are at low capillary numbers. Much less data are available at high capillary numbers corresponding to the condensate banks near production wells. Also, many of these authors have shown that steady state gas and condensate relative permeability data can be correlated with the ratio given in Eq. 10.8. The data presented in this section confirm and extend this correlation to a wider range of conditions and higher capillary numbers.

New steady-state relative permeability data have been measured over a wide range of capillary numbers including very high values corresponding to the near-well region. These measurements have been made on several reservoir rocks as well as outcrop rocks and over a range of temperature, pressure, connate water saturation and hydrocarbon composition typical of gas-condensate reservoirs. The relative permeability model developed by Pope *et al.* (2000) and described in Section 10.3 was tested using both new data and data from the literature.

Table 10.1 gives the rock properties for the new core flood experiments as well as those from the literature. Initially Non-Darcy flow effects were neglected in calculating gas relative permeabilities from the measured pressure drops. The effect of non-Darcy flow correction on gas relative permeabilities is presented in the Section 10.5. This correction is very significant in some cases.

10.4.1 Results for Sandstones

Figures 10.1 to 10.10 show gas and oil relative permeability data as a function of Capillary number for different k_{rg}/k_{ro} ratios. The new data extends the range of the Capillary numbers to the high values representative of flow near high-rate wells.

Figures 10.1 and 10.2 show the measured gas and oil relative permeability data measured on Berea sandstone (Experiment 17) for a k_{rg}/k_{ro} ratio of 2.1 for capillary numbers up to 10^{-3} . The experiment was conducted at 145°F using synthetic fluid mixture-1 (**Table 3.1**). Under some conditions non-Darcy flow can complicate the measurement of relative permeability at such high capillary numbers. Non-Darcy flow was avoided in these measurements by lowering the IFT between the gas and oil on the order of 0.05 dyne/cm. Lower IFT was obtained by keeping the core pressure close to the dew point pressure. With this low IFT, the flow rates required to give the desired capillary numbers are not high enough to cause significant non-Darcy flow. Details of the experiment are given in **Appendix B17**.

On the other hand measurements of Experiment 33 were done at extremely high flow rates ranging from 5,499 cc/hr to 25,841 cc/hr to achieve high capillary numbers. The measurements were done at a core pressure of 420 psig which is much lower than the dew point pressure (4398 psig) and thus results in IFT of about 12-13 dyne/cm between gas and condensate. As the pressure drop during the two-phase flow was very high, the fluid properties were calculated at the mean core pressure. The k_{rg}/k_{ro} ratio varied from 2.36 to 2.6. The results show very small change in relative permeability up to capillary number of 10^{-4} . Non-Darcy flow effects were neglected in calculating gas relative permeabilities from measured pressure drops. Effect of non-Darcy flow correction on gas

relative permeabilities is presented in the later sections. Details of the experiment are given in **Appendix B33**.

The new set of measured relative permeability data is at much higher capillary numbers (10^{-4} to 10^{-3}) and shows a significant increase in both gas and oil relative permeabilities for increasing capillary numbers greater than 10^{-4} . The gas relative permeability increased from about 0.1 to 0.4 as the capillary number increased from 10^{-4} to 10^{-3} . A similar increase was observed for the oil relative permeability. This increase in the relative permeability at high capillary number is due to the reduction in the residual saturations of both gas and oil (condensate) when the capillary number increases.

The plots also show gas and oil relative permeabilities reported in literature by Henderson *et al.* (2000) and Kumar *et al.* (2006) for a k_{rg}/k_{ro} ratio of about 2. Data on Reservoir cores B and C was measured in Chevron's research lab by Ayyalasomayajula (Bang *et al.*, 2006). Most of the data reported in literature at this PVT ratio or k_{rg}/k_{ro} ratio is at low capillary numbers and doesn't show a significant change in relative permeabilities because the capillary number is less than the critical capillary number.

Figures 10.3 and **10.4** show the measured gas and oil relative permeability data as well as the data from the literature as a function of capillary number for a k_{rg}/k_{ro} ratio of 1. This set of data shows almost constant value of gas and oil relative permeabilities for capillary numbers less than 10^{-4} and a steep increase in both the gas and oil relative permeability values for capillary numbers greater than 10^{-4} , which corresponds to the critical capillary number. The data of Cable and Mott (2003) using reservoir gas-condensate fluids and the data of Kumar *et al.* (2006) using synthetic gas-condensate fluids are in good agreement over a wide range of capillary numbers. This is an important observation since almost all of the data in the literature are for synthetic fluids. This shows that accurate gas and condensate relative permeabilities can be measured

using synthetic lab fluids modeled accurately to match the important PVT properties of the actual reservoir fluid. Non-Darcy flow effects were neglected by Kumar *et al.* (2006) and Cable (2003). Results presented in next section show that the true critical capillary number obtained after correcting gas relative permeability data for non-Darcy flow is much less than 10^{-4} .

Figures 10.5 and 10.6 show the dependence of gas and oil relative permeability on capillary number for reservoir sandstone with a k_{rg}/k_{ro} ratio of 4.10 (Exp#33). Measurements were conducted at extremely high flow rates ranging from 38,678 cc/hr to 46,427 cc/hr, to achieve high capillary numbers. The measurements were done at a core pressure of 200 psig which is much lower than the dew point pressure (4398 psig) and thus results in IFT of about 14 dyne/cm between gas and condensate. As the pressure drop during the two-phase flow was very high, the fluid properties were calculated at the mean core pressure. Again the non-Darcy flow effects were neglected in calculating gas relative permeabilities from measured pressure drops. Effect of non-Darcy flow correction on gas relative permeabilities is presented in the Section 10.5. Details of the experiment are given in **Appendix B33**. The plots also show gas and oil relative permeabilities reported in literature for k_{rg}/k_{ro} ratio in the range of 3 to 5.

Figures 10.7 and 10.8 show the measured relative permeability data for lean gas-condensate fluids corresponding to a k_{rg}/k_{ro} ratio in the range of 8 to 12. Relative permeability data for even leaner fluids corresponding to a k_{rg}/k_{ro} ratio in the range of 20 to 60 are shown in **Figures 10.9 and 10.10**. The data for k_{rg}/k_{ro} ratios of 8 to 12 and 20 to 60 were measured on two different reservoir sandstone cores (Reservoir A and Reservoir B1). The low values of gas relative permeability show that for even for such lean fluids (high k_{rg}/k_{ro} ratios) condensate blocking can be a serious problem.

The new sandstone data and the sandstone data reported in the literature for both reservoir and synthetic fluids was used to tune the relative permeability model described in Section 10.3. An attempt was made to fit all of the gas and oil relative permeability using only one set of model parameters for all rocks and fluids over the entire range of capillary numbers. **Table 10.2** gives the model parameters obtained after tuning the model to fit all of the data.

Figures 10.1 to 10.10 show the comparison of the measured gas and oil relative permeability data with the model curves. The comparison shows that the model curves fit the data over k_{rg}/k_{ro} ratios ranging from 1 to 60 and capillary numbers ranging from 10^{-7} to 10^{-3} reasonably well within experimental uncertainty. The model predicts low and almost constant gas and oil relative permeabilities for capillary numbers less than 10^{-4} as observed from the data. The match is equally good for low and high k_{rg}/k_{ro} ratios. An important observation is that the model is able to capture the sharply increasing relative permeability in the capillary number range of 10^{-4} to 10^{-3} , which represents the capillary numbers expected near high-rate gas-condensate wells.

10.4.2 Results for Limestones

The steady state relative permeability measurements for Texas Cream Limestone were done using synthetic fluid mixture-1 at 145 °F. The experiments were done at 1200 psig and 2600 psig corresponding to k_{rg}/k_{ro} ratios of 1.6 and 2.1. **Figures 10.11 and 10.12** show the measured gas and oil relative permeability data as a function of capillary number. The data for a k_{rg}/k_{ro} ratio of 1.6 are for capillary numbers on the order of 10^{-5} . The data at a ratio of 2.1 was measured over a capillary number range of 10^{-4} to 10^{-3} and show a significant increase in both gas and oil relative permeabilities with capillary number (details given in Appendix B16). This is the first set of limestone data reported

for such high capillary numbers. **Figures 10.11** and **10.12** also compare the new data with some of the data reported in literature, which show a similar behavior.

The gas and oil relative permeabilities are higher for this limestone than for the sandstones at low capillary numbers. However, gas and oil relative permeabilities are almost the same at high capillary numbers. The data for capillary numbers in the range of 10^{-5} to 10^{-3} were compared with the model curves using the same set of parameters used for sandstones (**Table 10.2**). **Figures 10.11** and **10.12** show that the model curve is close to the data at high capillary numbers, but is somewhat lower than most of the data at low capillary numbers.

High capillary number data measured on sandstone (Exp#17) and limestone (Exp# 16) were measured at core pressures close to the dew point pressure of the fluid, which resulted in low IFT between gas and condensate. This helped in achieving high capillary numbers without going to high flow rates. Thus non-Darcy flow effects on these measured relative permeabilities can be neglected without introducing much error. Most of the high capillary number data reported in literature, however was measured at high flow rates where non-Darcy flow effects become significant and have to be accounted for calculating the correct values of gas relative permeabilities.

10.5 EFFECT OF NON-DARCY FLOW ON GAS AND OIL RELATIVE PERMEABILITIES:

At high velocities the relative permeabilities for the flowing phases are dependent on two opposing effects, capillary number and non-Darcy flow. **Figure 10.13** shows a schematic of the effect of non-Darcy flow and capillary number on the two-phase flow pressure drop. As the flowing phase velocity increases, additional pressure drop is caused due to non-Darcy flow effects, which results in a reduction in its relative permeability. At the same time increasing capillary number decreases the pressure drop and thus results in

increase in relative permeability with increasing velocity. Thus, the relative permeability may increase or decrease with increasing velocity depending on the dominance of one effect over the other. Correlations defining the dependence of relative permeabilities on capillary number were described in Section 10.3. This section describes the approach developed and adopted in this work to account for non-Darcy flow effects.

Non-Darcy flow can be described using Forchheimer's equation:

$$\frac{\Delta P_j}{L} = \frac{\mu_j u_j}{k k_{rj}} + \beta_j \rho_j u_j^2 \quad (10.21)$$

where j represents the flowing phase i.e. either gas or condensate. β is the multi-phase flow non-Darcy coefficient, μ is the viscosity and ρ is the density of the flowing phase. ΔP is the measured steady state pressure drop for two-phase gas condensate flow. The second term on the right hand side of equation of 10.18 represents the contribution of non-Darcy flow in the pressure gradient. Thus, as the velocity increases the contribution of non-Darcy flow to the total pressure drop becomes significant. The above equation can be re-arranged and written as follows:

$$k_{rj} = \frac{\mu_j u_j}{k \Delta P} \left(1 + \frac{\beta_j \rho_j k k_{rj} u_j}{\mu_j} \right) \quad (10.22)$$

The correct gas and oil relative permeabilities corresponding to the measured pressure drop can be calculated using the equation 10.19. As the velocity increases, the effect on non-Darcy flow on relative permeabilities becomes significant. Equation 10.19 has relative permeability on both sides of the equation, which makes it iterative. The non-

Darcy multi-phase flow coefficient is the only other unknown in equation 10.19. Determination of the non-Darcy flow coefficient for multiphase flow from experimental data is much more complicated than it is for single-phase flow because it depends on fluid saturation and because the pressure drop also depends on the capillary number.

Figure 10.14 shows the experimental two-phase flow data plotted as $\Delta P/vL$ vs gas velocity. Based upon Forchheimer's equation, single-phase flow data should plot as a straight line with a positive slope equal to β . The measured data for two-phase flow show a negative slope, which indicates that the capillary number effects are more significant than the non-Darcy flow effects under these conditions. For Experiment-17 conducted at low flow rates and high capillary numbers, the slope has a high negative value indicating a strong dominance of capillary number effects over the non-Darcy flow effects. However, for Experiment 33 done at 200 psi core pressure and extremely high flow rates but lower capillary numbers, the slope has a low negative value indicating that capillary number and non-Darcy flow effects are almost equal.

Many different correlations have been reported in literature for calculating two-phase non-Darcy flow coefficients. But most of these are based on single-phase measurements and were simply extended to two-phase flow by coupling saturation with porosity to account for available pore space for the flowing phase. Geertsma's correlation (Geertsma *et al.*, 1974) is one of the widely used correlations for calculating the non-Darcy flow coefficient:

$$\beta_g = \frac{0.005}{(kk_{rg})^{0.5} (\phi(1 - S_{wi}))^{5.5}} \quad (10.23)$$

The coefficients and exponents were obtained from fitting single-phase flow data and then extended to gas flow at initial water saturation. For multi-phase flow with gas and oil flowing at initial water saturation, theoretically the $(1-S_{wi})$ term should be replaced with the saturation of the flowing phase, but the gas saturation is often not measured and is not needed in the pseudo pressure approach such as used in this study. Although the validity of equation 10.23 for multi-phase flow is uncertain for these reasons, it was assumed to still give the correct order of magnitude for the multiphase flow value of β and was therefore used in this study for lack of a better alternative.

Figure 10.15 compares the gas relative permeability measured in Experiment 33 before and after correcting for non-Darcy flow. Results show that the true gas relative permeability can be underestimated by almost a factor of 2 if it is calculated using the measured pressure drop and Darcy's law without taking non-Darcy flow effects into account. The error in true gas relative permeability (calculated using equation 10.22) increases with increasing gas velocity. This shows the increasing contribution of non-Darcy flow effect with increasing gas velocity and the importance of correcting gas relative permeability for non-Darcy flow or inertial flow.

Figure 10.16 shows the variation of corrected and uncorrected gas relative permeability measured on Berea sandstone (Exp#33) as a function of capillary number. The uncorrected gas relative permeability increased by only about 20% as the capillary number increased by about an order of magnitude (2×10^{-5} to 1.5×10^{-4}) whereas the gas relative permeability calculated using equation 10.19 increased by almost 100% (from 0.1 to 0.2). These results show that the critical capillary number is on the order of 10^{-5} and not 10^{-4} as indicated in the previous section when the calculations were done without correcting for the non-Darcy flow effects. The lower value is typical of the critical capillary number for sandstones (Delshad *et al.*, 1990).

Figure 10.17 shows the variation of corrected and uncorrected gas relative permeability measured in the propped fracture (Experiment-43). **Table 10.3** gives the properties of the propped fracture and the experimental conditions. Measurements were done at three different core pressures to get data for different PVT ratios. Gas relative permeability calculated using the measured pressure drop in Darcy's law shows a decreasing trend with capillary number. These results show that the effect of non-Darcy flow is extremely significant in these measurements since they were done at high flow rates up to a maximum flow rate of 33,622 cc/hr. Details of the experiment with the flow rates and measured pressure drops are given in **Appendix B43**.

The corrected gas relative permeabilities (calculated using equation 10.22) are significantly higher than the uncorrected gas relative permeabilities similar to what was observed for the Berea sandstone experiments. The gas relative permeability increased by almost 400% after correcting for non-Darcy flow effects at higher velocities or higher capillary numbers. The corrected gas relative permeability shows a small increase with Capillary Number for values up to about 7×10^{-3} but increases significantly as the capillary number is increased further. These results suggest that the critical capillary number for the unconsolidated sand (F35) used in the propped fracture is much higher than that for the consolidated Berea sandstone. No similar comparison for gas-condensate fluids could be found in the literature, but the higher critical capillary number is consistent with capillary desaturation data for water displacing oil in uniform unconsolidated sand.

10.5 REPLACING k_{rg}/k_{ro} RATIO WITH PVT RATIO TO ACCOUNT FOR NON-DARCY FLOW:

In Section 10.2 it was shown that the ratio of gas to oil relative permeability can be expressed as a function of fractional flow and fluid viscosities only as long as non-Darcy flow effects are insignificant. If the non-Darcy flow term is taken into account, the ratio of gas to oil relative permeability can be expressed as follows:

$$\frac{k_{rg}}{k_{ro}} = \frac{\mu_g f_g}{\mu_o f_o} \left(\frac{1 + \frac{\beta_g \rho_g k k_{rg} u_g}{\mu_g}}{1 + \frac{\beta_o \rho_o k k_{ro} u_o}{\mu_o}} \right) \quad (10.24)$$

For the experiments done in this study, the non-Darcy correction was negligible, so equation 10.21 simplifies to:

$$\frac{k_{rg}}{k_{ro}} = \frac{\mu_g f_g}{\mu_o f_o} \left(1 + \frac{\beta_g \rho_g k k_{rg} u_g}{\mu_g} \right) \quad (10.25)$$

Equation 10.22 gives the ratio of gas to oil relative permeability with non-Darcy flow effects taken into account and shows that it cannot be expressed in terms of the PVT ratio only as previously done by Chopra *et al.*, 1986; Whitson *et al.*, 1999; Mott *et al.*, 2000; Chowdhury *et al.*, 2003; Bang *et al.*, 2006, Kumar *et al.*, 2006 and others. The PVT ratio as defined in Section 10.2 is still valid and useful whereas the k_{rg}/k_{ro} ratio is not. A general approach using the PVT ratio, capillary number and a modified Reynolds number is developed in the next section.

10.6 RELATIVE PERMEABILITY EXPRESSED AS A FUNCTION OF THREE NON-DIMENSIONLESS GROUPS:

To take into account the factors affecting gas and oil (condensate) relative permeabilities, relative permeability has been expressed as function of three fundamental non-dimensionless groups; capillary number, modified Reynolds number and PVT ratio. capillary number has been explained in detail in Section 10.3. The modified Reynolds number is used to quantify the contribution of non-Darcy flow term. The modified Reynolds number (Ma and Ruth, 1997 and Mott *et al.* 2000) is defined as:

$$N_{Re} = \frac{\beta_g \rho_g k k_{rg} u_g}{\mu_g} \quad (10.26)$$

Equation 10.22 for calculating the true gas relative permeability can be expressed in terms of modified Reynolds Number as follows:

$$k_{rg} = \frac{\mu_g u_g}{k \Delta P} (1 + N_{Re}) \quad (10.27)$$

The gas relative permeability data corrected for non-Darcy flow was used to tune the capillary number dependent relative permeability model described in Section 10.3. An attempt was made to fit all of the gas and oil relative permeability using only one set of model parameters over the entire range of capillary numbers. Gas relative permeabilities reported in literature could not be corrected for non-Darcy flow as all the properties were not known to calculate true gas relative permeability from equation 10.19 or 10.24. Therefore, these results are based on the new set of data measured at high capillary numbers and high flow rates. **Table 10.4** gives the new model parameters obtained after tuning the model to fit all of the data.

Figure 10.18 shows the comparison of the corrected gas relative permeability and the model curves with the new set of parameters for PVT ratios of 2-3. The result shows that the model curves capture the trend of relative permeability with capillary number and fit the measured data over a wide range of capillary number. The model with the new set of parameters shows a critical capillary number on the order of 10^{-5} .

Figure 10.19 shows gas relative permeability model curves as a function of capillary number for different PVT ratios. **Figure 10.20** shows the model curves as a function of PVT ratios for different capillary numbers. **Figure 10.21** shows gas relative permeability model curves as a function of oil saturation for different capillary numbers. **Figure 10.22** shows that the oil saturation predicted by the model varies over a very narrow range of about 0.35 to 0.40 when the PVT ratio is 1. All curves were calculated using the same set of parameters given in **Table 10.4**. These curves can be used to get a quick first estimate of the steady state gas and oil relative permeability values in a condensate bank using nothing but PVT data to calculate the PVT ratio and the capillary number. The well productivity index can then be estimated from one of several simple models (Whitson *et al.* 1999 and Chowdhury *et al.* 2003).

10.7 SUMMARY

Relative permeability data for gas condensate fluids have been measured at high capillary numbers and Reynolds numbers corresponding to the near wellbore region of high flow rate gas-condensate wells. Relative permeability measured on both sandstone and limestone rocks show a strong dependence on capillary number at high velocities. At high velocities, the effect of non-Darcy flow can also become significant and result in a large error in the estimation of gas relative permeability if it is not accounted for

correctly. A new approach has been developed to correct the gas relative permeability for non-Darcy flow effects. As the non-Darcy flow becomes significant the widely used k_{rg}/k_{ro} ratio becomes invalid. Therefore, the relative permeability has been expressed as a function of capillary number, modified Reynolds number and PVT ratio in this study. A relative permeability model developed by Pope *et al.* (2000) has been tuned to fit all the corrected gas and oil relative permeabilities measured over a wide range of conditions using only one set of parameters.

Table 10.1: Sources of Relative Permeability Data on Sandstone and Limestone cores

Source	Rock Type	k, md	ϕ	S_{wi} %	Nc Range
This work	Berea Sandstone	130-230	20	0-50	6×10^{-6} - 1.2×10^{-3}
This work	Texas Cream Limestone	8-20	20	0	4×10^{-6} - 9×10^{-4}
This work	Propped Fractures	23,000- 57,000	36-43	0-40	
Bang <i>et al.</i> (2006)	Reservoir A (Sandstone)	5-23	14-16	20-22	4×10^{-7} - 3×10^{-5}
Bang <i>et al.</i> (2006)	Reservoir B1 (Sandstone)	3-51	10-13	8-20	5×10^{-7} - 3×10^{-5}
Bang <i>et al.</i> (2006)	Reservoir C (Sandstone)	40-50	16	26-50	1×10^{-5} - 2×10^{-5}
Al-Anazi <i>et al.</i> (SPE-77546)	Texas Cream Limestone	2-6	20	0-20	4×10^{-8} - 5×10^{-5}
Ayyalasomayajula <i>et al.</i> (SCA-2003-33)	Reservoir Sandstone	4-60	17	26-33	4×10^{-8} - 2×10^{-6}
Cable <i>et al.</i> (SCA-2003)	Outcrop Sandstone	12	20	5.3	6×10^{-6} - 2×10^{-4}
Henderson <i>et al.</i> (SPE-30770)	Berea Sandstone	92	19.8	26.4	2×10^{-5} - 9×10^{-5}
Kumar <i>et al.</i> (SPE-100529)	Berea and Reservoir	14-500	16-20	0-40	4×10^{-6} - 6×10^{-4}

	Sandstone				
Mott <i>et al.</i> (SPE-62932)	North Sea Sandstone	102.4	25.4	11.8	6×10^{-5} - 6×10^{-4}

Table 10.2: Relative permeability model parameters tuned to match relative permeability data without non-Darcy Correction

Model Parameters	Tuned Value
S_{wr}	0.25
S_{or}	0.3
S_{gr}	0.25
k_{ro}^o	0.3
k_{rg}^o	0.45
n_o	2
n_g	3
T_w	100
T_o	10,000,000
T_g	3,000,000
τ_w	1.1
τ_o	2
τ_g	2

Table 10.3 Properties of Sand filled propped fracture (Exp#43)

Matrix rock	Berea Sandstone
Proppant	30/50 Bauxite
Length, inches	7.875
Fracture width, cm	0.225
Fracture porosity, %	37.50
Fracture Pore Volume, cc	4.20
Total Pore Volume, cc	17.72
Fracture Permeability (k_g), Darcy	41.13

Table 10.4: Relative permeability model parameters tuned to match relative permeability data after non-Darcy Correction

Model Parameters	Tuned Value
S_{wr}	0.25
S_{or}	0.3
S_{gr}	0.25
k_{ro}^o	0.3
k_{rg}^o	0.45
n_o	2
n_g	3
T_w	100
T_o	100,000
T_g	300,000
τ_w	1.1
τ_o	1.5
τ_g	1.5

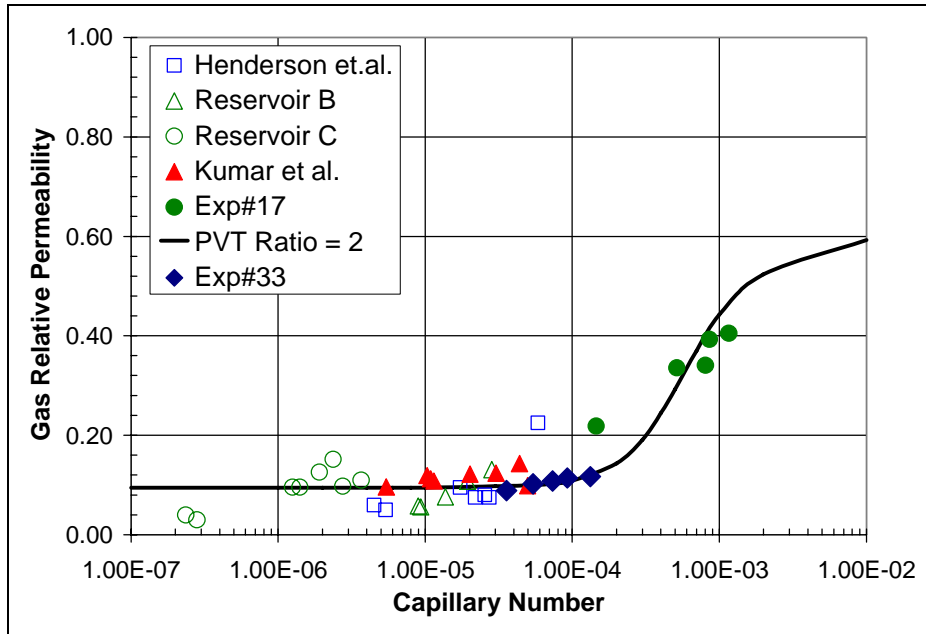


Figure 10.1: Comparison of measured gas relative permeability for $k_{rg}/k_{ro}=2$ with the relative permeability model

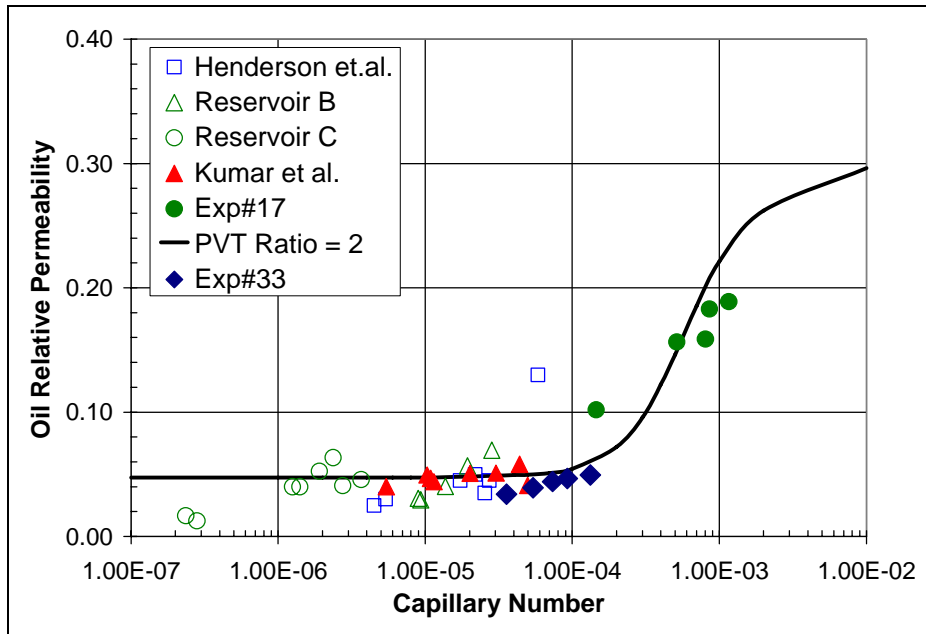


Figure 10.2: Comparison of measured oil relative permeability for $k_{rg}/k_{ro}=2$ with the relative permeability model

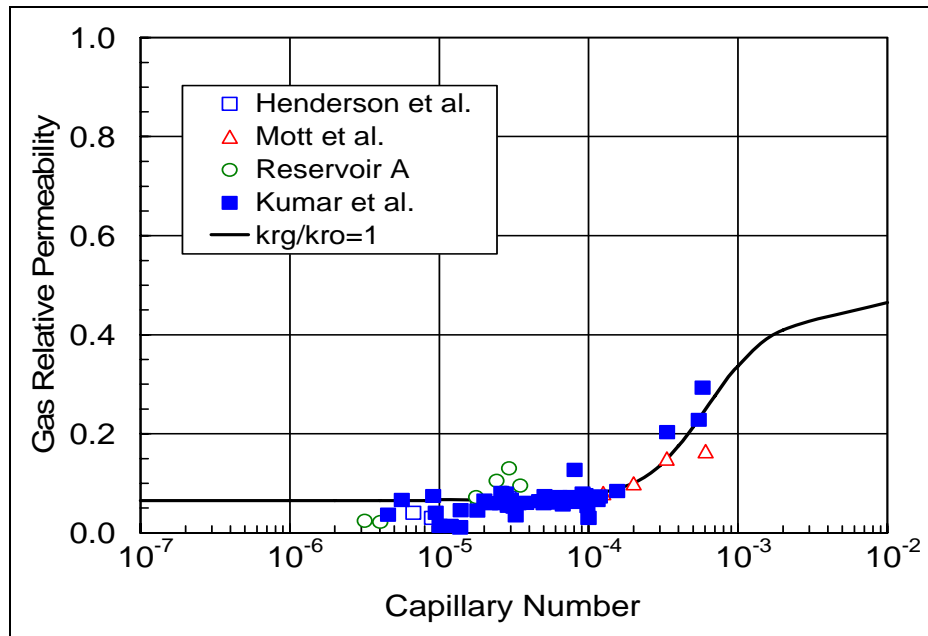


Figure 10.3: Comparison of measured gas relative permeability for $k_{rg}/k_{ro}=1$ with the relative permeability model

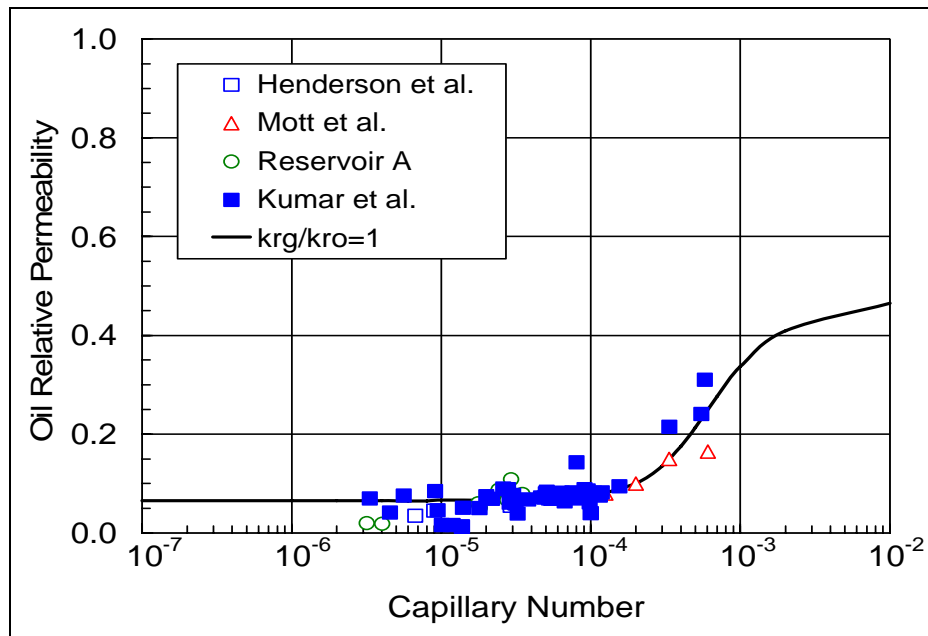


Figure 10.4: Comparison of measured oil relative permeability for $k_{rg}/k_{ro}=1$ with the relative permeability model

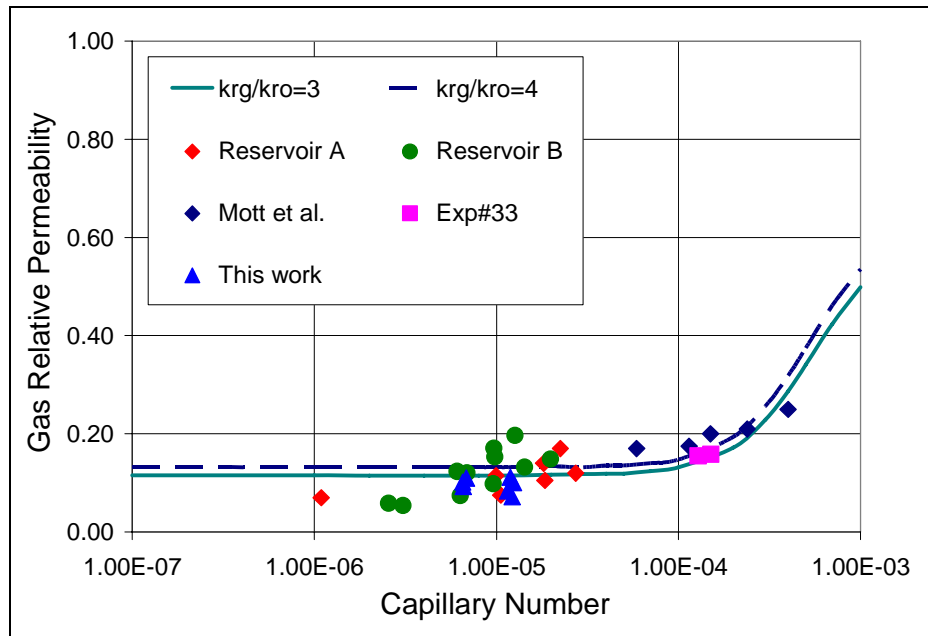


Figure 10.5: Comparison of measured gas relative permeability for $k_{rg}/k_{ro}=3$ to 4 with the relative permeability model

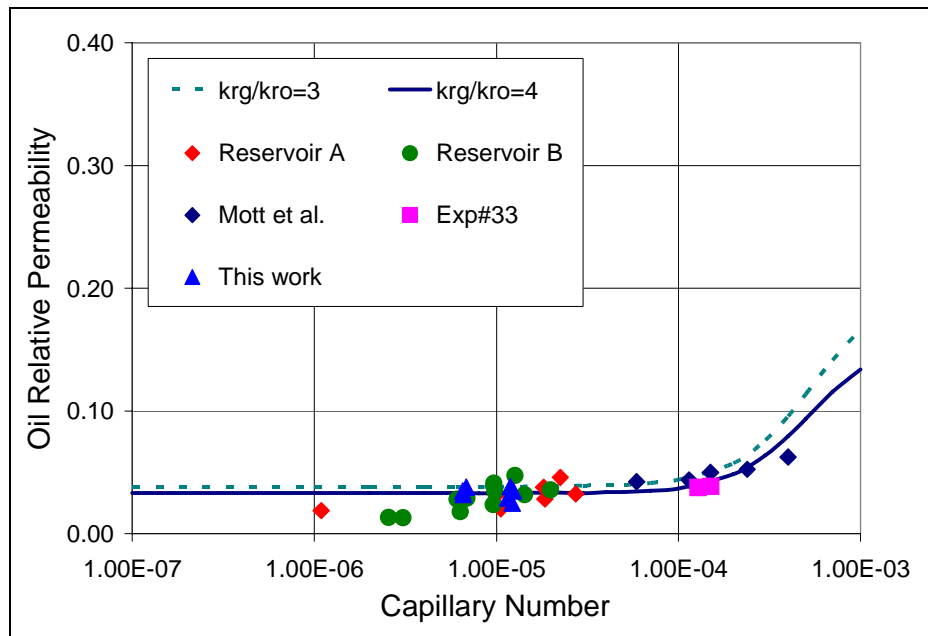


Figure 10.6: Comparison of measured oil relative permeability for $k_{rg}/k_{ro}=3$ to 4 with the relative permeability model

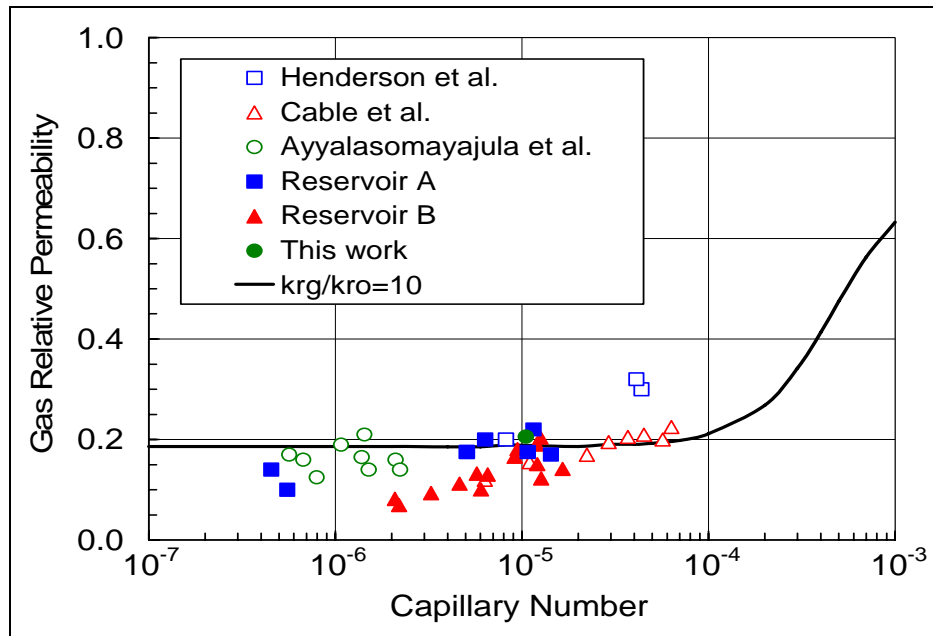


Figure 10.7: Comparison of measured gas relative permeability for $k_{rg}/k_{ro}=8$ to 10 with the relative permeability model

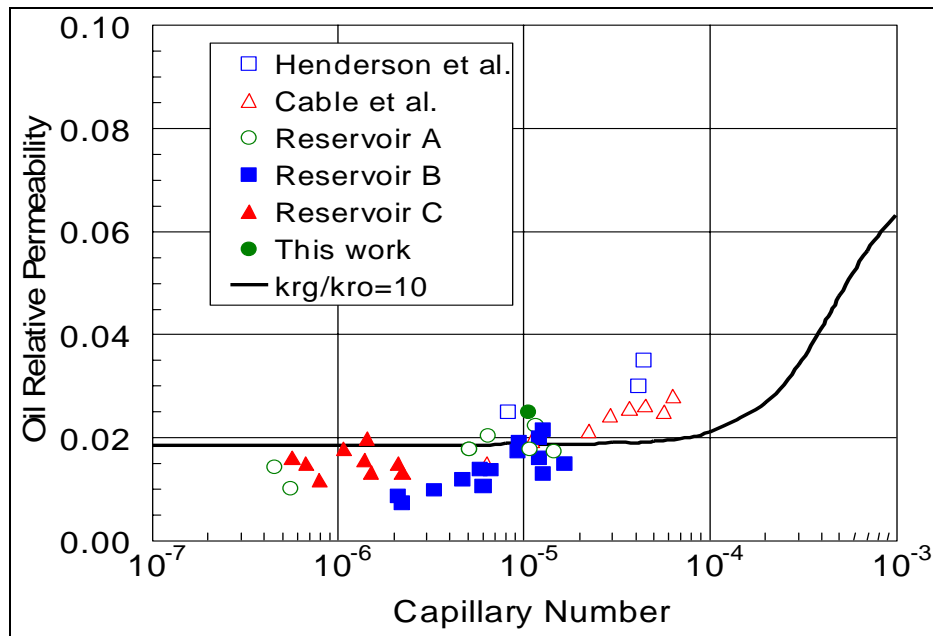


Figure 10.8: Comparison of measured oil relative permeability for $k_{rg}/k_{ro}=8$ to 10 with the relative permeability model

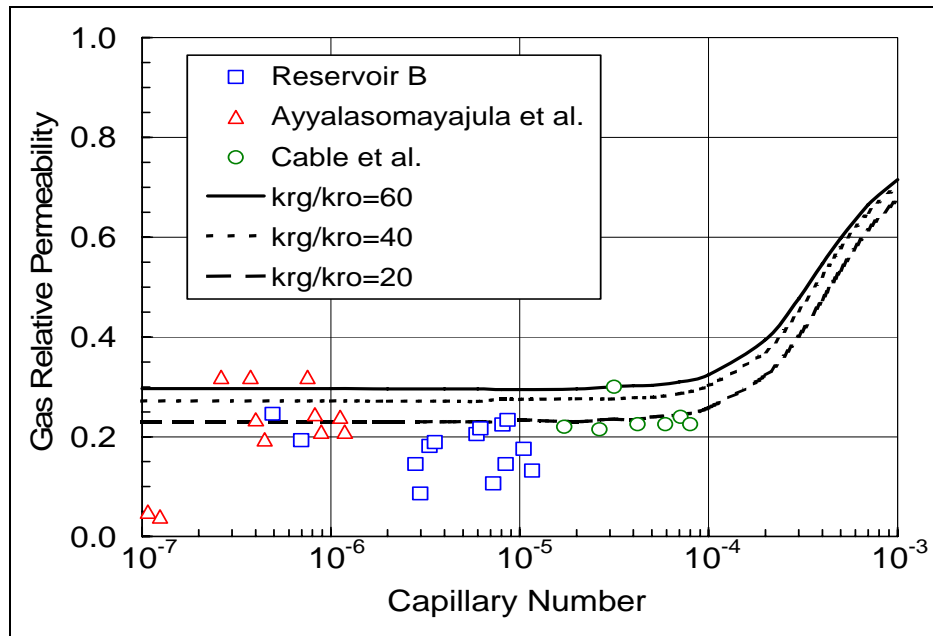


Figure 10.9: Comparison of measured gas relative permeability for $k_{rg}/k_{ro}=20$ to 60 with the relative permeability model

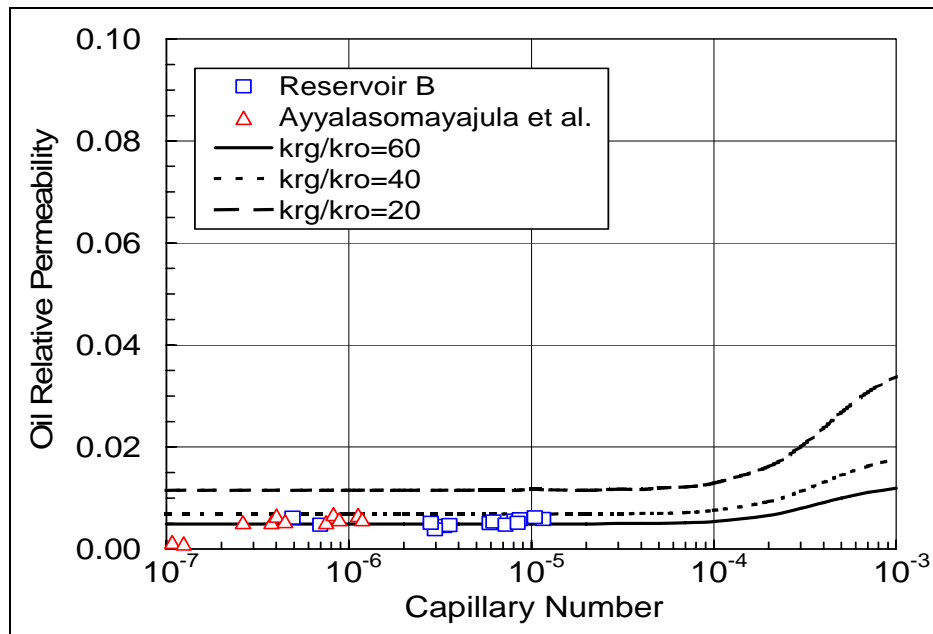


Figure 10.10: Comparison of measured oil relative permeability for $k_{rg}/k_{ro}=20$ to 60 with the relative permeability model

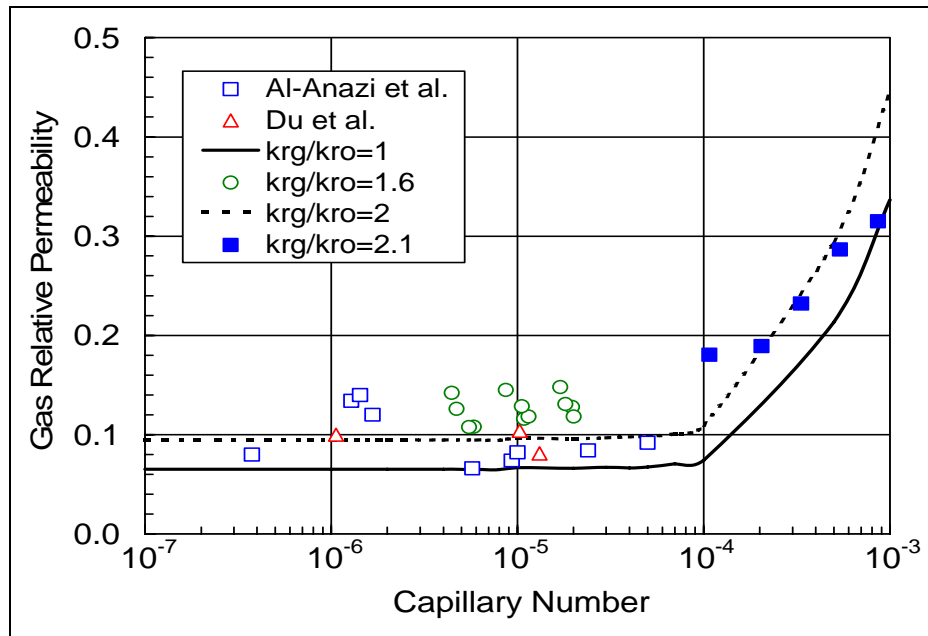


Figure 10.11: Comparison of gas relative permeability measured on limestone for $k_{rg}/k_{ro}=1$ and 2 with the relative permeability model

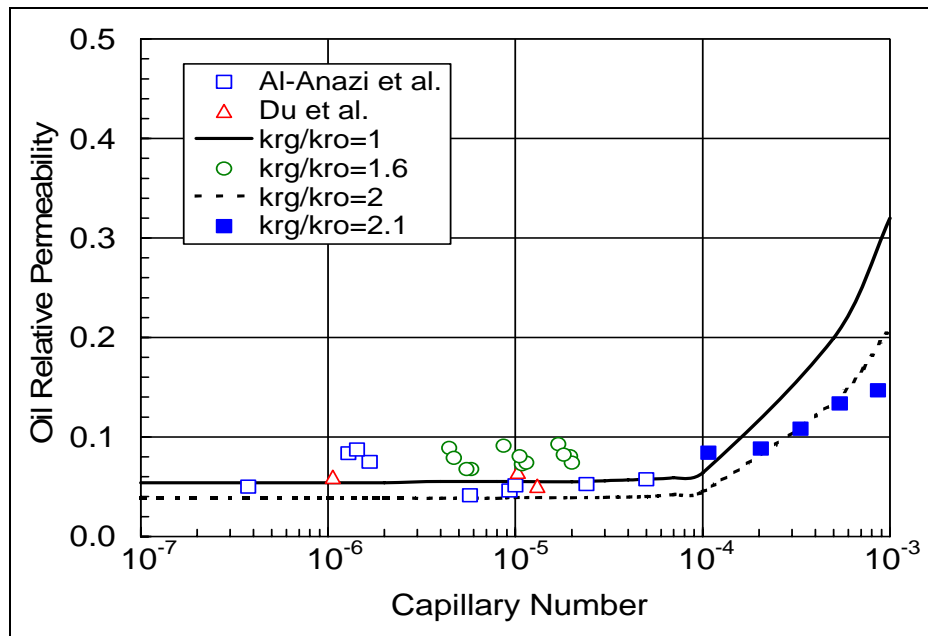


Figure 10.12: Comparison of oil relative permeability measured on limestone for $k_{rg}/k_{ro}=1$ and 2 with the relative permeability model

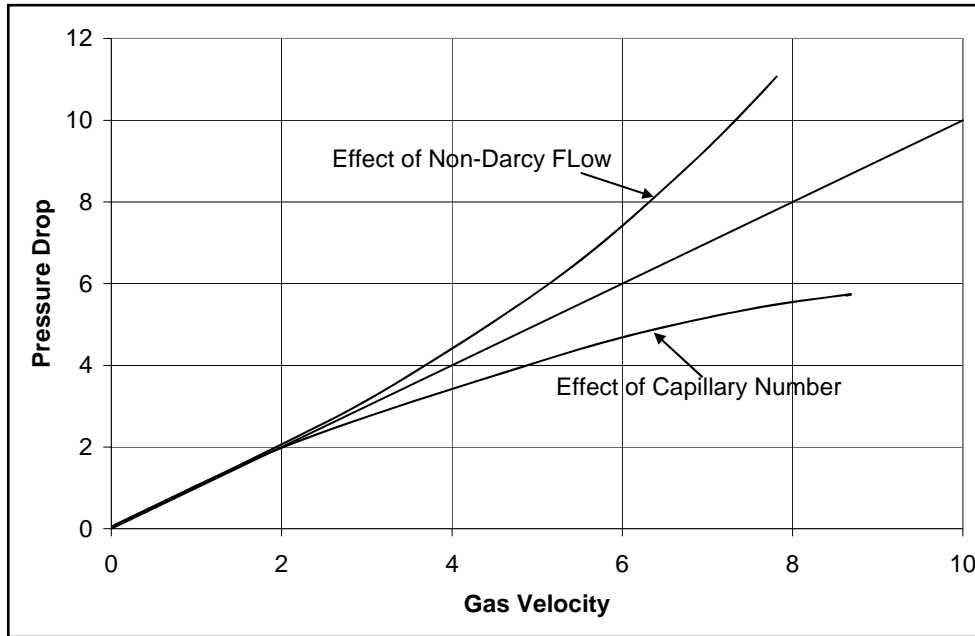


Figure 10.13: Effect of capillary number and non-Darcy flow at high gas velocities on gas relative permeability

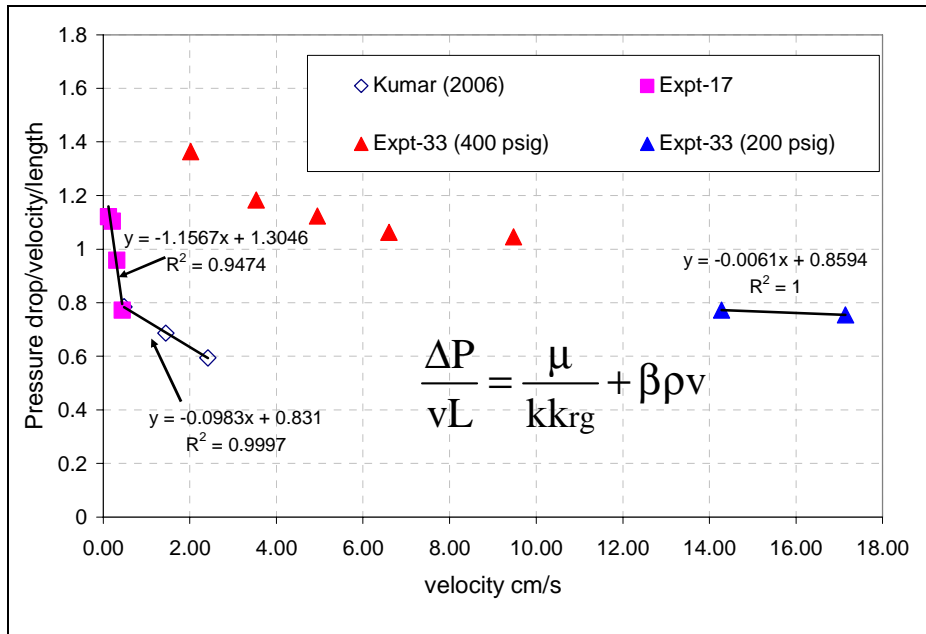


Figure 10.14: Combined effect of capillary number and non-Darcy flow on steady state pressure drop measurement for two-phase gas condensate flow

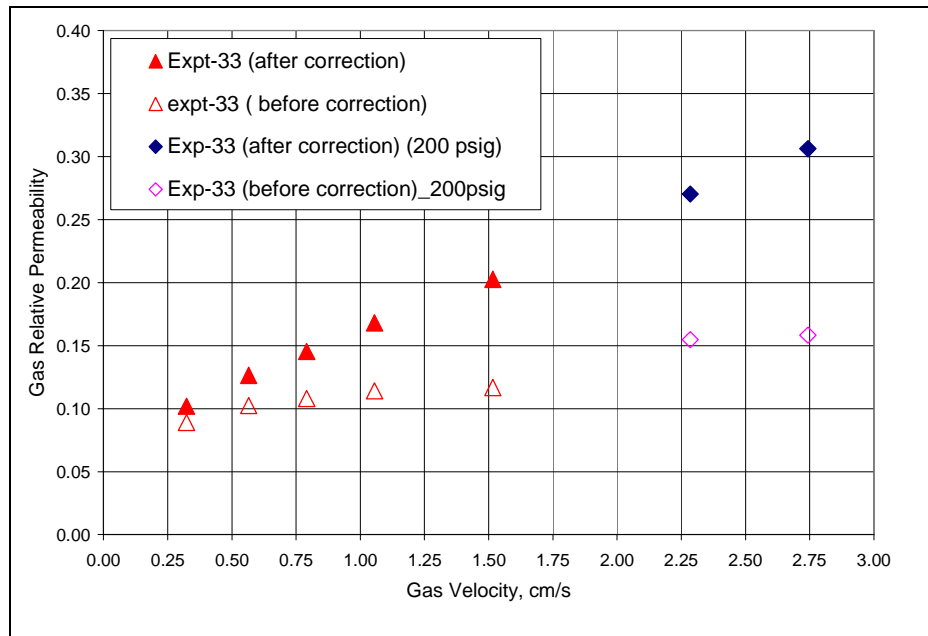


Figure 10.15: Comparison of gas relative permeability before and after correction for non-Darcy flow

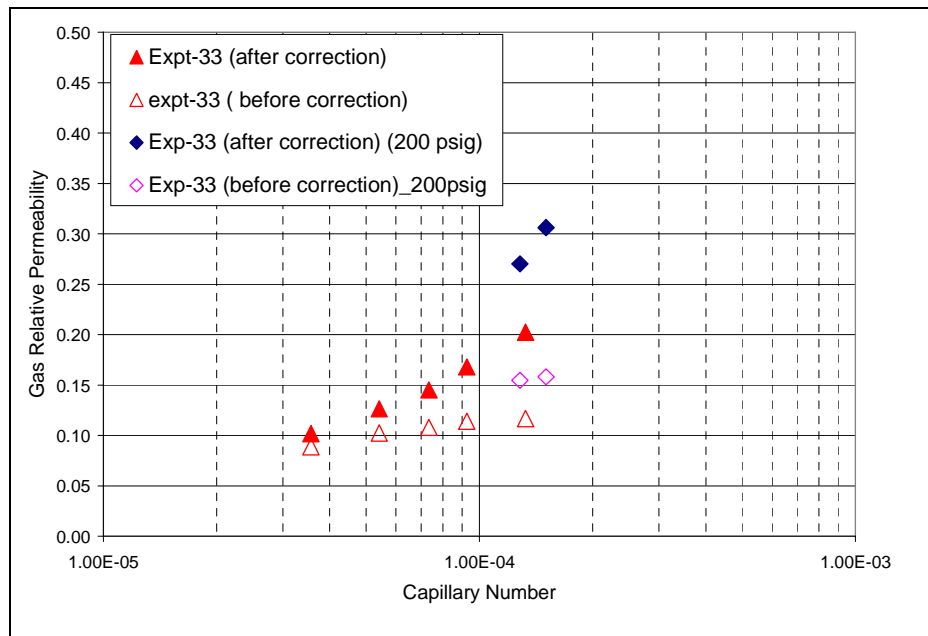


Figure 10.16: Effect of capillary number on corrected and non-corrected gas relative permeability

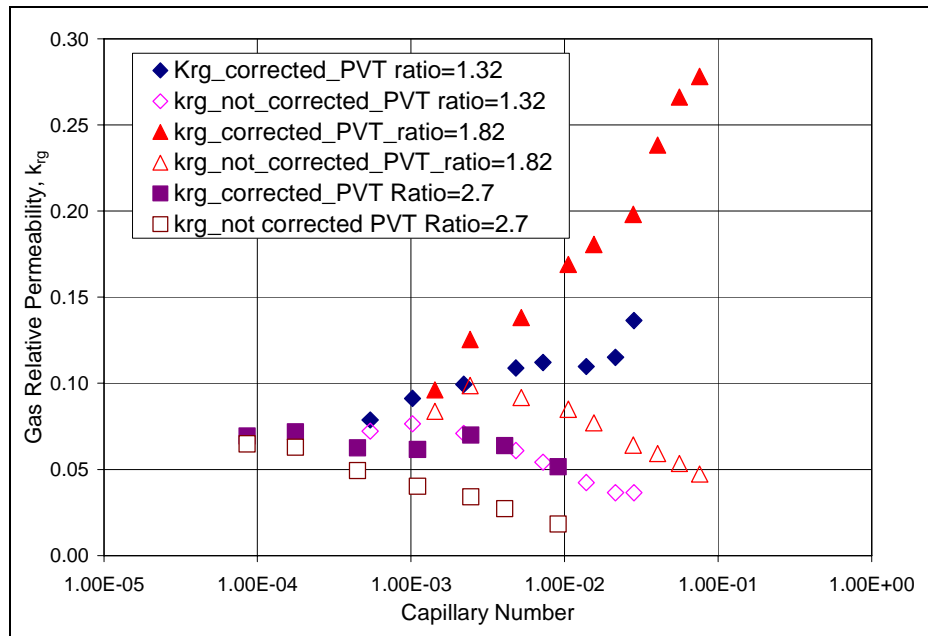


Figure 10.17: Effect of capillary number on corrected and non-corrected gas relative permeability measured at different PVT ratios on propped fracture (Exp#43)

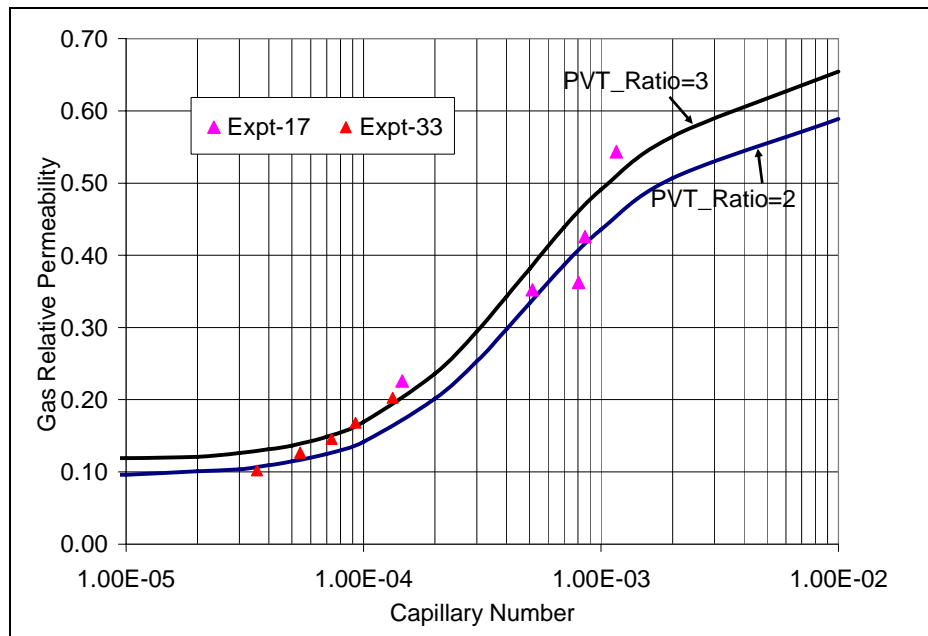


Figure 10.18: Comparison of corrected gas relative permeability with the modified relative permeability model for PVT ratio of 2 to 3

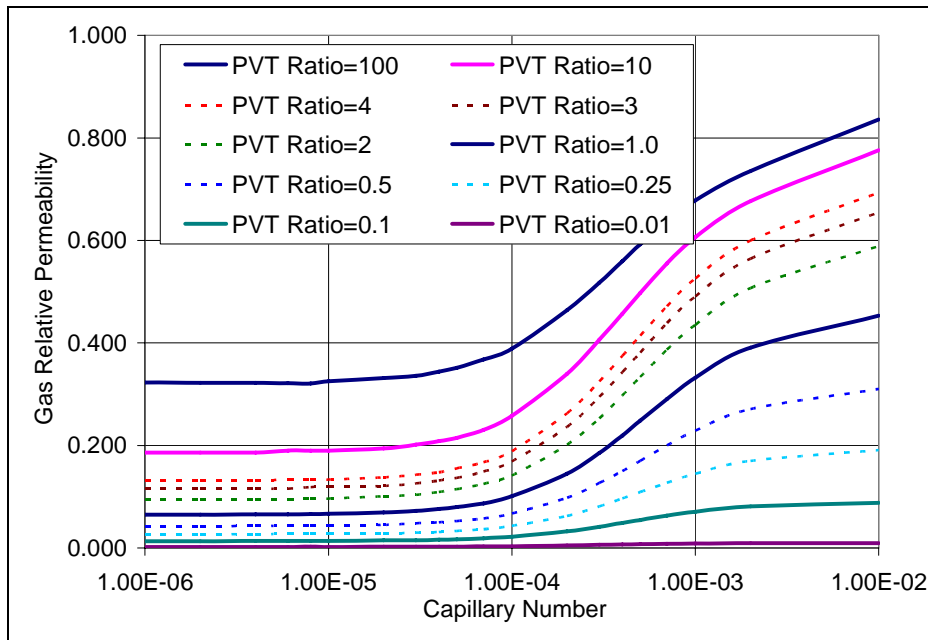


Figure 10.19: Gas relative permeability as a function of capillary number

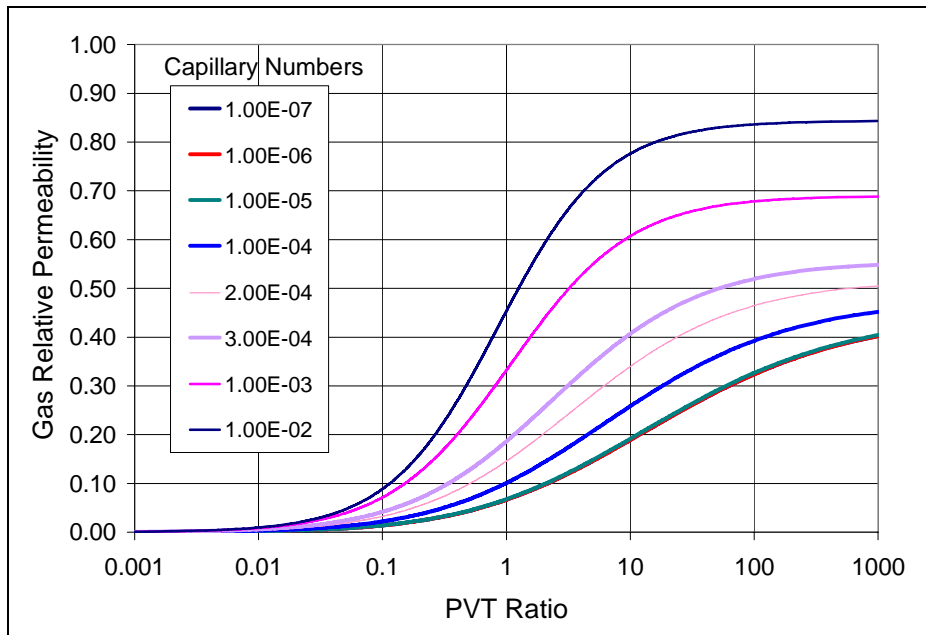


Figure 10.20: Gas relative permeability as a function of PVT Ratio

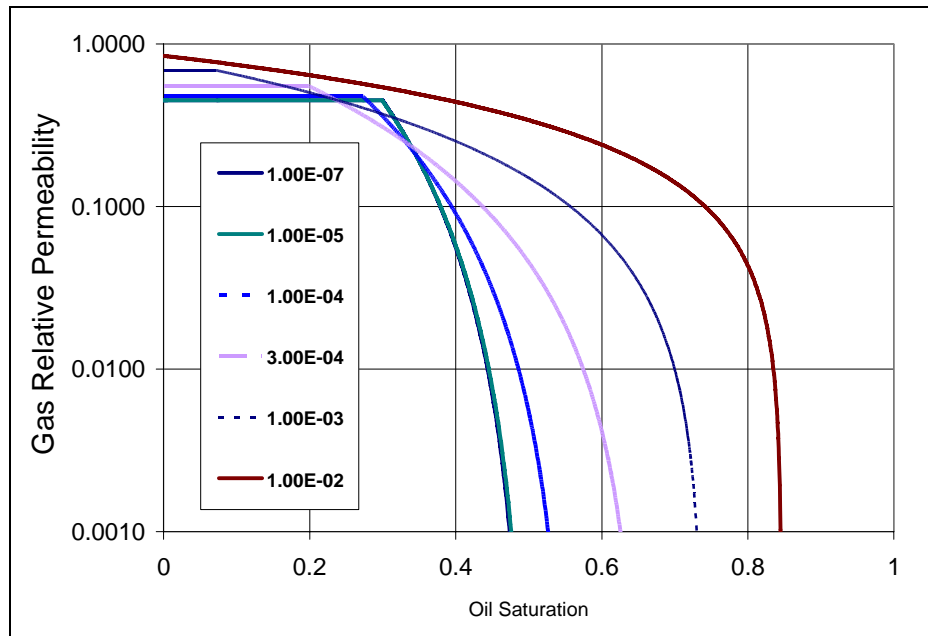


Figure 10.21: Gas relative permeability as a function of oil saturation and capillary number

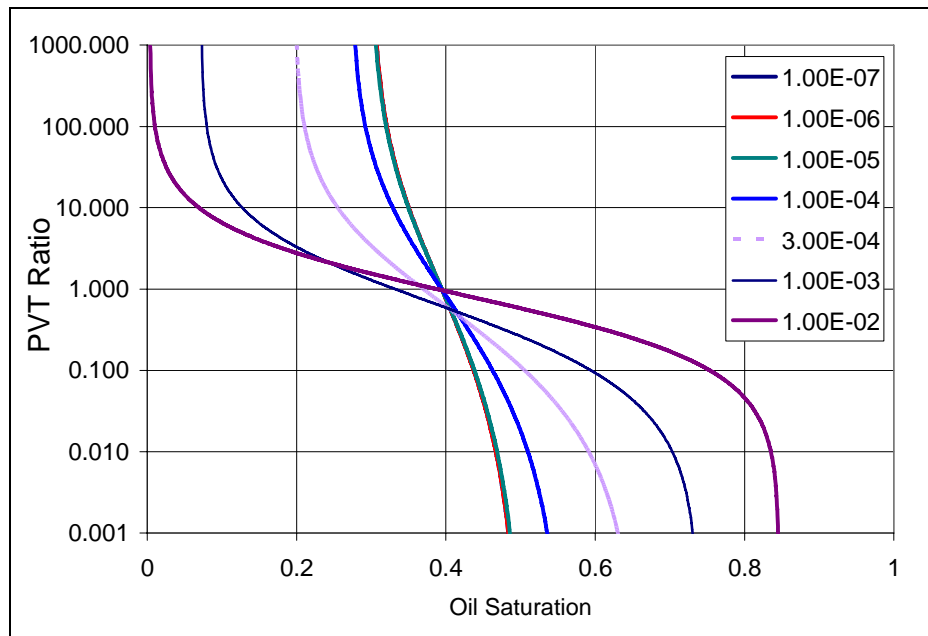


Figure 10.22: Oil saturation as a function of PVT ratio and capillary number

Chapter 11: Chemical Treatment of Limestone Rocks

Results presented and discussed in earlier chapters were mainly focused on sandstone rocks. This chapter presents the results of two-phase gas condensate flow measurements done on Limestone cores. The chapter also discusses the different chemicals evaluated to reduce the damage caused by condensate blocking and improve the relative permeability.

11.1 GAS RELATIVE PERMEABILITY MEASUREMENTS ON TEXAS CREAM LIMESTONE ROCKS:

Dynamic condensate accumulation coreflood experiments were performed on Texas Cream limestone cores over a temperature range of 145°F to 250°F. **Table 11.1** summarizes the experimental conditions of these measurements. **Figure 11.1** shows the pressure drop across a Texas Cream limestone core during the dynamic condensate accumulation at 1,200 psig and 145°F at flow rates varying from 274 cc/hr to 1011 cc/hr (Exp#1). Two-phase flood was conducted using synthetic gas mixture-1 (**Table 3.1**). There was no water present in the core. Details of the experiment are given in **Appendix B1**.

Figure 11.2 shows the pressure drop across a Texas Cream limestone core during dynamic condensate accumulation at 490 psig and 175°F at a flow rate of 579 cc/hr (Exp#48). Two phase flood was conducted using synthetic gas mixture-5 (**Table 3.5**). An initial water saturation of 14% was established in the core using synthetic Bruce brine. Details of the experiment are given in **Appendix B48**.

These results and those observed from other experiments conducted on Texas cream limestones (**Table 11.1**) show that gas relative permeability decreased by about 90% due to condensate build-up in the core. The reduction in gas relative permeability due to condensate dropout is therefore about the same as that observed for sandstone rocks for the same PVT ratios.

11.2 CHEMICAL TREATMENT OF TEXAS CREAM LIMESTONE ROCKS:

Dynamic condensate accumulation coreflood experiments were performed on Texas Cream limestone over a temperature range of 145°F to 250°F after chemical treatment. These experiments were performed to evaluate different chemicals for limestone. **Table 11.1** lists the different chemicals tested to treat limestone rocks.

Figure 11.3 shows the pressure drop during the dynamic condensate accumulation at 1,200 psig and 145°F at multiple flow rates varying from 274 cc/hr to 1011 cc/hr in Texas Cream limestone with no initial water saturation, before and after treating with chemical FC4432 (Exp#1). The core was treated using 2% FC4432 in a mixture of methanol and water. **Table 11.2** gives the composition of the treatment solution. The pressure drop during the treatment at 1,200 psig and 145°F is shown in **Appendix B1**. 17 pore volumes of the treatment solution was flowed through the core at 112 and 224 cc/hr. The treatment improved the gas and condensate relative permeability by a factor of 1.3 at the lower flow rate but the improvement factor dropped to 1.07 at the higher rate.

Figures 11.4 and **11.5** show the pressure drop during the dynamic condensate accumulation at 1,200 psig and 145°F at multiple flow rates varying from 276 cc/hr to 1019 cc/hr on Texas Cream limestone with no initial water saturation before and after chemical treatment respectively (Exp#2). The core was treated using 2% FC4430 in a

mixture of methanol and water. **Table 11.2** gives the composition of the treatment solution. The pressure drop during the treatment flood at 1,200 psig and 145°F is shown in **Appendix 2**. 17 pore volumes of the treatment solution was flowed through the core at 56 and 112 cc/hr. The treatment did not improve the relative permeability.

Chemical treatment using FC4430 in a mixture of methanol and water improved the gas and condensate relative permeability by a factor of 1.56-1.89 on dry Berea sandstone rocks. Thus, the above result shows that a different family of chemicals may be required to treat limestone rock because of the difference in the mineralogy of the rocks. Carbonate surfaces are positively charged and therefore anionic surfactants may adsorb more strongly on the limestone rock surface compared to non-ionic surfactants FC4430 and FC4432.

Some new chemicals, L16218 and L16209 from 3M corp were also tried for treating Texas Cream limestones rocks. **Table 11.1** summarizes the results of the chemical treatment using these two chemicals (Exp #4 and #5 respectively). Results show that chemical treatment did not improve gas and condensate relative permeabilities. Details of these experiments are given in **Appendix B4 and B5**.

A new chemical APG1430 from Advanced Polymer inc. was also tested. The chemical is a Fluorophosphate Ester. The chemical is supplied in an aqueous based solution by the vendor. **Table 11.1** summarizes the results of the chemical treatment using APG1430 on gas and condensate relative permeabilities (Exp #38). The chemical plugged the core during chemical treatment. Pressure drop across the core during the treatment flood is shown in **Appendix B38**.

Table 11.2 gives the treatment solutions used for the experiments conducted on Texas Cream limestone.

11.3 SUMMARY

Results of some exploratory experiments conducted to evaluate chemicals for treating limestone rocks have been presented in this chapter. Different chemicals FC4430, FC4432, L16209 and L16218 from 3M corp and APG1430 from Advanced polymer inc. were tried to treat Texas cream limestone rocks. No significant improvements in gas and condensate relative permeabilities were observed with any of the tried chemicals. Different approaches like activating limestone surfaces, using anionic surfactants, using different solvents to deliver the surfactant to rock surface should be tried for treating limestone surfaces.

Table 11.1: Summary of chemical treatments on Texas Cream Limestone cores

	Exp#1	Exp#2	Exp#4	Exp#5	Exp#12	Exp#48	Exp#38
Temperature, °F	145	145	145	145	250	175	175
Pressure, psig	1200	1200	1200	1200	1500	420	420
k _g , md	9	8	20	12	14	8	10
Swi%	0	0	0	0	0	14	20
Surfactant	FC4432	FC4430	L16218	L16209	L16218	136598- 106	APG1430
k _{rg} before treatment	0.091	0.121	0.094	0.108	0.098	0.110	0.121
k _{ro} before treatment	0.064	0.084	0.065	0.075	0.110	0.049	0.058
k _{rg} after treatment	0.119	0.121	0.115	0.125	0.111	0.130	xx
k _{ro} after treatment	0.084	0.085	0.079	0.087	0.125	0.056	xx
IF	1.31	1.0	1.22	1.15	1.13	1.18	plugged

Table 11.2: Treatment solution

Exp no.	Treatment solution
1	2% FC4432, 94% methanol, 4% water
2	2% FC4430, 78% methanol, 20% water
4	2% L16218, 94% methanol, 4% water
5	2% L16209, 94% methanol, 4% water
12	2% L16218, 94% methanol, 4% NH ₄ OH
48	2% surfactant (136598-106), 69% PG, 29%IPA
38	20% APG1430, 15% EGMBE, 15%IPA, 50% water

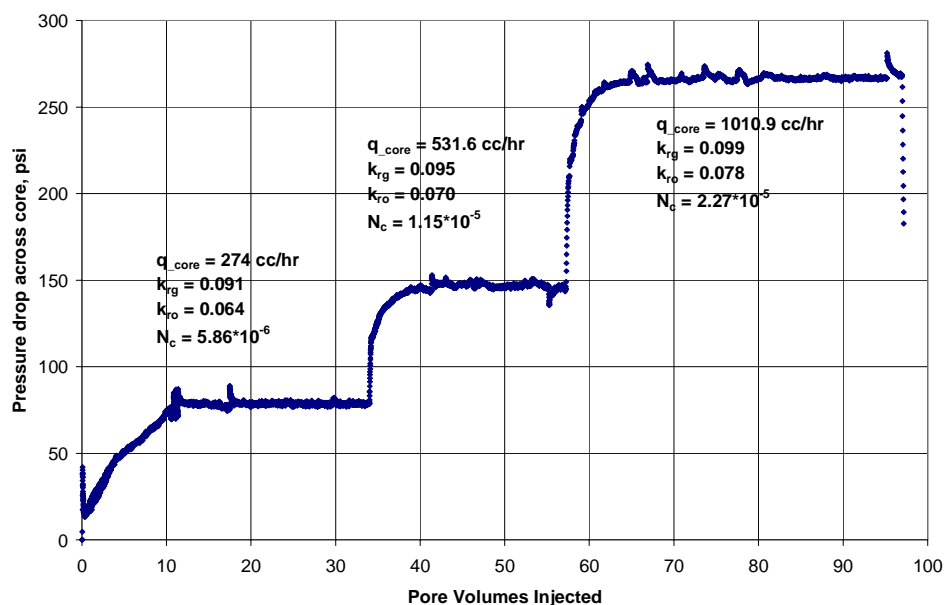


Figure 11.1: Pressure drop across TCL core during dynamic condensate accumulation at 145°F and 1200 psig (Exp#1)

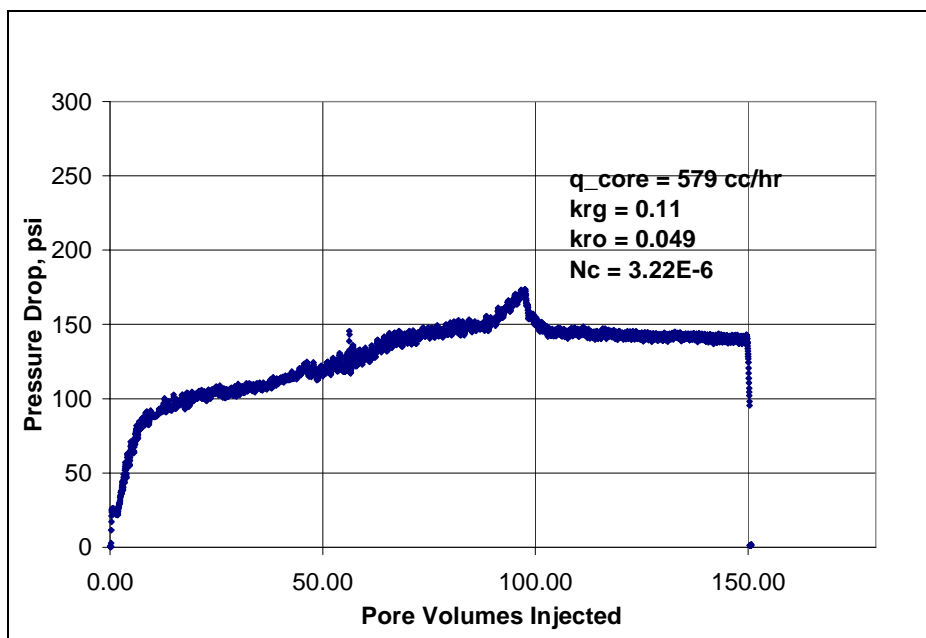


Figure 11.2: Pressure drop across TCL core during dynamic condensate accumulation at Swi-14% at 175°F and 420 psig (Exp#48)

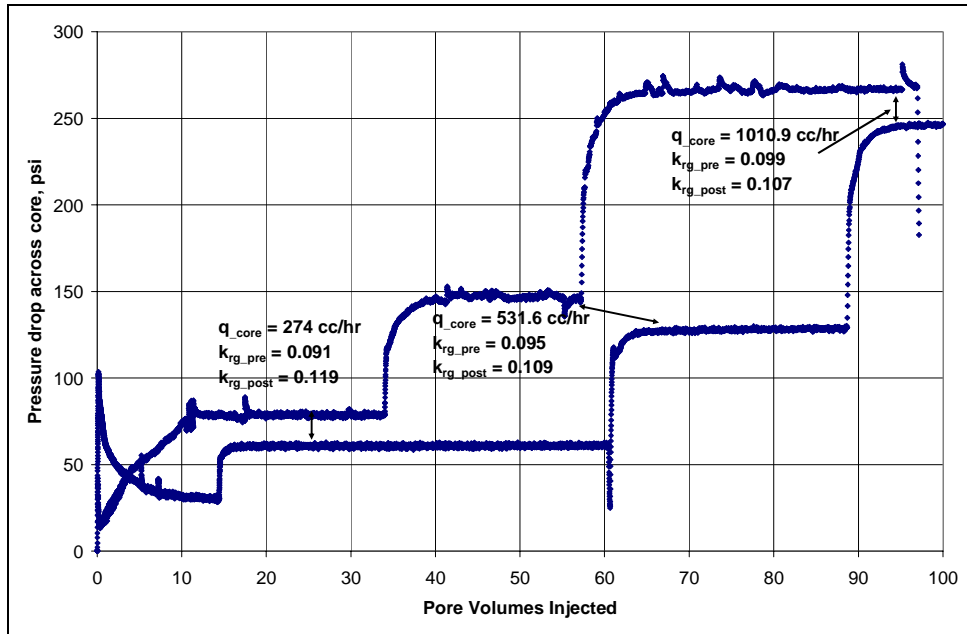


Figure 11.3: Effect of chemical treatment using FC4432 on gas relative permeability at 145°F and 1200 psig (Exp#1)

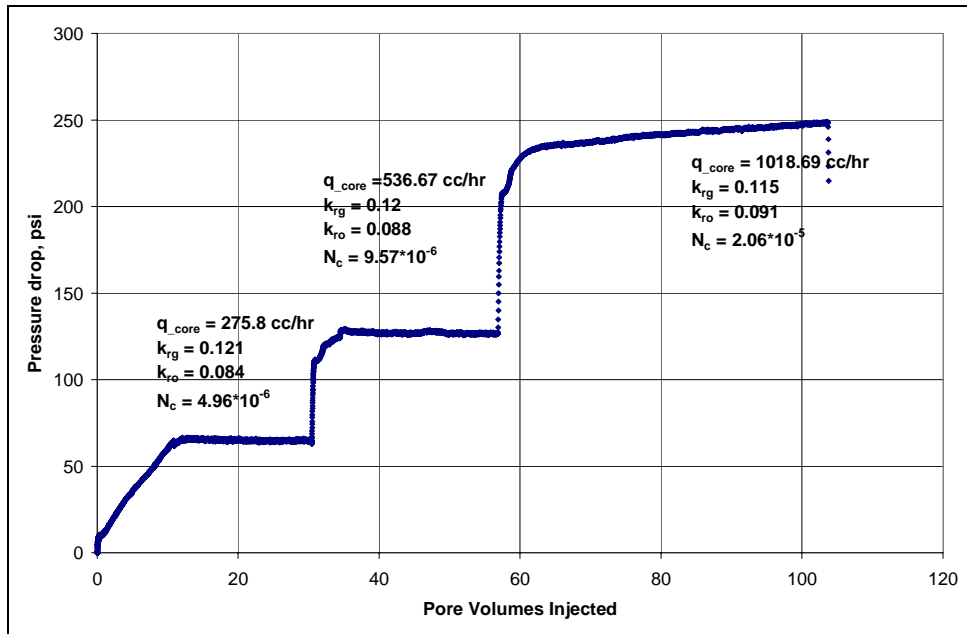


Figure 11.4: Pressure drop across TCL core during pre-treatment dynamic condensate accumulation at 145°F and 1200 psig (Exp#2)

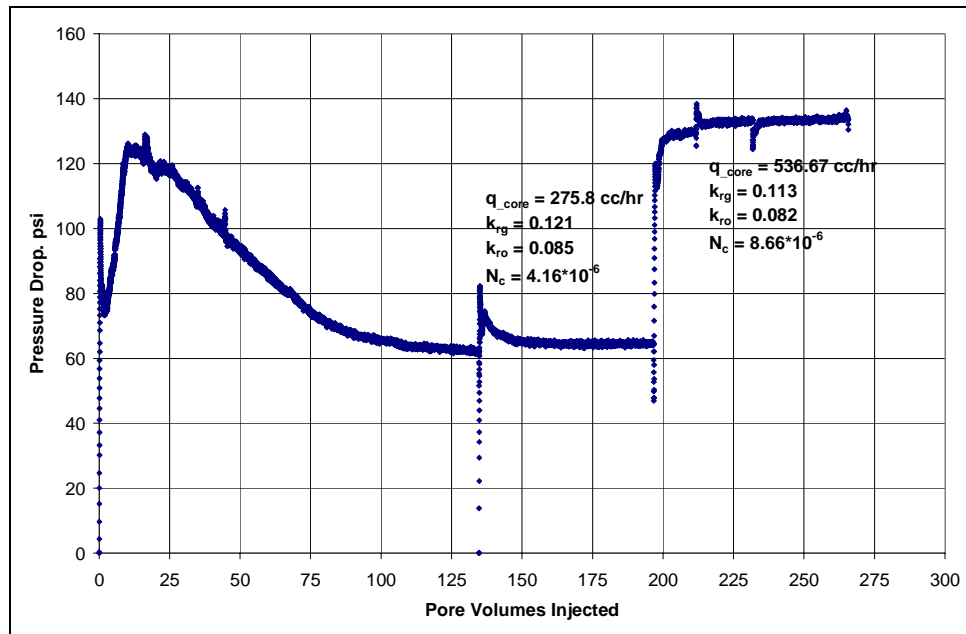


Figure 11.5: Pressure drop across TCL core during dynamic condensate accumulation at 145°F and 1200 psig after treating with FC4430 (Exp#2)

Chapter 12: Simulation study of chemical treatments to remove liquid blocking from gas reservoirs

This chapter presents a single-well simulation study of chemical treatments in gas-condensate wells. A description of the input data is first presented. The data include reservoir and fluid properties, numerical grid, relative permeability, initialization and well constraints. Studies were done for a multi-layered reservoir. The results of the simulations with and without chemical treatment are presented. The effect of different treatment volumes on the improvement in the productivity of a gas well is discussed next. The chapter also describes the simulation of the treatment injection process and the flow back of the injected solvents with produced reservoir fluids.

12.1 INTRODUCTION:

Predicting gas-condensate well deliverability is very complex. The difficulty arises due to large changes in the relative permeability near wells during and after accumulation of a condensate bank. The differential equations describing multiphase flow are highly non-linear and do not lend themselves to analytical solutions. As shown in Chapter 10, the gas and oil relative permeabilities in the near wellbore region are greatly affected by high capillary number and the non-Darcy flow. Thus the combined effects of phase behavior, relative permeability, capillary number and non-Darcy flow must be modeled to get accurate predictions of well deliverability.

The chemical treatment and well performance following chemical treatment is even more complicated to predict with a simulator since the rock properties of a treated zone differ from the untreated zone, which results in changes in relative permeability

after treatment. Also, a change in the phase behavior of reservoir fluids during the injection of treatment solution and chase gas must be simulated accurately. Kumar *et al.* (2006) presented some preliminary simulation studies done to evaluate the effect of chemical treatment on gas well productivity, but he did not attempt to model the injection and flow back of the solvents.

12.2 GEM COMPOSITIONAL SIMULATOR

The GEM compositional simulator was used to simulate the performance of gas-condensate wells before and after chemical treatment. GEM (version 2006.10) is Computer Modeling Group's (CMG) general equation-of-state compositional simulator. The GEM simulator can be run in explicit, fully implicit and adaptive implicit modes. The adaptive implicit option is particularly useful when high flow rates occur near the well or in stratified reservoirs with very thin layers. GEM uses AIMSOL, which is a linear solution routine based on incomplete Gaussian Elimination as a preconditioning step to the GMRES iterative solver. AIMSOL has been developed especially for adaptive implicit Jacobian matrices.

GEM uses either the Peng-Robinson or the Soave-Redlich-Kwong equation of state to predict the phase equilibrium compositions and densities of the oil and the gas phases. It also supports various models for computing related properties such as oil and gas viscosities. The quasi-Newton successive substitution method (QNSS) developed at CMG is used to solve the nonlinear equations associated with the flash calculations. A stability test based on a Gibbs energy analysis is used to determine the number of phases.

GEM uses CMG's Grid Module for interpreting the reservoir definition keywords used to describe a complex reservoir. There is a provision for variable thickness-variable depth type grids. One of the very helpful options in CMG is that of using local grid

refinement (LGR). LGR means some of the gridblocks in a particular range on the fundamental (main) grid will be replaced by a refined grid. Each refined grid will be made up of several small gridblocks that will together fill the space occupied previously by a parent gridblock. These refined gridblocks can be of variable size, and can be assigned different reservoir properties. LGR option is particularly helpful for simulating hydraulically fractured reservoirs (Mohan *et al.*, 2005).

The effect of capillary number on relative permeability can be modeled in GEM using the permeability model developed by Pope *et al.* (2000) and described in Chapter 10. High-velocity gas flow (non-Darcy flow) can be modeled in GEM with the Forchheimer equation. Non-Darcy flow coefficient β can be calculated from the correlations developed by Geertsma (1974), Evans (1988) or Frederick *et al.* (1994). As discussed in Chapter 10, Geertsma's correlation was used to calculate β .

12.3 SIMULATION MODEL SETUP

Coarse grid simulations do not accurately capture the steep changes in condensate saturation, relative permeability, pressure and so forth near the wells where they matter the most and dominate the production rates. Fine-grid compositional simulations or simulations using local grid refinement (LGR) near the wells are needed to accurately calculate the production.. However, these methods have the disadvantage of large run times, especially on full field problems with many zones and other complexities that make their use impractical for routine use on large problems. Therefore, single-well simulations are often done to model the condensate banking effects. These models can be calibrated to capture the effects near the well and the results can be used in the form of pseudo functions in large-scale simulation.

In this study, single-well simulations with a logarithmically distributed radial grid were used to model the effects of condensate and water blocking on well deliverability. This allows use of small grid blocks near the wellbore where they are needed most for numerical accuracy and large grid blocks away from the well where the effect of condensate banking is not significant on the production performance. The smallest grid block used around the well was 0.18 m (0.59 ft).

8.3.1 EOS Model and Fluid Properties

The Peng-Robinson EOS (Peng and Robinson, 1976) was used to model the phase behavior. Description of PREOS is given in **Chapter 3**. The characterized fluid composition of Bruce reservoir fluid is given in **Table 12.1**. The EOS parameters used for the fluid are given in **Table 12.2**. Volume shift parameters for the components were calculated using equation 3.20 (Chapter 3). **Figure 12.1** shows the calculated P-T phase envelope for the characterized reservoir fluid and **Figure 12.2** shows the calculated liquid dropout at the reservoir temperature (230°F). The maximum liquid dropout at 230°F is 11.5 %. The dew point pressure at 230°F is 5397 psig. **Figures 12.3** and **12.4** show the gas and oil viscosities calculated at 230°F (Herning and Zipperer model, 1936). **Figure 12.5** shows interfacial tension calculated at 230°F (Reid *et al.*, 1977).

Table 12.3 gives the binary interaction parameters between the components. Binary interaction coefficients (BICs) are used to take into account the non-ideal interaction between components that do not follow the ideal van der Waals mixing rule, e.g. polar components.

Table 12.2 also gives the EOS parameters for the solvents used in the treatment solution. The binary interaction parameters between ethanol and hydrocarbons were taken from Calsep's PVTsim database. 2-Butoxyethanol (ethylene glycol monobutyl

ether or EGMBE) is not in the PVTsim database, so the binary interaction parameters between it and the hydrocarbon components and also the volume shift parameters given for diethylene glycol were used since it is the closest glycol to 2-butoxyethanol in the PVTsim database. Therefore, there is a lot of uncertainty in these values and this could change some of the results significantly as discussed later.

12.3.2 Simulation Grid (Reservoir Model)

A simulation model with a drainage radius of 3500 ft and six layers (25x1x6) was used to represent the drainage area of a gas-condensate well in the Bruce field. **Figure 12.6** shows a 3D schematic of the simulation model. A magnified view of the refined grids near the well in layer 6 is shown in **Figure 12.7**. Gridblock sizes increase in a logarithmically away from the well. The smallest gridblock size was 0.59 ft (0.18 m) and the largest gridblock size farthest from the well was 1262 ft (385 m).

Table 12.4 gives the reservoir properties of the six layers used in the simulation model. The layers have different porosities and permeabilities representing the heterogeneous nature of the reservoir. Different water saturations were used in the six layers. Layer 6 is the most permeable layer and accounts for about 90% of the total formation kh (md-ft). Vertical permeability was taken as 0.01 times the horizontal permeability to model cross flow between the layers.

12.3.3 Initialization

Initial reservoir pressure and temperature are 5800.8 psi (39985.1 KPa) and 230°F. Initial water saturation varied from layer to layer as given in **Table 12.4**. The bottom hole flowing pressure was changed with time to match the production history of

the well. Well was produced at 2000 psig bottom hole flowing pressure for the first 4 years, then at 1000 psi for next 8 years and then finally the bottom hole flowing well pressure was decreased to 400 psi.

For the post-treatment simulation cases, the pressure and fluid composition (mole fractions) in each grid block at the end of the pretreatment simulation were taken as the initial composition for the post-treatment simulation. The water saturation in the treated zone or gridblocks was reduced to zero since the treatment solution miscibly displaces the water it contacts.

12.3.4 Relative Permeability Model

At high production rates, non-Darcy flow and changes in relative permeability with capillary number can be important. The model described in Chapter 10 modifies the relative permeability as per equations **10.14 to 10.17** to account for capillary number. The model parameters including endpoints for water, oil and gas relative permeability, residual saturations of the three phases, exponents for water, oil and gas relative permeability and different trapping parameters are given in **Table 10.2**. These model parameters were obtained by fitting a large set of relative permeability data measured over a wide range of capillary numbers and k_{rg}/k_{ro} ratios. The model was also validated against the data reported in literature.

Figure 12.8 shows the variation of the simulated gas and oil relative permeability close to the well after 13 years of production. **Figure 12.9** shows the capillary number calculated at the same time step (13 years). Results show that the capillary number close to the well for this case is only about 1×10^{-5} and thus smaller than the critical capillary number (Chapter 10). Therefore, the dependence of relative permeability on capillary number for this case can be neglected.

Results of **Figure 12.8** show that the gas relative permeability calculated by the simulator are much higher than those calculated from a carefully validated spreadsheet at the same capillary number and k_{rg}/k_{ro} ratio of 1.22. For a k_{rg}/k_{ro} ratio of 1.22, the measured gas relative permeability is about 0.066. Thus, some kind of an error in the simulator seems likely when using the capillary number option. The values computed by GEM with the capillary number turned off were correct and furthermore the capillary number does not matter in this case since the values were less than the critical capillary number, so subsequent simulations were done with the capillary number turned off. **Figure 12.10** compares the gas and oil relative permeabilities with the capillary number dependent relative permeability model option on and off. The gas relative permeability decreased from about 0.1 to 0.056 by turning the capillary number option off and the lower value is close to the measured value under these conditions.

To model the effect of chemical treatment, relative permeability curves were changed for the treated zones. This was done by defining a second rock type for the gridblocks representing the treated zone. **Table 12.5** gives the relative permeability model parameters before and after treatment. **Figure 12.11** compares the pre-treatment and post-treatment relative permeability curves. The parameters for post-treatment case were adjusted to give an improvement factor of 1.9 for capillary numbers ranging from $1E-7$ to $1E-4$. The choice of post-treatment relative permeability parameters is not based on a large amount of data and it is possible to get the same improvement factor with another set of parameters. The improvement factor of 1.9 is an average value based on the experiments done under Bruce conditions.

A third rock type was used to account for some improvement that will be obtained by pushing treatment solution deeper in the formation by the chase gas (discussed in the following section). The parameters for the third rock type were chosen to give a much

lower improvement factor of about 1.3. Parameters used for the third relative permeability model are given in **Table 12.5**.

Figure 12.12 compares the gas relative permeability in the near wellbore region with and without the treatment after 50 days. **Figure 12.13** compares the oil relative permeability in the near wellbore region with and without treatment after 50 days. The improvement factor changes along the distance from the wellbore as the saturation and pressure changes. This results in changing PVT ratio or k_{rg}/k_{ro} ratios and thus the improvement factor.

12.4 SIMULATION RESULTS

12.4.1 Base Case

Figures 12.14 and **12.15** show the gas and condensate production data of the gas condensate well AO3 in Bruce field since the beginning of production. The well had been producing for 13 years. The gas production for the first year was very high, about 25 MMSCF/day but it dropped to about 10 MMSCF/day after about 500 days of production and then further to about 5-6 MMSC/day after 1000 days. Thus the gas rate decreased by almost a factor of 5 due to the build up of high condensate saturation around the well and the decline in reservoir pressure. Over the last 10 years the gas production was been maintained around 5-6 MMSCF/day by reducing the bottom hole flowing pressure or tubing head pressure at the surface. Similar decline was observed for the oil/condensate production rates over the last 13 years of production.

Figure 12.16 shows the decline in average reservoir pressure during production. **Figure 12.17** shows the change in bottom hole flowing pressure. Average reservoir

pressure decreased from 5800 psi to about 2400 psi and correspondingly the bottom hole flowing pressure was decreased from 2000 psi to 400 psi over the 13 years of production.

Figures 12.14 and 12.15 show the simulated gas and oil production rates and compare them with the actual production data. Simulation results fail to capture the initial high gas production rates but closely match the gas production rate after about 1000 days of production. At the end of 13 years both the simulated and the actual gas rate are about 6 MMSCF/day. The calculated oil rate is however lower than the actual production rate by about 30%. The actual oil rate is 300 STB/day compared to 200 STB/day predicted from simulation after 13 years. **Figure 12.16** compares the decline in reservoir pressure with simulation results. The calculated average reservoir pressure is higher than the actual average reservoir pressure by about 1000 psi but the simulated pressure decline rate is almost same as that observed from the field data. **Figure 12.17** compares the simulated and actual flowing bottom hole pressure history. Bottom hole pressure was changed from 2000 psi to 1000 psi and then finally to 400 psi in the simulation model to match the change in flowing bottom hole pressure.

Figure 12.18 shows the calculated oil saturation profile after 100 days, 1000 days and 4745 days of production. The oil or condensate bank is small initially and builds up significantly around the wellbore with time. The condensate bank was only about 12m after 100 days but increased to about 32m after 1000 days. After 13 years (4745 days) condensate bank had buildup to almost 74m (242 ft) from the well. Also, as the average reservoir pressure had dropped below the dew-point pressure condensate had dropped out of gas phase resulting in two-phases throughout the reservoir.

12.4.2 Simulating Treatment Injection Process

Injection of treatment solution and chase gas was simulated to model the whole treatment process. For simulating treatment solution injection, a mixture of 70 wt% 2-butoxyethanol (EGMBE) and 30 wt% ethanol was injected in to the formation using an injector well-1 located in the same grid block as the production well. The ratios of the solvents were converted to mole %, which are 48% and 52% respectively. For simplicity, injection of surfactant along with the solvents was not simulated as the effect of surfactant on rock properties was already taken into account by changing the relative permeability curves for the treated grid blocks (zones). Also, the surfactant is not expected to have a significant effect on the phase behavior of the reservoir fluids unlike the injected solvents.

Amount of treatment solution was calculated from the radius around the well targeted for the treatment and the pore volume corresponding to that radius. As the simulation model has multiple layers with different kh md-ft, amount of treatment solution injected will go into the layers depending on their kh. As, Layer 6 accounts for about 90 of the total kh md-ft, almost all of the injected treatment solution will go into Layer 6 only. Therefore, for simplicity treatment solution was injected into Layer 6 only and the amount of treatment solution was calculated based on the pore volume corresponding to the treatment radius in Layer 6. Treatment solution was injected at a constant bottom hole injection rate of 228 cubic meters per day (1434 bbls/day). The time required for injection varied depending on the volume of treatment solution.

Injection of treatment solution was followed with the injection of chase gas. To simulate chase gas injections nitrogen, methane or separator gas was injected using a second injector well located in the same grid block as the producer and the first injector

well. 2MMSCF of chase gas was injected at a constant bottom hole pressure of 5000 psig.

Chase gas is injected to push out the injected treatment solution deeper into the formation. This can help in getting additional benefit of treating the part of the formation beyond the targeted treatment radius. As not all of the surfactant in the treatment solution gets adsorbed on the rock surface, by pushing the excess treatment solution into the untreated zone can help get some additional improvement. Also, by injecting chase gas at high pressure, energy is provided to the formation, which helps in getting the well back to production and avoid any problems due of liquid loading in the well due to large volume of treatment solution injected. **Figure 12.19** shows the bottom hole well pressure during the injection of treatment solution followed by chase gas for the case of treating 2.72m around the well.

The production well was then put back on production. Shut-in time after the treatment was not simulated as the actual adsorption of surfactant on the rock surface is not simulated here but just the effect of treatment on the relative permeabilities of gas and oil is modeled by changing the relative permeability curves.

12.4.3 Results of Chemical Treatment

Chemical treatment was then simulated to see the effect of improvement in gas and condensate relative permeability due to wettability alteration on the productivity of well at field scale. Effect of different treatment radii was studied to determine the optimum treatment radius and volume for this case. Effects of different chase gases and chase gas injection pressure were also studied to determine the optimum conditions for chase gas injection.

Figure 12.20 shows the effect of chemical treatment on gas production rate for different treatment radii. Studies were done for treatment radius of 1.69m, 2.17m, 2.72m and 4.2m. Improvement in gas production rate increased with the treatment radius. Gas production rate increased from 6 MMSCF/day to 8.1 MMSCF/day for a treatment radius of 1.69m and to 8.9 MMSCF/day for a treatment radius of 4.2m after 100 days of post-treatment production. **Figure 12.21** shows the effect of chemical treatment on oil production rate for different treatment radii. The oil production rate increased from 195 STB/day to 256 STB/day for a treatment radius of 1.69m and to 278 STB/day for a treatment radius of 4.2m after 100 days of post-treatment production.

Figure 12.22 shows increase in productivity index after the treatment for different treatment radii. In this work the PI (Productivity Index) has defined as

$$PI = q_{sc} / (P_{avg} - P_{wf}) \quad (12.1)$$

A more standard definition of PI is based on pseudo pressure $m(P)$ definition. Increasing the treatment radii from 1.69m to 4.2m increased the PI from 1.36 to 1.48 after 100 days of post-treatment production.

The results show that increasing the relative permeability by a factor of 1.9 in the treated zone does not increase the gas and condensate production rate by the same factor. This relatively smaller increase in productivity due to treatment is because the original condensate bank is almost 74m (region with oil saturation greater than 40%). The treatment reduces only a part of the damage caused by condensate block as the whole 74m of condensate bank is not treated. However, as most of the pressure gradient driving the flow is in the first few feet from the well, therefore a significant improvement in productivity can be observed by just treating few feet around the wellbore. Thus an

improvement of almost 50% can be obtained by treating radius corresponding to only about 5% of the condensate bank.

Treatment volumes injected for each case is given in **Table 12.6**. **Figure 12.23** shows the improvement in productivity index for different treatment radii. **Figure 12.24** shows the improvement in productivity index for different treatment volumes. Results show that increasing the treatment radius from 2.72m to 4.2m (i.e. increasing the treatment volume from 253 bbls to 594 bbls) does not significantly increase the productivity index but can increase the cost of the treatment significantly. Thus the optimum treatment radius for this case is 2.72m or the optimum treatment volume is 253 bbls. Thus for this case by just treating 2.72 m around the well can increase the productivity of the well by more than 40%, which makes the treatment extremely cost effective.

Figure 12.25 shows the net gas production with different treatment radius at different times after the treatment. Net gas production is the difference between post-treatment cumulative gas production and cumulative gas production without the treatment. **Figure 12.26** shows the net oil production with different treatment radius at different times after the treatment. Net oil production is the difference between post-treatment cumulative oil production and the cumulative oil production without the treatment. The results show that if the chemical treatment holds for one year, almost an additional 800 MMSCF of gas and 25000 STB of condensate can be produced.

12.4.4 Flow Back of Solvents

Simulating the displacement of injected solvents in the formation by the chase gas and the production of the solvents with the producing fluids is important. Displacement by chase gas is important to know how deep the solvents are pushed in the formation as

this may help in achieving extra benefit of the treatment. Predicting the flow back of solvents is important from the surface handling point of view. Results presented in this section are for the post-treatment case with a treatment radius of 2.72m.

Figure 12.27 shows the gas production rate and **Figure 12.28** shows the composition of the gas phase at surface conditions for the first few days after treatment. **Figure 12.29** shows the oil production rate and **Figure 12.30** shows the composition of the oil phase at surface conditions for the first few days after treatment. Results show that a surge in gas production is observed for the first couple of days, which is mainly due to the energy introduced in to the formation by injecting high pressured chase gas. Whereas, the liquid production rate is extremely low till the solvents are produced back and then increases by more than an order of magnitude. The simulation results show that most of injected ethanol is produced back within a day after resuming production and is mainly in the gas phase. 2-butoxyethanol mainly comes out in the liquid phase and takes about 18 days to produce back.

To test the sensitivity of solvent production to the EOS parameters like the binary interaction parameters, the BIC's between 2-butoxyethanol, ethanol and hydrocarbon components were changed to zero. The post-treatment case with 2.72m of treatment radius and nitrogen as the chase gas was simulated with other parameters kept same as the earlier case. **Figure 12.31** shows the gas production rate and **Figure 12.32** shows the composition of the gas phase at surface conditions for the first few days after treatment. **Figure 12.33** shows the oil production rate and **Figure 12.34** shows the composition of the oil phase at surface conditions for the first few days after treatment. Results show high liquid (oil) production right after resuming production after treatment unlike the previous case, which showed a long period of low liquid production after treatment. The new results show that most of the ethanol is produced in the gas phase and 2-

butoxyethanol (EGMBE) in the oil phase like the previous case. Ethanol is produced back within the first day after resuming production like the earlier case and 2-butoxyethanol is produced back within first 4-5 days unlike the earlier case where it took about 18 days to flow back.

These results show that the calculation of recovery of solvents is a strong function of EOS parameters like the binary interaction parameters between the 2-butoxyethanol, ethanol, the injected chase gas and the hydrocarbon components. A small change in these values can affect the phase behavior of injected solvents and the reservoir fluids significantly and thus partitioning of these solvents in the gas and oil phases. There is a lot of uncertainty in these values as no phase behavior data is available for these fluids under these reservoir conditions to tune the EOS model. Modeling of mixtures with polar components like alcohol and glycol becomes extremely difficult because of the non-ideal interaction between components and therefore PVT data at the experimental/reservoir conditions becomes extremely important. The actual EOS parameters can differ significantly from the values used in these simulations and the actual recovery of solvents may be different from the simulated results.

12.5 SUMMARY

Single well simulation studies were conducted in a compositional equation of state simulator GEM to evaluate the effect of chemical treatment on the productivity of liquid blocked gas wells. The base simulation model was history matched against the production data from the gas condensate well AO3 in Bruce field. The effect of chemical treatment was simulated by changing the relative permeability curves for the treated zone to account for the improvement in gas and condensate relative permeability by a factor of 1.9 after chemical treatment as observed from the coreflood results (**Chapters 6 and 7**).

Effect of different treatment radii on the improvement in gas and oil productivity was studied. The productivity index increases with the increase in treatment radius but there is a critical treatment radius after which increasing the treatment radius shows no significant improvement. For the studied case, the critical treatment radius was 2.72m for which the productivity index increased by a factor of 1.43.

The injection of the treatment solution followed by chase gas was simulated to design the optimum injection pressures and rates for both the treatment solution and the chase gas. The recovery of injected solvents has also been simulated. Ethanol is mainly produced back within a day after resuming production and is mainly produced in the gas phase. 2-Butoxyethanol mainly is produced back in the liquid phase. Calculation of the flow back period of solvents is a strong function of EOS parameters like the binary interaction parameters between the solvents and the hydrocarbons. PVT studies of the solvents with the hydrocarbon gas mixtures needs to be done to better understand the phase behavior of such mixtures and tune the EOS models to model such mixtures.

Table 12.1 Composition of characterized Bruce reservoir fluid

Component	Mole %
C1N ₂ CO ₂	77.11
C2	7.77
C3	3.98
C4	2.17
C5-C6	2.81
C7-C15	5.19
C16-C31	0.92
C32+	0.048

Table 12.2: Equation of states parameters for the characterized Bruce fluid and solvents

Component	Mw	Tc (k)	Pc (atm)	ω	Vshift	Parachors
C1N ₂ CO ₂	16.91	193.928	46.22	0.015	-0.12	76.9
C2	30.07	305.4	48.2	0.098	-0.06	108.9
C3	44.097	369.8	41.9	0.152	-0.16	151.9
C4	58.124	420.22	37.07	0.188	-0.09	188.9
C5-C6	78.79	481.18	33.06	0.253	-0.09	258.2
C7-C15	109.79	601.98	30.41	0.423	0.04	389.5
C16-C31	359.99	688.85	14.25	0.912	-0.29	735.9
C32+	609.96	973.711	8.01	1.355	0.18	1364.3
EGMBE	46.09	513.9	60.6	0.644	0.04	0
Ethanol	118.2	633.9	38.5	1.2	0.06	0
N ₂	28	126	33.5	0.04	-0.04	41

Table 12.3: Binary interaction coefficients between components

	C1N ₂ CO ₂	C2	C3	C4	C5-C6	C7-C15	C16-C31	C32+	EGMBE	Ethanol
C2	0.0061									
C3	0.0064	0.0008								
C4	0.0096	0.0023	0.0003							
C5-C6	0.0281	0.0034	0.0009	0.0012						
C7-C15	0.0928	0.0068	0.0022	0.0061	0.0009					
C16-C31	0.0817	0.0169	0.0381	0.013	0.0139	0.0075				
C32+	0.0579	0.096	0.0867	0.0338	0.0424	0.0303	0			
EGMBE	0	0.19	0.03	0	0	0.29	0.29	0.29		
Ethanol	0	0.2	0.2	0	0	0.2	0.2	0.2	0.18	
N ₂	0.08	0.08	0.08	0.08	0.08	0.08	0.08	0.08	0.5	0.2

Table 12.4: Reservoir Properties

Layers	Height, m	k, md	Porosity, %	Net to gross	Swi
1	43.73	0.03	12	0.1	0.5
2	27.08	0.15	14	0.1	0.35
3	13.93	0.02	12	0.1	0.15
4	21.79	1.42	16	0.3	0.15
5	25.67	0.31	13	0.1	0.15
6	15.49	10	11	1	0.15

Table 12.5: Pre and Post treatment relative permeability parameters

Corey's parameters	RPT-1 (Pre-Treatment)	RPT-2 (Post-Treatment)	RPT-3
S_{wr}	0.25	0.25	0.25
S_{or}	0.3	0.3	0.3
S_{gr}	0.25	0.25	0.25
k_{ro}^o	0.3	0.4	0.3
k_{rg}^o	0.45	0.6	0.5
n_o	2	1.45	1.6
n_g	3	1.7	1.2

Table 12.6: Volume of treatment solution for different treatment radii

Treatment radius, m	Treatment Volume, bbls	Improvement in PI after 100 days
1.69	96.1	1.36
2.17	158.5	1.39
2.72	252.7	1.43
4.2	593.8	1.48

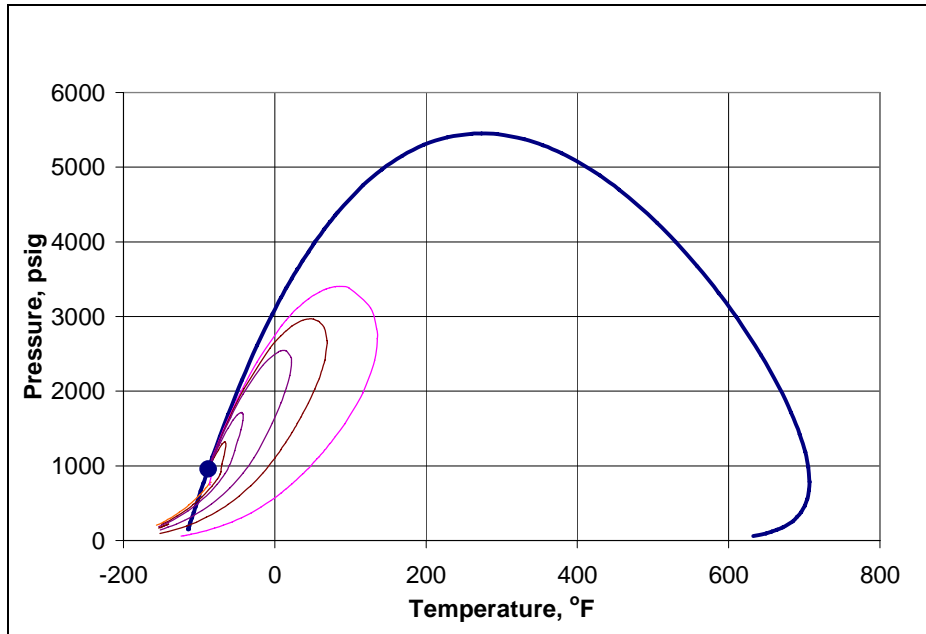


Figure 12.1: P-T phase diagram of Characterized Bruce reservoir fluid calculated using PREOS

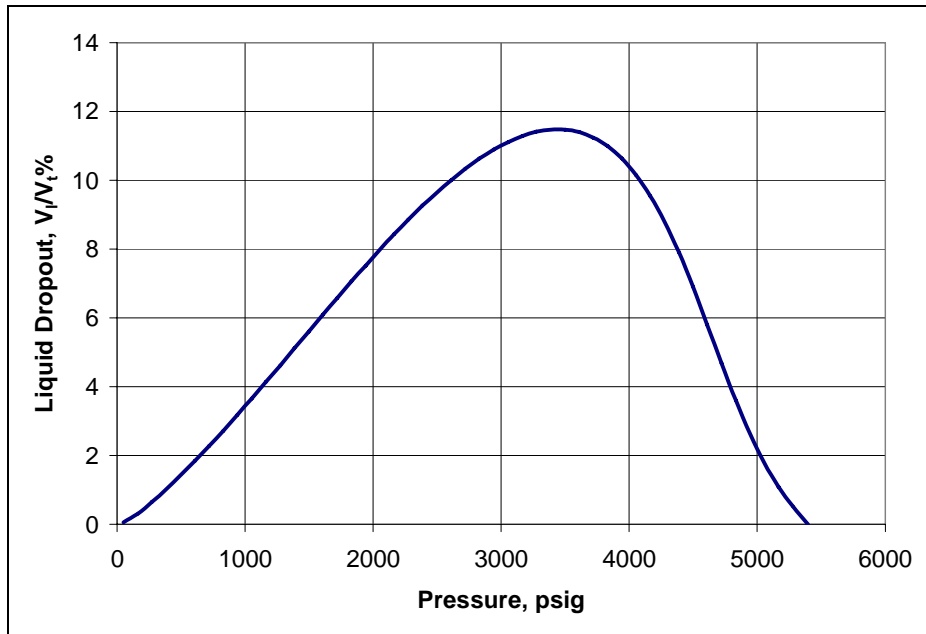


Figure 12.2: Liquid dropout of the Characterized Bruce reservoir fluid calculated using PREOS at 230°F

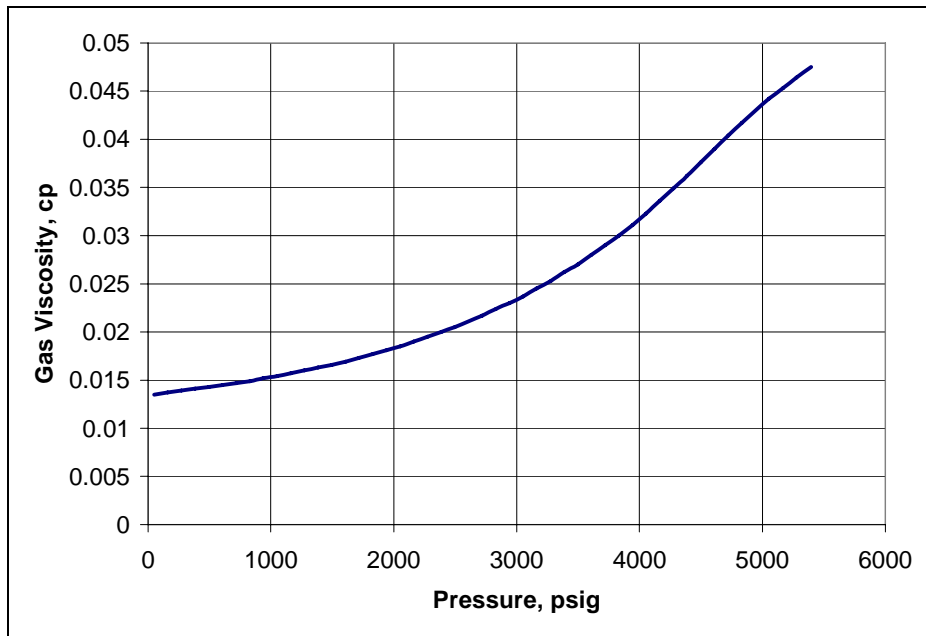


Figure 12.3: Gas viscosity of the Characterized Bruce reservoir fluid calculated using PREOS at 230°F

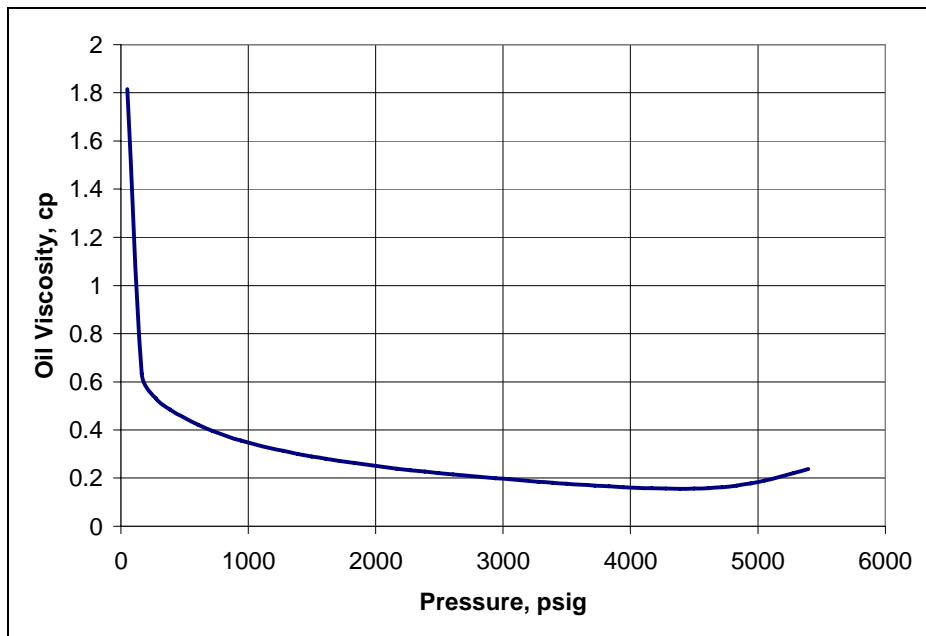


Figure 12.4: Oil viscosity of the Characterized Bruce reservoir fluid calculated using PREOS at 230°F

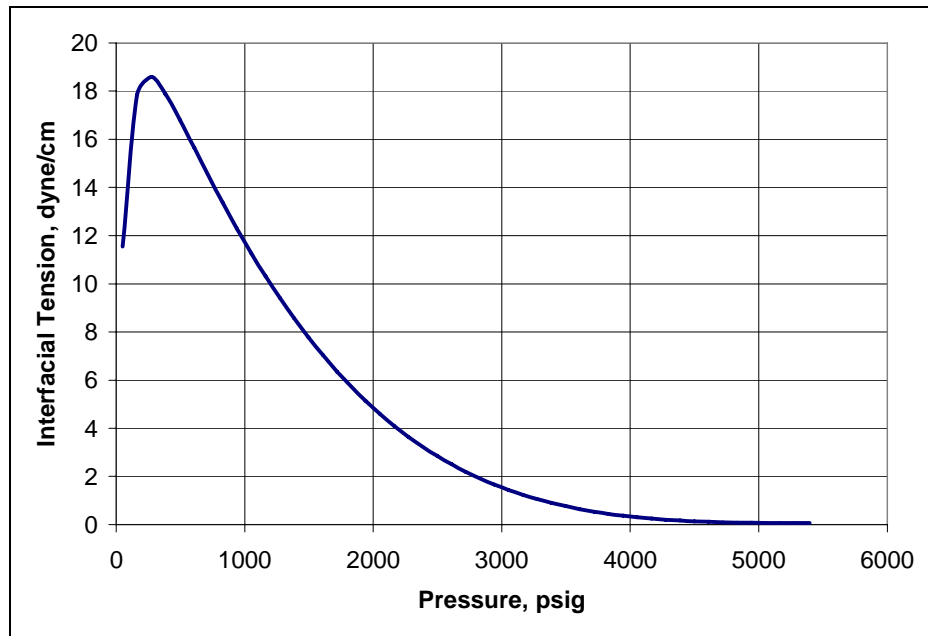


Figure 12.5: Interfacial tension between gas and oil calculated using PREOS at 230°F for the Characterized Bruce reservoir fluid

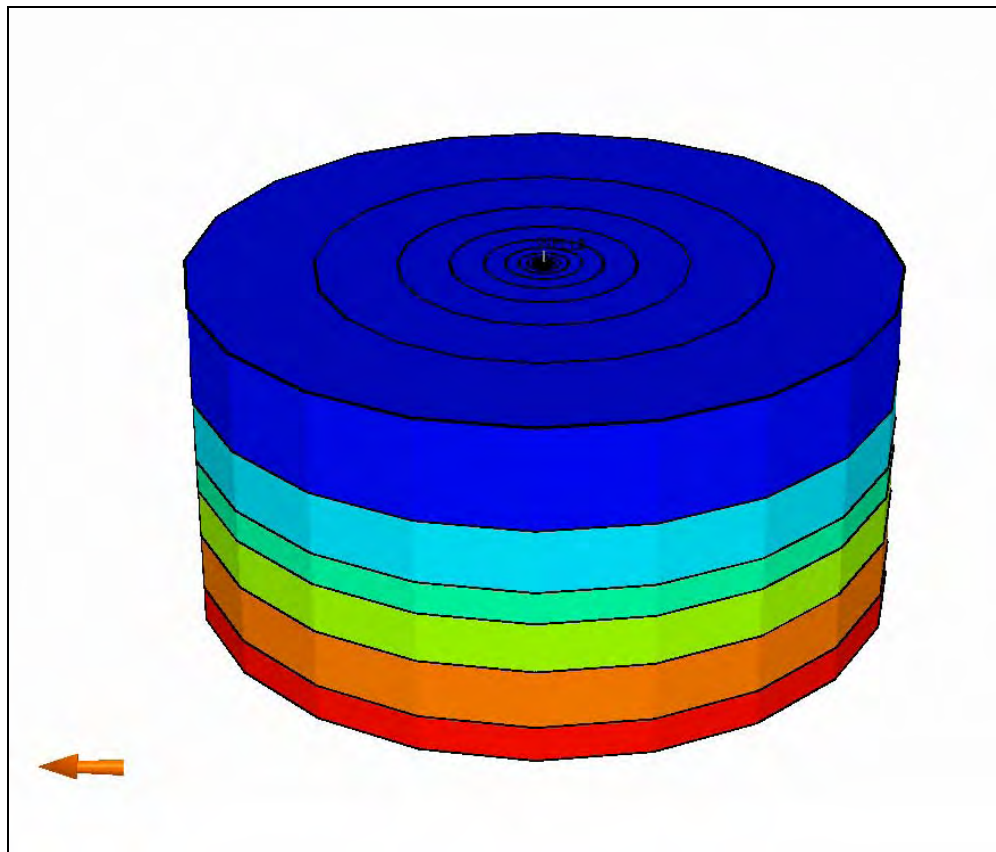


Figure 12.6: Schematic of the 6 layered simulation model for a gas condensate well in Bruce field

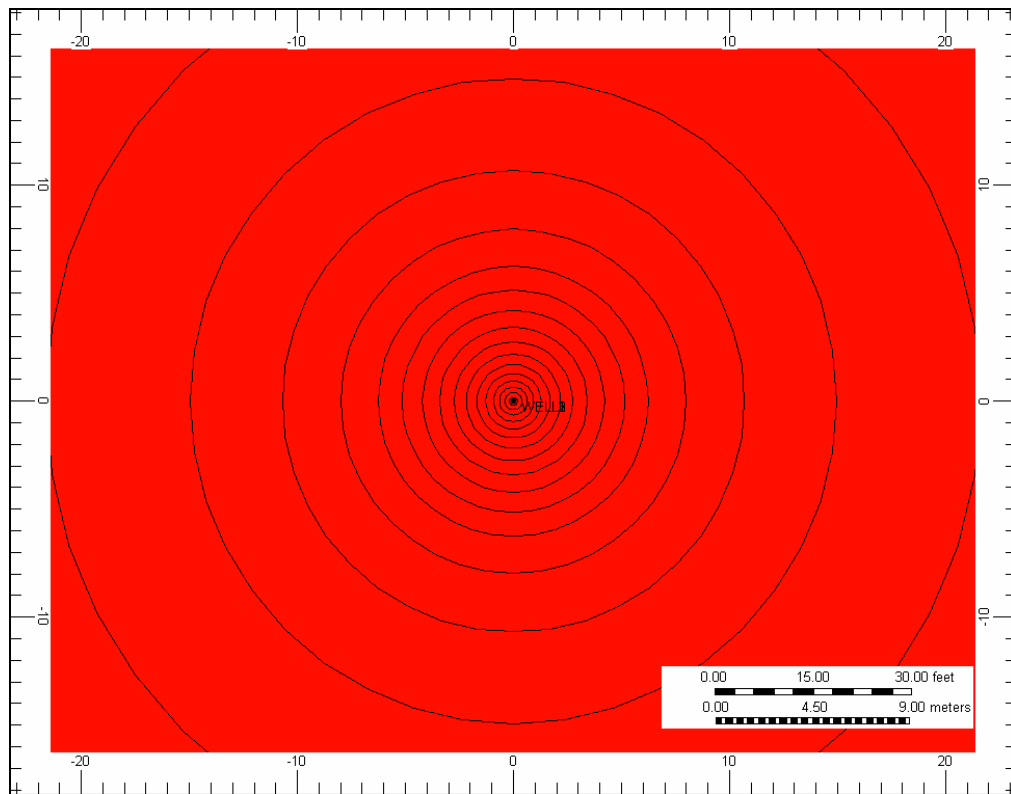


Figure 12.7: Schematic showing the refined grids near the well and increasing logarithmically away from the well

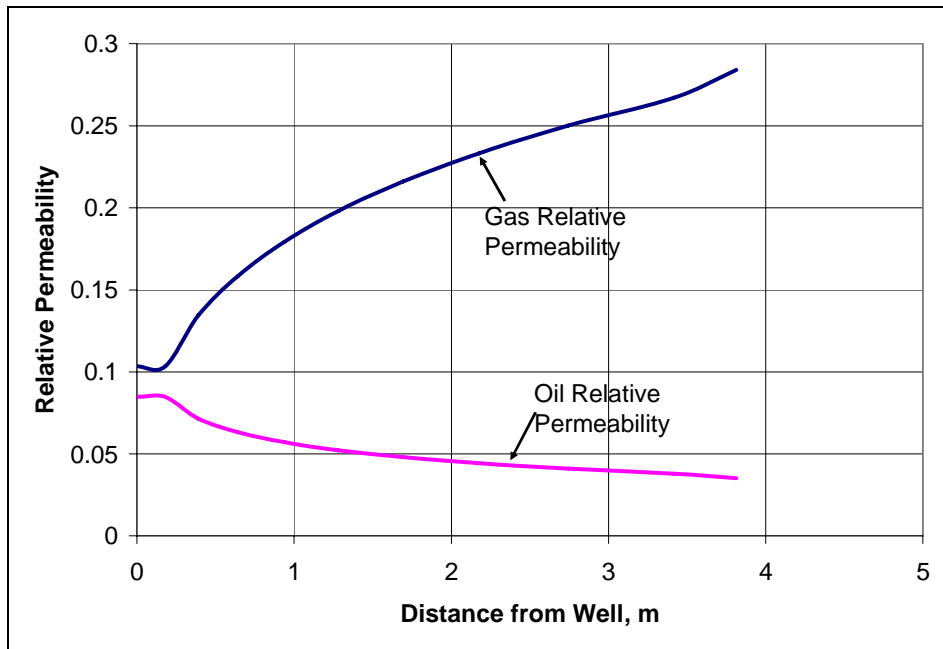


Figure 12.8: Gas and oil relative permeabilities calculated using the capillary number dependent relative permeability model after 13 years of production

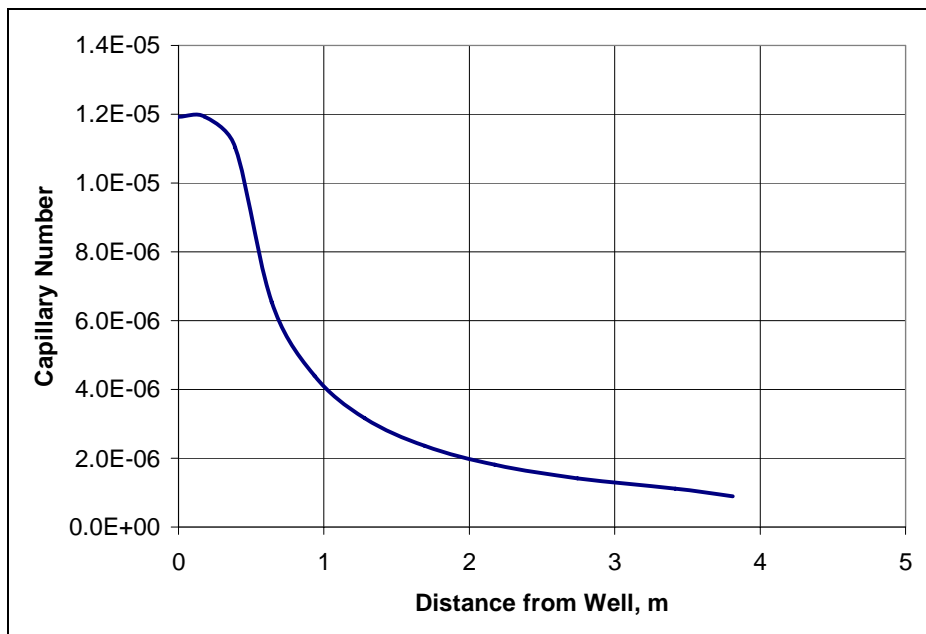


Figure 12.9: Capillary number calculated in the near wellbore region after 13 years of production

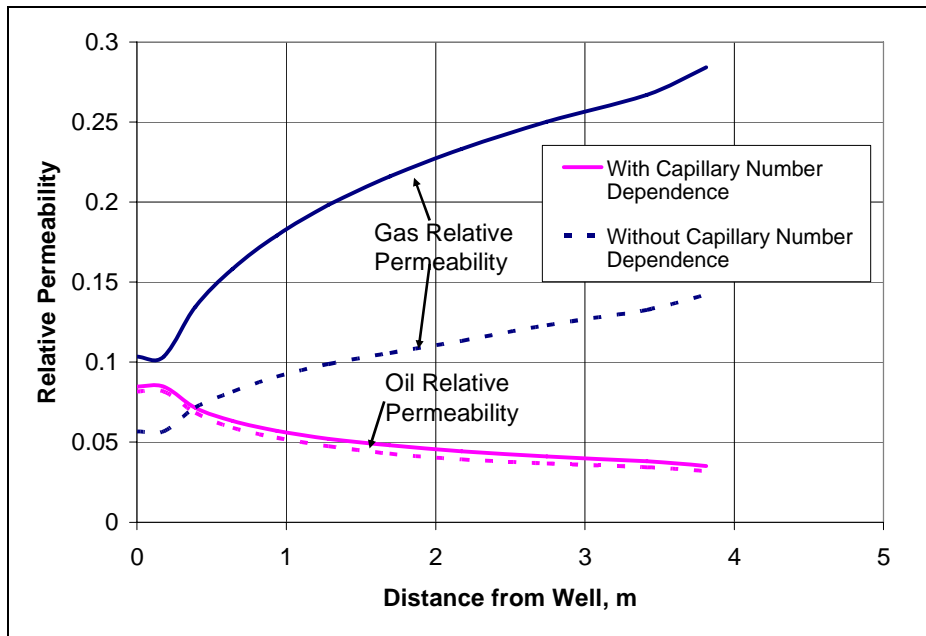


Figure 12.10: Comparison of gas and oil relative permeabilities calculated with the capillary number dependent relative permeability model option on and off

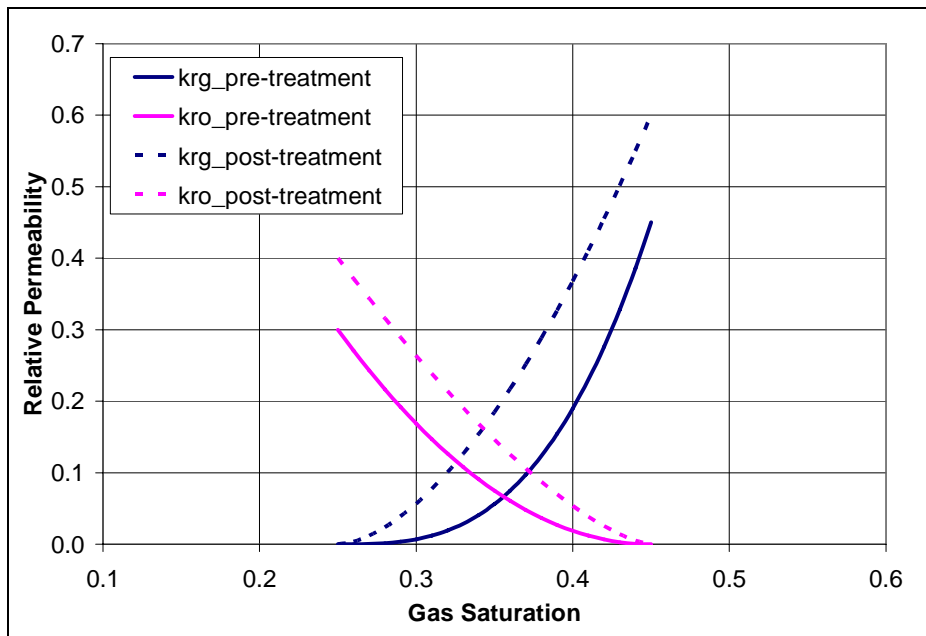


Figure 12.11: Comparison of pre and post-treatment relative permeability curves

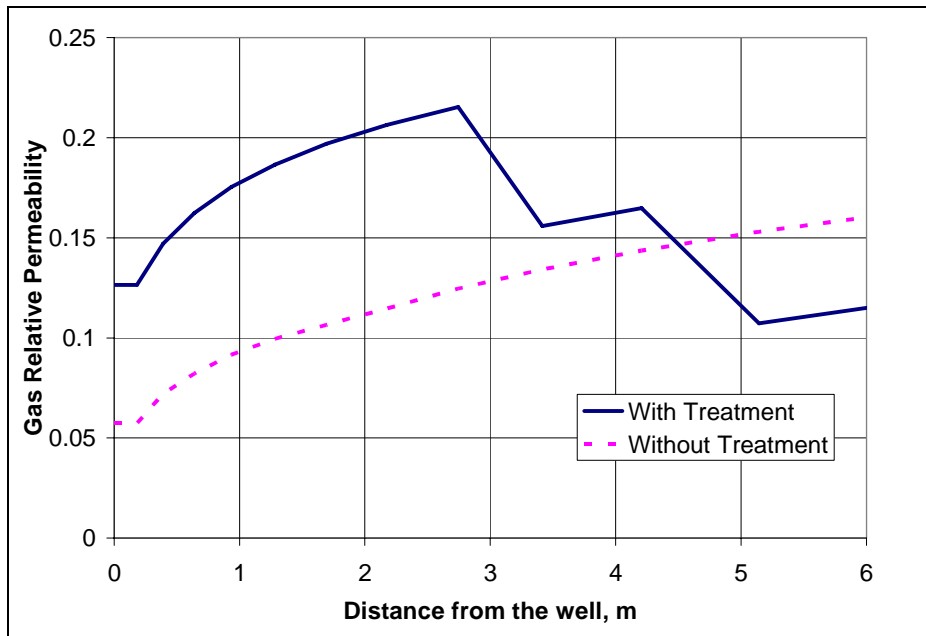


Figure 12.12: Comparison of gas relative permeability near the well with and without treatment after 50 days

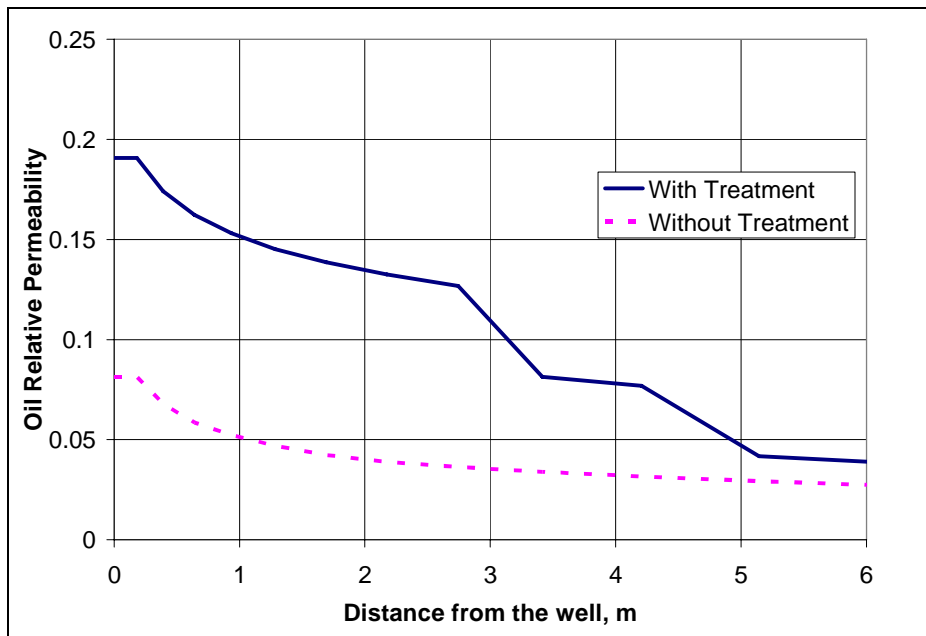


Figure 12.13: Comparison of oil relative permeability near the well with and without treatment after 50 days

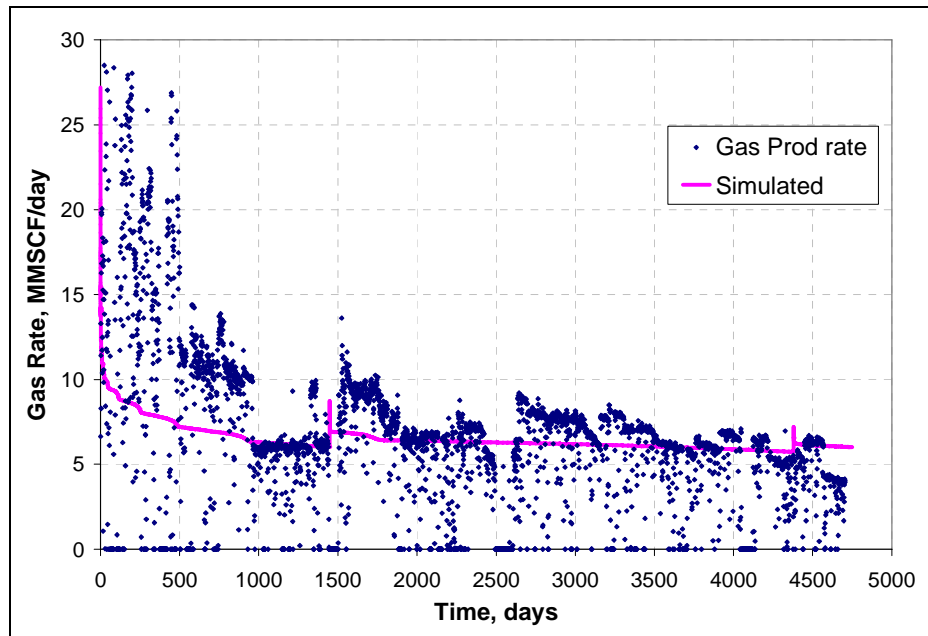


Figure 12.14: Comparison of simulated gas production rate with the actual production data of well AO3 of Bruce field

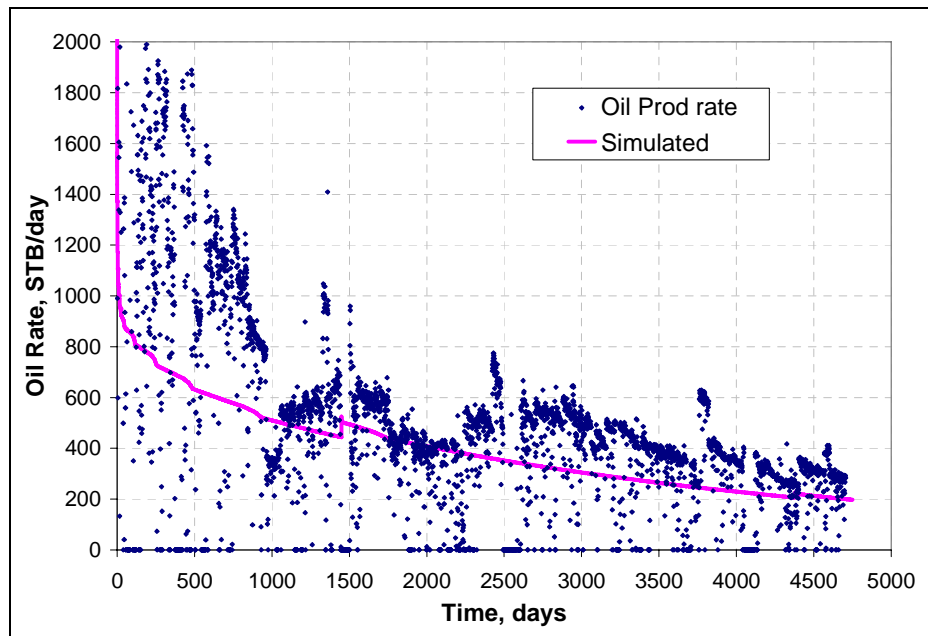


Figure 12.15: Comparison of simulated oil production rate with the actual production data of well AO3 of Bruce field

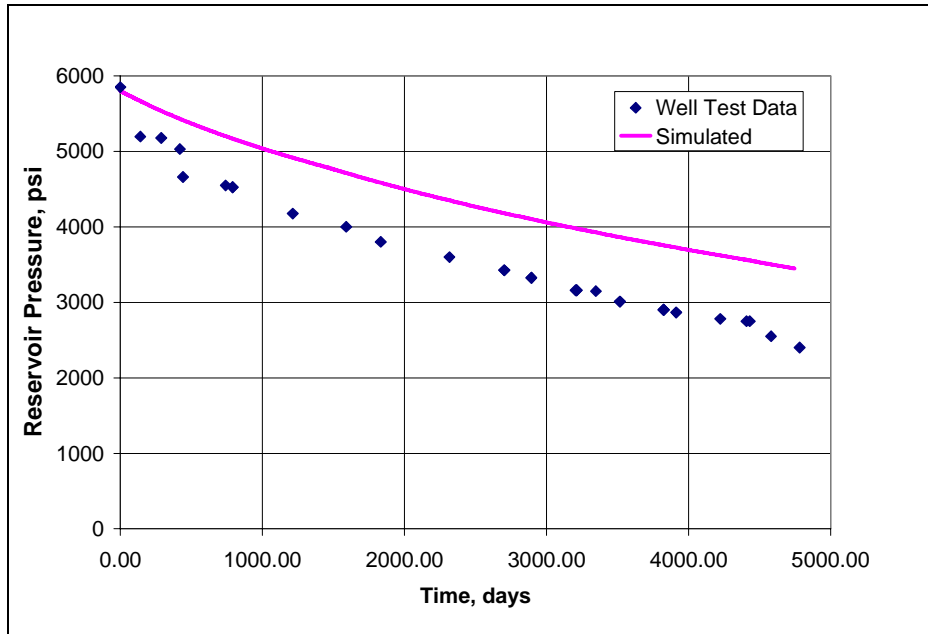


Figure 12.16: Comparison of simulated reservoir pressure depletion with the actual well test data

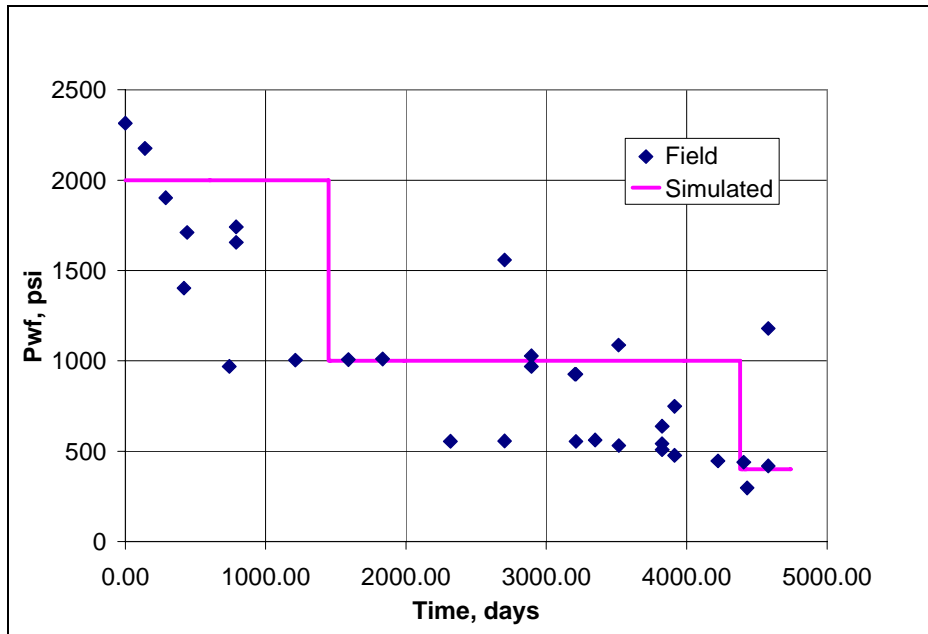


Figure 12.17: Flowing bottom hole pressure data and those used in simulation

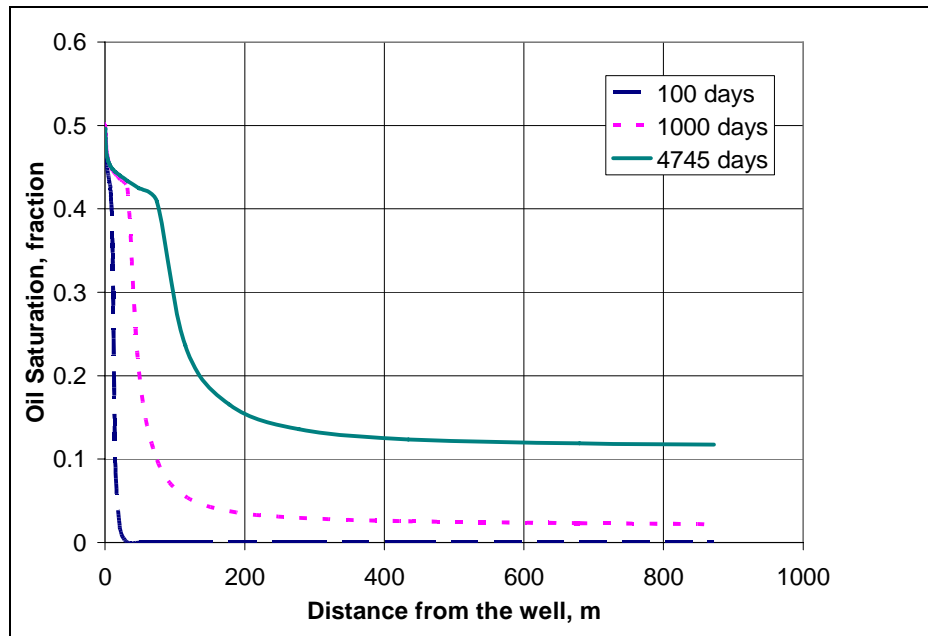


Figure 12.18: Oil saturation profile around the production well at different times

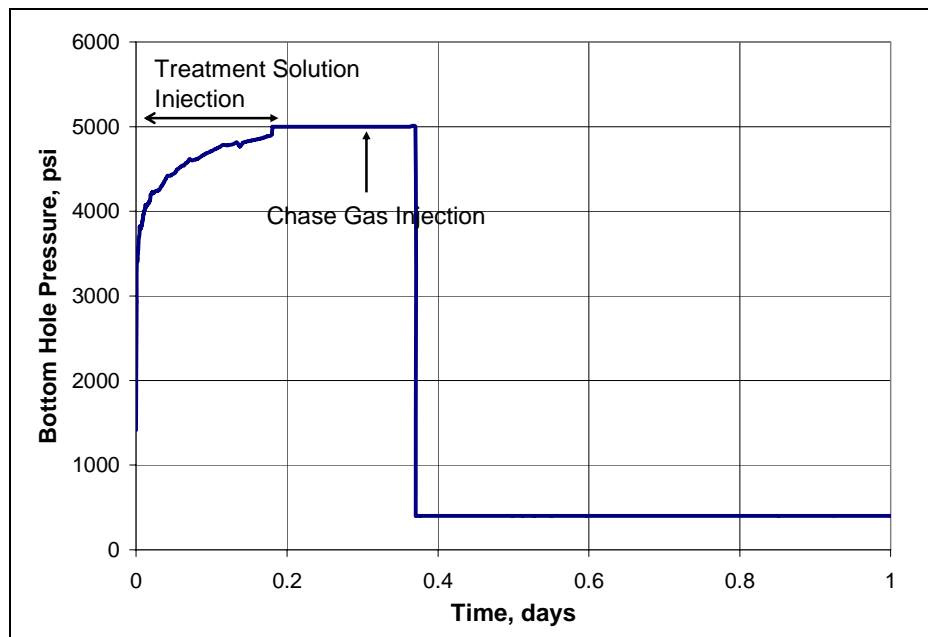


Figure 12.19: Simulated bottom hole pressure during the injection of treatment solution and chase gas

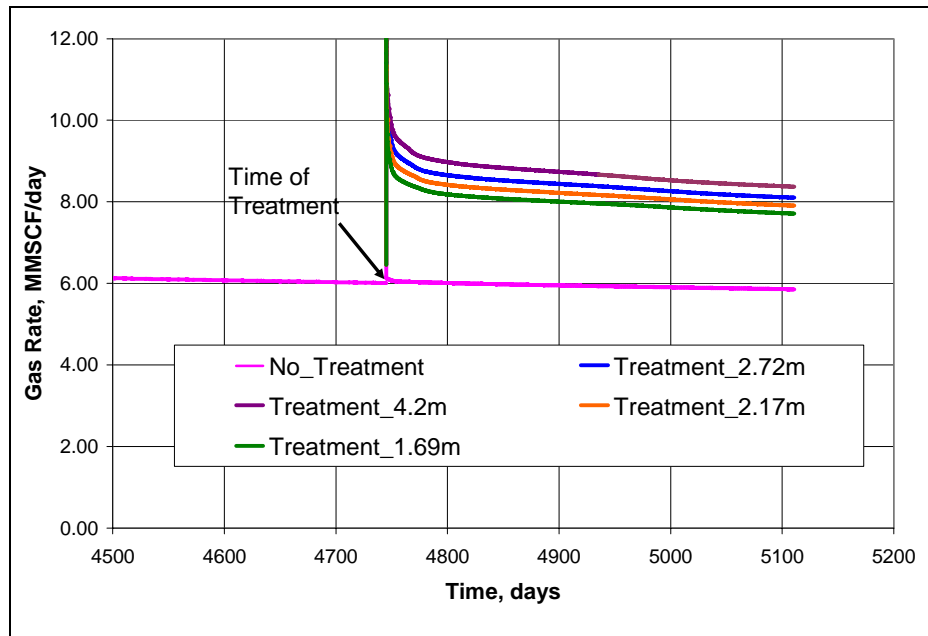


Figure 12.20: Effect of chemical treatment and treatment radii on gas production rate

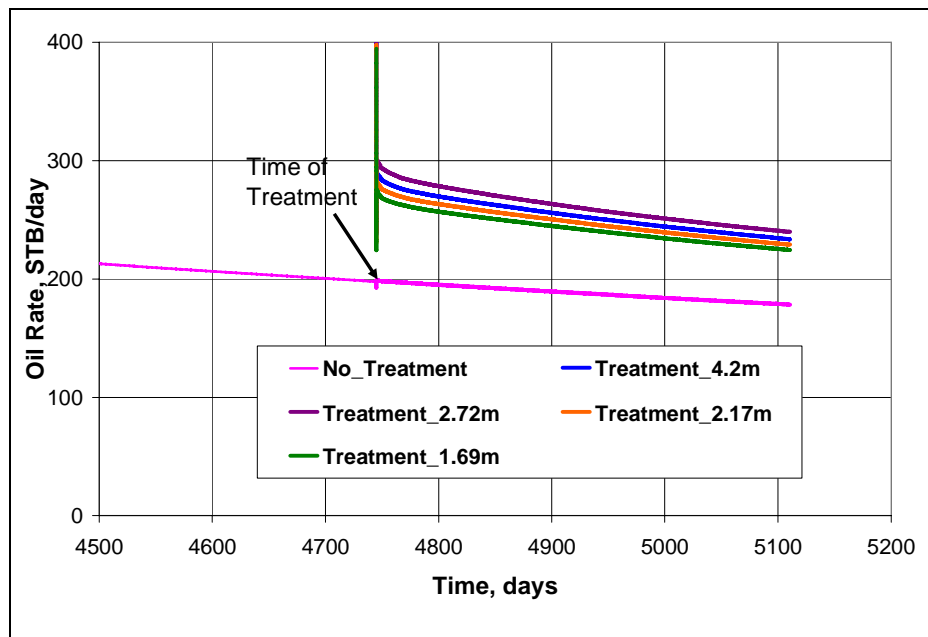


Figure 12.21: Effect of chemical treatment and treatment radii on oil production rate

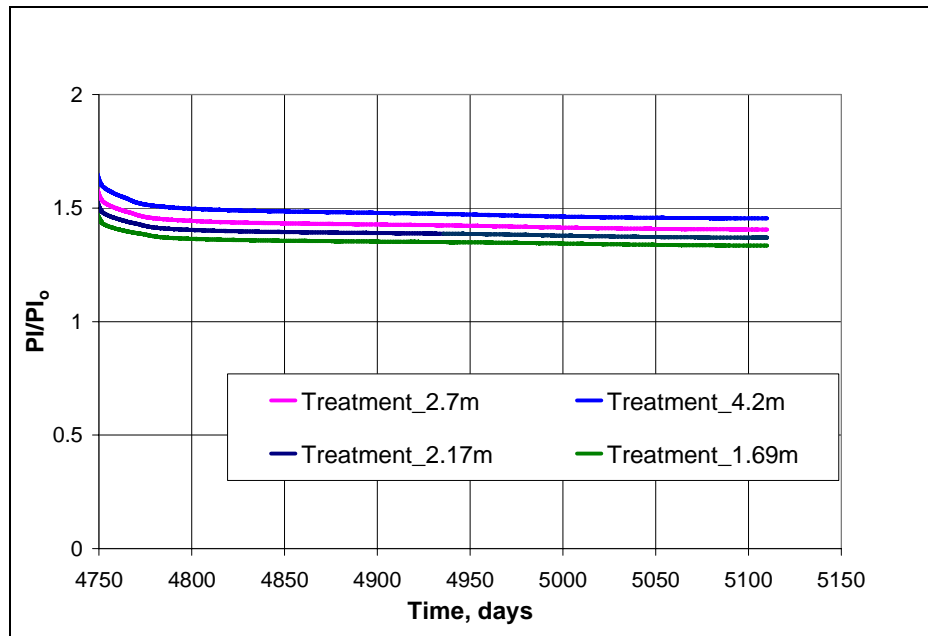


Figure 12.22: Improvement in productivity index due to chemical treatment for different treatment radii

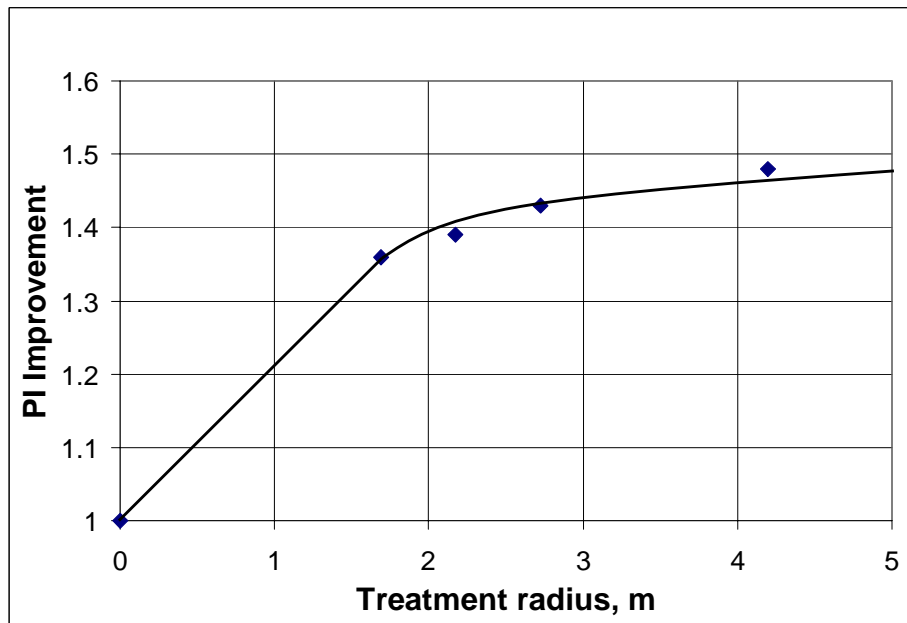


Figure 12.23: Effect of treatment radius on improvement in Productivity index

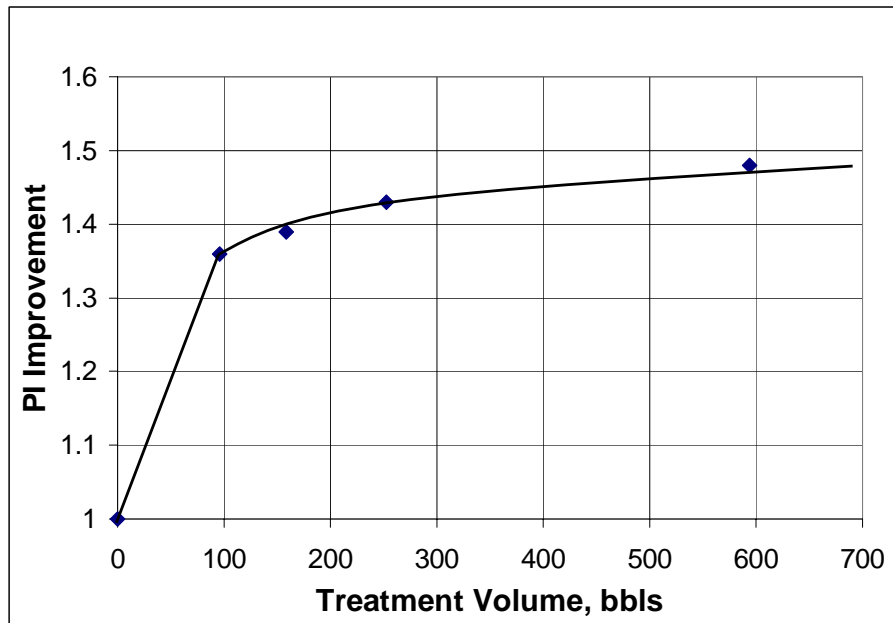


Figure 12.24: Effect of treatment volume on improvement in Productivity index

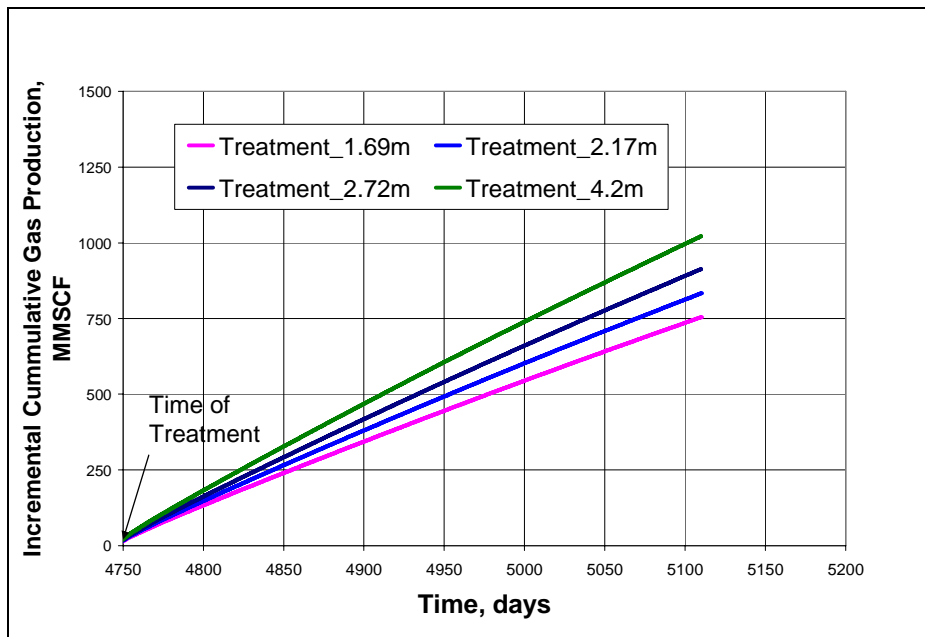


Figure 12.25: Effect of chemical treatment and treatment radii on net gas production

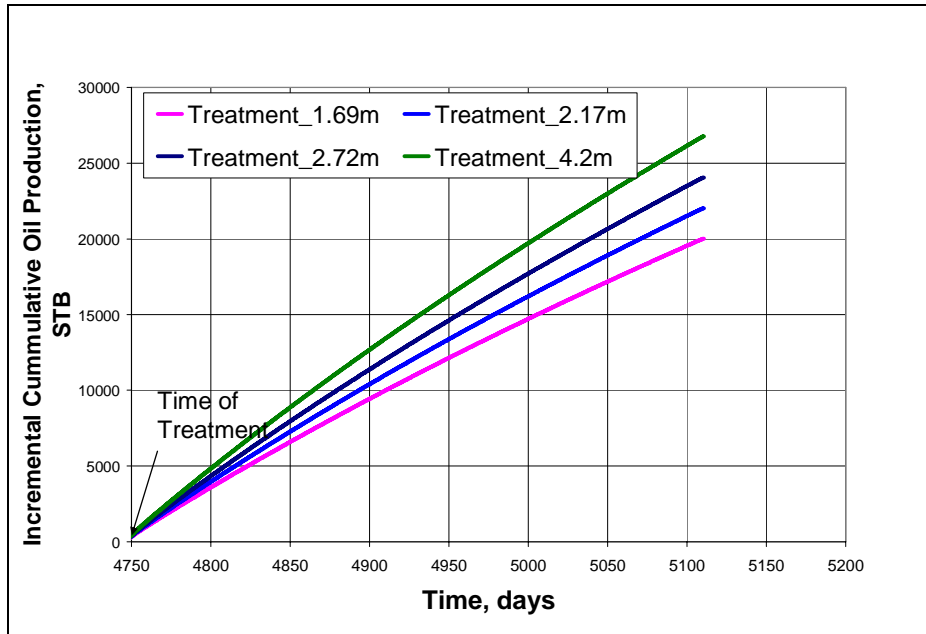


Figure 12.26: Effect of chemical treatment and treatment radii on net oil production

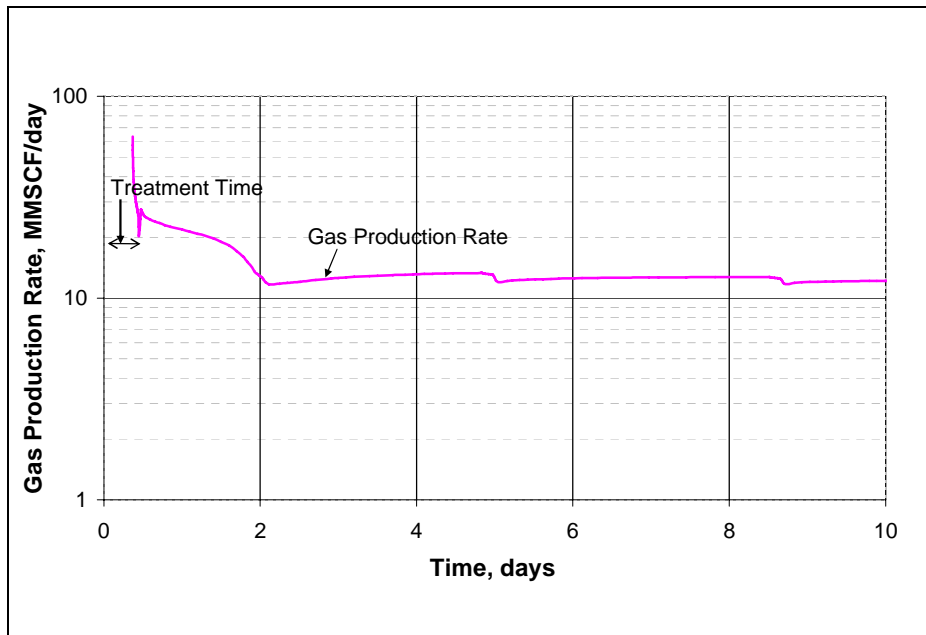


Figure 12.27: Initial high gas production for the first few days after treatment calculated using default BIC's from PVTSim

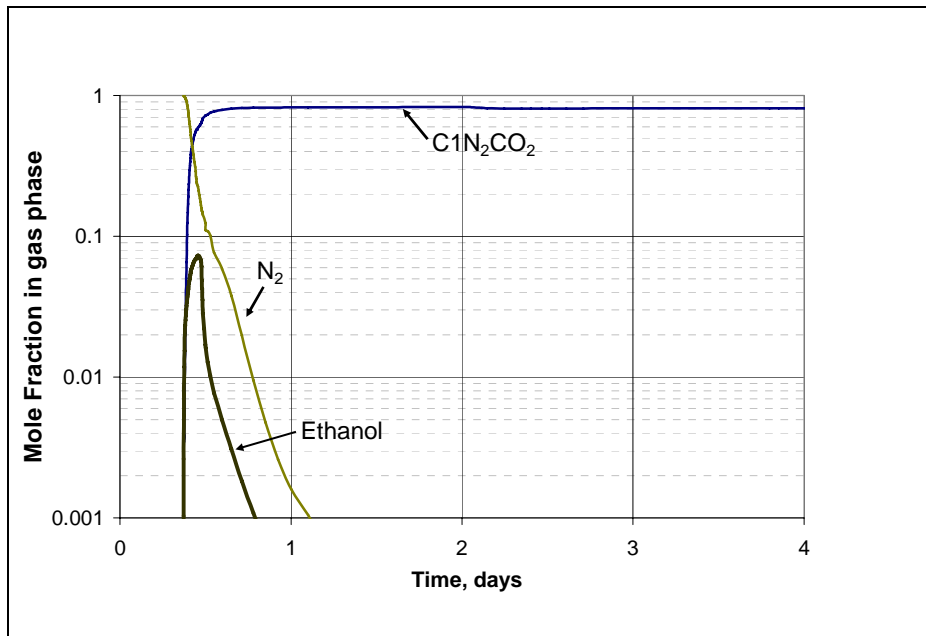


Figure 12.28: Flow back of solvents in the gas phase after treatment calculated using default BIC's from PVTsim

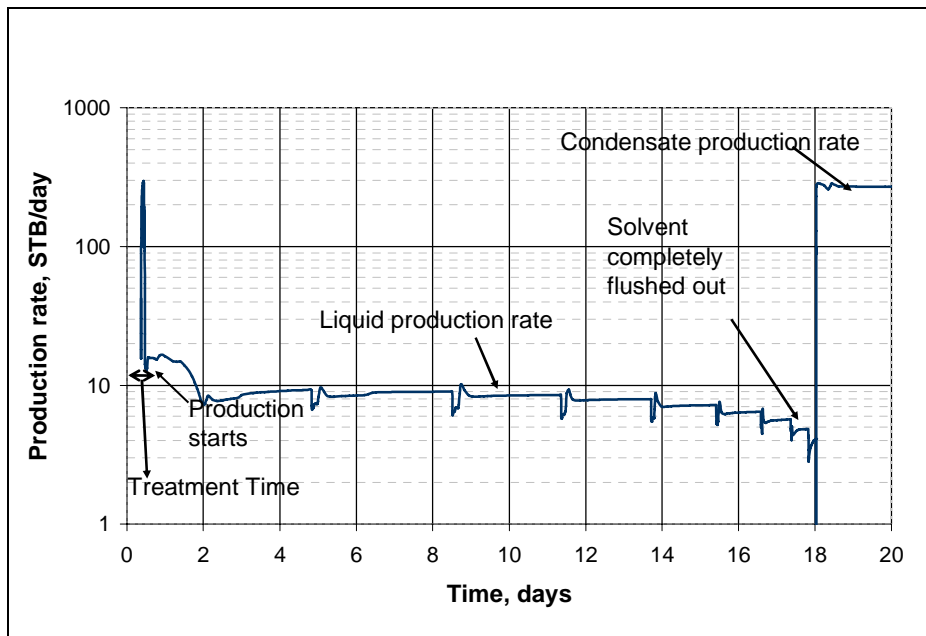


Figure 12.29: Initial low liquid production for the first few days after treatment calculated using default BIC's from PVTsim

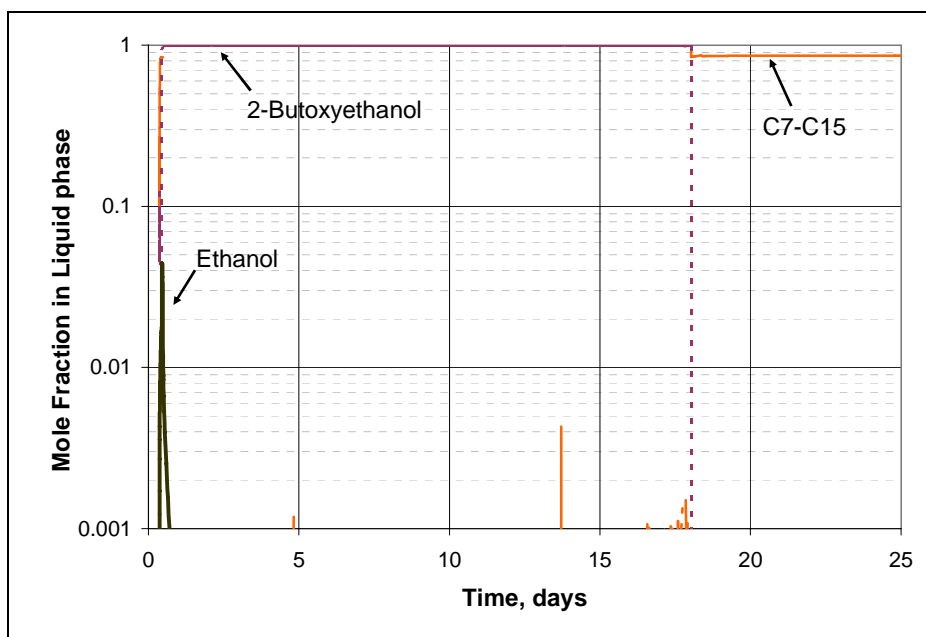


Figure 12.30: Flow back of solvents in the liquid phase after treatment calculated using default BIC's from PVTsim

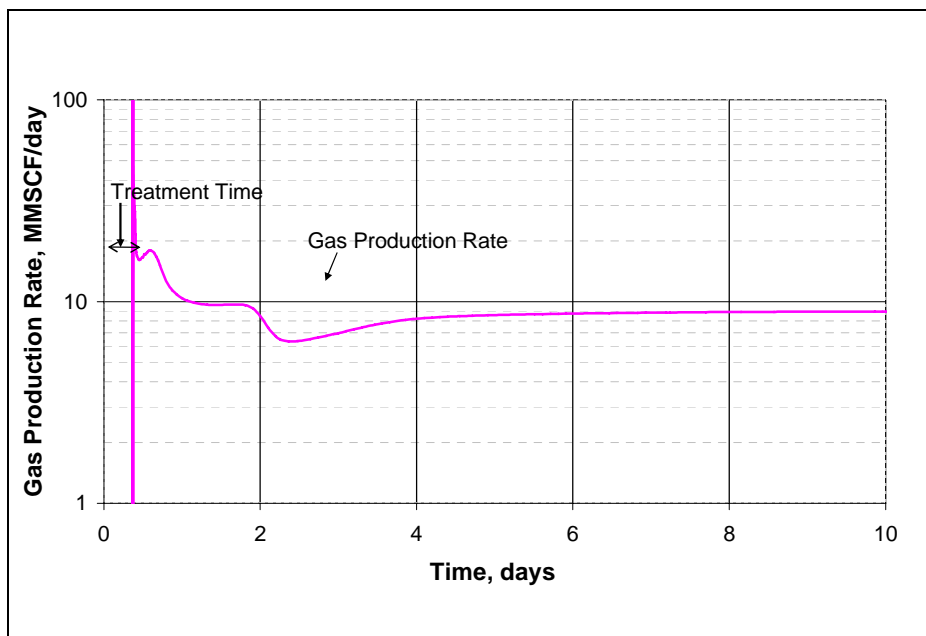


Figure 12.31: Gas production rate for the first few days after treatment calculated by changing the BIC's between solvents and hydrocarbons to zero

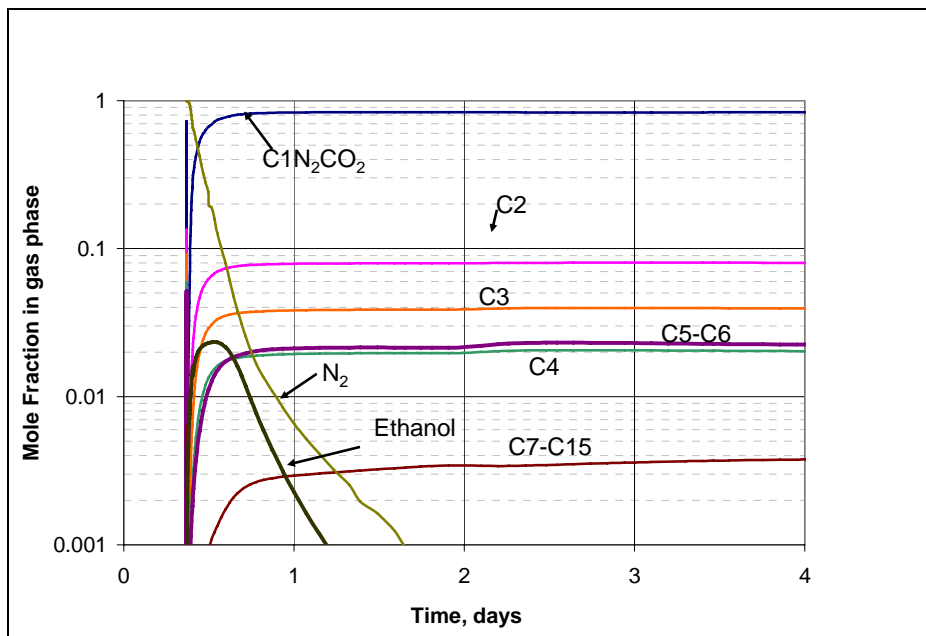


Figure 12.32: Composition of the the gas phase after treatment calculated by changing the BIC's between solvents and hydrocarbons to zero

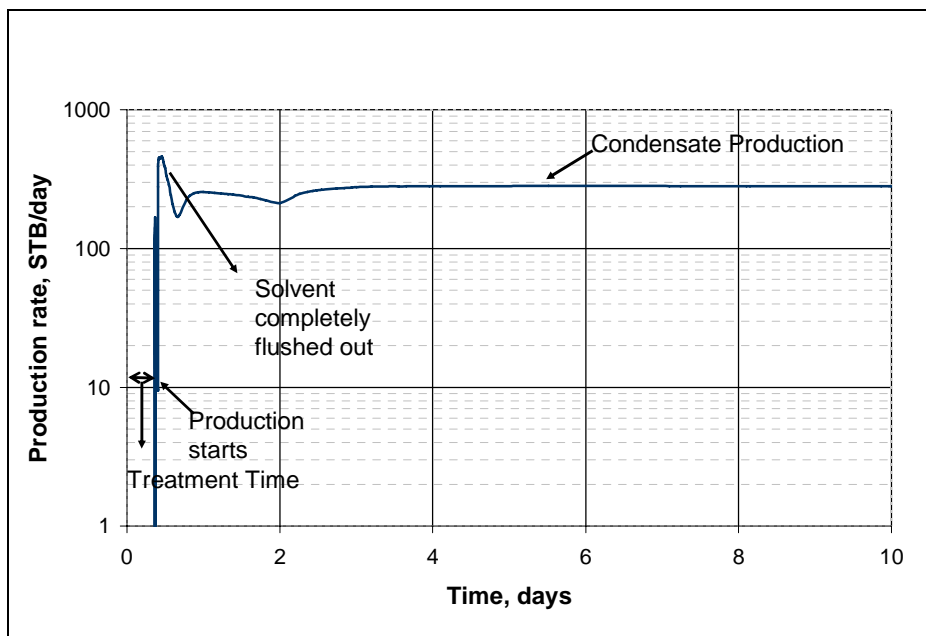


Figure 12.33: Oil production rate for the first few days after treatment calculated by changing the BIC's between solvents and hydrocarbons to zero

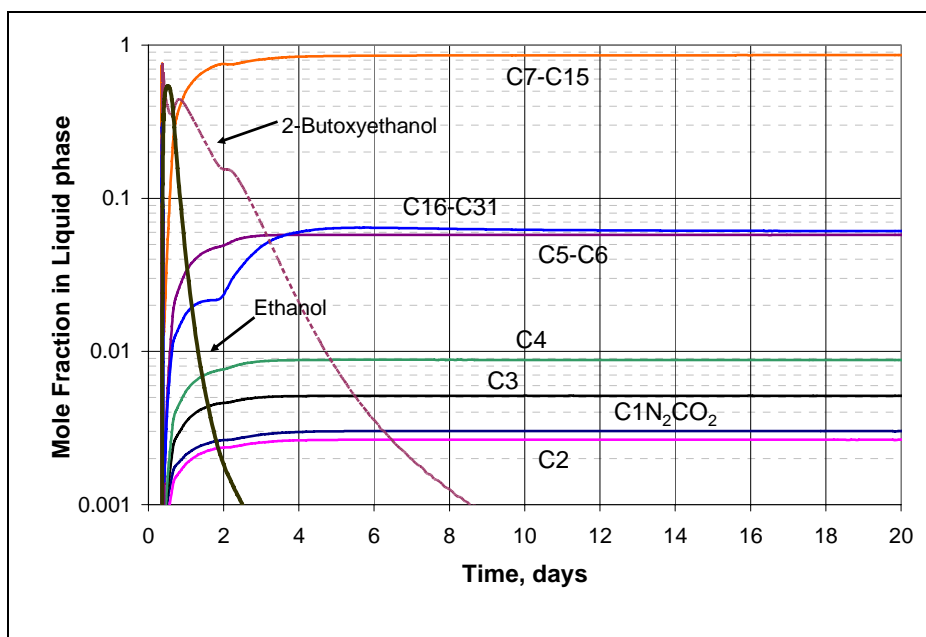


Figure 12.34: Composition of the oil phase after treatment calculated by changing the BIC's between solvents and hydrocarbons to zero

Chapter 13: Summary, Conclusions and Recommendations for Future Work

13.1: SUMMARY

The objective of this research work was to develop a successful chemical treatment for improving the productivity of liquid (condensate + water) blocked gas wells. The chemical treatment changes the wettability of water-wet or oil-wet sandstone rocks to neutral wet, and thus reduces the residual liquid saturations and increases the gas and oil relative permeability. A new experimental coreflood setup was designed and built to perform experiments at reservoir conditions. Experiments were performed over a temperature range of 140°F to 308°F and pressures up to 6000 psig. Coreflood experiments were conducted on Berea sandstones, reservoir rocks and Texas Cream limestones to study the effect of condensate and water blocking on gas relative permeabilities over a wide range of temperatures, pressures and fluid compositions. Gas relative permeability decreased by about 90% due to condensate dropout in both high and low permeability sandstone and limestone rocks. Reduction in gas relative permeability was more than 95% in presence of high connate water saturation and during the three-phase gas-oil-water steady state flow even for low fractional flows of water.

As shown in both this research and previous research at the University of Texas by Kumar (2006), chemical treatments using 3M's non-ionic fluoro-surfactant (FC4430) in methanol/water solvents increased both the gas and condensate relative permeability in dry sandstone rocks by about a factor of 1.6 to 1.9, but failed to give the same improvement in the presence of connate water. These results showed that methanol alone or in combination with water is not effective at solubilizing/displacing the brine and/or condensate while delivering the treatment solution.

This research shows that a major part of developing a successful chemical treatment for gas-condensate wells is the selection of appropriate solvents to deliver the surfactant to the rock surface in the presence of brine including high water saturations and high salinity. Choosing inappropriate solvents can result in the failure of the chemical treatment either due to the inefficiency of solvents in removing brine from the core or precipitation of surfactant and/or salt or a combination of any of these. A screening test based upon phase behavior studies of treatment solutions and brines was found to be effective in the selection of solvents for different reservoir temperatures, water and oil saturations and brine salinities. The selection of effective solvents thus turned out to be a critical step in the development of a practical field technology.

The chemical treatment using the same non-ionic polymeric fluoro-surfactant (3M's FC4430) in a mixture of either 2-butoxyethnaol/ethanol solvents or propylene glycol/Isopropanol solvents was found to be effective in increasing the gas and condensate relative permeability of both Berea sandstone and reservoir sandstones over a wide range of conditions. Chemical treatment increased the gas and condensate relative permeability by about a factor of about 2 for surfactant concentrations ranging from 0.1% and 2%. The adsorption of the surfactant on the rock surface increased from 1 mg/g of rock to 3 mg/ g of rock as the surfactant concentration in the treatment solution increased from 0.1% to 2%. The wettability of treated and untreated reservoir rocks was measured using the USBM method to determine the effect of the chemical treatment on the wettability.

Remarkably, the same chemical treatment was also found to be effective for removing the damage caused by water blocking in gas wells. The final gas permeability measured on treated cores was same as the initial gas permeability, which shows that the treatment did not damage the cores.

A novel approach has been developed for improving the multi-phase flow conductivity of propped fractures by surface modification of proppants. Relative permeability measurements for gas condensate fluids have been done for the first time on propped fractures at reservoir conditions. The same chemical treatment was also found to substantially increase the gas and condensate relative permeability in the propped fracture.

Preliminary experiments indicate that the chemical treatment developed for gas condensate reservoirs can be successfully extended for improving the productivity of volatile oil reservoirs. Both the gas and oil relative permeabilities increased by a factor of 2.7 to 2.9 after the treatment. Some exploratory measurements have also been conducted to test the possibility of improving the productivity of dead oil reservoirs by the chemical treatment.

In addition to the measurements made to test the effectiveness of the chemical treatments, systematic relative permeability measurements have been done on both sandstone and limestone cores over a wide range of conditions including high velocities typical of high-rate gas wells and corresponding to both high capillary numbers and non-Darcy flow. A new approach has been presented to express relative permeability as a function of three non-dimensionless terms; capillary number, modified Reynolds Number and a PVT ratio defined in this work for this purpose. A relative permeability model was calibrated against the measured relative permeability data at both low and high capillary numbers after correcting for non-Darcy flow effects.

A reservoir simulation study using CMG's compositional numerical reservoir simulator was done to assess the impact of chemical treatments on a well with condensate blocking. The chemical treatment was simulated by dividing the reservoir into two rock types, one treated region and other non-treated region. The effect of different treatment

radii on the improvement in well productivity was studied to get the optimum treatment radius. Injection of treatment solution and chase gas and the flow back of solvents were also simulated for the first time.

13.2: CONCLUSIONS

The major conclusions of this research work are:

1. A successful chemical treatment using non-ionic polymeric fluoro-surfactants (3M's FC4430 and X3) has been developed to remove the damage caused by water and/or condensate blocking in sandstone rocks.
2. Successful treatments of rocks with connate water required the tailoring of the solvent for the surfactant to tolerate the formation brine without precipitation of either the surfactant or the salts. A quick and simple screening method based upon visual observations of the phase behavior was used to select mixtures of 2-butoxyethanol/ethanol and propylene glycol/isopropanol for the reservoir conditions of interest in this study.
3. Chemical treatment increased the relative permeability of both gas and oil (condensate) by a factor of 1.75-2.4 on outcrop and reservoir sandstone rocks with connate water, including high salinity brines. The USBM wettability index for the treated cores is close to zero implying that the chemical treatment makes them neutral or mixed-wet.
4. Chemical treatment has been successfully tested for reducing the damage caused by water blocking in gas and gas condensate wells. Chemical treatment of reservoir cores with high initial water saturation increased the gas and condensate relative permeability by a factor of 3-4 and the relative permeability remained high even after injecting large volumes of brine.

5. Chemical treatment of sand based propped fractures increased the relative permeability of gas and oil by a factor of 1.6 to 2.5 over a wide range of capillary numbers. This is a novel approach of improving multi-phase flow conductivity of propped fractures and can increase the productivity of hydraulically fractured gas condensate wells.
6. The chemical treatment developed for gas condensate reservoirs has been successfully extended to volatile oil reservoirs that may face the same problem of two-phase flow in the near wellbore region, which reduces the productivity of well. The chemical treatment increased the oil and gas relative permeability for the volatile oil fluid by a factor of 2.7 - 2.9.
7. The relative permeability for gas condensate fluids has been modeled as function of three non-dimensionless terms; PVT ratio, capillary number and a modified Reynolds number. A gas-condensate relative permeability model has been tuned and validated against measured data over a wide range of conditions.
8. Single-well simulations of chemical treatments for a gas-condensate well showed an improvement of about 50% in the productivity index. The productivity index increases rapidly with an increase in treatment radius at first and then slowly, but finally beyond a certain radius no more improvement occurs.

13.3: FUTURE WORK

1. Possible future research topics for the chemical treatment of carbonate and sandstone rocks are as follows:

- A treatment solution that is effective in carbonate rocks should be developed since many of the world's hydrocarbon reservoirs are carbonate formations. Different surfactant chemistries such as high molecular weight anionic fluorinated surfactants should be tested for treating carbonate rocks. Also different approaches such as changing the solvents and/or activating the rock surface to get a stronger interaction between the rock and the surfactant should be tried.
- A better understanding of the mechanism and its variability with different rocks is needed and this will require more measurements of wettability, adsorption and so forth over a wide range of conditions using different chemicals.
- Test new surfactant types including some non-fluorinated chemistries for treating both condensate and water block removal in both formations and propped fractures.
- Test the applicability of the chemical treatment on tight rocks, with permeability less than 1md.
- Test the durability of the chemical treatment by flowing for even longer times than those presented in this study.
- Test the applicability of the chemical treatment for treating oil wet cores. Though most of the gas reservoirs are expected to be water-wet, a small fraction can be oil wet because of the minerals or other reasons.
- Measurement of the surfactant desorption rate from the rock surface. Desorption measurements are important to predict the long term durability of the treatment.

- Explore the possibility of using the chemical treatment for improving oil relative permeabilities for oil-water two-phase flow.
 - Evaluating new surfactants for treating different proppants such as bauxite. Exploring the possibility of injecting pre-treated proppants in the hydraulic fractures.
2. Possible future research topics for relative permeability modeling and simulation include the following:
- The models for multiphase flow non-Darcy flow need to be either validated or revised, which will require additional measurements as well.
 - Accurate EOS models are needed for the complex polar solvents and mixtures of these solvents with the hydrocarbons and brines in the reservoir so that more reliable simulation predictions of the treatment process can be made, and this also will require new phase behavior and PVT measurements.
 - The surfactant adsorption on different rocks should be modeled and incorporated into mechanistic simulations of the process.

Nomenclature

a	energy parameter of PREOS
a_{ii}	pure component energy parameter
A	Cross sectional area, cm^2
b	co-volume parameter of PREOS
b_i	pure component co-volume parameter
c	Peneloux volume correction
c'	temperature independent volume correction
c''	temperature dependent volume correction
f	fractional flow
k	Permeability, md
k_{rl}	relative permeability of phase l
k_{rl}^o	endpoint relative permeability of phase l
L	length
N_c	capillary number
N_T	Trapping number
n_p	number of phases
P	pressure (psi)
P_c	critical pressure (psi)
q	flow rate
R	gas constant
S_j	saturation of phase i
S_{jr}	residual saturation of phase i
T	temperature ($^{\circ}\text{F}$ or $^{\circ}\text{R}$)
T_c	critical temperature($^{\circ}\text{R}$)
T_l	Trapping parameter for phase l
T_{sc}	temperature at standard conditions ($^{\circ}\text{R}$)
V	volume fraction (Volume/Total volume)
x_i	mole fraction of component i in oil phase
y_i	mole fraction of component i in gas phase
z_i	overall mole fraction of component i

Greek Symbols

β	non-Darcy flow coefficient
β_j	non-Darcy two-phase flow coefficient
Δ	difference
σ	interfacial tension (dynes/cm)
ρ	density
ϕ	porosity
μ	Viscosity (cp)

Subscripts

l	displaced phase
l'	displacing phase
r	residual
g	gas
o	oil
w	water
s	spontaneous imbibition
f	Forced imbibition

Superscripts

high	High trapping number
low	Low trapping number
o	End point

Appendix A

Appendix A1 discusses the derivations of two-phase flow equations. Appendix A2 gives the phase behavior data for treatment solutions made of FC4430 in mixtures of either 2-butoxyethanol/ethanol or PG/IPA and different salinity brines. The section gives the data for different ratios of solvents in the treatment solution.

A1. FLOW RATES EQUATIONS

In coreflood experiments, two-phase flow was established by dropping the flowing pressure below the dewpoint while the upstream pressure was kept above the dewpoint pressure. This procedure allows dynamic condensate accumulation through the core. Therefore, it mimics formation of condensate bank in the near wellbore region in retrograde reservoirs. To achieve that the upstream backpressure regulator pressure was kept above the dew point pressure and the pressure of the downstream backpressure regulator was kept below the dew point pressure. The injection pump rate is not the rate that is flowing through the core due to the difference in the flashing pressure before and after the upstream backpressure regulator. In order to calculate the exact flow rates of both gas and condensate phases through the core, a mass balance needs to be performed across the upstream backpressure regulator.

Figure A1.1 shows a schematic diagram of the upstream backpressure regulator during two-phase flow using a flashing method. A mass balance across the upstream backpressure regulator can be represented as follows:

$$q \rho = q_g \rho_g + q_o \rho_o \quad (A.1)$$

where

q = total flow rate of gas mixture above dew point pressure

q_g = flow rate of gas-phase below dew point pressure

q_o = flow rate of oil-phase below dew point pressure

ρ = molar density of gas mixture above dew point pressure

ρ_g = molar density of gas-phase below dew point pressure

ρ_o = molar density of oil-phase below dew point pressure

The molar densities of both gas and oil phases were obtained using a flash calculation for the gas mixture at experimental condition. Since

$$q_{\text{core}} = \frac{q_g}{f_g} = \frac{q_o}{f_o} \quad (\text{A.2})$$

then

$$q \rho = \frac{f_g}{f_o} q_o \rho_g + q_o \rho_o \quad (\text{A.3})$$

multiplying Equation (A.3) by f_o and taking q_o as a common factor in the right-hand side results in

$$f_o q \rho = q_o (f_g \rho_g + f_o \rho_o) \quad (\text{A.4})$$

solving Equation (A.4) for q_o gives the flow rate of oil phase:

$$q_o = \frac{f_o q \rho}{f_o \rho_o + f_g \rho_g} \quad (\text{A.5})$$

doing the same procedure and solving for q_g drives the following equation for gas-phase flow rate:

$$q_g = \frac{f_g q \rho}{f_o \rho_o + f_g \rho_g} \quad (\text{A.6})$$

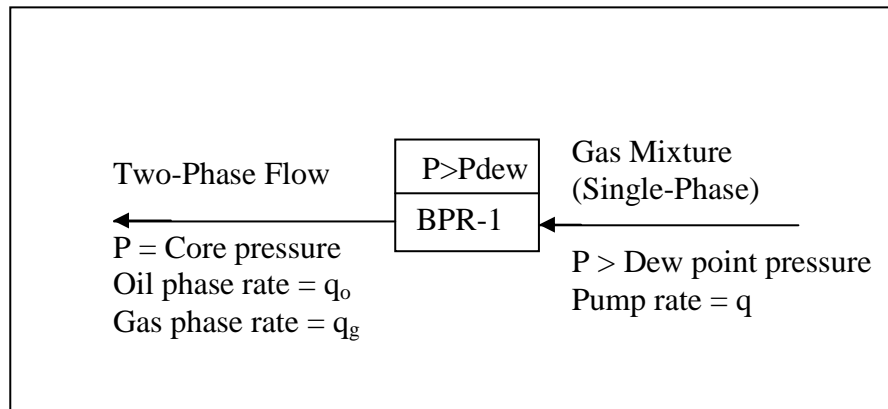


Figure A1.1: A schematic of the upstream back-pressure regulator (BPR-1) during two-phase flow

A2. PHASE BEHAVIOR DATA

Table A2.1: Composition of surfactant solution 1

Component	Weight %
FC4430	2
2-Butoxyethanol	69
Ethanol	29

Table A2.2: Composition of surfactant solution 2

Component	Weight %
FC4430	2
2-Butoxyethanol	49
Ethanol	49

Table A2.3: Composition of surfactant solution 3

Component	Weight %
FC4430	2
2-Butoxyethanol	29
Ethanol	69

Table A2.4: Composition of surfactant solution 4

Component	Weight %
FC4430	2
Propylene glycol	69
Iso-propanol (IPA)	29

Table A2.5: Composition of surfactant solution 5

Component	Weight %
FC4430	2
Propylene glycol	49
Iso-propanol (IPA)	49

Table A2.6: Composition of surfactant solution 6

Component	Weight %
FC4430	2
Propylene glycol	29
Iso-propanol (IPA)	69

Table A2.7: Composition of surfactant solution 7

Component	Weight %
FC4430	1
2-Butoxyethanol	69
Ethanol	29

Table A2.8: Composition of surfactant solution 8

Component	Weight %
FC4430	1
2-Butoxyethanol	49
Ethanol	49

Table A2.8: Solubility data for D.I. water and surfactant solution 1

Water Weight % in solution	25°C	60°C	80°C	100°C	120°C	150°C
10	clear	clear	clear	clear	clear	clear
20	clear	clear	clear	clear	clear	clear
30	clear	clear	clear	clear	clear	clear
40	clear	clear	clear	clear	clear	clear
50	clear	clear	clear	clear	clear	clear
60	clear	clear	clear	clear	clear	cloudy
70	clear	cloudy	-	-	-	-
80	cloudy					

Table A2.9: Solubility data for 25,000 ppm NaCl brine water and surfactant solution 1

Water Weight % in solution	25°C	60°C	80°C	100°C	120°C	150°C
10	clear	clear	clear	clear	clear	evaporated
20	clear	clear	clear	clear	clear	clear
30	clear	clear	clear	clear	clear	clear
40	clear	clear	clear	clear	clear	clear
50	clear	clear	clear	clear	clear	cloudy (2-phase)
60	clear	clear	clear	cloudy	-	-
70	clear	cloudy	-	-	-	-
80	cloudy					

Table A2.10: Solubility data for 50,000 ppm NaCl brine water and surfactant solution 1

Water Weight % in solution	25°C	60°C	80°C	100°C	120°C	150°C
10	clear	clear	clear	clear	clear	clear
20	clear	clear	clear	clear	clear	clear
30	clear	clear	clear	clear	clear	clear
40	clear	clear	clear	clear	clear	clear
50	clear	clear	clear	clear	clear	cloudy (2-phase)
60	clear	clear	cloudy	-	-	-
70	clear	cloudy	-	-	-	-
80	cloudy					

Table A2.11: Solubility data for 75,000 ppm NaCl brine water and surfactant solution 1

Water Weight % in solution	25°C	60°C	80°C	100°C	120°C	150°C
10	clear	clear	clear	clear	clear	evaporated
20	clear	clear	clear	clear	clear	evaporated
30	clear	clear	clear	clear	clear	evaporated
40	clear	clear	cloudy	-	-	-
50	clear	clear	cloudy	-	-	-
60	clear	cloudy	-	-	-	-
70	cloudy	-	-	-	-	-

Table A2.12: Solubility data for 100,000 ppm NaCl brine water and surfactant solution 1

Water Weight % in solution	25°C	60°C	80°C	100°C	120°C	150°C
10	clear	clear	salt ppt	-	-	-
20	clear	clear	clear	clear	cloudy	-
30	clear	clear	cloudy	-	-	-
40	clear	clear	cloudy	-	-	-
50	clear	clear	cloudy	-	-	-
60	clear	clear	cloudy	-	-	-
70	cloudy	-	-	-	-	-

* ppt:- precipitate

Table A2.13: Solubility data for 150,000 ppm NaCl brine water and surfactant solution 1

Water Weight % in solution	25°C
10	salt ppt
20	2-phase
30	2-phase
40	2-phase
50	2-phase

Table A2.14: Solubility data for D.I. water and surfactant solution 2

Water Weight % in solution	25°C	65°C	80°C	100°C	125°C
10	clear	clear	clear	clear	clear
20	clear	clear	clear	clear	clear
30	clear	clear	clear	clear	clear
40	clear	clear	clear	clear	clear
50	clear	clear	clear	clear	clear
60	clear	clear	clear	clear	cloudy
70	clear	cloudy	-	-	-
80	cloudy				

Table A2.15: Solubility data for 25,000 ppm NaCl Brine and surfactant solution 2

Water Weight % in solution	25°C	42°C	70°C	85°C	100°C	130°C
10	clear	clear	clear	clear	clear	clear
20	clear	clear	clear	clear	clear	clear
30	clear	clear	clear	clear	clear	clear
40	clear	clear	clear	clear	clear	clear
50	clear	clear	clear	clear	clear	clear
60	clear	clear	clear	cloudy	-	-
70	cloudy	-	-		-	-

Table A2.16: Solubility data for 50,000 ppm NaCl Brine and surfactant solution 2

Water Weight % in solution	25°C	70°C	80°C	100°C	125°C
10	clear	clear	clear	clear	clear
20	clear	clear	clear	clear	clear
30	clear	clear	clear	clear	clear
40	clear	clear	clear	clear	clear
50	clear	clear	clear	clear	clear
60	clear	cloudy	-	-	-
70	cloudy	-	-	-	-

Table A2.17: Solubility data for 75,000 ppm NaCl Brine and surfactant solution 2

Water Weight % in solution	25°C	65°C	80°C	100°C	125°C
10	clear	salt ppt	-	-	-
20	clear	clear	clear	clear	evaporated
30	clear	clear	clear	clear	clear
40	clear	clear	clear	clear	clear
50	clear	clear	clear	clear	clear
60	clear	cloudy	-	-	-
70	cloudy	-	-	-	-

Table A2.18: Solubility data for 100,000 ppm NaCl Brine and surfactant solution 2

Water Weight % in solution	25°C	65°C	80°C	100°C	125°C
10	salt ppt	-	-	-	-
20	clear	clear	clear	clear	clear
30	clear	clear	clear	clear	clear
40	clear	clear	clear	clear	evaporated
50	clear	clear	clear	clear	clear
60	clear	cloudy	-	-	-
70	cloudy	-	-	-	-

Table A2.19: Solubility data for 150,000 ppm NaCl Brine and surfactant solution 2

Water Weight % in solution	25°C	65°C	80°C	100°C	125°C
10	salt ppt	-	-	-	-
20	salt ppt	-	-	-	-
30	clear	clear	clear	clear	clear
40	clear	clear	clear	clear	evaporated
50	clear	clear	clear	clear	clear
60	clear	cloudy	-	-	-
70	cloudy	-	-	-	-

Table A2.20: Solubility data for D.I. water and surfactant solution 3

Water Weight % in solution	25°C	70°C	85°C	100°C	130°C
10	clear	clear	clear	clear	clear
20	clear	clear	clear	clear	clear
30	clear	clear	clear	clear	clear
40	clear	clear	clear	clear	clear
50	clear	clear	clear	clear	clear
60	clear	clear	clear	cloudy	-
70	cloudy	-		-	-

Table A2.21: Solubility data for 25,000 ppm NaCl Brine and surfactant solution 3

Water Weight % in solution	25°C	70°C	85°C	100°C	130°C
10	clear	clear	clear	clear	clear
20	clear	clear	clear	clear	clear
30	clear	clear	clear	clear	clear
40	clear	clear	clear	clear	clear
50	clear	clear	clear	clear	clear
60	clear	cloudy	-	-	-
70	cloudy	-		-	-

Table A2.22: Solubility data for 50,000 ppm NaCl Brine and surfactant solution 3

Water Weight % in solution	25°C	70°C	85°C	100°C	120°C	130°C
10	clear	clear	clear	clear	clear	clear
20	clear	clear	clear	clear	clear	clear
30	clear	clear	clear	clear	clear	clear
40	clear	clear	clear	clear	clear	clear
50	clear	clear	clear	clear	cloudy	-
60	clear	cloudy	-	-	-	-
70	cloudy	-	-	-	-	-

Table A2.23: Solubility data for 75,000 ppm NaCl Brine and surfactant solution 3

Water Weight % in solution	25°C	60°C	80°C	100°C	120°C	130°C
10	clear	clear	clear	clear	clear	clear
20	clear	clear	clear	clear	clear	clear
30	clear	clear	clear	clear	clear	clear
40	clear	clear	clear	clear	clear	clear
50	clear	clear	clear	clear	clear	clear
60	clear	cloudy	-	-	-	-
70	cloudy	-	-	-	-	-

Table A2.24: Solubility data for 100,000 ppm NaCl Brine and surfactant solution 3

Water Weight % in solution	25°C	60°C	80°C	100°C	110°C	130°C
10	clear	clear	clear	clear	salt ppt	-
20	clear	clear	clear	clear	salt ppt	-
30	clear	clear	clear	clear	clear	clear
40	clear	clear	clear	clear	clear	clear
50	clear	clear	clear	clear	clear	clear
60	clear	cloudy	-	-	-	-
70	cloudy	-	-	-	-	-

Table A2.25: Solubility data for 125,000 ppm NaCl Brine and surfactant solution 3

Water Weight % in solution	25°C	45°C	80°C	100°C	110°C	130°C
10	salt ppt	-	-	-	-	-
20	salt ppt	-	-	-	-	-
30	clear	clear	clear	clear	clear	clear
40	clear	clear	clear	clear	clear	clear
50	clear	clear	clear	clear	cloudy	-
60	clear	cloudy	-	-	-	-
70	cloudy	-	-	-	-	-

Table A2.26: Solubility data for 150,000 ppm NaCl Brine and surfactant solution 3

Water Weight % in solution	25°C	45°C	80°C	100°C	110°C	130°C
10	salt ppt	-	-	-	-	-
20	salt ppt	-	-	-	-	-
30	clear	clear	clear	clear	clear	clear
40	clear	clear	clear	clear	clear	clear
50	clear	clear	clear	clear	cloudy	-
60	clear	cloudy	-	-	-	-
70	cloudy	-	-	-	-	-

Table A2.27: Solubility data for 175,000 ppm NaCl Brine and surfactant solution 3

Water Weight % in solution	25°C	45°C	80°C	100°C	110°C
10	salt ppt	-	-	-	-
20	salt ppt	-	-	-	-
30	salt ppt	-	-	-	-
40	clear	clear	clear	clear	clear
50	clear	clear	clear	clear	cloudy
60	clear	cloudy	-	-	-
70	cloudy	-	-	-	-

Table A2.28: Solubility data for 200,000 ppm NaCl Brine and surfactant solution 3

Water Weight % in solution	25°C	45°C	80°C	100°C	110°C
10	salt ppt	-	-	-	-
20	salt ppt	-	-	-	-
30	salt ppt	-	-	-	-
40	salt ppt	-	-	-	-
50	clear	clear	clear	clear	cloudy
60	clear	cloudy	-	-	-
70	cloudy	-	-	-	-

Table A2.29: Solubility data for D.I. water and surfactant solution 4

Water Weight % in solution	25°C	45°C	80°C	100°C	120°C	160°C
10	clear	clear	clear	clear	clear	clear
20	clear	clear	clear	clear	clear	clear
30	clear	clear	clear	clear	clear	clear
40	clear	clear	clear	clear	clear	clear
50	clear	cloudy	-	-	-	-
60	cloudy	-	-	-	-	-
70	cloudy	-	-	-	-	-

Table A2.30: Solubility data for 25,000 ppm NaCl brine and surfactant solution 4

Water Weight % in solution	25°C	45°C	60°C	100°C	120°C	160°C
10	clear	clear	clear	clear	clear	clear
20	clear	clear	clear	clear	clear	clear
30	clear	clear	clear	clear	clear	clear
40	clear	clear	cloudy	-	-	-
50	clear	cloudy	-	-	-	-
60	cloudy	-	-	-	-	-

Table A2.31: Solubility data for 50,000 ppm NaCl brine and surfactant solution 4

Water Weight % in solution	25°C	40°C	60°C	100°C	120°C	160°C
10	clear	clear	clear	clear	clear	clear
20	clear	clear	clear	clear	clear	clear
30	clear	clear	clear	clear	clear	clear
40	clear	clear	cloudy	-	-	-
50	clear	cloudy	-	-	-	-
60	cloudy	-	-	-	-	-

Table A2.32: Solubility data for 75,000 ppm NaCl brine and surfactant solution 4

Water Weight % in solution	25°C	40°C	60°C	100°C	120°C	160°C
10	clear	clear	clear	clear	clear	clear
20	clear	clear	clear	clear	clear	clear
30	clear	clear	clear	clear	clear	clear
40	clear	clear	cloudy	-	-	-
50	clear	cloudy	-	-	-	-
60	cloudy	-	-	-	-	-

Table A2.33: Solubility data for 100,000 ppm NaCl brine and surfactant solution 4

Water Weight % in solution	25°C	40°C	60°C	100°C	120°C	160°C
10	clear	clear	clear	clear	clear	clear
20	clear	clear	clear	clear	clear	clear
30	clear	clear	clear	clear	clear	clear
40	clear	clear	cloudy	-	-	-
50	cloudy	-	-	-	-	-

Table A2.34: Solubility data for 125,000 ppm NaCl brine and surfactant solution 4

Water Weight % in solution	25°C	40°C	60°C	100°C	120°C	160°C
10	clear	clear	clear	clear	clear	clear
20	clear	clear	clear	clear	clear	clear
30	clear	clear	clear	clear	clear	clear
40	clear	clear	cloudy	-	-	-
50	cloudy	-	-	-	-	-

Table A2.35: Solubility data for 125,000 ppm NaCl brine and surfactant solution 4

Water Weight % in solution	25°C	40°C	60°C	100°C	120°C	160°C
10	clear	clear	clear	clear	clear	clear
20	clear	clear	clear	clear	clear	clear
30	clear	clear	clear	clear	clear	clear
40	clear	clear	cloudy	-	-	-
50	cloudy	-	-	-	-	-

Table A2.36: Solubility data for 150,000 ppm NaCl brine and surfactant solution 4

Water Weight % in solution	25°C	40°C	60°C	100°C	120°C	160°C
10	clear	clear	clear	clear	clear	clear
20	clear	clear	clear	clear	clear	clear
30	clear	clear	clear	clear	clear	clear
40	clear	clear	cloudy	-	-	-
50	cloudy	-	-	-	-	-

Table A2.37: Solubility data for 175,000 ppm NaCl brine and surfactant solution 4

Water Weight % in solution	25°C	40°C	60°C	100°C	120°C	160°C
10	clear	clear	clear	clear	clear	clear
20	clear	clear	clear	clear	clear	clear
30	clear	clear	clear	clear	clear	clear
40	clear	clear	cloudy	-	-	-
50	cloudy	-	-	-	-	-

Table A2.38: Solubility data for 200,000 ppm NaCl brine and surfactant solution 4

Water Weight % in solution	25°C	40°C	60°C	100°C	120°C	160°C
10	clear	clear	clear	clear	clear	clear
20	clear	clear	clear	clear	clear	clear
30	clear	clear	clear	clear	clear	clear
40	clear	clear	cloudy	-	-	-
50	cloudy	-	-	-	-	-

Table A2.39: Solubility data for 225,000 ppm NaCl brine and surfactant solution 4

Water Weight % in solution	25°C	40°C	60°C	100°C	120°C	160°C
10	clear	clear	clear	clear	clear	clear
20	clear	clear	clear	clear	clear	clear
30	clear	clear	clear	clear	clear	cloudy
40	clear	clear	cloudy	-	-	-
50	cloudy	-	-	-	-	-

Table A2.40: Solubility data for 250,000 ppm NaCl brine and surfactant solution 4

Water Weight % in solution	25°C	40°C	60°C	100°C	120°C	160°C
10	clear	clear	clear	clear	clear	clear
20	salt	-	-	-	-	-
30	salt	-	-	-	-	-
40	salt	cloudy,ppt	-	-	-	-
50	cloudy	-	-	-	-	-

*ppt - salt precipitation

Table A2.41: Solubility data for D.I. water and surfactant solution 5

Water Weight % in solution	25°C	60°C	80°C	100°C	120°C	160°C
10	clear	clear	clear	clear	clear	clear
20	clear	clear	clear	clear	clear	clear
30	clear	clear	clear	clear	clear	clear
40	clear	clear	clear	clear	clear	clear
50	clear	clear	clear	cloudy	-	-
60	clear	cloudy	-	-	-	-
70	cloudy	-	-	-	-	-

Table A2.42: Solubility data for 25,000 ppm NaCl brine and surfactant solution 5

Water Weight % in solution	25°C	60°C	80°C	100°C	120°C	160°C
10	clear	clear	clear	clear	clear	clear
20	clear	clear	clear	clear	clear	clear
30	clear	clear	clear	clear	clear	clear
40	clear	clear	clear	clear	clear	clear
50	clear	cloudy	-	-	-	-
60	cloudy	-	-	-	-	-

Table A2.43: Solubility data for 50,000 ppm NaCl brine and surfactant solution 5

Water Weight % in solution	25°C	60°C	80°C	100°C	120°C	160°C
10	clear	clear	clear	clear	clear	clear
20	clear	clear	clear	clear	clear	clear
30	clear	clear	clear	clear	clear	clear
40	clear	clear	clear	clear	clear	clear
50	clear	cloudy	-	-	-	-
60	cloudy	-	-	-	-	-

Table A2.44: Solubility data for 75,000 ppm NaCl brine and surfactant solution 5

Water Weight % in solution	25°C	60°C	80°C	100°C	120°C	160°C
10	clear	clear	clear	clear	clear	clear
20	clear	clear	clear	clear	clear	clear
30	clear	clear	clear	clear	clear	clear
40	clear	clear	clear	clear	clear	cloudy
50	clear	cloudy	-	-	-	-
60	cloudy	-	-	-	-	-

Table A2.45: Solubility data for 100,000 ppm NaCl brine and surfactant solution 5

Water Weight % in solution	25°C	60°C	80°C	100°C	120°C	160°C
10	clear	clear	clear	clear	clear	clear
20	clear	clear	clear	clear	clear	clear
30	clear	clear	clear	clear	clear	clear
40	clear	clear	clear	clear	clear	clear
50	clear	cloudy	-	-	-	-
60	cloudy	-	-	-	-	-

Table A2.46: Solubility data for 125,000 ppm NaCl brine and surfactant solution 5

Water Weight % in solution	25°C	60°C	80°C	100°C	120°C	160°C
10	clear	clear	clear	clear	clear	clear
20	clear	clear	clear	clear	clear	clear
30	clear	clear	clear	clear	clear	clear
40	clear	clear	clear	clear	clear	cloudy
50	clear	cloudy	-	-	-	-
60	cloudy	-	-	-	-	-

Table A2.47: Solubility data for 150,000 ppm NaCl brine and surfactant solution 5

Water Weight % in solution	25°C	60°C	80°C	100°C	120°C	160°C
10	clear	clear	clear	clear	clear	clear
20	clear	clear	clear	clear	clear	clear
30	clear	clear	clear	clear	clear	cloudy
40	clear	clear	clear	clear	clear	cloudy
50	clear	clear	cloudy	-	-	-
60	cloudy	-	-	-	-	-

Table A2.48: Solubility data for 175,000 ppm NaCl brine and surfactant solution 5

Water Weight % in solution	25°C	60°C	80°C	100°C	120°C	160°C
10	salt ppt	salt ppt	salt ppt	salt ppt	salt ppt	salt ppt
20	salt ppt	salt ppt	salt ppt	salt ppt	salt ppt	salt ppt
30	clear	clear	clear	clear	clear	cloudy
40	clear	clear	clear	clear	clear	cloudy
50	clear	cloudy	-	-	-	-
60	cloudy	-	-	-	-	-

*salt ppt – salt precipitation

Table A2.49: Solubility data for 200,000 ppm NaCl brine and surfactant solution 5

Water Weight % in solution	25°C	60°C	80°C	100°C	120°C	160°C
10	salt ppt	salt ppt	salt ppt	salt ppt	salt ppt	salt ppt
20	salt ppt	salt ppt	salt ppt	salt ppt	salt ppt	salt ppt
30	salt ppt	salt ppt	salt ppt	salt ppt	salt ppt	salt ppt
40	clear	clear	clear	clear	cloudy	-
50	clear	cloudy	-	-	-	-
60	cloudy	-	-	-	-	-

*salt ppt – salt precipitation

Table A2.50: Solubility data for 225,000 ppm NaCl brine and surfactant solution 5

Water Weight % in solution	25°C	60°C	80°C	100°C	120°C	160°C
10	salt ppt	salt ppt	salt ppt	salt ppt	salt ppt	salt ppt
20	salt ppt	salt ppt	salt ppt	salt ppt	salt ppt	salt ppt
30	salt ppt	salt ppt	salt ppt	salt ppt	salt ppt	salt ppt
40	salt ppt	salt ppt	salt ppt	salt ppt	cloudy, salt	-
50	clear	cloudy	-	-	-	-
60	cloudy	-	-	-	-	-

*salt ppt/salt – salt precipitation

Table A2.51: Solubility data for 250,000 ppm NaCl brine and surfactant solution 5

Water Weight % in solution	25°C	60°C	80°C	100°C	120°C	160°C
10	salt ppt	salt ppt	salt ppt	salt ppt	salt ppt	salt ppt
20	salt ppt	salt ppt	salt ppt	salt ppt	salt ppt	salt ppt
30	salt ppt	salt ppt	salt ppt	salt ppt	salt ppt	salt ppt
40	salt ppt	salt ppt	salt ppt	salt ppt	salt ppt	cloudy (evap)
50	salt ppt	cloudy, salt	-	-	-	-
60	cloudy	-	-	-	-	-

*salt ppt/salt – salt precipitation

Table A2.52: Solubility data for D.I. water and surfactant solution 6

Water Weight % in solution	25°C	60°C	80°C	100°C	120°C	160°C
10	clear	clear	clear	clear	clear	clear
20	clear	clear	clear	clear	clear	clear
30	clear	clear	clear	clear	clear	clear
40	clear	clear	clear	clear	clear	clear
50	clear	clear	clear	clear	clear	clear
60	clear	cloudy	-	-	-	-
70	cloudy	-	-	-	-	-

Table A2.53: Solubility data for 25,000 ppm NaCl brine and surfactant solution 6

Water Weight % in solution	25°C	60°C	80°C	100°C	120°C	160°C
10	clear	clear	clear	clear	clear	clear
20	clear	clear	clear	clear	clear	clear
30	clear	clear	clear	clear	clear	clear
40	clear	clear	clear	clear	clear	clear
50	clear	clear	clear	clear	clear	clear
60	clear	cloudy	-	-	-	-
70	cloudy	-	-	-	-	-

Table A2.54: Solubility data for 50,000 ppm NaCl brine and surfactant solution 6

Water Weight % in solution	25°C	60°C	80°C	100°C	120°C	160°C
10	clear	clear	clear	clear	clear	clear
20	clear	clear	clear	clear	clear	clear
30	clear	clear	clear	clear	clear	clear
40	clear	clear	clear	clear	clear	clear
50	clear	clear	clear	clear	clear	hazy
60	clear	cloudy	-	-	-	-
70	cloudy	-	-	-	-	-

Table A2.55: Solubility data for 75,000 ppm NaCl brine and surfactant solution 6

Water Weight % in solution	25°C	60°C	80°C	100°C	120°C	160°C
10	clear	clear	clear	clear	clear	clear
20	clear	clear	clear	clear	clear	clear
30	clear	clear	clear	clear	clear	clear
40	clear	clear	clear	clear	clear	clear
50	clear	clear	clear	hazy	cloudy	-
60	clear	cloudy	-	-	-	-
70	cloudy	-	-	-	-	-

Table A2.56: Solubility data for 100,000 ppm NaCl brine and surfactant solution 6

Water Weight % in solution	25°C	60°C	80°C	100°C	120°C	160°C
10	salt ppt	salt ppt	salt ppt	salt ppt	salt ppt	salt ppt
20	clear	clear	clear	clear	clear	clear
30	clear	clear	clear	clear	clear	clear
40	clear	clear	clear	clear	clear	clear
50	clear	clear	clear	hazy	cloudy	-
60	clear	cloudy	-	-	-	-
70	cloudy	-	-	-	-	-

*salt ppt – salt precipitation

Table A2.57: Solubility data for 125,000 ppm NaCl brine and surfactant solution 6

Water Weight % in solution	25°C	60°C	80°C	100°C	120°C	160°C
10	salt ppt	salt ppt	salt ppt	salt ppt	salt ppt	salt ppt
20	clear	clear	clear	clear	clear	clear
30	clear	clear	clear	clear	clear	cloudy, evap
40	clear	clear	clear	clear	clear	cloudy
50	clear	clear	clear	cloudy	-	-
60	clear	cloudy	-	-	-	-
70	cloudy	-	-	-	-	-

*salt ppt – salt precipitation

Table A2.58: Solubility data for 150,000 ppm NaCl brine and surfactant solution 6

Water Weight % in solution	25°C	60°C	80°C	100°C	120°C	160°C
10	salt ppt	salt ppt	salt ppt	salt ppt	salt ppt	salt ppt
20	salt ppt	salt ppt	salt ppt	salt ppt	salt ppt	salt ppt
30	clear	clear	clear	clear	clear	clear
40	clear	clear	clear	clear	clear	clear
50	clear	clear	clear	cloudy	-	-
60	clear	cloudy	-	-	-	-
70	cloudy	-	-	-	-	-

*salt ppt – salt precipitation

Table A2.59: Solubility data for 175,000 ppm NaCl brine and surfactant solution 6

Water Weight % in solution	25°C	60°C	80°C	100°C	120°C	160°C
10	salt ppt	salt ppt	salt ppt	salt ppt	salt ppt	salt ppt
20	salt ppt	salt ppt	salt ppt	salt ppt	salt ppt	salt ppt
30	salt ppt	salt ppt	salt ppt	salt ppt	salt ppt	salt ppt
40	clear	clear	clear	clear	clear	cloudy, evap
50	clear	clear	hazy	cloudy	-	-
60	hazy	cloudy	-	-	-	-
70	cloudy	-	-	-	-	-

*salt ppt – salt precipitation

Table A2.60: Solubility data for 200,000 ppm NaCl brine and surfactant solution 6

Water Weight % in solution	25°C	60°C	80°C	100°C	120°C	160°C
10	salt ppt	salt ppt	salt ppt	salt ppt	salt ppt	salt ppt
20	salt ppt	salt ppt	salt ppt	salt ppt	salt ppt	salt ppt
30	salt ppt	salt ppt	salt ppt	salt ppt	salt ppt	salt ppt
40	clear	clear	clear	clear	clear	clear
50	clear	clear	hazy	cloudy	-	-
60	cloudy	-	-	-	-	-

*salt ppt – salt precipitation

Table A2.61: Solubility data for 225,000 ppm NaCl brine and surfactant solution 6

Water Weight % in solution	25°C	60°C	80°C	100°C	120°C	160°C
10	salt ppt	salt ppt	salt ppt	salt ppt	salt ppt	salt ppt
20	salt ppt	salt ppt	salt ppt	salt ppt	salt ppt	salt ppt
30	salt ppt	salt ppt	salt ppt	salt ppt	salt ppt	salt ppt
40	salt ppt	salt ppt	salt ppt	salt ppt	salt ppt	salt ppt
50	clear	clear	hazy	cloudy	-	-
60	cloudy	-	-	-	-	-

*salt ppt – salt precipitation

Table A2.62: Solubility data for 250,000 ppm NaCl brine and surfactant solution 6

Water Weight % in solution	25°C	60°C	80°C	100°C	120°C	160°C
10	salt ppt	salt ppt	salt ppt	salt ppt	salt ppt	salt ppt
20	salt ppt	salt ppt	salt ppt	salt ppt	salt ppt	salt ppt
30	salt ppt	salt ppt	salt ppt	salt ppt	salt ppt	salt ppt
40	salt ppt	salt ppt	salt ppt	salt ppt	salt ppt	salt ppt
50	salt	hazy, salt	cloudy, salt	-	-	-
60	cloudy	-	-	-	-	-

*salt ppt – salt precipitation

Table A2.63: Solubility data for D.I. water and surfactant solution 7

Water Weight % in solution	25°C	60°C	80°C	100°C	120°C	160°C
10	clear	clear	clear	clear	clear	clear
20	clear	clear	clear	clear	clear	clear
30	clear	clear	clear	clear	clear	clear
40	clear	clear	clear	clear	clear	clear
50	clear	clear	clear	clear	clear	clear
60	clear	clear	clear	clear	clear	clear
70	clear	cloudy	-	-	-	-
80	cloudy	-	-	-	-	-

Table A2.64: Solubility data for 25,000 ppm NaCl brine and surfactant solution 7

Water Weight % in solution	25°C	60°C	80°C	100°C	120°C	160°C
10	clear	clear	clear	clear	clear	clear
20	clear	clear	clear	clear	clear	clear
30	clear	clear	clear	clear	clear	clear
40	clear	clear	clear	clear	clear	clear
50	clear	clear	clear	clear	clear	clear
60	clear	clear	clear	cloudy	-	-
70	clear	cloudy	-	-	-	-
80	cloudy	-	-	-	-	-

Table A2.65: Solubility data for 50,000 ppm NaCl brine and surfactant solution 7

Water Weight % in solution	25°C	60°C	80°C	100°C	120°C	160°C
10	clear	clear	clear	clear	clear	clear
20	clear	clear	clear	clear	clear	clear
30	clear	clear	clear	clear	clear	clear
40	clear	clear	clear	clear	clear	clear
50	clear	clear	clear	clear	clear	clear
60	clear	clear	cloudy	-	-	-
70	clear	cloudy	-	-	-	-
80	cloudy	-	-	-	-	-

Table A2.66: Solubility data for 75,000 ppm NaCl brine and surfactant solution 7

Water Weight % in solution	25°C	60°C	80°C	100°C	120°C	160°C
10	clear	clear	salt ppt	salt ppt	salt ppt	salt ppt
20	clear	clear	clear	clear	clear	clear
30	clear	clear	cloudy	-	-	-
40	clear	cloudy	-	-	-	-
50	clear	cloudy	-	-	-	-
60	clear	cloudy	--	-	-	-
70	cloudy	-	-	-	-	-

*salt ppt – salt precipitation

Table A2.67: Solubility data for 100,000 ppm NaCl brine and surfactant solution 7

Water Weight % in solution	25°C	60°C	80°C	100°C	120°C	160°C
10	salt ppt	salt ppt	salt ppt	salt ppt	salt ppt	salt ppt
20	clear	clear	clear	clear	clear	clear
30	clear	cloudy	-	-	-	-
40	clear	cloudy	-	-	-	-
50	clear	cloudy	-	-	-	-
60	cloudy	-	--	-	-	-

*salt ppt – salt precipitation

Table A2.68: Solubility data for 125,000 ppm NaCl brine and surfactant solution 7

Water Weight % in solution	25°C	60°C	80°C	100°C	120°C	160°C
10	salt ppt	salt ppt	salt ppt	salt ppt	salt ppt	salt ppt
20	clear	clear	clear	clear	clear	clear
30	clear	cloudy	-	-	-	-
40	cloudy	-	-	-	-	-

*salt ppt – salt precipitation

Table A2.69: Solubility data for 150,000 ppm NaCl brine and surfactant solution 7

Water Weight % in solution	25°C	60°C	80°C	100°C	120°C	160°C
10	salt ppt	salt ppt	salt ppt	salt ppt	salt ppt	salt ppt
20	salt ppt	salt ppt	salt ppt	salt ppt	salt ppt	salt ppt
30	cloudy, salt	-	-	-	-	-

*salt ppt/salt – salt precipitation

Table A2.70: Solubility data for 175,000 ppm NaCl brine and surfactant solution 7

Water Weight % in solution	25°C	60°C	80°C	100°C	120°C	160°C
10	cloudy, salt	-	-	-	-	-

*salt ppt/salt – salt precipitation

Table A2.71: Solubility data for D.I. water and surfactant solution 8

Water Weight % in solution	25°C	60°C	80°C	100°C	120°C	160°C
10	clear	clear	clear	clear	clear	clear
20	clear	clear	clear	clear	clear	clear
30	clear	clear	clear	clear	clear	clear
40	clear	clear	clear	clear	clear	clear
50	clear	clear	clear	clear	clear	clear
60	clear	clear	clear	clear	clear	clear
70	clear	cloudy	-	-	-	-
80	cloudy	-	-	-	-	-

Table A2.72: Solubility data for 25,000 ppm NaCl brine and surfactant solution 8

Water Weight % in solution	25°C	40°C	80°C	100°C	120°C	160°C
10	clear	clear	clear	clear	clear	clear
20	clear	clear	clear	clear	clear	clear
30	clear	clear	clear	clear	clear	clear
40	clear	clear	clear	clear	clear	clear
50	clear	clear	clear	clear	clear	clear

60	clear	clear	clear	cloudy	-	-
70	clear	cloudy	-	-	-	-
80	cloudy	-	-	-	-	-

Table A2.73: Solubility data for 50,000 ppm NaCl brine and surfactant solution 8

Water Weight % in solution	25°C	40°C	80°C	100°C	120°C	160°C
10	clear	clear	clear	clear	clear	clear
20	clear	clear	clear	clear	clear	clear
30	clear	clear	clear	clear	clear	clear
40	clear	clear	clear	clear	clear	clear
50	clear	clear	clear	clear	clear	cloudy
60	clear	clear	clear	cloudy	-	-
70	clear	cloudy	-	-	-	-
80	cloudy	-	-	-	-	-

Table A2.74: Solubility data for 75,000 ppm NaCl brine and surfactant solution 8

Water Weight % in solution	25°C	40°C	80°C	100°C	120°C	160°C
10	salt ppt	salt ppt	salt ppt	salt ppt	salt ppt	salt ppt
20	clear	salt ppt	salt ppt	salt ppt	salt ppt	salt ppt
30	clear	clear	clear	clear	clear	clear
40	clear	clear	clear	clear	clear	clear
50	clear	clear	clear	clear	clear	clear
60	clear	clear	cloudy	-	-	-
70	cloudy	-	-	-	-	-

Table A2.75: Solubility data for 100,000 ppm NaCl brine and surfactant solution 8

Water Weight % in solution	25°C	40°C	80°C	100°C	120°C	160°C
10	salt ppt	salt ppt	salt ppt	salt ppt	salt ppt	salt ppt
20	clear	clear	clear	clear	clear	salt ppt
30	clear	clear	clear	clear	clear	clear
40	clear	clear	clear	clear	clear	clear
50	clear	clear	clear	clear	clear	clear
60	clear	clear	cloudy	-	-	-
70	cloudy	-	-	-	-	-

Table A2.76: Solubility data for 125,000 ppm NaCl brine and surfactant solution 8

Water Weight % in solution	25°C	40°C	60°C	100°C	120°C	160°C
10	salt ppt	salt ppt	salt ppt	salt ppt	salt ppt	salt ppt
20	salt ppt	salt ppt	salt ppt	salt ppt	salt ppt	salt ppt
30	clear	clear	clear	clear	clear	clear
40	clear	clear	clear	clear	clear	clear
50	clear	clear	clear	clear	clear	clear
60	clear	clear	cloudy	-	-	-
70	cloudy	-	-	-	-	-

Table A2.77: Solubility data for 150,000 ppm NaCl brine and surfactant solution 8

Water Weight % in solution	25°C	40°C	60°C	100°C	120°C	160°C
10	salt ppt	salt ppt	salt ppt	salt ppt	salt ppt	salt ppt
20	salt ppt	salt ppt	salt ppt	salt ppt	salt ppt	salt ppt
30	clear	salt ppt	salt ppt	salt ppt	salt ppt	salt ppt
40	clear	clear	clear	clear	clear	cloudy
50	clear	clear	cloudy	-	-	-
60	clear	clear	cloudy	-	-	-
70	cloudy	-	-	-	-	-

Table A2.78: Solubility data for 175,000 ppm NaCl brine and surfactant solution 8

Water Weight % in solution	25°C	40°C	60°C	100°C	120°C	160°C
10	salt ppt	salt ppt	salt ppt	salt ppt	salt ppt	salt ppt
20	salt ppt	salt ppt	salt ppt	salt ppt	salt ppt	salt ppt
30	salt ppt	salt ppt	salt ppt	salt ppt	salt ppt	salt ppt
40	clear	clear	cloudy	-	-	-
50	clear	clear	cloudy	-	-	-
60	clear	cloudy	-	-	-	-
70	cloudy	-	-	-	-	-

Table A2.79: Solubility data for 175,000 ppm NaCl brine and surfactant solution 8

Water Weight % in solution	25°C	40°C	60°C	100°C	120°C	160°C
10	salt ppt	salt ppt	salt ppt	salt ppt	salt ppt	salt ppt
20	salt ppt	salt ppt	salt ppt	salt ppt	salt ppt	salt ppt
30	salt ppt	salt ppt	salt ppt	salt ppt	salt ppt	salt ppt
40	salt ppt	salt ppt	salt ppt	salt ppt	salt ppt	salt ppt
50	cloudy	-	-	-	-	-

Appendix B

This appendix summarizes all the coreflood experiments performed to measure two-phase and three-phase relative permeabilities and evaluate the effect of chemical treatment on relative permeabilities.

Appendix B1- Experiment No.1

Objective:

The objective of this experiment (Exp #1) was to investigate the effect of non-ionic polymeric fluoro-surfactant FC4432 treatment in improving the gas and condensate relative permeability on carbonate rock. The experiment was performed on an outcrop Texas Cream Limestone core at 145°F.

Experimental Results:

Initial permeability of the core was measured using nitrogen at 145°F. **Table B1.1** summarizes the properties of the core and the experimental conditions. **Figure B1.1** shows the nitrogen flood pressure drop measured across the plug and **Table B1.2** summarizes the results of the nitrogen flood. Synthetic fluid mixture-1 (Table 3.1) was used for the two-phase flow measurements.

The initial flood was done at a flowing core pressure of 1200 psig. **Figure B1.2** show the pressure drop across the core for the two-phase gas condensate flow at multiple rates. As, the pressure drop across the core was large, the fluid properties at the average core pressures were used for calculating relative permeabilities. **Table B1.3** gives the fluid properties of the synthetic fluid calculated using the Peng-Robinson EOS at the

average core pressures for different flow rates. **Table B1.4** summarizes the results of the initial two-phase flow.

The core was then treated with a non-ionic polymeric fluoro-surfactant FC4432. **Table B1.5** gives the composition of the treatment solution. **Figure B1.3** shows the measured pressure drop across the core during the injection of 18 pore volumes of treatment solution. The core was then shut-in for 24 hours. Post-treatment two-phase gas and condensate flow of the same gas mixture was then done under the same conditions as the initial two-phase flow. **Figure B1.4** shows the pressure drop across the core measured during the post-treatment two-phase flow at flowing pressures of 1200 psig. **Table B1.6** summarizes the results of the post-treatment two-phase flow.

The results show that the treatment had no significant effect on gas and condensate relative permeabilities. The improvement factor was about 1.3 at the lower rate but was almost one at higher rates.

Finally, the post-treatment permeability of the core was measured using methane to find out if the final gas permeability was as high as the initial gas permeability or if some damage might have been done. **Figure B1.5** shows the pressure drop across the core. The final gas permeability was 6.4 md.

Table B1.1: Core properties

Core	Texas Cream Limestone
Length, inches	8.01
Diameter, inches	0.972
Porosity, %	20.5
Pore volume, cc	20
Swi, %	0
Temperature, °F	145

Table B1.2: Result of methane flood

q_{core}, (cc/hr)	ΔP (psi)	k_g (md)
271	9.7	9.00
542	19.4	9.02
1084	38.9	8.99
Permeability, k_g (md)		9.00

Table B1.3: Synthetic fluid properties at experimental conditions

Pressure, psig	3000	1240		1280		1333	
Fluid Properties		Gas phase	Oil phase	Gas phase	Oil phase	Gas phase	Oil phase
ρ, g/cc	0.2724	0.0782	0.5152	0.0807	0.5122	0.851	0.5071
μ (cp)		0.0148	0.1271	0.015	0.125	0.0152	0.124
Volume fraction		0.9241	0.0759	0.927	0.079	0.9156	0.0844
IFT (dyne/cm)		3.617		3.438		3.14	

Table B1.4: Results of initial two-phase flow of gas and condensate

q_{pump}, cc/hr	112	224	448
$q_{\text{total core}}$, cc/hr	273.95	531.57	1010.92
$q_{\text{g core}}$, cc/hr	253.15	489.57	925.60
$q_{\text{o core}}$, cc/hr	20.79	41.99	85.32
ΔP, psi	79.16	147.74	266.58
k_{rg}	0.091	0.095	0.099
k_{ro}	0.064	0.070	0.078
Nc	5.86×10^{-6}	1.15×10^{-5}	2.27×10^{-5}
PVT Ratio	1.42	1.4	1.36

Table B1.5: Composition of treatment solution

Component	Mole%
FC4432	2
Methanol	94
D.I. water	4

Table B1.6: Results of post-treatment two-phase flow of gas and condensate

q_{pump}, cc/hr	112	224	448
q_{total core}, cc/hr	273.95	531.57	1010.92
q_{g core}, cc/hr	253.15	489.57	925.60
q_{o core}, cc/hr	20.79	41.99	85.32
ΔP, psi	60.75	127.93	247.44
k_{rg}	0.119	0.109	0.107
k_{ro}	0.084	0.08	0.084
Nc	4.47*10 ⁻⁶	9.4*10 ⁻⁶	1.82*10 ⁻⁵
K_{rg treated}/k_{rg untreated}	1.3	1.15	1.07

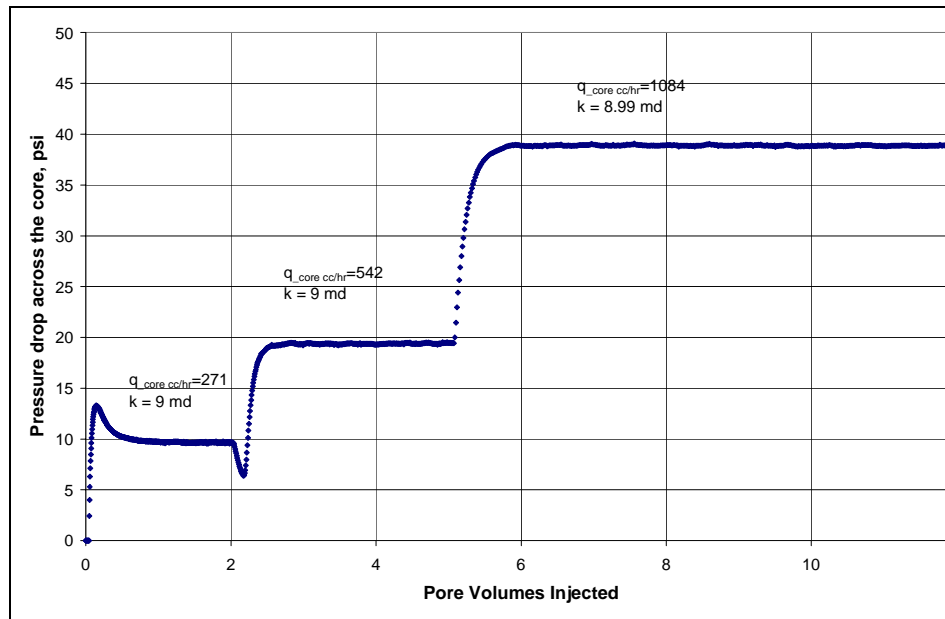


Figure B1.1: Pressure drop across the core during initial methane flood

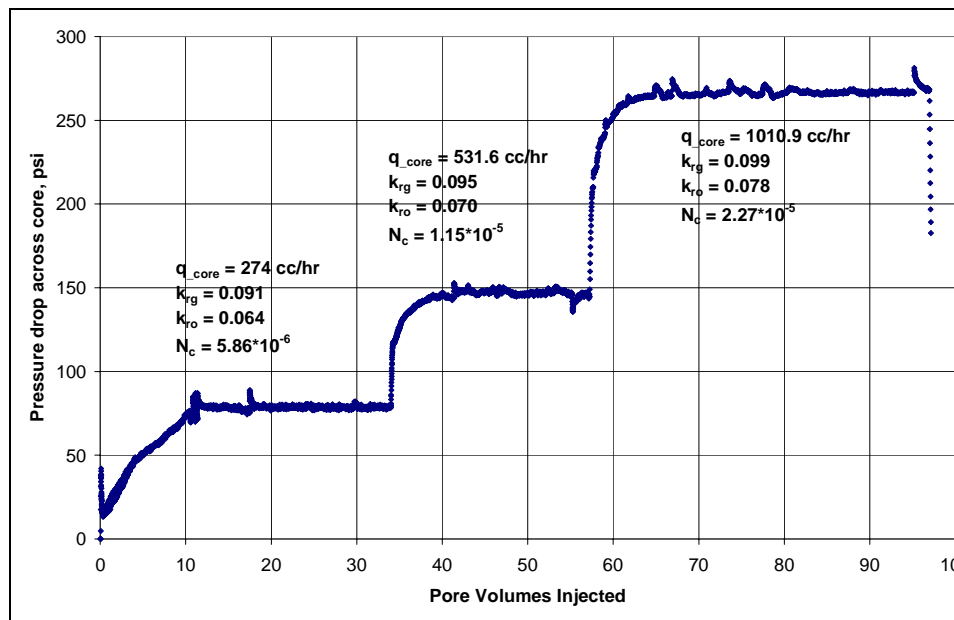


Figure B1.2: Pressure drop across the core during the initial two-phase flow at 1200 psig flowing pressure

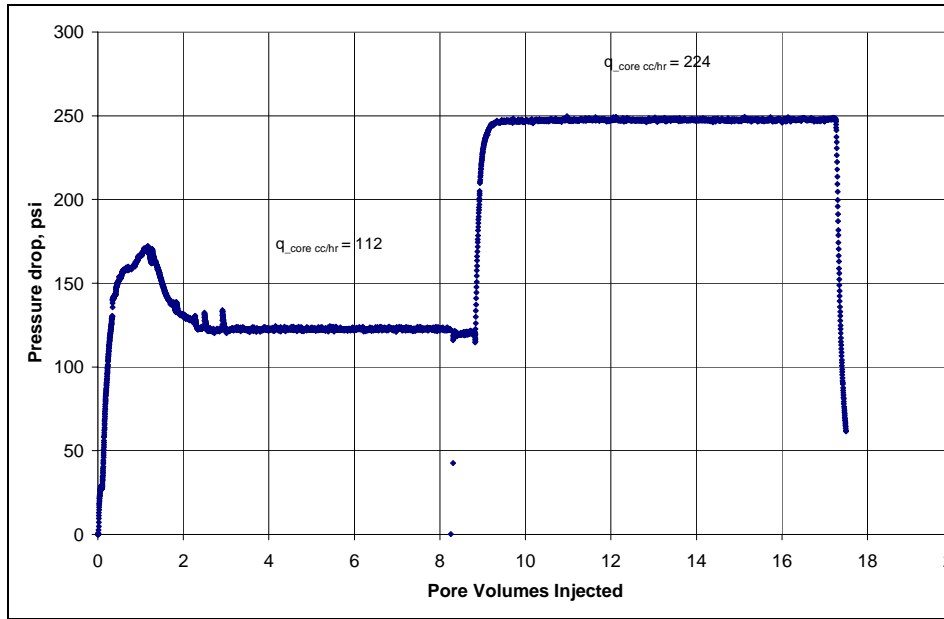


Figure B1.3: Pressure drop across the core during surfactant treatment

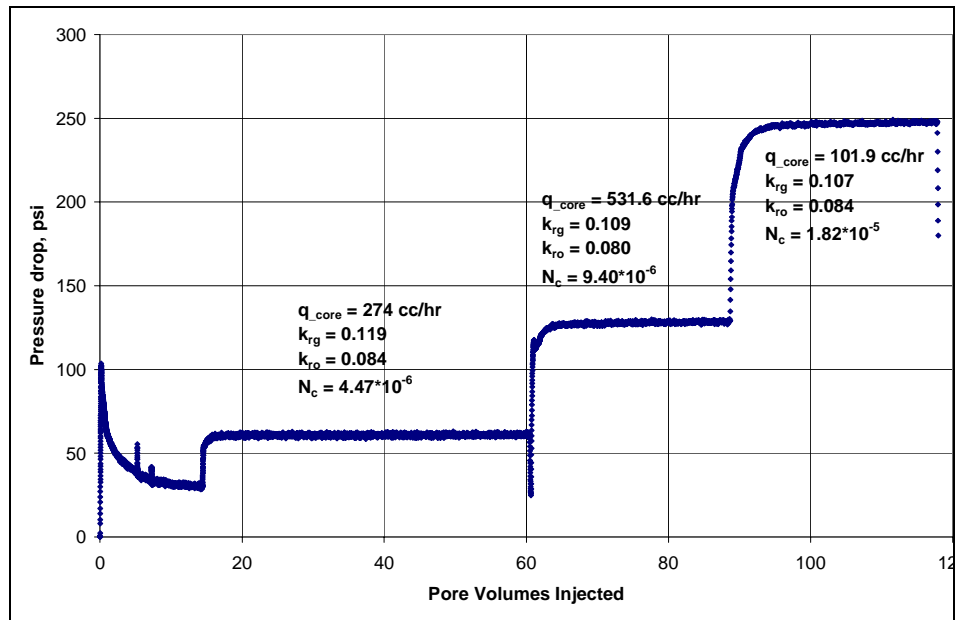


Figure B1.4: Pressure drop across the core during post-treatment two-phase flow at 1200 psig flowing pressure.

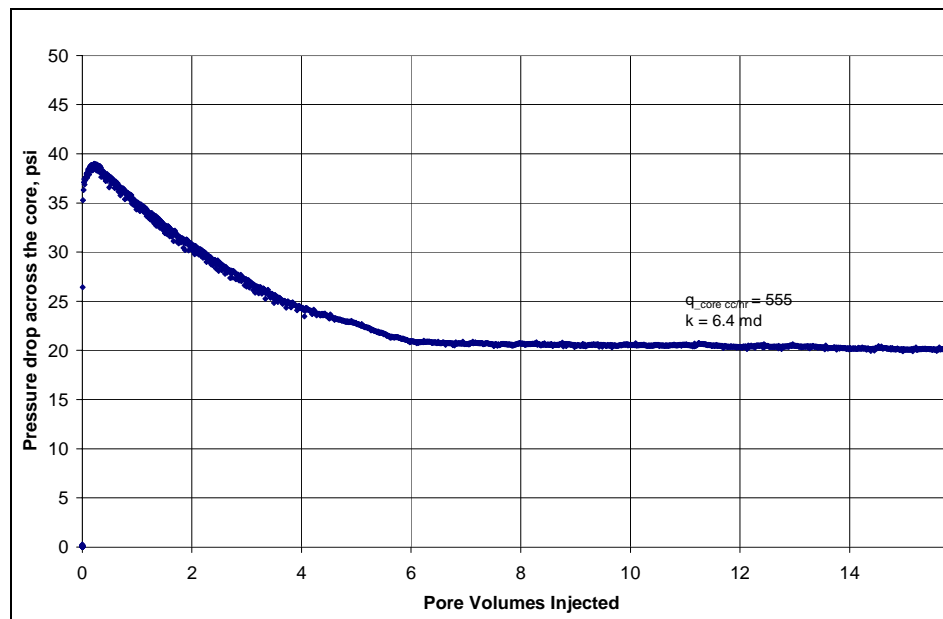


Figure B1.5: Pressure drop across the core during the final methane flood at 1200 psig.

Appendix B2- Experiment No.2

Objective:

The objective of this experiment (Exp #2) was to investigate the effect of non-ionic polymeric fluoro-surfactant FC4430 treatment in improving the gas and condensate relative permeability on carbonate rocks. The experiment was performed on an outcrop Texas Cream Limestone core at 145°F.

Experimental Results:

Initial permeability of the core was measured using methane at 145°F. **Table B2.1** summarizes the properties of the core and the experimental conditions. **Figure B2.1** shows the methane flood pressure drop measured across the plug and **Table B2.2** summarizes the results of the methane flood. Synthetic fluid mixture-1 (**Table 3.1**) was used for the two-phase flow measurements.

The initial flood was done at a flowing core pressure of 1200 psig. **Figure B2.3** shows the pressure drop across the core for the two-phase gas condensate flow at multiple rates. As, the pressure drop across the core was large; the fluid properties at the average core pressures were used for calculating relative permeabilities. **Table B2.4** gives the fluid properties of the synthetic fluid calculated using the Peng-Robinson EOS at the average core pressures for different flow rates. **Table B2.5** summarizes the results of the initial two-phase flow.

A solvent flood was then done to see if the presence of high water concentration in the solvent mixture damages the low permeability limestone core. **Figure B2.4** shows the measured pressure drop across the core during the injection of 17 pore volumes of methanol/water (80/20) mixture. This was followed with a two-phase gas condensate

flood. **Figure B2.5** shows the pressure drop across the core for the two-phase gas condensate flow after solvent flood. **Table B2.6** summarizes the results of the two-phase flow. The result shows that high concentration of water did not damage the core and the gas and condensate relative permeabilities were unchanged.

The core was then treated with a non-ionic polymeric fluoro-surfactant FC4430. **Table B2.7** gives the composition of the treatment solution. **Figure B2.6** shows the measured pressure drop across the core during the injection of 17 pore volumes of treatment solution. The core was then shut-in for 24 hours. Post-treatment two-phase gas and condensate flow of the same gas mixture was then done under the same conditions as the initial two-phase flow. **Figure B2.7** shows the pressure drop across the core measured during the post-treatment two-phase flow at flowing pressures of 1200 psig. **Table B2.8** summarizes the results of the post-treatment two-phase flow. The results show that the treatment had no effect on gas and condensate relative permeabilities. The improvement factor was about 1.

Finally, the post-treatment permeability of the core was measured using methane to find out if the final gas permeability was as high as the initial gas permeability or if some damage might have been done. **Figure B2.8** shows the pressure drop across the core. The final gas permeability was 6.3 md.

Table B2.1: Core properties

Core	Texas Cream Limestone
Length, inches	8
Diameter, inches	1
Porosity, %	20
Pore volume, cc	20.59
Swi, %	0
Temperature, °F	145

Table B2.2: Result of methane flood

q_{core}, (cc/hr)	ΔP (psi)	k_g (md)
277.75	8.1	7.91
555.5	16.19	7.91
1111	32.66	7.85
Permeability, k_g (md)		7.89

Table B2.3: Synthetic fluid properties at experimental conditions

Pressure, psig	3000	1232		1263		1324	
Fluid Properties		Gas phase	Oil phase	Gas phase	Oil phase	Gas phase	Oil phase
ρ, g/cc	0.2724	0.0777	0.5159	0.0799	0.5132	0.0844	0.5078
μ (cp)		0.0148	0.1276	0.0149	0.1257	0.0151	0.122
Volume fraction		0.9249	0.0751	0.922	0.078	0.9164	0.0836
IFT (dyne/cm)		3.66		3.495		3.184	

Table B2.4: Results of initial two-phase flow of gas condensate mixture

q_{pump}, cc/hr	112	224	448
$q_{\text{total core}}$, cc/hr	275.83	536.67	1018.69
$q_{\text{g core}}$, cc/hr	255.11	494.81	933.53
$q_{\text{o core}}$, cc/hr	20.71	41.86	85.16
ΔP, psi	64.89	126.58	248.55
k_{rg}	0.121	0.12	0.115
k_{ro}	0.084	0.088	0.091
Nc	4.69×10^{-6}	9.57×10^{-6}	2.06×10^{-5}
PVT Ratio	1.43	1.37	1.27

Table B2.5: Results of post-solvent flood two-phase flow of gas condensate mixture

q_{pump}, cc/hr	112
q_{total_core}, cc/hr	275.83
q_{g_core}, cc/hr	255.11
q_{o_core}, cc/hr	20.71
ΔP, psi	61.08
k_{rg}	0.128
k_{ro}	0.09
Nc	3.94*10 ⁻⁶
PVT Ratio	1.43

Table B2.6: Composition of treatment solution

Component	Mole%
FC4430	2
Methanol	78
D.I. water	20

Table B2.7: Results of post-treatment two-phase flow of gas condensate mixture

q_{pump}, cc/hr	112	224
q_{total core}, cc/hr	275.83	536.67
q_{g core}, cc/hr	255.11	494.81
q_{o core}, cc/hr	20.71	41.86
ΔP, psi	64.53	134.36
k_{rg}	0.121	0.113
k_{ro}	0.085	0.082
Nc	4.16*10 ⁻⁶	8.66*10 ⁻⁶
K_{rg treated}/k_{rg untreated}	1.00	0.94

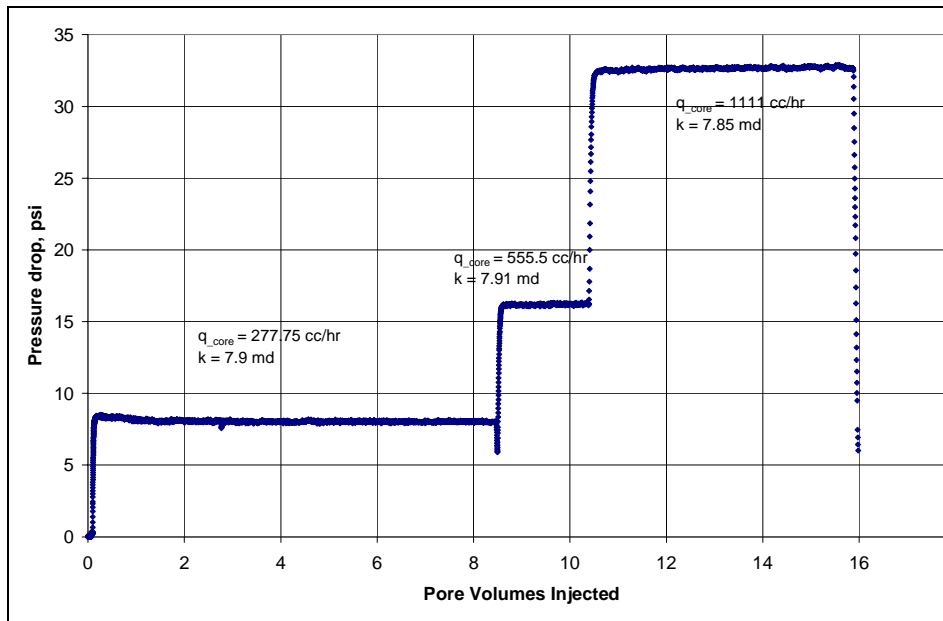


Figure B2.1: Pressure drop across the core during initial methane flood

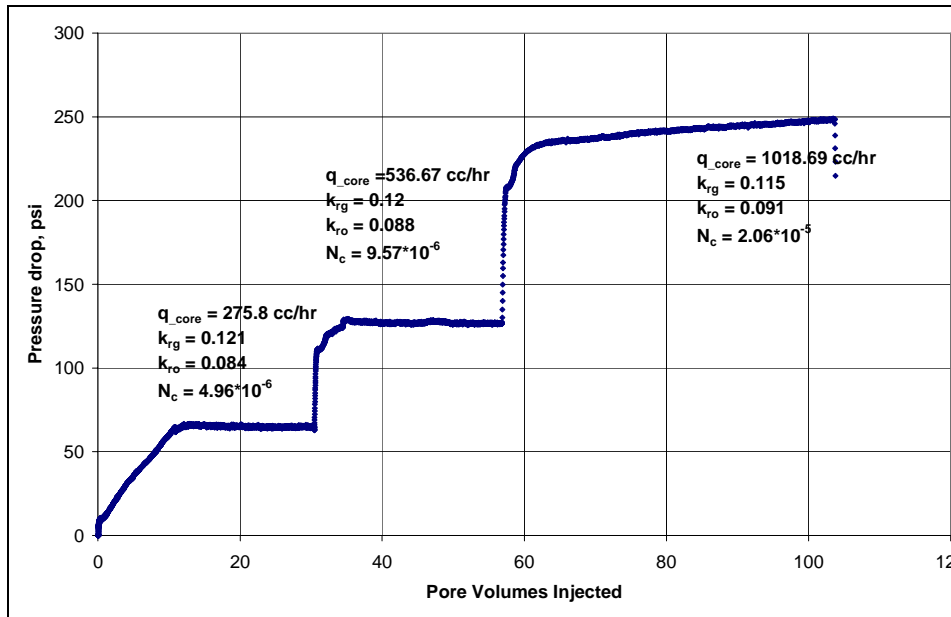


Figure B2.2: Pressure drop across the core during the initial two-phase flow at 1200 psig flowing pressure.

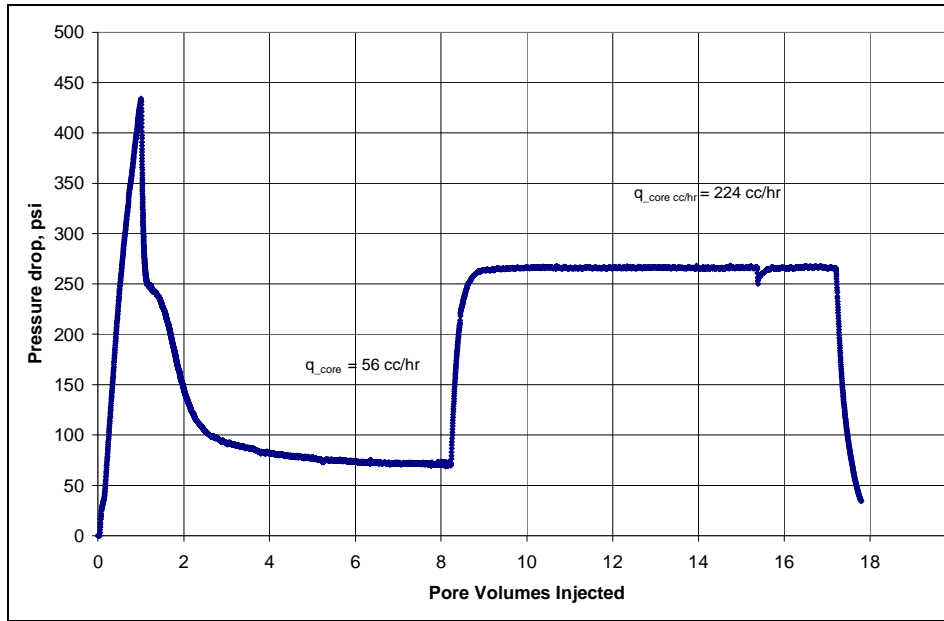


Figure B2.3: Pressure drop across the core during (methanol-water) solvent flood

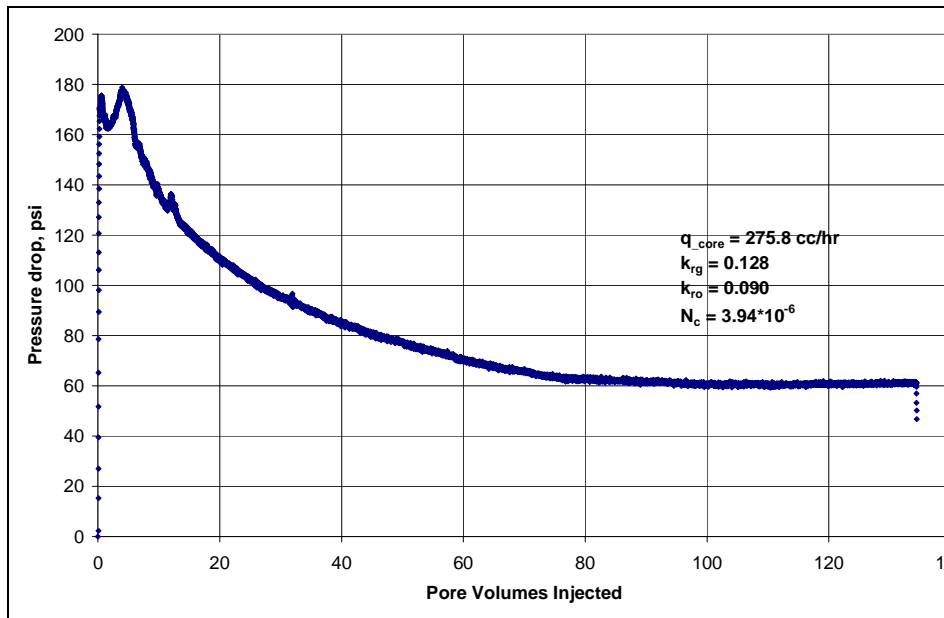


Figure B2.4: Pressure drop across the core during post- solvent flood two-phase flow at 1200 psig flowing pressure

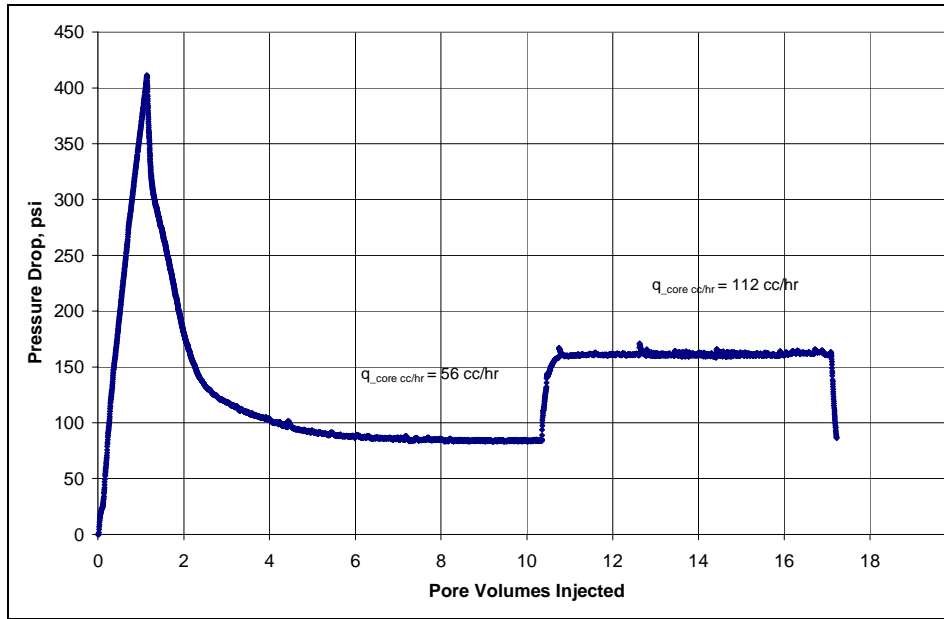


Figure B2.5: Pressure drop across the core during surfactant treatment.

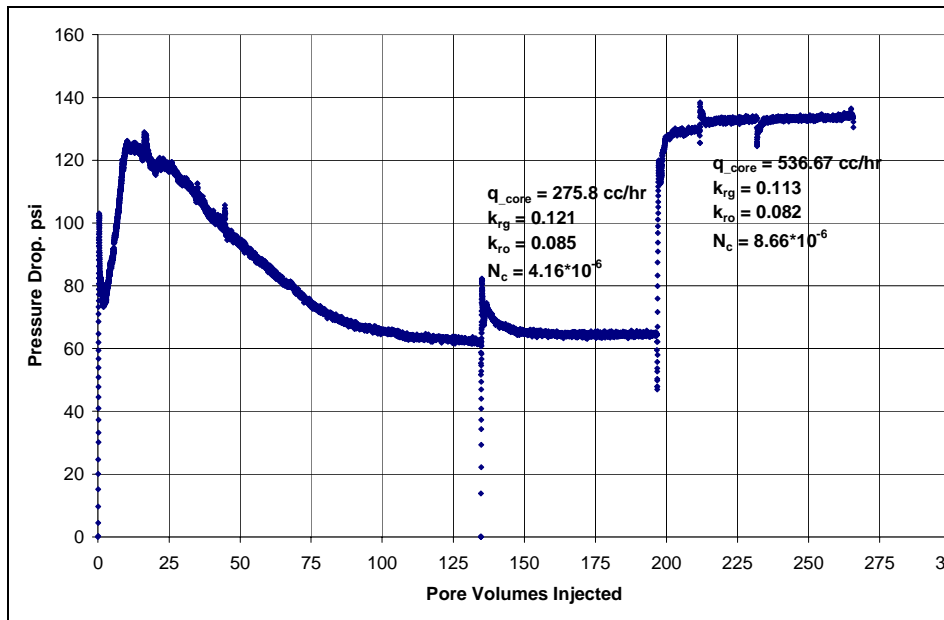


Figure B2.6: Pressure drop across the core during post-treatment two-phase flow at 1200 psig flowing pressure.

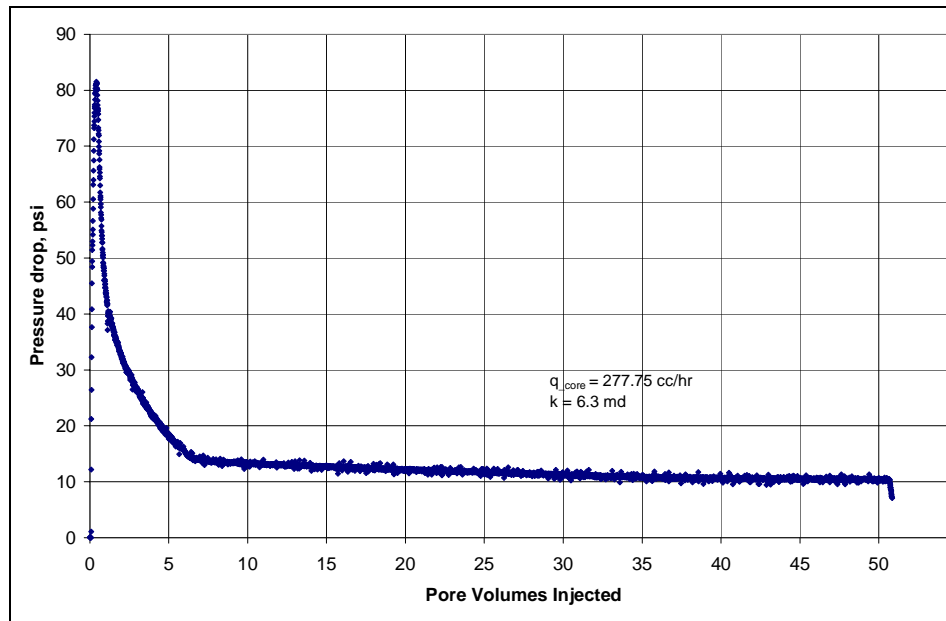


Figure B2.7: Pressure drop across the core during the final methane flood at 1200 psig.

B3- Experiment No.3

Objective:

The objective of this experiment was to test the effect of non-ionic polymeric fluoro-surfactant FC4430 treatment in improving the gas and condensate relative permeability on a dry sandstone rock and test the durability of the treatment. The experiment was performed on Berea sandstone core at 145°F.

Experimental Results:

Initial permeability of the core was measured using methane at 145°F. **Table B3.1** summarizes the properties of the core and the experimental conditions. **Figure B3.1** shows the methane flood pressure drop measured across the plug and **Table B3.2** summarizes the results of the methane flood. Synthetic fluid mixture-1 (Table 3.1) was used for the two-phase flow measurements.

The initial flood was done at a flowing core pressure of 1200 psig. **Figure B3.2** shows the pressure drop across the core for the two-phase gas condensate flow at multiple rates. **Table B3.3** gives the fluid properties of the synthetic fluid calculated using the Peng-Robinson EOS at the flowing core pressures. **Table B3.4** summarizes the results of the initial two-phase flow.

This was followed with an equilibrium gas flood to measure the gas end point relative permeability at residual condensate saturation. The equilibrium gas phase composition at 145°F and 1200 psig was calculated using PREOS. **Table B3.5** gives the equilibrium gas phase composition. **Figure B3.3** shows the pressure drop across the core for the equilibrium gas flood at multiple rates. **Table B3.6** summarizes the results of the pre-treatment equilibrium gas flood.

The core was then treated with a non-ionic polymeric fluoro-surfactant FC4430. **Table B3.7** gives the composition of the treatment solution. **Figure B3.4** shows the measured pressure drop across the core during the injection of 19 pore volumes of treatment solution. The treatment was done at a very low flow rate of 4cc/hr to increase the residence time of the chemical in the rock. The pressure drop during the surfactant treatment was extremely less because of the low flow rate. The core was then shut-in for 24 hours.

Post-treatment two-phase gas and condensate flow of the same gas mixture was then done under the same conditions as the initial two-phase flow. To test the durability of the chemical treatment, multiple batches of post-treatment gas condensate floods were done. **Figure B3.5** shows the pressure drop across the core measured during the post-treatment two-phase floods at flowing pressures of 1200 psig. The results show that the improvement factor was higher than 2 for the first couple of floods but the pressure drop kept increasing as more gas mixture was flown through the core. The pressure drop stabilized after flowing about 600 pore volumes through the core and the improvement factor dropped to about 1.6. Total of about 1350 pore volumes of gas mixture was flown through the core and the actual flowing time was 52 hours. The absolute time, actual time from the first post-treatment gas condensate flood to the last flood, was 183 hours. **Table B3.8** summarizes the results of the post-treatment two-phase flow. These results show that the treatment increased the gas and condensate relative permeability by a factor of 1.56 and the treatment is durable for large amount of flowing time.

This was followed with an equilibrium gas flood to measure the post-treatment gas end point relative permeability at the residual condensate saturation. **Figure B3.6** shows the pressure drop across the core for the equilibrium gas flood at multiple rates. **Table B3.9** summarizes the results of the post-treatment equilibrium gas flood.

Finally, the post-treatment permeability of the core was measured using methane to find out if the final gas permeability was as high as the initial gas permeability or if some damage might have been done. **Figure B3.7** shows the pressure drop across the core. The final gas permeability was 124.7 md.

Table B3.1: Core properties

Core	Berea Sandstone
Length, inches	8
Diameter, inches	1
Porosity, %	20
Pore volume, cc	20.59
Swi, %	0
Temperature, °F	145

Table B3.2: Result of methane flood

q_{core}, (cc/hr)	ΔP (psi)	k_g (md)
3586.76	4.87	151.64
7173.53	9.88	149.97
5123.95	7.14	147.97
Permeability, k_g (md)		149.76

Table B3.3: Synthetic fluid properties at experimental conditions

Pressure, psig	3000	1200	
Fluid Properties		Gas phase	Oil phase
ρ, g/cc	0.2724	0.0754	0.5186
μ (cp)		0.0147	0.1297
Volume fraction		0.9286	0.0714
IFT (dyne/cm)		3.835	

Table B3.4: Results of initial two-phase flow of gas condensate mixture

q_{pump}, cc/hr	192	320	448
$q_{\text{total core}}$, cc/hr	488.59	814.32	1140.04
$q_{\text{g core}}$, cc/hr	453.70	756.17	1058.64
$q_{\text{o core}}$, cc/hr	34.89	58.14	81.40
ΔP, psi	22.95	31.89	40.62
k_{rg}	0.032	0.038	0.042
k_{ro}	0.022	0.026	0.028
Nc	$3.00 \cdot 10^{-5}$	$4.17 \cdot 10^{-5}$	$5.31 \cdot 10^{-5}$
PVT Ratio	1.47	1.47	1.47

Table B3.5: Composition of the equilibrium gas mixture

Component	Mole%
Methane	88.99
n-Butane	10.22
n-Heptane	0.75
n-Decane	0.05

Table B3.6: Results of pre-treatment equilibrium gas flood

q_{pump}, cc/hr	192	448
q_{g core}, cc/hr	487.11	1136.58
ΔP, psi	3.31	7.43
k_{rg}	0.235	0.244
Nc	4.33*10 ⁻⁶	9.72*10 ⁻⁶

Table B3.7: Composition of treatment solution

Component	Weight %
FC4430	2
Methanol	94
D.I. water	4

Table B3.8: Results of post-treatment two-phase flow of gas condensate mixture

q_{pump}, cc/hr	192
q_{total_core}, cc/hr	488.59
q_{g_core}, cc/hr	453.70
q_{o_core}, cc/hr	34.89
ΔP, psi	14.72
k_{rg}	0.050
k_{ro}	0.034
Nc	1.92*10 ⁻⁵
K_{rg_treated}/k_{rg_untreated}	1.56

Table B3.9: Results of post-treatment equilibrium gas flood

q_{pump}, cc/hr	192	448
q_{g_core}, cc/hr	487.11	1136.58
ΔP, psi	1.63	4.19
k_{rg}	0.476	0.433
Nc	2.14*10 ⁻⁶	5.48*10 ⁻⁶

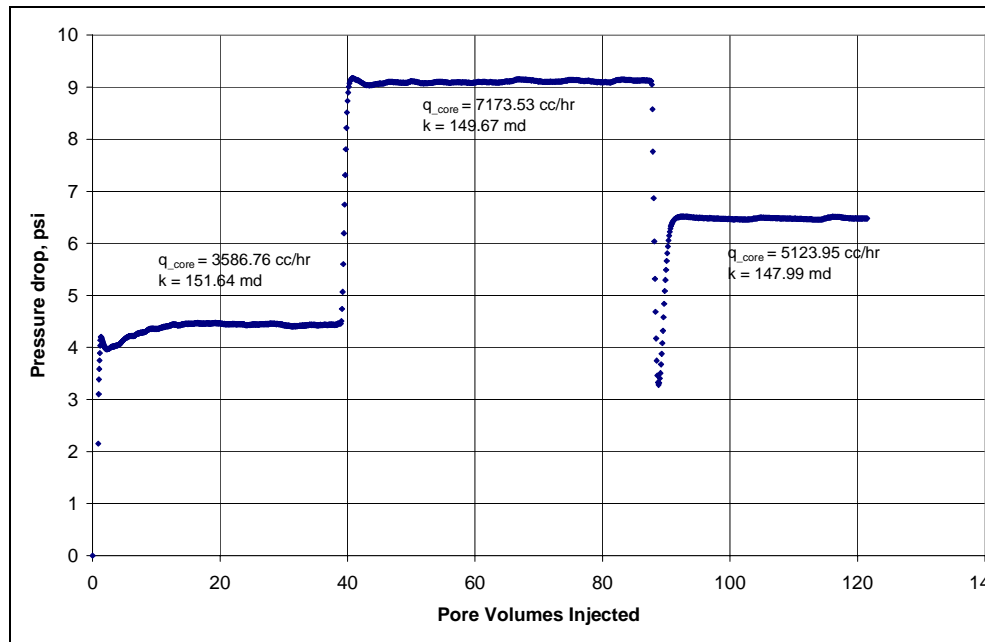


Figure B3.1: Pressure drop across the core during initial methane flood

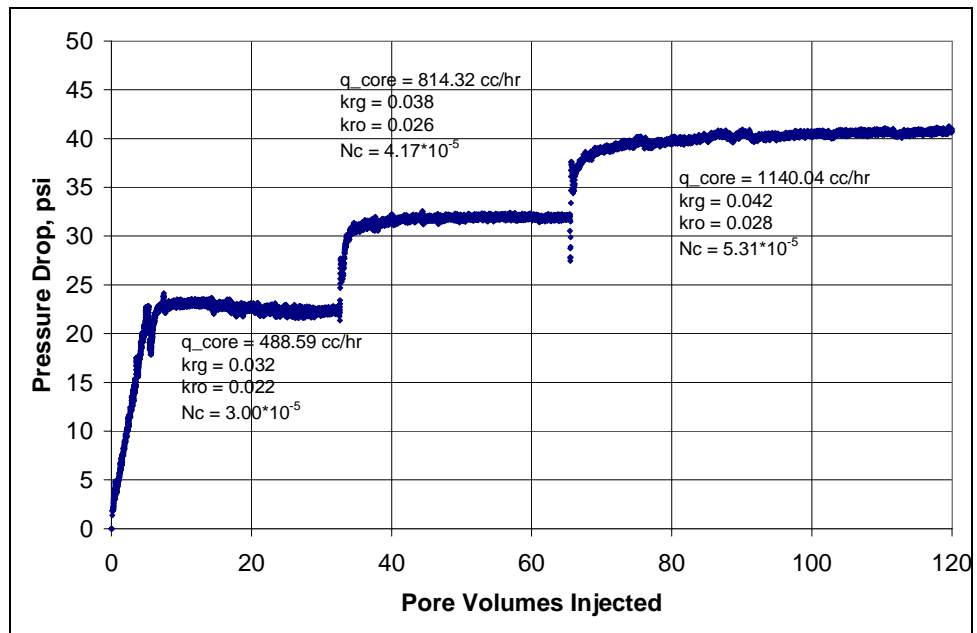


Figure B3.2: Pressure drop across the core during the initial two-phase flow at 1200 psig flowing pressure

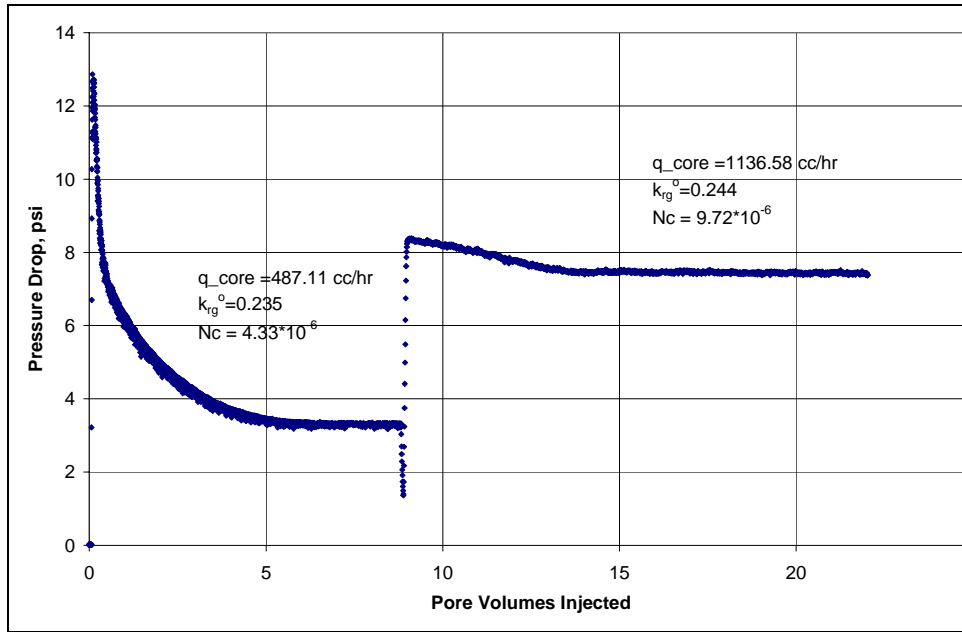


Figure B3.3: Pressure drop across the core during the pre-treatment equilibrium gas flood.

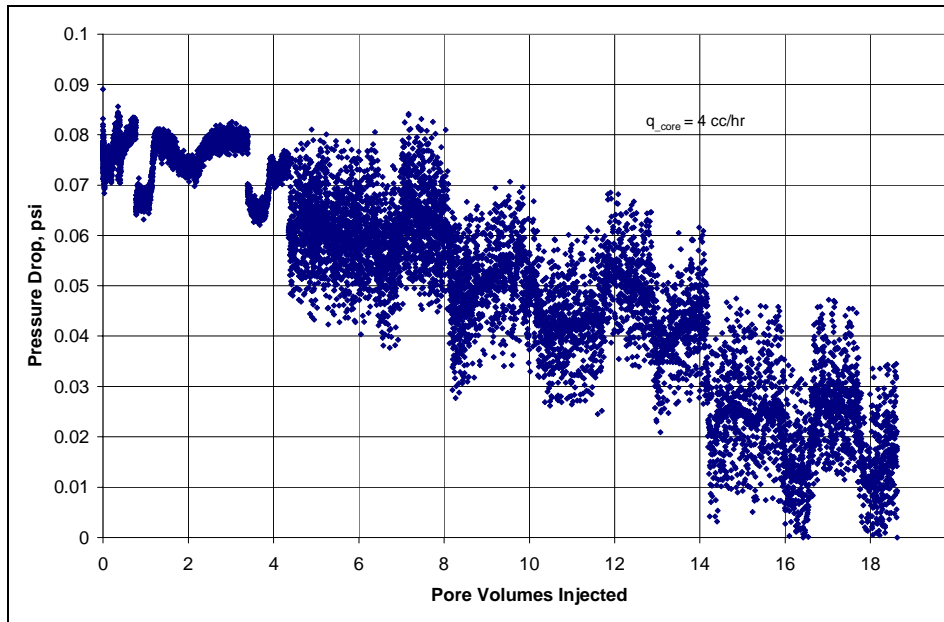


Figure B3.4: Pressure drop across the core during surfactant treatment.

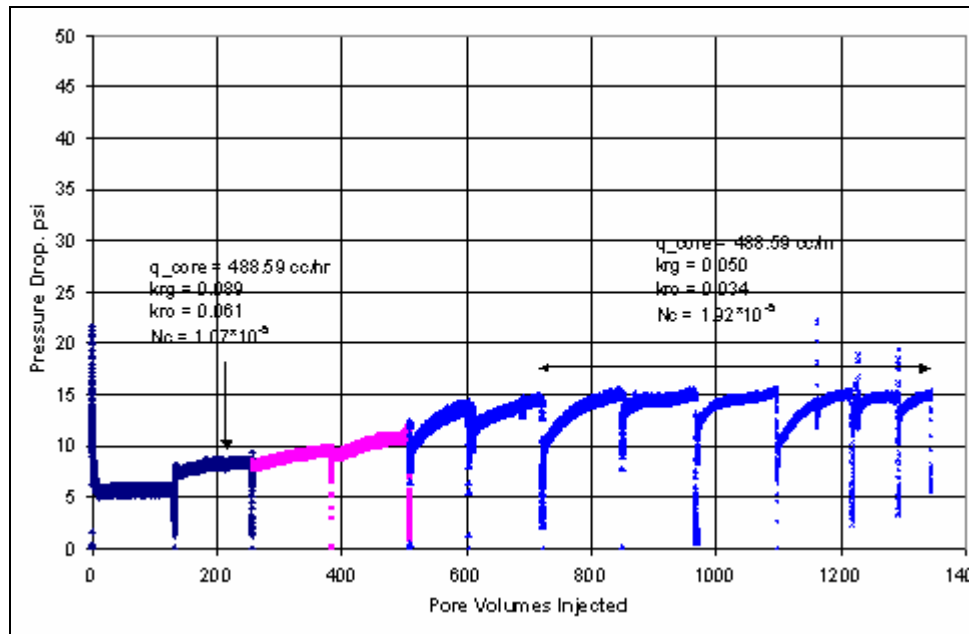


Figure B3.5: Pressure drop across the core during post-treatment two-phase flow at 1200 psig flowing pressure.

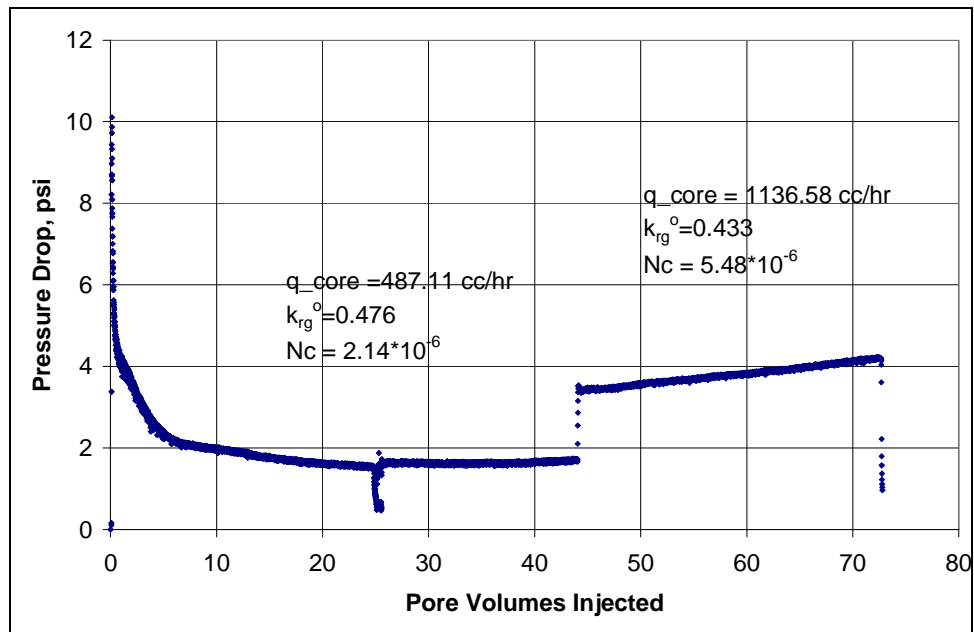


Figure B3.6: Pressure drop across the core during post-treatment equilibrium gas flood

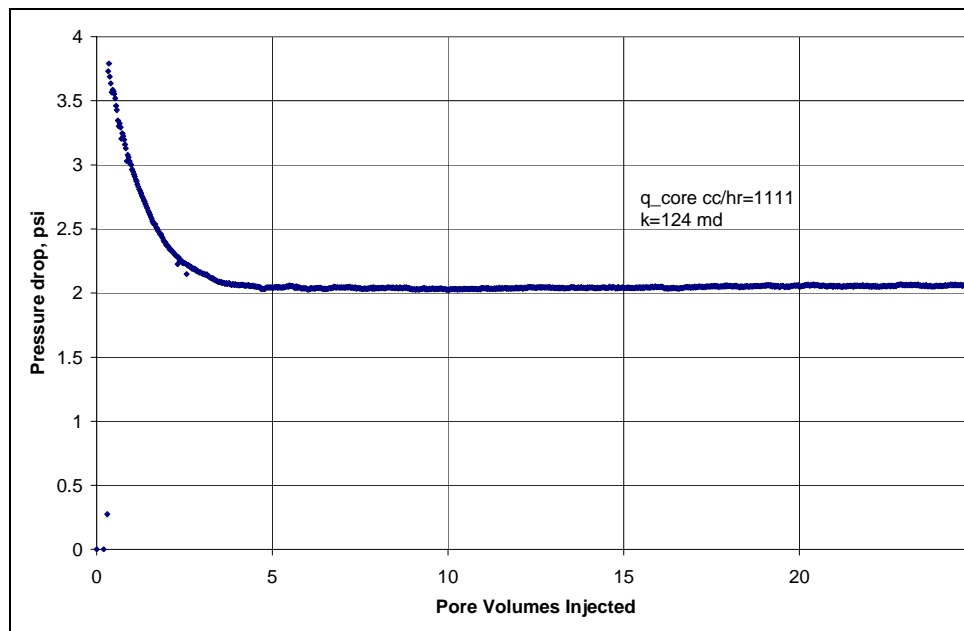


Figure B3.7: Pressure drop across the core during the final methane flood at 1200 psig

B4- Experiment No.4

Objective:

The objective of this experiment was to investigate the effect of polymeric fluoro-surfactant L16218 treatment in improving the gas and condensate relative permeability on carbonate rocks. The experiment was performed on an outcrop Texas Cream Limestone core at 145°F.

Experimental Results:

Initial permeability of the core was measured using methane at 145°F. **Table B4.1** summarizes the properties of the core and the experimental conditions. **Figure B4.1** shows the methane flood pressure drop measured across the plug and **Table B4.2** summarizes the results of the methane flood. Synthetic fluid mixture-1 (Table 3.1) was used for the two-phase flow measurements.

The initial flood was done at a flowing core pressure of 1200 psig. **Figure B4.3** shows the pressure drop across the core for the two-phase gas condensate flow at multiple rates. As, the pressure drop across the core was large; the fluid properties at the average core pressures were used for calculating relative permeabilities. **Table B4.3** gives the fluid properties of the synthetic fluid calculated using the Peng-Robinson EOS at the average core pressures for different flow rates. **Table B4.4** summarizes the results of the initial two-phase flow.

This was followed with an equilibrium gas flood to measure the gas end point relative permeability at residual condensate saturation. The equilibrium gas phase composition at 145°F and 1200 psig was calculated using PREOS. **Table B4.5** gives the equilibrium gas phase composition. **Figure B4.3** shows the pressure drop across the core

for the equilibrium gas flood at multiple rates. **Table B4.6** summarizes the results of the pre-treatment equilibrium gas flood.

The core was then treated with fluoro-surfactant L16218. **Table B4.7** gives the composition of the treatment solution. **Figure B4.4** shows the measured pressure drop across the core during the injection of 19 pore volumes of treatment solution. The treatment was done at a very low flow rate of 4cc/hr to increase the residence time of the chemical in the rock. The pressure drop during the surfactant treatment was extremely less because of the low flow rate. The core was then shut-in for 24 hours.

Post-treatment two-phase gas and condensate flow of the same gas mixture was then done under the same conditions as the initial two-phase flow. **Figure B4.5** shows the pressure drop across the core measured during the post-treatment two-phase flow at flowing pressures of 1200 psig. **Table B4.8** summarizes the results of the post-treatment two-phase flow. The results show that the treatment had no significant effect on gas and condensate relative permeabilities. The improvement factor was about 1.1 to 1.2.

This was followed with an equilibrium gas flood to measure the post-treatment gas end point relative permeability at the residual condensate saturation. **Figure B4.6** shows the pressure drop across the core for the equilibrium gas flood at multiple rates. **Table B4.9** summarizes the results of the post-treatment equilibrium gas flood.

Finally, the post-treatment permeability of the core was measured using methane to find out if the final gas permeability was as high as the initial gas permeability or if some damage might have been done. **Figure B4.7** shows the pressure drop across the core. The final gas permeability was 20.02 md.

Table B4.1: Core properties

Core	Texas Cream Limestone
Length, inches	8
Diameter, inches	1
Porosity, %	20
Pore volume, cc	20.59
Swi, %	0
Temperature, °F	145

Table B4.2: Result of methane flood

q_{core}, (cc/hr)	ΔP (psi)	k_g (md)
1111	12.43	20.63
2222	25.70	19.95
1587.15	18.11	20.22
Permeability, k_g (md)		20.27

Table B4.3: Synthetic fluid properties at experimental conditions

Pressure, psig	3000	1200		1235		1261	
Fluid Properties		Gas phase	Oil phase	Gas phase	Oil phase	Gas phase	Oil phase
ρ, g/cc	0.2724	0.0754	0.5186	0.0779	0.5156	0.0798	0.5133
μ (cp)		0.147	0.1297	0.0148	0.1274	0.0149	0.1258
Volume fraction		0.9277	0.0723	0.9246	0.0754	0.9222	0.0778
IFT (dyne/cm)		3.835		3.644		3.506	

Table B4.4: Results of initial two-phase flow of gas condensate mixture

q_{pump}, cc/hr	112	256	448
$q_{\text{total core}}$, cc/hr	283.95	628.79	1074.95
$q_{\text{g core}}$, cc/hr	263.42	581.38	991.32
$q_{\text{o core}}$, cc/hr	20.53	47.41	83.63
ΔP, psi	33.20	69.16	121.17
k_{rg}	0.094	0.100	0.098
k_{ro}	0.065	0.072	0.071
Nc	5.87×10^{-6}	1.29×10^{-5}	2.35×10^{-5}
PVT Ratio	1.45	1.39	1.38

Table B4.5: Composition of the equilibrium gas mixture

Component	Mole%
Methane	88.99
n-Butane	10.22
n-Heptane	0.75
n-Decane	0.05

Table B4.6: Results of pre-treatment equilibrium gas flood

q_{pump}, cc/hr	112	256
q_{g core}, cc/hr	284.15	469.48
ΔP, psi	5.86	12.78
k_{rg}	0.571	0.599
Nc	9.71*10 ⁻⁷	2.12*10 ⁻⁶

Table B4.7: Composition of treatment solution

Component	Weight %
L16218	2
Methanol	94
D.I. water	4

Table B4.8: Results of post-treatment two-phase flow of gas condensate mixture

q_{pump}, cc/hr	112	256
q_{total core}, cc/hr	283.95	628.79
q_{g core}, cc/hr	263.42	581.38
q_{o core}, cc/hr	20.53	47.41
ΔP, psi	27.13	61.07
k_{rg}	0.115	0.113
k_{ro}	0.079	0.081
Nc	4.49*10 ⁻⁶	1.01*10 ⁻⁵
K_{rg treated}/k_{rg untreated}	1.22	1.13

Table B4.9: Results of post-treatment equilibrium gas flood

q_{pump}, cc/hr	112	256
q_{g core}, cc/hr	284.15	469.48
ΔP, psi	5.82	11.59
k_{rg}	0.576	0.661
Nc	9.63*10 ⁻⁷	1.92*10 ⁻⁶

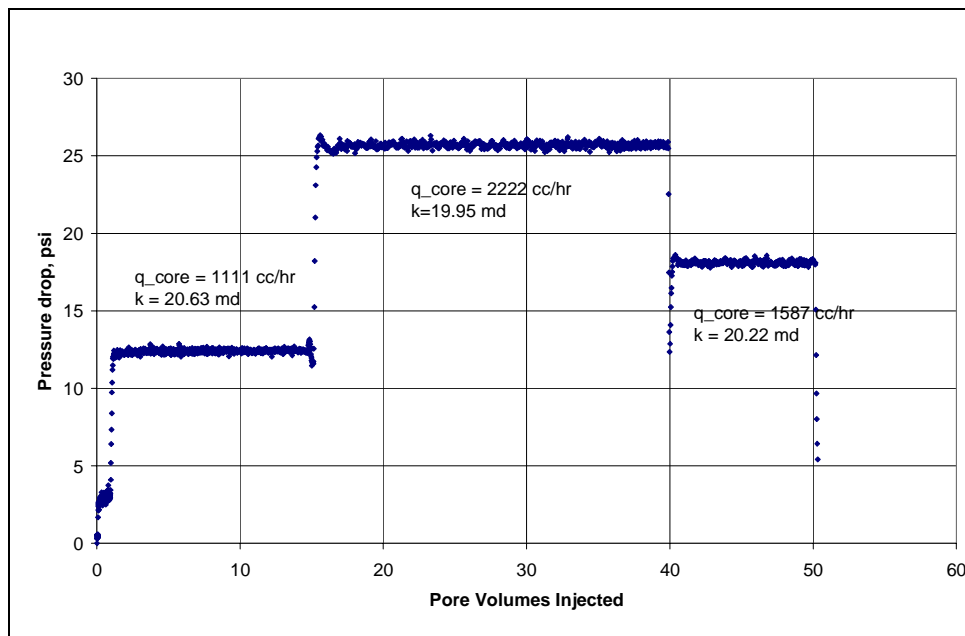


Figure B4.1: Pressure drop across the core during initial methane flood

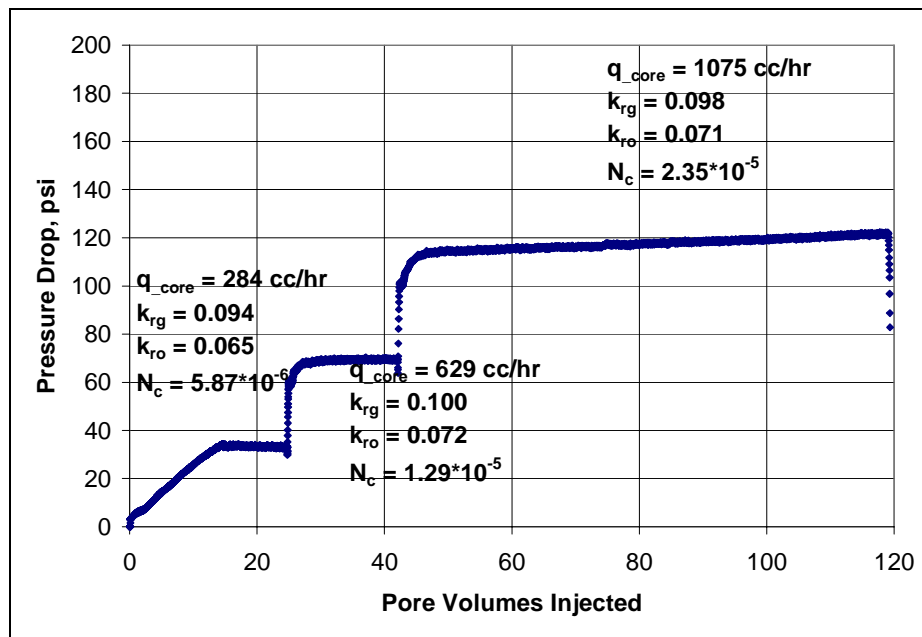


Figure B4.2: Pressure drop across the core during the initial two-phase flow at 1200 psig flowing pressure

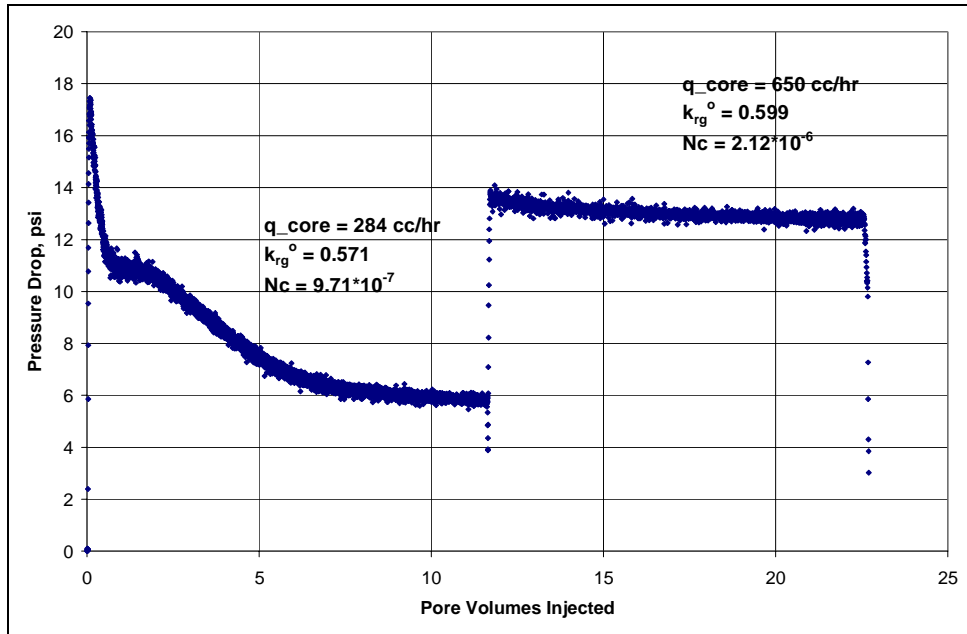


Figure B4.3: Pressure drop across the core during the pre-treatment equilibrium gas flood

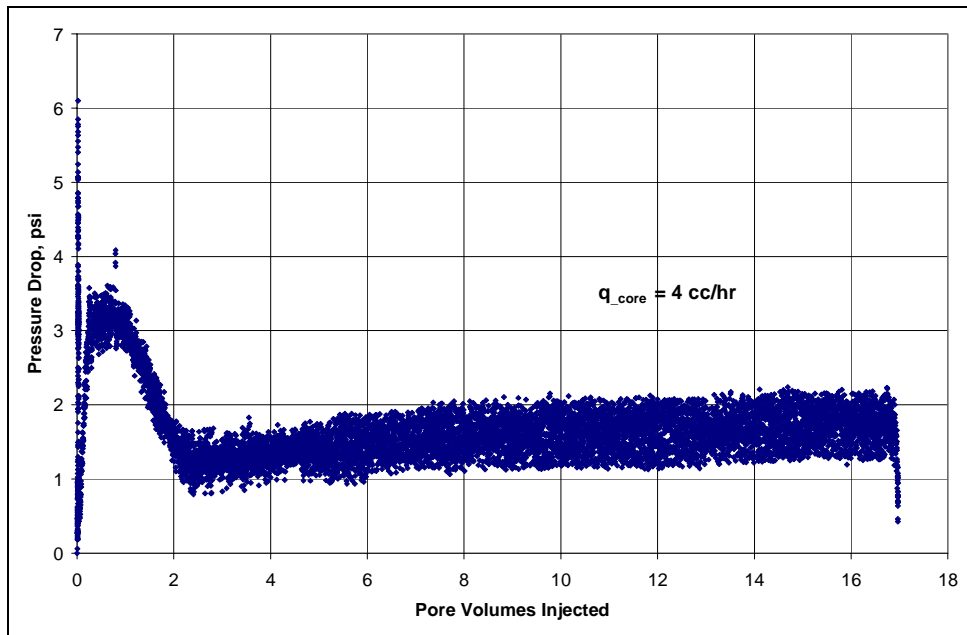


Figure B4.4: Pressure drop across the core during surfactant treatment

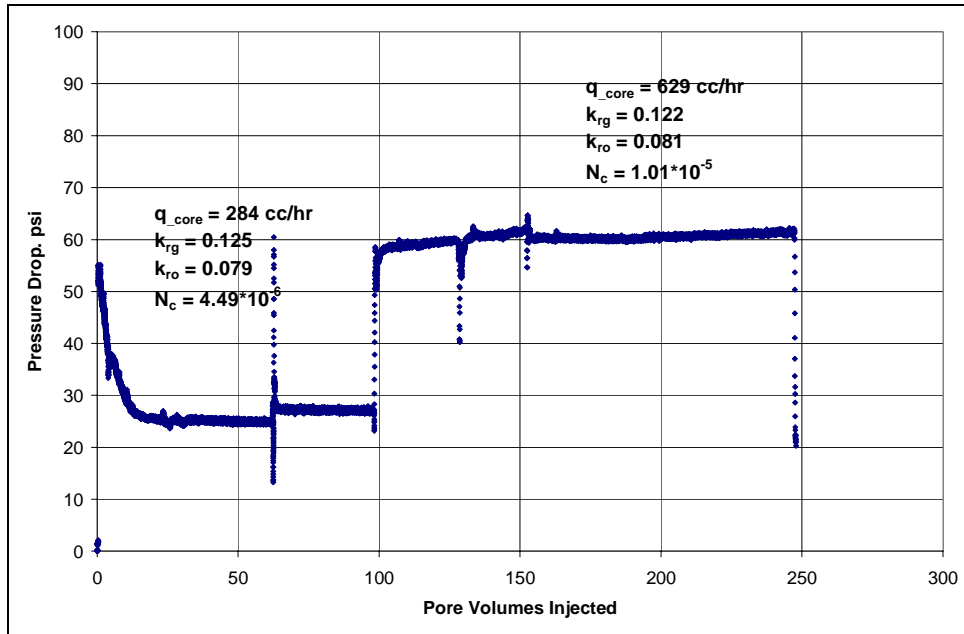


Figure B4.5: Pressure drop across the core during post-treatment two-phase flow at 1200 psig flowing pressure

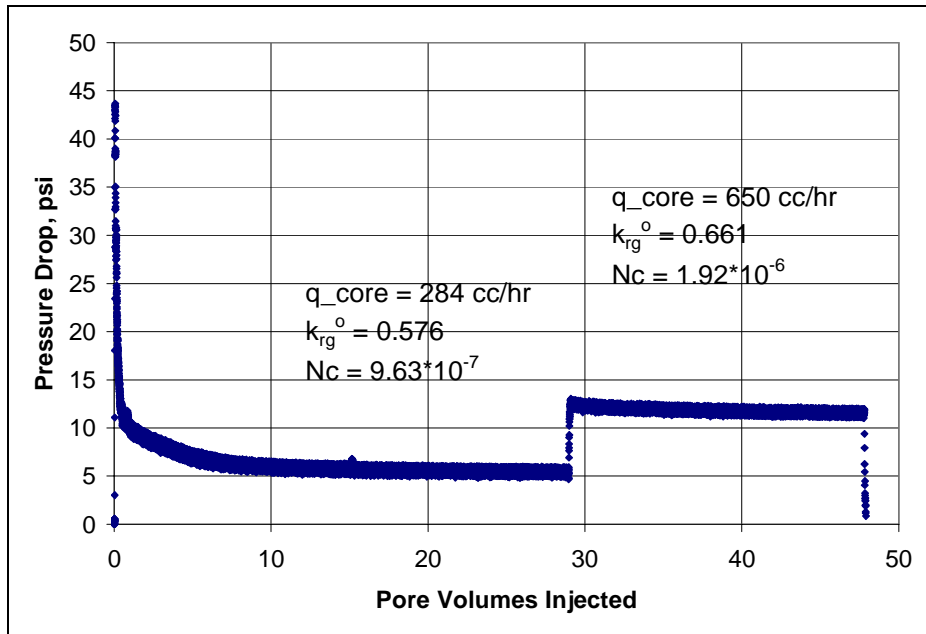


Figure B4.6: Pressure drop across the core during the post-treatment equilibrium gas flood

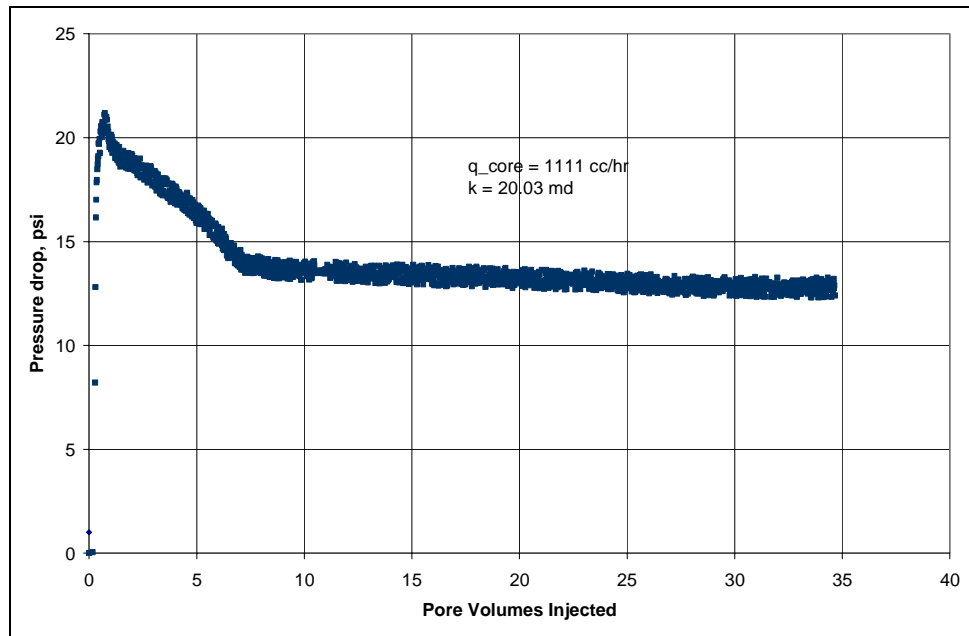


Figure B4.7: Pressure drop across the core during the final methane flood at 1200 psig

B5- Experiment No.5

Objective:

The objective of this experiment was to investigate the effect of fluoro-surfactant L16209 treatment in improving the gas and condensate relative permeability on carbonate rocks. The experiment was performed on an outcrop Texas Cream Limestone core at 145°F.

Experimental Results:

Initial permeability of the core was measured using methane at 145°F. **Table B5.1** summarizes the properties of the core and the experimental conditions. **Figure B5.1** shows the methane flood pressure drop measured across the plug and **Table B5.2** summarizes the results of the methane flood. Synthetic fluid mixture-1 (Table 3.1) was used for the two-phase flow measurements.

The initial flood was done at a flowing core pressure of 1200 psig. **Figure B5.2** shows the pressure drop across the core for the two-phase gas condensate flow at multiple rates. As, the pressure drop across the core was large; the fluid properties at the average core pressures were used for calculating relative permeabilities. **Table B5.3** gives the fluid properties of the synthetic fluid calculated using the Peng-Robinson EOS at the average core pressures for different flow rates. **Table B5.4** summarizes the results of the initial two-phase flow.

The core was then treated with a fluoro-surfactant L16209. **Table B5.5** gives the composition of the treatment solution. **Figure B5.3** shows the measured pressure drop across the core during the injection of 19 pore volumes of treatment solution. The

treatment was done at a very low flow rate of 4cc/hr to increase the residence time of the chemical in the rock. The core was then shut-in for 24 hours.

Post-treatment two-phase gas and condensate flow of the same gas mixture was then done under the same conditions as the initial two-phase flow. **Figure B5.4** shows the pressure drop across the core measured during the post-treatment two-phase flow at flowing pressures of 1200 psig. **Table B5.6** summarizes the results of the post-treatment two-phase flow. The results show that the treatment had no effect on gas and condensate relative permeabilities. The improvement factor was about 1.1.

Table B5.1: Core properties

Core	Texas Cream Limestone
Length, inches	8
Diameter, inches	1
Porosity, %	20
Pore volume, cc	20.59
Swi, %	0
Temperature, °F	145

Table B5.2: Result of methane flood

q_{core}, (cc/hr)	ΔP (psi)	k_g (md)
1111	21.38	11.99
2222	42.58	12.04
1269.7	24.61	11.91
Permeability, k_g (md)		11.98

Table B5.3: Synthetic fluid properties at experimental conditions

Pressure, psig	3000	1224		1254		1293	
Fluid Properties		Gas phase	Oil phase	Gas phase	Oil phase	Gas phase	Oil phase
ρ, g/cc	0.2724	0.0771	0.5166	0.0792	0.5139	0.0821	0.5105
μ (cp)		0.0148	0.1281	0.0149	0.1262	0.015	0.1238
Volume fraction		0.9256	0.0744	0.9229	0.0771	0.9193	0.0807
IFT (dyne/cm)		3.703		3.542		3.34	

Table B5.4: Results of initial two-phase flow of gas condensate mixture

q_{pump}, cc/hr	112	224	448
$q_{\text{total core}}$, cc/hr	277.86	618.68	1045.97
$q_{\text{g core}}$, cc/hr	257.19	570.98	961.56
$q_{\text{o core}}$, cc/hr	20.67	47.70	84.41
ΔP, psi	48.07	107.72	185.10
k_{rg}	0.108	0.108	0.106
k_{ro}	0.075	0.076	0.077
Nc	5.21×10^{-6}	1.22×10^{-5}	2.22×10^{-5}
PVT Ratio	1.44	1.41	1.38

Table B5.5: Composition of treatment solution

Component	Mole%
L16209	2
Methanol	94
D.I. water	4

Table B5.6: Results of post-treatment two-phase flow of gas condensate mixture

q_{pump}, cc/hr	112	112
q_{total core}, cc/hr	277.86	618.68
q_{g core}, cc/hr	257.19	570.98
q_{o core}, cc/hr	20.67	47.70
ΔP, psi	41.61	96.40
k_{rg}	0.125	0.12
k_{ro}	0.087	0.087
Nc	4.07*10 ⁻⁶	9.43*10 ⁻⁶
K_{rg treated}/k_{rg untreated}	1.15	1.11

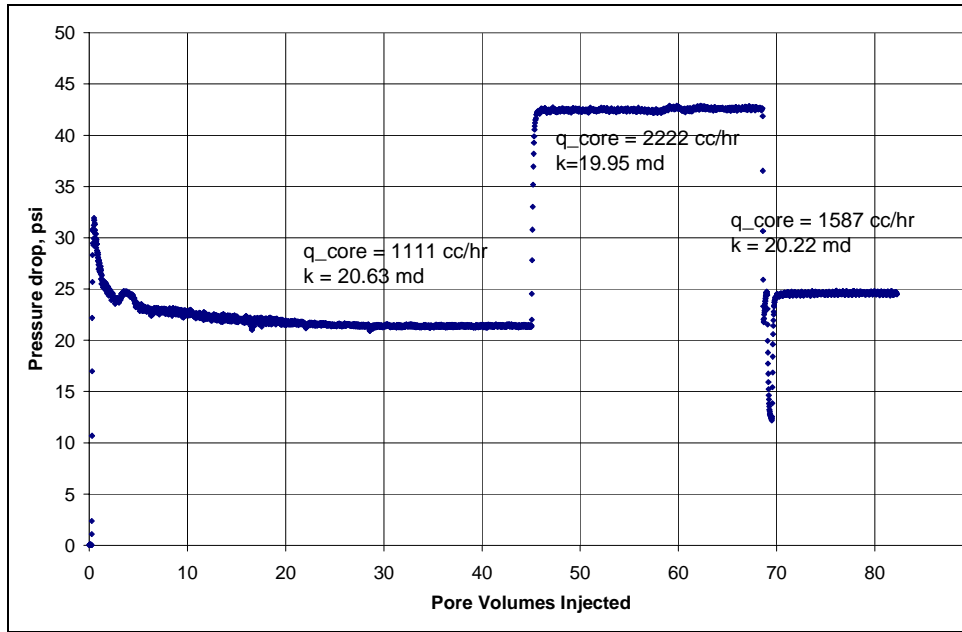


Figure B5.1: Pressure drop across the core during initial methane flood

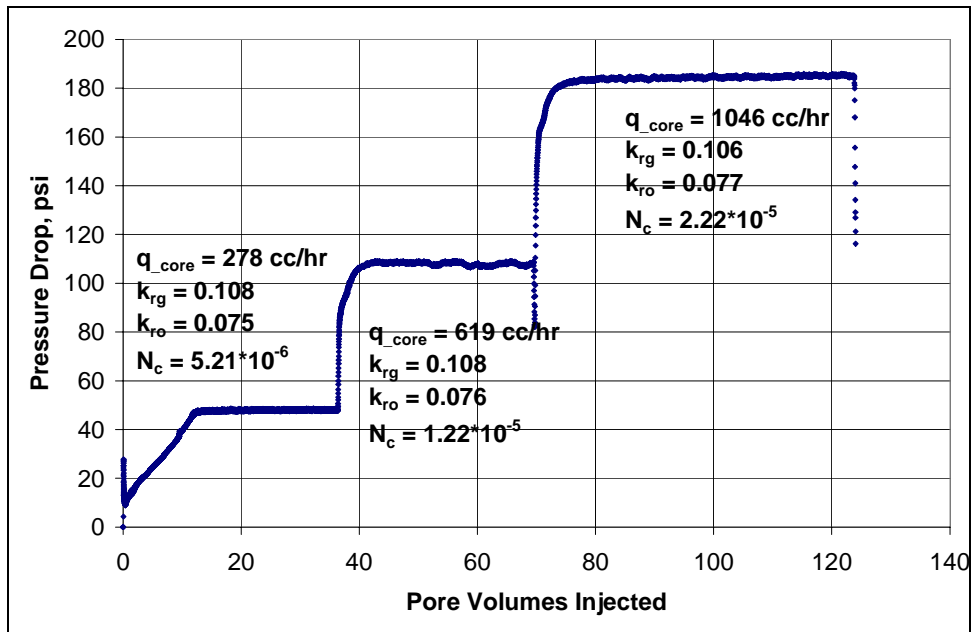


Figure B5.2: Pressure drop across the core during the initial two-phase flow at 1200 psig flowing pressure

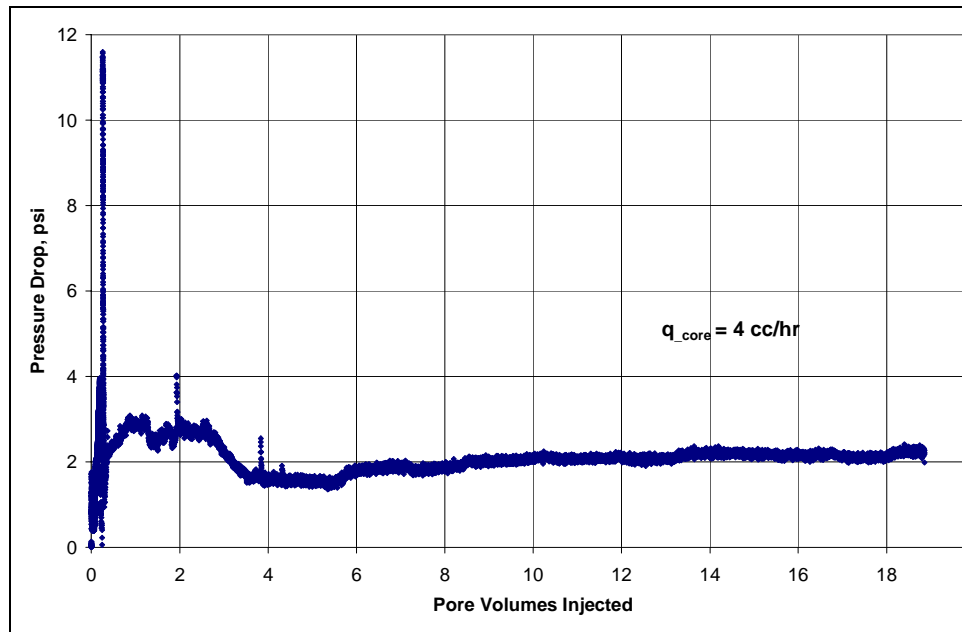


Figure B5.3: Pressure drop across the core during surfactant treatment

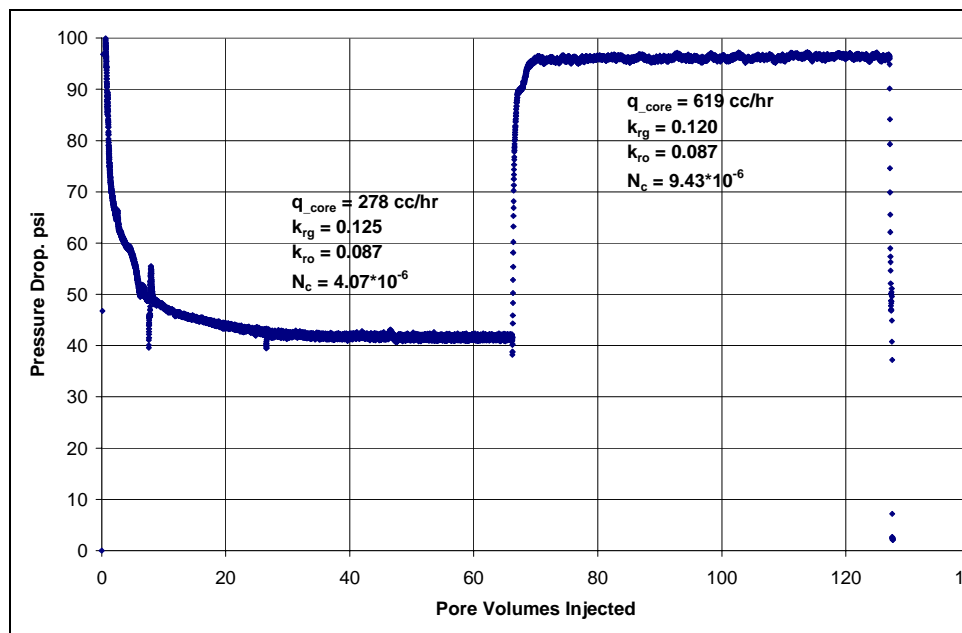


Figure B5.4: Pressure drop across the core during post-treatment two-phase flow at 1200 psig flowing pressure

B6- Experiment No.6

Objective:

The objective of this experiment was to investigate the effect of non-ionic polymeric fluoro-surfactant FC4430 treatment in improving the gas and condensate relative permeability on a reservoir sandstone rock in presence of initial water. The experiment was performed on a Britannia reservoir core (plug #13828.5) at 275°F.

Experimental Results:

Table B6.1 summarizes the properties of the core and the experimental conditions. Initial permeability of the core was measured using methane at 72°F. **Figure B6.1** shows the methane flood pressure total drop measured across the plug and across the top and bottom section. **Table B6.2** summarizes the results of the methane flood.

The initial water saturation of 26.1% was established by injecting 2.6 cc of brine in the vacuumed core. **Table B6.3** gives the composition of the synthetic brine used in this experiment. The temperature of the oven of then increased to 275°F but no pressure was kept on the core, which could have resulted in vaporization of water and precipitation of salt in the core. Methane flood was then done to measure the end point gas permeability and a reduction of about 17% in gas permeability was observed. **Figure B6.2** shows the methane flood pressure drop measured across the core and the sections. **Table B6.4** summarizes the results of the methane flood.

Synthetic fluid mixture-2 (Table 3.2) was used for the two-phase flow measurements. The initial flood was done with the upstream backpressure regulator set at 4650 psig and the downstream back pressure regulator set at 1500 psig. **Figure B6.3** shows the pressure drop across the core and the sections for the two-phase gas-

condensate flow. Three batches of gas mixture were flown through the core but steady state was not reached. This was primarily because the gas mixture was not a single phase at the start of the flood and more liquid was injected into the core during the end of the flood, which resulted in increasing pressure drop. This could be because the accumulator containing the gas mixture was not rocked and was not given sufficient time to get into equilibrium. **Table B6.5** gives the fluid properties of the synthetic fluid calculated using the Peng-Robinson EOS at the flowing core pressure. **Table B6.6** summarizes the results of the initial two-phase flow.

The core was then treated with a fluoro-surfactant FC4430. **Table B6.7** gives the composition of the treatment solution. **Figure B6.4** shows the measured pressure drop across the core during the injection of 23 pore volumes of treatment solution. The treatment was flowed at 32 cc/hr and the core was then shut-in for 24 hours. The pressure drop across the top section of the core during the treatment flood kept increasing indicating plugging at the inlet of the core.

Post-treatment two-phase of gas-condensate using the same gas mixture was then done under the same conditions as the initial two-phase flow. **Figure B6.8** shows the pressure drop across the core measured during the post-treatment two-phase flow at flowing pressures of 1500 psig. **Table B6.8** summarizes the results of the post-treatment two-phase flow. The results show that the pressure drop for the post-treatment two-phase flood was much higher than the pre-treatment two-phase flood. This was because of the plugging at the inlet of the core during the surfactant treatment. The pressure drop across the sections could not be measured because the pressure drop was higher than the range of the pressure transducers. The results thus showed that the core was plugged by the surfactant treatment.

Table B6.1: Core properties

Core	Britannia (Reservoir A), 16/26-B5 13828.6, SPL-B
Length, inches	4.5
Top Section, inches	2.25
Bottom Section, inches	2.25
Diameter, inches	1
Porosity, %	16.90
Pore volume, cc	9.79
Swi, %	26.1
Temperature, °F	275

Table B6.2: Result of methane flood

q_{core}, (cc/hr)	ΔP (psi)	k_g (md)
1330.42	3.55	45.17
2660.84	6.89	46.58
1900.60	4.482	51.15
Permeability, k_g (md)		47.63

Table B6.3: Synthetic Brine

Component	g/l
NaCl	59
CaCl ₂	16
MgCl ₂ .6H ₂ O	3.5

Table B6.4: Result of methane flood at Swi

q_{core}, (cc/hr)	P (psi)	k_g (md)
1378.46	4.10	40.51
2076.92	6.35	39.43
1661.54	4.91	40.82
Permeability, k_g (md)		40.25

Table B6.5: Synthetic fluid properties at experimental conditions

Pressure, psig	4650	1500	
Fluid Properties		Gas phase	Oil phase
ρ, g/cc	0.2052	0.0614	0.6015
μ (cp)		0.0165	0.2615
Volume fraction		0.9787	0.0213
IFT (dyne/cm)		5.168	

Table B6.6: Results of initial two-phase flow of gas condensate mixture

q_{pump}, cc/hr	256
q_{total_core}, cc/hr	720.55
q_{g_core}, cc/hr	705.20
q_{o_core}, cc/hr	15.35
ΔP, psi	22.37
k_{rg}	0.101
k_{ro}	0.035
Nc	8.70*10 ⁻⁶
PVT Ratio	2.89

Table B6.7: Composition of treatment solution

Component	Weight %
FC4430	2
Methanol	88
D.I. water	10

Table B6.8: Results of post-treatment two-phase flow of gas condensate mixture

q_{pump}, cc/hr	112	256
q_{total_core}, cc/hr	315.24	720.55
q_{g_core}, cc/hr	308.53	705.20
q_{o_core}, cc/hr	6.71	15.35
ΔP, psi	27.13	61.07
k_{rg}	0.036	0.037
k_{ro}	0.013	0.013
Nc	1.06×10^{-5}	2.38×10^{-5}
Improvement Factor		0.366

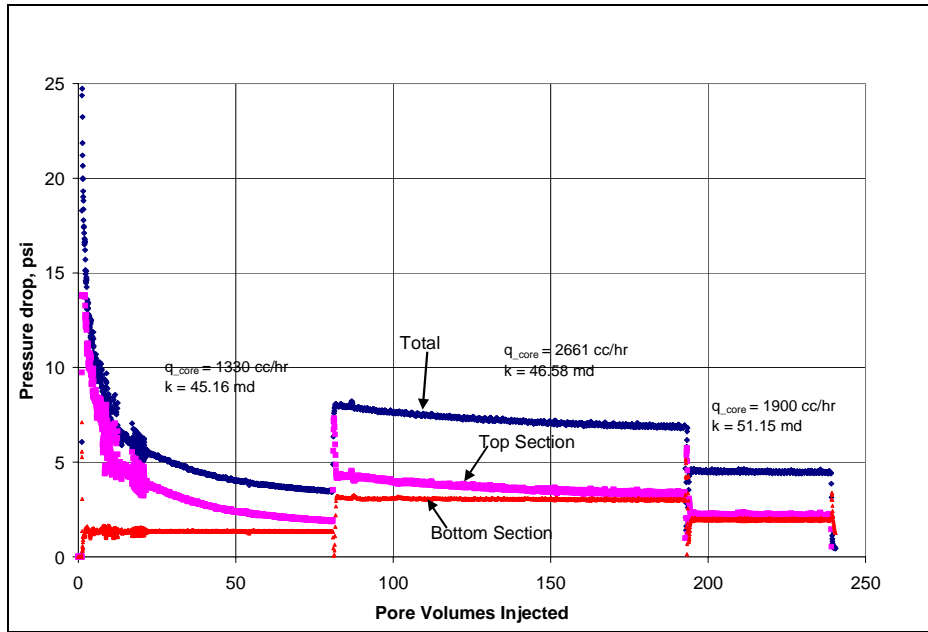


Figure B6.1: Pressure drop across the core and the sections during initial methane flood

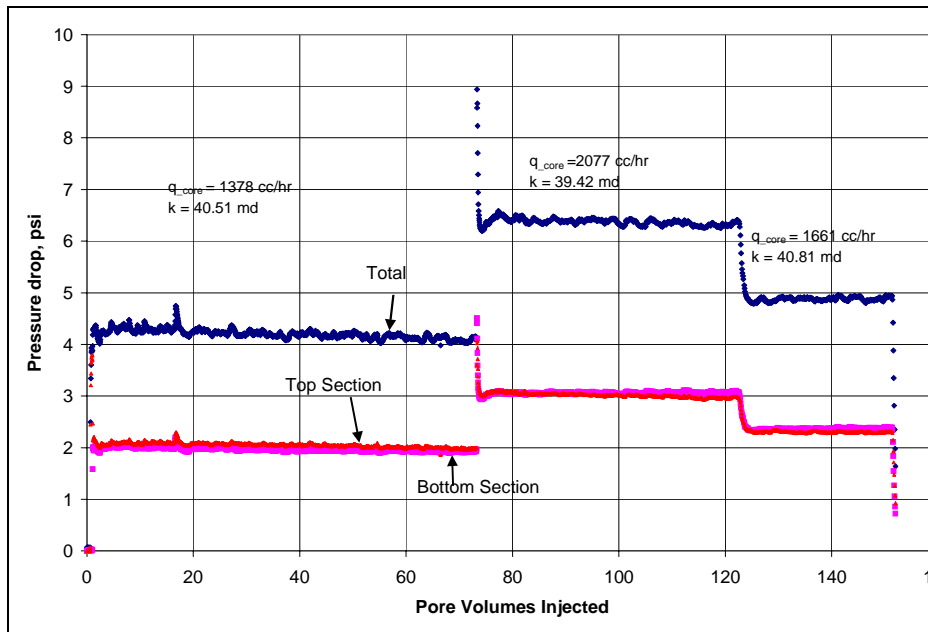


Figure B6.2: Pressure drop across the core and the sections during methane flood at $S_{wi}=26.1\%$

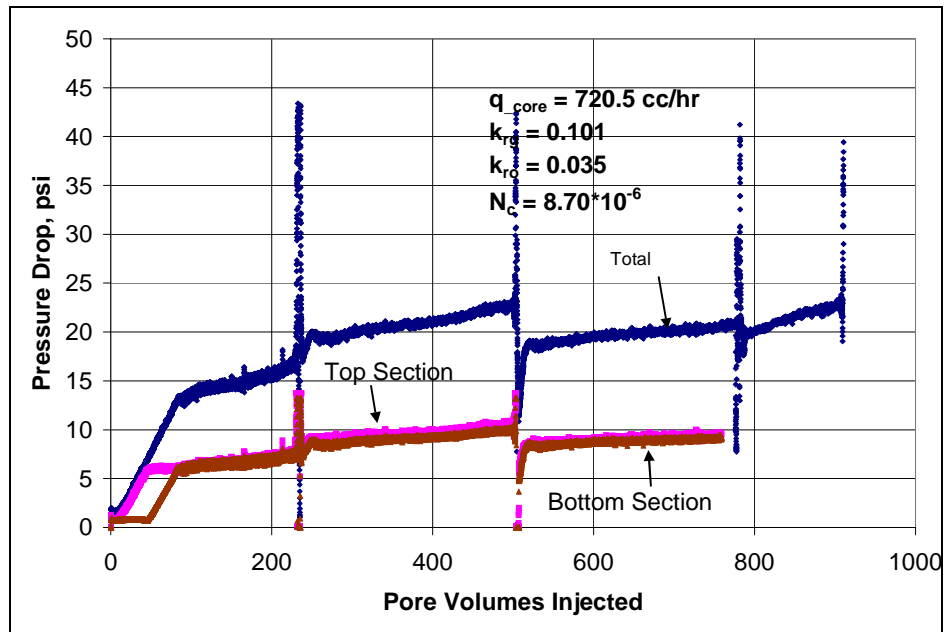


Figure B6.3: Pressure drop across the core and the sections during the initial two-phase flow at 275°F and 1500 psig

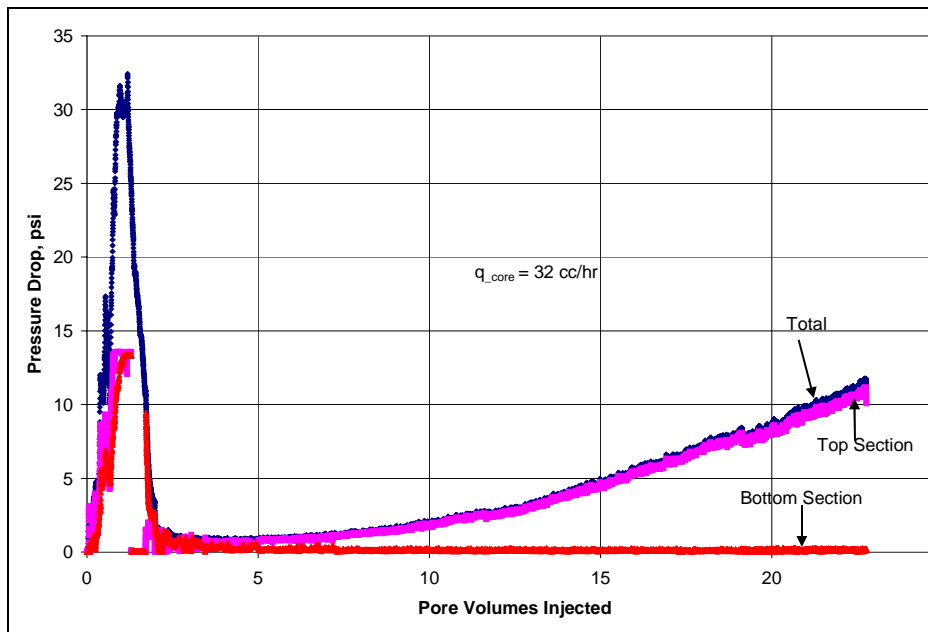


Figure B6.4: Pressure drop across the core and the sections during surfactant treatment

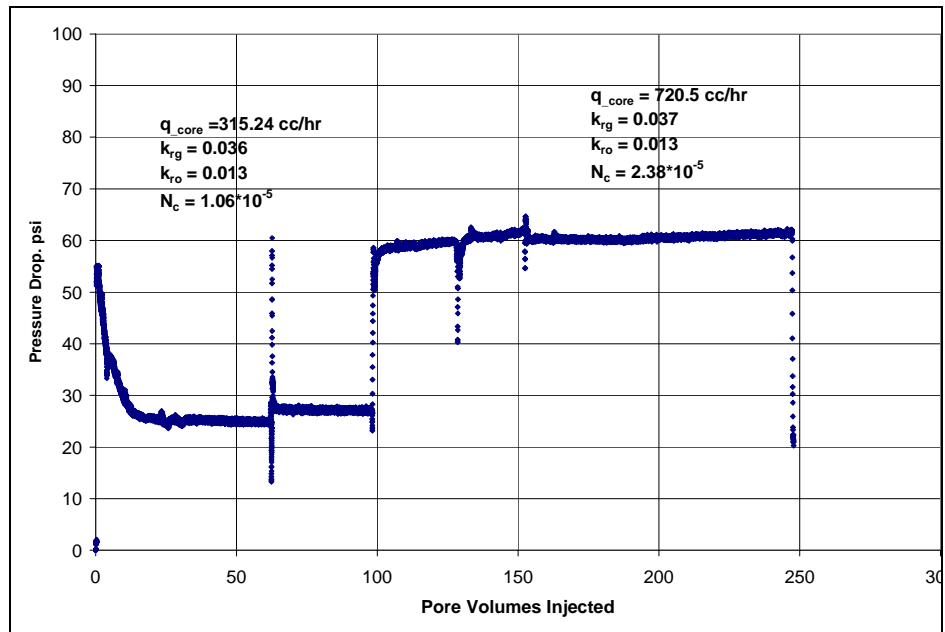


Figure B6.5: Pressure drop across the core and the sections during post-treatment two-phase flow at 275°F and 1500 psig

B7- Experiment No.7

Objective:

The objective of this experiment was to investigate the effect of non-ionic polymeric fluoro-surfactant FC4430 treatment in improving the gas and condensate relative permeability on a reservoir sandstone rock in presence of initial water. The experiment was performed on a Britannia reservoir core at 275°F. The plug used in Experiment-6 was re-used in this experiment.

Experimental Results:

Table B7.1 summarizes the properties of the core and the experimental conditions. Initial permeability of the core was measured using methane at 75°F. **Figure B7.1** shows the methane flood pressure total drop measured across the plug and across the top and bottom section. **Table B7.2** summarizes the results of the methane flood.

The initial water saturation of 26.1% was established by injecting 2.6 cc of brine in the vacuumed core and left to distribute uniformly for 1hour. **Table B7.3** gives the composition of the synthetic brine used in this experiment. The pressure of the core was raised to 500 psig and then the temperature of the oven was increased to 275°F. This was done to avoid any vaporization of water at high temperature. Methane flood was then done to measure the end point gas permeability. **Figure B7.2** shows the methane flood pressure drop measured across the core and the sections. The plot shows that water was not distributed uniformly throughout the core initially. The water saturation was higher at the inlet and this resulted in higher pressure drop in the top section. Flowing large volume of methane through the core distributed water more uniformly though the core. **Table B7.4** summarizes the results of the methane flood.

Synthetic fluid mixture-2 (Table 3.2) was used for the two-phase flow measurements. The initial flood was done with the upstream backpressure regulator set at 5140 psig and the downstream back pressure regulator set at 1500 psig. **Figure B7.3** shows the pressure drop across the core and the sections for the two-phase gas-condensate flow. Two batches of gas mixture were flown through the core but steady state was not reached. There was steady increase in the pressure drop initially and then a steep increase at the end of each flood. This was again because the gas mixture was not single phase at the start of the flood and more liquid was injected into the core during the end of the flood, which resulted in increasing pressure drop. The pressure drop at the end of the flood was used to calculate the relative permeabilities. **Table B7.5** gives the fluid properties of the synthetic fluid calculated using the Peng-Robinson EOS at the flowing core pressure. **Table B7.6** summarizes the results of the initial two-phase flow.

The core was then treated with a fluoro-surfactant FC4430. **Table B7.7** gives the composition of the treatment solution. **Figure B7.4** shows the measured pressure drop across the core during the injection of 21 pore volumes of treatment solution. The treatment was done at 32 cc/hr and the core was then shut-in for 24 hours.

Post-treatment two-phase of gas-condensate using the same gas mixture was then done under the same conditions as the initial two-phase flow. **Figure B7.5** shows the pressure drop across the core measured during the post-treatment two-phase flow at flowing pressures of 1500 psig. **Table B7.8** summarizes the results of the post-treatment two-phase flow. The results show that the pressure drop for the post-treatment two-phase flood was same as the pre-treatment two-phase flood. Thus, there was no improvement in gas and condensate relative permeability due to surfactant treatment. This was because of couple of reasons, the solvent was not effective in delivering surfactant in the presence of initial water and the core had already been treated before (in experiment -6).

Table B7.1: Core properties

Core	Britannia (Reservoir A), 16/26-B5 13828.6, SPL-B
Length, inches	4.5
Top Section, inches	2.25
Bottom Section, inches	2.25
Diameter, inches	1
Porosity, %	16.90
Pore volume, cc	9.79
Swi, %	26.1
Temperature, °F	275

Table B7.2: Result of methane flood

	Total		Top Section		Bottom Section	
q_{core}, (cc/hr)	ΔP (psi)	k_g (md)	ΔP (psi)	k_g (md)	ΔP (psi)	k_g (md)
1012.48	3.27	56.65	1.49	62.44	1.57	58.97
1446.4	5.00	53.00	2.22	59.80	2.34	56.78
2024.96	7.47	49.66	3.48	53.28	3.39	54.73
Permeability, k_g (md)		53.11		58.5		56.82

Table B7.3: Synthetic Brine

Component	g/l
NaCl	59
CaCl ₂	16
MgCl ₂ .6H ₂ O	3.5

Table B7.4: Result of methane flood at Swi

	Total		Top Section		Bottom Section	
q_{core}, (cc/hr)	ΔP (psi)	k_g (md)	ΔP (psi)	k_g (md)	ΔP (psi)	k_g (md)
1184.79	4.00	43.84	2.02	43.29	1.69	51.71
1692.56	5.95	42.17	3.03	41.38	2.5	50.05
2369.59	8.79	39.94	4.52	38.82	3.66	47.99
Permeability, k_g (md)		41.98		41.16		49.91

Table B7.5: Synthetic fluid properties at experimental conditions

Pressure, psig	5150	1500	
Fluid Properties		Gas phase	Oil phase
ρ, g/cc	0.2197	0.0614	0.6015
μ (cp)		0.0165	0.2615
Volume fraction		0.9787	0.0213
IFT (dyne/cm)		5.168	

Table B7.6: Results of initial two-phase flow of gas condensate mixture

	Total	Top Section	Bottom Section
q_{pump}, cc/hr	192	192	192
q_{total_core}, cc/hr	567.44	567.44	567.44
q_{g_core}, cc/hr	555.35	555.35	555.35
q_{o_core}, cc/hr	12.09	12.09	12.09
ΔP, psi	25.81	12.24	11.04
k_{rg}	0.062	0.065	0.072
k_{ro}	0.021	0.022	0.025
Nc	$1.15 \cdot 10^{-5}$	$1.44 \cdot 10^{-5}$	$1.29 \cdot 10^{-5}$
PVT Ratio	2.89		

Table B7.7: Composition of treatment solution

Component	Weight %
FC4430	2
Methanol	88
D.I. water	10

Table B7.8: Results of post-treatment two-phase flow of gas condensate mixture

q_{pump}, cc/hr	192
q_{total_core}, cc/hr	567.44
q_{g_core}, cc/hr	555.35
q_{o_core}, cc/hr	12.09
ΔP, psi	23.83
k_{rg}	0.067
k_{ro}	0.023
Nc	1.40*10 ⁻⁵
Improvement Factor	1.08

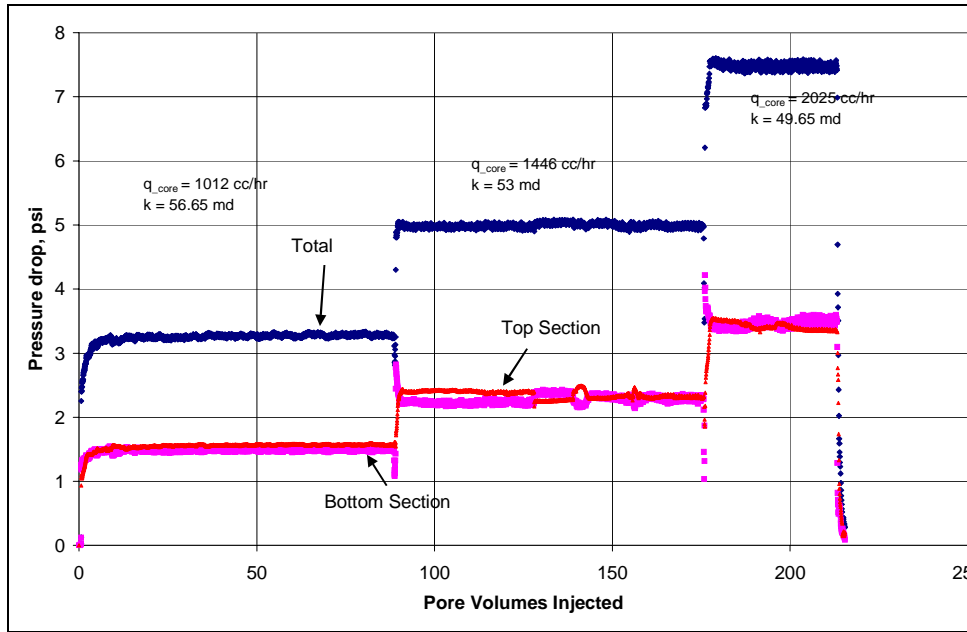


Figure B7.1: Pressure drop across the core and the sections during initial methane flood

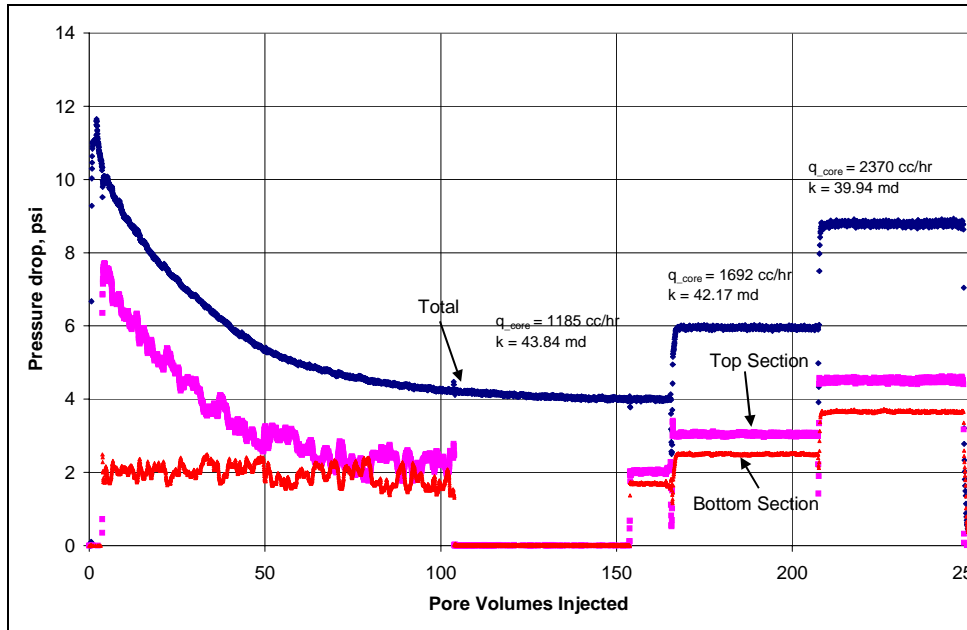


Figure B7.2: Pressure drop across the core and the sections during methane flood at $S_{wi}=26.1\%$

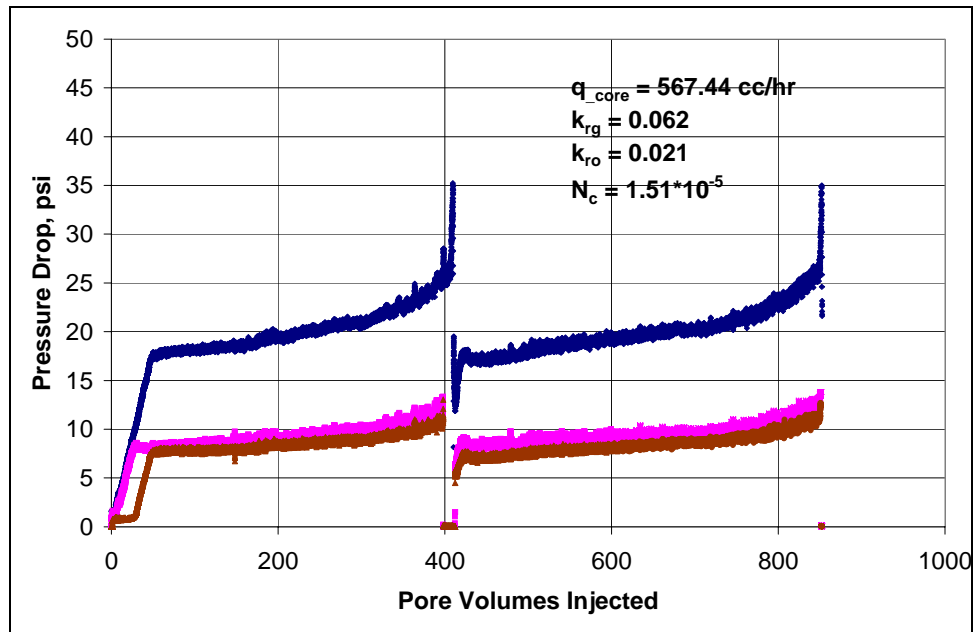


Figure B7.3: Pressure drop across the core and the sections during the initial two-phase flow at 275°F and 1500 psig

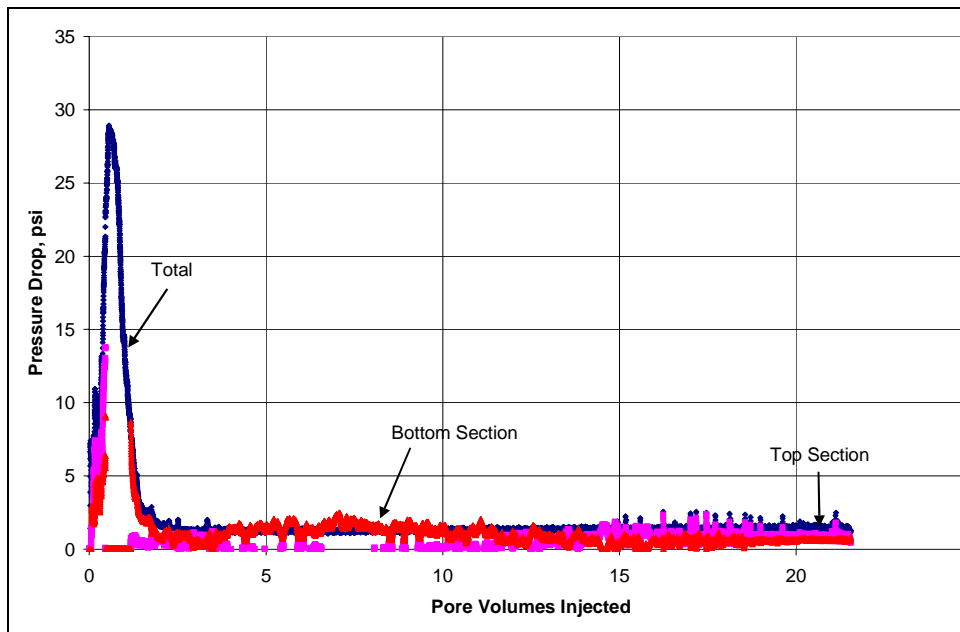


Figure B7.4: Pressure drop across the core and the sections during surfactant treatment

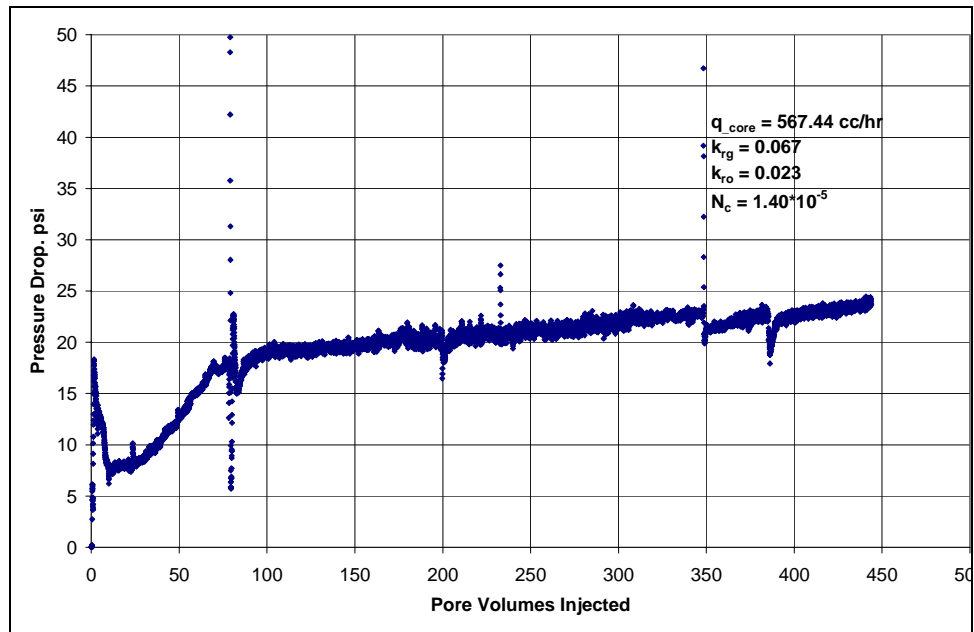


Figure B7.5: Pressure drop across the core and the sections during post-treatment two-phase flow at 275°F and 1500 psig

B8- Experiment No.8

Objective:

The objective of this experiment was to investigate the effect of non-ionic polymeric fluoro-surfactant FC4430 treatment in improving the gas and condensate relative permeability on a Berea sandstone rock in presence of initial water. The experiment was performed at 275°F.

Experimental Results:

Table B8.1 summarizes the properties of the core and the experimental conditions. Initial permeability of the core was measured using methane at 72°F. **Figure B8.1** shows the methane flood pressure total drop measured across the plug and across the top and bottom section. **Table B8.2** summarizes the results of the methane flood.

The initial water saturation of 26.1% was established by injecting 2.6 cc of brine in the vacuumed core. **Table B8.3** gives the composition of the synthetic brine used in this experiment. The pressure of the core was raised to 500 psig and then the temperature of the oven was increased to 275°F. This was done to avoid any vaporization of water at high temperature. Methane flood was then done to measure the end point gas permeability. **Figure B8.2** shows the methane flood pressure drop measured across the core and the sections. **Table B8.4** summarizes the results of the methane flood.

Synthetic fluid mixture-2 (Table 3.2) was used for the two-phase flow measurements. The initial flood was done with the upstream backpressure regulator set at 4650 psig and the downstream back pressure regulator set at 1550 psig. **Table B6.5** gives the fluid properties of the synthetic fluid calculated using the Peng-Robinson EOS at the flowing core pressure. **Figure B8.3** shows the pressure drop across the core and the

sections for the two-phase gas-condensate flow. **Table B8.6** summarizes the results of the initial two-phase flow.

Nine pore volumes of methanol/water (90/10) mixture was flowed thorough the core after the initial gas condensate two-phase flood. The pre-flush of methanol/water mixture was conducted before chemical treatment to flush out brine from the core. **Figure B8.4** shows the measured pressure drop across the core during pre-flush. The core was then treated with a fluoro-surfactant FC4430. **Table B8.7** gives the composition of the treatment solution. **Figure B8.5** shows the measured pressure drop across the core during the injection of 19 pore volumes of the treatment solution. The treatment was flowed at 32 cc/hr and the core was then shut-in for 24 hours.

Post-treatment two-phase of gas-condensate using the same gas mixture was then done under the same conditions as the initial two-phase flow. **Figure B8.6** shows the pressure drop across the core measured during the post-treatment two-phase flow at flowing pressures of 1500 psig. **Table B8.8** summarizes the results of the post-treatment two-phase flow. No improvement was observed due to chemical treatment.

Table B8.1: Core properties

Core	Berea Sandstone
Length, inches	8
Diameter, inches	1
Porosity, %	20.00
Pore volume, cc	20.59
Swi, %	26.1
Temperature, °F	275

Table B8.2: Result of methane flood

q_{core} , (cc/hr)	ΔP (psi)	k_g (md)
2420.14	6.08	129.55
1210.07	2.85	138.22
1728.67	4.27	131.89
Permeability, k_g (md)		130.31

Table B8.3: Synthetic Brine

Component	g/l
NaCl	59
CaCl ₂	16
MgCl ₂ .6H ₂ O	3.5

Table B8.4: Result of methane flood at Swi

q_{core}, (cc/hr)	ΔP (psi)	k_g (md)
1261.58	4.57	109.23
1802.26	6.61	108.04
Permeability, k_g (md)		108.64

Table B8.5: Synthetic fluid properties at experimental conditions

Pressure, psig	4750	1500	
Fluid Properties		Gas phase	Oil phase
ρ, g/cc	0.2082	0.0614	0.6015
μ (cp)		0.0165	0.2615
Volume fraction		0.9787	0.0213
IFT (dyne/cm)		5.168	

Table B8.6: Results of initial two-phase flow of gas condensate mixture

q_{pump}, cc/hr	128
q_{total_core}, cc/hr	364.58
q_{g_core}, cc/hr	356.82
q_{o_core}, cc/hr	7.77
ΔP, psi	7.77
k_{rg}	0.093
k_{ro}	0.032
Nc	6.56x10 ⁻⁶
PVT Ratio	2.90

Table B8.7: Composition of treatment solution

Component	Weight %
FC4430	2
Methanol	94
D.I. water	4

Table B8.8: Results of post-treatment two-phase flow of gas condensate mixture

q_{pump}, cc/hr	128
q_{total_core}, cc/hr	364.58
q_{g_core}, cc/hr	356.82
q_{o_core}, cc/hr	7.77
ΔP, psi	7.42
k_{rg}	0.097
k_{ro}	0.034
Nc	6.27x10 ⁻⁶
Improvement Factor	1.05

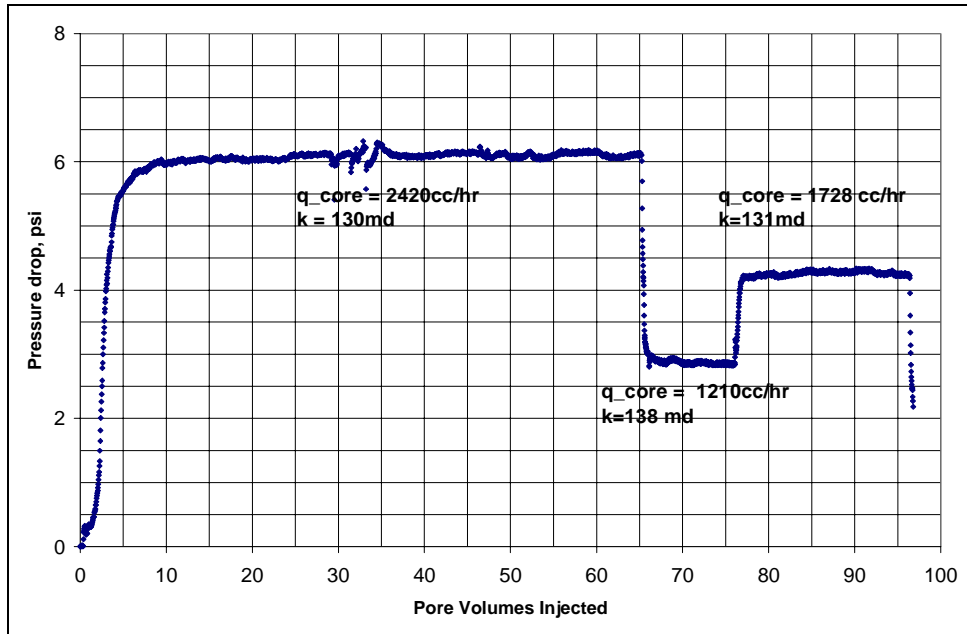


Figure B8.1: Pressure drop across the core during initial nitrogen flood

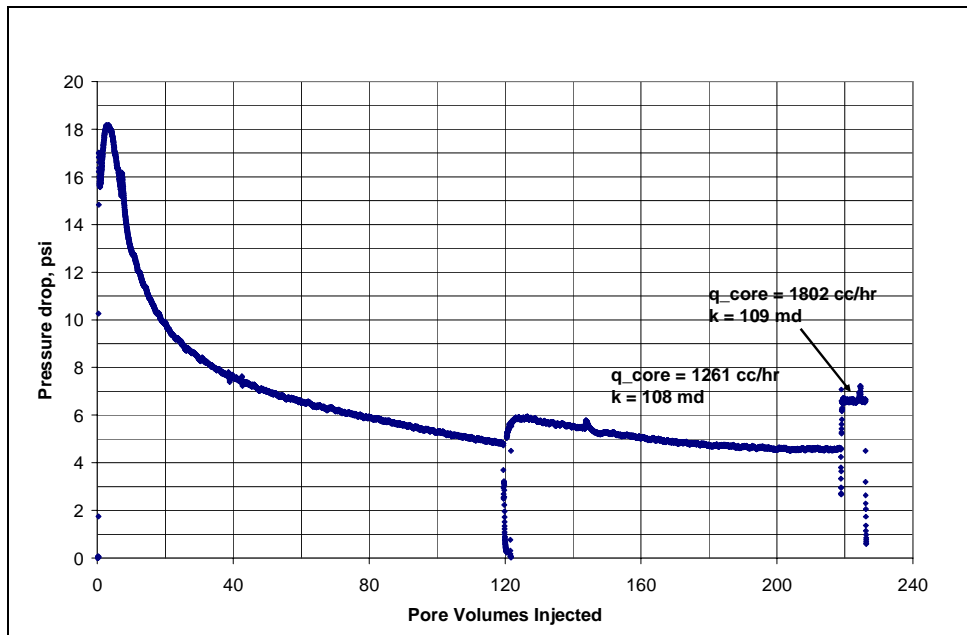


Figure B8.2: Pressure drop across the core during methane flood at $S_{wi}=26.1\%$

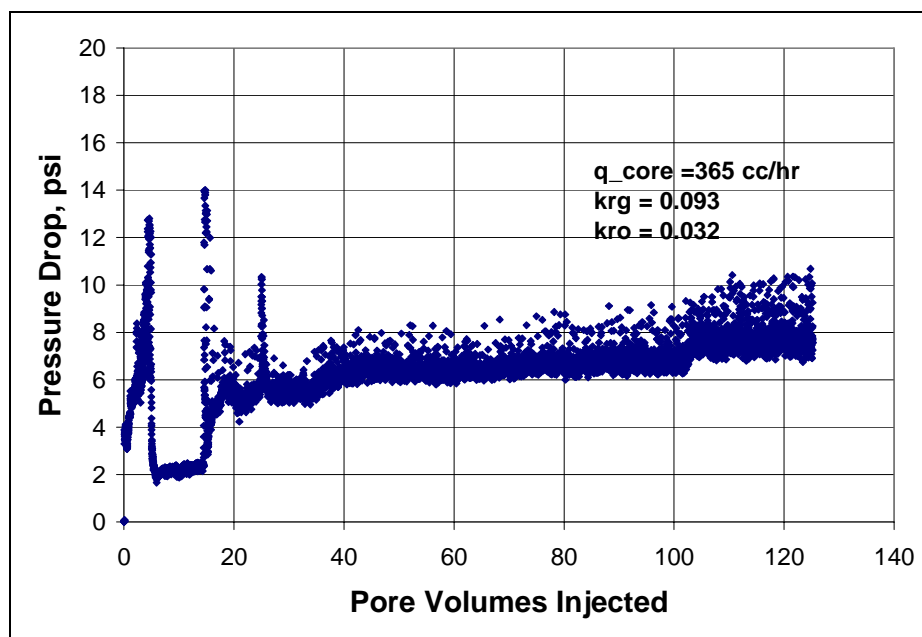


Figure B8.3: Pressure drop across the core during the initial two-phase flow at 275°F and 1500 psig

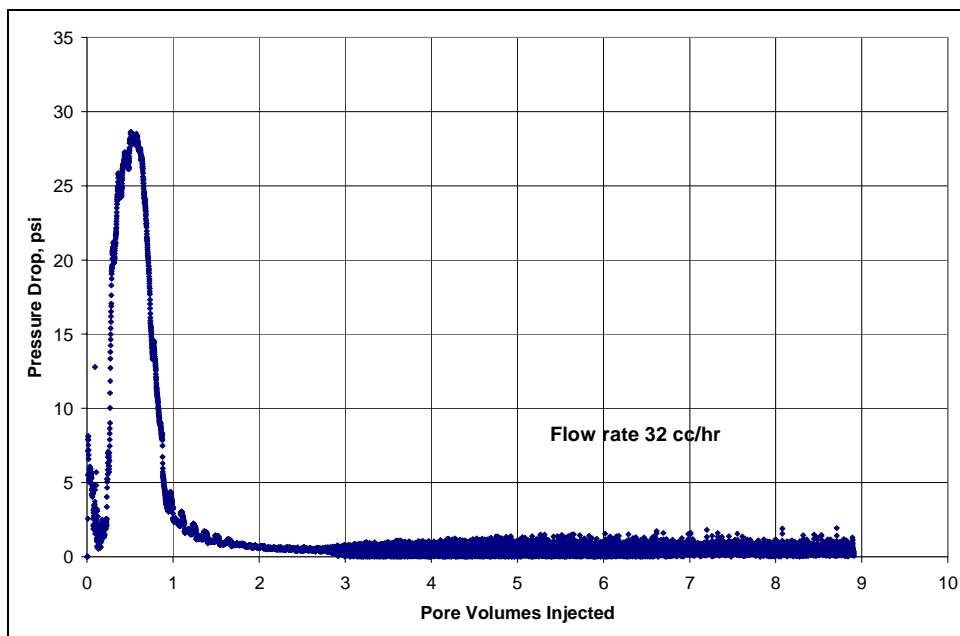


Figure B8.4: Pressure drop across the core during solvent preflush

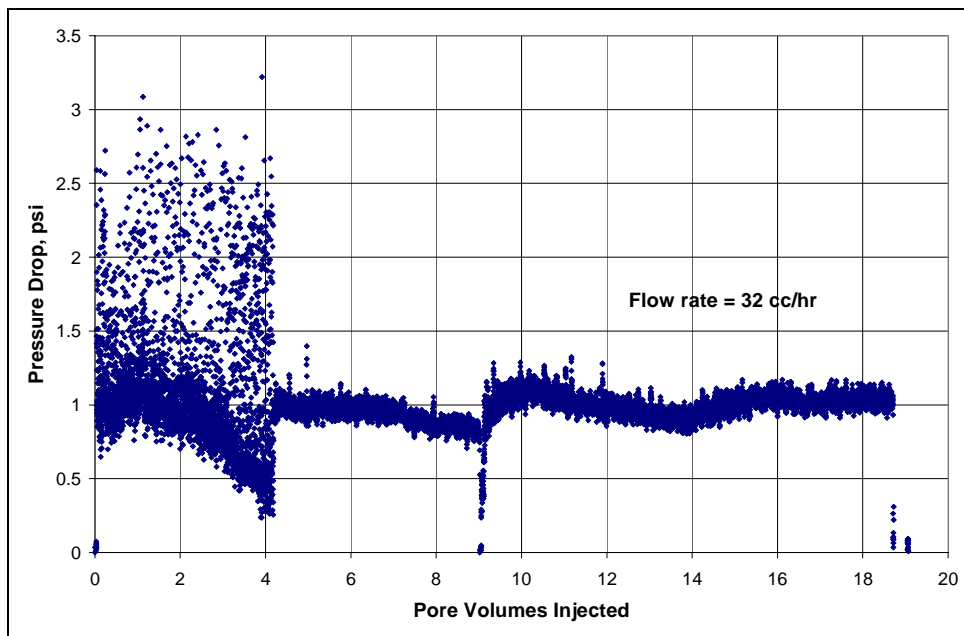


Figure B8.5: Pressure drop across the core during surfactant treatment

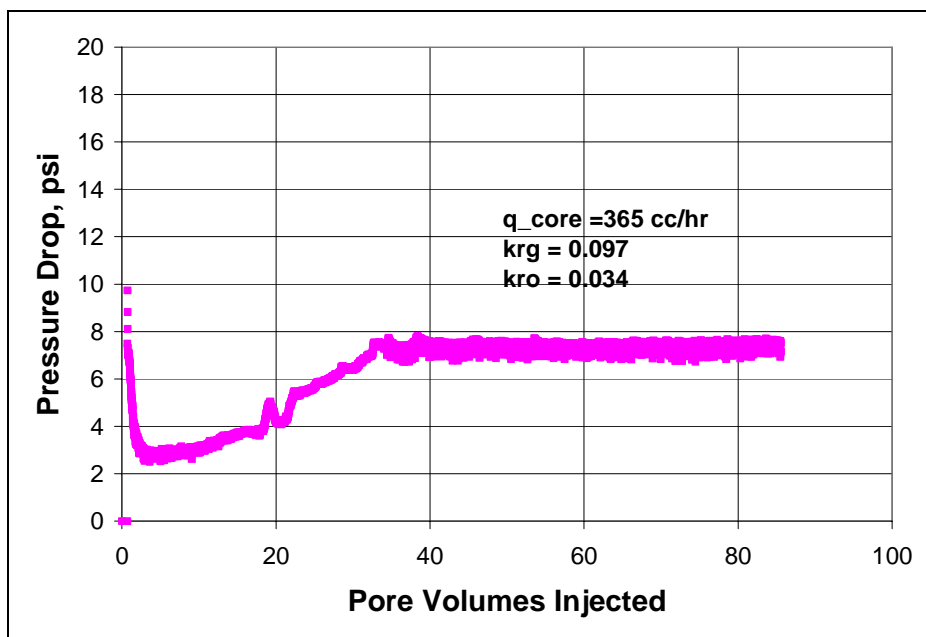


Figure B8.6: Pressure drop across the core and the sections during post-treatment two-phase flow at 275°F and 1500 psig

B9- Experiment No.9

Objective:

The objective of this experiment was to investigate the effect of non-ionic polymeric fluoro-surfactant FC4430 treatment in improving the gas and condensate relative permeability on a Berea sandstone rock in presence of initial water. The experiment was performed at 275°F.

Experimental Results:

Table B9.1 summarizes the properties of the core and the experimental conditions. Initial permeability of the core was measured using nitrogen at 75°F. **Figure B9.1** shows the pressure drop measured across the core during nitrogen flood. **Table B9.2** summarizes the results of the nitrogen flood.

The initial water saturation of 26.1% was established by injecting 2.6 cc of water in the vacuumed core. Nitrogen flood was then conducted to measure the gas end point relative permeability. **Figure B9.2** shows the pressure drop measured across the core. **Table B9.3** summarizes the results of the nitrogen flood. The pressure of the core was raised to 500 psig and then the temperature of the oven was increased to 275°F.

Synthetic fluid mixture-2 (Table 3.2) was used for the two-phase flow measurements. The initial flood was conducted with the upstream backpressure regulator set at 4650 psig and the downstream back pressure regulator set at 1500 psig. **Table B9.4** gives the fluid properties of the synthetic fluid calculated using the Peng-Robinson EOS at the flowing core pressure. **Figure B9.3** shows the pressure drop across the core during the two-phase gas-condensate flow. **Table B9.5** summarizes the results of the initial two-phase flow.

Nine pore volumes of methanol were flowed thorough the core after the initial gas condensate two-phase flood. The pre-flush of methanol was conducted before chemical treatment to flush out water from the core. **Figure B9.4** shows the measured pressure drop across the core during pre-flush. The core was then treated with a fluoro-surfactant FC4430. **Table B9.6** gives the composition of the treatment solution. **Figure B9.5** shows the measured pressure drop across the core during the treatment flood. The treatment solution was injected at 32 cc/hr and the core was then shut-in for 24 hours.

Post-treatment two-phase gas-condensate flood was then conducted under the same conditions as the initial two-phase flow. **Figure B9.6** shows the pressure drop across the core measured during the post-treatment two-phase flow at a flowing pressure of 1500 psig. **Table B9.7** summarizes the results of the post-treatment two-phase flow. No improvement was observed due to chemical treatment.

Table B9.1: Core properties

Core	Berea Sandstone
Length, inches	8
Diameter, inches	1
Porosity, %	20.00
Pore volume, cc	20.59
Swi, %	26.1
Temperature, °F	275

Table B9.2: Result of nitrogen flood

q_{core}, (cc/hr)	ΔP (psi)	k_g (md)
1805.94	2.59	227.27
902.97	1.266	232.32
1289.96	1.79	234.66
Permeability, k_g (md)		232.70

Table B9.3: Result of nitrogen flood at Swi

q_{core}, (cc/hr)	ΔP (psi)	k_g (md)
1261.58	4.57	109.23
1802.26	6.61	108.04
Permeability, k_g (md)		108.64

Table B9.4: Synthetic fluid properties at experimental conditions

Pressure, psig	4500	1500	
Fluid Properties		Gas phase	Oil phase
ρ, g/cc	0.2067	0.0614	0.6015
μ (cp)		0.0165	0.2615
Volume fraction		0.9787	0.0213
IFT (dyne/cm)		5.168	

Table B9.5: Results of initial two-phase flow of gas condensate mixture

q_{pump}, cc/hr	192	320
$q_{\text{total_core}}$, cc/hr	542.94	904.89
$q_{\text{g_core}}$, cc/hr	531.37	885.62
$q_{\text{o_core}}$, cc/hr	11.56	19.27
ΔP, psi	7.36	14.05
k_{rg}	0.084	0.074
k_{ro}	0.029	0.025
Nc	1.11×10^{-5}	2.12×10^{-5}
PVT Ratio	2.90	2.90

Table B9.6: Composition of treatment solution

Component	Weight %
FC4430	2
Methanol	94
D.I. water	4

Table B9.7: Results of post-treatment two-phase flow of gas condensate mixture

q_{pump}, cc/hr	192
q_{total_core}, cc/hr	542.94
q_{g_core}, cc/hr	531.37
q_{o_core}, cc/hr	11.56
ΔP, psi	7.28
k_{rg}	0.085
k_{ro}	0.029
Nc	1.10x10 ⁻⁵
Improvement Factor	1.01

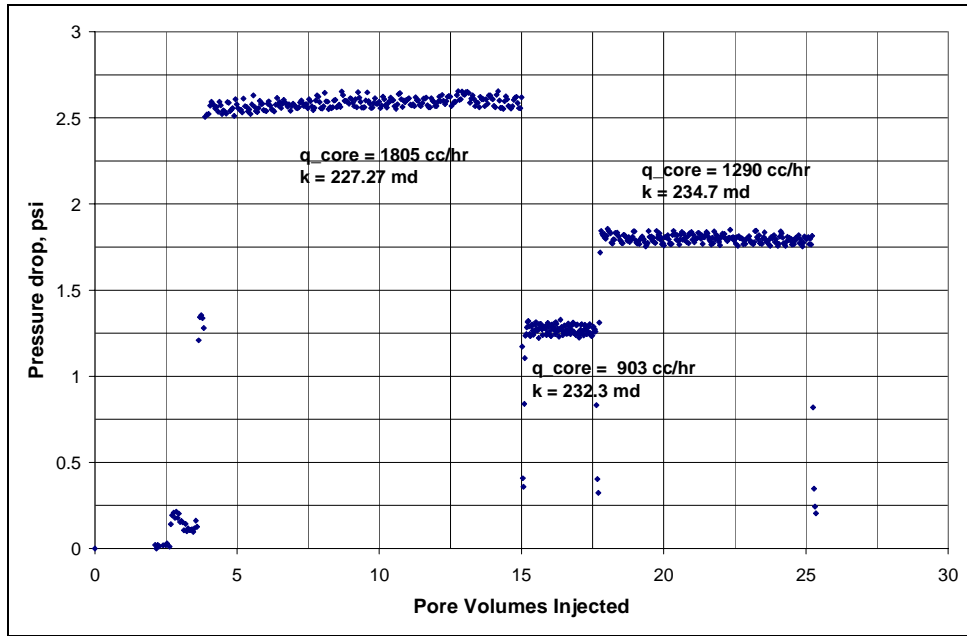


Figure B9.1: Pressure drop across the core during initial nitrogen flood

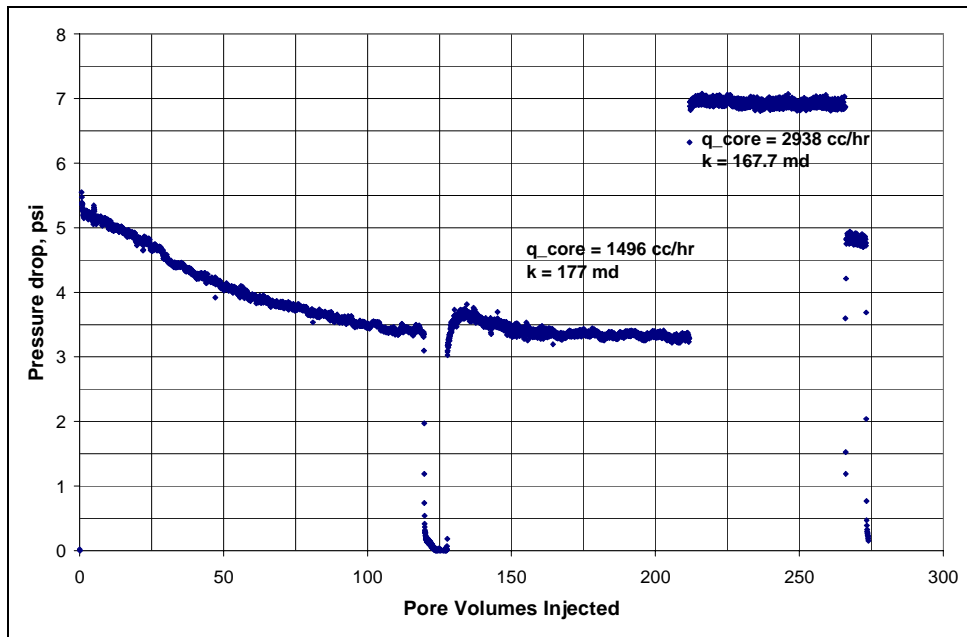


Figure B9.2: Pressure drop across the core during nitrogen flood at $S_{wi}=26.1\%$

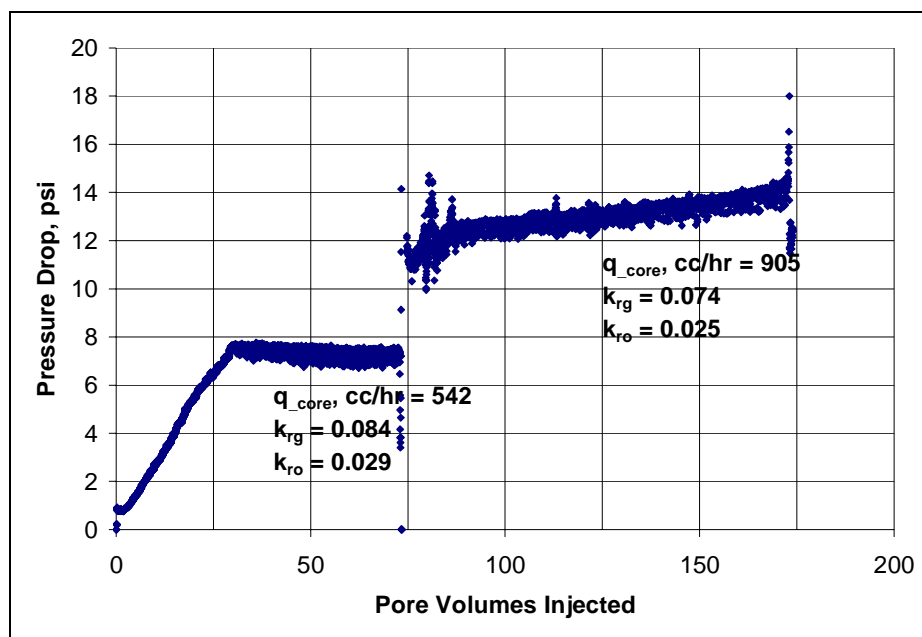


Figure B9.3: Pressure drop across the core during the initial two-phase flow at 275°F and 1500 psig

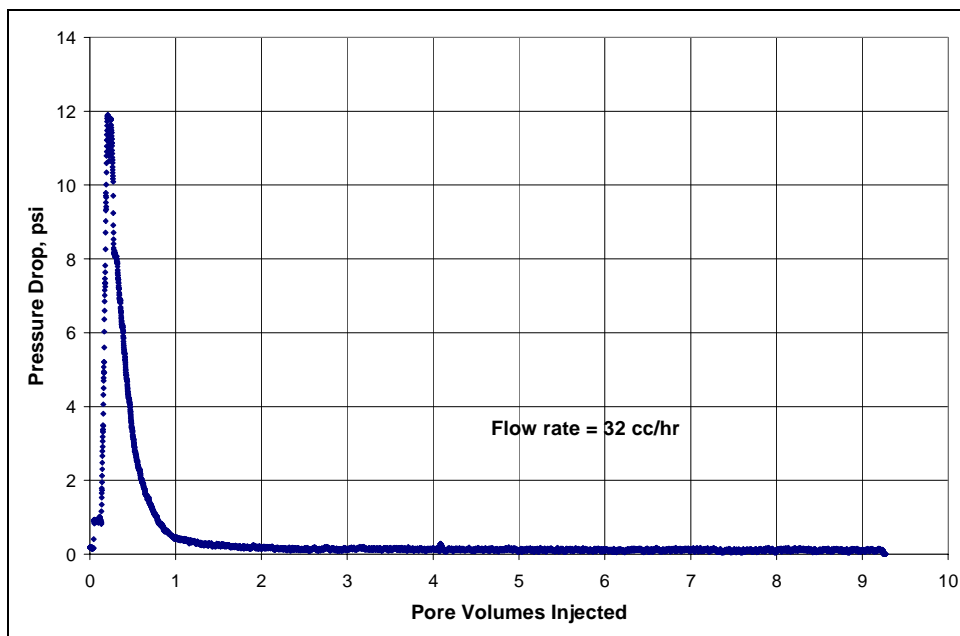


Figure B9.4: Pressure drop across the core during solvent preflush

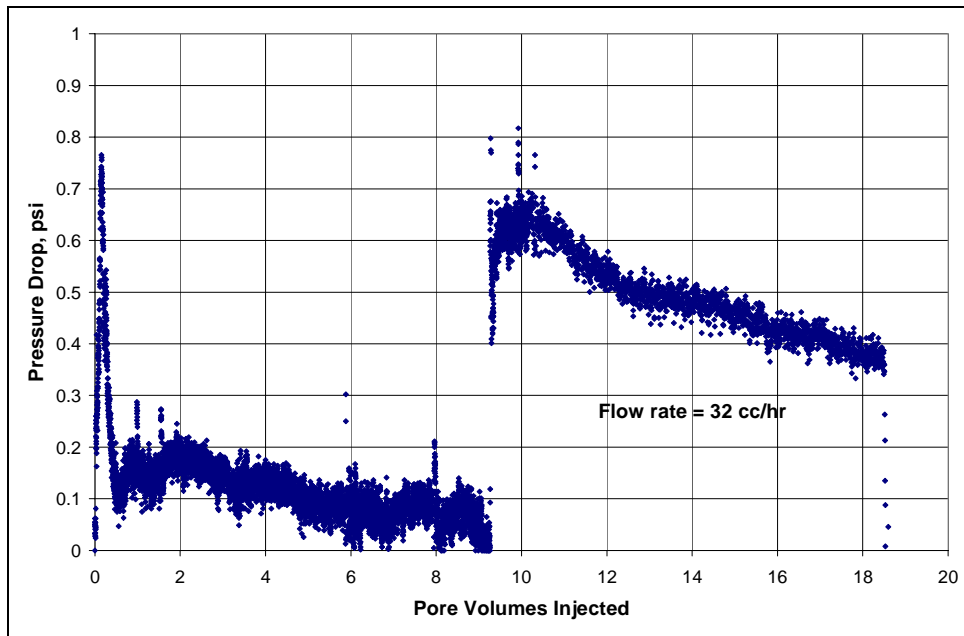


Figure B9.5: Pressure drop across the core during surfactant treatment

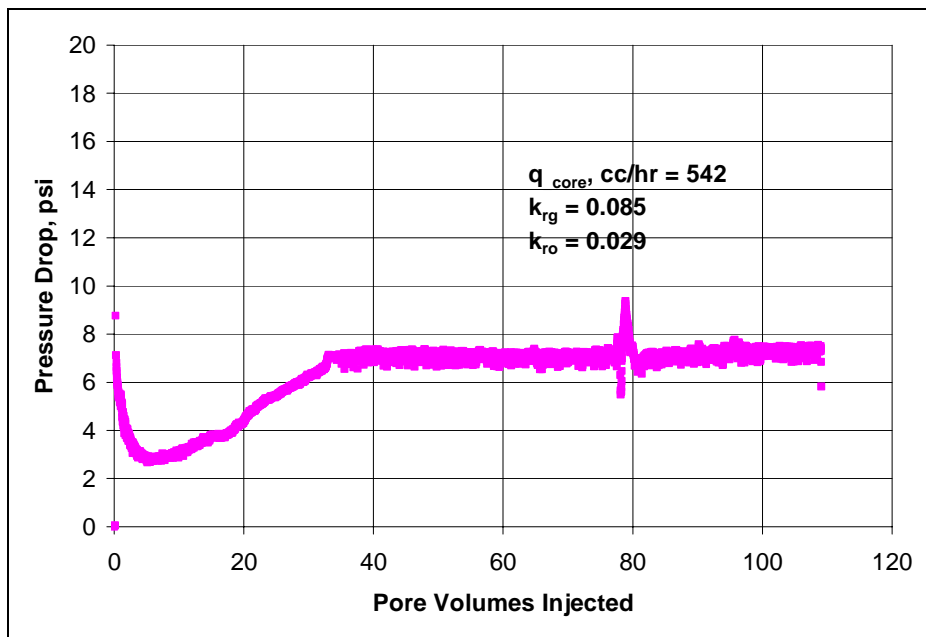


Figure B9.6: Pressure drop across the core during post-treatment two-phase flow at 275°F and 1500 psig

B10- Experiment No.10

Objective:

The objective of this experiment was to investigate the effect of non-ionic polymeric fluoro-surfactant FC4430 treatment in improving the gas and condensate relative permeability on a reservoir sandstone rock in presence of initial water. The experiment was performed at 275°F on a Britannia reservoir core (plug #16/26-B5).

Experimental Results:

Table B10.1 summarizes the properties of the core and the experimental conditions. Initial permeability of the core was measured using methane at 72°F. **Figure B10.1** shows the methane flood pressure total drop measured across the plug and across the top and bottom section. **Table B10.2** summarizes the results of the methane flood.

The initial water saturation was established by injecting 20 PV of brine into the core and then displacing it with nitrogen to reduce the water saturation to residual. **Table B10.3** gives the composition of the synthetic brine used in this experiment. **Figure B10.2** shows the nitrogen flood pressure drop measured across the core. **Table B10.4** summarizes the results of the nitrogen flood. The pressure of the core was raised to 500 psig and then the temperature of the oven was increased to 275°F.

Synthetic fluid mixture-2 (Table 3.2) was used for the two-phase flow measurements. The initial flood was done with the upstream backpressure regulator set at 4500 psig and the downstream back pressure regulator set at 1500 psig. **Table B10.5** gives the fluid properties of the synthetic fluid calculated using the Peng-Robinson EOS at the flowing core pressure. **Figure B10.3** shows the pressure drop across the core for

the two-phase gas-condensate flow. **Table B10.6** summarizes the results of the initial two-phase flow.

The core was then treated with a fluoro-surfactant FC4430. **Table B10.7** gives the composition of the treatment solution. **Figure B10.4** shows the measured pressure drop across the core during the injection of 20 pore volumes of the treatment solution. The treatment was flowed at 32 cc/hr and the core was then shut-in for 24 hours.

Post-treatment two-phase gas-condensate flow was conducted using the same gas mixture under the same conditions as the initial two-phase flow. **Figure B10.5** shows the pressure drop across the core measured during the post-treatment two-phase flow at flowing pressures of 1500 psig. **Table B10.8** summarizes the results of the post-treatment two-phase flow. No improvement was observed due to chemical treatment.

The core was re-treated with the treatment solution given in **Table B10.7**. 20 pore volumes of treatment solution was flowed through the core at 32 cc/hr and the core was then shut-in for 24 hours. **Figure B10.6** shows the pressure drop across the core during the treatment flood.

Post second treatment two-phase gas-condensate flow was conducted using the same gas mixture under the same conditions as the initial two-phase flow. **Figure B10.7** shows the pressure drop across the core measured during the post-treatment two-phase flow at flowing pressures of 1500 psig. **Table B10.9** summarizes the results of the post-treatment two-phase flow. No improvement was observed after the second chemical treatment either.

Table B10.1: Core properties

Core	Britannia (plug 16/26-B5)
Length, inches	4.5
Diameter, inches	1
Porosity, %	16.90
Pore volume, cc	9.79
Swi, %	30-50
Temperature, °F	275

Table B10.2: Result of methane flood

q_{core}, (cc/hr)	ΔP (psi)	k_g (md)
110.3.77	4.59	43.81
2207.53	10.24	39.27
1576.81	6.93	41.52
Permeability, k_g (md)		40.52

Table B10.3: Synthetic Brine

Component	g/l
NaCl	59
CaCl ₂	16
MgCl ₂ .6H ₂ O	3.5

Table B10.4: Result of methane flood at Swi

q_{core}, (cc/hr)	ΔP (psi)	k_g (md)
1103.77	8.63	23.31
2207.54	20.58	19.55
1579.82	13.19	21.79
Permeability, k_g (md)		20.72

Table B10.5: Synthetic fluid properties at experimental conditions

Pressure, psig	4500	1500	
Fluid Properties		Gas phase	Oil phase
ρ, g/cc	0.2006	0.0614	0.6015
μ (cp)		0.0165	0.2615
Volume fraction		0.9787	0.0213
IFT (dyne/cm)		5.168	

Table B10.6: Results of initial two-phase flow of gas condensate mixture

q_{pump}, cc/hr	192
q_{total_core}, cc/hr	528.3
q_{g_core}, cc/hr	517.05
q_{o_core}, cc/hr	11.25
ΔP, psi	26.11
k_{rg}	0.072
k_{ro}	0.025
Nc	1.22x10 ⁻⁵
PVT Ratio	2.90

Table B10.7: Composition of treatment solution

Component	Weight %
FC4430	2
Methanol	94
D.I. water	4

Table B10.8: Results of post-treatment two-phase flow of gas condensate mixture

q_{pump}, cc/hr	192
q_{total_core}, cc/hr	528.3
q_{g_core}, cc/hr	517.05
q_{o_core}, cc/hr	11.25
ΔP, psi	22.68
k_{rg}	0.083
k_{ro}	0.029
Nc	1.06x10 ⁻⁵
Improvement Factor	1.15

Table B10.9: Results of post second treatment two-phase flow of gas condensate mixture

q_{pump}, cc/hr	192
q_{total_core}, cc/hr	528.3
q_{g_core}, cc/hr	517.05
q_{o_core}, cc/hr	11.25
ΔP, psi	26.26
k_{rg}	0.072
k_{ro}	0.025
Nc	1.23x10 ⁻⁵
Improvement Factor	0.99

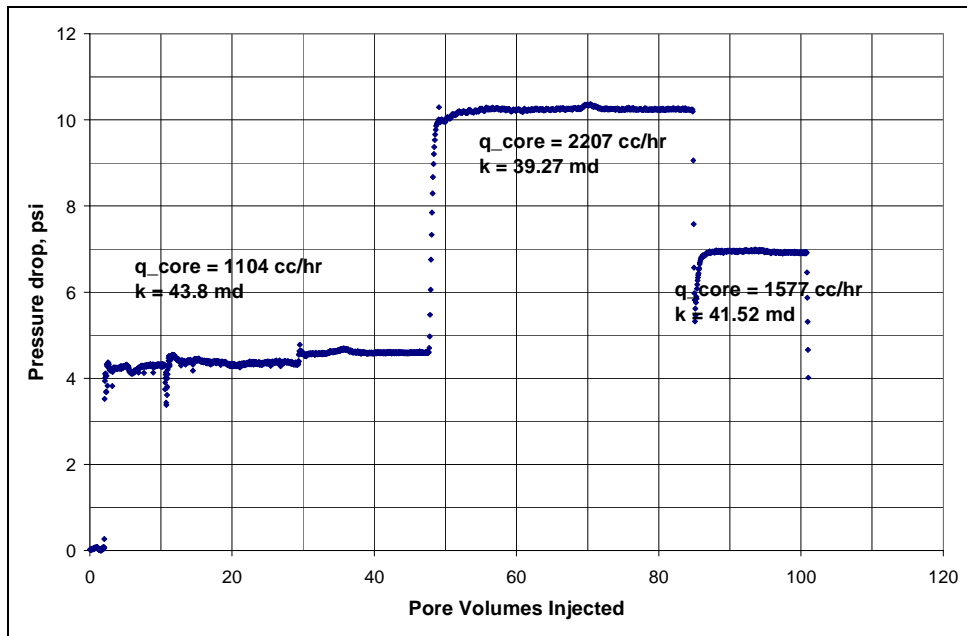


Figure B10.1: Pressure drop across the core during initial nitrogen flood

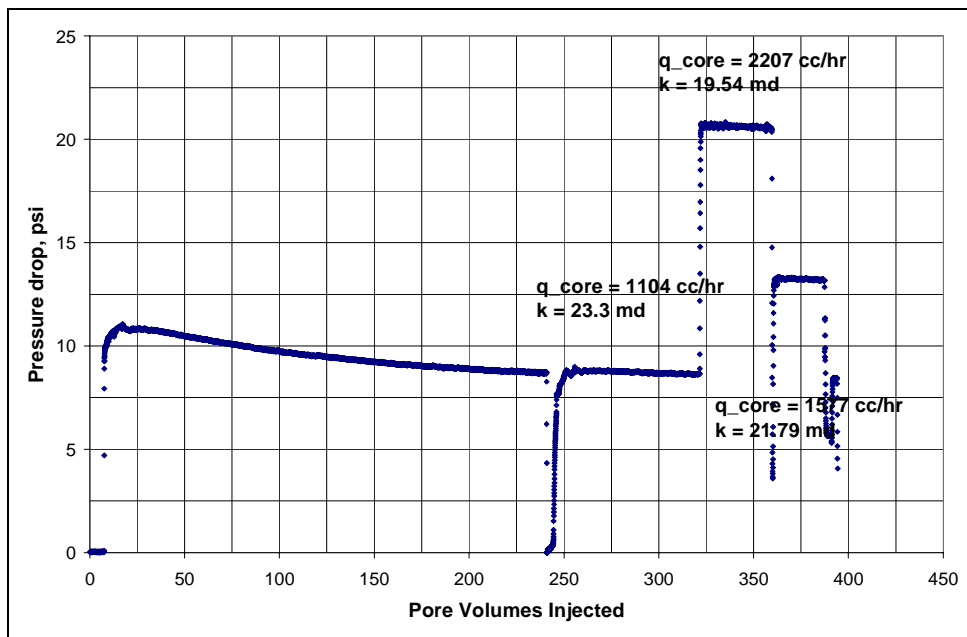


Figure B10.2: Pressure drop across the core during nitrogen flood at Sw_i

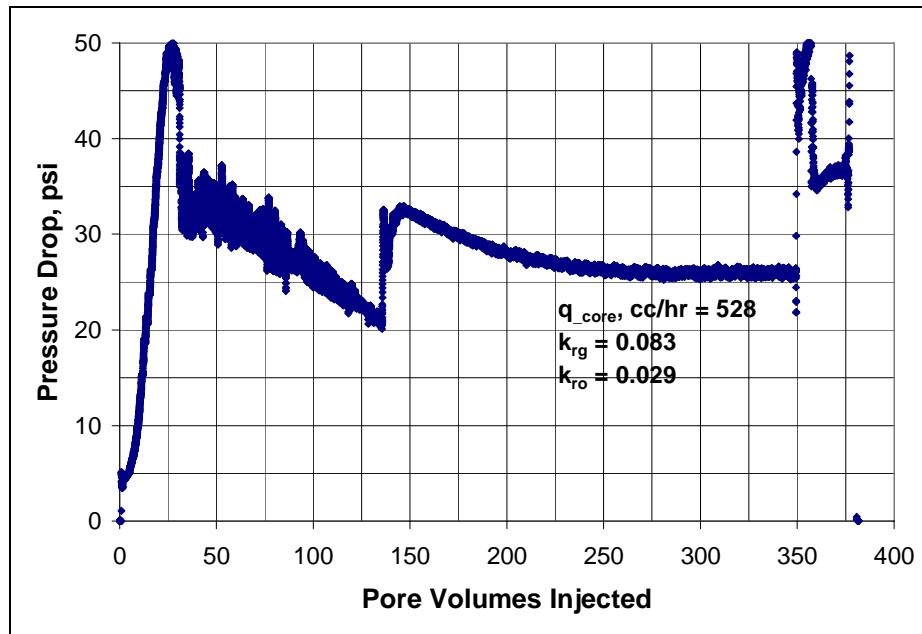


Figure B10.3: Pressure drop across the core during the initial two-phase flow at 275°F and 1500 psig

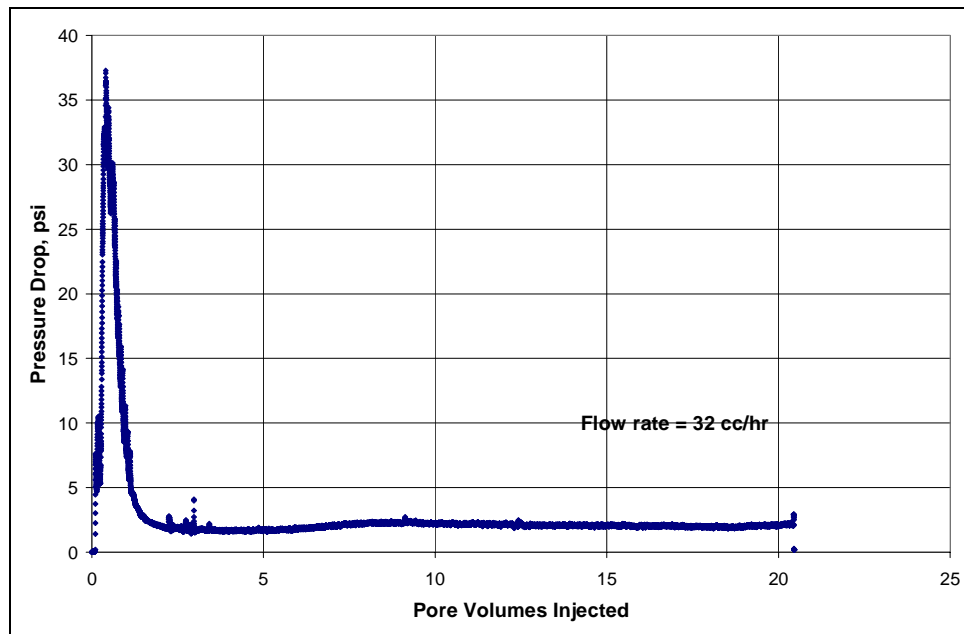


Figure B10.4: Pressure drop across the core during first surfactant treatment

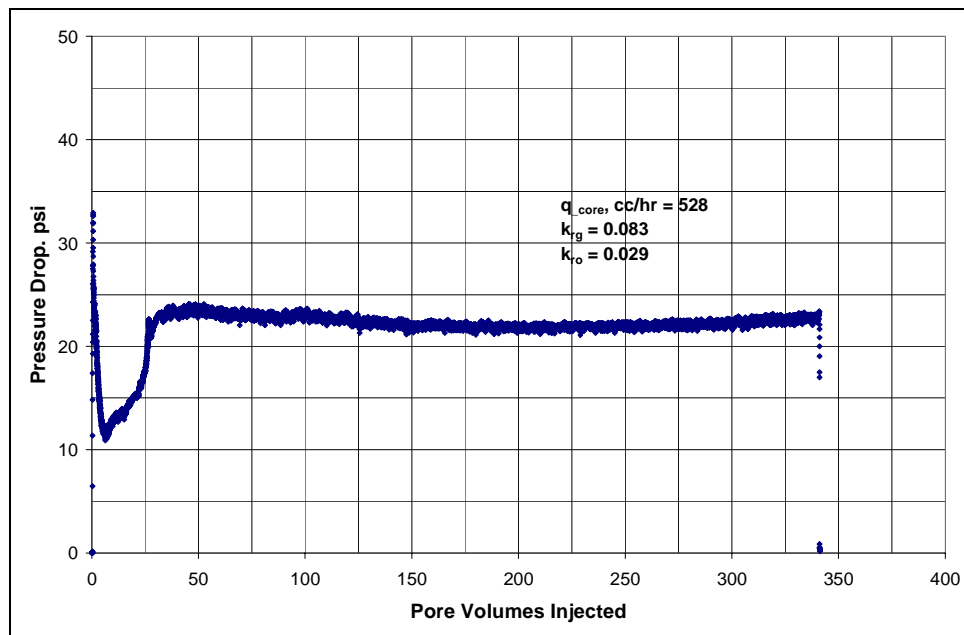


Figure B10.5: Pressure drop across the core during post-treatment two-phase flow at 275°F and 1500 psig

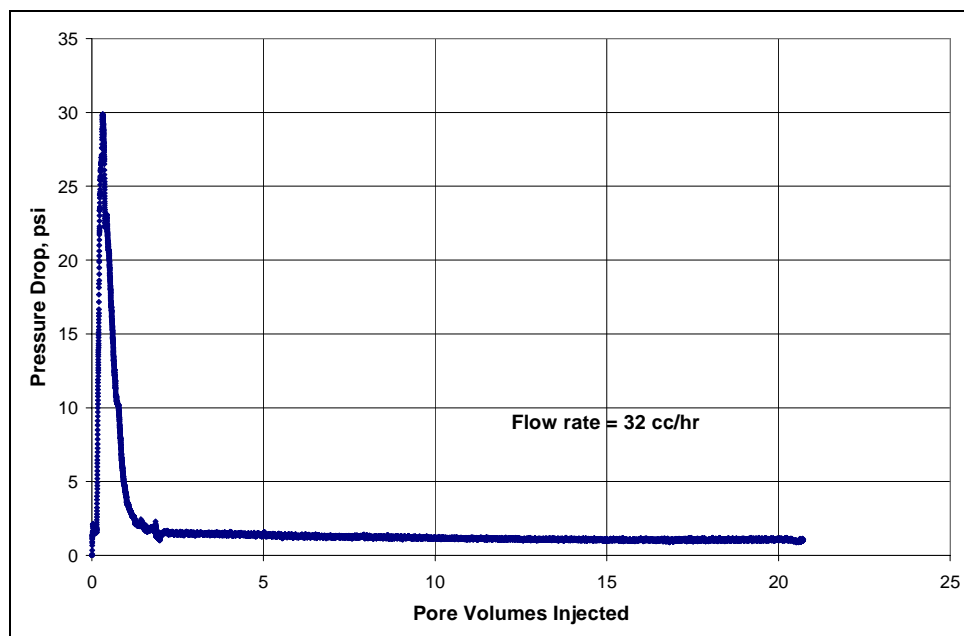


Figure B10.6: Pressure drop across the core during second surfactant treatment

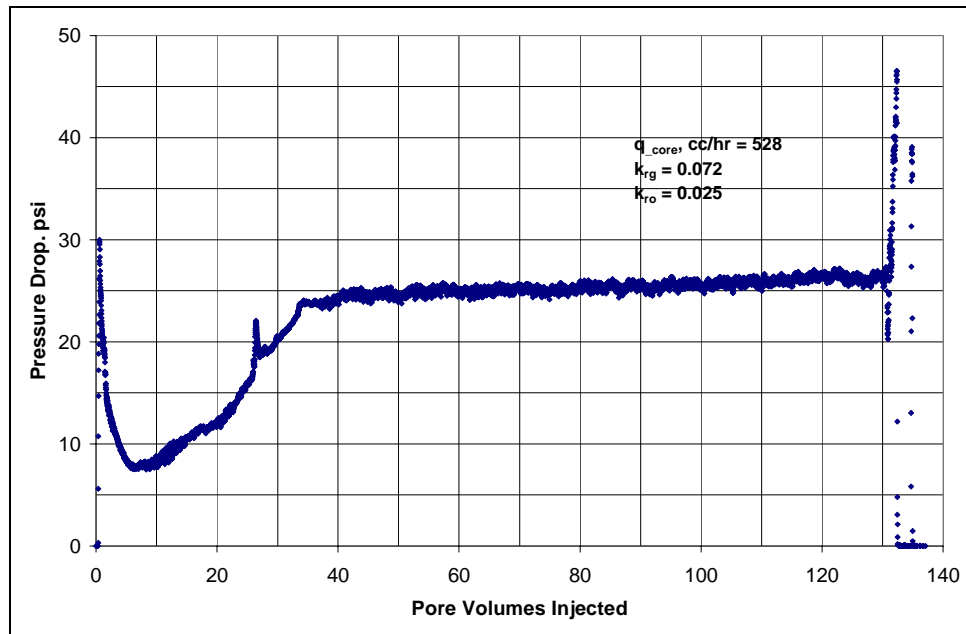


Figure B10.7: Pressure drop across the core during post-second treatment two-phase flow at 275°F and 1500 psig

B11- Experiment No.11

Objective:

The objective of this experiment was to test the effect of non-ionic polymeric fluoro-surfactant FC4430 treatment in improving the gas and condensate relative permeability on a dry sandstone rock and test the durability of the treatment at high temperature. The experiment was performed on Berea sandstone core at 250°F.

Experimental Results:

Table B11.1 summarizes the properties of the core and the experimental conditions. Initial permeability of the core was measured using nitrogen at 75°F. **Figure B11.1** shows the methane flood pressure total drop measured across the core. **Table B11.2** summarizes the results of the nitrogen flood.

Two-phase gas condensate floods were conducted using synthetic fluid mixture-3 (Table 3.3) at 250°F. The initial flood was conducted with the upstream backpressure regulator set at 4200 psig and the downstream back pressure regulator set at 1500 psig. **Table B11.3** gives the fluid properties of the synthetic fluid calculated using the Peng-Robinson EOS at the flowing core pressure. **Figure B11.2** shows the pressure drop across the core for the two-phase gas-condensate flood. **Table B11.4** summarizes the results of the initial two-phase flow.

The core was then treated with a fluoro-surfactant FC4430. **Table B11.5** gives the composition of the treatment solution. **Figure B11.3** shows the measured pressure drop across the core during the treatment flood. 20 PV of treatment solution was injected at 64 cc/hr and the core was then shut-in for 24 hours.

Post-treatment two-phase gas-condensate flow was conducted using the same gas mixture under the same conditions as the initial two-phase flow. To test the durability of the chemical treatment, multiple batches of post-treatment gas condensate floods were done. Figure B11.4 shows the pressure drop across the core measured during the post-treatment two-phase floods at flowing pressures of 1500 psig. Total of about 1060 pore volumes of gas mixture was flown through the core and the actual flowing time was 34 hours. The absolute time, actual time from the first post-treatment gas condensate flood to the last flood, was 231 hours. Table B11.6 summarizes the results of the post-treatment two-phase flow. Table B11.7 summarizes the results of all the post-treatment two-phase floods.

Table B11.1: Core properties and Experimental conditions

Core	Berea Sandstone
Length, inches	8
Diameter, inches	1
Porosity, %	20.0
Pore volume, cc	20.59
Swi, %	0
Temperature, °F	250

Table B11.2: Result of methane flood

q_{core}, (cc/hr)	ΔP (psi)	k_g (md)
1163.7	1.86	202.17
2327.40	3.98	189.55
4662.43	2.74	196.78
Permeability, k_g (md)		196.17

Table B11.3: Synthetic fluid properties at experimental conditions

Pressure, psig	4200	1500	
Fluid Properties		Gas phase	Oil phase
ρ , g/cc	0.2998	0.0711	0.5544
μ (cp)		0.0165	0.1651
Volume fraction		0.8989	0.1011
IFT (dyne/cm)		4.473	

Table B11.4: Results of initial two-phase flow of gas condensate mixture

q_{pump}, cc/hr	256
q_{total_core}, cc/hr	639.78
q_{g_core}, cc/hr	575.10
q_{o_core}, cc/hr	64.68
ΔP, psi	22.80
k_{rg}	0.035
k_{ro}	0.039
Nc	3.25×10^{-5}
PVT Ratio	0.89

Table B11.5: Composition of treatment solution

Component	Weight %
FC4430	2
Methanol	94
D.I. water	4

Table B11.6: Results of post-treatment two-phase flow of gas condensate mixture

q_{pump}, cc/hr	256
q_{total_core}, cc/hr	639.78
q_{g_core}, cc/hr	575.10
q_{o_core}, cc/hr	64.68
ΔP, psi	22.80
k_{rg}	0.066
k_{ro}	0.074
Nc	1.72x10 ⁻⁵
Improvement Factor	1.89

Table 11.7 summary of all the post-treatment two-phase floods

Post-treatment gas condensate flood	Pore Volumes Flowed	Cumulative flowing time, hrs	Absolute Time, hrs	Improvement Factor
1	105	3.60	3.6	2.78
2	248	8.10	14	2.28
3	361	11.65	64	2.09
4	466	15.30	80	2.07
5	580	18.95	86	1.93
6	692	22.55	101	1.92
7	810	26.06	126	1.88
8	950	30.56	135	1.94
9	1060	34.13	232	1.81

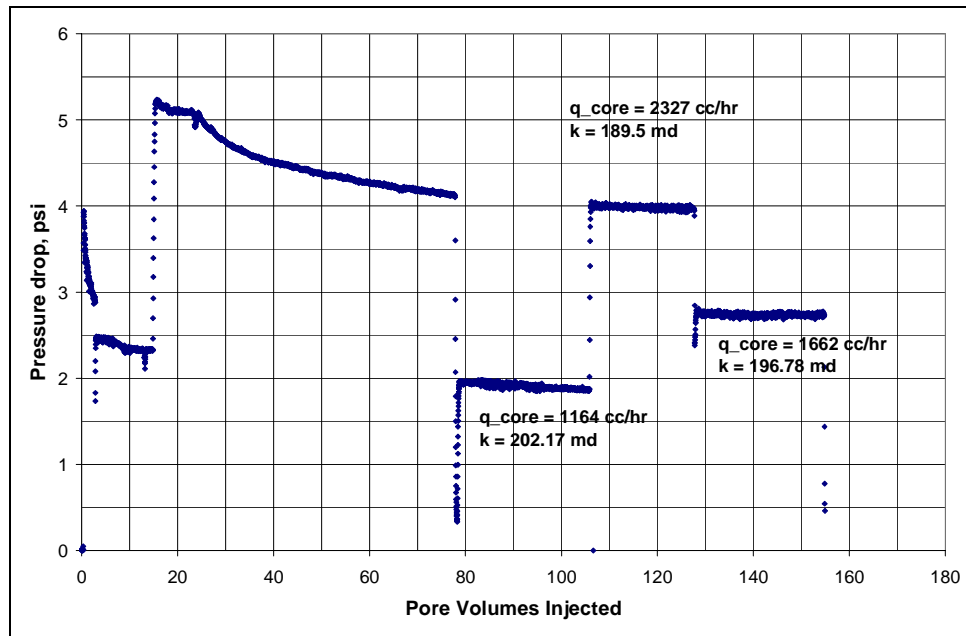


Figure B11.1: Pressure drop across the core during initial nitrogen flood

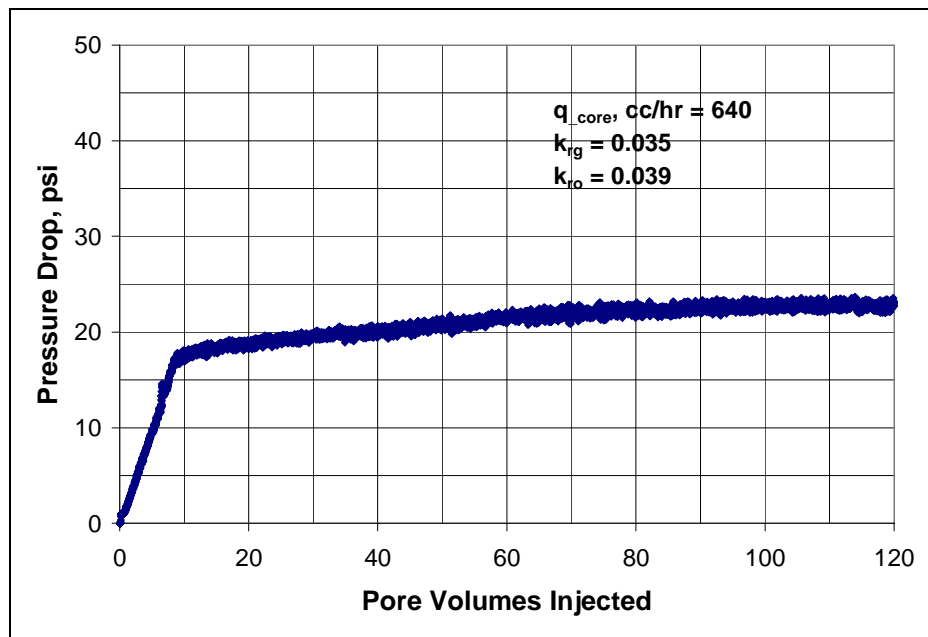


Figure B11.2: Pressure drop across the core during the initial two-phase flow at 250°F and 1500 psig

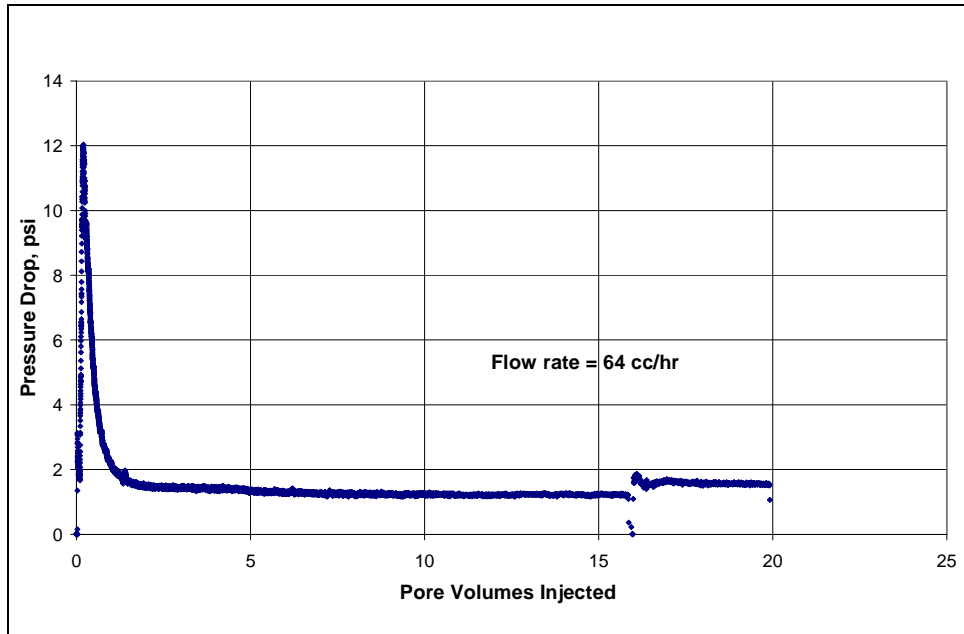


Figure B11.3: Pressure drop across the core during first surfactant treatment

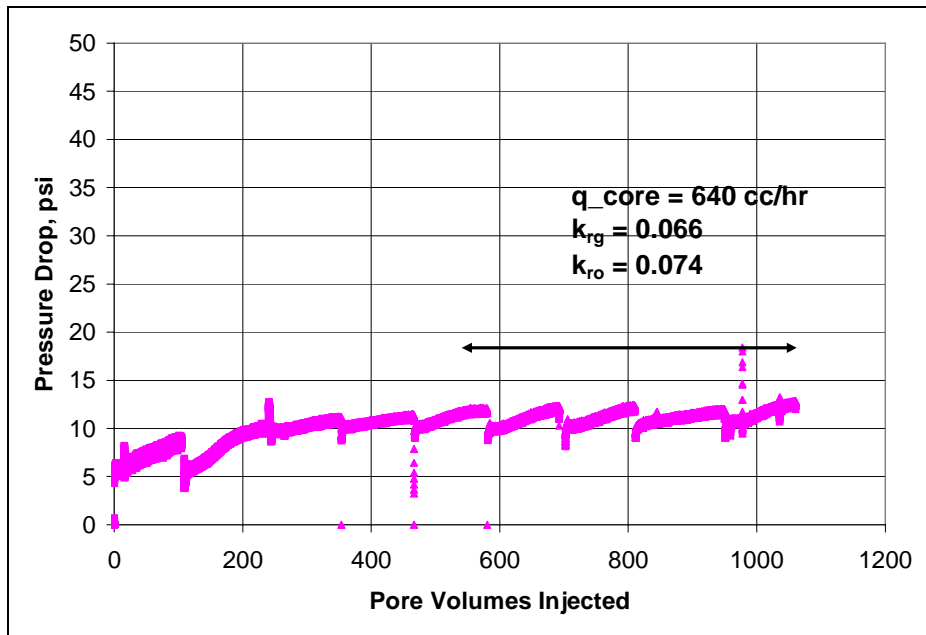


Figure B11.4: Pressure drop across the core during post-treatment two-phase floods at 250°F and 1500 psig

B12- Experiment No.12

Objective:

The objective of this experiment was to test the effect of surfactant L16218 treatment in improving the gas and condensate relative permeability on a Texas Cream limestone core. The experiment was performed at 250°F.

Experimental Results:

Table B12.1 summarizes the properties of the core and the experimental conditions. Initial permeability of the core was measured using nitrogen at 75°F. **Figure B11.1** shows the methane flood pressure total drop measured across the core. **Table B11.2** summarizes the results of the nitrogen flood.

Two-phase gas condensate floods were conducted using synthetic fluid mixture-3 (Table 3.3) at 250°F. The initial flood was conducted with the upstream backpressure regulator set at 4200 psig and the downstream back pressure regulator set at 1500 psig. **Table B12.3** gives the fluid properties of the synthetic fluid calculated using the Peng-Robinson EOS at the flowing core pressure. **Figure B12.2** shows the pressure drop across the core for the two-phase gas-condensate flood. **Table B12.4** summarizes the results of the initial two-phase flow.

The core was then treated with surfactant L16218 manufactured by 3M corp. **Table B12.5** gives the composition of the treatment solution. **Figure B12.3** shows the measured pressure drop across the core during the treatment flood. 18 PV of treatment solution was injected at 32 cc/hr and the core was then shut-in for 24 hours.

Post-treatment two-phase gas-condensate flow was conducted using the same gas mixture under the same conditions as the initial two-phase flow. Figure B12.4 shows the

pressure drop across the core measured during the post-treatment two-phase flow at flowing pressures of 1500 psig. Table B12.6 summarizes the results of the post-treatment two-phase flow.

Table B12.1: Core Properties and Experimental conditions

Core	Texas Cream Limestone
Length, inches	8
Diameter, inches	1
Porosity, %	20.0
Pore volume, cc	20.59
Swi, %	0
Temperature, °F	250

Table B12.2: Result of nitrogen flood

q_{core}, (cc/hr)	ΔP (psi)	k_g (md)
772.16	17.54	14.19
1647.28	36.36	14.61
2882.75	5.63	14.17
Permeability, k_g (md)		14.27

Table B12.3: Synthetic fluid properties at experimental conditions

Pressure, psig	4200	1500	
Fluid Properties		Gas phase	Oil phase
ρ, g/cc	0.2998	0.0711	0.5544
μ (cp)		0.0165	0.1651
Volume fraction		0.8989	0.1011
IFT (dyne/cm)		4.473	

Table B12.4: Results of initial two-phase flow of gas condensate mixture

q_{pump}, cc/hr	128	256	448
$q_{\text{total_core}}$, cc/hr	319.89	619.04	1058.65
$q_{\text{g_core}}$, cc/hr	287.55	585.10	1006.42
$q_{\text{o_core}}$, cc/hr	32.34	64.68	113.19
ΔP, psi	55.32	102.08	175.87
k_{rg}	0.089	0.103	0.102
k_{ro}	0.110	0.118	0.119
Nc	5.91×10^{-6}	1.09×10^{-5}	1.88×10^{-5}
PVT Ratio	0.89	0.89	0.89

Table B12.5: Composition of treatment solution

Component	Weight %
L16218	2
Methanol	94
D.I. water	4

Table B12.6: Results of post-treatment two-phase flow of gas condensate mixture

q_{pump}, cc/hr	128
q_{total_core}, cc/hr	319.89
q_{g_core}, cc/hr	287.55
q_{o_core}, cc/hr	32.34
ΔP, psi	48.90
k_{rg}	0.111
k_{ro}	0.125
Nc	5.22x10 ⁻⁶
Improvement Factor	1.13

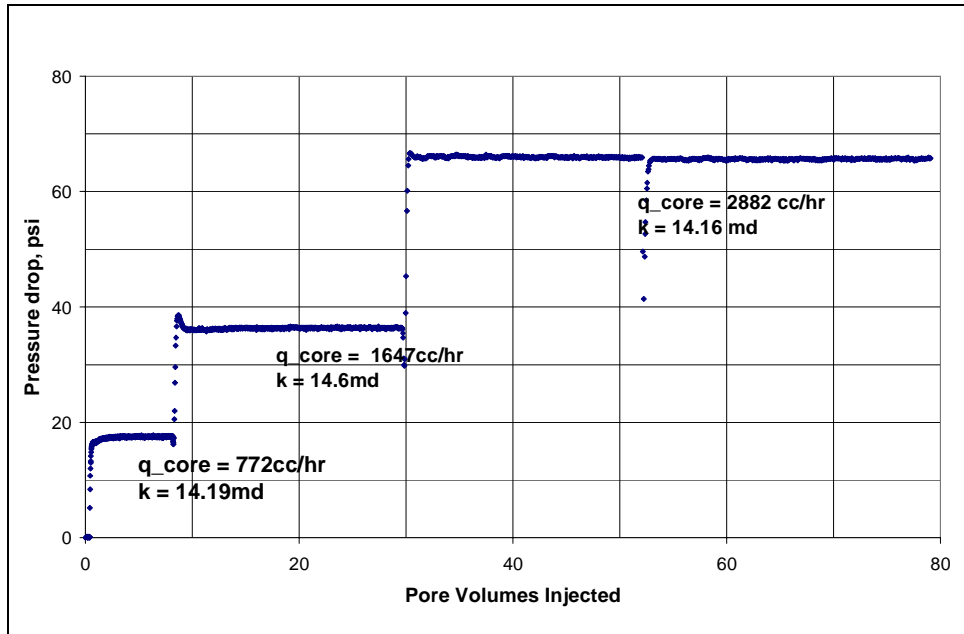


Figure B12.1: Pressure drop across the core during initial nitrogen flood

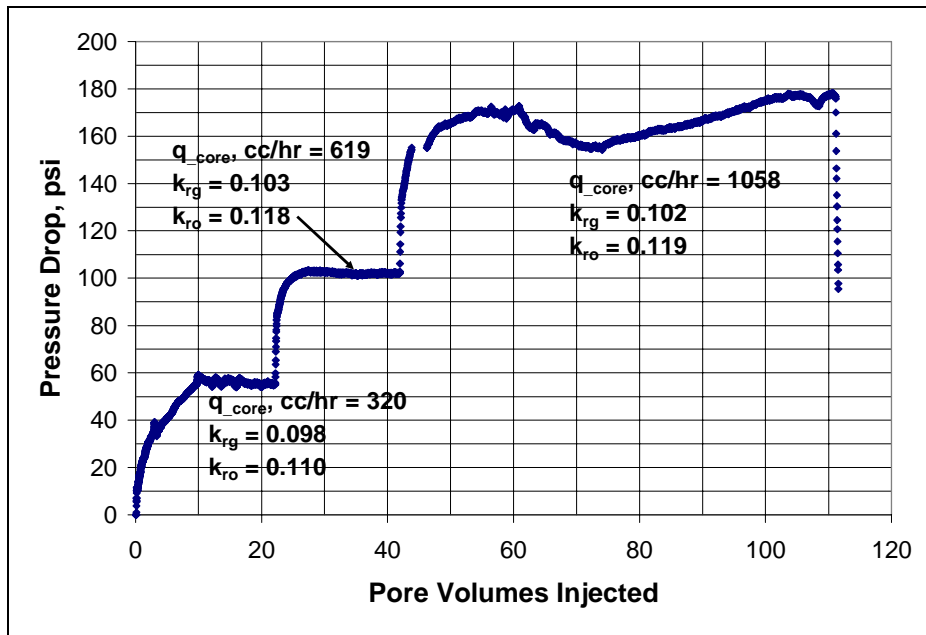


Figure B12.2: Pressure drop across the core during the initial two-phase flow at 250°F and 1500 psig

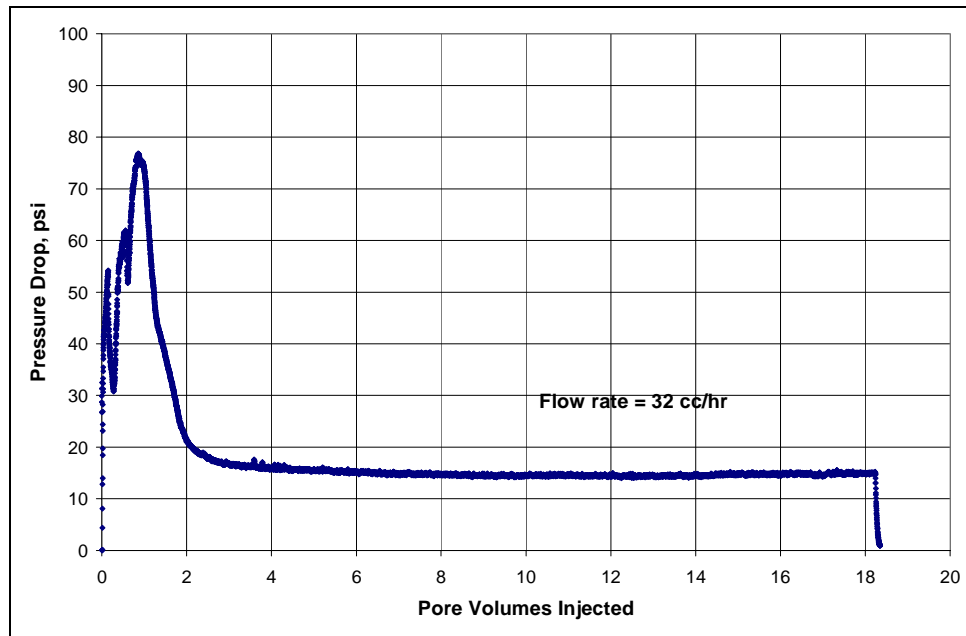


Figure B12.3: Pressure drop across the core during first surfactant treatment

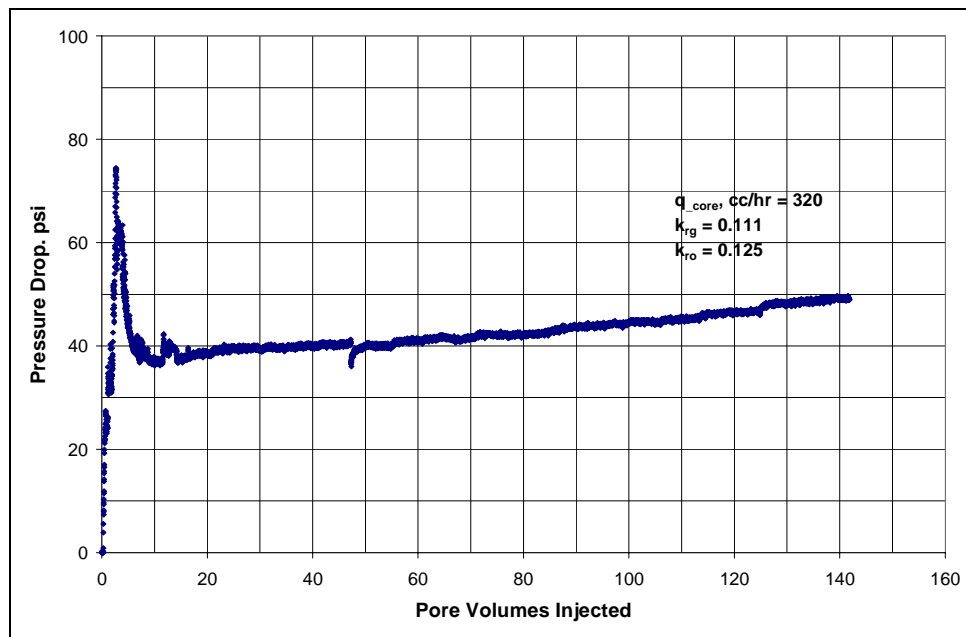


Figure B12.4: Pressure drop across the core during post-treatment two-phase floods at 250°F and 1500 psig

B13- Experiment No.13

Objective:

The objective of this experiment was to investigate the effect of non-ionic polymeric fluoro-surfactant FC4430 treatment in improving the gas and condensate relative permeability on a Berea sandstone rock in presence of initial water. The experiment was performed at 275°F.

Experimental Results:

Table B13.1 summarizes the properties of the core and the experimental conditions. Initial permeability of the core was measured using nitrogen at 72°F. **Figure B13.1** shows the pressure drop measured across the core during nitrogen flood. **Table B130.2** summarizes the results of the nitrogen flood.

The initial water saturation of 26.1% was established by injecting 5.2 cc of D.I. water in the vacuumed core. Nitrogen flood was then conducted to measure the end point gas permeability. **Figure B13.2** shows the pressure drop measured across the core. **Table B13.3** summarizes the results of the nitrogen flood. The pressure of the core was raised to 500 psig and then the temperature of the oven was raised to 275°F.

Synthetic fluid mixture-2 (Table 3.2) was used for the two-phase flow measurements. The initial flood was conducted with the upstream backpressure regulator set at 4500 psig and the downstream back pressure regulator set at 1500 psig. **Table B13.4** gives the fluid properties of the synthetic fluid calculated using the Peng-Robinson EOS at the flowing core pressure. **Figure B13.3** shows the pressure drop measured across the core for the two-phase gas-condensate flow. **Table B13.5** summarizes the results of the initial two-phase flow.

Nine pore volumes of methanol was flowed thorough the core after the initial gas condensate two-phase flood and then it was shut-in for 12 hours followed by nine more pore volumes of methanol. **Figure B13.4** shows the measured pressure drop across the core during pre-flush. A two-phase gas condensate flood was conducted under the same conditions as the initial two-phase flood to flush out methanol and establish condensate saturation in the core. **Figure B13.5** shows the pressure drop across the core during the post-solvent flush two-phase flow.

The core was then treated with a fluoro-surfactant FC4430. **Table B13.6** gives the composition of the treatment solution. **Figure B13.6** shows the measured pressure drop across the core during the treatment flood. 16 PV of treatment solution was injected at 32 cc/hr and the core was then shut-in for 24 hours.

Post-treatment two-phase gas-condensate flood was conducted under the same conditions as the initial two-phase flow. **Figure B13.7** shows the pressure drop across the core measured during the post-treatment two-phase flow at flowing pressures of 1500 psig. **Table B13.7** summarizes the results of the post-treatment two-phase flow.

The core was retreated with treatment solution given in Table B13.6. One pore volume of treatment solution was injected at 20 cc/hr. **Figure B13.8** shows the pressure drop across the core during the second treatment flood. The core was then shut-in for 24 hours.

Two-phase gas-condensate flood was then conducted under the same conditions as the initial two-phase flow. **Figure B13.9** shows the pressure drop across the core measured during the two-phase flood at a flowing pressures of 1500 psig. **Table B13.8** summarizes the results of the post-second treatment two-phase flood.

Methane flood was then conducted to measure the post-treatment permeability of the core. **Figure B13.10** shows the pressure drop across the core during methane flood. **Table B13.9** summarizes the results of methane flood.

The core was treated again with the treatment solution given in **Table B13.6**. 17 PV of treatment solution was injected at 32 cc/hr. **Figure B13.11** shows the pressure drop across the core during the third treatment flood. The core was then shut-in for 24 hours.

Two-phase gas-condensate flood was then conducted under the same conditions as the initial two-phase flow. **Figure B13.12** shows the pressure drop across the core during the two-phase flow at a flowing pressures of 1500 psig. **Table B13.10** summarizes the results of the post-third treatment two-phase flood.

10 PV of toluene was then injected at 32 cc/hr. Approximately 1.5 cc of water was produced from the core during the toluene flood. Two-phase gas condensate flood was then conducted under the same conditions as the initial two-phase flood to flush out toluene and establish condensate saturation in the core. **Figure B13.13** shows the pressure drop across the core during the post-toluene flush two-phase flow. **Table B13.11** summarizes the results of the post-toluene flood two-phase flow.

The core was treated again with the treatment solution given in **Table B13.6**. 17 PV of treatment solution was injected at 32 cc/hr. **Figure B13.14** shows the pressure drop across the core during the fourth treatment flood. The core was then shut-in for 24 hours.

Two-phase gas-condensate flood was then conducted under the same conditions as the initial two-phase flow. **Figure B13.15** shows the pressure drop across the core during the two-phase flow at a flowing pressures of 1500 psig. **Table B13.12** summarizes the results of the post-third treatment two-phase flood.

Table B13.1: Core properties

Core	Berea Sandstone
Length, inches	8
Diameter, inches	1
Porosity, %	20.00
Pore volume, cc	20.59
Swi, %	26.1
Temperature, °F	275

Table B13.2: Result of nitrogen flood

q_{core}, (cc/hr)	ΔP (psi)	k_g (md)
1240.7	2.88	139.82
2171.22	5.085	138.12
1550.88	3.69	136.21
Permeability, k_g (md)		138.05

Table B13.3: Result of nitrogen flood at Swi

q_{core}, (cc/hr)	ΔP (psi)	k_g (md)
1240.7	4.29	93.56

Table B13.4: Synthetic fluid properties at experimental conditions

Pressure, psig	4500	1500	
Fluid Properties		Gas phase	Oil phase
ρ, g/cc	0.2067	0.0615	0.6018
μ (cp)		0.0165	0.2639
Volume fraction		0.9787	0.0213
IFT (dyne/cm)		5.184	

Table B13.5: Results of initial two-phase flow of gas condensate mixture

q_{pump}, cc/hr	192	384
$q_{\text{total_core}}$, cc/hr	527.88	1055.75
$q_{\text{g_core}}$, cc/hr	516.79	1033.58
$q_{\text{o_core}}$, cc/hr	11.09	22.17
ΔP, psi	7.49	13.67
k_{rg}	0.102	0.112
k_{ro}	0.035	0.038
Nc	6.54×10^{-6}	1.19×10^{-5}
PVT Ratio	2.90	2.90

Table B13.6: Composition of treatment solution

Component	Weight %
FC4430	2
Methanol	94
D.I. water	4

Table B13.7: Results of post-treatment two-phase flow of gas condensate mixture

q_{pump}, cc/hr	192
q_{total_core}, cc/hr	527.88
q_{g_core}, cc/hr	516.79
q_{o_core}, cc/hr	11.09
ΔP, psi	5.53
k_{rg}	0.138
k_{ro}	0.047
Nc	4.82x10 ⁻⁶
Improvement Factor	1.36

Table B13.8: Results of post-second treatment two-phase flow of gas condensate mixture

q_{pump}, cc/hr	192	384
q_{total_core}, cc/hr	527.88	1055.75
q_{g_core}, cc/hr	516.79	1033.58
q_{o_core}, cc/hr	11.09	22.17
ΔP, psi	5.60	10.88
k_{rg}	0.136	0.140
k_{ro}	0.047	0.048
Nc	4.88x10 ⁻⁶	9.49x10 ⁻⁶
Improvement Factor	1.34	1.26

Table B13.9: Result of methane flood to measure post-treatment permeability

q_{core}, (cc/hr)	ΔP (psi)	k_g (md)
872.89	1.31	176.89
1745.80	2.55	181.39
2444.12	3.41	189.84
Permeability, k_g (md)		189.43

Table B13.10: Results of post-third treatment two-phase flow of gas condensate mixture

q_{pump}, cc/hr	192
q_{total_core}, cc/hr	527.88
q_{g_core}, cc/hr	516.79
q_{o_core}, cc/hr	11.09
ΔP, psi	5.78
k_{rg}	0.132
k_{ro}	0.045
Nc	5.052x10 ⁻⁶
Improvement Factor	1.29

Table B13.11: Results of two-phase flow of gas condensate mixture after toluene flood

q_{pump}, cc/hr	192
q_{total_core}, cc/hr	527.88
q_{g_core}, cc/hr	516.79
q_{o_core}, cc/hr	11.09
ΔP, psi	5.51
k_{rg}	0.139
k_{ro}	0.048
Nc	4.81x10 ⁻⁶
Improvement Factor	1.36

Table B13.12: Results of post-fourth treatment two-phase flow of gas condensate mixture

q_{pump}, cc/hr	192
q_{total_core}, cc/hr	527.88
q_{g_core}, cc/hr	516.79
q_{o_core}, cc/hr	11.09
ΔP, psi	4.87
k_{rg}	0.157
k_{ro}	0.054
Nc	4.25x10 ⁻⁶
Improvement Factor	1.54

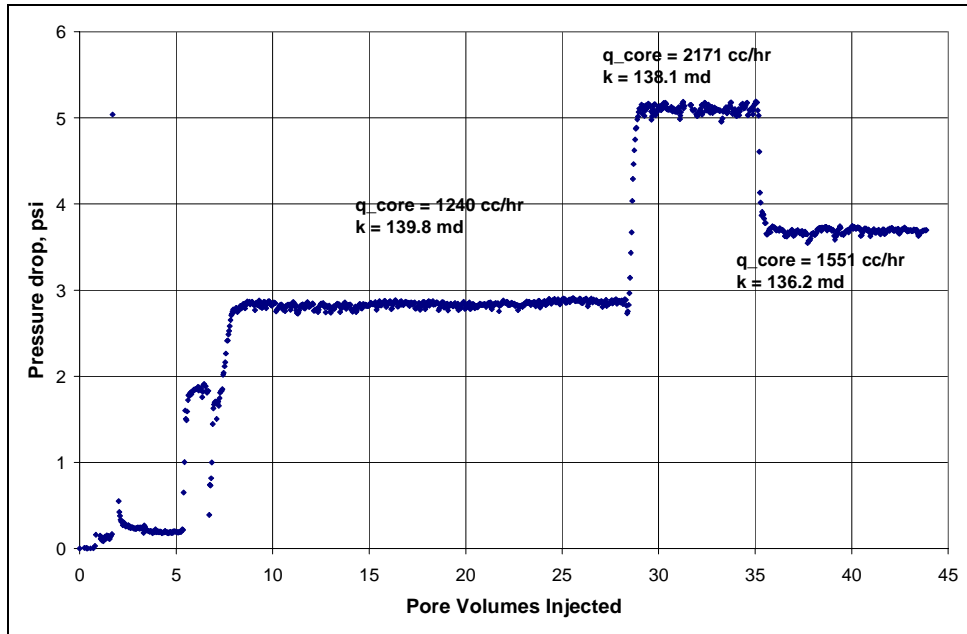


Figure B13.1: Pressure drop across the core during initial nitrogen flood

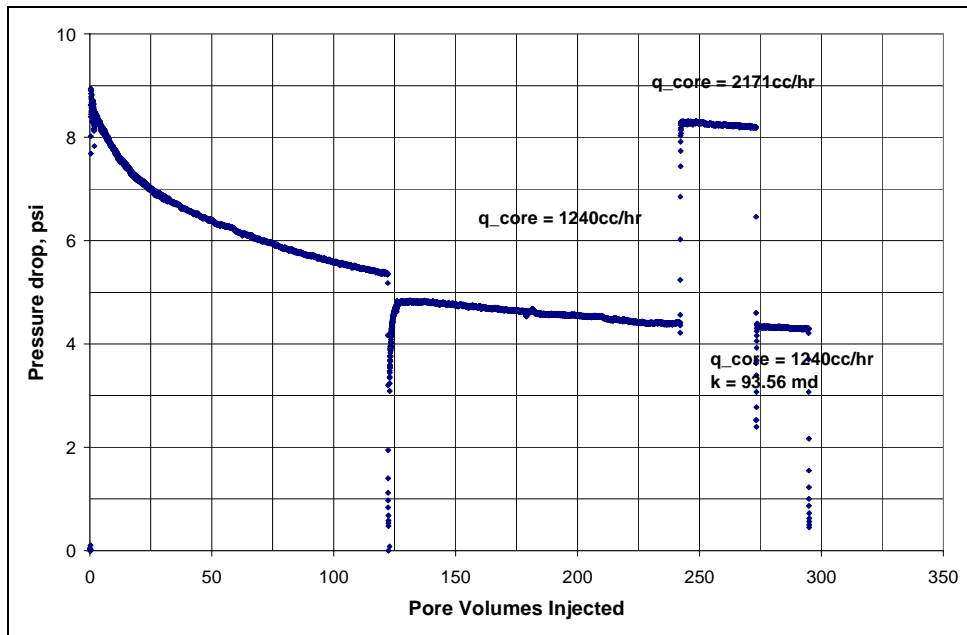


Figure B13.2: Pressure drop across the core during nitrogen flood at $Sw_i=26.1\%$

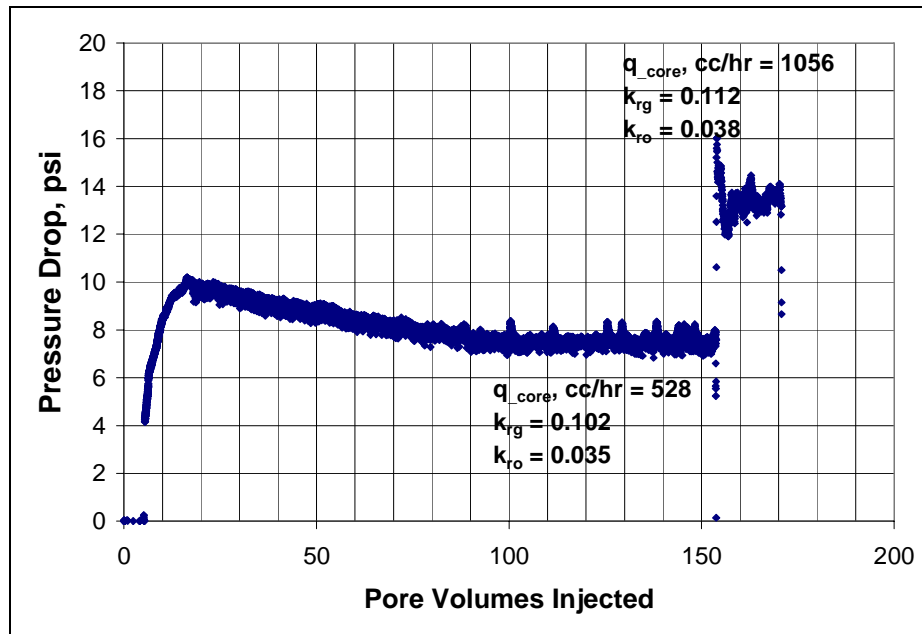


Figure B13.3: Pressure drop across the core during the initial two-phase flow at 275°F and 1500 psig

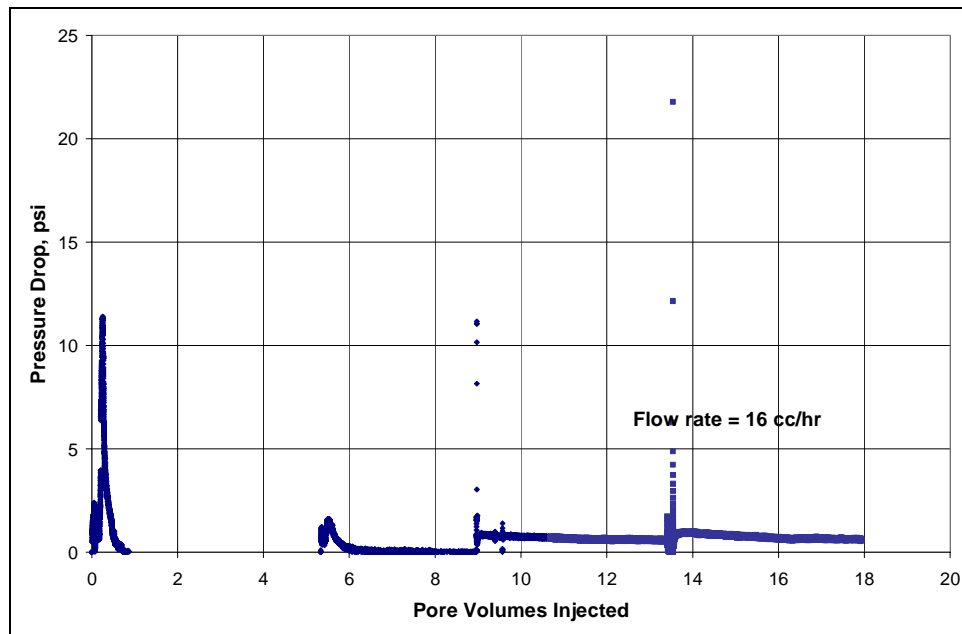


Figure B13.4: Pressure drop across the core during methanol preflush

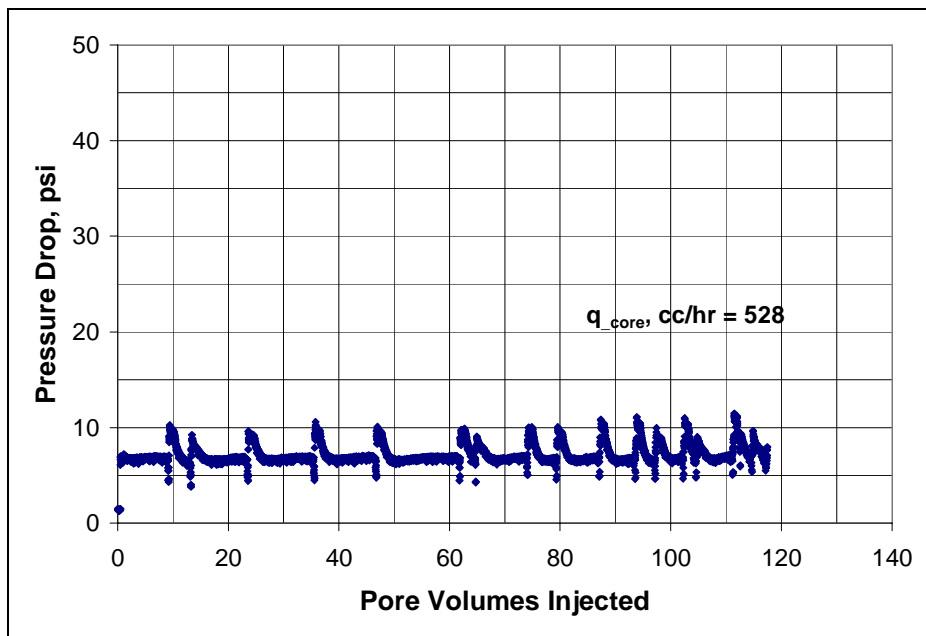


Figure B13.5: Pressure drop across the core during the two-phase flow at 275°F and 1500 psig after methanol pre-flush

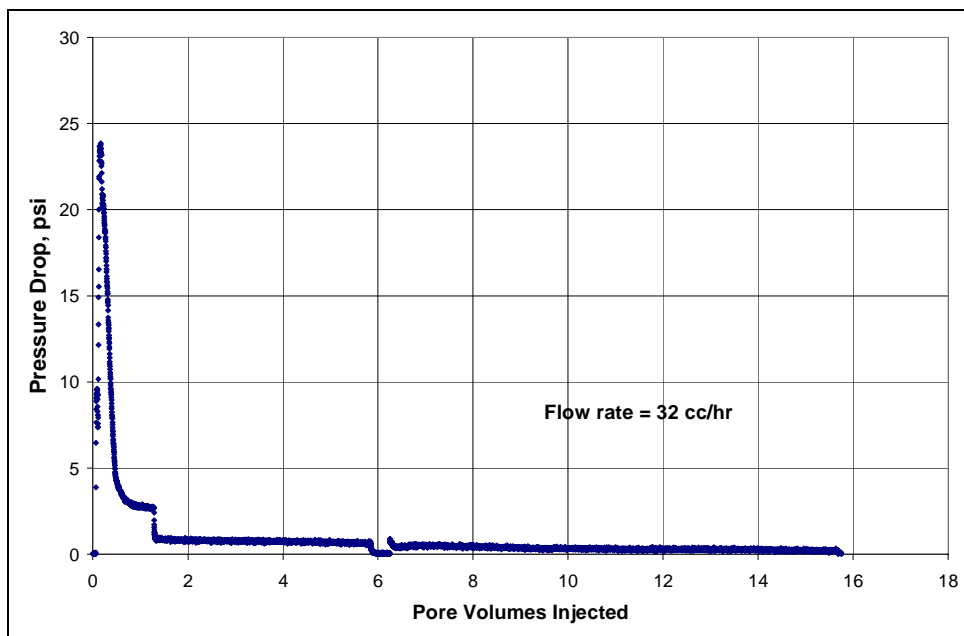


Figure B13.6: Pressure drop across the core during surfactant treatment

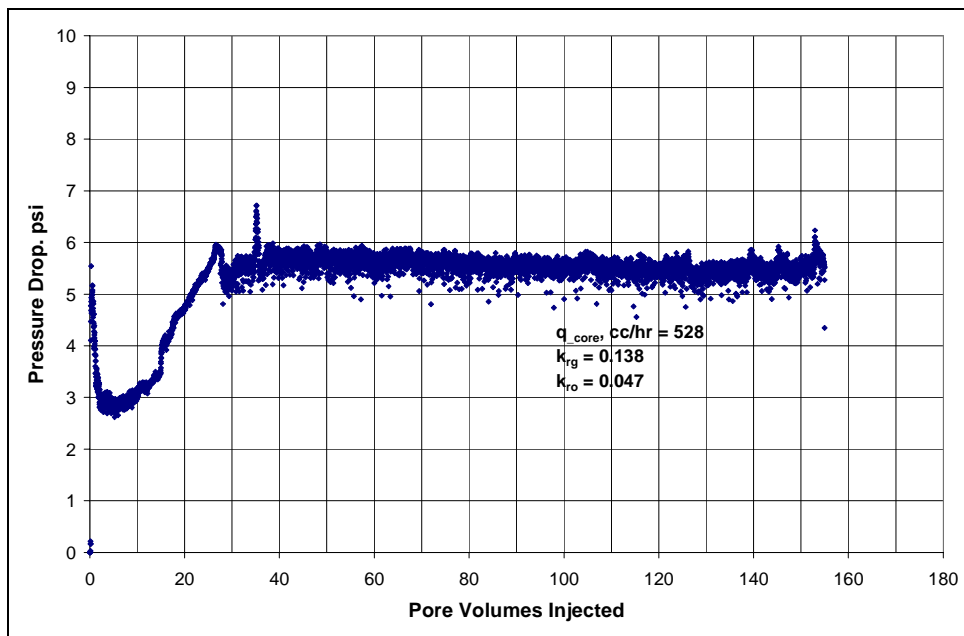


Figure B13.7: Pressure drop across the core during the post-first treatment two-phase flow at 275°F and 1500 psig

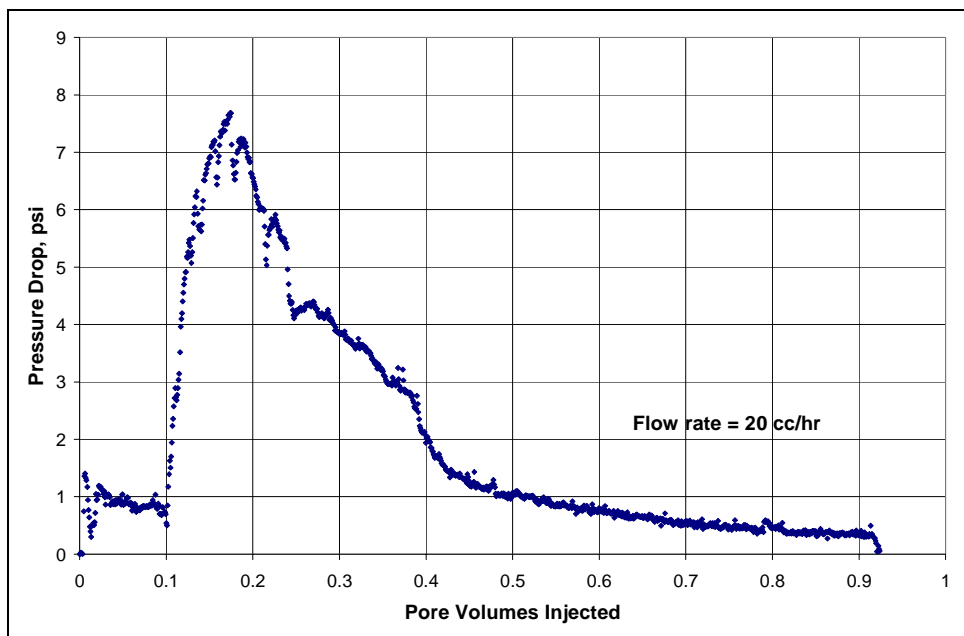


Figure B13.8: Pressure drop across the core during the second surfactant treatment

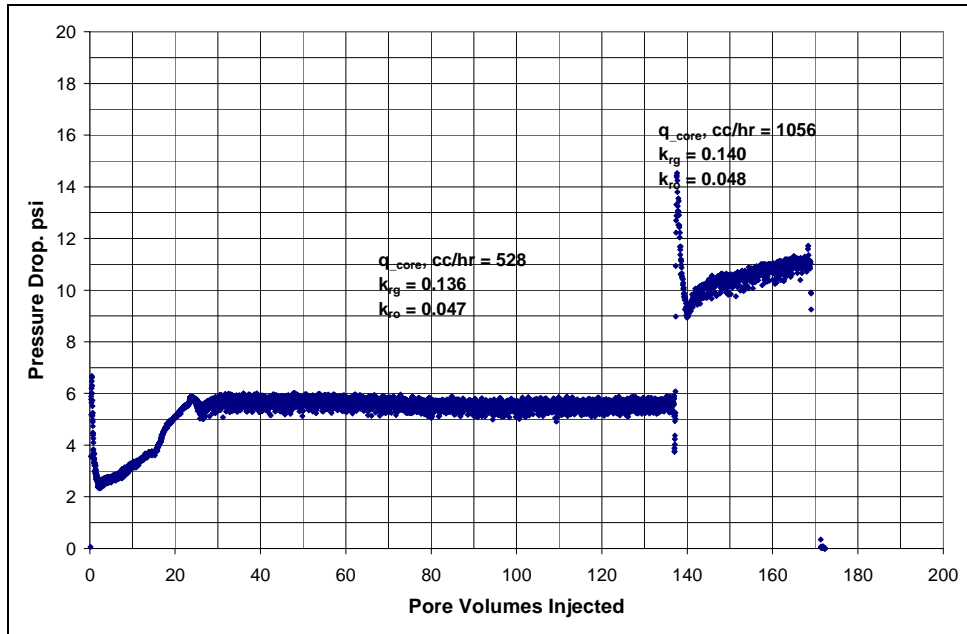


Figure B13.9: Pressure drop across the core during the post-second treatment two-phase flow at 275°F and 1500 psig

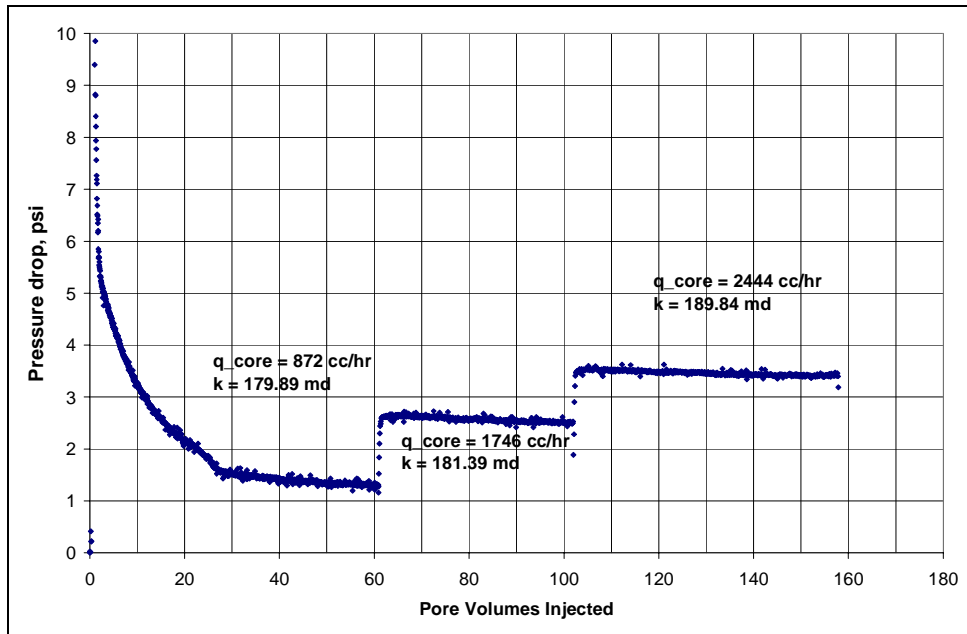


Figure B13.10: Pressure drop across the core during the methane flood at 275°F and 1500 psig to measure the post-treatment core permeability

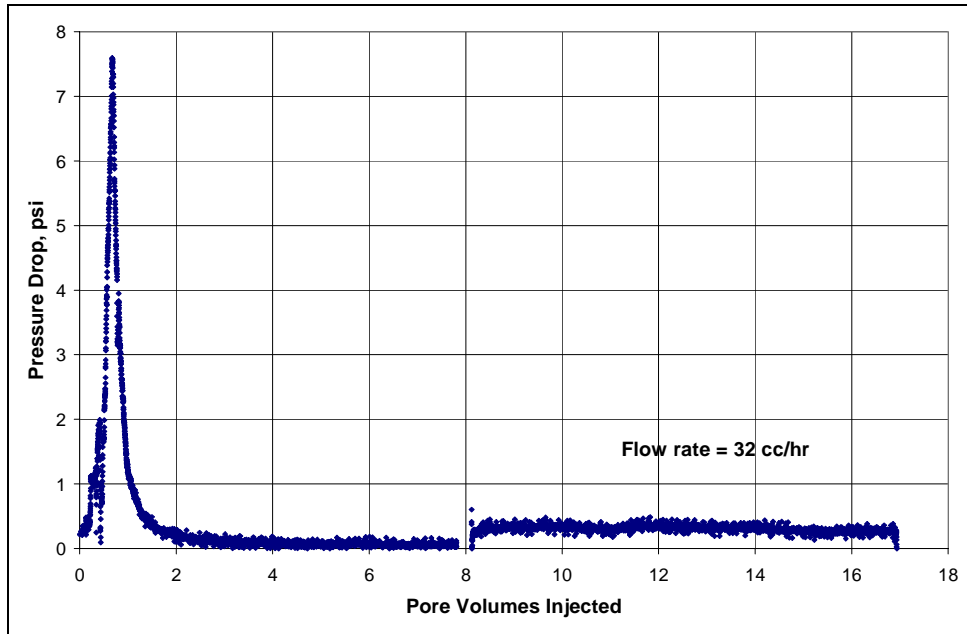


Figure B13.11: Pressure drop across the core during the third surfactant treatment

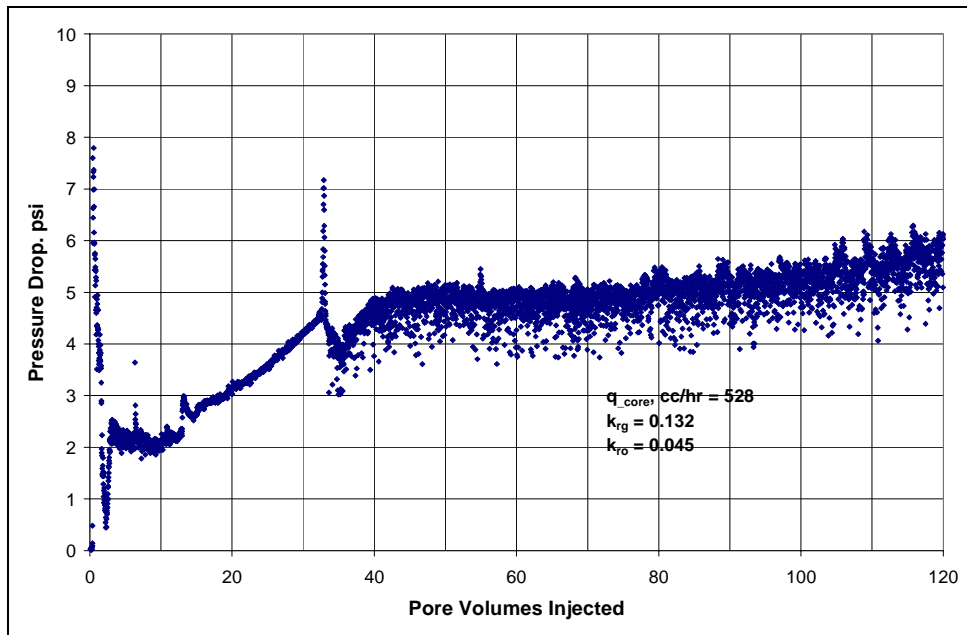


Figure B13.12: Pressure drop across the core during the post-third treatment two-phase flow at 275°F and 1500 psig

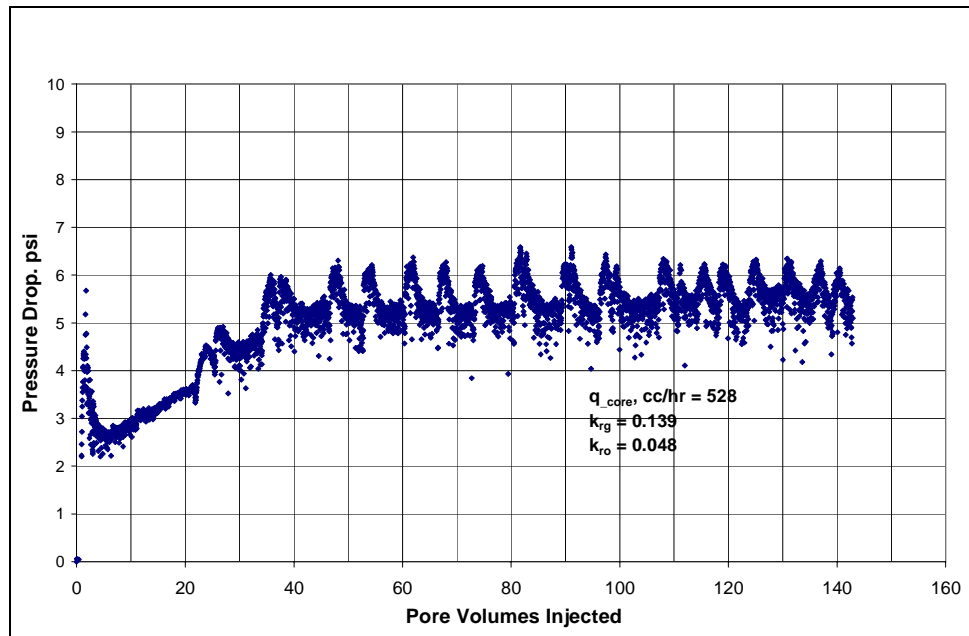


Figure B13.13: Pressure drop across the core during the two-phase flow at 275°F and 1500 psig after toluene flood

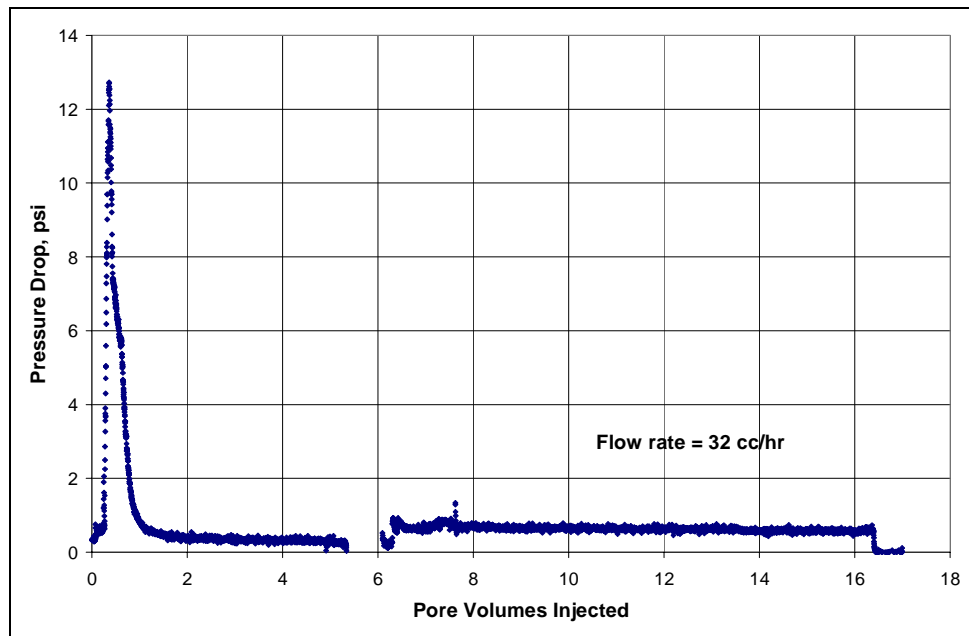


Figure B13.14: Pressure drop across the core during the fourth surfactant treatment

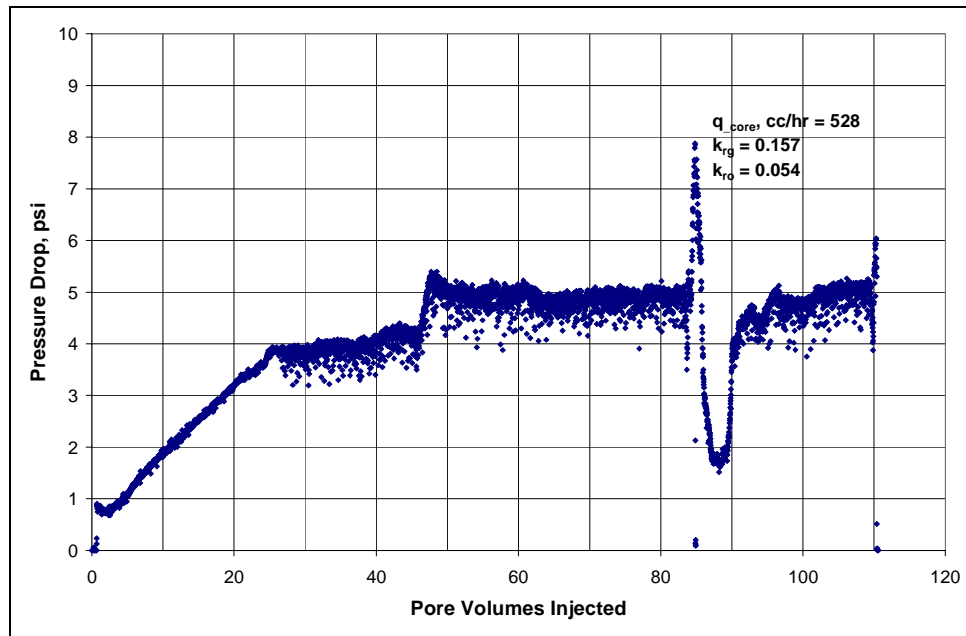


Figure B13.15: Pressure drop across the core during the post-fourth treatment two-phase flow at 275°F and 1500 psig

B14- Experiment No.14

Objective:

The objective of this experiment was to investigate the effect of fluoro-surfactant L19829 treatment in improving the gas and condensate relative permeability on a Berea sandstone rock in presence of initial water. The experiment was performed at 275°F.

Experimental Results:

Table B14.1 summarizes the properties of the core and the experimental conditions. Initial permeability of the core was measured using nitrogen at 75°F. **Figure B14.1** shows the pressure drop measured across the core during nitrogen flood. **Table B14.2** summarizes the results of the nitrogen flood.

The initial water saturation of 26.1% was established by injecting 2.6 cc synthetic Britannia brine (**Table B6.3**) in the vacuumed core. Nitrogen flood was then conducted to measure the gas end point relative permeability. **Figure B14.2** shows the pressure drop measured across the core. **Table B14.3** summarizes the results of the nitrogen flood. The pressure of the core was raised to 500 psig and then the temperature of the oven was increased to 275°F.

Synthetic fluid mixture-2 (**Table 3.2**) was used for the two-phase flow measurements. The initial flood was conducted with the upstream backpressure regulator set at 4750 psig and the downstream back pressure regulator set at 1500 psig. **Table B14.4** gives the fluid properties of the synthetic fluid calculated using the Peng-Robinson EOS at the flowing core pressure. **Figure B14.3** shows the pressure drop across the core during the two-phase gas-condensate flow. **Table B14.5** summarizes the results of the initial two-phase flow.

Sixteen pore volumes of methanol was flowed thorough the core after the initial gas condensate two-phase flood. **Figure B14.4** shows the measured pressure drop across the core during methanol pre-flush. Two-phase gas condensate flood was then conducted under the same conditions as the initial two-phase flood to flush out methanol and establish condensate saturation in the core. **Figure B14.5** shows the pressure drop across the core during the post-solvent flush two-phase flow.

The core was then treated with a fluoro-surfactant L19289. **Table B14.6** gives the composition of the treatment solution. **Figure B14.6** shows the measured pressure drop across the core during the treatment flood. The core was then shut-in for 24 hours.

Post-treatment two-phase gas-condensate flood was then conducted under the same conditions as the initial two-phase flow. **Figure B14.7** shows the pressure drop across the core measured during the post-treatment two-phase flow at a flowing pressure of 1500 psig. **Table B14.7** summarizes the results of the post-treatment two-phase flow. No improvement was observed after chemical treatment.

Table B14.1: Core properties

Core	Berea Sandstone
Length, inches	8
Diameter, inches	1
Porosity, %	20.00
Pore volume, cc	20.59
Swi, %	26.1
Temperature, °F	275

Table B14.2: Result of nitrogen flood

q_{core}, (cc/hr)	ΔP (psi)	k_g (md)
1520.69	3.22	154.05
3014.38	7.28	136.09
2025.79	4.77	138.43
Permeability, k_g (md)		141.64

Table B14.3: Result of methane flood at Swi

q_{core}, (cc/hr)	ΔP (psi)	k_g (md)
1485.89	3.16	186.17

Table B14.4: Synthetic fluid properties at experimental conditions

Pressure, psig	4750	1500	
Fluid Properties		Gas phase	Oil phase
ρ , g/cc	0.2008	0.0614	0.6018
μ (cp)		0.0165	0.2639
Volume fraction		0.9787	0.0213
IFT (dyne/cm)		5.184	

Table B14.5: Results of initial two-phase flow of gas condensate mixture

q_{pump}, cc/hr	210
q_{total_core}, cc/hr	577.36
q_{g_core}, cc/hr	565.24
q_{o_core}, cc/hr	12.12
ΔP, psi	7.48
k_{rg}	0.11
k_{ro}	0.038
Nc	6.84×10^{-6}
PVT Ratio	2.90

Table B14.6: Composition of treatment solution

Component	Weight %
L19289	2
Methanol	94
D.I. water	4

Table B14.7: Results of post-treatment two-phase flow of gas condensate mixture

q_{pump}, cc/hr	210
q_{total_core}, cc/hr	577.36
q_{g_core}, cc/hr	565.24
q_{o_core}, cc/hr	12.12
ΔP, psi	7.18
k_{rg}	0.114
k_{ro}	0.039
Nc	6.57x10 ⁻⁶
Improvement Factor	1.04

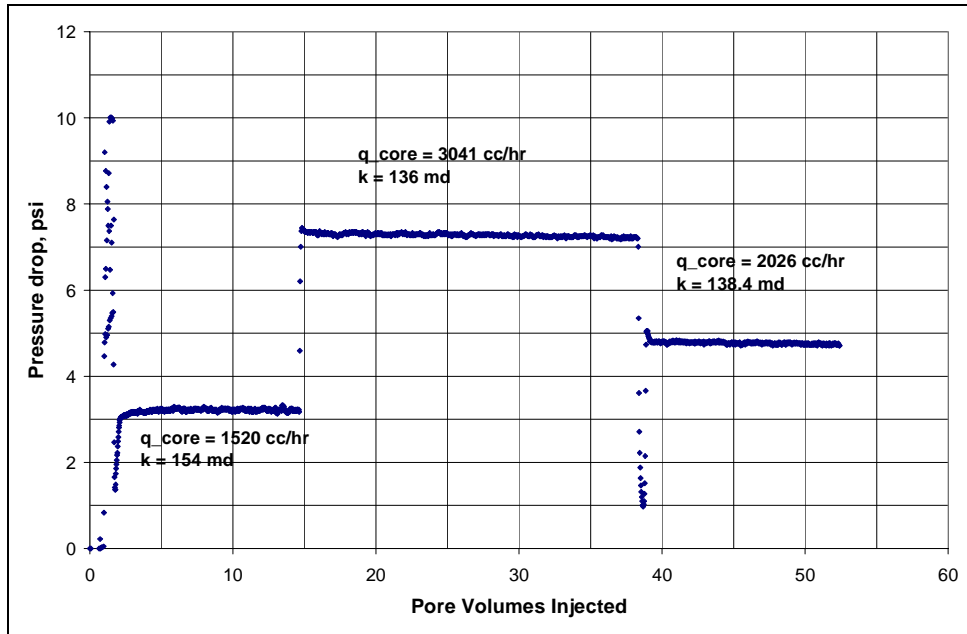


Figure B14.1: Pressure drop across the core during initial nitrogen flood

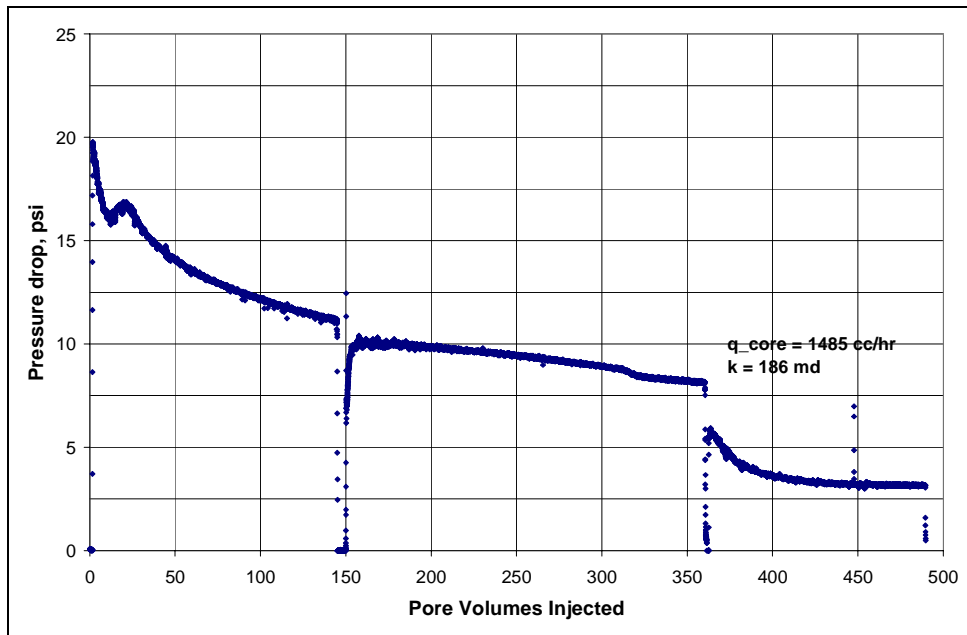


Figure B14.2: Pressure drop across the core during nitrogen flood at $Sw_i = 26.1\%$

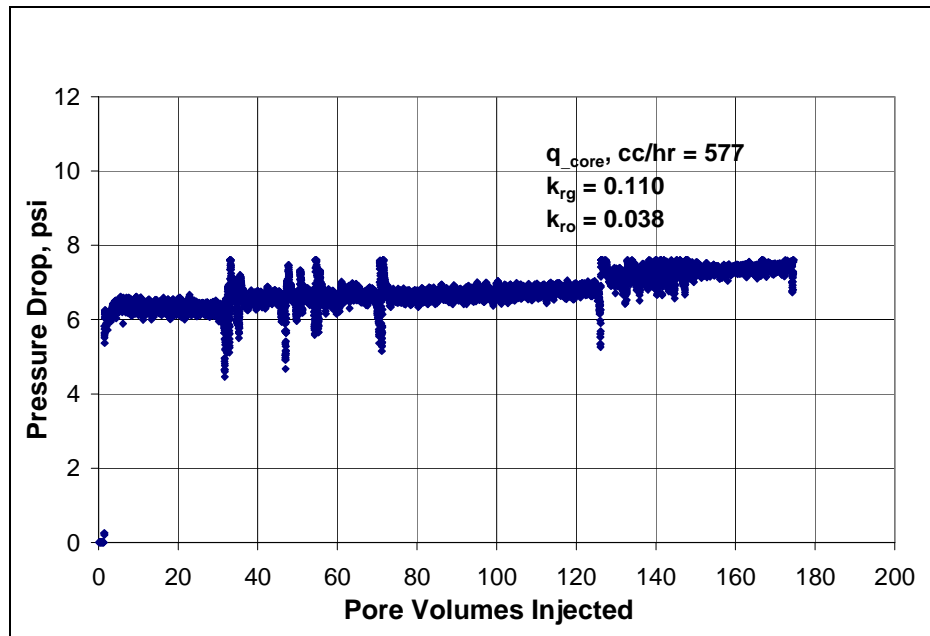


Figure B14.3: Pressure drop across the core during the initial two-phase flow at 275°F and 1500 psig

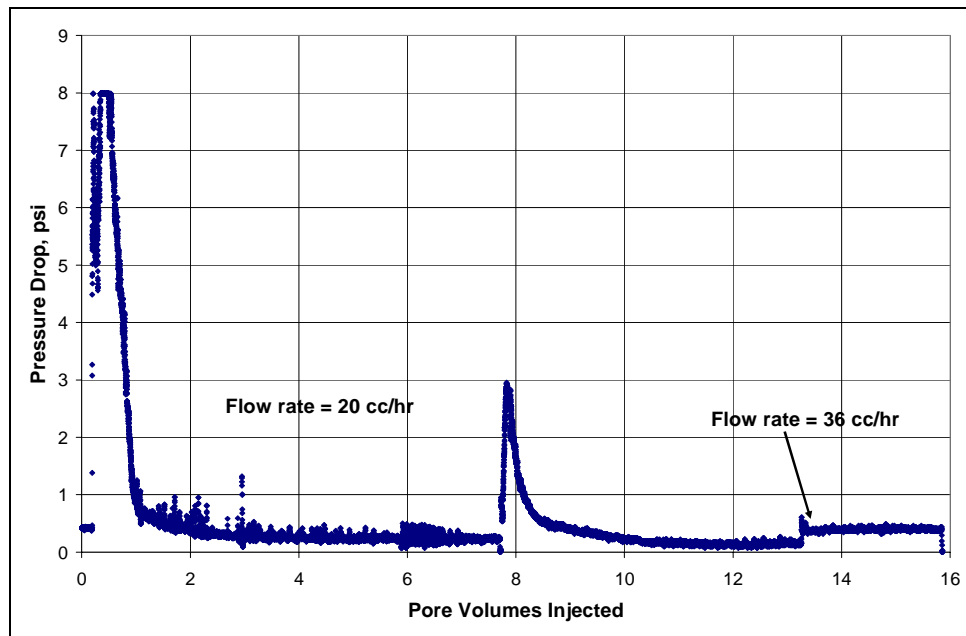


Figure B14.4: Pressure drop across the core during methanol preflush

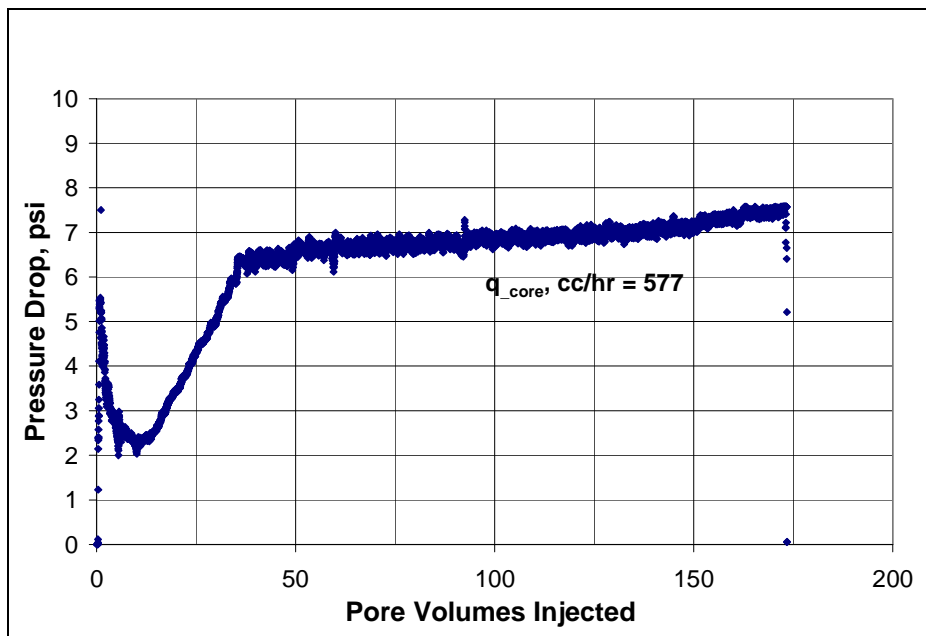


Figure B14.5: Pressure drop across the core during two-phase flow at 275°F and 1500 psig after methanol pre-flush

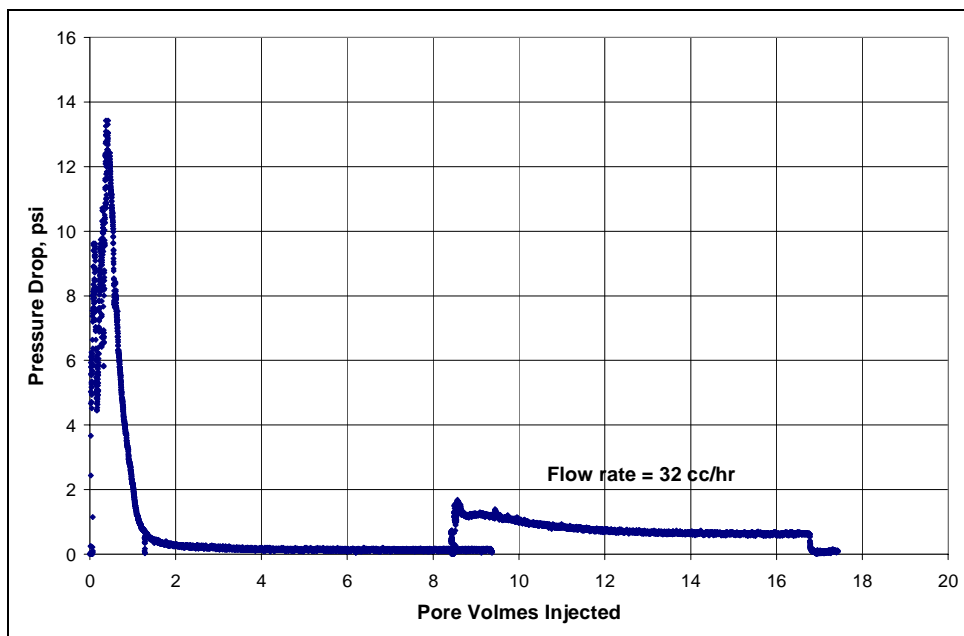


Figure B14.6: Pressure drop across the core during surfactant treatment

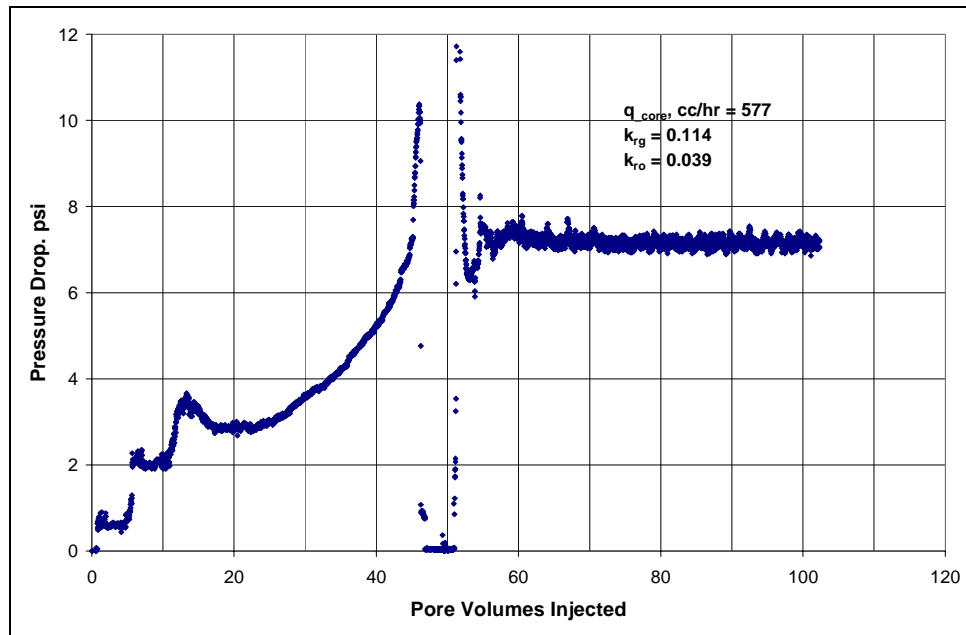


Figure B14.7: Pressure drop across the core during post-treatment two-phase flow at 275°F and 1500 psig

B15- Experiment No.15

Objective:

The objective of this experiment was to investigate the effect of chemical treatment using non-ionic polymeric fluoro-surfactant FC4430 treatment in improving the gas and condensate relative permeability on a Berea sandstone rock in presence of initial water. The experiment was performed at 275°F.

Experimental Results:

Table B15.1 summarizes the properties of the core and the experimental conditions. Initial permeability of the core was measured using nitrogen at 75°F. **Figure B15.1** shows the pressure drop measured across the core during nitrogen flood. **Table B15.2** summarizes the results of the nitrogen flood.

The core was fully saturated with synthetic Britannia brine (**Table B6.3**). Nitrogen flood was then conducted to reduce the water saturation in the core to residual and measure the end point gas relative permeability. **Figure B15.2** shows the pressure drop measured across the core. **Table B15.3** summarizes the results of the nitrogen flood. The pressure of the core was raised to 500 psig and then the temperature of the oven was raised to 275°F.

Synthetic fluid mixture-2 (Table 3.2) was used for the two-phase flow measurements. The initial flood was conducted with the upstream backpressure regulator set at 4500 psig and the downstream back pressure regulator set at 1500 psig. **Table B15.4** gives the fluid properties of the synthetic fluid calculated using the Peng-Robinson EOS at the flowing core pressure. **Figure B15.3** shows the pressure drop measured across

the core and the sections during the two-phase gas-condensate flow. **Table B15.5** summarizes the results of the initial two-phase flow.

Eight pore volumes of methanol were flowed thorough the core after the initial gas condensate two-phase flood and then it was shut-in for 12 hours followed by eight more pore volumes of methanol flood. **Figure B15.4** shows the measured pressure drop across the core during pre-flush. Two-phase gas condensate flood was conducted under the same conditions as the initial two-phase flood to flush out methanol and establish condensate saturation in the core. **Figure B15.5** shows the pressure drop across the core during the post-solvent flush two-phase flow. **Table B15.6** summarizes the results of the two-phase gas condensate flood conducted after methanol pre-flush.

The core was then treated with a fluoro-surfactant FC4430. **Table B15.7** gives the composition of the treatment solution. **Figure B15.6** shows the measured pressure drop across the core during the treatment flood. 19 PV of treatment solution was injected at 32cc/hr and the core was then shut-in for 24 hours.

Post-treatment two-phase gas-condensate flood was conducted under the same conditions as the initial two-phase flow. **Figure B15.7** shows the pressure drop across the core measured during the post-treatment two-phase flow at a flowing pressure of 1500 psig. **Table B15.8** summarizes the results of the post-treatment two-phase flow.

10 PV of toluene was then flowed through the core at 32cc/hr. 2.5cc of water was produced from the core during the toluene flood. **Figure B15.8** shows the pressure drop across the core measured during the toluene flood. Two-phase gas condensate flood was then conducted under the same conditions as the initial two-phase flood to flush out toluene and establish condensate saturation in the core. **Figure B15.9** shows the pressure drop across the core during the post-toluene flush two-phase flow. **Table B15.9** summarizes the results of the post-toluene flood two-phase flow.

The core was treated again with the treatment solution given in **Table B15.7**. 19 PV of treatment solution was injected at 32cc/hr. **Figure B15.10** shows the pressure drop across the core during the second treatment flood. The core was then shut-in for 24 hours.

Two-phase gas-condensate flood was then conducted under the same conditions as the initial two-phase flow. **Figure B15.11** shows the pressure drop across the core during the two-phase flow at a flowing pressure of 1500 psig. **Table B15.10** summarizes the results of the post-third treatment two-phase flood.

Table B15.1: Core properties

Core	Berea Sandstone
Length, inches	8
Diameter, inches	1
Porosity, %	20.00
Pore volume, cc	20.59
Swi, %	26.1
Temperature, °F	275

Table B15.2: Result of nitrogen flood

q_{core}, (cc/hr)	ΔP (psi)	k_g (md)
1085.61	1.19	295.58
1817.43	2.47	238.25
2714.04	3.63	242.07
3799.65	3.63	242.07
Permeability, k_g (md)		227.62

Table B15.3: Result of nitrogen flood at Swi

q_{core}, (cc/hr)	ΔP (psi)	k_g (md)
1017.76	3.28	100.41

Table B15.4: Synthetic fluid properties at experimental conditions

Pressure, psig	4500	1500	
Fluid Properties		Gas phase	Oil phase
ρ, g/cc	0.2008	0.0615	0.6018
μ (cp)		0.0165	0.2639
Volume fraction		0.9787	0.0213
IFT (dyne/cm)		5.184	

Table B15.5: Results of initial two-phase flow of gas condensate mixture

q_{pump}, cc/hr	210
$q_{\text{total_core}}$, cc/hr	577.36
$q_{\text{g_core}}$, cc/hr	565.24
$q_{\text{o_core}}$, cc/hr	12.12
ΔP, psi	8.89
k_{rg}	0.074
k_{ro}	0.025
Nc	1.33×10^{-5}
PVT Ratio	2.90

Table B15.6: Results of two-phase flow of gas condensate mixture after methanol pre-flush

q_{pump}, cc/hr	210	691
q_{total_core}, cc/hr	577.36	1889.80
q_{g_core}, cc/hr	565.24	1859.91
q_{o_core}, cc/hr	12.12	39.90
ΔP, psi	9.36	28.16
k_{rg}	0.070	0.077
k_{ro}	0.024	0.026
Nc	1.40x10 ⁻⁵	4.21x10 ⁻⁵
PVT Ratio	2.90	2.90

Table B15.7: Composition of treatment solution

Component	Weight %
FC4430	2
Methanol	94
D.I. water	4

Table B15.8: Results of post-treatment two-phase flow of gas condensate mixture

q_{pump}, cc/hr	210
q_{total_core}, cc/hr	577.36
q_{g_core}, cc/hr	565.24
q_{o_core}, cc/hr	12.12
ΔP, psi	8.07
k_{rg}	0.082
k_{ro}	0.028
Nc	1.21x10 ⁻⁵
Improvement Factor	1.01

Table B15.9: Results of two-phase flow of gas condensate mixture after toluene flood

q_{pump}, cc/hr	210	1011
q_{total_core}, cc/hr	577.36	2779.60
q_{g_core}, cc/hr	565.24	2721.23
q_{o_core}, cc/hr	12.12	58.37
ΔP, psi	6.62	38.01
k_{rg}	0.100	0.084
k_{ro}	0.034	0.029
Nc	9.90x10 ⁻⁶	5.68x10 ⁻⁵
Improvement Factor	1.34	-

Table B15.10: Results of post-second treatment two-phase flow of gas condensate mixture

q_{pump}, cc/hr	210
q_{total_core}, cc/hr	577.36
q_{g_core}, cc/hr	565.24
q_{o_core}, cc/hr	12.12
ΔP, psi	5.45
k_{rg}	0.121
k_{ro}	0.042
Nc	8.14x10 ⁻⁶
Improvement Factor	1.63

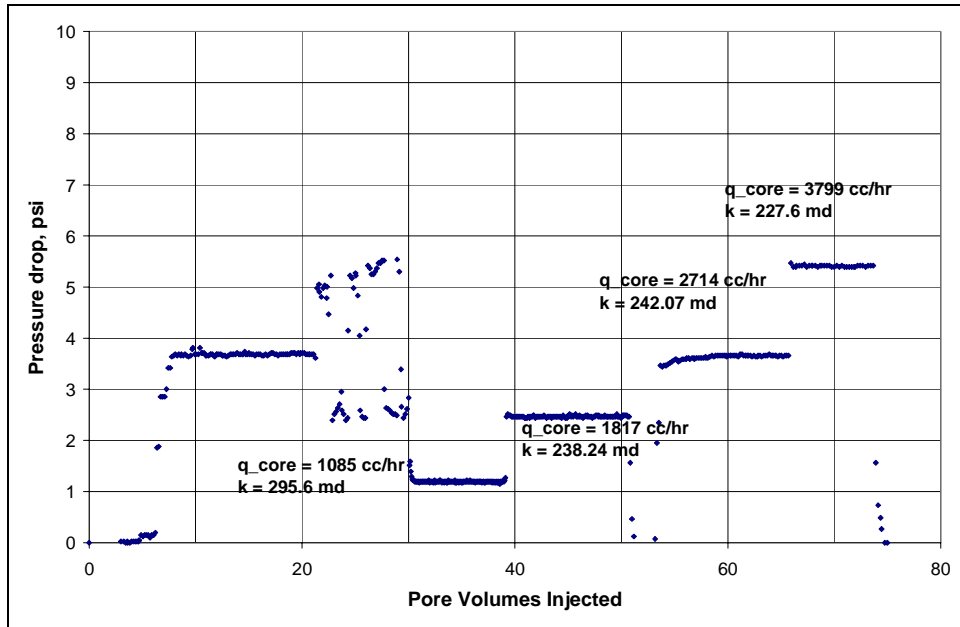


Figure B15.1: Pressure drop across the core during initial nitrogen flood

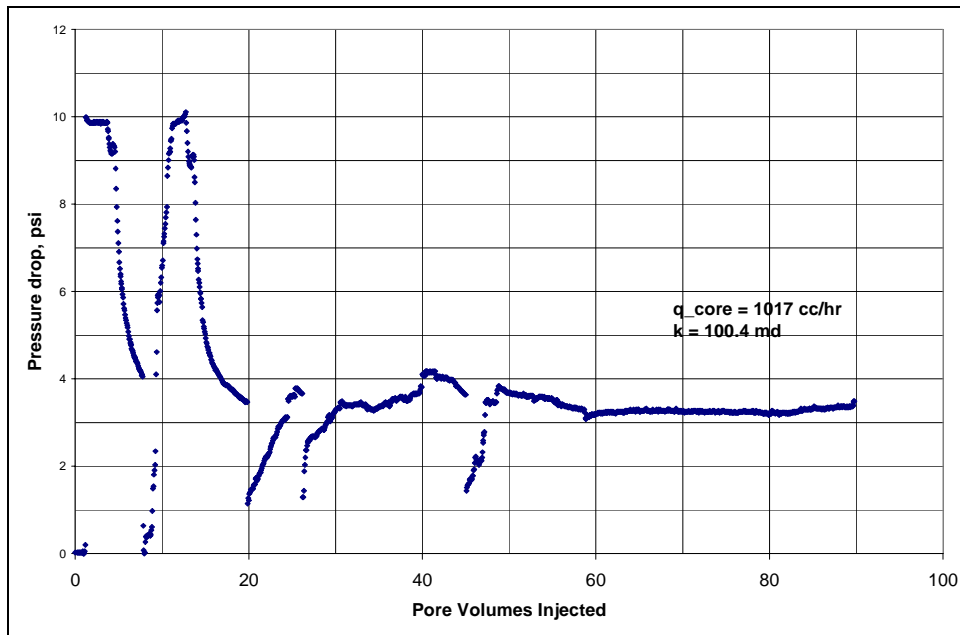


Figure B15.2: Pressure drop across the core during nitrogen flood at Sw_i

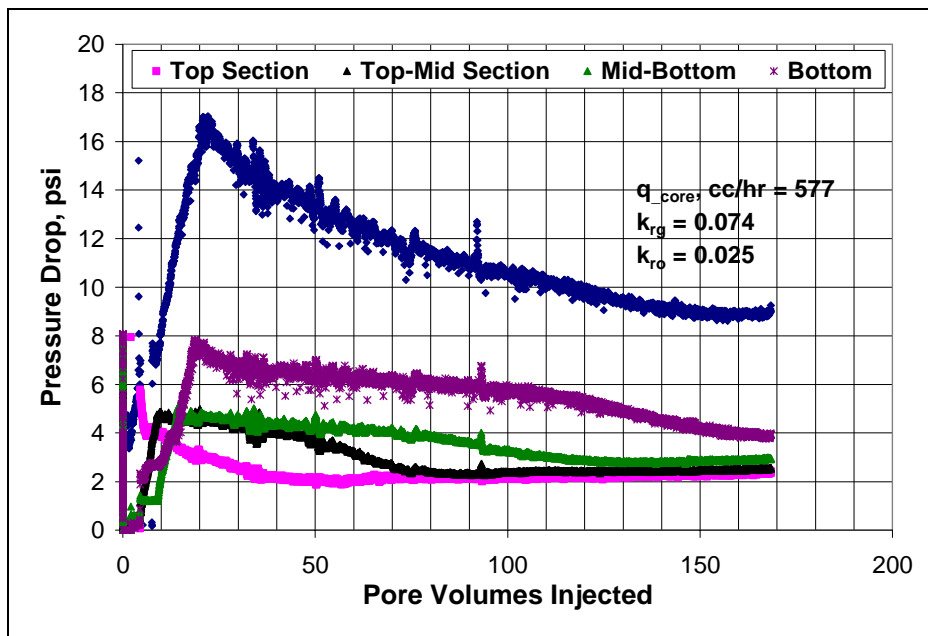


Figure B15.3: Pressure drop across the core during the initial two-phase flow at 275°F and 1500 psig

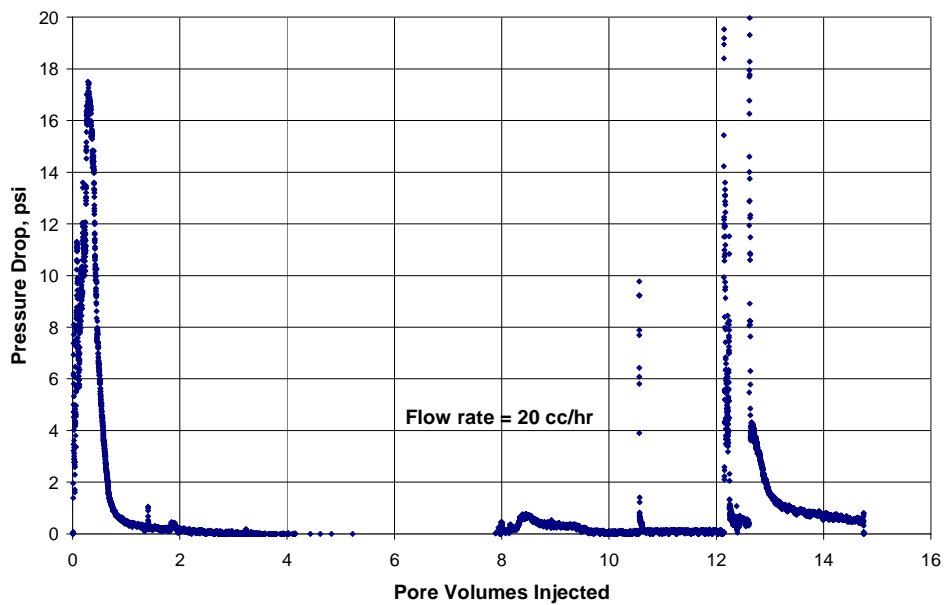


Figure B15.4: Pressure drop across the core during methanol preflush

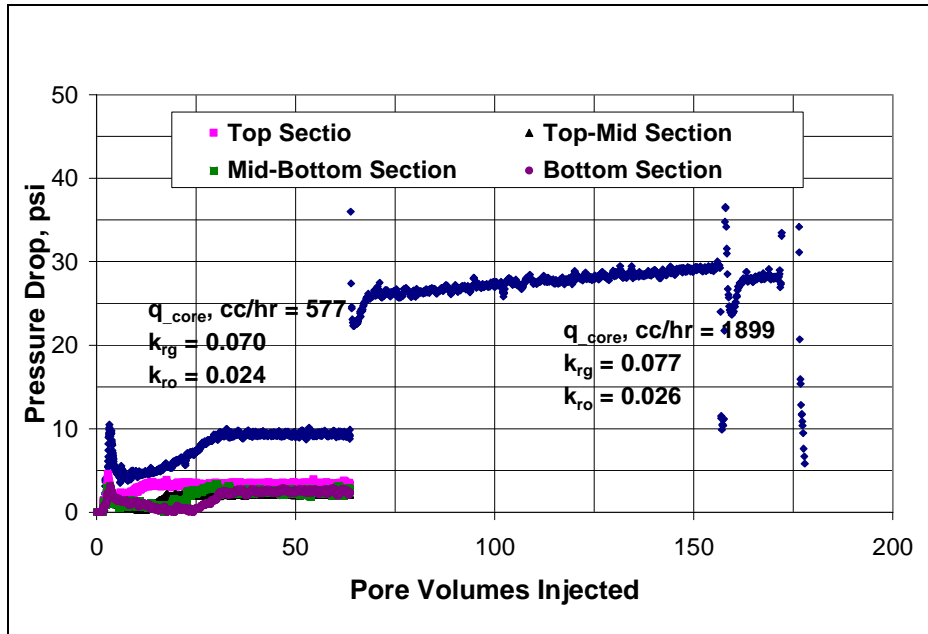


Figure B15.5: Pressure drop across the core during the two-phase flow at 275°F and 1500 psig after methanol pre-flush

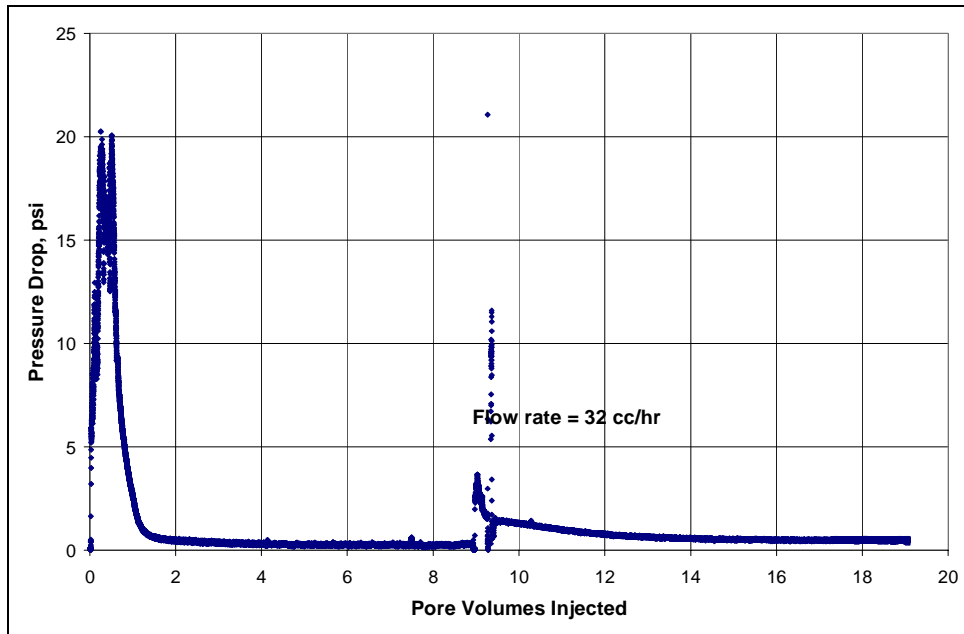


Figure B15.6: Pressure drop across the core during surfactant treatment

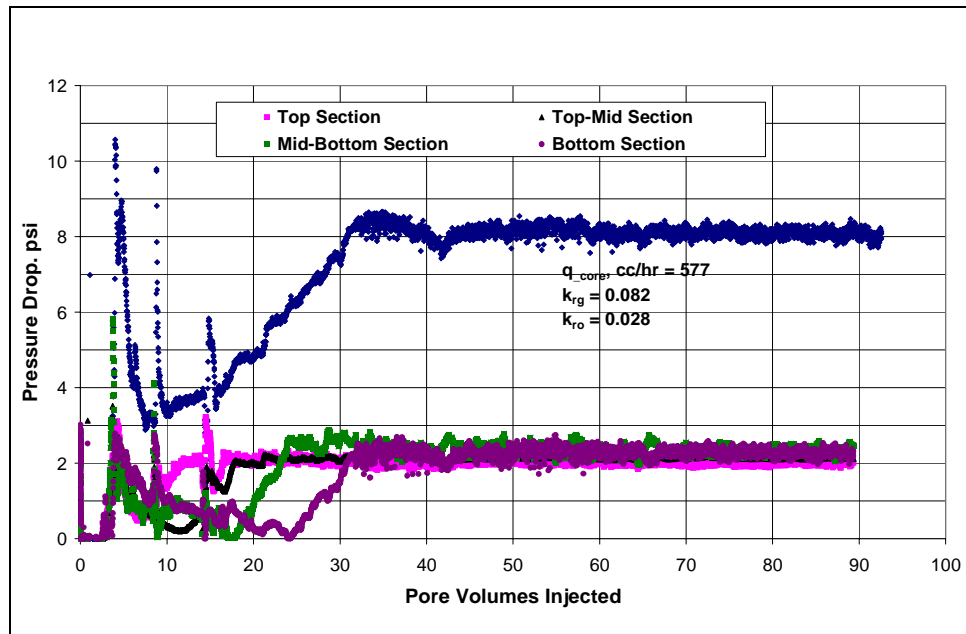


Figure B15.7: Pressure drop across the core during the post-first treatment two-phase flow at 275°F and 1500 psig

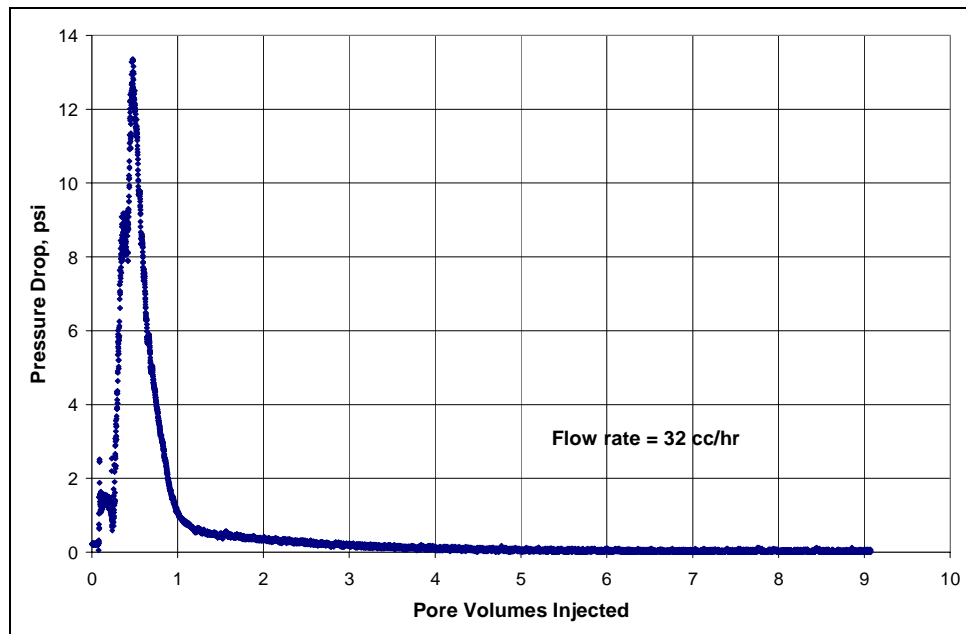


Figure B15.8: Pressure drop across the core during the toluene flood

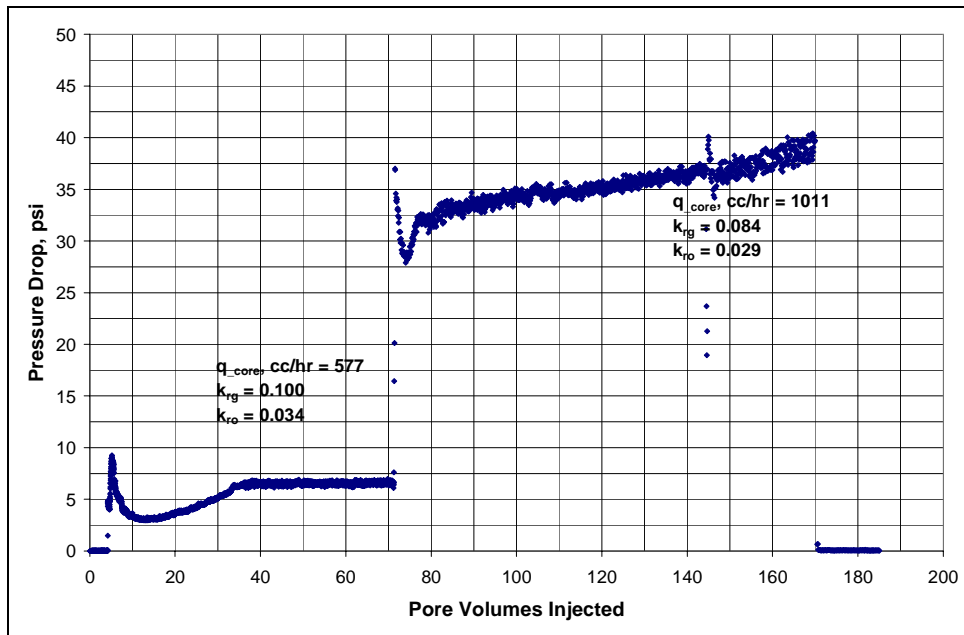


Figure B15.9: Pressure drop across the core during the two-phase flow at 275°F and 1500 psig after toluene flood

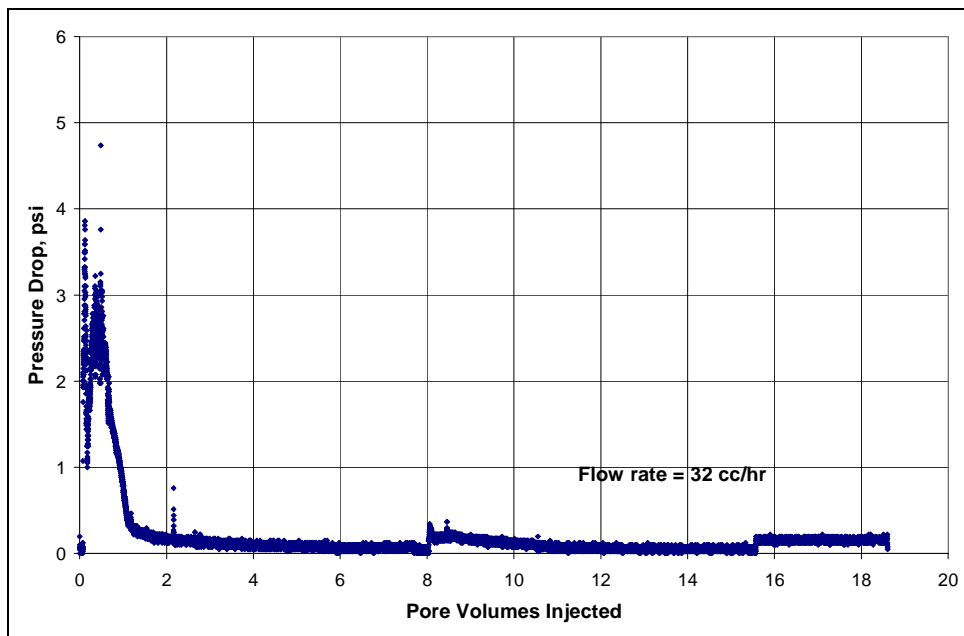


Figure B15.10: Pressure drop across the core during the second surfactant treatment

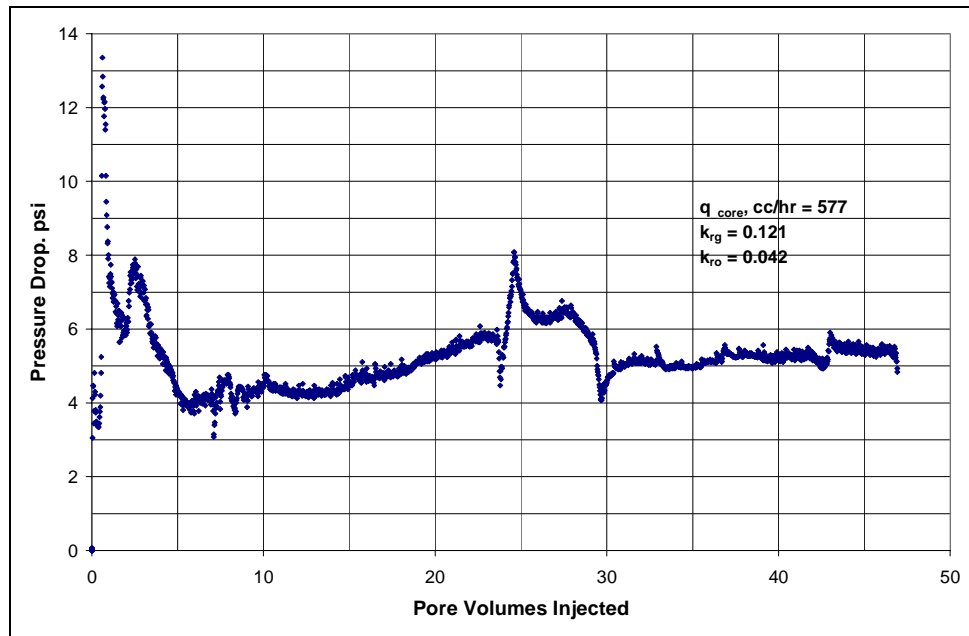


Figure B15.11: Pressure drop across the core during the post-second treatment two-phase flow at 275°F and 1500 psig

B16- Experiment No.16

Objective:

The objective of this experiment was to measure gas and condensate relative permeabilities at high capillary numbers. The experiment was performed on Texas cream limestone at 145°F.

Experimental Results:

Table B16.1 summarizes the properties of the core and the experimental conditions. Initial permeability of the core was measured using nitrogen at 75°F. **Figure B16.1** shows the pressure drop measured across the core during nitrogen flood. **Table B15.2** summarizes the results of the nitrogen flood.

Synthetic fluid mixture-1 (**Table 3.1**) was used for the two-phase flow measurements. The gas condensate floods were conducted with the upstream backpressure regulator set at 3600 psig and the downstream back pressure regulator set at 2600 psig. **Table B16.3** gives the fluid properties of the synthetic fluid calculated using the Peng-Robinson EOS at the flowing core pressure. **Figure B16.2** shows the pressure drop across the core during the two-phase gas-condensate flood done at multiple rates. **Table B16.4** summarizes the results of the two-phase floods.

Table B16.1: Core properties

Core	Texas Cream Limestone
Length, inches	8
Diameter, inches	1
Porosity, %	19.42
Pore volume, cc	20.00
Swi, %	0
Temperature, °F	145

Table B16.2: Result of nitrogen flood

q_{core}, (cc/hr)	ΔP (psi)	k_g (md)
529.68	8.46	20.29
1059.37	17.38	17.76
1853.89	31.54	19.05
Permeability, k_g (md)		19.26

Table B16.3: Synthetic fluid properties at experimental conditions

Pressure, psig	3600	2600	
Fluid Properties		Gas phase	Oil phase
ρ, g/cc	0.2985	0.2184	0.371
μ (cp)		0.0269	0.0592
Volume fraction		0.8252	0.1748
IFT (dyne/cm)		0.049	

Table B16.4: Results of gas condensate two-phase floods at 145°F and 2600 psig

q_{pump}, cc/hr	512	256	128	64	900
$q_{\text{total_core}}$, cc/hr	623.61	311.81	155.90	77.95	1096.20
$q_{\text{g_core}}$, cc/hr	514.61	257.30	128.65	64.33	904.58
$q_{\text{o_core}}$, cc/hr	109.01	54.50	27.25	13.63	191.62
ΔP, psi	40.28	24.86	15.26	8.00	64.41
k_{rg}	0.287	0.232	0.189	0.180	0.315
k_{ro}	0.134	0.108	0.088	0.084	0.147
Nc	5.40×10^{-4}	3.34×10^{-4}	2.05×10^{-4}	1.07×10^{-4}	8.64×10^{-4}
PVT Ratio	2.15	2.15	2.15	2.15	2.15

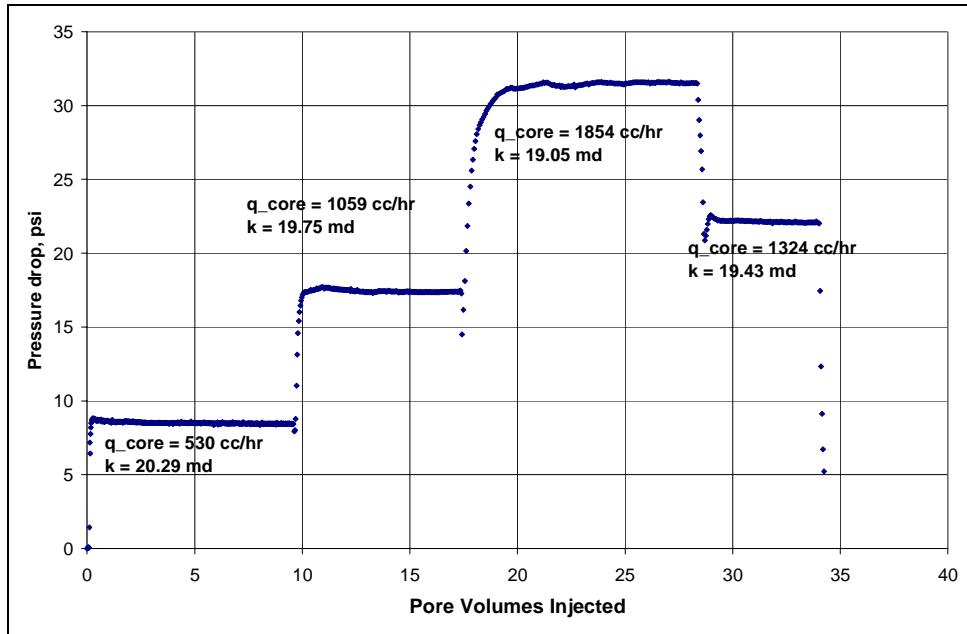


Figure B16.1: Pressure drop across the core during initial nitrogen flood

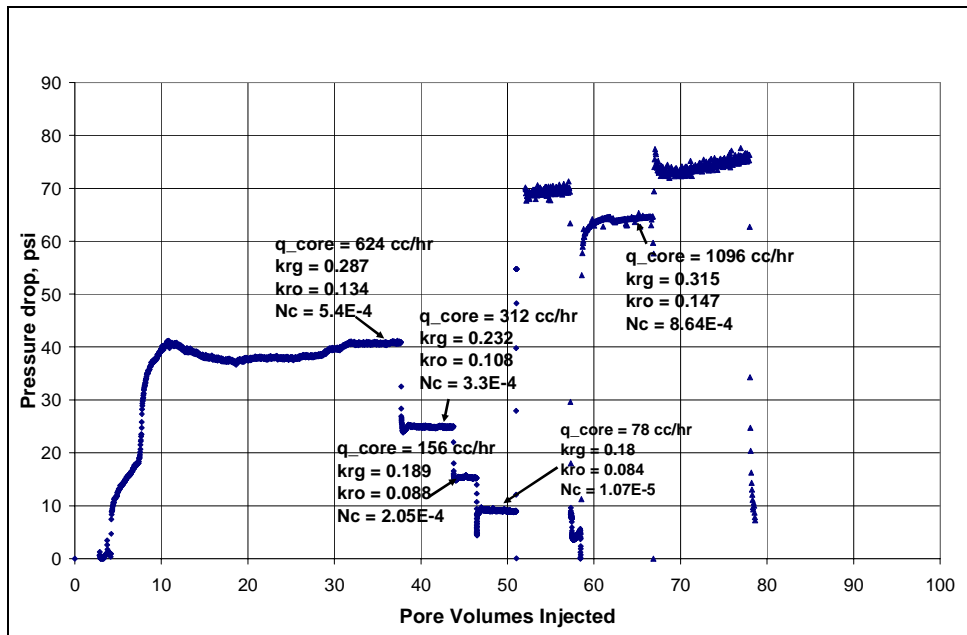


Figure B16.2: Pressure drop across the core during the two-phase floods at 145°F and 2600 psig

B17- Experiment No.17

Objective:

The objective of this experiment was to measure gas and condensate relative permeabilities at high capillary numbers. The experiment was performed on a Berea sandstone core at 145°F.

Experimental Results:

Table B17.1 summarizes the properties of the core and the experimental conditions. Initial permeability of the core was measured using nitrogen at 75°F. **Figure B17.1** shows the pressure drop measured across the core during nitrogen flood. **Table B17.2** summarizes the results of the nitrogen flood.

Synthetic fluid mixture-1 (**Table 3.1**) was used for the two-phase flow measurements. The gas condensate floods were conducted with the upstream backpressure regulator set at 3600 psig. The downstream back pressure regulator varied from 2580 psig to 2625 psig. **Table B17.3** gives the fluid properties of the synthetic fluid calculated using the Peng-Robinson EOS at the flowing core pressures. **Figure B17.2** shows the pressure drop across the core during the two-phase gas-condensate flood done at multiple rates. **Table B17.4** summarizes the results of the two-phase floods.

Table B17.1: Core properties

Core	Berea Sandstone
Length, inches	8
Diameter, inches	1
Porosity, %	19.42
Pore volume, cc	20.00
Swi, %	0
Temperature, °F	145

Table B17.2: Result of nitrogen flood

q_{core} , (cc/hr)	ΔP (psi)	k_g (md)
473.46	0.91	200.95
1190.01	2.21	207.38
Permeability, k_g (md)		204.17

Table B17.3: Synthetic fluid properties at experimental conditions

Pressure, psig	3600	2600	
Fluid Properties		Gas phase	Oil phase
ρ , g/cc	0.2985	0.2184	0.371
μ (cp)		0.0269	0.0592
Volume fraction		0.8252	0.1748

Table B17.4: Results of gas condensate two-phase floods at 145°F

BPR-2 pressure, psig	2625	2620	2600	2580	2600
IFT, dyne/cm	0.038	0.04	0.049	0.059	0.049
q_{pump}, cc/hr	448	750	1126	128	1574
q_{total_core}, cc/hr	538.83	901.56	1353.55	153.87	1892.08
q_{g_core}, cc/hr	444.40	743.97	1116.95	126.97	1561.34
q_{o_core}, cc/hr	94.14	157.59	236.60	26.90	330.74
ΔP, psi	2.86	4.71	6.14	1.25	6.91
k_{rg}	0.352	0.362	0.426	0.226	0.543
k_{ro}	0.156	0.159	0.183	0.102	0.189
Nc	5.14x10 ⁻⁴	8.05x10 ⁻⁴	8.56x10 ⁻⁴	1.45x10 ⁻⁴	1.16x10 ⁻³
PVT Ratio	2.15	2.15	2.15	2.15	2.15

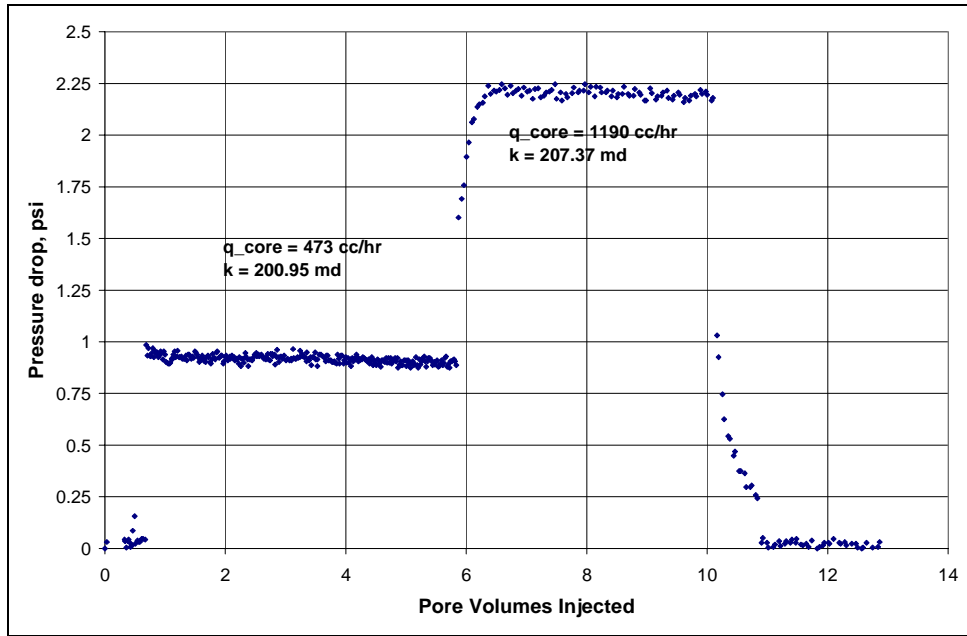


Figure B17.1: Pressure drop across the core during initial nitrogen flood

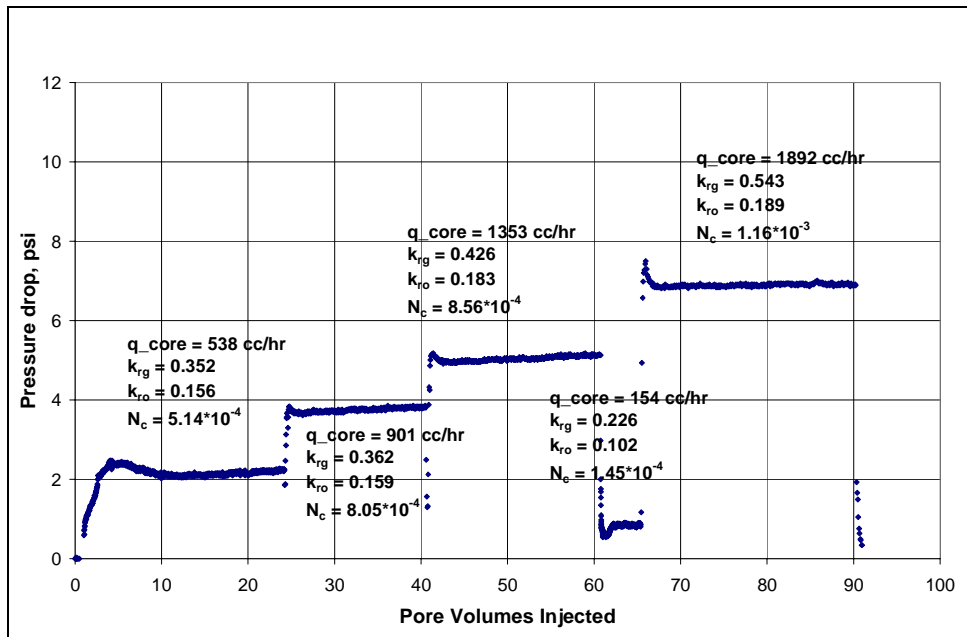


Figure B17.2: Pressure drop across the core during the two-phase floods at 145°F

B19- Experiment No.19

Objective:

The objective of this experiment was to investigate the effect of chemical treatment using the surfactant FC4430 delivered in a mixture of toluene/IPA/water in improving the gas and condensate relative permeability on a Berea sandstone rock in presence of initial water. The experiment was performed at 275°F.

Experimental Results:

Table B19.1 summarizes the properties of the core and the experimental conditions. Initial permeability of the core was measured using nitrogen at 75°F. **Figure B19.1** shows the pressure drop measured across the core during nitrogen flood. **Table B19.2** summarizes the results of the nitrogen flood.

The initial water saturation of 26% was established by injecting 2.6 cc of synthetic Britannia brine (**Table B6.3**) in the vacuumed core. Nitrogen flood was then conducted to measure the end point gas relative permeability. **Figure B19.2** shows the pressure drop measured across the core. **Table B19.3** summarizes the results of the nitrogen flood. The pressure of the core was raised to 500 psig and then the temperature of the oven was increased to 275°F.

Synthetic fluid mixture-2 (Table 3.2) was used for the two-phase flow measurements. The initial flood was conducted with the upstream backpressure regulator set at 4900 psig and the downstream back pressure regulator set at 1500 psig. **Table B19.4** gives the fluid properties of the synthetic fluid calculated using the Peng-Robinson EOS at the flowing core pressure. **Figure B19.3** shows the pressure drop across the core

during the two-phase gas-condensate flow. **Table B19.5** summarizes the results of the initial two-phase flow.

The core was then treated with the treatment solution (**Table B19.6**). **Figure B19.4** shows the measured pressure drop across the core during the treatment flood. The treatment solution was injected at 32cc/hr for the first 7 pore volumes and then at 128cc/hr for the next 12. The core was then shut-in for 24 hours.

Post-treatment two-phase gas-condensate flood was conducted under the same conditions as the initial two-phase flow. **Figure B19.5** shows the pressure drop across the core measured during the post-treatment two-phase flow at a flowing pressure of 1500 psig. **Table B19.7** summarizes the results of the post-treatment two-phase flow.

Table B19.1: Core properties

Core	Berea Sandstone
Length, inches	8
Diameter, inches	1
Porosity, %	20
Pore volume, cc	20.59
Swi, %	26.1
Temperature, °F	275

Table B19.2: Result of nitrogen flood

q_{core}, (cc/hr)	ΔP (psi)	k_g (md)
615.50	0.77	260.39
1231.01	1.76	226.94
2188.19	3.57	216.94
Permeability, k_g (md)		234.75

Table B19.3: Result of nitrogen flood at Swi

q_{core}, (cc/hr)	ΔP (psi)	k_g (md)
615.50	2.938	67.90
1231.01	5.99	66.61
2188.19	8.03	88.36
Permeability, k_g (md)		74.29

Table B19.4: Synthetic fluid properties at experimental conditions

Pressure, psig	4500	1500	
Fluid Properties		Gas phase	Oil phase
ρ, g/cc	0.2067	0.0615	0.6018
μ (cp)		0.0165	0.2639
Volume fraction		0.979	0.021
IFT (dyne/cm)		5.184	

Table B19.5: Results of the initial two-phase gas condensate flood

q_{pump}, cc/hr	256
$q_{\text{total_core}}$, cc/hr	703.83
$q_{\text{g_core}}$, cc/hr	689.05
$q_{\text{o_core}}$, cc/hr	14.78
ΔP, psi	13.95
k_{rg}	0.057
k_{ro}	0.019
Nc	1.22×10^{-5}
PVT Ratio	2.90

Table B19.6: Composition of treatment solution

Component	Weight %
FC4430	2
IPA	44
Toluene	44
D.I. water	10

Table B19.7: Results of post-treatment two-phase flow of gas condensate mixture

q_{pump}, cc/hr	256
q_{total_core}, cc/hr	703.83
q_{g_core}, cc/hr	689.05
q_{o_core}, cc/hr	14.78
ΔP, psi	10.60
k_{rg}	0.075
k_{ro}	0.026
Nc	9.24x10 ⁻⁶
Improvement factor	1.32

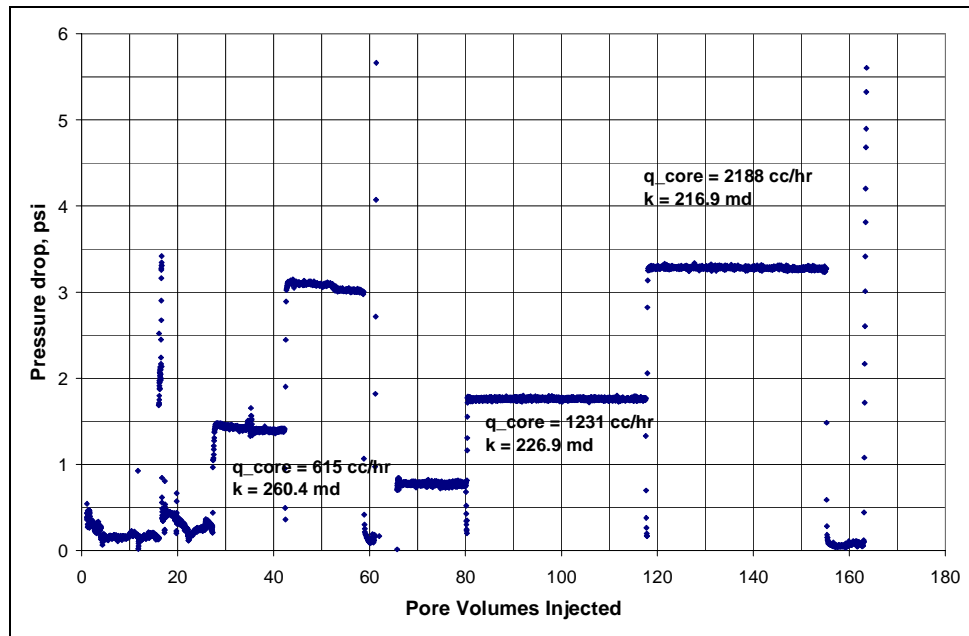


Figure B19.1: Pressure drop across the core during initial nitrogen flood

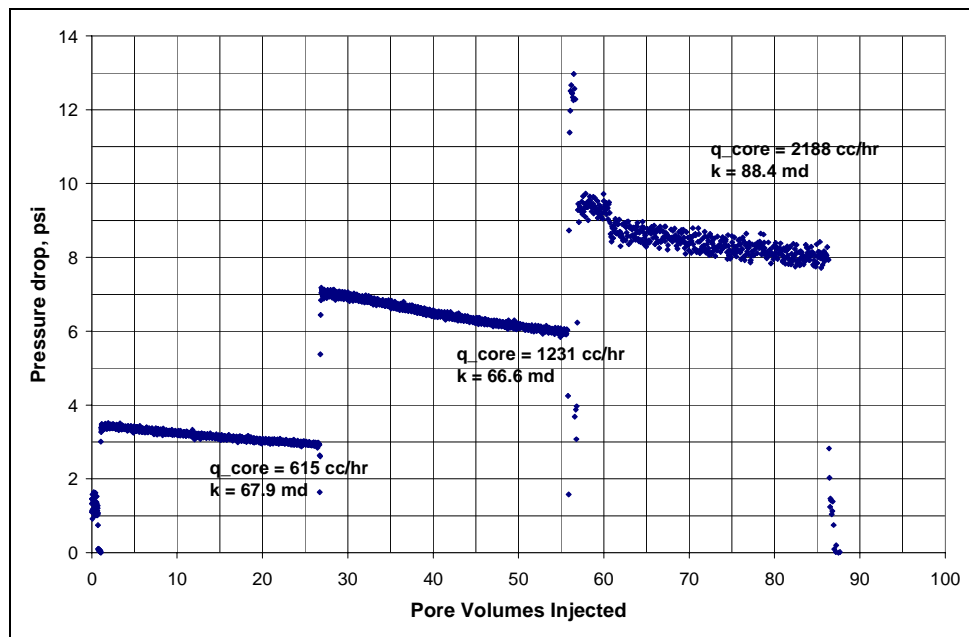


Figure B19.2: Pressure drop across the core during nitrogen flood at $Sw_i = 26.1\%$

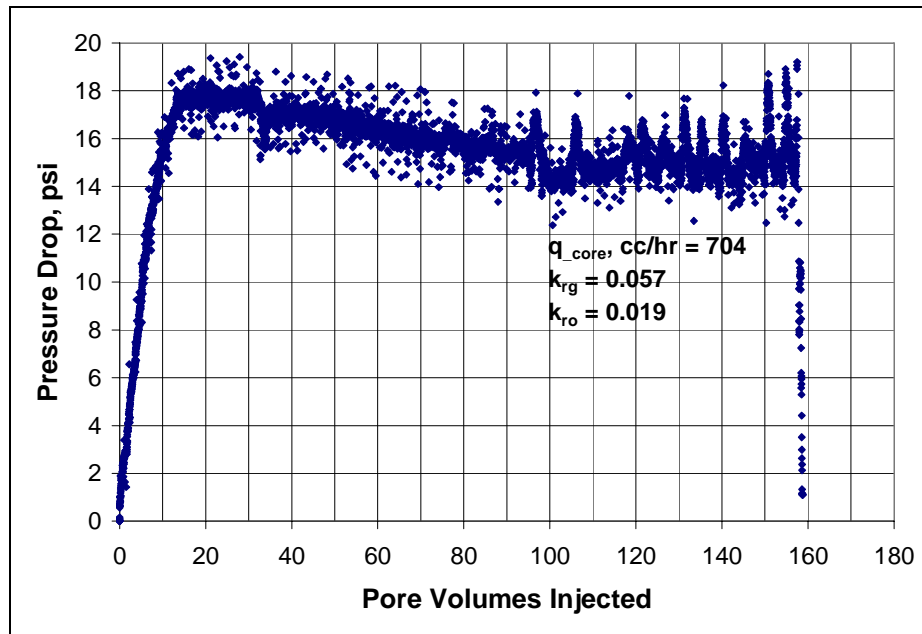


Figure B19.3: Pressure drop across the core during the initial two-phase flow at 275°F and 1500 psig

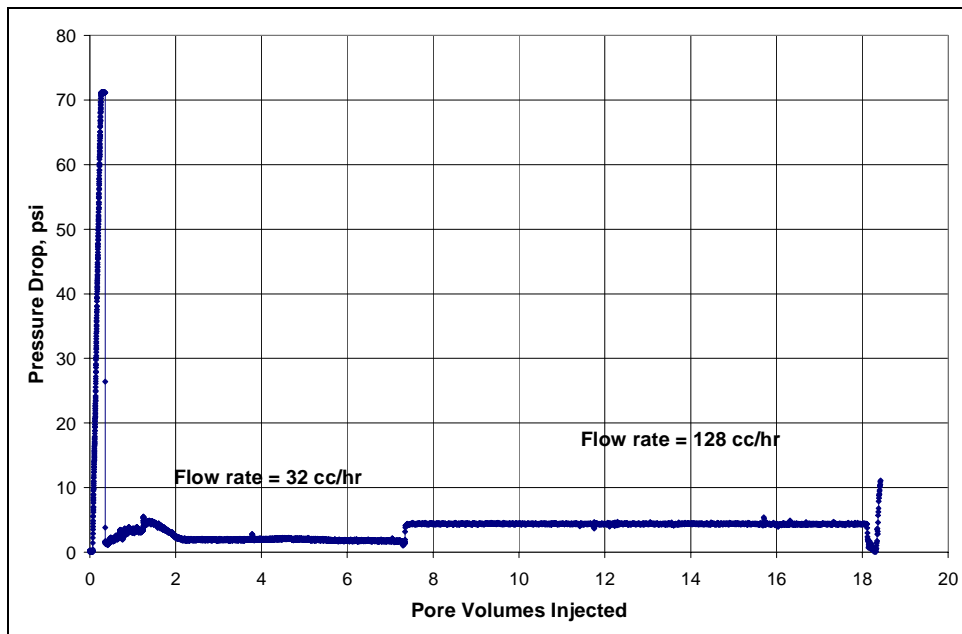


Figure B19.4: Pressure drop across the core during surfactant treatment

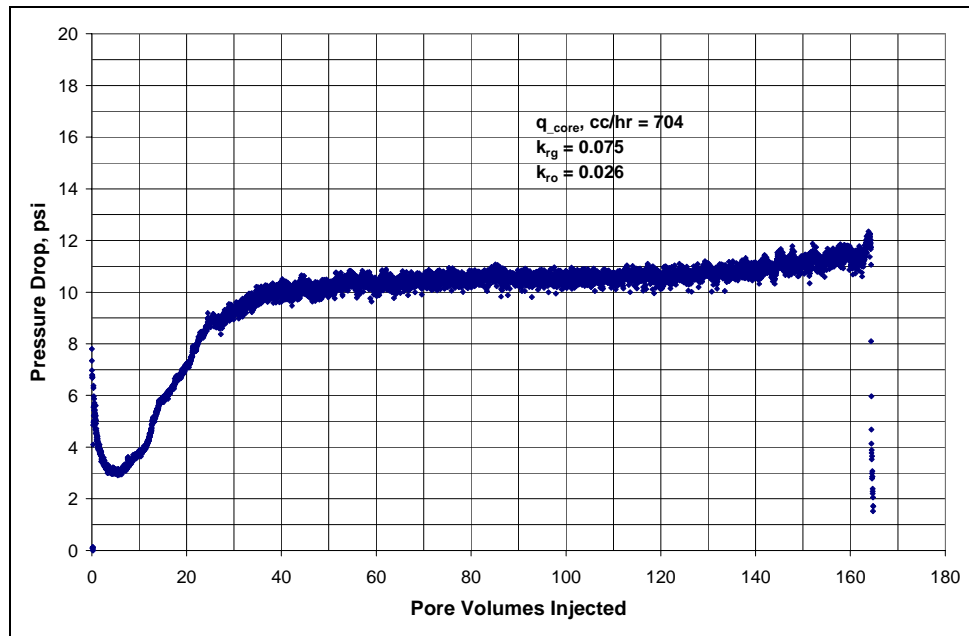


Figure B19.5: Pressure drop across the core during post-treatment two-phase flow at 275°F and 1500 psig

B20- Experiment No.20

Objective:

The objective of this experiment was to investigate the effect of chemical treatment using the surfactant FC4430 delivered in a mixture of IPA/water in improving the gas and condensate relative permeability on a Berea sandstone rock in presence of initial water. The experiment was performed at 275°F.

Experimental Results:

Table B20.1 summarizes the properties of the core and the experimental conditions. Initial permeability of the core was measured using nitrogen at 75°F. **Figure B20.1** shows the pressure drop measured across the core during nitrogen flood. **Table B20.2** summarizes the results of the nitrogen flood.

The initial water saturation of 26% was established by injecting 2.6 cc of synthetic Britannia brine (**Table B6.3**) in the vacuumed core. Nitrogen flood was then conducted to measure the end point gas relative permeability. **Figure B20.2** shows the pressure drop measured across the core and **Table B20.3** summarizes the results of the nitrogen flood. The pressure of the core was raised to 500 psig and then the temperature of the oven was increased to 275°F.

Synthetic fluid mixture-2 (**Table 3.2**) was used for the two-phase flow measurements. The initial flood was conducted with the upstream backpressure regulator set at 4900 psig and the downstream back pressure regulator set at 1500 psig. **Table B20.4** gives the fluid properties of the synthetic fluid calculated using the Peng-Robinson EOS at the flowing core pressure. **Figure B20.3** shows the pressure drop across the core

during the two-phase gas-condensate flow. **Table B20.5** summarizes the results of the initial two-phase flow.

The core was then treated with the treatment solution (**Table B20.6**). **Figure B20.4** shows the measured pressure drop across the core during the treatment flood. The treatment solution was injected at 32cc/hr. The core was then shut-in for 24 hours.

Post-treatment two-phase gas-condensate flood was conducted under the same conditions as the initial two-phase flow. **Figure B20.5** shows the pressure drop across the core measured during the post-treatment two-phase flow at a flowing pressure of 1500 psig. **Table B20.7** summarizes the results of the post-treatment two-phase flow.

Table B20.1: Core properties

Core	Berea Sandstone
Length, inches	8
Diameter, inches	1
Porosity, %	20
Pore volume, cc	20.59
Swi, %	26.1
Temperature, °F	275

Table B20.2: Result of nitrogen flood

q_{core}, (cc/hr)	ΔP (psi)	k_g (md)
656.70	0.93	228.95
1386.1	2.0	224.61
2432.94	3.73	211.51
Permeability, k_g (md)		221.69

Table B20.3: Result of nitrogen flood at Swi

q_{core}, (cc/hr)	ΔP (psi)	k_g (md)
600.96	2.88	67.62
1199.51	7.43	52.34
2229.39	13.25	54.54
Permeability, k_g (md)		58.17

Table B20.4: Synthetic fluid properties at experimental conditions

Pressure, psig	4500	1500	
Fluid Properties		Gas phase	Oil phase
ρ, g/cc	0.2067	0.0615	0.6018
μ (cp)		0.0165	0.2639
Volume fraction		0.979	0.021
IFT (dyne/cm)		5.184	

Table B20.5: Results of the initial two-phase gas condensate flood

q_{pump}, cc/hr	240.5
$q_{\text{total_core}}$, cc/hr	661.22
$q_{\text{g_core}}$, cc/hr	647.33
$q_{\text{o_core}}$, cc/hr	13.89
ΔP, psi	10.84
k_{rg}	0.073
k_{ro}	0.025
Nc	1.51×10^{-5}
PVT Ratio	2.90

Table B20.6: Composition of treatment solution

Component	Weight %
FC4430	2
IPA	88
D.I. water	10

Table B20.7: Results of post-treatment two-phase flow of gas condensate mixture

q_{pump}, cc/hr	240.5
q_{total_core}, cc/hr	661.22
q_{g_core}, cc/hr	647.33
q_{o_core}, cc/hr	13.89
ΔP, psi	10.50
k_{rg}	0.075
k_{ro}	0.026
Nc	1.47x10 ⁻⁵
Improvement factor	1.03

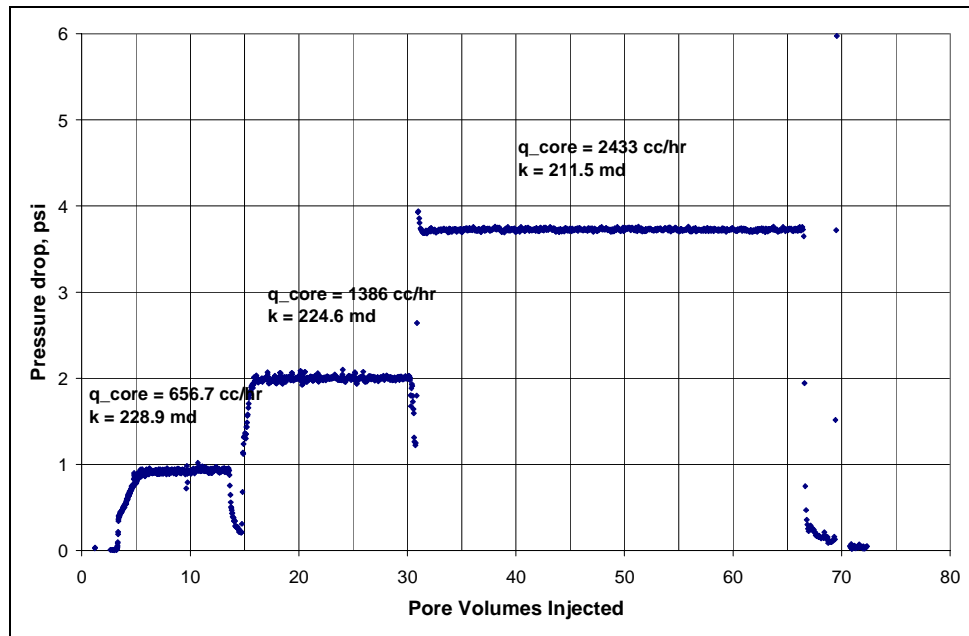


Figure B20.1: Pressure drop across the core during initial nitrogen flood

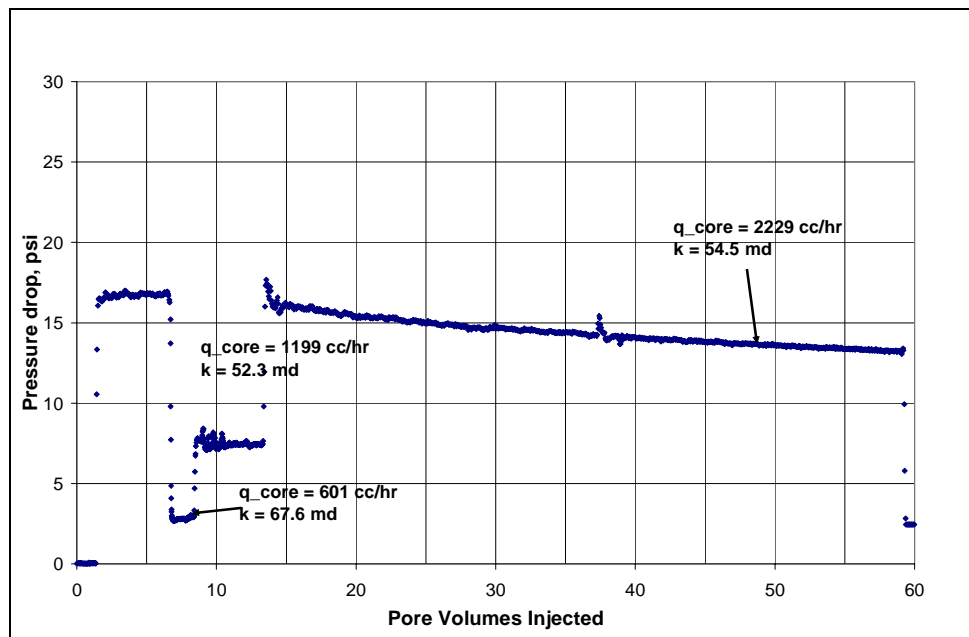


Figure B20.2: Pressure drop across the core during nitrogen flood at $Sw_i=26.1\%$

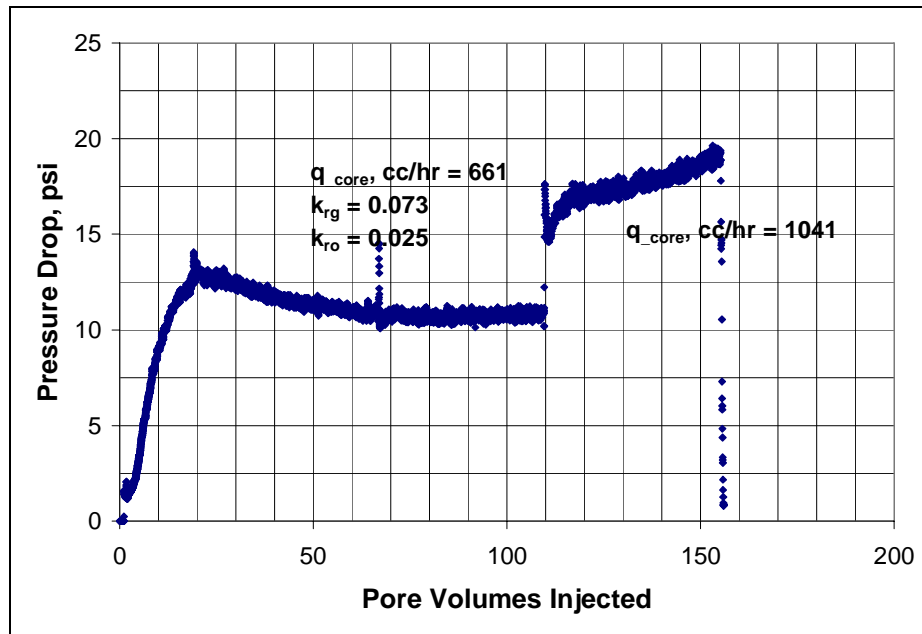


Figure B20.3: Pressure drop across the core during the initial two-phase flow at 275°F and 1500 psig

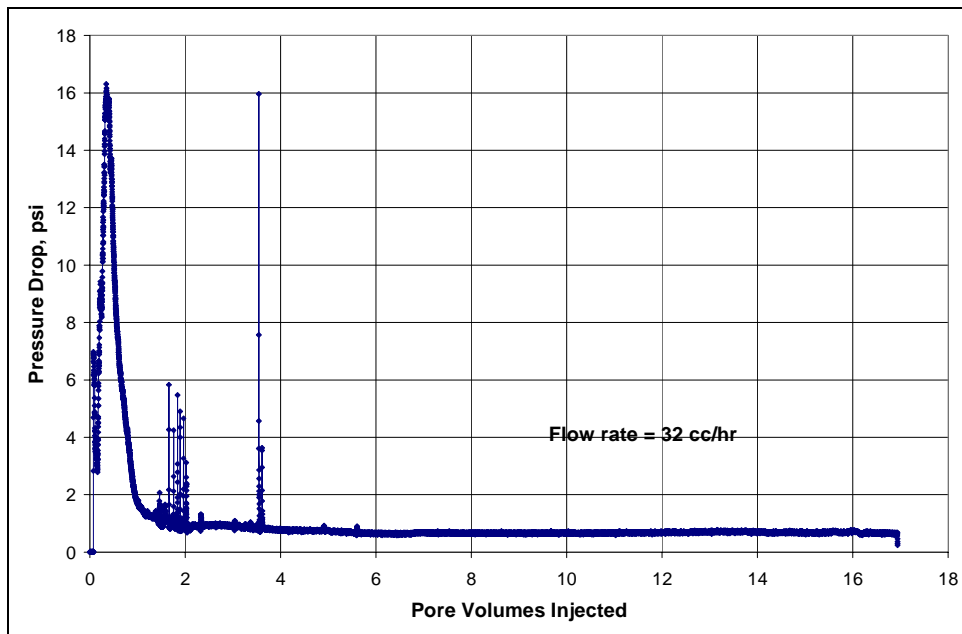


Figure B20.4: Pressure drop across the core during surfactant treatment

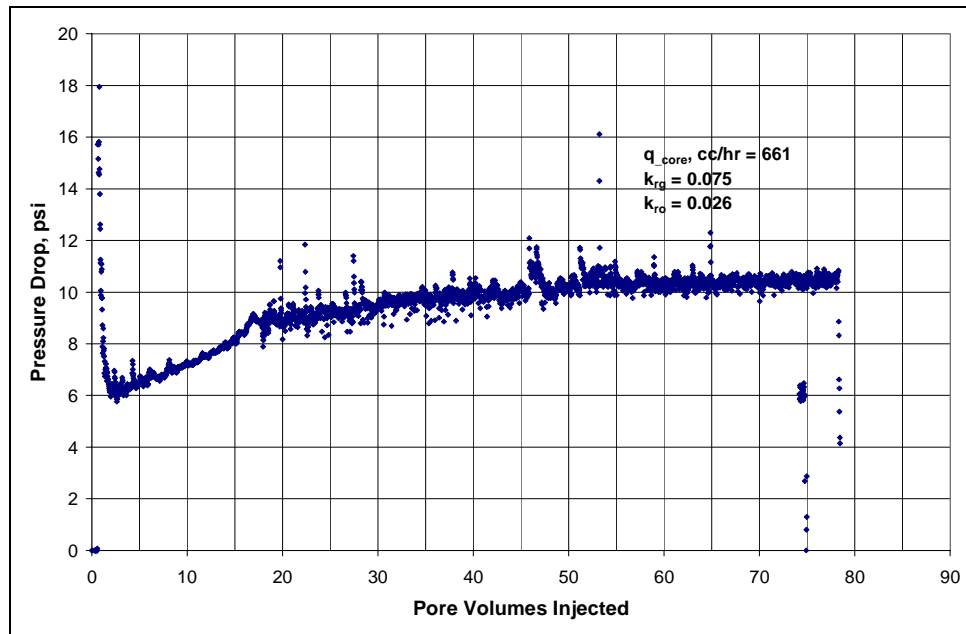


Figure B20.5: Pressure drop across the core during post-treatment two-phase flow at 275°F and 1500 psig

B21- Experiment No.21

Objective:

The objective of this experiment was to investigate the effect of chemical treatment using the surfactant FC4430 delivered in a mixture of 2-butoxyethanol/ethanol in improving the gas and condensate relative permeability on a Berea sandstone rock in presence of initial water. The experiment was performed at 175°F.

Experimental Results:

Table B21.1 summarizes the properties of the core and the experimental conditions. Initial permeability of the core was measured using nitrogen at 75°F. **Figure B21.1** shows the pressure drop measured across the core during nitrogen flood. **Table B21.2** summarizes the results of the nitrogen flood.

The initial water saturation of 19% was established by injecting 3.8 cc of synthetic Bruce brine (**Table B21.3**) in the vacuumed core. Nitrogen flood was then conducted to measure the end point gas relative permeability. **Figure B21.2** shows the pressure drop measured across the core and **Table B21.4** summarizes the results of the nitrogen flood. The pressure of the core was raised to 200 psig and then the temperature of the oven was increased to 175°F.

Synthetic fluid mixture-4 (**Table 3.4**) was used for the two-phase flow measurements. The initial flood was conducted with the upstream backpressure regulator set at 4970 psig and the downstream back pressure regulator set at 1985 psig. **Table B21.5** gives the properties of the synthetic fluid calculated using the Peng-Robinson EOS at the flowing core pressure. **Figure B21.3** shows the pressure drop across the core

during the two-phase gas-condensate flow. **Table B21.6** summarizes the results of the initial two-phase flow.

The core was then treated with the treatment solution (**Table B21.7**). **Figure B21.4** shows the measured pressure drop across the core during the treatment flood. The treatment solution was injected at 224cc/hr. The core was then shut-in for 15 hours.

Post-treatment two-phase gas-condensate flood was conducted under the same conditions as the initial two-phase flow. Figure B21.5 shows the pressure drop across the core measured during the post-treatment two-phase flow at a flowing pressure of 1985 psig. Table B21.8 summarizes the results of the post-treatment two-phase flow.

Table B21.1: Core properties

Core	Berea Sandstone
Length, inches	8
Diameter, inches	1
Porosity, %	20
Pore volume, cc	20.59
Swi, %	19
Temperature, °F	175

Table B21.2: Result of nitrogen flood

q_{core}, (cc/hr)	ΔP (psi)	k_g (md)
1137.17	2.19	168.89
1514.91	3.19	154.80
2274.38	4.57	162.04
Permeability, k_g (md)		162.89

Table B21.3: Synthetic Bruce brine

Component	g/l
NaCl	64.54
CaCl ₂	7.72
MgCl ₂ .6H ₂ O	1.67
KCl	0.66

Table B21.4: Result of nitrogen flood at Swi

q_{core} , (cc/hr)	ΔP (psi)	k_g (md)
1137.19	3.50	105.83

Table B21.5: Synthetic fluid properties at experimental conditions

Pressure, psig	4970	2000	
Fluid Properties		Gas phase	Oil phase
ρ , g/cc	0.2973	0.1025	0.5674
μ (cp)		0.017	0.1907
Volume fraction		0.9148	0.0852
IFT (dyne/cm)		3.107	

Table B21.6: Results of the initial two-phase gas condensate flood

q_{pump} , cc/hr	256
$q_{\text{total_core}}$, cc/hr	535.56
q_{g_core} , cc/hr	489.93
q_{o_core} , cc/hr	45.63
ΔP , psi	18.72
k_{rg}	0.045

k_{ro}	0.047
Nc	3.29x10 ⁻⁵
PVT Ratio	0.96

Table B21.7: Composition of treatment solution

Component	Weight %
FC4430	2
2-butoxyethanol	69
Ethanol	29

Table B21.8: Results of post-treatment two-phase flow of gas condensate mixture

q_{pump}, cc/hr	256
q_{total_core}, cc/hr	535.56
q_{g_core}, cc/hr	489.93
q_{o_core}, cc/hr	45.63
ΔP, psi	9.69
k_{rg}	0.087
k_{ro}	0.091
Nc	1.70x10 ⁻⁵
Improvement factor	1.93

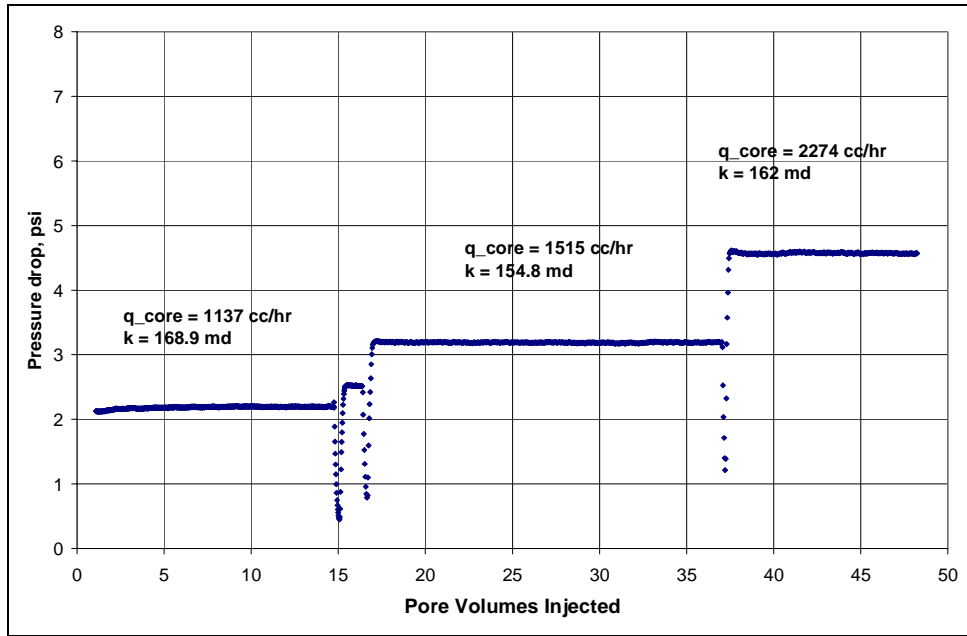


Figure B21.1: Pressure drop across the core during initial nitrogen flood

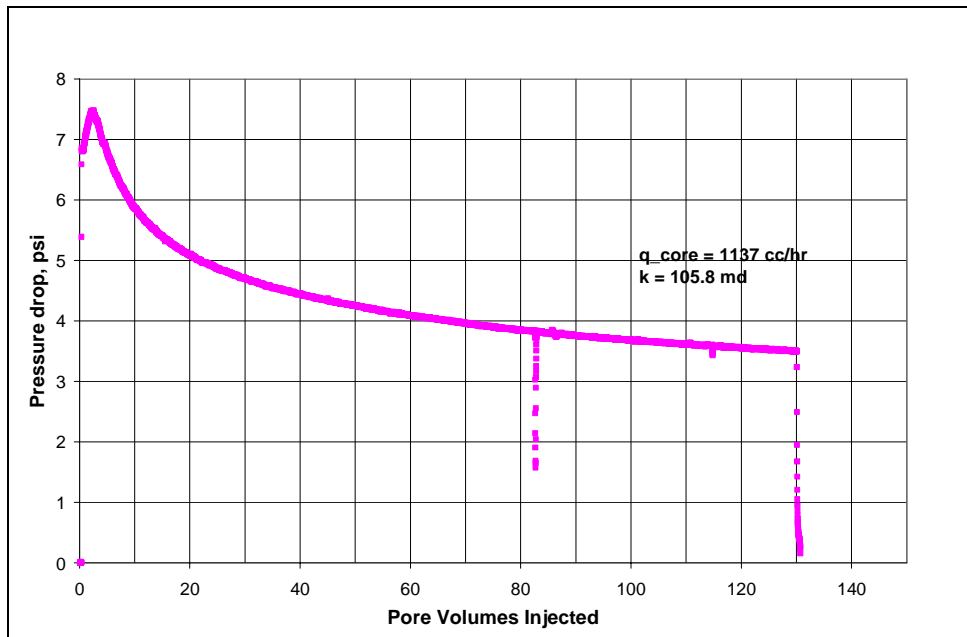


Figure B21.2: Pressure drop across the core during nitrogen flood at $S_{wi}=19\%$

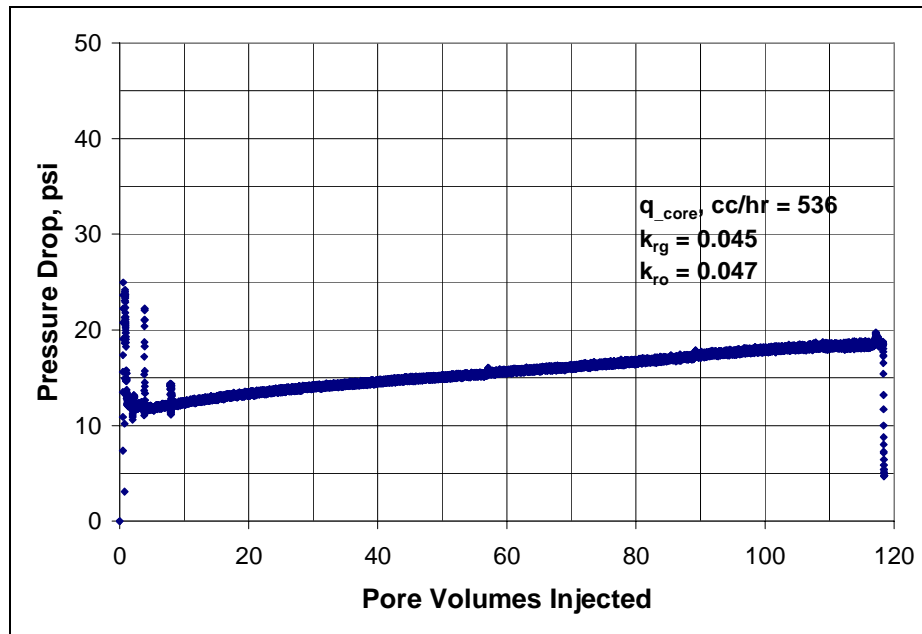


Figure B21.3: Pressure drop across the core during the initial two-phase flow at 175°F and 1985 psig

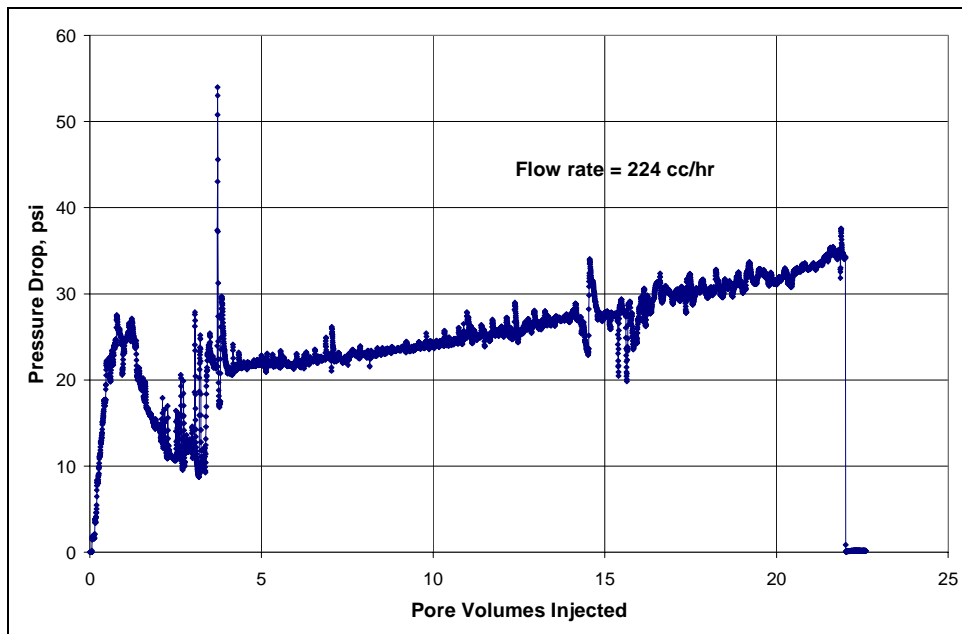


Figure B21.4: Pressure drop across the core during surfactant treatment

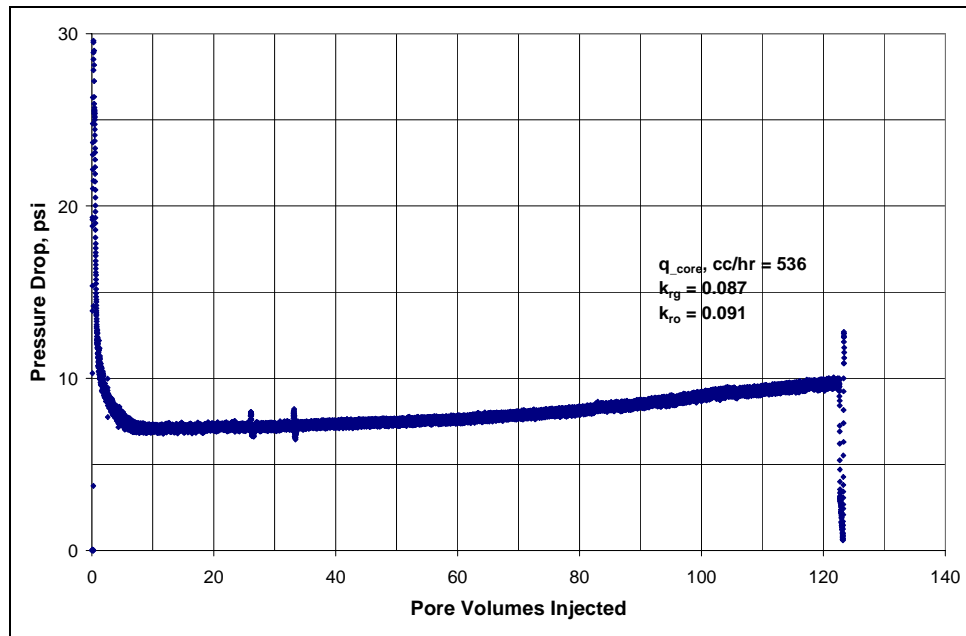


Figure B21.5: Pressure drop across the core during post-treatment two-phase flow at 175°F and 1985 psig

B23- Experiment No.23

Objective:

The objective of this experiment was to investigate the effect of chemical treatment using the surfactant FC4430 delivered in a mixture of 2-butoxyethanol/ethanol in improving the gas and condensate relative permeability on a reservoir sandstone rock in presence of initial water. The experiment was performed on Bruce reservoir cores (plugs #1 and #3) at 175°F.

Experimental Results:

Plugs #1 and #3 were stacked together vertically. **Table B23.1** summarizes the properties of the plugs and the experimental conditions. Initial permeability of the core (stacked plugs) was measured using nitrogen at 75°F. **Figure B23.1** shows the pressure drop measured across the core during nitrogen flood. **Table B23.2** summarizes the results of the nitrogen flood.

The initial water saturation of 19% was established by injecting 3.5 cc of synthetic Bruce brine (**Table B21.3**) in the vacuumed core. Nitrogen flood was then conducted to measure the end point gas relative permeability. **Figure B23.2** shows the pressure drop measured across the core and **Table B23.3** summarizes the results of the nitrogen flood. The pressure of the core was raised to 200 psig and then the temperature of the oven was increased to 175°F.

Synthetic fluid mixture-4 (**Table 3.4**) was used for the two-phase flow measurements. The initial flood was conducted with the upstream backpressure regulator set at 4950 psig and the downstream back pressure regulator set at 2000 psig. **Table B23.4** gives the properties of the synthetic fluid calculated using the Peng-Robinson EOS

at the flowing core pressure. **Figure B23.3** shows the pressure drop across the core during the two-phase gas-condensate flow. **Table B23.5** summarizes the results of the initial two-phase flow.

The core was then treated with the treatment solution (**Table B23.6**). **Figure B23.4** shows the measured pressure drop across the core during the treatment flood. The treatment solution was injected at 196cc/hr. The core was then shut-in for 15 hours.

Post-treatment two-phase gas-condensate flood was conducted under the same conditions as the initial two-phase flow. Two batches of gas mixture were used for the post-treatment two-phase flood. **Figure B23.5** shows the pressure drop across the core measured during the post-treatment two-phase floods at a flowing pressure of 2000 psig. **Table B23.7** summarizes the results of the post-treatment two-phase flow.

Methane flood was conducted to measure the post-treatment permeability of the core. **Table B23.8** summarizes the results and **Figure B23.6** shows the pressure drop measured across the stacked plugs during the methane flood at 175°F.

Table B23.1: Core properties

Core	Bruce Reservoir Core (plugs #1 and #3)
Length, inches (plug #1)	3.70
Length, inches ((plug #3))	2.86
Diameter, inches	1
Porosity, %	21.60
Pore volume, cc	18.25
Swi, %	19
Temperature, °F	175

Table B23.2: Result of nitrogen flood

q_{core} , (cc/hr)	ΔP (psi)	k_g (md)
27238.40	5.89	1129.75
23347.20	4.93	1157.49
15564.80	3.072	1238.54
Permeability, k_g (md)		1175.26

Table B23.3: Result of nitrogen flood at Swi

q_{core} , (cc/hr)	ΔP (psi)	k_g (md)
15564.80	3.83	993.48

Table B23.4: Synthetic fluid properties at experimental conditions

Pressure, psig	4950	2000	
Fluid Properties		Gas phase	Oil phase
ρ, g/cc	0.2973	0.1025	0.5674
μ (cp)		0.017	0.1907
Volume fraction		0.9148	0.0852
IFT (dyne/cm)		3.107	

Table B23.5: Results of the initial two-phase gas condensate flood

q_{pump}, cc/hr	512	900
$q_{\text{total_core}}$, cc/hr	1071.13	1882.84
$q_{\text{g_core}}$, cc/hr	979.87	1722.43
$q_{\text{o_core}}$, cc/hr	91.26	160.42
ΔP, psi	4.75	7.18
k_{rg}	0.04	0.047
k_{ro}	0.042	0.049
Nc	7.63×10^{-5}	1.15×10^{-4}
PVT Ratio	0.96	0.96

Table B23.6: Composition of treatment solution

Component	Weight %
FC4430	2
2-butoxyethanol	69
Ethanol	29

Table B23.7: Results of post-treatment two-phase flow of gas condensate mixture

q_{pump}, cc/hr	512
q_{total_core}, cc/hr	1071.13
q_{g_core}, cc/hr	979.87
q_{o_core}, cc/hr	91.26
ΔP, psi	3.12
k_{rg}	0.061
k_{ro}	0.064
Nc	5.01x10 ⁻⁵
Improvement Factor	1.53

Table B23.8: Result of methane flood to measure final permeability

q_{core}, (cc/hr)	ΔP (psi)	k_g (md)
12603.62	2.44	1263.11
18905.42	3.88	1191.94
22056.33	4.69	1150.37
Permeability, k_g (md)		1201.81

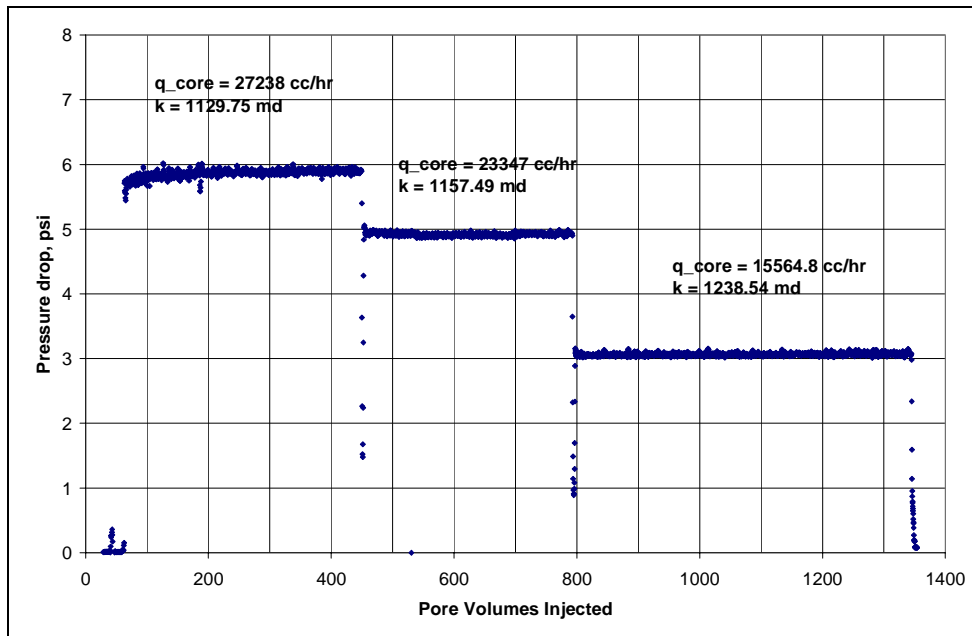


Figure B23.1: Pressure drop across the core during initial nitrogen flood

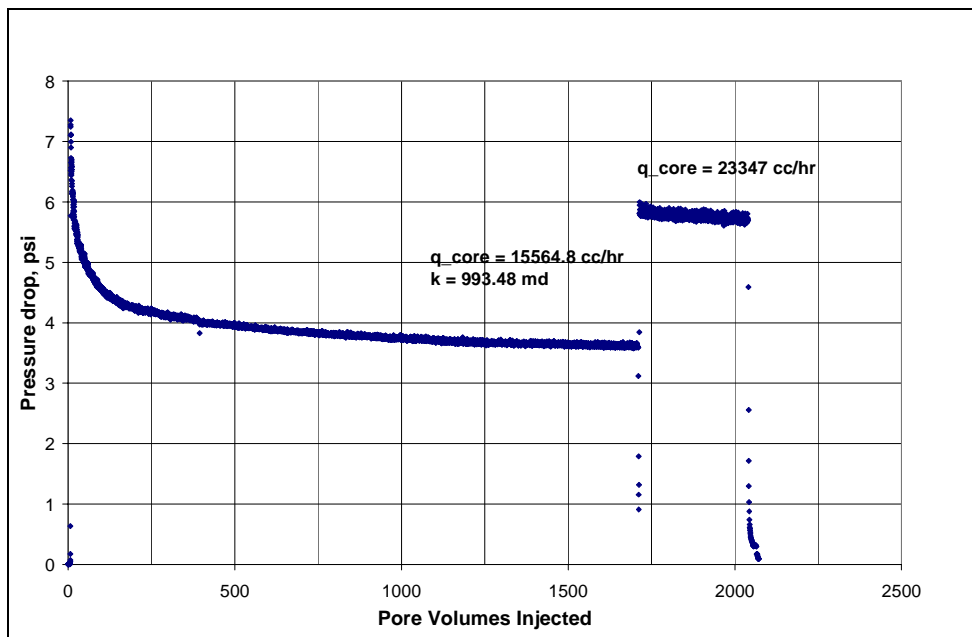


Figure B23.2: Pressure drop across the core during nitrogen flood at $S_{wi}=19\%$

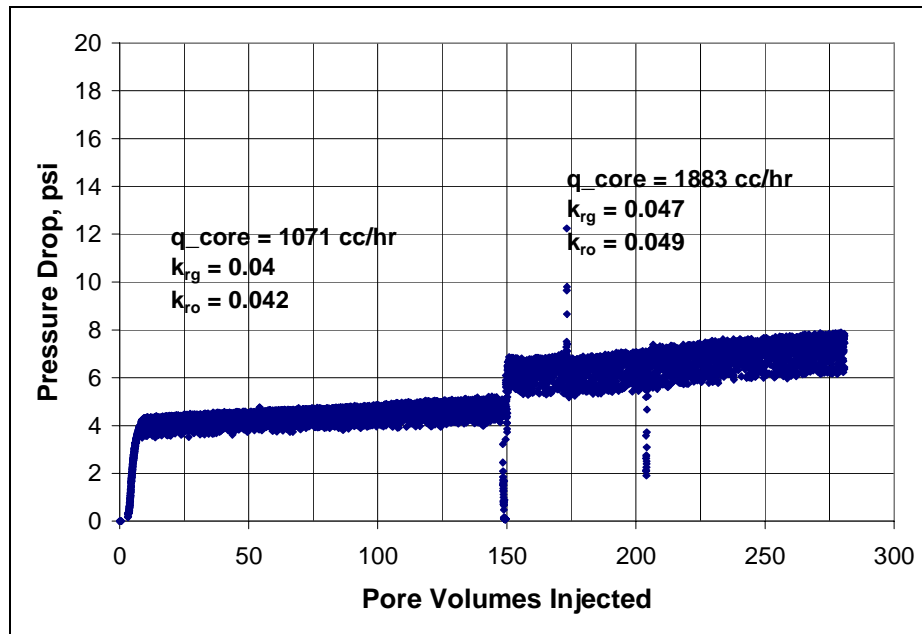


Figure B23.3: Pressure drop across the core during the initial two-phase flow at 175°F and 2000 psig

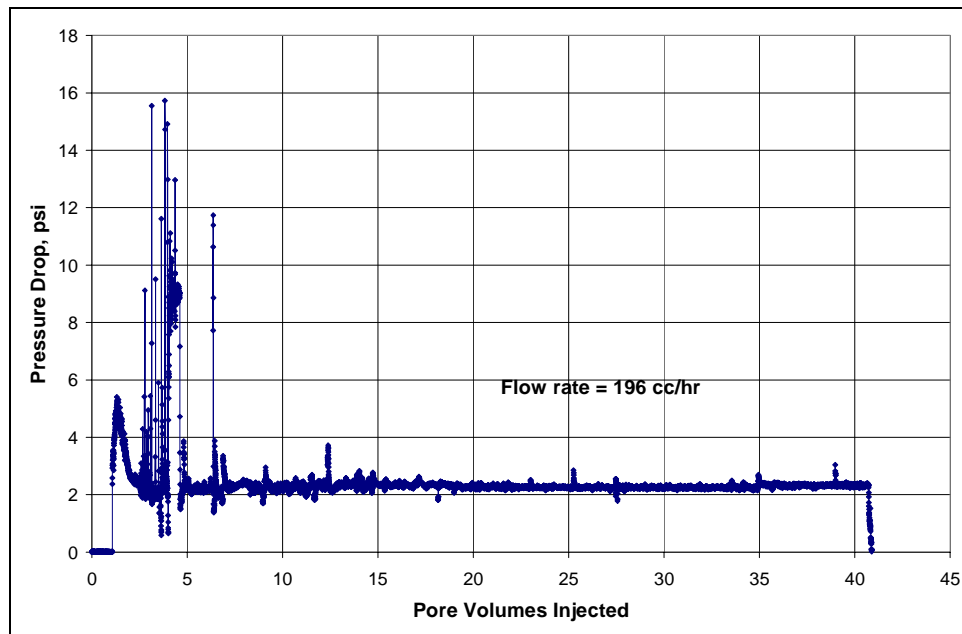


Figure B23.4: Pressure drop across the core during surfactant treatment

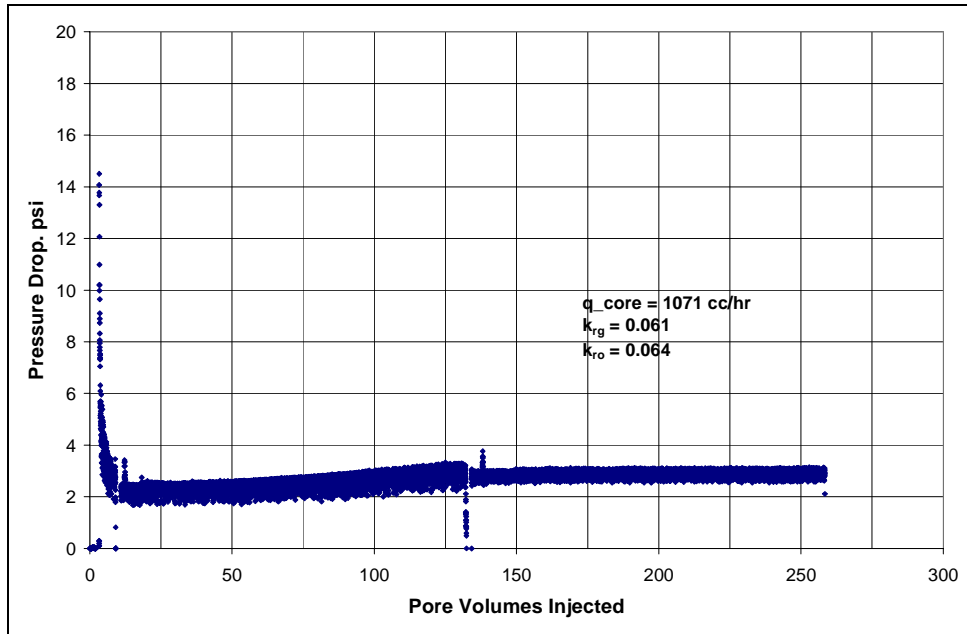


Figure B23.5: Pressure drop across the core during post-treatment two-phase flow at 175°F and 2000 psig

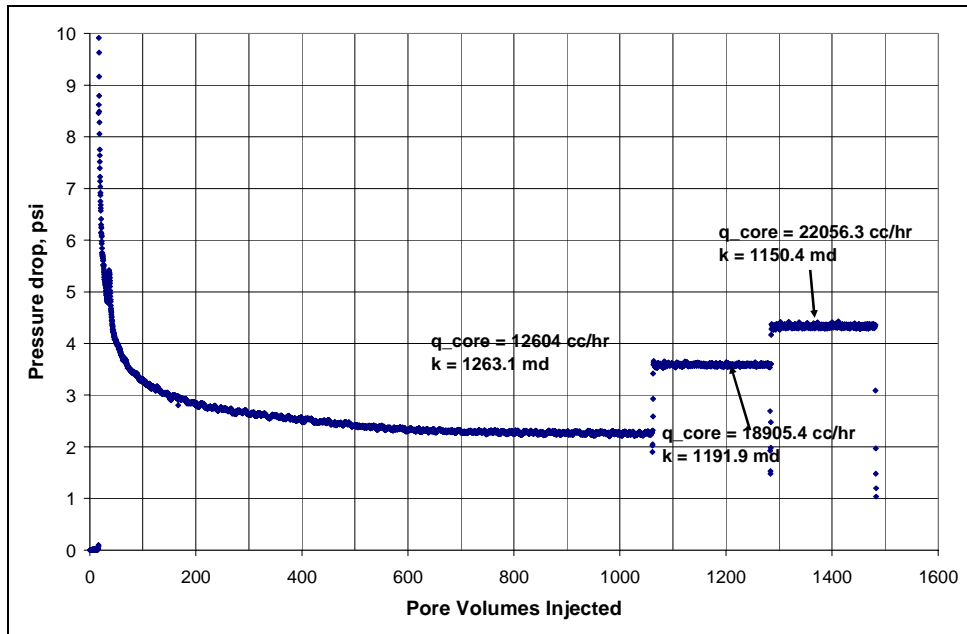


Figure B23.6: Pressure drop across the core during final methane flood

B24- Experiment No.24

Objective:

The objective of this experiment was to investigate the effect of chemical treatment using the surfactant FC4430 delivered in a mixture of 2-butoxyethanol/ethanol on the gas and condensate relative permeability on a reservoir sandstone rock in presence of initial water. The experiment was performed on Bruce reservoir core (plug 7) at 175°F.

Experimental Results:

The plug properties and the experimental conditions are summarized in **Table B24.1**. The initial brine saturation was established by BP using a porous plate method. Initial gas permeability of the rock at $S_{wi}=22\%$ was measured using water-saturated methane at 175°F and 1930 psig. Water-saturated methane was used to prevent vaporization of water by flowing methane. **Table B24.2** summarizes the results of the methane flood. **Figure B24.1** shows the methane flood pressure drop measured across the plug.

Synthetic fluid mixture-4 (**Table 3.4**) was used for the two-phase flow measurements. The initial flood was done at a flowing core pressure of 1930 psig and subsequently again at 460 psig so the measurements could be done at two different k_{rg}/k_{ro} ratios. For this fluid, the ratio of gas to condensate relative permeability is 0.96 at 1930 psig and 2.37 at 460 psig. **Table B24.3** gives the properties of the synthetic fluid calculated using the Peng-Robinson EOS at the flowing core pressures. **Figure B24.2** shows the pressure drop across the core for the two-phase flow at flowing pressures of 1930 psig and 460 psig. **Table B24.4** summarizes the results of the initial two-phase flow.

The core was then treated with the treatment solution (**Table B24.5**). **Figure B23.3** shows the measured pressure drop across the core during the treatment flood. The treatment solution was injected at 196cc/hr. The core was then shut-in for 15 hours.

Post-treatment two-phase gas-condensate flood was conducted under the same conditions as the initial two-phase flow. **Figure B23.4** shows the pressure drop across the core measured during the post-treatment two-phase floods at flowing pressures of 1930 psig and 460 psig. **Table B23.6** summarizes the results of the post-treatment two-phase flow.

Finally, the post-treatment permeability of the core was measured using methane to find out if the final gas permeability was as high as the initial gas permeability or if some damage might have been done. **Figure B24.5** shows the pressure drop across the core and **Table B23.7** summarizes the results. The initial gas permeability at $S_{wi}=22\%$ was 58.1 md. The final gas permeability was 71.7 md. The result implies that the treatment did not damage the permeability of the core.

Table B24.1: Core properties

Core	Bruce Reservoir Core (plug #7)
Length, inches (plug #7)	3.36
Diameter, inches	1
Porosity, %	15.00
Pore volume, cc	6.49
Swi, %	22
Temperature, °F	175

Table B24.2: Result of initial methane flood at Swi = 22%

q_{core}, (cc/hr)	ΔP (psi)	k_g (md)
1173.01	2.12	60.07
1466.26	2.71	58.76
2052.76	4.01	55.60
Permeability, k_g (md)		57.21

Table B24.3: Synthetic fluid properties at experimental conditions

Fluid Properties	1930 psig		460 psig	
	Gas	Oil	Gas	Oil
ρ, g/cc	0.0985	0.5713	0.0221	0.6592
μ (cp)	0.0167	0.1957	0.0133	0.3767
Volume fraction	0.9182	0.0818	0.9853	0.0147
IFT (dyne/cm)	3.107		12.133	

Table B24.4: Results of the initial two-phase gas condensate flood

BPR-2 pressure, psig	1930	460
q_{pump}, cc/hr	240	160
$q_{\text{total_core}}$, cc/hr	520.15	1511.76
$q_{\text{g_core}}$, cc/hr	477.60	1489.53
$q_{\text{o_core}}$, cc/hr	42.55	22.22
ΔP, psi	13.99	23.04
k_{rg}	0.067	0.102
k_{ro}	0.07	0.043
Nc	2.05×10^{-5}	8.66×10^{-6}
PVT Ratio	0.96	2.37

Table B24.5: Composition of treatment solution

Component	Weight %
FC4430	2
2-butoxyethanol	69
Ethanol	29

Table B24.6: Results of post-treatment two-phase flow of gas condensate mixture

BPR-2 pressure, psig	1930	460
q_{pump}, cc/hr	240	160
q_{total_core}, cc/hr	520.15	1511.76
q_{g_core}, cc/hr	477.60	1489.53
q_{o_core}, cc/hr	42.55	22.22
ΔP, psi	7.97	11.23
k_{rg}	0.118	0.209
k_{ro}	0.124	0.088
Nc	1.17x10 ⁻⁵	4.22x10 ⁻⁶
Improvement factor	1.75	2.05

Table B24.7: Result of methane flood to measure final permeability

q _{core} , (cc/hr)	ΔP (psi)	k _g (md)
2999.1	4.54	71.77

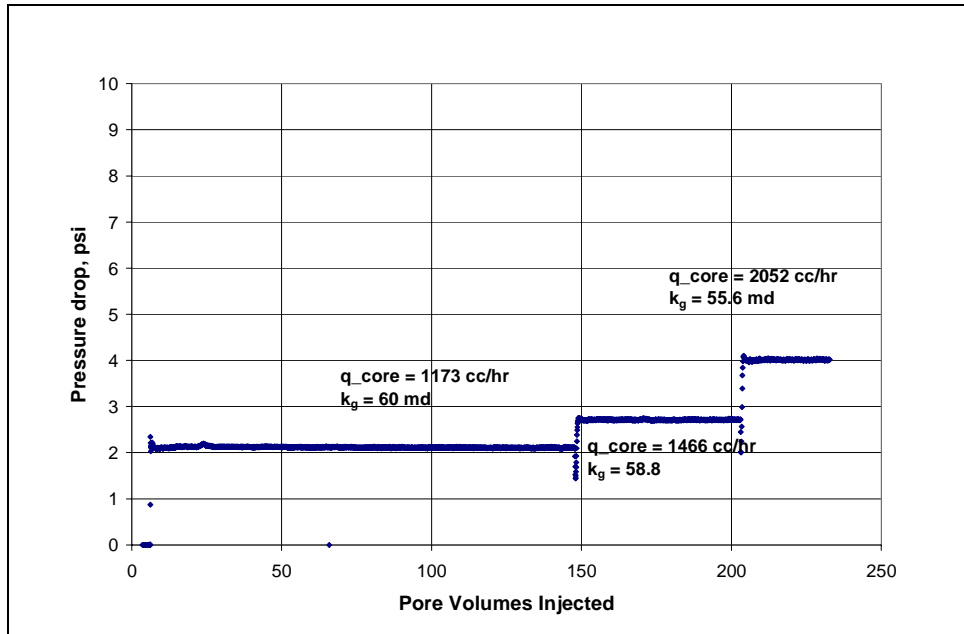


Figure B24.1: Pressure drop across the core during methane flood at $S_{wi}=22\%$

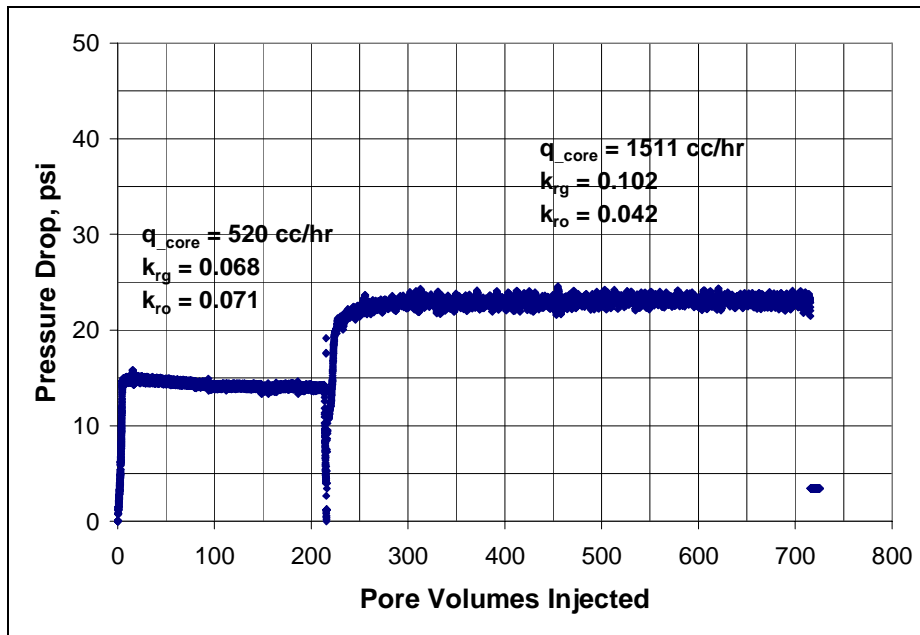


Figure B24.2: Pressure drop across the core during the initial two-phase flow at 1930 psig and 460 psig flowing pressures

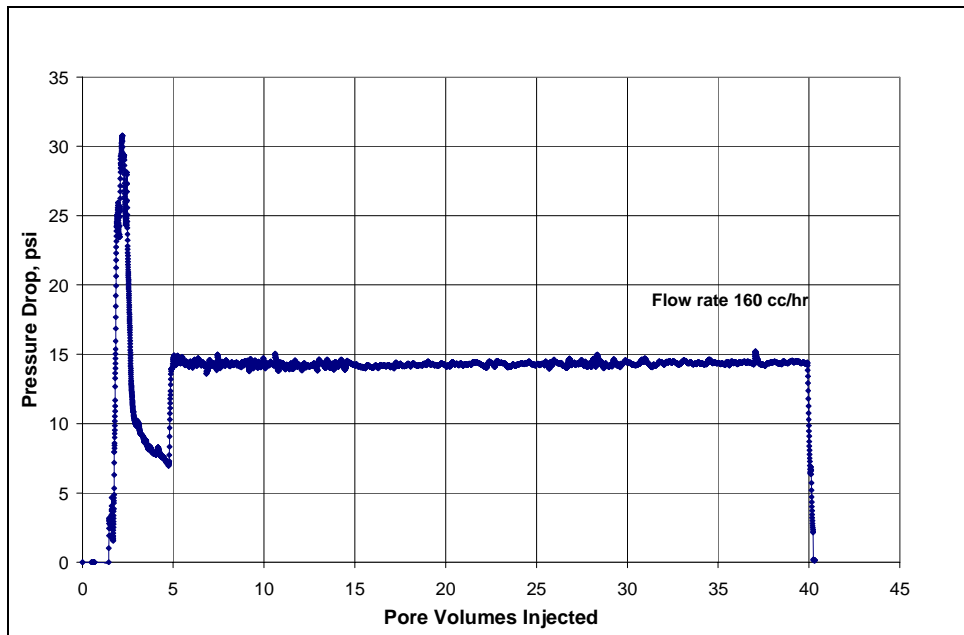


Figure B24.3: Pressure drop across the core during surfactant treatment

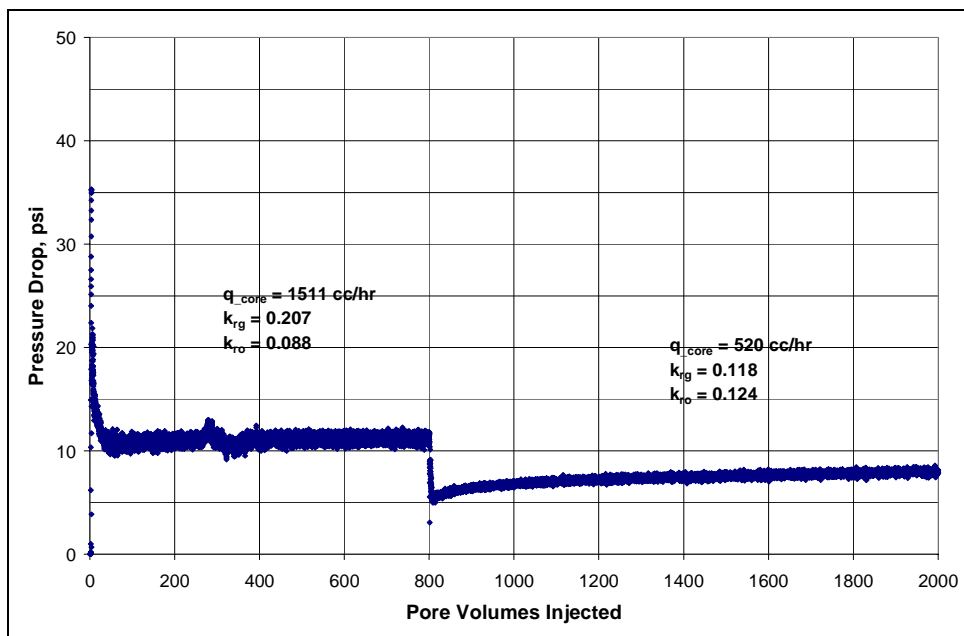


Figure B24.4: Pressure drop across the core during post-treatment two-phase flow at 1930 psig and 460 psig flowing pressures

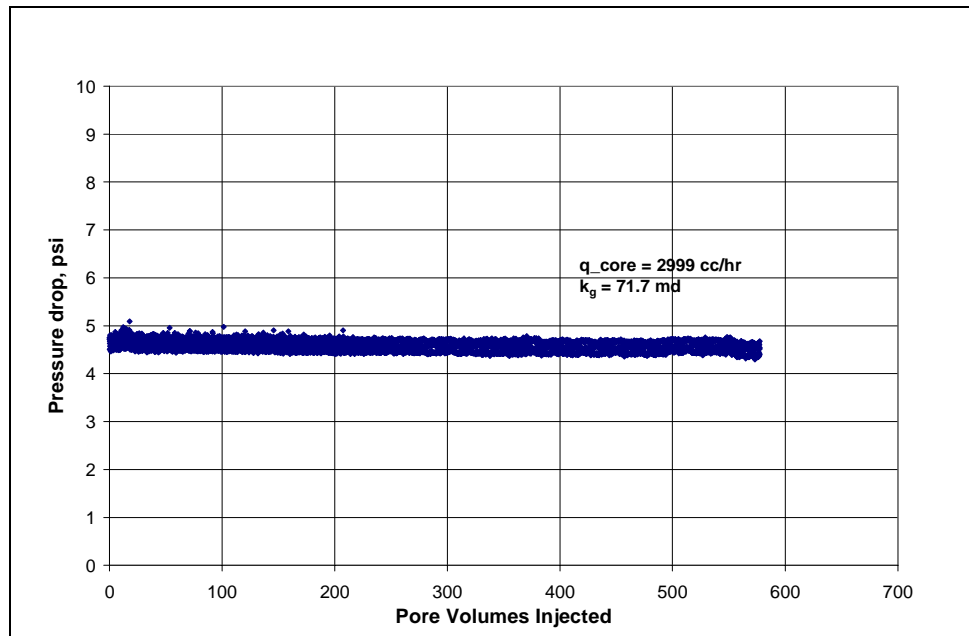


Figure B24.5: Pressure drop across the core during final methane flood

B25- Experiment No.25

Objective:

The objective of this experiment was to investigate the effect of chemical treatment using the surfactant FC4430 delivered in a mixture of 2-butoxyethanol/methanol in improving the gas and condensate relative permeability on a reservoir sandstone rock in presence of initial water. The experiment was performed on Hatter's Pond reservoir cores (plugs #18331A and #18331B) at 308°F.

Experimental Results:

Plugs #18331A and #18331B were stacked together vertically. **Table B25.1** summarizes the properties of the plugs and the experimental conditions. Initial permeability of the core (stacked plugs) was measured using nitrogen at 75°F. **Figure B25.1** shows the pressure drop measured across the core during nitrogen flood. **Table B25.2** summarizes the results of the nitrogen flood.

The initial water saturation of 20% was established by injecting 1.4 cc of synthetic Hatter's Pond brine (**Table B25.3**) in the vacuumed core. Nitrogen flood was then conducted to measure the end point gas relative permeability. **Figure B25.2** shows the pressure drop measured across the core and **Table B25.4** summarizes the results of the nitrogen flood. The pressure of the core was raised to 200 psig and then the temperature of the oven was increased to 308°F.

Synthetic fluid mixture-6 (**Table 3.6**) was used for the two-phase flow measurements. The initial flood was conducted with the upstream backpressure regulator set at 4180 psig and the downstream back pressure regulator set at 1140 psig. **Table B25.5** gives the properties of the synthetic fluid calculated using the Peng-Robinson EOS

at the flowing core pressure. **Figure B25.3** shows the pressure drop across the core during the two-phase gas-condensate flow. **Table B25.6** summarizes the results of the initial two-phase flow.

0.5 PV of 50/50 mixture of 2-butoxyethanol/methanol was flowed through the core at 12cc/hr. **Figure B25.4** shows the pressure drop across the core during the pre-flush. The core was then treated with the treatment solution (**Table B25.7**). **Figure B25.5** shows the measured pressure drop across the core during the treatment flood. The core was then shut-in for 15 hours.

Post-treatment two-phase gas-condensate flood was conducted under the same conditions as the initial two-phase flow. **Figure B25.6** shows the pressure drop across the core measured during the post-treatment two-phase flood at a flowing pressure of 1140 psig. **Table B25.8** summarizes the results of the post-treatment two-phase flow.

The core was retreated with treatment solution given in **Table B25.9**. **Figure B25.7** shows the pressure drop across the core during the second treatment flood. The core was then shut-in for 15 hours. Post-treatment two-phase gas-condensate flood was then conducted under the same conditions as the initial two-phase flow. **Figure B25.8** shows the pressure drop across the core measured during the two-phase flood after the second treatment. **Table B25.10** summarizes the results of the post-treatment two-phase flow. Finally, 8.5PV of toluene flood were flowed through the core. No water was produced from the core during toluene flood. **Figure B25.9** shows the pressure drop across the core during the toluene flood. **Table B25.11** gives the final permeability of the core calculated using the pressure drop measured during the toluene flood.

Table B25.1: Core properties

Core	Hatter's Pond Reservoir Core (plugs #18331A and #18331B)
Length, inches (plug #18331A)	2.75
Length, inches ((plug #18331B))	2.78
Diameter, inches	1
Porosity, %	9.30
Pore volume, cc	7.04
Swi, %	20
Temperature, °F	308

Table B25.2: Result of nitrogen flood

q_{core}, (cc/hr)	ΔP (psi)	k_g (md)
776.67	35.42	4.38
1560.27	83.94	3.81
2340.40	137.11	3.50
Permeability, k_g (md)		3.64

Table B25.3: Synthetic Hatter's Pond brine

Component	g/l
CaCl ₂ (6H ₂ O)	77.43
MgCl ₂ (6H ₂ O)	5.2
KCl	15.05
NaCl	89.92

Table B25.4: Result of nitrogen flood at Swi

q_{core}, (cc/hr)	ΔP (psi)	k_g (md)
780.13	92.24	1.74

Table B25.5: Synthetic fluid properties at experimental conditions

Pressure, psig	4150	1140	
Fluid Properties		Gas phase	Oil phase
ρ, g/cc	0.3443	0.0674	0.5347
μ (cp)		0.0166	0.1532
Volume fraction		0.9119	0.0881
IFT (dyne/cm)		3.632	

Table B25.6: Results of the initial two-phase gas condensate flood

q_{pump}, cc/hr	40
q_{total_core}, cc/hr	123.17
q_{g_core}, cc/hr	112.31
q_{o_core}, cc/hr	10.85
ΔP, psi	127.19
k_{rg}	0.043
k_{ro}	0.038
Nc	6.17x10 ⁻⁶
PVT Ratio	1.12

Table B25.7: Composition of treatment solution

Component	Weight %
FC4430	2
2-butoxyethanol	49
Methanol	49

Table B25.8: Results of post-treatment two-phase flow of gas condensate mixture

q_{pump}, cc/hr	40
q_{total_core}, cc/hr	123.17
q_{g_core}, cc/hr	112.31
q_{o_core}, cc/hr	10.85
ΔP, psi	118.22
k_{rg}	0.046
k_{ro}	0.041
Nc	5.74x10 ⁻⁶
Improvement Factor	1.08

Table B25.9: Composition of second treatment solution

Component	Weight %
FC4430	2
Methanol	98

Table B25.10: Results of two-phase flow of gas condensate mixture after second treatment

q_{pump}, cc/hr	40
q_{total_core}, cc/hr	123.17
q_{g_core}, cc/hr	112.31
q_{o_core}, cc/hr	10.85
ΔP, psi	128.60
k_{rg}	0.042
k_{ro}	0.038
Nc	6.24x10 ⁻⁶
Improvement Factor	0.99

Table B25.11: Result of toluene flood

q_{core}, (cc/hr)	ΔP (psi)	k_g (md)
67.27	166.5	1.12

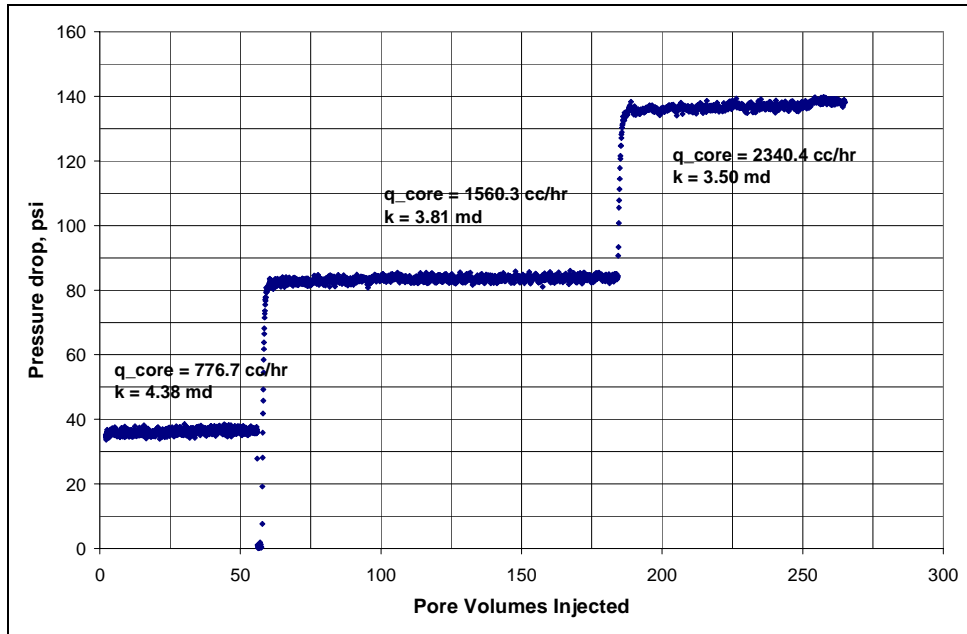


Figure B25.1: Pressure drop across the core during initial nitrogen flood

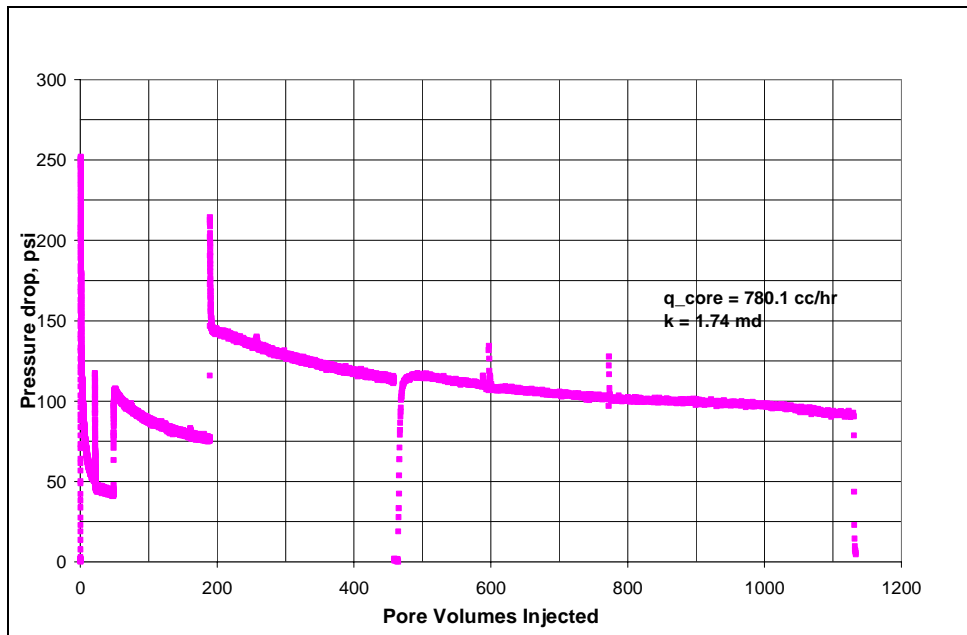


Figure B25.2: Pressure drop across the core during nitrogen flood at $Sw_i = 20\%$

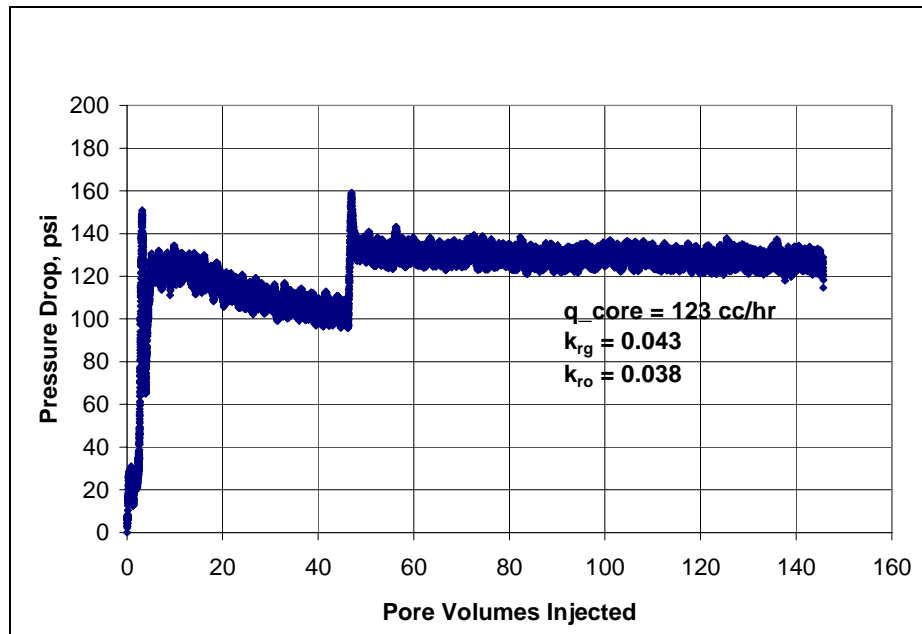


Figure B25.3: Pressure drop across the core during the initial two-phase flow at 308°F and 1140 psig

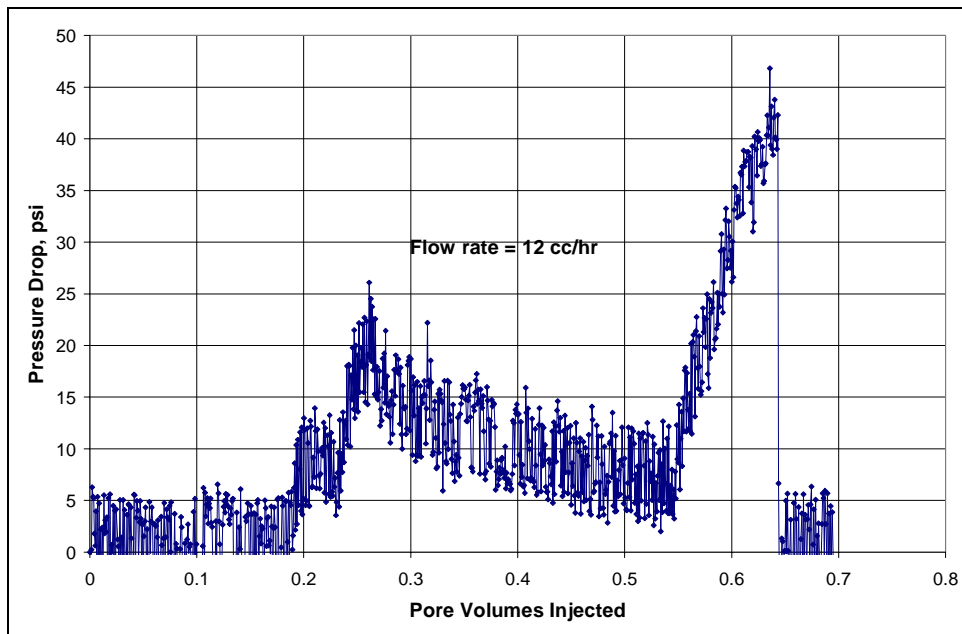


Figure B25.4: Pressure drop across the core during solvent pre-flush

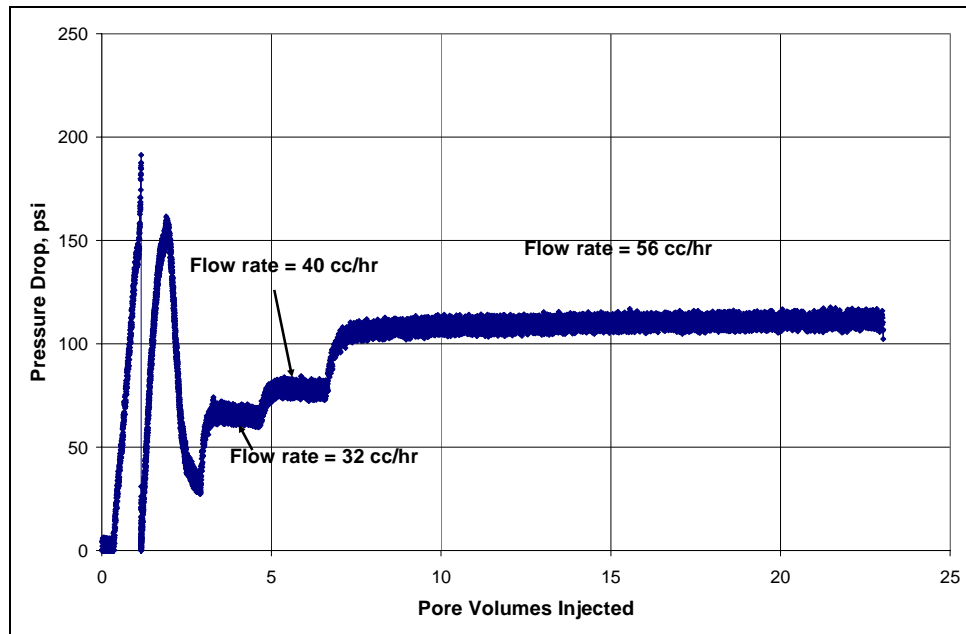


Figure B25.5: Pressure drop across the core during surfactant treatment

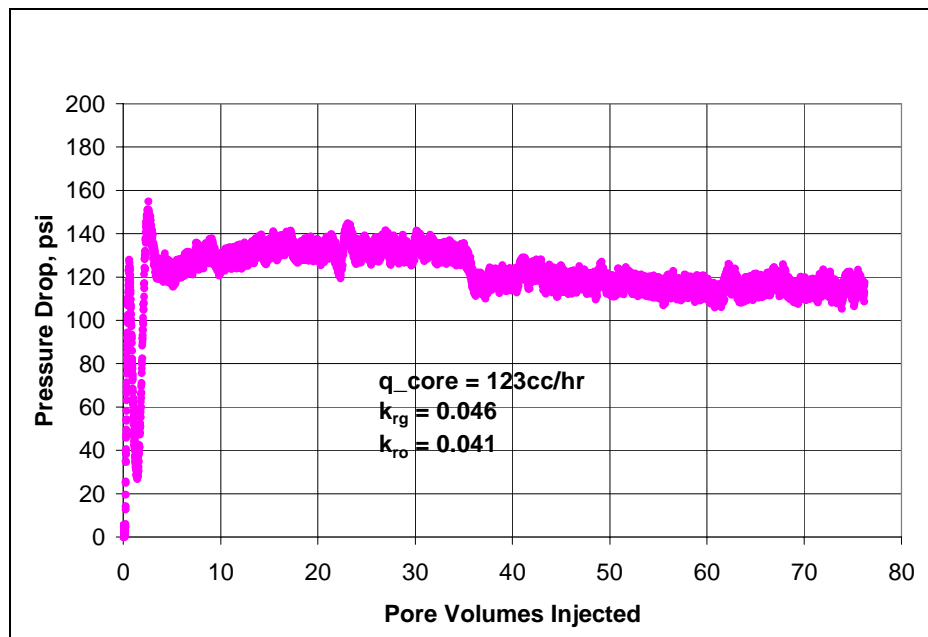


Figure B25.6: Pressure drop across the core during post-treatment two-phase flow at 308°F and 11400 psig

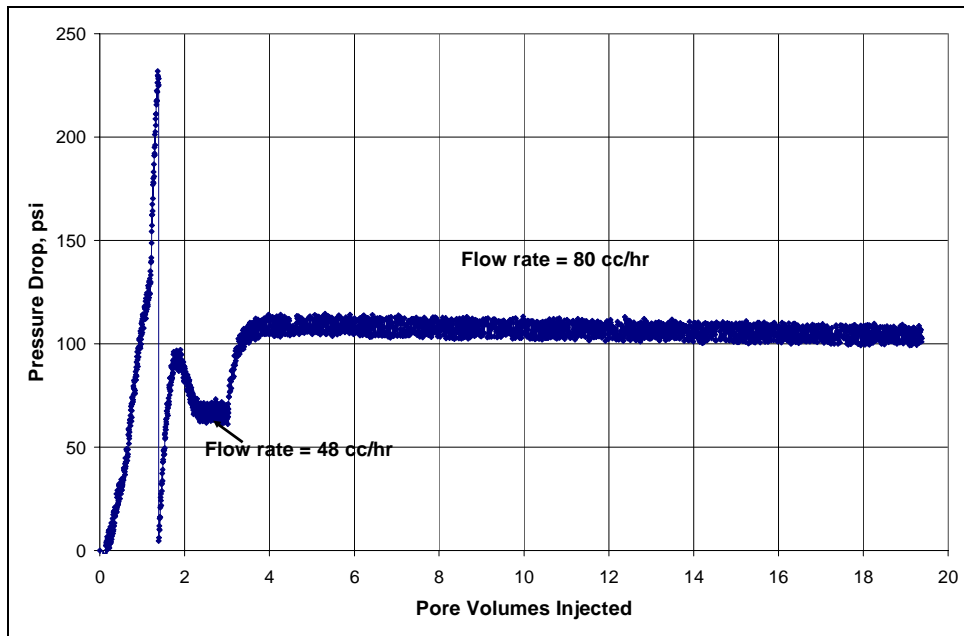


Figure B25.7: Pressure drop across the core during the second surfactant treatment

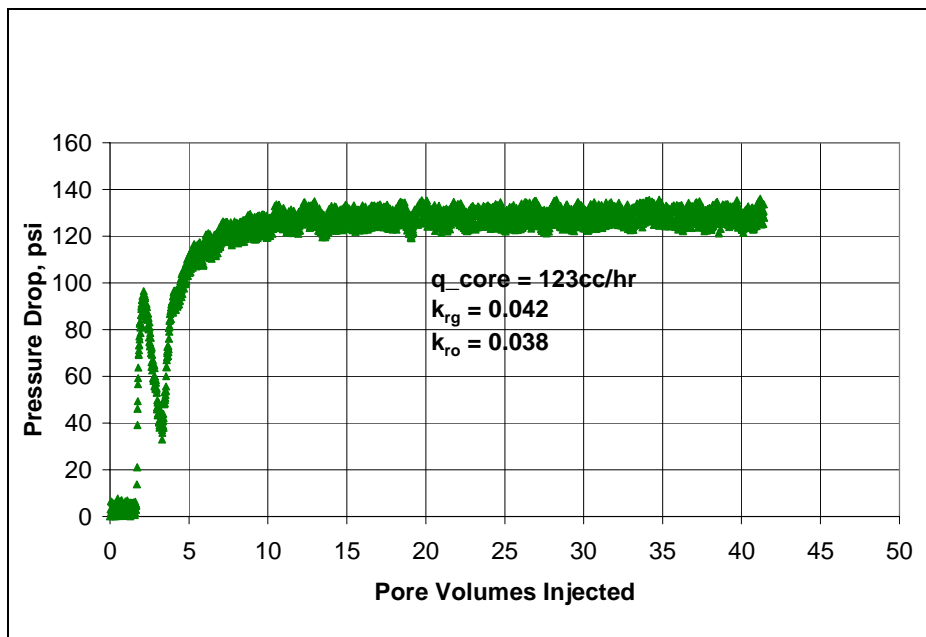


Figure B25.8: Pressure drop across the core during two-phase flow at 308°F and 11400 psig after second treatment

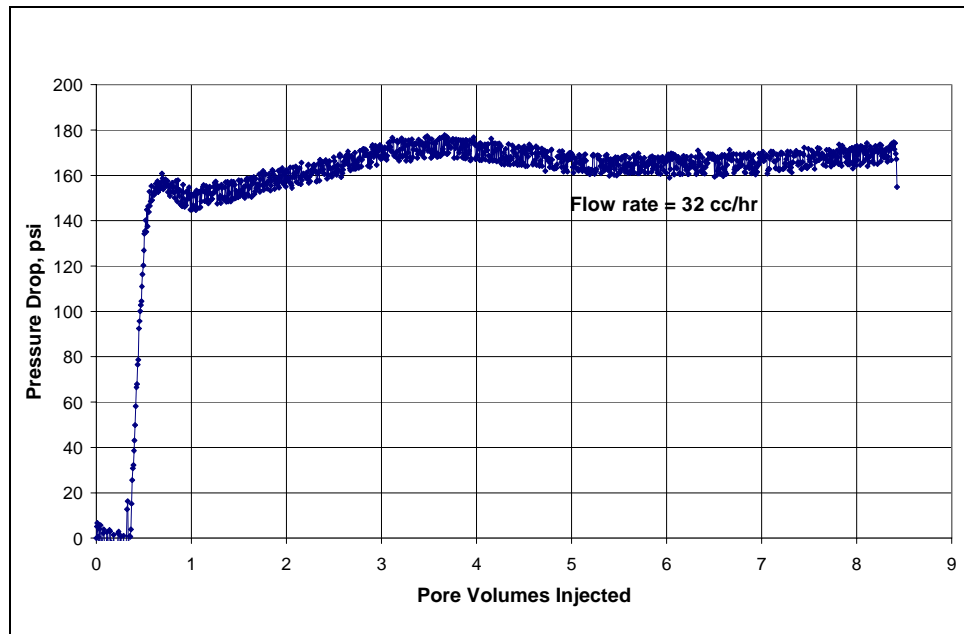


Figure B25.9: Pressure drop across the core during toluene flood

B26- Experiment No.26

Objective:

The objective of this experiment was to investigate the effect of chemical treatment using the surfactant FC4430 delivered in a mixture of 2-butoxyethanol/ethanol on three phase flow of gas, condensate and water. The experiment was performed on a Berea sandstone rock at 175°F.

Experimental Results:

Table B26.1 summarizes the properties of the core and the experimental conditions. Initial permeability of the core was measured using nitrogen at 75°F. **Figure B26.1** shows the pressure drop measured across the core during nitrogen flood. **Table B26.2** summarizes the results of the nitrogen flood.

The initial water saturation of 19% was established by injecting 3.8 cc of synthetic Bruce brine (**Table B21.3**) in the vacuumed core. Nitrogen flood was then conducted to measure the end point gas relative permeability. **Figure B26.2** shows the pressure drop measured across the core and **Table B26.3** summarizes the results of the nitrogen flood. The pressure of the core was raised to 200 psig and then the temperature of the oven was increased to 175°F.

Synthetic fluid mixture-4 (**Table 3.4**) was used for the two-phase flow measurements. The initial flood was conducted with the upstream backpressure regulator set at 4950 psig and the downstream back pressure regulator set at 400 psig. **Table B26.4** gives the properties of the synthetic fluid calculated using the Peng-Robinson EOS at the flowing core pressure. The two-phase flow was followed with a three-phase flow by co-injecting brine along with gas and condensate through the core at a fractional flow of 0.1

(fw=0.1). **Figure B26.3** shows the pressure drop across the core for the two-phase and three-phase flow. **Table B26.5** summarizes the results of the initial two-phase and three-phase flow.

The core was then treated with the treatment solution (**Table B26.6**). Treatment injection was started at 64cc/hr then increased to 160 and 225 cc/hr. The pressure drop started increasing indicating plugging in the core. The treatment was then injected in the reverse direction to remove any kind of plugging at the inlet face. **Figure B26.4** shows the measured pressure drop across the core during the treatment flood. The core was then shut-in for 15 hours.

Post-treatment two-phase and three-phase flows of the gas mixture with the same fractional flow of brine were then done under the same conditions as the pre-treatment two-phase and three-phase flow. **Figure B26.5** shows the pressure drop across the core measured during the post-treatment two-phase and three-phase flow at a flowing pressure of 400 psig. **Table B26.7** summarizes the results of the post-treatment floods.

Table B26.1: Core properties

Core	Berea Sandstone
Length, inches	3.70
Diameter, inches	1
Porosity, %	20.00
Pore volume, cc	20.59
Swi, %	19
Temperature, °F	175

Table B26.2: Result of nitrogen flood

q_{core}, (cc/hr)	ΔP (psi)	k_g (md)
1679.75	2.72	191.10
2519.63	4.14	188.19
2939.57	4.86	187.16
Permeability, k_g (md)		188.82

Table B26.3: Result of nitrogen flood at Swi

q_{core}, (cc/hr)	ΔP (psi)	k_g (md)
1679.75	2.70	192.23

Table B26.4: Synthetic fluid properties at experimental conditions

Pressure, psig	4940	400	
Fluid Properties		Gas phase	Oil phase
ρ, g/cc	0.2965	0.0193	0.6337
μ (cp)		0.0133	0.3883
Volume fraction		0.9876	0.0124
IFT (dyne/cm)		12.9	

Table B26.5: Results of the initial two-phase and three-phase floods

q_{pump}, cc/hr	160	40	20
$q_{\text{total_core}}$, cc/hr	1738.33	482.58	241.29
$q_{\text{g_core}}$, cc/hr	1716.77	429.19	214.60
$q_{\text{o_core}}$, cc/hr	21.56	5.39	2.69
$q_{\text{w_core}}$, cc/hr	0.00	48.00	24.00
f_w	0.00	0.10	0.10
ΔP, psi	21.54	141.16	96.99
k_{rg}	0.092	0.004	0.003
k_{ro}	0.034	0.001	0.001
k_{rw}	0.00	0.011	0.008
Nc	1.08×10^{-5}	-	-
PVT Ratio	2.73	-	-

Table B26.6: Composition of treatment solution

Component	Weight %
FC4430	2
2-butoxyethanol	69
Ethanol	29

Table B26.7: Results of post-treatment two-phase flow of gas condensate mixture

q_{pump}, cc/hr	160	20
q_{total_core}, cc/hr	1738.33	241.29
q_{g_core}, cc/hr	1716.77	214.60
q_{o_core}, cc/hr	21.56	2.69
q_{w_core}, cc/hr	0.00	24.00
f_w	0.00	0.10
ΔP, psi	23.42	115.49
k_{rg}	0.085	0.002
k_{ro}	0.031	0.001
k_{rw}	0.00	0.006
Nc	1.18x10 ⁻⁵	-
Improvement factor	0.92	-

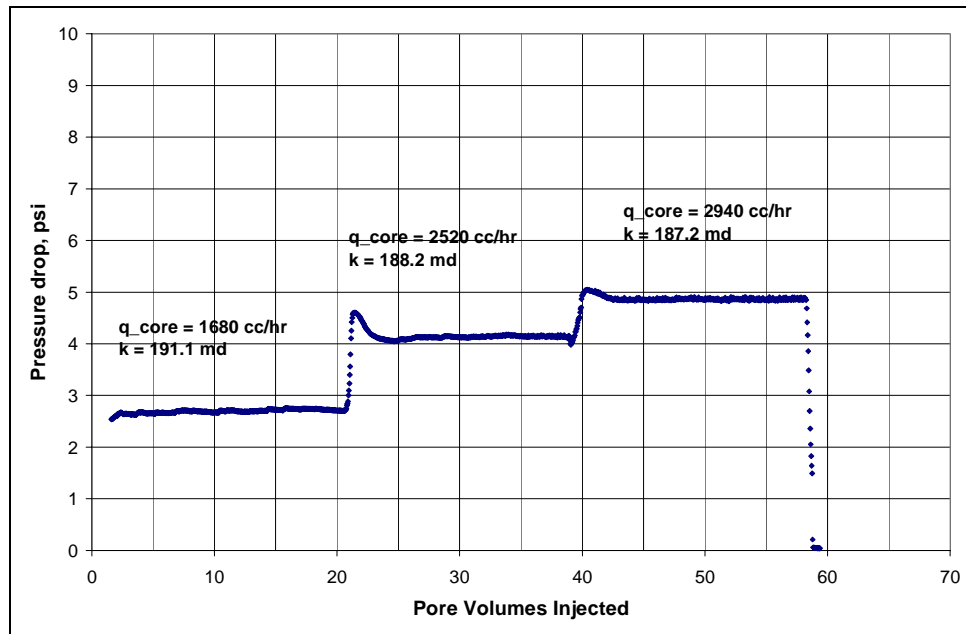


Figure B26.1: Pressure drop across the core during initial nitrogen flood

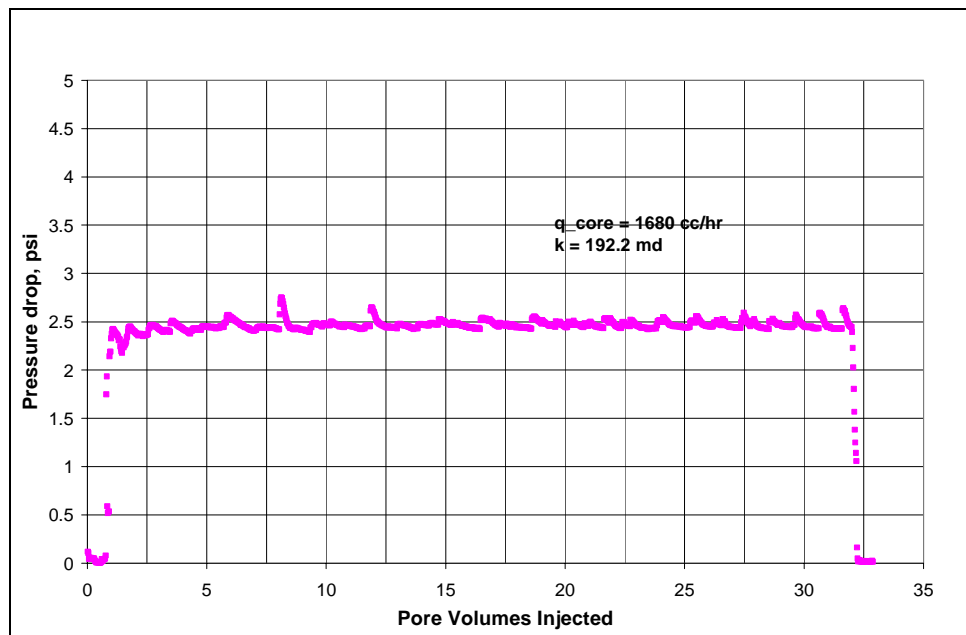


Figure B26.2: Pressure drop across the core during nitrogen flood at $S_{wi}=19\%$

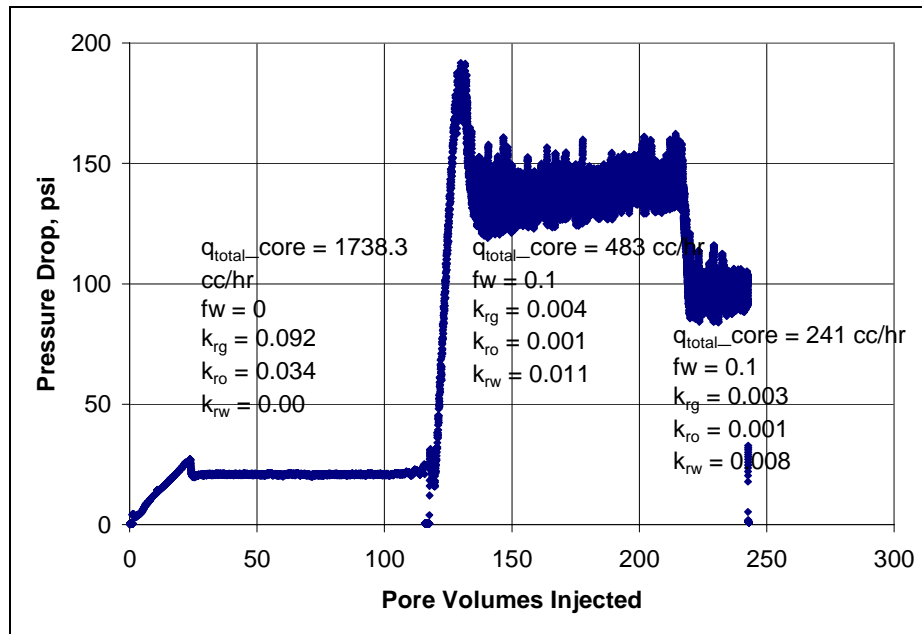


Figure B26.3: Pressure drop across the core during the initial two-phase and three-phase floods at 175°F and 400 psig

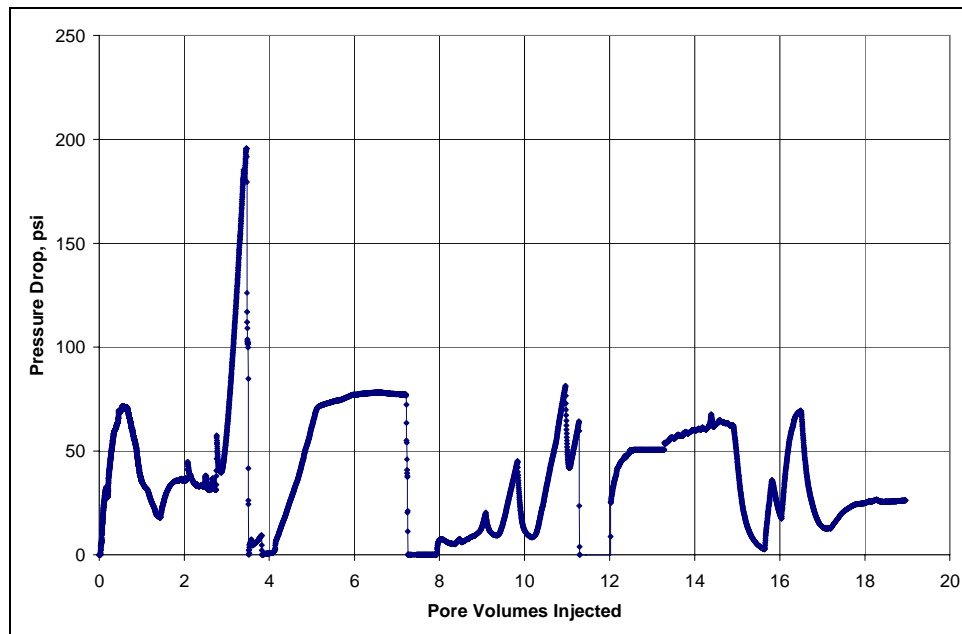


Figure B26.4: Pressure drop across the core during surfactant treatment

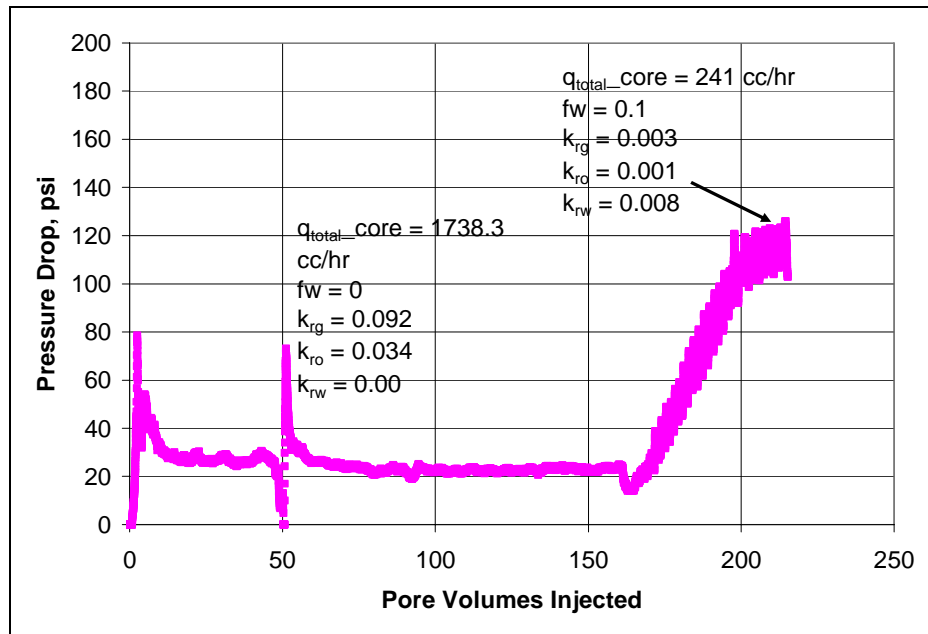


Figure B26.5: Pressure drop across the core during post-treatment two-phase and three-phase floods at 175°F and 400 psig

B27- Experiment No.27

Objective:

The objective of this experiment was to investigate the effect of chemical treatment using the surfactant FC4430 delivered in a mixture of 2-butoxyethanol/ethanol on the gas and condensate relative permeability on a reservoir sandstone rock in presence of initial water. The experiment was performed on Bruce reservoir core (plug #9) at 175°F.

Experimental Results:

The plug properties and the experimental conditions are summarized in **Table B27.1**. The initial brine saturation was established by BP using a porous plate method. Initial gas permeability of the rock at $S_{wi}=12\%$ was measured using water-saturated methane at 175°F and 1910 psig. Water-saturated methane was used to prevent vaporization of water by flowing methane. **Table B27.2** summarizes the results of the methane flood. **Figure B27.1** shows the methane flood pressure drop measured across the plug.

Synthetic fluid mixture-4 (**Table 3.4**) was used for the two-phase flow measurements. The initial flood was done at a flowing core pressure of 1915 psig and subsequently again at 550 psig so the measurements could be done at two different k_{rg}/k_{ro} ratios. For this fluid, the ratio of gas to condensate relative permeability is 0.96 at 1930 psig and 2.03 at 550 psig. **Table B27.3** gives the properties of the synthetic fluid calculated using the Peng-Robinson EOS at the flowing core pressures. **Figure B27.2** shows the pressure drop across the core for the two-phase flow at flowing pressures of

1915 psig and 550 psig. **Table B27.4** summarizes the results of the initial two-phase flow.

The core was then treated with the treatment solution (**Table B27.5**). **Figure B27.3** shows the measured pressure drop across the core during the treatment flood. The treatment solution was injected at 80 cc/hr and 160 cc/hr. The core was then shut-in for 185 hours.

Nitrogen flood was then conducted to flush out treatment solution from the core and imitate chase gas injection in field treatments. **Figure B27.4** shows the pressure drop across the core during chase gas injection.

Post-treatment two-phase gas-condensate flood was conducted under the same conditions as the initial two-phase flow. **Figure B27.5** shows the pressure drop across the core measured during the post-treatment two-phase floods at the flowing pressure of 550 psig. **Table B27.6** summarizes the results of the post-treatment two-phase flow.

Finally, the post-treatment permeability of the core was measured using methane to find out if the final gas permeability was as high as the initial gas permeability or if some damage might have been done. **Figure B27.6** shows the pressure drop across the core and **Table B27.7** summarizes the results.

Table B27.1: Core properties

Core	Bruce Reservoir Core (plug #9)
Length, inches (plug #7)	3.72
Diameter, inches	1
Porosity, %	15.00
Pore volume, cc	7.19
Swi, %	12
Temperature, °F	175

Table B27.2: Result of initial methane flood at Swi = 12%

q_{core}, (cc/hr)	ΔP (psi)	k_g (md)
1486.61	4.47	40.27
1842.92	5.72	39.03
2130.80	6.80	37.97
Permeability, k_g (md)		39.09

Table B27.3: Synthetic fluid properties at experimental conditions

Fluid Properties	1985sig		550ig	
	Gas	Oil	Gas	Oil
ρ, g/cc	0.0969	0.5729	0.0263	0.6528
μ (cp)	0.0167	0.1983	0.0135	0.3599
Volume fraction	0.9195	0.0805	0.9819	0.0181
IFT (dyne/cm)	3.455		11.347	

Table B27.4: Results of the initial two-phase gas condensate flood

BPR-2 pressure, psig	1985	550	550
q_{pump}, cc/hr	254	508	128
$q_{\text{total_core}}$, cc/hr	568.23	1136.46	1028.70
$q_{\text{g_core}}$, cc/hr	522.49	1044.98	1010.08
$q_{\text{o_core}}$, cc/hr	45.74	91.49	18.62
ΔP, psi	21.07	32.75	42.12
k_{rg}	0.081	0.104	0.063
k_{ro}	0.084	0.108	0.031
N_{c}	1.71×10^{-5}	2.66×10^{-5}	1.04×10^{-5}
PVT Ratio	0.96	0.96	2.03

Table B27.5: Composition of treatment solution

Component	Weight %
FC4430	2
2-butoxyethanol	69
Ethanol	29

Table B27.6: Results of post-treatment two-phase flow of gas condensate mixture

BPR-2 pressure, psig	550
q_{pump}, cc/hr	128
q_{total_core}, cc/hr	1028.70
q_{g_core}, cc/hr	1010.08
q_{o_core}, cc/hr	18.62
ΔP, psi	24.12
k_{rg}	0.110
k_{ro}	0.054
Nc	5.98x10 ⁻⁶
Improvement factor	1.75

Table B27.7: Result of methane flood to measure final permeability

q _{core} , (cc/hr)	ΔP (psi)	k _g (md)
2321.41	6.65	42.30

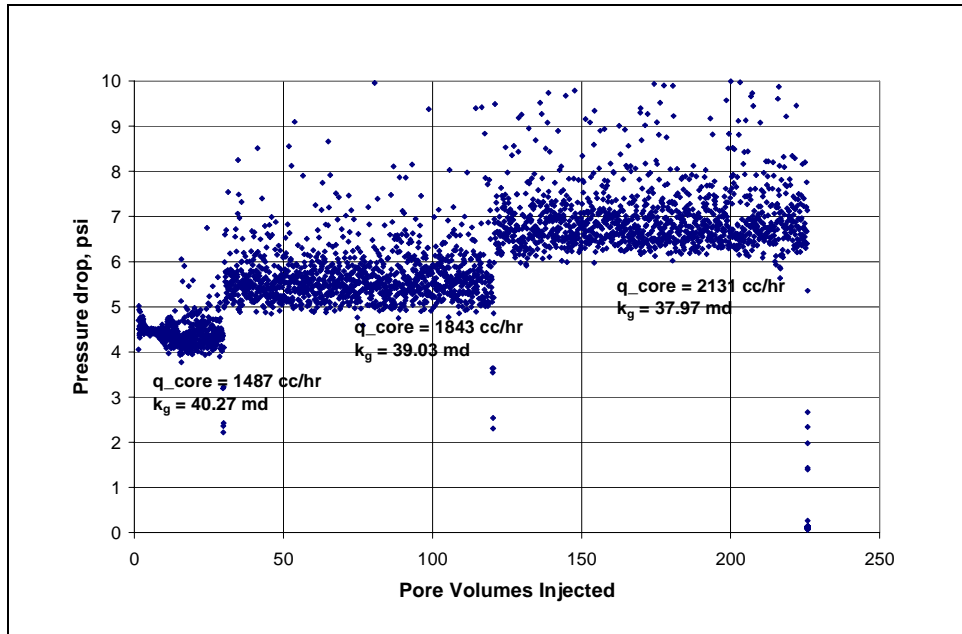


Figure B27.1: Pressure drop across the core during methane flood at $Sw_i=22\%$

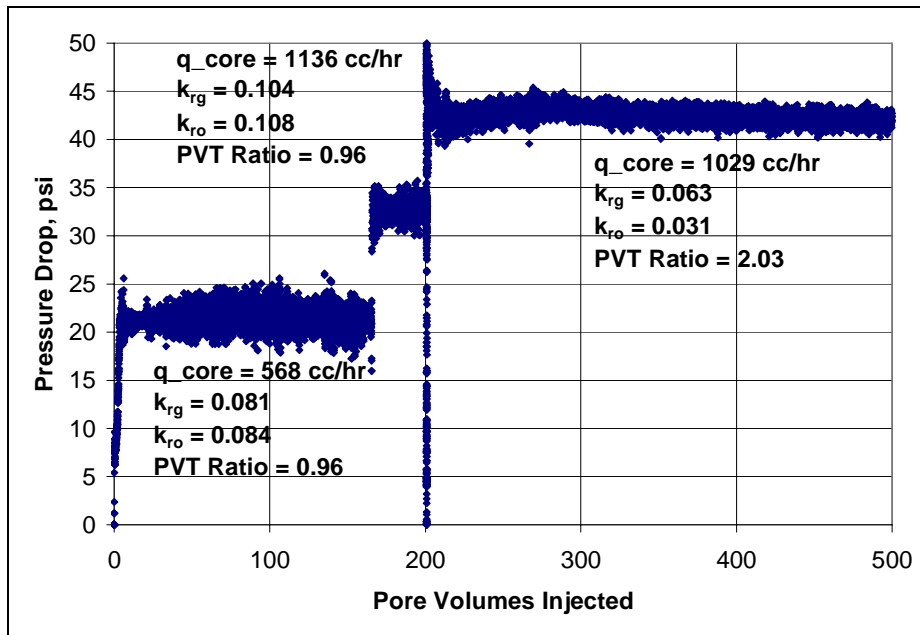


Figure B27.2: Pressure drop across the core during the initial two-phase flow at 1985 psig and 550 psig flowing pressures

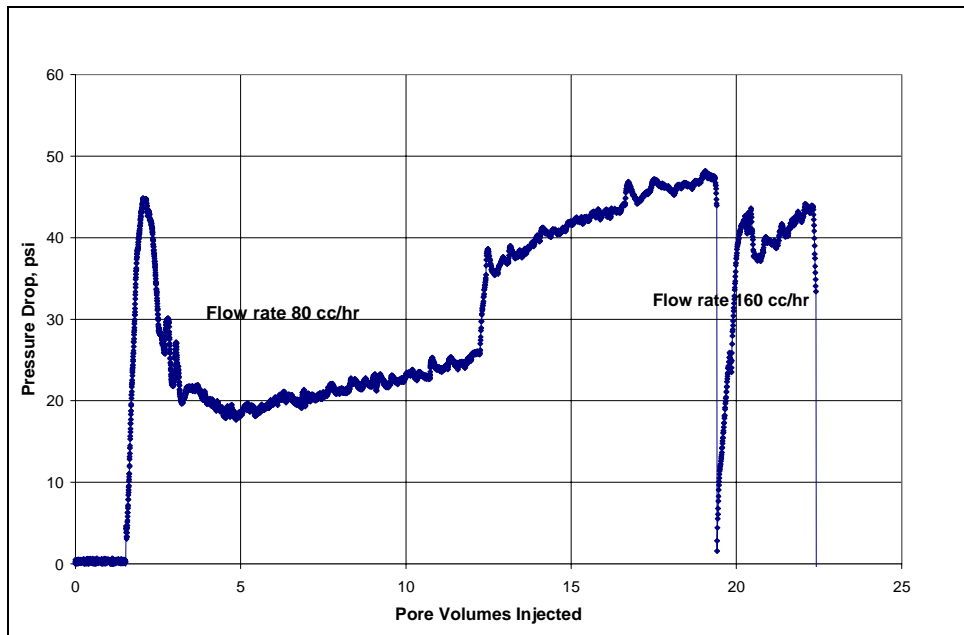


Figure B27.3: Pressure drop across the core during surfactant treatment

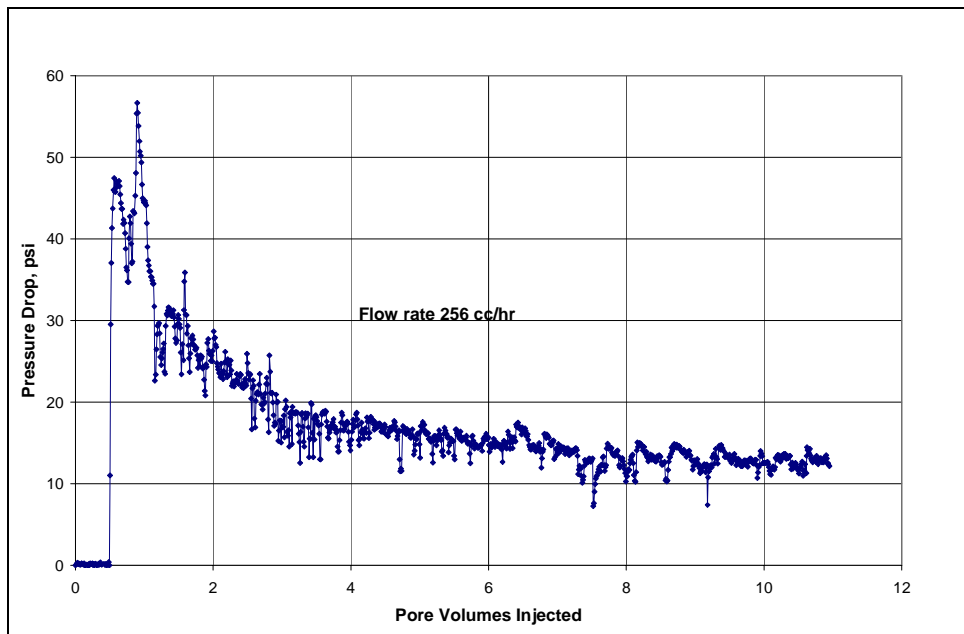


Figure B27.4: Pressure drop across the core during case gas injection

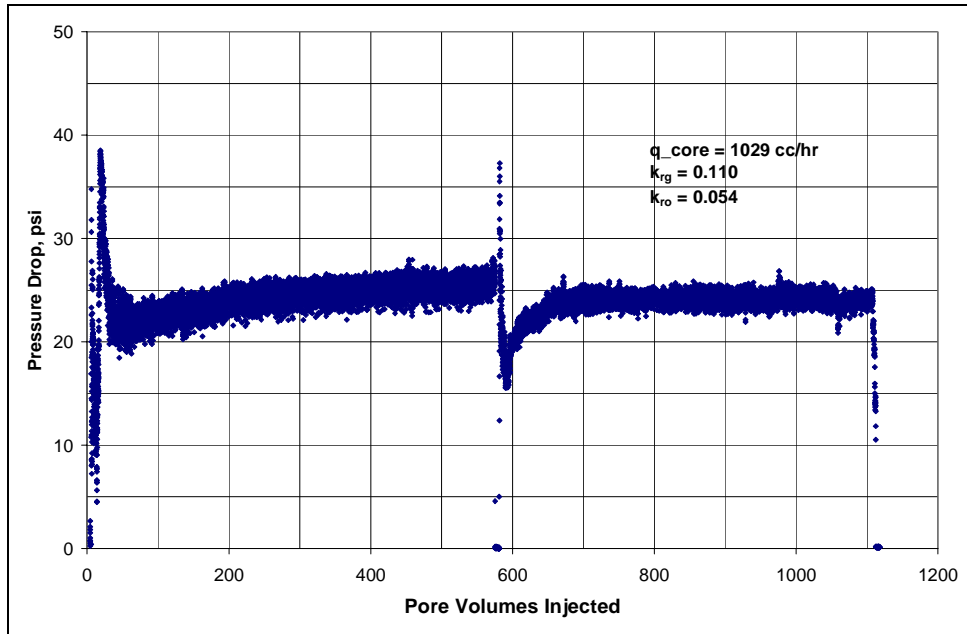


Figure B27.5: Pressure drop across the core during post-treatment two-phase flow at 550 psig

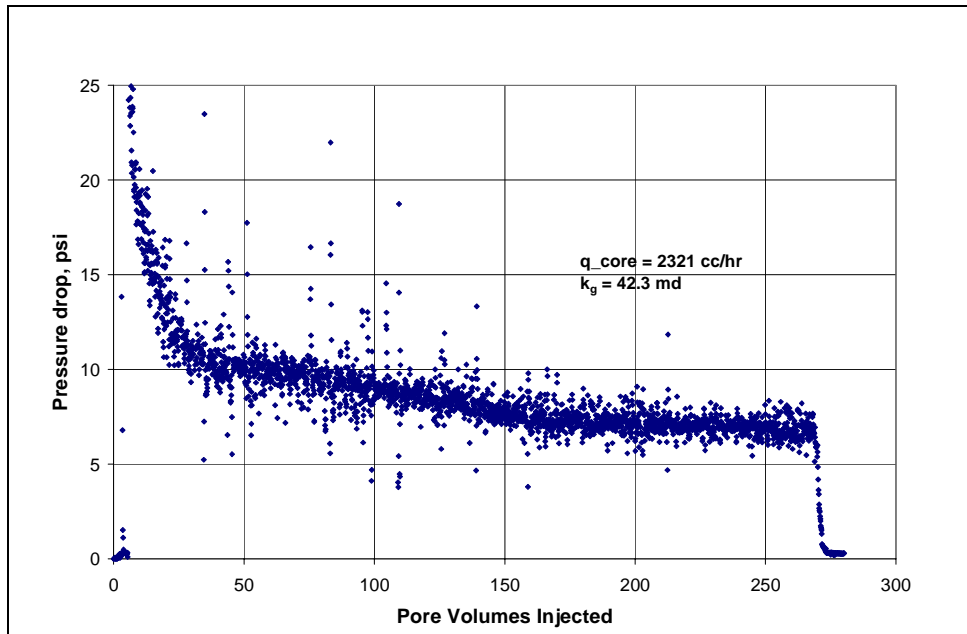


Figure B27.6: Pressure drop across the core during final methane flood

B28- Experiment No.28

Objective:

The objective of this experiment was to investigate the effect of chemical treatment on the gas and condensate relative permeability in presence of mobile water. The experiment was performed on a Berea core at 175°F.

Experimental Results:

Table B28.1 summarizes the properties of the core and the experimental conditions. Initial permeability of the core was measured using nitrogen at 75°F. **Figure B28.1** shows the pressure drop measured across the core during nitrogen flood. **Table B28.2** summarizes the results of the nitrogen flood.

The initial water saturation of 19% was established by injecting 3.8 cc of synthetic Bruce brine (**Table B21.3**) in the vacuumed core. Nitrogen flood was then conducted to measure the end point gas relative permeability. **Figure B28.2** shows the pressure drop measured across the core and **Table B28.3** summarizes the results of the nitrogen flood. The pressure of the core was raised to 200 psig and then the temperature of the oven was increased to 175°F.

Synthetic fluid mixture-4 (**Table 3.4**) was used for the two-phase flow measurements. The initial flood was conducted with the upstream backpressure regulator set at 4950 psig and the downstream back pressure regulator set at 400 psig. **Table B28.4** gives the properties of the synthetic fluid calculated using the Peng-Robinson EOS at the flowing core pressure. The two-phase flow was followed with a three-phase flow by co-injecting brine along with gas and condensate through the core at a fractional flow of 0.036 (fw=0.036). **Figure B28.3** shows the pressure drop across the core for the two-

phase and three-phase flow. **Table B28.5** summarizes the results of the initial two-phase and three-phase flow.

The core was then treated with the treatment solution (**Table B28.6**). Treatment was injected at 128 cc/hr. **Figure B28.4** shows the measured pressure drop across the core during the treatment flood. The core was then shut-in for 15 hours.

Post-treatment two-phase and three-phase flows of the gas mixture with the same fractional flow of brine were then done under the same conditions as the pre-treatment two-phase and three-phase flow. **Figure B28.5** shows the pressure drop across the core measured during the post-treatment two-phase and three-phase flow. **Table B28.7** summarizes the results of the post-treatment two-phase and three-phase flow.

A solvent flush (composition given in **Table B28.8**) was done to remove the water from the core and this was followed by two-phase flow of gas and condensate mixture (*condensate flood-3*). **Figure B28.6** shows the pressure drop across the core during the solvent flood-1. **Figure B28.7** shows the pressure drop for the condensate flood-3. **Table B28.9** summarizes the results of the condensate flood-3.

Then floods were done to analyze effect a small amount of water cross flow into a gas bearing rock on the gas and condensate relative permeabilities and how long does it take for the gas and condensate two-phase flow to reach steady state back. 2 PV's of the three-phases at $fw=0.036$ were flown through the core followed by two-phase flow of gas and condensate (*condensate flood-4*). **Figure B28.8** shows the pressure drop for the 2 PV's of three-phase flow followed by the two-phase flow. The results show the two-phase gas condensate flow reached steady state in about 30 PV's and the improvement factor was about the same as that for condensate flood-3. **Table B28.10** summarizes the results of the condensate flood-4.

Finally, the effect of large volume of flowing brine on the treatment was studied. 10 PV's of brine was flowed through the core followed by 10 PV's of the solvent (composition given in **Table B28.8**) to remove brine which was followed with the two-phase gas condensate flow (*condensate flood-5*) under the same conditions as the previous two-phase floods. **Figure B28.9** shows the pressure drop across the core during the injection of brine. **Figure B28.10** shows the pressure drop across the core during the solvent flood-2. **Figure B28.11** shows the pressure drop for the condensate flood-5. **Table B28.11** summarizes the results of the condensate flood-5.

The core was re-treated with the treatment solution (**Table B28.6**). **Figure B28.12** shows the pressure drop across the core during the second treatment flood. Plugging was observed during the treatment injection. The plugging was caused because of rust deposition at the inlet face of the core. Flowing large pore volumes of brine at high temperature through stainless steel tubing may have corroded the tubing.

The core was shut-in for 15 hours after the second treatment. Gas condensate flood was then done after the second treatment. **Figure B28.13** shows the pressure drop across the core during the gas condensate flood. **Table B28.12** summarizes the results of the gas condensate flood after second treatment.

Table B28.1: Core properties

Core	Berea Sandstone
Length, inches	3.70
Diameter, inches	1
Porosity, %	20.00
Pore volume, cc	20.59
Swi, %	19
Temperature, °F	175

Table B28.2: Result of nitrogen flood

q_{core}, (cc/hr)	ΔP (psi)	k_g (md)
2490.53	1.95	244.18
4358.43	3.76	222.22
3735.80	3.26	219.14
Permeability, k_g (md)		220.07

Table B28.3: Result of nitrogen flood at Swi

q_{core}, (cc/hr)	ΔP (psi)	k_g (md)
3113.17	3.00	198.50

Table B28.4: Synthetic fluid properties at experimental conditions

Pressure, psig	5200	420	
Fluid Properties		Gas phase	Oil phase
ρ, g/cc	0.303	0.0195	0.6633
μ (cp)		0.0133	0.3872
Volume fraction		0.9874	0.0126
IFT (dyne/cm)		3.107	

Table B28.5: Results of the initial two-phase and three-phase floods

q_{pump}, cc/hr	192	48
q_{total_core}, cc/hr	2106.92	546.73
q_{g_core}, cc/hr	2080.37	520.09
q_{o_core}, cc/hr	26.55	6.64
q_{w_core}, cc/hr	0.00	20.00
f_w	0.00	0.036
ΔP, psi	23.45	76.65
k_{rg}	0.085	0.007
k_{ro}	0.032	0.002
k_{rw}	0.000	0.007
Nc	5.37×10^{-5}	-
PVT Ratio	2.69	-

Table B28.6: Composition of treatment solution

Component	Weight %
FC4430	2
2-butoxyethanol	49
Ethanol	49

Table B28.7: Results of post-treatment two-phase flow of gas condensate mixture

q_{pump}, cc/hr	192	48
q_{total_core}, cc/hr	2106.92	546.73
q_{g_core}, cc/hr	2080.37	520.09
q_{o_core}, cc/hr	26.55	6.64
q_{w_core}, cc/hr	0.00	20.00
f_w	0.00	0.036
ΔP, psi	13.95	88.16
k_{rg}	0.143	0.006
k_{ro}	0.053	0.002
k_{rw}	0.00	0.0006
Nc	3.20x10 ⁻⁵	-
Improvement factor	1.68	0.87

Table B28.8- Composition of the solvent used to flush out brine

Component	wt%
2-Butoxyethanol	50
Ethanol	50

Table B28.9: Results of condensate flood-3

q_{pump}, cc/hr	192
q_{total_core}, cc/hr	2106.92
q_{g_core}, cc/hr	2080.37
q_{o_core}, cc/hr	26.55
ΔP, psi	15.12
k_{rg}	0.132
k_{ro}	0.049
Nc	3.47x10 ⁻⁵
Improvement factor	1.55

Table B28.10: Results of condensate flood-4

q_{pump}, cc/hr	192
q_{total_core}, cc/hr	2106.92
q_{g_core}, cc/hr	2080.37
q_{o_core}, cc/hr	26.55
ΔP, psi	15.82
k_{rg}	0.126
k_{ro}	0.047
Nc	3.63x10 ⁻⁵
Improvement factor	1.48

Table B28.11: Results of condensate flood-5

q_{pump}, cc/hr	192
q_{total_core}, cc/hr	2106.92
q_{g_core}, cc/hr	2080.37
q_{o_core}, cc/hr	26.55
ΔP, psi	17.83
k_{rg}	0.112
k_{ro}	0.042
Nc	3.47x10 ⁻⁵
Improvement factor	1.32

Table B28.12: Results of gas condensate flood after second treatment

q_{pump}, cc/hr	192
q_{total_core}, cc/hr	2106.92
q_{g_core}, cc/hr	2080.37
q_{o_core}, cc/hr	26.55
ΔP, psi	24.36
k_{rg}	0.082
k_{ro}	0.031
Nc	5.95x10 ⁻⁵
Improvement factor	0.96

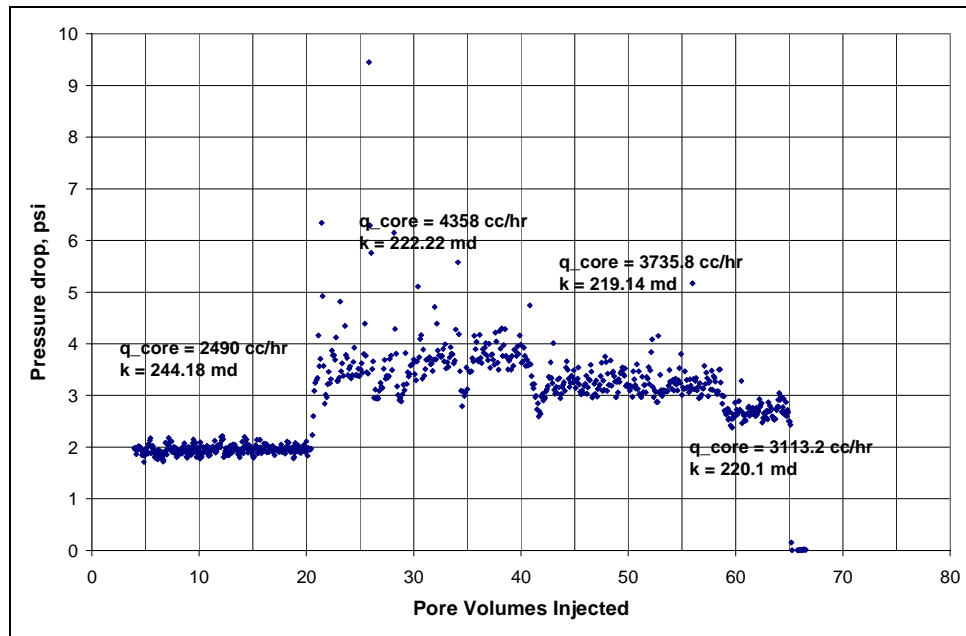


Figure B28.1: Pressure drop across the core during initial nitrogen flood

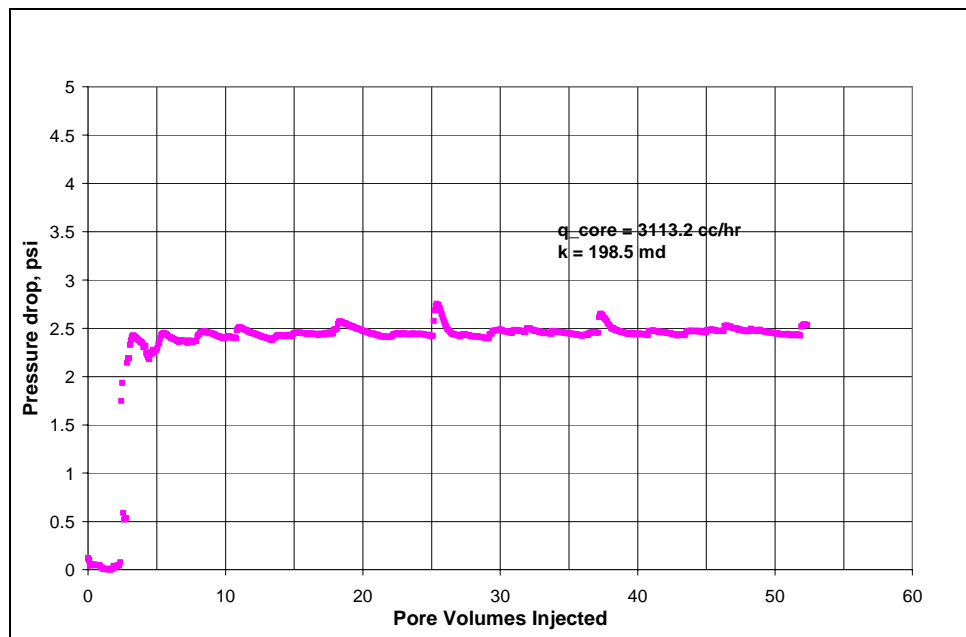


Figure B28.2: Pressure drop across the core during nitrogen flood at $S_{wi}=19\%$

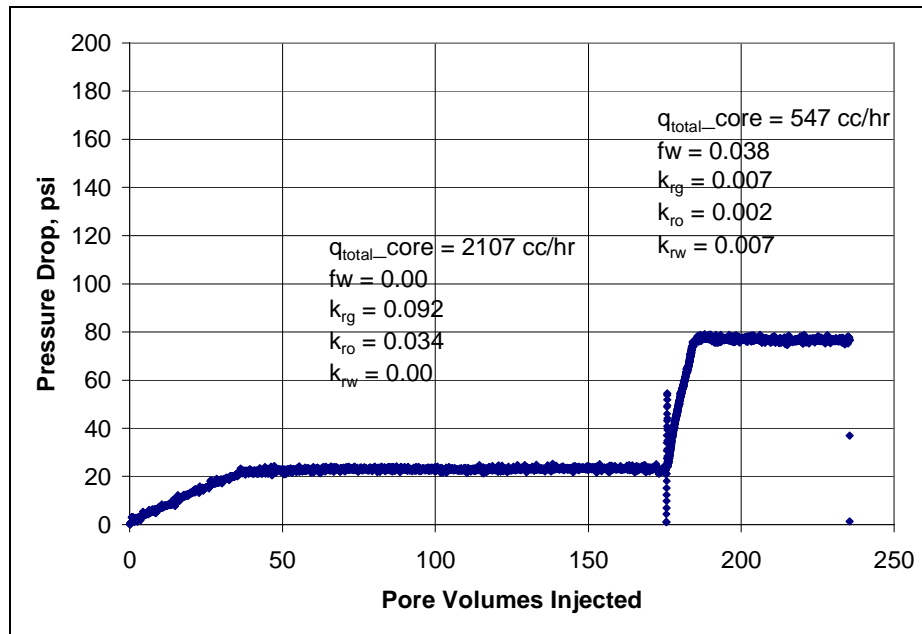


Figure B28.3: Pressure drop across the core during the initial two-phase and three-phase floods at 175°F and 420 psig

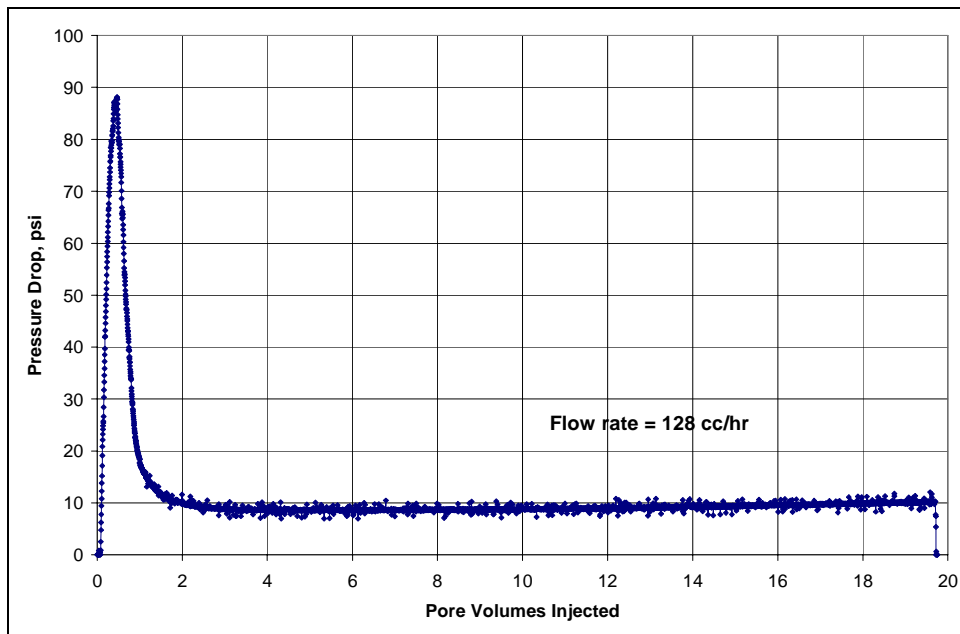


Figure B28.4: Pressure drop across the core during surfactant treatment

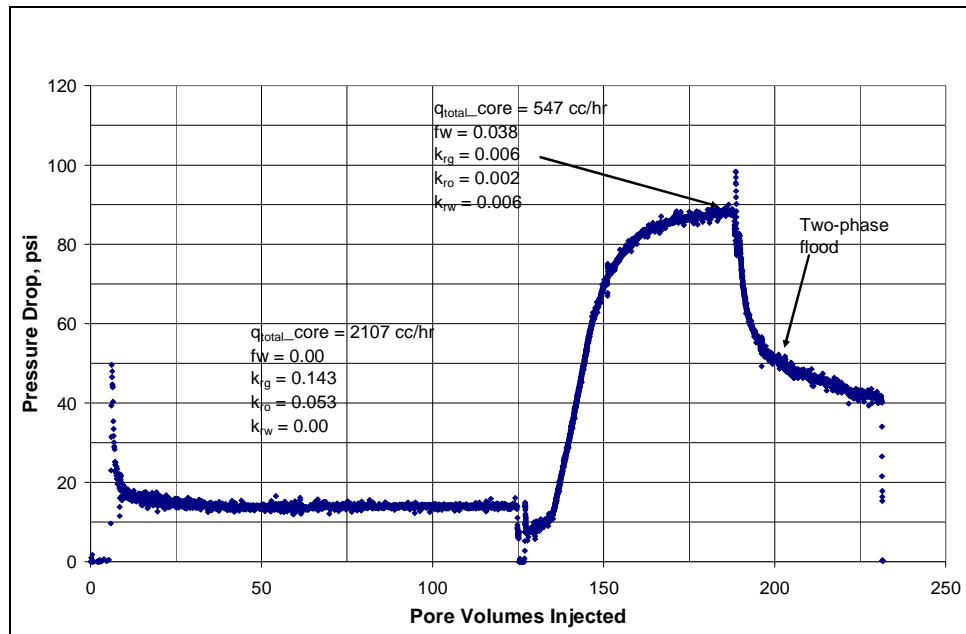


Figure B28.5: Pressure drop across the core during post-treatment two-phase and three-phase floods at 175°F and 420 psig

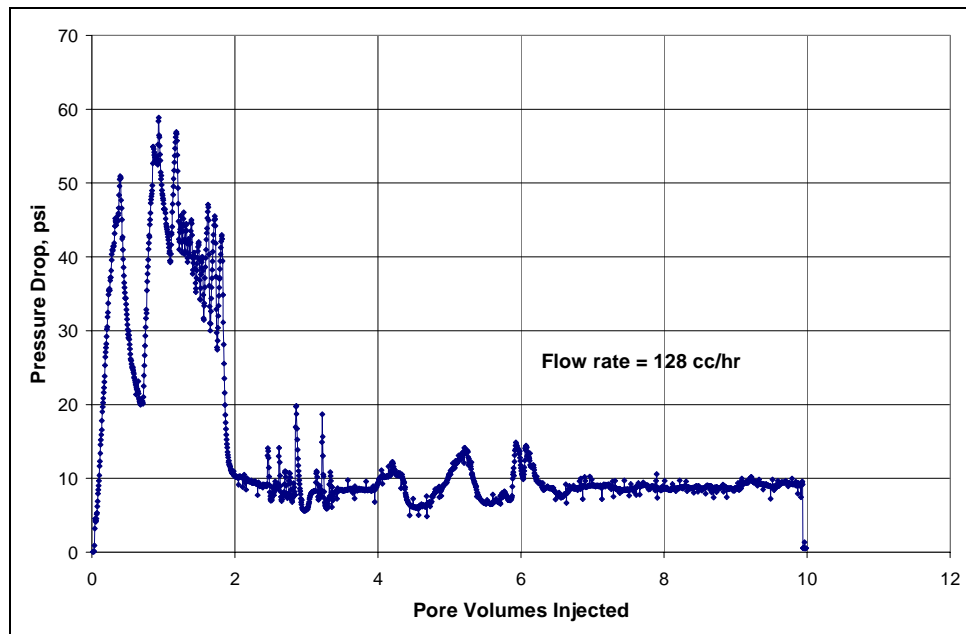


Figure B28.6: Pressure drop across the core during solvent flood-1

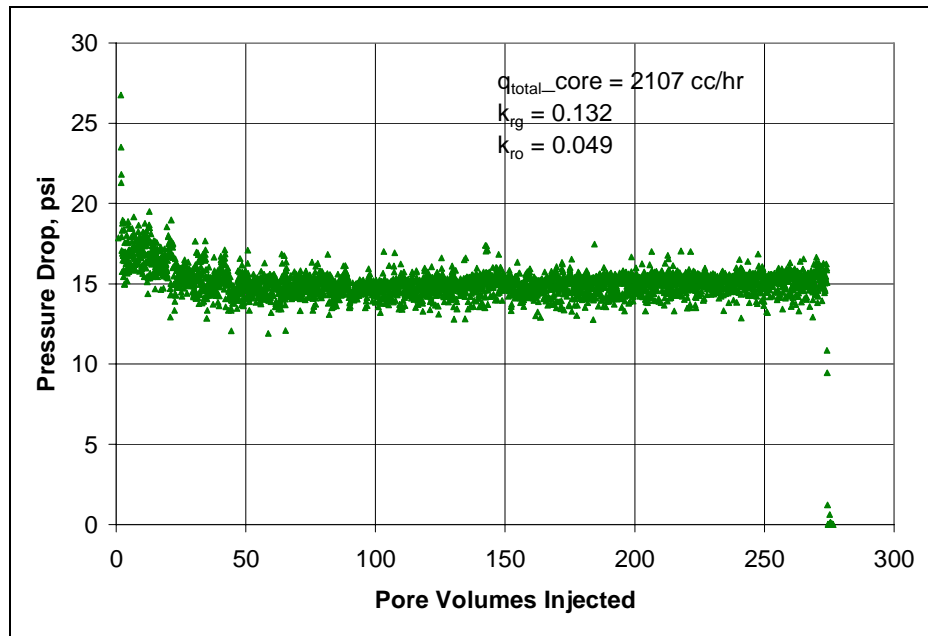


Figure B28.7: Pressure drop across the core during condensate flood-3

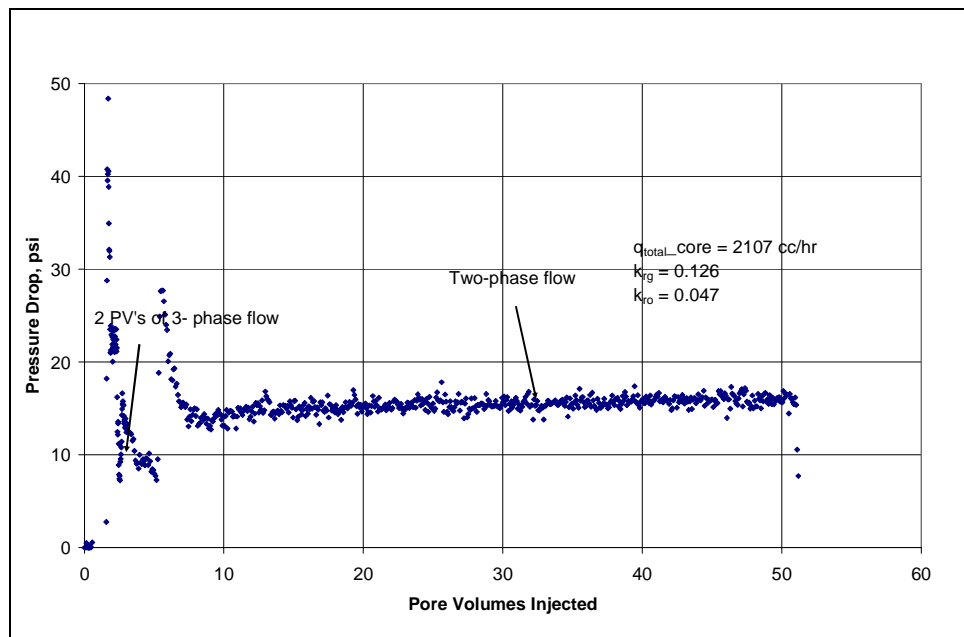


Figure B28.8: Pressure drop for 2PV's of three-phase followed by two-phase flow

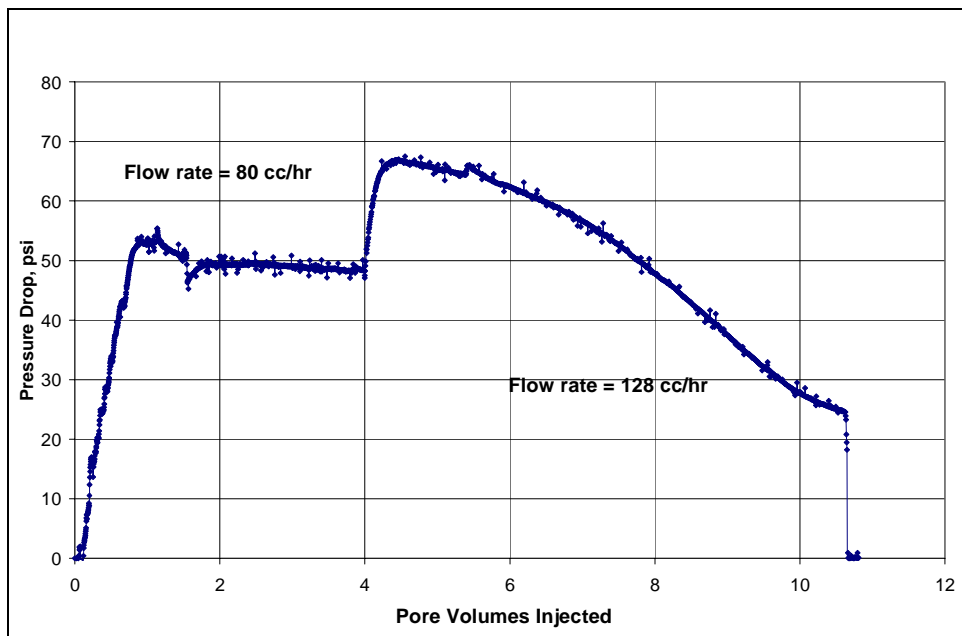


Figure B28.9: Pressure drop across the core during brine injection

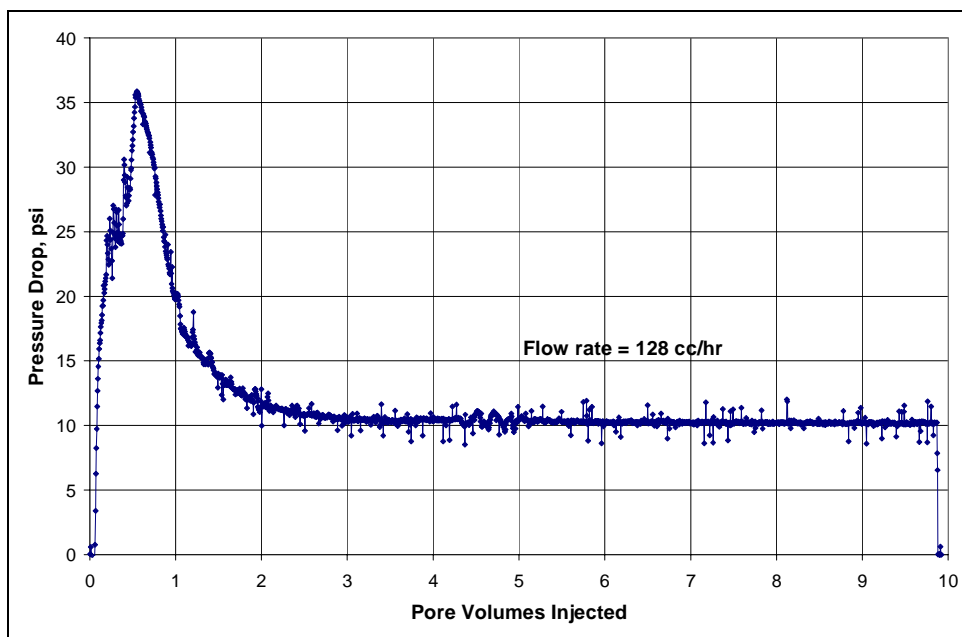


Figure B28.10: Pressure drop across the core during solvent flood-2

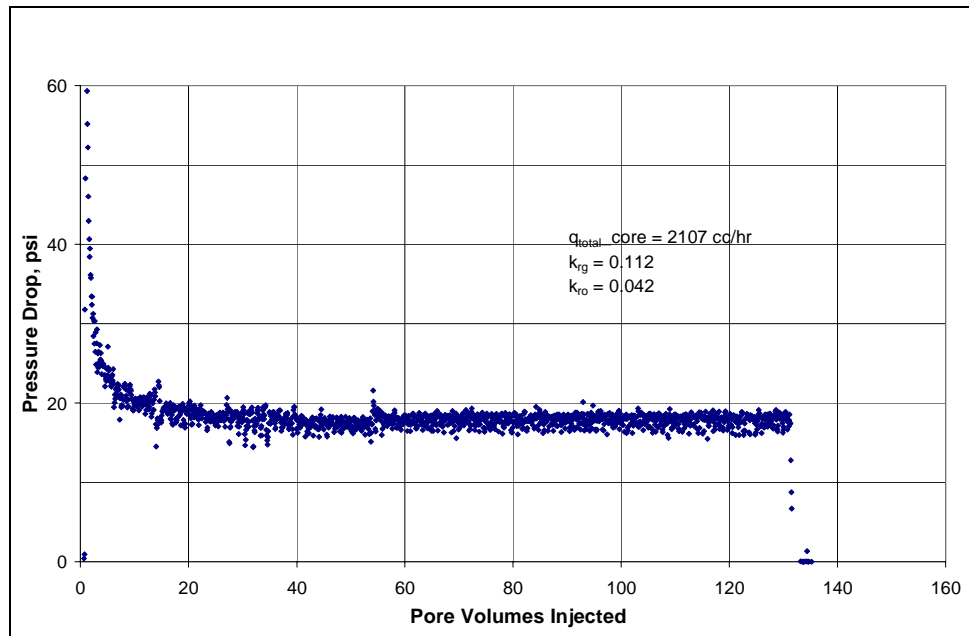


Figure B28.11: Pressure drop across the core during condensate flood-5

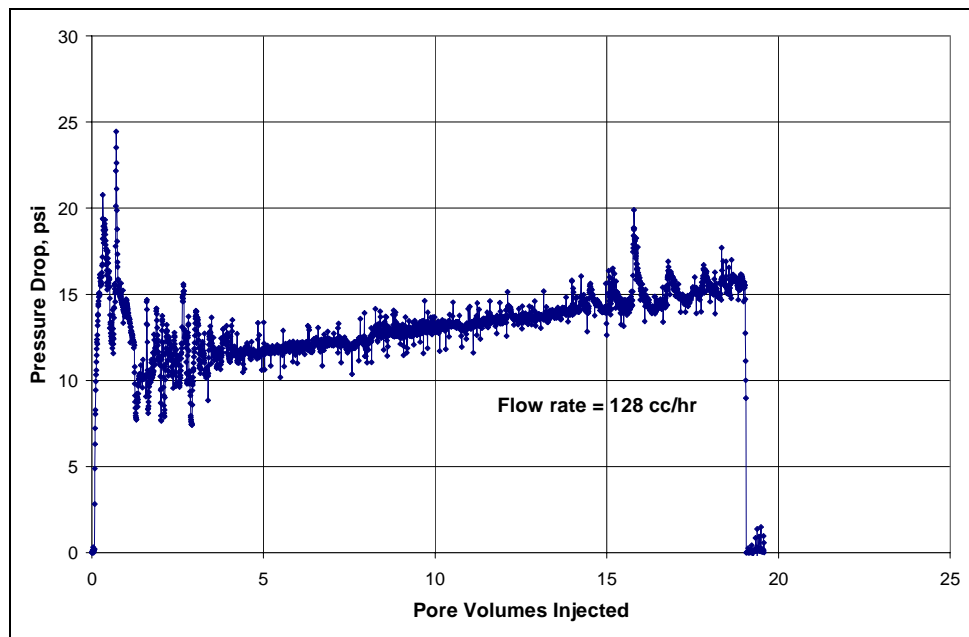


Figure B28.12: Pressure drop across the core during second chemical treatment

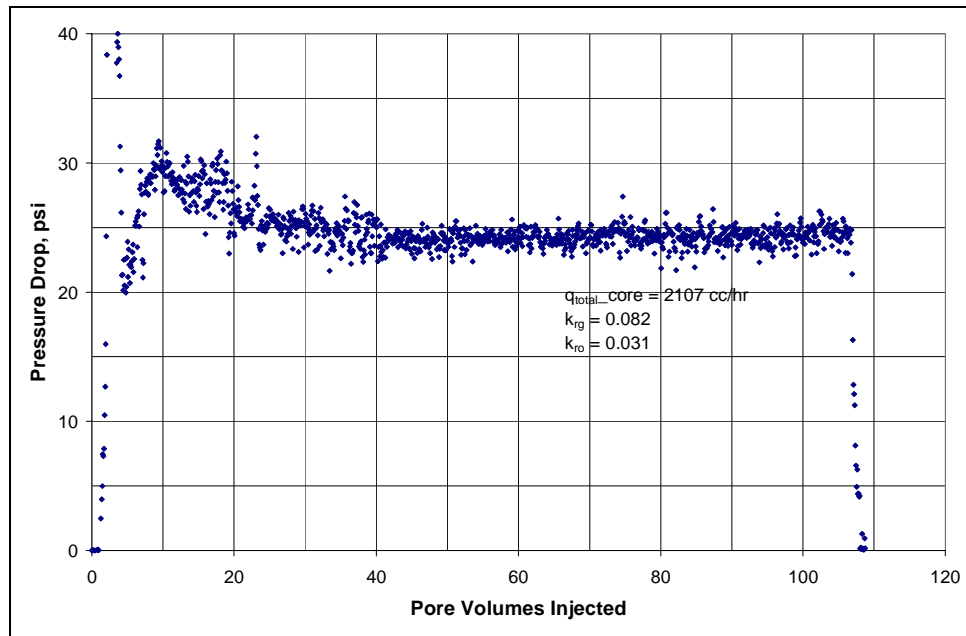


Figure B28.13: Pressure drop across the core during the gas condensate flood after second chemical treatment

B29- Experiment No.29

Objective:

The objective of this experiment was to investigate the effect of the chemical treatment using FC4430 on gas and condensate relative permeability measured on a propped fracture. The experiment was performed using Ottawa F35 sand as proppant at 279°F.

Experimental Results:

Reservoir B plug 7E was used as the matrix rock and Ottawa F35 sand was used as the proppant to fill the simulated fracture void. This sand has an average mesh size of about 35 corresponding to an average grain diameter of on the order of 0.02 cm.

Table B29.1 summarizes the properties of the propped fracture and the experimental conditions. Initial permeability of the propped fracture was measured using nitrogen at 75°F. **Figure B29.1** shows the pressure drop measured across the core during nitrogen flood. **Table B29.2** summarizes the results of the nitrogen flood. The average permeability of the fracture was calculated from the intercept of the plot of $(\Delta P/q)$ vs q . **Figure B29.2** shows the plot of $(\Delta P/q)$ vs q . As permeability of the fracture is 100 times more than the permeability of the rock matrix, most of the flow will be through the fracture and thus the pressure drop measured across the core will be same as the pressure drop across the fracture.

80 Pore volumes of synthetic brine (**Table B29.3**) was flowed through the fracture. **Figure B29.3** shows the pressure drop across the fracture during the brine flood. Nitrogen flood was then conducted to reduce the water saturation to residual and measure the end point gas relative permeability. **Figure B29.4** shows the pressure drop measured

across the fracture and **Table B29.4** summarizes the results of the nitrogen flood. The average permeability at S_{wi} was calculated from the intercept of the plot of $(\Delta P/v/l)$ vs velocity. **Figure B29.5** shows the plot of $(\Delta P/q)$ vs q . The temperature of the oven was increased to 279°F.

Synthetic fluid mixture-9 (**Table 3.9**) was used for the two-phase flow measurements. The initial flood was conducted with the upstream backpressure regulator set at 5500 psig and the downstream back pressure regulator set at 2600 psig. Net confining stress on the fracture was 1000 psi. **Table B29.5** gives the properties of the synthetic fluid calculated using the Peng-Robinson EOS at the flowing core pressure. Initial gas condensate flood was conducted at 542 cc/hr (core rate) and 291 cc/hr (core rate). **Figure B29.6** shows the pressure drop across the core during the two-phase gas-condensate flood. **Table B29.6** summarizes the results of the initial two-phase flow. The relative permeability data reported in this section has been corrected for non-Darcy flow effects.

14 pore volumes of solvent (70/30 mixture of PG/IPA) was flowed through the core at 157.5 cc/hr. **Figure B29.7** shows the pressure drop across the core during the solvent flood. Gas condensate flood was then conducted at multiple rates to measure steady state two-phase flow pressure drops. BPR#1 was set at 5500 psi and BPR#2 was set at 1500 psi. Overburden pressure was 3500 psi. **Figure B29.8** shows the pressure drop across the core during the two-phase gas-condensate flood after solvent flush. The pressure drops were higher than expected value and showed a lot of fluctuation at the higher flow rate. The direction of flow was then reversed to remove any kind of blockage from the fracture. **Figure B29.9** shows the pressure drop across the core during the two-phase gas-condensate flood after reversing the flow. **Table B29.7** summarizes the results of the post-solvent two-phase flow in the reverse direction.

The core was then treated with the treatment solution (**Table B29.8**). **Figure B29.10** shows the measured pressure drop across the core during the treatment flood. 40 PV of treatment solution was injected at 24 cc/hr and then 30 PV of treatment solution was injected at 384 cc/hr. The core was then shut-in for 15hours.

Post-treatment two-phase gas-condensate flood was conducted under the same conditions as the initial two-phase flow. The initial pressure drops were higher than the pre-treatment values. After injecting 2200 pore volumes of gas mixture the flow was again reversed to determine if sand blockage might be the reason of high pressure drop. **Figure B29.11** shows the pressure drop measured during the post-treatment gas condensate flood. **Table B29.9** summarizes the results of the post-treatment two-phase flow in the reverse direction.

Table B29.1: Core and fracture properties

Core	Reservoir B core (plug #7E)
Proppant	Ottawa F35 sand
Fracture Aperture, cm	0.22
Length, cm	4.66
Fracture width, cm	2.47
Porosity, %	36.07
Pore volume, cc	0.91
Swi, %	-
Temperature, °F	279

Table B29.2: Result of nitrogen flood

q_{core} , (cc/hr)	ΔP (psi)	k_g (Darcy)
5501.64	0.80	4.67
4126.23	0.48	5.84
2750.82	0.24	7.78
Permeability, k_g (md) (corrected for non Darcy)		23.38

Table B29.3: Composition of synthetic brine

Component	ppm
NaCl	225.2
CaCl ₂	1.5
KCl	3.1

Table B29.4: Result of nitrogen flood at Swi

q_{core} , (cc/hr)	ΔP (psi)	k_g (Darcy)
2750.82	0.39	4.79
1375.41	0.14	6.67
3439.00	0.57	4.10
Permeability, k_g (md) (corrected for non Darcy)		11.51

Table B29.5: Synthetic fluid properties at experimental conditions

Pressure, psig	5500	2600		1500	
Fluid Properties		Gas phase	Oil phase	Gas phase	Oil phase
ρ , g/cc	0.2231	0.1019	0.5781	0.057	0.630
μ (cp)		0.0189	0.2137	0.0165	0.3112
Volume fraction		0.9604	0.0396	0.9782	0.0218
IFT (dyne/cm)		2.335		2.416	

Table B29.6: Results of the initial two-phase gas condensate flood at 2600 psig

q_{pump}, cc/hr	292	157
q_{total_core}, cc/hr	542.00	291.00
q_{g_core}, cc/hr	520.54	279.48
q_{o_core}, cc/hr	21.46	11.52
ΔP, psi	0.90	0.70
k_{rg}	0.019	0.012
k_{ro}	0.008	0.005
Nc	1.31x10 ⁻³	1.02x10 ⁻³
PVT Ratio	2.14	2.14

TableB29.7: Results of the initial two-phase gas condensate flood after solvent flush at 1500 psig

q_{total_core}, cc/hr	514	815	1631	2899
q_{g_core}, cc/hr	502.79	797.23	1595.44	2835.80
q_{o_core}, cc/hr	11.21	17.77	35.56	63.20
ΔP, psi	0.19	0.26	0.55	1.20
k_{rg}	0.069	0.080	0.078	0.065
k_{ro}	0.028	0.032	0.030	0.025
Nc	2.68x10 ⁻⁴	3.67x10 ⁻⁴	7.76x10 ⁻⁴	1.69x10 ⁻³
PVT Ratio	2.38	2.38	2.38	2.38

Table B29.8: Composition of treatment solution

Component	Weight %
FC4430	2.0
Propylene Glycol	69
IPA	29

Table B29.9: Results of post-treatment two-phase flow of gas condensate mixture

q_{total_core}, cc/hr	514	815	1631	2899
q_{g_core}, cc/hr	502.79	797.23	1595.44	2835.80
q_{o_core}, cc/hr	11.21	17.77	35.56	63.20
ΔP, psi	0.11	0.17	0.37	0.84
k_{rg}	0.119	0.124	0.117	0.095
k_{ro}	0.048	0.049	0.045	0.035
Nc	1.55x10 ⁻⁴	2.40x10 ⁻⁴	5.22x10 ⁻⁴	1.18x10 ⁻³
Improvement factor	1.74	1.54	1.50	1.45

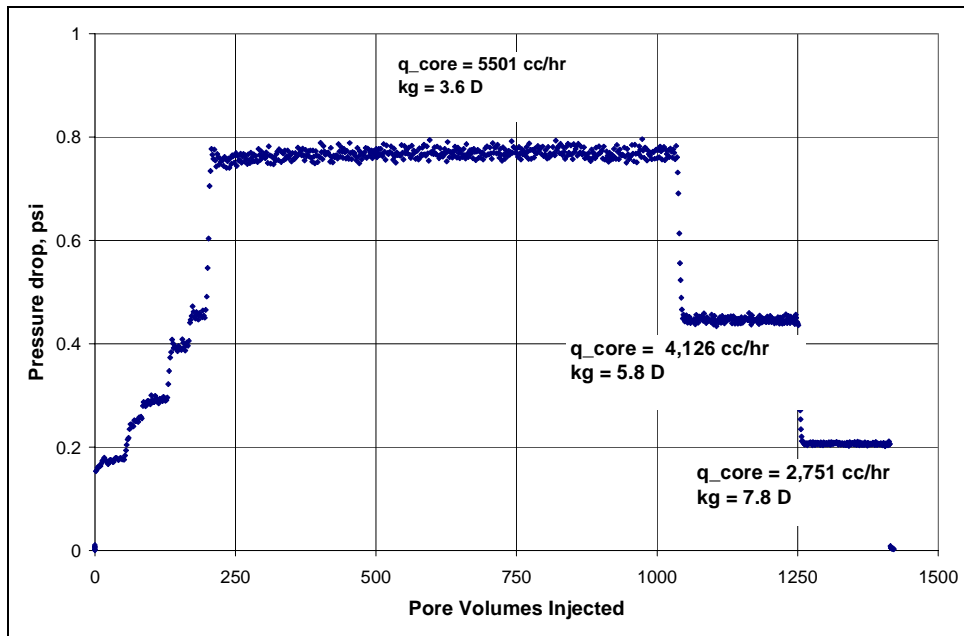


Figure B29.1: Pressure drop across the propped fracture during initial nitrogen flood

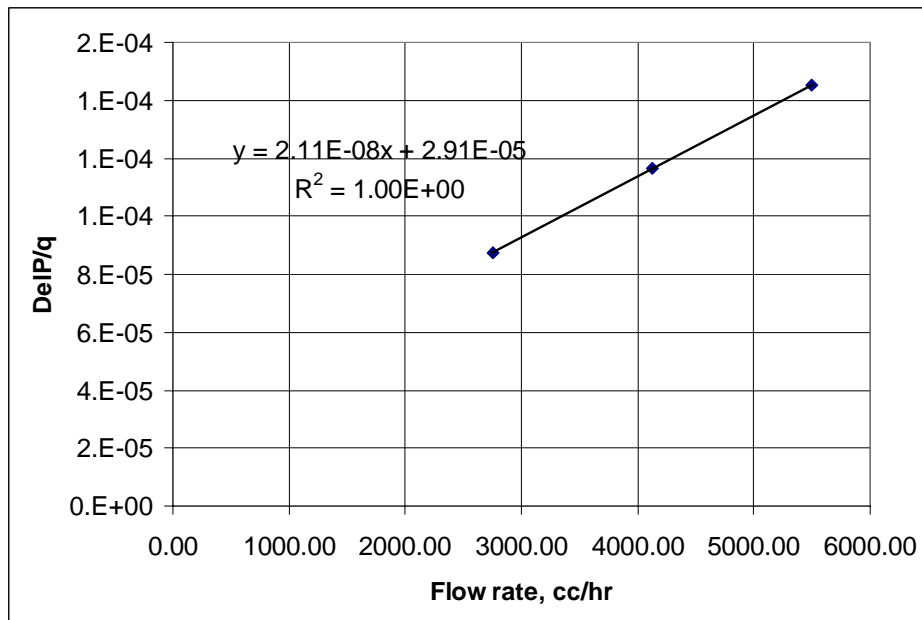


Figure B29.2: Correcting gas permeability measurement for non-Darcy flow

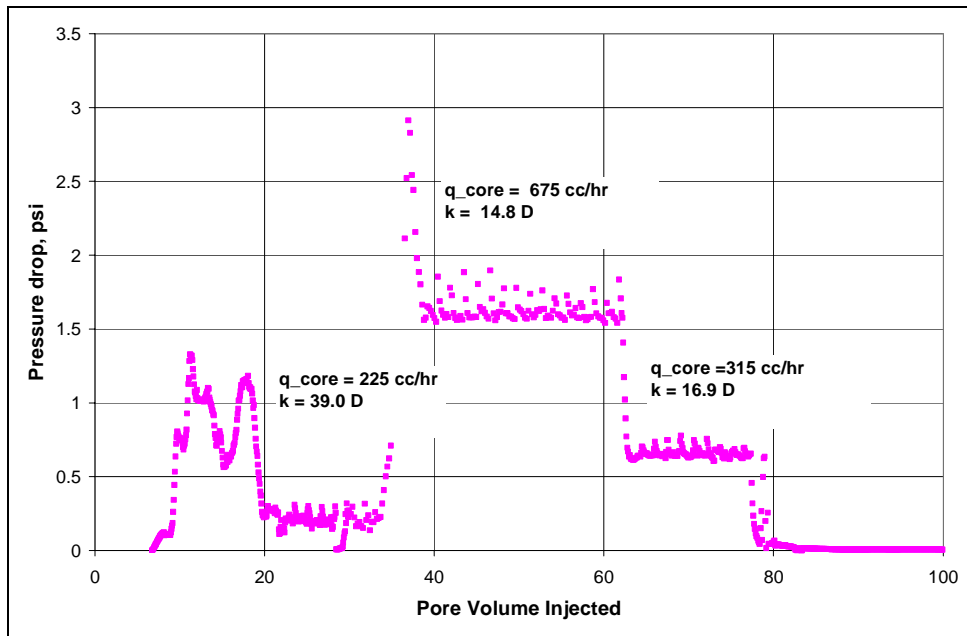


Figure B29.3: Pressure drop across the propped fracture during the brine flood

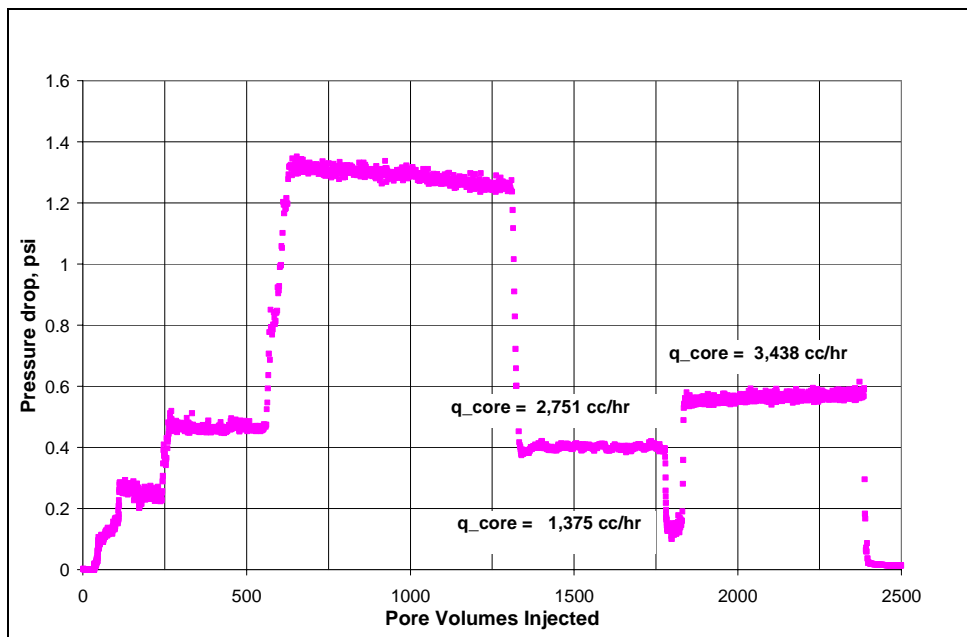


Figure B29.4: Pressure drop across the propped fracture during nitrogen flood at Swi

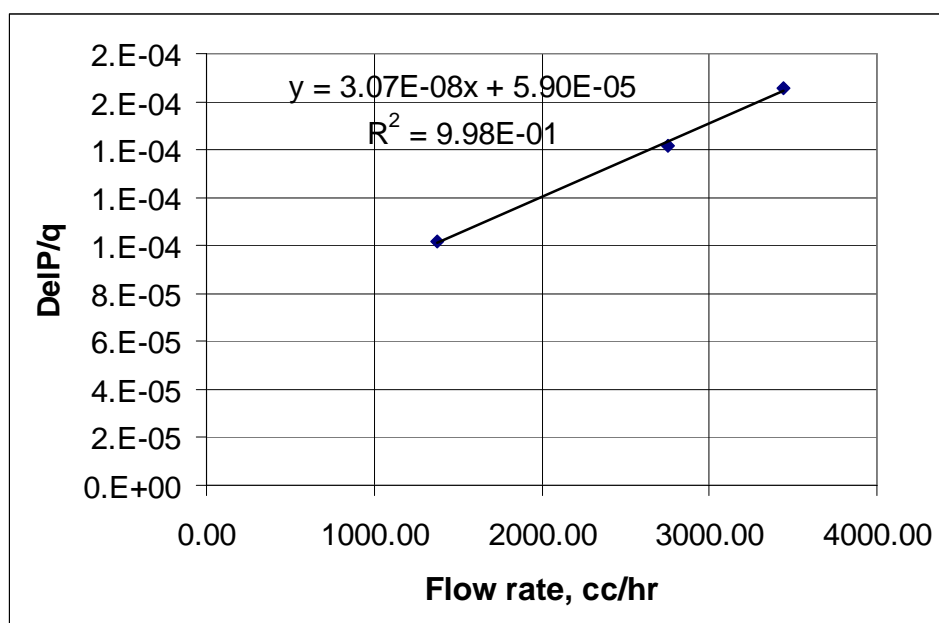


Figure B29.5: Correcting gas permeability measurement at S_{wi} for non-Darcy flow

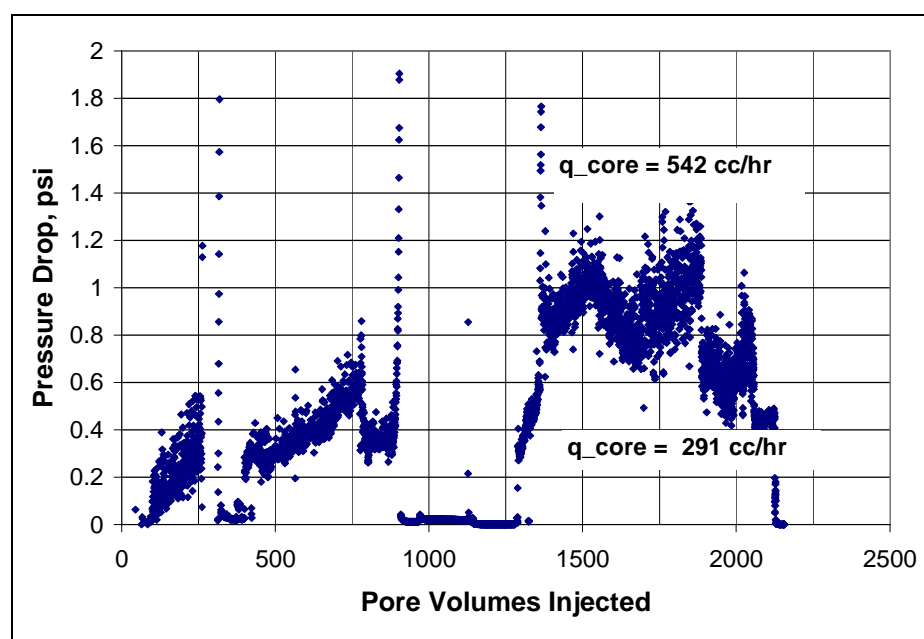


Figure B29.6: Pressure drop across the propped fracture during the initial two-phase flood at 279°F and 2600 psig

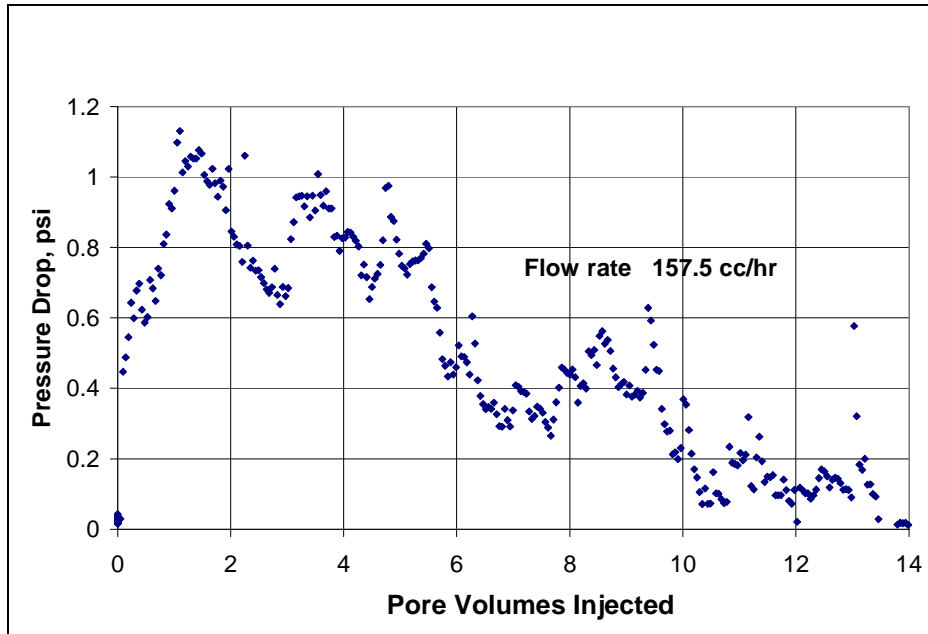


Figure B29.7: Pressure drop across the propped fracture during the solvent flood

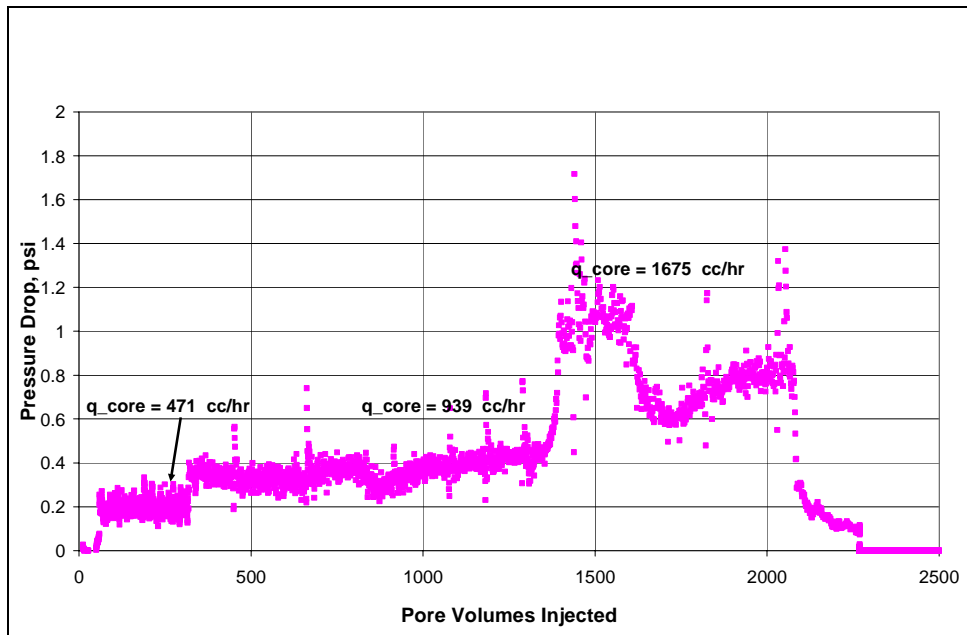


Figure B29.8: Pressure drop across the propped fracture during the gas condensate flood after solvent flush at 279°F and 1500 psig

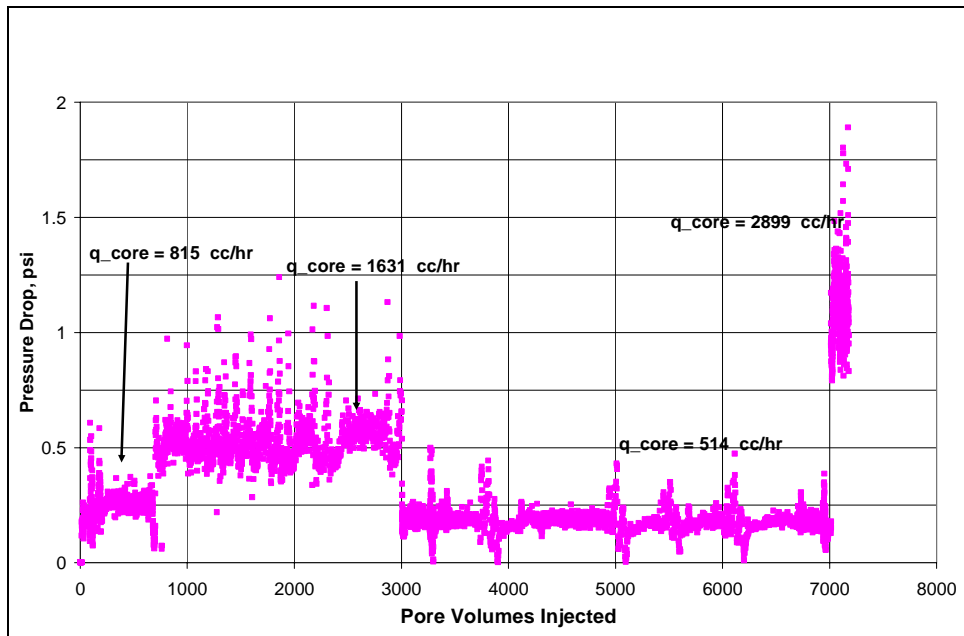


Figure B29.9: Pressure drop across the propped fracture during the gas condensate flood in the reverse flow direction at 279°F and 1500 psig

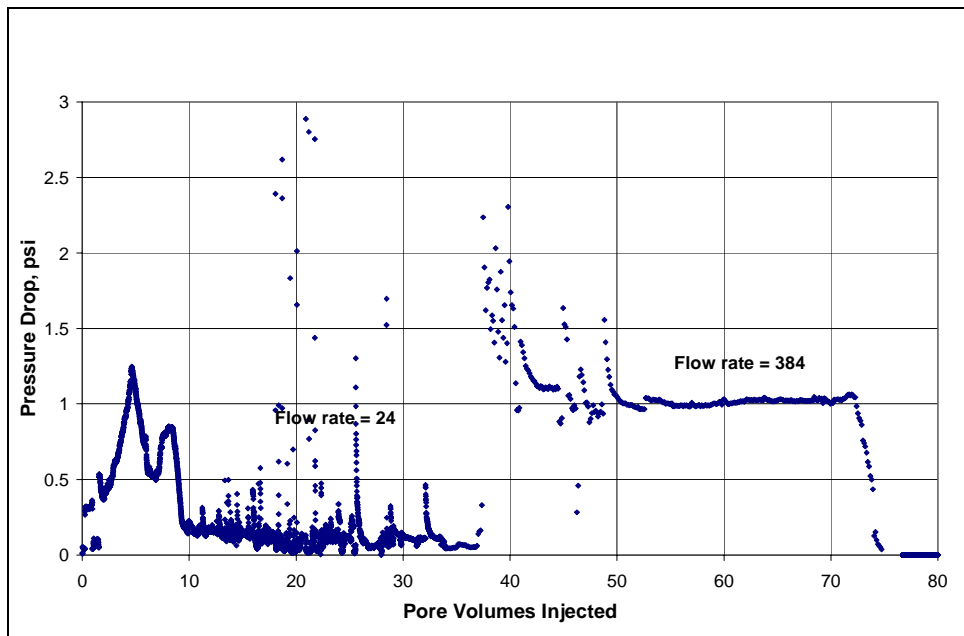


Figure B29.10: Pressure drop across the propped fracture during surfactant treatment

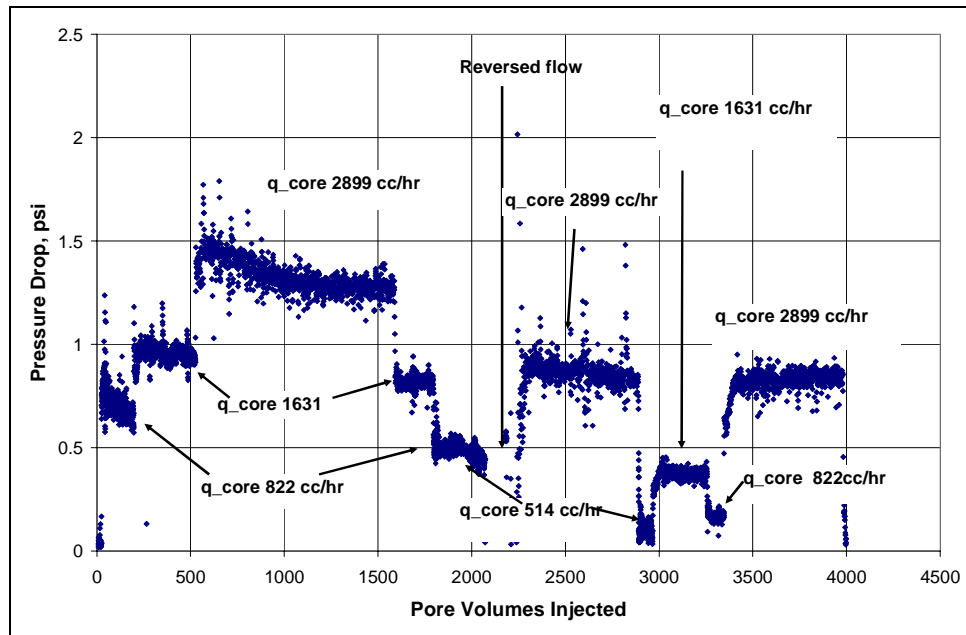


Figure B29.11: Pressure drop across the propped fracture during post-treatment two-phase flood at 279°F and 1500 psig

B30- Experiment No.30

Objective:

The objective of this experiment was to investigate the effect of chemical treatment using a new surfactant X3 on gas and condensate relative permeability in presence of mobile water. The experiment was performed on a Berea core at 175°F. To avoid problems of corrosion, sodium dithionite was added to brine.

Experimental Results:

Table B30.1 summarizes the properties of the core and the experimental conditions. Initial permeability of the core was measured using nitrogen at 75°F. **Figure B30.1** shows the pressure drop measured across the core during nitrogen flood. **Table B30.2** summarizes the results of the nitrogen flood.

The initial water saturation of 19% was established by injecting 3.8 cc of synthetic Bruce brine (**Table B21.3**) in the vacuumed core. Nitrogen flood was then conducted to measure the end point gas relative permeability. **Figure B30.2** shows the pressure drop measured across the core and **Table B30.3** summarizes the results of the nitrogen flood. The pressure of the core was raised to 200 psig and then the temperature of the oven was increased to 175°F.

Synthetic fluid mixture-4 (**Table 3.4**) was used for the two-phase flow measurements. The initial flood was conducted with the upstream backpressure regulator set at 5120 psig and the downstream back pressure regulator set at 420 psig. **Table B28.4** gives the properties of the synthetic fluid calculated using the Peng-Robinson EOS at the flowing core pressure. **Figure B30.3** shows the pressure drop across the core for the two-phase flow. **Table B30.5** summarizes the results of the initial two-phase flow.

The core was then treated with the treatment solution (**Table B30.6**). Treatment was injected at 128 cc/hr. **Figure B28.4** shows the measured pressure drop across the core during the treatment flood. The core was then shut-in for 15 hours.

Post-treatment two-phase flow of the gas mixture was then done under the same conditions as the pre-treatment two-phase flow. **Figure B30.5** shows the pressure drop across the core measured during the post-treatment two-phase. **Table B30.7** summarizes the results of the post-treatment two-phase flow.

The post-treatment gas condensate flood was followed with 2 pore volumes of three-phase flow of gas, condensate and brine at a fractional flow of brine equal to 0.038 ($f_w=0.038$). To avoid problems of corrosion, 0.02% of sodium dithionite was added to brine. This was followed with the gas condensate two-phase flow (*condensate flood-3*). **Figure B30.6** shows the pressure drop during the condensate flood-3. The pressure drop for the two-phase flow was lower than the pre-treatment two-phase flow but did not reach steady state even after flowing 140 pore volumes, suggesting that brine is not easily removed from the core. The flood was stopped for 1 hour and then restarted at the same rate. The pressure drop increased by almost 50% suggesting that some water from the lines went into the core. Some water was also produced in the effluent from the core. A solvent flush (*solvent flush-1*) (composition given in **Table B30.8**) was conducted at 128cc/hr to remove the brine from the core and this was followed by two-phase flow of gas condensate mixture (*condensate flood-4*). **Figures B30.7** and **B30.8** show the pressure drop for the solvent flush-1 and condensate flood-4 respectively. **Table B30.9** summarizes the results of condensate flood-4.

The core was then flooded with 1 PV of brine ($f_w=1$). **Figure B30.9** shows pressure drop during brine injection. The brine flood was followed with a solvent flush (*solvent flush-2*) (composition in **Table B30.8**) and finally with the two-phase gas

condensate flood (*condensate flood-5*). **Figures B30.10 and B30.11** show the pressure drop for the solvent flush-2 and condensate flood-45 respectively. **Table B30.10** summarizes the results of condensate flood-5.

Next, 10 PV's of brine was flowed through the core. **Figure B30.12** shows pressure drop during brine injection. Flowing such a large pore volume of brine (at a pressure gradient of 35psi/ft) can result in water saturation up to 60-80 % in the core. The brine flood was followed by 10 PV's of the solvent (*solvent flush-3*) to remove brine, which was followed with the two-phase gas condensate flow (*condensate flood-6*) under the same conditions as the previous two-phase floods. **Figures B30.13 and B30.14** show the pressure drop for the solvent flush-3 and condensate flood-6 respectively. The pressure drop for the two-phase flow and the effluent from the core showed that the solvent flush did not remove the brine completely and significant amount of it was still present in the core. To remove the remaining brine some more solvent was flushed through the core (*solvent flush-4*) at a lower rate of 64 cc/hr for the first four pore volumes compared to the earlier rates of 128 cc/hr. The lower rate gives more residence time for the solvent to mix with brine in the core and miscibly displace it. The rate was then increased back to 128 cc/hr after 4 pore volumes of injection. Gas condensate flood (*condensate flood-7*) was done after the solvent flush-4. **Figures B30.15 and B30.16** show the pressure drop for the solvent flush-4 and condensate flood-7 respectively. **Table B30.11** summarizes the results of condensate flood-7.

Table B30.1: Core properties

Core	Berea Sandstone
Length, inches	8.00
Diameter, inches	1
Porosity, %	20.02
Pore volume, cc	20.61
Swi, %	19
Temperature, °F	175

Table B30.2: Result of nitrogen flood

q_{core}, (cc/hr)	ΔP (psi)	k_g (md)
4232.42	5.90	218.31
3627.79	5.08	217.55
3023.16	4.22	217.88
Permeability, k_g (md)		217.49

Table B30.3: Result of nitrogen flood at Swi

q_{core}, (cc/hr)	ΔP (psi)	k_g (md)
4232.42	8.61	149.76

Table B30.4: Synthetic fluid properties at experimental conditions

Pressure, psig	5120	420	
Fluid Properties		Gas phase	Oil phase
ρ, g/cc	0.3008	0.0202	0.6621
μ (cp)		0.0133	0.3844
Volume fraction		0.9868	0.0132
IFT (dyne/cm)		12.496	

Table B30.5: Results of the initial two-phase flood

q_{pump}, cc/hr	192
$q_{\text{total_core}}$, cc/hr	2014.21
$q_{\text{g_core}}$, cc/hr	1987.62
$q_{\text{o_core}}$, cc/hr	26.59
ΔP, psi	30.49
k_{rg}	0.065
k_{ro}	0.025
Nc	1.78×10^{-5}
PVT Ratio	2.59

Table B30.6: Composition of treatment solution

Component	Weight %
X3	2
2-butoxyethanol	69
Ethanol	29

Table B30.7: Results of post-treatment two-phase flow of gas condensate mixture

q_{pump}, cc/hr	192
q_{total_cores}, cc/hr	2014.21
q_{g_cores}, cc/hr	1987.62
q_{o_cores}, cc/hr	26.59
ΔP, psi	16.18
k_{rg}	0.123
k_{ro}	0.047
Nc	9.43x10 ⁻⁶
Improvement factor	1.88

Table B30.8- Composition of the solvent used to flush out brine

Component	wt%
2-Butoxyethanol	70
Ethanol	30

Table B30.9: Results of condensate flood-4

q_{pump}, cc/hr	192
q_{total_core}, cc/hr	2014.21
q_{g_core}, cc/hr	1987.62
q_{o_core}, cc/hr	26.59
ΔP, psi	14.85
k_{rg}	0.134
k_{ro}	0.052
Nc	8.66×10^{-6}
Improvement factor	2.05

Table B30.10: Results of condensate flood-5

q_{pump}, cc/hr	192
q_{total_core}, cc/hr	2014.21
q_{g_core}, cc/hr	1987.62
q_{o_core}, cc/hr	26.59
ΔP, psi	16.41
k_{rg}	0.121
k_{ro}	0.047
Nc	9.56×10^{-6}
Improvement factor	1.86

Table B30.11: Results of condensate flood-7

q_{pump}, cc/hr	192
q_{total_core}, cc/hr	2014.21
q_{g_core}, cc/hr	1987.62
q_{o_core}, cc/hr	26.59
ΔP, psi	18.87
k_{rg}	0.105
k_{ro}	0.041
Nc	1.10×10^{-5}
Improvement factor	1.62

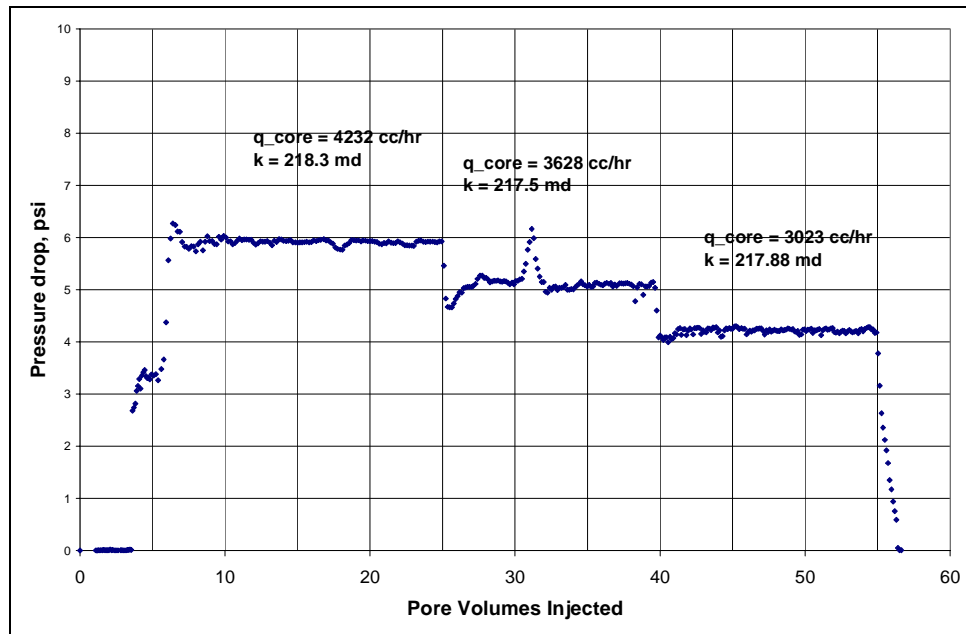


Figure B30.1: Pressure drop across the core during initial nitrogen flood

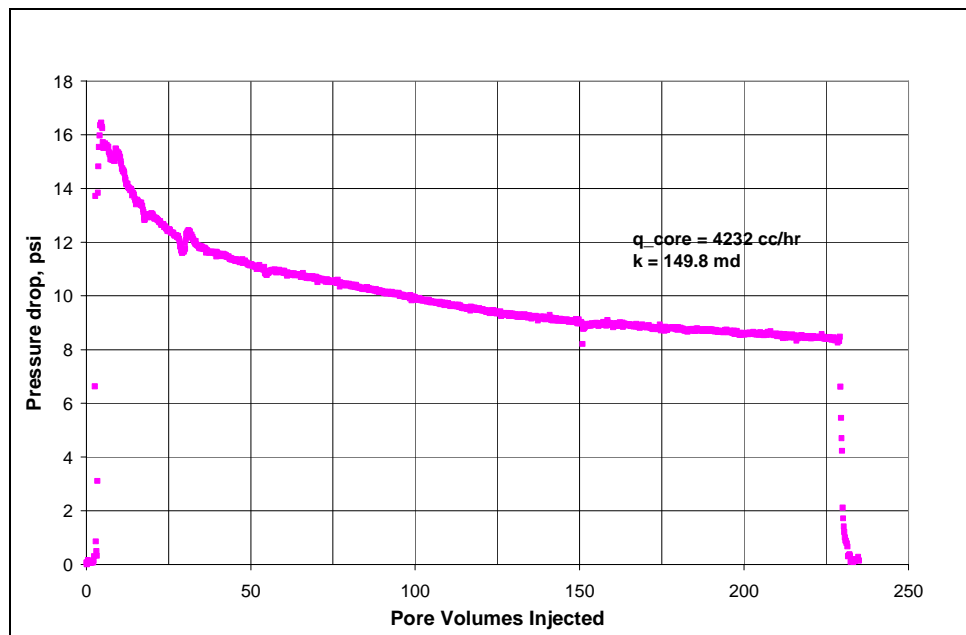


Figure B30.2: Pressure drop across the core during nitrogen flood at $Sw_i = 19\%$

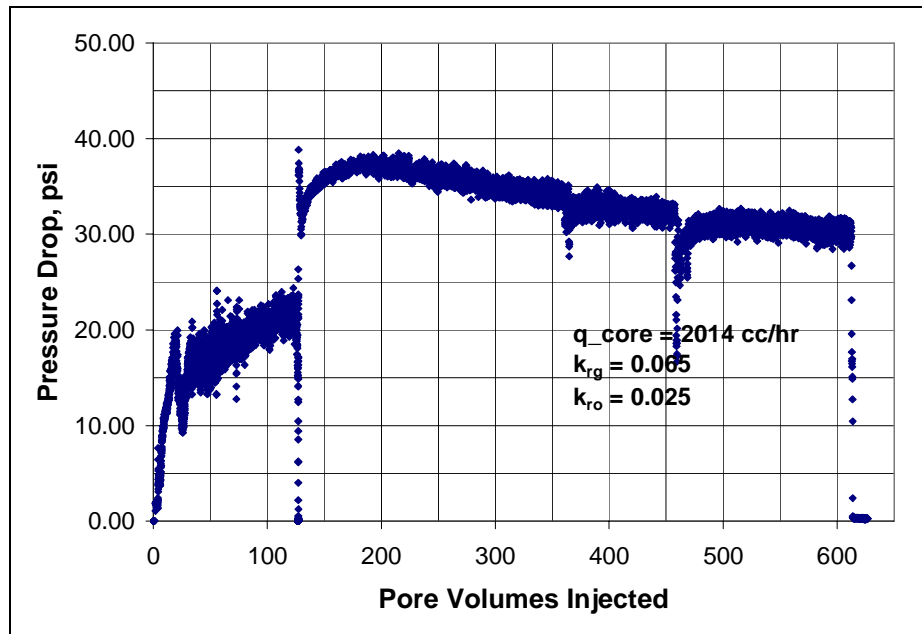


Figure B30.3: Pressure drop across the core during the initial gas condensate flood at 175°F and 420 psig

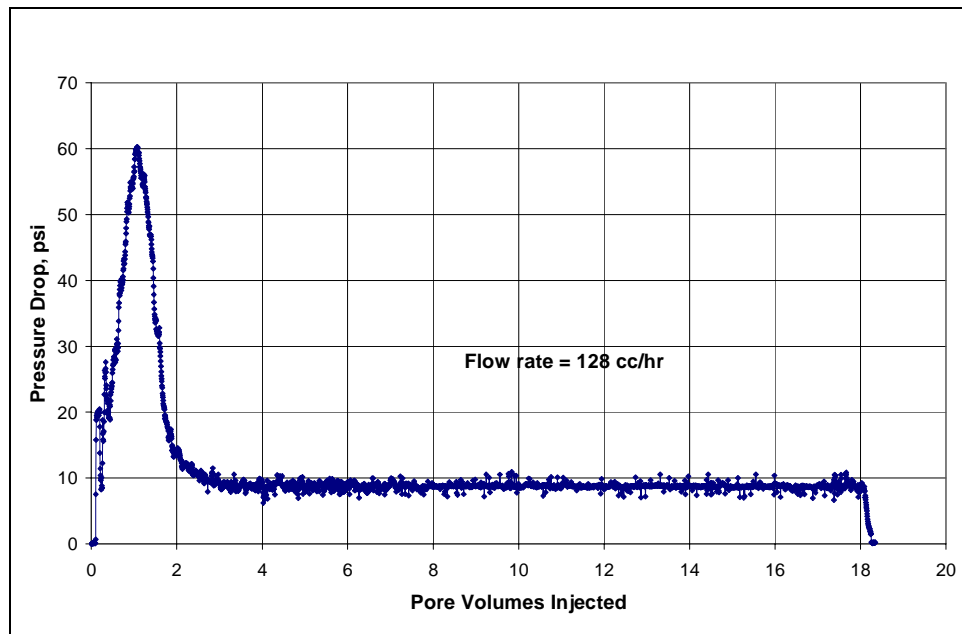


Figure B30.4: Pressure drop across the core during surfactant treatment

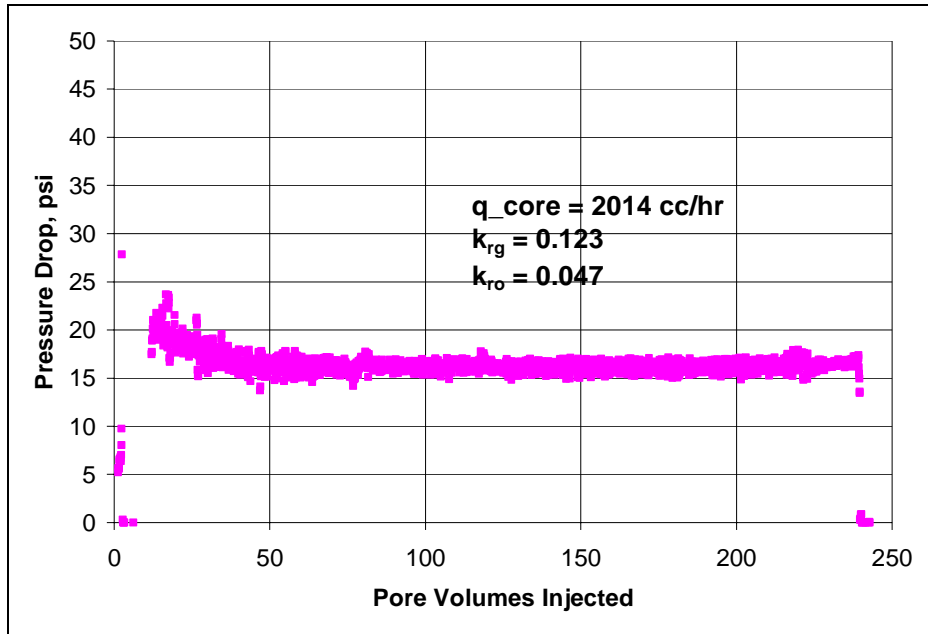


Figure B30.5: Pressure drop across the core during post-treatment gas condensate flood at 175°F and 420 psig

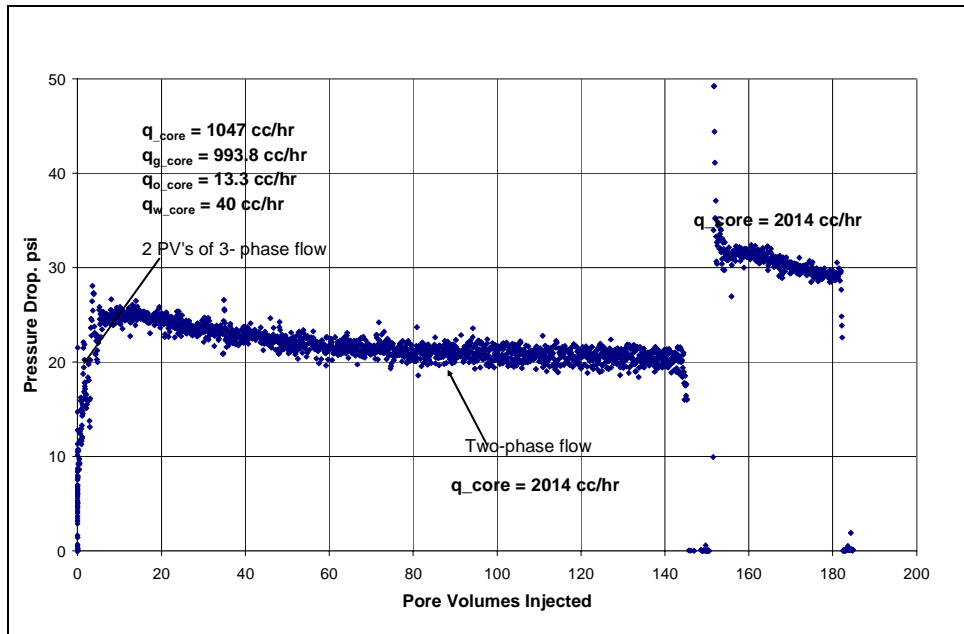


Figure B30.6: Pressure drop for 2PV's of three-phase followed by two-phase flow

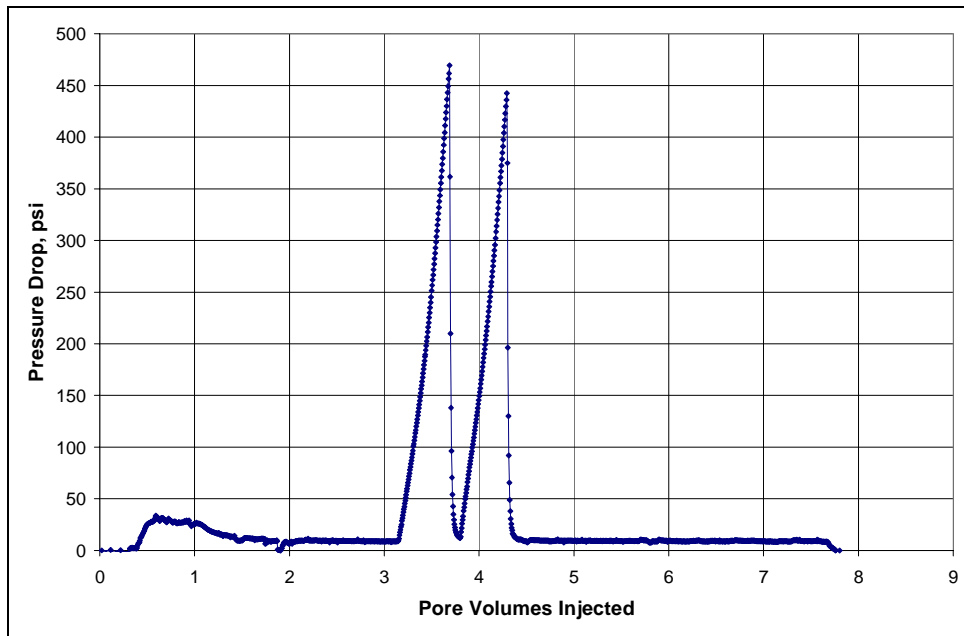


Figure B30.7: Pressure drop across the core during solvent flood-1

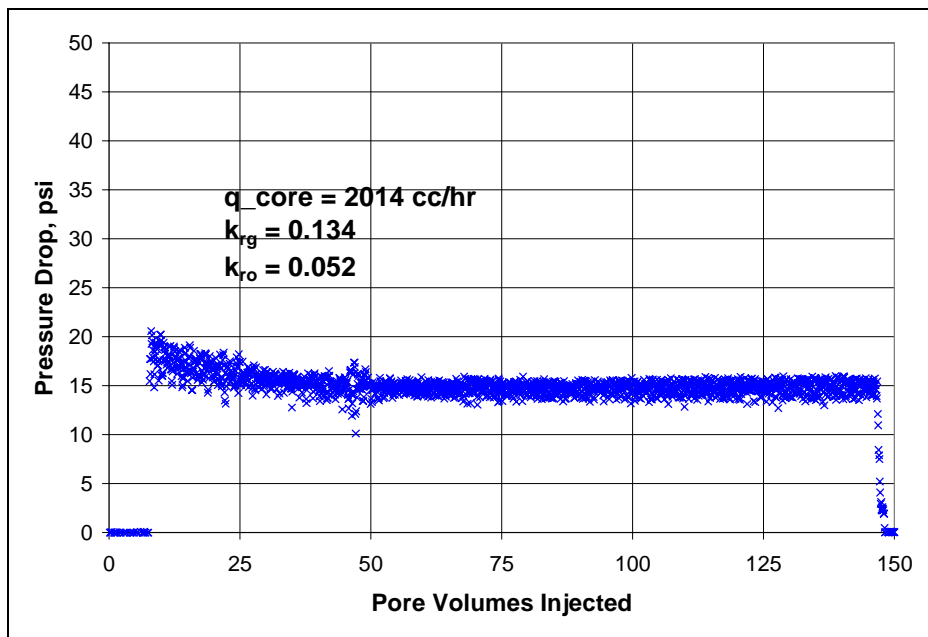


Figure B30.8: Pressure drop across the core during condensate flood-4

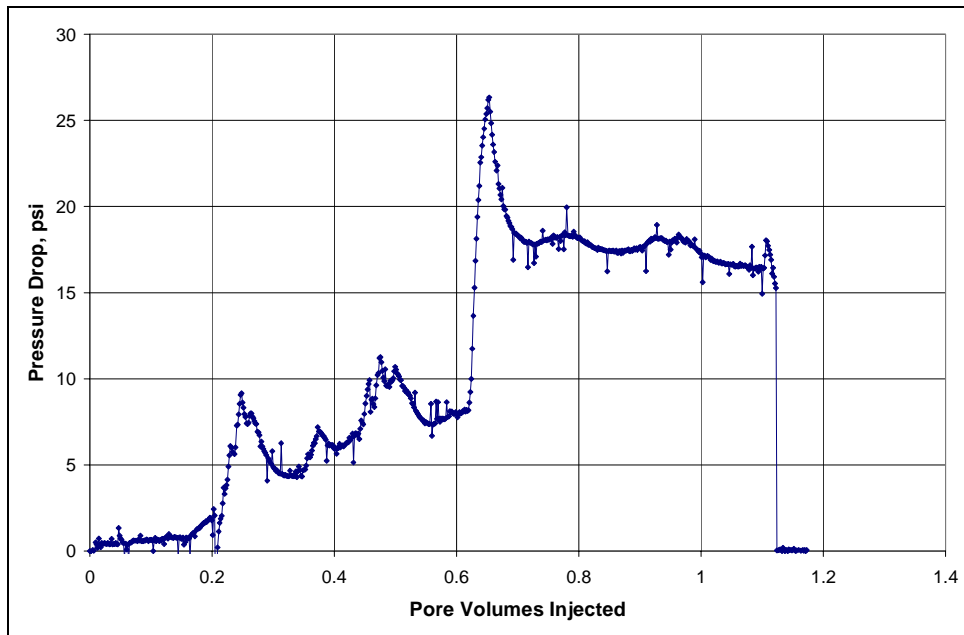


Figure B30.9: Pressure drop across the core during injection of 1 PV of brine

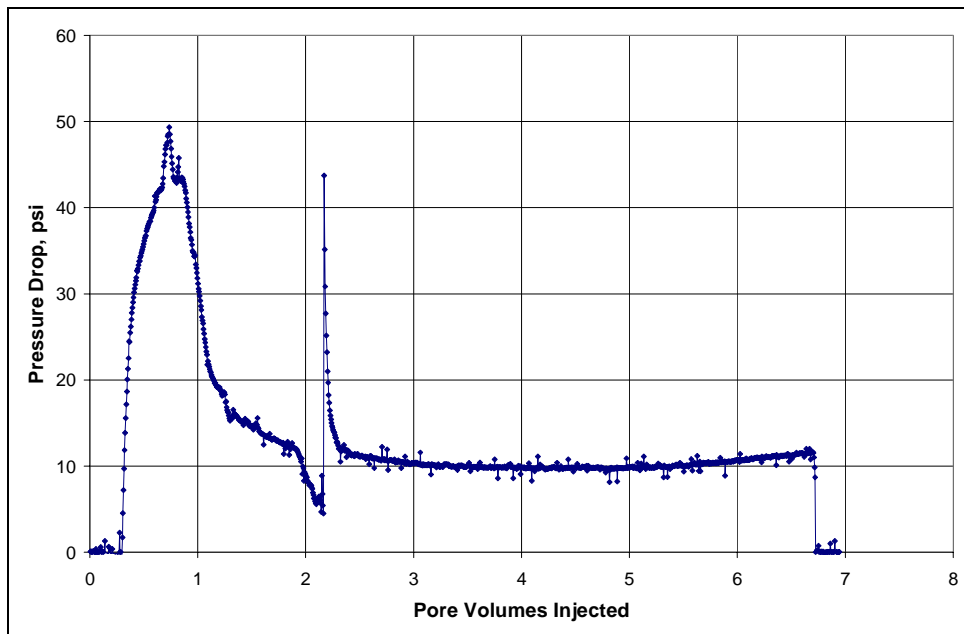


Figure B30.10: Pressure drop across the core during solvent flood-2

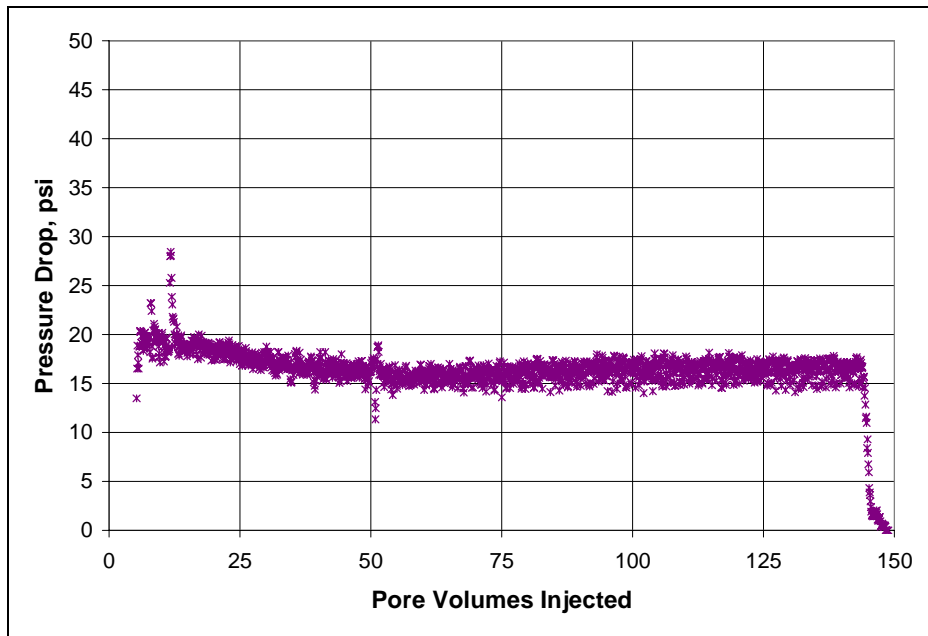


Figure B30.11: Pressure drop across the core during condensate flood-5

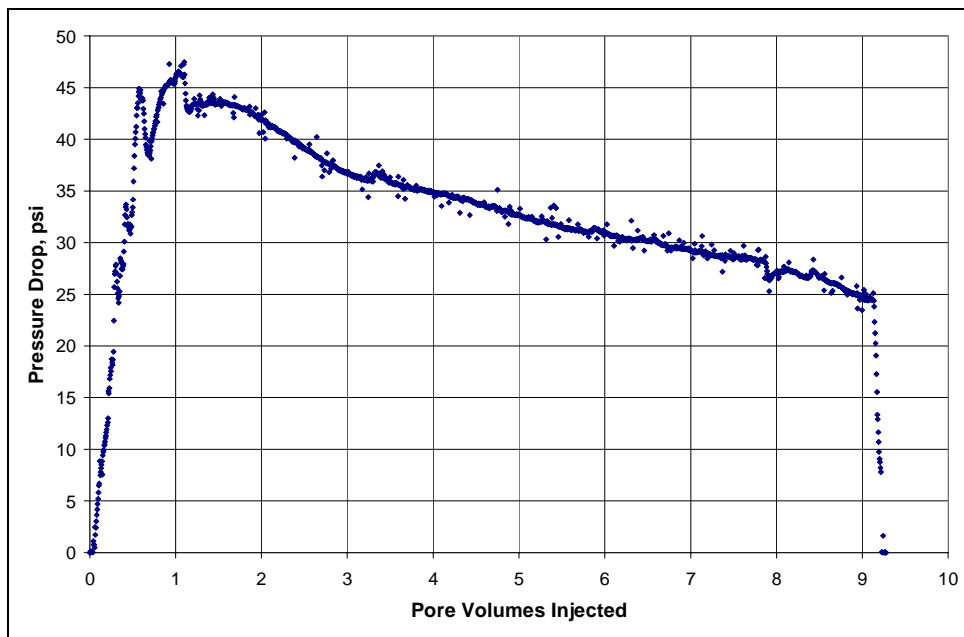


Figure B30.12: Pressure drop across the core during injection of 10 PV of brine

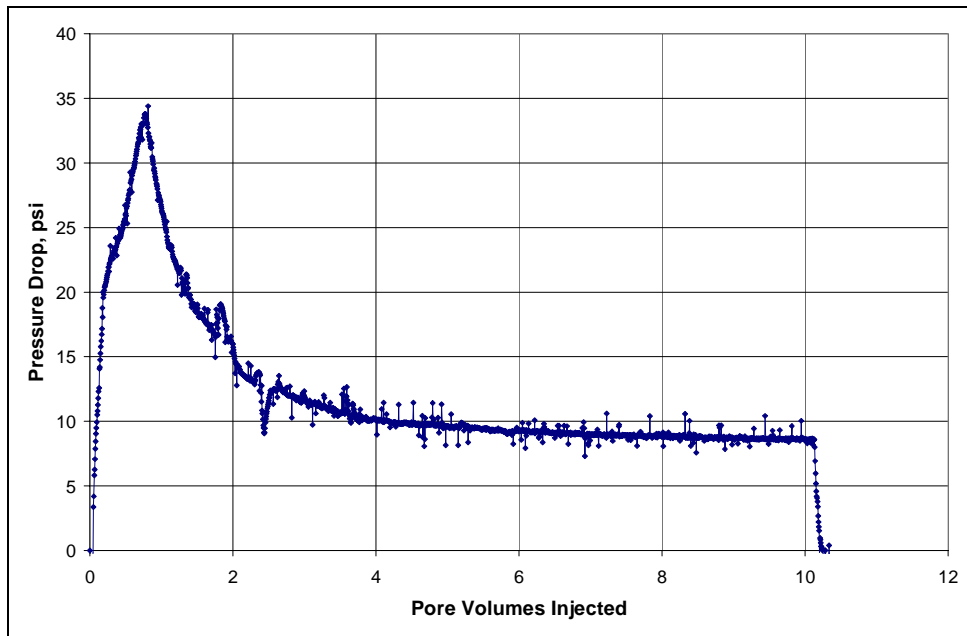


Figure B30.13: Pressure drop across the core during solvent flood-3

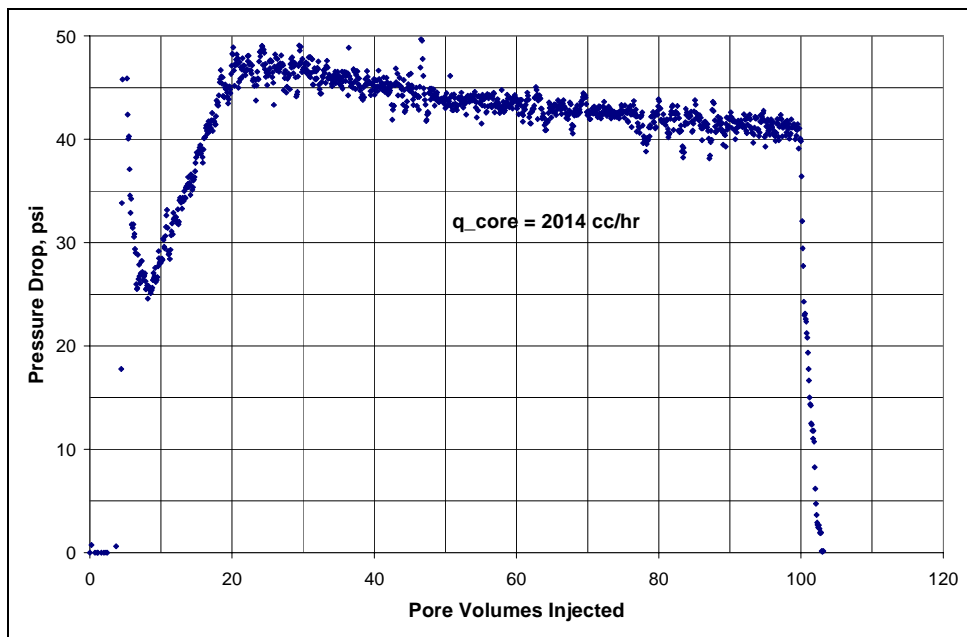


Figure B30.14: Pressure drop across the core during condensate flood-6

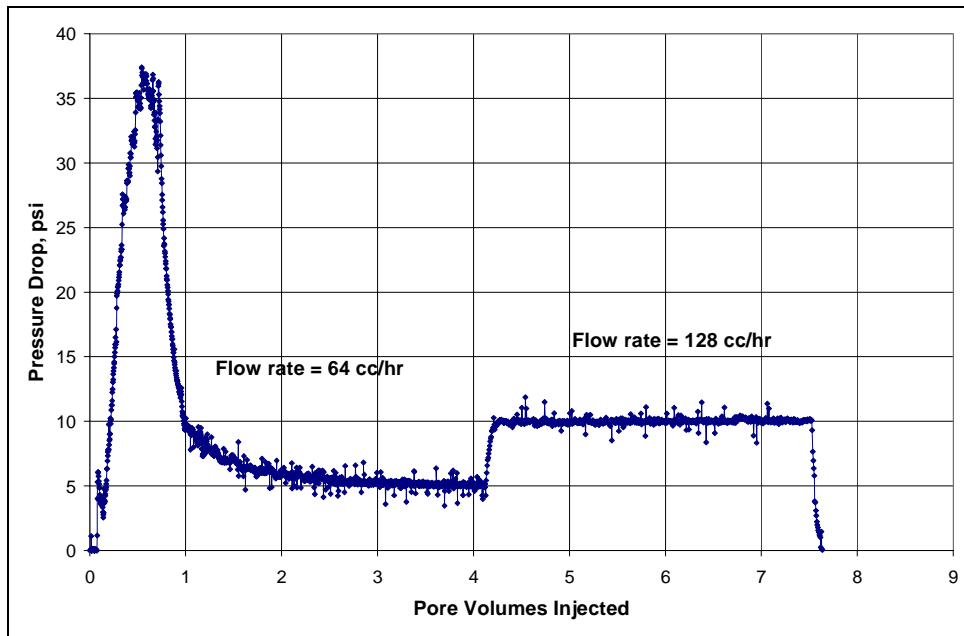


Figure B30.15: Pressure drop across the core during solvent flood-4

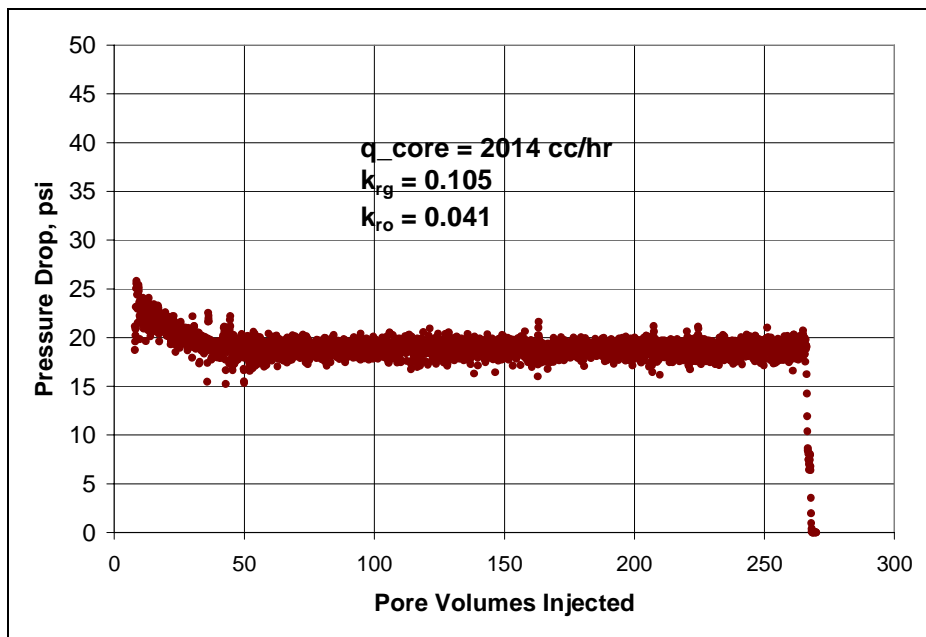


Figure B30.16: Pressure drop across the core during condensate flood-7

B31- Experiment No.31

Objective:

The objective of this experiment was to investigate the effect of the chemical treatment using FC4430 on gas and condensate relative permeability measured on a propped fracture. The experiment was performed using Ottawa F35 sand as proppant at 279°F.

Experimental Results:

Berea core was used as the matrix rock and Ottawa F35 sand was used as the proppant to fill the simulated fracture void. This sand has an average mesh size of about 35 corresponding to an average grain diameter of on the order of 0.02 cm.

Table B31.1 summarizes the properties of the propped fracture and the experimental conditions. Initial permeability of the propped fracture was measured using nitrogen at 75°F. Nitrogen flood was done at two core pressures, 1450 psig and 500 psig. **Figure B31.1** shows the pressure drop measured across the core during nitrogen flood. **Table B31.2** summarizes the results of the nitrogen flood. The average permeability of the fracture was calculated from the intercept of the plot of $(\Delta P/v/l)$ vs velocity. **Figure B31.2** shows the plot of $(\Delta P/v/l)$ vs velocity. As permeability of the fracture is 100 times more than the permeability of the rock matrix, most of the flow will be through the fracture and thus the pressure drop measured across the core will be same as the pressure drop across the fracture.

The initial water saturation of 25% was established by injecting 0.9 cc of 30,000 ppm NaCl brine in the vacuumed propped fracture. Nitrogen flood was then conducted to measure the end point gas relative permeability. **Figure B31.3** shows the pressure drop

measured across the fracture and **Table B31.3** summarizes the results of the nitrogen flood. The average permeability at S_{wi} was calculated from the intercept of the plot of $(\Delta P/v/l)$ vs velocity. **Figure B31.4** shows the plot of $(\Delta P/v/l)$ vs velocity. The temperature of the oven was increased to 279°F.

Synthetic fluid mixture-9 (**Table 3.9**) was used for the two-phase flow measurements. The initial flood was conducted with the upstream backpressure regulator set at 5500 psig and the downstream back pressure regulator set at 1400 psig. **Table B31.4** gives the properties of the synthetic fluid calculated using the Peng-Robinson EOS at the flowing core pressure. Initial gas condensate flood was started at a pump rate of 224 cc/hr at which the pressure drop across the core was approximately 4.0 psi. The pressure drop data was very noisy. Flow rate was decreased from 224 cc/hr, to 96 cc/hr, then 48 cc/hr and finally 24 cc/hr. The rate was then increased back to 224 cc/hr to see if the same pressure drop can be obtained. Initially the pressure increased back to 4 psi. The data then began to exhibit larger fluctuations followed by an increase in pressure drop to about 6 psi. **Figure B31.5** shows the pressure drop across the core during the two-phase gas-condensate flow. It was thought that the large fluctuations in the pressure data were because of plugging or blockage in the core or lines. The gas condensate flood was the flowed in the reverse direction. The steady state pressure drop for the gas condensate flood decreased compared to values obtained for the original flow. **Figure B31.6** shows the pressure drop across the core during the two-phase gas-condensate flow in the reverse direction. **Table B31.5** summarizes the results of the initial two-phase flow. The relative permeability data has been corrected for non-Darcy flow effects.

The core was then treated with the treatment solution (**Table B31.6**). **Figure B31.7** shows the measured pressure drop across the core during the treatment flood. 20 PV of treatment solution was injected at 80 cc/hr and then the last 10 PV of treatment solution was injected at 160 cc/hr. The core was then shut-in for 11 hours.

Post-treatment two-phase gas-condensate flood was conducted under the same conditions as the initial two-phase flow. The initial pressure drops at pump rates of 256 cc/hr and 903 cc/hr were significantly higher than the pre-treatment values. After injecting 1900 pore volumes of gas mixture the flow was again reversed to determine if sand blockage might be the cause. **Figure B31.8** shows the pressure drop measured during the post-treatment gas condensate flood.

The core was then re-treated with the treatment solution (**Table B31.6**). **Figure B31.9** shows the measured pressure drop across the core during the second treatment flood. 23 PV of treatment solution was injected at 80 cc/hr and the core was then shut-in for 1 hour.

Post-treatment two-phase gas-condensate flood was conducted under the same conditions as the initial two-phase flow. It was observed that small amount of treatment solution was produced in the effluent. **Figure B31.10** shows the pressure drop during the gas condensate flood after the second treatment. The pressure drop did not stabilize during the flood. A second gas condensate flood was then conducted under the same conditions. **Figure B31.11** shows the pressure drop during the second gas condensate flood after the second treatment. **Table B31.7** summarizes the results for the second gas condensate flood after the second treatment.

Finally, the post-treatment permeability of the fracture was measured using methane to find out if the final gas permeability was as high as the initial gas

permeability. **Figure B31.12** shows the pressure drop during the methane flood and **Table B31.8** summarizes the results.

Table B31.1: Core properties

Core	Berea Sandstone
Proppant	Ottawa F35 sand
Fracture Aperture, cm	0.24
Length, inches	8
Fracture width, cm	2.48
Porosity, %	36.66
Pore volume, cc	4.43
Swi, %	25
Temperature, °F	279

Table B31.2: Result of nitrogen flood

Core Pressure, psig	q_{core} , (cc/hr)	ΔP (psi)	k_g (Darcy)
500	3238.62	0.46	18.36
500	5397.71	0.95	14.87
500	7556.79	1.59	12.44
1420	1175.28	0.17	19.68
1420	1958.81	0.38	14.68
1420	2742.33	0.66	11.96
Permeability, k_g (md) (corrected for non-Darcy)			37.78
β (1/cm) = 8.44×10^3			

Table B31.3: Result of nitrogen flood at Swi

q_{core}, (cc/hr)	ΔP (psi)	k_g (Darcy)
1958.81	0.39	14.16
2742.33	0.69	11.38
1175.28	0.21	16.38
783.52	0.13	16.06
Permeability, k_g (md) (corrected for non Darcy)		33.02
β (1/cm) = 8.90x10³		

Table B31.4: Synthetic fluid properties at experimental conditions

Pressure, psig	5500	1450	
Fluid Properties		Gas phase	Oil phase
ρ, g/cc	0.2236	0.057	0.63
μ (cp)		0.0165	0.3112
Volume fraction		0.9872	0.0218
IFT (dyne/cm)		5.517	

Table B31.5: Results of the initial two-phase gas condensate flood

q_{pump}, cc/hr	64	128	256	512	896
q_{total_core}, cc/hr	205.93	411.86	823.72	1647.44	2883.03
q_{g_core}, cc/hr	201.44	402.88	805.76	1611.53	2820.18
q_{o_core}, cc/hr	4.49	8.98	17.96	35.91	62.85
ΔP, psi	0.23	0.30	0.45	0.96	2.53
k_{rg}	0.054	0.086	0.122	0.127	0.092
k_{ro}	0.022	0.034	0.046	0.043	0.028
Nc	5.34x10 ⁻⁵	6.87x10 ⁻⁵	1.03x10 ⁻⁴	2.20x10 ⁻⁴	5.81x10 ⁻⁴
PVT Ratio	2.38	2.38	2.38	2.38	2.38

Table B31.6: Composition of treatment solution

Component	Weight %
FC4430	2.0
Propylene Glycol	78.4
IPA	19.6

Table B31.7: Results of post-treatment two-phase flow of gas condensate mixture

q_{pump}, cc/hr	64	128	256	512	896
q_{total_core}, cc/hr	205.93	411.86	823.72	1647.44	2883.03
q_{g_core}, cc/hr	201.44	402.88	805.76	1611.53	2820.18
q_{o_core}, cc/hr	4.49	8.98	17.96	35.91	62.85
ΔP, psi	0.09	0.13	0.24	0.55	1.24
k_{rg}	0.134	0.184	0.204	0.178	0.138
k_{ro}	0.056	0.077	0.086	0.075	0.058
Nc	2.10x10 ⁻⁵	3.05x10 ⁻⁵	5.51x10 ⁻⁴	1.26x10 ⁻⁴	2.84x10 ⁻⁴
Improvement Factor	2.52	2.19	1.75	1.53	1.71

Table B31.8: Result of methane flood to measure final permeability

q_{core}, (cc/hr)	ΔP (psi)	k_g (Darcy)
1863.00	0.26	16.07
1241.00	0.17	16.38
Permeability, k_g (md) (corrected for non Darcy)		28.05

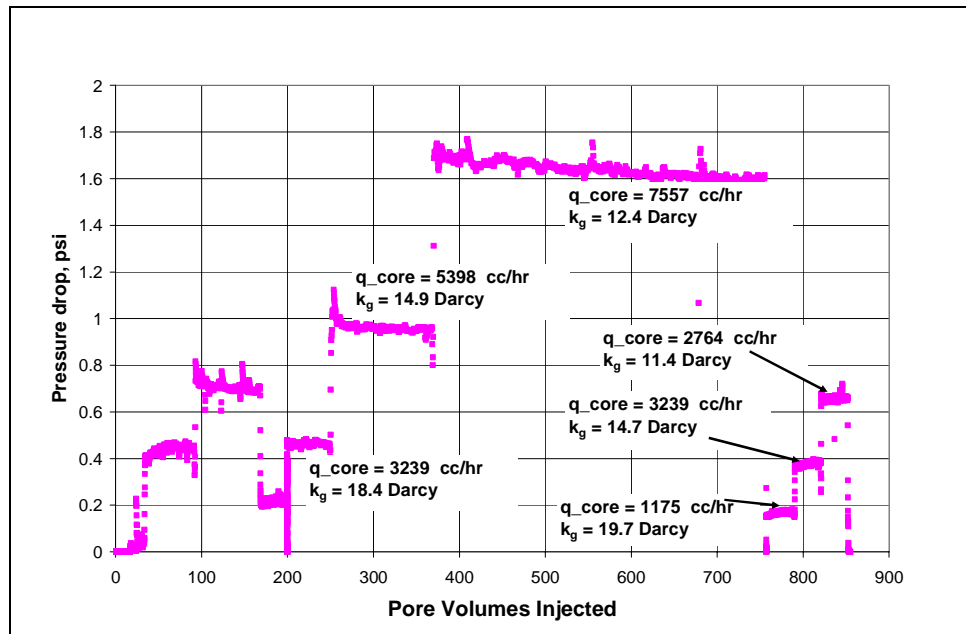


Figure B31.1: Pressure drop across the propped fracture during initial nitrogen flood

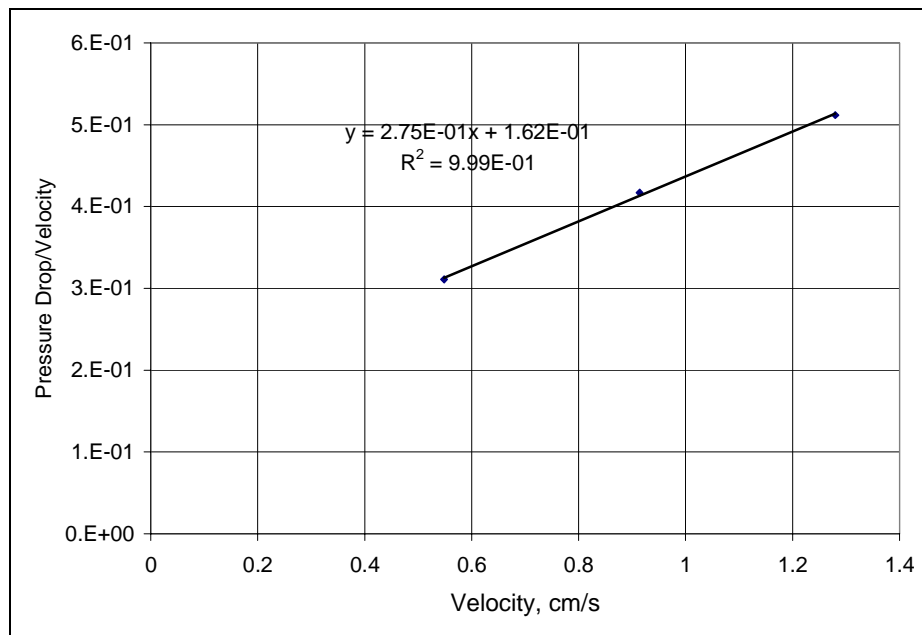


Figure B31.2: Correcting gas permeability measurement for non-Darcy flow

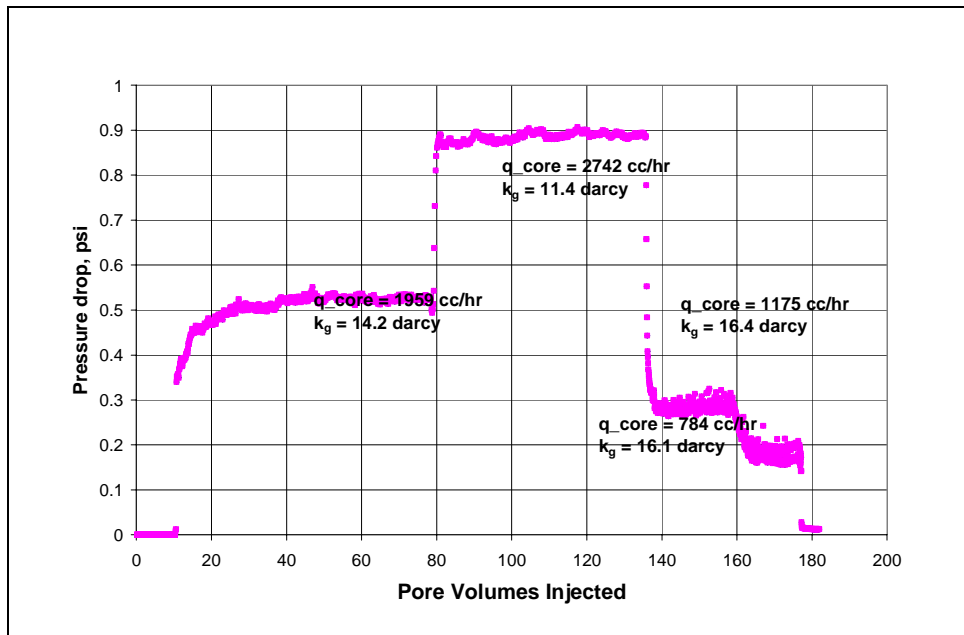


Figure B31.3: Pressure drop across the propped fracture during nitrogen flood at $Sw_i=25\%$

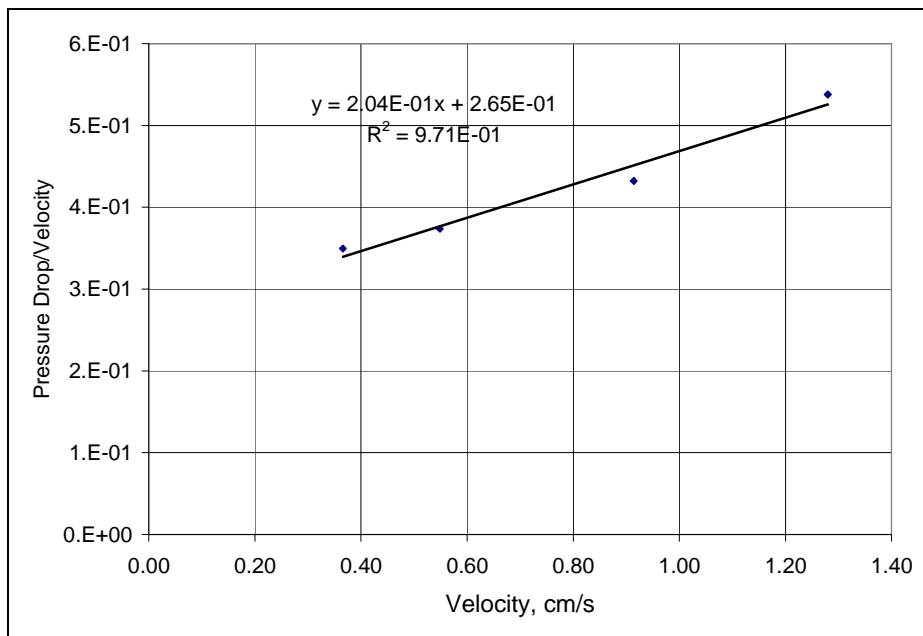


Figure B31.4: Correcting gas permeability measurement at $Sw_i=25\%$ for non-Darcy flow

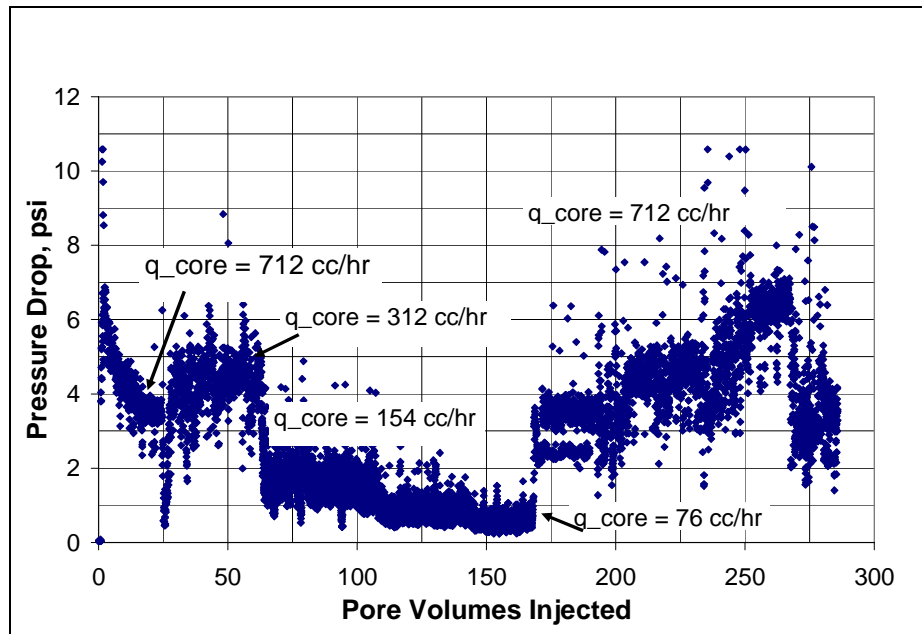


Figure B31.5: Pressure drop across the propped fracture during the initial two-phase flood at 279°F and 1450 psig

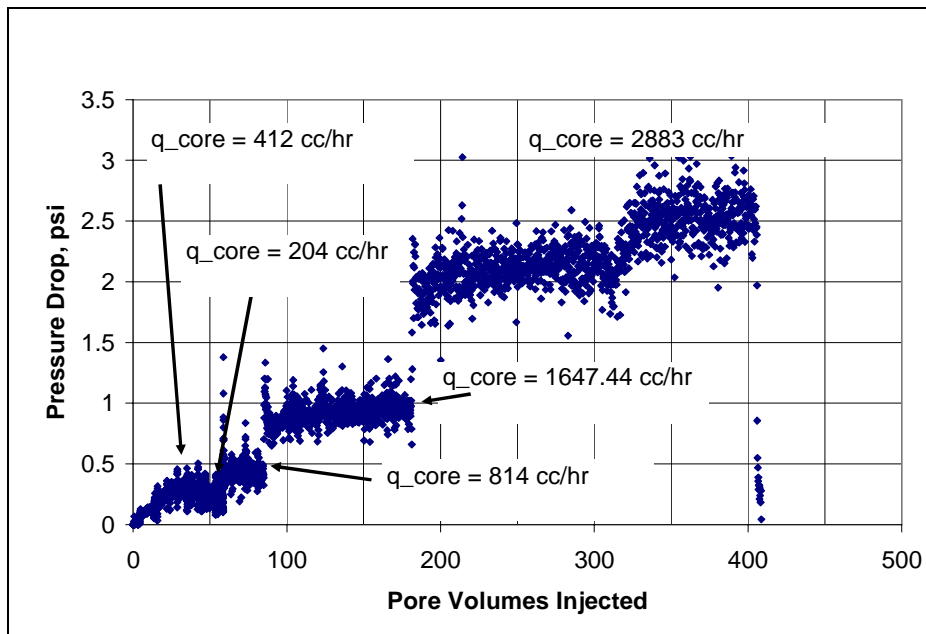


Figure B31.6: Pressure drop across the propped fracture during the initial two-phase flood in the reverse flow direction at 279°F and 1450 psig

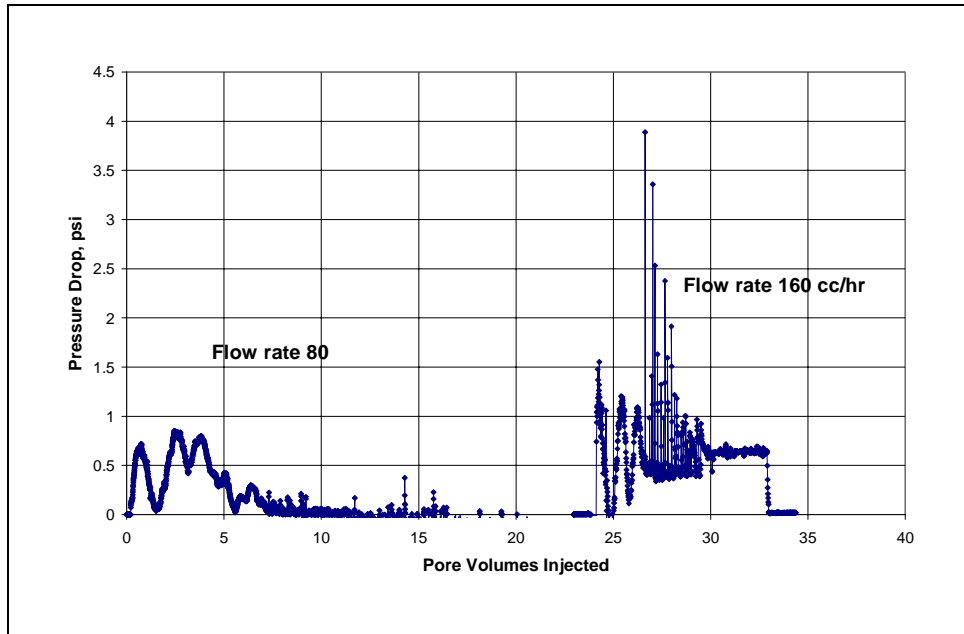


Figure B31.7: Pressure drop across the propped fracture during surfactant treatment

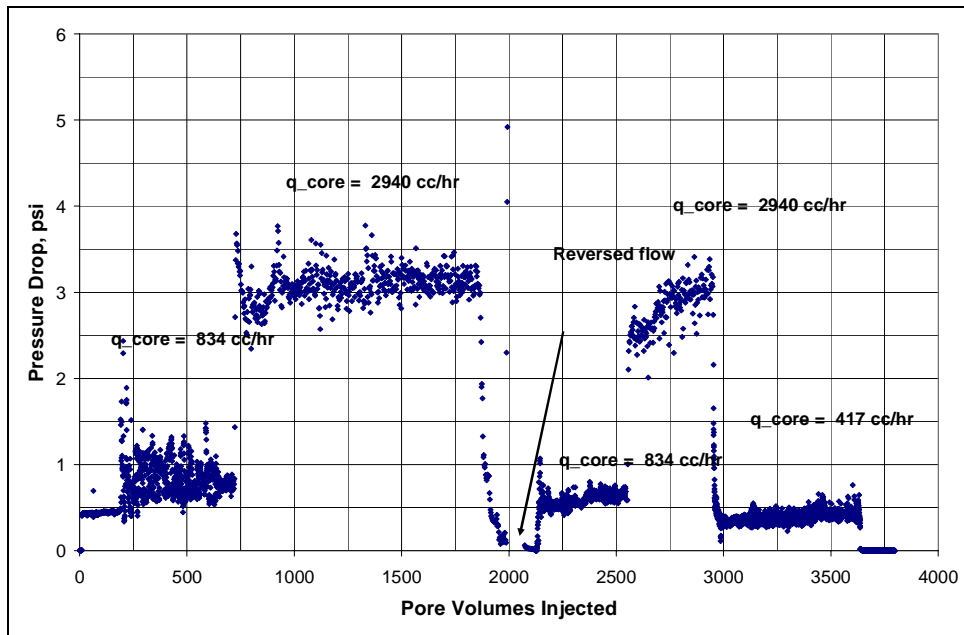


Figure B31.8: Pressure drop across the propped fracture during post-treatment two-phase flood at 279°F and 1450 psig

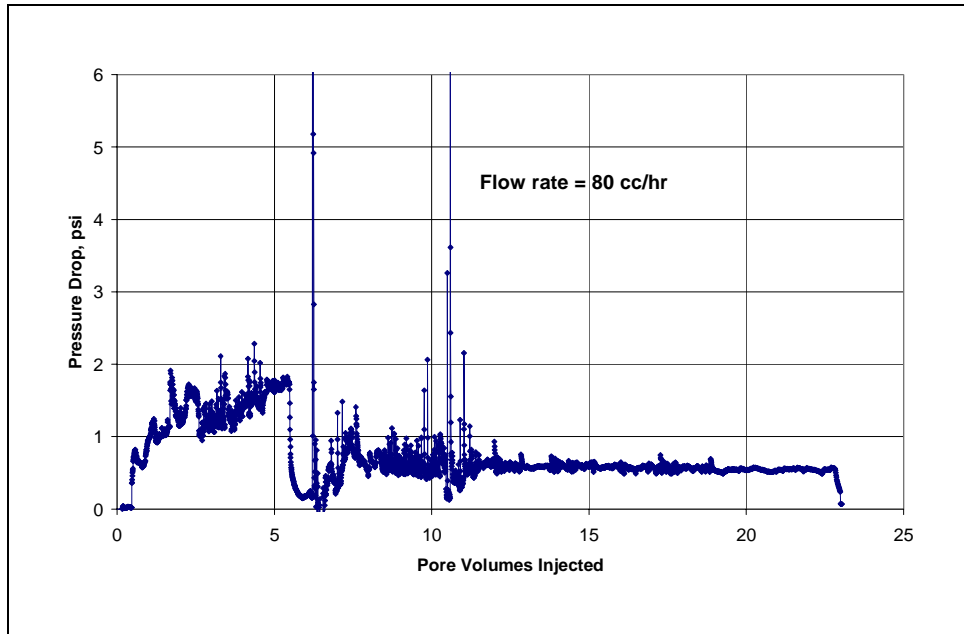


Figure B31.9: Pressure drop across the propped fracture during the second surfactant treatment

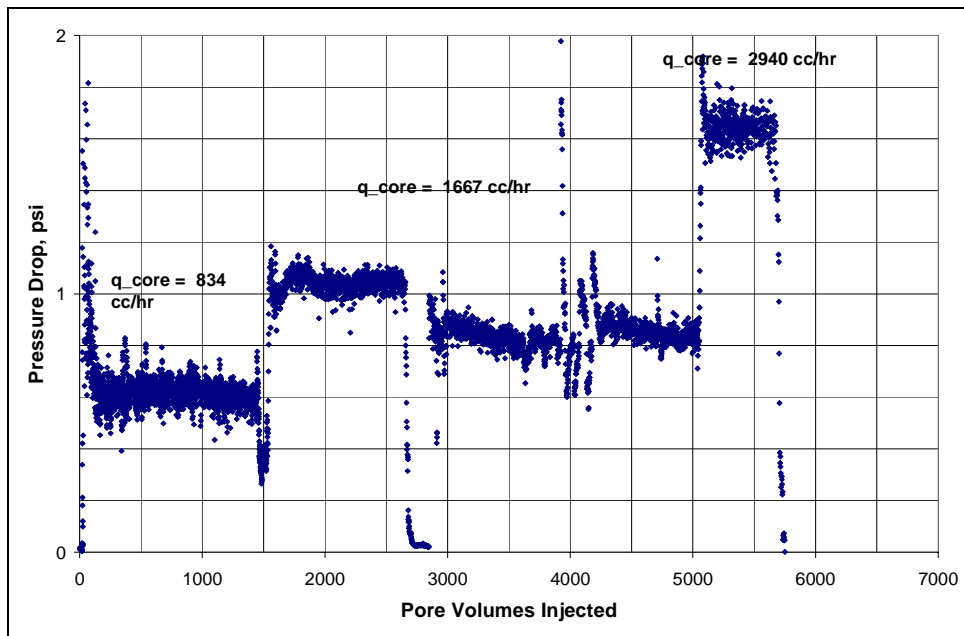


Figure B31.10: Pressure drop across the propped fracture during gas condensate flood after second treatment at 279°F and 1450 psig

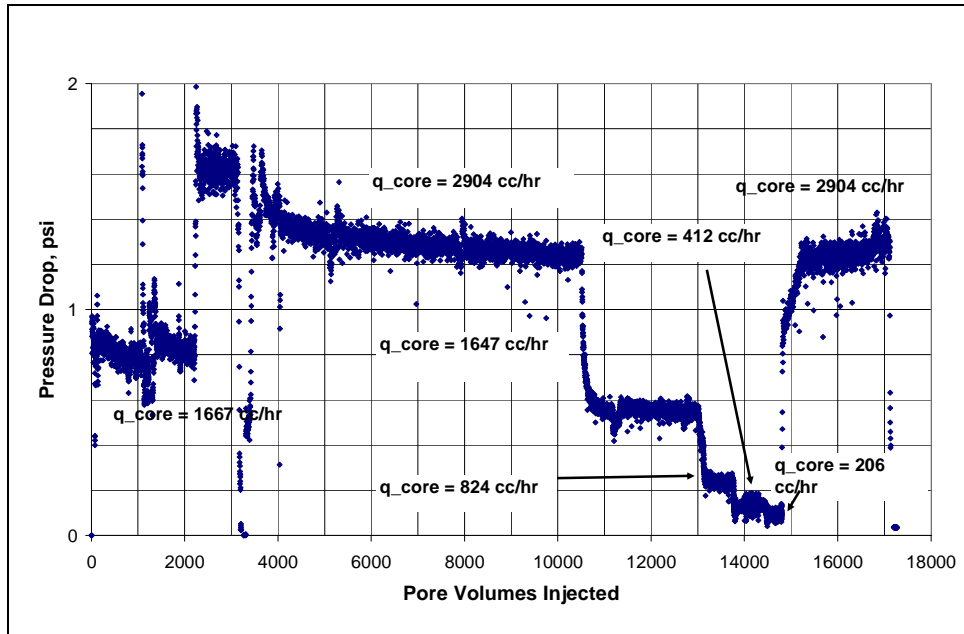


Figure B31.1: Pressure drop across the propped fracture during second gas condensate flood after second treatment at 279°F and 1450 psig

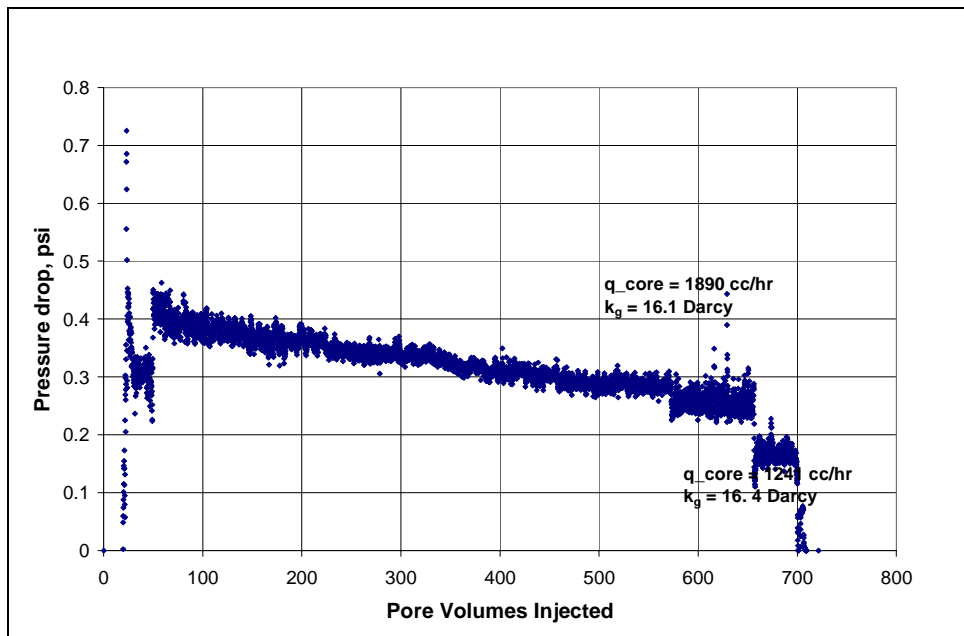


Figure B31.12: Pressure drop across the propped fracture during final methane flood

B33- Experiment No.33

Objective:

The objective of this experiment was to measure gas and condensate relative permeabilities at high velocities to capture the effect of capillary number and non-Darcy flow. The experiment was performed on a Berea sandstone core at 175°F.

Experimental Results:

Table B33.1 summarizes the properties of the core and the experimental conditions. Initial permeability of the core was measured using nitrogen at 75°F. **Figure B33.1** shows the pressure drop measured across the core during nitrogen flood. **Table B33.2** summarizes the results of the nitrogen flood.

The initial water saturation of 20% was established by injecting 1.9 cc of synthetic Bruce brine (**Table B21.3**) in the vacuumed core. Nitrogen flood was then conducted to measure the end point gas relative permeability. **Figure B33.2** shows the pressure drop measured across the core and **Table B33.3** summarizes the results of the nitrogen flood. The pressure of the core was raised to 200 psig and then the temperature of the oven was increased to 175°F.

Synthetic fluid mixture-5 (**Table 3.5**) was used for the two-phase flow measurements. The initial flood was done at a flowing core pressure of 420 psig and subsequently again at 200 psig so the measurements could be done at two different k_{rg}/k_{ro} ratios. The fluid properties were calculated at the average core pressures. **Figure B33.3** shows the pressure drop across the core during the two-phase gas-condensate flood done at multiple rates and multiple BPR-2 pressures. **Tables B33.4** and **B33.5** summarize the results of the two-phase floods done at 420 psig and 200 psig respectively.

Equilibrium gas flood was then conducted. **Table B33.6** gives the composition of the equilibrium gas mixture at 200 psig calculated using PREOS. **Figure B33.4** shows the pressure drop across the core and **Table B33.7** summarizes the results for the equilibrium gas flood.

The core was then treated with the treatment solution (**Table B33.8**). **Figure B33.5** shows the measured pressure drop across the core during the treatment flood. The treatment solution was injected at 128cc/hr. The core was then shut-in for 15 hours. Post-treatment two-phase gas-condensate flood was conducted. **Figure B33.6** shows the pressure drop across the core measured during the post-treatment two-phase floods at a flowing pressure of 420 psig. **Table B33.9** summarizes the results of the post-treatment two-phase flow.

Table B33.1: Core properties

Core	Berea Sandstone
Length, inches	4
Diameter, inches	0.98
Porosity, %	19.02
Pore volume, cc	9.50
Swi, %	20
Temperature, °F	175

Table B33.2: Result of nitrogen flood

q_{core} , (cc/hr)	ΔP (psi)	k_g (md)
2549.52	1.61	249.24
3186.90	2.03	246.19
4461.66	2.92	240.02
Permeability, k_g (md)		245.15

Table B33.3: Result of nitrogen flood at Swi = 20%

q_{core} , (cc/hr)	ΔP (psi)	k_g (md)
4461.66	4.13	169.99

Table B33.4: Results of gas condensate floods at 175°F and 420 psig

q_{pump}, cc/hr	512	896	1346	1796	2696
q_{total_core}, cc/hr	5499.43	9624.00	13477.68	17983.60	25841.43
q_{g_core}, cc/hr	5431.79	9505.63	13298.43	17744.41	25479.65
q_{o_core}, cc/hr	67.64	118.38	179.25	239.18	361.78
ΔP, psi	28.02	42.55	56.52	71.32	100.78
k_{rg} (corrected for non-Darcy)	0.102	0.127	0.145	0.168	0.203
k_{ro}	0.034	0.039	0.044	0.047	0.050
Nc	3.57x10 ⁻⁵	5.41x10 ⁻⁵	7.34x10 ⁻⁵	9.26x10 ⁻⁵	1.33x10 ⁻⁴
PVT Ratio	2.62	2.62	2.62	2.62	2.62

Table B33.5: Results of gas condensate floods at 175°F and 200 psig

q_{pump}, cc/hr	2246	2696
q_{total_core}, cc/hr	38677.88	46427.23
q_{g_core}, cc/hr	38399.40	46092.96
q_{o_core}, cc/hr	278.48	334.28
ΔP, psi	112.15	131.57
k_{rg} (corrected for non-Darcy)	0.270	0.306
k_{ro}	0.038	0.039
Nc	1.28x10 ⁻⁴	1.50x10 ⁻⁴
PVT Ratio	4.10	4.10

Table B33.6: Composition of equilibrium gas mixture at 200 psig and 175°F

Component	Mole%
Methane	93.39
n-propane	5.11
n-heptane	1.29
n-decane	0.204
n-pentadecane	0.002

Table B33.7: Results of equilibrium gas condensate floods at 175°F and 200 psig

q_{pump}, cc/hr	224	512	896	1500	2500
q_{g, core}, cc/hr	4997.28	11422.35	19989.11	33463.92	55773.20
ΔP, psi	4.90	10.00	15.50	25.50	47.00
k_{rg}^o	0.461	0.516	0.583	0.593	0.536
Nc	5.60x10 ⁻⁶	1.14x10 ⁻⁵	1.77x10 ⁻⁵	2.91x10 ⁻⁵	5.37x10 ⁻⁵

Table B33.8: Composition of treatment solution

Component	Weight %
FC4430	0.2
2-butoxyethanol	69.9
Ethanol	29.9

Table B33.9: Results of post-treatment gas condensate floods at 175°F and 420 psig

q_{pump}, cc/hr	512	1346	2696
q_{total_core}, cc/hr	5499.43	13477.68	25841.43
q_{g_core}, cc/hr	5431.79	13298.43	25479.65
q_{o_core}, cc/hr	67.64	179.25	361.78
ΔP, psi	21.21	49.90	91.50
k_{rg} (not-corrected for non-Darcy)	0.117	0.122	0.128
k_{ro}	0.045	0.051	0.056
Nc	2.70x10 ⁻⁵	6.48x10 ⁻⁵	1.19x10 ⁻⁴

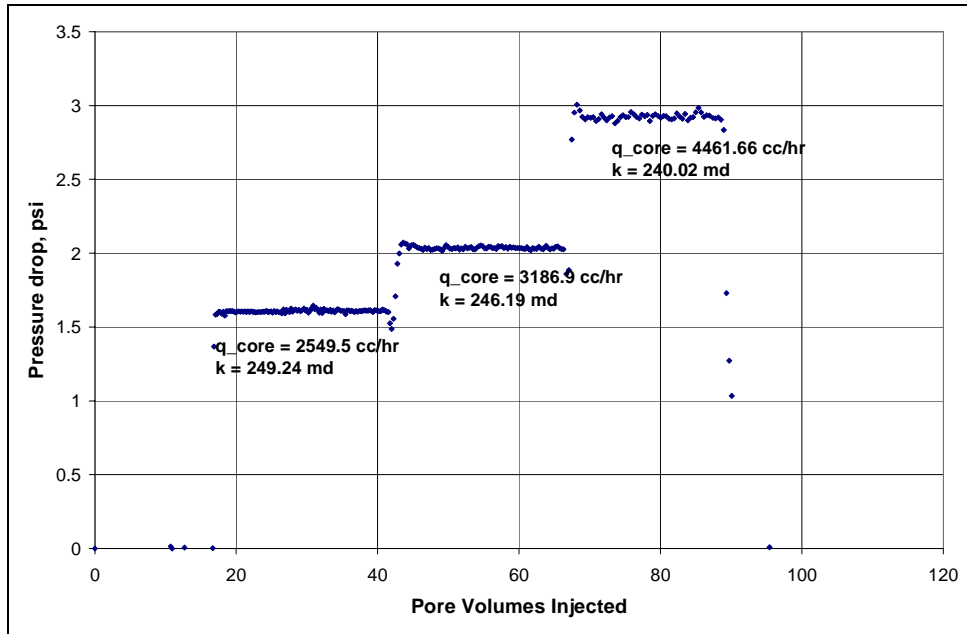


Figure B33.1: Pressure drop across the core during initial nitrogen flood

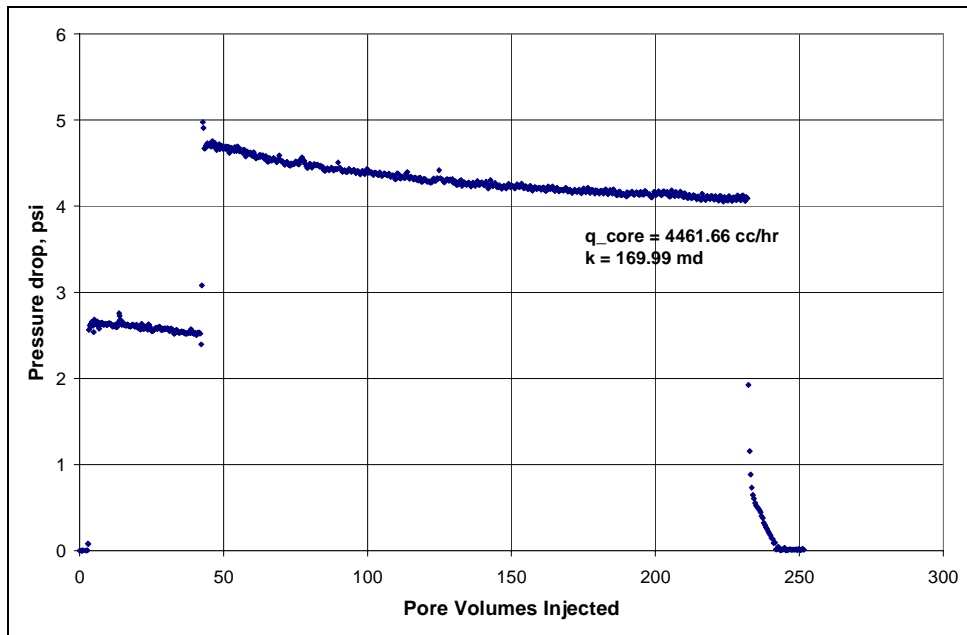


Figure B33.2: Pressure drop across the core during nitrogen flood at $S_{wi}=20\%$

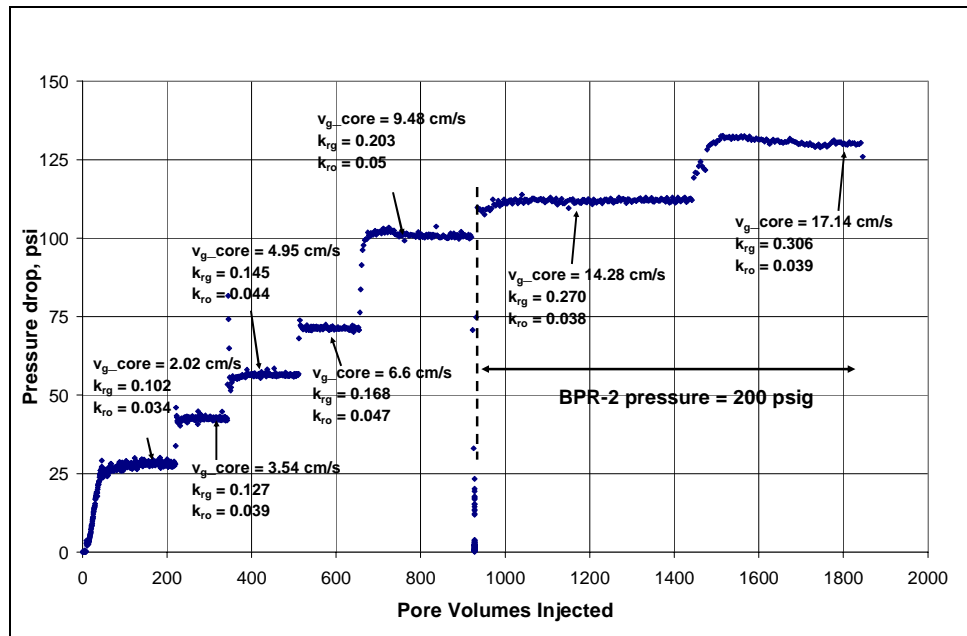


Figure B33.3: Pressure drop across the core during the gas condensate floods at 420 psig and 200 psig

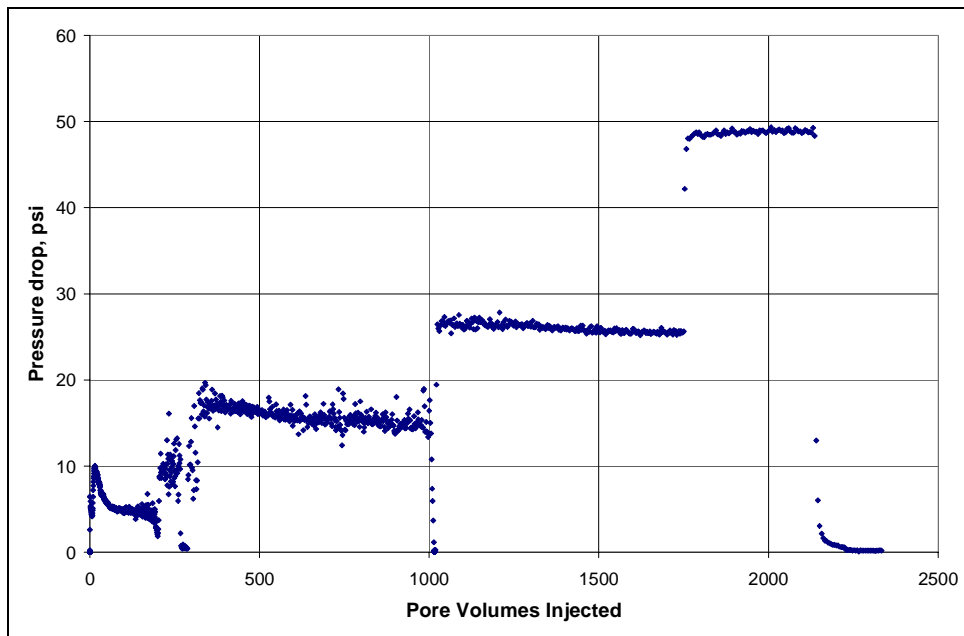


Figure B33.4: Pressure drop across the core during the equilibrium gas floods at 175°F and 200 psig

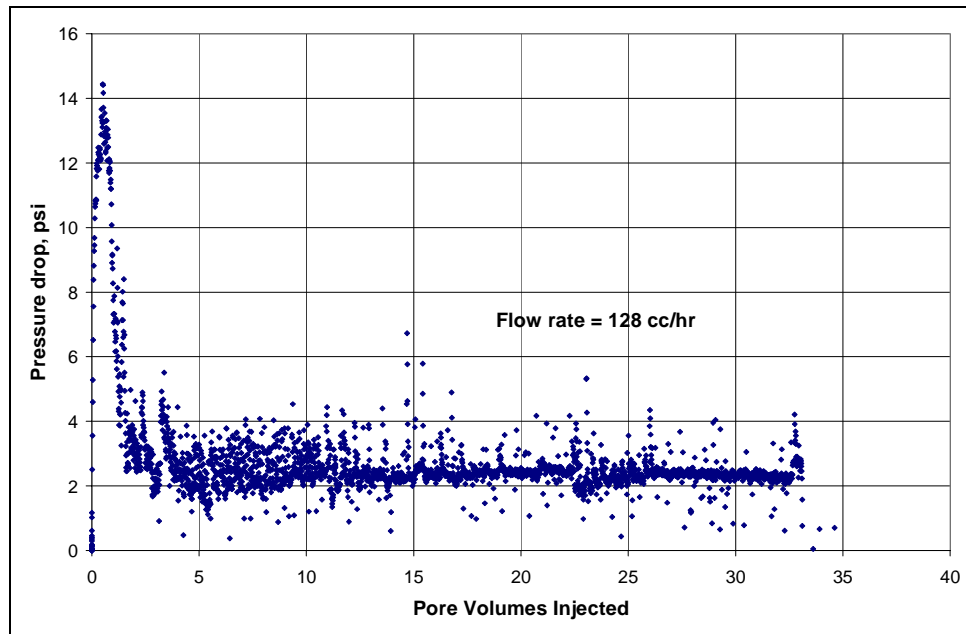


Figure B33.5: Pressure drop across the treatment flood

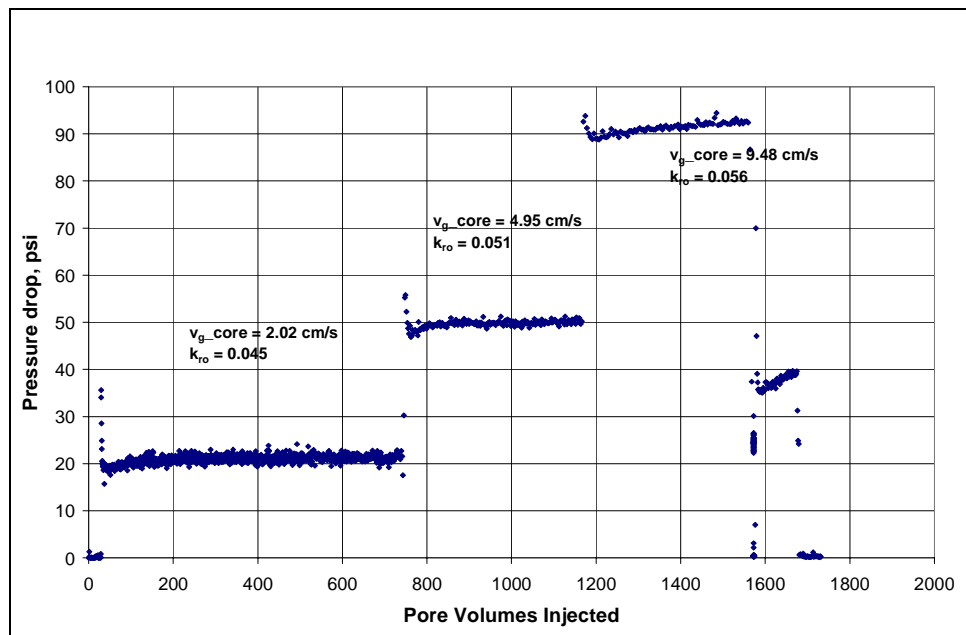


Figure B33.6: Pressure drop across the core during the post-treatment gas condensate floods at 175°F and 420 psig

B34- Experiment No.34

Objective:

The objective of this experiment was to investigate the effect of chemical treatment using the surfactant FC4430 in removing damage caused by water and condensate blocking in a reservoir core. The experiment was performed on Tunu reservoir core (plug #4) at 275°F.

Experimental Results:

First half of the experiment i.e. till the first surfactant treatment was performed by Ahmadi *et al.* (2008-09). **Table B34.1** summarizes the properties of the plugs and the experimental conditions. Initial permeability of the core (plug) was measured using methane at 275°F. **Figure B34.1** shows the pressure drop measured across the core during methane flood. **Table B34.2** summarizes the results of the methane flood.

15,000 ppm NaCl synthetic brine was used for establishing the initial water saturation. While injecting brine the whole core was saturated with the brine by mistake. Solvent flood using a 70/30 mixture of PG/IPA was done to remove the brine from the core. Figure B34.2 shows the pressure drop for the solvent flood. Methane was flowed through the core to remove the solvent. **Figure B34.3** shows the pressure drop for the methane flood done to remove solvent from the core. **Table B34.3** summarizes the results.

The initial water saturation of 30% was established by injecting 1.1 cc of 15,000 NaCl brine in the core at 1200 psig. To prevent corrosion problem 200 ppm of sodium dithionite was added to the brine in the accumulator. Nitrogen gas was bleed into the brine solution for five minutes to saturate the brine with nitrogen and remove any free oxygen before adding dithionite. Methane flood was then conducted to measure the end

point gas relative permeability. **Figure B34.4** shows the pressure drop measured across the core and **Table B34.4** summarizes the results of the methane flood.

Synthetic fluid mixture-8 (**Table 3.8**) was used for the two-phase flow measurements. The initial flood was conducted with the upstream backpressure regulator set at 4275 psig and the downstream back pressure regulator set at 1200 psig. **Table B34.5** gives the properties of the synthetic fluid calculated using the Peng-Robinson EOS at the flowing core pressure. **Figure B34.5** shows the pressure drop across the core during the two-phase gas-condensate flow. The pressure drop data was too noisy and the fluctuated by more than 60%. **Table B34.6** summarizes the results of the initial two-phase flow.

The core was then treated with the treatment solution (**Table B34.7**). **Figure B34.6** shows the measured pressure drop across the core during the treatment flood. The treatment solution was injected at 90 cc/hr. The core was then shut-in for 15 hours.

Post-treatment two-phase gas-condensate flood was conducted under the same conditions as the initial two-phase flow. The flood was done at multiple rates. **Figure B34.7** shows the pressure drop across the core measured during the post-treatment two-phase flood at a flowing pressure of 1200 psig. Treatment was still being produced in the effluent samples at the end of the gas condensate flood. A second batch of gas condensate mixture was then flowed through the core. **Figure B34.8** shows the pressure drop across the core during second gas condensate flood. **Table B34.8** summarizes the results of the second post-treatment gas condensate flood.

2 cc of brine was then injected into the core to establish a water saturation of 55% in the core. Brine injection was followed by gas condensate flood. **Figure B34.9** shows the pressure drop during the gas condensate flood. **Table B34.9** summarizes the results.

One PV of brine was then injected into the core. Brine injection was followed by gas condensate flood. **Figure B34.10** shows the pressure drop during the gas condensate flood. **Table B34.10** summarizes the results.

The core was re-treated with the treatment solution (**Table 34.7**). 20 PV of treatment solution was injected at 100 cc/hr. The core was then shut in for 15 hours. **Figure B34.11** shows the pressure drop during the second treatment flood.

Post second treatment gas-condensate flood was conducted under the same conditions as the initial two-phase flow. The flood was done at multiple rates. **Figure B34.12** shows the pressure drop across the core measured during the post-treatment two-phase flood at a flowing pressure of 1200 psig. **Table B34.11** summarizes the results of the gas condensate flood after the second treatment.

Methane flood was conducted to measure the post-treatment permeability of the core. **Table B34.12** summarizes the results and **Figure B34.13** shows the pressure drop measured across the plug during the methane flood at 275°F.

Table B34.1: Core properties

Core	Tunu Reservoir Core (plug #4)
Length, inches (plug #4)	1.95
Diameter, inches	1
Porosity, %	14.45
Pore volume, cc	3.63
Swi, %	30
Temperature, °F	275

Table B34.2: Result of methane flood

q_{core}, (cc/hr)	ΔP (psi)	k_g (md)
149.7	0.71	13.2
329.4	1.56	13.2
658.8	3.13	13.2
988.2	4.73	13.1
1197.8	5.78	13.0
1617.0	7.97	12.7
2006.3	10.13	12.4
2395.6	12.38	12.1
Permeability, k_g (md)		13.2

Table B34.3: Result of methane flood after solvent flush

q_{core}, (cc/hr)	ΔP (psi)	k_g (md)
2395.6	13.7	11.0

Table B34.4: Result of methane flood at Swi

q_{core}, (cc/hr)	ΔP (psi)	k_g (md)
658.8	3.97	10.4

Table B34.5: Synthetic fluid properties at experimental conditions

Pressure, psig	4275	1200	
Fluid Properties		Gas phase	Oil phase
ρ, g/cc	0.2008	0.0521	0.6054
μ (cp)		0.016	0.2447
Volume fraction		0.9843	0.0157
IFT (dyne/cm)		6.36	

Table B34.6: Results of the initial two-phase gas condensate flood

q_{pump}, cc/hr	180
q_{total_core}, cc/hr	594.6
q_{g_core}, cc/hr	585.27
q_{o_core}, cc/hr	9.34
ΔP, psi	28.50
k_{rg}	0.099
k_{ro}	0.024
Nc	8.13x10 ⁻⁶
PVT Ratio	4.10

Table B34.7: Composition of treatment solution

Component	Weight %
FC4430	2
Propylene Glycol	69
Isopropanol	29

Table B34.8: Results of post-treatment two-phase flow of gas condensate mixture

q_{pump}, cc/hr	180	675	900
q_{total_core}, cc/hr	594.60	2229.76	2973.01
q_{g_core}, cc/hr	585.27	2194.75	2926.34
q_{o_core}, cc/hr	9.34	35.01	46.68
ΔP, psi	25.00	65.00	74.50
k_{rg}	0.113	0.163	0.189
k_{ro}	0.028	0.040	0.046
Nc	7.13x10 ⁻⁶	1.85x10 ⁻⁵	2.13x10 ⁻⁵

Table B34.9: Results of post-treatment gas condensate flood after injecting 2 cc of brine

q_{pump}, cc/hr	180	675	1550
q_{total_core}, cc/hr	594.60	2229.76	5120.19
q_{g_core}, cc/hr	585.27	2194.75	5039.80
q_{o_core}, cc/hr	9.34	35.01	80.39
ΔP, psi	35.0	72.0	130.0
k_{rg}	0.081	0.147	0.187
k_{ro}	0.020	0.036	0.083
Nc	9.99x10 ⁻⁶	2.05x10 ⁻⁵	3.71x10 ⁻⁵

Table B34.10: Results of post-treatment gas condensate flood after injecting 1PV of brine

q_{pump}, cc/hr	180	675
q_{total_core}, cc/hr	594.60	2229.76
q_{g_core}, cc/hr	585.27	2194.75
q_{o_core}, cc/hr	9.34	35.01
ΔP, psi	28.0	68.0
k_{rg}	0.101	0.156
k_{ro}	0.025	0.038
Nc	7.99x10 ⁻⁶	1.94x10 ⁻⁵

Table B34.11: Results of gas condensate flood after second treatment

q_{pump}, cc/hr	180	675
q_{total_core}, cc/hr	594.60	2229.76
q_{g_core}, cc/hr	585.27	2194.75
q_{o_core}, cc/hr	9.34	35.01
ΔP, psi	45.0	81.0
k_{rg}	0.063	0.131
k_{ro}	0.024	0.091
Nc	1.28x10 ⁻⁵	2.31x10 ⁻⁵

Table B34.12: Result of methane flood to measure final permeability

q_{core}, (cc/hr)	ΔP (psi)	k_g (md)
2171.3	13.5	10.14
2573.39	16.2	10.02
643.35	3.7	10.96
Permeability, k_g (md)		10.37

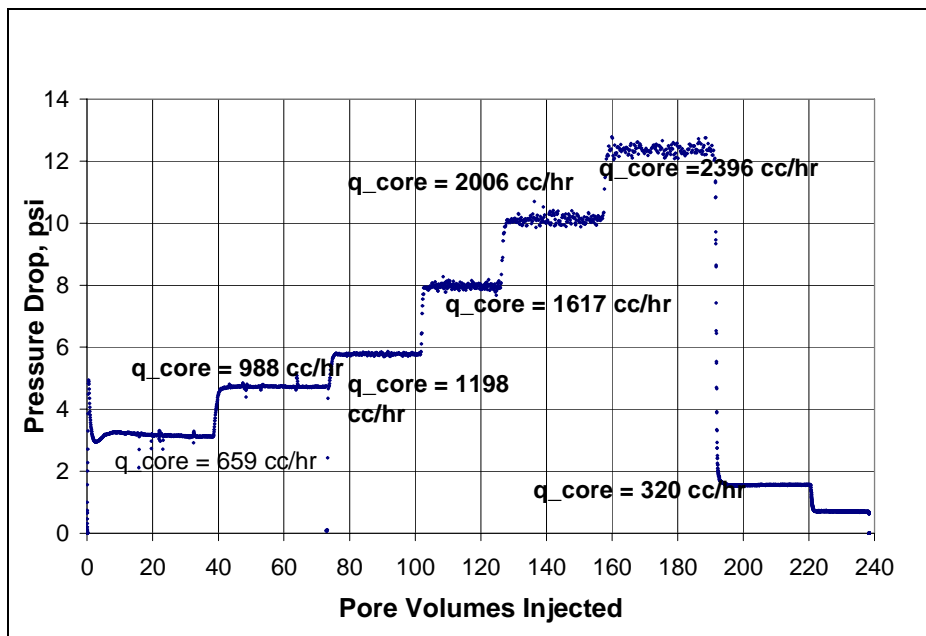


Figure B34.1: Pressure drop across the core during initial methane flood

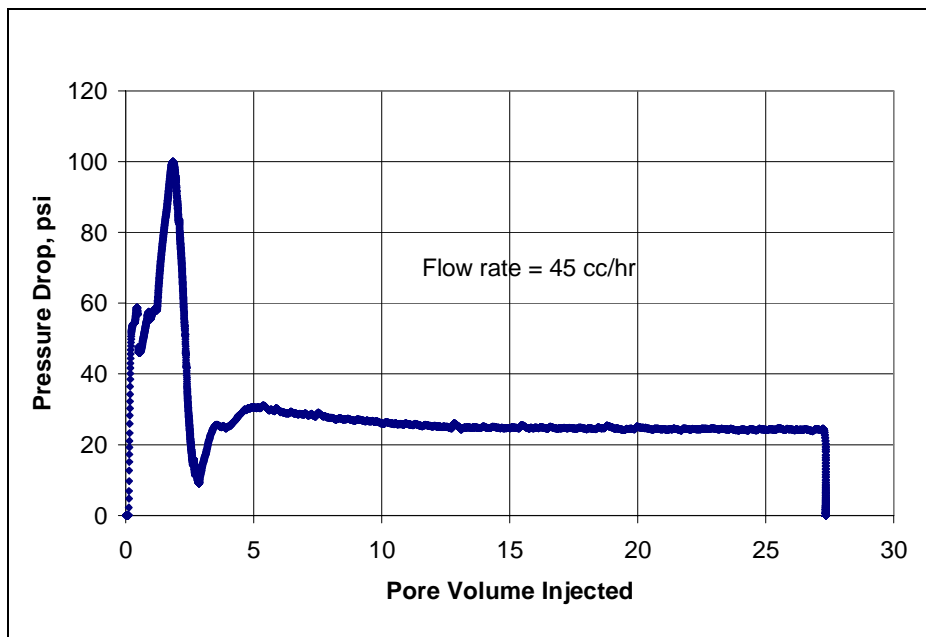


Figure B34.2: Pressure drop across the core during solvent flood

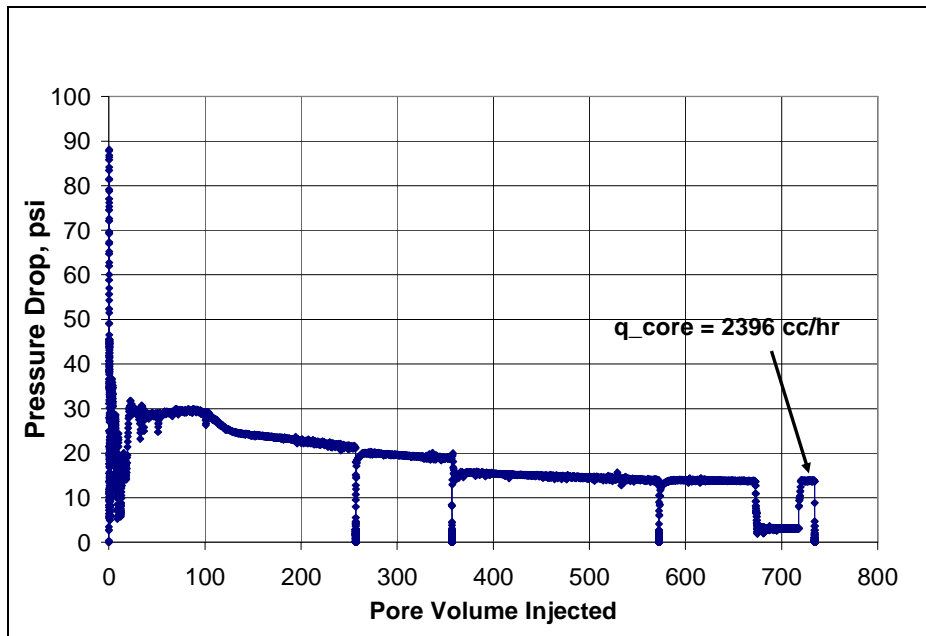


Figure B34.3: Pressure drop across the core during methane flood after the solvent flush

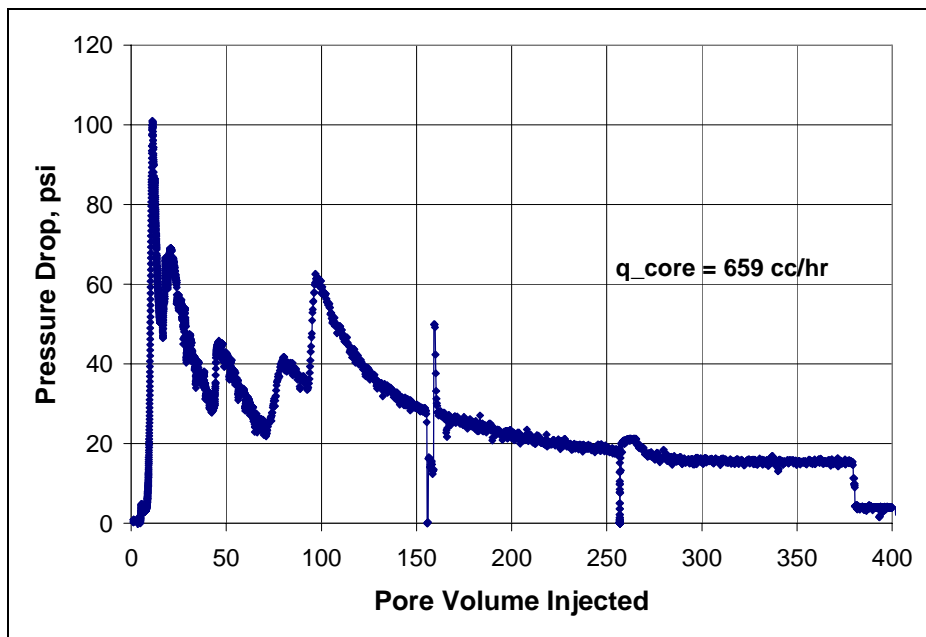


Figure B34.4: Pressure drop across the core during methane flood at $S_{wi}=30\%$

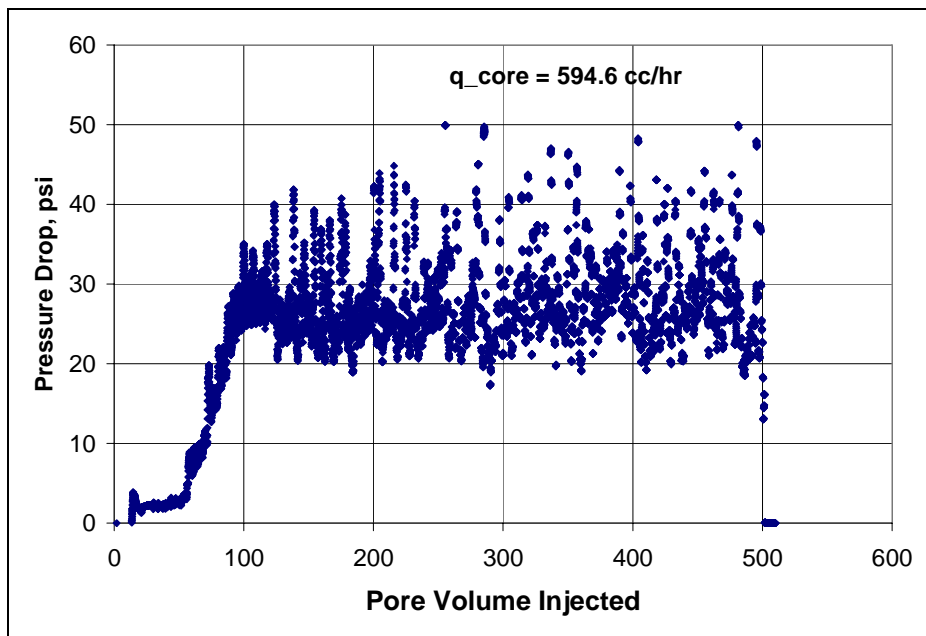


Figure B34.5: Pressure drop across the core during the initial gas condensate flood at 275°F and 1200 psig

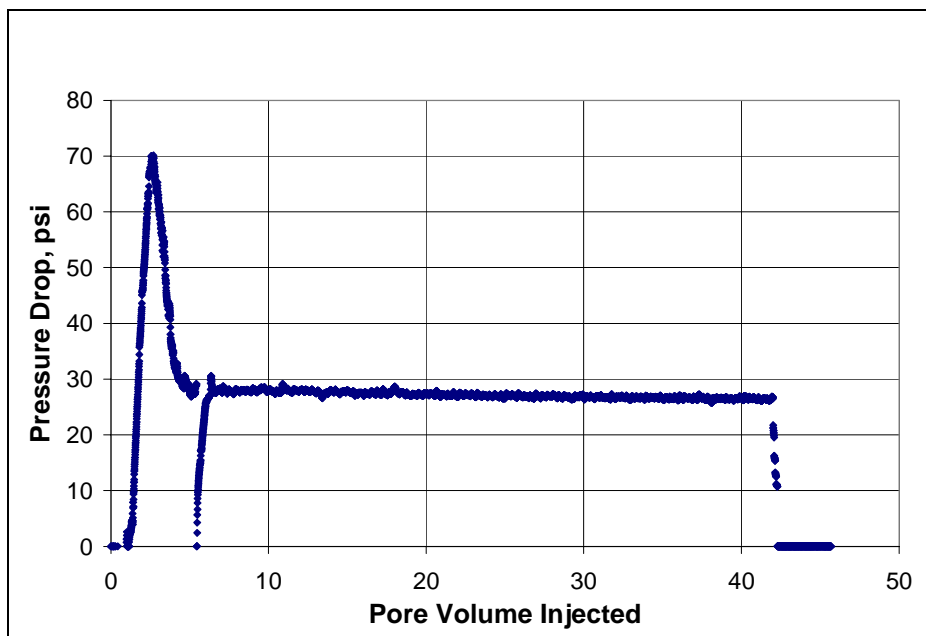


Figure B34.6: Pressure drop across the core during surfactant treatment

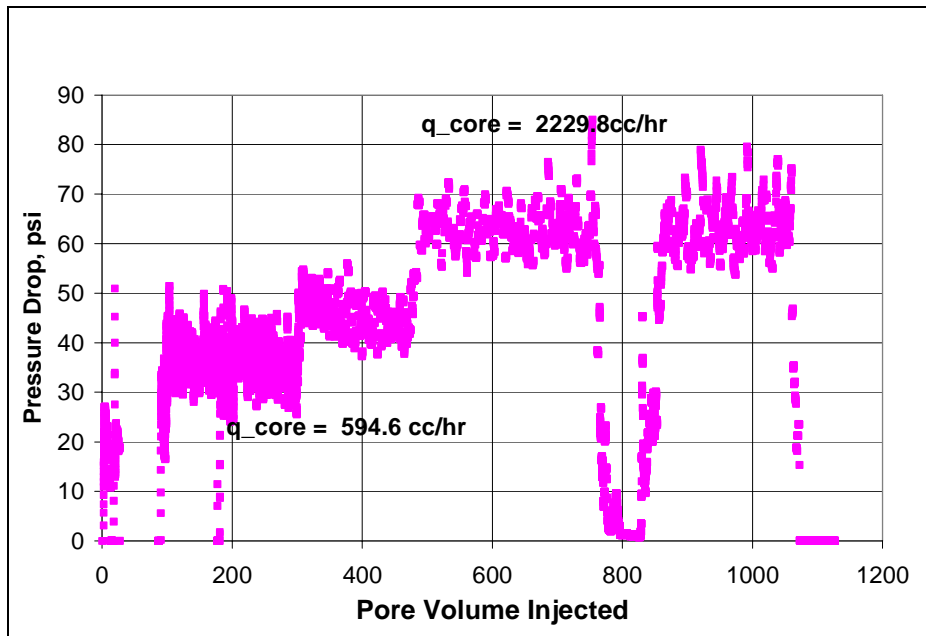


Figure B34.7: Pressure drop across the core during the first post-treatment gas condensate flood at 275°F and 1200 psig

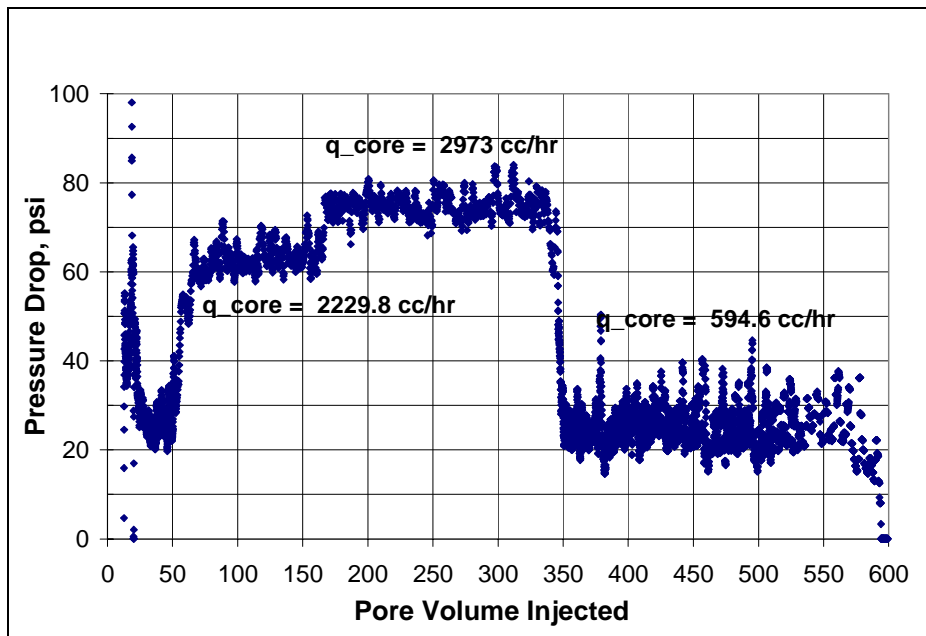


Figure B34.8: Pressure drop across the core during the second post-treatment gas condensate flood at 275°F and 1200 psig

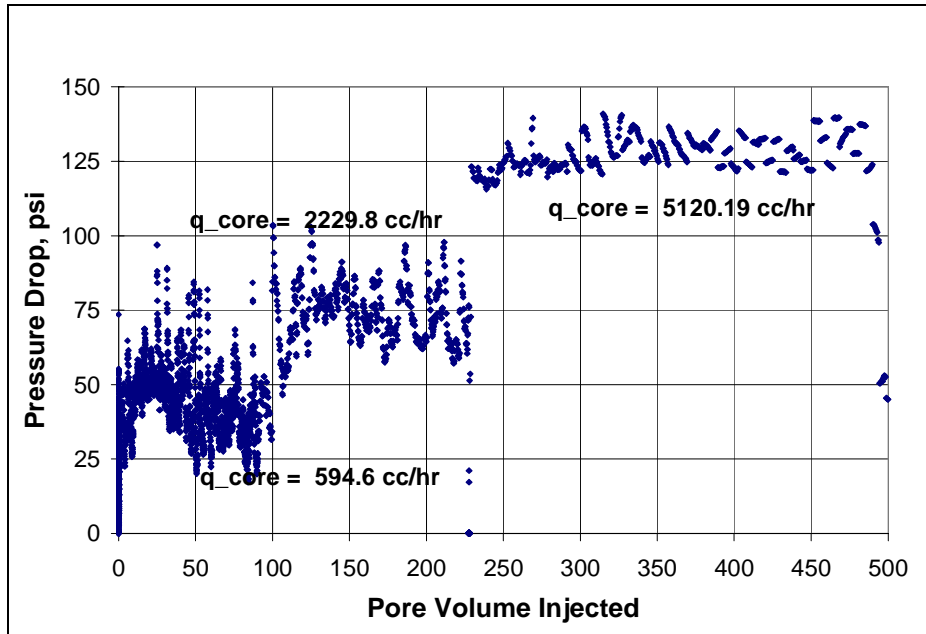


Figure B34.9: Pressure drop across the core during the post-treatment gas condensate flood after injecting 2 cc of brine at 275°F and 1200 psig

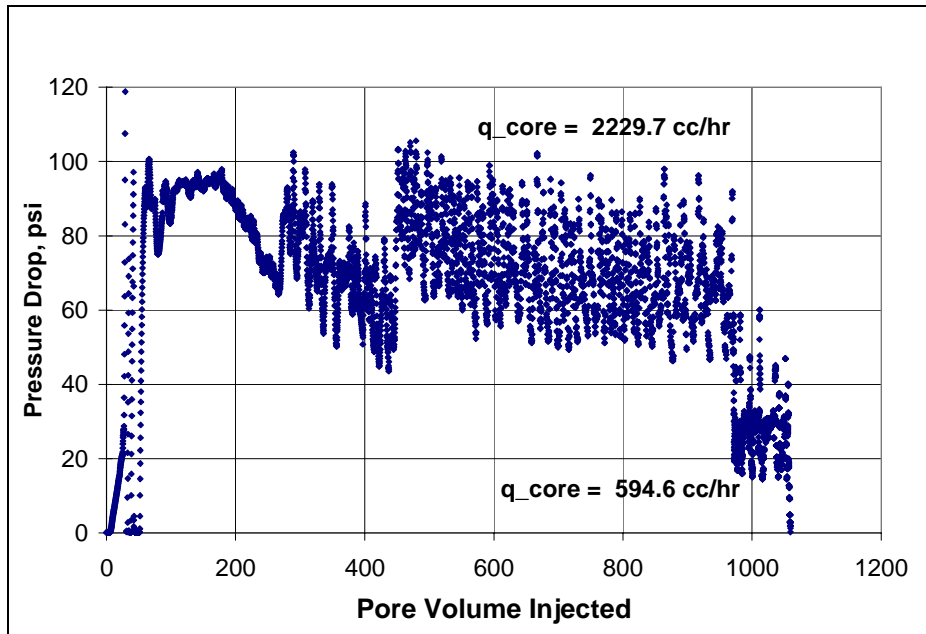


Figure B34.10: Pressure drop across the core during the post-treatment gas condensate flood after injecting 1PV of brine at 275°F and 1200 psig

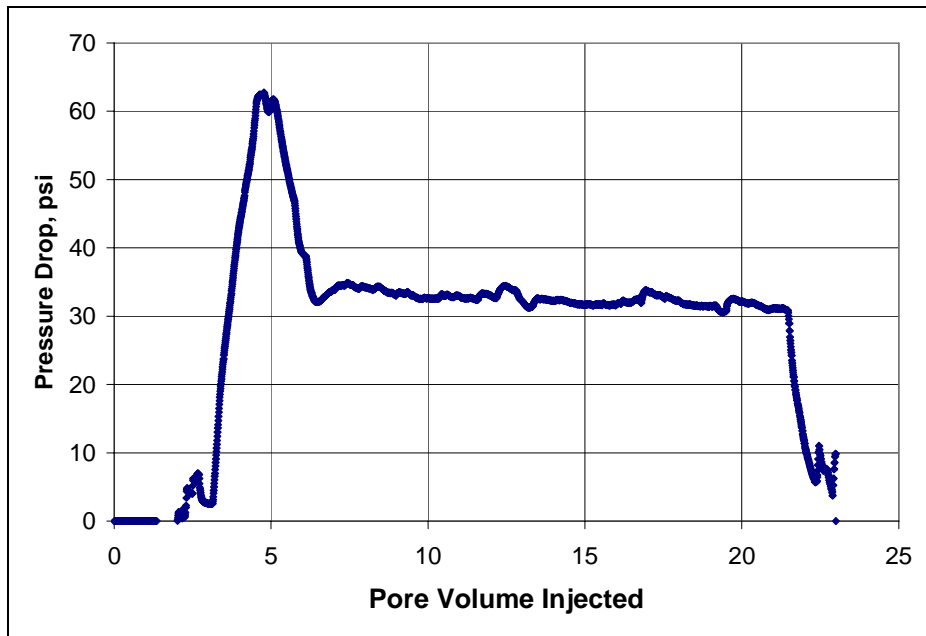


Figure B34.11: Pressure drop across the core during the second surfactant treatment

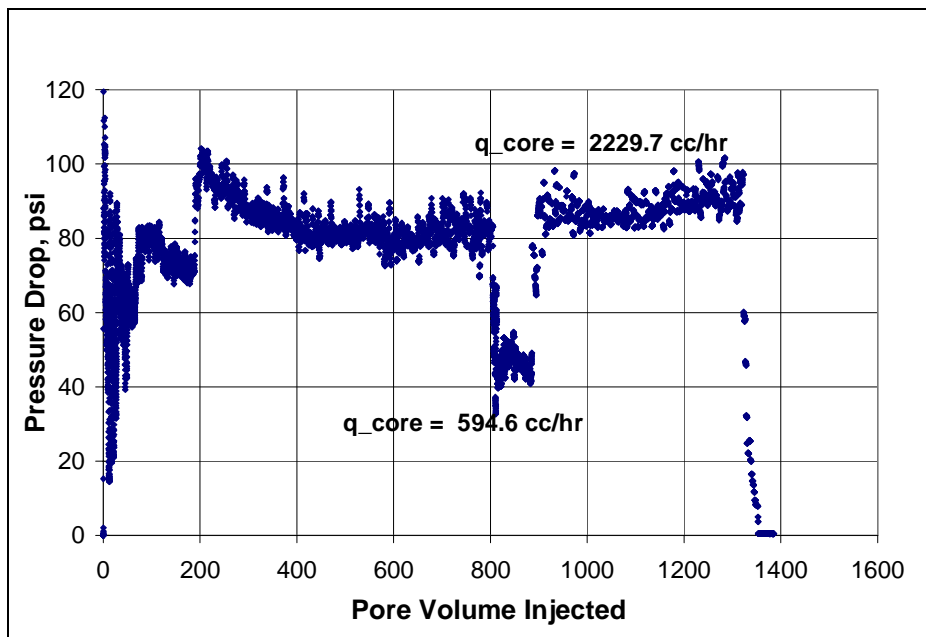


Figure B34.12: Pressure drop across the core during the gas condensate flood after the second treatment at 275°F and 1200 psig

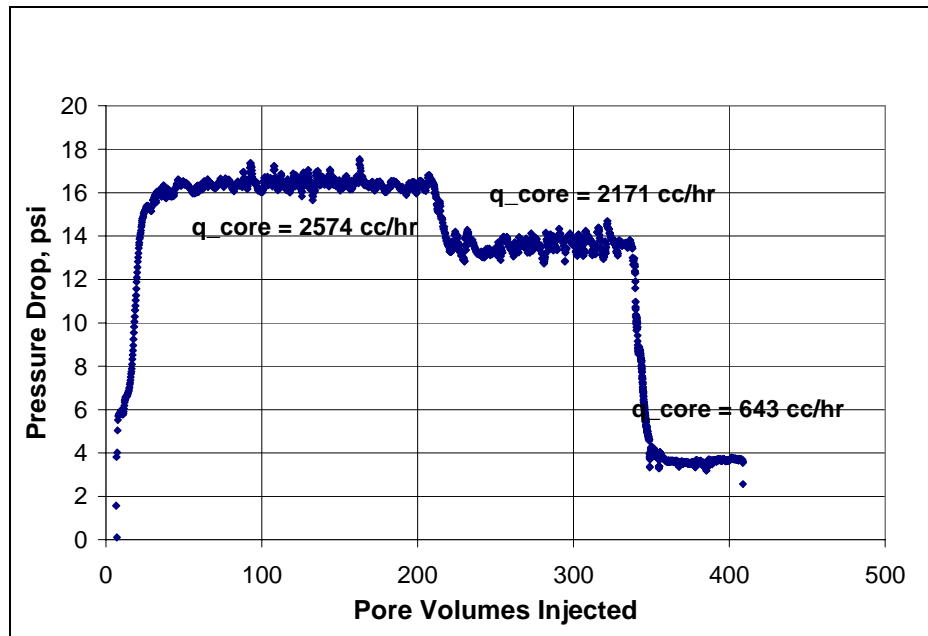


Figure B34.13: Pressure drop across the core during final methane flood

B35- Experiment No.35

Objective:

The objective of this experiment was to investigate the effect water blocking on an untreated reservoir core. The experiment was performed on a Tunu reservoir core (plug #7) at 275°F.

Experimental Results:

Table B35.1 summarizes the properties of the plug and the experimental conditions. Initial permeability of the core (plug) was measured using nitrogen at 75°F. **Figure B35.1** shows the pressure drop measured across the core during nitrogen flood. **Table B35.2** summarizes the results of the nitrogen flood. Temperature of the oven was then raised to 275°F. 2 cc of 1.5% KCl brine was then injected into the core at 225 cc/hr.

Synthetic fluid mixture-7 (**Table 3.7**) was used for the two-phase flow measurements. The gas condensate flood was conducted with the upstream backpressure regulator set at 4200 psig and the downstream back pressure regulator set at 1200 psig. **Table B35.3** gives the properties of the synthetic fluid calculated using the Peng-Robinson EOS at the flowing core pressure. **Figure B35.2** shows the pressure drop across the core during the two-phase gas-condensate flow. **Table B35.4** summarizes the results of the two-phase flow.

Table B35.1: Core properties

Core	Tunu Reservoir Core (plug #7)
Length, inches (plug #1)	2.05
Diameter, inches	1
Porosity, %	14.00
Pore volume, cc	3.69
Swi, %	55
Temperature, °F	275

Table B35.2: Result of nitrogen flood

q_{core}, (cc/hr)	ΔP (psi)	k_g (md)
2011.36	15.74	9.90
1206.82	8.92	10.49
4022.73	33.68	9.26
Permeability, k_g (md)		9.45

Table B35.3: Synthetic fluid properties at experimental conditions

Pressure, psig	4200	1200	
Fluid Properties		Gas phase	Oil phase
ρ, g/cc	0.1984	0.0522	0.6026
μ (cp)		0.0161	0.2378
Volume fraction		0.984	0.016
IFT (dyne/cm)		6.234	

Table B35.4: Results of the initial two-phase gas condensate flood

q_{pump}, cc/hr	45	90	180
$q_{\text{total_core}}$, cc/hr	146.35	292.69	585.38
$q_{\text{g_core}}$, cc/hr	144.00	288.01	576.02
$q_{\text{o_core}}$, cc/hr	2.34	4.68	9.37
ΔP, psi	46.94	64.13	86.61
k_{rg}	0.021	0.031	0.045
k_{ro}	0.005	0.007	0.011
Nc	9.73×10^{-6}	1.33×10^{-5}	1.80×10^{-4}
PVT Ratio	4.16	4.16	4.16

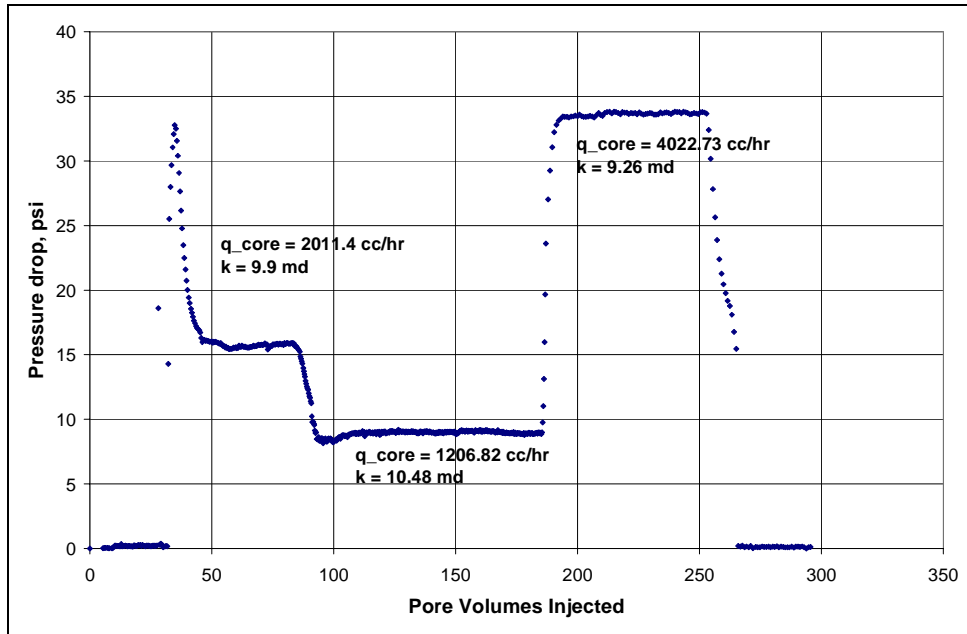


Figure B35.1: Pressure drop across the core during initial nitrogen flood

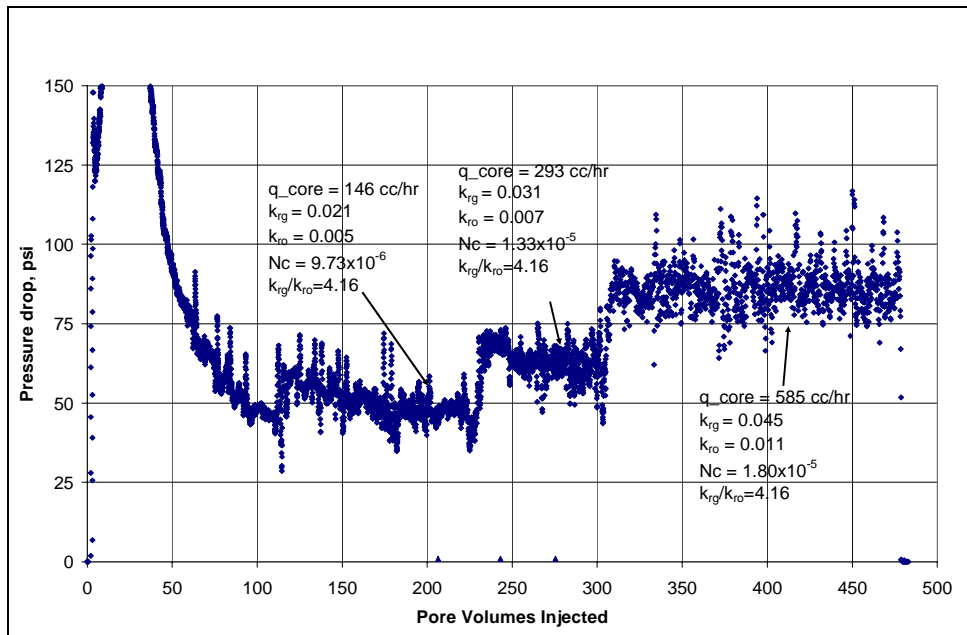


Figure B35.2: Pressure drop across the core during the gas condensate flow at 275°F and 1200 psig

B36- Experiment No.36

Objective:

The objective of this experiment was to investigate the effect of chemical treatment using a non-fluorinated surfactant #144927-75 on gas, condensate and water relative permeabilities. The experiment was performed on a Berea core at 175°F.

Experimental Results:

Table B36.1 summarizes the properties of the core and the experimental conditions. Initial permeability of the core was measured using nitrogen at 75°F. **Figure B36.1** shows the pressure drop measured across the core during nitrogen flood. **Table B36.2** summarizes the results of the nitrogen flood. Temperature of the oven was then raised to 175°F.

Two-phase gas-water flood ($f_w=0.037$) was conducted at 410 psig. Synthetic Bruce brine (**Table B21.3**) was used as the aqueous phase and methane as the gas phase. Brine was injected directly into the core whereas methane was flowed through the BPR-1 maintained at 1100 psig. An accumulator filled with methane at 400 psig was placed at the outlet of the core to collect all the liquid effluent from the core. This was done to prevent multi-phase flow through BPR-2, which can result in noisy data. **Table B36.3** gives the properties of methane and brine calculated using the Peng-Robinson EOS at the flowing core pressure. **Figure B36.2** shows the pressure drop across the core and **Table B36.4** summarizes the results of the initial two-phase gas-water flow. Methane flood was then conducted to reduce the water saturation in the core to residual and measure gas end point relative permeability at residual water saturation. **Figure B36.3** shows the pressure drop across the core and **Table B36.5** summarizes the results of the methane flood.

Synthetic fluid mixture-5 (**Table 3.5**) was used for the two-phase gas condensate flow measurements. The initial flood was conducted with the upstream backpressure regulator set at 5100 psig and the downstream back pressure regulator set at 410 psig. **Table B36.6** gives the properties of the synthetic fluid calculated using the Peng-Robinson EOS at the flowing core pressure. For higher pressure drops, the fluid properties were calculated at the average core pressures. **Figure B36.4** shows the pressure drop across the core during the two-phase gas-condensate flow. **Table B36.7** summarizes the results of the initial two-phase gas condensate flood.

The core was then treated with the treatment solution (**Table B36.8**). **Figure B36.5** shows the measured pressure drop across the core during the treatment flood. The treatment solution was injected at 120cc/hr for the first 10PV and then at 150 cc/hr. The core was then shut-in for 16 hours.

Post-treatment two-phase gas-condensate flood was conducted under the same conditions as the initial two-phase flow. **Figure B36.6** shows the pressure drop across the core measured during the post-treatment two-phase gas condensate floods at a flowing pressure of 410 psig. **Table B36.9** summarizes the results of the post-treatment gas condensate flow.

Methane flood was conducted to measure the post-treatment permeability of the core and remove condensate from the core. **Table B36.10** summarizes the results and **Figure B36.7** shows the pressure drop measured across the core during the methane flood at 175°F.

Post-treatment two-phase gas-water flood was conducted under the same conditions as the initial two-phase flow. **Figure B36.8** shows the pressure drop across the core measured during the post-treatment two-phase gas-water flood and **Table B36.11** summarizes the results.

Table B36.1: Core properties

Core	Berea Sandstone
Length, inches	7.94
Diameter, inches	0.99
Porosity, %	19.16
Pore volume, cc	19.27
Temperature, °F	175

Table B36.2: Result of nitrogen flood

q_{core}, (cc/hr)	ΔP (psi)	k_g (md)
3682.19	5.66	199.71
4602.73	7.17	197.14
5523.28	8.66	195.87
7364.37	11.72	192.93
Permeability, k_g (md)		196.41

Table B36.3: Synthetic fluid properties at experimental conditions

Pressure, psig	1100	410	
Fluid Properties		Gas phase	water phase
ρ, g/cc	0.0477	0.0165	0.9728
μ (cp)		0.0133	0.3596

Table B36.4: Results of the initial two-phase gas-water flood

q_{gas_pump}, cc/hr	225
q_{total_core}, cc/hr	633.55
q_{g_core}, cc/hr	609.55
q_{w_core}, cc/hr	24
fw	0.038
ΔP, psi	33.36
k_{rg}	0.02
k_{rw}	0.022

Table B36.5: Result of methane flood

q_{core}, (cc/hr)	ΔP (psi)	k_{rg}^o
2438.18	5.00	0.55
4876.36	10.00	0.55

Table B36.6: Synthetic fluid properties at experimental conditions

Pressure, psig	5100	410	
Fluid Properties		Gas phase	Oil phase
ρ, g/cc	0.2925	0.0192	0.6702
μ (cp)		0.0133	0.4098
Volume fraction		0.988	0.012
IFT (dyne/cm)		12.976	

Table B36.7: Results of the initial two-phase gas condensate flood

q_{pump}, cc/hr	250	500	1000
q_{total_core}, cc/hr	2707.13	4956.99	9639.67
q_{g_core}, cc/hr	2674.64	4891.07	9507.61
q_{o_core}, cc/hr	32.49	65.93	132.06
ΔP, psi	44.00	75.87	109.42
k_{rg}	0.068	0.073	0.097
k_{ro}	0.025	0.029	0.041
Nc	2.19x10 ⁻⁵	3.88x10 ⁻⁵	5.65x10 ⁻⁵
PVT Ratio	2.67	2.45	2.39

Table B36.8: Composition of treatment solution

Component	Weight %
Chemical #144927-75	2
2-Butoxyethanol	49
Ethanol	49

Table B36.9: Results of post-treatment gas condensate flood

q_{pump}, cc/hr	500	1000
q_{total_core}, cc/hr	4956.99	9639.67
q_{g_core}, cc/hr	4891.07	9507.61
q_{o_core}, cc/hr	65.93	132.06
ΔP, psi	64.00	113.00
k_{rg}	0.085	0.094
k_{ro}	0.035	0.040
Nc	3.28x10 ⁻⁵	5.83x10 ⁻⁵
Improvement Factor	1.19	0.97

Table B36.10: Result of methane flood to measure final permeability

q_{core}, (cc/hr)	ΔP (psi)	k_g (md)	k_{rg}^o
5490.91	7.00	172.16	0.88

Table B36.11: Results of the post-treatment two-phase gas-water flood

q_{gas_pump}, cc/hr	225
q_{total_core}, cc/hr	633.55
q_{g_core}, cc/hr	609.55
q_{w_core}, cc/hr	24
fw	0.038
ΔP, psi	35.16
k_{rg}	0.019
k_{rw}	0.021
Improvement factor	0.95

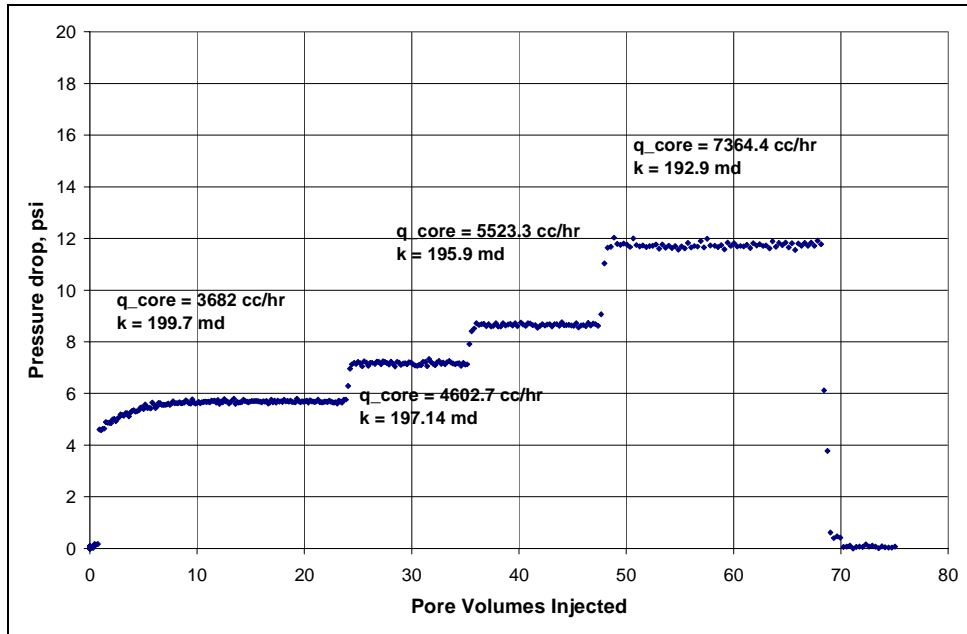


Figure B36.1: Pressure drop across the core during initial nitrogen flood

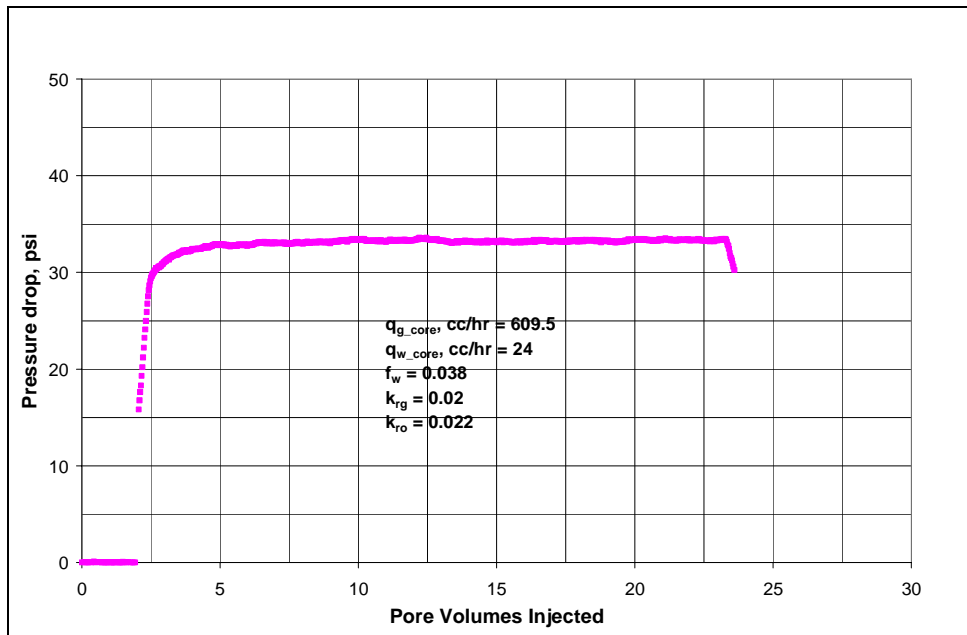


Figure B36.2: Pressure drop across the core during the initial two-phase gas-water flood ($f_w=0.038$) at 175°F and 410 psig

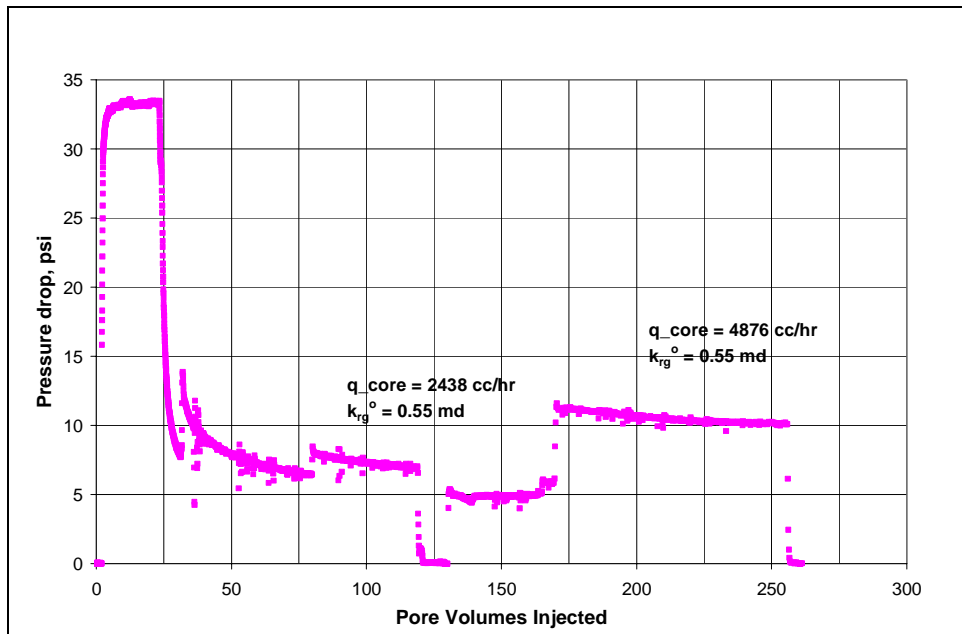


Figure B36.3: Pressure drop across the core during methane flood

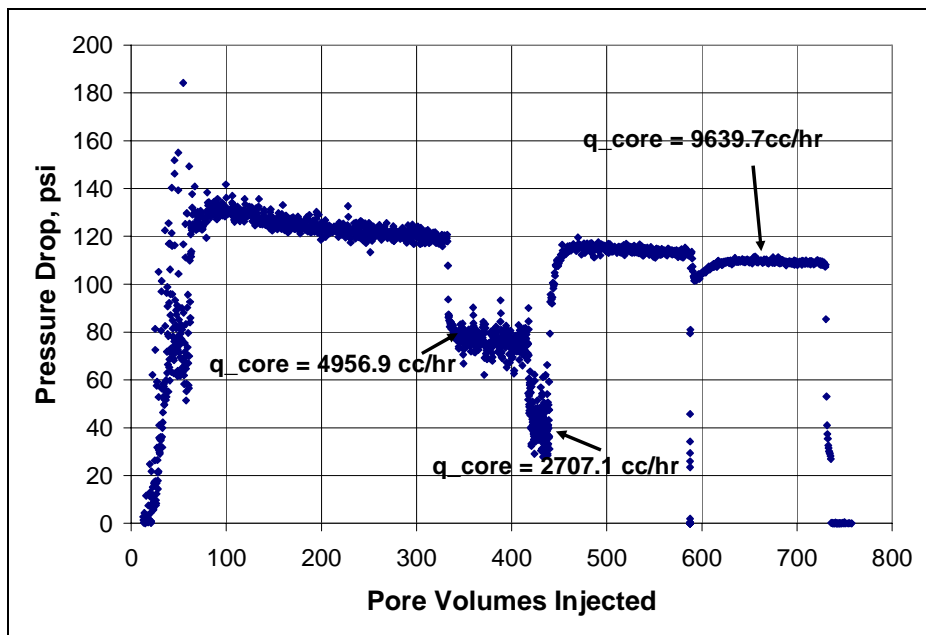


Figure B36.4: Pressure drop across the core during the initial gas condensate flood at 175°F and 410 psig

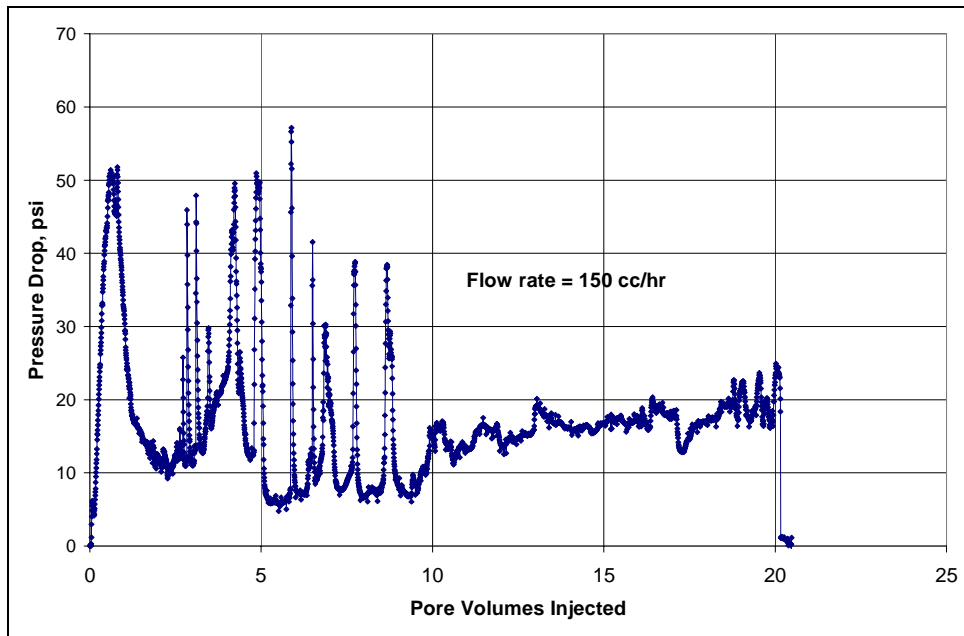


Figure B36.5: Pressure drop across the core during surfactant treatment

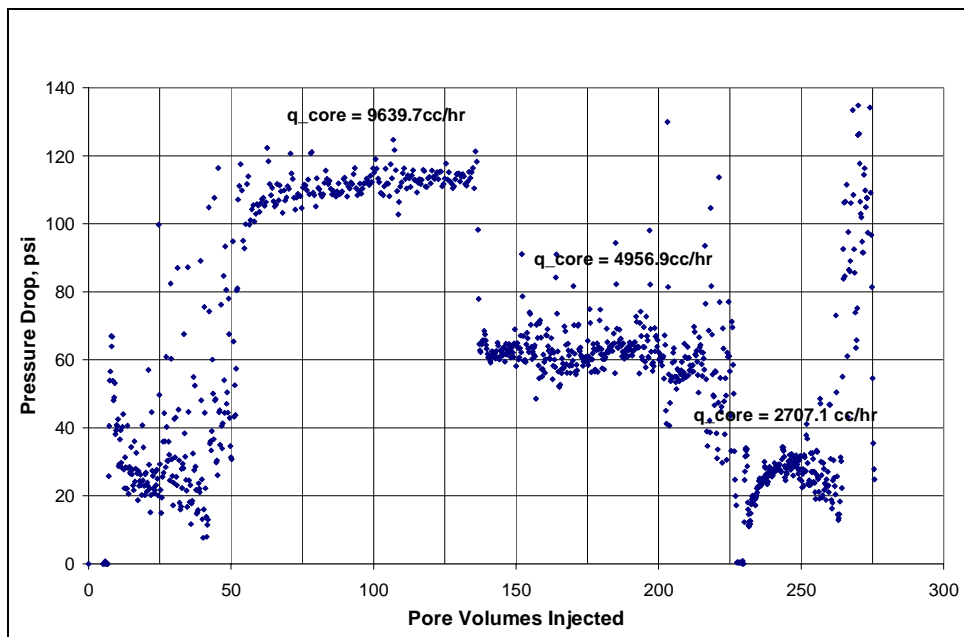


Figure B36.6: Pressure drop across the core during post-treatment gas condensate flood at 175°F and 410 psig

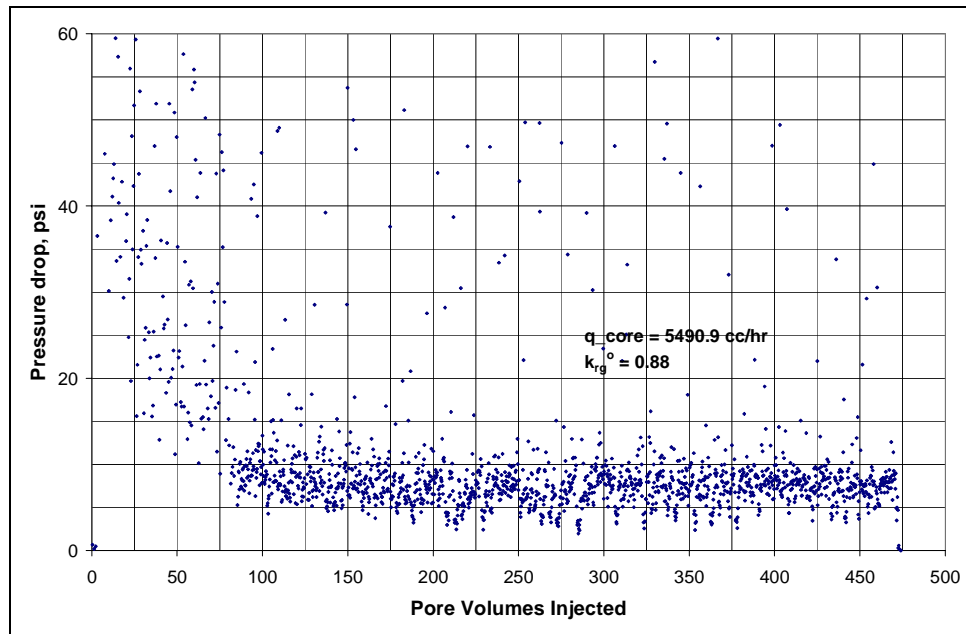


Figure B36.7: Pressure drop across the core during final methane flood

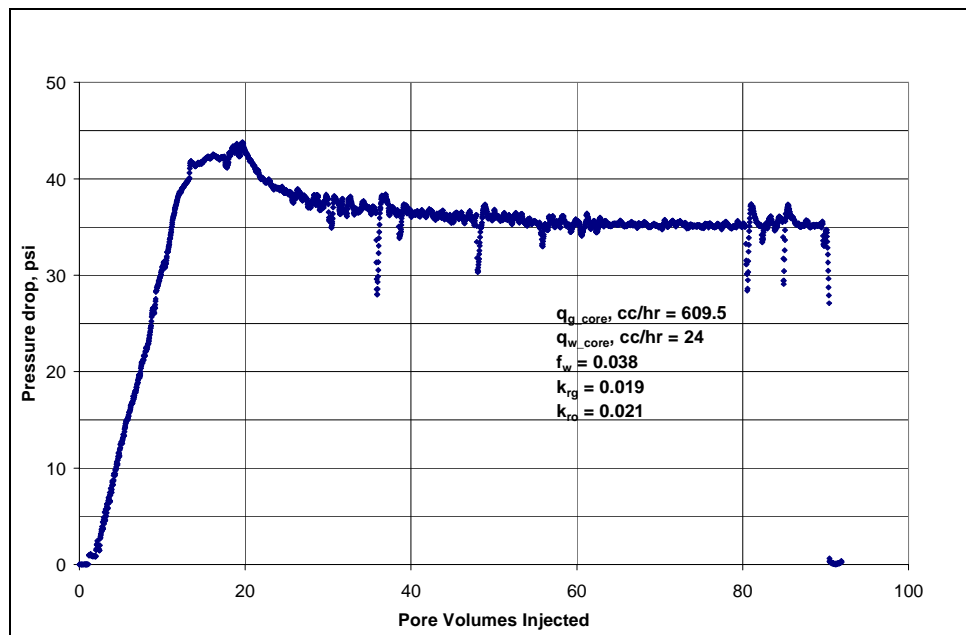


Figure B36.8: Pressure drop across the core during the post-treatment two-phase gas-water flood ($f_w=0.038$) at 175°F and 410 psig

B37- Experiment No.37

Objective:

The objective of this experiment was to investigate the effect of shut-in time on the chemical treatment using FC4430 in a mixture of 2-butoxyethanol and ethanol. The experiment was performed on a Berea core at 175°F.

Experimental Results:

Table B37.1 summarizes the properties of the core and the experimental conditions. Initial permeability of the core was measured using nitrogen at 75°F. **Figure B37.1** shows the pressure drop measured across the core during nitrogen flood. **Table B37.2** summarizes the results of the nitrogen flood.

The initial water saturation of 19% was established by injecting 1.7 cc of synthetic Bruce brine (**Table B21.3**) in the vacuumed core. Nitrogen flood was then conducted to measure the end point gas relative permeability. **Figure B37.2** shows the pressure drop measured across the core and **Table B37.3** summarizes the results of the nitrogen flood. The pressure of the core was raised to 200 psig and then the temperature of the oven was increased to 175°F.

Synthetic fluid mixture-5 (**Table 3.5**) was used for the two-phase flow measurements. The initial flood was conducted with the upstream backpressure regulator set at 5000 psig and the downstream back pressure regulator set at 400 psig. **Table B37.4** gives the properties of the synthetic fluid calculated using the Peng-Robinson EOS at the flowing core pressure. **Figure B37.3** shows the pressure drop across the core during the two-phase gas-condensate flow. **Table B37.5** summarizes the results of the initial two-phase flow.

The core was then treated with the treatment solution (**Table B37.6**). **Figure B37.4** shows the measured pressure drop across the core during the treatment flood. The treatment solution was injected at 196cc/hr. The core was then shut-in for 15 hours.

Post-treatment two-phase gas-condensate flood was conducted under the same conditions as the initial two-phase flow. **Figure B37.5** shows the pressure drop across the core measured during the post-treatment two-phase floods at a flowing pressure of 400 psig. **Table B37.7** summarizes the results of the post-treatment two-phase flow.

Table B37.1: Core properties

Core	Berea Sandstone
Length, inches	3.75
Diameter, inches	1
Porosity, %	17.98
Pore volume, cc	8.68
Swi, %	19
Temperature, °F	175

Table B37.2: Result of nitrogen flood

q_{core}, (cc/hr)	ΔP (psi)	k_g (md)
2586.83	1.50	245.70
5173.65	3.13	235.82
7760.48	4.92	225.30
Permeability, k_g (md)		237.88

Table B37.3: Result of nitrogen flood at Swi

q_{core}, (cc/hr)	ΔP (psi)	k_g (md)
5173.65	3.78	195.35

Table B37.4: Synthetic fluid properties at experimental conditions

Pressure, psig	5000	400	
Fluid Properties		Gas phase	Oil phase
ρ, g/cc	0.2898	0.0192	0.6702
μ (cp)		0.0133	0.4098
Volume fraction		0.988	0.012
IFT (dyne/cm)		12.976	

Table B37.5: Results of the initial two-phase gas condensate flood

q_{pump}, cc/hr	250	500
$q_{\text{total_core}}$, cc/hr	2682.14	5364.28
$q_{\text{g_core}}$, cc/hr	2649.96	5299.91
$q_{\text{o_core}}$, cc/hr	32.19	64.37
ΔP, psi	11.92	23.37
k_{rg}	0.096	0.098
k_{ro}	0.036	0.037
Nc	1.56×10^{-5}	3.06×10^{-5}
PVT Ratio	2.67	2.67

Table B37.6: Composition of treatment solution

Component	Weight %
FC4430	2
2-butoxyethanol	69
Ethanol	29

Table B37.7: Results of post-treatment two-phase flow of gas condensate mixture

q_{pump}, cc/hr	250	500
q_{total_core}, cc/hr	2682.14	5364.28
q_{g_core}, cc/hr	2649.96	5299.91
q_{o_core}, cc/hr	32.19	64.37
ΔP, psi	7.19	15.43
k_{rg}	0.160	0.149
k_{ro}	0.060	0.056
Nc	9.42×10^{-6}	2.02×10^{-5}
Improvement Factor	1.66	1.54

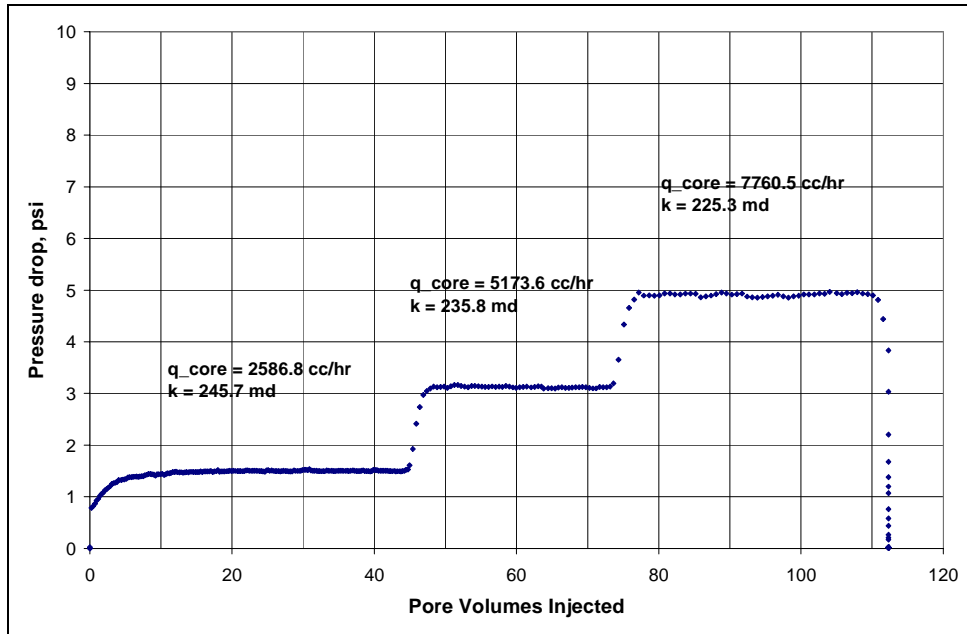


Figure B37.1: Pressure drop across the core during initial nitrogen flood

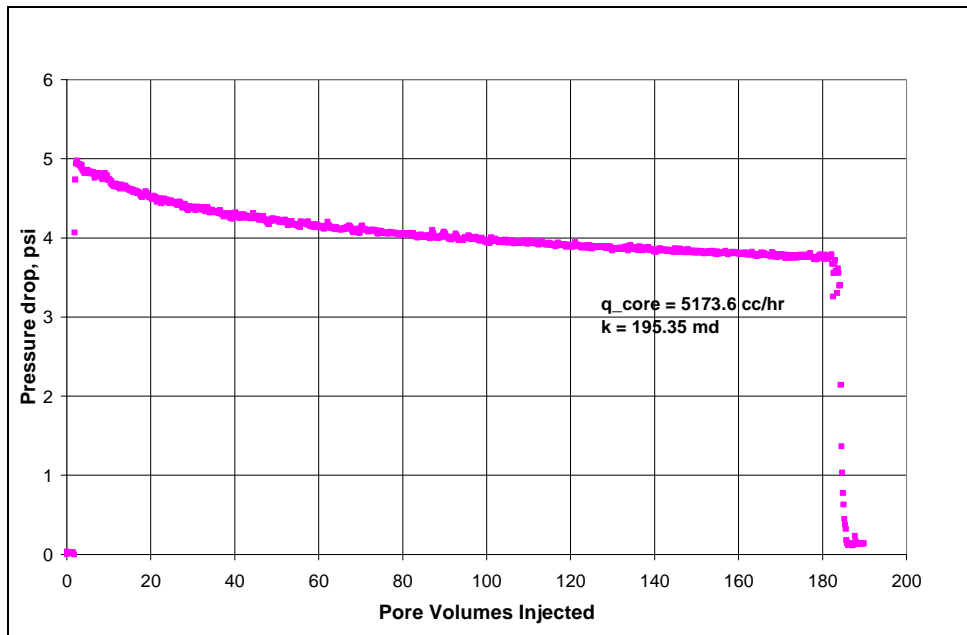


Figure B37.2: Pressure drop across the core during nitrogen flood at $Sw_i=19\%$

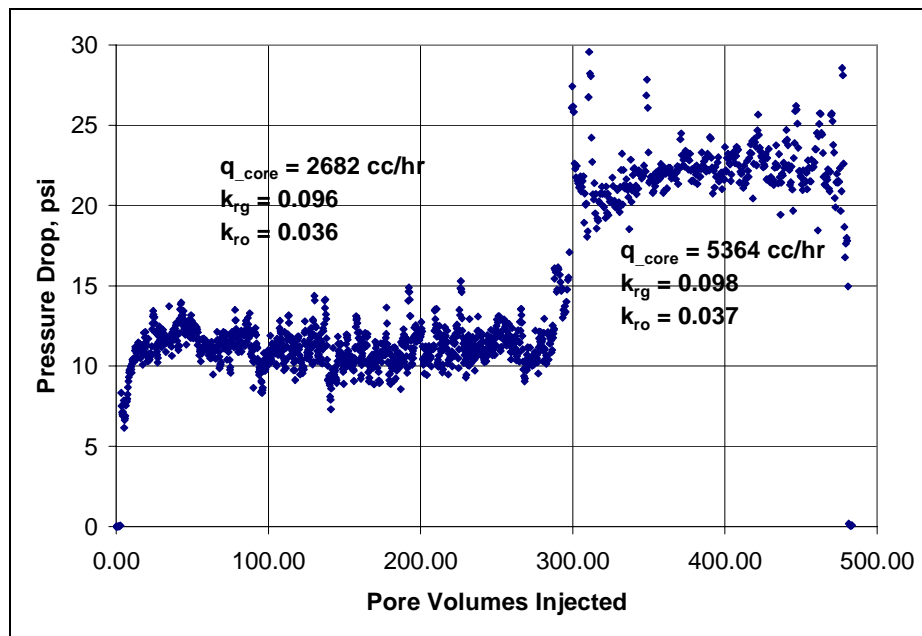


Figure B37.3: Pressure drop across the core during the initial two-phase flow at 175°F and 400 psig

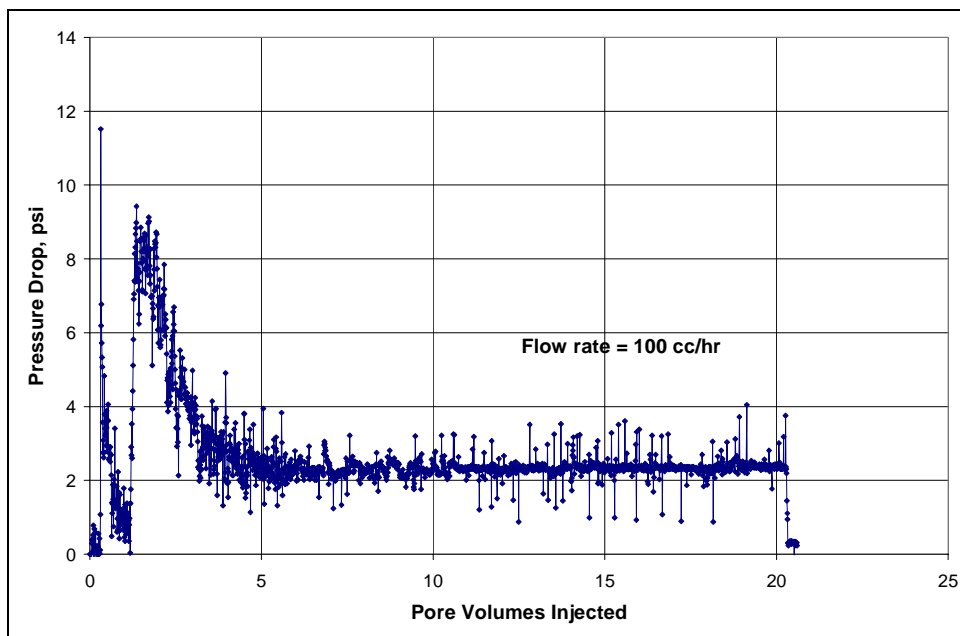


Figure B37.4: Pressure drop across the core during surfactant treatment

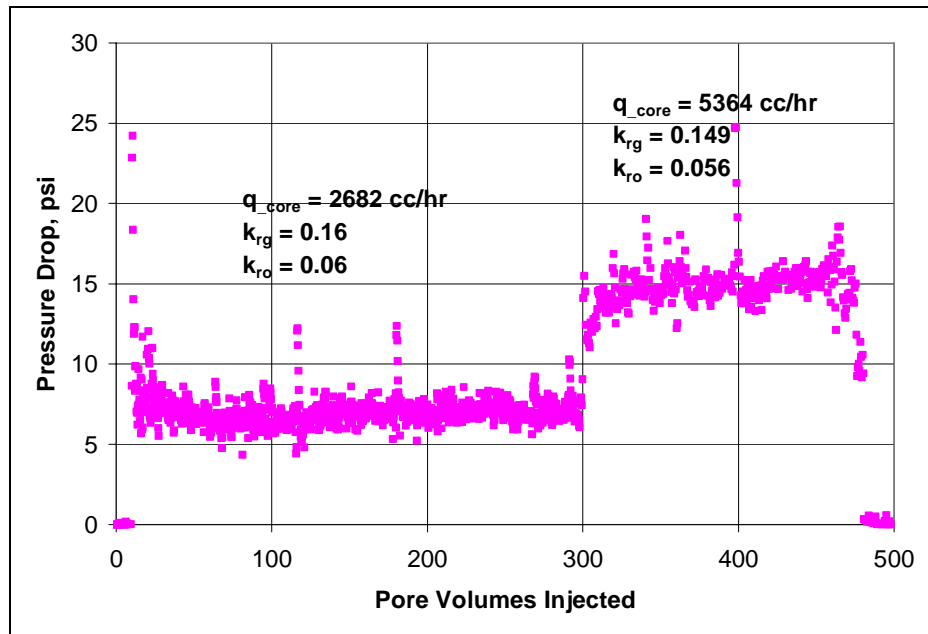


Figure B37.5: Pressure drop across the core during post-treatment two-phase flow at 175°F and 400 psig

B38- Experiment No.38

Objective:

The objective of this experiment was to investigate the effect chemical APG1430 from Advanced polymer inc. on gas and condensate relative permeability. The experiment was performed on a Texas Cream limestone core at 175°F.

Experimental Results:

Table B38.1 summarizes the properties of the core and the experimental conditions. Initial permeability of the core was measured using nitrogen at 75°F. **Figure B38.1** shows the pressure drop measured across the core during nitrogen flood. **Table B38.2** summarizes the results of the nitrogen flood.

The initial water saturation of 20% was established by injecting 2 cc of D.I. water in the vacuumed core. Nitrogen flood was then conducted to measure the end point gas relative permeability. **Figure B38.2** shows the pressure drop measured across the core and **Table B38.3** summarizes the results of the nitrogen flood. The pressure of the core was raised to 200 psig and then the temperature of the oven was increased to 175°F.

Synthetic fluid mixture-5 (**Table 3.5**) was used for the two-phase flow measurements. The initial flood was conducted with the upstream backpressure regulator set at 4900 psig and the downstream back pressure regulator set at 500 psig. **Table B38.4** gives the properties of the synthetic fluid calculated using the Peng-Robinson EOS at the flowing core pressure. **Figure B38.3** shows the pressure drop across the core during the two-phase gas-condensate flow. **Table B38.5** summarizes the results of the initial two-phase flow.

The core was then treated with the treatment solution (**Table B38.6**). The treatment solution was mixed using a magnetic mixer at 60°C for 2 hours and then mixed at room temperature for 2 more hours. The solution was single-phase at room temperature. **Figure B38.4** shows the measured pressure drop across the core during the treatment flood. The injection of treatment solution was started at 50 cc/hr but then dropped to 25 cc/hr as the pressure drop reached 120 psi. The effluent from the core became foamy after 7.5 PV of injection and the treatment flood was stopped. The core was then shut-in for 15 hours.

Post-treatment two-phase gas-condensate flood was started at a pump rate of 40cc/hr (331 cc/hr core rate). The pressure drop kept on increasing and reached 350-400 psi. The flood was then stopped. A solvent flush using a 50/50 mixture of 2-butoxyethanol/IPA was then done to clean out the core. The solvent flood was started at 50cc/hr then dropped to 25cc/hr and finally to 12.5cc/hr. The pressure drop still kept increasing indicating that the core is severely plugged.

Table B38.1: Core properties

Core	Texas Cream Limestone
Length, inches	4.02
Diameter, inches	1
Porosity, %	20.00
Pore volume, cc	10.34
Swi, %	20
Temperature, °F	175

Table B38.2: Result of nitrogen flood

q_{core}, (cc/hr)	ΔP (psi)	k_g (md)
740.49	11.38	10.00
1480.99	22.51	10.11
2221.48	33.99	10.04
Permeability, k_g (md)		10.04

Table B38.3: Result of nitrogen flood at Swi

q_{core}, (cc/hr)	ΔP (psi)	k_g (md)
1480.99	26.11	8.72

Table B38.4: Synthetic fluid properties at experimental conditions

Pressure, psig	5000	530		560	
Fluid Properties		Gas phase	Oil phase	Gas phase	Oil phase
ρ, g/cc	0.2898	0.0247	0.6627	0.0261	0.6608
μ (cp)		0.0134	0.3902	0.0135	0.3854
Volume fraction		0.9839	0.0161	0.9829	0.0171
IFT (dyne/cm)		11.945		11.696	

Table B38.5: Results of the initial two-phase gas condensate flood

q_{pump}, cc/hr	80	160
$q_{\text{total_core}}$, cc/hr	662.93	1254.77
$q_{\text{g_core}}$, cc/hr	652.26	1233.31
$q_{\text{o_core}}$, cc/hr	10.67	21.46
ΔP, psi	59.13	115.95
k_{rg}	0.121	0.117
k_{ro}	0.058	0.059
Nc	3.22×10^{-6}	6.50×10^{-6}
PVT Ratio	2.10	1.97

Table B38.6: Composition of treatment solution

Component	Weight %
APG-1430	20
2-butoxyethanol	15
IPA	15
D.I. water	50

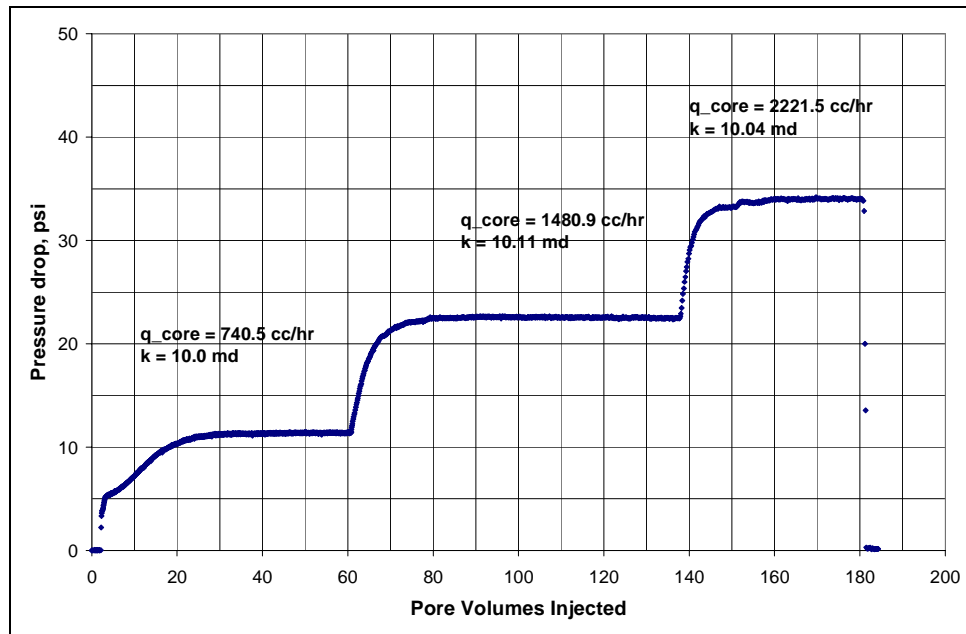


Figure B38.1: Pressure drop across the core during initial nitrogen flood

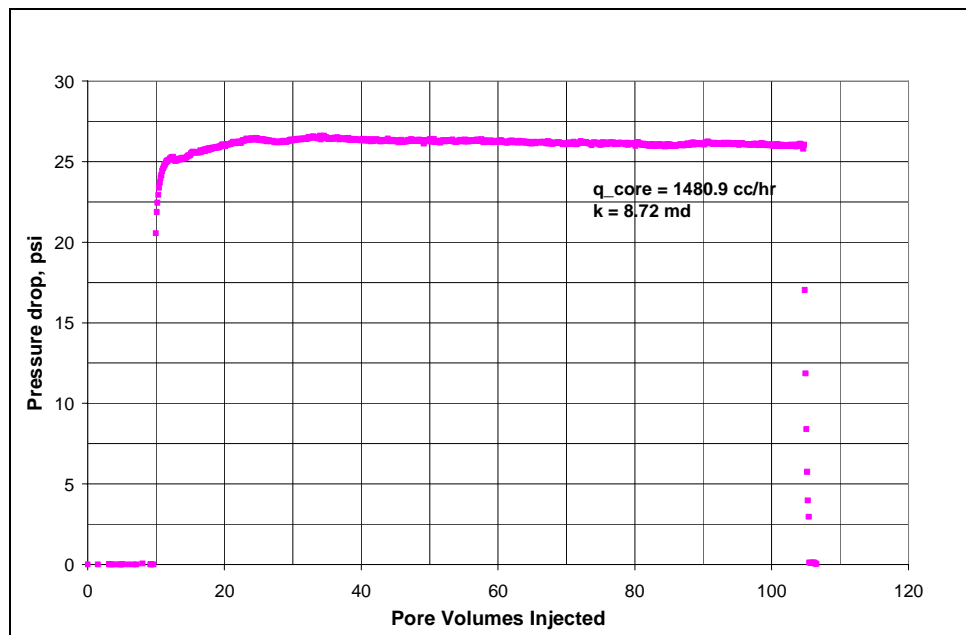


Figure B38.2: Pressure drop across the core during nitrogen flood at $Sw_i = 20\%$

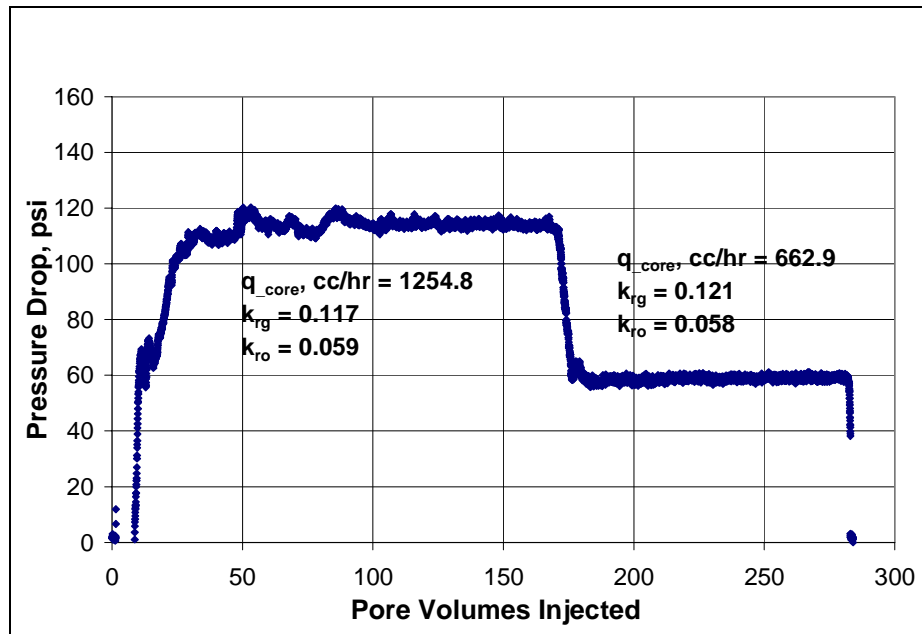


Figure B38.3: Pressure drop across the core during the initial two-phase flow at 175°F and 500 psig

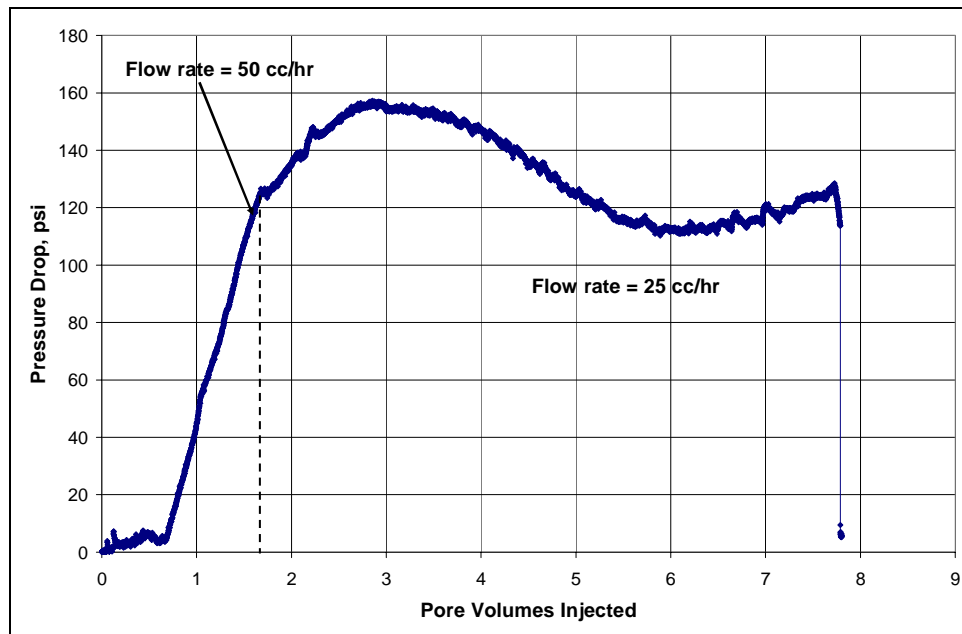


Figure B38.4: Pressure drop across the core during surfactant treatment

B39- Experiment No.39

Objective:

The objective of this experiment was to investigate the effect of chemical treatment on gas and condensate relative permeability on propped fractures. The experiment was performed using 30/50 Bauxite as proppant at 279°F.

Experimental Results:

Berea core was used as the matrix rock and 30/50 Bauxite was used as the proppant to fill the simulated fracture void. **Table B39.1** summarizes the properties of the propped fracture and the experimental conditions. Initial permeability of the propped fracture was measured using nitrogen at 75°F. Measurements were done at 1000 psi, 2000 psi, 3000 psi, 4000 psi, 5000 psi, 7000 psi and 9000 psi net confining stress. Measurements were done at multiple rates at each net confining stress to capture the effect of non-Darcy flow on single-phase gas permeability. **Figure B39.1** shows the pressure drop measured across the core during nitrogen flood at different net confining stress and flow rates. **Tables B39.2 to B39.8** summarize the results of the nitrogen flood at different net confining stress. The average permeability of the fracture was calculated from the intercept of the plot of $(\Delta P/q)$ vs velocity. **Figures B39.2 to B39.8** show the plot of $(\Delta P/q)$ vs velocity for data measured at different net confining stress.

Initial water saturation of 20% was established by injecting 0.9 cc of 30,000 ppm NaCl brine in the vacuumed core. Nitrogen flood was then conducted to measure the end point gas relative permeability. Nitrogen flood at S_{wi} was conducted at multiple flow rates and multiple net confining stresses. **Figure B39.9** shows the pressure drop across the fracture during the nitrogen flood. **Tables B39.9 to B39.12** summarize the results of

the nitrogen flood at different net confining stresses. The average gas permeability at S_{wi} was calculated from the intercept of the plot of $(\Delta P/q)$ vs q . **Figures B39.10 to B39.13** shows the plot of $(\Delta P/q)$ vs q for data measured at different net confining stress.

Synthetic fluid mixture-9 (**Table 3.9**) was used for the two-phase flow measurements. The gas condensate flood was done at a net confining stress of 1000 psi, 3000 psi and 5000 psi. The upstream backpressure regulator set at 5600 psig and the downstream back pressure regulator set at 1450 psig. **Table B39.13** gives the properties of the synthetic fluid calculated using the Peng-Robinson EOS at the flowing core pressure. **Figure B39.14** shows the pressure drop across the fracture measured during the initial gas condensate flood. **Tables B39.14, B39.15 and B39.16** summarize the results of gas condensate floods at a net confining stress of 1000 psi, 3000 psi and 5000 psi respectively. The relative permeability data has been corrected for non-Darcy flow effects.

The core was then treated with the treatment solution (**Table B39.17**). **Figure B39.15** shows the measured pressure drop across the core during the treatment flood. First 17 PV of treatment solution was injected at 100 cc/hr and the last 10 pore volumes of treatment solution was injected at 500 cc/hr. The core was then shut-in for 15 hours.

Post-treatment two-phase gas-condensate flood was conducted at a net confining stress of 1000 psig. **Figure B39.16** shows the pressure drop measured during the post-treatment gas condensate flood. **Table B39.18** summarizes the results for the gas condensate flood after the treatment.

The post-treatment permeability of the fracture was measured using methane to find out if the final gas permeability was as high as the initial gas permeability. **Figure B39.17** shows the pressure drop during the methane flood and **Table B39.19** summarizes the results.

The core was re-treated with the treatment solution (**Table B39.17**). **Figure B39.18** shows the measured pressure drop across the core during the second treatment flood. First 60 PV of treatment solution was injected at 100 cc/hr and the last 30 pore volumes of treatment solution was injected at 500 cc/hr. The core was then shut-in for 15 hours.

Post-treatment two-phase gas-condensate flood was conducted at a net confining stress of 1000 psig. **Figure B39.19** shows the pressure drop measured during the gas condensate flood after the second treatment.

Table B39.1: Core and fracture properties

Core	Berea Sandstone
Proppant	30/50 Bauxite
Fracture Aperture, cm	0.24
Length, inches	6
Fracture width, cm	2.48
Porosity, %	42.82
Pore volume, cc	4.45
Swi, %	20
Temperature, °F	279

Table B39.2: Result of nitrogen flood at a net confining stress of 1000 psig

q_{core}, (cc/hr)	ΔP (psi)	k_g (Darcy)
1014.14	0.066	38.74
2165.58	0.16	33.26
4164.57	0.49	20.88
5552.76	0.82	16.64
8329.15	1.66	12.33
Permeability, k_g (md) (corrected for non Darcy)		77.03
β (1/cm) = 4.25x10³		

Table B39.3: Result of nitrogen flood at a net confining stress of 2000 psig

q_{core}, (cc/hr)	ΔP (psi)	k_g (Darcy)
1014.14	0.066	38.76
2165.58	0.16	33.26
4164.57	0.48	21.32
5552.76	0.80	17.06
8329.15	1.66	12.33
Permeability, k_g (md) (corrected for non Darcy)		81.10
β (1/cm) = 4.26x10³		

Table B39.4: Result of nitrogen flood at a net confining stress of 3000 psig

q_{core}, (cc/hr)	ΔP (psi)	k_g (Darcy)
1014.14	0.076	33.66
2165.58	0.20	26.61
4164.57	0.54	18.95
5552.76	0.89	15.33
8329.15	1.86	11.00
Permeability, k_g (md) (corrected for non Darcy)		69.02
β (1/cm) = 4.71x10³		

Table B39.5: Result of nitrogen flood at a net confining stress of 4000 psig

q_{core}, (cc/hr)	ΔP (psi)	k_g (Darcy)
1014.14	0.076	33.66
2165.58	0.19	28.01
4164.57	0.56	18.27
5552.76	0.93	14.69
8329.15	1.93	10.60
Permeability, k_g (md) (corrected for non Darcy)		66.05
β (1/cm) = 4.90x10³		

Table B39.6: Result of nitrogen flood at a net confining stress of 5000 psig

q_{core}, (cc/hr)	ΔP (psi)	k_g (Darcy)
1014.14	0.081	31.58
2165.58	0.20	26.61
4164.57	0.57	17.95
5552.76	0.95	14.36
8329.15	1.94	10.55
Permeability, k_g (md) (corrected for non Darcy)		57.68
β (1/cm) = 4.80x10³		

Table B39.7: Result of nitrogen flood at a net confining stress of 7000 psig

q_{core}, (cc/hr)	ΔP (psi)	k_g (Darcy)
1014.14	0.081	31.58
2165.58	0.20	26.47
4164.57	0.61	16.89
5552.76	0.99	13.78
8329.15	2.04	10.01
Permeability, k_g (md) (corrected for non Darcy)		60.08
β (1/cm) = 5.17x10³		

Table B39.8: Result of nitrogen flood at a net confining stress of 9000 psig

q_{core}, (cc/hr)	ΔP (psi)	k_g (Darcy)
1014.14	0.083	30.82
2165.58	0.22	24.75
4164.57	0.62	16.51
5552.76	1.02	13.38
8329.15	2.07	9.89
Permeability, k_g (md) (corrected for non Darcy)		51.51
β (1/cm) = 5.07x10³		

Table B39.9: Result of nitrogen flood at Swi at a net confining stress of 1000 psig

q_{core}, (cc/hr)	ΔP (psi)	k_g (Darcy)
1014.14	0.095	26.93
2165.58	0.21	25.34
4164.57	0.60	17.06
5552.76	0.99	13.81
8329.15	2.06	9.94
Permeability, k_g (md) (corrected for non Darcy)		56.88
β (1/cm) = 5.11x10³		

Table B39.10: Result of nitrogen flood at Swi at a net confining stress of 3000 psig

q_{core}, (cc/hr)	ΔP (psi)	k_g (Darcy)
1014.14	0.09	28.43
2165.58	0.21	25.34
4164.57	0.62	16.51
5552.76	1.00	13.64
8329.15	2.11	9.70
Permeability, k_g (md) (corrected for non Darcy)		58.09
β (1/cm) = 5.28x10³		

Table B39.11: Result of nitrogen flood at Swi at a net confining stress of 5000 psig

q_{core}, (cc/hr)	ΔP (psi)	k_g (Darcy)
1014.14	0.10	25.58
2165.58	0.24	22.17
4164.57	0.66	15.50
5552.76	1.07	12.75
8329.15	2.25	9.10
Permeability, k_g (md) (corrected for non Darcy)		47.07
β (1/cm) = 5.42x10³		

Table B39.12: Result of nitrogen flood at Swi at a net confining stress of 7000 psig

q_{core}, (cc/hr)	ΔP (psi)	k_g (Darcy)
1014.14	0.105	24.36
2165.58	0.24	22.17
4164.57	0.66	15.50
5552.76	1.07	12.67
8329.15	2.22	9.22
Permeability, k_g (md) (corrected for non Darcy)		45.09
β (1/cm) = 5.30x10³		

Table B39.13: Synthetic fluid properties at experimental conditions

Pressure, psig	5600	1450	
Fluid Properties		Gas phase	Oil phase
ρ, g/cc	0.2236	0.057	0.63
μ (cp)		0.0165	0.3112
Volume fraction		0.9872	0.0218
IFT (dyne/cm)		5.517	

Table B39.14: Results of the initial two-phase gas condensate flood at net confining stress of 1000 psi

q_{pump}, cc/hr	200	400	800	1500	2200	3000
$q_{\text{total core}}$, cc/hr	643.53	1287.07	2574.13	4826.50	7078.86	9652.99
$q_{\text{g core}}$, cc/hr	629.50	1259.01	2518.02	4721.28	6924.54	9442.56
$q_{\text{o core}}$, cc/hr	14.03	28.06	56.12	105.22	154.32	210.44
ΔP, psi	0.13	0.28	0.82	2.06	3.80	6.20
k_{rg}	0.139	0.144	0.113	0.106	0.100	0.099
k_{ro}	0.052	0.048	0.033	0.025	0.02	0.016
Nc	7.07×10^{-5}	1.52×10^{-4}	4.46×10^{-4}	1.12×10^{-3}	2.07×10^{-3}	3.37×10^{-3}
PVT Ratio	2.38	2.38	2.38	2.38	2.38	2.38

Table B39.15: Results of the initial two-phase gas condensate flood at net confining stress of 3000 psi

q_{pump}, cc/hr	200	400	800	1500	2200
q_{total core}, cc/hr	643.53	1287.07	2574.13	4826.50	7078.86
q_{g core}, cc/hr	629.50	1259.01	2518.02	4721.28	6924.54
q_{o core}, cc/hr	14.03	28.06	56.12	105.22	154.32
ΔP, psi	0.18	0.40	0.98	2.27	4.00
k_{rg}	0.114	0.109	0.103	0.104	0.104
k_{ro}	0.043	0.038	0.031	0.025	0.021
Nc	8.53x10 ⁻⁵	1.95x10 ⁻⁴	4.78x10 ⁻⁴	1.11x10 ⁻³	1.95x10 ⁻³
PVT Ratio	2.38	2.38	2.38	2.38	2.38

Table B39.16: Results of the initial two-phase gas condensate flood at net confining stress of 5000 psi

q_{pump}, cc/hr	200	400	800	1500	2200
q_{total core}, cc/hr	643.53	1287.07	2574.13	4826.50	7078.86
q_{g core}, cc/hr	629.50	1259.01	2518.02	4721.28	6924.54
q_{o core}, cc/hr	14.03	28.06	56.12	105.22	154.32
ΔP, psi	0.19	0.49	1.10	2.60	4.40
k_{rg}	0.125	0.104	0.107	0.105	0.109
k_{ro}	0.048	0.037	0.033	0.026	0.023
Nc	7.74x10 ⁻⁵	2.00x10 ⁻⁴	4.48x10 ⁻⁴	1.06x10 ⁻³	1.79x10 ⁻³
PVT Ratio	2.38	2.38	2.38	2.38	2.38

Table B39.17: Composition of treatment solution

Component	Weight %
FC4430	1
Propylene glycol	69
Isopropanol	29

Table B39.18: Results of post-treatment gas condensate flood at a net confining stress of 1000 psig

q_{pump}, cc/hr	800	2200	3000
q_{total_core}, cc/hr	2574.13	7078.86	9652.99
q_{g_core}, cc/hr	2518.02	6924.54	9442.56
q_{o_core}, cc/hr	56.12	154.32	210.44
ΔP, psi	1.00	4.50	7.70
k_{rg}	0.090	0.080	0.073
k_{ro}	0.027	0.017	0.013
Nc	5.44x10 ⁻⁴	2.45x10 ⁻³	4.19x10 ⁻³
Improvement Factor	0.82	0.84	0.81

Table B39.19: Result of methane flood to measure final permeability

q_{core}, (cc/hr)	ΔP (psi)	k_g (Darcy)
1863.00	0.26	13.82
1241.00	0.17	14.07
Permeability, k_g (md) (corrected for non Darcy)		14.61

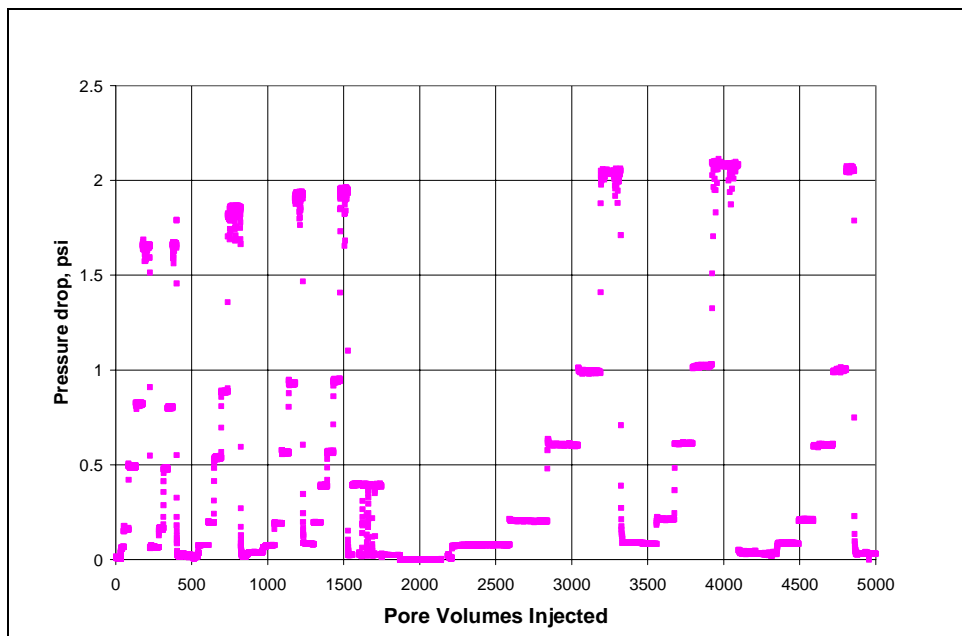


Figure B39.1: Pressure drop across the propped fracture during initial nitrogen flood at different net confining stresses

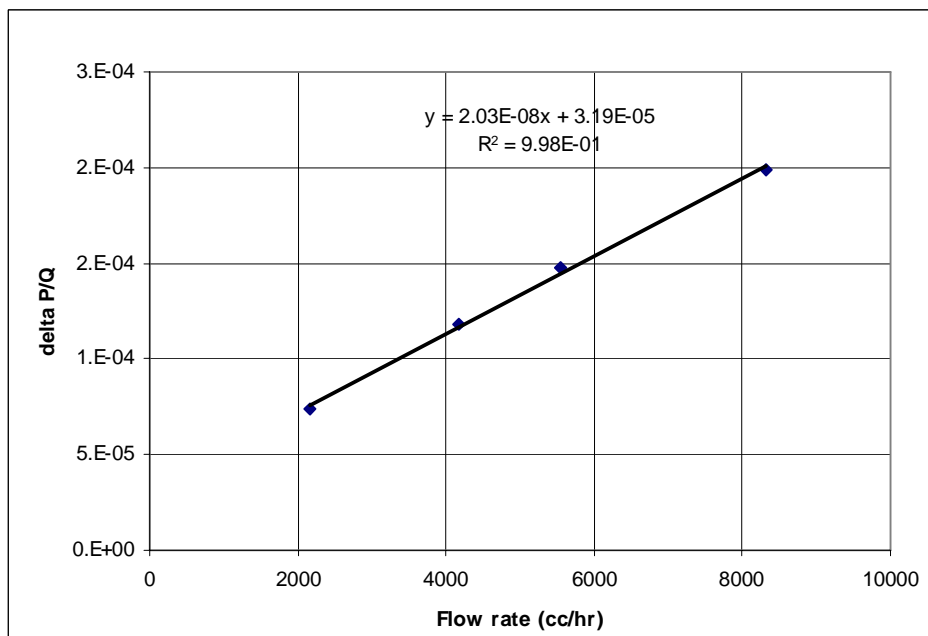


Figure B39.2: Correcting gas permeability measurement for non-Darcy flow at net confining stress of 1000 psig

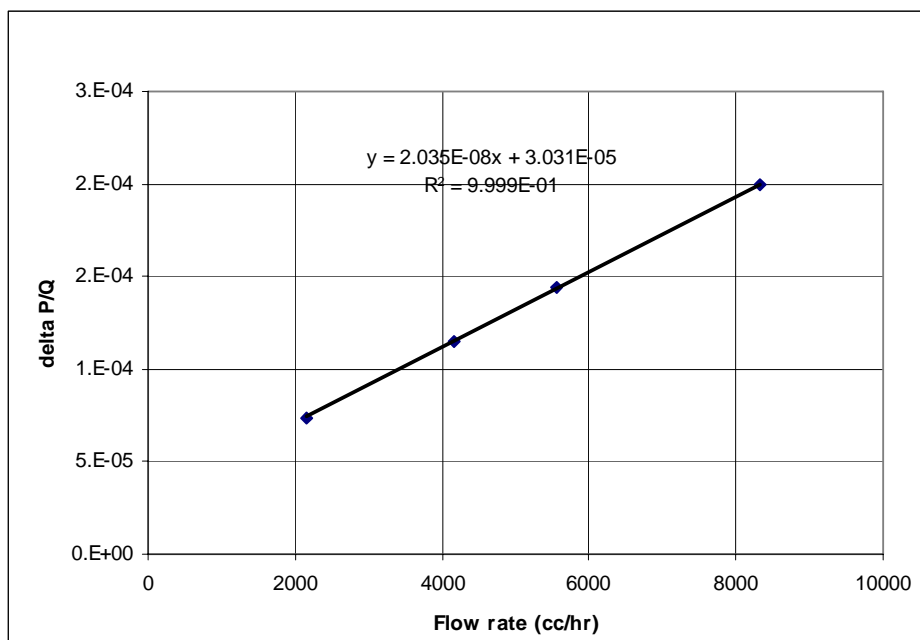


Figure B39.3: Correcting gas permeability measurement for non-Darcy flow at net confining stress of 2000 psig

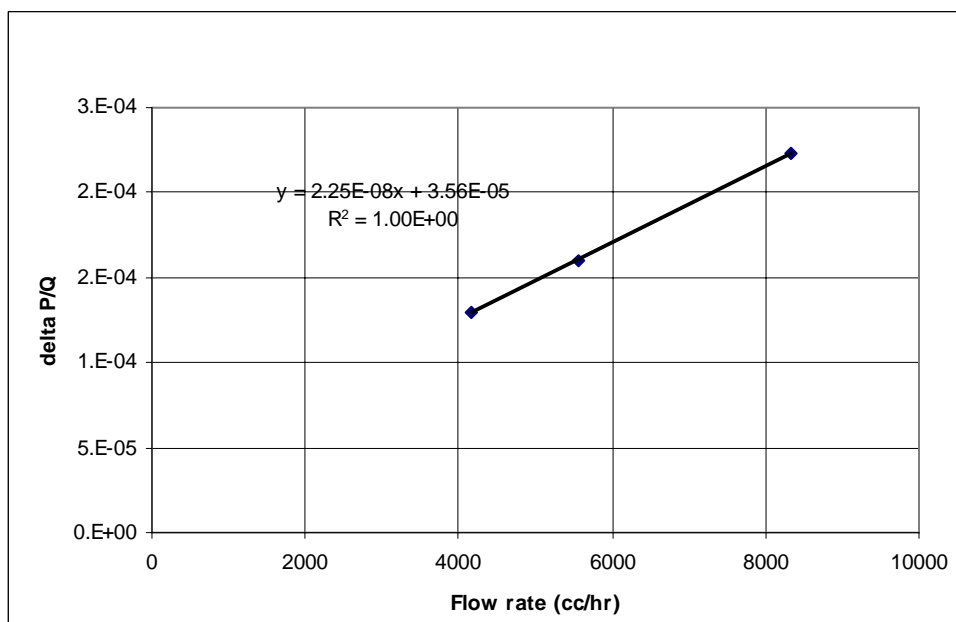


Figure B39.4: Correcting gas permeability measurement for non-Darcy flow at net confining stress of 3000 psig

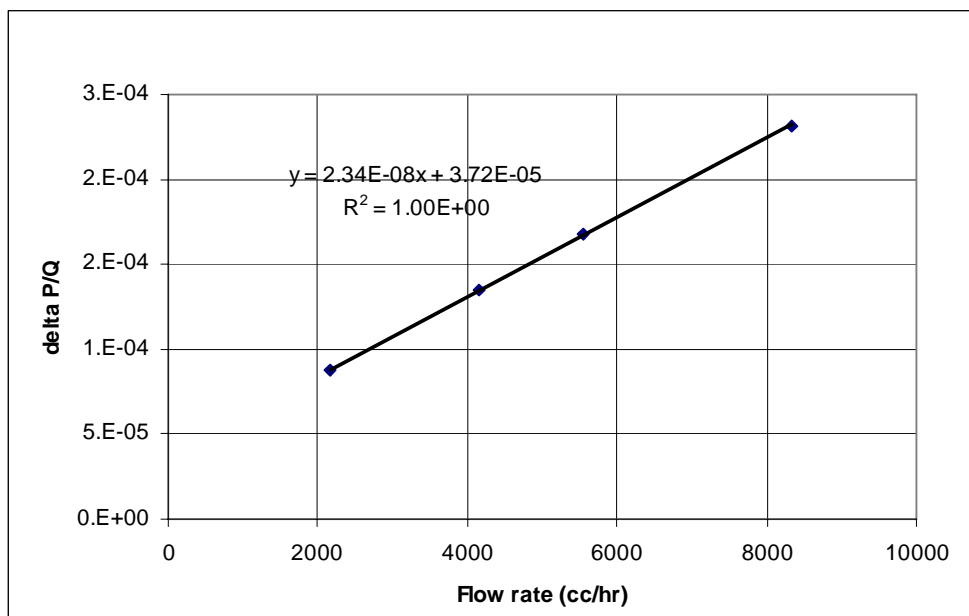


Figure B39.5: Correcting gas permeability measurement for non-Darcy flow at net confining stress of 4000 psig

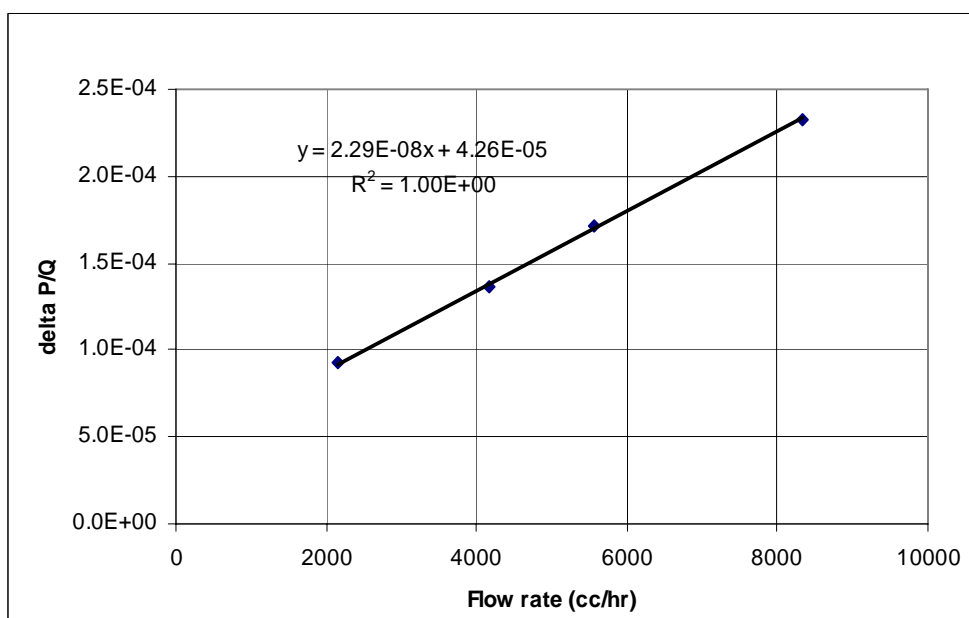


Figure B39.6: Correcting gas permeability measurement for non-Darcy flow at net confining stress of 5000 psig

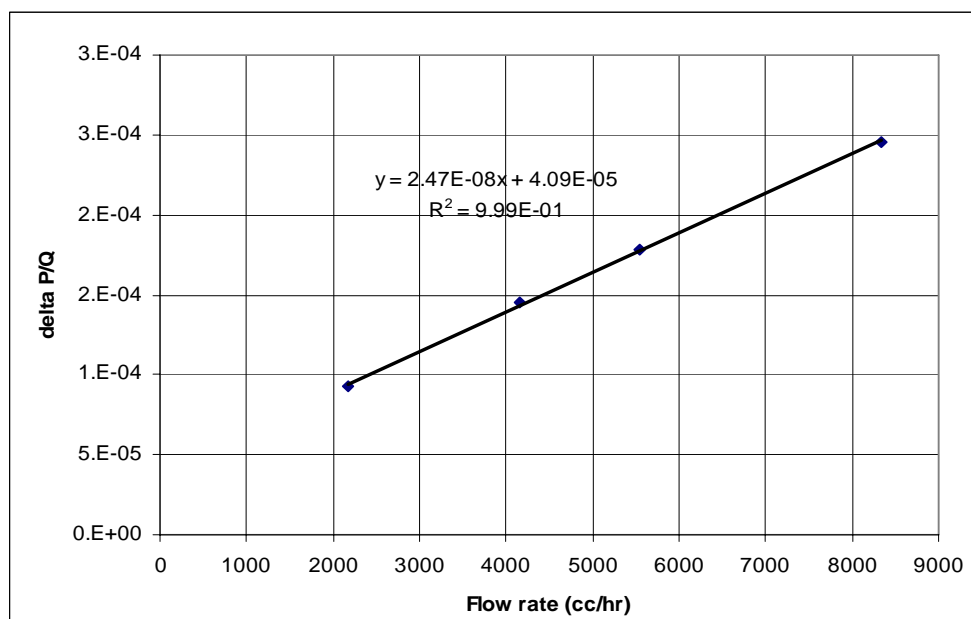


Figure B39.7: Correcting gas permeability measurement for non-Darcy flow at net confining stress of 7000 psig

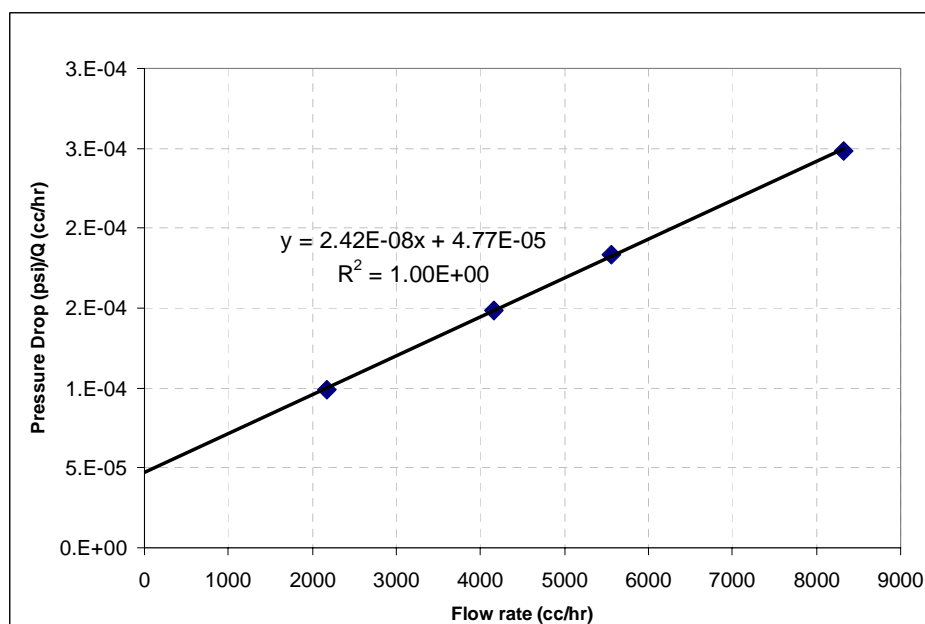


Figure B39.8: Correcting gas permeability measurement for non-Darcy flow at net confining stress of 9000 psig

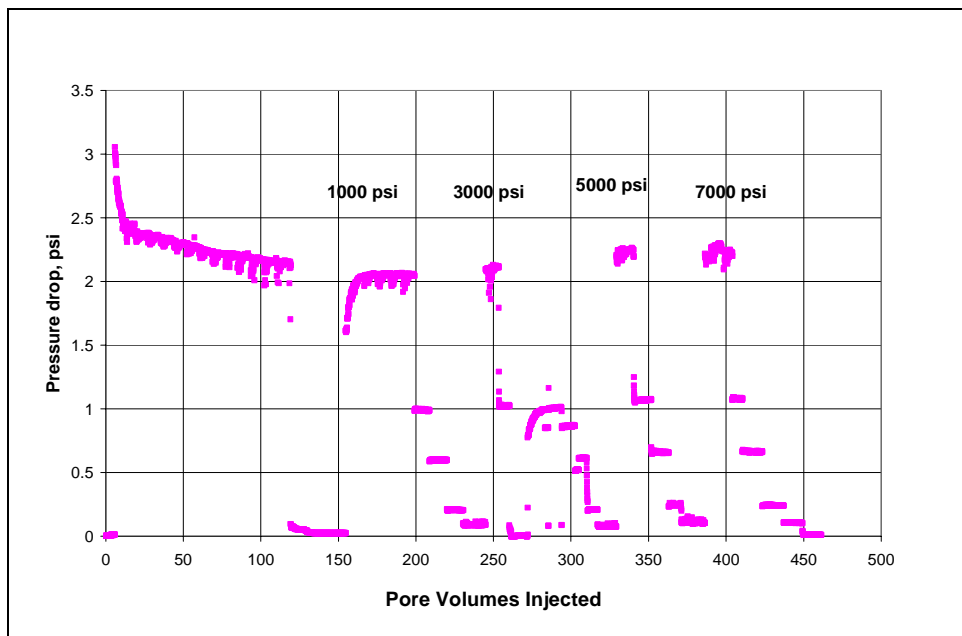


Figure B39.9: Pressure drop across the propped fracture during initial nitrogen flood at Swi at different net confining stresses

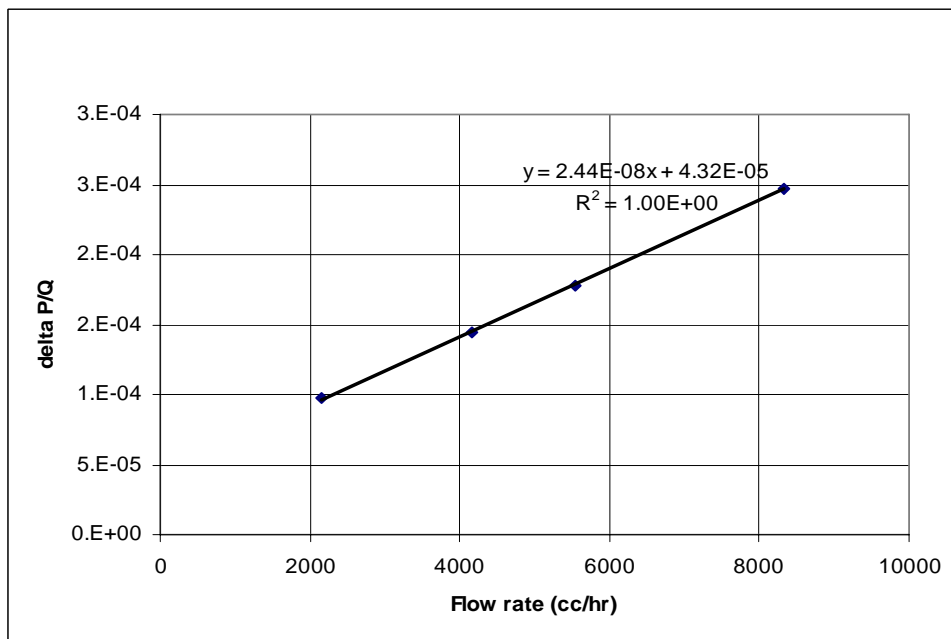


Figure B39.10: Correcting gas permeability measurement at Swi for non-Darcy flow at net confining stress of 1000 psig

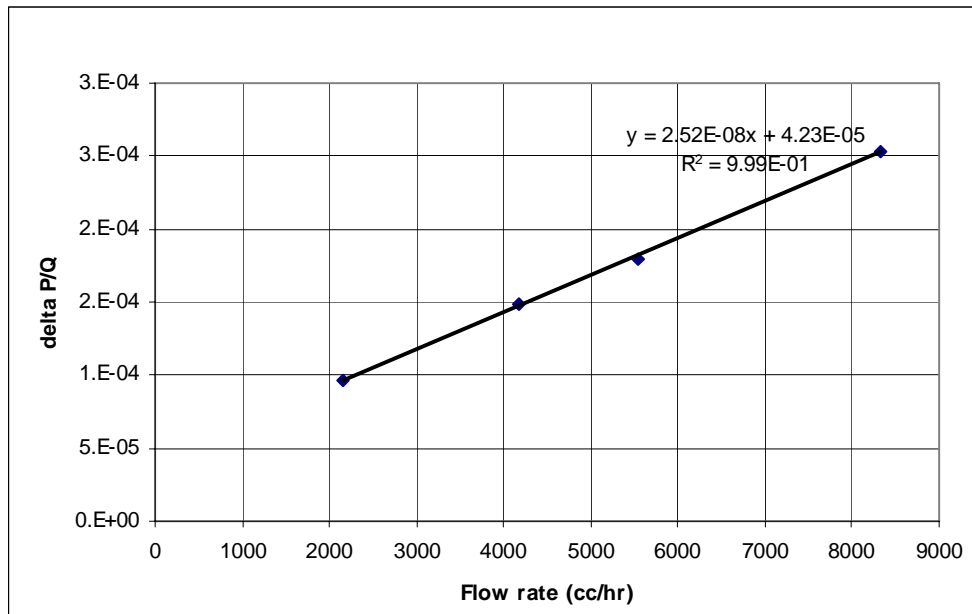


Figure B39.11: Correcting gas permeability measurement at S_{wi} for non-Darcy flow at net confining stress of 3000 psig

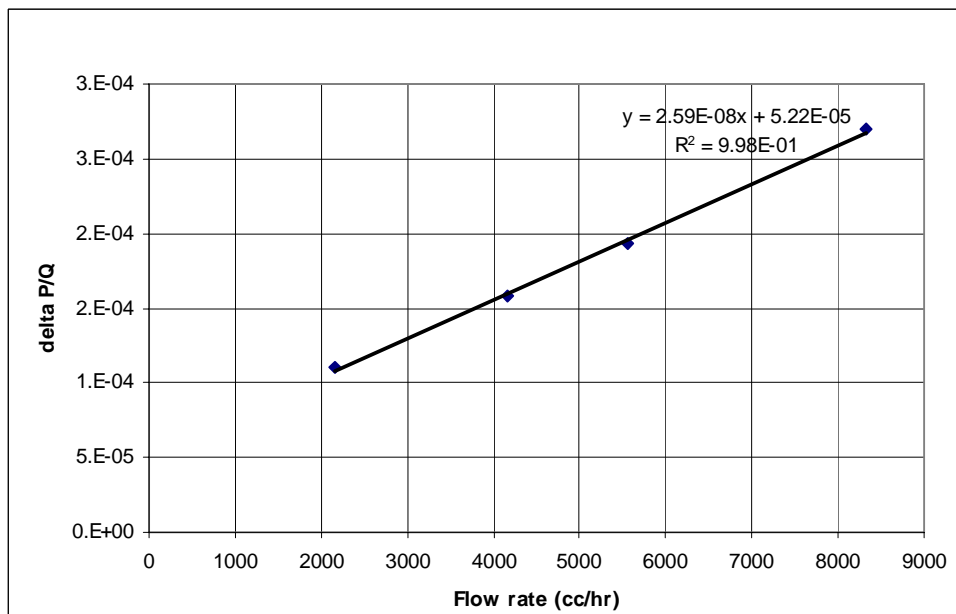


Figure B39.12: Correcting gas permeability measurement at S_{wi} for non-Darcy flow at net confining stress of 5000 psig

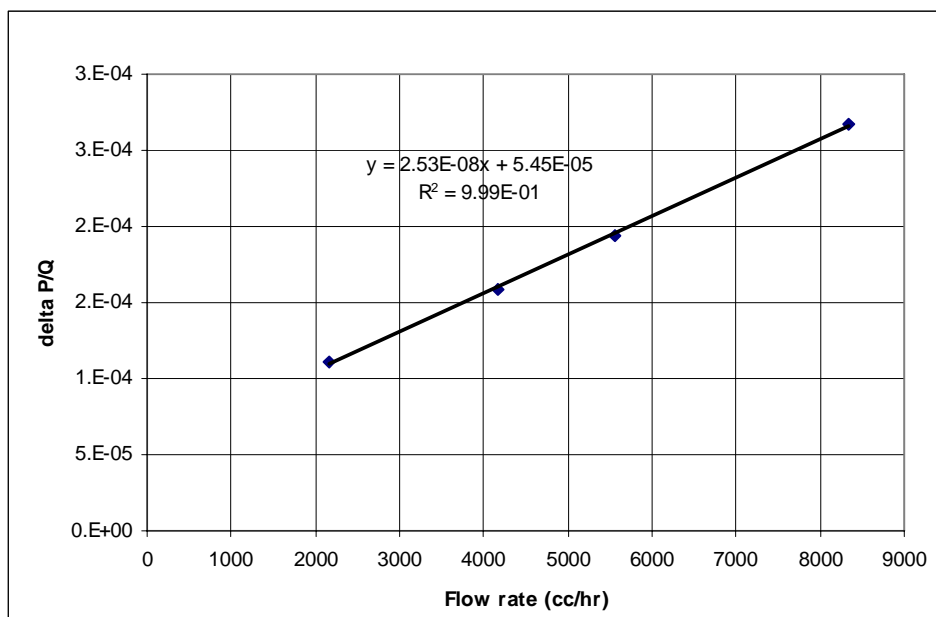


Figure B39.13: Correcting gas permeability measurement at S_{wi} for non-Darcy flow at net confining stress of 7000 psig

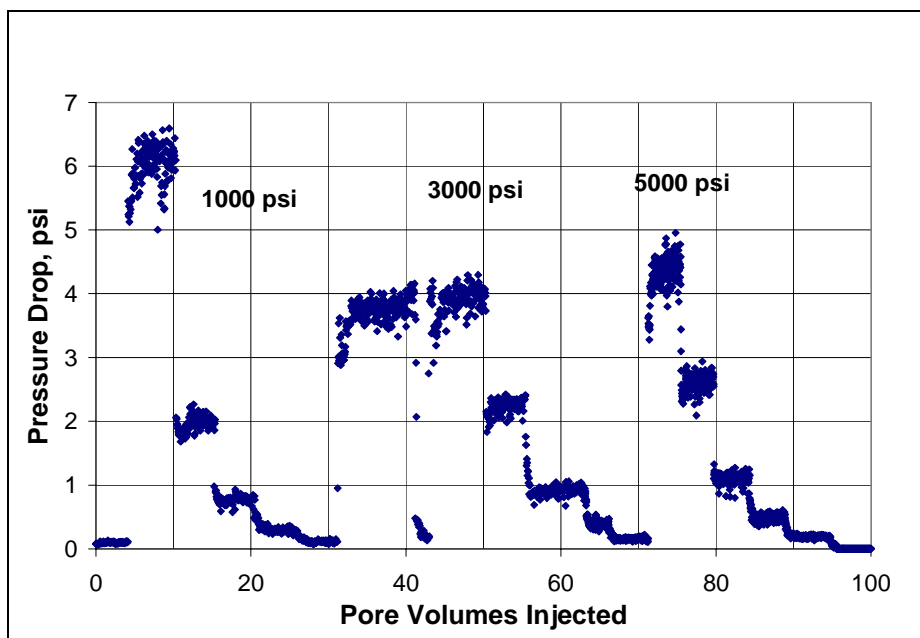


Figure B39.14: Pressure drop across the propped fracture during the initial gas condensate flood at 279°F and 1450 psig and different net confining stresses

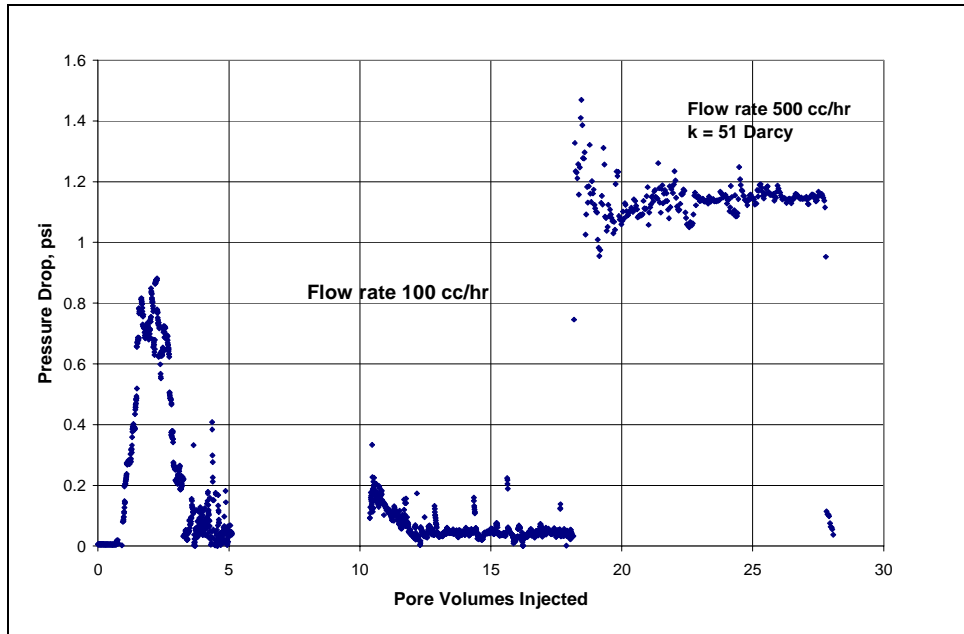


Figure B39.15: Pressure drop across the propped fracture during surfactant treatment

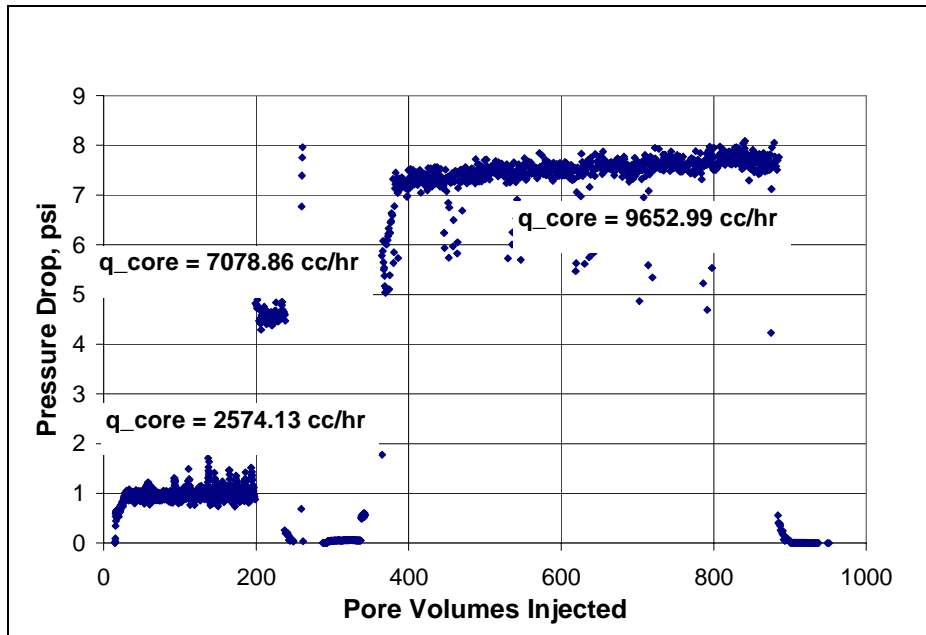


Figure B39.16: Pressure drop across the propped fracture during the post-treatment gas condensate flood at 275°F and 1450 psig and a net confining stress of 1000 psi

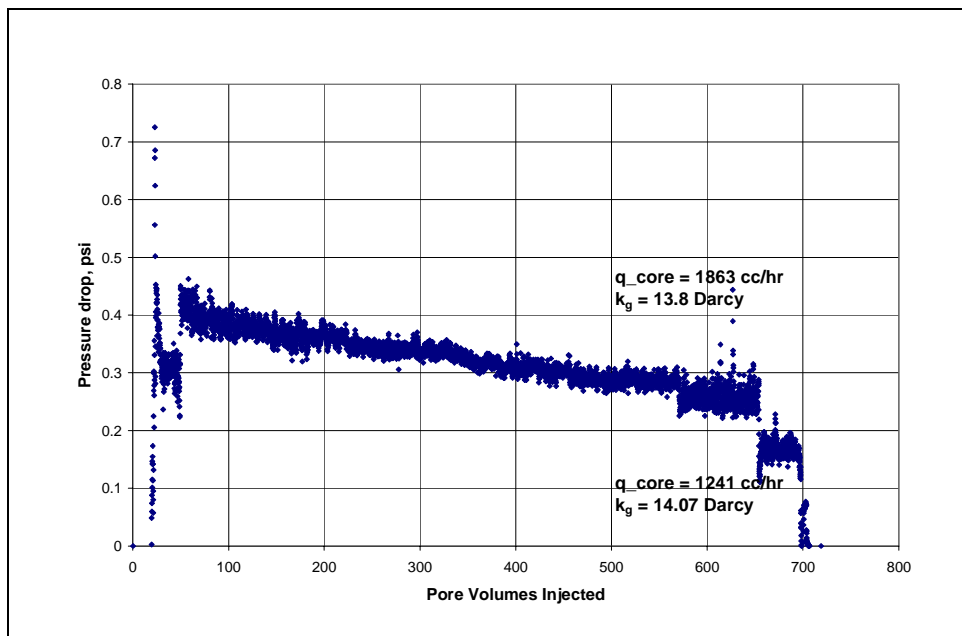


Figure B39.17: Pressure drop across the propped fracture during final methane flood

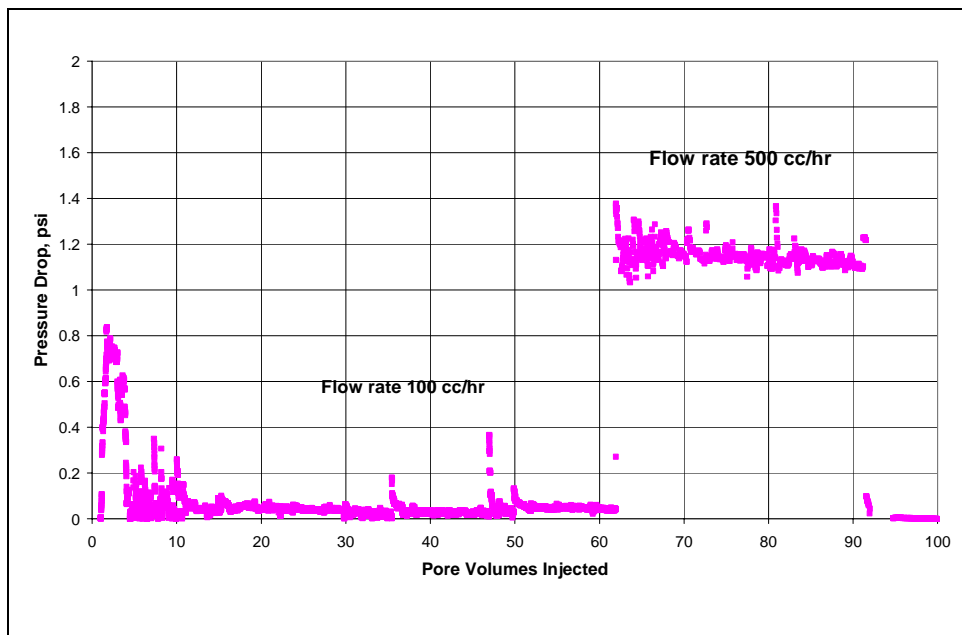


Figure B39.18: Pressure drop across the propped fracture during second surfactant treatment

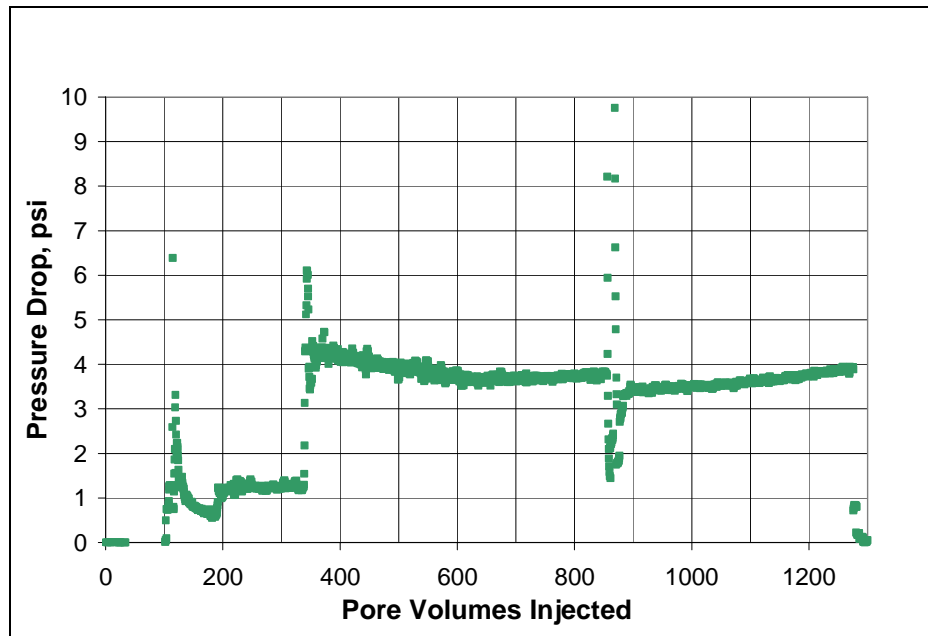


Figure B39.19 Pressure drop across the propped fracture during the gas condensate flood after second treatment

B40- Experiment No.40

Objective:

The objective of this experiment was to investigate the effect chemical FC4430L from 3M corp. on gas and condensate relative permeability. The experiment was performed on a Texas Cream limestone core at 175°F.

Experimental Results:

Table B40.1 summarizes the properties of the core and the experimental conditions. Initial permeability of the core was measured using nitrogen at 75°F. **Figure B40.1** shows the pressure drop measured across the core during nitrogen flood. **Table B40.2** summarizes the results of the nitrogen flood.

The initial water saturation of 20% was established by injecting 2.1 cc of D.I. water in the vacuumed core. Nitrogen flood was then conducted to measure the end point gas relative permeability. **Figure B40.2** shows the pressure drop measured across the core and **Table B40.3** summarizes the results of the nitrogen flood. The pressure of the core was raised to 200 psig and then the temperature of the oven was increased to 175°F.

Synthetic fluid mixture-5 (**Table 3.5**) was used for the two-phase flow measurements. The initial flood was conducted with the upstream backpressure regulator set at 4644 psig and the downstream back pressure regulator set at 9720 psig. **Table B40.4** gives the properties of the synthetic fluid calculated using the Peng-Robinson EOS at the flowing core pressure. **Figure B40.3** shows the pressure drop across the core during the two-phase gas-condensate flow. **Table B40.5** summarizes the results of the initial two-phase flow.

The core was then treated with the treatment solution (**Table B40.6**). **Figure B40.4** shows the measured pressure drop across the core during the treatment flood. The treatment solution was injected at 96cc/hr. The pressure drop kept increasing indicating plugging in the core. The rate was then dropped to 48 cc/hr after injecting 8PV of treatment solution. The pressure drop still kept on increasing and the flood was stopped after injecting 10 PV. The core was then shut-in for 18 hours. .

Post-treatment two-phase gas-condensate flood was started at a pump rate of 64 cc/hr (263 cc/hr core rate). The pressure was much higher than the initial flood. The gas mixture was then injected in the reverse direction. The gas mixture was injected at a pump rate of 128cc/hr. The pressured drop was still higher than the initial flood. The flood was then stopped. **Figure B40.5** shows the pressure drop across the core measured during the post-treatment two-phase floods. **Table B40.7** summarizes the results of the post-treatment two-phase flow.

The core was then re-treated with the treatment solution (**Table B40.6**). **Figure B40.6** shows the measured pressure drop across the core during the second treatment flood. The treatment solution was injected at 96cc/hr in the reverse direction. The pressure drop kept increasing indicating that the core is still plugged.

Post-treatment gas-condensate flood was conducted under the same conditions as the initial two-phase flow. **Figure B40.7** shows the pressure drop across the core measured during the gas condensate flood after the second treatment. **Table B40.7** summarizes the results of the gas condensate flood after the second treatment.

Table B40.1: Core properties

Core	Texas Cream Limestone
Length, inches	4.11
Diameter, inches	1
Porosity, %	20.00
Pore volume, cc	10.59
Swi, %	20
Temperature, °F	175

Table B40.2: Result of nitrogen flood

q_{core}, (cc/hr)	ΔP (psi)	k_g (md)
2415.44	21.49	17.60
3623.15	33.07	17.15
4830.87	45.16	16.75
Permeability, k_g (md)		17.02

Table B40.3: Result of nitrogen flood at Swi

q_{core}, (cc/hr)	ΔP (psi)	k_g (md)
2415.44	24.96	15.15

Table B40.4: Synthetic fluid properties at experimental conditions

Pressure, psig	4650	970	
Fluid Properties		Gas phase	Oil phase
ρ, g/cc	0.307	0.0445	0.5896
μ (cp)		0.0154	0.2045
Volume fraction		0.9446	0.0554
IFT (dyne/cm)		7.369	

Table B40.5: Results of the initial two-phase gas condensate flood

q_{pump}, cc/hr	128
$q_{\text{total_core}}$, cc/hr	526.06
$q_{\text{g_core}}$, cc/hr	496.92
$q_{\text{o_core}}$, cc/hr	29.14
ΔP, psi	63.50
k_{rg}	0.059
k_{ro}	0.046
N_{c}	9.55×10^{-6}
PVT Ratio	1.28

Table B40.6: Composition of treatment solution

Component	Weight %
FC4430L	2
2-Butoxyethanol	59
Ethanol	39

Table B40.7: Results of post-treatment two-phase flow of gas condensate mixture

q_{pump}, cc/hr	128	64
q_{total_core}, cc/hr	526.06	263.03
q_{g_core}, cc/hr	496.92	248.46
q_{o_core}, cc/hr	29.14	14.57
ΔP, psi	81.00	84.00
k_{rg}	0.046	0.023
k_{ro}	0.036	0.018
Nc	1.22x10 ⁻⁵	1.26x10 ⁻⁵
Improvement Factor	0.78	

Table B40.8: Results of post-treatment two-phase flow of gas condensate mixture

q_{pump}, cc/hr	128
q_{total_core}, cc/hr	526.06
q_{g_core}, cc/hr	496.92
q_{o_core}, cc/hr	29.14
ΔP, psi	76
k_{rg}	0.049
k_{ro}	0.038
Nc	1.14x10 ⁻⁵
Improvement Factor	0.84

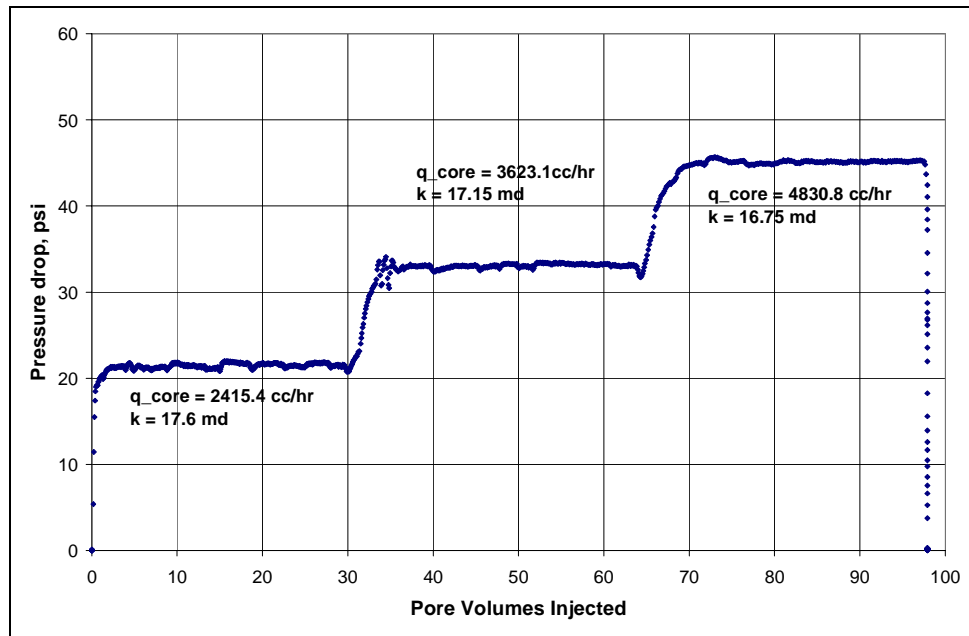


Figure B40.1: Pressure drop across the core during initial nitrogen flood

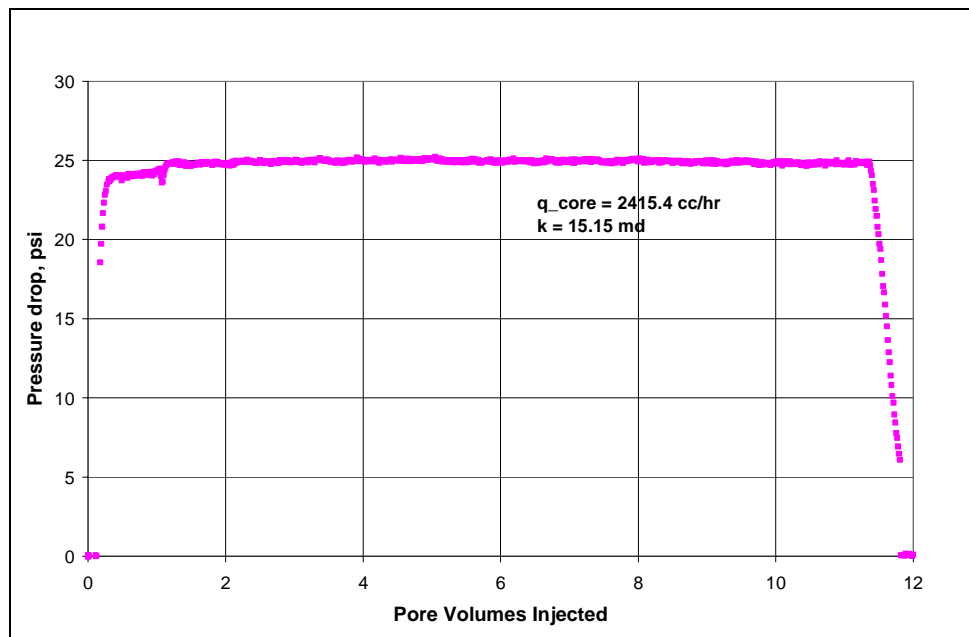


Figure B40.2: Pressure drop across the core during nitrogen flood at $S_{wi}=20\%$

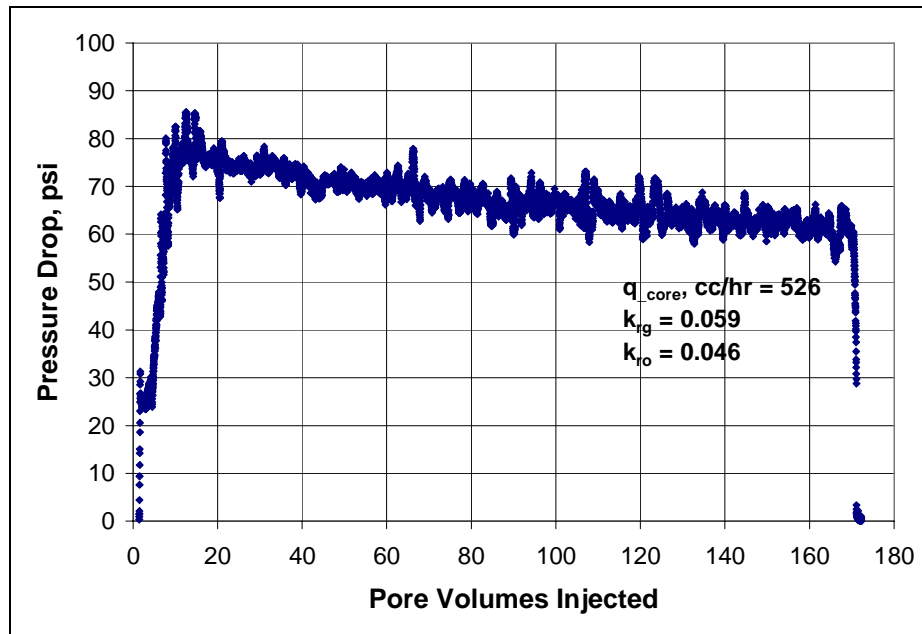


Figure B40.3: Pressure drop across the core during the initial two-phase flow at 175°F and 970 psig

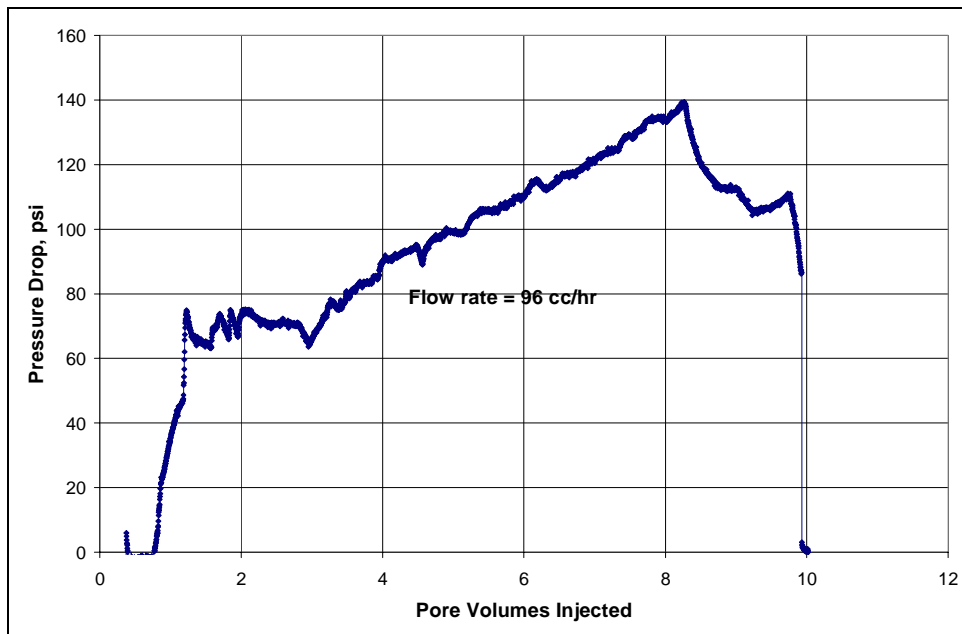


Figure B40.4: Pressure drop across the core during surfactant treatment

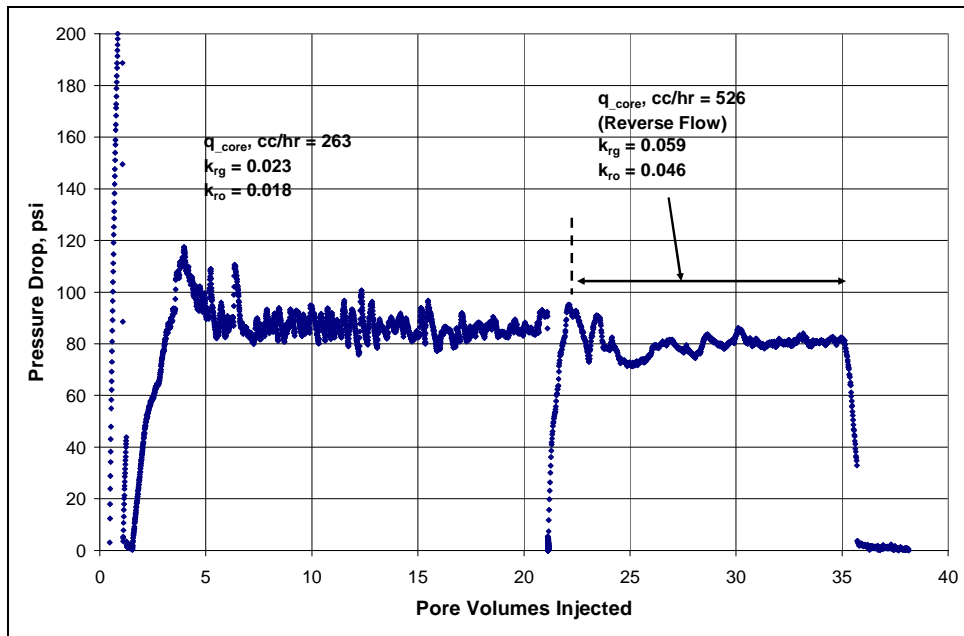


Figure B40.5: Pressure drop across the core during the post-treatment two-phase flow at 175°F and 970 psig

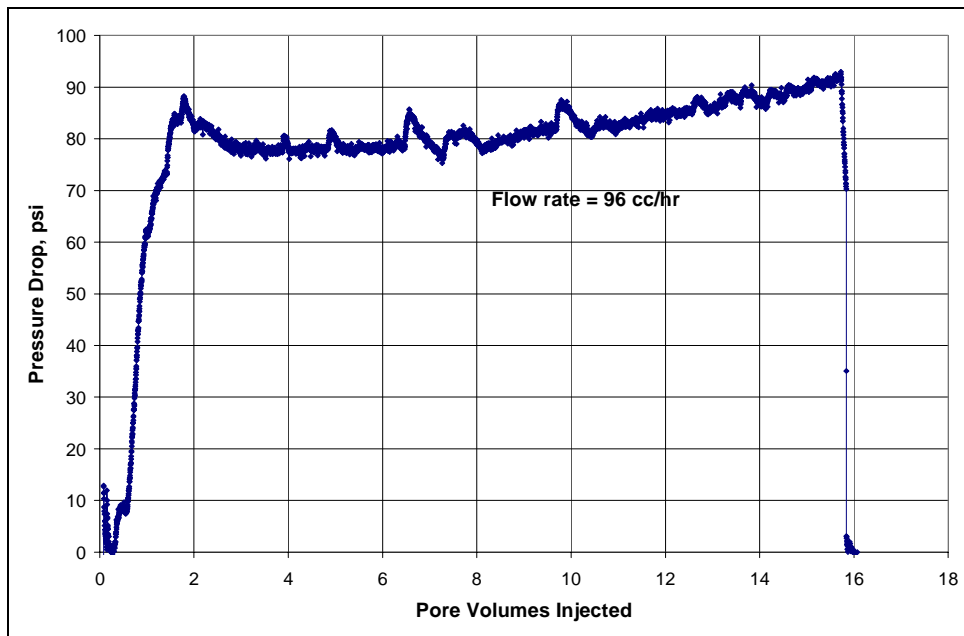


Figure B40.6: Pressure drop across the core during second surfactant treatment

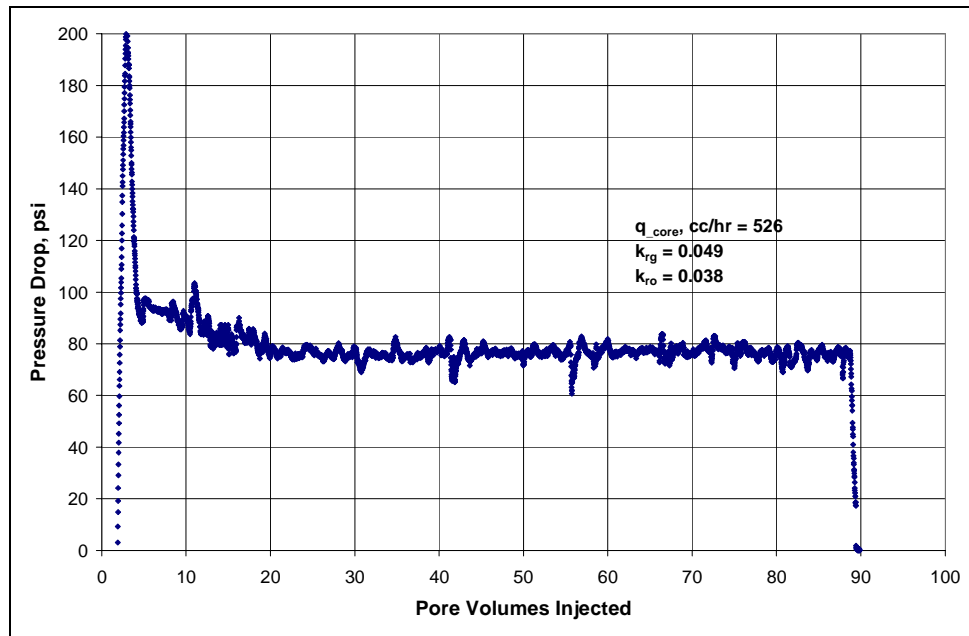


Figure B40.7: Pressure drop across the core during the gas condensate flood after the second treatment at 175°F and 970 psig

B41- Experiment No.41

Objective:

The objective of this experiment was to investigate the effect of surfactant concentration on the chemical treatment using FC4430 in a mixture of 2-butoxyethanol and ethanol. The experiment was performed on a Berea core at 175°F.

Experimental Results:

Table B41.1 summarizes the properties of the core and the experimental conditions. Initial permeability of the core was measured using nitrogen at 75°F. **Figure B41.1** shows the pressure drop measured across the core during nitrogen flood. **Table B41.2** summarizes the results of the nitrogen flood.

The initial water saturation of 20% was established by injecting 3.8 cc of synthetic Bruce brine (**Table B21.3**) in the vacuumed core. Nitrogen flood was then conducted to measure the end point gas relative permeability. **Figure B41.2** shows the pressure drop measured across the core and **Table B41.3** summarizes the results of the nitrogen flood. The pressure of the core was raised to 200 psig and then the temperature of the oven was increased to 175°F.

Synthetic fluid mixture-5 (**Table 3.5**) was used for the two-phase flow measurements. The initial flood was conducted with the upstream backpressure regulator set at 5150 psig and the downstream back pressure regulator set at 420 psig. **Table B41.4** gives the properties of the synthetic fluid calculated using the Peng-Robinson EOS at the flowing core pressure. **Figure B41.3** shows the pressure drop across the core during the two-phase gas-condensate flow. **Table B41.5** summarizes the results of the initial two-phase flow.

The core was then treated with the treatment solution (**Table B41.6**). **Figure B41.4** shows the measured pressure drop across the core during the treatment flood. The treatment solution was injected at 112 cc/hr. Effluent samples were collected for every 0.2 PV for the first 4 pore volumes and then every 0.4 PV. The core was then shut-in for 19 hours.

Post-treatment two-phase gas-condensate flood was conducted under the same conditions as the initial two-phase flow. **Figure B41.5** shows the pressure drop across the core measured during the post-treatment two-phase floods at a flowing pressure of 400 psig. **Table B41.7** summarizes the results of the post-treatment two-phase flow.

Table B41.1: Core properties

Core	Berea Sandstone
Length, inches	8
Diameter, inches	1
Porosity, %	19.09
Pore volume, cc	19.04
Swi, %	20
Temperature, °F	175

Table B41.2: Result of nitrogen flood

q_{core}, (cc/hr)	ΔP (psi)	k_g (md)
2679.88	3.06	275.38
4287.81	5.04	267.17
6565.71	7.82	263.95
Permeability, k_g (md)		268.83

Table B41.3: Result of nitrogen flood at Swi

q_{core}, (cc/hr)	ΔP (psi)	k_g (md)
4287.81	7.62	176.90

Table B41.4: Synthetic fluid properties at experimental conditions

Pressure, psig	5150	420	
Fluid Properties		Gas phase	Oil phase
ρ, g/cc	0.2925	0.0196	0.6696
μ (cp)		0.0133	0.4081
Volume fraction		0.9877	0.0123
IFT (dyne/cm)		12.976	

Table B41.5: Results of the initial two-phase gas condensate flood

q_{pump}, cc/hr	256
$q_{\text{total_core}}$, cc/hr	2713.54
$q_{\text{g_core}}$, cc/hr	2680.16
$q_{\text{o_core}}$, cc/hr	33.38
ΔP, psi	39.11
k_{rg}	0.057
k_{ro}	0.022
Nc	2.64×10^{-5}
PVT Ratio	2.62

Table B41.6: Composition of treatment solution

Component	Weight %
FC4430	1
2-butoxyethanol	69.5
Ethanol	29.5

Table B41.7: Results of post-treatment two-phase flow of gas condensate mixture

q_{pump}, cc/hr	256
q_{total_core}, cc/hr	2713.54
q_{g_core}, cc/hr	2680.16
q_{o_core}, cc/hr	33.38
ΔP, psi	16.58
k_{rg}	0.135
k_{ro}	0.052
Nc	1.12x10 ⁻⁵
Improvement Factor	2.36

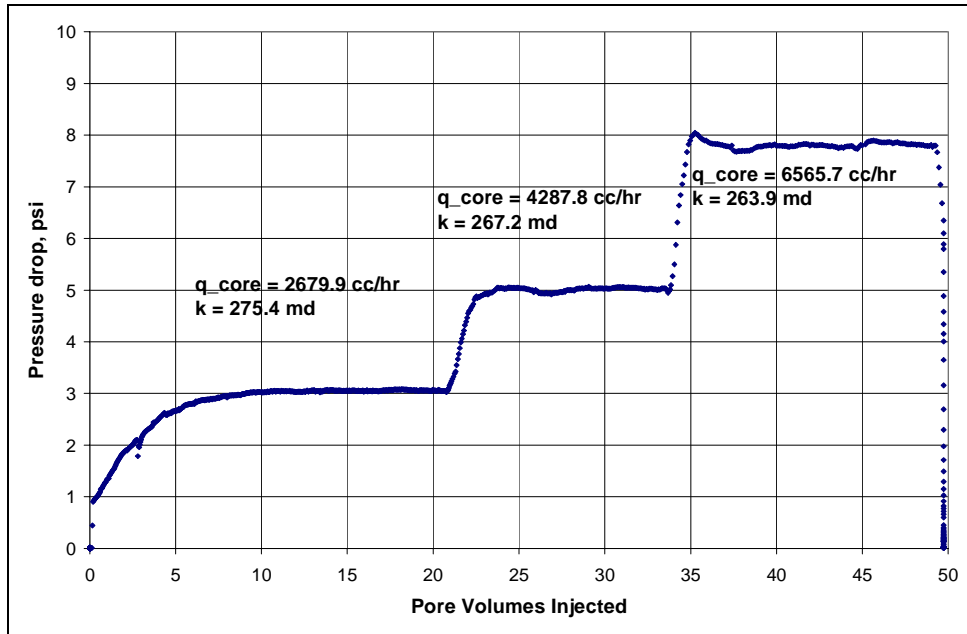


Figure B41.1: Pressure drop across the core during initial nitrogen flood

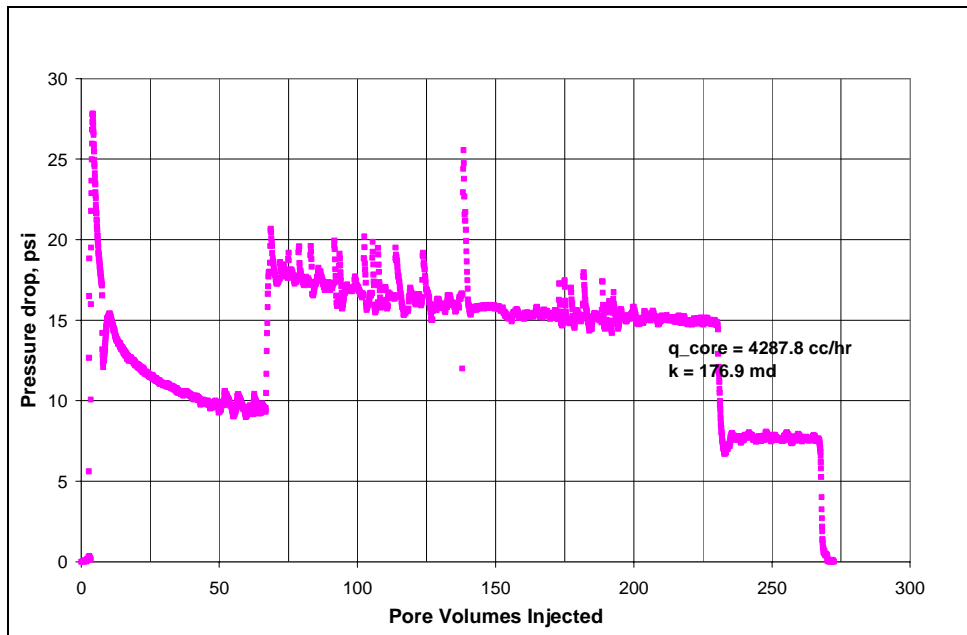


Figure B41.2: Pressure drop across the core during nitrogen flood at $Sw_i=19\%$

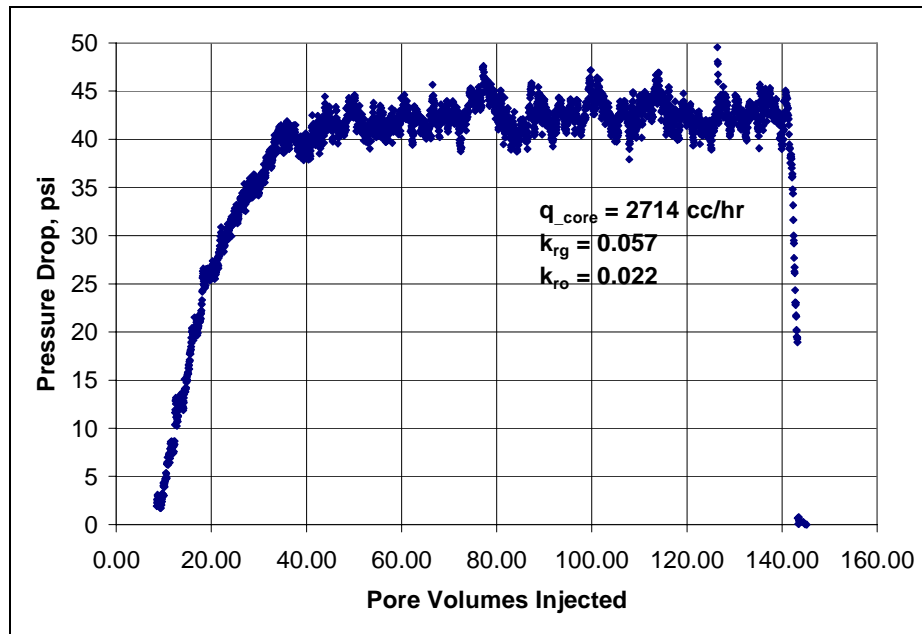


Figure B41.3: Pressure drop across the core during the initial two-phase flow at 175°F and 420 psig

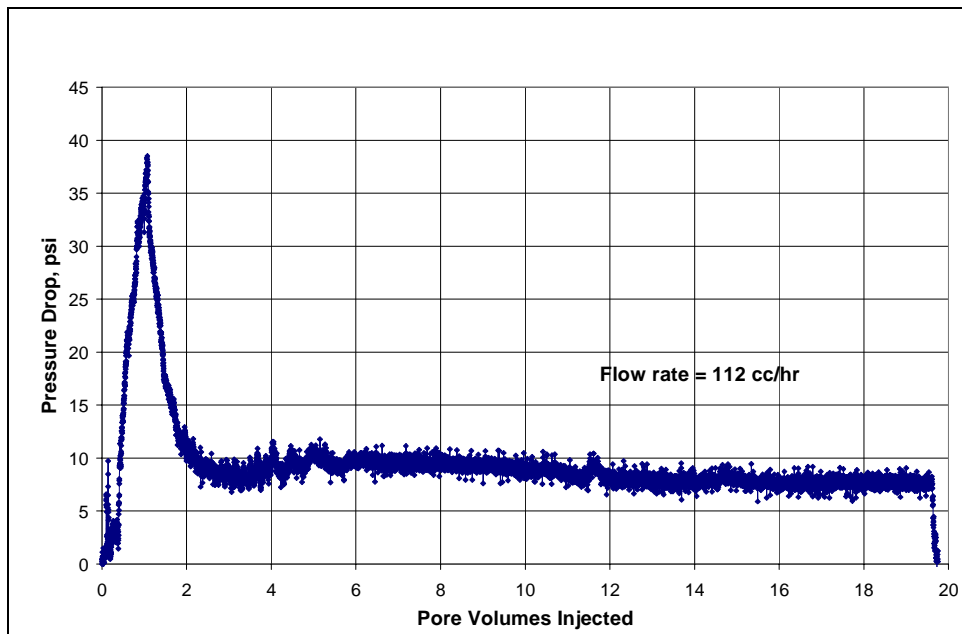


Figure B41.4: Pressure drop across the core during surfactant treatment

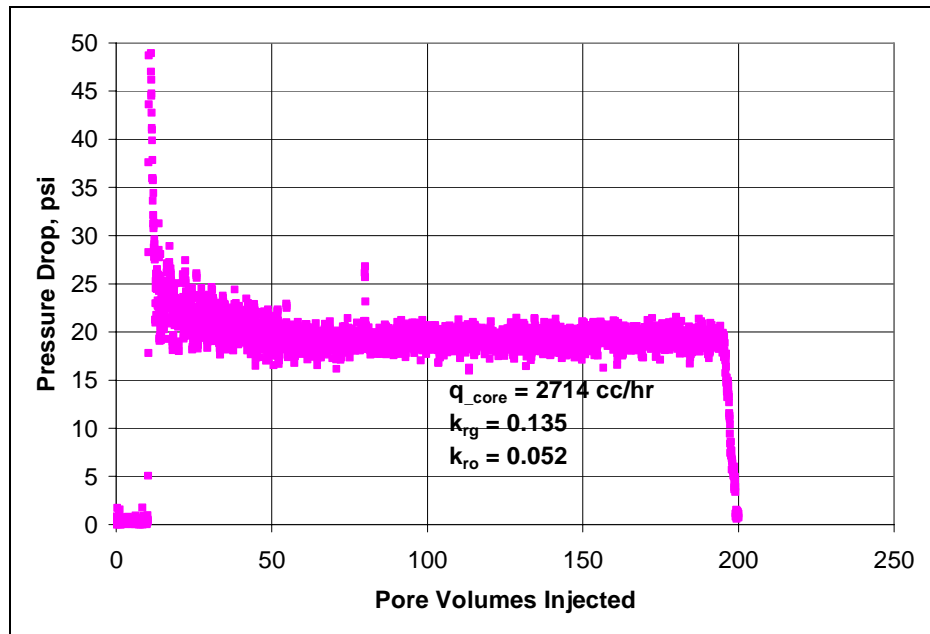


Figure B41.5: Pressure drop across the core during post-treatment two-phase flow at 175°F and 420 psig

B42- Experiment No.42

Objective:

The objective of this experiment was to investigate the effect of surfactant concentration (0.1 wt%) on the chemical treatment using FC4430 in a mixture of 2-butoxyethanol and ethanol. The experiment was performed on a Berea core at 175°F.

Experimental Results:

Table B42.1 summarizes the properties of the core and the experimental conditions. Initial permeability of the core was measured using nitrogen at 75°F. **Figure B42.1** shows the pressure drop measured across the core during nitrogen flood. **Table B42.2** summarizes the results of the nitrogen flood.

The initial water saturation of 20% was established by injecting 4 cc of synthetic Bruce brine (**Table B21.3**) in the vacuumed core. Nitrogen flood was then conducted to measure the end point gas relative permeability. **Figure B42.2** shows the pressure drop measured across the core and **Table B42.3** summarizes the results of the nitrogen flood. The pressure of the core was raised to 200 psig and then the temperature of the oven was increased to 175°F.

Synthetic fluid mixture-5 (**Table 3.5**) was used for the two-phase flow measurements. The initial flood was conducted with the upstream backpressure regulator set at 5150 psig and the downstream back pressure regulator set at 420 psig. **Table B41.4** gives the properties of the synthetic fluid calculated using the Peng-Robinson EOS at the flowing core pressure. **Figure B42.3** shows the pressure drop across the core during the two-phase gas-condensate flow. **Table B42.5** summarizes the results of the initial two-phase flow.

The core was then treated with the treatment solution (**Table B42.6**). **Figure B42.4** shows the measured pressure drop across the core during the treatment flood. 45 PV of treatment solution was injected at 128 cc/hr. Effluent samples were collected for every 0.2 PV for the first 10.8 pore volumes, every 0.4 PV for the next 8 pore volumes and finally every 0.8PV for the rest of the flood. The core was then shut-in for 14.5 hours.

Post-treatment two-phase gas-condensate flood was conducted under the same conditions as the initial two-phase flow. **Figure B42.5** shows the pressure drop across the core measured during the post-treatment two-phase flood at a flowing pressure of 420 psig. **Table B42.7** summarizes the results of the post-treatment two-phase flow.

Finally, the post-treatment permeability of the core was measured using methane to find out if the final gas permeability was as high as the initial gas permeability. **Table B42.8** summarizes the results.

Table B42.1: Core properties

Core	Berea Sandstone
Length, inches	8
Diameter, inches	1
Porosity, %	19.09
Pore volume, cc	19.04
Swi, %	20
Temperature, °F	175

Table B42.2: Result of nitrogen flood

q_{core}, (cc/hr)	ΔP (psi)	k_g (md)
2679.88	3.06	275.38
4287.81	5.04	267.17
6565.71	7.82	263.95
Permeability, k_g (md)		268.83

Table B42.3: Result of nitrogen flood at Swi

q_{core}, (cc/hr)	ΔP (psi)	k_g (md)
4287.81	7.62	176.90

Table B42.4: Synthetic fluid properties at experimental conditions

Pressure, psig	5150	420	
Fluid Properties		Gas phase	Oil phase
ρ, g/cc	0.2925	0.0196	0.6696
μ (cp)		0.0133	0.4081
Volume fraction		0.9877	0.0123
IFT (dyne/cm)		12.976	

Table B42.5: Results of the initial two-phase gas condensate flood

q_{pump}, cc/hr	256
$q_{\text{total_core}}$, cc/hr	2713.54
$q_{\text{g_core}}$, cc/hr	2680.16
$q_{\text{o_core}}$, cc/hr	33.38
ΔP, psi	39.11
k_{rg}	0.057
k_{ro}	0.022
Nc	2.64×10^{-5}
PVT Ratio	2.62

Table B42.6: Composition of treatment solution

Component	Weight %
FC4430	0.1
2-butoxyethanol	70
Ethanol	29.9

Table B42.7: Results of post-treatment two-phase flow of gas condensate mixture

q_{pump}, cc/hr	256
q_{total_core}, cc/hr	2713.54
q_{g_core}, cc/hr	2680.16
q_{o_core}, cc/hr	33.38
ΔP, psi	16.58
k_{rg}	0.135
k_{ro}	0.052
Nc	1.12x10 ⁻⁵
Improvement Factor	2.36

Table B42.8: Result of methane flood to measure final permeability

q _{core} , (cc/hr)	ΔP (psi)	k _g (md)
2913.39	4.20	214.58

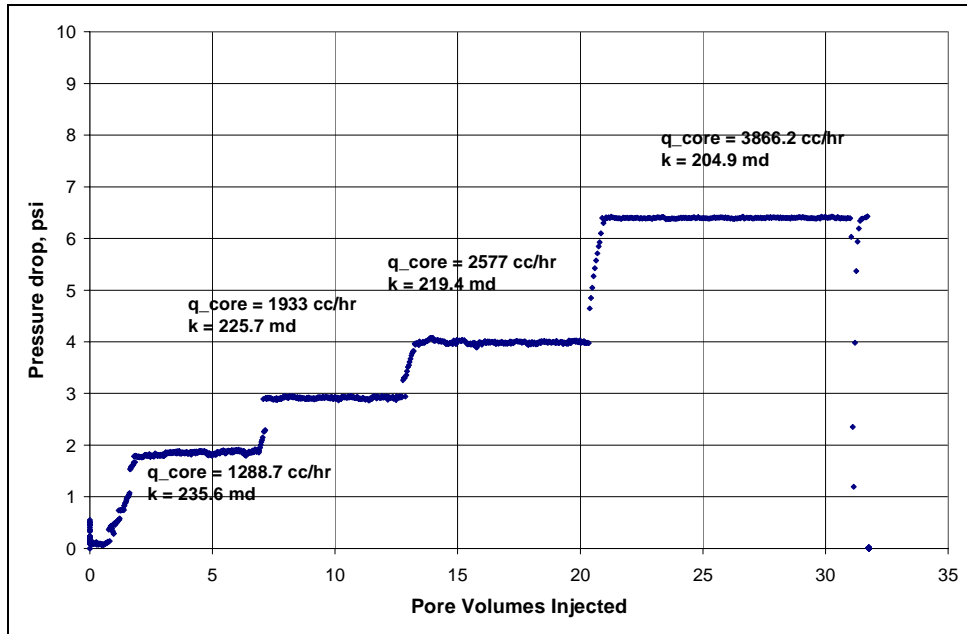


Figure B42.1: Pressure drop across the core during initial nitrogen flood

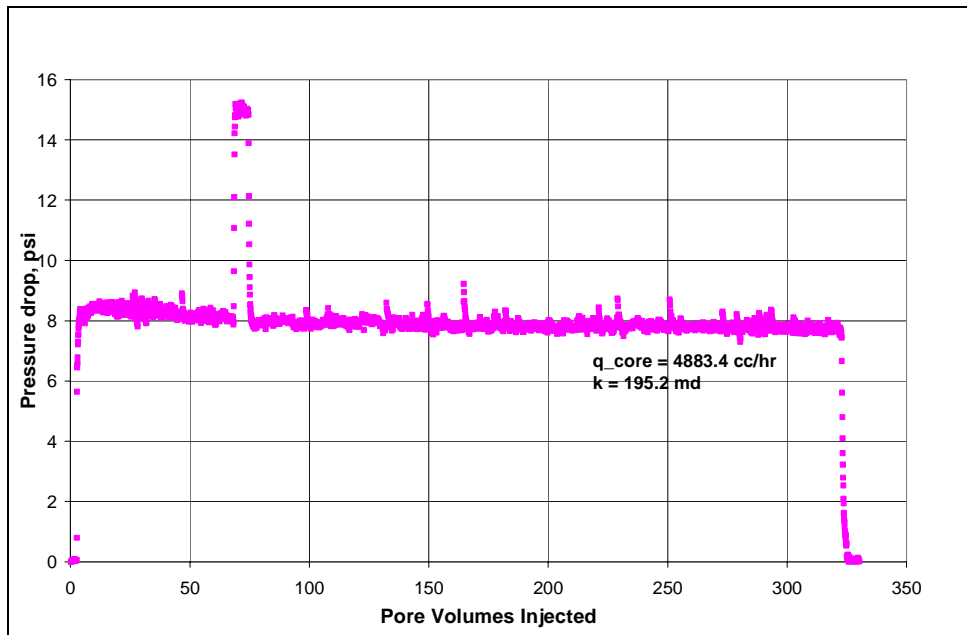


Figure B42.2: Pressure drop across the core during nitrogen flood at $Sw_i = 19\%$

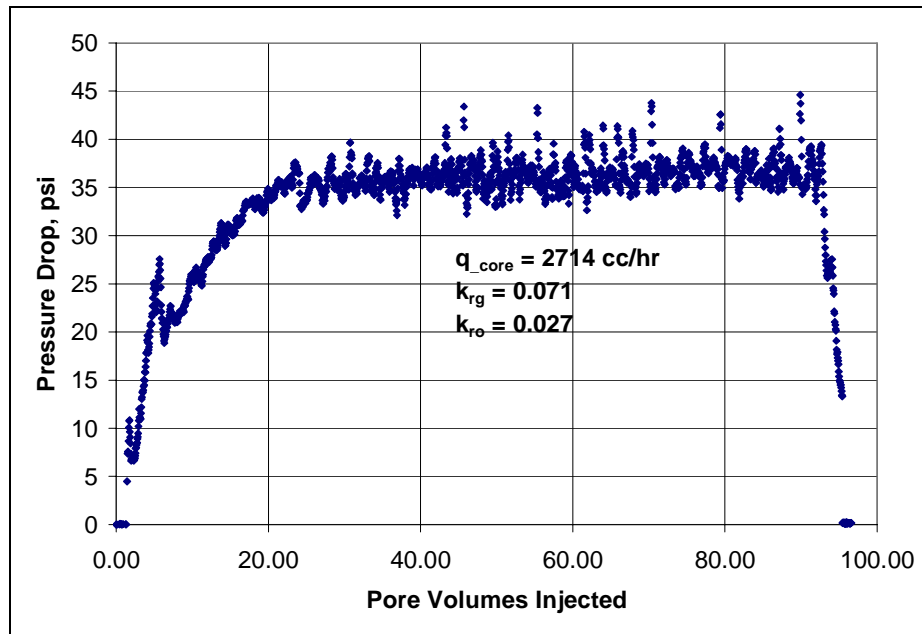


Figure B42.3: Pressure drop across the core during the initial two-phase flow at 175°F and 420 psig

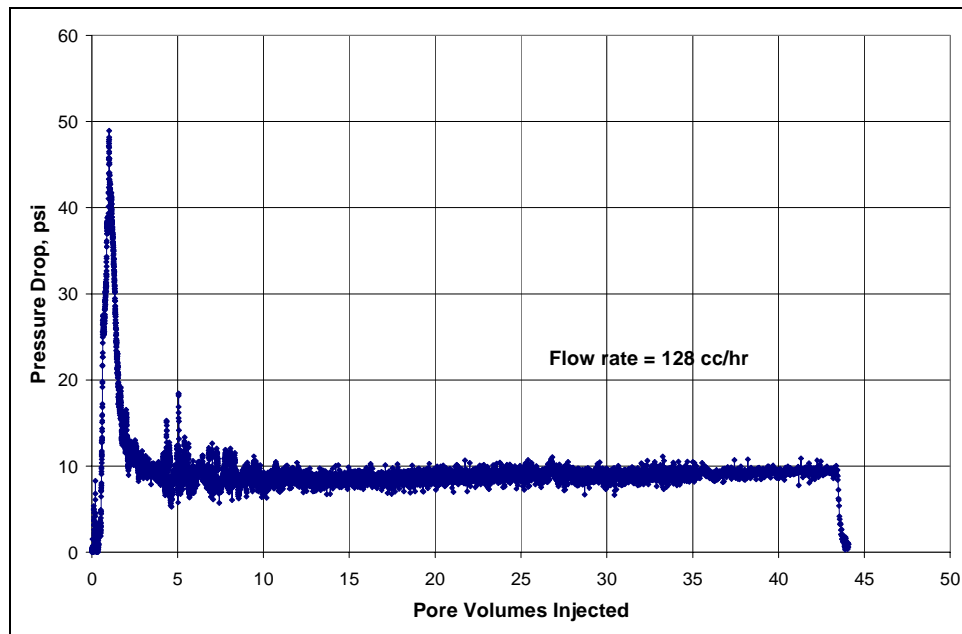


Figure B42.4: Pressure drop across the core during surfactant treatment

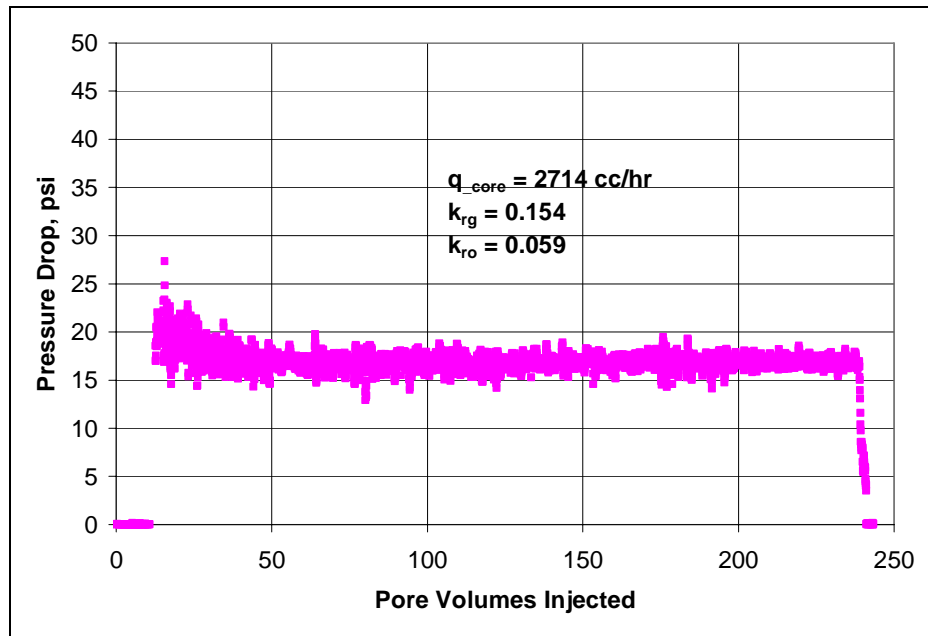


Figure B42.5: Pressure drop across the core during post-treatment two-phase flow at 175°F and 420 psig

B43- Experiment No.43

Objective:

The objective of this experiment was to investigate the effect of net-confining stress and non-Darcy flow on gas and condensate relative permeability measured on a propped fracture. The experiment was performed using Ottawa F35 sand as proppant at 175°F.

Experimental Results:

Berea core was used as the matrix rock and Ottawa F35 sand was used as the proppant to fill the simulated fracture void. This sand has an average mesh size of about 35 corresponding to an average grain diameter of on the order of 0.02 cm.

Table B43.1 summarizes the properties of the propped fracture and the experimental conditions. Initial permeability of the propped fracture was measured using nitrogen at 75°F. Measurements were done at 1000 psi, 2000 psi, 3000 psi, 4000 psi and 5000 psi of net confining stress. Measurements were done at multiple rates at each net confining stress to capture the effect of non-Darcy flow on single-phase gas permeability. **Figure B43.1** shows the pressure drop measured across the core during nitrogen flood at different net confining stress and flow rates. **Tables B43.2 to B43.6** summarize the results of the nitrogen flood at different net confining stress. The average permeability of the fracture was calculated from the intercept of the plot of $(\Delta P/v/l)$ vs velocity. **Figures B43.2 to B43.6** shows the plot of $(\Delta P/v/l)$ vs velocity for data measured at different net confining stress. As permeability of the fracture is 100 times more than the permeability of the rock matrix, most of the flow will be through the fracture and thus the pressure drop measured across the core will be same as the pressure drop across the fracture.

45 Pore volumes of synthetic Bruce brine (**Table B21.3**) was flowed through the fracture. Nitrogen flood was then conducted to reduce the water saturation to residual and measure the end point gas relative permeability. Nitrogen flood at Swi was conducted at multiple flow rates and multiple net confining stresses. **Figure B43.7** shows the pressure drop across the fracture during the nitrogen flood. **Tables B43.7 to B43.9** summarize the results of the nitrogen flood at different net confining stresses. The average gas permeability at Swi was calculated from the intercept of the plot of $(\Delta P/v/l)$ vs velocity. **Figures B43.8 to B43.10** shows the plot of $(\Delta P/v/l)$ vs velocity for data measured at different net confining stress.

Synthetic fluid mixture-5 (**Table 3.5**) was used for the two-phase flow measurements. The gas condensate flood was done at different core pressure to measure data at different PVT ratios and over a wide range of gas velocities. The first gas condensate flood was conducted with the upstream backpressure regulator set at 5200 psig and the downstream back pressure regulator set at 3200 psig. **Table B43.10** gives the properties of the synthetic fluid calculated using the Peng-Robinson EOS at the flowing core pressures. **Figure B43.11** shows the pressure drop across the fracture measured during the initial gas condensate flood at 3200 psig. Second gas condensate flood was done at core pressure of 3750 psig. **Figure B43.12** shows the pressure drop across the fracture measured during the initial gas condensate flood at 3750 psig. Third gas condensate flood was done at core pressure of 400 psig. **Figure B43.13** shows the pressure drop across the fracture measured during the initial gas condensate flood at 400 psig. The pressure drop during the gas condensate flood went as high as 85 psi. This high pressure gradient across the fracture can cause the sand to move and change the fracture properties such as its permeability. Gas condensate floods were then done at core pressures of 3200 psig and 3750 psig again. **Figures B43.14 and B43.15** show the

pressure drops during the gas condensate floods at 3200 psig and 3750 psig core pressures. **Tables B43.11, B43.12 and B43.13** summarize the results of gas condensate floods at 3200 psig, 3750 psig and 400 psig core pressures respectively. The relative permeability data has been corrected for non-Darcy flow effects.

The core was then treated with the treatment solution (**Table B43.14**). **Figure B43.16** shows the measured pressure drop across the core during the treatment flood. 90 PV of treatment solution was injected. The treatment solution was injected at 40 cc/hr for the first 38 pore volumes. The rate was then increased to 160 cc/hr and finally increased to 320 cc/hr. The core was then shut-in for 15 hours.

Post-treatment two-phase gas-condensate flood was conducted at the core pressure of 3200 psig. **Figure B43.17** shows the pressure drop measured during the post-treatment gas condensate flood. **Table B43.15** summarizes the results for the gas condensate flood after the treatment.

Finally, the post-treatment permeability of the fracture was measured using methane to find out if the final gas permeability was as high as the initial gas permeability. **Figure B43.18** shows the pressure drop during the methane flood and **Table B43.16** summarizes the results.

Table B43.1: Core and fracture properties

Core	Berea Sandstone
Proppant	Ottawa F35 sand
Fracture Aperture, cm	0.225
Length, inches	7
Fracture width, cm	2.49
Porosity, %	37.50
Pore volume, cc	4.20
Swi, %	-
Temperature, °F	175

Table B43.2: Result of nitrogen flood at a net confining stress of 1000 psig

q_{core}, (cc/hr)	ΔP (psi)	k_g (Darcy)
8329.15	2.34	10.12
5552.76	1.22	12.94
4164.57	0.74	15.99
2776.38	0.37	21.33
1388.19	0.16	24.66
Permeability, k_g (md) (corrected for non Darcy)		43.39
β (1/cm) = 4.65x10³		

Table B43.3: Result of nitrogen flood at a net confining stress of 2000 psig

q_{core}, (cc/hr)	ΔP (psi)	k_g (Darcy)
8329.15	2.34	10.12
5552.76	1.22	12.94
4164.57	0.74	15.99
2776.38	0.38	20.76
1388.19	0.17	23.21
Permeability, k_g (md) (corrected for non Darcy)		41.13
β (1/cm) = 4.26x10³		

Table B43.4: Result of nitrogen flood at a net confining stress of 3000 psig

q_{core}, (cc/hr)	ΔP (psi)	k_g (Darcy)
8329.15	2.40	9.86
5552.76	1.22	12.94
4164.57	0.75	15.78
2776.38	0.40	19.73
1388.19	0.18	21.92
Permeability, k_g (md) (corrected for non Darcy)		39.15
β (1/cm) = 4.21x10³		

Table B43.5: Result of nitrogen flood at a net confining stress of 4000 psig

q_{core}, (cc/hr)	ΔP (psi)	k_g (Darcy)
8329.15	2.45	9.66
5552.76	1.23	12.83
4164.57	0.76	15.57
2776.38	0.41	19.25
1388.19	0.19	20.76
Permeability, k_g (md) (corrected for non Darcy)		38.67
β (1/cm) = 4.46x10³		

Table B43.6: Result of nitrogen flood at a net confining stress of 5000 psig

q_{core}, (cc/hr)	ΔP (psi)	k_g (Darcy)
8329.15	2.60	9.10
5552.76	1.26	12.52
4164.57	0.84	14.09
2776.38	0.45	17.53
1388.19	0.20	19.73
Permeability, k_g (md) (corrected for non Darcy)		32.74
β (1/cm) = 4.58x10³		

Table B43.7: Result of nitrogen flood at Swi at a net confining stress of 1000 psig

q_{core}, (cc/hr)	ΔP (psi)	k_g (Darcy)
8329.15	2.90	8.16
5552.76	1.40	11.27
4164.57	0.91	13.01
2776.38	0.46	17.15
1388.19	0.19	20.76
Permeability, k_g (md) (corrected for non Darcy)		32.52
β (1/cm) = 5.57x10³		

Table B43.8: Result of nitrogen flood at Swi at a net confining stress of 3000 psig

q_{core}, (cc/hr)	ΔP (psi)	k_g (Darcy)
8329.15	3.05	7.76
5552.76	1.45	10.88
4164.57	0.95	12.46
2776.38	0.51	15.47
1388.19	0.20	19.73
Permeability, k_g (md) (corrected for non Darcy)		29.67
β (1/cm) = 5.69x10³		

Table B43.9: Result of nitrogen flood at Swi at a net confining stress of 5000 psig

q_{core}, (cc/hr)	ΔP (psi)	k_g (Darcy)
8329.15	3.25	7.28
5552.76	1.60	9.86
4164.57	1.00	11.84
2776.38	0.54	14.61
1388.19	0.20	19.73
Permeability, k_g (md) (corrected for non Darcy)		29.24
β (1/cm) = 6.25x10³		

Table B43.10: Synthetic fluid properties at experimental conditions

Pressure, psig	5200	3750		3200		400	
Fluid Properties		Gas phase	Oil phase	Gas phase	Oil phase	Gas phase	Oil phase
ρ, g/cc	0.2951	0.2089	0.4718	0.1721	0.5087	0.0187	0.6709
μ (cp)		0.0265	0.1071	0.0224	0.1331	0.0132	0.4115
Volume fraction		0.8804	0.1196	0.8818	0.1182	0.9883	0.0117
IFT (dyne/cm)		0.225		0.697		13.065	

Table B43.11: Results of the initial two-phase gas condensate flood at 3200 psig

q_{pump}, cc/hr	200	400	800	1500	2000	3000	4000	5000	6000
q_{total_core}, cc/hr	278.55	557.09	114.18	2089.09	2785.46	4178.19	5570.92	6963.65	8356.38
q_{g_core}, cc/hr	245.62	491.24	982.49	1842.16	2456.22	3684.33	4912.43	6140354	7368.65
q_{o_core}, cc/hr	32.92	65.85	131.70	246.93	329.24	496.86	658.48	823.10	987.72
ΔP, psi	0.27	0.51	1.10	2.40	3.60	6.90	10.70	14.10	18.80
k_{rg}	0.07	0.091	0.099	0.109	0.112	0.110	0.115	0.136	0.145
k_{ro}	0.055	0.058	0.054	0.046	0.041	0.032	0.028	0.026	0.023
Nc	5.42×10^{-4}	1.02×10^{-3}	2.21×10^{-3}	4.82×10^{-3}	7.23×10^{-3}	1.38×10^{-2}	2.15×10^{-2}	2.83×10^{-2}	3.77×10^{-2}
PVT	1.32	1.32	1.32	1.32	1.32	1.32	1.32	1.32	1.32
Ratio									

Table B43.12: Results of the initial two-phase gas condensate flood at 3750 psig

q_{pump} , cc/hr	200	400	800	1500	2000	3000	4000	5000	6000
$q_{\text{total_core}}$, cc/hr	245.57	491.13	892.26	1841.74	2455.66	3683.49	4911.32	6139.15	7366.98
$q_{\text{g_core}}$, cc/hr	216.20	432.39	864.78	1621.47	2161.96	3242.94	4323.92	5404.90	6485.89
$q_{\text{o_core}}$, cc/hr	29.37	58.74	117.48	220.27	293.70	440.55	587.39	734.24	881.09
ΔP , psi	0.23	0.39	0.84	1.70	2.50	4.50	6.50	9.00	12.20
k_{rg}	0.096	0.125	0.138	0.169	0.181	0.198	0.238	0.266	0.278
k_{ro}	0.048	0.057	0.053	0.049	0.045	0.037	0.034	0.031	0.027
Nc	1.43×10^{-3}	2.42×10^{-3}	5.22×10^{-3}	1.06×10^{-2}	1.55×10^{-2}	2.80×10^{-2}	4.04×10^{-2}	5.60×10^{-2}	7.59×10^{-2}
PVT Ratio	1.73	1.73	1.73	1.73	1.73	1.73	1.73	1.73	1.73

Table B43.13: Results of the initial two-phase gas condensate flood at 400 psig

q_{pump}, cc/hr	200	100	400	800	1500	2000	3000
q_{total core}, cc/hr	2241.49	1120.74	4482.97	8965.95	16811.15	22414.87	33622.30
q_{g core}, cc/hr	2215.26	1107.63	4430.52	8861.04	16614.46	22152.61	33228.92
q_{o core}, cc/hr	26.23	13.11	52.45	104.90	196.69	262.25	393.38
ΔP, psi	1.65	0.80	4.20	10.30	22.85	38.00	85.00
k_{rg}	0.072	0.069	0.063	0.062	0.070	0.064	0.052
k_{ro}	0.023	0.024	0.018	0.015	0.013	0.010	0.007
Nc	1.77x10 ⁻⁴	8.57x10 ⁻⁵	4.50x10 ⁻⁴	1.10x10 ⁻³	2.45x10 ⁻³	4.07x10 ⁻³	9.10x10 ⁻³
PVT Ratio	2.71	2.71	2.71	2.71	2.71	2.71	2.71

Table B43.14: Composition of treatment solution

Component	Weight %
FC4430	1
2-Butoxyethanol	69
Ethanol	29

Table B43.15: Results of post-treatment gas condensate flood at 3300 psig

q_{pump}, cc/hr	200
q_{total_core}, cc/hr	278.55
q_{g_core}, cc/hr	245.62
q_{o_core}, cc/hr	32.92
ΔP, psi	0.37
k_{rg}	0.053
k_{ro}	0.042
Nc	3.95x10 ⁻⁵
Improvement Factor	0.73

Table B43.16: Result of methane flood to measure final permeability

q _{core} , (cc/hr)	ΔP (psi)	k _g (Darcy)
1863.00	0.26	16.81
1241.00	0.17	17.13
Permeability, k_g (md) (corrected for non Darcy)		17.76

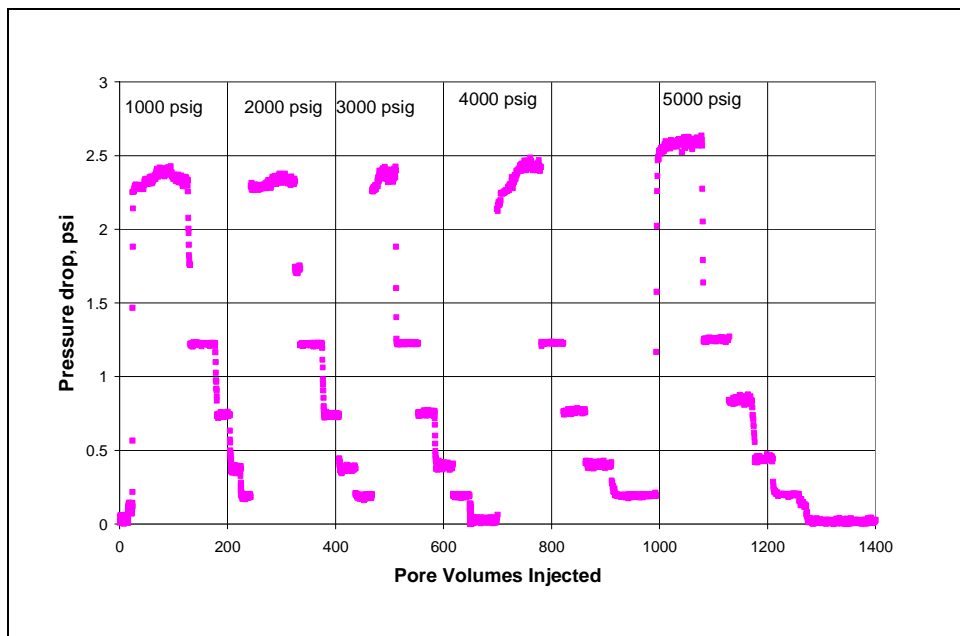


Figure B43.1: Pressure drop across the propped fracture during initial nitrogen flood at different net confining stresses

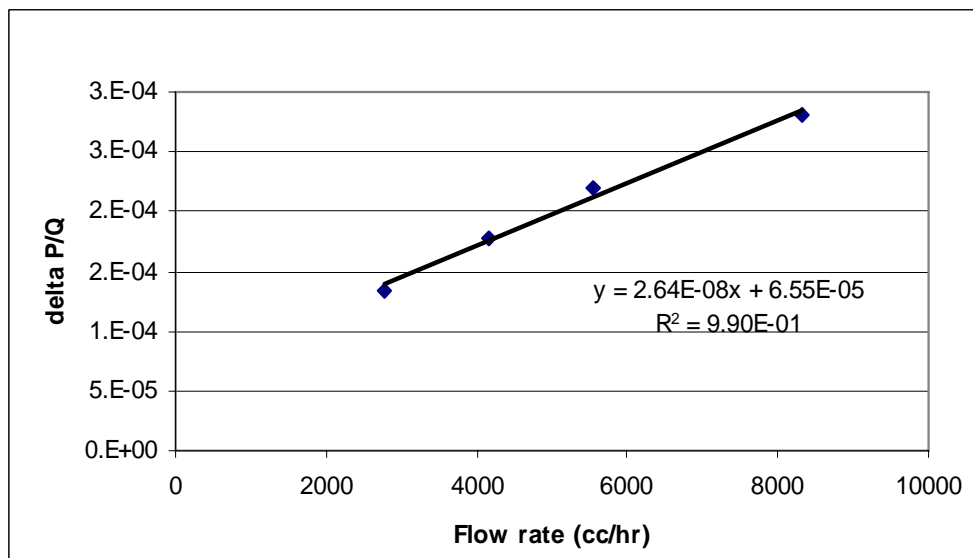


Figure B43.2: Correcting gas permeability measurement for non-Darcy flow at net confining stress of 1000 psig

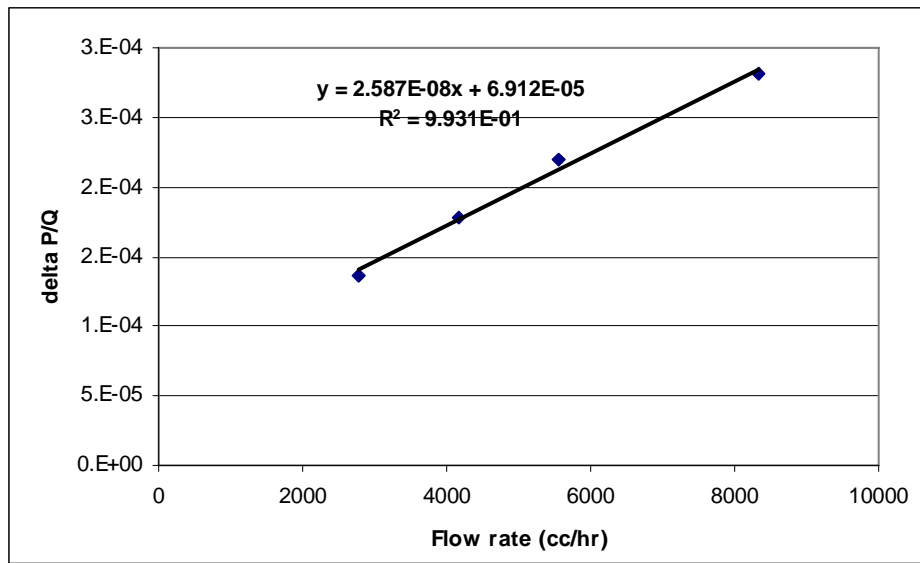


Figure B43.3: Correcting gas permeability measurement for non-Darcy flow at net confining stress of 2000 psig

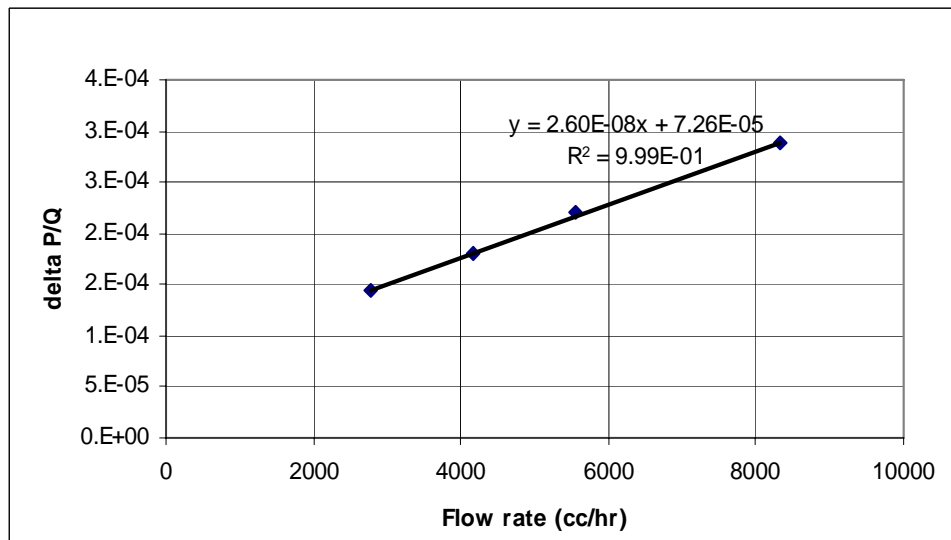


Figure B43.4: Correcting gas permeability measurement for non-Darcy flow at net confining stress of 3000 psig

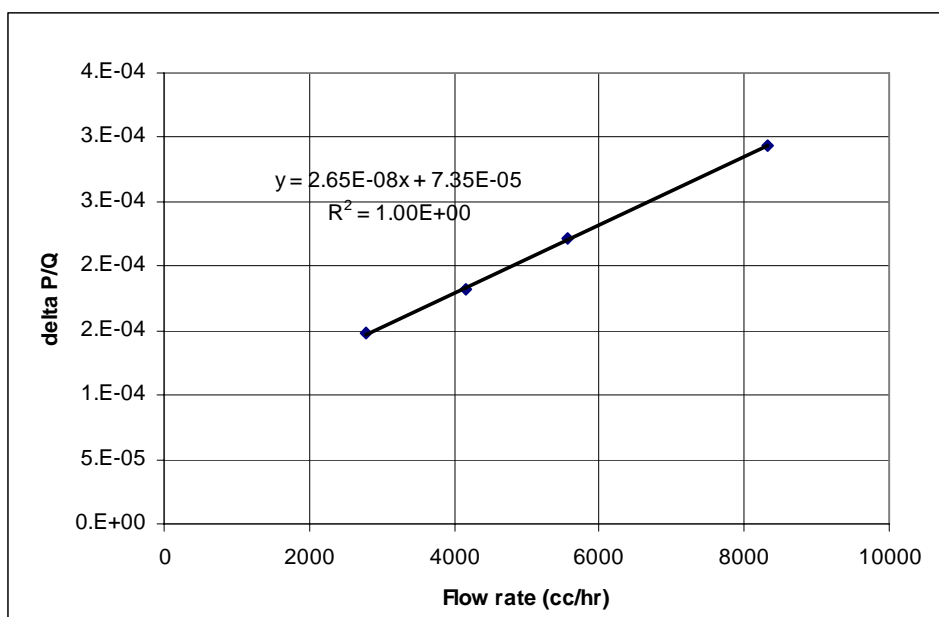


Figure B43.5: Correcting gas permeability measurement for non-Darcy flow at net confining stress of 4000 psig

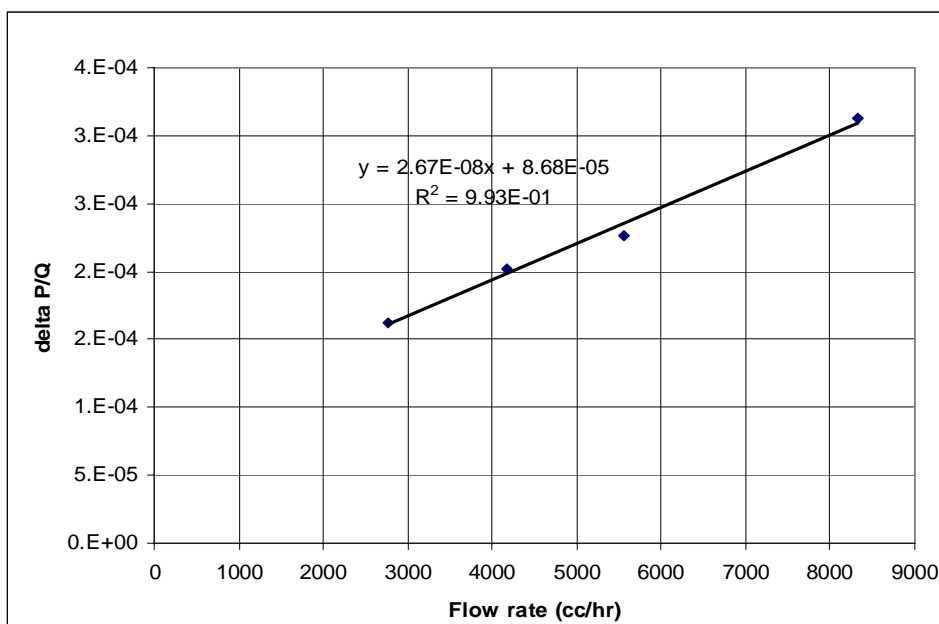


Figure B43.6: Correcting gas permeability measurement for non-Darcy flow at net confining stress of 5000 psig

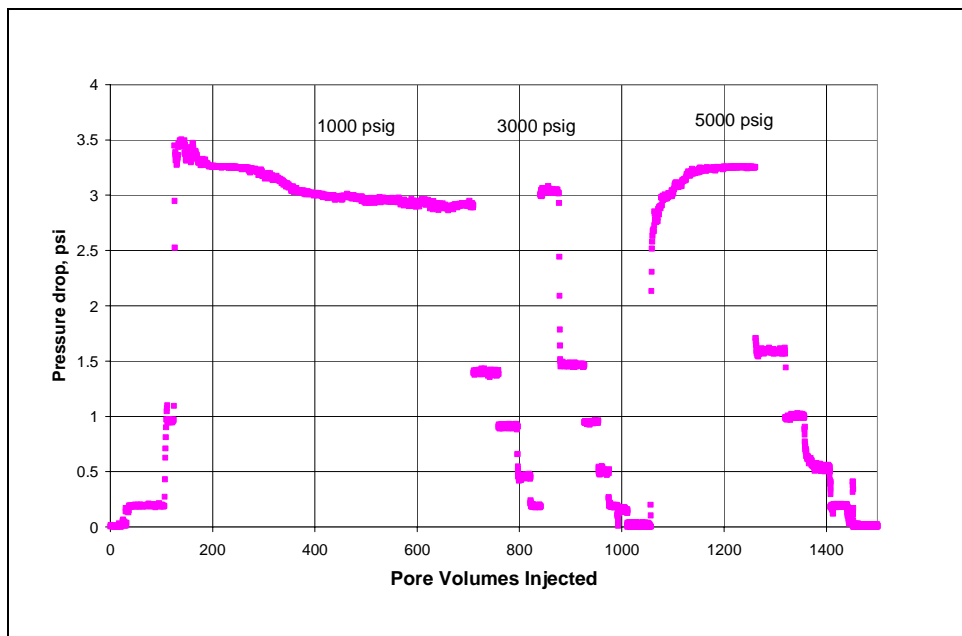


Figure B43.7: Pressure drop across the propped fracture during initial nitrogen flood at Swi at different net confining stresses

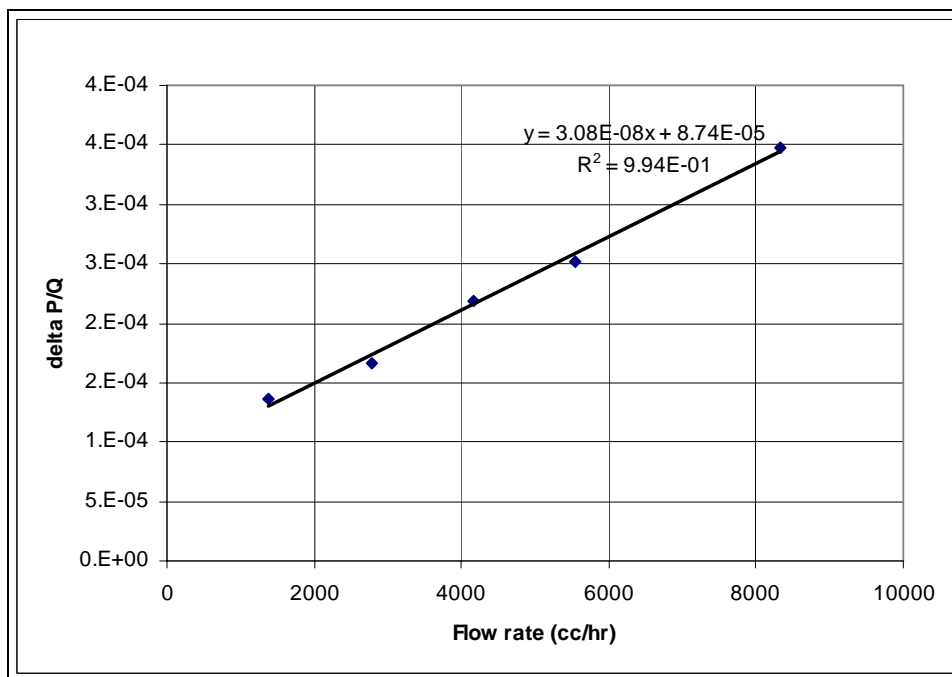


Figure B43.8: Correcting gas permeability measurement at Swi for non-Darcy flow at net confining stress of 1000 psig

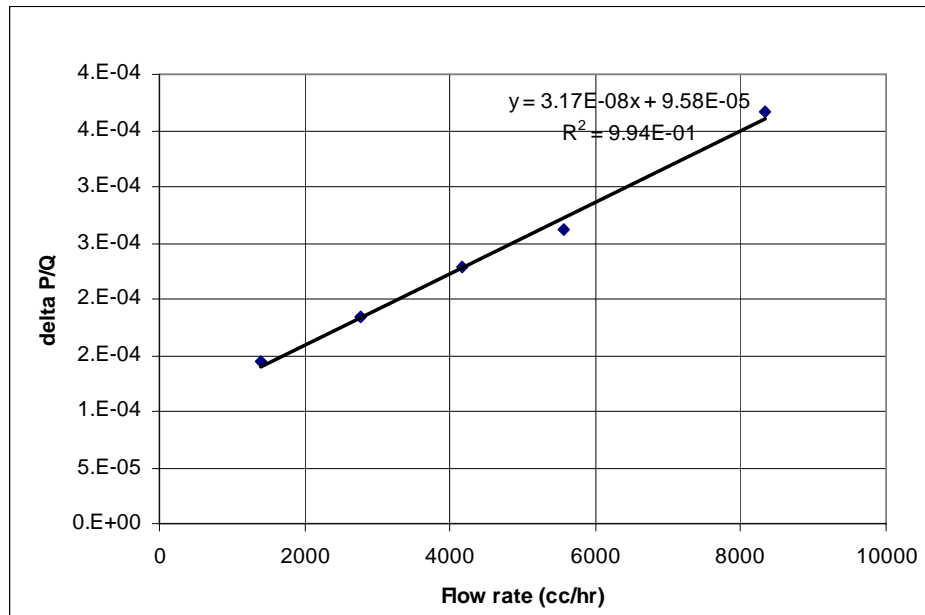


Figure B43.9: Correcting gas permeability measurement at S_{wi} for non-Darcy flow at net confining stress of 3000 psig

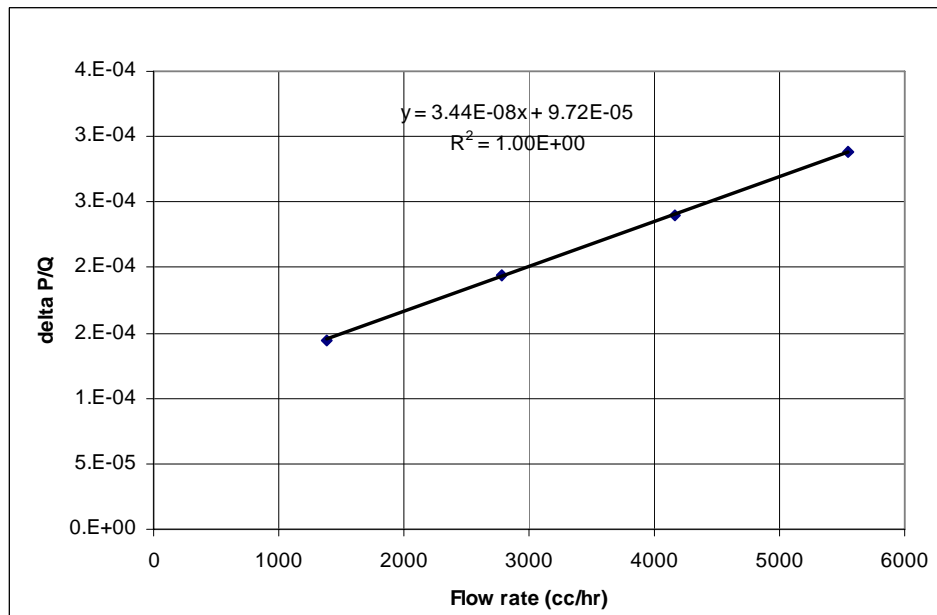


Figure B43.10: Correcting gas permeability measurement at S_{wi} for non-Darcy flow at net confining stress of 5000 psig

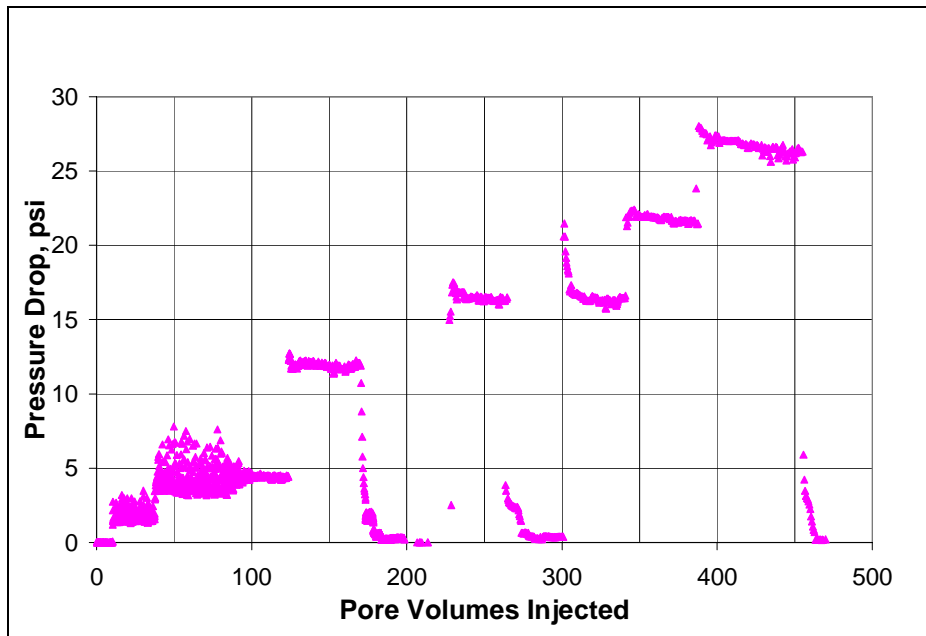


Figure B43.11: Pressure drop across the propped fracture during the initial gas condensate flood at 175°F and 3200 psig

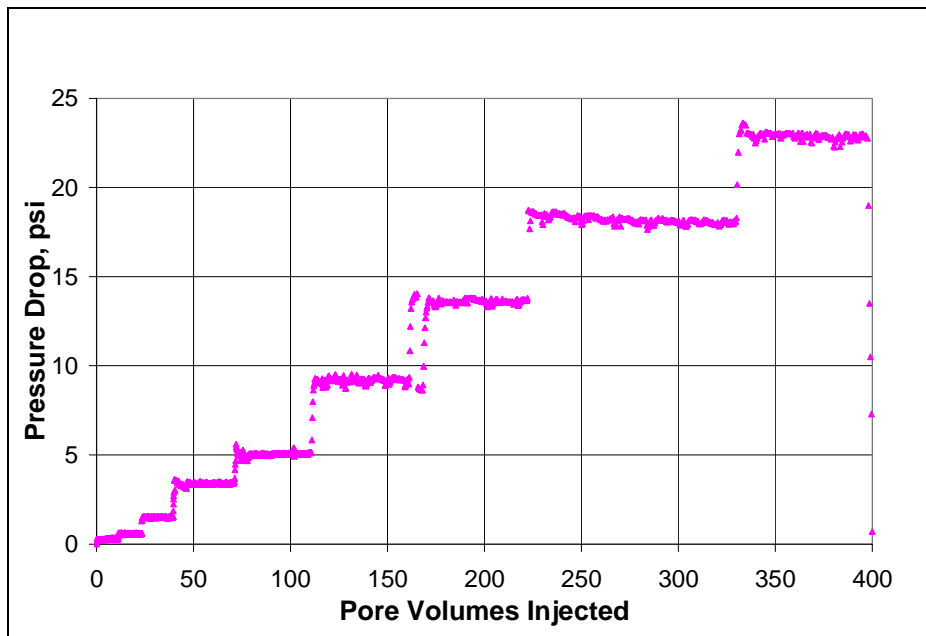


Figure B43.12: Pressure drop across the propped fracture during the initial gas condensate flood at 175°F and 3750 psig

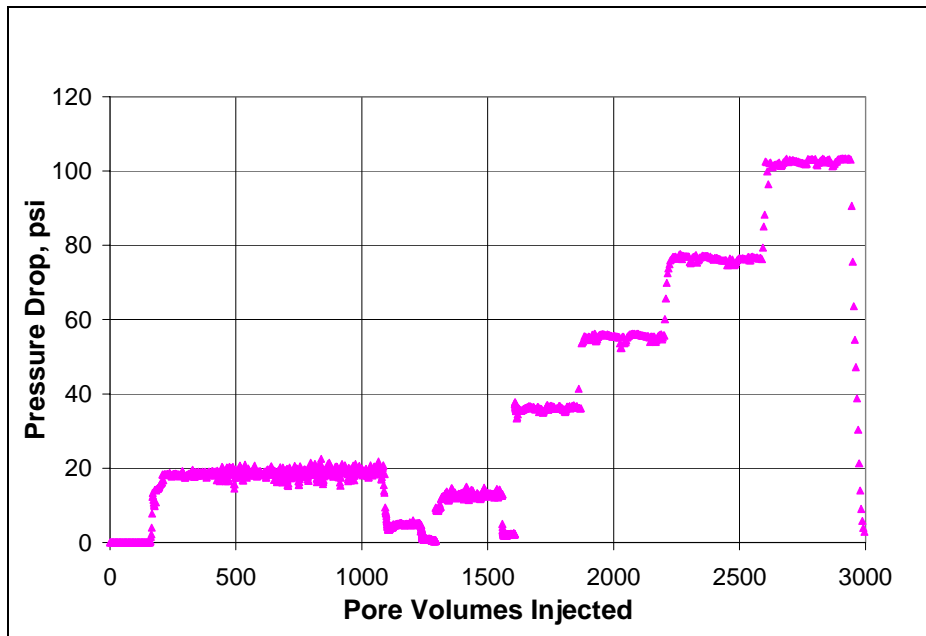


Figure B43.13: Pressure drop across the propped fracture during the initial gas condensate flood at 175°F and 400 psig

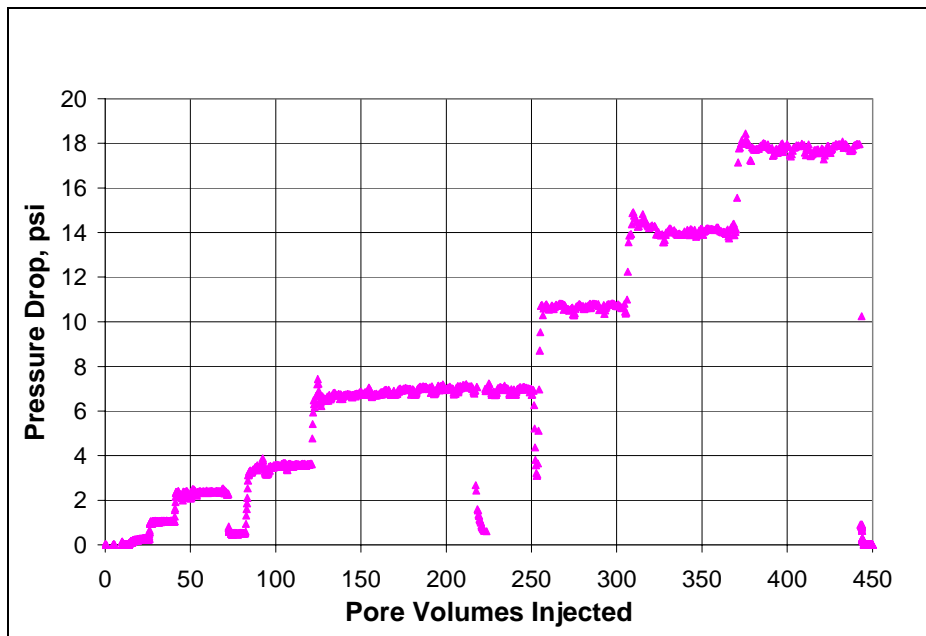


Figure B43.14: Pressure drop across the propped fracture during the second gas condensate flood at 175°F and 3200 psig

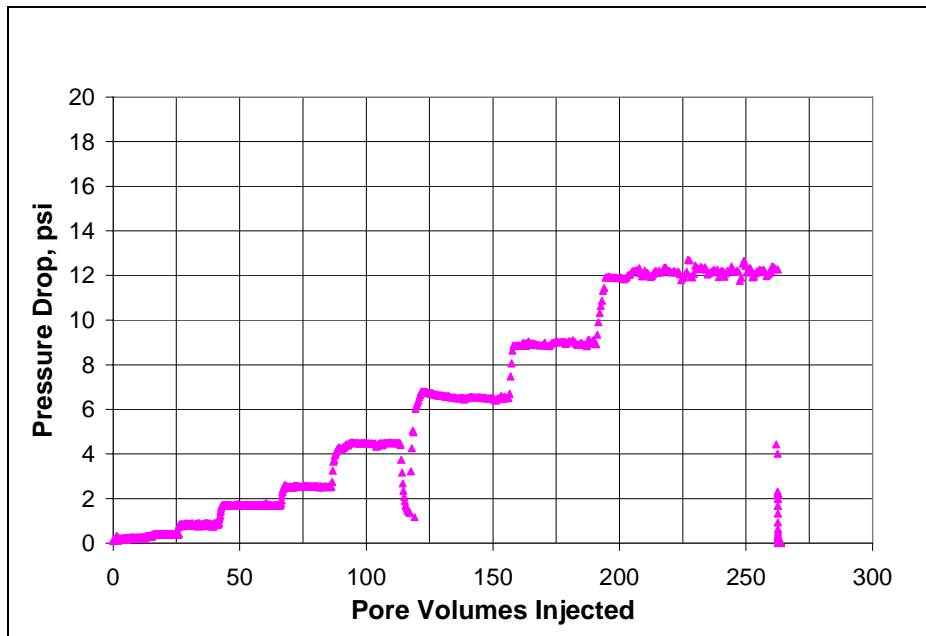


Figure B43.15: Pressure drop across the propped fracture during the second gas condensate flood at 175°F and 3750 psig

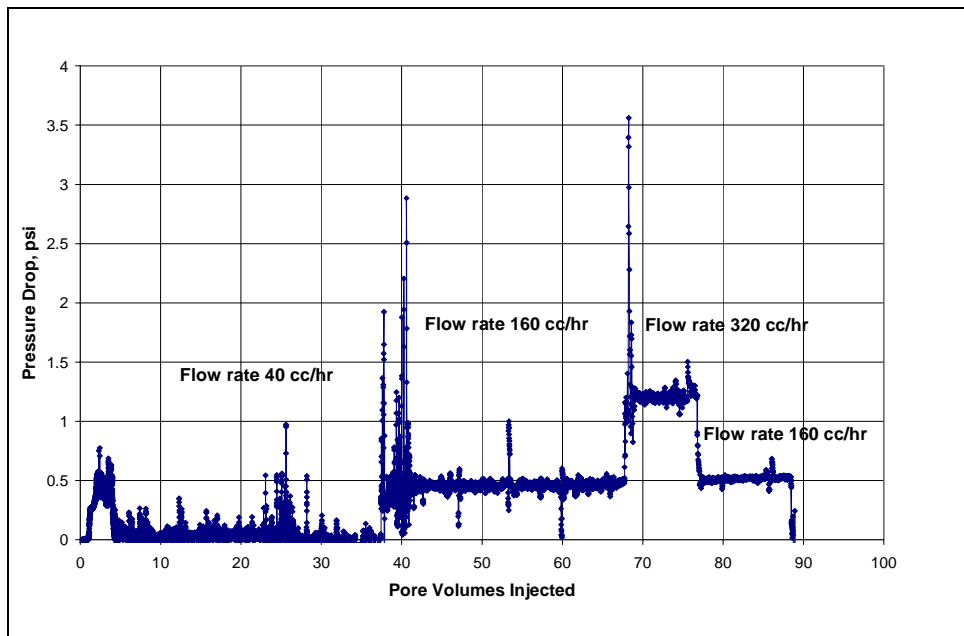


Figure B43.16: Pressure drop across the propped fracture during surfactant treatment

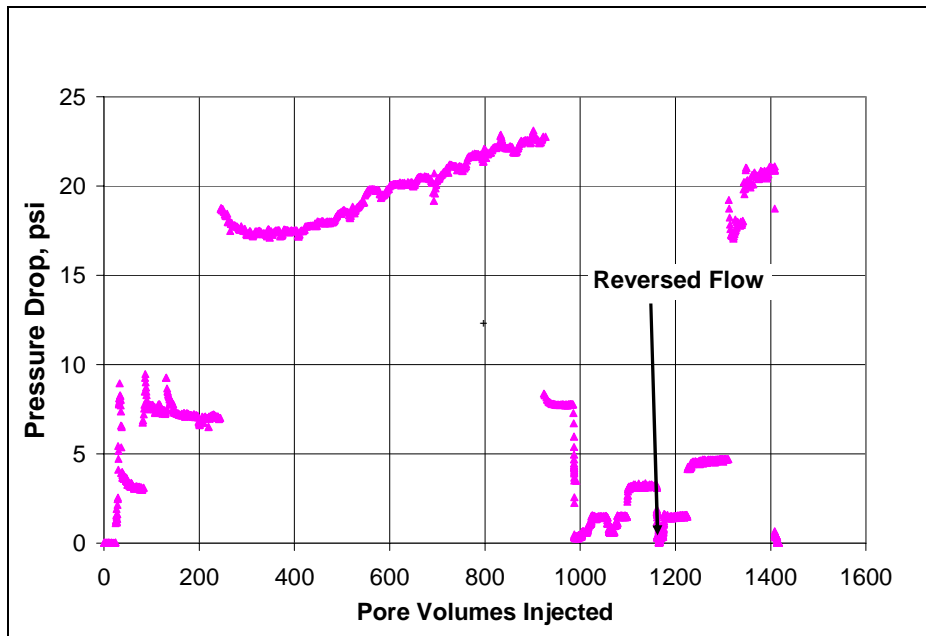


Figure B43.17: Pressure drop across the propped fracture during the post-treatment gas condensate flood at 175°F and 3200 psig

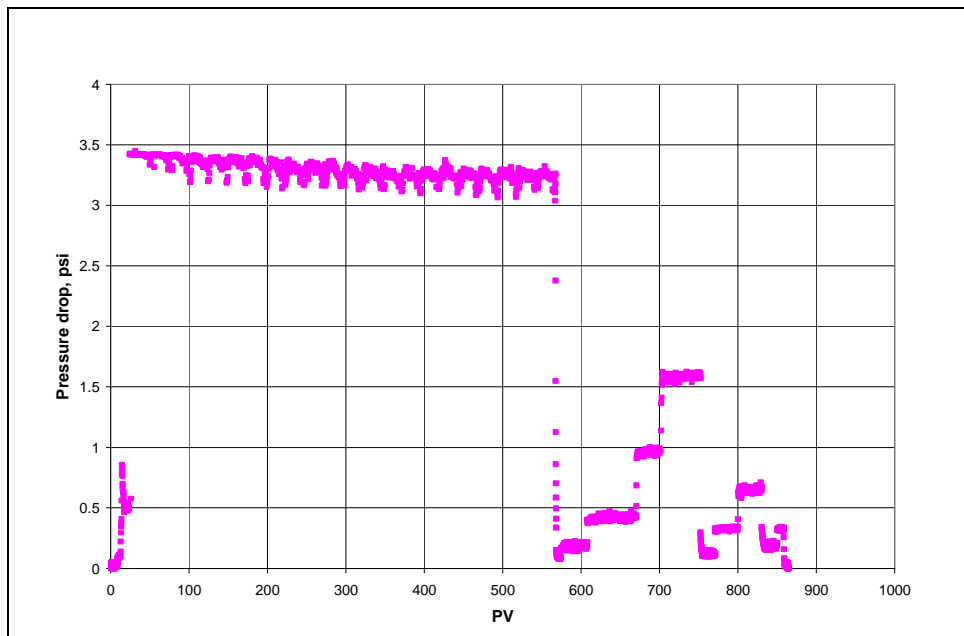


Figure B43.18: Pressure drop across the propped fracture during final methane flood

B45- Experiment No.45

Objective:

The objective of this experiment was to investigate the effect of chemical treatment using the surfactant FC4430 delivered in a mixture of 2-butoxyethanol/ethanol in improving the gas and condensate relative permeability on a reservoir sandstone rock in presence of initial water. The experiment was performed on a Bruce reservoir core (plug #8) at 175°F.

Experimental Results:

Plugs #8 and #10 had been contaminated with confining pump oil while loading up the core in the core holder. The plugs were cleaned by flowing 120 cc of methanol followed by 200 cc of toluene. This was followed by 120 cc of 50/50 mixture of methanol and toluene. The effluent from the toluene/methanol flood was cloudy indicating that the plugs were still contaminated. The plugs were left in this state for 9 months. Plug #8 was then further cleaned after 9 months for this experiment. The plug did not imbibe water but imbibed oil before cleaning. To clean the plug, 40 cc of 50/50 mixture of methanol/toluene was flowed through the core. The effluent was yellowish in color for the first few pore volumes and then became clear. The clear effluent indicated that all the confining oil was removed from the plug.

Table B45.1 summarizes the properties of the plug and the experimental conditions. Initial permeability of the core (plug) was measured using nitrogen at 75°F. **Figure B45.1** shows the pressure drop measured across the core during nitrogen flood. **Table B45.2** summarizes the results of the nitrogen flood.

The initial water saturation of 19% was established by injecting 1.4 cc of synthetic Bruce brine (**Table B21.3**) in the vacuumed core. Nitrogen flood was then conducted to measure the end point gas relative permeability. **Figure B45.2** shows the pressure drop measured across the core and **Table B45.3** summarizes the results of the nitrogen flood. The pressure of the core was raised to 200 psig and then the temperature of the oven was increased to 175°F.

Synthetic fluid mixture-5 (**Table 3.5**) was used for the two-phase flow measurements. The initial flood was conducted with the upstream backpressure regulator set at 5022 psig and the downstream back pressure regulator set at 400 psig. **Table B45.4** gives the properties of the synthetic fluid calculated using the Peng-Robinson EOS at the flowing core pressure. **Figure B45.3** shows the pressure drop across the core during the two-phase gas-condensate flow. **Table B45.5** summarizes the results of the initial two-phase flow.

The core was then treated with the treatment solution (**Table B45.6**). **Figure B45.4** shows the measured pressure drop across the core during the treatment flood. The treatment solution was injected at 80 cc/hr. The core was then shut-in for 12 hours.

Post-treatment two-phase gas-condensate flood was conducted under the same conditions as the initial two-phase flow. Two batches of gas mixture were used for the post-treatment two-phase flood. **Figure B45.5** shows the pressure drop across the core measured during the post-treatment two-phase flood at a flowing pressure of 400 psig. **Table B45.7** summarizes the results of the post-treatment two-phase flood.

Methane flood was conducted to measure the post-treatment permeability of the core. **Table B45.8** summarizes the results and **Figure B45.6** shows the pressure drop measured across the core during the methane flood at 175°F.

Table B45.1: Core properties

Core	Bruce Reservoir Core (plugs #8)
Length, inches (plug #8)	3.68
Diameter, inches	1
Porosity, %	15.30
Pore volume, cc	7.25
Swi, %	19
Temperature, °F	175

Table B45.2: Result of nitrogen flood

q_{core}, (cc/hr)	ΔP (psi)	k_g (md)
6742.54	7.36	127.73
4816.10	5.04	133.30
5869.62	6.17	132.63
Permeability, k_g (md)		131.22

Table B45.3: Result of nitrogen flood at Swi

q_{core}, (cc/hr)	ΔP (psi)	k_g (md)
11287.74	12.87	122.23

Table B45.4: Synthetic fluid properties at experimental conditions

Pressure, psig	5000	400	
Fluid Properties		Gas phase	Oil phase
ρ, g/cc	0.2898	0.0184	0.6714
μ (cp)		0.0132	0.4128
Volume fraction		0.9886	0.0114
IFT (dyne/cm)		13.127	

Table B45.5: Results of the initial two-phase gas condensate flood

q_{pump}, cc/hr	200	400	800
$q_{\text{total_core}}$, cc/hr	2242.67	4485.34	8970.68
$q_{\text{g_core}}$, cc/hr	2217.10	4434.21	8868.41
$q_{\text{o_core}}$, cc/hr	25.57	51.13	102.27
ΔP, psi	24.46	54.26	105.00
k_{rg}	0.069	0.062	0.064
k_{ro}	0.025	0.022	0.023
Nc	1.72×10^{-5}	3.81×10^{-5}	7.37×10^{-5}
PVT Ratio	2.77	2.77	2.77

Table B45.6: Composition of treatment solution

Component	Weight %
FC4430	2
2-Butoxyethanol	69
Ethanol	29

Table B45.7: Results of post-treatment two-phase flow of gas condensate mixture

	Based on initial permeability	Based on final permeability
q_{pump}, cc/hr	512	512
q_{total_core}, cc/hr	1071.13	1071.13
q_{g_core}, cc/hr	979.87	979.87
q_{o_core}, cc/hr	91.26	91.26
ΔP, psi	16.98	16.98
k_{rg}	0.099	0.128
k_{ro}	0.036	0.046
Nc	1.19x10 ⁻⁵	1.19x10 ⁻⁵
Improvement Factor	1.44	1.86

Table B45.8: Result of methane flood to measure final permeability

q _{core} , (cc/hr)	ΔP (psi)	k _g (md)
2913.39	4.00	101.50

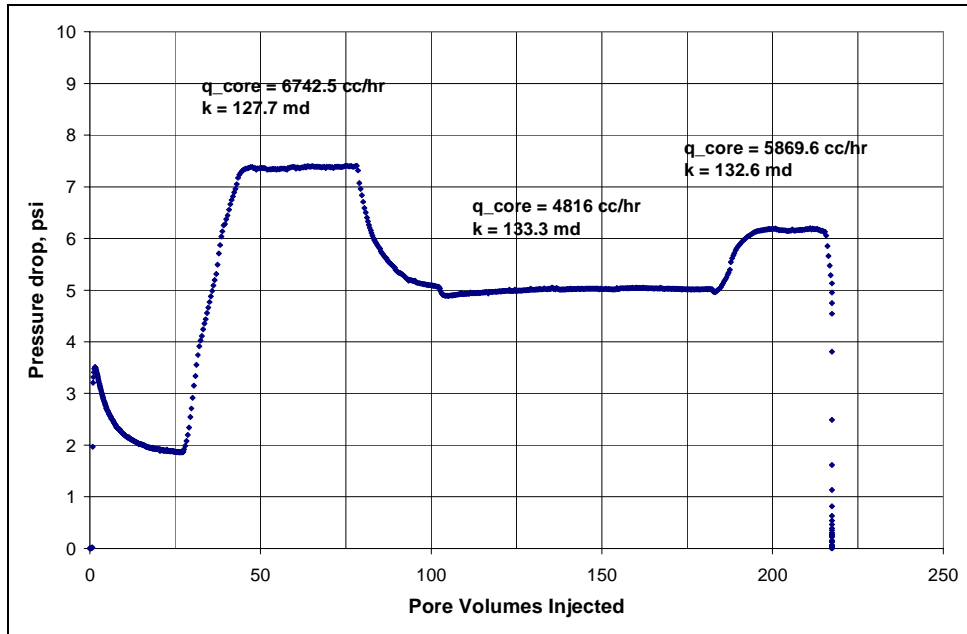


Figure B45.1: Pressure drop across the core during initial nitrogen flood

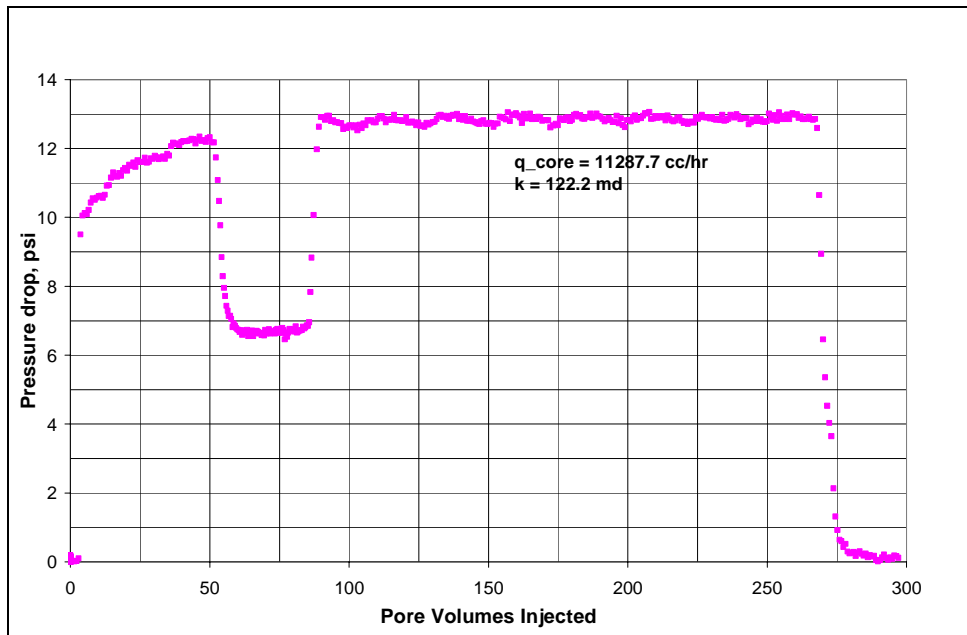


Figure B45.2: Pressure drop across the core during nitrogen flood at $Sw_i = 19\%$

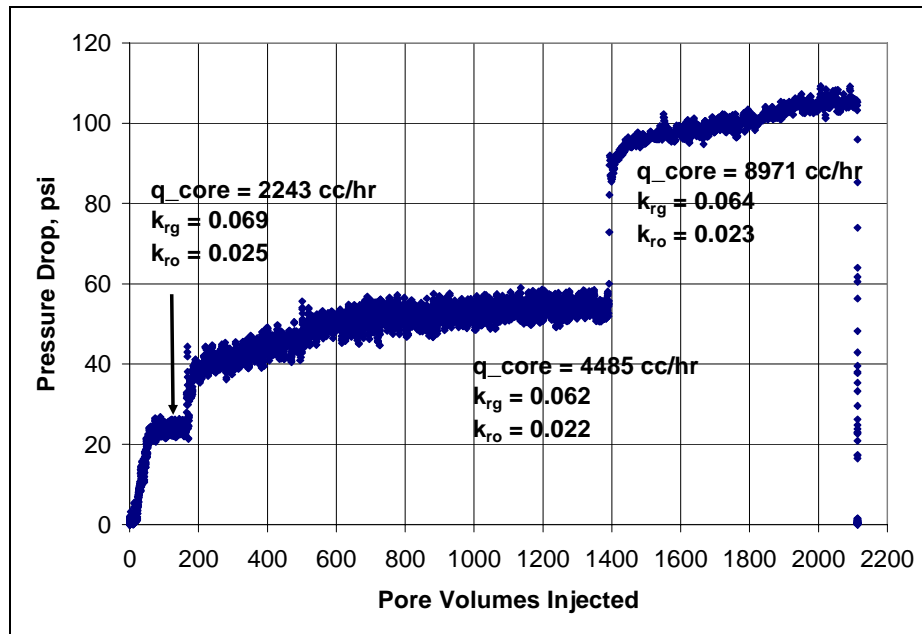


Figure B45.3: Pressure drop across the core during the initial two-phase flow at 175°F and 400 psig

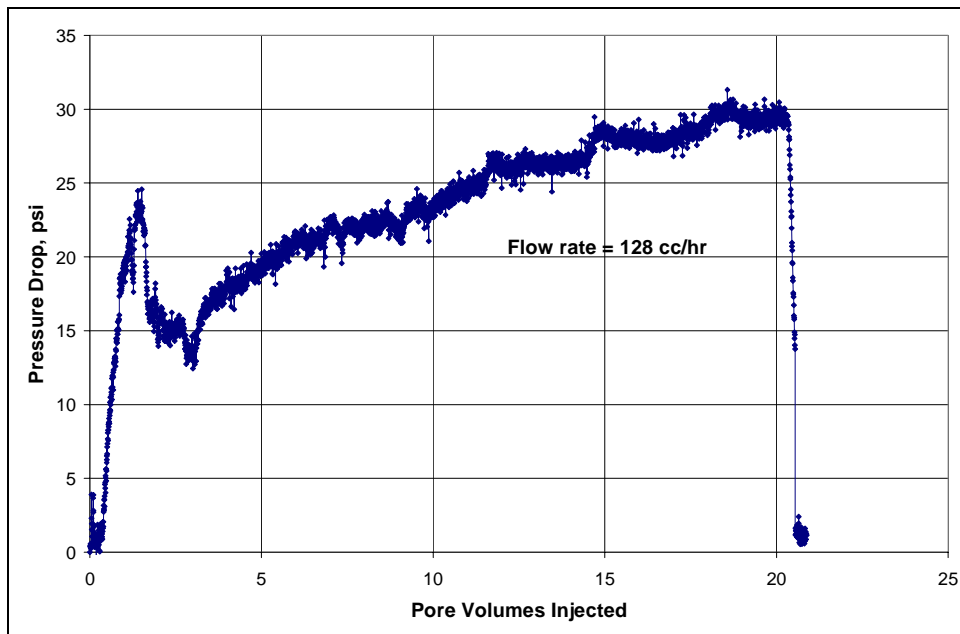


Figure B45.4: Pressure drop across the core during surfactant treatment

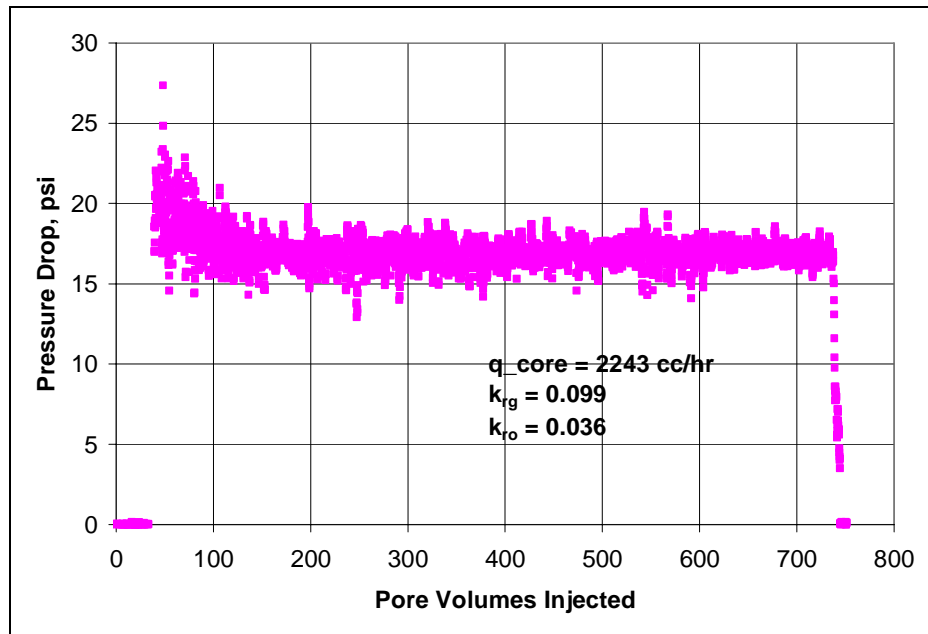


Figure B45.5: Pressure drop across the core during post-treatment two-phase flow at 175°F and 400 psig

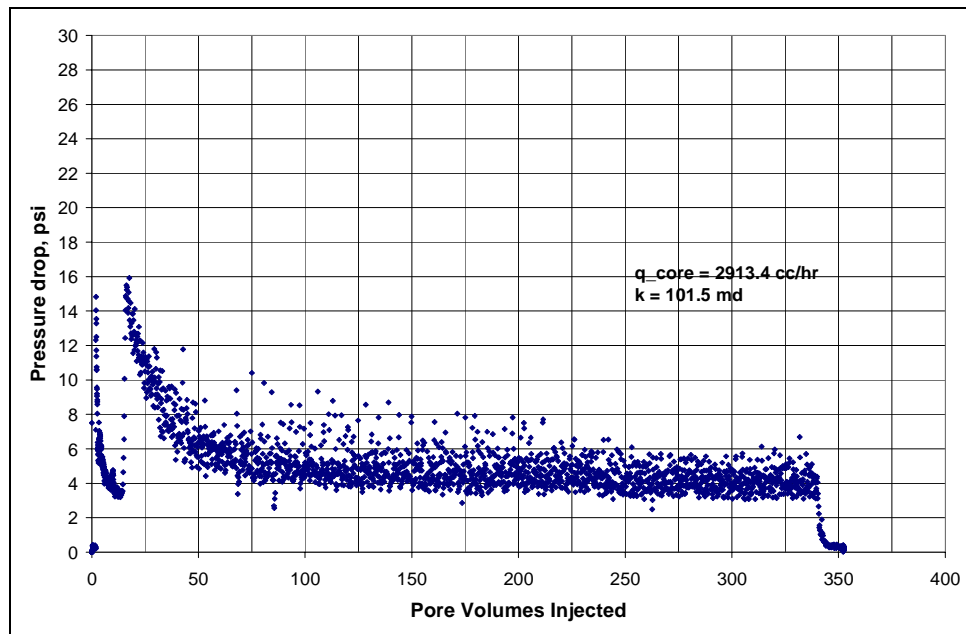


Figure B45.6: Pressure drop across the core during final methane flood

B46- Experiment No.46

Objective:

The objective of this experiment was to investigate the effect of chemical treatment using FC4430 on the gas and oil relative permeabilities for a volatile oil or a bubble point fluid. The experiment was done on Berea sandstone at 154°F.

Experimental Results:

Table B46.1 summarizes the properties of the core and the experimental conditions. Initial permeability of the core was measured using nitrogen at 75°F. **Figure B46.1** shows the pressure drop measured across the core during nitrogen flood. **Table B46.2** summarizes the results of the nitrogen flood.

The initial water saturation of 20% was established by injecting 4.4 cc of 25,000 ppm NaCl brine in the vacuumed core. Nitrogen flood was then conducted to measure the end point gas relative permeability. **Figure B46.2** shows the pressure drop measured across the core and **Table B46.3** summarizes the results of the nitrogen flood. The pressure of the core was raised to 200 psig and then the temperature of the oven was increased to 154°F.

A synthetic hydrocarbon mixture was designed to exhibit volatile oil or bubble point fluid behavior under the experimental conditions. **Table B46.4** gives the composition of the synthetic mixture. The initial flood was conducted with the upstream backpressure regulator set at 4460 psig and the downstream back pressure regulator set at 687 psig. **Table B46.5** gives the properties of the synthetic fluid calculated using the Peng-Robinson EOS at the flowing core pressure. **Figure B46.3** shows the pressure drop

across the core during the two-phase flow. **Table B46.6** summarizes the results of the initial two-phase flood.

The core was then treated with the treatment solution (**Table B42.7**). **Figure B46.4** shows the measured pressure drop across the core during the treatment flood. 19 PV of treatment solution was injected at 120 cc/hr. The core was then shut-in for 24 hours.

Post-treatment two-phase oil and gas flow of the same fluid mixture was then done under the same conditions as the initial two-phase flow. **Figure B46.5** shows the pressure drop across the core measured during the post-treatment two-phase flood at a flowing pressure of 687 psig. **Table B46.8** summarizes the results of the post-treatment two-phase flow.

Finally, the post-treatment permeability of the core was measured using methane to find out if the final gas permeability was as high as the initial gas permeability. **Figure B46.6** shows the pressure drop across the core and **Table B46.9** summarizes the results.

Table B46.1: Core properties

Core	Berea Sandstone
Length, inches	8
Diameter, inches	0.99
Dry Weight of the core	214.36
Porosity, %	20.19
Pore volume, cc	20.46
Swi, %	20
Temperature, °F	154

Table B46.2: Result of nitrogen flood

q_{core}, (cc/hr)	ΔP (psi)	k_g (md)
3739.06	4.65	247.23
5608.59	7.22	239.15
7478.13	9.91	232.30
Permeability, k_g (md)		236.68

Table B46.3: Result of nitrogen flood at Swi

q_{core}, (cc/hr)	ΔP (psi)	k_g (md)
7478.13	13.37	172.16
3739.06	6.09	188.78
5608.59	9.49	181.91
Permeability, k_g (md)		180.99

Table B46.4: Synthetic fluid mixture

Component	Mole%
Methane	75
Propane	12
n-Heptane	9
n-Decane	4

Table B46.5: Synthetic fluid properties at experimental conditions

Pressure, psig	4460	687	
Fluid Properties		Gas phase	Oil phase
ρ, g/cc	0.3782	0.0379	0.3782
μ (cp)		0.0133	
Volume fraction		0.9428	
IFT (dyne/cm)		9.64	

Table B46.6: Results of the initial two-phase gas-oil flood

q_{pump}, cc/hr	250	125
q_{total_core}, cc/hr	1340.73	670.37
q_{g_core}, cc/hr	1264.04	632.02
q_{o_core}, cc/hr	76.69	38.34
ΔP, psi	30.55	16.49
k_{rg}	0.038	0.035
k_{ro}	0.041	0.038
Nc	$2.51 \cdot 10^{-5}$	$1.36 \cdot 10^{-5}$
PVT Ratio	0.94	0.94

Table B46.7: Composition of treatment solution

Component	Weight %
FC4430	1
2-butoxyethanol	69.5
Ethanol	29.5

Table B46.8: Results of post-treatment two-phase gas-oil flood

q_{pump}, cc/hr	250	125
q_{total_core}, cc/hr	1340.73	670.37
q_{g_core}, cc/hr	1264.04	632.02
q_{o_core}, cc/hr	76.69	38.34
ΔP, psi	11.18	5.17
k_{rg}	0.104	0.113
k_{ro}	0.111	0.120
Nc	9.19*10 ⁻⁶	4.25*10 ⁻⁶
Improvement Factor	2.73	2.96

Table B46.9: Result of methane flood to measure final permeability

q_{core}, (cc/hr)	ΔP (psi)	k_g (md)
3101.42	3.50	272.64
4652.14	5.40	265.07
Permeability, k_g (md)	268.86	

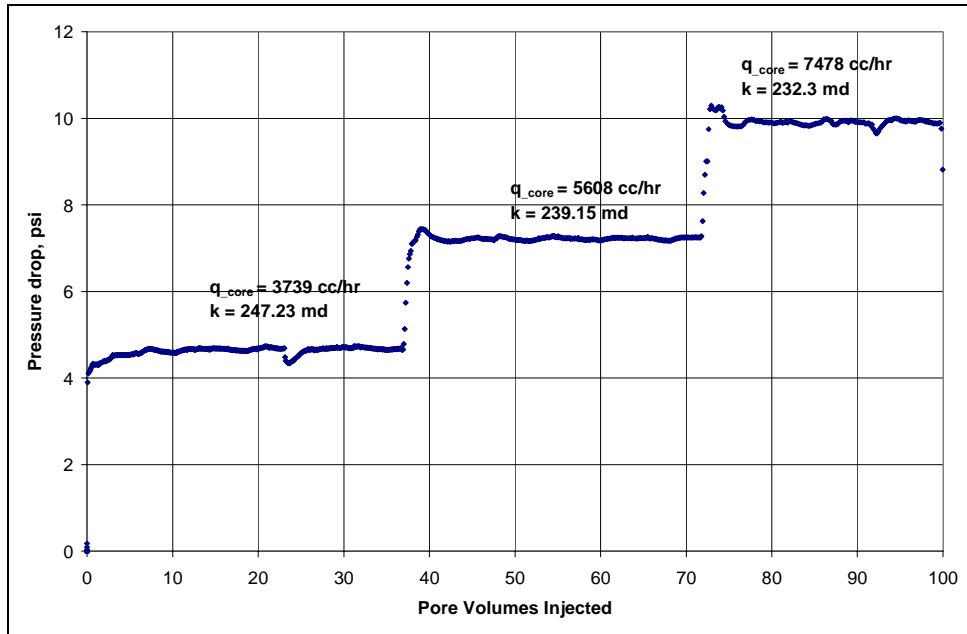


Figure B46.1: Pressure drop across the core during initial nitrogen flood

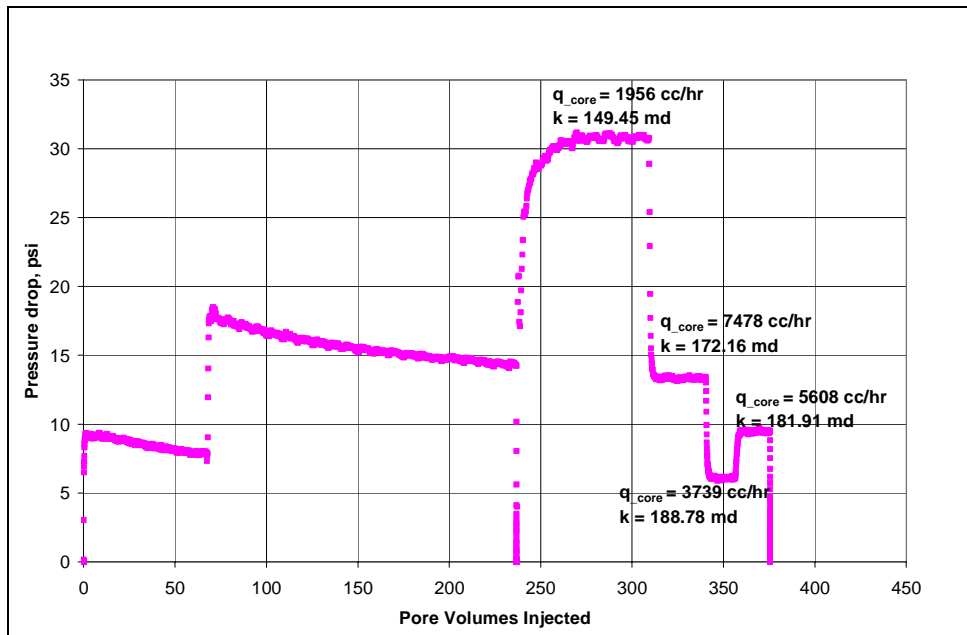


Figure B46.2: Pressure drop across the core during nitrogen flood at $Sw_i = 19\%$

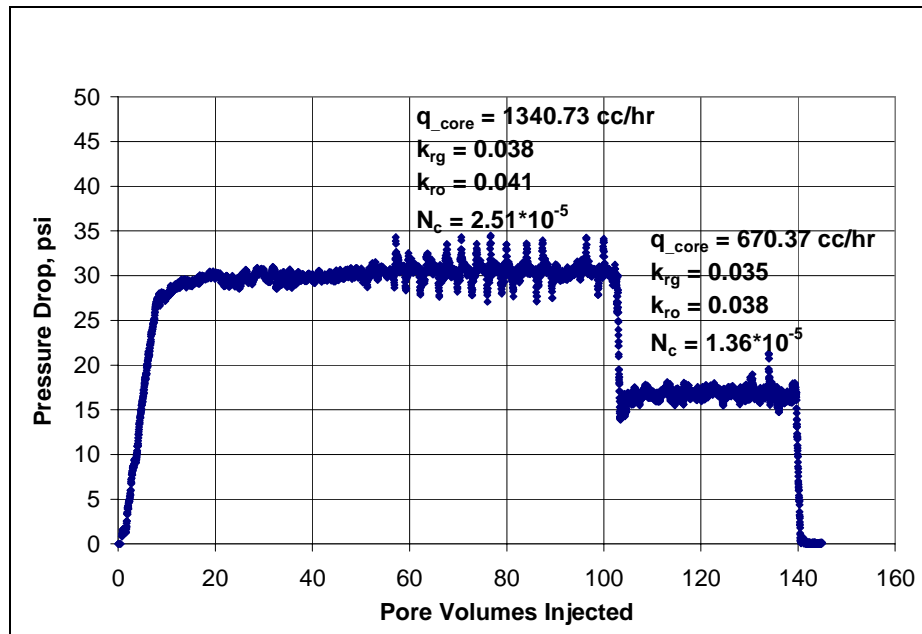


Figure B46.3: Pressure drop across the core during the initial two-phase flow at 154°F and 687 psig

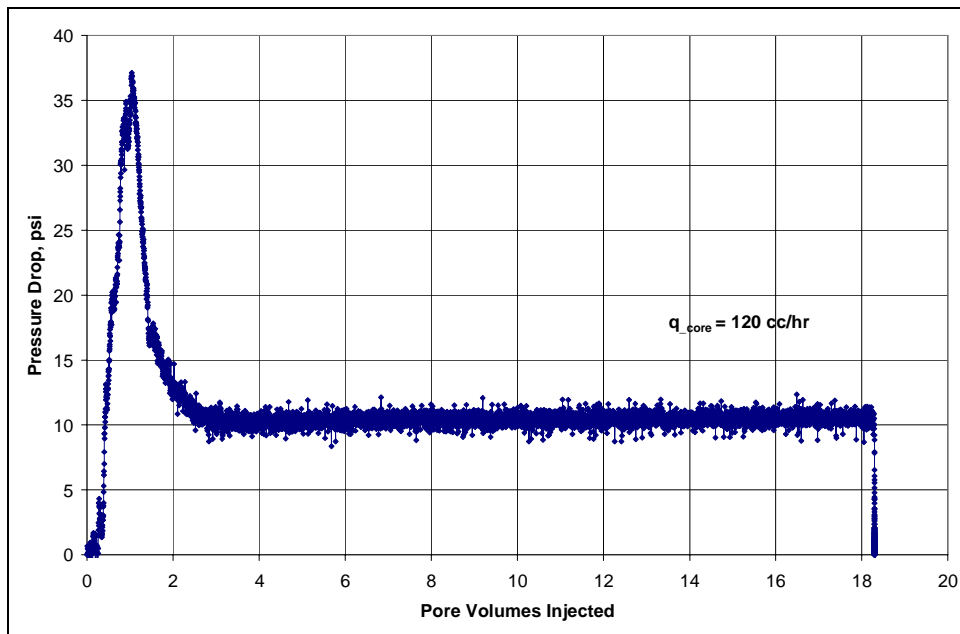


Figure B46.4: Pressure drop across the core during surfactant treatment

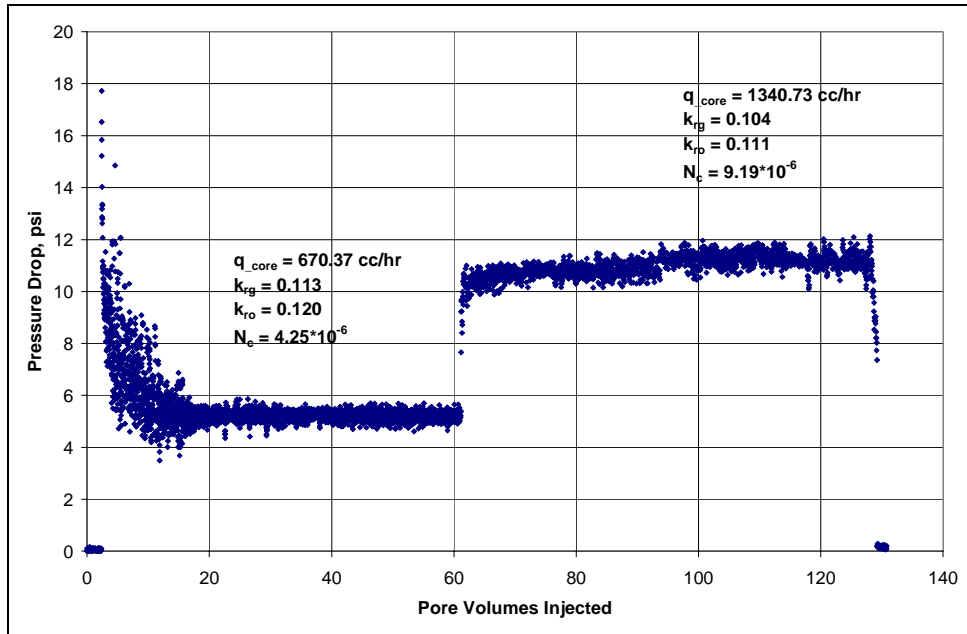


Figure B46.5: Pressure drop across the core during post-treatment two-phase flow at 154°F and 687 psig

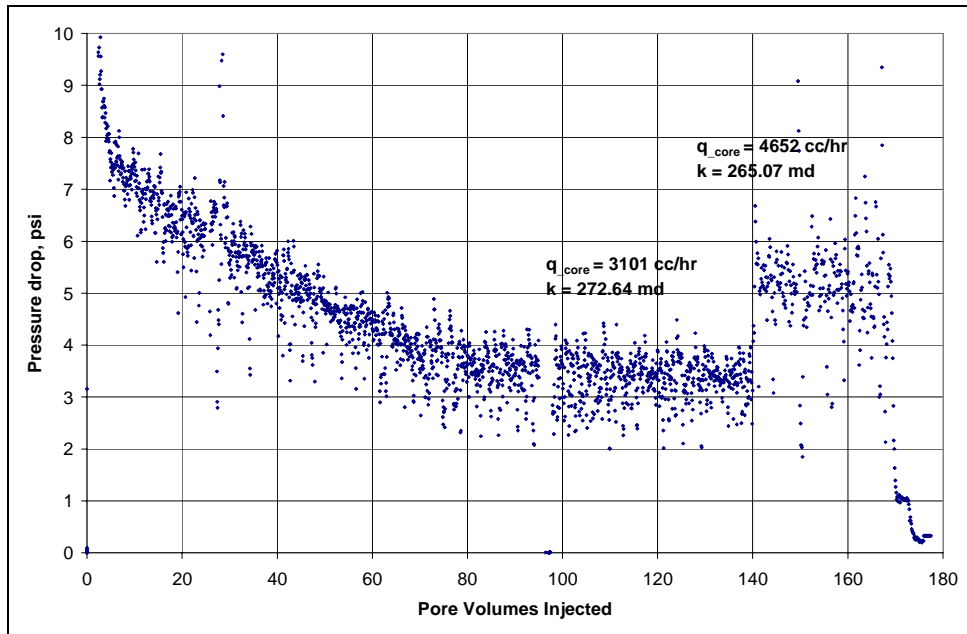


Figure B46.6: Pressure drop across the core during final methane flood

B47- Experiment No.47

Objective:

The objective of this experiment was to investigate the effect of chemical treatment using FC4430 on the oil and water relative permeabilities. The experiment was done on Berea sandstone at 140°F. 25,000 ppm NaCl brine was used as water and n-decane was used as oil.

Core Preparation

The Berea cores used were drilled to have a diameter of about 2 inches and around 1 foot in length. The length and diameter was recorded in addition to the rock mass. Polycarbonate end caps were machined with a 1/16 inch dead space to allow uniform flow across the rock face. These pieces were glued to the core with epoxy and dead space is calculated to be about 2 cc. This space was estimated from the volume of offset created by the end caps and rock faces in addition to the tubing segments and valves used at the inlet, both taps, and outlet. One end of the core was tapped and stood inside a 3 inch diameter lexan tube. The void space between the tube and the core was filled with epoxy. A 7:3 mix of resin and hardener was made with Epon Resin 828 and Versamid 125 Hardener and stirred with a glass rod. The core was allowed to cure for 24 hours. Holes for pressure taps were measured, drilled and threaded into the core at 5 cm from each face of the rock core. Swagelok bulkhead fittings were screwed into both end caps and pressure taps.

After attaching all the necessary Swagelok fittings, tubing and valves, the prepared core was pressure tested to 80 psi with regulated air. The core was then placed

under water in a trough to observe for leaks. If bubbles were apparent, the core was dried and epoxy was applied as needed to remedy the escaping air.

The epoxy coated core was prepared and pressure tested by Chris Britton. All the stainless steel tubing was replaced with nylon tubing. The upstream backpressure regulator was by-passed and the downstream back pressure regulator was set at 14 psi.

Experimental Results:

Table B47.1 summarizes the properties of the core and the experimental conditions. Vacuum was pulled on the core for 2 hours and 25,000 ppm NaCl brine was then injected into the vacuumed core. The pore volume of the core was determined from the volume of the brine imbibed. The pore volume was also calculated by weighing the core before and after saturating with brine. The temperature of the oven was raised to 140°F.

Initial permeability of the core was measured by flowing brine. **Figure B47.1** shows the pressure drop measured across the core and the sections during first brine flood. **Table B47.2** summarizes the results of the brine flood. Oil flood was then conducted to reduce the water saturation to residual. **Figure B47.2** shows the pressure drop measured across the core and the sections during first oil flood. **Table B47.3** summarizes the results of the oil flood. The effluent was collected and from the volume of water produced, the volume of water remaining in the core was determined and the residual water saturation was calculated. Second brine flood was then done to reduce the oil saturation to residual. The effluent was collected and from the volume of oil produced, the volume of oil remaining in the core was determined and the residual oil saturation was calculated. **Figure B47.3** shows the pressure drop measured across the core and the sections during second brine flood. **Table B47.4** summarizes the results of the second

brine flood. Second oil flood was then conducted to reduce the water saturation to residual again. This was done so that the fractional flow of oil and water can be started at from a smaller fractional flow of water and then increased in steps to measure the relative permeability curves during the imbibition cycle instead of drainage cycle. **Figure B47.4** shows the pressure drop measured across the core and the sections during second oil flood. **Table B47.5** summarizes the results of the second oil flood.

Two-phase oil-water flood was then conducted at different fractional flows. Steady state pressure drop was measured for $f_w = 0.24, 0.25, 0.49, 0.63, 0.62$ and 1.0 . **Figure B47.5** shows the pressure drop measured across the core and the sections during the two-phase oil-water flood at different fractional flows. The saturation at each fractional flow was estimated from the difference between the water injected and produced from the core. **Table B47.6** summarizes the results of the initial two-phase flood. The core was weighed after the flood at $f_w = 1$ and the residual oil saturation was calculated on mass basis. **Table B47.7** summarizes the result of residual oil saturation calculated on mass basis. An oil flood was then conducted to reduce the water saturation to residual. **Figure B47.6** shows the pressure drop measured across the core and the sections during third oil flood. **Table B47.8** summarizes the results of the third oil flood.

The core was then treated with the treatment solution (**Table B47.9**). Treatment solution was injected at 250 cc/hr for the first 4 PV and then at 500 cc/hr for the last 10 pore volumes. **Figure B47.7** shows the pressure drop across the core and the sections during the treatment flood.

An ethanol flood was then conducted to remove the treatment solution from the core. **Figure B47.8** shows the pressure drop across the core and the sections during the ethanol flood. An oil flood was then conducted to flush out ethanol **Figure B47.9** shows the pressure drop across the core and the sections during the oil flood. Brine flood was

then conducted to reduce the oil saturation to residual. **Figure B47.10** shows the pressure drop measured across the core and the sections during brine flood. **Table B47.10** summarizes the results of the brine flood. An oil flood was then conducted to reduce the water saturation to residual. **Figure B47.11** shows the pressure drop measured across the core and the sections during the oil flood. **Table B47.11** summarizes the results of the oil flood.

Post-treatment two-phase flow of oil and water was then done at different fractional flows of water. Steady state pressure drop was measured for $f_w = 0.2, 0.4, 0.5, 0.6, 0.8$ and 1.0 . **Figure B47.12** shows the pressure drop measured across the core and the sections during the post-treatment two-phase oil-water flood at different fractional flows. The saturation at each fractional flow was estimated from the difference between the water injected and produced from the core. **Table B47.12** summarizes the results of the post-treatment two-phase flood. The core was weighed after the flood at $f_w = 1$ and the residual oil saturation was calculated on mass basis. **Table B47.13** summarizes the result of residual oil saturation calculated on mass basis.

Table B47.1: Core Properties and Experimental Conditions

Core	Berea Sandstone
Length, inches	11.75
Length (Top Section), inches	1.875
Length (Top-Mid Section), inches	4
Length (Mid-Bottom Section), inches	4
Length (Bottom Section), inches	1.875
Diameter, inches	2
Mass of core + epoxy, gms	2568.19
Mass of brine saturated core, gms	2684.91
Mass of core at Sor	2673.26
Porosity, %	19.32
Pore volume, cc	116.85
Temperature, °F	140
Brine viscosity, cp (at 75°F)	0.913
Brine viscosity, cp (at 140°F)	0.468
Oil viscosity, cp (at 140°F)	0.5658
Brine density, g/cc (at 140°F)	0.98
Oil density, g/cc (at 140°F)	0.71

Table B47.2: Result of first brine flood at 500 c/hr

	ΔP (psi)	k (md)
Total	4.83	567.81
Top Section	1.00	434.72
Top-Mid Section	1.57	593.71
Mid-Bottom Section	1.46	641.57
Bottom Section	0.80	547.17

Table B47.3: Result of first oil flood at 500 c/hr

	ΔP (psi)	k (md)
Total	5.31	320.39
Top Section	0.56	483.55
Top-Mid Section	1.47	393.61
Mid-Bottom Section	1.49	386.47
Bottom Section	1.76	154.01
Water produced = 69.70 cc		
$S_{wr} = 0.40$		
$K_{ro}^o = 0.56$		

Table B47.4: Result of second brine flood at 250 c/hr

	ΔP (psi)	k (md)
Total	16.72	50.73
Top Section	4.48	25.01
Top-Mid Section	5.54	43.22
Mid-Bottom Section	4.52	52.98
Bottom Section	2.23	50.26
Oil produced = 21.40 cc		
Sor = 0.41		
$K_{rw}^o = 0.09$		

Table B47.5: Result of second oil flood at 250 c/hr

	ΔP (psi)	k (md)
Total	3.11	273.55
Top Section	0.196	691.00
Top-Mid Section	0.86	337.04
Mid-Bottom Section	0.76	380.25
Bottom Section	1.39	97.59
Water produced = 25 cc		
Swr = 0.37		
$kr_o^o = 0.48$		

Table B47.6: Results of the initial two-phase oil-water flood

q_{o_core}, cc/hr	63.80	186.43	125.57	90.50	111.0	0.00	0.00
q_{w_core}, cc/hr	20.60	62.14	122.14	152.00	182.67	242.33	250
f_w	0.24	0.25	0.49	0.63	0.62	1.00	1.00
ΔP, psi	2.99	8.84	13.10	15.76	18.98	242.33	250.00
k_{ro}	0.128	0.126	0.057	0.034	0.035	0.00	0.00
k_{rw}	0.034	0.035	0.046	0.048	0.048	0.060	0.060
Water produced, cc		32.13	47.90	63.20	60.30	103.10	
Water injected, cc		49.60	52.40	65.00	60.00	112.00	
Sw		0.52	0.56	0.58	0.57	0.65	0.64

Table B47.7: Saturation measured based on mass basis at the end of two-phase flow

Mass of core + epoxy after flood at $fw = 1$	2673.26
Mass of the fluid in the core	105.07
S_w	0.64
S_{or}	0.36

Table B47.8: Results of third oil flood

Water produced, cc	23.6
S_w	0.44
S_o	0.66

Table B47.9: Composition of treatment solution

Component	Weight %
FC4430	1
2-butoxyethanol	69.3
Ethanol	29.7

Table B47.10: Result of post-treatment brine flood at 250 c/hr

	ΔP (psi)	k (md)
Total	6.26	135.77
Top Section	0.668	168.00
Top-Mid Section	1.61	148.94
Mid-Bottom Section	2.53	94.58
Bottom Section	1.48	75.63
Water injected = 212 cc		
Water produced = 118.20 cc		
Sor = 0.31		
$K_{rw}^o = 0.24$		

Table B47.11: Result of post-treatment oil flood at 650 c/hr

	ΔP (psi)	k (md)
Total	4.55	485.85
Top Section	0.68	520.71
Top-Mid Section	1.49	503.00
Mid-Bottom Section	2.32	324.61
Bottom Section	0.98	359.57
Water produced = 53.50 cc		
Swr = 0.23		
$kr_o^o = 0.86$		

Table B47.12: Results of the initial two-phase oil-water flood

q_{o_core}, cc/hr	240	180	150	120	60	0
q_{w_core}, cc/hr	60	120	150	180	240	250
fw	0.2	0.4	0.5	0.6	0.8	1.0
ΔP, psi	8.06	13.63	16.30	19.00	24.50	23.60
k_{ro}	0.178	0.079	0.055	0.038	0.015	0.00
k_{rw}	0.037	0.044	0.046	0.047	0.049	0.00
Water produced, cc	20.82	38.10	58.00	52.70	101.40	97.60
Water injected, cc	46.80	44.20	60.20	54.00	104.20	100.30
Sw	0.45	0.50	0.52	0.53	0.56	0.58

Table B47.13: Saturation measured based on mass basis at the end of two-phase flow

Mass of core + epoxy after flood at fw = 1	2671.48
Mass of the fluid in the core	103.29
Sw	0.59
Sor	0.41

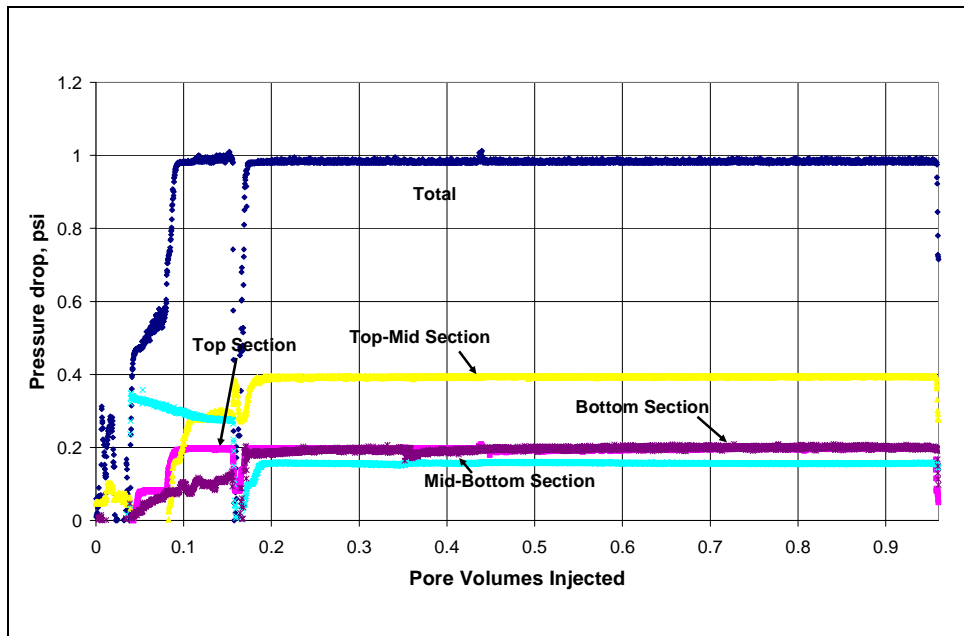


Figure B47.1: Pressure drop across the core and the sections during first brine flood

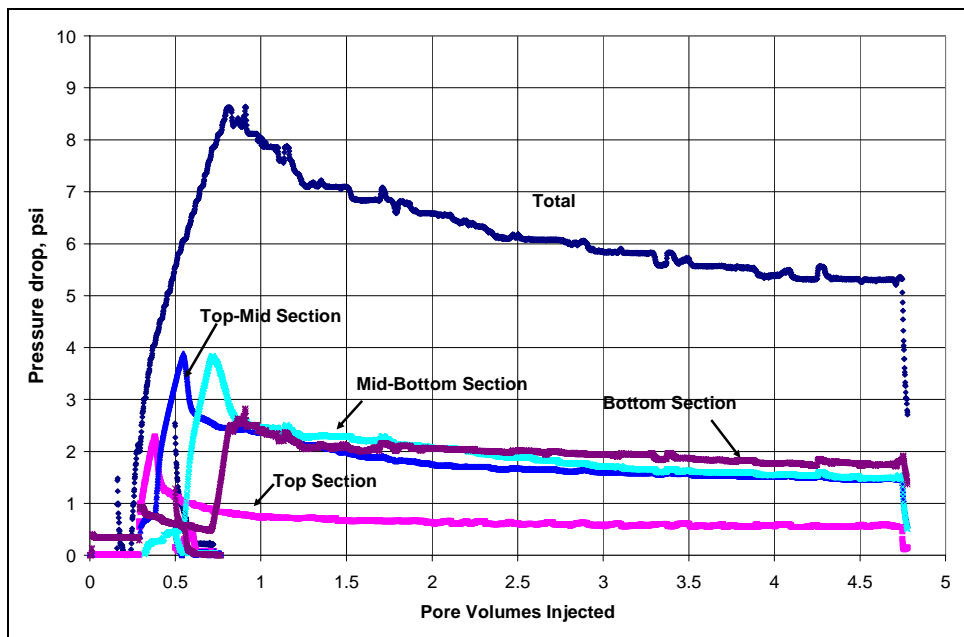


Figure B47.2: Pressure drop across the core and the sections during first oil flood

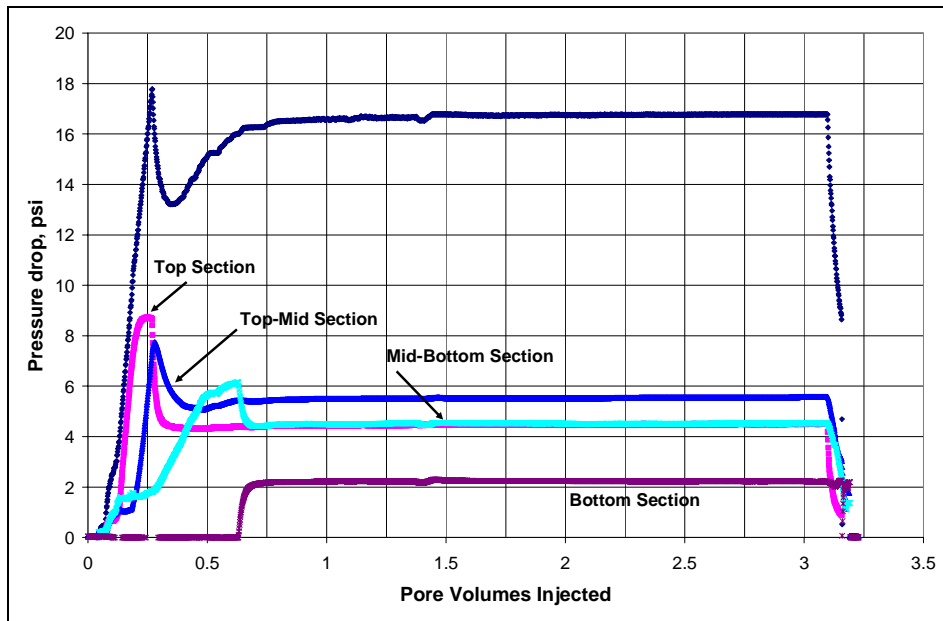


Figure B47.3: Pressure drop across the core and the sections during second brine flood

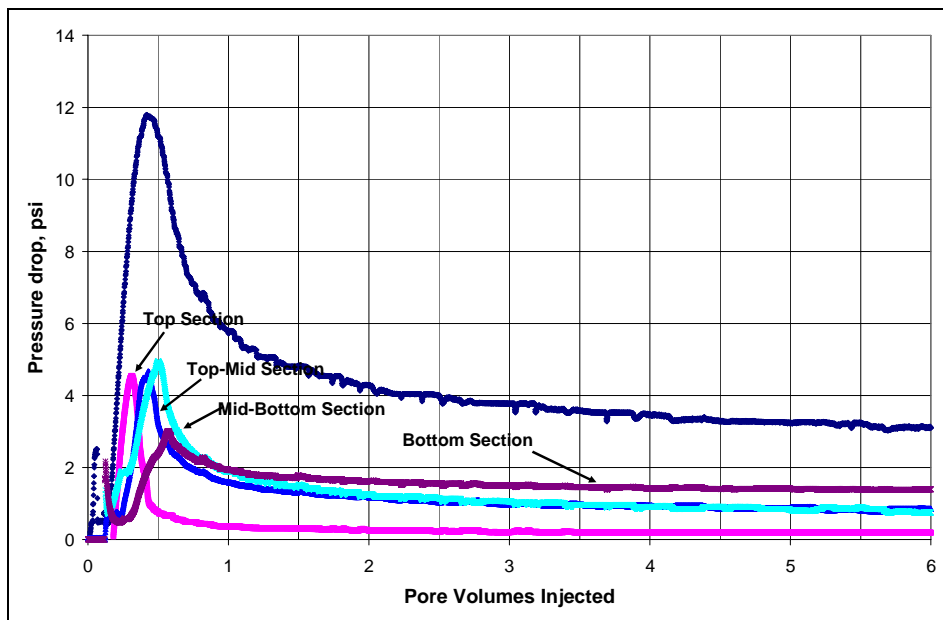


Figure B47.4: Pressure drop across the core and the sections during second oil flood

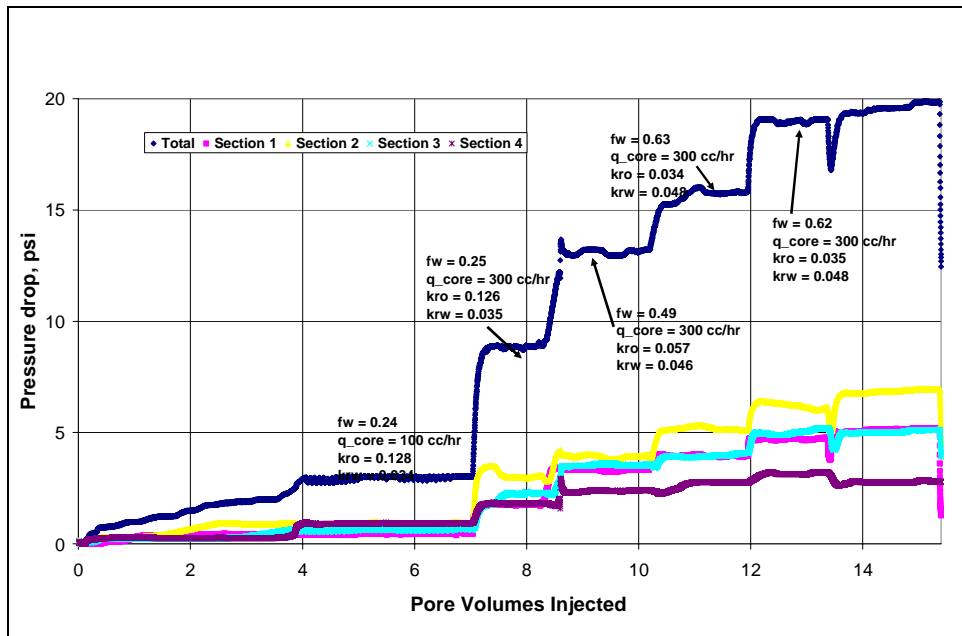


Figure B47.5: Pressure drop across the core and the sections during initial two-phase oil-water flood at different fractional flows

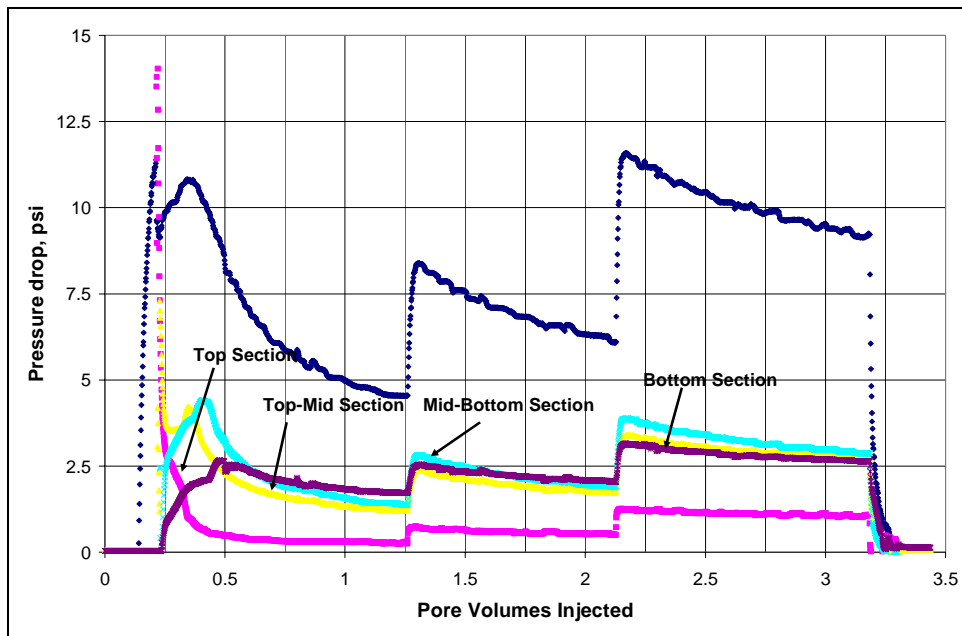


Figure B47.6: Pressure drop across the core and the sections during third oil flood

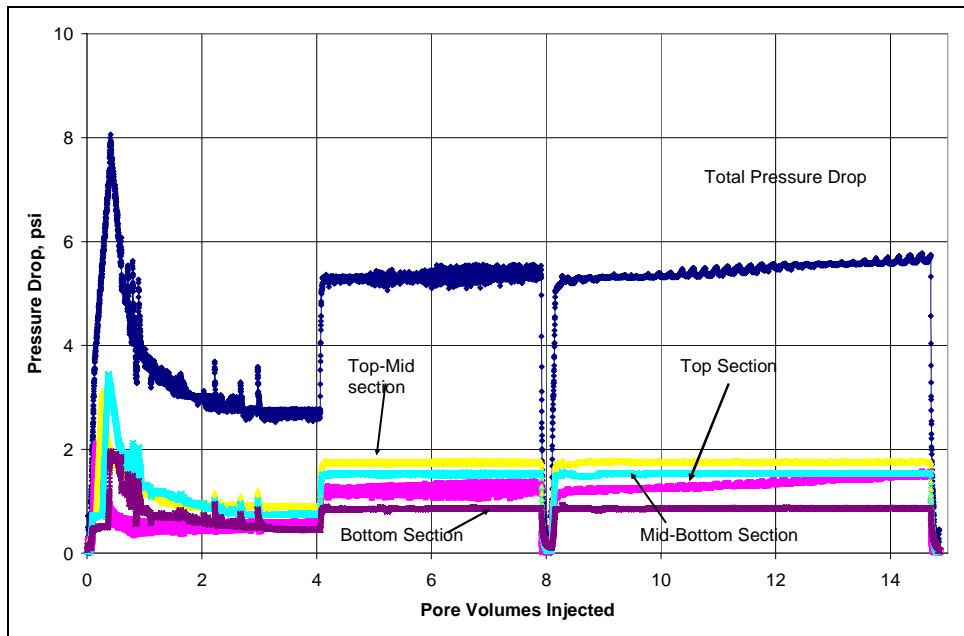


Figure B47.7: Pressure drop across the core and the sections during treatment flood

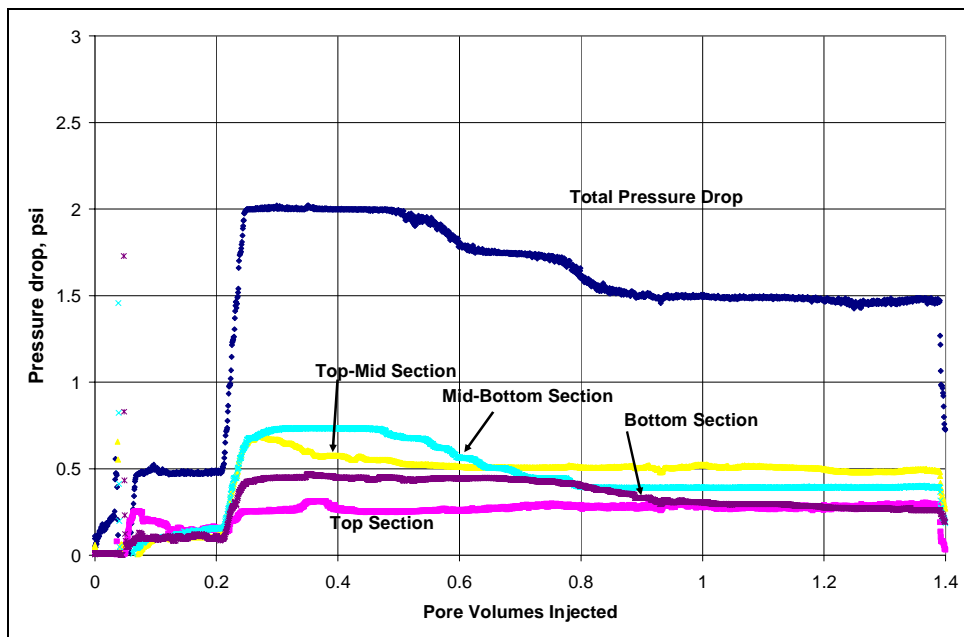


Figure B47.8: Pressure drop across the core and the sections during ethanol flood

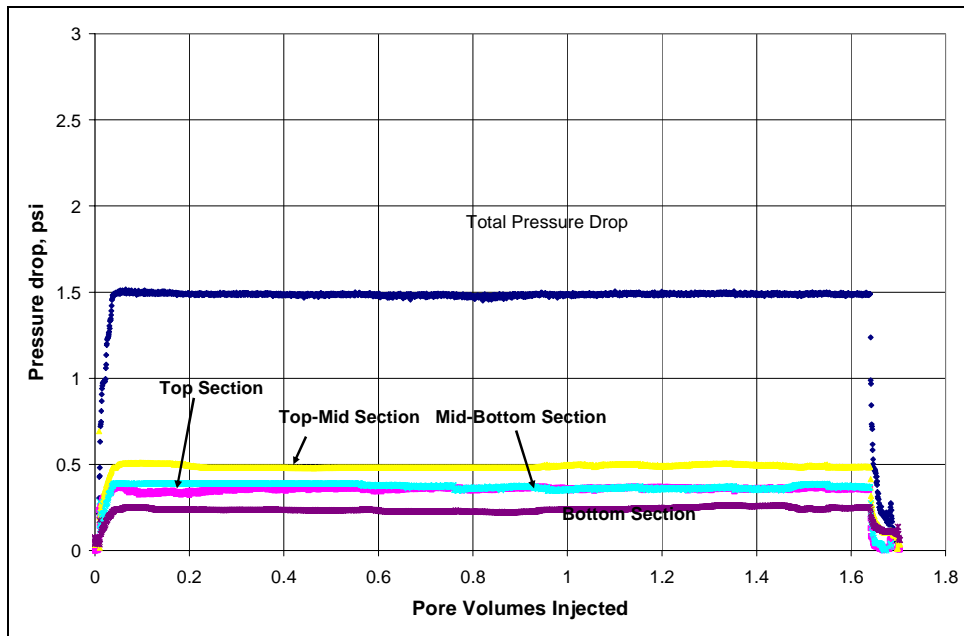


Figure B47.9: Pressure drop across the core and the sections during first post-treatment oil flood

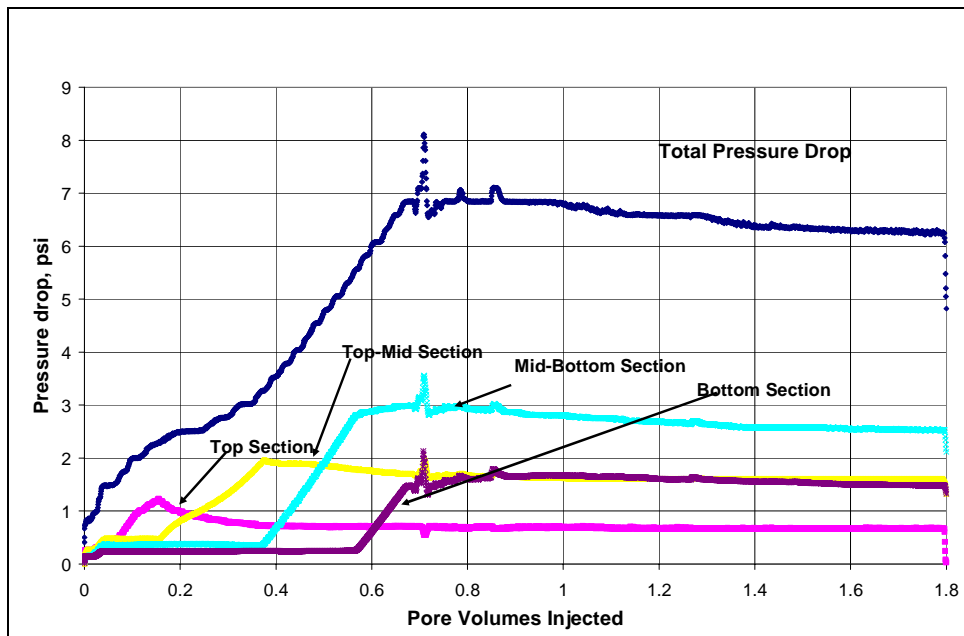


Figure B47.10: Pressure drop across the core and the sections during first post-treatment brine flood

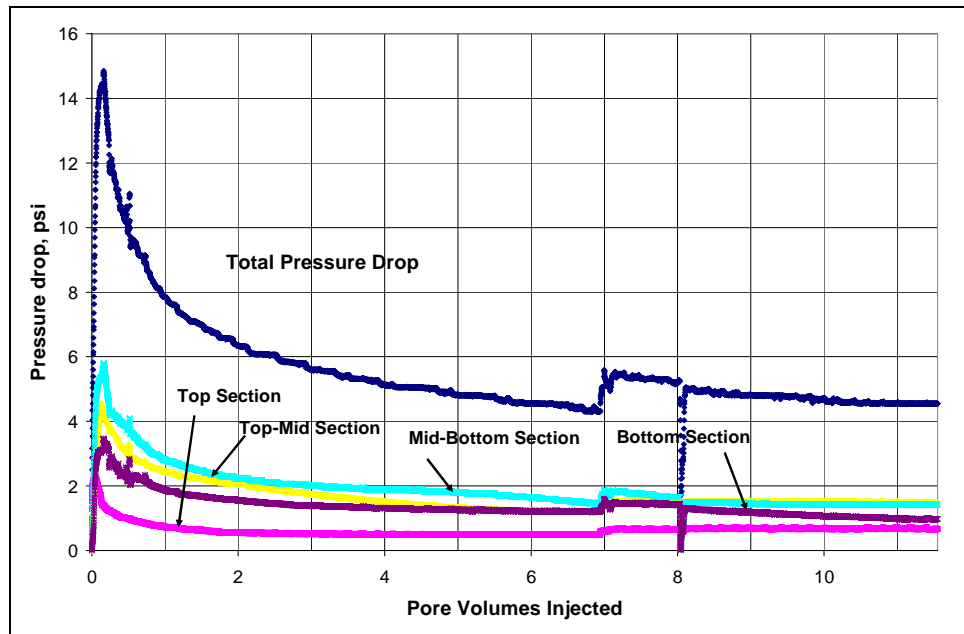


Figure B47.11: Pressure drop across the core and the sections during second post-treatment oil flood

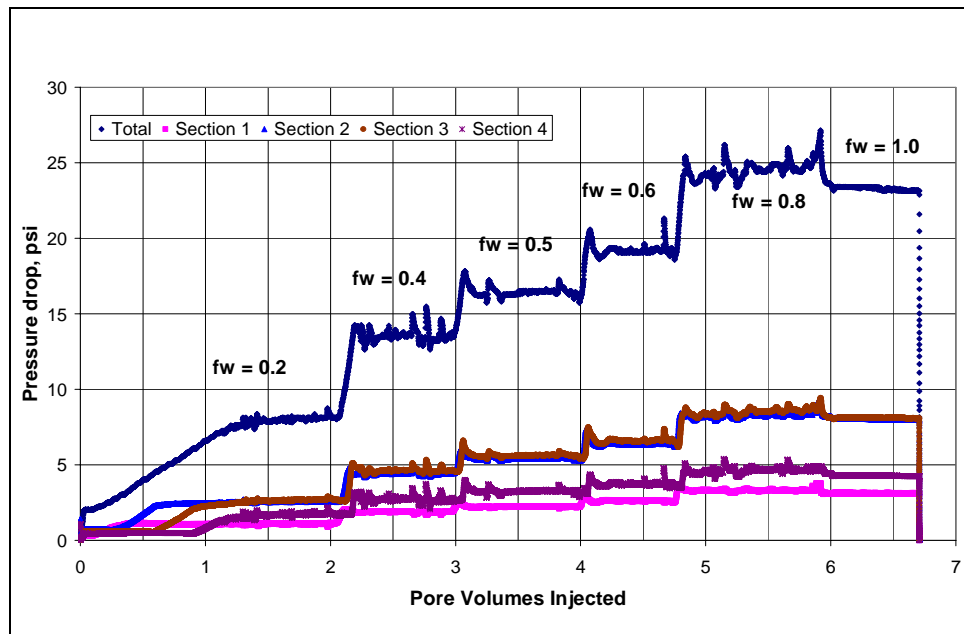


Figure B47.12: Pressure drop across the core and the sections during the post-treatment two-phase oil-water flood at different fractional flows

B48- Experiment No.48

Objective:

The objective of this experiment was to investigate the effect of chemical treatment using the surfactant #136598-106 from 3M Corp. on the gas and condensate relative permeability. The experiment was performed on a Texas Cream limestone core at 175°F.

Experimental Results:

Table B48.1 summarizes the properties of the core and the experimental conditions. Initial permeability of the core was measured using nitrogen at 75°F. **Figure B48.1** shows the pressure drop measured across the core during nitrogen flood. **Table B48.2** summarizes the results of the nitrogen flood.

The initial water saturation of 19% was established by injecting 3.8 cc of synthetic Bruce brine (**Table B21.3**) in the vacuumed core. Nitrogen flood was then conducted to measure the end point gas relative permeability. **Figure B48.2** shows the pressure drop measured across the core and **Table B48.3** summarizes the results of the nitrogen flood. The pressure of the core was raised to 200 psig and then the temperature of the oven was increased to 175°F.

Synthetic fluid mixture-4 (**Table 3.4**) was used for the two-phase flow measurements. The initial flood was conducted with the upstream backpressure regulator set at 5200 psig and the downstream back pressure regulator set at 420 psig. **Figure B48.3** shows the pressure drop across the core during the two-phase gas-condensate flow. As the pressure drop during the gas condensate flood was too high, the fluid properties were calculated at the average core pressure. **Table B48.4** gives the properties of the

synthetic fluid calculated using the Peng-Robinson EOS at the average core pressure. **Table B48.5** summarizes the results of the initial two-phase flow.

The core was then treated with the treatment solution (**Table B23.6**). **Figure B48.4** shows the measured pressure drop across the core during the treatment flood. The treatment flood was started at 64 cc/hr but then dropped to 32 cc/hr due to high pressure drop. The core was then shut-in for 15 hours.

Post-treatment two-phase gas-condensate flood was conducted under the same conditions as the initial two-phase flow. **Figure B48.5** shows the pressure drop across the core measured during the post-treatment two-phase floods at a flowing pressure of 420 psig. **Table B48.7** summarizes the results of the post-treatment two-phase flow.

Table B48.1: Core properties

Core	Texas Cream Limestone
Length, inches	7.91
Diameter, inches	0.99
Porosity, %	26.22
Pore volume, cc	26.29
Swi, %	19
Temperature, °F	175

Table B48.2: Result of nitrogen flood

q_{core}, (cc/hr)	ΔP (psi)	k_g (md)
574.04	21.05	8.34
956.73	36.31	8.06
1148.07	43.75	8.03
Permeability, k_g (md)		8.15

Table B48.3: Result of nitrogen flood at Swi

q_{core}, (cc/hr)	ΔP (psi)	k_g (md)
956.73	37.31	7.85

Table B48.4: Synthetic fluid properties at experimental conditions

Pressure, psig	5200	490	
Fluid Properties		Gas phase	Oil phase
ρ, g/cc	0.3034	0.0235	0.657
μ (cp)		0.0134	0.371
Volume fraction		0.9842	0.0158
IFT (dyne/cm)		11.867	

Table B48.5: Results of the initial two-phase gas condensate flood

q_{pump}, cc/hr	64
$q_{\text{total_core}}$, cc/hr	579.47
$q_{\text{g_core}}$, cc/hr	570.31
$q_{\text{o_core}}$, cc/hr	9.16
ΔP, psi	139.98
k_{rg}	0.110
k_{ro}	0.049
Nc	3.22×10^{-6}
PVT Ratio	2.25

Table B48.6: Composition of treatment solution

Component	Weight %
Surfactant #136598-106	2
Propylene glycol	69
Isopropanol	29

Table B48.7: Results of post-treatment two-phase flow of gas condensate mixture

q_{pump}, cc/hr	64
q_{total_core}, cc/hr	592.46
q_{g_core}, cc/hr	583.34
q_{o_core}, cc/hr	9.12
ΔP, psi	121.69
k_{rg}	0.130
k_{ro}	0.056
Nc	2.78x10 ⁻⁶
Improvement Factor	1.18

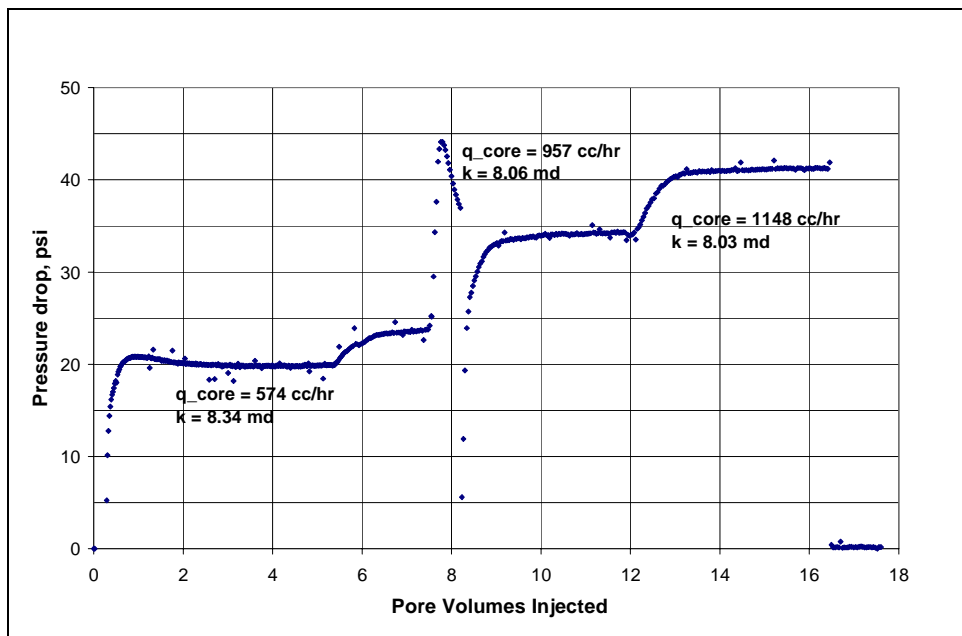


Figure B48.1: Pressure drop across the core during initial nitrogen flood

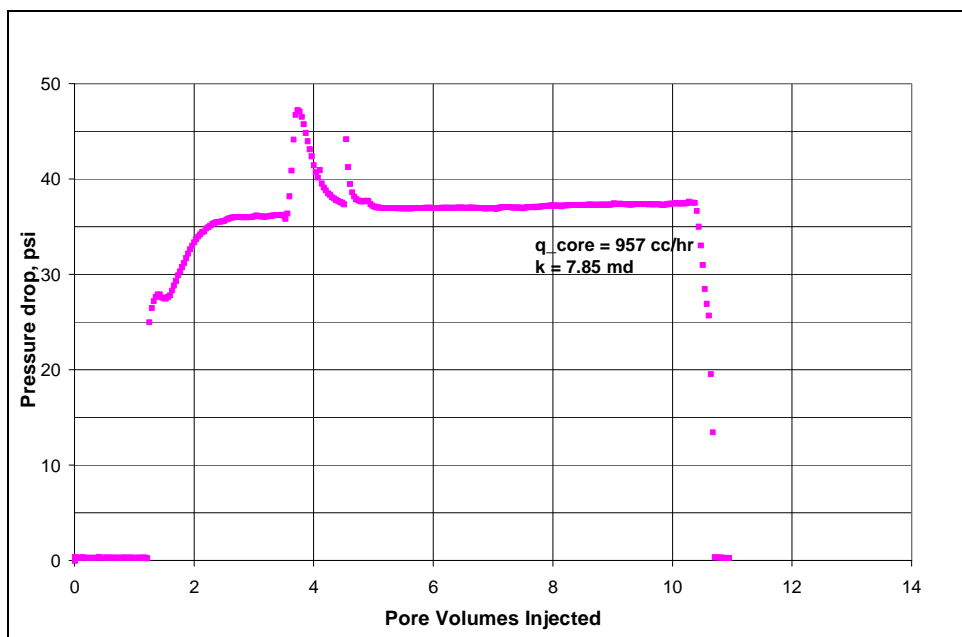


Figure B483.2: Pressure drop across the core during nitrogen flood at $S_{wi}=19\%$

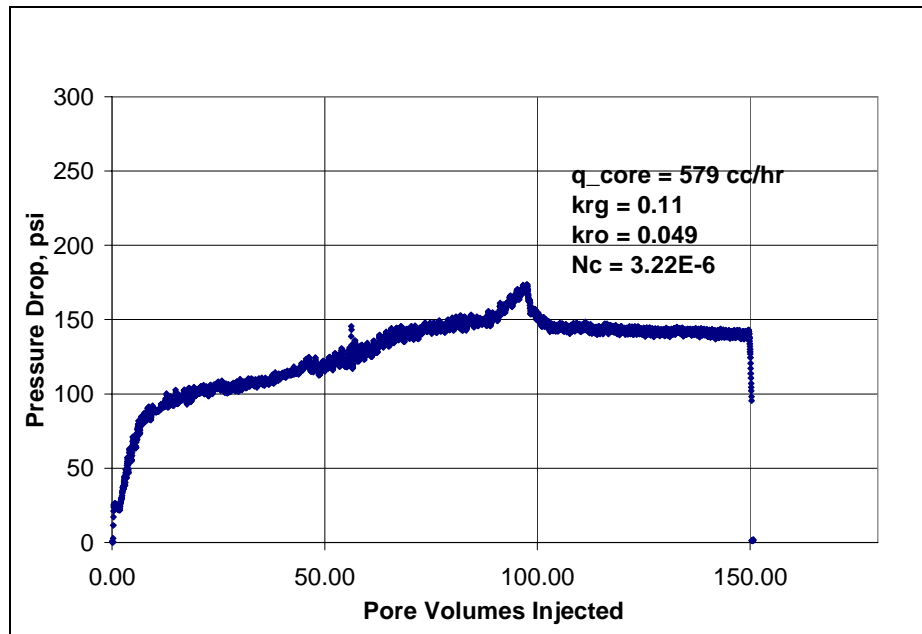


Figure B48.3: Pressure drop across the core during the initial two-phase flow at 175°F and 420psig

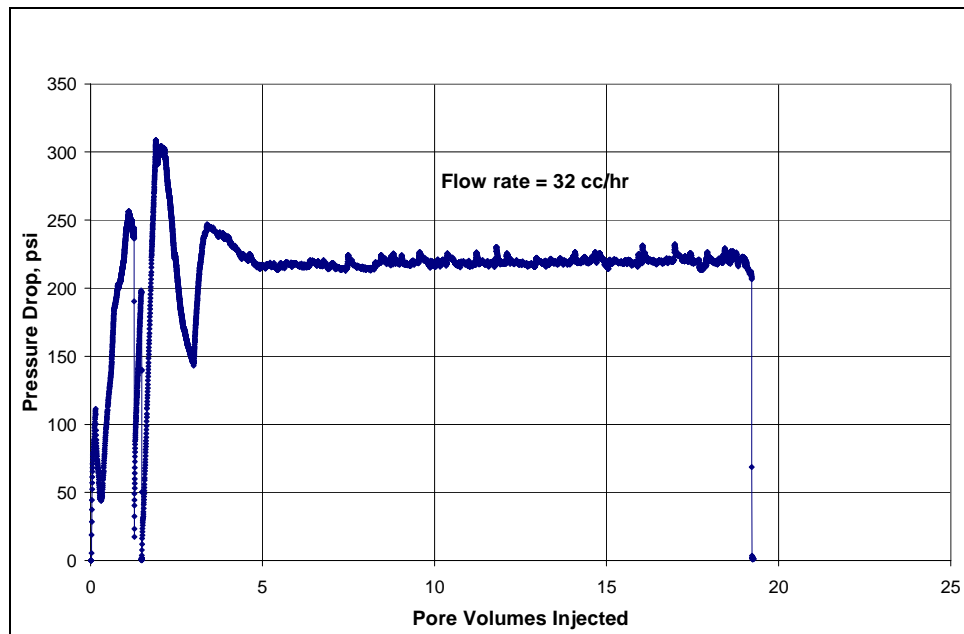


Figure B48.4: Pressure drop across the core during surfactant treatment

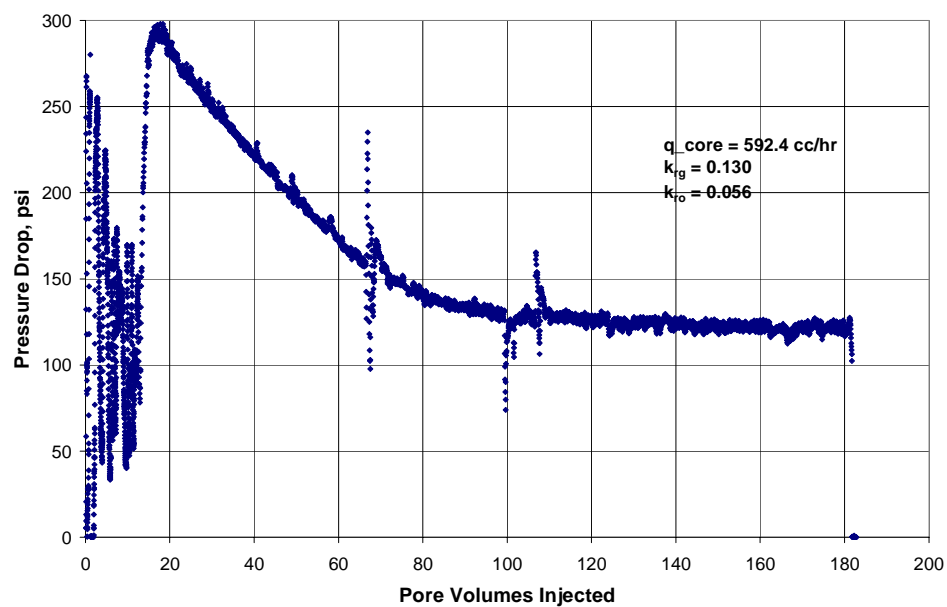


Figure B48.5: Pressure drop across the core during post-treatment two-phase flow at 175°F and 420 psig

Appendix C

This appendix gives a sample input files for the pre-treatment and post-treatment cases.

APPENDIX C1: SAMPLE INPUT FILE FOR THE BASE CASE:

RESULTS SIMULATOR GEM

RESULTS SECTION INOUT

DIM *MAXPERCENT_OF_FULLYIMPLICITBLOCKS 100

*TITLE1 'Bruce_Field_Pre_Treatment'

*INUNIT *SI

*INTERRUPT *INTERACTIVE

*RANGECHECK *ON

*XDR *ON

*MAXERROR 20

*WRST *TIME

*WPRN *WELL *TIME

*WPRN *GRID *TIME

*WSRF *WELL 1

*WSRF *GRID *TIME

*OUTPRN *WELL *ALL

*OUTPRN *WELL *PSPLIT

*OUTPRN *GRID DENG KRG SG VISG DENO KRO SO VISO PRES KRW SW SIG RHOG FRG
 RHOO CAPN VELOCRC Z 'C1N2CO2' Z 'C2' Z 'C3' Z 'C4' Z 'C5-C6' Z 'C7-C15' Z 'C16-C31' X 'C16-
 C31' Y 'C16-C31' Z 'C32+' X 'C32+' Y 'C32+'

*OUTPRN *RES *ALL

*OUTSRF *GRID DENG KRG SG VISG DENO KRO SO VISO PRES KRW SW SIG RHOG FRG
 RHOO CAPN VELOCRC Z 'C1N2CO2' Z 'C2' Z 'C3' Z 'C4' Z 'C5-C6' Z 'C7-C15' Z 'C16-C31' X 'C16-
 C31' Y 'C16-C31' Z 'C32+' X 'C32+' Y 'C32+'

*DIM *MDJCS 300

*OUTSRF *WELL PAVG

RESULTS XOFFSET 0.

RESULTS YOFFSET 0.

RESULTS ROTATION 0

**-----Reservoir Data-----

GRID RADIAL 25 1 6 *RW 0.05

KDIR DOWN

DI IVAR	0.179419	0.21160946	0.249575371	0.294352936	0.347164268
	0.409450746	0.482912351	0.569554071	0.671740614	0.792260957
	0.934404456	1.102050632	1.729117441	2.712985265	4.25667388
	6.678721318	10.47891375	16.44141567	25.79658119	40.47483588
	63.5050175	99.63937246	156.3341754	245.2883212	384.8573759

** Radial Blocks are in drainage radius=3500 ft

DJ *CON 360

DK KVAR 43.73780488 27.08841463 13.93292683 21.79878049 25.67073171
15.49695122

DTOP 25*3576.2 ** Depth of top zone is 11730 ft

RESULTS SECTION GRID

RESULTS SECTION NETPAY

RESULTS SECTION NETGROSS

*NETGROSS KVAR

0.1 0.1 0.1 0.3 0.1 1

RESULTS SECTION POR

RESULTS SECTION PERMS

**-----Porosity-----

POR KVAR

0.12 0.14 0.12 0.16 0.13 0.11

**-----

**\$ RESULTS PROP PERMI Units: md

**\$ RESULTS PROP Minimum Value: 0 Maximum Value: 16.22

**-----Permeability-----

PERMI KVAR 0.03 0.15 0.02 1.42 0.31 10 ** k=35md

PERMJ EQUALSI

PERMK KVAR 0.0003 0.0015 0.0002 0.0142 0.0031 0.1

*NULL *KVAR 1 1 1 1 1 1

RESULTS SECTION TRANS

RESULTS SECTION FRACS

RESULTS SECTION GRIDNONARRAYS

CPOR MATRIX 7.E-07

PRPOR MATRIX 39985.1

DCPOR MATRIX 0

RESULTS SECTION VOLMOD

RESULTS SECTION SECTORLEASE

RESULTS SECTION ROCKCOMPACTION

RESULTS SECTION GRIDOTHER

RESULTS SECTION MODEL

*MODEL *PR

*NC 10 10

*NONDARCY 1

*COMPNAME 'C1N2CO2' 'C2' 'C3' 'C4' 'C5-C6' 'C7-C15' 'C16-C31' 'C32+' 'EtOH' 'EGMBE'

*HCFLAG 0 0 0 0 0 0 0 0 0

*TRES 110.

*PCRIT 46.22 48.2 41.9 37.07 33.06 30.41 14.25 8.01 60.6 38.5

*TCRIT 193.928 305.4 369.8 420.222 481.183 601.978 688.85 973.711 513.9 633.9

*AC 0.015 0.098 0.152 0.188 0.2525 0.4229 0.9119 1.3549 0.644 1.2

*VCRIT 0.09857 0.148 0.203 0.25718 0.33592 0.63018 1.23499 2.49958 0.167 0.316

**VSHIFT -0.19 -0.14 -0.11 -0.09 -0.02 0.32 0.02 -0.13

*VSHIFT -0.12 -0.06 -0.16 -0.09 -0.09 0.04 -0.29 0.18 0.04 0.06

*ZCRIT 0.2209 0.2869 0.2826 0.2765 0.22 0.3099 0.3394 0.2754 0.25 0.25

*MW 16.91 30.07 44.097 58.124 78.79 109.79 359.99 609.96 46.09 118.2

*PCHOR 76.9 108.9 151.9 188.9 258.2 389.5 735.9 1364.3 0 0

*BIN

0.0061

0.0064 0.0008

0.0096 0.0023 0.0003

0.0281 0.0034 0.0009 0.0012

0.0928 0.0068 0.0022 0.0061 0.0009

0.0817	0.0169	0.0381	0.013	0.0139	0.0075			
0.0579	0.096	0.0867	0.0338	0.0424	0.0303	0		
0.00	0.19	0.03	0.00	0.00	0.29	0.29	0.29	
0	0.2	0.2	0	0	0.2	0.2	0.2	0.18

*MIXINGRULE 1

*PHASEID *DEN

*RHOW 39985

*CW 4.8E-07

*REFPW 101.3

*VISW 0.7

*PSAT 37525 ** kPA

RESULTS SECTION MODELARRAYS

RESULTS SECTION ROCKFLUID

*ROCKFLUID

RPT 1

*SWT

0.25	0.00	0.30
0.28	0.00	0.26
0.31	0.00	0.23
0.33	0.01	0.20
0.36	0.01	0.17
0.39	0.02	0.14

0.42	0.03	0.12
0.45	0.04	0.09
0.48	0.05	0.08
0.50	0.06	0.06
0.53	0.08	0.04
0.56	0.09	0.03
0.59	0.11	0.02
0.62	0.13	0.01
0.64	0.15	0.00
0.67	0.18	0.00
0.70	0.20	0.00

*SGT

0.25	0.00	0.30
0.26	0.00	0.26
0.28	0.00	0.23
0.29	0.00	0.20
0.30	0.01	0.17
0.31	0.01	0.14
0.33	0.02	0.12
0.34	0.04	0.09
0.35	0.06	0.08
0.36	0.08	0.06
0.38	0.11	0.04

0.39	0.15	0.03
0.40	0.19	0.02
0.41	0.24	0.01
0.43	0.30	0.00
0.44	0.37	0.00
0.45	0.45	0.00
0.50	0.70	0.00
0.60	0.86	0.00
0.70	0.92	0.00
0.80	0.95	0.00
0.85	0.97	0.00
1.00	1.00	0.00

*CROCK 7e-07 0 39985.1

**KRGAS *KRG

*KROIL *STONE2

*RTYPE *IJK

1:25 1 1:6 1

RESULTS SECTION ROCKARRAYS

RESULTS SECTION INIT

*INITIAL

*USER_INPUT

*NREGIONS 1

RESULTS SECTION INITARRAYS

SW *IJK

1:25 1 1 0.5

1:25 1 2 0.35

1:25 1 3:6 0.15

PRES CON 39985.1 ** kPa which is 5800.8 psi

ZGLOBALC 'C1N2CO2' CON 0.77108822

ZGLOBALC 'C2' CON 0.07774299

ZGLOBALC 'C3' CON 0.0398004

ZGLOBALC 'C4' CON 0.0217255

ZGLOBALC 'C5-C6' CON 0.0280703

ZGLOBALC 'C7-C15' CON 0.05189689

ZGLOBALC 'C16-C31' CON 0.0091876

ZGLOBALC 'C32+' CON 0.0004881

ZGLOBALC 'EtOH' CON 0.000001

ZGLOBALC 'EGMBE' CON 0.0000001

RESULTS SECTION INITARRAYS

RESULTS SPEC 'Water Saturation'

RESULTS SPEC SPECNOTCALCVAL 0

RESULTS SPEC REGION 'All Layers (Whole Grid)'

RESULTS SPEC REGIONTYPE 0

RESULTS SPEC LAYERNUMB 0

RESULTS SPEC PORTYPE 1

RESULTS SPEC CON 0.2

RESULTS SPEC STOP

RESULTS SECTION NUMERICAL

*NUMERICAL

*MAXSTEPS 500000

*DTMAX 1

*DTMIN 1.E-08

MAXCHANGE PRESS 1000

MAXCHANGE SATUR 0.01

MAXCHANGE GMOLAR 0.01

**PIVOT *ON

*ITERMAX 20

RESULTS SECTION NUMARRAYS

RESULTS SECTION GBKEYWORDS

RUN

DATE 2000 04 30

WELL 1 'WELL1'

WELL 2 'WELL2'

PRODUCER 'WELL1'

*PWELLBORE *MODEL

** wdepth wlen rough whtemp bhtemp wrad

3576.2 3576.2 0.0001 30.0 110.0 0.05

OPERATE MIN BHP 13786. CONT

GEOMETRY K 0.05 0.37 1. 0.

PERF GEOA 'WELL1'

1 1 1:6 1 OPEN

INJECTOR 'WELL2'

*INCOMP *SOLVENT 0 0 0 0 0 0 0 0.3 0.7

*OPERATE *MAX *BHF 37 ** cu.m/day

GEOMETRY K 0.05 0.37 1. 0.

PERF GEOA 'WELL2'

1 1 1:6 1 OPEN

WELL 3 'WELL3'

INJECTOR 'WELL3'

*INCOMP *SOLVENT 1 0 0 0 0 0 0 0 0 0

*OPERATE *MAX *BHF 1088 ** cu.m/day

GEOMETRY K 0.05 0.37 1. 0.

PERF GEOA 'WELL3'

1 1 1:6 1 OPEN

OPEN 'WELL1'

*SHUTIN 'WELL2'

*SHUTIN 'WELL3'

OPEN 'WELL1'

TIME 5

TIME 10

TIME 20

TIME 30

TIME 50

TIME 75

TIME 100

TIME 200

TIME 365

TIME 500
TIME 750
TIME 1000
TIME 1449
*ALTER 1
6893
TIME 1500
TIME 1825
TIME 2000
TIME 2500
TIME 3000
TIME 3650
TIME 4015
TIME 4380
ALTER 1
2757
TIME 4500
TIME 4600
TIME 4745
STOP

APPENDIX C2: SAMPLE INPUT FILE FOR THE POST-TREATMENT CASE:

** Treatment radius=2.7m

RESULTS SIMULATOR GEM

RESULTS SECTION INOUT

**DIM *MDGRID

DIM *MAXPERCENT_OF_FULLYIMPLICITBLOCKS 100

*TITLE1 'Bruce_Field_Post_Treatment'

*INUNIT *SI

*INTERRUPT *INTERACTIVE

*RANGECHECK *ON

*XDR *ON

*MAXERROR 20

*WRST *TIME

*WPRN *WELL *TIME

*WPRN *GRID *TIME

*WSRF *WELL 1

*WSRF *GRID *TIME

*OUTPRN *WELL *ALL

*OUTPRN *WELL *PSPLIT

*OUTPRN *GRID DENG KRG SG VISG DENO KRO SO VISO PRES KRW SW SIG RHOG FRG
RHO0 CAPN VELOCRC Z 'C1N2CO2' Z 'C2' Z 'C3' Z 'C4' Z 'C5-C6' Z 'C7-C15' Z 'C16-C31' X 'C16-
C31' Y 'C16-C31' Z 'C32+' X 'C32+' Y 'C32+'

*OUTPRN *RES *ALL

*OUTSRF *GRID DENG KRG SG VISG DENO KRO SO VISO PRES KRW SW SIG RHOG FRG
RHO0 CAPN VELOCRC Z 'C1N2CO2' Z 'C2' Z 'C3' Z 'C4' Z 'C5-C6' Z 'C7-C15' Z 'C16-C31' X 'C16-
C31' Y 'C16-C31' Z 'C32+' X 'C32+' Y 'C32+'

*DIM *MDJCS 300

*OUTSRF *WELL PAVG

RESULTS XOFFSET 0.

RESULTS YOFFSET 0.

RESULTS ROTATION 0

**-----Reservoir Data-----

GRID RADIAL 25 1 6 *RW 0.05

KDIR DOWN

DI IVAR	0.179419	0.21160946	0.249575371	0.294352936	0.347164268
	0.409450746	0.482912351	0.569554071	0.671740614	0.792260957
	0.934404456	1.102050632	1.729117441	2.712985265	4.25667388
	6.678721318	10.47891375	16.44141567	25.79658119	40.47483588
	63.5050175	99.63937246	156.3341754	245.2883212	384.8573759

** Radial Blocks are in meteres drainage radius=3500 ft

DJ *CON 360

DK KVAR 43.73780488 27.08841463 13.93292683 21.79878049 25.67073171

15.49695122

DTOP 25*3576.2

** Depth of top zone is 11730 ft

RESULTS SECTION GRID

RESULTS SECTION NETPAY

RESULTS SECTION NETGROSS

*NETGROSS KVAR

0.1 0.1 0.1 0.3 0.1 1

RESULTS SECTION POR

RESULTS SECTION PERMS

**-----Porosity-----

POR KVAR

0.12 0.14 0.12 0.16 0.13 0.11

**-----

**\$ RESULTS PROP PERMI Units: md

**\$ RESULTS PROP Minimum Value: 0 Maximum Value: 16.22

**-----Permeability-----

PERMI KVAR 0.03 0.15 0.02 1.42 0.31 10 ** k=35md

PERMJ EQUALSI

PERMK KVAR 0.0003 0.0015 0.0002 0.0142 0.0031 0.1

*NULL *KVAR 1 1 1 1 1 1

RESULTS SECTION TRANS

RESULTS SECTION FRACS

RESULTS SECTION GRIDNONARRAYS

CPOR MATRIX 7.E-07

PRPOR MATRIX 39985.1

DCPOR MATRIX 0

RESULTS SECTION VOLMOD

RESULTS SECTION SECTORLEASE

RESULTS SECTION ROCKCOMPACTION

RESULTS SECTION GRIDOTHER

RESULTS SECTION MODEL

*MODEL *PR

*NC 11 11

*NONDARCY 1

*COMPNAME 'C1N2CO2' 'C2' 'C3' 'C4' 'C5-C6' 'C7-C15' 'C16-C31' 'C32+' 'EtOH' 'EGMBE' 'N2'

*HCFLAG 0 0 0 0 0 0 0 0 0 0

*TRES 110.

*PCRIT 46.22 48.2 41.9 37.07 33.06 30.41 14.25 8.01 60.6 38.5 33.5

*TCRIT 193.928 305.4 369.8 420.222 481.183 601.978 688.85 973.711 513.9 633.9 126

*AC 0.015 0.098 0.152 0.188 0.2525 0.4229 0.9119 1.3549 0.644 1.2 0.04

*VCRIT 0.09857 0.148 0.203 0.25718 0.33592 0.63018 1.23499 2.49958 0.167 0.316
0.089

**VSHIFT -0.19 -0.14 -0.11 -0.09 -0.02 0.32 0.02 -0.13

*VSHIFT -0.12 -0.06 -0.16 -0.09 -0.09 0.04 -0.29 0.18 0.04 0.06
-0.04

*ZCRIT 0.2209 0.2869 0.2826 0.2765 0.22 0.3099 0.3394 0.2754 0.25 0.25 0.28

*MW 16.91 30.07 44.097 58.124 78.79 109.79 359.99 609.96 46.09 118.2 28

*PCHOR 76.9 108.9 151.9 188.9 258.2 389.5 735.9 1364.3 0 0 41

*BIN

0.0061

0.0064 0.0008

0.0096 0.0023 0.0003

0.0281 0.0034 0.0009 0.0012

0.0928 0.0068 0.0022 0.0061 0.0009

0.0817 0.0169 0.0381 0.013 0.0139 0.0075

0.0579 0.096 0.0867 0.0338 0.0424 0.0303 0

0.00 0.19 0.03 0.00 0.00 0.29 0.29 0.29

0 0.2 0.2 0 0 0.2 0.2 0.2 0.18

0.08 0.08 0.08 0.08 0.08 0.08 0.08 0.08 0.5 0.2

*MIXINGRULE 1

*PHASEID *DEN

*RHOW 39985

*CW 4.8E-07

*REFPW 101.3

*VISW 0.7

*PSAT 37525 ** kPA

RESULTS SECTION MODELARRAYS

RESULTS SECTION ROCKFLUID

*ROCKFLUID

RPT 1

*SWT

0.25	0.00	0.30
0.28	0.00	0.26
0.31	0.00	0.23
0.33	0.01	0.20
0.36	0.01	0.17
0.39	0.02	0.14
0.42	0.03	0.12
0.45	0.04	0.09
0.48	0.05	0.08
0.50	0.06	0.06
0.53	0.08	0.04
0.56	0.09	0.03
0.59	0.11	0.02
0.62	0.13	0.01
0.64	0.15	0.00
0.67	0.18	0.00
0.70	0.20	0.00

*SGT

0.25	0.00	0.30
0.26	0.00	0.26
0.28	0.00	0.23
0.29	0.00	0.20
0.30	0.01	0.17
0.31	0.01	0.14
0.33	0.02	0.12
0.34	0.04	0.09
0.35	0.06	0.08
0.36	0.08	0.06
0.38	0.11	0.04
0.39	0.15	0.03
0.40	0.19	0.02
0.41	0.24	0.01
0.43	0.30	0.00
0.44	0.37	0.00
0.45	0.45	0.00
0.50	0.70	0.00
0.60	0.86	0.00
0.70	0.92	0.00
0.80	0.95	0.00
0.85	0.97	0.00
1.00	1.00	0.00

**CROCK 7e-07 0 39985.1

**KRGAS *KRG

*KROIL *STONE2

*RPT 2

*SWT

0.25	0.00	0.40
------	------	------

0.28	0.00	0.26
------	------	------

0.31	0.00	0.23
------	------	------

0.33	0.01	0.20
------	------	------

0.36	0.01	0.17
------	------	------

0.39	0.02	0.14
------	------	------

0.42	0.03	0.12
------	------	------

0.45	0.04	0.09
------	------	------

0.48	0.05	0.08
------	------	------

0.50	0.06	0.06
------	------	------

0.53	0.08	0.04
------	------	------

0.56	0.09	0.03
------	------	------

0.59	0.11	0.02
------	------	------

0.62	0.13	0.01
------	------	------

0.64	0.15	0.00
------	------	------

0.67	0.18	0.00
------	------	------

0.70	0.20	0.00
------	------	------

*SGT

0.25	0	0.4
0.26	0.003684685	0.3713293
0.27	0.011971576	0.343329903
0.28	0.023850992	0.316022085
0.29	0.038895763	0.289427953
0.3	0.056839377	0.263571729
0.31	0.077492098	0.238480103
0.32	0.100708693	0.214182686
0.33	0.1263727	0.190712565
0.34	0.154387647	0.168107037
0.35	0.184671671	0.146408571
0.36	0.217154004	0.125666101
0.37	0.251772558	0.105936833
0.38	0.288472202	0.087288828
0.39	0.327203491	0.069804885
0.4	0.367921703	0.053588674
0.41	0.410586093	0.038775151
0.42	0.455159309	0.025550084
0.43	0.50160692	0.014192536
0.44	0.549897039	0.005194772
0.45	0.6	0
1	1	0

*RPT 3

*SWT

0.25	0.00	0.3
0.28	0.00	0.26
0.31	0.00	0.23
0.33	0.01	0.20
0.36	0.01	0.17
0.39	0.02	0.14
0.42	0.03	0.12
0.45	0.04	0.09
0.48	0.05	0.08
0.50	0.06	0.06
0.53	0.08	0.04
0.56	0.09	0.03
0.59	0.11	0.02
0.62	0.13	0.01
0.64	0.15	0.00
0.67	0.18	0.00
0.70	0.20	0.00

*SGT

0.25	0	0.3
0.26	0.00125	0.276362443
0.27	0.005000001	0.253459907
0.28	0.011250002	0.231308471
0.29	0.020000003	0.209925519
0.3	0.031250004	0.189329932
0.31	0.045000005	0.16954232
0.32	0.061250006	0.150585317
0.33	0.080000007	0.132483947
0.34	0.101250008	0.11526609
0.35	0.125000009	0.098963095
0.36	0.151250009	0.083610589
0.37	0.180000009	0.069249597
0.38	0.211250009	0.055928109
0.39	0.245000009	0.043703405
0.4	0.281250008	0.032645647
0.41	0.320000007	0.022843848
0.42	0.361250006	0.014416747
0.43	0.405000004	0.00753566
0.44	0.451250002	0.002485841
0.45	0.5	0
1	1	0

**CROCK 7e-07 0 39985.1

**KRGAS *KRG

*KROIL *STONE2

** Change in relative permeability curves for the treated zones**

*RTYPE *IJK

1:25 1 1:6 1

1:8 1 6 2

9:10 1 6 3

RESULTS SECTION ROCKARRAYS

RESULTS SECTION INIT

*INITIAL

*USER_INPUT

*NREGIONS 1

RESULTS SECTION INITARRAYS

SW *IJK

1:25 1 1 0.5

1:25 1 2 0.35

1:25 1 3:6 0.15

1:8 1 6 0.0000001

PRES ALL

INCLUDE 'Pre_Treatment_1 Pressure Time 4745.txt'

** Initial composition of each component is taken from the final time step of the base case as an include file**

ZGLOBALC 'C1N2CO2' ALL

INCLUDE 'Pre_Treatment_1 Global Mole Fraction(C1N2CO2) Time 4745.txt'

ZGLOBALC 'C2' ALL

INCLUDE 'Pre_Treatment_1 Global Mole Fraction(C2) Time 4745.txt'

ZGLOBALC 'C3' ALL

INCLUDE 'Pre_Treatment_1 Global Mole Fraction(C3) Time 4745.txt'

ZGLOBALC 'C4' ALL

INCLUDE 'Pre_Treatment_1 Global Mole Fraction(C4) Time 4745.txt'

ZGLOBALC 'C5-C6' ALL

INCLUDE 'Pre_Treatment_1 Global Mole Fraction(C5-C6) Time 4745.txt'

ZGLOBALC 'C7-C15' ALL

INCLUDE 'Pre_Treatment_1 Global Mole Fraction(C7-C15) Time 4745.txt'

ZGLOBALC 'C16-C31' ALL

INCLUDE 'Pre_Treatment_1 Global Mole Fraction(C16-C31) Time 4745.txt'

ZGLOBALC 'C32+' ALL

INCLUDE 'Pre_Treatment_1 Global Mole Fraction(C32+) Time 4745.txt'

ZGLOBALC 'EtOH' CON 0.000001

ZGLOBALC 'EGMBE' CON 0.0000001

RESULTS SECTION INITARRAYS

RESULTS SPEC 'Water Saturation'

RESULTS SPEC SPECNOTCALCVAL 0

RESULTS SPEC REGION 'All Layers (Whole Grid)'

RESULTS SPEC REGIONTYPE 0

RESULTS SPEC LAYERNUMB 0

RESULTS SPEC PORTYPE 1

RESULTS SPEC CON 0.2

RESULTS SPEC STOP

RESULTS SECTION NUMERICAL

*NUMERICAL

*MAXSTEPS 500000

*DTMAX 0.1

*DTMIN 1.E-10

MAXCHANGE PRESS 3500

MAXCHANGE SATUR 0.05

MAXCHANGE GMOLAR 0.05

**PIVOT *ON

*ITERMAX 20

RESULTS SECTION NUMARRAYS

RESULTS SECTION GBKEYWORDS

RUN

DATE 2000 04 30

WELL 1 'WELL1'

WELL 2 'WELL2'

WELL 3 'WELL3'

PRODUCER 'WELL1'

*PWELLBORE *MODEL

** wdepth wlen rough whtemp bhtemp wrad

3576.2 3576.2 0.0001 30.0 110.0 0.05

OPERATE MIN BHP 2757. CONT

Monitor MAX BHP 3000

GEOMETRY K 0.05 0.37 1. 0.

PERF GEOA 'WELL1'

1 1 1:6 1 OPEN

INJECTOR 'WELL2'

*INCOMP *SOLVENT 0 0 0 0 0 0 0 0.52 0.48 0

*OPERATE *MAX *BHF 228 ** cu.m/day

GEOMETRY K 0.05 0.37 1. 0.

PERF GEOA 'WELL2'

1 1 6 1 OPEN

INJECTOR 'WELL3'

*INCOMP *SOLVENT 0 0 0 0 0 0 0 0 0 1

*OPERATE *MAX *BHP 34455 ** cu.m/day, injecting 2MMSCF of chase gas

GEOMETRY K 0.05 0.37 1. 0.

PERF GEOA 'WELL3'

1 1 6 1 OPEN

SHUTIN 'WELL1'

SHUTIN 'WELL3'

OPEN 'WELL2'

TIME 0.18

SHUTIN 'WELL2'

OPEN 'WELL3'

TIME 0.37

SHUTIN 'WELL3'

OPEN 'WELL1'

TIME 0.5

TIME 1

TIME 2

TIME 3

TIME 4

TIME 5

TIME 7

TIME 10

TIME 20

TIME 30

TIME 50

TIME 75

TIME 100

TIME 200

TIME 365

STOP

References

- Abel, W., Jackson, R.F. and Wattenbarger, R.A.: "Simulation of a Partial Pressure Maintenance Gas Cycling Project with a Compositional Model, Carson Creek Field, Alberta," *JPT* (January 1970), 38-46.
- Afidick, D., Kaczorowski, N.J. and Bette, S.: "Production Performance of Retrograde Gas Reservoir: A Case Study of the Arun Field," paper SPE 28749 presented at the 1994 SPE Asia Pacific Oil and Gas Conference, Melbourne, Australia, Nov. 7-10.
- Ahmadi, M.: "Chemical Treatment for Reducing Impairment due to Condensate and/or Water Blocking in Gas wells," PhD Dissertation, The University of Texas at Austin, expected 2008-09.
- Ahmed, H., Banbi, EL., Aly, A.M., Lee, W.J. and McCain, W.D.: "Investigation of Waterflooding and Gas Cycling for Developing a Gas Condensate Reservoir," paper SPE 59772, presented at SPE/CERI Gas Technology Symposium, Alberta, Canada, April 3-5, 2000.
- Ahmed, T., Evans, J., Kwan, R. and Vivian, T.: "Wellbore Liquid Blockage in Gas-Condensate Reservoirs", SPE51050, presented at the 1998 SPE Eastern Regional Meeting held in Pittsburgh, PA, 9-11 November.
- Ahmed, T.H.: "Comparative Study of Eight Equation of State for Predicting Hydrocarbon Volumetric Phase Behavior," paper SPE 15673, presented at SPE Annual Technical Conference, New Orleans, October 5 – 6, 1986.
- Al-Anazi, Hamoud: "Experimental Measurements of Condensate Blocking and Treatments in Low and High Permeability Cores," Ph.D. dissertation, The University of Texas At Austin (2003).
- Al-Anazi, H. A., Pope, G. A. and Sharma, M. M.: "Laboratory Measurement of Condensate Blocking and Treatment for Both Low and High Permeability Rocks", paper SPE 77546, presented at the SPE Annual Technical Conference and Exhibition, San Antonio, TX, 29 September-2 October 2002.
- Al-Anazi, H. A., Sharma, M. M. and Pope, G. A.: "Revaporization of condensate with methane flood", paper SPE 90860, presented at the SPE International Petroleum Conference, Puebla, Mexico, 8-9 November 2004.

- Al-Anazi, Hamoud, Walker, Jacob G., Walker, Pope, Gary A., Pope, Sharma, Mukul M., Sharma, Hackney, David F. Hackney: "A Successful Methanol Treatment in a Gas-Condensate Reservoir: Field Application", SPE 80901, presented at the SPE Production and Operations Symposium held in Oklahoma City, Oklahoma, U.S.A., 22-25 March 2003.
- Al-Hashim, H.S. and Hashmi, S.S.: "Long Term Performance of Hydraulically Fractured Layered Rich Gas Condensate Reservoir," paper SPE 64774, presented at SPE International Oil and Gas Conference and Exhibition, Beijing, China, November 7-9, 2000.
- Amott, E. Trans. AIME 1959, 216, 156-192
- Anderson, G.A.: "Simulation of Chemical Flood Enhanced Oil Recovery Processes Including the Effects of Reservoir Wettability," MS Thesis, The University of Texas at Austin, May 2006
- Arcia, M.E, Rodriguez, F. and Madail, W.: "Estimation of Saturation Pressure Through Wellbore Measurements," paper SPE 90186, presented at the 2004 SPE Annual Technical Conference and Exhibition, Houston, TX, September 26-29.
- Asar Hamza and Handy L.L.: "Influence of Interfacial Tension on Gas/Oil Relative Permeability in a Gas-Condensate System", SPERE, February 1988
- Ayyalasomayajula, S. P.: "Prediction of Bulk and Interfacial Thermodynamic Properties of Polar Mixtures by Statistical Associating Fluid Theory," Ph.D. dissertation, The University of Texas at Austin, 2003.
- Ayyalasomayajula, P., Sharma, R., Walker, J.G., Sharma, M.M. and Pope, G.A.: "Phase Behavior Modeling of Hydrocarbon-Methanol-Water Mixtures by Peng-Robinson and SAFT Equations of State," paper SPE 77575 presented at the 2002 SPE Annual Technical Conference and Exhibition, San Antonio, TX, September 29 - October 2.
- Ayyalasomayajula P., Silpngarmmlers N., Berroteran J., Sheffield J. and Kamath J.: "Condensate Relative Permeability Data For Well Deliverability Predictions For A Deep Marine Sandstone Reservoir," paper SCA 2003-33.
- Ayyalasomayajula P, Silpngarmmlers N and Kamath J: "Well Deliverability Predictions for a Low Permeability Gas Condensate Reservoir," paper SPE 95529, presented at the SPE Annual Technical Conference and Exhibition, Dallas, October 9-12, 2005.
- Baker, L.E.: "Review of Three-Phase Relative Permeability Literature: Data and Correlation Methods," Report, Amoco Production Co. February 1987

- Bang, V.: "Phase Behavior Study of Hydrocarbon-Water-Alcohol Mixtures," M.S. Thesis, The University Of Texas At Austin (2005).
- Bang,V, Pope, G.A. and Sharma, M.M.: "Phase Behavior Study of Hydrocarbon-Water-Alcohol Mixtures at Reservoir Conditions", SPE 102100 presented at the SPE Annual Technical Conference and Exhibition, San Antonio, TX, 24-27 September 2006.
- Bang,V, Kumar, V., Ayyalasomayajula, P., Pope, G.A. and Sharma, M.M.: "Relative Permeability of Gas/Condensate Fluids: A General Correlation", SPE 102741, presented at the SPE Annual Technical Conference and Exhibition, San Antonio, TX, 24-27 September 2006.
- Baran, J.: Discussion in private communication, 2006
- Bardon, C. P. and Longeron D. G: "Influence of Very Low Interfacial Tension on Relative Permability", SPEJ (October 1980), pp 391-401.
- Barnum, R.S., Brinkman, F.P., Richardson, T.W. and Spillette, A.G.: "Gas Condensate Reservoir Behavior: Productivity and Recovery Reduction Due to Condensation," paper SPE 30767 presented at the 1995 SPE Annual Technical Conference and Exhibition, Dallas, TX, October 22-25.
- BP.: "Statistical Review of World Energy," World Wide Web Address: <http://bp.com>, 2007
- Boom, W., Wit, K., Zeelenberg, J.P.W., Weeda, H.C. and Maas, J.G.: "On the Use of Model Experiments for Assessing Improved Gas-Condensate Mobility Under Near-Wellbore Flow Conditions," paper SPE 36714 presented at the 1996 SPE Annual Technical Conference and Exhibition, Denver, Colorado, October 6-9.
- Bourbiaux, B.J. and Limborg, S.G.: "An Integrated Experimental Methodology for a Better Prediction of Gas-Condensate Flow Behavior," paper SPE 28931 presented at the SPE 69th Annual Technical Conference and Exhibition, New Orleans, LA, September 25-28, 1994.
- Brownell L. E. and Katz, D.L.: "Flow of Fluids through Porous Media-Part II", Chem. Eng. Pros., 43 11, 601-612 (1947).
- Cable A., Mott, R. and Spearing, M.: "X-Ray in-situ saturation in gas condensate relative permeability studies", SCA 2003.
- Chen H. L., Wilson S. D. and Monger-McClure: "Determination of Relative Permeability and Recovery for North Sea Gas Condensate Reservoir", SPEREE August 1999 (pg. 393-402)

- Chen, J., Hirasaki, G. and Flaum, M.: "Study of Wettability Alteration From NMR: Effect of OBM on Wettability and NMR Responses," 8th International Symposium on Reservoir Wettability, May 2004
- Chen, J., Hirasaki, G. and Flaum, M.: "NMR wettability indices: Effect of OBM on wettability and NMR responses," Journal of Petroleum Science and Engineering vol. 52, June 2006 (pg 161-171)
- Chopra, A.K., and Carter, R. D.: "Proof of the Two-Phase Steady-State Theory for Flow through Porous Media," paper SPE 14472, SPE Formation Evaluation, December 1986
- Chowdhury N.S.: "Reservoir Simulation of Asphaltene Precipitation and of Gas Condensates," MS thesis, The University of Texas at Austin, December 2003.
- Chowdhury N.S, Sharma, R., Pope, G.A. and Sepehrnoori, K.: "A Semi-Analytical Method to Predict Well Deliverability in Gas Condensate Reservoirs," paper SPE 90320, to be presented at SPE Annual Technical Conference, Houston, TX, September 26-29, 2004.
- Civan, Faruk: "Modeling Well Performance Under Non equilibrium Deposition Conditions", SPE 67234, presentation at the SPE Production and Operations Symposium held in Oklahoma City, Oklahoma, 24-27 March 2001.
- Cullick, A.S., Lu, H.S., Jones, L.G., Cohen, M.F. and Watson, J.P.: "WAG May Improve Gas Condensate Recovery," paper SPE 19114, presented at 1989 SPE Gas Technology Symposium, Dallas, Texas, June 7-9
- Cvetkovic, B., Economides, M.J., Mining U. L., Omrcen, B., and Longaric, B.: "Production from Heavy Gas Condensate Reservoirs," paper SPE 20968, European Petroleum Conference, October 21-24, The Hague, Netherlands, 1990
- Danesh, A., Henderson, G.D., Krinis, D., and Peden, J.M.: "Experimental Investigation of Retrograde Condensation in Porous Media at Reservoir Conditions," paper SPE 18316 presented at SPE Annual Technical Conference and Exhibition, October 2-5, Houston, Texas, 1989
- Delshad, M.: "Trapping of Micellar Fluids in Berea Sandstone," PhD dissertation, The University of Texas At Austin (1990).
- Donaldson, E.C., Thomas, R.D. and Lorenz, R.B.: "Wettability Determination and its Effect on Recovery Efficiency," Society of Petroleum Engineering Journal, 1969, Vol. 9, 13-20
- Du, L., Walker, J.G., Pope, G.A., Sharma, M.M. and Wang, P.: "Use of Solvents to Improve the Productivity of Gas Condensate Wells," paper SPE 62935 presented

- at the 2000 SPE Annual Technical Conference and Exhibition, Dallas, TX, October 1-4.
- Elliot, S., Hsu, H.H., O'Hearn T., Sylvester, I.F. and Vercesi, R.: "The Giant Karachaganak Field, Unlocking Its Potential," *Oilfield Review* 10, no. 3 (Autumn 1998): 16-25.
- Elsharkawy, A.M., Yosef, S.Kh., Hashem, S. and Alikhan, A.A.: "Compressibility Factor for Gas Condensates," paper SPE 59704, presented at SPE 2000 Permian Basin Oil and Gas Recovery Conference, Midland, Texas, March 21-23.
- Engineer, R.: "Cal Canal Field, California: Case History of a Tight and Abnormally Pressured Gas Condensate Reservoir," paper SPE 13650 presented at the 1985 SPE California Regional Meeting, Bakersfield, CA, March 27-29.
- Fahes, M. and Firoozabadi: "Wettability alteration to intermediate gas wetting in gas/condensate reservoirs at high temperatures," paper SPE 96184 presented at the SPE Annual Technical Conference and Exhibition, Dallas, TX, October 9-12, 2005.
- Fevang, Ø. and Whitson, C.H.: "Modeling Gas-Condensate Well Deliverability," paper SPE 30714, presented at SPE Annual Technical Conference, Dallas, October – 22-25, 1995.
- Fevang, Ø. and Whitson, C.H.: "Modeling Gas-Condensate Well Deliverability," *SPE* (Nov. 1996).
- Fevang, Ø. and Whitson, C.H.: "Guidelines for Choosing Compositional and Black-Oil Models for Volatile Oil and Gas- Condensate Reservoirs," paper SPE 63087, presented at SPE Annual Technical Conference, Dallas, October 1-4, 2000.
- Fevang Ø.: "Gas Condensate Flow Behavior And Sampling", Ph.D. dissertation, The University Of Trondheim (1995).
- Fishlock, T.P. and Smith, R.A.K.: "Three-phase studies of gas condensate flow behavior", SPE Advanced Technology Services, Vol 1. 1993.
- Fishlock, T.P. and Probert, C.J.: "Waterflooding of Gas-Condensate Reservoirs," paper SPE 35370, presented at 1996 SPE/DOE Symposium on Improved Oil Recovery, Tulsa, Oklahoma, April 21-24.
- Garzon, F. O., Al-Anazi, H.A., Leal, J. A., and Al-Faifi, M.G: "Laboratory and filed trial results of condensate banking removal in retrograde gas condensate reservoirs: Case study," paper SPE 102558 presented at the SPE Annual Technical Conference and Exhibition, San Antonio, TX, September 25-27, 2006.

- Gatlin, C.: "The Miscible Displacement of Oil and Water From Porous Media by Various Alcohols," Ph.D. Dissertation, The Pennsylvania State University, August 1959.
- Geertsma, J.: "Estimating the Coefficient of Inertial Resistance through Consolidated Porous Media," Society of Petroleum Engineers Journal, October 1974, 445-450.
- GEM: "General equation of states modeling," compositional simulator, Version 2006.1, Computer Modeling Group.
- Gravier, J.F., Lemouzy, P., Barroux, C., and Abed, A.F.: "Determination of Gas-Condensate Relative Permeability on Whole Cores Under Reservoir Conditions," paper SPE 11493, SPE Formation Evaluation, v 1, n 1, p 9-15, February 1986.
- Ham, J.D. and Eilerts, C.K.: "Effect of saturation on mobility of low liquid-vapor ratio fluids," SPEJ, March 1967
- Haniff, M.S., and Ali, J.K.: "Relative Permeability and Low Tension Fluid Flow in Gas Condensate Systems," paper SPE 20917 presented at European Petroleum Conference, October 21-24, The Hague, Netherlands, 1990
- Henderson, G.D., Danesh, A., Tehrani, D.H. and Peden, J.M.: "An Investigation Into the Processes Governing Flow and Recovery in Different Flow Regimes in Gas Condensate Reservoirs," paper SPE 26661 presented at the 68th Annual Technical Conference and Exhibition of the SPE, Houston, Texas, 3-6 October 1993.
- Henderson, G. D., Danesh, A., Tehrani, D. H., Al-Shaidi, S. and Peden, J. M.: "Measurement and Correlation of Gas Condensate Relative Permeability by the Steady-State Method", SPEREE (April 1998).
- Henderson, G.D., Danesh, A., Tehrani, D. H., Al-Shaidi, S., Peden, J.M.: "Measurement and Correlation of Gas Condensate Relative Permeability by the Steady-State Method" SPE 30770, presented at the SPE Annual Technical Conference & Exhibition, Dallas, TX, U.S.A., 22-25 October, 1995.
- Henderson, G. D., Danesh, A., Tehrani, D. H., and Al-Kharusi, B: "The Relative Significance of Positive Coupling and Inertial Effects on Gas Condensate Relative Permeabilities at High Velocity", paper SPE 62933 presented at the SPE Annual Technical Conference and Exhibition, Dallas, TX, October 1-4, 2000.
- Henderson, G.D., Danesh, A., and Peden, J.M.: "Waterflooding of Gas Condensate Fluids in Cores Above and Below the Dewpoint," SPE 22636, presented at the SPE Annual Technical Conference & Exhibition, Dallas, TX, U.S.A., 6-9 October, 1991.

- Herning, F. and Zipperer, L.: Gas und Wasserfach v79, 49 (1936)
- Hoier, L., Cheng, N., and Whitson, C.H.: "Miscible Gas Injection in Undersaturated Gas-Oil Systems," SPE 90379, presented at the SPE Annual Technical Conference & Exhibition, Houston, TX, U.S.A., 26-29 September, 2004.
- Huron, M. J. and Vidal, J.: "New Mixing Rules in Simple Equation of State for Representing Vapor-Liquid Equilibria of Strongly Non-Ideal Mixtures", Fluid Phase Equilibria, 3, 1979, p 255-271.
- Jadhunandan, P.P. and Morrow, N.R.: "Effect of Wettability on Waterflood Recovery for Crude-Oil/Brine/Rock Systems," paper SPE 22597, October 1991.
- Jamaluddin, A.K.M., Thomas, S.Y.J., D'Cruz, D., and Nighswander, J.: "Experimental and Theoretical Assessment of Using Propane to Remediate Liquid Buildup on Condensate Reservoirs," paper SPE 71526 presented at the 2001 SPE Annual Technical Conference and Exhibition, New Orleans, LO, September 30-October 3.
- Kalaydjian, F.J-M, Bourbiaux, B.J. and Lombard, J-M.: "Predicting gas-condensate reservoir performance: how flow parameters are altered when approaching production wells". SPE 36715, presented at the 1996 SPE Annual Technical Conference and Exhibition held in Denver, Colorado, U.S.A., 6-9.
- Kissa, E.: "Flourinated Surfactants and Repellents," Surfactant science series, v 97, 2nd edition, Marcel Dekker, 2001
- Kumar, R.: "Productivity Improvement of Gas-Condensate Wells by Fracturing", MS thesis, The University of Texas at Austin, August 2000.
- Kumar V: "Chemical Stimulation of Gas Condensate Reservoir: An Experimental and Simulation Study" Ph.D. dissertation, The University of Texas at Austin (2006).
- Kumar, V., Pope, G.A. and Sharma, M.M.: "Improving the Gas and Condensate Relative Permeability Using Chemical Treatments", SPE 100529 presented at the 2006 SPE Gas Technology Symposium, Calgary, Alberta, Canada, May 15-17.
- Kumar, V., Bang, V., Pope, G.A., Sharma, M.M., Ayyalasomayajula, P.S., Kamath, J.: "Chemical Stimulation of Gas-Condensate Reservoirs", SPE 102669 presented at the SPE Annual Technical Conference and Exhibition, San Antonio, TX, 24-27 September 2006.
- Kokal, S., Mohammad Al-Dokhi and Selim, S.: "Phase Behavior of Gas Condensate/Water System", SPE62931, presentation at the 2000 SPE Annual Technical Conference and Exhibition held in Dallas, Texas, 1-4 October 2000.

- Kossack, C.A. and Opdal, S.T.: "Recovery of Condensate from a Heterogeneous Reservoir by Injection of a Slug of Methane Followed by Nitrogen," paper SPE 18265 presented at 1986 SPE Annual Technical Conference and Exhibition, Houston, TX, October 23.
- Lawson, J.B.: "The Adsorption of Non-ionic and Anionic Surfactants on Sandstone and Carbonate," paper SPE 7052
- Li, K. and Firoozabadi, A.: "Experimental study of wettability alteration to preferential gas wetting in porous media and its effects," SPERE (April 2000), 139–149.
- Liu, Y., Zheng, H., Huang, G. and Zhongyuan, G.L.: "Improving production in gas/condensate reservoirs by wettability alteration to gas wetness," paper SPE 99739, presented at 2006 SPE Symposium on Improved Oil Recovery, Tulsa, Oklahoma, April 22-26, 2006
- Lindeloff, N, Michael L. and Michelsen: "Phase Envelope Calculations for Hydrocarbon-Water Mixtures", paper SPE77770, presented at the SPE Annual Technical Conference and Exhibition, San Antonio, Texas, 29 September-2 October 2002.
- Lolon, E.P., McVay, D.A. and Schubarth, S.K.: "Effect of Fracture Conductivity on Effective Fracture Length," paper SPE 84311, presented at 2003 SPE Annual Technical Conference, Denver, Colorado, October 5-8.
- Looney, M.D., Haynes, L.L. and Thomas, A.R.: "Core/Fluid Study, Hatters Pond Field, Mobile County, AL" Technical Memorandum, E&P Technology dept, Texaco, January 1995
- Luo, K., Shi, L., Zeng, X., Chen, G., Dai, Z. and Liu, N.: "Experimental Investigation in Revaporization of Retrograde Condensate by Lean Gas Injection," paper SPE 68683 presented at the SPE Asia – Pacific Oil and Gas Conference, Jakarta, Indonesia, April 17-19, 2000.
- Ma, H. and Ruth, D.: "Physical Explanations of Non-Darcy Effects for Fluid Flow in Porous Media," SPE Formation Evaluation Journal, March 1997.
- Marker, M.F.: "Simulation of the Use of Solvents in Gas-Condensate Reservoirs," MS Thesis, Technical University of Denmark, Fall 2000.
- Mohan, J: "Modeling of Gas Condensate Wells with and without Hydraulic Fractures," MS Thesis, The University of Texas at Austin, August 2005.
- Mohan, J., Pope, G.A. and Sharma, M.M.: "Effect of Non-Darcy Flow on Well Productivity in a Hydraulically Fractured Gas/Condensate Well", SPE 103025 presented at the SPE Annual Technical Conference and Exhibition, San Antonio, TX, 24-27 September 2006.

- Mohanty, K.K., Adibhatla, B.: "Effect of Surfactants on Wettability of near-wellbore Regions of Gas Reservoirs, SPE Wettability conference, Houston, TX, May 2004.
- Marokane, D., Logmo-Ngog, A.B. and Sarkar, R.: "Applicability of Timely Gas Injection in Gas Condensate Fields To Improve Well Productivity", SPE75147, presented at the SPE/DOE Thirteenth Improved Oil Recovery Symposium, Tulsa, Oklahoma, 13-17 April 2002.
- Mott, R., Cable, A. and Spearing, M.: "A New Method for Measuring Relative Permeabilities for Calculating Gas Condensate Well Deliverability," paper SPE 56484 presented at the 1999 SPE Annual Technical Conference and Exhibition, Houston, TX, October 3-6.
- Mott, R., Cable, A. and Spearing, M.: "Measurements and Simulation of Inertial and High Capillary Number Flow Phenomena in Gas-Condensate Relative Permeability," paper SPE 62932 presented at the 2000 SPE Annual Technical Conference and Exhibition, Dallas, TX, October 1-4.
- Mott, Robert: "Engineering Calculations of Gas Condensate Well Productivity", SPE 77551, SPE Annual Technical Conference and Exhibition held in San Antonio, Texas, 29 September-2 October 2002.
- Mukerud, P.K.: "Measurement of Relative Permeability and Flow Properties of a Gas Condensate System during Pressure Depletion and Pressure Maintenance," paper SPE 19071 presented at SPE Gas Technology Symposium, 7-9 June, Dallas, Texas, 1989
- Nagarajan, N. R, Honarpour, M. M., Sampath, K., and McMichael, D.: "Comparison of Gas-Condensate Relative Permeability Using Live Fluid vs. Model Fluids," SCA2004-09, 2004
- Narayanaswamy, G: "Well Productivity of Gas Condensate Reservoir", MS Thesis, The University of Texas at Austin, August 1998.
- Narayanaswamy, G., Pope, G.A. and Sharma, M.M.: "Effect of Heterogeneity on the Non-Darcy Flow Coefficient," paper SPE 39979.
- Narayanaswamy, G., Pope, G.A. and Sharma, M.M.: "Predicting Gas Condensate Well Productivity Using Capillary Number and Non-Darcy Effects," paper SPE 51910 presented at the 1999 SPE Reservoir Simulation Symposium, Houston, TX, February 14-17.
- Narayanaswamy, G., Pope, G.A. and Sharma, M.M.: "Effect of Heterogeneity on the Non-Darcy Flow Coefficient," paper SPE 56881.

- Noh, M. and Firoozabadi, A.: "Effect of Wettability on High-Velocity Coefficient in Two-Phase Gas/Liquid Flow," paper SPE 102773 presented at SPE Annual Technical Conference and Exhibition, San Antonio, TX, 24-27 September 2006.
- Owolabi, O.O. and Watson, R.W.: "Effects of Rock-Pore Characteristics on Oil Recovery at Breakthrough and Ultimate Oil Recovery in Water-Wet Sandstones," SPE 26935, November 1993.
- Panga, M.K.R. and Ooi, Y.S.: "Wettability Alteration for Water-Block Prevention in High Temperature Gas Wells," paper SPE 100182 presented at SPE Europec/EAGE Annual Conference and Exhibition, 12-15 June, Austria, 2006
- Panga, M.K.R, Ismail, S., Pascal, C. and Samuel, M.: "Preventive Treatment for Enhancing Water Removal from Gas Reservoirs by Wettability Alteration," paper SPE 105367 presented at SPE Middle East Oil and Gas Conference, 11-14 March, Bahrain, 2007
- Pederson, K.S., Michelson, M.L. and Fredhium, A.O., (1996) Fluid Phase Equilibria 126, 13-28.
- Pederson, K.S. and Milter, J.: "Phase Equilibrium Between Gas Condensate and Brine at HT/HP Conditions," paper SPE 90309, presented at SPE Annual Technical Conference, Houston, TX, September 26 – 29, 2004.
- Peng, D. Y. and Robinson, D. B.: "A New Two Constant Equation of State", Ind. Eng. Chem. Fundamen., Vol. 15, No. 1, 59-64, 1976.
- Pope, G.A. and Baran, J.: "Method of Obtaining Treatment Composition for Removing the Productivity of Hydrocarbon Producing Wells," U.S patent application, filed 08/23/2006.
- Pope, G.A., Wu, W., Narayanaswamy, G., Delshad, M., Sharma, M.M. and Wang, P.: "Modeling Relative Permeability Effects in Gas-Condensate Reservoirs," paper SPE 49266, presented at SPE Annual Technical Conference, New Orleans, September 27 – 30, 1998.
- Pope, G.A., Wu, W., Narayanaswamy, G., Delshad, M., Sharma, M.M. and Wang, P.: "Modeling Relative Permeability Effects in Gas-Condensate Reservoirs With a New Trapping Model", SPE 62497, published in SPEREE, April 2000.
- Rai, R.R.: "Gas Condensates Relative Permeability Parametric Study and Core Flood Simulation" Thesis, The University of Texas at Austin, December 2003.
- Reid, R.C., Prausnitz, J.M., and Sherwood, T.K.: "The Properties of Gases and Liquids," pg-614, 3rd Edition, McGraw-Hill, New York, 1977.

- Saevareid, A., Whitson, C.H. and Fevang, ø., and.: "An Engineering Approach To Measuring And Modeling Gas Condensate Relative Permeabilities," paper presented at the 1999 SCA conference held in Goldon, CO, Aug. 2-4, 1999.
- Sänger, P. and Hagoort, J.: "Recovery of Gas Condensate by Nitrogen Injection Compared with Methane Injection," *SPEJ* (March 1998), 26-33.
- Sarkar, R., Danesh A.S. and Todd, A. C.: "Phase Behavior Modeling of Gas-Condensate Fluids Using an Equation of State:" paper SPE 22714 presented at 66th Annual Technical Conference and Exhibition of the Society of Petroleum Engineers, Dallas, TX, October 6-9, 1991.
- Schmidt, G. and Wenzel, H.: "A Modified Van der Waal Type Equation of State," *Chem. Eng. Sci.*, Vol. 135, PP 1503-1512, 1980.
- Schramm, L.L.: "Surfactants: Fundamentals and Applications in the Petroleum Industry," Cambridge University press, 2000.
- Settari, A., Bachman, R.C., Hovem, K. and Paulson, S.G.: "Productivity of Fractured Gas Condensate Wells – A Case Study of Smorbukk Field," paper SPE 35604, presented at Gas Technology Conference, Calgary, Canada, 28 April – 1 May, 1996.
- Sharma M.M. and Wunderlich, R.W.: "The Alteration of Rock Properties Due to Interactions with Drilling Fluid Components," paper SPE 14302, presented at SPE Annual Technical Conference and Exhibition, Las Vegas, 22-26 Sep 1985
- Sharma M.M. and Wunderlich, R.W.: "The Alteration of Rock Properties Due to Interactions with Drilling Fluid Components," *Journal of Petroleum Science and Engineering* Vol.1, April 1987 (pg 127-143)
- Sharma M.M. and Filoco, P.R.: "Effect of Brine Salinities and Crude-oil Properties on Oil Recovery and Residual Saturations," *SPE Journal* Vol.5, No.3, September 2000 (pg 293-300)
- Sharma, R.: "Modeling Gas Condensate Reservoir and Development of a New Hybrid Well Model," MS Thesis, The University of Texas at Austin, May 2003.
- Smits, R.M.M., N. van der Post, Al Shaidi, S.M., "Accurate Prediction of Well Requirements in Gas Condensate Fields," SPE 68173, SPE Middle East Oil Show, 17-20 March, Bahrain, 2001
- Soave, G.: "Equilibrium Constants From a Modified Redlich-Kwong Equation of State", *Chem. Eng. Sci.* (1972) 27, p 1197-1203.

- Sohrabi, M., Henderson, G.D., Tehrani, D.H. and Danesh, A.: "Visualisation of Oil Recovery by Water Alternating Gas (WAG) Injection Using High Pressure Micromodels – Water-Wet System," paper SPE 63000, presented at 2000 SPE Annual Technical Conference and Exhibition, Dallas, Texas, October 1-4, 2000.
- Tang, G.Q. and Firoozabadi, A.: "Relative Permeability Modification in Gas Liquid Systems Through Wettability Alteration to Intermediate Gas-Wetting," paper SPE 62934 presented at the 2000 Annual Technical Conference and Exhibition held in Dallas, TX, Oct. 1-4, 2000.
- Tang, G.Q. and Firoozabadi, A.: "Relative Permeability Modification in Gas Liquid Systems Through Wettability Alteration to Intermediate Gas-Wetting," SPEREE (2002).
- Walker, J.G.: "Laboratory Evaluation of Alcohols and Surfactants to Increase Production from Gas-Condensate Reservoirs," M.S. Thesis, The University of Texas at Austin, December 2000.
- Wang P. and Pope G.A.: "Proper Use of Equations of State for Compositional Reservoir Simulation," paper SPE 69071, Distinguished Author Series, JPT, July 2001.
- Wang, P., Pope, G. A. and Sepehrnoori, K., "Development of Equations of State for Gas Condensates for Compositional Petroleum Reservoir Simulation," *In Situ*, 24 (2&3) 2000

Vita

Vishal Bang was born in Amravati, Maharashtra, India on 2nd September 1980, the son of Mr. Shyam Sundar Bang and Mrs. Shobha Bang. After completing his high school education at Birla Vidya Niketan, New Delhi, India, in 1998, he entered Maharashtra Institute of Technology, Pune, India. He graduated with a Bachelors degree in Petroleum Engineering in July 2002. He worked as a Production Engineer in GeoEnpro Petroleum Ltd., India for 4 months. In January 2003, he entered the Graduate School at the University of Texas at Austin. He was awarded a Masters Degree in Petroleum Engineering on May 2005. Then, he was admitted in the PhD program in Petroleum Engineering at the University of Texas at Austin. Vishal did summer internships with ConocoPhillips and ExxonMobil during his graduate studies at the University of Texas at Austin.

Permanent address: M-63, Greater Kailash-2,
New Delhi-110048, India

This dissertation was typed by the author.